

# INDIAN JOURNAL OF PHYSICS

VOL. 44

No. 1

AND

VOL. 53

PROCEEDINGS

No. 1

OF THE

INDIAN ASSOCIATION FOR THE CULTIVATION OF SCIENCE

*(Edited in collaboration with the Indian Physical Society).*

JANUARY 1970

---

PUBLISHED BY THE  
INDIAN ASSOCIATION FOR THE CULTIVATION OF SCIENCE  
JADAVPUR, CALCUTTA-32

## BOARD OF EDITORS

F. C. AULUCK	D. N. KUNDU
K. BANERJEE	B. D. NAG CHAUDHURI
D. BASU	R. RAMANNA
D. M. BOSE	K. R. RAO
S. N. BOSE	S. C. SIKKAR
S. D. CHATTERJEE	B. N. SRIVASTAVA
S. R. KHASTGIR	A. R. VERMA
D. S. KOTHARI	A. BOSE ( <i>Hon. Secretary</i> )

## EDITORIAL COLLABORATORS

R. K. ASUNDI	S. N. GHOSH	N. K. SAHA
G. N. BHATTACHARYA	S. GUPTA	N. N. SAHA
J. N. BHAR	G. S. KASTHA	D. SHARMA
V. G. BHIDE	R. C. MAZUMDAR	VIKRAM A. SARABHAI
H. N. BOSE	Y. G. NAIK	R. K. SEN
S. K. CHAKRABORTY	S. R. PALIT	A. K. SEN GUPTA
J. S. CHATTERJEE	T. PRADHAN	NAND LAL SINGH
N. N. DAS GUPTA	B. RAMACHANDRA RAO	N. R. TAWDE
J. DHAR	H. RAKSHIT	B. V. THOSAR *
A. K. DUTTA	A. K. RAY CHOUDHURY	P. VENKATESWABLU
S. DUTTA MAZUMDAR	A. K. SAHA	R. VIJAYRAGHAVAN

## RATES OF ADVERTISEMENT

<i>Ordinary page</i>	<i>One insertion</i>		<i>Six insertions</i>		<i>12 insertions</i>	
	India	Foreign	India	Foreign	India	Foreign
Full page	Rs. 75/-	\$ 30	Rs. 375/-	\$ 150	Rs. 720/-	\$ 288
Half page	„ 40/-	„ 18	„ 200/-	„ 80	„ 380/-	„ 152
Quarter page	„ 22/-	„ 88				
<i>Cover (back inside)</i>						
Full page	Rs. 130/-	\$ 52	Prorata		Prorata	
Half page	Rs. 70/-	„ 28				
<i>Page facing text matter</i>						
Full page	Rs. 90/-	\$ 36	„		„	
Half page	Rs. 50/-	„ 20				
<i>Page facing front inside cover</i>						
Full page	Rs. 90/-	\$ 36	„		„	
Half page	Rs. 50/-	„ 20				
<i>Page facing inside back cover</i>						
Full page	Rs. 90/-	\$ 36	„		„	
Half page	Rs. 50/-	„ 20				

N. B.—Rates are exclusive of the cost of blocks.

**Annual Subscription**—Inland Rs. 40.00 ; Foreign \$ 14.00 per volume

Cost of reprints (without cover) : Rs. 5 per page per 50 copies.



Regd. No. C-90

# INDIAN JOURNAL OF PHYSICS

VOL. 44

AND

## PROCEEDINGS

OF THE

Indian Association for the Cultivation of Science, Vol. 53

*(Edited in Collaboration with the Indian Physical Society)*

CONTENTS, SUBJECT INDEX AND AUTHOR INDEX, 1970

( With Sixteen Plates )

IJPYAS 44 (1-12) 1-666 (1970)

Published by the Registrar, Indian Association for the Cultivation of Science,  
Jadavpur, Calcutta-32 and printed by Prokash Chandra Chakroberty,  
Eka Press, 204/1, B. T. Road, Calcutta-35

**1970**

## BOARD OF EDITORS

F. C. AULUCK	D. N. KUNDU
K. BANERJEE	B. D. NAG CHAUDHURI
D. BASU	R. RAMANNA
D. M. BOSE	K. R. RAO
S. N. BOSE	S. C. SIKKAR
S. D. CHATTERJEE	B. N. SRIVASTAVA
S. R. KHASTGIR	A. R. VERMA
D. S. KOTHARI	A. BOSE ( <i>Hon. Secretary</i> )

## EDITORIAL COLLABORATORS

R. K. ASUNDI	S. N. GHOSH	N. K. SAHA
G. N. BHATTACHARYA	S. GUPTA	N. N. SAHA
J. N. BHAR	G. S. KASTHA	D. SHARMA
V. G. BHIDE	R. C. MAZUMDAR	VIKRAM A. SARABHAI
H. N. BOSE	Y. G. NAIK	R. K. SEN
S. K. CHAKRABORTY	S. R. PALIT	A. K. SEN GUPTA
J. S. CHATTERJEE	T. PRADHAN	NAND LAL SINGH
N. N. DAS GUPTA	B. RAMACHANDRA RAO	N. R. TAWDE
J. DEAR	H. RAKSHIT	B. V. THOSAR
A. K. DUTTA	A. K. RAY CHOUDHURY	P. VENKATESWARLU
S. DUTTA MAZUMDAR	A. K. SAHA	R. VIJAYRAGHAVAN

# INDIAN JOURNAL OF PHYSICS VOL. 44, 1970

## CONTENTS

### No. 1. January

	PAGE
1. On mechanical response in a piezoelectric plate characterized by a diffusion and subjected to a prescribed polarization gradient—Alok Chakrabarty .. .. .	1
2. On the assignment of vibration frequencies of ortho-, meta- and para-resols—J. Jha and S. Chattopadhyay .. .. .	9
3. Gamma ray spectroscopy of $^{187m}\text{W}$ —B. P. Pathak, S. C. Gujrathi and S. K. Mukherjee .. .. .	19
4. Problem of screw dislocation in a non-homogeneous transversely isotropic annular disc—Sanjib Kumar Chakrabarti .. .. .	30
5. Infrared spectrum of anhydrous citric acid in the solid state-I.—K. Mallikarjuna Rao and C. K. Narayanaswamy .. .. .	34
6. Effect of radiative heat transfer on the propagation of cylindrical shock waves—T. D. Varma .. .. .	39
7. Unsteady heat distribution in an orthotropic rectangular rod moving along the direction of its length—M. P. Gupta and V. P. Saxena ..	48

### LETTERS TO THE EDITOR—

1. Field measurements in dc and hf gas discharges—D. R. Gupta and G. L. Gupta .. .. .	57
2. Polarized absorption spectrum of $\text{Fe}^{3+}$ doped in $\text{CsCdCl}_3$ at $77^\circ\text{K}$ —Ranjit Kr. Saha, A. Bose and Mihir Chowdhury .. .. .	59
3. Statistically linear mass relation of elementary particles and its representation by a polynomial curve fitting equation—B. J. Bhattacharjee	60
4. Hydrogen excitation in $\text{H}-\alpha$ collision by second Born approximation—Jayasri Chowdhury (née Sen) and D. M. Bhattacharya .. .. .	63
5. On parameter estimation of Gibb's canonical distribution—C. G. Chakrabarti .. .. .	65
6. Effective atomic numbers for scattering processes of gamma rays in alloys—M. Sriramchandra Murty, M. N. Sectaramanath, J. Rama Rao and K. Parthasaradhi .. .. .	68

## No. 2. February

	PAGE
8. On wide-band communication techniques using pseudo-random and orthogonal sequences-I.—N. B. Chakraborti, A. K. Mukherjee and N. Pal .. .. .	71
9. ESR and optical absorption studies on certain copper complexes (Plate 1)—P. V. Gopalakrishna Murthy .. .. .	91
10. Linear flow of heat in a semi-infinite-finite solid—S. K. Ghosh and D. Bhattacharya .. .. .	101
11. Some special studies on dynamic response of a simply supported beam to impact loads (Plate 2)—R. N. Das .. .. .	108
12. Magnetic studies on natural crystals of wolframite (Fe, Mn) WO <sub>4</sub> —S. R. Guha Thakurta .. .. .	117
13. The $\pi$ - $\pi^*$ emission spectra of three isomeric fluorophenols in the near ultraviolet region (Plates 3-5)—(Miss) J. V. Shukla, K. N. Upadhya and S. K. Tiwari .. .. .	128

## LETTERS TO THE EDITOR—

7. Microwave relaxation and association of n-octanol—F. F. Hanna and K. N. Abdel-Nour .. .. .	137
8. X-ray crystallographic data for some organic compounds—M. P. Gupta and S. M. Prasad .. .. .	138
9. Application of Rao's rule to liquified inert gases—A. Qadeer, M. N. Sharma and A. S. Varma .. .. .	141
BOOK REVIEWS .. .. .	143

## No. 3, March

14. Force constants and mean amplitudes of vibration of octahedral halo-anions of IVB group elements—H. S. Singh, A. N. Pandey, B. P. Singh and Nitish K. Sanyal .. .. .	147
15. Glauber approximation in inelastic e-H scattering—A. S. Ghosh and N. C. Sil .. .. .	153
16. Second positive bands of N <sub>2</sub> in the after-glow of N <sub>2</sub> and O <sub>2</sub> mixture (Plate 6)—S. N. Ghosh, A. N. Srivastava and R. V. Shukla .. .. .	162
17. Effects of external circuit on heat transfer in MHD channel flow—V. M. Soundalgekar, B. V. Rao, D. D. Haldavnekar and R. S. Iyer .. .. .	172

	PAGE
18. Modular spark chamber (Plate 7)—Samir Ghosh, J. P. Mundra and D. Majumdar .. .. .	188
19. Unsteady hydromagnetic free convection past a vertical flat plate—Ioan Pop .. .. .	194
20. $E_2$ -transition probabilities in even nuclei—M. S. Rajput and A. Augusthy .. .. .	198
21. Capture cross-section of 14 MeV neutrons—Manjushree Majumder ..	204
LETTERS TO THE EDITOR—	
10. Near ultraviolet absorption spectrum of meta-methoxy phenol (Plate 8)—C. G. Rama Rao, B. R. K. Reddy and P. Tiruvenganna Rao ..	212
11. Comment on a note on the linear flow of a viscous incompressible conducting fluid past an infinite flat plate with constant suction in the presence of a transverse magnetic field.—V. V. Ramana Rao ..	213
BOOK REVIEWS .. .. .	215

**No. 4. April**

22. The $r$ -centroids of diatomic molecules from true potential energy curves—V. K. Vaidyan and C. Santaram .. .. .	217
23. On motions of test-particles in Kerr metric—K. D. Krori ..	227
24. Generation and properties of multilevel pseudo-random sequences—N. B. Chakraborti and A. K. Mukherjee .. .. .	232
25. Exact partition function of Ising model in magnetism in one, two and three dimensions in non-zero field—D. D. Das .. .. .	244
26. Neutron bound $S$ -state in Woods-Saxon potential—Chhaya Ganguly	253
27. A coincidence method for absolute measurement of incident energy of electrons—P. K. Bhattacharya and M. R. Bhiday .. .. .	258
LETTERS TO THE EDITOR—	
12. Modulation effects in NMR—C. Raghavendra Rao .. .. .	264
13. Vibrational spectra of o- and m-methystyrenes—V. N. Verma and Kamalash Singh .. .. .	265
14. A preliminary report on the structures of glycocyamine hemihydrate, diglycine monopicrate and 4-(N-phenyl piperizino)-6-methoxy quinaldine—Sankarananda Guha .. .. .	267
BOOK REVIEWS .. .. .	270

## No. 5. May

	PAGE
28. The Raman spectrum of cyclohexylbenzene (Plate 9)—R. N. Bapat ..	273
29. Classical distributions of charged dust—A. K. Dutta .. ..	278
30. Theory of operation of the magnetic crescograph—Arun Kumar Gupta and S. D. Chatterjee .. ..	283
31. Covalency reduction factors in $D_{4h}$ symmetry and estimation of bonding parameters from magnetic data—D. Mazumdar and U. S. Ghosh ..	292
32. Triple gamma cascade studies in $W^{182}$ from the decay of $Ta^{182}$ —U. S. Pande and B. P. Singh .. ..	300
33. Analysis of observed grain density in nuclear emulsions—R. K. Gaur and A. P. Sharma .. ..	308

## LETTER TO THE EDITOR—

15. Elastic scattering of fast electrons by nitrogen-14—G. Banerjee ..	319
--	-----

BOOK REVIEWS .. ..	323
--------------------	-----

## No. 6 June

34. Use of a logarithmic form of potential in the studies on metals—J. Behari .. ..	325
35. Ionization potentials and Rydberg series in Kr I sequence—M. S. Z. Chaghtai and Zahid Ali .. ..	330
36. Electron collision frequency in Martian ionosphere—D. C. Agarwal ..	336
37. Electronic spectra of 2, 4-xylene in different states—D. Marjit ..	339
38. On the energy loss in Čerenkov radiation—N. D. Sen Gupta ..	346
39. Measurement of diurnal cosmic ray intensity variation at Calcutta with a meson telescope—(Mrs.) Sarama Alexander and S. D. Chatterjee	350
40. The influence of a slowly varying axial magnetic field on the stability of a gravitating cylinder—P. K. Bhat .. ..	356

## LETTERS TO THE EDITOR—

16. Dielectric relaxation of 1- and 2-naphthaldehydes from microwave absorption measurements—F. F. Hanna and K. N. Abdel-Nour ..	367
--	-----

## Contents

*v*

	PAGE
17. Thermodynamic functions of the three isometric aminophenols— V. N. Verma .. .. .	369
18. Transient free convection flow with constant suction—V. V. Ramana Rao .. .. .	372
BOOK REVIEWS .. .	374

### No. 7. July

41. Rotational structure in the $^1\Pi-^1\Sigma^+$ transition of $CS^{34}$ molecule (Plates 10-13)—A. K. Chaudhury, K. N. Upadhyaya and S. N. Thakur ..	375
42. Nonlinear interaction of electromagnetic waves in a magnetized electron beam—G. S. Bajwa and K. M. Srivastava .. ..	386
43. Cherenkov type of radiation in an anisotropic electron plasma—R. M. Khan .. .. .	392
44. Dielectric function of degenerate plasma at relativistic temperatures—P. Misra and K. C. Roy .. .. .	399
45. Free convection flow of elastico-viscous liquid from horizontal plate—Shankar Prasad Mishra and Jyotirmoy Sinha Roy .. ..	405
46. Measurement of the differential elastic scattering cross-section of 662 keV gamma rays in lead—H. S. Sahota and B. S. Sood ..	415

#### LETTERS TO THE EDITOR—

19. Lattice energy and thermal expansion of diatomic crystals—V. K. Dixit and M. N. Sharma .. .. .	419
20. Gamma-gamma directional correlations of the 552-134 keV cascade in $Re^{187}$ —M. L. Narasimha Raju, A. Khayoom and D. L. Sastry ..	423
BOOK REVIEWS .. .	423

### No. 8. August

47. The binding energy calculation of triton with Faddeev equation in separable approximation—Gita Purkayastha, S. N. Banerjee and N. C. Sil ..	425
48. Elastic scattering of electrons and positrons by helium atom—G. Banerji and N. C. Sil .. .. .	431
49. On the electrical resistivities of pyrolytic graphite—A. R. Saha, P. K. Banerjee and A. K. Das .. .. .	438

	PAGE
50. Significant structure theory and thermodynamic properties of liquid carbonyl fluoride and trifluorophosphine—R. V. Gopala Rao and T. Nammalvar .. .. .	445
51. Dielectric relaxation of some large aromatic molecules in benzene from microwave absorption measurements—F. F. Hanna and K. N. Abdel-Nour .. .. .	451
52. Oscillations of inhomogeneous bounded plasma—Tushar Ray ..	457
53. A note on heat transfer due to the motion of a gradually accelerated plate—Rama Shankar Rath and Bhimsen Mahapatra ..	463
54. Spin of 4.8 MeV level of Be <sup>9</sup> —M. K. Saxena .. .. .	466
LETTERS TO THE EDITOR—	
21. A note on the level structure of <sup>199</sup> Au—M. N. Seetharamanath, B. R. Sastry and K. Parthasaradhi .. .. .	469
22. Forced convection flow past a plate with variable thermal conductivity—P. C. Sinha .. .. .	471
BOOK REVIEWS .. .. .	474

### No. 9. September

55. Spin- $\frac{1}{2}$ formalism for two level problems—H. G. Venkatesh and L. P. Dixit .. .. .	475
56. Double-boundary-layer concept in free-convection at high Prandtl numbers—Sreedhan Roy .. .. .	488
57. Lattice properties of heavier halides—I—D. C. Gupta and M. N. Sharma ..	495
58. The emission spectrum of indium monobromide (Plates 14-15)—A. Lakshminarayana and P. B. V. Harnath .. .. .	504
LETTERS TO THE EDITOR—	
23. Reliability of anode as a reference point of probe potentials in dc gas discharge—D. R. Gupta and G. L. Gupta .. .. .	511
24. Effect of rubber ingredients on its dielectric properties—F. F. Hanna, A. A. Yehia and A. Abou-Bakr .. .. .	514
25. Comparison of experimental and theoretical pair cross-sections near the threshold—J. Rama Rao, M. Sriramachandra Murty and K. Parthasaradhi .. .. .	516



## *Contents*

	PAGE
26. Some comments on exact function of Ising model in magnetism in one, two and three dimensions in non-zero field—V. P. Desai ..	518
BOOK REVIEWS .. .. .	520

### **No. 10. October**

59. Potential function for diatomic molecules—S. M. Mirajkar ..	521
60. Line and continuum spectra of H. F. at Alibag during quiet and disturbed period—A. K. Sen .. .. .	532
61. The effect of salinity on the apparent dielectric constant values of rock specimens—S. Rangachari .. .. .	537
62. Flow of a power law fluid in a rotating straight pipe-1 : Determination of flow field—Kanaka Raju .. .. .	544
63. Propagation of oblique shock waves in troposphere—V. P. Singh and Prem Kumar .. .. .	554

#### LETTERS TO THE EDITOR—

27. Crystal and molecular structure of piperidine hydrochloride—J. K. Datta Gupta .. .. .	561
28. A note concerning second and third order optical and magneto-optical activity—Debashis Mukherjee and Mihir Chowdhury ..	565
BOOK REVIEWS	568

### **No. 11. November**

64. Interaction of electromagnetic field with matter (angular momentum basis)—B. S. Rajput .. .. .	569
65. Response of a moving coil galvanometer in a vacuum tube circuit—S. D. Chatterjee and Arun Kumar Gupta .. .. .	579
67. Dielectric function of a magnetoactive degenerate plasma at relativistic temperature—P. Misra and K. C. Roy .. .. .	596
68. Magnetic properties of bismuth telluride ( $\text{Bi}_2\text{Te}_3$ ) crystals—S. R. Guha Thakurta and A. K. Bose .. .. .	601

#### LETTERS TO THE EDITOR—

29. Search for nuclear penetration in the internal conversion process of the 53 keV transition in $^{144}\text{Pr}$ —H. S. Sahota .. .. .	609
---	-----

	PAGE
30. Binding energy of hypernuclei from $K^-$ -capture (Plate 16)—T. Roy and I. K. Daffri .. .. .	610
31. A report on the crystal structure of 5-benzene sulphonamido 3-phenyl 1-2-4 triazole—Dilip Kumar Nag and Sankarananda Guha ..	613
BOOK REVIEWS	615

### No. 12. December

69. Entry-length flow in a vortical cooled pipe—S. N. Singh and R. N. Pandey .. .. .	617
70. Stability of a Homopolar device—P. K. Bhat and M. P. Srivastava ..	625
71. Quadrupole hyperfine effects in microwave spectrum of $SF_6Cl$ —K. S. R. Murty and A. K. Mohanty .. .. .	635
72. A new logarithmic form of overlap repulsion for the heavier salts—K. P. Pande, K. D. Misra and M. N. Sharma .. .. .	641
73. Hydromagnetic source flow—M. A. A. Khan and R. B. Srivastava ..	647

#### LETTERS TO THE EDITOR—

22. Infrared spectrum of dichlorosilicon-phthalocyanine—S. C. Mathur, Jai Singh and A. C. Krupnick .. .. .	657
33. Crystal and molecular structure of p-dimethylaminobenzaldehyde hydrobromide—J. K. Datta Gupta and N. N. Saha .. .. .	660

BOOK REVIEWS	664
--------------	-----

ERRATA AND ADDENDUM	666
---------------------	-----

# AUTHOR INDEX

(L) indicates Letter to the Editor

AUTHOR	SUBJECT	PAGE
<b>A</b>		
Abdel-Nour K. N.	See Hanna F. F.	137
Abdel-Nour K. N.	See Hanna F. F.	367
Abdel-Nour K. N.	See Hanna F. F.	451
Abou-Bakr A.	See Hanna F. F.	514
Agarwal D. C.	Electron collision frequency in Martian ionosphere	336
Alexander Saramma (Mrs.) , Chatterjee S. D.	Measurement of diurnal cosmic ray intensity variation at Calcutta with a meson telescope	350
Ali Zahid	See Chaghtai M. S. Z.	330
Augusthy A.	See Rajput M. S.	198
<b>B</b>		
Bajwa G. S. & Srivastava K. M.	Nonlinear interaction of electro- magnetic waves in a magnetized electron beam	386
Banerjee G.	Elastic scattering of fast electrons by nitrogen-14 (L)	319
Banerjee G. & Sil N. C.	Elastic scattering of electrons and positrons by helium atom	431
Banerjee P. K.	See Saha A. R.	438
Banerjee S. N.	See Purkayastha Gita	425
Bapat R. N.	The Raman spectrum of cyclo- hexylbenzene (Plate 9)	273
Behari J.	Use of a logarithmic form of potential in the studies on metal	325
Bhat P. K.	The influences of a slowly vary- ing axial magnetic field on the stability of a gravitating cylinder	356

( ix )

AUTHOR	SUBJECT	PAGE
Bhat P. K. & Srivastava M. P.	Stability of a Homopolar device	625
Bhattacharjee B. J.	Statistically linear mass relation of elementary particles and its representation by a polynomial curve fitting equation (L)	60
Bhattacharya D.	See Ghosh S. K.	101
Bhattacharya D. M.	See Chowdhury (née Sen) Jayasri	63
Bhattacharya P. K. & Bhiday M. R.	A coincidence method for absolute measurement of incident energy of electrons	258
Bhiday M. R.	See Bhattacharya P. K.	258
Boso A.	See Shaha Ranajit Kr.	59
Boso A. K.	See Guha Thakurta S. R.	601

**C**

Chaghtai M. S. Z. & Ali Zahid	Ionization potentials and Rydberg series in Kr I sequence	330
Chakrabarti C. G.	On parameter estimation of Gibb's canonical distribution	65
Chakrabarti Sanjib Kumar	Problem of screw dislocation in a non-homogeneous transversely isotropic annular disc	30
Chakraborti N. B. & Mukherjee A. K.	Generation and properties of multi-level pseudo-random sequences	232
Chakraborti N. B., Mukherjee A. K. & Pal N.	On wide band communication techniques using pseudo-random and orthogonal sequences-I	71
Chakrabarty Alok	On mechanical response in a piezoelectric plate characterized by a diffusion and subjected to a prescribed polarization gradient	1
Chatterjee S. D.	See Alexander Saramma (Mrs.)	350
Chatterjee S. D.	See Gupta Arun Kumar	283
Chatterjee S. D. & Gupta Arun Kumar	Response of a moving-coil galvanometer in vacuum tube circuit	579
Chattopadhyay S.	See Jha J.	9

AUTHOR	SUBJECT	PAGE
Chaudhury A. K., Upadhy K. N. Thakur S. N.	Rotational structure in the $^1\Pi-^1\Sigma^+$ transition of $\text{CS}^{34}$ molecule (Plates 10-13)	375
Chowdhury (née Sen) Jayasri & Bhattacharya D. M.	Hydrogen excitation in $\text{H}-\alpha$ colli- sion by second Born approximation	63
Chowdhury Mihir	See Mukherjee Debashis	565
Chowdhury Mihir	See Shaha Ranjit Kr.	59

**D**

Daftri I. K.	See Roy T.	610
Das A. K.	See Saha A. R.	438
Das D. D.	Exact partition function of Ising model in magnetism in one, two and three dimensions in non-zero field	244
Das R. N.	Some special studies on dynamic response of a simply supported beam to impact loads (Plate 2)	108
Datta A. K.	Classical distribution of charged dust	278
Datta Gupta J. K. & Saha N. N.	Crystal and molecular structure of piperidine hydrochloride ( <i>L</i> )	561
Datta Gupta J. K. & Saha N. N.	Crystal and molecular structure of p-dimethylamino-benzaldehyde hydrobromide ( <i>L</i> )	660
Desai V. P.	Some comments on exact parti- tion function of Ising model in magnetism in one, two and three dimensions in non-zero field ( <i>L</i> )	518
Dixit L. P.	See Venkatesh H. G.	475
Dixit V. K. & Sharma M. N.	Lattice energy and thermal expan- sion of diatomic crystals ( <i>L</i> )	419

**G**

Ganguly Chhaya	Neutron bound <i>S</i> -states in Woods- Saxon potential	253
Gaur R. K. & Sharma A. P.	Analysis of observed grain density in nuclear emulsions	308

AUTHOR	SUBJECT	PAGE
Ghosh A. S. & Sil N. C.	Glauber approximation in inelastic-H scattering	153
Ghosh Samir, Mundra J. P. & Majumdar D.	Modular spark chamber (Plate 7)	188
Ghosh S. K. & Bhattacharya D.	Linear flow of heat in a semi-infinite-finite solid	101
Ghosh S. N., Srivastava, A. N. & Shukla R. V.	Second positive bands of $N_2$ in the afterglow of $N_2$ and $O_2$ mixture (Plate 6)	162
Ghosh U. S.	See Majumdar D.	292
Guha Sankarananda	A preliminary report on the structures of glycocyamine hemihydrate, diglycine monopycricrate and 4-(N-phenyl piperizino)-6-methoxy quinaldine (L)	267
Guha Sankarananda	See Nag Dilip Kumar	613
Guha Thakurta S. R.	Magnetic studies on natural crystals of wolframite ( $Fe, Mn$ ) $WO_4$	117
Guha Thakurta S. R. & Bose A. K.	Magnetic properties of bismuth telluride ( $Bi_2Te_3$ ) crystal	601
Gujrathi, S. C.	See Pathak B. P.	19
Gupta Arun Kumar	See Chatterjee S. D.	579
Gupta Arun Kumar & Chatterjee S. D.	Theory of operation of the magnetic crecograph	283
Gupta D. C. & Sharma M. N.	Lattice properties of heavier halides-I	495
Gupta D. R. & Gupta G. L.	Field measurements in dc and hf gas discharges (L)	57
Gupta D. R. & Gupta G. L.	Reliability of anode as a reference point of probe potentials in dc gas discharge (L)	511
Gupta G. L.	See Gupta D. R.	57
Gupta G. L.	See Gupta D. R.	511
Gupta M. P. & Prasad S. M.	X-ray crystallographic data for some organic compounds (L)	138

AUTHOR	SUBJECT	PAGE
Gupta M. P. & Saxena V. P.	Unsteady heat distribution in an orthotropic rectangular rod moving along the direction of its length	48
<b>H</b>		
Haldavnekar D. D.	See Soundalgekar V. M.	171
Hanna F. F. & Abdel-Nour K. N.	Microwave relaxation and association of n-octanol ( <i>L</i> )	137
Hanna F. F. & Abdel-Nour K. N.	Dielectric relaxation of 1- and 2-naphthaldehydes from microwave measurements ( <i>L</i> )	367
Hanna F. F. & Abdel-Nour K. N.	Dielectric relaxation of some large aromatic molecules in benzene from microwave absorption measurements	451
Hanna F. F., Yehia A. A. & Abou-Bakr A.	Effect of rubber ingredients on its dielectric properties ( <i>L</i> )	514
Harnath P. B. V.	See Lakshminarayana A.	504
<b>I</b>		
Iyer R. S.	See Soundalgekar V. M.	172
<b>J</b>		
Jha J. & Chattopadhyay S.	On the assignment of vibration frequencies of ortho-, meta, and para-cresols	9
<b>K</b>		
Khan M. A. A. & Srivastava R. S.	Hydromagnetic source flow	647
Khan R. M.	Cherenkov type of radiation in an anisotropic electron plasma	392
Khayyoom A.	See Raju M. L. Narasimha	421
Krori K. D.	On motions of test-particles in Kerr metric	277
Krupnick A. C.	See Mathur S. C.	657
Kumar Prem	See Singh V. P.	554

AUTHOR	SUBJECT	PAGE
<b>L</b>		
Lakshminarayana A. & Harnath P. B. V.	The emission spectrum of in- dium monobromide (Plates 14-15)	504
<b>M</b>		
Mahapatra Bhimsen	See Rath Rama Sankar	463
Majumdar D.	See Ghosh Samir	188
Majumdar D. & Ghosh U. S.	Covalency reduction factors in $D_{4h}$ symmetry and estimation of bonding paramoters from magnetic data	292
Majumder Manjushree	Capture cross-section of 14MeV neutrons	204
Marjit D.	Electronic spectra of 2, 4-xyle- nol in different states	339
Mathur S. C., Singh Jai & Krupnick A. C.	Infrared spectrum of dichlorosi- licon-phthalocyanine (L)	657
Mirajkar S. M.	Potential function for diatomic molecules	521
Mishra Shankar Prasad & Sinha Roy Jyotirmoy	Free convection flow of elastico- viscous liquid from horizontal plate	405
Misra K. D.	See Pande K. P.	641
Misra P. & Roy K. C.	Dielectric function of degenerate plasma at relativistic tem- peratures	399
Misra P. & Roy K. C.	Dielectric function of a magne- toactive degenerate plasma at relativistic temperature	596
Mohanty A. K.	See Murty K. S. R.	635
Mukherjee A. K.	See Chakraborti N. B.	71
Mukherjee A. K.	See Chakraborti N. B.	232
Mukherjee Debashis & Chowdhury Mihir	A note concerning second and third order optical and mag- neto-optical activity (L)	565
Mukherjee S. K.	See Pathak B. P.	19



# Author Index

xxv

AUTHOR	SUBJECT	PAGE
Mundra J. P.	See Ghosh Samir	188
Murthy P. V. Gopalakrishna	ESR and optical absorption studies on certain copper complexes (Plate 1)	91
Murty K. S. R. & Mohanty A. K.	Quadrupole hyperfine effects in microwave spectrum of $\text{SF}_6\text{Cl}$	635
Murty M. Sriramachandra	See Rao J. Rama	516
Murty M. Sriramachandra, Seetaramanath M. N., Rao J. Rama & Parthasaradhi K.	Effective atomic numbers for scattering process of gamma rays in alloys (L)	68
<b>N</b>		
Nag Dilip Kumar & Guha Sankarananda	A report on the crystal structure of 5-benzene sulphonamido 3-phenyl 1-2-4-triazole (L)	613
Nammalvar T.	See Rao R. V. Gopala	445
Narayanaswamy C. K.	See Rao K. Mallikarjuna	34
<b>P</b>		
Pal N.	See Chakraborti N. B.	71
Pande U. S. & Singh B. P.	Triple gamma cascade studies in $\text{W}^{182}$ from the decay of $\text{Ta}^{182}$	300
Pandey A. N.	See Singh H. S.	147
Pandey K. P., Mishra K. D. & Sharma M. N.	A new logarithmic form of overlap repulsion for the heavier salts	641
Pandey R. N.	See Singh S. N.	617
Parthasaradhi K.	See Murty M. Sriramachandra	68
Parthasaradhi K.	See Rao J. Rama	516
Parthasaradhi K.	See Seetaramanath M. N.	469
Pathak B. P., Gujrathi S. C. & Mukherjee S. K.	Gamma ray spectroscopy of $^{185\text{m}}\text{W}$	19
Pop Ioan	Unsteady hydromagnetic free convection past a vertical flat plate	194
Prasad S. M.	See Gupta M. P.	138

AUTHOR	SUBJECT	PAGE
Purkayastha Gita, Banerjee S. N. & Sil N. C.	The binding energy calculation of triton with Faddeev equation in separable approximation	425
<b>Q</b>		
Quadeor A., Sharma M. N. & Varma A. S.	Application of Rao's rule to liquified inert gases ( <i>L</i> )	141
<b>R</b>		
Rajput B. S.	Interaction of electromagnetic field with matter (angular momentum basis)	569
Rajput M. S. & Augusthy A.	$E_2$ -transition probabilities in even nuclei	198
Raju Kanaka	Flow of a power law fluid in a rotating straight pipe-I: Determination of flow field	544
Raju M. L. Narasimha, Khayyoom A. & Sastry D. L.	Gamma-gamma directional correlations of the 552-134 keV cascade in $\text{Re}^{187}$ ( <i>L</i> )	421
Rangachari S.	The effect of salinity on the apparent dielectric constant values of rock specimens	537
Rao B. V.	See Soundalgekar V. M.	171
Rao C. G. Rama, Reddy B. R. K. & Rao P. Tiruvenganna	Near ultraviolet absorption spectrum of meta-methoxy phenol (Plate 8) ( <i>L</i> )	212
Rao C. Raghavendra	Modulation effects in NMR ( <i>L</i> )	264
Rao J. Rama	See Murty M. Sriramchandra	68
Rao J. Rama, Murty M. Sriramchandra & Parthasaradhi K.	Comparison of experimental and theoretical pair cross-sections near the threshold ( <i>L</i> )	516
Rao K. Mallikarajuna & Narayanaswamy C. K.	Infrared spectrum of anhydrous citric acid in solid state-I	34
Rao P. Tiruvenganna	See Rao C. G. Rama	212
Rao R. V. Gopala & Nammalvar T.	Significant structure theory and thermodynamic properties of liquid carbonyl fluoride and trifluoro-phosphine	445

# *Author Index*

*xvii*

AUTHOR	SUBJECT	PAGE
Rao V. V. Ramana	Comment on a note on the linear flow of a viscous incompressible conducting fluid past an infinite flat plate with constant suction in the presence of a transverse magnetic field ( $L$ )	213
Rao V. V. Ramana	Transient free convection flow with constant suction ( $L$ )	372
Rath Rama Sankar & Mahapatra Bhimsen	A note on heat transfer due to motion of a gradually accelerated plate	463
Ray Tushar	Oscillations of an inhomogeneous bounded plasma	457
Reddy B. R. K.	See Rao C. G. Rama	212
Roy K. C.	See Misra P.	399
Roy K. C.	See Misra P.	596
Roy Sreedhan	Double-boundary-layer concept in free-convection at high Prandtl numbers	488
Roy T. & Daftri I. K.	Binding energy of hyper nuclei from $K^-$ -capture (Plate 16)	610

## **S**

Saha A. R., Banerjee P. K. & Das A. K.	On the electrical resistivities of pyrolytic graphite	438
Saha N. N.	See Datta Gupta J. K.	561
Saha N. N.	See Datta Gupta J. K.	660
Sahota H. S.	Search for nuclear penetration in the internal conversion process of the 53 keV transition in $^{144}\text{Pr}$ ( $L$ )	609
Sahota H. S. & Sood B. S.	Measurement of the differential elastic scattering cross-section of 662 keV gamma rays in lead	415
Santaram C.	See Vaidyan V. K.	217
Sanyal Nitish K.	See Singh H. S.	147
Sastry B. R.	See Seetaramanath M. N.	469

AUTHOR	SUBJECT	PAGE
Sastry D. L.	See Raju M. L. Narasimha	421
Saxena M. K.	Spin of 4.8 MeV level of $\text{Bc}^8$	466
Saxena V. P.	See Gupta P. M.	48
Seetaramanath M. N.	See Murty M. Sriramchandra	68
Sectaramanath M. N., Sastry B. R. & Parthasaradlu K.	A note on the level structure of $^{199}\text{Au}$ (L)	469
Sen A. K.	Line and continuum spectra of H. F. at Alibag during quiet and disturbed periods	532
Sen Gupta N. D.	On the energy loss in Čerenkov radiation	346
Shaha Ranajit Kr., Bose A. & Chowdhury Mihir	Polarized absorption spectrum of $\text{Fe}^{2+}$ doped in $\text{CsCdCl}_3$ at $77^\circ\text{K}$ (L)	59
Sharma A. P.	See Gaur R. K.	308
Sharma M. N.	See Dixit V. K.	449
Sharma M. N.	See Gupta D. C.	495
Sharma M. N.	See Pande K. P.	641
sharma M. N.	See Qadeer A.	141
Shukla (Miss) J. V., Upadhy K. N. & Tiwari S. K.	The $\pi - \pi^*$ emission spectra of three isomeric fluorophenols in the near ultraviolet region (Plates 3-5)	128
Shukla R. V.	See Ghosh S. N.	162
Sil N. C.	See Banerji G.	431
Sil N. C.	See Ghosh A. S.	153
Sil N. C.	See Purkayastha Gita	425
Singh B. P.	See Pande U. S.	300
Singh B. P.	See Singh H. S.	147
Singh H. S., Pandey A. N., Singh B. P. & Sanyal Nitish Kr.	Force constants and mean ampli- tudes of vibration of octahedral halo-anions of IVB group elements	147
Singh Jai	See Mathur S. C.	657
Singh Kamalesh	See Verma V. N.	265
Singh S. N. & Pandey R. N.	Entry-length flow in a vertical cooled pipe	617

AUTHOR	SUBJECT	PAGE
Singh V. P. & Kumar Prem	Propagation of oblique shock waves in the troposphere	554
Sinha P. C.	Forced convection flow past a plate with variable thermal conductivity ( <i>L</i> )	471
Sinha Roy Jyotirmoy	See Mishra Shankar Prasad	405
Sood B. S.	See Sahota H. S.	415
Soundalgekar V. M., Rao B. V., Haldavnekar D. D. & Iyer R. S.	Effects of external circuit on heat transfer in MHD channel flow	172
Srivastava A. N.	See Ghosh S. N.	162
Srivastava K. M.	See Bajwa G. S.	386
Srivastava M. P.	See Bhat P. K.	625
Srivastava R. B.	See Khan M. A. A.	647
<b>T</b>		
Thakur S. N.	See Chaudhury A. K.	375
Tiwari S. K.	See Shukla (Miss) J. V.	128
<b>U</b>		
Upadhya K. N.	See Shukla (Miss) J. V.	128
Unadhva K. N.	See Chaudhury A. K.	375
<b>V</b>		
Vaidyan V. K. & Santaram C.	The $r$ -centroids of diatomic molecules from true potential energy curves	217
Varma A. S.	See Qadeer A.	141
Varma T. D.	Effect of radiative heat transfer on the propagation of cylindrical shock waves	39
Venkatesh H. G. & Dixit L. P.	Spin- $\frac{1}{2}$ formalism for two-level problems	475
Verma V. N.	Thermodynamic functions of three isomeric aminophenols ( <i>L</i> )	369
Verma V. N. & Singh Kamalesh	Vibrational spectra of o- and m-methylstyrenes ( <i>L</i> )	265
<b>Y</b>		
Yehia A. A.	See Hanna F. F.	514

# SUBJECT INDEX

(*L*) Indicates Letter to the Editor

SUBJECT	AUTHOR	PAGE
<b>A</b>		
Apparent dielectric constant values of rock specimens—The effect of salinity on the	S. Rangachari	537
<b>B</b>		
Book Reviews	143, 215, 270, 323, 374, 424, 474, 520, 568, 615, 664	
<b>C</b>		
Capture cross-section of 14 MeV neutrons	Manjushree Mazumder	204
Charged dust—Classical distribution of	A. K. Dutta	278
Cherenkov type of radiation in an anisotropic electron plasma	R. M. Khan	392
Covalency reduction factors in $D_{4h}$ symmetry and estimation of bonding parameters from magnetic data	D. Majumdar & U. S. Ghosh	292
Crystal and molecular structure of piperidine hydrochloride—( <i>L</i> )	J. K. Datta Gupta & N. N. Saha	561
Crystal and molecular structure of p-dimethylaminobenzaldehyde hydrobromide ( <i>L</i> )	J. K. Datta Gupta & N. N. Saha	660
Crystal structure of 5-benzene sulphonamido 3-phenyl 1-2-4 triazole—A report on the ( <i>L</i> )	Dilip Kumar Nag & Sankarananda Guha	613
<b>D</b>		
Degenerate plasma at relativistic temperatures—Dielectric function of	P. Misra & K. C. Roy	399

# Subject Index

xxi

SUBJECT	AUTHOR	PAGE
Dielectric properties—Effect of rubber ingredients on its ( <i>L</i> )	F. F. Hanna, A. A. Yehia & A. Abou-Bakr	514
Dielectric relaxation of 1- and 2-naphthaldehydes from microwave absorption measurements ( <i>L</i> )	F. F. Hanna & K. N. Abdel-Nour	367
Dielectric relaxation of some large aromatic molecules in benzene from microwave absorption measurements	F. F. Hanna & K. N. Abdel-Nour	451
Differential elastic scattering cross-section of 662 keV gamma rays in lead—Measurement of the	H. S. Sahota & B. S. Sood	415
Diurnal cosmic energy intensity variation at Calcutta with a meson telescope—Measurement of	(Mrs.) Saramma Alexander & S. D. Chatterjee	350
Dynamic response of a simple supported beam to impact loads—Some special studies on (Plate 2)	R. N. Das	108
<b>E</b>		
$E_2$ -transition probabilities in even nuclei	M. S. Rajput & A. Augsthy	198
Elastic scattering of fast electrons by nitrogen-14 ( <i>L</i> )	G. Banerji	319
Electrical resistivities of pyrolytic graphite—On the	A. R. Saha, P. K. Banerjee & A. K. Das	438
Electromagnetic waves in a magnetized electron beam—Nonlinear interaction of	G. S. Bajwa & K. M. Srivastava	386
Electron collision frequency in Martian ionosphere	D. C. Agarwal	336
Electronic spectra of 2, 4-xyleneol in different states	D. Marjit	339

SUBJECT	AUTHOR	PAGE
Emission spectrum of indium mono-bromide—The (Plates 14-15)	A. Lakshminarayana & P. B. V. Harnath	504
Energy loss in Čerenkov radiation— On the	N. D. Sen Gupta	346
Entry-length flow in a vertical cooled pipe	S. N. Singh & R. N. Pandey	617
Errata and Addendum		666
ESR and optical absorption studies on certain copper complexes (Plate 1)	P. V. Gopalakrishna Murthy	91
Experimental and theoretical pair cross-sections near the threshold—Comparison of ( <i>L</i> )	J. Rama Rao, M. Sriramchandra Murty & K. Parthasaradhi	516
<b>F</b>		
Faddeév equation in separable approximation—The binding energy calculation of triton with	Gita Purkayastha, S. N. Banerjee & N. C. Sil	425
Field measurements in dc and hf gas discharges ( <i>L</i> )	D. R. Gupta & G. L. Gupta	57
Flow of elastico-viscous liquid from horizontal plane—Free convection	Shankar Prasad Mishra & Jyotirmoy Sinha Roy	405
Forced convection flow past a plate with variable thermal conductivity ( <i>L</i> )	P. C. Sinha	471
Free-convection at high Prandtl numbers—Double-boundary-layer concept	Sreedhan Roy	488
<b>G</b>		
Gamma ray spectroscopy of $^{186m}\text{W}$	B. P. Pathak, S. C. Gujrathi & S. K. Mukherjee	19
Gamma-gamma directional correlations of the 552-134 keV cascade in $\text{Re}^{187}$	M. L. Narasimha Raju, A. Khayyoom & D. L. Sastry	421



# Subject Index

xxvii

SUBJECT	AUTHOR	PAGE
Gibbs' canonical distribution—On parameter estimation of ( <i>L</i> )	C. G. Chakrabarti	65
Glauber approximation in inelastic e-H scattering	A. S. Ghosh & N. C. Sil	153
Grain density in nuclear emulsions—Analysis of observed	R. K. Gaur & A. P. Sharma	308
<b>H</b>		
Heat transfer due to the motion of a gradually accelerated plate—A note on	Rama Shankar Rath & Bhimsen Mahapatra	463
Heat transfer in MHD channel flow—Effects of external circuit on	V. M. Soundalgekar, B. V. Rao, D. D. Haldavnekar & R. S. Iyer,	172
Hydrogen excitation in H- $\alpha$ collision by second Born approximation ( <i>L</i> )	Jayasri Chowdhury (née Sen) & D. M. Bhattacharya	63
Hydromagnetic source flow	M. A. A. Khan & R. S. Srivastava	647
Hypernuclei from K-capture—Binding energy of (Plate 16) ( <i>L</i> )	T. Roy & I. K. Daftri	610
Incident energy of electrons—A coincidence method for absolute measurement of	P. K. Bhattacharya & M. R. Bhiday	258
Infrared spectrum of anhydrous citric acid in the solid state-I	K. Mallikarjuna Rao & C. K. Narayanaswamy	34
Infrared spectrum of dichlorosilicon-phthalocyanine ( <i>L</i> )	S. C. Mathur, Jai Singh & A. C. Krupnick	657
Inhomogeneous bounded Oscillations of an	Tushar Ray	457

SUBJECT	AUTHOR	PAGE
Interaction of electromagnetic field with matter (angular momentum basis)	B. S. Rajput	569
Internal conversion process of the 53 keV transition in $^{144}\text{Pr}$ —Search for nuclear penetration in the ( <i>L</i> )	H. S. Sahota	609
Ionization potentials and Rydberg series in Kr I sequence	M. S. Z. Chaghtai & Zahid Ali	330
<b>L</b>		
Lattice energy and thermal expansion of diatomic crystals ( <i>L</i> )	V. K. Dixit & M. N. Sharma	419
Lattice properties of heavier halides-I	D. C. Gupta & M. N. Sharma	495
Level structure of $^{199}\text{Au}$ —A note on ( <i>L</i> )	M. N. Seetaramanath, B. R. Sastry & K. Parthasaradhi	469
Line and continuum spectra of H.F. at Alibag during quiet and disturbed period	A. K. Sen	532
Linear flow of a viscous incompressible conducting fluid past an infinite flat plate with constant suction in the presence of a transverse magnetic field—Comment on a note on the ( <i>L</i> )	V. V. Ramana Rao	213
Linear flow of heat in a semi-infinite solid	S. K. Ghosh & D. Bhattacharya	101
Logarithmic form of potential in the studies on metals—Use of a	J. Behari	325
<b>M</b>		
Magnetic crescograph—Theory of operation of the	Arun Kumar Gupta & S. D. Chatterjee	283
Magnetic properties of bismuth telluride ( $\text{Bi}_2\text{Tc}_3$ ) crystals	S. R. Guha Thakurta & A. K. Bose	601

# Subject Index

xxv

SUBJECT	AUTHOR	PAGE
Magnetic studies on natural crystals of wolframite (Fe, Mn) $\text{WO}_4$	S. R. Guha Thakurta	117
Magnetoactive degenerate plasma at relativistic temperature—Dielectric function of a	P. Misra & K. C. Roy	596
Mass relation of elementary particles and its representation by a polynomial curve fitting equation—Statistically linear ( $L$ )		60
Microwave-relaxation and association of n-octanol ( $L$ )	F. F. Hanna & K. N. Abdel-Nour	137
Microwave spectrum of $\text{SF}_5\text{Cl}$ —Quadrupole hyperfine effects in	K. S. R. Murty & A. K. Mohanty	635
Modular spark chamber (Plate 7)	Samir Ghosh, J. P. Mundra & D. Mazumdar	188
Modulation effect in NMR( $L$ )	C. Raghavendra Rao	264
Motions of test-particles in Kerr metric—On	K. D. Krori	227
Moving-coil galvanometer in a vacuum tube circuit—Response of a	S. D. Chatterjee & Arun Kumar Gupta	579
Multilevel pseudo-random sequences—Generation and properties of	N. B. Chakraborti & A. K. Mukherjee	232

## N

Near ultra-violet absorption spectrum of meta-methoxy phenol (Plate 8) ( $L$ )	C. G. Rama Rao, B. R. K. Reddy & P. Tiruvenganna Rao	212
Non-homogeneous transversely isotropic annular disc—Problem of screw dislocation in a	Sanjit Kumar Chakrabarti	30

SUBJECT	AUTHOR	PAGE
<b>O</b>		
Oblique shock waves in the troposphere— Propagation of	V. P. Singh & Prem Kumar	554
Orthotropic rectangular rod moving along the direction of its length— Unsteady heat distribution in an	P. M. Gupta & V. P. Saxena	48
Overlap repulsion for the heavier salts— A new logarithmic form of	K. P. Pande, K. D. Misra & M. N. Sharma	641
<b>P</b>		
$\pi-\pi^*$ emission spectra of three isomeric fluorophenols in the near ultraviolet region—The (Plates 3-5)	(Miss) J. V. Shukla, K. N. Upadhyaya & S. K. Tiwari	128
$^1\Pi-^1\Sigma^+$ transition of $\text{CS}^{34}$ molecule— Rotational structure in (Plates 10-13)	A. K. Chaudhury, K. N. Upadhyaya & S. N. Thakur	375
Partition function of Ising model in magnetism in one, two and three dimensions in non-zero field—Exact	D. D. Das	244
Partition function of Ising model in magnetism in one, two and three-di- mensions in non-zero field—Some comments on exact ( <i>L</i> )	V. P. Desai	518
Piezoelectric plate characterized by a diffusion and subjected to a prescribed polarization gradient—On mechanical response in a	Alok Chakrabarty	1
Polarized absorption spectrum of $\text{Fe}^{2+}$ doped in $\text{CsCdCl}_3$ at $77^\circ\text{K}$ ( <i>L</i> )	Ranjit Kr. Shaha, A. Bose & Mihir Chowdhury	59
Potential function for diatomic mole- cules	S. M. Mirajkar	521

SUBJECT	AUTHOR	PAGE
Power law fluid in a rotating straight pipe—Flow of a—I : Determination of flow field	Kanaka Raju	544
Probe potentials in dc gas discharge—Reliability of anode as reference point of ( <i>L</i> )	D. R. Gupta & G. L. Gupta	511
Propagation of cylindrical shock waves—Effect of radiative heat transfer on the	T. D. Varma	39
<b>R</b>		
<i>r</i> -centroids of diatomic molecules from true potential energy curves—The	V. K. Vaidyan & C. Santaram	217
Raman spectra of cyclohexylbenzene—The (Plate 9)	R. N. Bapat	273
Rao's rule to liquified inert gases—Application of ( <i>L</i> )	A. Qadeer, M. N. Sharma & A. S. Varma	141
<b>S</b>		
Scattering processes of gamma rays in alloys—Effective atomic number for ( <i>L</i> )	M. Sriramachandra Murty, M. N. Seetaramanath J. Rama Rao & K. Parthasaradhi	68
Second and third order optical and magneto-optical activity—A note concerning ( <i>L</i> )	Debashis Mukherjee & Mihir Chowdhury	565
Second positive bands of $N_2$ in the afterglow of $N_2$ and $O_2$ mixture (Plate 6)	S. N. Ghosh, A. N. Srivastava & R. V. Shukla	162
Slowly varying axial magnetic field on the stability of a gravitating cylinder—The influence of a	P. K. Bhat	356

SUBJECT	AUTHOR	PAGE
Spin- $\frac{1}{2}$ formalism for two-level problems	H. G. Venkatesh & L. P. Dixit	475
Spin of 4.8 MeV level of Be <sup>9</sup>	M. K. Saxena	466
Stability of a Homopolar device	P. K. Bhat & M. P. Srivastava	625
Structures of glycocyamine hemihydrate, diglycine monopierate and 4-(N-phenyl piperizino)—6-methoxy quinaldine—A preliminary report on the (L)	Sankarananda Guha	267
Structure theory and thermodynamic properties of liquid carbonyl fluoride and trifluorophosphine—Significant	R. V. Gopala Rao & T. Nammalvar	445
<b>T</b>		
Thermodynamic functions of the three isomeric aminophenols (L)	V. N. Verma	369
Transient free convection flow with constant suction (L)	V. V. Ramana Rao	372
Triple gamma cascade <sup>182</sup> studies in W from the decay of Ta <sup>182</sup>	U. S. Pande & B. P. Singh	300
<b>U</b>		
Unsteady hydromagnetic free convec- tion past a vertical flat plate	Ioan Pop	194
<b>V</b>		
Vibration frequencies of ortho-, meta- and para-cresols—On the assign- ment of	J. Jha & S. Chattopadhyay	
Vibration of octahedral halo-anions of IVB groups elements—Force constants and mean amplitudes of	H. S. Singh, A. N. Pandey, B. P. Singh & Nitish K. Sanyal	147
Vibrational spectra of o-and m-methyl- styrenes (L)	V. N. Verma & Kamallesh Singh	265

*Subject Index**xxix*

SUBJECT	AUTHOR	PAGE
<b>W</b>		
Wide-band communication techniques using pseudo-random and orthogonal sequences-I—On	N. B. Chakraborti, A. K. Mukherjee & N. Pal	71
Woods-Saxon potential—Neutron bound <i>S</i> -state in	Chhaya Ganguly	253
<b>X</b>		
X-ray crystallographic data for some organic compounds ( <i>L</i> )	M. P. Gupta & S. M. Prasad	138





# INDIAN JOURNAL OF PHYSICS

VOL. 44

No. 1

AND

VOL. 53

PROCEEDINGS

No. 1

OF THE

INDIAN ASSOCIATION FOR THE CULTIVATION OF SCIENCE

*(Edited in collaboration with the Indian Physical Society).*

JANUARY 1970

PUBLISHED BY THE

INDIAN ASSOCIATION FOR THE CULTIVATION OF SCIENCE

JADAVPUR, CALCUTTA-32



## On mechanical response in a piezoelectric plate characterized by a diffusion and subjected to a prescribed polarization gradient

ALOK CHAKRABARTY

*Department of Physics, S. A. Jaipuria College, Calcutta-5*

(Received 10 March 1969—Revised 26 March 1970)

The paper is concerned with the mechanical response in a piezoelectric plate transducer under constant voltage input across it; the plate being characterized by a prescribed diffusion and subjected to an exponentially decaying polarization gradient.

### INTRODUCTION

The studies of piezoelectric transducer from the point of view of mechanics of continuous media are largely due to Redwood (1961), Mason (1950), Filipezynski (1956), Sinha (1963, 1965 and 1967), Giri (1966), Das (1967), Chakrabarty (1968, 1969) and others. This article is a similar attempt seeking to investigate the mechanical response due to a constant voltage input under a prescribed diffusion and characterised by an exponentially decaying polarization gradient. The analysis presented here conforms to the line of investigation undertaken by the above-mentioned authors. It has been found that the method of Laplace transform facilitates the solution of the problem.

### PROBLEM, FUNDAMENTAL EQUATION AND BOUNDARY CONDITION

Let  $x = 0$  and  $x = X$  be the extremities of a piezoelectric plate in the direction of its thickness (taken as the  $X$ -axis), excited by a constant voltage  $\phi_0$  at its ends. The transducer is characterised by an exponentially decaying polarization gradient. Let there be a cavity excited by a field defined by  $e^{-kx}$ ,  $\delta(t)$ ,  $k$  being a constant and  $\delta(t)$  is the well known Dirac's Delta function. The plate is taken as rigidly backed at  $x = X$ .

The equations of state for the plate, (Redwood 1961) are

$$T_1 = c_{11} \frac{\partial \xi}{\partial x} + e_{11} E_1 \quad (1)$$

$$P_1 = e_{11} \frac{\partial \xi}{\partial x} + k_{11} E_1 \quad (2)$$

where  $T_1$  = stress,  $c_{11}$  = average stiffness co-efficient,  $\xi$  = mechanical deformation at any point  $x$ ,  $e_{11}$  = piezoelectric constant,  $P_1$  = polarization vector and  $k_{11}$  = electric susceptibility.

# Alok Chakrabarty

In accordance with our assumption, we have

$$\frac{\partial P_1}{\partial x} = -P_0 e^{-rt} \quad (3)$$

so that by suitable choice

$$P_1 = -P_0 x e^{-rt} \quad (4)$$

where  $P_0$  is a constant and  $r$  is a decaying factor. This assumption is justified by experimental facts (Swann, 1950).

Eliminating  $E_1$  from (1) and (2) we have

$$T_1 = a \frac{\partial \xi}{\partial x} + \frac{e_1}{k_{11}} P_1 \quad (5)$$

where  $a = c_{11} - e_{11}^2/k_{11}$

Differentiating (5) and using (4) we get

$$\frac{\partial T_1}{\partial x} = a \frac{\partial^2 \xi}{\partial x^2} - \frac{e_{11} P_0}{k_{11}} e^{-rt} \quad (6)$$

Using (6) with Newton's equation

$$\rho \frac{\partial^2 \xi}{\partial t^2} - \frac{\partial T_1}{\partial x} = e^{-kx} \cdot \delta(t)$$

we have

$$\rho \frac{\partial^2 \xi}{\partial t^2} - a \frac{\partial^2 \xi}{\partial x^2} + \frac{e_{11} P_0}{k_{11}} e^{-rt} = e^{-kx} \cdot \delta(t) \quad (7)$$

Equation (7) constitutes the fundamental equation of the problem.

The boundary conditions are that both the displacement and force are continuous at the end  $x = 0$  of the transducer. Also the transducer being rigidly backed at  $x = X$ , the mechanical displacement at  $x = X$  must be zero.

## SOLUTION OF THE PROBLEM

Taking Laplace transform (7) of parameter  $s (s > 0)$

$$\text{who have} \quad \frac{\partial^2 \xi}{\partial x^2} - \frac{\rho}{a} s^2 \xi = \frac{1}{a} \left[ \frac{e_{11} P_0}{k_{11}} \cdot \frac{1}{s+r} - e^{-kx} \right] \quad \dots (8)$$

Solving (8) we get

$$\xi = A e^{-\frac{v}{v} x} + B e^{-\frac{v}{v} x} - \frac{e_{11} P_0}{k_{11} \rho \cdot s^2 (s+r)} + \frac{e^{-kx}}{\rho \{s^2 - (kv)^2\}} \quad \dots (9)$$

where  $A$  and  $B$  are constants of integration and  $v^2 = a/\rho$ , and it is assumed that  $\xi(0) = 0$ ,  $\xi'(0) = 0$ .

To evaluate  $A$  and  $B$  from the boundary conditions, we attach two mechanical systems 1 and 2 as assumed by Rodwood (1961) to the extremities  $x = 0$  and  $x = X$ . We denote the corresponding entities,  $A_1, B_1$  and  $A_2, B_2$  by the symbols 1 and 2, respectively. In that case, since the transducer is rigidly backed,

$$A_2 = B_2 = 0 \quad \text{and} \quad A_1 = 0 \quad (10)$$

Also continuity of displacement at  $x = 0$ , gives

$$\bar{\xi}(0) = \bar{\xi}_1(0)$$

$$\text{i.e.} \quad A + B - \frac{e_{11}P_0}{k_{11}\rho} \cdot \frac{1}{s^2(s+r)} + \frac{1}{\rho\{s^2 - (kv)^2\}} = B_1 \quad \dots \quad (11)$$

$$\text{where} \quad \bar{\xi}_1(x) = B_1 e^{\frac{s}{v}x} \quad \dots \quad (12)$$

Again for a rigidly backed transducer  $\bar{\xi}(X) = 0$ .

$$\text{Hence} \quad A e^{-\frac{s}{v}X} + B e^{\frac{s}{v}X} - \frac{e_{11}P_0}{k_{11}\rho} \cdot \frac{1}{s^2(s+r)} + \frac{e^{-kX}}{\rho\{s^2 - (kv)^2\}} = 0 \quad \dots \quad (13)$$

Using (1), (3) and the relation  $E_1 = D_1 - 4\pi P_1$ , we have

$$T_1 = c_{11} \frac{\partial \xi}{\partial x} + e_{11} \frac{Q_1}{YZ} + 4\pi e_{11} P_0 x e^{-rt} \quad \dots \quad (14)$$

where  $D_1 = \frac{Q_1}{YZ}$ ,  $Y$  is length of the transducer along  $Y$ -axis,  $Z$  its length along  $Z$ -axis, and  $Q_1$  is the charge.

Taking Laplace transform of (14) and using (9) we have

$$\bar{T}_1(0) = c_{11} \left[ -\frac{s}{v}A + \frac{s}{v}B - \frac{k}{\rho} \cdot \frac{1}{s^2 - (kv)^2} \right] + e_{11} \frac{\bar{Q}_1}{YZ} \quad \dots \quad (15)$$

If  $T$  stands for the stress for the medium towards the left of the transducer (i.e., at  $x = 0$ ) then from (12)

$$\bar{T} = \frac{sc}{v} B_1 e^{\bar{v}} \quad \dots \quad (16)$$

$c$  being a similar constant as  $c_{11}$ .

$$\text{Hence} \quad \bar{T}(0) = \frac{sc}{v} B_1 \quad \dots \quad (17)$$

For continuity of stress at  $x = 0$ , we have from (15) and (17)

$$c_{11} \left[ -\frac{s}{v} A + \frac{s}{v} B - \frac{k}{\rho} \cdot \frac{1}{s^2 - (kv)^2} \right] + e_{11} \frac{Q_1}{YZ} = s \frac{c}{v} B_1 \quad \dots (18)$$

Again

$$\begin{aligned} \bar{V} &= -(\bar{V}_X - \bar{V}_0) = \int_0^X \bar{E} dx \\ &= \int_0^X (\bar{D}_1 - 4\pi \bar{P}_1) dx \end{aligned}$$

$$\text{Hence,} \quad \bar{\phi}_0 = \frac{\bar{Q}_1}{YZ} X + \frac{4\pi P_0}{s+r} \cdot \frac{X^2}{2} \quad \dots (19)$$

since the voltage across the transducer is given by  $\phi_0$

Substituting the value of  $B_1$  from (11) in (18) and then eliminating  $\bar{Q}_1$  from (18) and (19) we get a relation connecting  $A$  and  $B$ . Using this relation along with (13) we get the values of  $A$  and  $B$ . The values of  $A$  and  $B$  are given by the following expressions

$$A = \frac{l_2 m_3 - l_3 e^{-\frac{s}{v} X}}{l_1 e^{\frac{s}{v} X} - l_2 e^{-\frac{s}{v} X}} \quad \text{and} \quad B = \frac{l_3 e^{-\frac{s}{v} X} - l_1 m_3}{l_1 e^{-\frac{s}{v} X} - l_2 e^{\frac{s}{v} X}} \quad \dots (20)$$

where

$$\left. \begin{aligned} l_1 &= -\frac{1}{v}(c_{11} + c), \quad l_2 = -\frac{1}{v}(c - c_{11}) \\ l_3 &= \left[ \frac{c}{\rho v} - \frac{c_{11} k}{\rho} \right] \cdot \frac{1}{s\{s^2 - k^2 v^2\}} + \frac{e_{11} P_0 c}{v} \cdot \frac{1}{s^2(s+r)} - \frac{c}{\rho v} \cdot \frac{1}{s^2 - k^2 v^2} \\ &\quad + \frac{e_{11} \phi_0}{s^2} - \frac{2\pi P_0 e_{11} X^2}{s(s+r)} \\ m_3 &= -\frac{e_{11} P_0}{k_{11} \rho} \cdot \frac{1}{s^2(s+r)} + \frac{e^{-kX}}{\rho\{s^2 - (kv)^2\}} \end{aligned} \right\} (20A)$$

Substituting the values of  $A$  and  $B$  in (9) we have

$$\xi = \frac{\left( l_2 m_3 - l_3 e^{-\frac{s}{v} X} \right) e^{-\frac{s}{v} X} + \left( l_3 e^{-\frac{s}{v} X} - l_1 m_3 \right) e^{-\frac{s}{v} X}}{l_1 e^{\frac{s}{v} X} - l_2 e^{-\frac{s}{v} X}} + [\bar{m}_3]_{X=X} \quad (20B)$$

It is simple to detect that  $\xi = 0$  when  $x = X$ . This must be the case, since the transducer is rigidly backed at  $x = X$ .

The inversion being too complicated, we find it for a particular value of  $x$ , say  $X/2$ . This is to be done by the methods of approximation. We restrict to approximation followed by Redwood (1961) and find

$$\bar{\xi}_X = \frac{l_2}{l_1} m_3 e^{-\frac{3xX}{2v}} - \frac{l_3}{l_1} e^{-\frac{3xX}{2v}} - m_3 e^{-\frac{xX}{2v}} - \frac{l_3}{l_1} e^{-\frac{xX}{2v}} + [m_3]_{X=\frac{X}{2}} \quad (21)$$

Substituting for  $l_3$  and  $m_3$  and taking inverse transform we have

$$\begin{aligned} \xi_{\frac{X}{2}} = & \frac{l_2}{l_1} \frac{e_{11}P_0}{k_{11}\rho} \left[ \frac{1}{r} \left( t - \frac{3X}{2v} \right) - \frac{1}{r^2} + \frac{1}{r^2} e^{-r \left( t - \frac{3X}{2v} \right)} \right] + \frac{l_2 e^{-\frac{kX}{2}}}{l_1 \rho} \frac{\sinh \left[ kv \left( t - \frac{3X}{2v} \right) \right]}{kv} \\ & - \frac{1}{l_1} \left[ \left( \frac{c_{11}k}{\rho} - \frac{c}{\rho v} \right) \cdot \frac{1}{k^2 v^2} \left\{ 1 - \cosh kv \left( t - \frac{3X}{2v} \right) \right\} + \frac{e_{11}P_0 c}{v} \left\{ \frac{1}{r} \left( t - \frac{3X}{2v} \right) \right. \right. \\ & \left. \left. - \frac{1}{r^2} + \frac{1}{r^2} e^{-r \left( t - \frac{3X}{2v} \right)} \right\} - \frac{c}{\rho v} \frac{\sinh kv \left( t - \frac{3X}{2v} \right)}{kv} + e_{11}\phi_0 \left( t - \frac{3X}{2v} \right) \right] \\ & - 2\pi P_0 e_{11}X^2 \left\{ \frac{1}{r} - \frac{1}{r} e^{-r \left( t - \frac{3X}{2v} \right)} \right\} - \frac{1}{l_1} \left[ \left( \frac{c_{11}k}{\rho} - \frac{c}{\rho v} \right) \frac{1}{k^2 v^2} \right. \\ & \left. \left\{ 1 - \cosh kv \left( t - \frac{X}{2v} \right) \right\} + \frac{e_{11}P_0 c}{v} \left\{ \frac{1}{r} \left( t - \frac{X}{2v} \right) - \frac{1}{r^2} + \frac{1}{r^2} e^{-r \left( t - \frac{X}{2v} \right)} \right\} \right. \\ & \left. - \frac{c}{\rho v} \frac{\sinh kv \left( t - \frac{X}{2v} \right)}{kv} + e_{11}\phi_0 \left( t - \frac{X}{2v} \right) - 2\pi P_0 e_{11}X^2 \left\{ \frac{1}{r} - \frac{1}{r} e^{-r \left( t - \frac{X}{2v} \right)} \right\} \right] \\ & + \frac{e_{11}P_0}{k_{11}\rho} \left[ \frac{1}{r} \left( t - \frac{X}{2v} \right) - \frac{1}{r^2} + \frac{1}{r^2} e^{-r \left( t - \frac{X}{2v} \right)} \right] - \frac{e^{-kX}}{\rho kv} \sinh \left\{ kv \left( t - \frac{X}{2v} \right) \right\} \\ & - \frac{e_{11}P_0}{k_{11}\rho} \left\{ \frac{1}{r} t - \frac{1}{r^2} + \frac{1}{r^2} e^{-rt} \right\} + \frac{e^{-\frac{kX}{2}}}{\rho kv} \sinh kv t \end{aligned} \quad (22A)$$

for  $t > \frac{3X}{2v}$ .

$$\begin{aligned} \text{and } \xi_{\frac{X}{2}} = & -\frac{1}{t_1} \left[ \left( \frac{c_{11}k}{\rho} - \frac{c}{\rho v} \right) \cdot \frac{1}{k^2 v^2} \left\{ 1 - \cosh kv \left( t - \frac{X}{2v} \right) \right\} \right. \\ & \left. + \frac{e_{11}P_0 c}{v} \left\{ \frac{1}{r} \left( t - \frac{X}{2v} \right) - \frac{1}{r^2} + \frac{1}{r^2} e^{-r \left( t - \frac{X}{2v} \right)} \right\} - \frac{c}{\rho v} \frac{\sinh kv \left( t - \frac{3X}{2v} \right)}{kv} \right] \end{aligned}$$

$$\begin{aligned}
& + e_{11} \phi_0 \left( t - \frac{3X}{2v} \right) - 2\pi P_0 e_{11} X^2 \left\{ \frac{1}{r} - \frac{1}{r} e^{-r \left( t - \frac{X}{2v} \right)} \right\} \\
& + \frac{e_{11} P_0}{k_{11} \rho} \left[ \frac{1}{r} \left( t - \frac{X}{2v} \right) - \frac{1}{r^2} + \frac{1}{r^2} e^{-r \left( t - \frac{X}{2v} \right)} \right] - \frac{e^{-k_2 X}}{\rho k v} \sinh \left\{ k v \left( t - \frac{X}{2v} \right) \right\} \\
& - \frac{e_{11} P_0}{k_{11} \rho} \left[ \frac{1}{r} t - \frac{1}{r^2} + \frac{1}{r^2} e^{-r t} \right] + \frac{e^{-k_2 X}}{\rho k v} \sinh k v t \quad (22B)
\end{aligned}$$

for  $\frac{X}{2v} < t < \frac{3X}{2v}$ .

and

$$\xi_{\frac{X}{2}} = \frac{1}{\rho k v} e^{-k_2 X} \sinh k v t - \frac{e_{11} P_0}{k_{11} \rho} \left[ \frac{1}{r} t - \frac{1}{r^2} + \frac{1}{r^2} e^{-r t} \right] \quad (22C)$$

for  $t < \frac{X}{2v}$ .

Relations (22A) (22B) and (22C) gives the expression for the mechanical response at  $x = \frac{X}{2}$ . This shows that the mechanical response is partly constant, partly linear and it partly decays exponentially with time. It also varies as hyperbolic sine function of time.

#### DISPLACEMENT OF THE SURFACE at $x = 0$

When  $x = 0$ , equation (20B) takes the form

$$\bar{\xi}_{x=0} = \frac{\left( (l_2 m_3 - l_3 e^{-\frac{s}{v} X}) + (l_3 e^{-\frac{s}{v} X} - l_1 m_3) \right)}{l_1 e^{-\frac{s}{v} X} - l_2 e^{-\frac{s}{v} X}} + [\bar{m}_3]_{X=0}$$

Following the same approximations, we have

$$\xi_{x=0} = \frac{l_2 - l_1}{l_1} m_3 e^{-\frac{s}{v} X} - \frac{1}{l_1} l_3 + \frac{1}{l_1} l_3 e^{-\frac{s}{v} X} + [m_3]_{X=0}$$

After taking invorse transform we get

$$\xi_{x=0} = \frac{1}{l_1} \left[ \left( \frac{c_{11} k}{\rho} - \frac{c}{\rho v} \right) \cdot \frac{1}{k^2 v^2} \left\{ 1 - \cosh k v \left( t - \frac{2X}{v} \right) \right\} + \frac{e_{11} P_0 c}{v} \left\{ \frac{1}{r} \left( t - \frac{2X}{v} \right) \right\} \right]$$



$$\begin{aligned}
 & -\frac{1}{r^2} + \frac{1}{r^2} e^{-r(t-\frac{2X}{v})} \left\} - \frac{c}{\rho k v^2} \sinh kv \left( t - \frac{2X}{v} \right) + e_{11} \phi_0 \left( t - \frac{2X}{v} \right) \right. \\
 & - 2\pi P_0 e_{11} X^2 \left\{ \frac{1}{r} - \frac{1}{r^2} e^{-r(t-\frac{2X}{v})} \right\} \left. - \frac{1}{l_1} \left[ \left( \frac{c_{11}k}{\rho} - \frac{c}{\rho v} \right) \frac{1}{k^2 v^2} (1 - \cosh kv t) \right. \right. \\
 & + \frac{e_{11} P_0 c}{v} \left\{ \frac{1}{r} t - \frac{1}{r^2} + \frac{1}{r^2} e^{-rt} \right\} - \frac{c}{\rho k v^2} \sinh kv t + e_{11} \phi_0 t - 2\pi P_0 e_{11} X^2 \left( \frac{1}{r} - \frac{1}{r^2} e^{-rt} \right) \left. \right] \\
 & + \frac{l_2 - l_1}{l_1} \left[ -\frac{e_{11} P_0}{k_{11} \rho} \left\{ \frac{1}{r} \left( t - \frac{x}{v} \right) - \frac{1}{r^2} + \frac{1}{r^2} e^{-r(t-\frac{x}{v})} \right\} + \frac{1}{\rho k v} e^{-kx} \cdot \sinh kv \left( t - \frac{x}{v} \right) \right. \\
 & \left. - \frac{e_{11} P_0}{k_{11} \rho} \left[ \frac{1}{r} t - \frac{1}{r^2} + \frac{1}{r^2} e^{-rt} \right] + \frac{1}{\rho k v} \sinh kv t \right] \quad \left[ \text{for } t > \frac{2X}{v} \right] \quad \dots \quad (23A)
 \end{aligned}$$

and

$$\begin{aligned}
 \xi_{x=0} = & -\frac{1}{l_1} \left[ \left( \frac{c_{11}k}{\rho} - \frac{c}{\rho v} \right) \cdot \frac{1}{k^2 v^2} (1 - \cosh kv t) + \frac{e_{11} P_0 c}{v} \left( \frac{1}{r} t - \frac{1}{r^2} + \frac{1}{r^2} e^{-rt} \right) \right. \\
 & \left. - \frac{c}{\rho k v^2} \sinh kv t + e_{11} \phi_0 t - 2\pi P_0 e_{11} X^2 \left( \frac{1}{r} - \frac{1}{r^2} e^{-rt} \right) \right] + \frac{l_2 - l_1}{l_1} \\
 & \left[ -\frac{e_{11} P_0}{k_{11} \rho} \left\{ \frac{1}{r} \left( t - \frac{x}{v} \right) - \frac{1}{r^2} + \frac{1}{r^2} e^{-r(t-\frac{x}{v})} \right\} + \frac{e^{-kx}}{\rho k v} \sinh kv \left( t - \frac{x}{v} \right) \right] \\
 & - \frac{e_{11} P_0}{k_{11} \rho} \left[ \frac{1}{r} t - \frac{1}{r^2} + \frac{1}{r^2} e^{-rt} \right] + \frac{1}{\rho k v} \sinh kv t \quad \dots \quad (23B)
 \end{aligned}$$

for

$$\frac{X}{v} < t < \frac{2X}{v}$$

and

$$\begin{aligned}
 \xi_{x=0} = & -\frac{1}{l_1} \left[ \left( \frac{c_{11}k}{\rho} - \frac{c}{\rho v} \right) \cdot \frac{1}{k^2 v^2} (1 - \cosh kv t) + \frac{e_{11} P_0 c}{v} \left( \frac{1}{r} t - \frac{1}{r^2} + \frac{1}{r^2} e^{-rt} \right) \right. \\
 & \left. - \frac{c}{\rho k v^2} \sinh kv t + e_{11} \phi_0 t - 2\pi P_0 e_{11} X^2 \left( \frac{1}{r} - \frac{1}{r^2} e^{-rt} \right) \right] \\
 & - \frac{e_{11} P_0}{k_{11} \rho} \left[ \frac{1}{r} t - \frac{1}{r^2} + \frac{1}{r^2} e^{-rt} \right] + \frac{1}{\rho k v} \sinh kv t \quad \text{for } t < \frac{X}{v} \quad \dots \quad (23C)
 \end{aligned}$$

Evidently the response omitted by the transducer is by and large similar to the one discussed earlier at the point  $x = \frac{X}{2}$ .

The response is evidently zero at  $t = 0$ .

## DISCUSSION

It is clear from each of the above expressions that the mechanical response of the transducer owing to prescribed electric excitations is dominated by the decay factor in the polarization gradient, whatever be the range of time. Moreover, for a large decay factor the responses do not exhibit the transient characteristics and remain uninfluenced by the polarization constant. In the general case, it is obvious from above, the effects due to the prescribed polarization are not coupled with those due to prescribed diffusion. Further, while the prescribed polarization gradient accentuates the damping part of the response, the diffusion does not necessarily do so, for large values of  $r$  and  $k$ .

All these facts bring out some of the physical aspects of the vibration of the transducer which will hold with or without numerical calculations.

## ACKNOWLEDGEMENT

The author expresses his gratitude to Dr. D. K. Sinha for help and guidance while preparing the paper

## REFERENCES

- Chakrabarty A. 1968 *Prajnan*, 2, No. 2 & 3, 37.  
 Chakrabarty A. 1969 *CZEC Jour. Phys.* 13-19, 131.  
 Das N. C. 1967 *Ind Jour. Theor. Phys.*, 41, 611.  
 Filipezynski, L. 1956 *Proc. Conf. Ultrasonics, Pol Acad. Scs.*, Warsaw, 29.  
 Guri R.R. 1966 *Roum Techs. Scs.*, 11, 253.  
 Mason W. P. 1948 *Piezoelectric crystals and their applications to ultrasonics*, D Van Nostrand Co. Inc. New York.  
 Redwood M. 1961 *Jour. Acoust. Amer*, 33, 527  
 Sinha D. K. 1965 *Ind. Jour. Theor. Phys.*, 11, 93.  
 Sinha D. K. 1967 *Proc. Ind. Acad. Scs.* LXV, 136.  
 Sinha D. K. 1965 *Proc. Natl Inst. Sc. Ind.* 31A, 395  
 Swann W. F. F. 1950 *Jour. Frank. Inst.*, 210, 250.

## On the assignment of vibration frequencies of ortho-, meta- and para-cresols

By J. JHA AND S. CHATTOPADHYAY

Optics Department, Indian Association for the Cultivation of Science,  
Calcutta-32

(Received 26, May 1969; revised 10 December, 1969)

The assignment of vibration frequencies of three isomeric cresols in the region  $200-700\text{ cm}^{-1}$  has been made. Some of the inconsistencies in the vibrational assignments of the frequencies between  $700-1680\text{ cm}^{-1}$  for all the three molecules made by previous workers have been pointed out and suitable alternative assignments for them have been proposed.

### INTRODUCTION

The Raman spectra of ortho-, meta- and para-cresols in the liquid state have been investigated by several workers (Kohlrausch & Pongratz 1933, Magat 1936, Biswas 1955) and a partial assignment of the Raman frequencies is given in the literature (Mecke-Korkhof 1951). Later, the infrared absorption spectra of para-cresol and a large number of para-di-substituted benzene compounds in the frequency interval  $650\text{ cm}^{-1}$ – $1650\text{ cm}^{-1}$  were studied by Garrigou-Lagrange *et al.* (1958), who also made assignments of the observed vibration frequencies. Recently, similar investigations in the case of ortho- and meta- disubstituted benzenes including ortho- and meta-cresols have been carried out respectively by Brigodiot & Lobas (1965) and by Garrigou-Lagrange *et al.* (1966). In view of the facts that some of the vibrational assignments of para-cresol proposed by Garrigou-Lagrange *et al.* (1958) are inconsistent with the states of polarisation of the Raman lines and strengths of the infrared absorption bands corresponding to the proposed modes of vibration and that assignments of vibrational frequencies below  $500\text{ cm}^{-1}$  for all the three isomers and especially for ortho-cresol have not been made earlier, it was thought worthwhile to attempt complete assignments of all the vibration frequencies of the three isomeric molecules observed in Raman scattering and in infrared absorption. For this purpose the Raman spectra of the three compounds in liquid state and the infrared absorption spectra of the pure liquids and their solutions in suitable solvents have been reinvestigated. A discussion of the results obtained is presented in this paper.

### EXPERIMENTAL

Chemically pure samples of ortho-, meta- and para-cresols obtained from E. Merck (Germany) were subjected to fractional distillation and the proper fractions were distilled under reduced pressure. The distilled liquids were

dehydrated before use. Guaranteed reagent quality carbon tetrachloride and chloroform were properly dehydrated and used as solvents for infrared absorption studies. The Raman spectra of the pure liquids, the states of polarisation of the Raman lines, and the infrared absorption spectra of the pure compounds in the liquid state and in solutions were studied by methods described earlier (Chattopadhyay & Jha, 1968). All the Raman spectra were recorded on a Fuess glass spectrograph having a dispersion of  $13\text{ \AA/mm}$  and  $19\text{ \AA/mm}$  in the Hg  $4047\text{ \AA}$  and  $4358\text{ \AA}$  regions, respectively, while the infrared absorption spectra were studied on a Perkin Elmer Model 21 double beam spectrophotometer provided with rocksalt optics.

### RESULTS

The Raman frequency shifts ( $\Delta\nu\text{ cm}^{-1}$ ) their relative intensities and states of polarisation for all the three liquids together with the positions of the infrared absorption bands ( $\nu\text{ cm}^{-1}$ ) and their relative strengths in the case of the pure liquids and their solutions are given in tables 1, 2 and 3. For any compound the Raman shifts recorded in the table are the averages of all the data available in the literature and those obtained in the present investigation. For comparison the data of the infrared absorption bands reported by previous workers have also been included in the tables. The tables contain the assignments of the vibration frequencies proposed by the present authors together with those given by previous investigators. Since many of the vibrational assignments made by previous workers do not require any modification the assignment of only those vibration frequencies for which no assignment has been made by previous workers is discussed in the following paragraph. Moreover, the inconsistencies in the assignment of some of the frequencies of vibration published in the literature are pointed out and suitable assignments for them have been suggested. Unless otherwise stated, the mode numbers of benzene mentioned in the text and in the tables are those due to Pitzer & Scott (1943).

#### a) *Para-cresol*

From table 1, it is seen that for the molecule of para-cresol there are six vibration frequencies below  $650\text{ cm}^{-1}$  which have not been assigned by Garrigou-Lagrange *et al.* (1958). However, the frequencies  $465\text{ cm}^{-1}$  and  $644\text{ cm}^{-1}$  have been assigned by Moko-Kerkhof (1951), to modes 6A and 6B respectively, of benzene with which the present authors are in agreement. The very weak Raman line  $406\text{ cm}^{-1}$  observed by Biswas (1955) certainly corresponds to mode 16A of benzene, while the weak broad Raman line  $282\text{ cm}^{-1}$  (Biswas, 1955) may arise from the modes 16B and 18B of benzene. This assignment has been made on the basis of a calculation of the vibrational frequencies of para-xylene and some other para-dihalobenzenes by Schmidt *et al.* (1960). Following the same authors the medium intensity broad and depolarised Raman line  $338\text{ cm}^{-1}$  has been assigned to the modes 9B and 10B. According to Moko-Kerkhof (1951) this line originates

from a mode involving in-plane bending motions of the substituents very similar to that in mode 15 of Stojiljkovic & Whiffen (1958) though contribution from mode 10 due to the same authors cannot be entirely ruled out. The weak Raman line  $510\text{ cm}^{-1}$  in accordance with the calculation of Schmidt *et al.* (1960) has been assigned to mode 11 of benzene.

Garrigou-Lagrange *et al.* (1958) have assigned the medium intensity polarised Raman line  $824\text{ cm}^{-1}$  having its counterpart in the strong infrared band at  $826\text{ cm}^{-1}$  to mode 10A of benzene. This mode in  $C_{2v}$  symmetry is inactive in the infrared absorption and also being an out of plane vibration cannot give rise to a polarised Raman line. Therefore, the weak Raman line at  $809\text{ cm}^{-1}$  (Garrigou-Lagrange *et al.* 1958) has been assigned to this mode of vibration. The frequency  $824\text{ cm}^{-1}$  is believed to correspond to mode 12 of benzene and following Sirkar & Bishui (1968) the strong polarised Raman line at  $844\text{ cm}^{-1}$  is assigned to mode 1 of benzene.

The weak Raman line at  $969\text{ cm}^{-1}$ , for which no corresponding infrared band has been observed, is assigned to mode 17A of benzene. This is in keeping with the infrared inactive nature of this mode in  $C_{2v}$  symmetry though according to the calculation of Schmidt *et al.* (1960) this line might also have originated from mode 5 of benzene. From the above considerations the assignment of the infrared bands at  $922\text{ cm}^{-1}$  and  $985\text{ cm}^{-1}$ , to modes 5 and 17A respectively, of benzene by Garrigou-Lagrange *et al.* (1958) does not seem satisfactory.

The two polarised Raman lines of medium intensity at  $1216\text{ cm}^{-1}$  and  $1255\text{ cm}^{-1}$  have been assigned by Garrigou-Lagrange *et al.* (1958) to modes  $e$  and  $e'$  of Kohlrausch. All para-substituted toluenes show a Raman line with a frequency shift of about  $1210\text{ cm}^{-1}$  while in all para-substituted phenols a Raman line at about  $1255\text{ cm}^{-1}$  is observed. So it may be concluded that in the case of paracresol the line  $1216\text{ cm}^{-1}$  originates from a mode of vibration involving the motion of the methyl group and the other line  $1253\text{ cm}^{-1}$  is due to a mode which involves the motion of the hydroxyl group. Moreover, in the present case there is no infrared absorption band corresponding to the line  $1216\text{ cm}^{-1}$  while a strong infrared band  $1258\text{ cm}^{-1}$  corresponding to the Raman line  $1253\text{ cm}^{-1}$  has been observed. These facts indicate that in the mode of vibration giving rise to the former line, the displacements of the nuclei are symmetrical but in the latter case some asymmetry in the displacements occurs. It is suggested that these two lines originate from modes of vibration similar to the mode  $q$  proposed by Randle & Whiffen (1955) in the case of mono-substituted benzenes. In one of these modes the trigonal displacements of 1, 3, 5 carbon atoms are coupled with the stretching of C-CH<sub>3</sub> bond and in the other similar coupling takes place between the stretching of the C-OH bond and the trigonal mode involving 2, 4, 6 carbon atoms. These are designated by the symbols  $q$  and  $q'$ , respectively.

Garrigou-Lagrange *et al.* (1958) have assigned the infrared band at  $1430\text{ cm}^{-1}$  to mode 14 of benzene. Though this is in accordance with the infrared active

nature of the mode in benzene the frequency is somewhat higher than that of benzene. Moreover, it may be noted that in the case of the two other cresols there are weak Raman lines at  $1440\text{ cm}^{-1}$  which are most conveniently assigned to asymmetric CH bending mode of the methyl group in these molecules. Accordingly, the infrared band  $1434\text{ cm}^{-1}$  has been assigned to asymmetric CH bending mode in the methyl group and the strong infrared band at  $1360\text{ cm}^{-1}$  due to the pure liquid has been assigned to mode 14 of benzene.

In the Raman spectrum of para-cresol, as in the case of two other cresols, a medium intensity polarised Raman line at  $2889\text{ cm}^{-1}$  has been observed. This has been assigned to symmetric C-H stretching vibration in the methyl group of the molecule. The assignments of asymmetric CH stretching vibrations and other C-H stretching vibrations of the phenyl ring are shown in table 1.

(b) *Meta-cresol*

The Raman spectrum of meta-cresol shows four Raman lines with frequency shifts below  $400\text{ cm}^{-1}$  (table 2) for which no assignment has been made by Garrigou-Lagrange *et al* (1966). In proposing assignment of these lines we have been guided by the calculations of Bogomolov (1962) in the case of meta-xylene and those of Nonnenmacher & Mecke (1961) for meta-derivatives of benzene including meta-xylene and resorcinol. These calculations show that the frequency of both the modes 11 and 10A of benzene are reduced and that the frequency of the latter mode is slightly higher than that of the former. Accordingly, the frequencies  $214$  and  $241\text{ cm}^{-1}$  have been assigned to mode 11 and 10A, respectively. Moreover, Bogomolov (1962) has shown that in the case of meta-xylene the frequencies of mode 9A and 15 of benzene are considerably lowered, but they are higher than those corresponding to the modes 11 and 10A. With these considerations the depolarised Raman lines at  $304\text{ cm}^{-1}$  and  $565\text{ cm}^{-1}$  are assigned to modes 9A and 15, respectively.

Garrigou-Lagrange *et al* (1966) have not given any assignment of the strong polarised Raman line at  $735\text{ cm}^{-1}$ . It is believed to originate in a vibration similar to mode *r* (Randle & Whiffen 1955) in which both the substituents move with the carbon atoms. The trigonal *p* mode (Randle and Whiffen 1955) evidently, gives rise to the very strong polarised Raman line at  $1000\text{ cm}^{-1}$ . It may be noted that this line has been assigned by Garrigou-Lagrange *et al*, (1966) to mode 1 of benzene.

The weak Raman line at  $850\text{ cm}^{-1}$  and the strong infrared band at  $818\text{ cm}^{-1}$  are assigned to the modes 5 and 18B of benzene, respectively. The strong infrared band at  $928\text{ cm}^{-1}$  is believed to arise from mode 17B of benzene while mode 17A of benzene gives rise to the weak Raman line at  $956\text{ cm}^{-1}$ .

In the spectra of meta-cresol there are two vibration frequencies at  $1246\text{ cm}^{-1}$  and  $1280\text{ cm}^{-1}$  of which the former is observed as a strong absorption band in the

infrared spectrum of the pure liquid while the latter is found to appear both as a weak polarised Raman line and a strong infrared band of about the same frequency Garrigou-Lagrange *et al.* (1966) did not observe the band  $1246\text{ cm}^{-1}$  while the band  $1281\text{ cm}^{-1}$  has been assigned by them to mode  $e'$  of Kohlrausch. Though the two frequencies in question appear to correspond to the frequencies  $1210$  and  $1253\text{ cm}^{-1}$  of para-cresol, it is doubtful whether they originate in similar modes of vibration in the two molecules, because the modes  $e$  and  $e'$  of Kohlrausch cannot possibly occur in the case of meta-cresol.

Following the mode of assignments in the case of meta-disubstituted benzenes by Bogomolov (1962) the frequency  $1281\text{ cm}^{-1}$  is assigned to vibration 13 in which there is symmetric in-phase stretching of C-CH<sub>3</sub> and C-OH bonds while the other frequency  $1246\text{ cm}^{-1}$  may be attributed to vibration 7B where such stretching of the two bonds takes place in opposite phases.

It can be seen from table 2 that there are two strong absorption bands at  $1495$  and  $1514\text{ cm}^{-1}$  in the infrared spectra of meta-cresol in the liquid state and in its solution in chloroform Garrigou-Lagrange *et al.* (1966) who also studied the infrared absorption spectra of solutions of meta-cresol, observed a number of bands between  $1460$ - $1520\text{ cm}^{-1}$  and assigned the bands  $1460$  and  $1490\text{ cm}^{-1}$ , to modes 19A and 19B respectively, of benzene. As these two bands have not been observed in the present investigation either in the spectra of the pure liquid or of its solutions, this assignment does not seem satisfactory and therefore, the bands  $1495$  and  $1514\text{ cm}^{-1}$  have been assigned to modes 19A and 19B, respectively.

The assignment of the vibrational modes of the methyl group and some of the modes involving stretching of the CH bonds of the ring is also shown in table 2.

#### c) *Ortho-cresol*

The assignment of the vibration frequencies of ortho-cresol in the region  $650$ - $1650\text{ cm}^{-1}$  made by Brigodiot & Lebas (1965) is given in table 3. Excepting a few, most of the assignments have not been changed in the present investigation. However, none of the Raman frequencies below  $700\text{ cm}^{-1}$  has been assigned by the above authors, though Mecke-Kerkhof (1951) have given assignment for some of these lines. According to Mecke-Kerkhof the moderately strong depolarised Raman line  $529\text{ cm}^{-1}$  arises from mode 6B of benzene while mode 6A of benzene gives rise to the medium intensity polarised Raman line at  $585\text{ cm}^{-1}$ . This is indicated in the table. Mecke-Kerkhof (1951) also assigned two vibrational frequencies in the range  $200$ - $450\text{ cm}^{-1}$  observed in the case of many other ortho-substituted benzenes, to two modes of vibration involving in-plane deformations of the bonds connecting the substituents to the ring. In the case of ortho-cresol the Raman line  $275\text{ cm}^{-1}$  probably corresponds to one of these modes. This frequency has been assigned to mode 18A of benzene.

Kovner & Bogomolov (1959) have calculated all the vibrational frequencies of ortho-xylene and calculations for the out of plane vibrations of ortho-xylene and some other ortho-disubstituted benzenes are given by Nonnenmacher & Mecke (1961). Following these calculations, the depolarised Raman line  $189\text{ cm}^{-1}$  assigned to modes  $10B$  of benzene and the weak Raman line  $442\text{ cm}^{-1}$  is assigned to mode  $16B$  of benzene. Assignments of other weak Raman lines have not been attempted.

The strong and polarised Raman line  $749\text{ cm}^{-1}$  and the strong infrared absorption band  $710\text{ cm}^{-1}$  are assigned to the modes 1 and 12 of benzene. Following the calculations of Kovner & Bogomolov (1959) and those of Nonnenmacher & Mecke (1961) the strong infrared band  $750\text{ cm}^{-1}$  is assigned to mode 11, while the depolarised Raman line  $847\text{ cm}^{-1}$  corresponding to the strong infrared band  $842\text{ cm}^{-1}$  is assigned to mode 5. These are shown in table 3.

The Raman spectrum of ortho-cresol in the liquid state show two polarised Raman lines of medium intensity at  $1237$  and  $1255\text{ cm}^{-1}$ . The infrared spectrum of the liquid shows two strong bands at  $1242$  and  $1255\text{ cm}^{-1}$  corresponding to the two Raman lines and a third strong band at  $1208\text{ cm}^{-1}$ . All these bands are also observed in the infrared spectra of ortho-cresol solutions. Brigodiot & Lebas (1965) who did not observe the infrared band  $1242\text{ cm}^{-1}$  assigned the bands  $1208\text{ cm}^{-1}$  and  $1255\text{ cm}^{-1}$  to modes  $e$  and  $e'$  of Kohlrausch. For reasons already stated in the case of meta-cresols, the author suggests that the two vibration frequencies be assigned to modes  $20B$  and  $7B$  of benzene. It is believed that the band  $1208\text{ cm}^{-1}$  which may correspond to the frequency  $1205\text{ cm}^{-1}$  of para-cresol arises from an in-plane OH deformation mode.

Some other minor changes made in the assignment given by Brigodiot & Lebas (1965) are indicated in table 3. The assignments of the vibrational frequencies of the methyl group and some of CH stretching vibrations of the ring are given in the same table.

#### ACKNOWLEDGEMENT

The authors express their gratitude to Professor G. S. Kastha, D.Sc. for his continued guidance. One of the authors (J.J.) thanks the authorities of the Indian Association for the Cultivation of Science for providing facilities for the investigation.



TABLE I Para-cresol

Raman Shift ( $\Delta \text{ cm}^{-1}$ )	Infrared bands		( $\nu \text{ cm}^{-1}$ )		Assignment	
Pure liquid	Pure liquid	Solution in $\text{CCl}_4$	Pure liquid	Solution	Garrigou- Lagrange	Present work
	Present authors		Garrigou-Lagrange <i>et al.</i> (1958)	(1958)	<i>et al.</i> (1958)	
*282 (0 <i>b</i> )						16 <i>B</i> /18 <i>B</i>
338 (3 <i>b</i> ) <i>D</i>						10 <i>B</i> /9 <i>B</i>
*406 (0)						16 <i>A</i>
465 (2) <i>P</i>						6 <i>A</i>
510 (1)						11
644 (5) <i>D</i>						6 <i>B</i>
701 (1)	702 <i>m</i>	700 <i>w</i>	703	702	4	4
741 (1)	738 <i>s</i>		739	738		5
				749		
*809 (0)				804		10 <i>A</i>
	814 <i>vs</i>	816 <i>s</i>		817	11/17 <i>B</i>	17 <i>B</i>
824 (3) <i>P</i>		826 <i>s</i>			10 <i>A</i>	12 ( <i>r'</i> )
844 (6) <i>P</i>	842 <i>s</i>	840 <i>s</i>	843	843	<i>d</i>	1( <i>r</i> )
		929 <i>w</i>		922	5	
				949		
969 (0)				985		17 <i>A</i>
						17 <i>A</i> /5
1018 (0)	1018 <i>w</i>		1017	1016	18 <i>A</i>	18 <i>A</i>
1039 (0)	1040 <i>w</i>		1043	1046	substituent	substituent
	1104 <i>s</i>	1105 <i>w</i>	1105	1101		
**1118 (4)		1110 <i>w</i>	1115	1112	15	15
1170 (2) <i>P</i>	1172 <i>s</i>	1177 <i>s</i>	1172	1170	9 <i>A</i>	9 <i>A</i>
*1205 (2)				1205	substituent	$\delta(\text{OH})$
1216 (4) <i>P</i>				1212	<i>c</i>	<i>q</i> (Kandle & Whiffon,
	1235 <i>sb</i>		1235			<i>q'</i> 1955)
1255 (2) <i>P</i>		1258 <i>s</i>		1254	<i>c</i>	
				1284		
1297 (1)	1292 <i>w</i>		1306	1292	3	3
	1340 <i>msb</i>	1346 <i>w</i>	1343	1338		
	1360 <i>sb</i>	1360 <i>mb</i>	1364	1368		14
1381 (4) <i>P</i>	1375 <i>msb</i>			1382	substituent	$\delta_s(\text{CH}_3)$
	1444 <i>m</i>	1436 <i>w</i>		1430	14	$\delta_a(\text{CH}_3)$
1460 (0) <i>D</i>		1468	1460	1468	19 <i>B</i>	19 <i>A</i>
1517 (0 <i>b</i> )	1514 <i>vs</i>	1516 <i>vs</i>		1515	19 <i>A</i>	19 <i>B</i>
				1572		
1596 (2) <i>D</i>	1600 <i>m</i>	1602 <i>msb</i>		1598	8 <i>B</i>	8 <i>B</i>
1614 (4) <i>D</i>	1614 <i>m</i>	1618 <i>ms</i>		1618	8 <i>A</i>	8 <i>A</i>
+2889 (3) <i>P</i>						$\nu_s(\text{CH}_3)$
2920 (4) <i>P</i>						$\nu_a(\text{CH}_3)$
3014 (2) <i>P</i>	}				}	$\nu(\text{CH})$
3037 (2) <i>P</i>						
3060 (6) <i>P</i>						

\*Data from Biswas (1955)

\*\*Data from Garrigou-Lagrange *et al.* (1958)

+ Observed in the present investigation.

TABLE 2 Meta-cresol

Raman shift ( $\Delta\nu$ cm <sup>-1</sup> )	Infrared bands		(ν cm <sup>-1</sup> )		Assignment
Pure Liquid	Pure liquid	CHCl <sub>3</sub> Present Authors	Pure liquid Garrigou- Lagrango <i>et al.</i> (1966)	Garrigou- Lagrango <i>et al.</i> (1966)	Present work
214 (3b)D					11
241 (4b)D					10A
304 (2)D			307		9A
			442	16B	16B
518 (3)P			517	ν <sub>c</sub>	6A
541 (2)P			537	ν <sub>c</sub>	6B
565 (1)D			560		15
	688 s	688 s	686	4	4
735 (0)P	740 mb		734		r (Randle & Whiffen, 1955)
	756 s		768		
			776	11	10B
778 (0)	776 vs				18B
	181 s	820 vs			5
850 (0)	844 m	846 s	842		
			854	17B	
	880 w	882 w	872		
			925	17A	
	928 s	930 s	928		17B
+956			959		17A
1000 (10)P	1000 w	1004 m	1000	1	p (Randle & Whiffen, 1955)
+1039 (0)	1042	1043 m	1039	substituent	substituent
			1080	18B	
1085 (2)P	1086 w	1086 wb	1086	18A	18A
	1106 m	1108 s			substituent?
			1154		
1161 (4b)D	1100 vs	1160 vsb	1164	9B	9B
			1178		
			1186	δ(OH) free	
			1286	δ(OH) assoc.	
	1246 vs		1267	3	7B
1280 (2)P	1280 vs	1286 vs	1281		13
			1305		
		1314 m	1309	14	
	1345 sb	1334 s			14
1381 (4)P	1385 w	1386 msh	1377	δ <sub>s</sub> (CH <sub>3</sub> )	δ <sub>s</sub> (CH <sub>3</sub> )
			1403		
1441 (0)	1440 m	1444 ssh	1436	δ <sub>a</sub> (CH <sub>3</sub> )	δ <sub>a</sub> (CH <sub>3</sub> )
			1460	19A	
		1470 sb	1470		
			1490	19B	
	1495 s	1498 s	1500		19A
	1514 vs	1516 vs			19B
			1520		
			1538		
			1590	8A	
1592 (2)D	1594 vs	1600 vs			8A
			1596		
1615 (6)D	1615 ssh		1613		8B
		1620 ssh	1619		
++2871 (3)P					ν <sub>s</sub> (CH <sub>3</sub> )
2922 (4)P					ν <sub>a</sub> (CH <sub>3</sub> )
3050 (2)P? } ++3061 (7b)P }					{ ν (CH)

+ Data from Biswas (1955).

++Observed in the present work.

TABLE 3 Ortho-cresol

Raman shift ( $\Delta\nu$ $\text{cm}^{-1}$ )		Infrared bands ( $\nu$ $\text{cm}^{-1}$ )		Assignment	
Pure Liquid	Pure liquid Present authors	Solution in $\text{CCl}_4$	Pure liquid Brigodiot & Lebas (1965)	Brigodiot & Lebas (1965)	Present work
189 (4b) <i>D</i>					10B
275 (3) <i>D</i>					18A
311 (0)					
442 (0)					16 B
529 (4) <i>D</i>					6B
585 (5) <i>P</i>					6A
* 646 (0)					
* 695 (0)			688		4
* 711 (0)	710 <i>s</i>	710 <i>s</i>	709 (50)	4	12
749 (10) <i>P</i>	750 <i>vs</i>		748 (397)		1, 11
			810		
847 (1) <i>D</i>	842 <i>vs</i>	842 <i>vs</i>	842 (75)	10 B	5
			922 (11)		
	928 <i>m</i>	930 <i>w</i>	926 (11)	17 B	17 B
986 (2b)	984 <i>m</i>	980 <i>wb</i>	984 (14)	5	17 A
			1017		
1044 (6) <i>P</i>	1044 <i>s</i>	1040 <i>msh</i>	1038 (34)	18 B	18B
			1043 (30)	substituent	
*1094 (1)					
1107 (1)	1108 <i>vs</i>	1104 <i>s</i>	1102 (130)	9B	substituent ?
1150 (4b) <i>D</i>	1156 <i>ssh</i>	1153 <i>msh</i>	1149 <i>sh</i>		9 B
	1170 <i>vs</i>	1168 <i>vs</i>	1164 (115)	9A/15	
	1208 <i>vsb</i>	1210 <i>vs</i>	1205 (118)	e	8(OH)
			1216 (64)		
1237 (4b) <i>P</i>	1242 <i>vsb</i>	1244 <i>vsch</i>			7B
1255 (3b) <i>P</i>	1255 <i>vs</i>	1256 <i>vs</i>	1254 (119)	e'	20B
	1300 <i>m</i>	1300 <i>m</i>	1299 (29)	14/3	3
	1330 <i>s</i>	1329 <i>s</i>	1324 (90)		
	1350 <i>msh</i>	1350 <i>w</i>			14
1381 (3) <i>D</i>	1388 <i>w</i>	1384 <i>w</i>	1380 (18)		$\delta_s(\text{CH}_3)$
1440 (1) <i>D</i>	1450 <i>msh</i>		1443 (33)	substituent	$\delta_a(\text{CH}_3)$
*1471 (1)	1466 <i>s</i>	1467 <i>s</i>	1462 (72)	substituent/10A	19A
**1484 (0b)	1496 <i>vs</i>	1495 <i>s</i>	1492 (85)	19B	19B
	1505 <i>ssh</i>		1508 (66)		2 x 750
1510 (1)	1515 <i>ssh</i>	1515 <i>msh</i>			
1592 (4) <i>D</i>	1592 <i>vs</i>	1593 <i>s</i>	1587 (65)	8A	8A
1615 (7) <i>D</i>	1610 <i>msh</i>	1612 <i>msh</i>	1608 (23)	8B	8B
**2865 (2) <i>P</i>					$\nu_s(\text{CH}_3)$
2020 (3b) <i>P</i>					$\nu_a(\text{CH}_3)$
3054 (6b) <i>P</i> }					} $\nu(\text{CH})$
3073 (3b) }					

\*Data taken from Biswas (1955).

\*\*Observed in the present investigation.

## REFERENCES

- Biswas D. C. , 1955, *Ind J Phys* , **29**, 262  
Bogomolov A. M. , 1962, *Optics and Spectroscopy (English translation)* **13**, 90  
Brigodiot M & Lobas J M , 1965, *J Chim Phys* , **62**, 347  
Chattopadhyay S. & Jha J., 1968, *Ind. J. Phys.* **42**, 610  
Garrigou-Lagrange C., Chohata M. & Lascombe J , 1966, *J. Chim Phys.*, **63**, 552.  
Garrigou-Lagrange C., Lebas J M & Jorien M L , 1958, *Spectrochim Acta.*, **12**, 305.  
Kohlrausch K. W F & Pongratz A , 1938, *Monatsch. Chem* , **63**, 427  
Kovner M. A & Bogomolov A M., 1959, *Optik u. Spectroskop*, **7**, 751.  
Mugat M., 1936, *Table of Constants and Numerical Data*  
Mecke-Kerkhof. 1951, *Landolt Bornstein Tables. Auf. 6, Band 1, Teil 2.*  
Nonnenmacher G. & Mecke R., 1961, *Spectrochim. Acta*, **17**, 1049  
Pitzer K. S & Scott D. H , 1943, *J Amer Chem. Soc.*, **65**, 803.  
Randle R. R. & Whiffen D H , 1955, *Molecular Spectroscopy, Institute of Petroleum, London*, 111  
Schmidt E. W., Brandmuller J & Nonnenmacher G., 1960, *Z Elektrochim.*, **64**, 726.  
Sarkar S C & Bishui P. K , 1968, *Ind J Phys.*, **42**, 1.  
Stojiljkovic A., & Whiffen D. H , 1958, *Spectrochim. Acta*, **12**, 47.

## Gamma ray spectroscopy of $^{185m}\text{W}$

By B. P. PATHAK, S. C. GUJRATHI\* AND S. K. MUKHERJEE

*Sahu Institute of Nuclear Physics, Calcutta, India*

(Received 19 January—Revised 13 August 1970)

The gamma decay characteristics of  $^{185m}\text{W}$  have been investigated using Ge(Li) and NaI(Tl) spectrometers. The samples of  $^{185m}\text{W}$  were produced through  $^{186}\text{W}(n, 2n)^{185m}\text{W}$  reaction by irradiating tungsten oxide enriched in  $^{186}\text{W}$  (97.8%), with 14.8 MeV neutrons. A half-life of  $1.65 \pm 0.05$  min was assigned to its decay. Gamma rays with 66.2, 94.5, 107.9, 122.3, 131.8, 164.7, 174.1 and 188.3 keV energies were found decaying with 1.65 min half-life. The results of singles and coincidence measurements have been incorporated into a decay scheme. The levels of 75d  $^{185}\text{W}$  populated by the decay of 1.65 min  $^{185m}\text{W}$  are established at 0, 23.6, 66.2, 93.8, 174.1 and 188.3 keV. The 1.65 min isomeric state is placed at 198.0 keV. The results of the present measurements are found to be consistent with those obtained in a recent work.

### INTRODUCTION

Duffield *et al* (1950) first produced  $^{185m}\text{W}$  by neutron capture reaction on  $^{184}\text{W}$ . They assigned a half-life of 1.85 min by studying the decay of 75 keV conversion electron peak. Poe (1955) reported 60, 130 and 175 keV gamma rays due to  $^{185m}\text{W}$ , using a NaI(Tl) detector, but he did not report a decay scheme. The first attempt to undertake a complete study of the decay scheme was made by Morinaga & Nagatani (1960). They reported gamma rays of 75, 100, 125, 175 and 230 keV decaying with 1.6 min half-life. The levels of 75d  $^{185}\text{W}$  populated by the decay of  $^{185m}\text{W}$  were suggested at 0, 100 and 175 keV. The 1.6 min isomeric state was placed at 300 keV. Erskine (1965) identified a number of low lying levels in  $^{185}\text{W}$  by  $^{184}\text{W}(d, p)^{185}\text{W}$  reaction. Martin *et al* (1966) reported the  $1/2^- [510]$  intrinsic state at  $\sim 15$  keV by studying the neutron capture reaction on  $^{184}\text{W}$ . Recently a systematic study of the decay of  $^{185m}\text{W}$  was made by Daly *et al* (1969) employing high resolution gamma ray spectrometers. They established a number of new gamma ray transitions and determined their energies within an error of less than 0.3. In contrast to Morinaga's report, they suggested the 1.7 min isomer at 197.8 keV.

The purpose of the present investigation is related to the interests of the authors in the high resolution gamma ray spectroscopy in the low energy region. The preliminary part of this work was reported previously at the Low Energy Nuclear Physics Symposium, Bombay, by Pathak *et al* (1968). In this report

\*Present Address: Department of Chemistry, Simon Fraser University, Burnaby-2, B. C., Canada.

an attempt was made to fit the observed gamma rays with the help of known levels of  $^{186}\text{W}$  from earlier works (Morinaga *et al* 1960, Erskine 1965). The appearance of the recent report by Daly *et al* (1969) prompted the authors to perform more detailed measurements with special attention to the intensity determination and the gamma-gamma coincidence experiments. By applying necessary corrections for the absorption of the gamma radiations in different media coming in between the source and the detector, the correct intensities of the low energy gamma rays were obtained. These intensities are an improvement on those reported earlier. Gamma-gamma coincidence experiments were performed with narrow gates and the new improved results led to the modification of the earlier decay scheme tentatively proposed by the authors (Pathak *et al* 1968).

#### PREPARATION OF SOURCE AND HALF-LIFE MEASUREMENT

The sources of  $^{185\text{m}}\text{W}$  were obtained through  $(n, 2n)$  reaction on enriched (97.8%) samples of  $^{186}\text{W}$ , by irradiating with 14.8 MeV neutrons in an average flux of  $\sim 10^{10}$  neutrons per sec per  $\text{cm}^2$ . For each bombardment the target sample was placed in a thin polythene bag, and placed between the layers of a cadmium sheet. After irradiation, the polythene bag containing the sample was transferred for the measurements. In general the counting began  $\sim 30$  sec after the irradiation. Radioactive sources of  $^{183\text{m}}\text{Hf}$  ( $T_{1/2} = 91\text{d}$  and  $64\text{min}$ ; Bakluu *et al* 1966),  $^{186}\text{Ta}$  ( $T_{1/2} = 10.5\text{min}$ ; Gujrathi *et al* 1968) and  $^{185\text{g}}\text{W}$  ( $T_{1/2} = 75\text{d}$ ) were produced besides  $^{185\text{m}}\text{W}$ , by  $(n, \alpha)$ ,  $(n, p)$  and  $(n, 2n)$  reactions, respectively, during the neutron irradiation of  $^{186}\text{W}$ . The radiations due to these isotopes presented no serious problem to our measurements. The production of longer lived activities was minimised by keeping the duration of irradiation to two minutes only. Most of the contributions due to the activities with half-lives of the order of hours and days were subtracted along with the background. The radiations from the  $10.5\text{min}$   $^{186}\text{Ta}$  could be identified and were taken care of by proper adjustments of the irradiation and the data accumulation timings. Thin W-foils (0.025 mm) were used for the accurate study of self-absorption, to apply necessary corrections.

To measure the half-life of  $^{185\text{m}}\text{W}$ , enriched  $^{186}\text{W}$  was bombarded for 5 min and the decay of beta rays and the converted electron intensities was studied under a Geiger-Müller counter. The existence of activities with half-lives  $1.65 \pm 0.05\text{min}$ , and  $10.5 \pm 0.5\text{min}$  along with an almost constant background due to longer lived activities was obtained (figure 1a). The  $1.65 \pm 0.05\text{min}$  half-life was assigned to  $^{185\text{m}}\text{W}$  and the  $10.5 \pm 0.5\text{min}$  activity was attributed to the decay of  $^{186}\text{Ta}$ . These assignments were further confirmed by studying the decay of photopeak intensity of each gamma ray using NaI(Tl) and Ge(Li) detectors. To confirm the half-lives of the longer lived portion of the activities, enriched  $^{186}\text{W}$  was bombarded for one hour and the decay was followed using a low background Geiger-Müller counter (background = 2 counts per min). Radiations

with half-lives 10.5 min, 65 min and  $\sim 75\text{d}$  were detected (figure 1b), which could be assigned to  $^{180}\text{Ta}$ ,  $^{183}\text{Hf}$ , and  $^{185}\text{W}$ , respectively.

In the experiments described in the following sections, an enriched sample of  $^{185}\text{W}$  weighing  $\sim 140\text{ mg}$  was used in repeated bombardments. The irradiation time in all the cases was kept to be about 2 min to reduce the production of impurity activities due to longer-lived radioactive isotopes. To have a reasonably good counting statistics a method of repeated bombardments and accumulations was adopted. After each irradiation four spectra were recorded for successive intervals of 1.5 min the first one being started about 30 sec after the irradiation. The subtraction of the fourth spectra from the first three removed most of the effects of background and longer-lived radiations. The difference spectra contained contributions mainly due to 1.65 min activity and a small fraction due to 10.5 min  $^{180}\text{Ta}$ . The decay of  $^{180}\text{Ta}$  has been carefully studied (Gujrathi *et al* 1968, Monmand *et al* 1969, Pathak *et al* 1970). Its contribution was accounted for in all the measurements. The interference due to radiations from 65 min and 75d activities was not detectable.

#### SINGLE GAMMA RAY SPECTRA

To study the gamma ray spectra of  $^{185m}\text{W}$  both enriched  $^{185}\text{W}$  and natural W-foils of a very high purity grade were used. The spectra were first studied using a  $7.6\text{ cm} \times 7.6\text{ cm}$  NaI(Tl) detector. Photopeaks at 60, 130 and 175 keV were found to decay with an average half-life of 1.65 min. Figure 2a shows the gamma ray spectra recorded for successive intervals of 3 min. The decay of individual photopeak intensities is shown in figure 2b. For the detailed study of gamma ray spectra a  $4\text{ cm}^2$  area  $\times 5\text{ mm}$  depletion depth Ge(Li) detector was employed. The energy resolution (FWHM) of the system was 2.8 keV for the 121.8 keV peak of  $^{152}\text{Eu}$ .

Most of the gamma rays emitted by 1.6 min  $^{185}\text{W}$  are of low energy and the behaviour of the Ge(Li) detector for such gamma rays is expected to be complicated due to absorption in the layers of different elements in between the source and the detector. Therefore, it was felt necessary to study the low energy response of the Ge(Li) detector used in the present work before using it for the spectrometry of very low energy gamma rays. With the conventional mounting of the source on the top of the detector, a sharp fall in the apparent photopeak efficiency for gamma rays having their energies below 80 keV is noted. This phenomenon can be understood in terms of the absorption in the following two media.

(i) A part of the low energy gamma radiation is absorbed in the sample itself. This absorption becomes prominent if the sample used is thick or of high atomic number. The samples used for the gamma ray spectroscopy of  $^{185m}\text{W}$  were either tungsten foil or oxide enriched in  $^{185}\text{W}$ . The percentage absorption

in the half-thickness of the sample was studied. A sharp increase in the percent absorption with decrease in gamma ray energy below  $\sim 100$  keV was noted.

(ii) The other absorbing medium is the dead layer of detector. The thickness of dead layer of the Ge(Li) detector used in the present investigation, has been quoted as 0.5 mm by the manufacturers. A sizeable portion of the gamma rays below 50 keV gets absorbed in this layer, thereby reducing the apparent photopeak efficiency.

The enclosures for the Ge(Li) detectors, provided by the manufacturers, are in general made of thin aluminium sheet. The atomic number for aluminium is 13, whereas, for Ge it is 32. Therefore, the absorption of gamma rays in the Ge dead layer should be several times more than that in the aluminium container. An alternative, to avoid the entry through the dead layer would be side entry, as suggested by Mukherjee (1969). The method of side entry for detection of protons was utilized by Gruhn *et al* (1969) to minimize the energy loss and straggling in penetrating the window. This is done by mounting source on the side of the detector, outside the enclosure, in such a position that the central part of the depleted region faces the source. To study the effect of absorption in the dead layer of the detector, gamma spectra of several standard calibrating sources, emitting low energy gamma radiations, were recorded with side and top entries, respectively. The photopeaks of gamma rays below 50 keV were far more intense in the spectrum recorded with side entry, as compared to one recorded with top entry. Figures 3a and 3b show the gamma ray spectra of  $^{133}\text{Ba}$  recorded with top and side entries, respectively. The difference in the relative intensities of the X-ray peaks as compared to the 80 keV peak in the two spectra is remarkable. As a result of these studies it was found that the absorption of low energy gamma rays in the dead layer is more prominent than in the aluminium wall. However, there are certain disadvantages with the side entry which make its use restricted only to strong sources. Firstly, the enclosure is at a good distance from the detector and secondly the sensitive area of the detector facing the source is quite small as compared to the top entry. These two facts lead to a very small solid angle being subtended by the detector at the source. Therefore, the overall detection efficiency is highly reduced. Figure 4 shows the variation of the relative photopeak efficiency with energy, for the side and top entries. In finding these curves the photopeak efficiency for 81.1 keV gamma ray was assumed to be 1 in both cases. It is remarkable to note that compared to the top entry the relative photopeak efficiency is higher for the side entry on both sides of 80 keV. However, the difference on the low energy side is more pronounced. The exact shape of the bent portion just below 80 keV could not be determined unambiguously due to the unavailability of well-studied very low energy gamma ray sources with closely spaced gamma rays around 80 keV and below. From the nature of the photopeak efficiency curves it is noted that the spectroscopy with the side entry



is advisable for gamma rays below 50 keV. The method will be more effective with detectors contained in thin and smallest possible diameter enclosures. The increase in the relative photopeak efficiency of high energy radiation may be attributed to the thicker depletion region seen by a gamma ray traversing the detector laterally.

The gamma ray spectra of  $^{185m}\text{W}$  were studied with both the side and top entries. The main purpose of studying the gamma spectra with side entry was to look for the low energy gamma rays whose existence has been predicted in an earlier work (Daly *et al* 1969). Figures 5a and 5b show the spectra recorded with the top and side entries respectively. A remarkable difference between the two spectra is in relative intensities of 59.2 and 66.2 keV photopeaks. In the spectrum taken with top entry the heights of these two peaks are almost equal but in the one taken with side entry the height of 59.2 keV is appreciably more. However, photopeaks corresponding to the low energy gamma rays suggested by Daly *et al* (1969) could not be observed in any of the spectra. No clear indication could be obtained even for the 42.7 keV gamma ray. To study the decay of photopeak intensities, spectra were recorded in the four sections of the 512-channel analyzer for successive intervals of 1.5 mm (figure 6). In figure 7 the decay mode of each gamma ray is shown. Several such measurements led to the assignment of 1.65 min as half-life of  $^{185m}\text{W}$ . The intensity of 198.0 keV gamma ray decayed with a half-life longer than 1.65 min but shorter than 10.5 min and therefore, it was inferred that a part of the intensity of 198.0 keV gamma ray is due to 10.5 min  $^{186}\text{Ta}$  and the rest comes from the summing of 131.8 and 66.2 keV gamma rays.

#### ENERGY AND INTENSITY MEASUREMENTS OF GAMMA RAYS

As the gamma rays emitted by 1.6 min  $^{185m}\text{W}$  are of very low energies special care had to be taken to account for the nonlinearity of multichannel analyzer below 50 channels, absorption of the radiations in the  $^{186}\text{W}$  sample used for the neutron irradiation, the window and the dead layer of the detector. The non-linear channels of the 512-channel analyzer were excluded by recording the spectrum unbiased and with a good dispersion. As all the gamma rays involved in this work are below 200 keV, spectra could be recorded in a single energy setting. The energy dispersion of the spectrometer was so adjusted that the  $K_{\alpha}$  X-ray peak was observed near 100 channels. The rise time of the output pulse from the ORTEC model 118A, FET preamplifier is very small ( $\sim 100$  ns), whereas, the decay time is very large ( $\sim 50\mu\text{s}$ ). Therefore, with different counting rates different portions of the pulse due to a radiation overlap with the succeeding radiation, thereby causing a shift in the energy calibration of the multichannel analyzer with the change in counting rate. To exclude the possibility of any such shift  $^{185m}\text{W}$  gamma spectra were recorded along with a  $^{133}\text{Ba}$  source of suitable

strength. Assuming the energies of  $^{133}\text{Ba}$  gamma rays quoted in the recent reports by Gurfinkel *et al* (1967) as standard, the accurate energies of the strong peaks were determined. In another run  $^{185\text{m}}\text{W}$  alone was used to record the spectra to observe the weak photpeaks distinctly. The energies of strong peaks determined in the previous experiments were used to determine the energies of the weak radiations. A linear relation of the form  $E = a + bx$ , where  $E$  is the energy corresponding to the channel  $x$  and  $a$  and  $b$  are constants, was used. The values of  $a$  and  $b$  were determined over the whole energy range used and the linearity of the detector response was confirmed.

It has been observed (Hollander 1966) that for Ge(Li) detectors a double logarithmic plot of efficiency *versus* energy is a straight line over the range of 100 keV to several MeV. Below 100 keV though the intrinsic efficiency of the Ge(Li) detector is expected to be high, due to excessive absorption in the container and the dead layer the apparent efficiency goes down rapidly with the energy. Thus besides self absorption in the sample the observable intensity of low energy gamma rays is further reduced due to the apparent poor efficiency. In the present work, since all the gamma rays in question are of low energy, sizeable correction due to these effects was necessary. The low energy response of the detector was studied using the X-rays and the gamma rays from  $^{133}\text{Ba}$  and  $^{152}\text{Eu}$ . An energy *versus* photpeak efficiency curve obtained for the energy range of interest is shown in figure 4. To account for the absorption of the low energy radiations in the sample itself the following procedure was adopted. Enriched  $^{186}\text{W}$  was packed in a thin polythene bag and irradiated with fast neutrons. Before putting it on the detector it was uniformly spread and two folded. Then it was mounted on the detector along with a  $^{133}\text{Ba}$  source of suitable strength. The energies and the relative intensities of the observed gamma rays were obtained by usual methods described earlier. To obtain the correction factor for absorption of gammas of different energies the percentage absorption of gammas of different energies in half thickness of the sample was studied in the following manner. Spectrum of  $^{133}\text{Ba}$  was recorded for 90 min by putting it on the top of the detector in a particular position. Then keeping the geometry the same the unfolded  $^{186}\text{W}$  sample (to make the thickness half of what was used for recording  $^{185\text{m}}\text{W}$  gamma spectra) was put under it and the spectrum was analysed for the same interval (90 min). The percentage reduction in the intensity of each gamma ray was calculated and an energy *versus* percentage absorption curve was obtained. The percentage absorption of  $^{185\text{m}}\text{W}$  gamma rays was determined using this curve. To confirm the results obtained after self-absorption correction further experiments were necessary because the sample of the  $\text{WO}_3$  enriched in  $^{186}\text{W}$  used in the above measurements was in the powder form resulting in non-uniformity in the thickness after spreading in the polythene bag used for packing. To do this the measurements described above were repeated using two W-foils of same dimensions. At the first instance, both the foils were irradiated with 14 MeV

neutrons and gamma spectra were recorded by mounting these foils one above the other on the detector. Next, the energy *versus* percentage absorption curves were obtained by putting each foil separately, one at a time, under a  $^{133}\text{Ba}$  source. An average of the two measurements was taken as the true value. The corrected intensities by the above two methods were consistent within the limits of experimental error.

A gamma spectrum taken with a Ge(Li) detector can be regarded as consisting of two distinct parts, (1) the continuous "base-line" and (2) individual peaks. The peaks are so narrow that the base-line under each peak can be assumed to be smooth curve or even linear. The continuity of the base line is broken under the peaks. Therefore, to determine the base line counts under a peak, the base-line is interpolated maintaining the smooth shape. After subtracting the base line isolated peaks are obtained. To find the peak position in terms of the channel numbers the centroids of the peaks were determined. Their energies were determined by taking the energies of  $^{152}\text{Eu}$  (Malinzen *et al* 1967) and  $^{133}\text{Ba}$  (Gurfinkel *et al* 1967) as standard. A linear relation of the form described above was used. To determine the intensities of gamma rays, the area under each photopeak was determined by summing the counts in an isolated peak. The relative photopeak efficiencies for different gamma energies were found from the curve shown in figure 4. The corrections for the self-absorption were applied in the manner described earlier. The intensity of 66.2 keV radiation was normalised to 100 and other intensities were determined with respect to it. The number 100 was chosen to make the intensities obtained in the present work directly comparable to those reported by Daly *et al* (1969). Table 1 shows the energies and relative intensities of the gamma

TABLE 1. Measured energies and relative intensities of gamma rays emitted by  $^{185m}\text{W}$

Energy in KeV		Relative intensity	
Present work	Daly <i>et al</i> (1969)	Present work	Daly <i>et al</i> (1969)
$59.2 \pm 0.2$	WX-ray	$112 \pm 22$	$99 \pm 9 \text{ K}_\alpha$
$66.2 \pm 0.2$	$66.1 \pm 0.2$	100 (standard)	100 (standard)
$94.5 \pm 0.3$	$94.3 \pm 0.3$	$2.1 \pm 0.2$	$1.6 \pm 0.2$
$107.9 \pm 0.3$	$107.7 \pm 0.3$	$7.7 \pm 0.8$	$5.3 \pm 0.5$
$122.3 \pm 0.3$	$122.1 \pm 0.3$	$2.1 \pm 0.2$	$1.6 \pm 0.2$
$131.8 \pm 0.2$	$131.7 \pm 0.2$	$80 \pm 8$	$66 \pm 4$
$164.7 \pm 0.3$	$164.5 \pm 0.3$	$11 \pm 1$	$9.9 \pm 1.0$
$174.1 \pm 0.2$	$173.8 \pm 0.2$	$58 \pm 6$	$58 \pm 4$
$188.3 \pm 0.3$	$188.1 \pm 0.2$	$14.7 \pm 1.5$	$14.5 \pm 1.4$

rays from  $^{185m}\text{W}$  obtained in the present work along with those reported by Daly *et al* (1969). A good consistency is noted between the values obtained by the two groups.

As 66.2 keV gamma ray is close to the K-absorption edge, accurate absorption corrections could not be applied as the behaviour of absorption coefficient is not well studied in this region. The gamma ray spectra were also studied by placing the source at a somewhat larger distance ( $\sim 5$  cm). The relative intensity of 198.0 keV photoppeak was found to decrease with the increase of source-to-crystal distance and therefore, it was attributed to summing of 131.8 and 66.2 keV gamma rays. As the intensity of 198.0 keV gamma ray is very poor and also contains a part of its intensity due to  $^{186}\text{Ta}$ , conclusions drawn about its nature were ambiguous. However, assuming it as a sum peak, the decay scheme proposed by Daly *et al* (1969) is nicely explained.

In the analysis of the observed gamma ray spectra, possible interference of Compton edges and back-scattered peaks with the genuine photoppeaks was also taken into account. The Compton edge of 164.7 keV gamma ray should be located around 66 keV, but as 66.2 keV transition is far more intense than 164.7 keV gamma ray, a negligible error is expected in finding the intensity of 66.2 keV gamma ray due to the presence of this Compton edge. To account for the effect of back-scattering the positions of back-scattered peaks were calculated. Although the energy of 188.3 keV gamma ray after back-scattering becomes very close to 107.9 keV, back-scattered peaks due to intense 174.1 and 131.8 keV gamma rays could not be observed and any back-scattered peak due to weak 188.3 keV radiation is almost ruled out. Therefore, 107.9 keV photoppeak was identified as a genuine gamma ray. In finding the intensity of 66.2 keV gamma ray the contribution due to W X-rays was calculated using the relative yields of  $K_{\alpha}$  and  $K_{\beta}$  X-rays (Lederer *et al* 1967).

#### THE GAMMA-GAMMA COINCIDENCE STUDIES

The gamma-gamma coincidence data were obtained using two scintillation NaI(Tl) detectors. A 5 cm dia  $\times$  5 cm thick NaI(Tl) crystal was used for selecting the gating pulses and another 7.6 cm  $\times$  7.6 cm NaI(Tl) crystal was employed as an analyzer detector. Both the detectors were coupled to R.C.A.8054 photomultipliers. The signals from the two gamma detectors were fed to a slow-fast coincidence circuit. The pulses from the analyzer detector were recorded in a Nuclear Data 512-channel analyzer gated by the coincidence signal. The detectors were placed 2.5 cm apart in a lead chamber facing each other. The sample holder was placed at the centre of a graded lead anti back-scattering which was placed between the two detectors. The NaI(Tl) crystals were covered with lucite plates of suitable thickness to stop beta rays and the converted electrons. As the singles counting rate was low, the accidental coincidences were expected to be negligible.

therefore, no corrections were applied for its contribution. A series of measurements were performed to confirm the observed coincidence spectra. All the intense gamma rays observed in the single crystal NaI(Tl) spectra were selected one by one in the gate and the coincident gamma spectra were studied.

Figures 8a and 8b show the gamma spectra in coincidence with 66.2 and 131.8 keV gamma rays, respectively. In figure 8a intense peaks are observed at 60 and 132 keV while in figure 8b only 60 keV peak is intense. In both the spectra a weak peak at  $\sim 30$  keV is observed. This may be partly due to I K X-rays. The broad peak at 208 keV was found to decay with 10.5 min half-life of  $^{186}\text{Ta}$ . As suggested by Morinaga *et al* (1960), we tried to search the coincidence between 66.2 and 174.1 keV gamma rays and also between 131.8 and 174.2 keV transitions. In the first series of experiments comparatively wider windows were selected and a very weak coincidence was observed between 174.1 and 131.8 keV gammas. Although this was consistent with the reports of Morinaga *et al* the situation was ambiguous as the observed coincidence could be due to Compton scattered electrons of other gamma rays. To resolve this ambiguity gamma-gamma coincidence experiments were repeated with narrow gates of single channel analyzers. Even after increasing the resolving time of the electronic set up to  $4\mu\text{sec}$  no coincidence could be observed between 131.8 and 174.1 keV gamma rays. The results of these coincidence measurements led to the modification of the tentative decay scheme reported earlier by the authors (Pathak *et al* 1968).

### DISCUSSION

The results of singles and coincidence measurements are summarised in the decay scheme shown in figure 9. In the decay scheme suggested by Morinaga & Nagatani (1960) the levels of  $^{185}\text{W}$  were shown at 0, 100 and 175 keV. The 1.6 min isomer was suggested at 300 keV. These assignments were supported by indications of coincidence between 175 and 125 keV gammas. It was further confirmed by the existence of a peak at 230 keV which was identified as a sum peak of 175 keV transition and the K X-ray emitted as a result of the conversion of 125 keV gamma ray. The multipolarity of the 125 keV transition was inferred as E3 and hence a fairly large K conversion coefficient ( $\sim 1.7$ ) was expected, thereby increasing the sum probability.

In the present investigation the gamma rays of 66.2, 94.5, 107.9, 131.8, 164.7, 174.1 and 188.3 keV were observed. As no coincidence could be observed between 131.8 and 174.1 keV transitions, the 131.8–174.1 keV cascade was ruled out. However, the 66.2 and 131.8 keV gammas were found coincident, and therefore, the 198.0 keV peak was identified as sum peak due to 131.8 and 66.2 keV gamma rays. No gamma ray decaying with 1.6 min half-life could be identified around 230 keV. A level at 66.1 keV in  $^{185}\text{W}$  has been reported by Daly *et al* (1969) whereas, no excited state at 131.8 keV is known. Therefore, we suggest a level at 66.2 keV

and the observed gamma ray of 66.2 keV is shown connecting this level and the ground state. The 1.65 min isomer is shown at 198.0 keV. These assignments are further supported by relative intensities and expected conversion coefficients of these transitions. The 174.1 keV transition is not in coincidence with any intense gamma ray, therefore a level at 174.1 keV is suggested to accommodate this gamma ray as a transition to ground state. A 23.9 keV gamma ray is shown by a dotted line, connecting isomeric state and the 174.1 keV level. It could not be observed in singles Ge(Li) spectra but the coincidence experiments indicate the existence of gamma ray of  $\sim 30$  keV (figure 8). The energy difference between the 188.3 and 122.3 keV gamma rays suggests that there should be a level at 188.3 keV and the above gammas could be placed between this level and the ground state and the 66.2 keV levels, respectively. The 107.9 keV gamma ray is very weak in the singles Ge(Li) spectrum as compared to 174.1 keV transition. In the decay scheme it is shown connecting 66.2 and 174.1 keV levels. The levels, so far proposed, explain all the singles and coincidence gamma spectra except 164.7 and 94.5 keV gamma rays.

Neutron deficient nuclei in the mass region around 185 have their ground state as  $1/2^-$  [510] while those with excess neutrons exhibit  $3/2^-$  [512]. Assuming the deformation parameter  $\delta \simeq 0.2$ , as suggested by Morinaga *et al* (1960), from the Nilsson diagram one expects  $1/2^-$  [510] or  $3/2^-$  [512] as ground state of  $^{185}\text{W}$ . The  $\beta$ -decay of  $^{75}\text{d}$   $^{185}\text{W}$  to the ground state ( $5/2^+$  [402]) of  $^{185}\text{Re}$  has a  $\log ft$  value of 6.5, whereas, the decay to the first excited state ( $7/2^+$ ) has the value 8.4 and there is no decay to the  $9/2^+$  level. The  $\log ft$  value of the decay to the ground state suggests the ground state spin of  $^{185}\text{W}$  as  $3/2^-$  [512]. In the recent report of Daly *et al* (1969) the spin of the ground state of  $^{185}\text{W}$  has been experimentally confirmed as  $3/2^-$  [512] intrinsic state and also justified by theoretical considerations. In Nilsson diagram  $3/2^-$  [512] and  $1/2^-$  [510] states are closely spaced, and therefore  $3/2^-$  being a ground state,  $1/2^-$  is expected at low excitation energy. Martin *et al* (1966) observed a gamma ray of 15 keV in the study of  $^{184}\text{W}(n, \gamma)$  reaction. They identified it as due to transition from  $1/2^-$  [510] to the ground state. Erskine (1965) suggested a level with spin  $1/2^-$  at 13.6 keV. Recently Daly *et al* (1969) could explain the observed gamma ray spectra with this level at 23.6 keV. We put this level at 23.6 keV to explain the observed singles and coincidence spectra. The 164.7 keV transition is shown between 188.3 and 23.6 keV levels. A level at 93.8 keV is suggested to accommodate the 94.5 keV gamma ray. A 93.8 keV gamma ray is included by dotted lines between this level and the ground state. The 23.9 and 9.7 keV transitions, shown by dotted lines in figure 9, could not be observed in the singles gamma ray spectra. However, a peak at about 30 keV was identified in coincidence with 66.2 and 131.8 keV transitions. This probably includes the 23.6 keV gamma ray. The presence of these transitions is essential to understand the relative intensities of the gamma transitions. The spins and the parities of the excited levels have been assigned with the help of previous

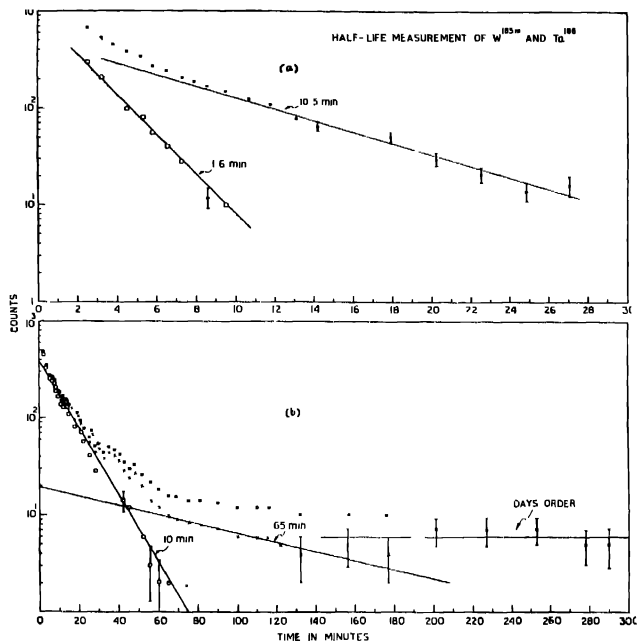


Figure 1a Half-life measurement of the short lived  $^{185m}\text{W}$ . Figure 1b long lived activities produced by the fast neutron irradiation of  $^{186}\text{W}$ .

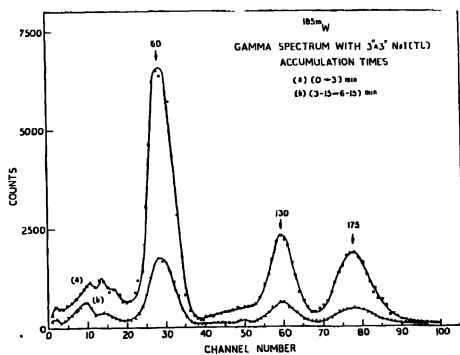


Figure 2a. Subtracted gamma ray spectra of 1.65 min  $^{185m}\text{W}$  taken with a 7.6 cm  $\times$  7.6 cm NaI(Tl) detector for successive intervals of 3 min. The sources of  $^{185m}\text{W}$  were obtained by irradiating enriched  $^{186}\text{W}$  with fast neutrons.

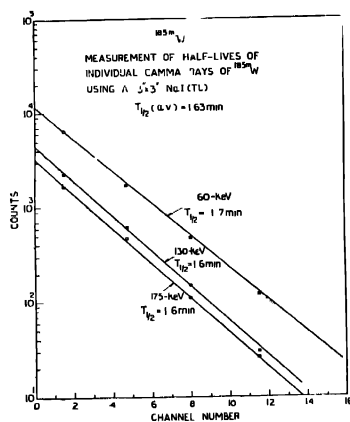


Figure 2b Decay of photopeak intensities of 1.65 min  $^{185m}\text{W}$  gamma rays using 7.6 cm  $\times$  7.6 cm NaI(Tl) detector

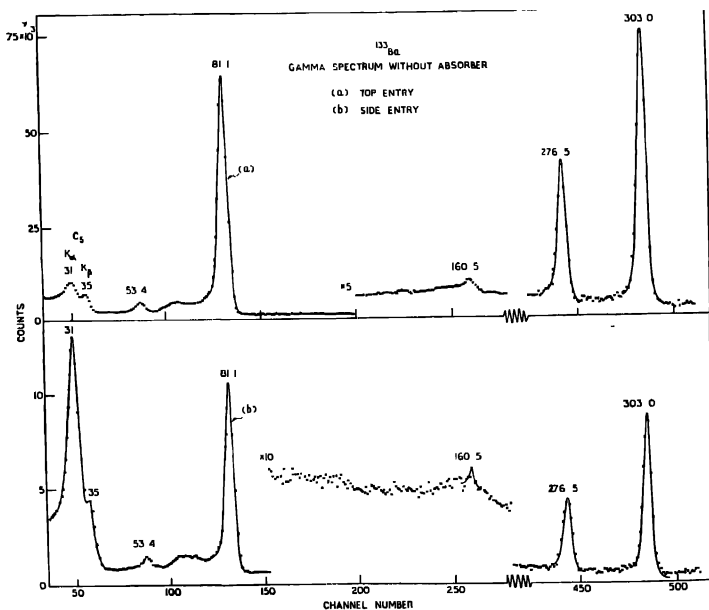


Figure 3 Gamma rays spectra of  $^{192}\text{Ba}$  recorded using a 4 cm<sup>2</sup> area  $\times$  5 mm deep Ge(Li) detector with figure 3a top entry and figure 3b side entry. A remarkable enhancement in the apparent detection efficiency for the Cs x-rays in the side entry gamma spectrum is noted.



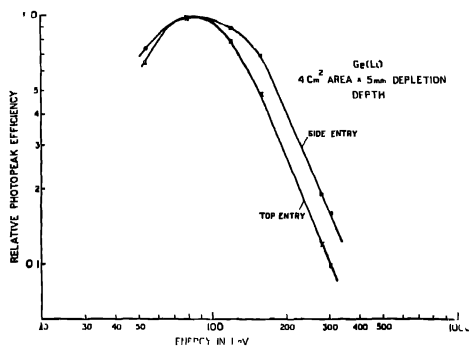


Figure 4 Energy versus photoppeak efficiency curve for a  $2\text{ cc}$  detector with figure 4a top entry and figure 4b side entry.

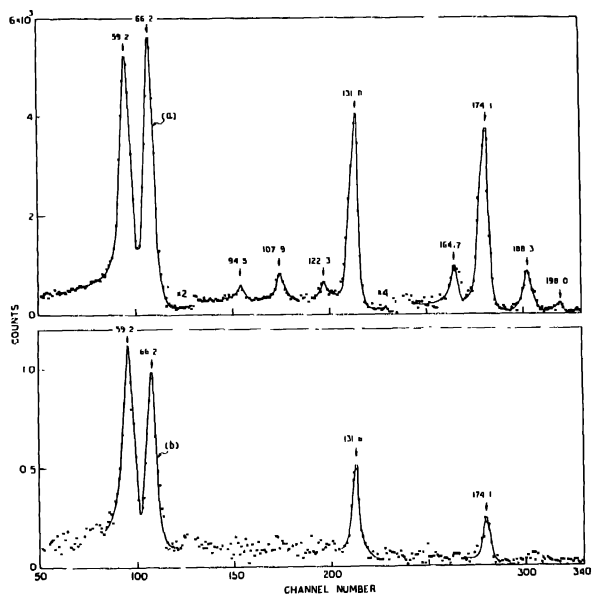


Figure 5. Gamma-ray spectra of  $185\text{mW}$  recorded in an expanded energy scale using a  $4\text{ cm}^2$  area  $\times 5\text{ mm}$  depletion depth  $\text{Ge(Li)}$  detector with figure 5a top entry and figure 5b side entry. In both the cases enriched samples of  $^{186}\text{W}$  were irradiated to obtain the sources of  $185\text{mW}$ .

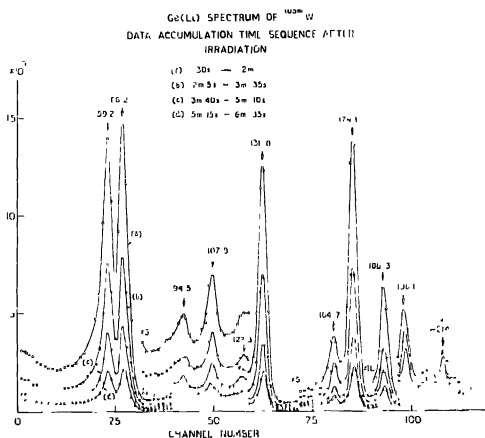


Figure 6. Gamma ray spectra of  $^{185}\text{mW}$  taken with a 2cc Ge(Li) detector for successive values of 1.5 min in the four sections of the analyzer memory. The spectra were corrected for background and longer lived activities produced during the irradiation of  $^{185}\text{mW}$ .

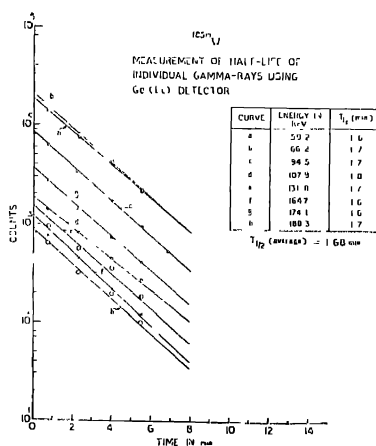


Figure 7. Half-life measurement of  $^{185}\text{mW}$  by studying the decay of gamma ray photopeak intensities using a Ge(Li) detector.

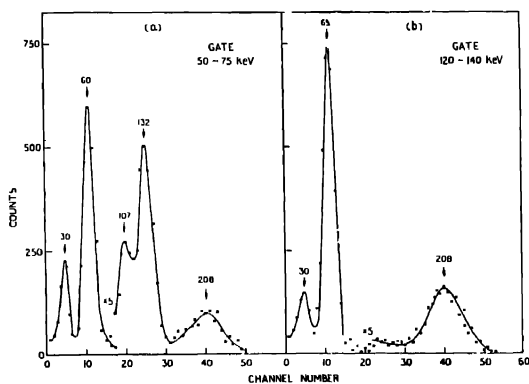


Figure 8. Gamma ray spectra in coincidence with figure 8a 66.2 and figure 8b 131.8 keV gamma rays

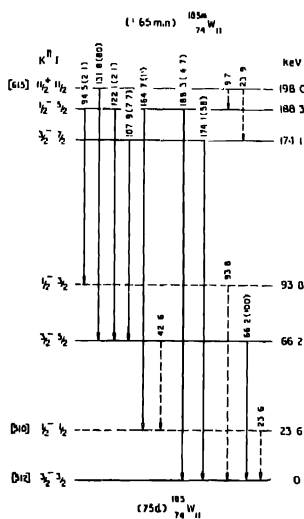


Figure 9. Proposed decay scheme of 1.65 min  $^{185m}\text{W}$ .



reports (Morinaga *et al* 1960, Daly *et al* 1969), especially one due to Daly *et al* (1969). The proposed decay scheme is consistent with the latter report.

The authors wish to acknowledge their sincere gratitude to Professor D. N. Kundu for his kind interest and to Professor P. N. Mukherjee for his stimulating discussion and helpful suggestions.

*Note added* After this paper was communicated a report on the decay of  $^{185m}\text{W}$  has appeared in Can. J. Phys. **48** (1970) 502, by S. C. Gujrathi and J. M. D'Auria. Our results are in good agreement with those reported in the above paper.

#### REFERENCES

- Bakhru H. & Mukherjee S. K. 1966 *Phys. Rev.*, **142**, 719.  
 Daly P. J., Kleinheinz P. & Casten R. F. 1969 *Nucl. Phys.*, **123A**, 186.  
 Duffield R. B., Hsiao L. & Sloth E. N. 1950 *Phys. Rev.*, **79**, 1011.  
 Eiskine J. R. 1965 *Phys. Rev.*, **138**, B66.  
 Gruhn C. R., Kuo T., Maggiori C., Freedom B., Samuelson L. & Chander J. 1969 *IEEE Trans. Nucl. Sci.* **NS-15**, 337.  
 Gujrathi S. C., Pathak B. P., Murty K. S. N. & Mukherjee S. K. 1968 *Proc. Nucl. Phys. Symp. Madras*, 343.  
 Gurfinkel Y. & Notten A. 1967 *Nucl. Instr. Methods*, **57**, 173.  
 Hollander J. M. 1966 *Nucl. Instr. Methods*, **43**, 65.  
 Lederer C. M. *et al* *Table of Isotopes*, VI ed. 1967 John Wiley & Sons.  
 Malmsten G., Nilson O. & Anderson I. 1967 *Arkiv. Fysik*, **33**, 361.  
 Martin M. J., Harvey J. A. & Slaughter S. G. 1966 *Oak Ridge National Laboratory Report*, ORNL-3924 (Unpublished).  
 Monand E., Blachot J. & Moussa A. 1969 *Nucl. Phys.*, **A184**, 321.  
 Morinaga H. & Nagatani K. 1960 *Nucl. Phys.*, **19**, 327.  
 Mukherjee P. 1969 Private communication.  
 Pathak B. P., Gujrathi S. C. & Mukherjee S. K. 1968 *Proc. Nucl. Phys. Symp.*, Bombay, 293.  
 Pathak B. P., Murty K. S. N., Mukherjee S. K. & Gujrathi S. C. 1970 *Phys. Rev.*, **C1**, 1477.  
 Poe A. J. 1955 *Phil. Mag.*, **46**, 611.

## Problem of screw dislocation in a non-homogeneous transversely isotropic annular disc

BY SANJIB KUMAR CHAKRABARTI

*Department of Mathematics, Chandernagore College, West Bengal,  
India*

(Received 28 July 1969—Revised 30 January 1970)

Expressions for stresses and displacements in the case of a screw dislocation in an annular disc of non-homogeneous transversely isotropic material have been calculated in this paper. The amount of energy necessary for forming the dislocation is also calculated. Stresses have been calculated numerically for different cases.

### INTRODUCTION

Effects of dislocations on crystals were studied by Forty (1951), Dawson & Vand (1950, 1951). Thereafter Eshelby & Stroh (1951) discussed different cases of straight screw dislocation in a thin plate and disc and in an infinite body. In the present case, the problem of screw dislocation in a non-homogeneous transversely isotropic annular disc has been considered.

### SOLUTION OF THE PROBLEM

Here we use the cylindrical co-ordinates  $r, \theta, z$ .  $u_r, u_\theta, u_z$  are the displacement components and  $\tau_{rr}, \tau_{r\theta}, \tau_{\theta z}$ , etc., the stress components,  $c_{44}, c_{66}$  being the elastic constants. Let the disc be bounded by  $r_1 \leq r \leq r_2$  and  $z = \pm d$ .

Now we know that for a screw dislocation in an infinite transversely isotropic body along the  $Z$ -axis, the non-vanishing displacement and stress components are

$$\begin{aligned} u_z &= \frac{b}{2\pi} \cdot \theta, \\ \tau_{\theta z} &= \frac{c_{66}b}{2\pi} \end{aligned} \quad \dots (1)$$

For screw dislocation in a disc, the tractions on the plane  $sz = \pm d$  must vanish. We have for transversely isotropic material (Love 1944)

$$\begin{aligned} - \frac{\partial u_r}{\partial z} \\ \tau_{\theta z} = c_{66} \left( \frac{\partial u_\theta}{\partial r} - \frac{u_\theta}{r} \right) \end{aligned} \quad \dots (2)$$

Let us suppose

$$c_{44} = c'_{44}r^l, \quad c_{66} = c'_{66}r^l, \quad \dots \quad (3)$$

$c'_{44}, c'_{66}, l$  being constants.

The equation of equilibrium that does not vanish is

$$\frac{\partial \tau_{r\theta}}{\partial r} + \frac{\partial \tau_{\theta z}}{\partial z} + \frac{2\tau_{r\theta}}{r} = 0. \quad \dots \quad (4)$$

This equation with (2) and (3) reduces to

$$\frac{\partial^2 u_\theta}{\partial r^2} + \frac{l+1}{r} \frac{\partial u_\theta}{\partial r} - (l+1) \frac{u_\theta}{r^2} + K^2 \frac{\partial^2 u_\theta}{\partial z^2} = 0, \quad \dots \quad (5)$$

where 
$$K^2 = \frac{c'_{44}}{c'_{66}}.$$

Let  $u_\theta = e^{imz} \cdot U(r)$ ,  $m$  being an arbitrary constant.

Then (5) becomes

$$\frac{\partial^2 U}{\partial r^2} + \frac{l+1}{r} \frac{\partial U}{\partial r} - (l+1) \frac{U}{r^2} - K^2 m^2 U = 0.$$

Again, the substitution  $U = r^p \cdot V$  reduces the equation to

$$\frac{\partial^2 V}{\partial r^2} + \frac{l+1+2p}{r} \frac{\partial V}{\partial r} + \left\{ \frac{(p-1)(l+1+p)}{r^2} - K^2 m^2 \right\} V = 0, \quad \text{which for}$$

$$p = -\frac{l}{2}, \quad r = \frac{t}{km} \quad \text{becomes} \quad \frac{\partial^2 V}{\partial t^2} + \frac{1}{t} \frac{\partial V}{\partial t} - \left\{ \frac{\left(\frac{l}{2}+1\right)^2}{t^2} + 1 \right\} V = 0.$$

The solution of this equation is 
$$V = AI_{\frac{l}{2}+1}(t) + BK_{\frac{l}{2}+1}(t).$$

Therefore, 
$$u_\theta = e^{imz} r^{-\frac{l}{2}} \cdot \left[ AI_{\frac{l}{2}+1}(Kmr) + BK_{\frac{l}{2}+1}(Kmr) \right] \quad \dots \quad (6)$$

Thus in our case the non-vanishing displacement and stress components can be written as

$$u_\theta = -\frac{b}{2\pi} \frac{z}{r} + r^{-\frac{l}{2}} \sum_{n \text{ odd}} \left[ A_n I_{\frac{l}{2}+1} \left( \frac{Kn\pi r}{2d} \right) + B_n K_{\frac{l}{2}+1} \left( \frac{Kn\pi r}{2d} \right) \right] \sin \frac{n\pi z}{2d},$$

$$u_z = \frac{b}{2\pi} \theta,$$

$$\begin{aligned}\tau_{\theta z} &= \frac{c'_{44}\pi}{2d} r^{\frac{l}{2}} \sum_{n \text{ odd}} n \left[ A_n I_{\frac{l}{2}+1} \left( \frac{Kn\pi r}{2d} \right) + B_n K_{\frac{l}{2}+1} \left( \frac{Kn\pi r}{2d} \right) \right] \cos \frac{n\pi z}{2d}, \\ \tau_{r\theta} &= \frac{c'_{46}b}{\pi} r^{l-z} z + \frac{c'_{46}K\pi}{2d} r^{\frac{l}{2}} \sum_{n \text{ odd}} n \left[ A_n I_{\frac{l}{2}+2} \left( \frac{Kn\pi r}{2d} \right) \right. \\ &\quad \left. - B_n K_{\frac{l}{2}+2} \left( \frac{Kn\pi r}{2d} \right) \right] \sin \frac{n\pi z}{2d} \quad \dots \quad (7)\end{aligned}$$

The conditions on the boundary are  $\tau_{r\theta} = 0$  on  $r = r_1$  and on  $r = r_2$ .

These give rise to

$$A_n I_{\frac{l}{2}+2} \left( \frac{Kn\pi r_1}{2d} \right) - B_n K_{\frac{l}{2}+2} \left( \frac{Kn\pi r_1}{2d} \right) = -\frac{16bd^2}{K\pi^4 n^3} r_1^{\frac{l}{2}-2} \sin \frac{n\pi}{2},$$

$$\text{and} \quad A_n I_{\frac{l}{2}+2} \left( \frac{Kn\pi r_2}{2d} \right) - B_n K_{\frac{l}{2}+2} \left( \frac{Kn\pi r_2}{2d} \right) = -\frac{16bd^2}{K\pi^4 n^3} r_2^{\frac{l}{2}-2} \sin \frac{n\pi}{2}.$$

Solving, we get

$$A_n = \frac{16bd^2}{K\pi^4 n^3} \sin \frac{n\pi}{2}.$$

$$\frac{r_2^{\frac{l}{2}-2} K_{\frac{l}{2}+2} \left( \frac{Kn\pi r_1}{2d} \right) - r_1^{\frac{l}{2}-2} K_{\frac{l}{2}+2} \left( \frac{Kn\pi r_2}{2d} \right)}{I_{\frac{l}{2}+2} \left( \frac{Kn\pi r_1}{2d} \right) K_{\frac{l}{2}+2} \left( \frac{Kn\pi r_2}{2d} \right) - I_{\frac{l}{2}+2} \left( \frac{Kn\pi r_2}{2d} \right) K_{\frac{l}{2}+2} \left( \frac{Kn\pi r_1}{2d} \right)} \dots (8)$$

$$B_n = \frac{16bd^2}{K\pi^4 n^3} \sin \frac{n\pi}{2}.$$

$$\frac{r_2^{\frac{l}{2}-2} I_{\frac{l}{2}+2} \left( \frac{Kn\pi r_1}{2d} \right) - r_1^{\frac{l}{2}-2} I_{\frac{l}{2}+2} \left( \frac{Kn\pi r_2}{2d} \right)}{I_{\frac{l}{2}+2} \left( \frac{Kn\pi r_1}{2d} \right) K_{\frac{l}{2}+2} \left( \frac{Kn\pi r_2}{2d} \right) - I_{\frac{l}{2}+2} \left( \frac{Kn\pi r_2}{2d} \right) K_{\frac{l}{2}+2} \left( \frac{Kn\pi r_1}{2d} \right)} \dots (8)$$

Thus with these values of  $A_n$ ,  $B_n$ , the displacement and stresses are given by (7).

The energy required to form the dislocation in the annulus is given by

$$W = \frac{1}{2} b \int_{-d}^{+d} dz \int_{r_1}^{r_2} \tau_{\theta z} dr$$



$$= \sum_{n \text{ odd}} c'_{44} b \sin \frac{n\pi}{2} \int_{r_1}^{r_2} r^{\frac{l}{2}} \left[ A_n I_{\frac{l}{2}+1} \left( \frac{Kn\pi r}{2d} \right) + B_n K_{\frac{l}{2}+1} \left( \frac{Kn\pi r}{2d} \right) \right] dr,$$

$A_n, B_n$  being given by (8).

#### NUMERICAL CALCULATION

Let us calculate the stresses on  $z = 0$  plane in the crystal topaz due to dislocation.

For this material, we have

$$c'_{44} = 1100 \text{ dynes/cm}^2, \quad c'_{66} = 1350 \text{ dynes/cm}^2$$

So that 
$$K = \sqrt{\frac{22}{97}}$$

In particular, we take  $r_1 = 1 \text{ cm}$ ,  $r_2 = 2 \text{ cm}$  and  $d = 10 \text{ cm}$

The variations of  $\tau_{\theta z}$  on  $z = 0$  plane with the variation of  $r$  for different values of  $l$  are given in table 1.

TABLE I

$r \text{ (in cm)}$		1.0	1.1	1.5	2.0
$\left. \begin{array}{l} \frac{\pi^3}{8 c'_{44} b} [\tau_{\theta z}]_{z=0} \\ \text{(in dynes/cm}^2 \text{)} \end{array} \right\}$	(i) $l = -2$	38.349	34.746	25.242	18.838
	(ii) $l = 0$	-4.198	-4.447	-6.703	-9.158
	Homogeneous case				
	(iii) $l = 2$	-25.149	-29.865	-78.908	-188.797

The author expresses his grateful thanks to Dr. A. Chakrabarty of Jadavpur University for his kind help in the preparation of this paper.

#### REFERENCES

- Love, A. E. H. 1944 *Mathematical Theory of Elasticity* Dover publication.  
 Dawson, I. M. & Vand, V. 1950 *Nature* **165**, 295; 1951 *Proc. Roy. Soc. A*, **206**, 555.  
 Porty, A. J. 1951 *Phil. Mag.* (7), **42**, 670.  
 Eshelby, J. D. & Stroh, A. N. 1951 *Phil. Mag.* **42**, 1401.

## Infrared spectrum of anhydrous citric acid in the solid state—I

By K. MALLIKARJUNA RAO AND C. K. NARAYANASWAMY

*Department of Physics, Indian Institute of Technology, Madras-36*

(Received 12 August revised 14 October and  
12 December 1969)

The infrared spectra of anhydrous citric acid in mull and in KBr matrix have been recorded in the range  $700\text{--}4000\text{ cm}^{-1}$  with a Perkin-Elmer Infrared Spectrophotometer, model 221 equipped with sodium chloride optics. The observed frequencies are assigned tentatively to their respective characteristic groups. The frequencies due to the hydrogen bonds in the unit cell, are assigned with reference to the data known from Hadzi (1965). The results are reported in this communication.

### INTRODUCTION

There are only a few investigations that are to be found in the literature on the infrared and Raman spectra of citric acid either in solution or in the solid state. Passerini (1935) and Duval (1955) have recorded the infrared spectrum in the solid state without presenting any analysis. There is no investigation reported on the infrared spectrum of citric acid in solution. Edsall (1937) has investigated the Raman spectrum in solution and has reported the Raman frequencies without any analysis except indicating the  $\text{C}=\text{O}$  and  $\text{CH}_2$  frequencies. Nisi (1931), Thatte *et al* (1936) and Canal *et al* (1938) have investigated the Raman spectrum of citric acid monohydrate in the solid state. Nisi has confined himself to the region of water of crystallization only and reported the same. Thatte *et al* have photographed the Raman spectrum in the molten state and discussed the  $\text{O}=\text{C}-\text{O}$  group frequencies only. Canal *et al* have photographed the spectrum using powder technique and reported the data without any analysis. The authors have attempted to analyse the vibrational spectrum of this molecule in the solid state. Thus they have recorded the infrared spectrum of anhydrous citric acid in mull and in KBr matrix and have assigned the frequencies to their respective characteristic groups.

### EXPERIMENTAL

Citric acid monohydrate of AR grade from S. Merck & Co. was procured and purified by repeated recrystallization. A hot saturated solution of the substance in distilled water at about  $70^\circ\text{C}$  was cooled slowly to room temperature over several days. It is known that citric acid becomes anhydrous above the temperature  $36.7^\circ\text{C}$  and so we have obtained the crystals of anhydrous citric acid by the

above process of cooling. This anhydrous citric acid was used to record the spectra in mull as well as with a KBr pellet. The spectra are reproduced in figures 1 and 2.

### RESULTS

The observed frequencies with assignments are given in table 1. Also a pictorial diagram of anhydrous citric acid molecule is given in figure 3a. The Raman frequencies of citric acid in the polycrystalline state from Landolt and Bornstein tables (1951) are also given for comparison.

### DISCUSSION

Anhydrous citric acid with the chemical formula  $C_6H_8O_7$  is a tribasic acid with an OH group attached to the middle carbon atom. There is no data available on the molecular symmetry of this molecule in the free state. The crystal structure has been fully worked out by Nordman *et al* (1960).

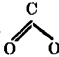
To facilitate understanding of the assignment of observed frequencies to their functional groups, a few salient details on the structure of the anhydrous citric acid molecule are given here. The aliphatic chain  $C_1-C_5$  is approximately planar, but is slightly bent away from the carboxyl  $O_6C_6O_6$ . All the carboxyls are coplanar with their  $\alpha$ -carbons. The carboxyl group  $O_1C_1O_2$  is at an angle of  $3.3^\circ$ , while the carboxyl  $O_3C_3O_4$  is approximately at right angles to that plane. There is approximate parallelism between the carboxyl  $O_5C_5O_5$  to the plane  $C_2C_3O_3$ , containing the  $\alpha$ -hydroxyl. In the unit cell the carboxyl group  $O_1C_1O_2$  is connected by two equivalent hydrogen bonds to an equivalent group across a centre of symmetry, i.e., the bonding is of the dimer type.

The free state symmetry of the molecule is only  $C_1$  and the site symmetry is also  $C_1$  although we could consider  $C_s$  to be the approximate site symmetry from the view point of the structural details already given above. Since in the present work we have aimed at only the characteristic group frequency assignments and not the assignment of symmetry species of the modes of vibration, the site symmetry has not been discussed further. The observed frequencies are discussed below in terms of their functional groups.

#### $CH_2$ frequencies

The antisymmetric stretching frequencies of this group appear in the region  $2920-2948\text{ cm}^{-1}$  as a broad region of absorption and the symmetric stretching frequencies appear in the region  $2885-2895\text{ cm}^{-1}$  in the mull spectrum. These frequencies are absent in the KBr pellet spectrum and this may be so because the pressure applied might be too high and some solid state reaction might take place between KBr and the substance. The region  $1100-1400\text{ cm}^{-1}$  is a little bit complicated, in the case of carboxylic acids having a number of COOH groups and because of waggings of  $CH_2$  group some of the skeletal frequencies and carboxyl group frequencies appear in this region. So in this region assignments

TABLE 1 Infrared frequencies of anhydrous citric acid from mull and KBr pellet spectra, with tentative assignments, 700–4000  $\text{cm}^{-1}$  region.

Raman freqs. from Landolt & Bornstein (1951)		Infrared freqs. present authors		Assignment
Freq. $\text{cm}^{-1}$	Intensity	Freq. $\text{cm}^{-1}$	Intensity	
419	(1)	—	—	
—		687	<i>w</i>	 Angle deformation
—		775	<i>m</i>	$\text{CH}_2$ rocking
870	(1)	928 } 937 }	<i>w</i> } <i>w</i> }	C-C bending and OH out of plane bending.
—		960	<i>w</i>	$\text{CH}_2$ rocking
—		1044 } 1073 }	<i>w</i> } <i>w</i> }	C-O stretches of C-OH
1071	(1)	1207	<i>m</i>	C-C stretching.
		1280	<i>m</i>	C-O stretching of carboxyl
		1307	<i>vw</i>	$\text{CH}_2$ wagging
		1328 } 1342 }	<i>m</i> }	OCO bending of COOH
		1407 } 1413 }	<i>m</i> } <i>m.br</i> }	$\text{CH}_2$ scissoring
1442	(1)	1425	<i>m.br</i>	C-O stretching
		1430	<i>m</i>	C-OH deformation
		1460	<i>m</i>	$\text{CH}_2$ scissoring
		1689 } 1695 } 1704 }	<i>m</i> } <i>vs</i> }	C = O stretching
		1715	<i>vs</i>	—
1739	(0)	1730 } 1741 } 1740 }	<i>vs</i> }	OH stretching lowered due to hydrogen bonding.
		2325 } 2340 }	<i>kinks</i> }	—
		2630 } 2650 }	<i>vw br</i> }	OH frequencies lowered due to hydrogen bonding
		2734 } 2776 }	<i>vvw.br</i>	—
		2845 } 2860 }	<i>s.br</i>	—
		2885	<i>s</i>	$\text{CH}_2$ stretching
2984	(b)	2920 } 2948 }	<i>m.br</i>	$\rightarrow$ $\text{CH}_2$ stretching
		3203 } 3277 } 3343 } 3367 } 3485 }	<i>m.br</i> } <i>s</i> } <i>m</i> } <i>vw</i> } <i>s.sh</i> }	O-H stretchings (fundamentals and overtones and combinations)

are made in comparison with the assignments for adipic acid due to Anantanarayanan (1964). The other frequencies of this group appear at 1400, 1413, 1407  $\text{cm}^{-1}$  assigned to  $\text{CH}_2$  scissoring modes and at 1307  $\text{cm}^{-1}$  a broad band assigned to  $\text{CH}_2$  wagging modes. The rocking vibrations of this group appear at 960 and 775  $\text{cm}^{-1}$ .

#### *COOH frequencies*

The frequencies at 1689, 1694 and 1704  $\text{cm}^{-1}$  are attributed to  $\text{C}=\text{O}$  stretchings of this group. These frequencies are in accordance with the fact that there is dimerization in the unit cell. From the literature it is known that the dimer type molecule will give  $\text{C}=\text{O}$  stretching frequencies in the range 1690–1720  $\text{cm}^{-1}$ . The other frequencies of this group, namely  $\text{C}-\text{O}$  stretchings appear at 1280, 1425  $\text{cm}^{-1}$ , the  $\text{COO}$  angle bendings of  $\text{COOH}$  group appear at 1328, 1342  $\text{cm}^{-1}$  and the angle deformation frequencies appear at 687  $\text{cm}^{-1}$ . The assignments are given in table 1.

#### *C—OH frequencies*

$\text{C}-\text{O}$  stretchings of this group appear at 1073, 1044  $\text{cm}^{-1}$  and the  $\text{C}-\text{OH}$  in plane bending appears at 1430  $\text{cm}^{-1}$ . These are given the assignments in comparison with other compounds containing  $\text{C}-\text{OH}$  group.

#### *C—C frequencies*

It is known from the anhydrous citric acid molecular structure given in figure 3a that the molecule consists of a zig-zag chain of carbon atoms and so one should expect the  $\text{CC}$  group to give rise to stretchings and bendings. The frequency at 1207  $\text{cm}^{-1}$  is attributed to the stretching vibration of this group and the band at 928  $\text{cm}^{-1}$  is attributed to the bendings of this group.

#### *Hydrogen bond frequencies*

The range of these frequencies is identified using the details available from Hadzi (1965). According to Hadzi these bands form a characteristic trio near 2800, 2500 and 1900  $\text{cm}^{-1}$ , if the carboxyl groups act as proton donors but they are somewhat lower (about 2700, 2200, 1600  $\text{cm}^{-1}$ ) for hydrogen phosphate and similar groups. Thus the frequencies in the range 2776 to 2325  $\text{cm}^{-1}$  and the frequencies at 1749 to 1730  $\text{cm}^{-1}$  assigned to the  $\text{OH}$  stretches are lowered due to hydrogen bonding. Except for identifying the range of these frequencies, any other discussion is difficult in the absence of studies on single crystals.

#### ACKNOWLEDGEMENT

The authors wish to thank the Director, Regional Research Laboratory, Hyderabad, for having permitted them to record the spectra reported in this paper. One of the authors (K. Mallikarjuna Rao) wishes to express his gratitude to the Director, Indian Institute of Technology, Madras, for the grant of a Research Fellowship.

## REFERENCES

- Anantanarayanan V. 1964 *Spectrochim. Acta.* **20**, 197.  
Canal S & Pierre Peyrot 1938 *Compt. Rend* **206**, 1179.  
Duval C. 1955 *Anal. Chim Acta.* **13**, 427.  
Edsall J. T. 1937 *J. Chem. Phys.* **5**, 508.  
Hadzi D., 1965, *Pure and Appl. Chem.*, **11**, 435.  
Landolt & Bornstein 1961 *Springer Verlag & Co. (Berlin)*, *Band 1, Teil 2*, 534.  
Nisi H. 1931 *Jap. J. Phys.* **7**, 1  
Nordman E., Weldon A. S. & Patterson A. L , 1960 *Acta. Cryst.* **13**, 418.  
Passerini L. 1935 *Gazz. Chim Ital.* **65**, 502  
Thatte V. N & Ashedkar W. 1936 *Z Physik*, **100**, 466.

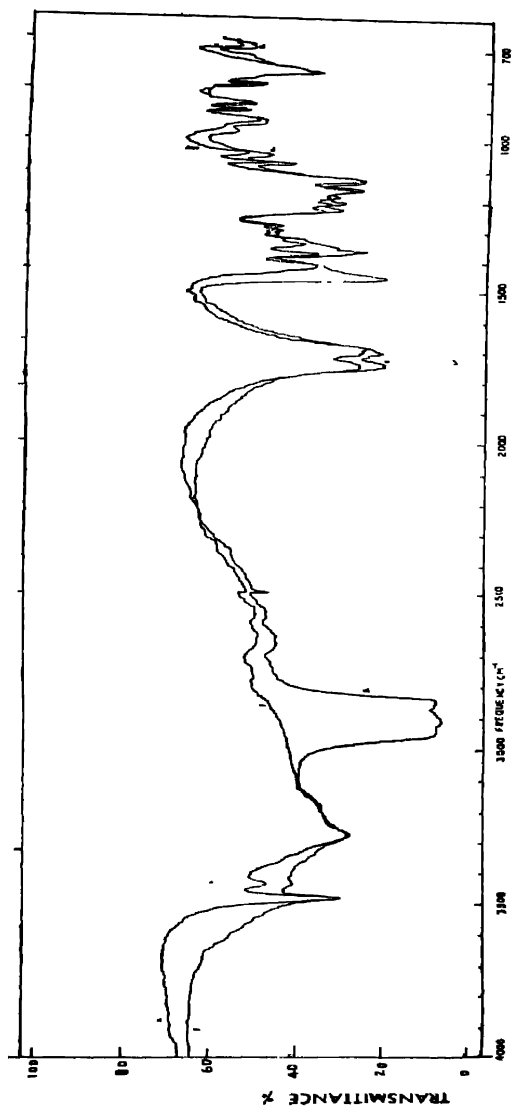


Figure 1. Infrared spectrum of anhydrous citric acid :

(1) KBr pellet spectrum (2) mull spectrum, 700—4000  $\text{cm}^{-1}$  ; NaCl optics, PE IRS—Model 221.

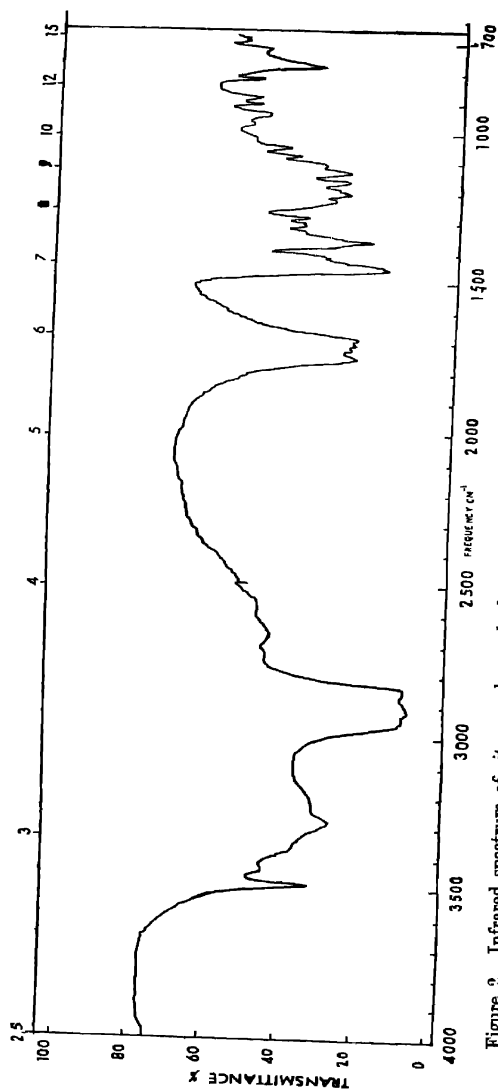


Figure 2. Infrared spectrum of citric acid monohydrate, mull spectrum; 700—4000  $\text{cm}^{-1}$ , NaCl optics PE IRS—Model 221.



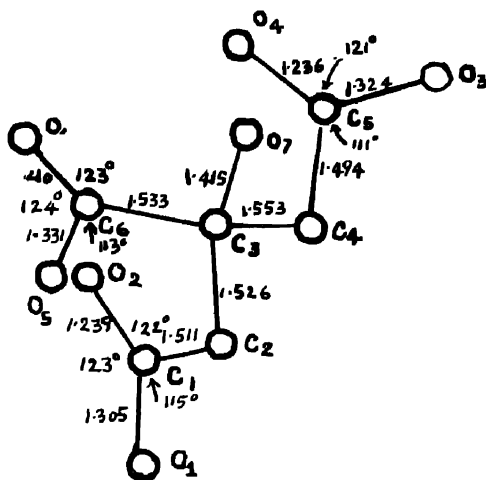


Figure 3a, Anhydrous citric acid molecule with H atoms removed.

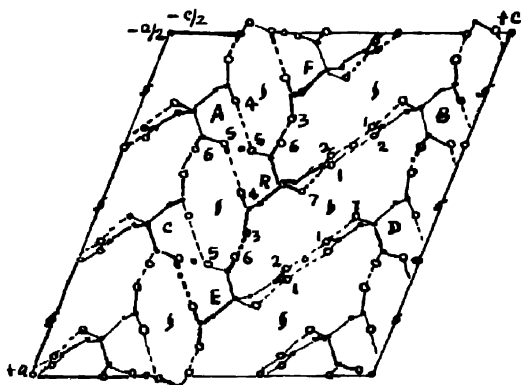


Figure 3b. Hydrogen bonding and molecular packing in anhydrous citric acid unit cell. Unit cell-dimensions:  $a = 12.82\text{\AA}$ ,  $b = 5.62\text{\AA}$ ,  $c = 11.54\text{\AA}$ ,  $\beta = 111.2^\circ$  space group  $C2h$ ,  $Z = 4$  molecules.



## Effect of radiative heat transfer on the propagation of cylindrical shock waves

By T. D. VARMA\*

*Defence Science Laboratory, Delhi, India*

*Received 21 August 1969—Revised 30 November 1969 and 2 February 1970*

A similarity solution for the propagation of intense cylindrical shock waves has been obtained. By the introduction of radiative heat flux the singularity in a solution of Lin (1954) is removed. It is observed that the type of configuration obtained and also the rate of propagation of the bounding shock depends on the amount of energy released and the density of the ambient air.

### INTRODUCTION

Under certain physical conditions it is some times found that temperatures are high enough for the hydrodynamics to be affected by radiation terms namely radiation flux, energy and pressure. Equations governing the flow in these circumstances were formulated by Thomas (1930). Marshak (1958) obtained similarity solutions of the radiation hydrodynamic equations for particular cases, when there was a plane symmetry and radiation energy and pressure were negligible although the flux was important, the cases he considered are those of (a) constant density (b) constant pressure and (c) power law time dependence of temperature. The extent to which problems in radiation hydrodynamics might be tackled by similarity methods was investigated by Elliot (1960). In particular he studied the problem of an intense point explosion and it was found that the type of configuration obtained as well as the rate of propagation of the bounding shock was dependent on the amount of energy released, and on the density of the ambient air; in this respect the solution differed from that obtained using only the hydrodynamic equations.

Lin (1954) and Sedov (1959) investigated the flow behind a cylindrical disturbance bounded by a strong shock wave which resulted from the instantaneous release of a finite amount of energy per unit length along a line. An exact analytical solution of this problem was obtained by Chakraborty (1962). In these solutions there was a singularity at the axis of symmetry where both temperature and temperature gradient became infinite. This singularity could be removed by introducing heat flux in the problem.

In the present paper we have extended Elliot's analysis to investigate the flow behind a cylindrical shock wave. Radiative heat flux is included in the

\*Present address: Defence Research Laboratory (Materials), Post Box No. 320, Kanpur-4.

problem, though we assume that the temperatures are low enough to justify neglecting radiation energy and pressure compared to material energy and pressure. We have used the diffusion approximation for the radiation flux. The losses of energy from the disturbance are neglected, which makes the total energy of the blast a constant

### FUNDAMENTAL EQUATIONS

The flow is governed by the usual hydrodynamic equations with some modifications to include radiation flux. The radiation pressure and energy are neglected as compared to material pressure and energy, but at the same time it is assumed that the temperature of the matter or more precisely the radiation density is so high that the energy transfer is accomplished basically by radiation

The equations of continuity, momentum and energy for cylindrical symmetry are

$$\frac{\partial \rho}{\partial t} + \frac{1}{r} \cdot \frac{\partial}{\partial r} (r \rho u) = 0 \quad \dots (2.1)$$

$$\frac{\partial u}{\partial t} + u \frac{\partial u}{\partial r} + \frac{1}{\rho} \frac{\partial p}{\partial r} = 0 \quad \dots (2.2)$$

$$\rho \left( \frac{\partial E}{\partial t} + u \frac{\partial E}{\partial r} \right) - \frac{\rho}{\rho} \left( \frac{\partial \rho}{\partial t} + u \frac{\partial \rho}{\partial r} \right) + \frac{1}{r} \frac{\partial}{\partial r} (r F) = 0 \quad \dots (2.3)$$

where  $p$ ,  $\rho$ ,  $u$  and  $E$  denote the pressure, density, material velocity and internal energy per unit mass, respectively, and  $F$  is the flux of radiation

For an ideal gas we have

$$\left. \begin{aligned} E &= \frac{p}{(\gamma-1)\rho} \\ p &= \rho \bar{R} T \end{aligned} \right\} \quad \dots (2.4)$$

Also assuming local thermodynamic equilibrium and taking the radiative diffusion approximation we have,

$$F = -\frac{4\lambda}{3} \frac{\partial}{\partial r} (\sigma T^4) \quad \dots (2.5)$$

where  $\sigma$  is the Stefan-Boltzmann constant and  $\lambda$  the mean free path of radiation.

### SIMILARITY TRANSFORMATIONS

We now introduce the similarity assumptions for this flow as follows

$$\begin{aligned} u &= R^a \Phi_1, & \rho &= \rho_0 \psi \\ p &= \rho_0 R^b f_1, & F &= \rho_0 R^c \xi_1 \end{aligned} \quad \dots (3.1)$$

where  $R$  is the radius of the shock wave forming the outer edge of the disturbance,  $\rho_0$  the density of the undisturbed atmosphere,  $\Phi_1$ ,  $\psi$ ,  $f_1$  and  $\xi_1$  are functions of  $\eta$  where,

$$\eta = r/R$$

Substituting (3.1) in (2.1) we get

$$\frac{1}{\eta} \{ \Phi_1 + (\psi/\psi')(\Phi'_1 + \Phi_1/\eta) \} = R^{-\alpha} \frac{dR}{dt} \quad (3.2)$$

The left hand side is a function of  $\eta$  only whereas the right hand side a function of  $t$  only. This can be satisfied if

$$R^{-\alpha} \cdot \frac{dR}{dt} = A \text{ (constant)} \quad (3.3)$$

Substituting (3.2), (3.3) in (2.2) we get

$$\psi [A\alpha\Phi_1 + (\Phi_1 - A\eta)\Phi'_1] R^{2\alpha} + f'_1 R^\beta = 0 \quad \dots (3.4)$$

In order that the equation may be satisfied identically we must have  $\beta = 2\alpha$

Finally equation (2.3) is transformed to

$$[2\alpha A f_1 + (\Phi_1 - A\eta) f'_1 + \gamma f_1 (\Phi'_1 + \Phi_1/\eta)] R^{3\alpha} + (\gamma - 1) \frac{R^\delta}{\eta} \cdot \frac{d}{d\eta} (\eta \xi_1) = 0$$

we find that  $\delta = 3\alpha$  so as to satisfy the above equation identically.

Equation (3.2), (3.4) and (3.5) may be reduced to non-dimensional form by substituting

$$\begin{aligned} \Phi_1 &= A\Phi \\ f_1 &= A^2 f \\ \xi_1 &= A^2 \xi \end{aligned} \quad \dots (3.6)$$

The resulting equations which contain only one parameter  $\gamma$  are

$$(\Phi' + \Phi/\eta) + (\Phi - \eta)\psi'/\psi = 0 \quad \dots (3.7)$$

$$(\Phi - \eta)\Phi' + \alpha\Phi = -f'/\psi \quad \dots (3.8)$$

$$2\alpha f + (\Phi - \eta)f' + \gamma f(\Phi' + \Phi/\eta) + \frac{(\gamma - 1)}{\eta} \cdot \frac{d}{d\eta} (\eta \xi) = 0 \quad \dots (3.9)$$

We shall now discuss the similarity form of the equation introduced by the flux of radiation (equation 2.5). The mean free path of radiation, in general, is a complicated function of temperature and density. However, to simplify the problem it is assumed that  $\lambda$  can be written in a form of power law.

$$\lambda = \lambda_1 T^m (\rho/\rho_0)^n \quad \dots \quad (3.10)$$

$$\text{where} \quad T = \frac{p}{\bar{R}\rho} = \frac{A^2 R^{2\alpha}}{\bar{R}} \cdot (f/\psi) \quad \dots \quad (3.11)$$

Substituting (3.1), (3.6), (3.10) and (3.11) in (2.5) we get

$$R^{3\alpha} \xi = - \frac{16\sigma\lambda_1}{3\rho_0} A^{2m+5} \cdot (\bar{R})^{-(m+4)} (f)^{-(m+3)} \psi^{n-m-5} (f'\psi - f\psi') R^{2\alpha(m+4)-1} \quad (3.12)$$

This can be satisfied if  $3\alpha = 2\alpha(m+4)-1$ , which gives

$$m = -\frac{5}{2} + \frac{1}{2\alpha} \quad \dots \quad (3.13)$$

We therefore have

$$\xi = -K f^{-(m+3)} \psi^{n-m-5} (f'\psi - f\psi') \quad \dots \quad (3.14)$$

where

$$K = \frac{16\sigma\lambda}{3\rho_0} A^{2m+5} (\bar{R})^{-(m+4)}$$

The constant  $\alpha$  is determined from total energy consideration and  $n$  is then determined by fitting the mean free path law (equation 3.10) to mean free path-temperature data.

#### TOTAL ENERGY CONSIDERATIONS

The values of  $A$  and  $\alpha$  are determined from the rate of change of total energy of the configuration. Suppose the disturbance lies between radii  $hR$  and  $R$  where  $h$  is a constant and  $0 \leq h < 1$ . Then the total energy is given by

$$\begin{aligned} E_T &= 2\pi \int_{hR}^R (E + \frac{1}{2}u^2) \rho r dr \\ &= 2\pi \rho_0 A^2 R^{2\alpha+2} \int_h^1 \psi \left\{ \frac{f}{(\gamma-1)\psi} + \frac{1}{2}\Phi^2 \right\} \eta d\eta \quad \dots \quad (4.1) \end{aligned}$$

$$\text{i.e.} \quad E_T = \rho_0 A^2 B R^{2\alpha+2} \quad \dots \quad (4.2)$$

If  $E_T$  remains constant with time, then we have  $\alpha = -1$  and

$$A^2 = \frac{E_T}{B\rho_0} \quad \dots \quad (4.3)$$

In this case it is possible to get a first integral from equations (3.7) to (3.9)

$$\xi = (\eta - \Phi) \psi \left[ \frac{f}{(\gamma-1)\psi} + \frac{1}{2}\Phi^2 \right] - f\Phi + \frac{\text{constant}}{\eta} \quad \dots \quad (4.4)$$

# SHOCK CONDITIONS

We are considering here a problem where the disturbance is bounded by a strong shock front. Three boundary conditions are provided by relations at the shock and the remaining one by the value of the flux at some fixed boundary. We then have a double boundary value problem.

The three conditions at the shock are given by the principles of conservation of mass, momentum and energy across the shock, namely,

$$\rho_s(U-u_s) = \rho_0 U = m_s \quad \dots \quad (5.1)$$

$$p_s - p_0 = m_s \cdot u_s \quad \dots \quad (5.2)$$

$$E_s + \frac{p_s}{\rho_s} + \frac{1}{2}(U-u_s)^2 - \frac{F_s}{m_s} = E_0 + \frac{p_0}{\rho_0} + \frac{1}{2}U^2 - \frac{F_0}{m_s} \quad \dots \quad (5.3)$$

where suffixes  $s$  and  $o$  denote conditions behind and in front of the shock, respectively, and  $U$  is the shock velocity. We consider a very strong shock wave and as such  $F_0 = P_0 = 0$ , we get

$$u_s = \frac{\mu-1}{\mu} U \quad (5.4)$$

$$p_s = \frac{\mu-1}{\mu} \rho_0 U^2 \quad (5.5)$$

$$\text{where} \quad \mu = \rho_s / \rho_0 \quad (5.6)$$

Also equation (5.3) simplifies to

$$F_s = \frac{\mu-1}{\mu^2} \left[ \frac{\gamma+1}{\gamma-1} - \mu \right] m_s U^2 \quad (5.7)$$

If we put terms in their similarity form we get

$$f_s = \Phi_s = \frac{\psi_s - 1}{\psi_s} \quad (5.8)$$

and

$$\xi_s = (\psi_s - 1) \left[ \frac{\gamma+1}{\gamma-1} - \psi_s \right] \left[ 2\psi_s^i \right] \quad (5.9)$$

From (5.9)  $\xi_s$  is determined in terms of  $\psi_s$ . If  $\xi_s$  were known explicitly in terms of  $f_s$  and  $\psi_s$  then (5.8) and (5.9) would be sufficient to determine  $\psi_s$  and all other quantities behind the shock, when it involves a derivative as in the case of (2.5) we require another boundary condition to determine  $\psi_s$ .

## THE SOLUTION

Equation (3.7) and (3.8) for  $\alpha = -1$  become

$$(\Phi + \Phi/\eta) + (\Phi - \eta)\psi'/\psi = 0 \quad \dots (6.1)$$

$$(\Phi - \eta)\Phi' - \Phi = -f'/\psi \quad \dots (6.2)$$

Instead of (3.9) we use the energy integral (4.4) which becomes

$$\xi = (\eta - \Phi)\psi \left[ \frac{f}{(\eta - 1)\psi} + \frac{1}{2} \Phi^2 \right] - f\Phi \quad \dots (6.3)$$

For  $\alpha = -1$ , equation (3.13) gives  $m = -3$ , the mean free path is then given by

$$\lambda = \lambda_1 T^{-2} \left( \frac{\rho}{\rho_0} \right)^n \quad \dots (6.4)$$

Since we have introduced radiative diffusion in the problem the mean free path of radiation is restricted in the form given by equation (6.4). This restriction fortunately allows for a variation of mean free path which is not unrealistic for temperature in air under  $10^6^\circ\text{C}$ . Equation (6.4) was fitted to the well known data for variation of mean free path in air with temperature and we got for  $n$  a value  $\approx -3/2$ . Equation (3.14) then gives

$$\xi = -K\psi^{-7/2}(f'\psi - f\psi') \quad \dots (6.5)$$

where,

$$K = \frac{16\sigma\lambda}{3\rho_0}(A\bar{R})^{-1}$$

Eliminating  $f'$  and  $\psi'$  with the help of (6.1) and (6.2), equation (6.5) gives

$$\Phi' \left[ (\Phi - \eta) - \frac{f}{\eta\psi(\Phi - \eta)} \right] = \Phi \left[ 1 + \frac{f}{\eta\psi(\Phi - \eta)} \right] + \frac{\xi\psi^{3/2}}{K} \quad \dots (6.6)$$

If for any value of  $\eta$ ,  $f$ ,  $\Phi$ ,  $\psi$  and  $\xi$  are known their values can be computed step by step for other values of  $\eta$ .

Two of the boundary conditions required in integrating these equations are the shock relations (5.8). The third shock condition (5.9) is automatically satisfied by  $\xi$  which is given by the relation (6.3) or (6.5). Assuming no heat source at the centre the third boundary condition is  $\xi = 0$  at  $\eta = 0$ .

We, therefore, have a double boundary value problem. By suitably scaling the variables we can reduce it to a single boundary problem. We assume that



pressure and density are finite and non-zero at the axis of symmetry *i.e.* at  $\eta = 0$ ,  $f = f_0$  and  $\psi = \psi_0$ , and make the following transformations.

$$\begin{aligned}\bar{\Phi} &= \epsilon_0 \Phi, & \bar{\eta} &= \epsilon_0 \eta, & \bar{\psi} &= \psi/\psi_0 \\ \bar{f} &= f/f_0, & \bar{\xi} &= \frac{\epsilon_0 \xi}{f_0}\end{aligned} \quad \dots (6.7)$$

where  $c_0 = \psi_0/f_0$  ... (6.8)

Making use of these transformations, equations (6.1), (6.2) (6.3) and (6.6) become

$$(\bar{\Phi} - \bar{\eta})\bar{\psi}'/\bar{\psi} = -(\bar{\Phi}' + \bar{\Phi}/\bar{\eta}) \quad \dots (6.9)$$

$$(\bar{\Phi} - \bar{\eta})\bar{\Phi}' - \bar{\Phi} = -\bar{f}/\bar{\psi} \quad \dots (6.10)$$

$$\bar{\xi} = (\bar{\eta} - \bar{\Phi})\bar{\psi} \left[ \frac{\bar{f}}{(\gamma-1)\bar{\psi}} + \frac{1}{2}\bar{\Phi}^2 \right] - \bar{f}\bar{\Phi} \quad \dots (6.11)$$

$$\left[ (\bar{\Phi} - \bar{\eta}) - \frac{\bar{f}}{\bar{\psi}(\bar{\Phi} - \bar{\eta})} \right] \bar{\Phi}' = \bar{\Phi} \left[ 1 + \frac{\bar{f}}{\bar{\eta}\bar{\psi}(\bar{\Phi} - \bar{\eta})} \right] + \frac{\bar{\xi}\bar{\psi}^{3/2}}{\bar{K}} \quad \dots (6.12)$$

where,  $\bar{K} = Kf_0^{-1}\psi_0^{-3/2}$

The boundary conditions become

$$\left. \begin{aligned}\bar{\Phi} &= \bar{\xi} = 0 \\ \bar{\psi} &= \bar{f} = 1\end{aligned} \right] \quad \text{at } \bar{\eta} = 0 \quad \dots (6.13)$$

To find at that value of  $\bar{\eta}$  the bounding shock occurs we used the shock conditions (5.8). The shock will occur where

$$\bar{\eta} = \epsilon_0 \eta = \epsilon_0 \quad \dots (6.14)$$

$$\bar{\Phi} = \epsilon_0 \Phi = \epsilon_0 \left( \frac{\psi_s - 1}{\psi_s} \right) \quad \dots (6.15)$$

and  $\bar{f}/\bar{\psi} = \frac{\epsilon_0^3 f}{\psi} = \epsilon_0^2 \left( \frac{\psi_s - 1}{\psi_s} \right) \quad \dots (6.16)$

Hence the shock occurs where

$$\bar{f}/\bar{\psi} = \bar{\Phi}(\bar{\eta} - \bar{\Phi}) \quad \dots (6.17)$$

and the values of the scaling factors and the density ratio across the shock can be obtained from (6.14), (6.15) and (6.8).

Analytical solution of the equations (6.9) to (6.12) near the axis of symmetry was obtained. It is of the form

$$\begin{aligned}\bar{\Phi} &= a_0 \bar{\eta}^3, \quad \bar{\psi} = 1 + 2a_0 \bar{\eta}^2 \\ \bar{f} &= 1 + a_0 \bar{\eta}^4\end{aligned}\quad \dots \quad (6.18)$$

where

$$a_0 = \frac{1}{4\bar{K}(\gamma-1)}$$

The approximate solution near the centre of symmetry given by (6.18) shows that

$$\bar{\Phi}' = \bar{f}' = \bar{\psi}' = 0 \quad \text{when} \quad \bar{\eta} = 0 \quad \dots \quad (6.19)$$

and substituting these values of the derivatives at the centre, integration can be carried out by numerical means to obtain the variation of  $\bar{\Phi}$ ,  $\bar{f}$ ,  $\bar{\psi}$  and  $\bar{\xi}$  with increasing  $\bar{\eta}$ , for various values of  $\bar{K}$ .

#### DISCUSSION OF RESULTS

For the explosion in air, the value of  $\gamma$  was taken as 1.2, this being approximately true for pressures of 10 to  $10^4$  atmospheres and temperatures between 20,000 and 200,000°K. A series of values of  $\bar{K}$ , the constant introduced by the expression for radiation diffusion were used. The variation of  $\bar{\Phi}$ ,  $\bar{f}$ ,  $\bar{\psi}$ ,  $\bar{\xi}$  and  $\bar{R}T$  with  $\bar{\eta}$  is given in figures 1 to 5. Dotted curves give Lin's solution for  $\gamma = 1.2$ .

For  $\bar{K} = 500$  the effect of heat flux is substantial throughout the disturbance. The point of maximum heat flux is at the shock and the temperature is rendered almost uniform by transport of radiation energy. In this case the density ratio across the shock is 2.79, compared with 11 when there is no radiation at the shock so that the mass of air just inside the shock is less and an appreciable amount of engulfed material lies in the central part of the disturbance.

As  $\bar{K}$  is decreased the point of maximum flux moves inwards from the shock and radiation becomes negligible in the outer regions of the disturbance. The value of the density ratio across the shock also increases as  $\bar{K}$  is decreased, for  $\bar{K} = 100$  and 10 the density ratio being 3.85 and 10.83, respectively. For  $\bar{K} = 10$ , most of the engulfed air lies in a thin shell behind the shock and the pressure profile is approximately the same as that of no radiation flux case.

The particle velocity at the shock front decreases as  $\bar{K}$  is increased. As one moves from the shock front towards the axis of symmetry, the particle velocity at first decreases very rapidly and then tends to zero as the axis of symmetry is approached. Moreover, for a higher value of  $\bar{K}$ , the particle velocity approaches the axis at points closer to the shock front.

# T. D. Varma

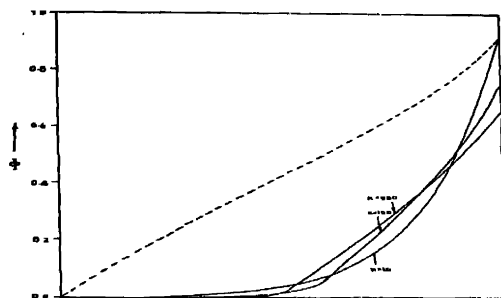


Figure 1. Variation of fluid velocity with radius.

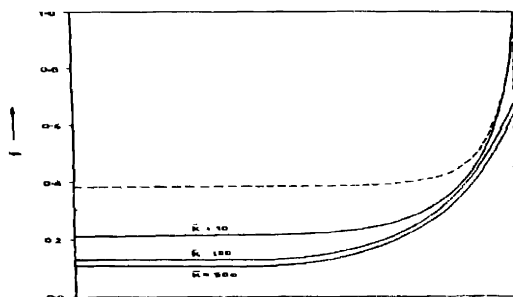


Figure 2. Variation of pressure with radius.

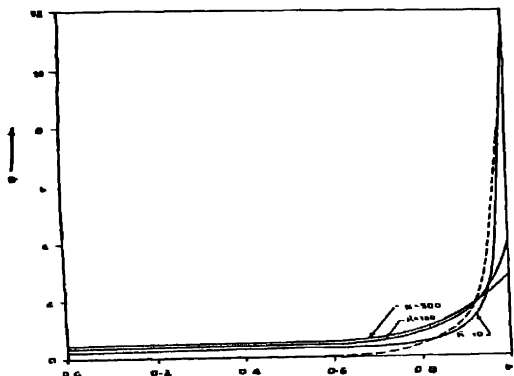


Figure 3. Variation of fluid density with radius.

# T. D. Varma

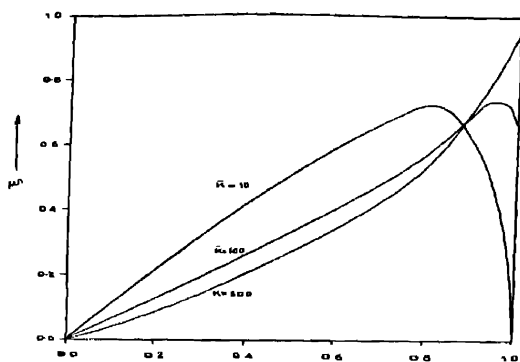


Figure 4. Variation of heat flux with radius.

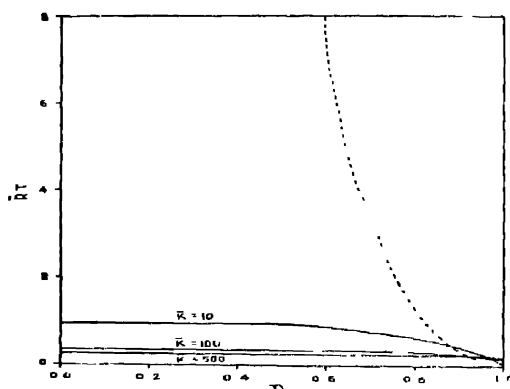


Figure 5. Variation of temperature with radius.

### CONCLUSIONS

When the effect of radiative heat flux is considered in the problem of an intense cylindrical explosion, it is found that the type of configuration obtained as well as the rate of propagation of the bounding shock depends on the amount of energy released and on the density of the ambient air. For a high energy explosion the solution is considerably affected by the radiative heat flux.

### ACKNOWLEDGEMENTS

The author is grateful to Dr. G. S. Bajwa for his constant encouragement and advice. Thanks are also due to the Director, Defence Science Laboratory, for permission to publish this paper.

### REFERENCES

- Chakraborty P. K. 1962 *Proc. Nat. Ins. Sci. India* **28**, 683.  
Elliot L. A. 1960 *Proc. Roy. Soc. A*, **258**, 287.  
Lin S. C. 1954 *J. Appl. Phys.* **25**, 54.  
Marshak R. E. 1958 *Phys. Fluids* **1**, 24.  
Sedov L. I. 1959 *Similarity and Dimensional Methods in Mechanics*, Academic Press, New York.  
Thomas L. H. 1930 *Quart. J. Math.* **1**, 239.

## Unsteady heat distribution in an orthotropic rectangular rod moving along the direction of its length\*

By P. M. GUPTA AND V. P. SAXENA\*\*

*Department of Applied Mathematics, S. A. Technological Institute,  
Vidisha, Madhya Pradesh, India*

*Received 15 July 1970*

In this paper partial differential equation governing heat conduction in a moving orthotropic solid rod with square cross section has been solved. The finite rod is initially kept at a given temperature and temperatures at both ends are supposed to be known. Some examples and their numerical calculations have also been added to indicate applications of the solution.

### INTRODUCTION

The problems of energy distribution in anisotropic and orthotropic solids are of practical importance. Such problems occur when we consider heat conduction in crystals, rocks, wood and laminated materials such as transformer cores etc.

Carslaw & Jaeger (1959) suggested a few problems of these solids treated under ordinary conditions. But in applied physics we come across many cases in which it is required to determine unsteady temperature distribution in orthotropic solids of different shapes moving in conductive media. No mathematical treatment of such problems has been considered so far.

In this paper we attempt to solve a partial differential equation governing heat conduction in a moving orthotropic solid rod with square cross section having a source situated inside it. Initially the solid is kept at a prescribed temperature and the temperatures of both extreme bases are known.

In one simple case of boundary and initial conditions we have calculated and computed numerical values of the temperature and subsequently discussed its variations with respect to important variable quantities.

### EQUATION OF MOTION AND BOUNDARY CONDITIONS

The partial differential equation of heat condition in a solid moving along the direction of z-axis with a constant velocity  $U$ , is given by

$$\frac{\partial}{\partial x} \left[ K_x \frac{\partial u}{\partial x} \right] + \frac{\partial}{\partial y} \left[ K_y \frac{\partial u}{\partial y} \right] + \frac{\partial}{\partial z} \left[ K_z \frac{\partial u}{\partial z} \right] - U \frac{\partial u}{\partial z} + Q(x, y, z, t) = c \frac{\partial u}{\partial t} \quad \dots (1)$$

---

\*The work has been supported by the Council of Scientific and Industrial Research, India.

\*\*Present address: Department of Mathematics, M.A. College of Technology, Bhopal-7.

## Unsteady heat distribution in an orthotropic rectangular etc. 49

where  $K_x, K_y, K_z$  are conductivities along the directions of the principal axes,  $Q(x, y, z, t)$  is intensity of continuous source of heat situated at the point  $x, y, z$ .

Consider a rod of length  $l$  with a square cross section and let the material be orthotropic in  $xy$  plane, assuming,

$$K_x = k(1-x^2), \quad K_y = k(1-y^2), \quad K_z = k$$

$$Q(x, y, z, t) = (c_1 + c_2 x) \frac{\partial u}{\partial x} + (c_3 + c_4 y) \frac{\partial u}{\partial y} + au + b + \rho(x, y, z, t); \quad \dots (2)$$

$c_1, c_2, c_3, c_4, a$  and  $b$  are constants and  $\rho(x, y, z, t)$  is an arbitrary function of  $xyz$  and  $t$ .

The mathematical statement of the conditions are given by

$$\begin{aligned} u(x, y, 0, t) &= \phi(x, y, t), \quad t > 0; \quad u(x, y, z, 0) = \psi(x, y, z); \\ u(x, y, l, t) &= 0, \quad t > 0. \end{aligned} \quad (3)$$

There is no radiation from the long sides of the rod. The equations of both side ends are given below.

### SOLUTION OF THE PROBLEM

To solve the problem we use the Jacobi transform of two variables as defined by Saxena (In press) :

$$\begin{aligned} J\{h(x, y)\} &= \int_{-1}^1 \int_{-1}^1 (1-x)^\alpha (1+x)^\beta (1-y)^\gamma (1+y)^\delta P_m^{(\alpha, \beta)}(x) \\ &\quad \times P_n^{(\gamma, \delta)}(y) h(x, y) dx dy \end{aligned} \quad \dots (4)$$

provided  $\alpha, \beta, \gamma, \delta > -1$ .

The inversion formula of the above transform gives

$$h(x, y) = \sum_{m=0}^{\infty} \sum_{n=0}^{\infty} (\delta_m \delta_n')^{-1} P_m^{(\alpha, \beta)}(x) P_n^{(\gamma, \delta)}(y) J\{h(x, y)\} \quad \dots (5)$$

where

$$\delta_m = \frac{2^{\alpha+\beta+1} \Gamma(m+\alpha+1) \Gamma(m+\beta+1)}{m! (\alpha+\beta+2m+1) \Gamma(m+\alpha+\beta+1)}, \quad \delta_n' = \frac{2^{\gamma+\delta+1} \Gamma(n+\gamma+1) \Gamma(n+\delta+1)}{n! (\gamma+\delta+2n+1) \Gamma(n+\gamma+\delta+1)} \quad (5a)$$

Also, we have the following theorem :

If (i) the function  $h(x, y)$  and its partial derivatives  $\frac{\partial h}{\partial x}, \frac{\partial h}{\partial y}$  are bounded almost continuous in the square  $-1 \leq x \leq 1, -1 \leq y \leq 1$ ,

(ii) the second derivatives  $\frac{\partial^2 h}{\partial x^2}$  and  $\frac{\partial^2 h}{\partial y^2}$  are bounded and integrable at each point of the square given in (i)

(iii) the Jacobi transform of two variables of  $h(x, y)$  exists,

and

$$(iv) \lim_{x \rightarrow \pm 1} (1-x)^{\alpha+1}(1+x)^{\beta+1} h(x, y) = \lim_{x \rightarrow \pm 1} (1-x)^{\alpha+1}(1+x)^{\beta+1} \frac{\partial h}{\partial x} = 0,$$

$$\lim_{y \rightarrow \pm 1} (1-y)^{\gamma+1}(1+y)^{\delta+1} h(x, y) = \lim_{y \rightarrow \pm 1} (1-y)^{\gamma+1}(1+y)^{\delta+1} \frac{\partial h}{\partial y} = 0$$

then,

$$J\{h(x, y)\} = -\{m(m+\alpha+\beta+1) + n(n+\gamma+\delta+1)\} J\{h(x, y)\} \quad \dots \quad (6)$$

where

$$C\{h(x, y)\} = (1-x)^{-\alpha}(1+x)^{-\beta} \frac{\partial}{\partial x} \left\{ (1-x)^{\alpha+1}(1+x)^{\beta+1} \frac{\partial h}{\partial x} \right\}$$

$$+ (1-y)^{-\gamma}(1+y)^{-\delta} \frac{\partial}{\partial y} \left\{ (1-y)^{\gamma+1}(1+y)^{\delta+1} \frac{\partial h}{\partial y} \right\},$$

Now substituting the values of  $K_x, K_y, K_z$  and  $Q$  from (2) in (1) with the assumptions

$$\alpha = -\frac{c_1+c_2}{2k}, \quad \beta = -\frac{c_1-c_2}{2k}, \quad \gamma = -\frac{c_3+c_4}{2k}, \quad \delta = -\frac{c_3-c_4}{2k},$$

taking Jacobi transform of two variables of the same equation and using (6) we obtain

$$\frac{\partial^2 u_J}{\partial z^2} - \frac{U}{k} \frac{\partial u_J}{\partial z} - A u_J = \frac{c}{k} - B - \rho_J(z, t), \quad \dots \quad (7)$$

where

$$u_J(z, t) = J\{u(x, y, z, t)\}, \quad \rho_J(z, t) = J\{\rho(x, y, z, t)\},$$

$$A = m(m+\alpha+\beta+1) + n(n+\gamma+\delta+1) - a/k \text{ and } B = b\delta_m\delta_n'. \quad \dots \quad (7a)$$

The conditions (3) reduce to

$$u_J(0, t) = \phi_J(t), \quad u_J(l, t) = 0 \text{ and } u_J(z, 0) = \psi_J(z) \quad \dots \quad (8)$$

where

$$\phi_J(t) = J\{\phi(x, y, t)\} \text{ and } \psi_J(z) = J\{\psi(x, y, z)\}.$$

Here we use the well known Laplace transform defined as

$$L\{h(t)\} = \int_0^\infty e^{-pt} h(t) dt \quad \dots \quad (9)$$



and the following inversion formula associated with the transform :

$$h(t) = \frac{1}{2\pi i} \int_{\nu-i\infty}^{\nu+i\infty} e^{pt} L\{h(t)\} dp, \quad \nu > 0. \quad \dots (10)$$

Also we have

$$L \left\{ \frac{\partial^n h(t)}{\partial t^n} \right\} = p^n L\{h(t)\} - p^{n-1} h(0) - p^{n-2} h'(0) - \dots - h^{(n-1)}(0). \quad \dots (11)$$

Multiplying (7) by  $e^{-pt}$  and integrating with respect to  $t$  from 0 to  $\infty$  and using (11) we get

$$\frac{d^2 v}{dz^2} - \frac{U}{k} \frac{dv}{dz} - \left( A + \frac{cp}{k} \right) v = -\frac{c}{k} \psi_J(z) - \sigma(z, p) - \frac{B}{p}, \quad \dots (12)$$

where

$$v(z, p) = L\{u_J(z, t)\}, \quad \sigma(z, p) = L\{\rho_J(z, t)\}$$

Now, with the help of the conditions

$$v(0, p) = \theta(p), \quad v(l, p) = 0 \quad \dots (13)$$

where

$$\theta(p) = L\{\phi_J(t)\},$$

the solution of (12) is obtained as

$$\begin{aligned} v(z, p) = & \frac{\{\theta(p) - \eta(0, p)\} e^{\frac{Uz}{2k}} \sinh \left\{ \left( \frac{U^2}{4k^2} + A + \frac{cp}{k} \right)^{\frac{1}{2}} (l-z) \right\}}{\sinh \left\{ \left( \frac{U^2}{4k^2} + A + \frac{cp}{k} \right)^{\frac{1}{2}} l \right\}} \\ & + \frac{\eta(l, p) e^{-\frac{Uz}{2k}} \cosh \left\{ \left( \frac{U^2}{4k^2} + A + \frac{cp}{k} \right)^{\frac{1}{2}} z \right\}}{\sinh \left\{ \left( \frac{U^2}{4k^2} + A + \frac{cp}{k} \right)^{\frac{1}{2}} l \right\}} \\ & + \frac{1}{2} \left( \frac{U^2}{4k^2} + A + \frac{cp}{k} \right)^{-\frac{1}{2}} \eta(z, p) + B \left( A + \frac{cp}{k} \right)^{-1} \end{aligned} \quad \dots (14)$$

where

$$\begin{aligned} \eta(z, p) = & \frac{1}{\lambda_1 - \lambda_2} \left[ e^{\lambda_1 z} \int_0^z e^{-\lambda_1 z} \left\{ \frac{c}{k} \psi_J(z) + \sigma(z, p) \right\} dz \right. \\ & \left. - e^{\lambda_2 z} \int_0^z e^{-\lambda_2 z} \left\{ \frac{c}{k} \psi_J(z) + \sigma(z, p) \right\} dz \right], \\ \lambda_1 = & \frac{U}{2k} - \left( \frac{U^2}{4k^2} + A + \frac{cp}{k} \right)^{\frac{1}{2}}, \quad \lambda_2 = \frac{U}{2k} + \left( \frac{U^2}{4k^2} + A + \frac{cp}{k} \right)^{\frac{1}{2}}. \end{aligned}$$

In this way we obtain the value of  $v(z, p)$  in terms of the known quantities. The value of  $u(x, y, z, t)$  can be obtained with the help of (10) and consequently using the inversion formula (5).

The value of  $v(z, p)$  thus obtained is in a complicated form. Here we calculate its value for a simple case.

Let

$$\psi(x, y, z) = 0, \quad \rho(x, y, z, t) = 0, \quad \phi(x, y, t) = 100xy$$

In this case we have

$$v(z, p) = D_J e^{\frac{Uz}{2k}} \frac{\sinh \left\{ \left( \frac{U^2}{4k^2} + A + \frac{cp}{k} \right)^{\frac{1}{2}} (l-z) \right\}}{p \sinh \left\{ \left( \frac{U^2}{4k^2} + A + \frac{cp}{k} \right)^{\frac{1}{2}} l \right\}} + \frac{kB}{c} \left( \frac{kA}{c} + p \right)^{-1} \quad \dots (15)$$

where

$$D_J = J(100xy)$$

Using the inversion theorem (10) and the well known result

$$L(e^{-\alpha t}) = \frac{1}{p+\alpha}$$

we arrive at

$$u_J(z, t) = D_J e^{\frac{Uz}{2k}} \cdot \frac{1}{2\pi i} \int_{\nu-i\infty}^{\nu+i\infty} \frac{e^{pt} \sinh \left\{ \left( \frac{U^2}{4k^2} + A + \frac{cp}{k} \right)^{\frac{1}{2}} (l-z) \right\}}{p \sinh \left\{ \left( \frac{U^2}{4k^2} + A + \frac{cp}{k} \right)^{\frac{1}{2}} l \right\}} dp + \frac{kB}{c} e^{-\frac{kA}{c} t} \quad \dots (16)$$

The integrand of (16) has simple poles at  $p = 0$  and for

$$l \left( \frac{U^2}{4k^2} + A + \frac{cp}{k} \right)^{\frac{1}{2}} = n\pi i, \quad n = 0, 1, 2, \dots$$

that is

$$p = -\frac{U^2}{4kc} - \frac{kA}{c} - \frac{kn^2\pi^2}{l^2c}, \quad n = 1, 0, 2, \dots$$

Evaluating the residues at these poles we get

$$u_J(z, t) = D_J e^{\frac{Uz}{2k}} \frac{\sinh \left\{ \left( \frac{U^2}{4k^2} + A \right)^{\frac{1}{2}} (l-z) \right\}}{\sinh \left\{ \left( \frac{U^2}{4k^2} + A \right)^{\frac{1}{2}} l \right\}}$$

$$+ \frac{2D_J \pi}{l^2} e^{\frac{U_z}{2k}} \sum_{r=1}^{\infty} \frac{(-1)^r r \sin\{r\pi(l-z)/l\} e^{-\left(\frac{U^2}{4k} + \frac{kr^2\pi^2}{l^2c}\right)t}}{\left(\frac{U^2}{4k^2} + \frac{r^2\pi^2}{l^2}\right)} + \frac{kB}{c} e^{-\frac{kA}{c}t} \quad \dots \quad (17)$$

Finally, applying the inversion formula (5) we obtain

$$u(x, y, z, t) = \sum_{m=0}^{\infty} \sum_{n=0}^{\infty} (\delta_m \delta_n^1)^{-1} P_m^{(\alpha, \beta)}(x) P_n^{(\gamma, \delta)}(y) \times \left[ D_J \frac{U_z}{2k} \frac{\sinh \left\{ \left( \frac{U^2}{4k^2} + A \right)^{\frac{1}{2}} (l-z) \right\}}{\sinh \left\{ \left( \frac{U^2}{4k^2} + A \right)^{\frac{1}{2}} l \right\}} + \frac{kB}{c} e^{-\frac{kA}{c}t} + \frac{2D_J \pi}{l^2} e^{\frac{U_z}{2k}} \sum_{r=0}^{\infty} \frac{(-1)^r r \sin\{r\pi(l-z)/l\} e^{-\left(\frac{U^2}{4k} + \frac{kr^2\pi^2}{l^2c}\right)t}}{\left(\frac{U^2}{4k^2} + \frac{r^2\pi^2}{l^2}\right)} \right] \quad \dots \quad (18)$$

where  $\delta_m$  and  $\delta_n^1$  are given in (5a) and  $A$  and  $B$  are given in (7a).

Now if  $t$  tends to infinity i.e., allowing it to reach steady state conditions and substituting the value of  $D$  obtained with the help of (15) the integrals

$$\int_{-1}^1 (1-x)^{\alpha}(1+x)^{\beta} x P_0^{(\alpha, \beta)}(x) dx = 2^{\alpha+\beta+1}(\beta-\alpha) \times \frac{\Gamma(\alpha+1)\Gamma(\beta+1)}{\Gamma(\alpha+\beta+3)} \quad \dots \quad (19)$$

$$\int_{-1}^1 (1-x)^{\alpha}(1+x)^{\beta} x P_1^{(\alpha, \beta)}(x) dx = 2^{\alpha+\beta+2} \frac{\Gamma(\alpha+2)\Gamma(\beta+2)}{\Gamma(\alpha+\beta+4)} \quad \dots \quad (20)$$

$$\int_{-1}^1 (1-x)^{\alpha}(1+x)^{\beta} x P_m^{(\alpha, \beta)}(x) dx = 0 \text{ for } m > 1 \quad \dots \quad (21)$$

we arrive at

$$u(x, y, z, t)_{t \rightarrow \infty} = \frac{100e^{\frac{U_z}{2k}}}{(\alpha+\beta+2)(\gamma+\delta+2)} \times \left[ \frac{(\beta-\alpha)(\delta-\gamma) \sinh \left\{ \left( \frac{U^2}{4k^2} - \frac{\alpha}{k} \right)^{\frac{1}{2}} (l-z) \right\}}{\sinh \left\{ \left( \frac{U^2}{4k^2} - \frac{\alpha}{k} \right)^{\frac{1}{2}} l \right\}} \right]$$

$$\begin{aligned}
& + \frac{(\beta - \alpha)\{(\gamma + \delta + 2)y + \gamma - \delta\} \sinh \left\{ \left( \frac{U^2}{4k^2} - \frac{a}{k} + \gamma + \delta + 2 \right)^{\frac{1}{2}} (l - z) \right\}}{\sinh \left\{ \left( \frac{W^2}{4k^2} - \frac{a}{k} + \gamma + \delta + 2 \right)^{\frac{1}{2}} l \right\}} \\
& + \frac{(\delta - \gamma)\{(\alpha + \beta + 2)x + \alpha - \beta\} \sinh \left\{ \left( \frac{U^2}{4k^2} - \frac{a}{k} + \alpha + \beta + 2 \right)^{\frac{1}{2}} (l - z) \right\}}{\sinh \left\{ \left( \frac{U^2}{4k^2} - \frac{a}{k} + \alpha + \beta + 2 \right)^{\frac{1}{2}} l \right\}} \\
& + \frac{\{(\alpha + \beta + 2)x + \alpha - \beta\}\{(\gamma + \delta + 2)y + \gamma - \delta\}}{\sinh \left\{ \left( \frac{U^2}{4k^2} - \frac{a}{k} + \alpha + \beta + \gamma + \delta + 4 \right)^{\frac{1}{2}} l \right\}} \\
& \times \sinh \left\{ \left( \frac{U^2}{4k^2} - \frac{a}{k} + \alpha + \beta + \gamma + \delta + 4 \right)^{\frac{1}{2}} (l - z) \right\} \Bigg] \quad \dots \quad (22)
\end{aligned}$$

Further in the expression (2) of the intensity  $Q(x, y, z, t)$  we take

$$c_1 = c_3 = k, \quad c_2 = c_4 = 0$$

which gives

$$\alpha = \beta = \gamma = \delta = -\frac{1}{2}$$

In this case the expression (22) reduces to

$$u(x, y, z) = 100xye^{\frac{2k}{U}} \frac{U_z \sinh \left\{ \left( \frac{U^2}{4k^2} - \frac{a}{k} + 2 \right)^{\frac{1}{2}} (l - z) \right\}}{\sinh \left\{ \left( \frac{U^2}{4k^2} - \frac{a}{k} + 2 \right)^{\frac{1}{2}} l \right\}} \quad \dots \quad (23)$$

where

$$u(x, y, z) = u(x, y, z, t)_{t \rightarrow \infty}$$

Here we discuss two different cases depending on the values of  $U$ ,  $k$  and  $a$ .

Case 1 : 
$$a > \frac{U^2}{4k} + 2k.$$

This case may arise when  $a$  remains constant and the motion of the solid is slow or  $U$  is known and  $k$  large

For the sake of convenience we take

$$\frac{a}{k} = \frac{U^2}{4k^2} + \frac{7}{4}, \quad l = \pi;$$

so that the expression (23) takes the form

$$u(x, y, z) = 100xye^{\frac{U_z}{2k}} \cos \frac{z}{2} \quad \dots \quad (24)$$

The *Isothermal Surfaces* for  $u = T$  are given as

$$xye^{\frac{Uz}{2k}} \cos \frac{z}{2} = \frac{T}{100} \quad \text{for } U > 0 \quad \dots (25)$$

$$xy \cos \frac{z}{2} = \frac{T}{100} \quad \text{for } U = 0 \quad \dots (26)$$

In the later case the *Isothermal Curves* at the plane  $z = \frac{2\pi}{3}$  are shown in figure 1, for  $T = 5, 10, 20, 25, 30$  and  $40$ . The variation of temperature in this case along any line parallel to the  $z$ -axis will be a simple cosine curve.

In the general case ( $U > 0$ ), the variation is shown in figure 2, We have considered the line  $x = y = 0.5$  and the cases  $U/k = 1$  and  $U/k = 2$ .

If we give different values to the velocity  $U$  we obtain different values of temperature considered at certain fixed points.

TABLE 1. Temperature corresponding to different values of  $U/k$  at 0.2, 0.1 and  $2\pi/3$ .

$U/k$	0	0.3	0.6	0.9	1.2	1.5	1.8	2.1	2.4	2.7	3.0
$u$	1	1.37	1.87	2.56	3.51	4.81	6.59	9.02	12.34	16.90	23.14

Case 2 : 
$$\alpha < \frac{U^2}{4k} + 2k.$$

This case may come for rapid motions of the solid or small values of  $k$ . For simplicity we take

$$\frac{U^2}{4k^2} = \frac{a}{k} - 1$$

so that expression (23) takes the form

$$u(x, y, z) = 100xye^{\frac{Uz}{2k}} \sinh(l-z)/\sinh l \quad \dots (27)$$

Isothermal surfaces are of form

$$xye^{\frac{Uz}{2k}} \sinh(l-z) = \text{constant}, \quad \text{for } U > 0 \quad \dots (28)$$

and

$$xy \sinh(l-z) = \text{constant}, \quad \text{for } U = 0 \quad \dots (29)$$

Variations of temperature along the direction of z-axis is shown in figures 3A and 3B.

The examples and numerical calculations for unsteady state distributions and more general conditions may lead to certain interesting results of practical importance. These results will be reported elsewhere.

#### REFERENCES

- Carslaw H. S., & Jaeger J. C., 1959 *Conduction of Heat in Solids* Oxford University Press.  
Saxena V. P., *Jacobi Transform of Two Variables and Heat Conduction in a Square Lamina*,  
*Vikram Math. Jour.* (In press).

ISOTHERMAL CURVES

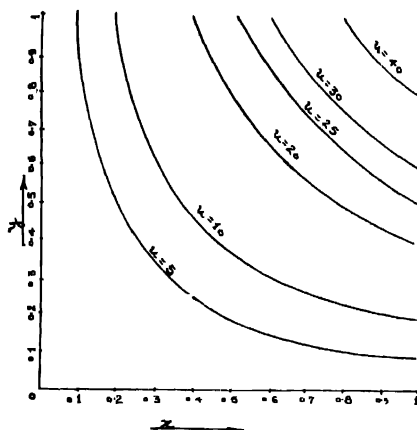


Figure 1. Isothermal curves at the plane  $z = \frac{2\pi}{3}$  for  $U = 0$ .

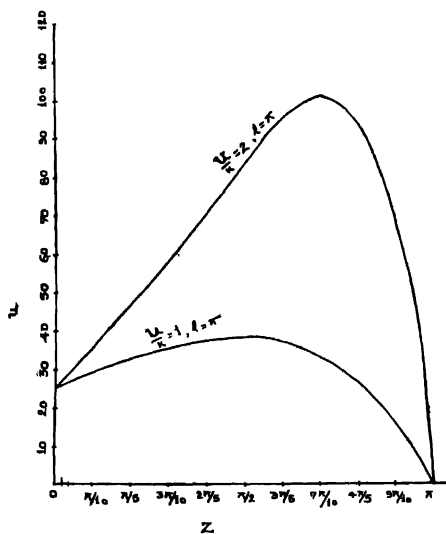


Figure 2. Curves showing variations of  $u$  along the line  $x = y = 0.5$  for  $U/k = 1$  and  $U/k = 2$ .

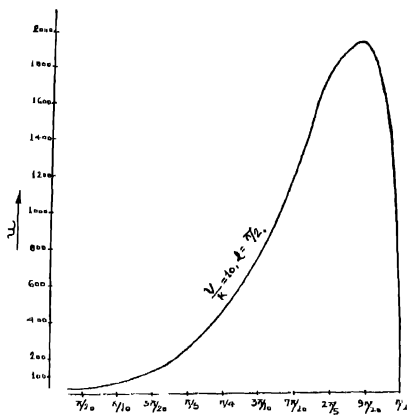


Figure 3A. The variation of temperature along the line  $x = y = 0.5$  for  $U/k = 10$ ,  $l = \frac{\pi}{9}$ .

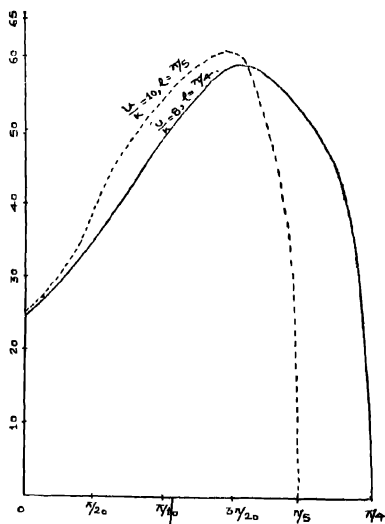


Figure 3B. The variation of temperature along the line  $x = y = 0.5$  for  $U/k = 10$ ,  $l = \frac{\pi}{5}$  and  $U/k = 8$ ,  $l = \frac{\pi}{4}$ .



## Letters to the Editor

### Field measurements in d. c. & h. f. gas discharges

By D. R. GUPTA AND G. L. GUPTA

Department of Physics, University of Jodhpur, Jodhpur

(Received 8 September 1969—Revised 25 February and 18 July 1970)

Engel and Stoenbeck (1934) have given a theoretical equation for the field strength  $E$  in the plasma of gas discharges :

$$E = \sqrt{\frac{2\sqrt{\pi}}{3}} \cdot \frac{2.405}{R} \sqrt{\frac{kT_e V_i}{e}} \cdot \sqrt{1 + \frac{Z V_a}{V_i}} \quad (1)$$

where  $b_+$  and  $b_e$  are mobilities of positive ions and electrons,  $Z$  is the number of inelastic collisions for ionisation,  $V_a$  the mean excitation voltage,  $k$  the Boltzmann's constant,  $V_i$  the ionisation potential,  $T_e$  the electron temperature,  $e$  the electronic charge and  $R$  the radius of the tube.

Further, the minimum field in the very high frequency region of the discharge was obtained by Brown and MacDonald (1951) by equating the number of ionising collisions to the number of collisions to diffuse out of the tube. Thus for the h.f. plasma where the frequency of the field is smaller than the collision frequency, the field strength  $E$  is obtained from the equation,

$$E = \frac{4}{\sqrt{3\pi}} \cdot \frac{1}{\lambda} \cdot \sqrt{\frac{kT_e V_i}{e}} \quad (2)$$

where  $\lambda$  is the diffusion length given by

$$\left(\frac{1}{\lambda}\right)^2 = \left(\frac{\pi}{L}\right)^2 + \left(\frac{2.405}{R}\right)^2 \quad (3)$$

where  $L$  represents the length of the discharge tube.

Kojima, *et al* (1953) have pointed out that equation (2) does not contain the frequency of the field and that it may, therefore, be applicable to d.c. field too. Both the equations (1) and (2) indicate that  $E \cdot R_e = \text{constant}$ ,  $R_e$  being the equivalent radius of the discharge tube given by,  $R_e = 2.405\lambda$ . The value of  $E \cdot R_e$  was calculated by Kojima *et al* for a discharge in argon.

This note presents the field strength in discharges in argon and neon at various pressures on the basis of the determination of the electron temperature under d.c. conditions.

A series of careful and systematic experiments conducted in the plasma of neon gas (and in argon too) established that the values of electron temperature obtained by Gupta (1956) with Langmuir probes are reliable in the pressure region of 0.0062–0.77 mm of mercury. Using probes of thin wire (diameter—0.045 to 0.116 mm) kept in the positive column of d.c. discharges of current density 0.7 to  $3.5 \times 10^{-3}$  ampere/cm<sup>2</sup>, he measured electron currents for varying potentials of probes with respect to the anode, and the electron temperatures were obtained from the usual semi-log plots. The design of suitable probe for this purpose has also been described (Gupta 1956).

From the observations made with argon, the values of the field strength under given discharge conditions have been calculated by the equation (2) mentioned above and the results in tabulated form are given below.

Table 1. For argon

Pressure $p$ (mm. Hg.)	$pR_e$ (mm. Hg. cm.)	$T_e$ (experimental value for d.c. plasma) °K	Mean free path in cm.	$E/p$ volt/cm. mm. Hg.	$ER_e$ in volts
0.0096	0.028	85,000	4.44	1200	33.60
0.013	0.038	31,000	3.28	535.3	20.34
0.77	2.25	14,100	0.055	6.071	13.68

This study has been extended by the authors to experimental observations for d.c. discharges in neon gas for which the results are given below.

Table 2. For neon

Pressure $p$ (mm. Hg.)	$pR_e$ (mm. Hg. cm.)	$T_e$ (experimental value for d.c. plasma) °K	Mean free path in cm.	$E/p$ volt/cm. mm. Hg.	$ER_e$ in volts
0.036	0.105	61,800	2.30	319.4	33.62
0.064	0.187	55,500	1.29	170.0	31.84
0.096	0.281	42,800	0.863	99.65	27.98
0.34	0.994	31,000	0.244	23.96	23.81
0.67	1.959	25,200	0.124	11.03	21.56

## REFERENCES

- Engel A. V. & Streenbeck M. 1934 *Elektrische Gasentladungen* Berlin, part II, pp. 85 and 87.  
 Brown S. C. & MacDonald A. D. 1951 *Phys. Rev.* **76**, 1620.  
 Kojima S., Takayama K. & Shimauchi A. 1953 *J. Phys. Soc. Japan* **8**, 55.  
 Gupta G. L. 1956 *Raj. Univ. Phys. Sc. Studies (India)* **I & II**, 34, 51.

## Polarised absorption spectrum of $\text{Fe}^{2+}$ doped in $\text{CsCdCl}_3$ at 77°K

BY RANAJIT KR. SHAHA AND A. BOSE

*Indian Association for the Cultivation of Science, Jadavpur, Calcutta-32*

AND

MIHIR CHOUDHURY

*Presidency College, Calcutta-12*

(Received 31 March, 1970)

In order to study the energy levels of  $\text{Fe}^{2+}$  in a ligand field provided by an octahedron of chloride ions, we have grown a single crystal of  $\text{Fe}^{2+}$ -doped  $\text{CsCdCl}_3$  from melt at 485°C by Stock-Berger's method. The crystal structure of  $\text{CsCdCl}_3$  has been reported by Siegel and Gobert (1964). The space group is  $C_6/mmc$ ,  $Z = 6$ . Six  $\text{Cl}^-$  ions form a trigonally distorted octahedron around the central metal ion. The polarised absorption spectrum of the doped single crystal, cooled to 77°K in a cold-finger type dewar, was measured with Zeiss VSU-2 spectrophotometer.

The electronic ground term  $^5D$  of  $\text{Fe}^{2+}$ , which incidentally is the only quintet term for the  $d^6$  configuration, splits under the octahedral crystalline field into an upper doublet  $^5E_g$  and a lower triplet  $^5T_{2g}$  state. The separation between them gives the measure of  $10 Dq$ . The small trigonal field present in  $\text{CsCdCl}_3$  splits the lower triplet further into a singlet  $^5A_1(C_{3v})$  and a doublet  $^5E(C_{3v})$  leaving the upper  $^5E_g(O_h)$  unsplit (figure 1). The upper state might be split by the spin-orbit interaction or by the combined action of the trigonal field and spin-orbit interaction, but such splittings should be small ( $< 100 \text{ cm}^{-1}$ , Low 1960). A large splitting of the upper  $E_g$  state, may, however, be caused by tetragonal Jahn-Teller distortion through the vibronic mechanism. Figure 2 shows the recorded polarised spectrum at 77°K.

We have assigned the absorption band at  $6452 \text{ cm}^{-1}$  to the  $^5T_{2g} \rightarrow ^5E_g$  transition and calculated the observed  $Dq$  to be  $\sim 645 \text{ cm}^{-1}$ . This is low in comparison with the  $Dq$  observed with  $\text{Fe}^{2+}$  in oxide ( $\sim 1030 \pm 20 \text{ cm}^{-1}$ , Low 1960) and in  $\text{OH}^-$  complex ( $\sim 1080 \text{ cm}^{-1}$ , Cotton & Mayers, 1960). This low value of  $Dq$  is obviously due to the large  $\text{Cd-Cl}$  distance in our case ( $2.59 \text{ \AA}$ ) and the difference in the ionic radii of  $\text{Fe}^{2+}$  ( $0.83 \text{ \AA}$ ) and  $\text{Cd}^{2+}$  ( $1.03 \text{ \AA}$ ). It is interesting to note that the present octahedral value of  $Dq$  is comparable to the tetrahedral  $Dq \sim 510 \text{ cm}^{-1}$  observed for  $\text{FeCl}_4^{2-}$  in chloride melt ( $\text{LiCl-KCl}$ , Gruen and McBeth 1962).

The absorption spectrum at 77°K (figure 2) shows that  ${}^6T_{2g} \rightarrow {}^5E_g$  band splits into two components at 5210  $\text{cm}^{-1}$  and 6370  $\text{cm}^{-1}$ . This splitting is presumably due to the Jahn-Teller distortion of the upper  ${}^5E_g$  state. The lack of polarisation of the bands agrees with this assignment. The separation of 1160  $\text{cm}^{-1}$  of the components, which measures the magnitude of the Jahn-Teller distortion, is less than that observed for  $\text{Fe}^{2+}$  surrounded by an octahedron of  $(\text{OH})^-$  ions ( $\sim 2000 \text{ cm}^{-1}$  Liehr & Ballhausen 1958). This is in conformity with the low strength of the crystal field in the present case.

In addition, we have observed a band at 25040  $\text{cm}^{-1}$  with high extinction coefficient. This is ascribed to the charge-transfer transition involving transfer of an electron from the Cl-ligand to the metal ion. In the molecular orbital scheme it is assigned to the transition (figure 3)  $t_{2u}(\text{ligand}) \rightarrow t_{2g}(\text{metal})$ . The direct product of  $t_2 \times t_2$  breaks into  $T_1, T_2, A_1, A_2$ . Under  $C_{3v}$  symmetry there should be three transitions polarised perpendicular to  $C$  and one transition polarised along  $C$ . From the observed polarised spectrum at 77°K (figure 2) it is seen that there are two transitions in the  $C_\perp$  direction at 25160  $\text{cm}^{-1}$  and 24390  $\text{cm}^{-1}$  and there is one transition at 25565  $\text{cm}^{-1}$  in the  $C_\parallel$  direction. The magnitude of the trigonal field splitting is estimated to be nearly 400  $\text{cm}^{-1}$ .

The authors have undertaken the magnetic susceptibility and anisotropy measurement to corroborate the above finding.

#### REFERENCES

- Cotton F. A. & Meyers M. D. 1960, *J. Am. Chem. Soc.* **82**, 5023.  
 Gruen D. M. & McBeth R. 1962, *Nature*, **194**, 468.  
 Gruen D. M. & McBeth R. 1963, *Pure and Applied Chemistry*, **6**, No. 1, 23.  
 Low W. 1960, *Phys. Rev.* **118**, 1130.  
 Liehr A. D. & Ballhausen C. J. 1958, *Ann. Phys. (N.Y.)* **3**, 304.

*Indian J. Phys.* **44**, 60-63, (1970)

### Statistically linear mass relation of elementary particles and its representation by a polynomial curve fitting equation

By B. J. BHATTACHARJEE

*St. Anthony's College, Shillong, India*

(Received 31 March—Revised 21 July 1970)

It is found that when the atomic weights of elements are plotted against the atomic numbers, a parabolic curve is obtained for the first 86 elements which however does not hold for the rest of the elements (figure 1). In the case of elementary

Figure 1 displays two IR spectra, labeled C1 and C2, showing transmittance versus wavenumber. The x-axis for both spectra ranges from 2000 to 1000  $\text{cm}^{-1}$ . Spectrum C1 (top) shows two distinct peaks at 2356.6  $\text{cm}^{-1}$  and 2439.6  $\text{cm}^{-1}$ . Spectrum C2 (bottom) shows two distinct peaks at 1650  $\text{cm}^{-1}$  and 1550  $\text{cm}^{-1}$ .

Figure 2. Polarised absorption spectra of  $\text{Fe}^{2+}$  in  $\text{CsCdCl}_3$  at 77°K.

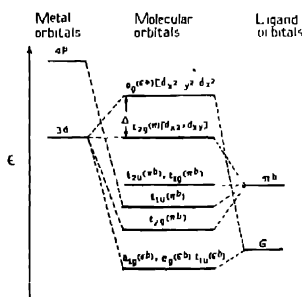


Figure 3. Molecular orbital energy level diagram for metal hexachlorides.

particles it seems to us (Bhattacharjee 1970) that excluding photon family, as their rest mass is zero or nearly so, we may ascribe a number for each elementary particle in the order of increasing mass. Let us call this number as 'Elementary particle number' (E.P.No.), as in the case of atomic number of elements. However, its physical meaning remains to be clarified. Plotting this number against respective 'Rest Mass' (R.M.) we find a parabolic curve (figure 2a). Thus the majority of elementary particles can be represented by a single curve. The overall symmetry of the curve suggests that there is a definite relation between E.P. No. and R.M. of the particles. It is true that a few points exhibit large deviations from the fundamental curve. These deviations can perhaps be eliminated if we have more elementary particles in these regions. On this basis, after postulating 9 more particles (Set 2), we have drawn the curve 2(b) which shows an overall symmetry.

The following numbers indicate the R.M. in MEV of Elementary particles :

For figure 2a. (Set 1) : .511(e), 106( $\mu$ ), 137( $\pi$ ), 496( $\kappa$ ), 548( $\eta$ ), 750( $d\pi$ ), 782( $\eta$ ), 888( $\kappa$ ), 937( $N$ ), 1020( $\eta$ ), 1115( $\Lambda$ ), 1193( $\Sigma$ ), 1238( $\Delta$ ), 1250( $\eta$ ), 1290( $\pi$ ), 1318( $\Xi$ ), 1385( $\Sigma$ ), 1405( $\Lambda$ ), 1515( $\kappa$ ), 1512( $N$ ), 1520( $\Lambda$ ), 1530( $\Xi$ ), 1605( $\Xi$ ), 1660( $\Sigma$ ), 1676( $\Omega$ ), 1688( $N$ ), 1815( $\Lambda$ ), 1860( $\eta$ ), 1890( $\Sigma$ ), 1920( $\Delta$ ), 1980( $\Xi$ ), 2015( $\Lambda$ );

For figure 2b (Set 2) : 0.511, 106, 137, 220 $p$ , 300 $p$ , 370 $p$ , 430 $p$ , 496, 548, 640 $p$ , 700 $p$ , 750, 782, 888, 939, 1020, 1060 $p$ , 1115, 1193, 1238, 1250, 1290, 1318, 1385, 1405, 1450, 1512, 1520, 1530, 1600, 1660, 1676, 1700, 1725 $p$ , 1775 $p$ , 1815, 1860, 1890, 1920, 1980, 2020

(Numbers associated with  $p$  are the particles postulated and other symbols have the conventional meaning).

The curves that have been drawn from considerations of the similarity in behaviour between elements and elementary particles agree well figuratively. We believe that the interpretation of the data indicates a compelling evidence that the linear mass relation should be given by a polynomial curve fitting equation, viz.

$$Y = A + BX + CX^2 + DX^3 \dots$$

where  $Y$  is E.P. No.,  $X$  is R.M.,  $A, B, C, D$  etc are constants. Obviously our prime interest will be the values of  $A, B, C$  etc. The values as obtained by electronic computer are given in table 1 for elements and elementary particles.

It is reasonable to expect that the values should fit into the above equation. Unfortunately the agreement is not good. The aim of this report, however, is to show (1) that the above is a novel method of approach, and (2) that the actual values of  $A, B, C$ , etc may offer some insight into the internal structure of elementary particles. Moreover (3) there is a purely statistical relation for elementary

particles and (4) also some similarity between elements and elementary particles, both being amenable to a curve fitting equation.

Table 1a. For elements

	2nd order	3rd order	4th order	5th order
A	-1.22831800	1.66207100	.38558000	-1.13840700
B	2.07051030	1.67414130	1.96004910	2.45843820
C	.00587743	.01746495	.00250491	-.03775392
D		-.00009085	.00018220	.00143930
E			-.00000160	-.00001826
F				.00000007

Table 1b. For elementary particles

Set I	2nd order	3rd order	4th order	5th order *
A	24.38707000	-215.30540000	-277.63580000	-219.49380000
B	106.76421000	187.76053000	220.96462000	177.46715000
C	-1.50055740	-7.54324520	-11.91073600	-3.24074600
D		.12207461	.32579282	-.35805610
E			-.00308669	.02003633
F				-.00028028

Set II	2nd order	3rd order	4th order	5th order
A	-56.13346000	-102.51284000	-52.32042000	-43.59700000
B	74.73282300	87.23702000	65.66401000	60.32073600
C	-.62255894	-1.35796390	.88921120	1.73883200
D		.01167310	-.07087805	-.12398310
E			.00098278	.00239492
F				-.00001345



B. J. Bhattacharjee

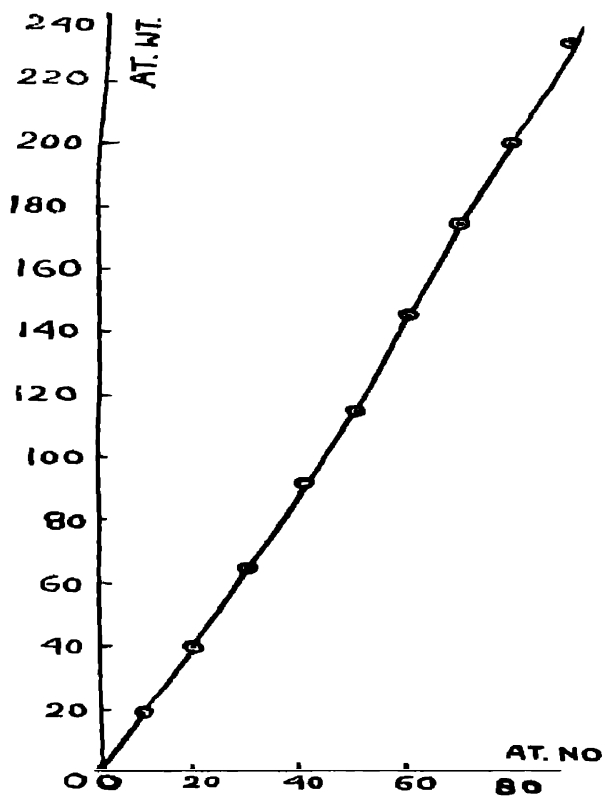


Fig. 1.

B. J. Bhattacharjee

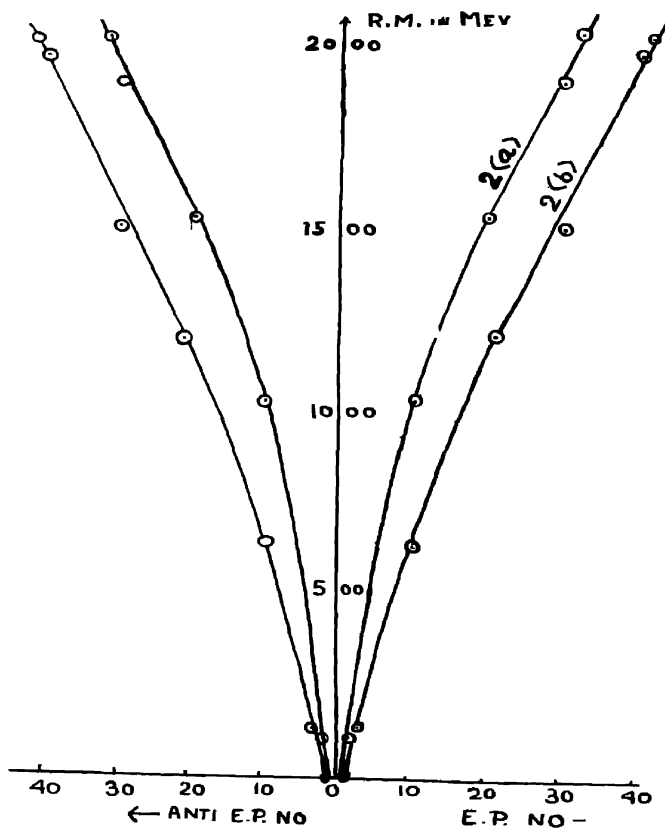


Fig. 2.

The author is thankful to Dr. G. P. Bhattacharjee and Dr. S. K. Dutta Roy for their interest and help in the work. He also thanks the authorities of the Indian Institute of Technology, Kharagpur, India, for providing facilities for using the electronic computer.

#### REFERENCES

- Bhattacharjee B. J. 1970 *Proc. 57th Ind. Sc. Cong. Part III, Section III*, 37.  
Fickinger W. J. & Sternheimer R. M. 1965 *Phys. Rev.* **139**, 413 and 1020.  
Gellmann M., Chew G. F. & Rosenfeld A. H. 1964 *Scientific American* **210**, 74.

*Indian J. Phys.* **44**, 63–65 (1970)

### Hydrogen excitation in H- $\alpha$ collision by second Born approximation

BY JAYASRI CHOWDHURY (née) SEN AND D. M. BHATTACHARYA

*Department of Theoretical Physics,*

*Indian Association for the Cultivation of Science, Calcutta—32*

(Received 31 March 1970)

Previous investigations on the excitation of atomic hydrogen by alpha particle have been made by Bates (1959). Using the impact parameter treatment he has shown that the introduction of allowance for distortion leads to much smaller cross-sections than those obtained by the first Born approximation at low and moderate energies. The purpose of our present work is to investigate the same problem in the second Born approximation and to compare our findings with the previous results.

We consider  $\alpha$ -particle  $B$  to be moving with a constant velocity  $v$  in a straight line and the target nucleus to be at rest at  $A$ . The Hamiltonian  $H$  corresponding to the motion of the electron is given by

$$H = -\frac{1}{2}\nabla^2 - \frac{1}{r_A} - \frac{2}{r_B} \quad (\text{in atomic units})$$

The total electronic wave function may be represented by the expansion

$$\Psi(r, t) = \sum_n a_n(t) \psi_n$$

where  $\psi_n = \phi_n(r) \exp(-ie_n t)$ ,

$\phi_n(r)$  and  $e_n$  being the eigenfunctions and eigenenergies of the hydrogen atom.

The collision is then described by the time-dependent Schrödinger equation  $H\Psi(t) = i \frac{\partial}{\partial t} \Psi(t)$ . Proceeding in the customary manner it can be shown that

$$\frac{d}{ds} a_m(s) = i \sum F_{mn} a_n(s) \quad (1)$$

where

$$s = vt$$

$$F_{mn} = - \int \bar{\psi}_m V_i \psi_n dV$$

and  $V_i = -2/r_B$ , is the perturbing potential

The cross section for excitation from ground state to  $m$ -th state is

$$Q_m = 2\pi \int_0^\infty |a_m|^2 p dp, \quad p \text{ being the impact parameter.}$$

From equation (1) together with the initial conditions

$$a_1(-\infty) = 1$$

and

$$a_n(-\infty) = 0, \quad n \neq 1$$

we have,

$$a_m(s) = \delta_{m1} + \frac{i}{v} \sum \int_{-\infty}^s F_{m1n} a_n ds \quad (2)$$

The 1st Born approximation for  $a_m$  is given by

$$a_m(s) = \delta_{m1} + \frac{i}{v} \int_{-\infty}^s F_{m1} ds \quad (3)$$

From (2) and (3) the second Born approximation is obtained. Neglecting the effect of all states other than the ground state and the final state  $m$ , we obtain

$$a_m(\infty) = \frac{i}{v} \int_{-\infty}^\infty F_{m1} ds$$

$$+ \frac{1}{v^2} \int_{-\infty}^\infty \left\{ \left( \int_{-\infty}^s F_{11} ds_1 \right) F_{m1} + \left( \int_{-\infty}^s F_{m1} ds_1 \right) F_{m1} \right\} ds$$

The total expression for cross section in the Born approximation is

$$Q = \int_0^\infty \left[ \frac{1}{v^2} \left( \int_{-\infty}^\infty F_{m1R} ds \right)^2 - \frac{2}{v^3} \left( \int_{-\infty}^\infty F_{m1R} ds \right) \right. \\ \left. \left( \int_{-\infty}^\infty \left\{ \left( \int_{-\infty}^s F_{11} ds_1 \right) F_{m1} + \left( \int_{-\infty}^s F_{m1} ds_1 \right) F_{m1} \right\} ds \right) \right] p dp \quad (4)$$

In equation (4) we have neglected the two terms of the fourth order in interaction energy. Since other terms of the same order would also come from higher Born

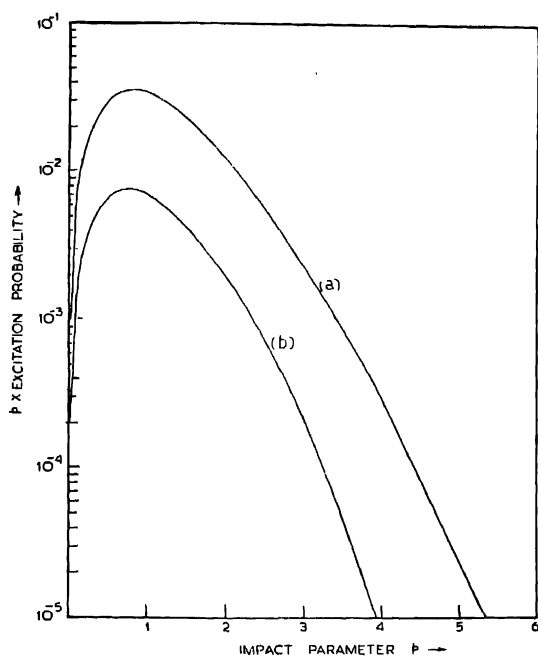


Figure 1. The product of excitation probability and the impact parameter  $p$  against  $p$   
 (a) For  $1s-2s$  excitation at  $1412 \text{ keV}$   
 (b) For  $1s-3s$  excitation at  $1412 \text{ keV}$ .

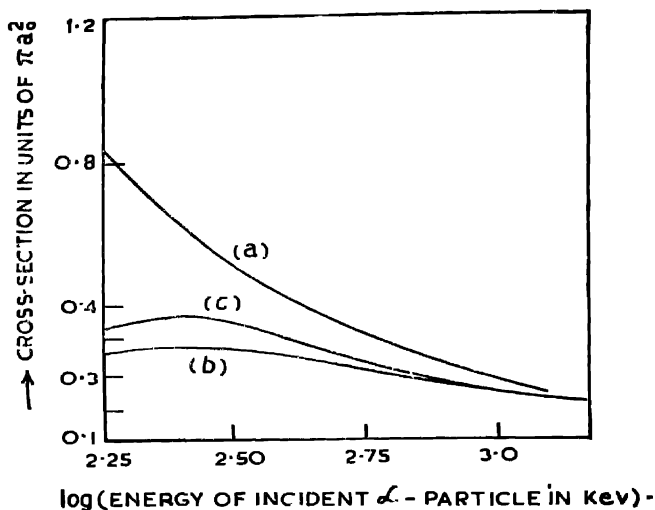


Figure 2. Excitation cross sections for  $1s-2s$  transition by  
(a) 1st Born, (b) distortion, and (c) 2nd Born approximations.

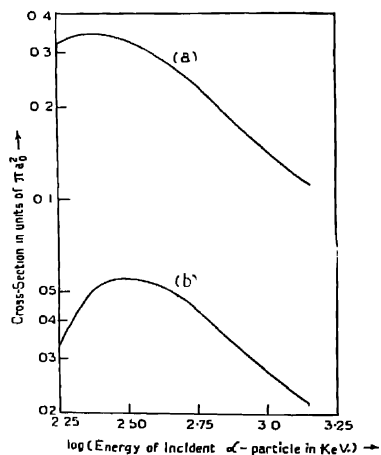


Figure 3. Second Born excitation cross sections for  
(a)  $1s-2s$  transition  
(b)  $1s-3s$  transition.

approximation and such terms are not known, hence for consistency those two terms are not included.

In figure 1 we have plotted the product of the excitation probabilities and the impact parameter  $p$  against  $p$  at the incident energy 1412  $keV$ .

In figure 2 we have compared the cross-sections obtained from first Born distortion and second Born approximation for  $1s\text{-}2s$  transition. It is seen that at about 1000  $keV$  incident energy, the cross-section due to 1st Born, 2nd Born and the distortion approximation are almost the same. As the energy decreases, the discrepancy between the results of the 1st Born and the distortion increases, where the second Born results are comparatively close to the distortion results.

Figure 3 shows our results of the cross-section of  $1s\text{-}2s$  and  $1s\text{-}3s$  excitations. It is found that  $1s\text{-}3s$  excitation cross-section is much lower than that of  $1s\text{-}2s$  excitation.

This work is preliminary to a series of investigations of Alpha-Hydrogen Collision where we propose to take into account the capture state of  $He^+$  as well.

The authors are thankful to Dr. N. C. Sil and Prof. D. Basu for helpful discussions.

#### REFERENCE

Bates D. R. 1950 *Proc. Phys. Soc. A*, **73**, 227.

*Indian J. Phys.* **44**, 65-67, (1970)

### On parameter estimation of Gibbs' canonical distribution

BY C. G. CHAKRABARTI

*Department of Mathematics, F. C. College, Diamond Harbour, West Bengal.*

(Received 26 March—Revised 20 July 1970)

In this note first considering Gibbs' canonical distribution as a simple statistical distribution, the fluctuation of temperature has been obtained using the asymptotic properties of maximum-likelihood estimate. Secondly, Einstein's formula for the fluctuation probability has been derived purely from statistical consideration.

After Gibbs, we consider a system in equilibrium as a small part of a large system exchanging its energy with its environment (heat bath). In this case the

system may be considered as a sample and let  $n$  (assumed sufficiently large) be the number of components (molecules etc.) having the energies  $\epsilon_i$  ( $i = 1, 2, \dots, n$ ). For the development of statistical theory each energy-component is taken to obey the exponential distribution as

$$dF(\epsilon, \theta) = e^{-\theta\epsilon} d\Omega(\epsilon) | \phi(\theta) \quad (1)$$

where  $\phi(\theta) = \sum e^{-\theta\epsilon} d\Omega(\epsilon)$  and  $\Omega(\epsilon)$  is a suitable positive measure. In usual statistical mechanics (Khinchin, 1949)  $d\Omega(\epsilon)$  is the number of microscopic states of the system of energy lying between  $\epsilon$  and  $\epsilon + d\epsilon$  and  $\Omega(\epsilon)$  is usually called structure function.

The likelihood function  $L$  for the system (sample) is given by

$$L(\epsilon_1, \epsilon_2, \dots, \epsilon_n; \theta) = e^{-\theta \sum_{i=1}^n \epsilon_i} \Omega(\sum_{i=1}^n \epsilon_i) | \Phi_n(\theta) \quad (2)$$

Where  $\Phi_n(\theta) = \phi_1(\theta)\phi_2(\theta)\dots\phi_n(\theta)$  and the maximum-likelihood estimate of  $\theta$  is given by

$$\frac{\partial \log L}{\partial \theta} = 0 \quad \text{or} \quad \bar{\epsilon} + \frac{d}{d\theta} \log \Phi_n(\theta) = 0 \quad (2a)$$

Let  $\hat{\theta}$  be the maximum-likelihood estimate of  $\theta$  which is thus taken to be the parameter corresponding to the equilibrium state of the system.

$F(\epsilon, \theta)$  being regular (Wilks, 1962) and equation (2a) having a unique solution (Khinchin 1949), the maximum-likelihood estimate  $\hat{\theta}$  of  $\theta$  for large values of  $n$  has a distribution which is asymptotically normal  $N[\theta, 1/nB^2(\theta, \theta)]$  (Wilks 1962). Thus for large  $n$ ,

$$\text{var}(\hat{\theta}) = \frac{1}{nB^2(\hat{\theta}, \hat{\theta})} = \frac{1}{\left(\frac{\partial \log L}{\partial \theta}\right)^2} \quad (3)$$

Where  $\left(\frac{\partial \log L}{\partial \theta}\right)^2 = H(\theta)$  is the Fisher's information contained in the sample.

As a system in Statistical Physics contains a large number of components, the appropriate formula for determination of fluctuation of parameter  $\hat{\theta}$  is given by

$$\text{var}(\hat{\theta}) = 1 \left/ \left( \frac{\partial \log L}{\partial \theta} \right)^2 \right. = 1/\text{var}(E)$$

where  $E$  is the total energy of the system.



On writing  $\hat{\theta} = 1/kT$ , we have,

$$\text{var}(T) = \left( \frac{dT}{d\hat{\theta}} \right)^2 \text{var}(\hat{\theta}) = \frac{k^2 T^4}{\text{var}(\bar{E})} = \frac{kT^2}{c_v} \quad (4)$$

which is of the same form as that for the fluctuation of temperature given by Landau and Lifshitz (1958). Thus this  $T$  may be identified with the temperature.

Let now there be a spontaneous transition of the equilibrium state corresponding to the parametric value  $\hat{\theta}$  (hereafter denoted by  $\theta$ ) to a neighbouring non-equilibrium state corresponding to the parametric value  $\theta + \Delta\theta$ . Let us now introduce a measure of divergence (or distance) between the two states of equilibrium and non-equilibrium, according to Rao (1945)

$$\Delta s^2 = H(\theta)\Delta\theta^2 - nB^2(\theta, \theta)\Delta\theta^2 \quad (5)$$

But  $\Delta s = \sqrt{n}B(\theta, \theta)\Delta\theta$  is normal  $N(0, 1)$  for large  $n$  (Wilks 1962). Thus we may define the fluctuation probability by

$$P(\Delta s) = \omega \alpha e^{-\frac{1}{2}\Delta s^2}$$

Since

$$\frac{1}{2}\Delta s^2 = \frac{1}{2}H(\theta)\Delta\theta^2 = \overline{\log L(\bar{E}, \theta)} - \overline{\log L(\bar{E}, \theta + \Delta\theta)}$$

(Kullback 1959) if  $S$  and  $S + \Delta S$  be the thermodynamic entropies of the states corresponding to the parametric values  $\theta$  and  $\theta + \Delta\theta$ , then  $\Delta S = \frac{1}{2}kH(\theta)\Delta\theta^2$  gives the entropy difference between the equilibrium and non-equilibrium states. So the thermodynamic fluctuation probability becomes

$$\omega = \omega_0 e^{\Delta S} \quad (6)$$

which is Einstein's formula for the fluctuation probability.

I express my deep gratitude to Dr. M. Dutta, University of Calcutta, for help in the preparation of this note.

# REFERENCES

- Khinchin A. I. 1949 *Mathematical foundation of statistical mechanics*, Dover Publication.  
 Kullback S. 1959 *Information theory and statistics*, John Wiley and Sons, N.Y.  
 Landau & Lifshitz 1958 *Statistical Physics*, Pergamon Press.  
 Rao C. R. 1945 *Bull. Cal. Math. Soc.* **37**, 81.  
 Wilks S. S. 1962 *Mathematical statistics*, John Wiley and Sons, N.Y.

## Effective atomic numbers for scattering processes of gamma rays in alloys

By M. SHRIRAMCHANDRA MURTY, M. N. SEETARAMANATH, J. RAMA RAO  
AND K. PARTHASARADHI

*The Laboratories for Nuclear Research, Andhra University, Waltair,  
India*

(Received 10 July 1970)

An effective atomic number for gamma ray interaction is defined for a material composed of several elements, to represent the attenuation properties of the material. Unlike the atomic number in the case of an element, the effective atomic number of such a material is not a unique number, since it assumes different values for different interaction processes. However, it has been shown (Parthasaradhi 1968) that the effective atomic number defined for a particular partial process is quite unique and retains its identity over a considerable energy range. Hence, more attention is devoted to the study of these partial effective atomic numbers (Visweswara Rao *et al* 1968, Parthasaradhi *et al* 1969) for various alloys. In these investigations (Parthasaradhi 1968) no discrimination seems to have been made between coherent and incoherent scattering processes, with the hope that the effect due to this indiscrimination in the energy region considered is small on the effective atomic number for total scattering process. Further, no attempt seems to have been made to determine partial effective atomic number for coherent scattering except at 30 keV in water and perspex (Parthasaradhi 1968). It is therefore felt that a detailed study of the effective atomic numbers for coherent and incoherent scattering processes separately in the energy region 0.1 to 1.33 MeV might be interesting. For this purpose two alloys of tin and a heavier element (Pb) and two of tin and a lighter element (Cu) in different proportions are chosen and the results are reported in this note.

As in previous investigations (Parthasaradhi 1968) the incoherent scattering cross-sections for the elements Pb, Sn and Cu are obtained by subtracting the other theoretical partial cross-sections (Plechaty 1968, Schmickely *et al* 1967) including the coherent scattering cross-sections (Plechaty) from the total experimental gamma ray cross-sections reported by McCrary *et al* (1967), Colgate (1952), Wyard (1952) and Parthasaradhi *et al* (1968). From these, the cross-sections in the alloys are determined using the sum rule. Making use of these effective cross-sections, the effective atomic numbers in alloys for incoherent scattering process are determined at the various energies by interpolation from the plots of cross-section *versus* atomic number. Since experimental total coherent scattering cross-sections

are not available the effective atomic numbers for this process are determined, in a similar manner as described above, utilizing the theoretical cross-sections reported by Plechaty. The values of the incoherent and coherent scattering cross-sections of the alloys are given in table 1 and the deduced values of the effective atomic numbers are presented in table 2.

**TABLE 1.** Coherent and incoherent scattering cross-sections in alloys (in barns/atom)

Energy (keV)		Solder	Solder (soft)	Bell metal	Bronze
		Pb 67% Sn 33%	Pb 40% Sn 60%	Sn 25% Cu 75%	aluminium Sn 10% Cu 90%
100	Incoherent	—	—	15.0	11.8
	Coherent	—	—	6.3	3.69
279	Incoherent	22.5	20.2	11.4	9.2
	Coherent	6.3	4.35	0.84	0.49
412	Incoherent	20.2	17.7	9.4	7.9
	Coherent	2.85	1.97	0.40	0.23
662	Incoherent	16.6	14.7	8.15	6.6
	Coherent	1.08	0.75	0.15	0.09
1332	Incoherent	12.2	10.6	5.8	4.8
	Coherent	0.28	0.19	0.033	0.02

**TABLE 2.** Effective atomic numbers for incoherent and coherent scattering processes of gamma rays

Energy (keV)		Solder	Solder (soft)	Bell metal	Bronze
		Pb 67% Sn 33%	Pb 40% Sn 60%	Sn 25% Cu 75%	aluminium Sn 10% Cu 90%
100	Incoherent	—	—	32 ± 1	27 ± 1
	Coherent	—	—	33	27
279	Incoherent	64 ± 2	57 ± 2	32 ± 1	26 ± 1
	Coherent	69	61.5	33.5	27
412	Incoherent	64 ± 2	56 ± 2	31.5 ± 1	26 ± 1
	Coherent	69	61	33	27
662	Incoherent	65 ± 2	58 ± 2	32 ± 1	26 ± 1
	Coherent	69	61	33.5	27
1332	Incoherent	66 ± 1	58 ± 1	32 ± 0.5	26 ± 0.5
	Coherent	69	61	33	27

It can be seen from table 2 that the effective atomic number for each scattering process retains its identity over the energy region considered within the limits of errors. There is a significant difference between the two effective atomic numbers in the two alloys composed of Pb and Sn, while the difference is not discernible in the other two alloys composed of Sn and Cu. It thus appears that in alloys consisting of heavy elements the effective atomic numbers for coherent and incoherent scattering processes have to be treated separately.

Two of the authors (M.S.M. and M.N.S.) are grateful to the Department of Atomic Energy, Government of India, for awarding them Research Fellowships.

#### REFERENCES

- Colgate S. A. 1952 *Phys. Rev.* **87**, 592.  
 McCrary J. H. *et al* 1967 *Phys. Rev.* **153**, 307  
 Parthasaradhi K. 1968 *Indian Jour. Pure & Appl. Phys.* **6**, 574.  
 Parthasaradhi K. 1968 *Indian Jour. Pure & Appl. Phys.* **6**, 609.  
 Parthasaradhi K. *et al* 1969 *Jour. Phys. A*, **2**, 245.  
 Parthasaradhi K. *et al* 1969 *Indian Jour. Pure & Appl. Phys.* **7**, 389.  
 Plechaty E. L. 1968 *Photon Cross-section Compilation*, Lawrence Radiation Laboratory, California (Private communication). These values are taken from McMaster W. H., Del Grande, Kerr N., Mallett J. H., Scofield N. E., Cahill R. & Hubbell J. H. 1967, *UCRL-50174*.  
 Schmickley R. D., *et al* 1967 *Phys. Rev.* **164**, 104.  
 Visweswara Rao V. *et al* 1968 *Indian Jour. Pure & Appl. Phys.* **6**, 643.  
 Ward S. J. 1952 *Phys. Rev.* **87**, 165.

# INDIAN JOURNAL OF PHYSICS

VOL. 44

No. 2

AND

VOL. 53

PROCEEDINGS

No. 2

OF THE

INDIAN ASSOCIATION FOR THE CULTIVATION OF SCIENCE

*(Edited in collaboration with the Indian Physical Society).*

FEBRUARY 1970

PUBLISHED BY THE

INDIAN ASSOCIATION FOR THE CULTIVATION OF SCIENCE

JADAVPUR, CALCUTTA-32



## On wide-band communication techniques using pseudo-random and orthogonal sequences-I.

By N. B. CHAKRABORTI, A. K. MUKHERJEE\* AND N. PAL

*Department of Electronics and Electrical Communication Engineering,  
Indian Institute of Technology, Kharagpur, West Bengal*

(Received 14 October 1966—Revised 11 November 1967, 30 August 1968  
and 12 January 1970)

In this paper properties of pseudo-random and orthogonal codes are discussed. Methods of their generation and techniques of application of such codes for communication, simplifications of existing Modem by using techniques of maximum amplitude selection, time compression, code-frequency time-matrixing, sequential technique for estimation and decoding are briefly described.

### 1. INTRODUCTION

Considerable interest has recently been aroused in wide-band Communication techniques (Golomb 1965, Harmuth 1960, 1961, Chakraborti 1964, Costas 1959), which are finding application in space communications and telemetry, random access, and secure military communications. One well known reason for increasing emphasis on spread spectrum techniques is that when the signal to noise ratio is necessarily low the only way of ensuring reliable communication is to exchange time-bandwidth product for power. Such large WT communication techniques require that the time and band-width have been spread in such a way as to enable the signals received over a given transmission channel to be compressed in the receiver processor to occupy again the minimum time and frequency intervals of the modulation. The object of this paper is two-fold. (i) To briefly review some techniques of spread-spectrum communication and (ii) present some of our own work. In the second category how the spread-spectrum techniques can be combined with existing modulation methods and can also be used to develop new efficient methods of modulation are described.

An obvious way of increasing the frequency occupancy of a message waveform having a given bandwidth is to modulate a larger number of coherent carriers by the message. Evidently such coherent carriers could be replaced by any alternating waveform of known structure and bandwidth. Pseudo-random (P.r.) and orthogonal code sequences provide such waveforms. Properties of such sequences and methods of generating them are considered in Sec. 1.

---

\* Present address: Institute of Radio Physics and Electronics, University of Calcutta, 92 Acharya Prafulla Chandra Road, Calcutta-9.

In time-frequency dispersal-accumulation techniques it seems imperative to employ pulse digital techniques for the purpose of matched filtering. Amongst pulse-digital modulation techniques  $M$ -ary, binary, pulse time modulation and delta modulation in conjunction with P.R. or orthogonal codes are discussed in Sec. II. Application of P.R. codes for determination of impulse response of a system is also discussed here.

Problems associated with synchronous as well as asynchronous multiplexing are considered in Sec. III. Techniques of synchronization in respect of the R.F. carrier phase, bit period and timing have also been discussed.

P.R. codes find an important application in random access shared channel communication, where a large number of signals carrying different messages share the same channel, every user having immediate access to all other users without central switching and each user being capable of separating signals intended from the total traffic present. Problems of multiplexing in such addressing and modulation techniques are considered in Sec. III. Waveform division multiplexing, time frequency matrixing, and code-frequency time matrixing applicable for binary PPM and DM are discussed.

It is felt that the quasi-Barker codes, the technique of maximum amplitude selection, code-frequency time matrixing and the sequential technique for decoding and estimation constitute useful new concepts.

## 2. P.R. SEQUENCES AND THEIR PROPERTIES

Processes characterised by unpredictable changes in time and exhibiting variations from observation to observation, which no amount of effort or control in the course of a trial can remove, are called random processes. However these processes also show regularities called statistical properties in a long series of trials. The statistical properties associated with random noise are the probability distribution of the amplitude and the auto-correlation function. In contrast, when a finite number of measurements of an ensemble determine the entire behaviour of the representative of an ensemble the process is called deterministic.

A pseudo-random time series is a deterministic time series having a finite number of states with known probability distribution, transition probabilities and specified transition times. The properties such a time series have in common with random noise are (a) an apparently bewildering complexity of wave form, (b) a peaked auto-correlation function and (c) a nearly zero average value if the time interval of observation is long compared with the correlation time.

It is known that the interval between the zero crossings of a noise waveform is a random function of time. It is not possible to regenerate such a characteristic and one has therefore to store the replica of transmitted noise waveform if



any coherent reception technique is to be employed. Since each part of the noise waveform is unpredictable and the length of the sample of the noise waveform must be large compared to the correlation period, the storage capacity of the processor must be very large. Pseudo-random sequences, on the other hand, can be generated deterministically. Further the peak factor of those sequences can be made quite small. Hence for purposes of application, P.r. sequences are preferred to samples of noise waveform.

P.r. sequences are specified by the number of states (corresponding to binary, ternary, quaternary, etc. systems), the probability distribution of the states, the minimum time interval between two successive transitions and the length of the sequence. Pseudo-random sequences of binary digits with equal probability of the states have been investigated for reasons of simplicity and suitability for application. Here a sequence is designated as binary if it consists of two states, i.e., presence and absence of a pulse (denoted respectively by 1 and 0).

Binary P.r. sequences can be generated by means of shift registers and modulo-two-adders. A device consisting of a consecutive binary storage positions, which shift the contents of each position, to the next in time, is termed a shift register. A modulo-2 adder is a logic circuit, which gives with two inputs  $A$  and  $B$  the Boolean output  $A\bar{B} + \bar{A}B$ . If the two inputs differ i.e., (01, or 10) then we get an output (1) and when the inputs are the same (11 or 00) then there is no output (0).

As an example one may consider a system consisting of a shift register with three storage positions and with the initial condition 101 and a mod-2 adder with its inputs from the first and third storage positions. If the output of the adder is fed back to first then for an initial condition 101 it goes through the succession of states 101, 010, 001, 100, 110, 111, 011, 101, ... and so on. The eighth state of course is the same as the initial condition set. So, at each of the shift registers and the modulo-2 adder we will get a sequence of ONES and ZEROS which repeat after a period of 7 units of the clock. At the three shift registers we will get outputs of (1001110), (0100111), ..., (1010011).

If on the other hand the inputs to the Mod-2 adder are the outputs of the second and third shift register, the sequence obtained is again of length 7, but assuming the same initial condition the output of the first shift register will be 0100011.

In general, the length of the sequence depends on the number of shift registers and the specific sequences obtained are determined by the logic.

It can be shown that the maximum period is  $L = 2^n - 1$ . The output sequences of this category are called maximal-length shift register sequences (Huffman 1956, Peterson 1961).

Special features of these sequences are :

- (1) In each period numbers of zeros and ones differ by at most unity.
- (2) Among runs of "one" and "zero" in the fine structure one-half runs of each kind are of length one. One fourth runs of each kind are of length 2, one-eighth of length 3 and so on.
- (3) Mod-2 sum of two such sequences is another such sequence.
- (4) If the period of such a sequence be considered term by term with any cyclic shift of itself, the number of agreements differs from the number of disagreements by at most one.

#### *Generation of maximal length binary sequences*

It has been discussed earlier how shift registers and modulo-2 adder can be used to generate the P.r. sequences. If the unit delay of the shift register be represented by  $D$ , then the law of formation of the sequence of length 7 is (a)  $F(D) = I(+)D(+)D^3 = 0$  or  $I(+)D^2(+)D^3 = 0$ . The two conditions imposed give rise to two different sequences. The length of the sequence in both the cases is 7 (as  $2^3 - 1 = 7$ ) and the the expression  $I(+)D(+)D^3$  and  $I(+)D^2(+)D^3$  are both prime factors. If the expression  $F(D)$  can be factorized then that condition if imposed on a sequence generator will give rise to a sequence of length  $2n^1 - 1$  where  $n^1$  is the highest power amongst the factors.

#### *Generation of any periodic sequence*

As mentioned earlier, a shift register can be converted into a sequence generator by including a feedback loop, which computes a new term based on the previous terms. If the sequence is specified, it is in general possible to obtain from the truth table (table 1) the logic for generating a given sequence, starting from any permissible initial condition. The logic for maximal length sequence of length  $L = 2^n - 1$  is given below for several values of  $n$ .

TABLE 1.

No. of stages (n)	Length of sequence (L)	Feedback from stages
3	7	2,3 or 1,3
4	15	3,4 or 1,4
5	31	3,5 or 1,3,4,5 or 1,2,3,5
6	63	5,6
7	127	4,7 or 6,7
8	255	2,3,4,5
9	511	5,9
10	1023	7,10

Generation of sequence of periods given by  $L < 2^n - 1$  is facilitated by the knowledge that all periods from 1 to  $2^n$  can be obtained from an  $n$  stage register with appropriate logic circuit. For example to obtain a sequence of length 11 one may start with a system for generation of a sequence of length 15 and derive appropriate output from a logical function generator to skip, route or recycle.

The block diagram for a sequence generator of length 11 or 13 is shown in figure 1.

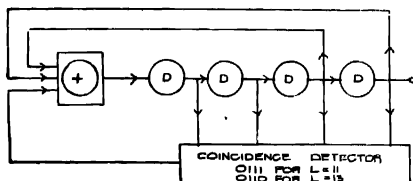


Figure 1. Schematic diagram of a P.R. sequence generator indicated mod-2-adder and D indicates delay unit. The coincidence detector is a logic circuit which gives an output (ONE) for the condition stated.

It may be mentioned that such sequence generators may be very conveniently used to count down by any factor.

To obtain sequences having large periods it is advisable to combine two or more sequences of smaller periods rather than realise it in a single stage.

When a sequence of a P.R. series passes through a band limited system (such as a filter) the shape of the pulses changes considerably. This change is maximum in case of transitions and is obviously small when the same state (one or zero) is continued. Such waveform distortion results in a considerable departure of the correlator output from the desired. This difficulty can be overcome if we can so arrange that the unit signals in every bit period are identical. In this case the change of shape is uniform for each bit and so all the properties of combinations of the series remain unaltered. This can be accomplished if we sample the series by pulse train of equal repetition rate but of shorter duration.

#### *Optimum correlation code for time modulation or ranging (Barker and Quasi-Barker codes)*

Some members of P.R. codes have the property that the correlation side lobe in the matched filter output is quite small. Barker(1953) has shown that there are sequences for which the correlation side lobe is as small as  $1/L$ . Such sequences are known only for length  $L = 3, 7, 11$  and  $13$ . It is possible to combine two or more Barker sequences to generate a new sequence in the following way. A

sequence of given length ( $m$ ) forms group or block. A new sequence of length ( $n$ ) is then constructed taking this group as a unit. Unfortunately, the side lobe amplitude in such case is rather high, being the larger of  $1/m$  and  $1/n$ . It seems therefore useful to enquire whether long sequences exist for which the minimum correlation side lobe is restricted to  $2/L$  or  $3/L$ . The study shows that some P.r. sequences have such property *e.g.*, for sequence of length 19, (1001001100001010111) matched filter output is 1, 0, -1, -2, 1, -2, -1, 2, -1, 0, -3, 0, 1, -2, 1, 0, -1, -2, 19. Similarly, for sequence of length 23 (0110, 0110, 01010000, 111101) matched filter output is -1, 2, -1, -2, 1, 2, -1, 0, 1, 0, -3, 2, -1, -2, -1, 0, -3, -2, 1, 0, -3, 0, 23). Such sequences are grouped here as quasi-Barker sequences.

### *Orthogonal codes and their properties*

It has been observed earlier that the cross-correlation output between any two signals of the same family of P.r. sequences is  $1/L$ . There is another class of signals which have zero cross-correlation between them. These are called orthogonal signals.

The most familiar example of an orthogonal code is a trigonometric orthogonal code. But in case of these type of codes the peak factor is large. Binary orthogonal codes are available which have very good peak factor. Such codes are generally related to orthogonal matrices which have been discussed by Paley and others. Paley (1933) has shown that orthogonal matrices of order  $m$  can be formed if either of the following conditions is satisfied.

- (a)  $m = 2^k$
- (b)  $m = p+1$ ,  $p$  is a prime and  $p \equiv 3 \pmod{4}$
- (c)  $m = 2^k(p+1)$ ,  $p$  is prime.
- (d)  $m = 2^k(p^h+1)$ ,  $p$  is an odd prime,  $m$  is divisible by 4.

Instead of quadratic residue  $\pmod{p}$  we consider quadratic residue in Galois field of polynomial,  $\pmod{p_0}$ ,  $\pmod{f(x)}$  where  $f(x)$  is an irreducible polynomial of degree  $h$ . Thus for instance,  $x^h = 3 \pmod{4}$   $k = 0$ .

- (e)  $m = 2^k p(p+1)$ ,  $p \equiv 3 \pmod{4}$  and  $p$  is prime.

Let us consider an example of an orthogonal matrix belonging to group (b), i.e.,  $m = p+1$ , where  $p$  is a prime number and  $p \equiv 3 \pmod{4}$ . The coefficient  $A_{ij}$  of the orthogonal matrix will be taken to be 1, if  $(i-j)$  satisfies the condition that it is a quadratic residue of the prime number, i.e., if a number  $x$  (say) such that  $x^2 - k = 0 \pmod{p}$  exists, where  $k$  equals  $(i-j)$ . Further  $A_{ij}$  may be taken to be equal to -1 and  $A_{io}$  or  $A_{oi}$  is equal to 1. One row of the orthogonal matrix constructed in the manner indicated with  $m = 12$  can be represented as 111100010010.

If we require the signals to be resolved in frequency then we will choose such signals which have power spectrum distinct and different for different members of the codes. But if we require resolution in time then the power spectrum should be the same for different codes but they should have distinct wave-shapes with reasonable separability in time.

P.r. sequence can never be used where we require resolution in frequency but orthogonal code can be used for both. It will be observed that while orthogonality is independent of interchange of columns, the actual value of the cross-correlator output for a given shifts may be minimised by such interchange.

### *Generation of orthogonal codes*

As mentioned earlier orthogonal trigonometric codes may be generated by combining trigonometric functions which have the same fundamental periods. Obviously the functions  $\cos wt$ ,  $\cos 2wt$ ,  $\dots$   $\cos nwt$ ,  $\sin wt$ ,  $\sin 2wt$   $\dots$   $\sin nwt$  are mutually orthogonal. Linear combinations of these functions will also be found to be orthogonal if appropriate weighting factors are used. For instance

$$f1(t) = \cos wt + \cos 2wt + \cos 3wt + \cos 4wt \quad \text{and}$$

$$f2(t) = \cos wt - \cos 2wt + \cos 3wt - \cos 4wt$$

are mutually orthogonal.

The difference between primary and combination functions is that the spectral regions occupied by the primary functions are different while for the combination functions the spectral regions occupied overlap.

Binary orthogonal sequences can be obtained by combining short pulses of appropriate duration, sign and delays to obtain different codes. One obvious method of obtaining several short pulses is to excite a number of monostable multivibrators in a chain, each pulse being generated from the trailing edge of the previous pulse and then to add them with proper sign.

An easier approach to this problem, as shown in figure 2, is to use the waveform obtained from dividers formed by a chain of bistable multivibrator operated serially, these waveforms constituting members of an orthogonal family. The rest of the members are obtainable from mod-2 sum of the primary members. This type of system can produce code family of length  $L = 2^n$ .

If the length  $L \neq 2^n$ , then this idea is no longer suited. However, a general technique is available for generating binary orthogonal codes. This consists of adding a single pulse of proper polarity at the start of a P.r. code of length  $(L-1)$ . The first position of these codes is always the pulse added, whereas the next  $(L-1)$  positions correspond to the one of the P.r. sequences. This idea can also be extended for sequences having length  $L = 2^n$ .

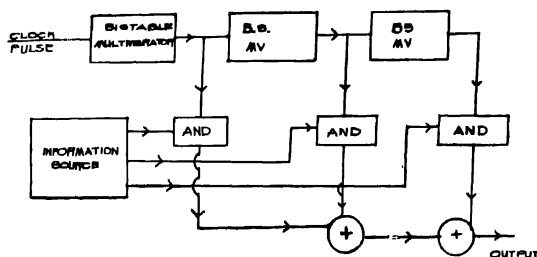


Figure 2. Schematic diagram of an orthogonal sequence generator employing binary flip-flops and logic circuits.

### 3. COMMUNICATION BY P.R. CODES

We have already observed that P.R. and orthogonal sequences have the following important properties—(a) these permit time-compression by a very large factor and have good resolution in time, it being possible to resolve sequences separated in time by an interval equal to the period, (b) sequences belonging to the same family and synchronous in time can be separated out with little or no mutual interference, and (c) it is possible to accumulate the signal voltages of all the individual signals spread over in time, so that the signal strength at the instant of matching is equal to  $LS$  where  $L$  is the sequence length and  $S$  is the signal voltage in any bit period, while the resultant noise voltage due to incoherent summation will be equal to  $\sqrt{L}N$  where  $N$  is the noise voltage in any bit period. These properties recommend the use of such sequences particularly in situations where signal to noise ratio is very small for ranging application and time modulation, waveform multiplexing in binary modulation and the so-called  $M$ -ary modulation.

In this section we wish to discuss the application of wideband codes P.R. or orthogonal, for communications and the advantages arising from such applications.

#### *M-ary Modulation*

We shall first consider  $M$ -ary modulation technique which is known to be an optimum coding method. In  $M$ -ary modulation, one of  $M$  alternative sequences is transmitted at a given time in accordance with the given state of the message source. These sequences, like samples of noise waveform, have little or no cross correlation if the integration is carried out over the appropriate time interval. In the receiver the decision with regard to which sequence has been sent is made on the basis of the comparison between the outputs of  $M$  correlators. For speech signal, analogue speech signal is first sampled and quantized and then the sampled signal is converted into pulse code. This p.c.m. code is now used as the initial

condition of the P.r. sequence generator or orthogonal sequence generator. Thus we get different sequences according to different amplitudes of the sample speech signal.

The technique of reception and decoding almost always employs matched filtering technique. In this type of reception we shall require as many receiver processors as there are possible sequences, a particular processor corresponding to a specific sequence. The decision with regard to which sequence has been transmitted will have to be made on the basis of magnitude of the output of the matched filters and the sequence that gives the largest output will be selected. A correspondence between the line selected and the analogue voltage may then be established.

To decide which sequence has been transmitted, the technique available is to use the parallel detection method where the received input signal is multiplied with all the possible sequences and the averages of the multiplied outputs are noted. The average of the multiplied outputs are sampled and the samples are fed to a decision circuit to determine which has the maximum value. This maximum is an indication of which sequence has been transmitted. Figure 3 shows the mechanization of a maximum likelihood decoder. For such a decoder we will require as many multipliers, integrators and samples as there are possible sequences. The size of the decoder becomes unwieldy if the number of sequences is large.

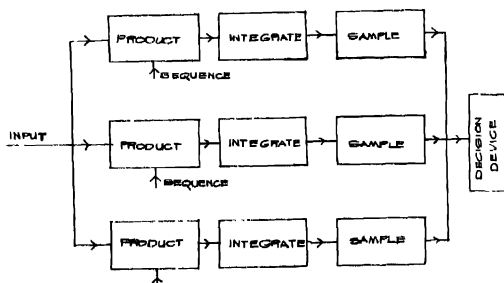


Figure 3. An optimal parallel decoder for M-ary modulations.

The size of the decoder can be minimised to a great extent if we use the serial technique in which the signal is compressed in time by means of a time compressor (Weber 1964), the compressed signal is stored and correlated with the different time shifted versions of the receiver P.r. sequence serially, the correlation outputs occurring serially being then examined for maximum amplitude. To achieve this the time of occupancy of each original signal component must be reduced to at least  $T/n$ , where  $n$  is the number of samples to be accommodated.

In such a technique of detection, the number of multipliers, integrators and samplers can be reduced to one only, whatever be the possible number of sequences to be received. In the parallel detection method one must have all the time shifted replicas of the sequence present simultaneously. Such a scheme is purely impractical especially when the length of the sequence is large. But in the case of serial decoding as one will be testing the sequence serially, the receiver sequence generator need be the conventional maximal length sequence generator. The schematic diagram for such a detection technique is shown in figure 4.

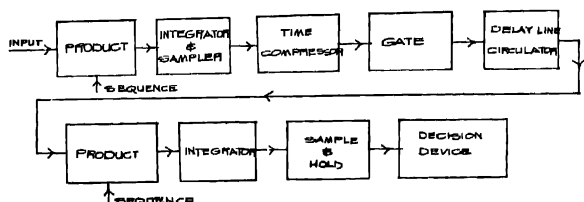


Figure 4. Schematic diagram of a serial decoder for M-ary modulation.

The received signal is first integrated and the integrated outputs at the end of each bit are sampled and these samples are then compressed in time. If  $T'$  secs be the bit period of original sequence of length  $L$  then after the time compression each sequence will only be occupying  $T$  secs. Then this compressed sequence whose period is also  $T$  has bit period  $T/L$ . It is clear that for such processing we are to have the input received sequence present for a period till all the time shifted replicas of the sequence are tested. For this purpose we use a delay line type circulator whose delay is equal to  $T'(1 - 1/L)$ . This enables correlation of the input in the receiver sequences time shifted by units of one bit period. After all the sequences are serially tested we require the circulator to be discharged and ready for testing of the next sequence. Now the minimum discharge time of a delay line is equal to the amount of delay produced by it. So, the total time taken for a full operation is  $(LT' + 2T)$ ,  $(LT' + T)$  for testing and approximately another  $T$  for discharging. Thus while the coding is done we must have a gap of  $2T'$  seconds after each sequence of period  $nT'$  seconds.

The output of the multiplier is integrated and sampled at instants of matching for the different sequences and stored. When all the results have accumulated the same decision technique as used in the case of parallel method is employed.

#### *Maximum amplitude selection*

In  $M$ -ary communication the decision process involves determination of the particular code word on the basis of comparison between the output of matched filters. This requires selection of line giving maximum amplitude from amongst



*M* lines. The similarity to selection diversity switching may be noted here. For the purpose, all the line amplifiers should have an automatic gain control arrangement operated by the average amplitude. This type of common degeneration may be combined with individual amplitude dependent regeneration for accentuating the difference in level between the outputs of different lines. If it so happens that even after such treatment more than one line has an output exceeding the threshold, the amplifiers associated with this may be biased by the average of the outputs to eliminate all but the strongest component.

One technique which seems promising is to use multi-level *FM* in the receiver, that is, to use the outputs of the different 'alphabet' channels to amplitude modulate a set of carriers displaced in frequency and utilize strong signal capture phenomenon for the threshold decision circuit

### *Binary modulation*

In case of binary modulation there will be only two states to transmit. These two states may be (a) a sequence or its absence, (b) alternate polarity of the same sequence, and (c) one of two orthogonal sequences.

Amongst these bipolar mode seems to be the desirable mode of operation. The two-sequence mode results in a more complex receiver, while off-on mode does not give the best SNR. In the bipolar mode the selected sequence will have a positive polarity for a positive polarity of the input, the sequence generator being timed in accordance with the timing sequence of the transmitter. In such operation it is desirable to select a Barker (1953) type code for the sequence, for such codes have the best available correlation properties. In the receiver one need have a matched filter matched to the particular Barker code transmitted and the reception technique must be a synchronous one suited for reception of bipolar signals.

### *Pulse position modulation*

As mentioned earlier P.r. codes having very good resolution in time are eminently suited for use in ranging and hence in pulse position modulation. For obtaining P.P.M. signals analogue speech signal is first processed by a threshold circuit to remove voltage below a certain amplitude. This processed signal is now amplified and sampled. The sampled signal is then used to position modulate the pulses. If now the position modulated pulses are used to trigger the P.r. sequence generator (preferably a Barker code) then we will get sequences having the starting point varying in proportion to the amplitude of the sample.

In case of reception the knowledge of which sequence is being transmitted must be built into the receiver. The receiver is to decide from the correlator output about the starting time of the sequence. Here one may usefully employ matched filter technique to find the time of occurrence of the maximum amplitude of pulse.

A method of determining this is to use the technique of a voltage saw-tooth reset by the matched filter output. In this case a saw-tooth wave generator is triggered at the beginning of each frame. The matched filter output pulse if it exceeds certain threshold level is used to reset the saw-tooth wave generator. The maximum amplitude obtained by the saw-tooth generator is then a measure of time of occurrence. Such a simple technique is directly applicable provided the probability of spurious signal exceeding the selected threshold is very small. A modification of the above for finding the time of occurrence of a pulse having the maximum amplitude in a selected time interval in the presence of spurious pulse and interference is however available. In this case the input pulses are applied to a peak charging diode; if the incoming pulse has an amplitude greater than the value of the voltage across the peak measuring device, a pulse of short duration is generated by the comparator. The output of the comparator is used to reset the free-running saw-tooth generator. The synchronised voltage for the saw tooth generator is obtained from p.r.f. generator as in figure 5.

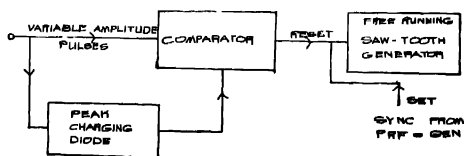


Figure 5. Arrangement for selecting the pulse having maximum amplitude.

### *Delta modulation*

P.r. or orthogonal codes may be employed with any pulse modulation system by replacing the single pulse ordinarily used by the sequence. The additional unit required in such a case is a matched filter at the receiver. In the case of Delta modulation ( $\Delta-M$ ) or Delta-Sigma ( $\Delta-\Sigma$ ) the pulse obtained from the conventional modulator may be used to obtain P.r. or orthogonal sequences of desired length. It should be observed that time gating for synchronous  $\Delta-M$  in the output of the matched filter of the receiver provides in this case a very useful technique of interference reduction. In fact  $\Delta-M$  is indeed a viable technique for random access. It is the simplest analogue to digital conversion technique and has all the well known advantages of digital communication. It has a low pulse rate and low duty cycle compared with other digital modulation. Further, one has only to transmit pulses of one polarity and techniques for removal of redundancy can be readily incorporated which together enable realization of a duty factor of about 0.30.

*P.r. sequence as a test signal*

It is well known that impulse response of a linear system can be determined by cross-correlating the input and the output if the input is white noise. From the convolution theorem one has

$$y(t) = \int_0^{\infty} x(t-t_1)h(t_1)dt_1$$

where  $y(t)$  and  $x(t)$  are the output and the input respectively and  $h(t)$  is the impulse. Multiplying both sides by  $x(t-\tau)$  and integrating one gets,

$$\phi_{yx}(\tau) = \int \phi_{xx}(\tau-t_1)h(t_1)dt_1$$

if  $\phi_{xx}(\tau-t_1) = \delta(\tau-t_1)$ , then  $h(\tau) \approx \phi_{yx}(\tau)$ .

It is obvious that pseudo-random waveforms with their highly peaked autocorrelation function approaching a delta function provide a better alternative than pure noise signals for the purpose of system identification, because of the simplicity of generation, storage and processing of the experimental data.

### 3. MULTIPLEXING AND RANDOM ACCESS

Pulse-digital modulation systems may be classified as synchronous or a synchronous according as there is time synchronism between the events or not, *i.e.* the time of arrival of the signal or the instant of time when the transition occurs in a precisely known period.

Channels are ordinarily multiplexed by means of either frequency division or time division multiplexing. A different technique of multiplexing can however be realized by means of orthogonal or pseudo-orthogonal codes in combination with time frequency matrixing. This type of multiplexing is usually asynchronous as its operation does not depend on allocation of specific time slots to the different signals and their synchronous routing at the receiving terminal.

Asynchronous systems find use in so called "Random Access" communication. In a random access system signals arise from sources dispersed in a random manner in location and time and users are allowed access as desired to a wide band channel and should be able to separate signals intended for them from the common channel. Obviously, the multiplexing here must also include a type of "addressing".

We intend to discuss here the technique of multiplexing that may be employed for binary modulation, P.P.M. and  $\Delta-M$ .

In case of binary modulation one may use what may be called waveform division multiplexing where different signals in the channel are allocated specific waveform codes. These waveform codes are selected in such a way that the filters matched to the different waveforms at receiving end are able to select only the desired wave and reject the others. An important parameter in this connection

is the peak height of the mutual correlation between the different wave-forms, which obviously must be kept below a certain maximum. This consideration precludes the use of members of pseudo-random code derived, for example, from a maximal length sequence unless only a few of the total number of possible sequences which are widely separated in time are used.

*Further it is found that even for orthogonal codes the maximum value of the cross-correlation output may be as large as  $L/2$ , where  $L$  is the length of the sequence, although the output of the correlator due to any undesired code is zero at the instant of matching. This causes severe mutual interference in asynchronous code division multiplexing. This problem is absent in synchronous multiplexing as in this case the outputs are observed only at precisely known instant of matching. One may in a large measure remove this difficulty by using time frequency matrixing, where code modulated bursts at different frequencies are arranged in a specific order in time for a given signal. Consider that the total signal time is divided into three intervals  $T_1$ ,  $T_2$ , and  $T_3$  which can be occupied by pulsed sinusoids of frequency  $f_1$ ,  $f_2$ , and  $f_3$ . For a particular channel one may allocate the matrix element  $f_1T_1$ ,  $f_2T_2$ , and  $f_3T_3$ . At the receiver particular signal can be selected by delaying the output at frequency  $f_1$ ,  $f_2$  by  $T_3 - T_1$  and  $T_3 - T_2$  and combining the output at three frequencies. The resultant output will obviously be large, only for this particular matrix element. For combining the outputs two approaches are available—pre-detection and post detection combination. In the case of pre-detection combination, the r.f. outputs at the three frequencies may be brought to the same frequency and phase lock circuits may be employed to phase the three signals and add them. The combined output is then fed to the matched filter detection and decision circuit. In the case of post detection combination the outputs at the three frequencies are fed to the matched filter detected, added and applied to decision circuit.*

The above mentioned multiplexing technique can be employed in channels using binary phase-shift keying (PSK). In the case of code division multiplexing, it is necessary to distribute the static phases of the carrier uniformly over  $2\pi$  radians in order that the peak factor of the sum signal could be kept within a reasonable limit. It is instructive in this connection to find the mean, r.m.s. and peak of the amplitude of the sum of  $N$  bipolar voltages (a) if the r.f. reference phase is the same for all and (b) if the r.f. phases are distributed uniformly for  $2\pi$  radians.

For P.P.M. system using P.r. codes several techniques of multiplexing are available. One may for example use different codes obtainable from a code generator for multiplexing the channel. The code selected should obviously be such as to give rise to small mutual interference. The advantage arising from such multiplexing is that the amount of permissible range of time modulation is large and is given by  $T_r - LT$  where  $T_r$  is the repetition period,  $L$  the length of the

TABLE 2

	N = 4		N = 6		N = 8	
	(a)	(b)	(a)	(b)	(a)	(b)
Max	4	2.8	6	$\sqrt{12}$	8	5.2
rms	2	2	$\sqrt{6}$	$\sqrt{4.5}$	2.19	2.8
mean	3/2	7/4	15/8	15/8	3.43	2.4

sequence and  $T$  is the bit period. Further, such a system does not require synchronization and can therefore be used for random access communication. There will however be some amount of mutual interference between the channels, the magnitude of which will depend on the total number of active channels at a given time, the cross-correlation property of the codes and the signal statistics at different channels. It should be reasonable to expect that the different signals arising from different sources will be uncorrelated and consequently the actual interference can be thought of as due to randomly time modulated pulse trains. Time frequency matrixing using the same code, preferably a Barker or a quasi-Barker one may also be employed.

It should be realized that sometimes different interfering signals together may give rise to particular  $f-t$  ordering of code thus producing a false output. To reduce the amount of false output one has to select only a limited number of possible combination of  $f-t$  codes which can be formed with the given set of frequencies.

#### Code-frequency-time matrixing

In frequency time matrixing, the distinct addresses available depend on the number  $m$  of distinct frequencies used. Although this number would appear to be large, the actual usable combinations are rather few if false addressing is to be kept low. For example, using three frequencies one finds that acceptable combinations are instead of eight only three, provided by the cyclic permutation i.e.  $(f_1t_1, f_2t_2, f_3t_3)$ ,  $(f_2t_1, f_3t_2, f_1t_3)$  and  $(f_3t_1, f_1t_2, f_2t_3)$ . It will be observed that the contribution from any interfering source to the desired address is at least  $1/m$  times the correlation peak, where  $m$  is the number of frequencies used. Identical remarks apply, *mutatis mutandis*, to code time matrixing.

In code-frequency-time matrixing one can take advantage of the quasi-orthogonality between the selected code and frequency-time ordering to realize combination addresses with very small mutual interference. If we take three mutually orthogonal codes and three distinct frequencies the following three combinations  $(M_1f_1t_1, M_2f_2t_2, M_3f_3t_3)$ ,  $(M_3f_2t_1, M_1f_3t_2, M_2f_1t_3)$  and  $(M_2f_3t_1, M_3f_1t_2, M_1f_2t_3)$

$M_1 f_1(t_2)$ , obtained by taking the diagonal elements of the admissible  $M$  and  $f$  matrices, will be found to have excellent resistance to interference.

### *Synchronization*

A digital receiver requires timing information in order to interpret the received signal sequences properly; when the value has become fully, each symbol in the sequence must be sampled at a time established and is not in a condition of transition

It will be recalled that an optimum receiver correlates received code word with the locally generated replica. Consequently, the instant in time in which one received word ends and the successive word begins must be known accurately. Besides, a suitable carrier for coherent demodulation must also be established and maintained. Thus there are three parameters to be synchronized, r.f. carrier, phase and frequency, word timing and bit timing. Techniques of r.f. synchronization are quite well established (Chakraborti & Biswas 1964, Chakraborti & Dutta 1966, 1967, Chakraborti 1964, Costas 1959) and will not be considered here.

To find word timing an automatic time control arrangement using a differential coincidence circuit may be used. In such a case one finds two correlations : (a) the correlation  $R_1(t) = \overline{f_i(t)}\overline{f_r(t)}$  between the input  $f_i(t)$  and the replica at the receiver  $f_r(t)$  and (b)  $R_2(t) = f_i(t)[f_r(t-T) - f_r(t+T)]$  where  $T$  is one bit period. The product of these correlations is then used to control the timing of the function. Such a technique may be termed self-synchronizing technique. Another technique is to insert an auxiliary synchronizing pattern periodically in the channel. If a pattern is chosen which cannot occur as part of the data sequence then position identification of the pattern establishes synchronization. It is obviously desirable to make the correlation between all the data sequences and the synchronizing pattern as small as possible. A satisfactory synchronizing pattern is one which gives very small output of the matched filter except at the instant of matching. Use of Barker sequence and quasi-Barker sequence seem appropriate here.

For synchronization when bipolar modulation with a single Barker or quasi-Barker code is employed the arrangement shown in figure 6(a) may be used. When the signal as transmitted contains the code component, that is, the transmitted signal is obtained by mod-2 addition of the code and the clock, the arrangement marked may be used. Another r.f. phase lock circuit applicable for bipolar phase modulation is shown in figure 6(b).

### *Sequential technique*

An important consideration here is the time required to effect acquisition of the code or synchronization. The Auto-correlation function of a P.r. sequence does not provide any indication during the search process of which way or how

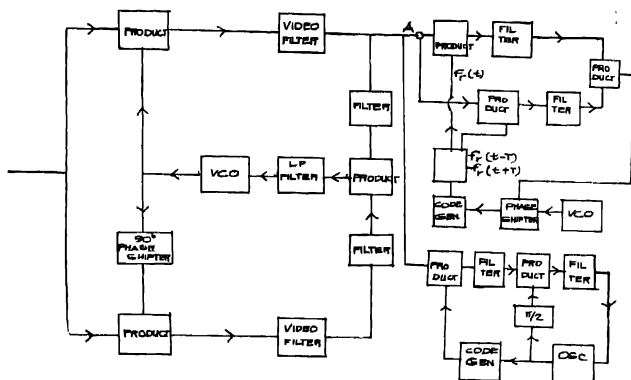


Figure 6(a) Schematic diagram of a circuit for achieving R.F. Phase lock and synchronization of the bit period and timing. Circuit to the left of  $A_1$  represents a typical phase lock circuit for bipolar A.M.

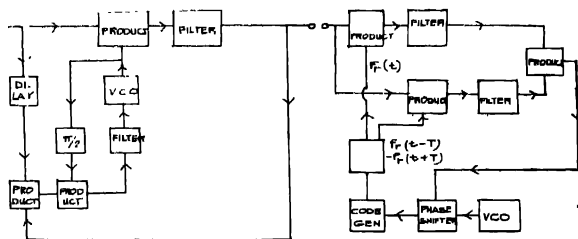


Figure 6(b) An alternative form of the phase lock circuit for bipolar modulation.

far to shift the local replica in order to bring about coincidence once it is outside the working zone. One has therefore to make trial correlation and find which code-shifts yield the highest correlation. The acquisition time therefore is rather very high compared to the information bits ( $\log 2L$ ), while in the absence of noise the sequences is completely determinable from one trial inspection of  $n$  digits. When the signal energy relative to the background noise is sufficiently high, the number of trials can be sufficiently reduced if the code is made up of several short sub-codes that can be acquired individually.

It will be recognized that in the absence of noise optimum acquisition technique is to introduce the first  $n$  received bits as the initial conditions of the receiver sequence generator which will then continue to produce a sequence approximately in phase with the incoming sequence. Errors arising may be corrected by the

tracking loop. However as the input invariably contains noise, it is necessary to find, by means of cross-correlation between the input sequence and the receiver sequence, whether initial estimate is correct. If the agreement between the two is not good, new data may be introduced and the process repeated in such a way as to (taking advantage of the longer integration time) enable rapid acquisition. New trials made on introduction of the new data need not destroy the information obtained from earlier trials. In such sequential estimation technique the length of the trial, which must be kept above a minimum to avoid false alarm and false dismissal, depends upon input signal to noise ratio. The acquisition time can therefore be kept small if the SNR is adequate.

### *Matched filter technique*

Matching means optimization of a receiving system to extract the desired signal from a noise background maximising the signal to noise ratio. In essence matched filter technique is the same as correlation detection technique. There is a variety of ways by which the optimization process can be physically effected but some of them can be thought as correlators and others as matched filters.

The matched filter processors depend on (1) the nature of the signal, (2) the accompanying noise statistics and the way it combines with the signal and (3) the optimization required. The first two are essentially *a priori* data and the third one is the choice of criterion. Generally, the choices are all based on the energy calculation, i.e., on some form of maximization of signal energy to that of the noise. Usually the matched filter design is obtained by maximization of signal to noise ratio (S/N matched filter).

### *Matched filter for a specific binary sequence*

When the specific binary sequence of length  $L$  is being received the output of the matched filter at the instant of matching must equal  $L$  times the amplitude of each unit. This requires that the impulse response of the matched filter be a time reversed replica of the input sequence. For a binary sequence of 0100111 (zero signifies negative polarity) the impulse response of the matched filter must be 1110010. The output of the matched filter is then  $-1, 0, -1, 0, -1, 0, 7, 0, -1, 0, -1, 0, -1$ .

Such matched filter may be easily realized by means of delay line having seven taps, with the delay between consecutive taps being equal to the delay between unit signals of the binary sequence, and the output obtained at the different taps being combined with appropriate polarity.

It is well known that a tapped delay line with resistor weights at each tap constitutes a linear filter. The array of resistors with different amplifiers for obtaining positive and negative value represents the impulse response of the filters.



The delay line accepts the incoming signal translating it across the spatially distributed resistor weights. The maximum output at the adder occurs at the instant when the desired signal fills the delay line.

The delay line may take a variety of forms (i) analogue LC or ultrasonic delay line or (ii) digital delay line. The ultrasonic delay line is essentially a band pass delay line and may consist of an array of barium titanate transducers coupled to any sonic solid media having small dispersion. If the input signal is translated down in frequency to video infinitely clipped and sampled then the analogue delay line may be replaced by a digital delay line such as shift register, operated by a clock having a repetition period equal to the required unit delay. The advantage of a digital delay line is that at each tap (trigger stage) the signal is regenerated and that precise timing can be achieved consistent with accuracy inherent in digital technique. Digital shift register permits the realization of extremely long high speed matched filter. Further the system is very readily adjustable for variable bit period while this poses a serious problem in any analogue delay line. The principal disadvantage is that as the input signal at a relatively low level has to be clipped, threshold effect causing suppression of the signal by the noise sets in. Finally for a band pass matched filter two video matched filters one each for the two quadrature channels will be needed.

#### *Concluding remarks :*

In this paper we have discussed only the basic concepts involved in the utilization of P.r and orthogonal codes in spread spectrum communication. Detailed experimental investigation of the concepts and practical embodiment of such utilization will be described in communications to follow. One point may still be made. The problem of generation and encoding is quite simple; the decoding technique on the other hand is quite complex. It would seem desirable to concentrate efforts on serial decoding (section 2) and sequential estimation aimed at simplification of circuitry and reduction of processing time.

#### ACKNOWLEDGEMENT

A part of this work was done at the Institute of Radio Physics and Electronics, Calcutta. The authors are grateful to Prof. G. S. Sanyal for his kind interest and encouragement. Their thanks are due to Dr. J. Das and Mr. R. C Ganguli for helpful discussions.

#### REFERENCES

- Barker, R. H. 1953 *Communication Theory*, W. Jackson (Editor) Butterworths Scientific Publications, London, 273.  
Chakraborti, N.-B. & Biswas, B.N. 1964 *Indian J. Phys.* **38**, 148.  
Chakraborti, N.B. & Dutta, A.K. 1966 *Indian J. Phys.* **41**, 501.

- Chakraborti, N.B. & Dutta, A.K. 1967 *Indian J. Phys.* 41, 87.
- Chakraborti, N.B. 1964 *Proc. I.E.E.E.* 52, 1248.
- Costas, J. P. 1959 *Proc. I.R.E.* 47, 2058.
- Golomb, S. W. 1965 *Digital Communication with Space Application*. Prentice Hall Inc. Englewood Cliffs, N. J.
- Harmuth, H. F. 1960 *Proc. I.E.E.*, 107, 242, Monograph No. 369E.
- Harmuth, H. F. 1961 *Proc. I.E.E.*, 108, 139, Monograph No. 405E.
- Huffman, D. A. 1956 *3rd. London Symposium on Information Theory*. Cherry Ed. Butterworths Scientific Publications, London, 77
- Middleton, D. 1960 *Statistical Communication Theory*. Mc-Graw Hill Book Co. New York.
- Paley, P. E A C 1933 *Journal of Mathematics and Physics*. 12, 311.
- Peterson, W. W. 1961 *Error Correcting Codes*. John Wiley Sons Inc.
- Shannon, C. E. 1949 *Proc. I.R.E.* 37, 10
- Weber, S. 1964 *Modern Digital Circuit*. Mc-Graw Hill Book Co., New York.
- Woodward, P. M. 1955 *Probability and Information Theory with Application to Radar*. Pergamon Press Ltd, London.

## ESR and optical absorption studies on certain copper complexes

By P. V. GOPALAKRISHNA MURTHY

*Department of Physics, Andhra University, Waltair, India*

(Received 7 November 1969—Revised 11 May 1970)

(Plate—1)

ESR and optical absorption studies are made in the four copper complexes: 1. Copper bis-(ethylenediamine) thiocyanate, 2. Copper bis-(ethylenediamine) fluoborate, 3. Copper dipyridine thiocyanate, 4. Copper tetrapyridine fluoborate. For the first two, both single crystal and powder measurements have been made. The principal  $g$ -values are estimated from an analysis of the observations in all the complexes. A considerable covalency in the metal ligand bonding is indicated.

### INTRODUCTION

ESR studies of different copper complexes with ligands such as  $H_2O$ ,  $N_2$  and  $O_2$  etc. have been the subject of a large number of investigations (Bleaney *et al* 1949, Abe *et al* 1956, Rajan 1962, 1963, Rajan *et al* 1963). In particular, Maki *et al* (1959) and later Neimann *et al* (1961) have shown in their analysis of the ESR spectra of a number of these complexes, the importance of this method in understanding the nature of the bonding of the copper ion with its ligands. Among these complexes the ethylene-diamine derivatives are of interest, as in these the copper ions are surrounded by nitrogen atoms of ethylenediamine, resulting in a considerable covalency in the metal ligand bonding, different from that in ordinary  $[Cu(H_2O)_6]^{2+}$  complexes (Bose *et al* 1964, Ghosh *et al* 1965). The present work deals with measurements at room temperature on four such complexes, which have not yet been investigated. These are copper bis-(ethylenediamine) thiocyanate,  $Cu(en)_2(SCN)_2$ , copper bis-(ethylenediamine) fluoborate,  $Cu(en)_2(BF_4)_2$ , copper dipyridine thiocyanate,  $Cu(py)_2(SCN)_2$  and copper tetrapyridine fluoborate,  $Cu(py)_4(BF_4)_2$ , for the first three of which, crystal structure data are available in literature (hereafter these will be referred to by their respective numbers given earlier). In the case of 1 and 2, single crystals as well as powder samples are studied. One advantage in each of these two crystals is that there is only one molecule in the unit cell and hence, the ESR spectra are expected to be simple without the complications that arise from the overlapping of spectra when there are two or more ions in the unit cell. An analysis of the experimental results has been attempted in terms of symmetry considerations that could be inferred from the known crystal structure. For 3 and 4 the other two substances, only powder specimens are investigated since difficulties

have been experienced in obtaining them in the form of good single crystals suitable for investigation.

Optical absorption measurements have been made on all the four substances in solution. The results are given in the following sections.

### EXPERIMENTAL

The ESR measurements have been carried out with the spectrometer used previously by the author (1968). The optical absorption measurements have been made on a Hilger U.V.I (ultraviolet and visible) spectrophotometer in the range 350m $\mu$  to 700m $\mu$ .

The complexes are prepared as in previous investigations on their crystal structure. The methods of preparation and the known crystal structures are briefly given below.

#### 1. $Cu(en)_2(SCN)_2$

This is prepared (Bruce *et al* 1964) by the addition of stoichiometric amount of ethylenediamine to an aqueous solution of copper sulphate at room temperature. Conversion to the thiocyanate is then done by the slow addition of barium thiocyanate solution with rapid stirring and filtering off the precipitate of barium sulphate. The filtrate is vacuum dried over anhydrous calcium chloride. Violet prismatic crystals of the anhydrous compound are then obtained by slow cooling of a hot methanol solution. The crystals are tablets on (101) elongated in  $b$  direction, reported by Bruce *et al* (1964) as belonging to the triclinic system of space group  $P\bar{1}$ , the lattice constants being:  $a = 7.352 \text{ \AA}$ ,  $b = 9.364 \text{ \AA}$ ,  $c = 6.585 \text{ \AA}$ ,  $\alpha = 86^\circ 56'$ ,  $\beta = 113^\circ 25'$ ,  $\gamma = 125^\circ 08'$  density  $\rho = 1.57$   $Z = 1$ .

#### 2. $Cu(en)_2(BF_4)_2$

This has been prepared by dissolving basic copper carbonate in fluoboric acid and adding ethylenediamine. Violet coloured crystals separate out. These are recrystallized from methanol solution. Single crystals of required size are obtained by slow evaporation of the solution. These are (Brown *et al* 1968) also triclinic, of space group  $P\bar{1}$ , with the following lattice constants:  $a = 7.42 \text{ \AA}$ ,  $b = 8.22 \text{ \AA}$ ,  $c = 5.92 \text{ \AA}$ ,  $\alpha = 100^\circ 54'$ ,  $\beta = 105^\circ 12'$ ,  $\gamma = 106^\circ 00'$ ,  $\rho = 1.84$   $Z = 1$ .

#### 3. $Cu(py)_2(SCN)_2$

Green coloured copper dipyridine thiocyanate, insoluble in water, is obtained by the reaction of copper sulphate with potassium thiocyanate and pyridine (Encyclopedia of Chemical Reactions. Vol III, Article II 1285, 1949). According to Porai-Koshits *et al* (1959) the crystals are monoclinic and belong to the space group  $C_2/m$  with two molecules in the unit cell.

4.  $\text{Cu}(\text{py})_4(\text{BF}_4)_2$ .

The preparation of this sample given by Ibers (1953) is similar to the fluoborate, the ethylene diamine having been replaced by pyridine. A fine deep blue crystalline substance is obtained and it is purified by recrystallization from ethanol solution. Although for this compound detailed crystal data are not available a morphological study reported by Ibers indicates an orthorhombic bipyramidal type of structure of space group  $P2_12_12_1$ , there being four molecules in the unit cell.

## RESULTS

A (1) *Single crystals of 1 and 2*

The ESR observations on single crystals could be taken only on the first two compounds. In both these triclinic crystals, a set of orthogonal axes,  $a^*$ ,  $b^*$ ,  $c^*$  have been chosen in order to facilitate the evaluation of the  $g$ -tensor from experimental observations. These are related to the crystallographic axes  $a$ ,  $b$  and  $c$  as follows:  $c^* = c$ ,  $b^*$  axis is in the  $bc$  plane and perpendicular to the  $c$ -axis,  $a^*$  is perpendicular to  $b^*c^*(=bc)$  plane. The angular variation of the ESR spectrum is studied in the planes,  $b^*c^*(=bc)$  and  $a^*b^*$  (a plane perpendicular to  $c$ -axis) and  $ac$  plane. The angular variations of  $g^2$  in the  $a^*b^*$  and  $b^*c^*$  planes in the first (1) and second (2) crystal, respectively, are shown in figures 1 and 2.

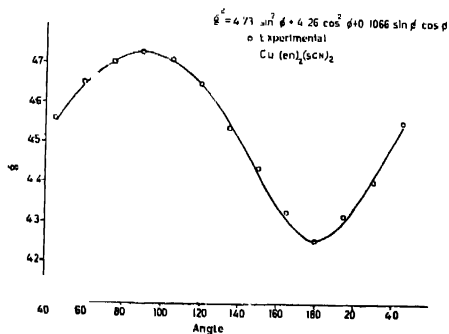


Figure 1.  $g^2$  variation in  $\text{Cu}(\text{en})_2(\text{SCN})_2$  in  $a^*b^*$  plane.

As the crystals contain one molecule in the unit cell, a simple direct method is adopted for the calculation of the  $g$ -tensor, as was done in the case of dibarium copper formate tetrahydrate (Ramasubba Reddy *et al* (1957), which also crystallizes in the triclinic system and contains only one molecule in the unit cell. This

procedure is based generally on those developed earlier by Pryce (1950), Weil *et al* (1958) and by Bose *et al* (1964).

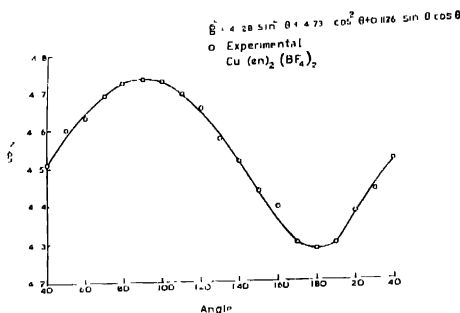


Figure 2  $g^2$  variation in  $\text{Cu(en)}_2(\text{BF}_4)_2$  in  $b^*c^*$  plane.

If  $I_1$ ,  $I_2$  and  $I_3$  are the direction cosines of the magnetic field with respect to  $a^*$ ,  $b^*$  and  $c^*$  axes, we have,

$$g^2 = \sum_{ij=1,2,3} A_{ij} I_i I_j = A_{11} I_1^2 + A_{22} I_2^2 + A_{33} I_3^2 + 2A_{12} I_1 I_2 + 2A_{23} I_2 I_3 + 2A_{31} I_3 I_1 \quad (1)$$

where  $A_{ij}$ 's are the components of the  $g^2$ -tensor (symmetric) in the  $a^*b^*c^*$  system. When these coefficients are known, the principal  $g$ -values are found by diagonalizing the matrix A. The three roots of the secular equation

$$\det [A - \lambda I] = 0 \quad \dots (2)$$

are the squares of the principal  $g$ -values

In  $b^*c^*$  plane, if  $\theta$  is the angle between the magnetic field and  $c^*$ -axis, then

$$I_1 = 0, I_2 = \sin \theta, I_3 = \cos \theta$$

and the above equation simplifies to

$$g^2 = A_{22} \sin^2 \theta + A_{33} \cos^2 \theta + 2A_{23} \sin \theta \cos \theta \quad \dots (3)$$

The  $g^2$  values along  $c^* = c$  axis and  $b^*$  axis gives  $A_{33}$  and  $A_{22}$ .  $A_{23}$  is obtained by the least square fit method from the above equation (3). The values obtained in the two crystals 1 and 2 are

$$A_{22} = 4.26 \quad A_{33} = 4.26 \quad A_{23} = 0.05299 \quad \text{for } 1$$

$$A_{22} = 4.28 \quad A_{33} = 4.73 \quad A_{23} = 0.0563 \quad \text{for } 2$$

In the  $a^* b^*$  plane if  $\phi$  is the angle between the magnetic field and the  $b^*$  axis then

$$I_1 = \sin \phi, I_2 = \cos \phi \quad I_3 = 0$$

so that

$$g^2 = A_{11} \sin^2 \phi + A_{22} \cos^2 \phi + 2A_{12} \sin \phi \cos \phi \quad \dots (4)$$

The values  $A_{22}$  is taken from  $b^* c^*$  plane.  $A_{11}$  is obtained from the  $g^2$ -value along  $a^*$  axis. As in the  $b^* c^*$  plane the value of  $A_{12}$  is obtained by least square fit method using the equation (4). This gives

$$A_{11} = 4.73 \quad A_{12} = 0.0533 \quad \text{for } 1$$

$$A_{11} = 4.28 \quad A_{12} = 0.0622 \quad \text{for } 2$$

In the  $ac$  plane along  $a$ -axis, the expression for  $g^2$  contains all the coefficients of which five are already known. Further the direction cosines of the  $a$ -axis with respect to  $a^*$ ,  $b^*$  and  $c^*$  axes are given by (using the known crystal structure data).

$$I_3^a = \cos \beta = -0.3969 \quad I_2^a = \cos \gamma \cos (\alpha - 90) = -0.5746$$

$$I_1^a = 1 - [(I_3^a)^2 - (I_2^a)^2]^{1/2} = 0.7156^* \quad \text{for } 1$$

$$I_3^a = 0.2622 \quad I_2^a = -0.2736 \quad I_1^a = 0.9255^* \quad \text{for } 2.$$

Using the value of  $g^2$  along  $a$ -axis the sixth coefficient  $A_{13}$  is obtained as

$$A_{13} = 0.2094 \text{ and } 0.2162 \text{ respectively for 1 and 2.}$$

The  $g^2$  tensor  $|A|$  with respect to the coordinate system  $a^*$ ,  $b^*$ ,  $c^*$  is therefore

$$A = \begin{vmatrix} (4.73 - \lambda) & 0.0533 & 0.2094 \\ 0.0533 & (4.26 - \lambda) & 0.0529 \\ 0.2094 & 0.0529 & (4.26 - \lambda) \end{vmatrix} \quad \text{for } 1,$$

and

$$A = \begin{vmatrix} (4.28 - \lambda) & 0.0622 & 0.2162 \\ 0.0622 & (4.28 - \lambda) & 0.0563 \\ 0.2162 & 0.0563 & (4.73 - \lambda) \end{vmatrix} \quad \text{for } 2.$$

\*As is generally customary in these calculations the positive sign has been adopted. However further calculation has shown that the adoption of the negative sign does not lead to any appreciable change in the result.

The solution for  $\lambda$  for the resulting respective cubic equations

$$\lambda^3 - 13.25\lambda^2 + 58.3978\lambda - 86.6274 = 0 \text{ for } 1$$

$$\lambda^3 - 13.29\lambda^2 + 59.2536\lambda - 87.4252 = 0 \text{ for } 2.$$

give the following three  $g$ -values.

$$g_3 = 2.197 \quad g_2 = 2.064 \quad g_1 = 2.041 \text{ for } 1$$

$$g_3 = 2.201 \quad g_2 = 2.071 \quad g_1 = 2.045 \text{ for } 2$$

In both the cases a nearly tetragonal symmetry is indicated. The difference between  $g_2$  and  $g_1$  in both cases is considered to be slightly greater than due to experimental error. The principal  $g$ -values are

$$g_{||} = 2.20 \quad g_{\perp} = 2.05 \text{ for } 1$$

$$g_{||} = 2.20 \quad g_{\perp} = 2.058 \text{ for } 2.$$

The angles  $\theta_i$  between the axis of symmetry and the  $a^*b^*c^*$  axes are obtained from the equation

$$A_{ii} = g_{||}^2 \cos^2 \theta_i + g_{\perp}^2 \sin^2 \theta_i \quad \dots \quad (5)$$

where  $i = 1, 2$ , and  $3$ . These are given below together with the orientation of all the  $g_i$ 's with respect to the chosen system (table 1).

The values of  $\theta_{c^*}$  are also deduced from the respective crystal structure data of the two compounds, these are  $80^\circ$  and  $34^\circ$  respectively, in good agreement with the experimental values

Table 1 Principal  $g$ -values and their orientations with respect to the chosen axes,  $a^*$ ,  $b^*$  and  $c^*$

Substance	Principal $g$ -values	Angle with respect to		
		$a^*$	$b^*$	$c^*$
$\text{Cu}(\text{en})_2(\text{SCN})_2$	$g_3 = 2.197$	$24^\circ 36'$	$73^\circ 10'$	$71^\circ 47'$
	$g_2 = 2.064$	$72^\circ 19'$	$25^\circ 28'$	$72^\circ 13'$
	$g_1 = 2.041$	$72^\circ 38'$	$70^\circ 38'$	$-26^\circ 31'$
	$g_{\perp} = 2.05$			
	$g_{  } = 2.20$			$75^\circ 00'$
				$(80^\circ)^+$
$\text{Cu}(\text{en})_2(\text{BF}_4)_2$	$g_3 = 2.201$	$67^\circ 54'$	$76^\circ 52'$	$24^\circ 58'$
	$g_2 = 2.071$	$72^\circ 00'$	$24^\circ 58'$	$74^\circ 46'$
	$g_1 = 2.045$	$28^\circ 58'$	$70^\circ 36'$	$69^\circ 29'$
	$g_{\perp} = 2.058$			
	$g_{  } = 2.20$			$35^\circ 15'$
				$(34^\circ)^+$

(<sup>+</sup>) Values obtained from crystal structure data.



(2) *The powder*

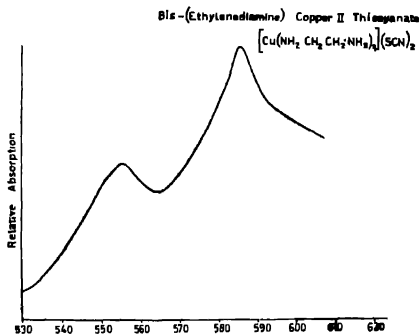
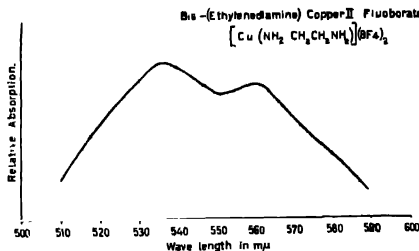
ESR absorption of crystalline powder samples of the above two compounds has shown asymmetry in the line shape, as may be seen from figures 3(I) and 3(II) (Plate 1). The shapes are similar to those obtained by Kneubuhl (1960) in substances with two principal  $g$ -values  $g_{\parallel}$  and  $g_{\perp}$ . The following values are deduced from the derivative tracings

	$\text{Cu(en)}_2(\text{SCN})_2$	$\text{Cu(en)}_2(\text{BF}_4)_2$
$g_{\parallel}$	2.19	2.20
$g_{\perp}$	2.03	2.07

3) *Optical absorption studies*

Optical absorption of these two substances in aqueous solution of 0.01 percent has given two distinct peaks in each (figures 4 and 5) at the following wave numbers.

$\text{Cu(en)}_2(\text{SCN})_2$	$\text{Cu(en)}_2(\text{BF}_4)_2$
$18018 \text{ cm}^{-1}$	$18691 \text{ cm}^{-1}$
$17094 \text{ cm}^{-1}$	$17857 \text{ cm}^{-1}$

Figure 4. Optical absorption spectrum of  $\text{Cu(en)}_2(\text{SCN})_2$ .Figure 5. Optical absorption spectrum of  $\text{Cu(en)}_2(\text{BF}_4)_2$ .

From these absorption frequencies the covalency reduction factors are obtained using the following expressions of Bose *et al* (1965) and of Ghosh *et al* (1967) and of Pal *et al* (1968).

$$g_{||} = 2 \left\{ 1 - \frac{4R'_{||}K'_{||}\lambda}{(E_3 - E_1)} - \frac{R^2\lambda^2}{2(E_2 - E_1)^2} - \frac{2R_{\perp}R'_{\perp}K'_{||}\lambda^2}{(E_2 - E_1)(E_3 - E_1)} \right\}$$

$$g_{\perp} = 2 \left\{ 1 - \frac{R_{\perp}K_{\perp}\lambda}{(E_2 - E_1)} - \frac{R_{\perp}\lambda^2(R_{\perp} - R_{||}K_{\perp})}{2(E_2 - E_1)^2} - \frac{2R_{||}^2\lambda^2}{(E_3 - E_1)^2} - \frac{R_{||}\lambda^2(R_{\perp}K'_{\perp} - R'_{\perp}K_{\perp})}{(E_2 - E_1)(E_3 - E_1)} \right\} \quad \dots \quad (6)$$

where  $\lambda$  is taken as  $-828 \text{ cm}^{-1}$  for copper and  $R_{||}$ ,  $R_{\perp}$  and  $K_{||}$ ,  $K_{\perp}$  are spin orbit and orbital reduction factors respectively, arising out of the covalency effect in the metal ligand bonding.  $(E_2 - E_1)$  and  $(E_3 - E_1)$  are the ligand field splittings.

The parameters appearing in the above expressions are  $R_{||}$ ,  $R'_{||}$ ,  $R_{\perp}$ ,  $R'_{\perp}$ ,  $K_{||}$ ,  $K'_{||}$  and  $K_{\perp}$ ,  $K'_{\perp}$  and simplifying approximations are made which make very little difference in the ultimate calculations. Since the primed and unprimed parameters appear in the third order expressions for  $g_{||}$  and  $g_{\perp}$ , the covalency reduction factors associated with the matrix elements between the two  $d(\tau)$  orbitals and that between  $d(\tau)$  and  $d(\rho)$  orbitals are the same:  $d(\tau)$  and  $d(\rho)$  are the atomic orbitals ( $d_{xy}$ ,  $d_{yz}$ ,  $d_{zx}$ ) and ( $d_{3z^2-r^2}$ ,  $d_{x^2-y^2}$ ) where the quantities given in the brackets are the five degenerate states of the free ion. Therefore  $R_{||} = R'$  etc.

In this case much simplification can be made due to the fact that from ESR and optical absorption data only the products of  $R_{||}K_{||}$  and  $R_{\perp}K_{\perp}$ , but not the individual quantities, are obtained. Therefore the above expressions can be written by neglecting all the terms except the first two and they are as follows

$$g_{||} = 2 \left[ 1 - \frac{4R_{||}K_{||}\lambda}{(E_3 - E_1)} \right]$$

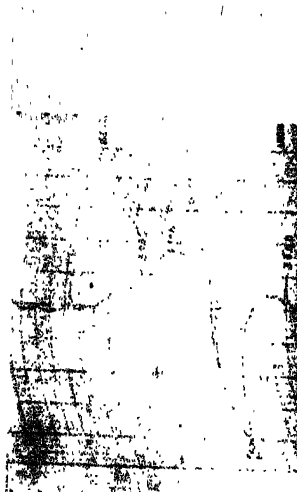
$$g_{\perp} = 2 \left[ 1 - \frac{R_{\perp}K_{\perp}\lambda}{(E_2 - E_1)} \right] \quad (7)$$

The values of  $R_{||}K_{||}$  and  $R_{\perp}K_{\perp}$  for the two crystals are given below. The results indicate a considerable covalency in the metal ligand bonding.

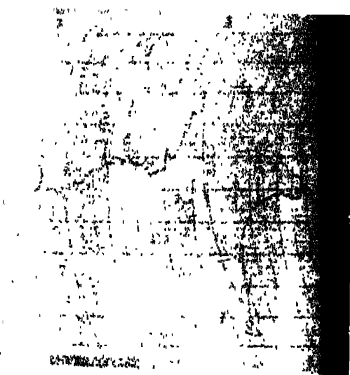
	$\text{Cu(en)}_2(\text{SCN})_2$	$\text{Cu(en)}_2(\text{BF}_4)_2$
$R_{  }K_{  }$	0.52	0.54
$R_{\perp}K_{\perp}$	0.54	0.64



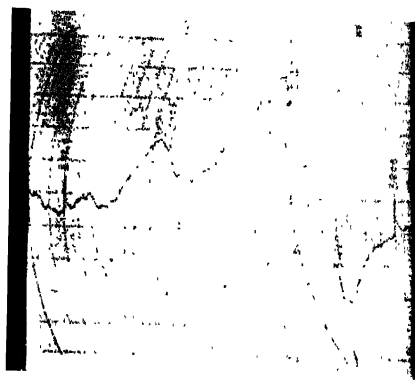
I



II



III



IV

Figure 3. Derivative tracings of powder samples  
I.  $\text{Cu}(\text{en})_2(\text{SCN})_2$ , II.  $\text{Cu}(\text{en})_2(\text{BF}_4)_2$ , III.  $\text{Cu}(\text{Py})_2(\text{SCN})_2$  and  
IV.  $\text{Cu}(\text{Py})_2(\text{BF}_4)_2$



## B. Powder patterns of 3 and 4

The derivative curves obtained for the powder specimens of the two pyridine compounds are also shown in figures (3) and (4). The respective principal  $g$ -values that are deduced and the absorption frequency in the case of  $\text{Cu}(\text{py})_4(\text{BF}_4)_2$  together with the estimated value of the covalency factor, are given below for  $\text{Cu}(\text{py})_2(\text{SCN})_2$  no clear absorption peak has been observed.

Since only one peak is obtained in the absorption in 4, the  $RK$  value is estimated by taking the average  $g$ -value and using the approximate equation

$$g_{av} = \left( \frac{g_{\parallel}^2 + 2g_{\perp}^2}{3} \right)^{1/2} = 2 - \frac{4\lambda RK}{\Delta E} \quad \dots (8)$$

where the following approximations have been made:  $R_{\parallel}K_{\parallel} \approx R_{\perp}K_{\perp} \approx RK$  which is strictly valid when  $\pi$ -bonding is neglected, and  $E_2 - E_1 \approx E_3 - E_1 \approx \Delta E$

3. $\text{Cu}(\text{py})_2(\text{SCN})_2$	4. $\text{Cu}(\text{py})_4(\text{BF}_4)_2$
$g_{\parallel} = 2.28$	$g_{\parallel} = 2.30$
$g_{\perp} = 2.02$	$g_{\perp} = 2.02$
	$\Delta E = 14493 \text{ cm}^{-1}$
	$RK = 0.54$

As in the first two compounds, the  $RK$  value indicates considerable covalency in the metal ligand bonding in  $\text{Cu}(\text{py})_4(\text{BF}_4)_2$ . But the value may be considered to be only approximate

## ACKNOWLEDGEMENT

The author is grateful to Prof. K. Rangadhama Rao for his keen interest in the work and various helpful suggestions.

## REFERENCES

- Abe, H. & Ono, K. 1956 *J. Phys. Soc. Japan* **11**, 947.  
 Bloaney, B., Penrose, R. P. & Plumpton Botty, I. 1949 *Proc. Roy. Soc. A*, **198**, 406.  
 Bose, A., Ghosh, U. S., Bagchi, R. N. & Pal, A. K. 1964 *Indian J. Phys.* **38**, 361.  
 Bose, A., Lahiry, S. & Ghosh, U. S. 1965 *J. Phys. Chem. Solids* **26**, 1747.  
 Brown, D. S., Lee, J. D. & Melson, B. G. A. 1968 *Acta Cryst.* **24**, 730.  
 Bruce, W., Brown, D. S. & Lingafelter, E. C. 1964 *Acta Cryst.* **17**, 254.  
 Gopalakrishna Murthy, P. V. 1968 *Indian J. Phys.* **42**, 136.  
 Ghosh, U. S. & Bagchi, R. N. 1962, *Indian J. Phys.* **36**, 538.  
 Ghosh, U. S., Bagchi, R. N., Pal, A. K. & Mitra, S. N. 1967 *Indian J. Phys.* **41**, 286.  
 Ghosh, U. S., Pal, A. K. & Bagchi, R. N. 1965 *J. Phys. Chem. Solids* **26**, 2041.  
 Ibers, J. A. 1953 *Acta Cryst.* **6**, 367.  
 Kneubuhl, F. K. 1960 *J. Chem. Phys.* **33**, 1074.  
 Maki, A. H. & McGrahey, B. R. 1958 *J. Chem. Phys.* **29**, 31 and 35.

- Neimann, R. & Kovilson, K. 1961 *J. Chem. Phys.* **35**, 156.
- Pal, A. K. Mitra, S. N. & Sengupta, P. 1968 *J. Chem. Phys.* **48**, 5219.
- Porai-Koshits, M. A. & Tishchenko, G. N. 1959 *Kristallografiya* **4**, 239 or *Soviet Phys. Cryst.* **4**, 210.
- Pryce, M. H. L. 1950 *Proc. Phys. Soc. A*, **63**, 25.
- Rajan, R. 1962 *J. Chem. Phys.* **36**, 1901.
- Rajan, R. 1963 *Physica*, **29**, 1195.
- Rajan, R. & Ramasubba Reddy, T. 1963 *J. Chem. Phys.* **39**, 1140.
- Ramasubba Reddy, T. & Srinivasan, R. 1967 *Proc. Ind. Acad. of Sciences* **96**, 304.
- Weil, J. & Anderson, J. H. 1958 *J. Chem. Phys.* **28**, 864.

## Linear flow of heat in a semi-infinite-finite solid

By S. K. GHOSH and D. BHATTACHARYA

*Department of Engineering Physics, Jadavpur University.*

*(Received 8 November 1969—Revised 25 March 1970)*

A problem on conduction of heat in semi-infinite-finite solid has been solved following Heaviside's Operational method. Unlike Laplace transformation methods which involve complicated transformations and solutions, the present method finds the correct solution in a simple way. Expressions for temperature distribution in a finite and infinite solid are easily obtained. Special cases of a thin film attached to a long solid having wide applications in Engineering to the theory of thin films have been worked out from the general theory.

### INTRODUCTION

In solving the general problem of heat conduction through a semi-infinite-finite solid we take the following simplifying assumptions.

1. Heat flow through the solid is linear *i.e.*, one dimensional.
2. The media in the two regions are isotropic as regards conductivity, density, specific heat.
3. We neglect the loss of heat in our calculations.
4. There is no thermal resistance at the point of contact. Symbols used are as follows :

$v_1$ ,  $k_1$ ,  $\rho_1$ ,  $c_1$  and  $h_1$  are the temperature, conductivity, density, specific heat and diffusivity respectively, in the finite region, *i.e.*  $-l < x < 0$ , and  $v_2$ ,  $k_2$ ,  $\rho_2$ ,  $c_2$  and  $h_2$  are the corresponding quantities in the infinite region, *i.e.*  $x > 0$ .

$l$  = Length of the finite region.

$x$  = Variable measured along the direction of propagation of heat-flux.

$V$  = Temperature of the source, *i.e.* at  $x = -l$ .

$t$  = Variable time, and

$$D = \frac{d}{dt}.$$

### METHOD OF SOLUTION

The differential equations to be solved are

$$\frac{\partial^2 v_1}{\partial x^2} - \frac{1}{h_1} \frac{\partial v_1}{\partial t} = 0, \quad -l < x < 0, \quad t > 0 \quad (1)$$

$$\frac{\partial^2 v_2}{\partial x^2} - \frac{1}{h_2} \frac{\partial v_2}{\partial t} = 0, \quad x > 0, \quad t > 0 \quad (2)$$

Assuming that there is no contact resistance at the surface of separation  $x = 0$ , the boundary conditions are

$$k_1 \frac{\partial v_1}{\partial x} = k_2 \frac{\partial v_2}{\partial x}, \quad x = 0, \quad t > 0 \quad \dots (3)$$

$$v_1 = v_2, \quad x = 0, \quad t > 0 \quad \dots (4)$$

With initial temperature zero and  $x = -l$  kept at  $V$  for  $t > 0$  equations (1) and (2) in operational form becomes,

$$\frac{\partial^2 v_1}{\partial x^2} - \frac{D}{h_1} v_1 = 0, \quad -l < x < 0 \quad \dots (5)$$

$$\frac{\partial^2 v_2}{\partial x^2} - \frac{D}{h_2} v_2 = 0, \quad x > 0 \quad \dots (6)$$

Let us put  $\frac{D}{h_1} = q_1^2$  and  $\frac{D}{h_2} = q_2^2$  then the equations (5) and (6) become

$$\frac{\partial^2 v_1}{\partial x^2} - q_1^2 v_1 = 0 \quad \dots (7)$$

$$\frac{\partial^2 v_2}{\partial x^2} - q_2^2 v_2 = 0 \quad \dots (8)$$

The solutions of equations (7) and (8) are

$$v_1 = A \cosh q_1 x + B \sinh q_1 x \quad \dots (9)$$

$$v_2 = C \cosh q_2 x + D \sinh q_2 x \quad \dots (10)$$

Where  $A$ ,  $B$ ,  $C$  and  $D$  constants to be determined from boundary conditions in (3) and (4) and are as follows :

$$A = \frac{V}{\cosh q_1 l + \frac{k_2 q_2}{k_1 q_1} \sinh q_1 l} \quad \dots$$

$$B = -\frac{k_2 q_2 V}{k_1 q_1 \cosh q_1 l + k_2 q_2 \sinh q_1 l}$$

$$C = \frac{q_1 k_1 V}{k_1 q_1 \cosh q_1 l + q_2 k_2 \sinh q_1 l}$$

$$D = -\frac{k_1 q_1 V}{k_1 q_1 \cosh q_1 l + k_2 q_2 \sinh q_1 l}$$



Now substitution in equation (9) and (10) yields

$$v_1 = V \frac{\cosh q_1 x - \sigma \sinh q_1 x}{\cosh q_1 l + \sigma \sinh q_1 l} \quad \dots \quad (9.1)$$

$$v_2 = V \frac{e^{-q_2 x}}{\cosh q_1 l + \sigma \sinh q_1 l} \quad \dots \quad (10.1)$$

where  $\sigma$  is a constant and given by

$$\sigma = \frac{k_2 q_2}{k_1 a_1} = \left( \frac{k_2 \rho_2 c_2}{k_1 \rho_1 c_1} \right)^{\frac{1}{2}}$$

Expanding the hyperbolic sines and cosines and simplifying,

$$v_1 = \frac{V \cdot e^{-q_1(x+l)} (1 - m e^{2q_1 x})}{(1 - m e^{-2q_1 l})} \quad \dots \quad (11)$$

$$v_2 = \frac{2V}{1+\sigma} \frac{e^{-q_2 x} e^{-q_1 l}}{(1 - m e^{-2q_1 l})} \quad \dots \quad (12)$$

where  $m = \frac{\sigma-1}{\sigma+1}$ , a constant.

To know the variation of  $v_1$  and  $v_2$  with time we express  $q_1$  and  $q_2$  in terms of  $D$ , operating on Heaviside unit function  $H(t)$  and remembering that

$$\begin{aligned} H(t) &= 0, & t < 0; \\ H(t) &= 1, & t > 0. \end{aligned}$$

the equations (11) and (12) turn out to be

$$\begin{aligned} v_1 = V \{ & e^{-D^1(x+l)/(h_1)^{\frac{1}{2}}} + m e^{-D^1(x+3l)/(h_1)^{\frac{1}{2}}} + m^2 e^{-D^1(x+5l)/(h_1)^{\frac{1}{2}}} + \dots \\ & - \{ m e^{-D^1(l-x)/(h_1)^{\frac{1}{2}}} + m^2 e^{-D^1(3l-x)/(h_1)^{\frac{1}{2}}} + m^3 e^{-D^1(5l-x)/(h_1)^{\frac{1}{2}}} + \dots \} \} H(t) \quad \dots \quad (13) \end{aligned}$$

$$\begin{aligned} v_2 = \frac{2V}{1+\sigma} \left[ & e^{-D^1 \left\{ \frac{x}{(h_2)^{\frac{1}{2}}} + \frac{l}{(h_1)^{\frac{1}{2}}} \right\}} + m e^{-D^1 \left\{ \frac{x}{(h_2)^{\frac{1}{2}}} + \frac{3l}{(h_1)^{\frac{1}{2}}} \right\}} \right. \\ & \left. + m^2 \cdot e^{-D^1 \left\{ \frac{x}{(h_2)^{\frac{1}{2}}} + \frac{5l}{(h_1)^{\frac{1}{2}}} \right\}} + \dots \right] H(t) \quad \dots \quad (14) \end{aligned}$$

$$\therefore v_1 = V \sum_{n=0}^{\infty} (m)^n \left\{ \operatorname{erfc} \frac{(2n+1)l+x}{2(h_1 t)^{\frac{1}{2}}} - m \cdot \operatorname{erfc} \frac{(2n+1)l-x}{2(h_1 t)^{\frac{1}{2}}} \right\} \quad \dots \quad (15)$$

$$\text{and} \quad v_2 = \frac{2V}{1+\sigma_{n-1}} \sum_{n=1}^{\infty} (m)^n \operatorname{erfc} \left\{ \frac{kx + (2n+1)l}{2(h_1 t)^{\frac{1}{2}}} \right\} \quad \dots \quad (16)$$

$$\text{where} \quad k = \left( \frac{h_1}{h_2} \right)^{\frac{1}{2}}$$

Again, the temperature gradient at the surface is found to be

$$\left( \frac{\partial v_1}{\partial x} \right)_x = -l_1 = \frac{-V}{(\pi h_1 t)^{\frac{1}{2}}} \left[ 1 + 2 \sum_{n=1}^{\infty} (m)^n e^{-\frac{n^2 l^2}{h_1 t}} \right] \quad \dots \quad (17)$$

For large value of time the exponential may be replaced by unity and we have

$$\begin{aligned} \left( \frac{\partial v_1}{\partial x} \right)_x &= -\frac{V}{(\pi h_1 t)^{\frac{1}{2}}} \{1 + 2m(1 + m + m^2 + \dots)\} \\ &= -\frac{V}{(\pi h_1 t)^{\frac{1}{2}}} \left( 1 + \frac{2m}{1-m} \right) \\ &= -\frac{V}{(\pi h_1 t)^{\frac{1}{2}}} \left( \frac{k_2 \rho_2 c_2}{k_1 \rho_1 c_1} \right)^{\frac{1}{2}} \quad \dots \quad (18) \end{aligned}$$

The equation (18) is in agreement with that obtained by Carslaw & Jaeger (1959) who used this equation for a correct estimate of the age of the earth. Taking the case of granite and air as the composition of earth and the surrounding thin film of air, the quantity  $\left( \frac{k_2 \rho_2 c_2}{k_1 \rho_1 c_1} \right)^{\frac{1}{2}}$  comes out to be nearly 450. A similar observation was made by Carslaw & Jaeger

#### SPECIAL CASES

*Case 1.* When  $l$  is small, that is, when a thin film of another substance is attached to the semi-infinite medium, expanding the hyperbolic functions and retaining only upto the first power of  $l$  we have from equation (10.1)

$$v_2 = \frac{V}{1+\sigma q_1 l} \cdot e^{-q_2 x} = \frac{hV}{h+q_2} \cdot e^{-q_2 x}, \quad \text{where} \quad h = \frac{k_1}{k_2 l}.$$

The Operational solution of the above equation will be

$$v_2 = V \left[ \operatorname{erfc} \frac{x}{2(h_2 t)^{\frac{1}{2}}} - e^{hx + h_2 t h^2} \times \operatorname{erfc} \left\{ \frac{x}{2(h_2 t)^{\frac{1}{2}}} + h(h_2 t)^{\frac{1}{2}} \right\} \right] \quad \dots \quad (19)$$

The equation (19) is computed by using the following data :

The material of the film is cork of conductivity  $k_1 = 0.0001$  and diffusivity  $h_1 = 0.0014$ . The second material is taken to be copper whose conductivity  $k_2 = 0.93$  and diffusivity  $h_2 = 1.14$ . The temperature  $v_2$  is calculated in

the specimen at different distances  $x = 10$  cm,  $x = 50$  cm,  $x = 100$  cm, after one hour when the temperature is assumed to be steady.

A theoretical graph is drawn between the film thickness *vs.* temperature on the infinite region at different distances. This is shown in figure 1. At a

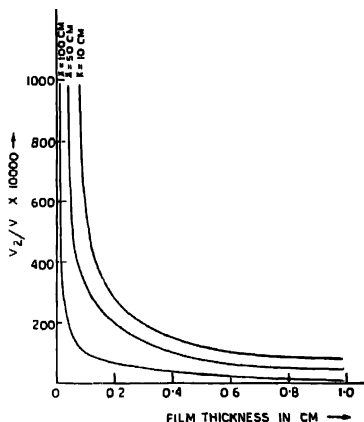


Figure 1

given value of  $x$  increasing the film thickness decreases the value of temperature. At low value of thickness, in all the three cases, the temperature rapidly falls to a lower value.

*Case 2.* Retaining the terms upto  $l^2$ , we have from equation (10.1).

$$v_2 = V \frac{e^{-q_2 x}}{\frac{l^2 D}{2 h_1} + \frac{\sigma l D}{(h_1)^2} + 1} = V \frac{e^{-q_2 x}}{\frac{l^2 h_2}{2 h_1} \cdot \frac{q_2^2 + \frac{1}{h}}{q_2 + 1}} = h' V \frac{e^{-q_2 x}}{h' q_2^2 + q_2 + \frac{h}{h'}}$$

where 
$$h' = \frac{l^2 h h_2}{2 h_1}.$$

$$v_2 = \frac{hV}{h'} \cdot \frac{e^{-q_2 x}}{\left[ q_2^2 + \frac{1}{h'} q_2 + \frac{h}{h'} \right]} \quad \dots (20)$$

Now two case may arise :

I. When the roots of the equation  $q_2^2 + \frac{1}{h'} q_2 + \frac{h}{h'} = 0$  are real and unequal,

i.e. when  $\left(\frac{1}{h'}\right)^2 > \frac{4h}{h'}$  and given by

$$[-\alpha, -\beta] = -\frac{\frac{1}{h'} \pm \left\{ \left(\frac{1}{h'}\right)^2 - \frac{4h}{h'} \right\}^{\frac{1}{2}}}{2}$$

then by the method of partial fraction, equation (20) becomes

$$v_2 = \frac{hV}{h'(\beta - \alpha)} \left\{ \frac{e^{-q_2 x}}{q_2 + \alpha} - \frac{e^{-q_2 x}}{q_2 + \beta} \right\} \quad (20.1)$$

The Operational solution of the equation (20.1) will be

$$\begin{aligned} v_2 &= \frac{hV}{h'(\beta - \alpha)} \left[ \frac{1}{\alpha} \operatorname{erfc} \frac{x}{2(h_2 t)^{\frac{1}{2}}} - \frac{1}{\alpha} e^{\alpha x + h_2 t \alpha^2} \right. \\ &\quad \times \operatorname{erfc} \left\{ \frac{x}{2(h_2 t)^{\frac{1}{2}}} + \alpha(h_2 t)^{\frac{1}{2}} \right\} - \frac{1}{\beta} \operatorname{erfc} \frac{x}{2(h_2 t)^{\frac{1}{2}}} \\ &\quad \left. + \frac{1}{\beta} e^{\beta x + h_2 t \beta^2} \times \operatorname{erfc} \left\{ \frac{x}{2(h_2 t)^{\frac{1}{2}}} + \beta(h_2 t)^{\frac{1}{2}} \right\} \right] \quad (20.2) \end{aligned}$$

II When the roots of the equation  $q_2^2 + \frac{1}{h'} q_2 + \frac{h}{h'} = 0$  are real and equal

i.e., when  $\left(\frac{1}{h'}\right)^2 = \frac{4h}{h'}$  or  $4hh' = 1$ .

$$-\alpha = -\beta = -\frac{1}{2h'}$$

then the equation (20) can be written as

$$v_2 = \frac{hV}{h'} \frac{e^{-q_2 x}}{\left(q_2 + \frac{1}{2h'}\right)^2} \quad \dots \quad (20.3)$$

The Operational solution of  $v_2$  in equation (20.3)

$$\begin{aligned} v_2 &= \frac{hV}{h'} \left[ 4h'^2 \operatorname{erfc} \frac{x}{2(h_2 t)^{\frac{1}{2}}} - 4h' \left(\frac{h_2 t}{\pi}\right)^{\frac{1}{2}} e^{-\frac{x^2}{4h_2 t}} \right. \\ &\quad \left. - 4h'^2 \left( 1 - \frac{x}{2h'} - \frac{2h_2 t}{4h'^2} \right) e^{\frac{x}{2h'} + \frac{h_2 t}{4h'^2}} \times \operatorname{erfc} \left\{ \frac{x}{2(h_2 t)^{\frac{1}{2}}} + \frac{(h_2 t)^{\frac{1}{2}}}{2h'} \right\} \right] \end{aligned}$$

$$v_2 = \frac{hV}{h'} - 4h'^2 \left[ \operatorname{erfc} \frac{x}{2(h_2t)^{1/2}} - \frac{1}{h'} \left( \frac{h_2t}{\pi} \right)^{1/2} \cdot e^{-\frac{x^2}{4h_2t}} \right. \\ \left. - \left( 1 - \frac{x}{2h'} - \frac{2h_2t}{4h'^2} \right) \cdot e^{\left( \frac{x}{2h'} + \frac{h_2t}{4h'^2} \right)} \right] \times \operatorname{erfc} \left\{ \frac{x}{2(h_2t)^{1/2}} + \frac{(h_2t)^{1/2}}{2h'} \right\} ]$$

Since  $4hh' = 1$ .

$$v_2 = V \left[ \operatorname{erfc} \frac{x}{2(h_2t)^{1/2}} - \left( \frac{h_2t}{\pi} \right)^{1/2} \cdot e^{-\frac{x^2}{4h_2t}} \right. \\ \left. - \left( 1 - \frac{x}{2h'} - \frac{h_2t}{2h'^2} \right) e^{\left( \frac{x}{2h'} + \frac{h_2t}{4h'^2} \right)} \right] \times \operatorname{erfc} \left\{ \frac{x}{2(h_2t)^{1/2}} + \frac{(h_2t)^{1/2}}{2h'} \right\} \quad \dots \quad (20.4)$$

### CONCLUSION

The equations (19) and (20) give approximately the temperature at any depth in the semi-infinite region bounded either by a thin film or a film of finite thickness having definite thermal capacity. The equation (20.4) shows that the temperature  $v_2$  is independent of the conductivity of the thin film. This clearly indicates the development of new thermoplastic device satisfying the condition  $\Delta hh' = 1$ , i.e.  $k_2\rho_2c_2 = 2k_1\rho_1c_1$

Further work on the heat flow in composite solid in which the conductivities vary with distance and the rate of heat production also varies with depth is under consideration

### REFERENCE

- Carslaw H. S. & Jaeger J. C. 1959, *Conduction of Heat in Solid* (Oxford Pub.), pp. 319-329.  
 Jeffreys H. & Jeffreys, B. 1966, *Methods of Mathematical Physics* (Camb. Pub.).

## Some special studies on dynamic response of a simply supported beam to impact loads

By R. N. DAS

University College of Engineering, Burla, Orissa

(Received 17 November 1969—Revised 17 February 1970)

(Plate—2)

In this paper broad aspects of impact between a uniform beam supported at its ends and a transversely impinging load at its midspan have been analysed. The effect of the striking velocity of the load on the duration of impact in the light of Hertz's (1927) theory is discussed. The range of application of Cox's (1856) theory with respect to "mass ratio" has been explained. The vibration pattern of the beam, the duration of impact and the energy absorbed by the beam during impact are studied in details both theoretically and experimentally. Photographic method of measurement has been used in the experiments. Experimental results are in excellent agreement with the theory.

### INTRODUCTION

Investigations on the beam-impact problem have been made by Cox (1856), Timoshenko (1956), Hoppman (1948), Banerjee (1966a) and others. Recently the author & Mishra (1968) following the deductions of Banerjee (1966a) has developed a general theory on transverse impact on a simply supported beam. In the present investigation the author using various beam-load combinations has made some special studies in details concerning the displacement, period of vibration, the energy of the beam and the duration of impact for a simply supported beam under central impact. Further, the results of the present analysis of the author have been compared with those of Cox's (1856) theory. Theoretical results have been verified experimentally employing photographic method of measurement.

### THEORY

Let us consider a uniform beam of length  $l$ , mass  $M$ , Young's modulus  $E_1$ , and moment of inertia about the neutral axis  $I$ , simply supported at its ends  $x = 0$  and  $x = l$  and transversely struck at mid-span ( $x = a = l/2$ ) by a load of mass  $m$  with a striking velocity  $V_0$ .

*Displacement of the beam and pressure of impact of the load.*

The analysis of Das (1968) yields the following expressions given by equations. (1) to (4).

$$\frac{2 \sinh \gamma_s \cdot \sin \gamma_s}{\sinh \gamma_s \cdot \sin^2 \frac{\gamma_s}{2} - \sin \gamma_s \cdot \sinh^2 \frac{\gamma_s}{2}} = \frac{m \cdot \gamma_s}{1 - \frac{E_1}{E_2} \cdot \frac{m \cdot \gamma_s^4}{M \cdot l^3}} \quad \dots (1)$$

$$q_s = \gamma_s^2 \left( \frac{E_1 I}{M l^3} \right)^{\frac{1}{2}} \quad \dots \quad (2)$$

$$y_a = 4V_0 \Sigma \frac{A_s}{q_s} \cdot \sin q_s t \quad \dots \quad (3.1)$$

$$y_1 = 4V_0 \Sigma \frac{\left( \sinh \gamma_s \cdot \sin \frac{\gamma_s}{2} \cdot \sin \gamma_s \frac{x}{l} - \sin \gamma_s \cdot \sinh \frac{\gamma_s}{2} \cdot \sinh \gamma_s \frac{x}{l} \right)}{\sinh \gamma_s \cdot \sin^2 \frac{\gamma_s}{2} - \sin \gamma_s \cdot \sinh^2 \frac{\gamma_s}{2}} \times \frac{A_s}{q_s} \sin q_s t \quad \dots \quad (3.2)$$

$$y_2 = 4V_0 \Sigma \frac{\left[ \sinh \gamma_s \cdot \sin \frac{\gamma_s}{2} \cdot \sin \gamma_s \left( 1 - \frac{x}{l} \right) - \sin \gamma_s \cdot \sinh \frac{\gamma_s}{2} \cdot \sinh \gamma_s \left( 1 - \frac{x}{l} \right) \right]}{\sinh \gamma_s \cdot \sin^2 \frac{\gamma_s}{2} - \sin \gamma_s \cdot \sinh^2 \frac{\gamma_s}{2}} \times \frac{A_s}{q_s} \sin q_s t \quad \dots \quad (3.3)$$

$$\frac{1}{\gamma_s} = 1 + 2 \frac{M}{m} + \frac{\gamma_s}{\coth \gamma_s - \cot \gamma_s} \quad (\text{for hard load}) \quad \dots \quad (3.4)$$

$$P = -4mV_0 \Sigma B_s \cdot q_s \cdot \sin q_s t \quad \dots \quad (4.1)$$

$$\frac{1}{B_s} = 1 + \frac{3mq_s^2}{E_2} + \frac{m\gamma_s^2}{4M} \left[ \frac{1}{\cos \gamma_s + 1} - \frac{1}{\cosh \gamma_s + 1} \right] \quad \dots \quad (4.2)$$

where,  $\gamma_s$  = pure number (for  $s = 1, 2, 3, \dots$  etc.) representing different modes of vibration,  $q_s$  = circular frequency of the vibrating beam,  $y_a$  = displacement of the beam at the struck point ( $x = a = l/2$ ),  $y_1$  = displacement of the beam at any point  $x < l/2$ ,  $y_2$  = displacement of the beam at any point  $x > l/2$ ,  $P$  = pressure of impact (impact force) of the load,  $t$  = variable time,  $E_2$  = shape elastic factor (elastic constant other than Young's modulus, Banerjee 1966a) of the load.

#### *Duration of impact and its dependence on the striking velocity of the load*

In the present analysis the duration of impact  $\phi_0$  is defined as the time elapsed from the instant the beam and the load come in contact to the instant the contact terminates. In case of "multiple contact" it is therefore the duration of first contact.

Considering Hertz's theory of impact the duration of impact can be divided into three distinct periods, namely First Hertz, Hooke and Second Hertz, respectively, as has been done by Ghosh (1940) and Banerjee (1966c).

$$\text{During each Hertz period, } P = -k_0 u^{3/2} \quad \dots (5)$$

$$\text{During the Hooke period, } P = -E_2 u \quad \dots (6)$$

where  $k_0$  = Hertz constant, and  $u$  = compression of the load.

The duration of Hooke period  $\phi$  is the lowest positive root of  $t$  other than zero, obtained from equations (4) by solving  $P = 0$ . The duration of each Hertz period  $\tau_0$  as given by Ghosh (1940) and Banerjee (1966c) is  $\tau_0 = u_0/V_0$ ; (7) where,  $u_0$  is the limiting value of  $u$  at the end of each Hertz period. Thus, the total duration of impact is  $\phi_0 = \phi + 2\tau_0 = \phi + 2u_0/V_0$  ... (8)

#### *Energy of the beam*

From equation (3.1) the velocity of the load at any instant during impact is

$$V_t = \frac{dy_a}{dt} = 4V_0 \Sigma A_s \cos q_s t \quad \dots (9)$$

The energy absorbed by the beam is assumed to be the energy lost by the striking load during impact and is given by  $\frac{1}{2}m(V_0^2 - V_f^2)$ , where  $V_f$  = velocity of the load at the termination of final contact and can be obtained from equation (9). The initial energy of the load is  $\frac{1}{2}mV_0^2$ . Thus, the energy absorbed ratio of the beam (i.e., the ratio of the energy absorbed by the beam to the initial energy of the load)  $\mu$  is given by  $\mu = 1 - (V_f/V_0)^2$  ... (10)

#### *Impact on the beam at its midspan by a large striking mass*

When the mass of the striking load is very large in comparison with the mass of the struck beam (i.e.  $m/M$  is large), equation (1) indicates that for  $s = 2, 3$ , etc.,  $\gamma_s$  will tend to assume values  $5\pi/2, 9\pi/2$ , etc., approximately, and the values of  $\gamma_s/(\coth \gamma_s/2 - \cot \gamma_s/2)$  will tend to infinity. So no other terms except the fundamental ( $s = 1$ ) will be present (since  $A_s = 0$  for  $s = 2, 3, \dots$  etc.) as given by equation (3.4).  $\gamma_1$  will be approximately  $\pi/2$  and the value of  $\gamma_1/(\coth \gamma_1/2 - \cot \gamma_1/2)$  will be approximately 3.

Thus, combining equations (3.4) and (9) the final velocity  $V_f$  of the beam and the load after the termination of contact for  $\gamma_1 = \pi/2$  is

$$V_f = - \frac{V_0}{1 + \frac{1}{2} \cdot \frac{M}{m}} \quad \dots (11)$$

Equation (11) can be well compared with the expression of Cox given by

$$V_f = - \frac{V_0}{1 + \frac{17}{35} \cdot \frac{M}{m}} \quad \dots (12)$$

in which  $(17/35) M$  is the reduced mass of the beam.



The deflected shape of the beam carrying a concentrated load at midspan ( $a = l/2$ ) can be written as

$$\delta_1 = \delta_a \left[ 3 \left( \frac{x}{l} \right) - 4 \left( \frac{x}{l} \right)^3 \right] \quad \dots \quad (13.1)$$

$$\delta_2 = \delta_a \left[ 3 \left( \frac{l-x}{l} \right) - 4 \left( \frac{l-x}{l} \right)^3 \right] \quad \dots \quad (13.2)$$

where,  $\delta_1$  and  $\delta_2$  are the static displacement of the beam at any point  $x < l/2$  and  $x > l/2$  respectively, and  $\delta$  is the static displacement at  $x = a = l/2$ . Using Maclaurin's expansion series equations (3.2) and (3.3) for the fundamental mode of vibration ( $s = 1$ ) may be written as

$$y_1 \approx y_a \left[ c_1 \left( \frac{x}{l} \right) - c_2 \left( \frac{x}{l} \right)^3 \right] \quad \dots \quad (14.1)$$

$$y_2 \approx y_a \left[ c_1 \left( \frac{l-x}{l} \right) - c_2 \left( \frac{l-x}{l} \right)^3 \right] \quad \dots \quad (14.2)$$

where  $y_a$  is given by equation. (3.1)

$$c_1 = \gamma_1 \left[ \frac{\sinh \gamma_1 \cdot \sin \frac{\gamma_1}{2} - \sin \gamma_1 \cdot \sinh \frac{\gamma_1}{2}}{\sinh \gamma_1 \cdot \sin^2 \frac{\gamma_1}{2} - \sin \gamma_1 \cdot \sinh^2 \frac{\gamma_1}{2}} \right] \quad \dots \quad (14.3)$$

$$c_2 = \frac{\gamma_1^3}{6} \left[ \frac{\sinh \gamma_1 \cdot \sin \frac{\gamma_1}{2} + \sin \gamma_1 \cdot \sinh \frac{\gamma_1}{2}}{\sinh \gamma_1 \cdot \sin^2 \frac{\gamma_1}{2} - \sin \gamma_1 \cdot \sinh^2 \frac{\gamma_1}{2}} \right] \quad \dots \quad (14.4)$$

For  $\gamma_1 \leq \pi/2$ ,  $c_1$  and  $c_2$  are found to be approximately 3 and 4, respectively. Thus, as indicated by equations (13) and (14), the deflection curve of the beam during impact due to a large striking mass has almost the same shape as the static deflection curve. With this assumption Cox had developed an expression for dynamic deflection of a simply supported beam due to a falling load at the centre ( $a = l/2$ ) of the beam which may be written as

$$y_a = \delta_a + \left[ \delta_a^2 + \delta_a \times \frac{V_0^2}{g \left( 1 + \frac{17}{35} \cdot \frac{M}{m} \right)} \right] \quad \dots \quad (15.1)$$

where,  $\delta_a = \frac{mgl^3}{48E_1I}$ ,  $g$  = acceleration due to gravity. With the help of equation (1) the value of  $m/M$  for  $\gamma_1 = \pi/2$  is found to be 7.4. ... (15.2)

Thus, the equations (12) and (15) as given by Cox theory can be rightly employed if the ratio of the mass of the load to the mass of the beam (*i.e.*  $m/M$ ) equals or exceeds 7.4. Compared to this the author's analysis is perfectly general and equations (3) and (9) can be utilized for all *mass ratios*.

### EXPERIMENTS

Particulars of beams and hammers used in experiments are given in table 1 and 2 respectively

TABLE 1. Particulars of beams.

Beam	Material	Length (cm)	Diameter (cm)	Weight (gm)	$E_1$ (kg/cm <sup>2</sup> )
$B_1$	Mild steel	90	1.27	869	$2.07 \times 10^6$
$B_3$	Brass	90	1.27	953	$0.95 \times 10^6$

TABLE 2. Particulars of hammers (spherical)

Hammer	Material	Weight (gm)	Radius at contact surface (cm)
$H_1$	Mild steel	908.0	2.95
$H_2$	Mild steel	294.4	2.00
$H_4$	Mild steel	268.5	1.98
$H_4$	Mild steel	213.6	1.91
$H_5$	Mild steel	106.0	1.47
$H_6$	Brass	294.4	2.00

The experimental results of this investigation presented in tables 4 and 5 and figures 2 and 3 are entirely based on the photographic method as has been used by Banerjee (1964). The set up and procedure for obtaining photographs are exactly the same as employed by Das & Mishra (1968). A camera box with a narrow vertical slit in its front face and a tuning fork (100 cycles per sec) are placed parallel to the beam with the slit exactly behind the struck point. The hammer is allowed to drop from the desired height above the beam. Light from a carbon arc lamp is focussed to the slit of the camera box to obtain photographs of the motion of the beam and hammer and also of the pointer of the vibrating tuning fork on the running photographic paper pinned on a photo

carrier (sliding inside the camera box). A few of the photographs so obtained are shown in figure. 1 (Plate 2) and their details in table 3.

TABLE 3. Details of photographs

Beam-hammer	$B_1-H_2$	$B_1-H_2$	$B_1-H_1$	$B_1-H_6$	$B_1-H_3$	$B_2-H_2$
Striking velocity cm/sec	100	200	200	200	200	200
Reference to figure 1 (Plate 2)	A	B	C	D	E	F

For finding the energy absorbed by the beam during impact due to a particular hammer the experimental arrangement is similar to that used by Banerjee (1966b). The velocity  $V_0$  before impact and the velocity  $V_f$  after impact are calculated, respectively, from the measured drops and the corresponding rebound heights of the hammer. The experimental values of the energy-absorbed ratio  $\mu$  of the beam (table 6) are obtained from equation (10).

## RESULTS

For a particular beam-hammer combination equation (1) is solved graphically and then using the method of successive approximation closer results for the values of  $\gamma_s$  ( $s = 1, 2, 3$ , etc.) are obtained. Accordingly the results of the present theory are given in tables 5 and 6 and figures. 2 to 4.

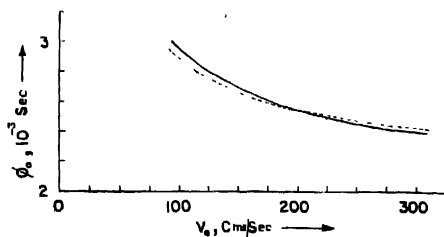


Figure 2. Theoretical (equation 8). --- Experimental (from Plate 2). Variation of the duration of impact ( $\phi_0$ ) with the striking velocity  $V_0$  for the beam  $B_1$  struck at midspan by hammer  $H_2$ .

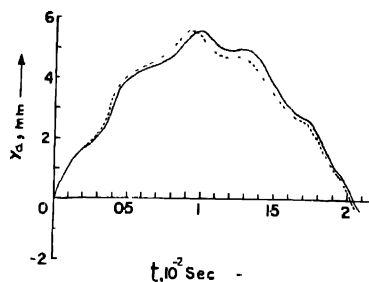


Figure 3 | Theoretical (equation 3.1) --- Experimental (figure 1B Plate 2). Time vs. displacement curves of the struck point (midspan). Beam  $B_1$ , hammer  $H_2$ ,  $V_0=200$  cm/s/Sec.

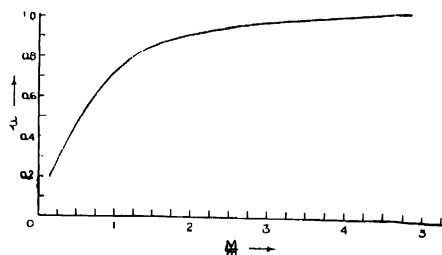


Figure 4. Theoretical curve (equation 10) of the energy-absorbed ratio  $M$ , vs. 'mass-ratio'  $M/m$  for the beam  $B_1$  struck at midspan

TABLE 4. Experimental values of the duration of impact  $\phi_0$  and maximum displacement ( $y_a$  max) at the struck point (midspan) of the beam for different striking velocities  $V_0$

$V_0$ (cm/sec)		100	150	200	250	300
$\phi_0$ ( $10^{-3}$ sec)	Beam $B_1$	2.89	2.66	2.55	2.48	2.43
	Hammer $H_2$					
	Beam $B_1$	2.98	2.74	2.62	2.55	2.50
	Hammer $H_2$					
$y_a$ max (mm)						
	Beam $B_1$	2.762	4.182	5.540	6.934	8.331
	Hammer $H_2$					

TABLE 5. Comparison of theoretical and experimental results for various beam-hammer combinations. The beam is struck at midspan with  $V_0 = 200$  cm/sec

Beam-hammer		$B_1-H_1$	$B_1-H_2$
Maximum displacement at struck point $y_a$ max, mm	Present theory equation (3.1)	12.23	5.492
	Cox Theory equation (15.1)	12.55	5.487
	Experiment	12.27	5.540
One-half of the period of vibration $\tau$ , sec	Present theory equation (3.1)	0.0280	0.0204
	Experiment	0.0273	0.0202

TABLE 6. Theoretical and experimental values of the energy-absorbed ratio ( $\mu$ ) of the beam  $B_1$  struck at midspan.

Hammer	Theoretical (Equation 10)	Experimental
$H_1$	0.7219	0.7396
$H_2$	0.9581	0.9614

### DISCUSSION OF RESULTS

1. For a particular beam-hammer combination the duration of impact diminishes in magnitude as the striking velocity of the hammer increases (table 4 and figure 2)

2. For hammers of different materials having equal weight and equal radius at contact surface striking a particular beam with equal striking velocity the duration of impact is different (table 4). These small variations are due to the difference in the elastic properties of the striking hammers.

3. For the beam struck by a particular hammer with different striking velocities the ratio between the amplitudes of experimental time-displacement curves (and thus the maximum displacement) of the beam and the corresponding striking velocity of the hammer is nearly the same (table 4). This is in full agreement with the theory given by equation (3.1).

4. The general shape of vibration curves of a particular beam struck by hammers of equal mass but of different elasticity is almost alike (figures 1B and 1D Plate 2).

5 The vibration patterns of beams of different materials (hence different masses) having same length and cross-section are almost similar, the ratio of the mass of the beam to the mass of the hammer being equal in each case (figures 1E and 1F Plate 2).

6. For a particular beam, as the mass of the hammer decreases, the ratio of the loss of energy to the initial energy of the hammer, *i.e.* the energy-absorbed ratio of the beam tends to assume a constant maximum value (figure 4).

7 For a simply supported beam struck at midspan, the Cox theory can be rightly applied when the ratio of the mass of the load to the mass of the beam equals or exceeds 7.4.

### CONCLUSION

Outside the duration of impact the motion of the beam given by displacement equation (3.1) will be affected due to the detachment of the load and its subsequent contacts with the beam (*i.e.* due to 'multiple contact'). Thus the results of the present theory given in figures 3 and 4 and tables 5 and 6 are to be slightly modified. This aspect is at present under the study of the author and will be reported in a subsequent paper.

### ACKNOWLEDGEMENT

The author is grateful to Dr. B. B. Banerjee, University College of Engineering, Burla, for valuable suggestions, and to Dr. M. Ghosh, City College, Calcutta, for interest in this work. Thanks are due to Prof. B. Mahapatra, Principal, University College of Engineering, for providing facilities for experiments. He also wishes to express his appreciation to Sri A. V. Acharyulu of the Civil Engineering Department of the College for drawings in the paper.

### REFERENCES

- Banerjee, B. B. 1964 *Ind. Jour. Phys.* **38**, 99.  
 1966a *Ind. Jour. Phys.* **40**, 198.  
 1966b *Ind. Jour. Phys.* **40**, 221.  
 1966c *Ind. Jour. Phys.* **40**, 215.  
 Cox, H. 1856 *Trans. Cam. Philos. Soc.* **9**, 73.  
 Das, R. N. & Mishra, K. 1968 *Jour. Inst. Eng. (India)*, **49**, 29.  
 Ghosh, M. 1940 *Ind. Jour. Phys.* **14**, 495.  
 Hertz, H. 1927, *Mathematical Theory of Elasticity*, Love, A. E. H. Cambridge University Press, 4th edition, p. 193.  
 Hoppman, W. H. 1948 *Jour. of Appl. Mech.* **15**, 125.  
 Timoshenko, S. 1956 *Vibration Problem in Engineering*, 3rd edition, p. 411, C. Van Nostrand Company Inc. Princeton, NJ.

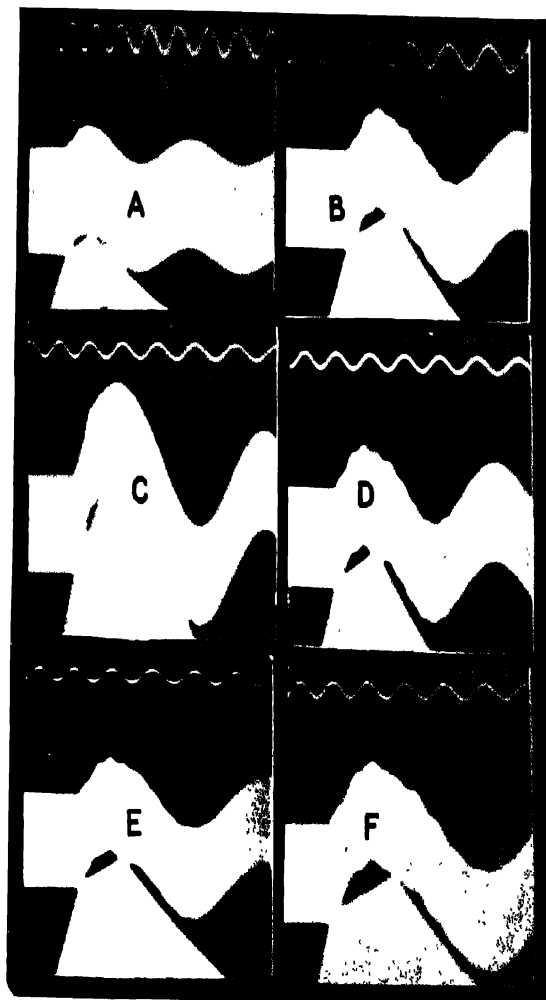


Figure 1. Photographs at the struck point (mid span) of the beams.





## Magnetic studies on natural crystals of wolframite (Fe,Mn)WO<sub>4</sub>

By S. R. GUHA THAKURTA

Department of Magnetism, Indian Association for the Cultivation of  
Science, Calcutta-32

(Received, 2 December, 1969)

The anisotropy and susceptibility of the naturally occurring single crystals of wolframite (Fe,Mn)WO<sub>4</sub> were measured over the temperature range from 90°K to 700°K. Although wolframite is a mixed crystal of Fe<sup>3+</sup> and Mn<sup>2+</sup> ions, the magnetic behaviour of each type could be separately obtained by assuming a perfect Curie law and magnetic isotropy for Mn<sup>2+</sup> in this mixed system. The anisotropy and susceptibility due to Fe<sup>3+</sup> ion only, calculated from those of the observed values of the mixed crystal were then compared with the theory worked out on the method based on Abragam & Pryce and Bose *et al.* Both the spin-orbit coupling coefficient and the effective orbital reduction factors along and perpendicular to the trigonal axis of symmetry of the ion are reduced anisotropically from its free ion value indicating anisotropic overlapping of the central charge clouds of Fe<sup>3+</sup>(3d<sup>5</sup>) with *s*- and *p*-charge clouds of the surrounding oxygen ligands. Inferences have been drawn regarding the marked variation of the anisotropic ligand field with temperature.

### INTRODUCTION

Wolframite [(Fe, Mn)WO<sub>4</sub>], the chief ore of tungsten occurs in nature in the form of crystals commonly of tabular form, belonging to the monoclinic system and having perfect cleavage along the (010) plane. From some preliminary magnetic measurements (Spoker & Mitchell 1958) with powdered samples at room temperature only, it has been found to be highly paramagnetic. But no further investigations with single crystals and at different temperatures which are essential for understanding its paramagnetic behaviour have yet been reported. We have therefore undertaken an extensive series of measurements of the magnetic anisotropies and susceptibilities of some well developed natural crystals of wolframite over a wide range of temperature (90°K to 700°K) and the present communication gives an account of these measurements as well as a discussion of the results in the light of the existing theories (Abragam & Pryce 1951, Bose *et al* 1961, 1965).

### EXPERIMENTAL

**Samples.** Good samples of single crystals were cleaved out from a specimen of wolframite obtained from the collection of Late Professor K. S. Krishnan in this Association. A chemical analysis of the sample yielded the following results :

SiO <sub>2</sub>	—	0.68%
FeO	—	14.58%
MnO	—	9.15%
WO <sub>3</sub>	—	75.50%

i.e., (0.614 FeO, 0.386 MnO)  $\text{WO}_3$  as the composition of the wolframite sample, used in our investigation.

The reported structural data of wolframite (Wyckoff, 1965) as given below have also been verified here by X-rays.

Crystal system : monoclinic space group :  $C_{2h}^4 (P2/c)$

Unit cell dimensions .  $a = 4.82$ ,  $b = 5.76$ ,  $c = 4.97$ ,  $\beta = 90^\circ 53'$

There are two molecules in the unit cell, one being derived from the other by reflection in the (010) plane. From X-ray data it has been found that the octahedron of six oxygen atoms surrounding each  $\text{Fe}^{2+}$  or  $\text{Mn}^{2+}$  ion, has an approximate trigonal symmetry. It is important to note here that the  $\text{Mn}^{2+}$  ion shows practically no anisotropy compared to the  $\text{Fe}^{2+}$  ion (Krishnan *et al* 1936, 1938) so that the anisotropy of the crystal may be safely treated as arising from the  $\text{Fe}^{2+}$  ion only. The mean susceptibility is contributed by both the ions according to their individual effective moments and concentration in the crystal. It is however, known that the effective moment of octahedral  $\text{Mn}^{2+}$  is very close to its spin only value and obeys Curie-law very closely. Thus, as will be seen later the peculiarities in the anisotropy and susceptibility behaviours of the crystal will be mainly the features of the  $\text{Fe}^{2+}$  ion contained in it.

#### MEASUREMENTS OF ANISOTROPY

The magnetic anisotropy of the crystal was measured by the usual 'null deflection' method of Dutta (1956) which is a much more precise modification of the 'critical torque' method of Krishnan *et al* (1936). The crystal was first suspended with  $b$ -axis vertical. The crystal being monoclinic with  $\beta \simeq 90^\circ$  and  $b$ -axis coinciding with the principal crystalline susceptibility  $\chi_3$ , we have from the measurement with this suspension

$$\Delta\chi = \chi_1 - \chi_2 \quad \dots (1)$$

where  $\Delta\chi$  is the anisotropy in the horizontal plane, (010) in this case and  $\chi_1$  and  $\chi_2$  are the maximum and minimum principal crystalline susceptibilities, respectively, in this plane. The sample crystal was in the form of an approximately circular disc, the plane of the disc being parallel to (010) plane. With such a sample  $a$ -axis or  $c$ -axis could not be recognised in the  $a$ - $c$  plane and hence the usual procedure could not be adopted for further measurement of anisotropy with some other known axis vertical. Hence we adopted the following procedure. An arbitrary line was marked on the sample disc and its orientation with respect to  $x_1$  axis was noted (at different temperatures) during measurements with  $b$ -axis vertical (see Datta 1956).

The crystal was then suspended with this arbitrary line in the  $a$ - $c$  plane vortical. The crystal was found to set with  $b$ -axis perpendicular to the magnetic field. From measurements with this suspension we obtain

$$\Delta\chi = (\chi_1 - \chi_3) - (\chi_1 - \chi_2) \cos^2\theta \quad \dots (2)$$

where  $\theta$  is the angle between the arbitrary line and  $\chi_1$  direction.

#### PRINCIPAL IONIC ANISOTROPIES

From the above values of crystalline anisotropies the principal ionic anisotropy (which as already mentioned refers to the  $\text{Fe}^{2+}$  ion) can be obtained as follows.

$$K_{\parallel} - K_{\perp} = 2(\chi_1 - \chi_2) - (\chi_1 - \chi_3) \quad \text{when } K_{\parallel} < K_{\perp} \quad \dots (3)$$

$$\text{or } K_{\perp} - K_{\parallel} = (\chi_1 - \chi_2) + (\chi_1 - \chi_3) \quad \text{when } K_{\perp} < K_{\parallel} \quad \dots (4)$$

where  $K$  is the principal ionic susceptibility along the trigonal axis of the  $\text{Fe}^{2+}\text{O}_6$  cluster and  $K_{\perp}$  is that perpendicular to that axis.

$$\left. \begin{aligned} \text{Also, } \cos 2\phi &= \frac{\chi_1 - \chi_3}{K_{\parallel} - K_{\perp}} \quad \text{when } K_{\parallel} > K_{\perp} \\ \text{and } \cos 2\phi &= \frac{(\chi_1 - \chi_2) - (\chi_1 - \chi_3)}{K_{\perp} - K_{\parallel}} \quad \text{when } K_{\parallel} < K_{\perp} \end{aligned} \right\} \quad \dots (5)$$

where  $2\phi$  is the angle between the symmetry axes of two magnetically inequivalent ions in the unit cell. The sign of  $|K_{\parallel} - K_{\perp}|$  can be determined from epr results or in some cases from magnetic anisotropies. Thus our magnetic investigation unambiguously shows that  $K_{\perp} > K_{\parallel}$ , the other alternative  $K_{\parallel} > K_{\perp}$  leading to an absurd value of  $\cos 2\phi > 1$ . This peculiarity of the ionic magnetic ellipsoid is common to many ferrous salts (Guha Thakurta *et al* 1966).

#### MEASUREMENTS OF SUSCEPTIBILITY

We have measured the mean susceptibility  $\bar{\chi}$  with powdered samples of wolframite. For this purpose the crystals were finely powdered in an agate mortar and tightly packed in a quartz container. The container was suspended in between the poles of an electromagnet from one end of the beam of a sensitive jewel-pivoted microbalance (Das, 1963) and the susceptibility was measured in the manner already described by her. The values are corrected as usual for diamagnetism.

#### MEASUREMENTS AT DIFFERENT TEMPERATURES

For low temperature measurement of  $\Delta\chi$ 's and  $\bar{\chi}$ , the specimens were kept suspended in the experimental chamber of a gas-flow type of cryostat (Bosc 1947),

the temperatures being recorded by a calibrated copper-constantan thermo-couple. For high temperature measurements the specimens were suspended in a tubular electric furnace with non-inductive windings, the temperature being recorded by a calibrated chromel-alumel thermo-couple.

Table I. Anisotropy and susceptibility of  $(\text{Fe, Mn})\text{WO}_4$ 

Temp. in °K	$\theta$	$(\chi_1 - \chi_2) \times 10^6$	$(\chi_1 - \chi_3) \times 10^6$	$(K_1 - K_2) \times 10^6$	$2\phi$	$\chi \times 10^6$
90	26°6'	5970	6930	12900	94°16'	41098
100	26°18'	5016	5924	10940	94°46'	36932
150	27°42'	2748	3352	6100	95°41'	24722
200	27°7'	1855	2295	4150	96°5'	18622
250	30°24'	1370	1710	3080	96°22'	14932
300	31°42'	1076	1354	2430	96°33'	12480
350	33°00'	827	1048	1875	96°53'	10693
400	34°24'	640	815	1455	96°56'	9399
450	35°42'	505	645	1150	97°40'	8376
500	37°00'	381	491	872	97°12'	7548
550	38°12'	293	377	670	97°18'	6886
600	39°24'	211.5	273.5	485	97°24'	6273
650	40°30'	161	209	370	97°27'	5793
700	41°36'	116	149	265	97°29'	5361

## THEORY OF THE LIGAND FIELD OF WOLFRAMITE

Wolframite is a mixed crystal of  $\text{FeWO}_4$  and  $\text{MnWO}_4$ . The  $\text{Fe}^{2+}$  or  $\text{Mn}^{2+}$  ion is surrounded by six oxygens forming a slightly trigonally distorted octahedron. Now,  $\text{FeO}$  or  $\text{MnO}$  single crystals are antiferromagnetic, the Neel temperature being 198°K and 122°K, respectively (Bizette 1956). But in wolframite within the range of our experiment (700°K to 90°K), no antiferromagnetic behaviour was observed. This is apparently due to the fact that the distance between  $\text{Fe}^{2+}$ — $\text{Fe}^{2+}$  or  $\text{Mn}^{2+}$ — $\text{Mn}^{2+}$  is much greater here because of the presence of intervening diamagnetic tungsten atoms so that the exchange interaction is comparatively much weaker. Moreover,  $\text{Fe}^{2+}$  being in  $D$  state and  $\text{Mn}^{2+}$  in  $S$  state, any antiferromagnetic exchange between them, if present, will be also very weak. It is to be noted that the observed magnetic behaviour of the substance does not favour the strong field scheme, since  $\text{Fe}^{2+}(3d^6)$  becomes diamagnetic and  $\text{Mn}^{2+}(3d^5)$  becomes single spin system under this scheme. The very large observed value about 5.477 BM for effective magnetic moment of the combined system at room temperature definitely precludes this possibility. We should therefore treat the crystal field behaviour of the system under the usual weak field scheme.

Since  $\text{Mn}^{2+}(3d^5)$  is an  $S$  state ion, its anisotropy will be negligible ( $\sim 0.1\%$  of the mean susceptibility, Krishnan & Banerji 1936). So the observed anisotropy

may be regarded as due to  $\text{Fe}^{2+}$  alone. Again the susceptibility of  $S$ -state  $\text{Mn}^{2+}$  will follow very closely the Curie's law (Van Vleck & Penney 1934), having effective magnetic moment 5.916 BM. Hence, subtracting the susceptibility of  $\text{Mn}^{2+}$  from the observed susceptibility of the crystal (with due consideration of the percentage composition) we get that of  $\text{Fe}^{2+}$  only. The ligand field having no effect on the  $\text{Mn}^{2+}$  ion to a high approximation, the susceptibility and anisotropy obtained for  $\text{Fe}^{2+}$  only are then treated with the ligand field theory of  $\text{Fe}^{2+}$  ion.

### THEORY OF THE LIGAND FIELD IN $\text{Fe}^{2+}$ ION

From X-ray data, it is found that the  $\text{Fe}^{2+}$  ion is under a predominant cubic field with a small superimposed trigonal component. Under the predominant cubic component of the ligand field, the five-fold orbital degeneracy of the ground state  $3d^6 {}^5D$  of  $\text{Fe}^{2+}$  ion in the free state is split up into an orbital doublet  ${}^5E_{2g}$  and a triplet  ${}^5T_{2g}$ , the triplet lying lower.

In calculating the energy levels of  $\text{Fe}^{2+}$  complex we employ the technique of Abragam & Pryce (1951) in treating the  ${}^5T_2$  state as an effective  ${}^5P$  state with a fictitious orbital angular momentum quantum number  $l' = 1$  and effective Lande factors  $-\alpha_{||}$ ,  $-\alpha_{\perp}$  ( $||$ ,  $\perp$  to the trigonal axis), and then apply the trigonal component of the field ( $V_t$ ) and spin orbit ( $\xi L \cdot S$ ) perturbations  $[-\alpha_{||}\xi_{||}L'_zS_z - \alpha_{\perp}\xi_{\perp}(L'_xS_x + L'_yS_y)]$  together. The effect of admixture of the upper  ${}^5E_2$  state enters through  $\alpha_{||}$ ,  $\alpha_{\perp}$ .

The finite structure energy levels arising out of the splitting of the cubic orbital triplet  ${}^5T_{2g}$  under the combined action of the axial component of the ligand field and the spin-orbit interaction are given by (Bose & Rai, 1965)

$$\begin{aligned} E_0 &= \frac{1}{2}[(\alpha_{||}\xi_{||} + \Delta) - \{(\alpha_{||}\xi_{||} - \Delta)^2 + 24\alpha_{\perp}^2\xi_{\perp}^2\}^{\frac{1}{2}}] \\ E_1 &= \alpha_{||}\xi_{||}x_1 \\ E_2 &= \frac{1}{2}[(\Delta - \alpha_{||}\xi_{||}) - \{(\Delta + \alpha_{||}\xi_{||})^2 + 8\alpha_{\perp}^2\xi_{\perp}^2\}^{\frac{1}{2}}] \\ E_3 &= \alpha_{||}\xi_{||}x_3 \\ E_4 &= \alpha_{||}\xi_{||} \\ E_5 &= \frac{1}{2}[(\alpha_{||}\xi_{||} + \Delta) + \{(\alpha_{||}\xi_{||} - \Delta)^2 + 24\alpha_{\perp}^2\xi_{\perp}^2\}^{\frac{1}{2}}] \\ E_6 &= \alpha_{||}\xi_{||}x_6 \\ E_7 &= \frac{1}{2}[(\Delta - \alpha_{||}\xi_{||}) + \{(\Delta + \alpha_{||}\xi_{||})^2 + 8\alpha_{\perp}^2\xi_{\perp}^2\}^{\frac{1}{2}}] \\ E_8 &= -2\alpha_{||}\xi_{||} \end{aligned}$$

where  $x_j$ 's ( $j = 1, 3, 6$ ) are the roots of cubic equation

$$x^3 - (2 + \eta)x^2 + (2\eta - 5\rho^2)x + 6\rho^2 = 0,$$

here

$$\rho = \frac{\alpha_{\perp}\xi_{\perp}}{\alpha_{||}\xi_{||}}; \quad \eta = \frac{\Delta}{\alpha_{||}\xi_{||}}$$

and  $\Delta$  is the trigonal field separation between the split components (a doublet and a singlet) of the triplet  ${}^5T_{2g}$

The corresponding eigen states are .

$$\begin{aligned}
 \psi_0 &= a_0 |1, -1\rangle + b_0 |0, 0\rangle + a_0 | -1, 1\rangle \\
 \psi_1 &= a_1 |1, 0\rangle + b_1 |0, 1\rangle + c_1 | -1, 2\rangle \\
 \psi_{-1} &= a_1 | -1, 0\rangle + b_1 |0, -1\rangle + c_1 |1, -2\rangle \\
 \psi_2 &= b_2 |1, 1\rangle + a_2 |0, 2\rangle \\
 \psi_{-2} &= b_2 | -1, -1\rangle + a_2 |0, -2\rangle \\
 \psi_3 &= a_3 |1, 0\rangle + b_3 |0, 1\rangle + c_3 | -1, 2\rangle \\
 \psi_{-3} &= a_3 | -1, 0\rangle + b_3 |0, -1\rangle + c_3 |1, -2\rangle \\
 \psi_4 &= 1/\sqrt{2} |1, -1\rangle - 1/\sqrt{2} | -1, 1\rangle \\
 \psi_5 &= b_0/\sqrt{2} |1, -1\rangle - \sqrt{2} a_0 |0, 0\rangle + b_0/\sqrt{2} | -1, 1\rangle \\
 \psi_6 &= a_0 |1, 0\rangle + b_0 |0, -1\rangle + c_0 | -1, 2\rangle \\
 \psi_{-6} &= a_0 | -1, 0\rangle + b_0 |0, -1\rangle + c_0 |1, -2\rangle \\
 \psi_7 &= a_2 |1, 1\rangle - b_2 |0, 2\rangle \\
 \psi_{-7} &= a_2 | -1, -1\rangle - b_2 |0, -2\rangle \\
 \psi_8 &= |1, 2\rangle \\
 \psi_{-8} &= | -1, -2\rangle
 \end{aligned}$$

where

$$\begin{aligned}
 a_0 &= \frac{\sqrt{3} \alpha_1 \xi_1}{(\alpha_{||} \xi_{||} - E_0)} b_0 ; & 2a_0^2 + b_0^2 &= 1 \\
 a_j &= -\frac{\sqrt{3}(2\alpha_{||}\xi_{||} - E_j)}{\sqrt{2}E} & a_j^2 + b_j^2 + c_j^2 &= 1 \\
 b_j &= \frac{2\alpha_{||}\xi_{||} - E_j}{\sqrt{2}\alpha_1 \xi_j} c_j ; & j &= 1, 3, 6
 \end{aligned}$$

and 
$$a_2 = \frac{\sqrt{2}\alpha_1 \xi_1}{\Delta - E_2} b_2 ; \quad a_2^2 + b_2^2 = 1$$

On these fine structure energy levels we apply the magnetic perturbation  $[\beta H_x(-\alpha_1 l_x + 2S_x) + \beta H_y(-\alpha_1 l_y + 2S_y) + \beta H_z(-\alpha_{||} l_z + 2S_z)]$  to get the expressions for magnetic susceptibilities. If we then expand the energy in powers of the field strength  $H$ , we get,

$$W = W_0^{(0)} + W_0^{(1)}H + W_0^{(2)}H^2 + \dots,$$

where the first term is the unperturbed energy, the second and the third terms are the first-order and second order Zeeman energy terms, respectively. Then,

the magnetic susceptibility upto the second order is given by (Van Vleck 1932),

$$K_p = N \frac{\sum_i [W_i^{(1)2}/kT - 2W_i^{(2)}] \exp(-W_i^{(0)}/kT)}{\sum_i \exp(-W_i^{(0)}/kT)}, \quad (p = \parallel \text{ or } \perp)$$

where  $N$  is the Avogadro number and  $k$  is the Boltzmann constant.

Final expressions for  $K_{\parallel}$  and  $K_{\perp}$  have been given by Bose & Rai (1965). The expressions being very lengthy, we do not present them again here.

#### COMPARISON OF THE EXPERIMENTAL RESULTS WITH THEORY AND DISCUSSIONS

The mean susceptibility and anisotropy of some of the  $\text{Fe}^{2+}$  salts measured by different authors are given below for comparison

Table 1

Salts	Temp °K	$\bar{K} \times 10^6$	$\Delta K \times 10^6$
$^1\text{Fe}(\text{NH}_4\text{SO}_4)_2 \cdot 6\text{H}_2\text{O}$	300	12080	2620 ( $K_{\parallel} > K_{\perp}$ )
	100	36380	22040
$^2\text{Fe}(\text{KNO}_3)_2 \cdot 6\text{H}_2\text{O}$	300	11790	3913 ( $K_{\parallel} > K_{\perp}$ )
	100	35980	24470
$^*\text{FeSiF}_6 \cdot 6\text{H}_2\text{O}$	300	12470	2854 ( $K_{\perp} > K_{\parallel}$ )
	100	38800	14570
$^{++}(\text{Fe, Mn})\text{WO}_4$	300	11150	2430 ( $K_{\perp} > K_{\parallel}$ )
	100	32625	10940

<sup>1</sup>Mukhopadhyay *et al* (to be published); <sup>\*</sup>Mazumdar, 1966; <sup>++</sup>Present author.

It will be seen that for the first and third crystals the anisotropies are of same sign to the present case and the order of  $\bar{K}$  is also the same indicating similar ligand fields in them. The experimental anisotropy and susceptibility of  $\text{Fe}^{2+}$  ion (of wolframite) are compared with the theoretically computed values in table 2.

In theoretical computation we have derived by trial and error a set of values for  $\alpha_{\parallel}k_{\perp}$ ,  $\alpha_{\perp}k_{\parallel}$ ,  $\alpha_{\parallel}\zeta_{\parallel}$ ,  $\alpha_{\perp}\zeta_{\perp}$  and  $\Delta$ , which gives the best fit with both the anisotropy and the susceptibility data, assuming that the first four parameters are independent of temperature. This is true for the absolute values to a good degree of approximation since the predominant cubic field mainly arises from the nearest strongly bound neighbours, but the anisotropy in  $\alpha$ 's  $k$ 's and  $\zeta$ 's may be dependent on temperature in the same way as  $\Delta$ . Since the explicit relation between these anisotropic factors are not known, to avoid too many temperature dependent parameters, we throw the entire burden of the thermal dependence on  $\Delta$  which may then cause this effect to be somewhat exaggerated. Our main purpose,

however, is to show the rough magnitude of this dependence hence we are justified in taking  $\Delta$  as the only variable with temperature.

In our case  $\Delta$  is negative. If we take  $\Delta$  as positive the doublet  $|\pm 1\rangle$  occupy the lowest position giving  $g_{\parallel} > g_{\perp}$  ( $g_{\perp} \approx 0$ ) which implies  $K_{\parallel} > K_{\perp}$ . But our magnetic measurement definitely shows that  $K_{\perp} > K_{\parallel}$ ; also we failed to fit the susceptibility and anisotropy data simultaneously, with any reasonable values of the parameters if  $\Delta$  is taken as positive. Hence, we have fitted the experimental data with  $\Delta$  negative which is consistent with the case of trigonally distorted  $\text{FeSiF}_6 \cdot 6\text{H}_2\text{O}$  (Bose & Rai, 1965). With  $\Delta$  negative, the singlet  $E_0$  lies lowest. Moreover, the energy levels  $E_i$ ,  $i = 0, 1, 2, \dots, 8$ , follow the sequence in order of increasing values as calculated from our results given in table 3, agreeing with the sequence reported by Eicher (1963).

Table 2. Comparison of the theoretical and experimental values of  $(K_{\perp} - K_{\parallel})$  and  $\bar{K}$  with :

$$\alpha_{\perp} k_{\perp} = 0.8, \quad \alpha_{\perp} \xi_{\perp} = -80 \text{ cm}^{-1}$$

$$\alpha_{\parallel} k_{\parallel} = 0.7, \quad \alpha_{\parallel} \xi_{\parallel} = -77 \text{ cm}^{-1}.$$

Temperature °K	$-\Delta \text{ (cm}^{-1}\text{)}$	$(K_{\perp} - K_{\parallel})$ $\times 10^6$	$\bar{K} \times 10^6$
90	950	12960 (12900)	36523 (30350)
100	960	10997 (10940)	32879 (32625)
150	925	6135 (6100)	22084 (21914)
200	890	4186 (4150)	16654 (16507)
250	850	3097 (3080)	13402 (13308)
300	800	2436 (2430)	11208 (11150)
400	700	1466 (1455)	8493 (8427)
500	580	877 (872)	6812 (6789)
600	450	489 (485)	5647 (5629)
700	300	268 (265)	4834 (4800)

The values in the parenthesis are the experimental values.

$\Delta$  is found to vary with temperature *e.g.*,  $\Delta = 950 \text{ cm}^{-1}$  at  $90^\circ\text{K}$  to  $\Delta = 300 \text{ cm}^{-1}$  at  $700^\circ\text{K}$ . We find that unless  $\Delta$  is varied with temperature the agreement of theoretical with experimental values at all but one temperature is poor with any



reasonable single set of parameters. The variation of  $\Delta$  with temperature is possibly connected with the change in the strength of the crystal field with temperature, which is also corroborated by the variation of  $\theta$  and  $\phi$  with temperature, indicating rotation of the magnetic ellipsoid in the crystal.

Table 3. Energy of the ligand field levels in  $\text{cm}^{-1}$ 

Temp. $^{\circ}\text{K}$	$E_0$	$E_1$	$E_2$	$E_3$	$E_7$	$E_8$				
90	-950	-992.0	-984.9	-962.3	-140.3	-77.0	-35.0	21.3	89.3	154.0
300	-800	-849.7	-841.4	-814.4	-137.9	-77.0	-27.3	25.3	91.4	154.0
700	-300	-414.0	-400.0	-331.3	-117.1	-77.0	37.0	63.1	108.6	154.0

The variation of  $\Delta$  (from  $90^{\circ}\text{K}$  to  $700^{\circ}\text{K}$ ) is about 68%. This large variation of  $\Delta$  as already mentioned is perhaps somewhat exaggerated and can be perceptibly reduced by varying  $\alpha$ 's,  $k$ 's and  $\zeta$ 's with temperature, but then there will be too many parameters for unique solution of their values from the limited experimental data.

Table 1 shows that  $\theta$  changes by about  $15^{\circ}$  while  $\phi$  changes by about  $3^{\circ}$  only within the range of temperature from  $90^{\circ}\text{K}$  to  $700^{\circ}\text{K}$ . This shows that the ions rotate appreciably about an axis approximately parallel to the  $b$ -axis of the crystal as the temperature changes. A rotation of the ion about an axis parallel to  $b$ -axis will not be reflected in the values of  $\phi$ , but it will manifest itself appreciably in the value of  $\theta$ . This rotation affects the packing of the lattice with consequent changes in the anisotropic part of the ligand field with temperature.

The values of the parameters ( $\Delta$ ,  $\alpha_{\parallel}k_{\parallel}$ ,  $\alpha_1 k_1$ ,  $\alpha_{\parallel}\zeta_{\parallel}$ ,  $\alpha_1 \zeta_1$ ) in table 4 are of the expected order of magnitude as observed in other bivalent iron salts.

Table 4. Comparison of the field parameters of different salts.

Salts	$\Delta$ $\text{cm}^{-1}$ at 300°K	$\Delta$ $\text{cm}^{-1}$ at 100°K	$\alpha_{\parallel}k_{\parallel}$	$\alpha_1 k_1$	$\alpha_{\parallel}\zeta_{\parallel}$ $\text{cm}^{-1}$	$\alpha_1 \zeta_1$ $\text{cm}^{-1}$
$\text{Fe}(\text{NH}_4\text{SO}_4)_2 \cdot 6\text{H}_2\text{O}$	-400		0.9	0.9	-80	-80
$\text{Fe}(\text{KSO}_4)_2 \cdot 6\text{H}_2\text{O}$	660	260	0.8	0.7	-88	-80
$\text{FeSiF}_6 \cdot 6\text{H}_2\text{O}$	-685	-815	0.8	0.8	-87	-90
$(\text{Fe}, \text{Mn})\text{WO}_4$	-800	-950	0.7	0.8	-77	-80

By comparison of the above values it is apparent that the axial field (tetragonal) splitting in the second Tutton salt is of opposite sign to our case, also the variations

with temperature are different in the same range. The other parameters are not very different showing that the covalency effect is more or less the same. The several parameters in the fluosilicate (trigonal distortion) compare very well with the present case in magnitude (also in sign for  $\Delta$ ) as is to be expected. Thus in spite of the very different structure of the two crystals, the ligand fields and the magnetic behaviours are in good general agreement. The values of  $\alpha_{||}$  &  $\alpha_{\perp}$  in the case of trigonally distorted  $\text{Fe}^{2+}$  ion is expected to deviate from unity somewhat more than in the tetragonal case. However, we cannot exactly evaluate  $\alpha_{||}$  &  $\alpha_{\perp}$  in our case. Under the circumstances, taking them approximately equal to unity, the spin-orbit coupling coefficient comes out as reduced on the average by about 23% from its free ion value  $-103 \text{ cm}^{-1}$ , due to overlap of the central  $3d$  charge cloud with the surrounding  $s$  and  $p$ -charge clouds of the ligand oxygen atoms. The overlap is likely to be anisotropic; hence the reductions in the spin-orbit coupling and the effective orbital factor are taken to be anisotropic in comparing the experimental data.

*g-values* The lowest level  $E_0$  is singlet, followed by the doublet  $E_1$ ,  $\sim 10 \text{ cm}^{-1}$  higher up. The expressions for  $g$ -values are as follows :

$$g_{||} = \{(4 + \alpha_{||}k_{||})c_1^2 + 2b_1^2 - \alpha_{||}k_{||}a_1^2\}$$

$$g_{\perp} = \{2\sqrt{3}a_1a_0 - \alpha_{\perp}k_{\perp}(a_1b_0 + b_1a_0) + 2\sqrt{3}b_1b_0 + 2\sqrt{2}c_1a_0\}$$

No experimental resonance data for  $g_{||}$  and  $g_{\perp}$  on wolframite are available. But from our magnetic susceptibility data at  $300^\circ\text{K}$  we can calculate  $g_{||}$  and  $g_{\perp}$  as  $g_{||} = 2.0508$  and  $g_{\perp} = 3.7527$ . From these values the calculated mean  $g$ -value comes out as  $3.285$  which may be compared with the mean  $g$  value of Low's result,  $g = 3.42$  (Low & Weger 1960) for  $\text{Fe}^{2+}$  ion embedded in  $\text{MgO}$ , in which the field has purely cubic symmetry, and with  $2.99$  calculated from the observed  $g$ -values ( $g_{||} = 8.97$ ,  $g_{\perp} = 0$ ) for  $\text{FeF}_2$  embedded in  $\text{ZnF}_2$  (Tinkham, 1956), where  $\text{Fe}^{2+}$  ions have approximately tetragonal symmetry. The difference is quite appreciable and is to be expected in view of the different ligand fields in these crystals.  $g$ -values of  $\text{FeSiF}_6$  calculated from magnetic susceptibility ( $g_{||} = 2.01$ ,  $g_{\perp} = 3.76$ ,  $\bar{g} = 3.30$ , Bose and Rai, 1955, Mazumdar, 1966), where the symmetry of  $\text{Fe}^{2+}$  ions is trigonal, compare much better with the present crystal.

#### ACKNOWLEDGMENT

The author expresses his gratefulness to Shri A. K. Dutta for suggesting the problem and his constant guidance throughout the course of work. He is indebted to Prof. A. Bose for taking keen interest in the work. He is also thankful to Dr U. S. Ghosh for valuable and stimulating discussions and Mr. M. Saha for his assistance in the work. Thanks are also due to Dr D. R. Dasgupta for some helpful discussions regarding the structure and composition of the sample.

## REFERENCES

- Abragam A. & Pryce M. H. L. 1951 *Proc. Roy. Soc. A* **205**, 135.  
Bizotte H. 1946 *Ann. Phys. Paris*, **1**, 133.  
Bose A. 1947 *Indian J. Phys.* **21**, 275.  
Bose A., Chakrabarty, A. S. & Chatterjee, R. 1961 *Proc. Roy. Soc. A* **261**, 43, 207.  
Bose A. & Rai R. 1965 *Indian J. Phys.* **39**, 176.  
Das S. 1963, *Indian J. Phys.* **37**, 582.  
Dutta S. K. 1956 *D. Phil. Thesis (Calcutta University)*.  
Fischer H. 1963 *Z. Physik* **171**, 582.  
Guha Thakurta D. & Mukhopadhyay D. 1966 *Indian J. Phys.* **40**, 69.  
Krishnan K. S. & Banerjee S. 1936 *Phil. Trans. Roy. Soc. A* **235**, 843  
Krishnan K. S. & Mookherji A. 1938 *Phil. Trans. Roy. Soc. A* **237** 135.  
Low W. & Weger M. 1960 *Phys. Rev.* **118**, 1130.  
Mazumdar M. 1966 *D. Phil. Thesis (Calcutta University)*.  
Spoker E. M. & Mitchell D. R. 1958 *Mining Eng* **10**, 373.  
Tinkham M. 1956 *Proc. Roy. Soc. A* **236**, 535  
Van Vleck J. H. & Penney G. 1934 *Phil. Mag.* **17**, 961.  
Wyckoff R. W. G. 1965 *Crystal structures*, Interscience Publishers, **3**, 43, 64

## The $\pi-\pi^*$ emission spectra of three isomeric fluorophenols in the near ultraviolet region

By (Miss) J. V. SHUKLA, K. N. UPADHYA and S. K. TIWARI

*Department of Spectroscopy, Banaras Hindu University, Varanasi-5*

(Received 5 December 1969—Revised 20 March and 8 August 1970)

(Plates 3—5)

The emission spectra of three isomeric fluorophenols have been recorded by means of an uncondensed transformer discharge on a Zeiss Medium Quartz Spectrograph. The spectra of ortho, meta and para-fluorophenols lie in the regions of 36950–34250  $\text{cm}^{-1}$ , 37410–33090  $\text{cm}^{-1}$  and 35770–30870  $\text{cm}^{-1}$  respectively. Assuming  $C_s$  symmetry for ortho and meta, and  $C_{2v}$  symmetry for para isomer, vibrational analyses have been proposed for the observed bands in each case.

### INTRODUCTION

The emission spectra of polyatomic molecules have been less thoroughly studied because of the rapid dissociation of the molecules before radiative emission. However, in benzene and some substituted benzenes it has been possible to obtain these spectra by means of controlled uncondensed transformer discharge. In continuation of our earlier work on substituted benzenes, the present paper deals with the emission spectra of three isomeric fluorophenols. Vibrational frequencies of para-fluorophenol have been theoretically interpolated by Kohlrausch (1947). Infrared and Raman studies of the fluorophenols in liquid phase have been made by Wittek (1935), Kohlrausch (1942) and Jakobson & Brewer (1962), whereas, the ultraviolet absorption studies have been made by Hodgcn (1943), Deardon & Forber (1959) and Tiwari (1963, 1966). Some bands of the emission spectra of *p*-fluorophenol have been studied by Tripathi *et al* (1963, 1968). High resolution studies on some of the absorption bands of *p*-fluorophenol have been carried out recently by Thakur & Tiwari (1968). It seems no emission study has been reported till now on all the isomers.

### EXPERIMENTAL

The chemicals were obtained from the Eastman Kodak Organic Chemical Company and purified before use. The spectra were excited by means of an uncondensed transformer discharge through the flowing vapour of the substance. The experimental details were similar to those reported earlier from this laboratory (Tiwari & Upadhyaya 1968). The discharge glow was quite feeble, hence the bands were recorded on Kodak I-0 plates by a Zeiss Medium Quartz Spectrograph using a slit width of 0.03 mm and giving an exposure of nearly 30 hrs in each case. The fluorescence spectrum of para fluorophenol has been obtained free from impurity spectrum. This spectrum was excited by the 2846.4 Å atomic

line of iron produced in spark. The details of the apparatus are as described by Bass & Sponer (1950). The fluorescence bands were recorded on the Medium Quartz Spectrograph using  $40\mu$  slit width on Kodak I-O plate and giving 80 hrs exposure.

### RESULTS

The emission spectra of ortho, meta and para-fluorophenols lie in regions  $36950-34250\text{ cm}^{-1}$ ,  $37410-33090\text{ cm}^{-1}$  and  $35770-30870\text{ cm}^{-1}$  are shown in figures 1, 2 and 3, respectively. In all the three cases a weak continuum is superimposed over the entire spectrum. The fluorescence spectrum of *p*-fluorophenol lies in the region  $35120-31260\text{ cm}^{-1}$ . In each case bands are quite sharp and degraded to the red side.

Para-fluorophenol belongs to  $C_{2v}$  point group and ortho and meta isomers belong to  $C_s$  point group. Under this assumption, the thirty three normal modes of vibration can be divided into  $12a_1+10b_1+3a_2+8b_2$  in  $C_{2v}$  point group and  $23a'+10a''$  in  $C_s$  point group. The electronic transitions involved in these three isomers correspond to  ${}^1A_{1g}-{}^1B_{2u}$  forbidden transition in benzene which becomes  ${}^1A'-{}^1A'$  in  $C_s$  and  ${}^1A_1-B_2^1$  in  $C_{2v}$  symmetry. The transition is an allowed  $\pi-\pi^*$  type with their transition moments lying in the molecular plane and expected to give strong (0, 0) band in all the three cases. It is observed that the (0, 0) band in the emission spectrum of the ortho derivative is weak, while in the other cases these are strong.

The (0, 0) band in the spectra of ortho, meta and para isomers are assigned at  $36803\text{ cm}^{-1}$ ,  $36625\text{ cm}^{-1}$  and  $35123\text{ cm}^{-1}$  respectively. The magnitude in each case is in agreement with their respective absorption spectra (Hedgen 1943, Tiwari 1966). In all the three spectra the ring vibration is dominating in comparison with the other mode, the magnitudes being  $857$ ,  $1008$  and  $855\text{ cm}^{-1}$  in *o*-, *m*- and *p*-isomers, respectively. The intensity of the corresponding band in ortho is weaker than in meta and para-isomers. The other  $C=C$  stretching vibrations corresponding to  $1596\text{ cm}^{-1}$  vibration of benzene appears with strong intensity in all the three spectra. The magnitudes are  $1603$ ,  $1616$  and  $1522$ , respectively, and all have totally symmetric character.

Of the substituent sensitive mode, C—F stretching is observed at  $1268$ ,  $1275$  and  $1241\text{ cm}^{-1}$  in *o*-, *m*- and *p*-isomer, respectively. These frequencies combine with totally symmetric vibration in each case as expected. The C—F planar bending is observed in meta compound only, whereas the O—H planar bending is observed in all the three compounds. The latter mode is prominent in the meta isomer only.

The C—C—C trigonal bending mode corresponding to the  $b_{1u}$  (1010) vibration of benzene appears very strongly in the infra-red, Raman and ultra-violet absorption spectra of orthofluorophenol. The strong band at  $36040\text{ cm}^{-1}$

associated with a frequency  $763\text{ cm}^{-1}$  can very well be attributed to this mode of vibration. The same mode of vibration in *p*-fluorophenol has been observed in a band at  $34377\text{ cm}^{-1}$  associated with a frequency  $746\text{ cm}^{-1}$ . However, in the emission spectrum of *m*-fluorophenol no such frequency could be observed. The detailed analyses of the spectra of ortho, meta and para are given in tables 1, 2 and 3, respectively.

Table 1

Relative Intensity	Wavenumbers in $\text{cm}^{-1}$		Difference from (0,0) in $\text{cm}^{-1}$	Assignments
	Absorption	Emission		
4	36951	36955	+ 152	0+152
3	36868	36873	+ 70	0+152-89
5	36800	36803	0	0-0
2	36774	36772	- 31	0-31
4	36712	36714	- 89	0-89
1	36658	36660	- 134	0-284+152
4	36612	36618	- 185	0-2×89
5	36519	36519	- 284	0-284
4		36427	- 376	0-284-89
4	36400	36390	- 413	0-562+152
3	36329	36329	- 474	0-284-2×89
9	36240	36241	- 562	0-562
2		36209	- 594	0-562-31
1		36181	- 622	0-162-2×31
3	36147	36144	- 659	0-562-89
1		36097	- 706	0-143-562
10	36036	36040	- 763	0-763
5	36003	36003	- 800	0-763-31
3	35954	35953	- 850	0-850, 0-763-89
1	35900	35898	- 905	0-763-143
8		35777	-1026	0-1026
7		35687	-1116	0-2×562, 0-1026-89
2		35646	-1167	0-2×562-31
6		35613	-1190	0-1190, 0-1026-2×89
7		35535	-1268	0-1268
6		35476	-1327	0-562-703
3		35447	-1356	0-1268-89
5		35395	-1408	0-562-763-89
5		35370	-1433	0-1026-562+152
5		35342	-1461	0-1461, 0-1026-562+152-31
3		35272	-1531	0-2×763
2		35200	-1603	0-1603
2		35151	-1652	0-2×763-143
2		35135	-1668	0-2×763-28+152
2		35043	-1760	0-2×763-143-89
2		35002	-1801	0-2×763-284
3		34977	-1826	0-1268-562
1		34914	-1889	0-1603-284
2		34857	-1946	0-1603-284-2×31
4		34771	-2032	0-763-1268
4		34690	-2113	0-763-1268-89
2		34630	-2173	0-763-1268-143
1		34584	-2219	0-763-1268-2×89
1		34544	-2259	0-763-1268-143-89
1		34497	-2306	0-763-1268-285
1		34350	-2453	0-1603-850
1		34320	-2483	0-1603-850-31
1		34305	-2498	0-2×1026-2×89-284
1		34271	-2532	0-2×1268

Table 2

Relative Intensity	Wavenumbers in $\text{cm}^{-1}$		Difference from (0,0) in $\text{cm}^{-1}$	Assignments
	Absorption	Emission		
1	37349	37349	+ 724	0+724
1	37280	37281	+ 656	0+724-61
1	37319	37222	+ 597	0+724-2 $\times$ 61
3	37149	37149	+ 524	0+524
4	37048	37039	+ 414	0+2 $\times$ 210
4	36991	36994	+ 369	0+2 $\times$ 210-49
1	36974	36975	+ 350	0+2 $\times$ 210-61
4	36942	36940	+ 315	0+2 $\times$ 210-2 $\times$ 49
1	36876	36889	+ 264	0+2 $\times$ 210-3 $\times$ 49
1	36844	36845	+ 220	0+2 $\times$ 210-4 $\times$ 49
10	36835	36835	+ 210	0+210
8	36768	36778	+ 153	0+210-61
6	36731	36734	+ 109	0+210-2 $\times$ 49
1	36694	36690	+ 65	0+210-3 $\times$ 49
7	36622	36625	0	0-0
6	36570	36576	- 49	0-49
6	36565	36564	- 61	0-61
6	36525	36527	- 98	0-2 $\times$ 49
4	36772	36502	- 123	0-2 $\times$ 61
5	36411	36475	- 150	0-3 $\times$ 49
2	36428	36430	- 195	0-4 $\times$ 49
5	36411	36410	- 215	0-215
5		36321	- 304	0-215-2 $\times$ 49
3		36255	- 370	0-215-2 $\times$ 49-61
5		36195	- 430	0-2 $\times$ 215
5		36175	- 450	0-450
10	36095	36094	- 531	0-531
5	36050	36055	- 570	0-531-49
4	35990	35991	- 634	0-531-2 $\times$ 49
3	35944	35942	- 683	0-531-3 $\times$ 49
8	35880	35888	- 737	0-737
8	35831	35831	- 794	0-737-61
6		35771	- 854	0-737-2 $\times$ 61
4		35705	- 920	0-737-3 $\times$ 61
3		35676	- 949	0-737-215
7		35617	- 1008	0-1008
6		35567	- 1058	0-1008-49, 0-2 $\times$ 531
3		35498	- 1127	0-2 $\times$ 531-61
1		35441	- 1184	0-2 $\times$ 531-2 $\times$ 61
3		35398	- 1227	0-1227, 0-1008-215
4		35350	- 1275	0-1275
1		35297	- 1328	0-1275-49
1		35246	- 1379	0-1275-2 $\times$ 49
1		35213	- 1412	0-1275-3 $\times$ 49
2		35184	- 1441	0-1008-2 $\times$ 215
6		35143	- 1482	0-2 $\times$ 737
7	35090	35090	- 1535	0-1008-531
3		35009	- 1616	0-1616
5		34885	- 1740	0-1008-737
4		34828	- 1797	0-1008-737-49
3		34785	- 1840	0-1008-737-2 $\times$ 49
3		34578	- 2047	0-2 $\times$ 1008-49
5		34551	- 2074	0-1008-2 $\times$ 531
1		34522	- 2103	0-2 $\times$ 1008-2 $\times$ 49
2		34481	- 2144	0-531-1616
2		34423	- 2202	0-531-1616-61
2		34358	- 2267	0-531-1616-2 $\times$ 61
2		34295	- 2330	0-3 $\times$ 531-737
2		34080	- 2545	0-2 $\times$ 1275

Table 2 (continued)

Relative Intensity	Wavenumbers in $\text{cm}^{-1}$		Difference from (0,0) in $\text{cm}^{-1}$	Assignments
	Absorption	Emission		
2		34031	-2594	$0-1008-3 \times 531$ , $0-2 \times 1275-49$
2		33967	-2658	$0-1008-3 \times 531-61$
2		33983	-2642	$0-737-2 \times 1008$
2		33822	-2803	$0-737-2 \times 1008-61$
2		33775	-2850	$0-3061+210$
2		33715	-2910	$0-3061+210-61$
2		33564	-3061	$0-3061$
1		33516	-3109	$0-3061-61$
1		33359	-3266	$0-2 \times 1127-1008$
1		33315	-3310	$0-2 \times 1127-1008-49$
1		33295	-3330	$0-2 \times 1127-1008-61$
1		33116	-3509	$0-3061-450$
1		33052	-3573	$0-3061-450-61$

Table 3

Relative Intensity	Frequencies in $\text{cm}^{-1}$			Difference from (0,0) in $\text{cm}^{-1}$	Assignments
	Absorption	Fluorescence	Emission		
1	35801		35803	+ 800	$0+2 \times 340$
1	35778		35370	+ 654	$0+2 \times 340-32$
1	35716		35711	+ 596	$0+2 \times 340-3 \times 32$
1	35683		35683	+ 560	$0+2 \times 340-4 \times 32$
1	35610		35629	+ 506	$0+3 \times 340-479-32$
1	35578		35573	+ 450	$0+2 \times 340-448$
3	35540		35541	+ 418	$0+418$
3	35474		35478	+ 355	$0+418-70$
3	35468		35463	+ 340	$0+340$
3	35324		35327	+ 204	$0+2 \times 340-448-32$ , $0+340-2 \times 70$
2	35287		35292	+ 169	$0+2 \times 340-448-2 \times 32$
2	35255		35256	+ 133	$0+2 \times 340-448-3 \times 32$
6	35236		35235	+ 102	$0+112$
8	35122	35120	35123	0	$0-0$
3	35093	35083	35091	- 32	$0-32(448-418)$
2	35080		35058	- 65	$0-2 \times 32$
8	35049	35050	35053	- 70	$0-70$
5	35016	35004	35018	- 105	$0-70-32, 0-3 \times 32$
1	34995		34998	- 125	$0-4 \times 32$
2	34990	34985	34987	- 136	$0-2 \times 70$
2	34693	34964	34952	- 171	$0-2 \times 70-32$
1	34920		34917	- 206	$0-3 \times 70$



Table 3 (continued)

Relative Intensity	Frequencies in $\text{cm}^{-1}$			Difference from (0,0) in $\text{cm}^{-1}$	Assignments
	Absorption	Fluorescence	Emission		
1	34885	34896	34888	- 235	0-2 $\times$ 70-3 $\times$ 32
1	34856		34851	- 272	0-4 $\times$ 70
1	34788	34783	34783	- 340	0-5 $\times$ 70
7	34671		34675	- 448	0-448
7	34641	34650	34644	- 479	0-479, 0-448-32
3	34619		34614	- 509	0-479-32
3	34592		34609	- 514	0-855+340
2	34571		34572	- 551	0-855+340-32
1	34539	34541	34536	- 587	0-479-3 $\times$ 32
1	34488		34490	- 633	0-746+112
1	34428		34426	- 697	0-746+112-70
10	34376	34375	34377	- 746	0-746
1		34333	34329	- 794	0-846-32
10	34262	34267	34268	- 855	0-855
9	34234	34230	34238	- 885	0-855-32
8	34210	34204	34211	- 912	0-855-2 $\times$ 32
6	34197	34179	34184	- 939	0-855-3 $\times$ 32
1	34160		34153	- 970	0-855-4 $\times$ 32
1			34111	-1012	0-855-5 $\times$ 32
1	34022		34021	-1102	0-1102
1	33971		33979	-1144	0-1102-32
1			33954	-1169	0-1102-70
1			33919	-1204	0-1204, 0-1102-70-30
6	33860		33882	-1241	0-1241
5				-1256	0-1256
4			33849	-1274	0-1241-32
5		33840	33839	-1284	0-1284
5		33792	33801	-1322	0-1284-32
3	33755		33764	-1359	0-1284-70
2			33740	-1383	0-1284-70-32
1			33658	-1465	0-1284-2 $\times$ 70-32
1			33601	-1522	0-1522
0.5			33565	-1558	0-1522-32
1			33523	-1600	0-746-855
4			33418	-1705	0-2 $\times$ 855
3			33385	-1738	0-2 $\times$ 85-32
1			33343	-1780	0-2 $\times$ 855-2 $\times$ 32
1			33316	-1807	0-2 $\times$ 855-32-70
1		33282	33280	-1843	0-2 $\times$ 855-2 $\times$ 32-70
1			33247	-1876	0-2 $\times$ 855-3 $\times$ 32-70
1			33162	-1961	0-855-1102
1		33074	33084	-2039	0-1284-746
1		33051	33051	-2072	0-1284-746-32

Table 3 (continued)

Relative Intensity	Frequencies in $\text{cm}^{-1}$			Difference from (0,0) in $\text{cm}^{-1}$	Assignments
	Absorption	Fluorescence	Emission		
2		33021	33020	-2103	0-855-1241
2		32982	32992	-2131	0-855-1241-32
2			32952	-2171	0-855-1241-70
1		32862	32860	-2263	0-746-1522
1			32773	-2350	0-2 $\times$ 746-855
3		32658	32658	-2465	0-746-2 $\times$ 855
2 3			32599	-2524	0-746-2 $\times$ 855-70
3			32548	-2575	0-3 $\times$ 855
1			32523	-2600	0-3 $\times$ 855-32
1			32483	-2640	0-3 $\times$ 855-70
1			32420	-2703	0-746-855-11023
3			32355	-2708	0-1241-1522
1			32293	-2830	0-1241-1522-70
1			32216	-2907	0-1241-1522-2 $\times$ 70
1		32142	32139	-2984	0-1241-1522-3 $\times$ 70
2		32067	32074	-3049	0-3049
2			32043	-3080	0-3049-32
2			32007	-3116	0-3049-2 $\times$ 32
2			31970	-3153	0-3049-3 $\times$ 32
2		31698	31701	-3422	0-4 $\times$ 855
1		31674	31671	-3452	0-4 $\times$ 855-32
1			31645	-3478	0-4 $\times$ 855-2 $\times$ 32
1		32546	31562	-3561	0-3049-479-32
1		31496	31494	-3629	0-3629
.		31300	31318	-3805	0-746-3049
1			31287	-3836	0-746-3049-32
1		31256	31260	-3863	0-746-3049-2 $\times$ 32
1			31230	-3893	0-746-3049-3 $\times$ 32

A correlation of the observed fundamental frequencies of the three isomers in the ground state along with the corresponding values in the respective infrared, Raman and ultra-violet absorption are given in table 4.

In disubstituted benzenes, Sklar (1942) has shown that the transition moment is maximum with the para isomer. A study of emission bands shows that *p*-fluorophenol gives rich emission in comparison with ortho- and meta-isomers. It is also observed that in the *p*-isomer the bands are in groups which are separated, whereas, in the meta-isomer this character is less prominent and in the ortho- it is least so. The superposing continuum is strong in ortho- and weak in meta- and para-isomers. No plausible explanation can be given about the origin of this continuum.

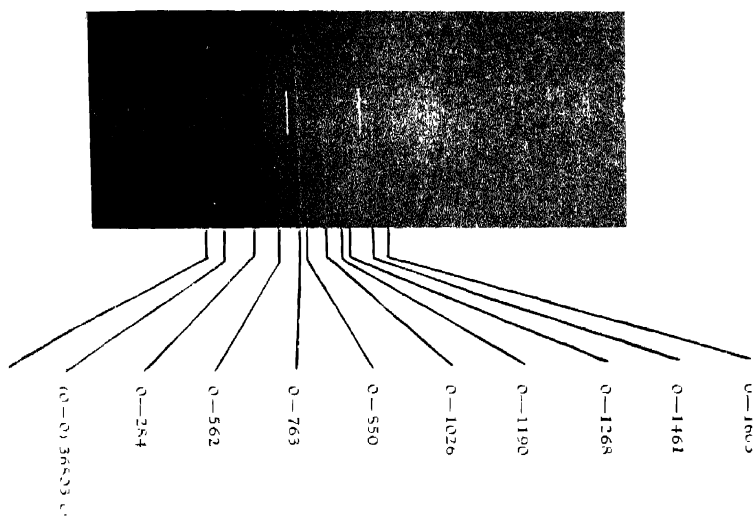


Figure 1. The Emission Spectrum of o-Fluorophenol.

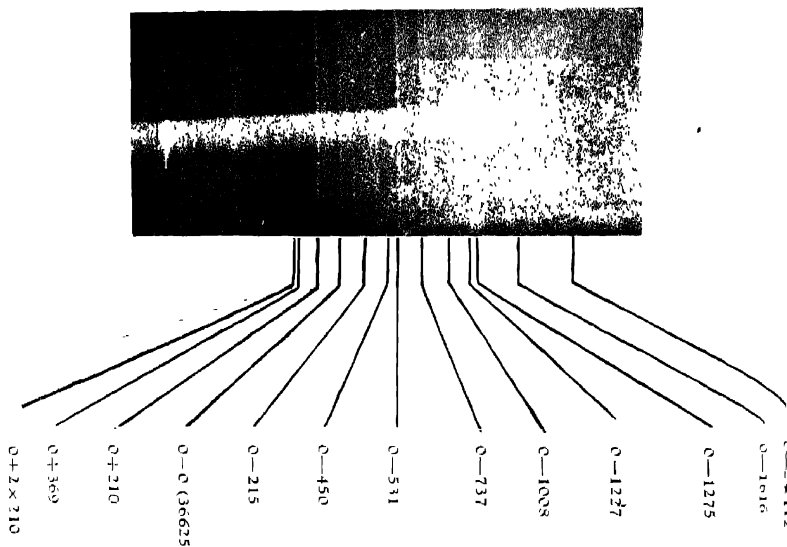


Figure 2. The Emission Spectrum of m-Fluorophenol.

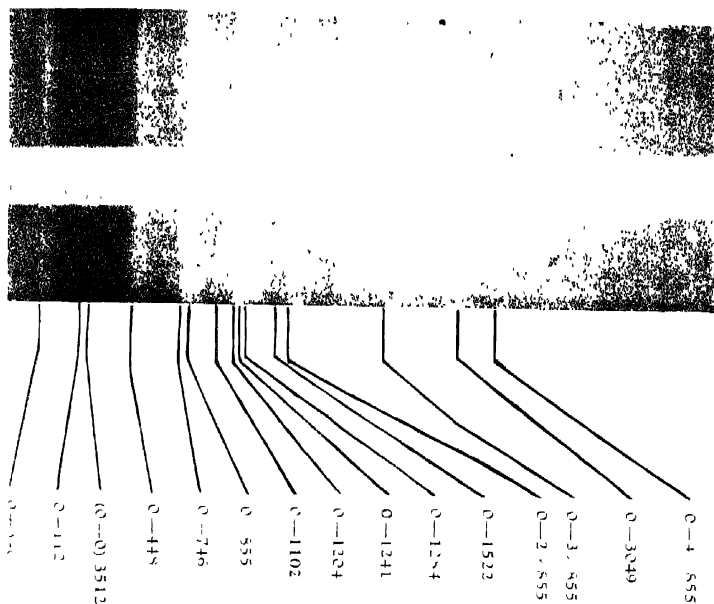


Figure 3. Emission Spectrum of p-Fluorophenol



Table 4. Correlation of the ground state vibrational frequencies of three isomeric fluorophenols.

Assignments	Benzene Frequencies (in $\text{cm}^{-1}$ )	O-fluorophenol frequencies (in $\text{cm}^{-1}$ )			M-fluorophenol frequencies (in $\text{cm}^{-1}$ )			P-fluorophenol frequencies (in $\text{cm}^{-1}$ )		
		I.R.	Raman	Emission	I.R.	Raman	Emission	I.R.	Raman	Fluorescence
C-C o.p. bending	404( $e_{2u}$ )		285	284( $a''$ )		220	215( $a''$ )			
O-H o.p. vibration										
C-OH i.p. bending								450	450	448( $b_1$ )
C-C-C i.p. bending	606( $e_{2g}$ )				456		450( $a'$ )	460	465	478( $a_1$ )
C-C-C i.p. bending	606( $e_{2g}$ )	573	580	562( $a'$ )	536	530	531( $a'$ )			
C-C-C i.p. bending, Trigonal	1010( $b_{1u}$ )	764	760	763( $a'$ )				750	750	746( $a_1$ )
C-F i.p. bending					740	740	737( $a'$ )			
Ring breathing	992( $a_{1g}$ )	859	850( $a'$ )		1006	1000	1008( $a'$ )	835	854	855( $a_1$ )
C-H i.p. bending	1037( $e_{1u}$ )	1030	1026( $a'$ )					1099	1092	1102( $a_1$ )
O-H i.p. bending	1188		1190( $a'$ )		1229		1227( $a'$ )	1212	1201	1204( $b_1$ )
C-F stretching	1266		1266( $a'$ )		1275		1275( $a'$ )	1240	1229	1241( $a_1$ )
C-H i.p. bending	1326( $a_{2g}$ )							1294	1284	1282
C = C stretching	1485( $e_{1u}$ )	1460	1461( $a'$ )							
C = C stretching	1585( $e_{2g}$ )	1605	1603( $a'$ )		1610		1616( $a'$ )	1530	1509	1522( $a_1$ )
C-H stretching					3040		3061( $a'$ )	3045		3053
O-H stretching	3062( $a_{1g}$ )							3661		3624

N.B. i.p. = in plane, o.p. = out of plane.

## ACKNOWLEDGEMENTS

Authors are thankful to Prof. N. L. Singh and Dr. D. K. Rai for their interest in the work and to Dr. K. P. R. Nair for help in preparing this paper. One of them (J. V. S.) thanks the Council of Scientific Industrial Research, New Delhi, for financial assistance.

## REFERENCES

- Deardon, J. R. & Forber, W. F. 1950 *Can. J. Chem.* **37**, 1294.  
 Hodgson, H. H. 1943 *J. Chem. Soc.* 380.  
 Jakobsen, R. J. & Brewer, E. J. 1962 *Appl. Spectry* **16**, 32.  
 Kohlrausch K. W. F., Hertz, E. & Vogel, R. 1947 *Monatsh. Chem.* **76**, 200.  
 Sharma, D. & Tripathy, L. N. 1963 *Ind. J. Pure Appl. Phys.* **1**, 229.  
 Sklar, A. L. 1942 *J. Chem. Phys.* **10**, 135.  
 Sponer, H. & Bass, A. M. 1950 *Optical Soc. Am.* **40**, 389.  
 Thakur, S. N. 1968 *Ph.D. Thesis*, Banaras Hindu University.  
 Tiwari, S. K. 1963 *Nature*, **200**, 1202.  
                     1966 *Ph.D. Thesis* Banaras Hindu University.  
 Tiwari, S. K. & Upadhyaya, K. N. 1968 *Ind. J. Pure Appl. Phys.* **6**, 698.  
 Tripathy, L. N. 1968 *Ind. J. Pure Appl. Phys.* **6**, 151.  
 Verma, P. K. 1965 *Ind. J. Pure and Appl. Phys.* **3**, 70.  
 Wittok, H. 1935, *S.B. Bayer Akad. Wiss.* **144**, 417.



## Letters to the Editor

### Microwave relaxation and association of n-octanol

By F. F. HANNA AND K. N. ABDEL-NOUR

Microwave Laboratory, National Research Centre, Dokki, Cairo, U.A.R.

(Received 16 June 1970)

The dielectric constant  $c'$  and dielectric loss  $c''$  of n-octanol in heptane solutions have been measured for six concentrations between 0.0082 and 0.1738 mole-fraction at wavelengths 0.22, 1.25, 3.24, 10 and 25 cm and at 6, 20, 40 and 60°C.

Also, the static dielectric constant  $\epsilon_0$  has been measured and is plotted in figure 1. The relation is not linear indicating that associates are formed and behave in the concentrated solutions in a different manner than that in the dilute solutions.

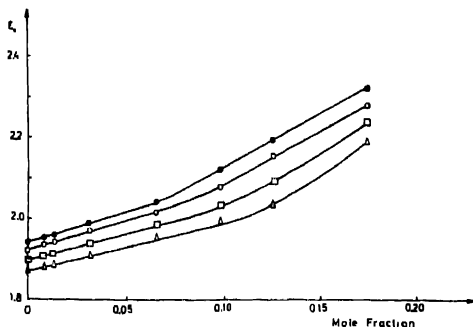


Figure 1. n-Octyl alcohol in heptane at  $\bullet$ —6°C,  $\circ$ —20°C,  $\square$ —40°C,  $\Delta$ —60°C.

Preliminary analysis of the absorption curves obtained gave three Debye terms for both dilute and concentrated solutions having relaxation times  $\tau_1$ ,  $\tau_2$  and  $\tau_3$  and weights  $G_1$ ,  $G_2$  and  $G_3$ .

From the dilute solutions, the short relaxation time  $\tau_3$  is found to be independent of temperature and concentration and lies around 0.6 psec and so it belongs to the rotation of the OH-group while the relaxation times  $\tau_1$  and  $\tau_2$  (around 38 and 6 psec respectively, at 20°C for the concentration 0.0082 mole-fraction) belong to the molecule as a whole.  $\tau_1$  which has a small weight  $G_1$ , results from the rotation of the long chain molecule with a dipole at the end, i.e. rotation around a short axis.

For the concentrated solutions,  $\tau_3$  (3.50 psec at 20°C for 0.1738 mole-fraction) is of the same order as that obtained for OH-group in pure *n*-octanol by Garg & Smyth (1965) and is temperature dependent.  $\tau_1$  (652 psec at 20°C for 0.1738 mole-fraction) is large and may be due to the rupture of hydrogen bonds inside the associated chain.  $\tau_2$  (34 psec for the same concentration and temperature) has about the same value as  $\tau_1$  in the dilute solutions should be connected with the rotation of the single molecules or to the ones at the end of the associated chains.  $G_0$  increases with the increase in temperature which demonstrates the decomposition or loosening of the association with increase in temperature.

From figure 1 and the results of analysis, it is clear that associates are formed because the OH-group lies at the end of the chain and hence is subjected to intermolecular interaction, unlike the case of 3,5-dimethyl 3-hexanol (Hanna & Abdel-Nour 1970) where the associates are hardly detectable as the OH-group lies within the molecule and is shielded against the intermolecular interaction.

Detailed results will be given after measuring  $\epsilon'$  and  $\epsilon''$  at meter waves to subtract the contribution of the lower dispersion region from the microwave measurements for accurate evaluation of the results.

The authors thank Prof. M. Mokhtar for his encouragement and to Prof. C. P. Smyth for allowing one of us (Abdel-Nour) to take the measurements in his laboratory.

#### REFERENCES

- Garg, S. K. & Smyth, C. P. 1965 *J. Phys. Chem.* 69, 1294  
 Hanna, F. F. & Abdel-Nour, K. N. 1970 under preparation for publication.

*Indian J. Phys.* 44, 138-140, (1970)

### X-ray crystallographic data for some organic compounds

By M. P. GUPTA AND S. M. PRASAD

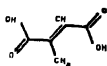
*Department of Physics, University of Ranchi, Ranchi-8*

(Received 22 June 1970)

As a part of programme for determining structures of simple organic molecules and their derivatives, we have investigated a number of molecules and the present note reports some preliminary results.

#### 1. Potassium mesaconate $\text{KC}_6\text{H}_5\text{O}_4$ .

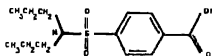
This is acid potassium salt of the dicarboxylic mesaconic acid  $\text{C}_6\text{H}_5\text{O}_4$  with stereochemical formula;



The crystal is transparent and platy in habit, belonging to the triclinic system with  $a = 6.23 \text{ \AA}$ ,  $b = 7.33 \text{ \AA}$ ,  $c = 3.97 \text{ \AA}$ ,  $\alpha = 87^\circ 36'$ ,  $\beta = 107^\circ 30'$ ,  $\gamma = 98^\circ 20'$ ,  $V = 170.95 \text{ \AA}^3$ ,  $\rho_{\text{calc}} = 1.63 \text{ gm/ml}$ ,  $\rho_{\text{obs}} = 1.62 \text{ gm/ml}$ . Number of molecules in the unit cell  $Z = 1$ . Linear absorption coefficient for copper  $K_\alpha$  radiation  $= 63.99 \text{ cm}^{-1}$ . As there is only one molecule in the unit cell and the molecule itself is noncentrosymmetric, the space group is uniquely fixed as  $P1$ . Complete zonal and three dimensional X-ray data have been collected using Weissenberg photography and the structure solved in projections. Refinement of the structure by three-dimensional least squares is in progress.

## 2. Probenecid $\text{C}_{13}\text{H}_{10}\text{O}_4\text{NS}$

This is a monocarboxylic acid with the stereochemical formula:



and crystallizes out of a solution in chloroform. The crystal is platy and colourless and belongs to the triclinic system with  $a = 7.53 \text{ \AA}$ ,  $b = 19.51 \text{ \AA}$ ,  $c = 5.31 \text{ \AA}$ ,  $\alpha = 102^\circ 8'$ ,  $\beta = 99^\circ 6'$ ,  $\gamma = 93^\circ 5'$ ,  $V = 750.4 \text{ \AA}^3$  and  $\rho_{\text{calc}} = 1.27 \text{ gm/ml}$ ,  $\rho_{\text{obs}} = 1.25 \text{ gm/ml}$ . The number of molecules in the unit cell  $Z = 2$ . Linear absorption coefficient for  $\text{CuK}_\alpha$  radiation  $\mu = 19.56 \text{ cm}^{-1}$ . Statistical intensity tests, morphology and number of formula units in the cell all indicate the space group to be centrosymmetric  $P\bar{1}$ . We have collected complete zonal and three-dimensional X-ray diffraction data using Weissenberg photography, and a three-dimensional Patterson synthesis is now in progress to locate the sulphur atom.

## 3. O-Aceto benzoic acid $\text{C}_9\text{H}_8\text{O}_3$

It is crystallized out of a solution in alcohol in the form of elongated plate. The stereochemical formula of the compound is

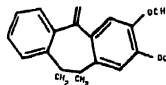


The crystal is orthorhombic with  $a = 9.53 \text{ \AA}$ ,  $b = 5.22 \text{ \AA}$ ,  $c = 15.82 \text{ \AA}$ ,  $V = 787.0 \text{ \AA}^3$ ,  $\rho_{\text{calc}} = 1.38 \text{ gm/ml}$ ,  $\rho_{\text{obs}} = 1.36 \text{ gm/ml}$ . The number of molecules in the unit cell  $Z = 4$ . Linear absorption coefficient for copper  $K_\alpha$  radiation  $\mu = 8.88 \text{ cm}^{-1}$ . The only space group absences are  $h00$ ,  $h = 2n+1$ ,  $0k0$ ,  $k = 2n+1$ ,  $00l$ ,  $l = 2n+1$ ,

This fixes the space group uniquely as  $P2_12_12_1$ . The crystal structure investigation is in progress

4 *Dimethoxy di-benzo suberone*  $C_{17}H_{16}O_3$ .

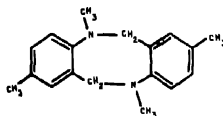
The compound with the stereochemical formula



is of interest because of the central seven-membered ring. The crystal is needle shaped and orthorhombic with  $a = 16.56 \text{ \AA}$ ,  $b = 21.48 \text{ \AA}$  and  $c = 7.56 \text{ \AA}$ ,  $\rho_{calc} = 1.322 \text{ gm/ml}$ ,  $\rho_{obs} = 1.285 \text{ gm/ml}$ . The number of molecules in the unit cell  $Z = 8$ . The linear absorption co-efficient for copper  $K_\alpha$  radiation  $\mu = 7.38 \text{ cm}^{-1}$ . The space group absences are  $0kl$  with  $k = 2n+1$ ,  $h0l$  with  $l = 2n+1$  and  $hkl$  with  $h = 2n+1$ . This fixes the space group uniquely as  $Pbca$ . We have collected complete three-dimensional X-ray diffraction data with Weissenberg photography and obtained an approximate solution for the structure. Since we suspect disorder in the structure it is still under our investigation.

5. *1-methyl 9-methyl 5, 6, 11, 12-tri-hydro 5, 11-dimethylphenhomazine*  $C_{18}H_{20}N_2$ .

The compound with the stereochemical formula



is of interest because of the central eight-membered ring. The crystal is platy in habit and belongs to the monoclinic system, with  $a = 10.13 \text{ \AA}$ ,  $b = 7.36 \text{ \AA}$ ,  $c = 20.66 \text{ \AA}$ ,  $\beta = 105^\circ 40'$ ,  $V = 1483 \text{ \AA}^3$ ,  $\rho_{calc} = 1.18 \text{ gm/ml}$ . Number of molecules in the unit cell  $Z = 4$ . The linear absorption coefficient for copper  $K_\alpha$  radiation  $\mu = 8.43 \text{ cm}^{-1}$ . Space group absences are  $h0l$  when  $l = 2n+1$ ,  $0k0$  when  $k = 2n+1$ . This fixes the space group uniquely as  $P2_1/c$ . We have collected complete three-dimensional X-ray diffraction data for the compound using Weissenberg photography and got an approximate solution of its structure in the  $0kl$  projection. Further work to refine the structure is in progress.

## Application of Rao's rule to liquified inert gases

By A. QADEER, M. N. SHARMA AND A. S. VARMA

*Physics Department, Lucknow University, Lucknow-7, India*

(Received 21 July 1970)

A considerable amount of work has been done on the propagation of ultrasonic waves in organic liquids and liquid mixtures by Parthasarthy (1935), Mikhalov (1949), Kudryavtsev (1951) and Bergmann (1956). However, no attempt has been made to investigate the propagation of ultrasonic waves at the liquefaction temperature of the inert and polar gases. On the basis of experimental data Rao (1940) has suggested an empirical relation connecting the temperature coefficient of velocity of sound  $\alpha_c$  and the temperature coefficient of volume  $\alpha_v$  and may be written as

$$\frac{\alpha_c}{\alpha_v} = -\lambda \quad \dots (1)$$

where  $\lambda$  is a constant known as Rao's empirical constant and has been found to be practically equal to +3 for most of the organic liquids.

In the present investigation, the authors have verified the Rao's rule in the case of liquid helium and argon at their liquefaction temperature on the basis of the interaction-potential approach. Various potential energy functions have been suggested for the interaction between the atoms or molecules. The simplest of them is the inverse form of the overlap interaction. In terms of volume the inverse potential form may be written as

$$\phi(v) = -\alpha v^{-\mu} + \beta v^{-\nu} \quad \dots (2)$$

where  $\alpha, \beta, \mu$  and  $\nu$  are constants of the potential energy functions and  $v$  is the molar volume.

The equation of state of a gas for the condensed system may be expressed as

$$p = \frac{kT}{v} - \frac{\partial \phi}{\partial v} \quad \dots (3)$$

Using equation (3) the following relation for  $\lambda$  the Rao's constant has been obtained

$$\lambda = -\frac{\alpha_c}{\alpha_v} = 1 - K \frac{\nu+2}{\mu} \quad \dots (4)$$

where

$$K = \frac{1 - \frac{k \left( \frac{1}{\alpha_v} - 2T \right)}{\beta v(v+1)(v+2)v^{-\nu}} - \frac{\alpha \mu(\mu+1)(\mu+2)v^{\nu-\mu}}{\beta v(v+1)(v+2)}}{1 + \frac{kT}{\beta v(v+1)(v+2)v^{-\nu}} - \frac{\alpha \mu(\mu+1)v^{\nu-\mu}}{\beta v(v+1)}}$$

The computed values of  $\lambda$  employing equation (4) for liquid helium and liquid argon are presented in table 1. These values of  $\lambda$  have been utilized to derive the following equations for the velocity of sound at the temperature of liquefaction

$$\frac{MC^{\frac{1}{3}}}{d} = R \text{ for helium} \quad \dots (5)$$

$$\frac{MC^{\frac{1}{3}}}{d} = R \text{ for argon} \quad \dots (6)$$

where  $M$  is the molecular weight,  $C$  the velocity of ultrasonic waves in the substance,  $d$  the density of the substance and  $R$  is an additive constant which depends upon chemical constitution of the substance but is independent of temperature. For other liquified gases the work is in progress and will be published shortly.

TABLE 1. Values of  $\lambda$  for liquid helium and liquid argon.

Substance	Temperature in °K	Using equations (4) and (5)
Liquid helium	4.2	2.0724
Liquid argon	87	3.0012

## REFERENCES

- Borgmann, L. 1956 *Ultrasonics*, IL  
 Kudryavtsev, B. B. 1962 *Applications of Ultrasonic Methods to Physico-Chemical Studies*, Gostekhizdat.  
 Mikhaylov, I. G. 1949 *The Propagation of Ultrasonic Waves in Liquids*, Gostekhizdat.  
 Purthasarathy 1935 *Proc. Indian Acad. Sci.* **A2**, 497.  
 Rao, Rama 1940 *Indian J. Phys.*, **14**, 109.

## BOOK REVIEWS

### *Arc Physics*

Max. F. Hoyaux.,

pp 305+xiii Springer-Verlag, Berlin-Heidelberg, New York (1968).

Recently quite a few good textbooks on plasma physics have been published. Here is one exclusively on 'Arc Physics' written by a physicist with very strong engineering background. Author says "This is an introduction on the elementary level" Actually the physics of the electric arc is an extremely complicated mixture of different kind of phenomena, skillful use of E. M. theory, Statistical mechanics, Magnetohydrodynamics etc. are required to explain the observed facts. This is a well written book by an expert and surely will be found useful to many in the field as well as to students. Introductory remarks in different chapters are excellent. In addition to general remarks they contain criticism and warns the reader about the scope and limitations of the theories discussed in the particular chapter.

The book is divided into three parts. The first part contains a very well written discussion on the theory of positive column and general theory of Arc Plasma. (According to the present reviewer this is the best part of the book). The second part deals with wall and electrode phenomena. The third part describes plasma diagnostics. It is felt that some of the methods (like temperature determination) given are too brief, this may be due to author's intention to keep the size of the book reasonable. Unlike other texts of this type no extensive bibliography is presented here as the author does not 'sport' in this hobby.

B. C.

### *The Physical Basis of Ultrahigh Vacuum*

P. A. Redhead, J. P. Hobson and E. V. Kornelsen ;

Chapman and Hall Ltd., London, 1968, Price £5.5s net in U.K.

It is well known that ultrahigh vacuum (uhv) i.e. the region of pressure below  $10^{-9}$  torr is needed for various important scientific and technological purposes, as for example, in systems for plasma physics research, accelerator vacuum systems, cryogenic systems, space simulators, production of thin films and other solid state devices, and in experiments requiring atomically clear surfaces or high gas purity, also certain other systems of smaller volumes required for scientific research. In order to understand the phenomena in uhv systems and in uhv technology, knowledge of different disciplines, namely, surface physics and chemistry, thermodynamics, electron and ion-impact physics, cryogenics, electronics etc. are required. Therefore, to deal with the physical basis of uhv in a single volume is a formidable task indeed. The authors, who are members of a wellknown group of workers in the field attempted to achieve this in the present volume. They have dealt with the physical processes involved in uhv phenomena, pressure measurement in those systems, production of uhv and examples of uhv. But nowhere the authors have attempted to deal with the practical or technological aspect of the subject. They have, however, taken great pains in clearly explaining the physical principles involved in the production, measurement and maintenance of uhv in various systems. The volume will therefore be a useful handbook for all workers, scientists or technologists, in the field of uhv, for whom a knowledge of the basic principles involved in the phenomena are essentially needed.

A. K. D.

*Transfer and Storage of Energy by Molecules: Vol. 1 Electronic Energy*

G. M. Burnett and A. M. North, Wiley-Interscience, 1969—227 pages.

The book is an attempt to collect and systematize the results of the work done in various branches of science on Energy Transfer in Molecules which are published in different specialised journals. In view of the growing importance of the energy transfer in chemistry, biology and solid state, a book which tries to bridge the gap between spectroscopists and chemical kineticists is definitely welcome. The book consists of four review articles on electronic energy transfer, and it will be followed by Vol 2 and Vol. 3 of the series discussing vibrational and rotational energy transfer, respectively. The first article of the book by Cundall discusses the conversion of electronic energy to vibrational and translational forms as deduced from experiments in the gas phase on atoms and diatomic & polyatomic molecules. The third article by Koorwell & Wilkinson emphasizes the work done in the condensed phase with organic polyatomic molecules, and discusses fluorescence, phosphorescence, triplet-triplet absorption and photochemical yield in relation to the properties of electronically excited states. This article overlaps to some extent with the first article, and the two perhaps could have been combined into one to present the materials in a more systematic fashion. The second article of the book by J. N. Bradley essentially discusses the reverse problem of conversion of other forms of energy to electronic energy as deduced from shock wave studies, while the fourth and the last article discusses the problems connected with the transfer of large amounts of energy from highly energised particles and radiation. All the articles are well-written and can be easily followed by physical organic chemists. However, I feel that an article on theories of radiationless process and energy transfer, and another on experimental techniques would have helped to bring completeness to the discussion. The articles emphasize the basic idea involved but make no attempt to be exhaustive, or to collect all the work done up-to-date.

The book will be a good addition to a chemical library.

M. C.

*The World of Mars*

V. A. Firsoff, 1969, pp 128, price 7sh 6d, Oliver & Boyd, Edinburgh.

This little book covers practically the entire information available on the planet Mars up-to-date. The author is himself a wellknown worker in Areology and speaks with authority and conviction on the subject. The writing is informative, instructive and intriguing. The confrontation between telescopic and other earthbound instrumental observations and the close range but limited observations by Mariner 4 probe, has been critically discussed to show the pitfalls in arriving at conclusions on Martian geography, geology, meteorology and ecology derived from either class of data. The mysteries of Schiaparelli's "Canals", the seasonal color and topological variations, some of the most intriguing and controversial subjects on Mars, have been given as logical an explanation as is to be expected, considering all the conflicting data. A layman to fully appreciate the book would be expected to have a fairly good knowledge of several associated subjects, but for the specialist it should be a source of pleasure to go through and ruminate over the many problems of Mars, only the fringe of which appears to have been touched as yet. There seems to be now little logical doubt that Mars contains plant and bacterial life and the necessary factors for their sustenance. Whether the "canals" of Mars



are really subterranean aqueducts, whether some of the observed mushrooming clouds on Mars are from nuclear explosions or whether the mysterious twin satellites of Mars are really huge spacecrafts, indicating existence and activities of Martians, such conclusions according to the author are improbable but not impossible. But without more unambiguous data it is still premature to build up a theory of the Martian World, and the day is perhaps not very far off when manned spacecrafts going round or landing on Mars or Lunokhod type robots roaming round Martian landscape will settle all controversy. Until then most of the theories on Mars are to remain "not proven for the time being" as the author very cautiously asserts.

A. B.

### *Atomic Spectra*

H. G. Kuhn, F.R.S., Second Edition 1969,  
Longmans Green & Co. Ltd.,  
London & Harlow, pp. 472+xviii, price 105sh.

This book on Atomic Spectra by Dr. Kuhn is a departure from the previous standard books on this subject. His method of exposition of the subject is also different. In the second chapter he has given the outlines of the theoretical methods required for the understanding of the mechanics of the atom which, as he himself has pointed out, is not meant to be a complete exposition of the complex mathematical techniques of quantum mechanics.

In succeeding chapters he has systematically expounded the methods applied for the elucidation of the atomic spectra starting from the simple spectra of hydrogen and hydrogen-like atoms through those of helium, alkali metals, alkaline earth metals, trivalent elements and ending in the complex spectra of higher members of the periodic table. All the concepts have been neatly developed giving the necessary mathematical treatments wherever necessary and illustrating the subjects with diagrams, tables and photographs of the spectra.

Dr. Kuhn has elaborately discussed the very important aspects of linear and quadratic Stark effects and those of Zeeman effects in simple, doublet and complex spectra.

In two special chapters he has dealt exclusively the subjects of hyperfine structure, isotope shift, width and shape of spectral lines on which he himself has made many contributions. The importance of the radiofrequency methods for studying the hyperfine structures has been specially discussed though the details of the experimental methods have been left out for obvious reasons.

The addition of many recently developed aspects of the atomic spectra such as Lamb shift in hydrogen, deuterium, singly ionised helium and doubly ionised lithium, atomic beam resonance, optical bumping, auto-ionisation etc., have made the book more up-to-date, though according to the author himself, it has not been possible to include all the new materials of current researches within the framework of the book.

This book though meant for more advanced undergraduate and graduate students, undoubtedly will be of much help to research workers in the field of atomic spectra. Moreover, the large number of references included in the bibliography has increased the usefulness of the book. This book is a valuable addition to the existing works on Atomic Spectra.

G. S. K.

*Spectra and Energy Levels of Rare Earth Ions in Crystals*

Gerhard H. Dieke,

Interscience Publishers, 1968, 401 pages.

G. H. Dieke is one of the pioneers who have done extensive investigations of the properties of the rare earth ions in crystals. Before World War II, the main interest was confined to Uranyl compounds for obvious reasons. After the war availability of pure rare earth compounds in good quantity resulted in a spurt of investigations on these ions. When lasers were invented in the early sixties, the potential use of rare earth ions as active material for lasers was recognised and now a good many people are working in this field. Dieke and his co-workers have made decisive contributions.

The book under review is mainly concerned with the optical properties of rare earth ions in crystals. It is mainly based on the author and his co-workers work and includes many unpublished results. Experimental procedures are lucidly presented and a large amount of experimental data is incorporated. The necessary theoretical methods are developed in a concise way in appropriate places. References are very extensive and useful. One can say without reservations that this is an important and welcome addition to the existing literature in this field.

A. S. C.

## BOOKS RECENTLY RECEIVED FOR REVIEW

- An Introduction to Liquid Helium*, J. Wilks, £ 2.40, Clarendon Press, Oxford, England.  
*Glass Lasers*, K. Patek, £ 6.50, London Iliffe Books, (Butterworth & Co.), London.  
*Atomic and Nuclear Physics. An introduction in S. I. Units*, Ed. T. A. Littlefield and N. Thorley, £ 0.75, English Language and Book Society and Van Nostrand Reinhold Co. London.  
*Thin film Physics*, O. S. Heavens, £ 2.00, Methuen and Co. Ltd., London.  
*Electron Diffraction*, T. B. Rymer, 50s, Methuen & Co. Ltd., London.  
*Nuclear and Particle Physics Annual (Vol. 1)*, Ed. Leon Lederman and Joseph Weneser, \$30.60, Gordon and Breach Science Publishers Ltd., London.  
*Topics in Theoretical Physics*, Ed. Christofer Cronstrom, \$ 36.00, Gordon and Breach Science Publishers, London.  
*Astrophysics and General Relativity, Vol. 1*, Ed. M. Chretien, S. Deser and J. Goldstein, \$ 21.00, Gordon and Breach Science Publishers, London.  
*Photophysics of Aromatic molecules*, John B. Birks, John Wiley & Sons, New York.  
*Mathematical and theoretical Physics, Vols. 1 and 2*, Egil A. Hylleraas, Vol. \$15.00, Vol. 2-15.00, John Wiley and Sons, New York.  
*Symmetry Principles and Atomic Spectroscopy*, Brian G. Wybourne, \$ 17.50, John Wiley & Sons, New York.  
*Applied Matrix and Tensor Analysis*, John A. Eisele and Rober M. Mason, John Wiley & Sons, New York.  
*Properties of Matter*, B. H. Flowers and E. Mendoza, \$ 15.50, John Wiley & Sons, New York.  
*Fundamentals of Aeronomy*, R. C. Whitton and I. G. Poppoff, \$ 14.95, John Wiley & Sons, New York.

# INDIAN JOURNAL OF PHYSICS

VOL. 44

No. 3

AND

VOL. 53

PROCEEDINGS

No. 3

OF THE

INDIAN ASSOCIATION FOR THE CULTIVATION OF SCIENCE

*(Edited in collaboration with the Indian Physical Society).*

MARCH 1970

PUBLISHED BY THE

INDIAN ASSOCIATION FOR THE CULTIVATION OF SCIENCE

JADAVPUR, CALCUTTA-32



## Force constants and mean amplitudes of vibration of octahedral haloanions of IV B group elements

By H. S. SINGH, A. N. PANDEY, B. P. SINGH and NITISH K. SANYAL

*Department of Physics, University of Gorakhpur, Gorakhpur*

(Received 12 December 1969)

General quadratic force constants for octahedral haloanions of  $O_h$  point group have been determined using IR and Raman spectral data. The trends in the force constants and vibrational frequencies have been discussed and compared with those corresponding to  $MX_4$  type molecules. The mean-square amplitude quantities and mean amplitudes of vibration for the bonded as well as non-bonded atoms for chloro- and bromoanions have been evaluated at three temperatures,  $T = 0^\circ$ ,  $298^\circ$  and  $500^\circ\text{K}$ .

### INTRODUCTION

Recently, the spectra of a large number of complexes of transition elements have been studied both theoretically and experimentally specially to understand the 'anomalous' intensity pattern of the fundamental frequencies (Woodward & Creighton 1961) consequences of different  $d$  orbital occupancies and Jahn-Teller effects. Adam & Newton (1968) studied the Raman and I. R. spectra of octahedral chloroanions of IVB group elements and calculated the force constants employing Urey-Bradley force field. Further Brisdon *et al* (1969) observed the Raman and I. R. spectra of chloro- and bromo-anions of IVB group elements and reported valence force constants on the basis of their vibrational studies of chloro- and bromo-anions of IVB group elements. Due to the increasing importance of the haloanions in the transition metal complexes, it was thought worthwhile to compute general quadratic force constants for the octahedral chloroanions ( $\text{TiCl}_6^{2-}$ ,  $\text{ZrCl}_6^{2-}$  and  $\text{HfCl}_6^{2-}$ ) in order to study the nature of bonding in the octahedral chloroanions, and also to compare the vibrational frequencies and force constants with those of the corresponding tetrahedral molecules. Further, the generalized mean-square amplitude quantities and mean amplitudes of vibration for bonded as well as non-bonded distances have been evaluated.

### METHOD

The ions of the type  $\text{MX}_6^{2-}$  ( $X = \text{Cl}, \text{Br}$ ) possess  $O_h$  symmetry and the fundamental vibrations are distributed as,  $(1a_{1g} + 1e_g + 2f_{1u} + 1f_{2g} + 1f_{2u})$ , where  $a_{1g}$ ,  $e_g + f_{2g}$  are Raman active and  $f_{1u}$  is infrared active, while  $f_{2u}$  is inactive in both.

The generalized quadratic potential field constant and the symmetrized mean-square amplitudes of vibrations were evaluated as in our earlier paper

(1969a, 1969b). The fundamental frequencies employed in the present computations were taken from literature (Adam & Newton 1968, Brisdon *et al* 1969) and are presented in table 1 along with computed bond distances. The  $\nu_6(f_{2u})$  fundamental frequencies in case of bromoanions were evaluated by employing modified valence force constants reported by Brisdon *et al* (1969).

TABLE 1. Fundamental frequencies of octahedral haloanions (in  $\text{cm}^{-1}$ )

Ion	$\nu_1$	$\nu_2$	$\nu_3$	$\nu_4$	$\nu_5$	$\nu_6$	M-X bond length (in Å)
$\text{TiCl}_6^{2-}$	331	284	330	193	194	142	2.31
$\text{ZrCl}_6^{2-}$	327	237	290	150	153	90	2.44
$\text{HfCl}_6^{2-}$	333	237	288	145	157	80	2.43
$\text{TiBr}_6^{2-}$	192	141	268	121	110	77 94	
$\text{ZrBr}_6^{2-}$	198	141.7	226	114	116	82.18	
$\text{HfBr}_6^{2-}$	201	157	193	112	116	82 18	

## FORCE CONSTANTS

The force constants, computed here using the general quadratic potential function, are presented in table 2. The symbols have their usual meanings as explained in our earlier papers (1969a, 1969b). The reported constants reproduce the observed frequencies very well.

TABLE 2. Force constants (in  $m$  dynes/Å)

Force constant	$\text{TiCl}_6^{2-}$	$\text{ZrCl}_6^{2-}$	$\text{HfCl}_6^{2-}$
$f_a$	1.527	1.305	1.419
$f_{dd}$	0.100	0.177	0.190
$f_{dx} - f_{da''}$	0.106	0.055	0.040
$f_x - f_{aa''}$	0.187	0.124	0.134
$f_{ax} - f_{ax''}$	-0.005	0.000	0.003
$f_{xa'} - f_{aa''}$	-0.012	0.019	0.034
$f_{dd'}$	0.358	0.321	0.134

Neglecting the small difference in M-Cl stretching constant  $f_d$  for  $\text{TiCl}_6^{2-}$ , which is due to the use of ammonium instead of tetraethylammonium salt, it may be noted that  $f_d$  varies inversely with M-Cl bond length estimated from Pauling covalent radii (1960). This is anticipated for elements of a group when oxidation states are equal. Similar trend in UBFF stretching constant ( $K$ ) has

also been reported by Adam & Newton (1968). It is also apparent from the table that the stretching of the bond varies for different complexes. The bond-bond interaction constant  $f_{dd}$  increases with the increase of atomic weight of the central atom while the reverse trend is observed for the  $f_{da}$  constant. The deformation constant,  $f_{aa}$ , for Zr and Hf-chloroanions is approximately the same.

A comparison of the force constants of  $\text{MCl}_6^{2-}$  ions with those of the corresponding  $\text{MCl}_4$  molecules (Muller & Krebs 1967 and Nagarajan, 1964) in table 3

TABLE 3. Comparison of force constants and frequencies of  $\text{MX}_4$  molecules and  $\text{MX}_6^{2-}$  ions.

Species	Force constants ( $m$ dynes/ $\text{\AA}$ )			Frequencies ( $\text{cm}^{-1}$ )	
	$f_a$	$f_{da}$	$f_a - f_{aa}'''$	$\nu_1$	$\nu_5$
$\text{TiCl}_4$	2.59	0.19	0.11	389	140
$\text{TiCl}_6^{2-}$	1.53	0.10	0.19	331	194
$\text{ZrCl}_4$	2.56	0.17	0.09	383	120
$\text{ZrCl}_6^{2-}$	1.31	0.18	0.12	327	153
$\text{HfCl}_4$	2.42	0.03	0.07	347	94
$\text{HfCl}_6^{2-}$	1.42	0.19	0.13	333	157

shows that the stretching constants for the octahedral chloroanions are less than those for tetrahedral molecules, indicating a loosening of the bonds in  $\text{MCl}_6^{2-}$  ions. An opposite trend is noticed for  $f_{da}$  and the bending constants except for  $\text{TiCl}_6^{2-}$  due to different salt used in spectral studies. Further, a greater force is required to open the  $\text{Cl}-\hat{\text{M}}-\text{Cl}$  angle in  $\text{MCl}_6^{2-}$  ion as compared with the  $\text{MCl}_4$  molecules.

#### TREND IN FREQUENCIES

The stretching frequency  $\nu_1(\alpha_{1g})$  for the ions under investigation is nearly the same. In the case of Zr and Hf, all the frequencies are approximately the same. A comparison of the frequencies of the  $\text{MCl}_6^{2-}$  ions with  $\text{MCl}_4$  molecules in table 3 indicates that the symmetrical stretching frequencies of the ions are less than those of the molecules while for bending frequencies the behaviour is opposite.

#### MEAN AMPLITUDES OF VIBRATION

The generalized mean-square amplitude quantities, viz. mean-square parallel amplitude  $\langle \Delta z^2 \rangle$  and mean-square perpendicular amplitudes  $\langle \Delta x^2 \rangle$  and

$\langle \Delta y^2 \rangle$  at three temperatures  $T = 0^\circ$ ,  $T = 298^\circ$  and  $500^\circ\text{K}$  are given in table 4. The mean amplitude of vibration for bonded as well as nonbonded atom pairs at temperatures  $T = 0^\circ$ ,  $298^\circ$  and  $500^\circ\text{K}$  are given in table 5. The mean amplitude of vibration for bonded atom pairs increases with the increase of mass of the central atom for chloro- and bromo-anions while the corresponding force constants show a reverse trend (1969). The mean amplitude quantities for non-bonded distances in general also increase. On the other hand, as one moves from chloro- to bromospecies for the same element, the mean

TABLE 4. Generalized mean-square amplitude quantities in  $10^{-4}\text{\AA}^2$  for octahedral haloanions.

Ion	Distance	Symbol	Mean-square amplitude quantities		
			$T = 0^\circ\text{K}$	$T = 298^\circ\text{K}$	$T = 500^\circ\text{K}$
$\text{TiCl}_6^{2-}$	Ti-Cl	$\langle \Delta z^2 \rangle$	25.834	39.957	60.211
		$\langle \Delta x^2 \rangle$	34.361	80.046	128.310
		$\langle \Delta y^2 \rangle$	34.361	80.046	128.310
	Cl-Cl (linear)	$\langle \Delta z^2 \rangle$	31.887	51.921	79.218
		$\langle \Delta x^2 \rangle$	24.501	56.088	90.052
		$\langle \Delta y^2 \rangle$	24.501	56.088	90.052
	Cl-Cl (non-linear)	$\langle \Delta z^2 \rangle$	87.246	165.142	257.249
		$\langle \Delta x^2 \rangle$	75.788	139.263	215.828
		$\langle \Delta y^2 \rangle$	45.722	129.481	211.136
	Zr-Cl	$\langle \Delta z^2 \rangle$	23.672	40.711	62.786
		$\langle \Delta x^2 \rangle$	38.606	131.082	215.315
		$\langle \Delta y^2 \rangle$	38.606	131.082	215.315
$\text{ZrCl}_6^{2-}$	Cl-Cl (linear)	$\langle \Delta z^2 \rangle$	36.431	66.458	103.528
		$\langle \Delta x^2 \rangle$	31.065	87.886	143.411
		$\langle \Delta y^2 \rangle$	31.065	87.886	143.411
	Cl-Cl (non-linear)	$\langle \Delta z^2 \rangle$	81.864	212.056	341.579
		$\langle \Delta x^2 \rangle$	68.171	173.683	279.185
		$\langle \Delta y^2 \rangle$	68.344	200.792	481.795
$\text{HfCl}_6^{2-}$	Hf-Cl	$\langle \Delta z^2 \rangle$	20.593	35.676	55.095
		$\langle \Delta x^2 \rangle$	36.209	138.557	228.581
		$\langle \Delta y^2 \rangle$	36.209	138.557	228.581
	Cl-Cl (linear)	$\langle \Delta z^2 \rangle$	36.255	66.014	102.791
		$\langle \Delta x^2 \rangle$	30.275	83.669	136.290
		$\langle \Delta y^2 \rangle$	30.275	83.669	136.290
	(Cl - - Cl) (non-linear)	$\langle \Delta z^2 \rangle$	69.962	192.254	329.625
		$\langle \Delta x^2 \rangle$	56.754	167.113	271.159
		$\langle \Delta y^2 \rangle$	74.550	353.330	586.607



TABLE 4 (contd.)

Ion	Distance	Symbol	Mean-square; amplitude quantities		
			$T = 0^\circ\text{K}$	$T = 298^\circ\text{K}$	$T = 500^\circ\text{K}$
$\text{TiBr}_6^{2-}$	Ti-Br	$\langle \Delta z^2 \rangle$	23.876	49.384	78.115
		$\langle \Delta x^2 \rangle$	32.716	111.492	182.759
		$\langle \Delta y^2 \rangle$	32.716	111.492	182.759
	Br-Br	$\langle \Delta z^2 \rangle$	27.263	77.740	126.797
		(linear) $\langle \Delta x^2 \rangle$	19.170	73.867	122.112
		$\langle \Delta y^2 \rangle$	19.170	73.867	122.112
	Br-Br	$\langle \Delta z^2 \rangle$	86.076	222.053	357.165
		(non-linear) $\langle \Delta x^2 \rangle$	78.715	191.870	307.430
		$\langle \Delta y^2 \rangle$	36.634	182.348	303.354
$\text{ZrBr}_6^{2-}$	Zr-Br	$\langle \Delta z^2 \rangle$	19.575	44.877	71.928
		$\langle \Delta x^2 \rangle$	26.739	99.036	163.245
		$\langle \Delta y^2 \rangle$	26.739	99.036	163.245
	Br..Br	$\langle \Delta z^2 \rangle$	26.943	76.216	124.252
		(linear) $\langle \Delta x^2 \rangle$	18.179	66.614	109.933
		$\langle \Delta y^2 \rangle$	18.179	66.614	109.933
	Br..Br	$\langle \Delta z^2 \rangle$	66.440	189.907	308.753
		(non-linear) $\langle \Delta x^2 \rangle$	58.760	163.678	265.656
		$\langle \Delta y^2 \rangle$	34.750	164.335	273.068
$\text{HfBr}_6^{2-}$	Hf-Br	$\langle \Delta z^2 \rangle$	16.580	40.065	64.609
		$\langle \Delta x^2 \rangle$	22.424	89.396	153.667
		$\langle \Delta y^2 \rangle$	22.424	89.396	153.667
	Br..Br	$\langle \Delta z^2 \rangle$	24.902	65.021	105.473
		(linear) $\langle \Delta x^2 \rangle$	18.179	66.614	109.933
		$\langle \Delta y^2 \rangle$	18.179	66.614	109.933
	Br..Br	$\langle \Delta z^2 \rangle$	52.842	166.206	278.025
		(non-linear) $\langle \Delta x^2 \rangle$	122.482	137.608	230.786
		$\langle \Delta y^2 \rangle$	34.750	164.335	273.068

amplitudes of vibration for bonded as well as non-bonded linear distances in general increases. The quantities corresponding to non-linear non-bonded distances show an opposite behaviour. In the case of octahedral titanium chloro- and bromo-anions such variation has not been observed due to reasons stated earlier. The mean amplitude quantities increase with temperature as expected.

TABLE 5. Mean amplitude quantities in  $10^{-2}$  Å for octahedral chloroanions and bromoanions.

Ion	Distance	Mean amplitude quantities		
		$T = 0^\circ\text{K}$	$T = 298^\circ\text{K}$	$T = 500^\circ\text{K}$
$\text{TiCl}_6^{2-}$	Ti-Cl	5.083	6.321	7.760
	Cl...Cl	5.647	7.206	8.900
	(linear)			
	Cl...Cl	9.341	12.852	16.039
$\text{ZrCl}_6^{2-}$	Zr-Cl	4.865	6.381	7.924
	Cl...Cl	6.036	8.132	10.175
	(linear)	9.048	14.662	18.482
	(non-linear)			
$\text{HfCl}_6^{2-}$	Hf-Cl	4.538	5.973	7.423
	Cl...Cl	6.021	8.125	10.139
	(linear)			
	Cl...Cl	8.364	13.866	18.156
$\text{TiBr}_6^{2-}$	Ti-Br	4.886	7.027	8.838
	Br...Br	5.221	8.817	11.260
	(linear)			
	Br...Br	9.326	14.902	18.899
$\text{ZrBr}_6^{2-}$	Zr-Br	4.242	6.699	8.841
	Br...Br	5.191	8.730	11.146
	(linear)			
	Br...Br	8.151	13.781	17.571
$\text{HfBr}_6^{2-}$	Hf-Br	4.072	6.330	8.038
	Br...Br	4.990	8.064	10.270
	(linear)			
	Br...Br	7.269	12.896	16.674
	(non-linear)			

## ACKNOWLEDGEMENT

The authors are thankful to Professor D. Sharma for encouragement. Financial assistance provided by The Council of Scientific & Industrial Research, New Delhi, to two of us (HSS and ANP) is thankfully acknowledged.

## REFERENCES

- Adams D. M., & Newton D. C. 1968 *J. Chem. Soc. A*, 2262.  
 Brisdon B. J., Ozin G. A. & Walton R. A. 1969 *J. Chem. Soc. A*, 342.  
 Muller A., & Krobs B. 1967 *J. Mol. Spectry*, **24**, 180.  
 Nagarajan G. 1964 *Indian J. Pure Appl. Phys.* **2**, 145.  
 Pandey A. N., Singh H. S., & Sanyal N. K. 1969a *Curr. Sci.* **38**, 108.  
 Pauling L. 1960 *The Nature of the Chemical Bond*, Cornell University Press, N.Y. 3rd Edn.  
 Sanyal N. K., Singh H. S., & Pandey A. N. 1969b *Indian J. Phys.* **43**, 361.  
 Woodward L. A., & Creighton J. A. 1961 *Spectrochim. Acta* **17**, 594.

## Glauber approximation in inelastic e-H scattering

By A. S. GHOSH and N. C. SIL

*Department of Theoretical Physics,*

*Indian Association for the Cultivation of Science, Jadavpur, Calcutta-32*

(Received 24 December 1969)

Glauber approximation has been applied to calculate the total and the differential cross sections for  $1s-2s$  and  $1s-2p$  excitations in e-H scattering. In the intermediate energy region, our results for the total cross section of  $1s-2p$  excitation are in better agreement with the experimental observations than other existing theoretical results. In the case of  $1s-2p$  excitation the total cross section curve almost coincides with the experimental findings. The differential cross sections for both the cases are more sharply peaked in the forward direction than those in Born approximation.

### INTRODUCTION

With the recent developments in the experimental techniques, considerable theoretical interests have been focussed upon electron-atom collisions. Electron-hydrogen system is theoretically the simplest one and as such has been most extensively studied. In the case of inelastic electron-hydrogen (e-H) collision process, there are long standing marked differences between the experimental results and the theoretical findings. There was no appreciable improvement in the theoretical results in spite of repeated attempts. Akerib & Borowitz (1961) have applied the impulse approximation to the inelastic e-H scattering. A new method, which explicitly takes into account the repulsion between the atomic and incident electrons in the choice of the total wave function, has been introduced by Vainshtein, Presnyakov & Sobelman (1963). Ochkur (1963) has given a modified form of Born-Oppenheimer approximation allowing for exchange interaction. Recently (1969), he has presented an improved version of this previous work. Sloan & Moore (1968) have given a theoretical formulation for both the elastic and inelastic processes based on Foddeev equation (1961) for three particle scattering. This approximation amounts to an unitarized Born approximation with the exchange effect taken into account. Several workers (Damburg & Peterkof 1962, Burke, Schey & Smith 1963) have applied the close coupling approximation to the e-H scattering problem. This approximation, though theoretically sound, is laborious in practice and the results obtained in the case of the inelastic processes are not upto the expectation.

The purpose of the present paper is to make an analysis of the inelastic ( $1s-2s$  and  $1s-2p$ ) electron-hydrogen scattering processes. The dynamical basis of our calculation is the multiple scattering model proposed by Glauber (1959). This approximation is extensively used in nuclear and particle physics Bessel

& Wilkin 1968, Harrington 1968). In atomic physics, it has been applied to elastic electron-hydrogen scattering (Franco 1968, Tai *et al* 1969). Glauber approximation is based on Eikonal approximation. The latter applies to the scattering by a fixed potential and is thereby restricted to single scattering whereas Glauber approximation takes account of multiple scattering. Contrary to the method of impulse approximation the interaction between the incident electron and the proton has been taken into account in the present method.

We have calculated the  $1s-2s$  and  $1s-2p$  excitation cross sections in e-H collision covering the energy region 10.6 eV to 200 eV.

### THEORY

We consider the target proton to be infinitely heavy and the origin of the co-ordinate to be placed at the position of the proton. Let  $\mathbf{r}$  denote the position vector of the atomic electron and  $\mathbf{b}$  be the impact parameter vector relative to the origin. In Glauber approximation, the amplitude of scattering  $F_{fi}(\alpha)$  for the process in which the hydrogen atom undergoes a transition from an initial state  $i$  with wave function  $\phi_i$  to a final state  $f$  with wave function  $\phi_f$  is given by (Franco 1968)

$$F_{fi}(\alpha) = \frac{ik_0}{2\pi} \int \phi_f^*(\mathbf{r}) \Gamma(\mathbf{b}, \mathbf{r}) \phi_i(\mathbf{r}) \exp(i\mathbf{q} \cdot \mathbf{b}) d^2b \, d\mathbf{r}, \quad (1)$$

where  $\mathbf{q} = \mathbf{k}_0 - \mathbf{k}_1$ ,  $\mathbf{k}_0$  and  $\mathbf{k}_1$  being, respectively, the momenta of the incident and scattered electron. The double integration with respect to  $d^2b$  is over the plane perpendicular to the incident beam direction.  $\Gamma(\mathbf{b}, \mathbf{r})$  has the form (Glauber 1959)

$$\Gamma(\mathbf{b}, \mathbf{r}) = 1 - \exp(2i\chi(\mathbf{b})), \quad \dots (2)$$

where  $\chi(\mathbf{b})$  is the phase shift corresponding to the impact parameter  $\mathbf{b}$ . According to Glauber, the phase shift due to a number of scattering centres is just the sum of the individual phase shifts due to each, taken separately, of course, at the appropriate values of the impact parameters. Thus for the case of e-H scattering we may write (Franco 1968)

$$\begin{aligned} \Gamma(\mathbf{b}, \mathbf{r}) &= 1 - \exp \left[ \left( -\frac{iZe^2}{v} \right) \int_{-\infty}^{\infty} \{ (b^2 + \zeta^2)^{-1} - [(b-s)^2 + (\zeta-Z)^2]^{-1} \} d\zeta \right] \\ &= 1 - \left( \frac{|\mathbf{b}-\mathbf{s}|}{b} \right)^{2i\pi} \end{aligned}$$

with  $\mathbf{r} = \mathbf{s} + \mathbf{z}$ , where  $\mathbf{s}$  is the component of  $\mathbf{r}$  perpendicular to the incident beam and  $n = e^2/\hbar v$ ,  $v$  being the velocity of the incident electron.

Next we calculate the scattering amplitudes for the two different cases under consideration.

(A) (1s-2s) case :

Here the initial and final states are, respectively, the 1s and 2s states of hydrogen atom;

i.e.,  $\phi_{1s}(r) = (\pi a_0^3)^{-1} \exp(-r/a_0)$  and  $\phi_{2s}(r) = (2^3 a_0^3 \pi)^{-1} \left(1 - \frac{r}{2a_0}\right) \exp(-r/2a_0)$ , where  $a_0$  is the Bohr radius.

We take  $\mathbf{q}$  to be perpendicular to the incident momentum  $\mathbf{k}_0$  (figure 1), this assumption (Bessel & Wilkin 1968) is justified in Glauber's model which is applicable to small angle scattering at high energy.

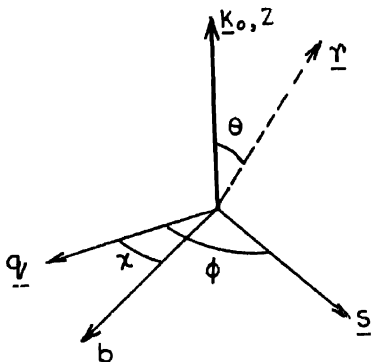


FIGURE 1. Coordinate system used for inelastic e-H scattering.

Substituting the expressions for  $\phi_{1s}(r)$ ,  $\phi_{2s}(r)$  and  $\Gamma(\mathbf{b}, \mathbf{r})$  and changing integration variables from  $\phi, \chi$  to  $\phi' (= \phi - \chi)$ ,  $\chi$  we can write equation (1) as

$$F_H(\alpha) = \frac{ik_0}{2^{5/2}\pi^2 a_0^3} \int \left(1 - \frac{\sqrt{s^2 + z^2}}{2a_0}\right) \exp\left(-\frac{3}{2a_0} \sqrt{s^2 + z^2}\right) \\ \left[1 - \left(\frac{b^2 + s^2 - 2bs \cos \phi'}{b^2}\right)^{1/2}\right] \exp(iqb \cos \chi) bs \, db \, d\chi \, dz \, d\phi'$$

Integrating with respect to  $\chi$  we have

$$F_{II}(\alpha) = \frac{ik_0}{2^{3/2}\pi a_0^3} \int \left(1 - \frac{\sqrt{s^2 + z^2}}{2a_0}\right) \exp\left(-\frac{3}{2a_0} \sqrt{s^2 + z^2}\right) \\ \left[1 - \left(\frac{b^2 + s^2 - 2bs \cos \phi'}{b^2}\right)^n\right] J_0(qb) \times bs \, db \, dz \, ds \, d\phi'$$

where the integration with respect to  $b$  is over the interval  $(0, \infty)$ . We perform the angular integration with respect to  $\phi'$  and obtain

$$F_{II}(\alpha) = \frac{ik_0}{\sqrt{2}a_0^3} \int \left(1 - \frac{\sqrt{s^2 + z^2}}{2a_0}\right) \exp\left(-\frac{3}{2a_0} \sqrt{s^2 + z^2}\right) \\ \left[1 - \left(\frac{2s}{b}\right)^n G(y)\right] J_0(qb) bs \, dz \, db \, ds,$$

where  $G(y) = y^{-n}(1-y^2)^{\frac{1}{2}n} {}_2F_1\left(\frac{1}{2} + \frac{1}{2}in, 1 + \frac{1}{2}in, 1, y^2\right)$  and  $y = \frac{2bs}{b^2 + s^2} \cdot {}_2F_1$  being the hypergeometric function. Now we perform the integration with respect to  $z(-\infty, \infty)$  and get

$$F_{II}(\alpha) = \frac{2''ik_0}{\sqrt{2}a_0^3} \int \left[ \frac{4}{3} {}_3K_1\left(\frac{3}{2a_0} s\right) - \frac{s^2}{2a_0} K_2\left(\frac{3}{2a_0} s\right) \right] \times \left[1 - \left(\frac{2s}{b}\right)^n G(y)\right] \\ \times J_0(qb) bs \, db \, ds \quad \dots (4)$$

where  $K_1$  and  $K_2$  are the Bessel functions of the third kind. The integration with respect to  $s$  is over the interval  $(0, \infty)$ . Introducing the polar variables  $r, \theta$  given by  $b = r \cos \theta$  and  $s = r \sin \theta$ , to the integral (4) and evaluating the radial integration we have

$$F_{II}(\alpha) = -\frac{2^{11}ik_0\alpha}{3^5 \times \sqrt{2}} \int_0^{\pi/2} \sin^3 \theta \cos \theta \left[ \sin^4 \theta - \frac{28}{9} (a_0 q)^2 \cos^2 \theta \sin^2 \theta + \frac{64}{81} (a_0 q)^4 \cos^4 \theta \right] \\ \times \left( \sin^2 \theta + \frac{4}{9} (a_0 q)^2 \cos^2 \theta \right)^{-5} \\ \times \left[1 - \left(|\cos 2\theta| / |\cos \theta|^2\right)^n |\cos 2\theta| {}_2F_1\left(\frac{1}{2} + \frac{1}{2}in, \frac{1}{2}in + 1, 1; \sin^2 2\theta\right)\right] d\theta \quad \dots (5)$$

(B) (1s-2p) case.

Here the possible final states, with  $k_0$  as the polar axis, are

$$\phi_{2p, \pm 1}(r) = (2^6 \pi a_0^5)^{-1/2} r \exp(-r/2a_0) \sin \theta \exp(\pm i\phi)$$

$$\phi_{2p, 0}(r) = (2^5 \pi a_0^5)^{-1/2} r \exp(-r/2a_0) \cos \theta$$

One can easily find that the factor  $r \cos \theta$  that appears in the wave function for 2p0, makes the corresponding matrix elements vanish. Further, it can be

shown that the cross sections for the other two states are the same. Therefore we need calculate only a single scattering amplitude. As in the previous case we now substitute the expressions for  $\phi_{1s}(r)$ ,  $\phi_{2p,-1}(r)$  and  $\Gamma(\mathbf{b}, \mathbf{r})$  in equation (1) and obtain

$$F_{f1}(\alpha) = \frac{ik_0}{2^4\pi^2 a_0^4} \int s \exp\left(-\frac{3}{2a_0} \sqrt{s^2+z^2}\right) \left[1 - \left(\frac{b^2+s^2-2bs \cos \phi'}{b^2}\right)^n\right] \\ \exp(iq b \cos \chi + i\chi) \exp(i\phi') bs db d\chi dz ds d\phi'$$

Integrating with respect to  $\chi$  we obtain

$$F_{f1}(\alpha) = \frac{-k_0}{2^3\pi a_0^4} \int s^2 \exp\left(-\frac{3}{2a_0} \sqrt{s^2+z^2}\right) \left[1 - \left(\frac{b^2+s^2-2bs \cos \phi'}{b^2}\right)^n\right] \\ \times J_1(qb) b db dz ds d\phi'$$

Performing the integration with respect to  $\phi'$  we get

$$F_{f1}(\alpha) = \frac{-in k_0}{2^3 a_0^4} \int s^2 \exp\left(-\frac{3}{2a_0} \sqrt{s^2+z^2}\right) \left(\frac{2s}{b}\right)^{in} G(y) J_1(qb) b db ds dz$$

$$\text{where} \quad G(y) = y^{1-in} {}_2F_1\left(\frac{1}{2}-\frac{1}{2}in, 1-\frac{1}{2}in, 2; y^2\right)$$

$$\text{and} \quad y = \frac{2bs}{b^2+s^2}$$

Following the same procedure as in 1s-2s, we finally get the scattering amplitude as

$$F_{f2}(\alpha) = -\frac{i2^{12}nk_0a_0^2}{3^6} \int_0^{\pi/2} (a_0q) \sin^5 \theta \cos^3 \theta (\cos \theta)^{-2in} \\ \times (\sin^2 \theta - \frac{4}{9} (a_0q)^2 \cos^2 \theta) (\sin^2 \theta + \frac{4}{9} (a_0q)^2 \cos^2 \theta)^{-5} \\ \times {}_2F_1\left(\frac{1}{2}-\frac{1}{2}in, 1-\frac{1}{2}in, 2; \sin^2 2\theta\right) d\theta \quad \dots (6)$$

The differential cross-section for a particular transition is obtained by the relation

$$I(\alpha) = \frac{k_f}{k_i} |F_{f1}(\alpha)|^2 \quad \dots (7)$$

The total cross section for the process is given by

$$Q = 2\pi \int_0^\pi [F(\alpha)] \sin \alpha d\alpha \quad \dots (9)$$

## RESULTS AND DISCUSSION

We have calculated the differential cross sections for  $1s-2s$  and  $1s-2p$  excitations with the help of the equations (5), (6) and (7). The integration in equations (5) and (6) have been done numerically using a 16-point Gaussian quadrature. In figure 2, we have compared our results for the differential cross sections for  $1s-2s$  excitation at incident energies 50, 100, and 200 eV with the corresponding results of the first Born approximation (FBA). Table 1 furnishes

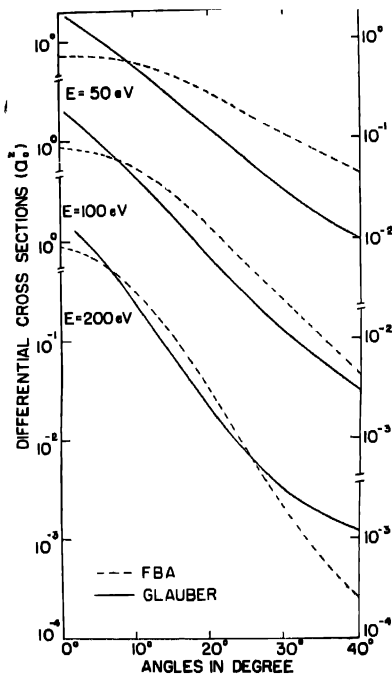


FIGURE 2. Excitation differential cross-sections of hydrogen  $2s$  level in the first Born and Glauber approximations.

Table 1. Differential cross-sections per unit solid angle in units of  $a_0^2$  per steradian for excitation of  $2p$  level of hydrogen.

Electron Energy (eV)	Cosine of angle of scattering					
	0.9999	0.996	0.985	0.939	0.868	0.750
50	32.00	20.99	7.56	0.04	0.17	0.03
100	83.51	22.56	4.22	0.25	0.03	0.004
200	259.30	12.70	1.44	0.03	0.003	0.0004



the calculated values of the differential cross-section for  $1s$ - $2p$  excitation at different values of the cosine of the angle of scattering for these incident energies.

In the calculation of the total cross-section we have carried out the integration with respect to the cosine of the angle of scattering numerically. Depending upon the nature of the integrand we have divided the total range of integration  $(-1, 1)$  into suitable sub-intervals. In each of the sub-intervals a 16 point Gaussian quadrature has been used. In table 2, we have compared our values

Table 2. Excitation total cross-sections  $2s$  and  $2p$  levels of Hydrogen (in units of  $\pi a_0^2$ ) in Born, Ochkur and Glauber approximations.

Excited states	E(eV)	30	40	60	100	200
$2s$	Born	—	—	—	0.057	0.029
	Ochkur	0.123	0.106	0.081	0.053	0.028
	Glauber	0.080	0.081	0.072	0.0515	0.028
$2p$	Born	—	—	—	0.73	0.47
	Ochkur	1.12	1.09	0.95	0.73	0.48
	Glauber	0.796	0.843	0.787	0.637	0.462

for the total cross-sections for both the cases at different incident energies with the corresponding values obtained by using Ochkur (1969) and Born approximations. In figures 3 and 4, we have shown our results for the total cross-

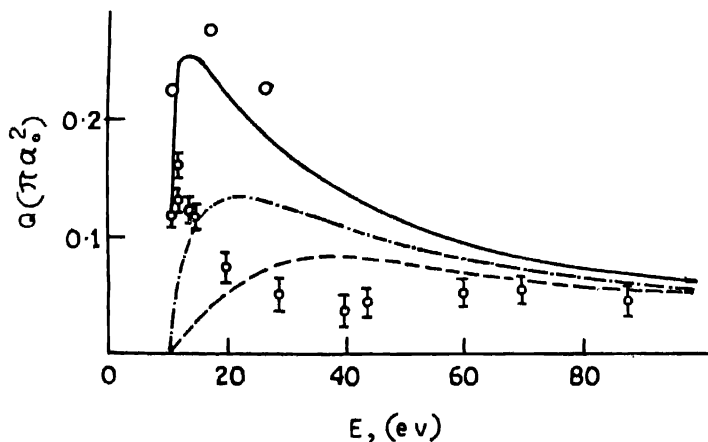


FIGURE 3. Total excitation cross-sections of the hydrogenic  $2s$  level in  $eH$  scattering. Solid line—Born approximation without exchange; small circles—close coupling approximation (Damburg *et al* 1962) with consideration of  $1s$ - $2s$ - $2p$ -levels; Chained curve—Ochkur approximation (1969); dotted lines—present calculation; circles with error indicated—experiment.

sections of  $1s-2s$  and  $1s-2p$  processes, respectively, together with the corresponding existing theoretical curves and compared them with the experimental findings (Fite *et al* 1959, 1960, Lichten 1961).

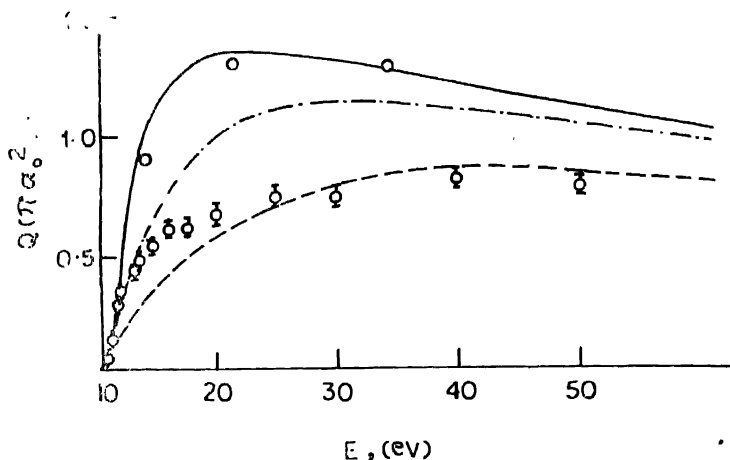


FIGURE 4. Total excitation cross-sections of the hydrogenic  $2p$  level in  $e$ -H scattering. Solid line—Born approximation without exchange; small circles—close coupling approximation (Damburg *et al.* 1962) with consideration of  $1-2s-2p$  levels; Chained curve—Ochkur approximation (1969), dotted line—present calculation, circles with error indicated—experiment.

The differential cross sections obtained in Glauber approximation are more sharply peaked in the forward direction at every energy than those given by the first Born approximation. With the increase of the incident energy, our results give closer agreement with those of the first Born approximation. This is in conformity with the observation of Tai *et al.* (1969)

The calculated values for the total cross section for  $1s-2s$  excitation agree more closely with the experimental findings than the results of other theoretical calculations in the intermediate energy range. However, near the threshold energy, our results deviate considerably from the experimental findings. It does not reproduce the peak at the threshold. The theoretical curve for the total cross-section for  $1s-2p$  excitation in Glauber approximation almost coincides with the experimental observations even upto energies as low as 25 eV; below this energy, however, there is a slight discrepancy. For both the cases under consideration, it appears from the table 2 that above 200 eV the theoretical results in first Born, Ochkur (1969) and Glauber approximations are almost



## Second positive bands of $N_2$ in the afterglow of $N_2$ and $O_2$ mixture

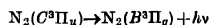
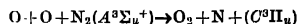
By S. N. GHOSH, A. N. SRIVASTAVA AND R. V. SHUKLA

*J. K. Institute of Applied Physics and Technology, University of Allahabad,  
Allahabad, India*

(Received 30 December 1969)

(Plate—6)

The second positive bands of  $N_2$  were observed in the afterglow of  $N_2$  and  $O_2$  mixture and were studied spectroscopically, photometrically and microphotometrically. Effect of temperature on the intensity of bands at  $3371\text{\AA}$  and  $3577\text{\AA}$  of  $N_2$  2PG system is small. Quenching cross-sections for the above by  $N_2$  and  $O_2$  are of the order of  $10^{-14}\text{ cm}^2$  and  $10^{-16}\text{ cm}^2$ , respectively. Excitation mechanism of these bands in the laboratory has been proposed as follows :



### INTRODUCTION

Mecke & Lindau (1924) and Coster *et al* (1933) observed the second positive bands of  $N_2$  in the discharge of  $N_2$  and air and also in arcs at low pressures. These bands were also excited by bombarding  $N_2$  molecules by ions (Philpot *et al* 1961, Ghosh *et al* 1965). In the pink afterglow excited in highly pure  $N_2$ , the presence of the bands was detected and their excitation was discussed by Prag & Clark (1963). The afterglow excited in  $N_2$  of ordinary purity contains mainly first positive bands and very weak second positive bands (Young & Black 1966). Barth & Kaplan (1957) observed the  $N_2$  second positive bands in the afterglow of  $N_2$  containing 2 percent of oxygen.

To understand the excitation mechanism of these bands in the afterglow and their characteristics, the present investigation was undertaken.

### EXPERIMENTAL ARRANGEMENT AND OBSERVATIONS

The experimental system described elsewhere (Ghosh *et al* 1969a) has been used omitting the sodium vapouring chamber (figure 1).  $N_2$  and  $O_2$  gases were used directly from cylinder without purification. These gases were 99.5% pure. Oxygen gas was introduced through the needle valve  $N'$  and was dissociated by discharge from a microtherm before it entered the reaction chamber. The

$N_2$  gas was introduced through the other needle valve  $N''$ . After adjusting the flow rates of  $N_2$  and  $O_2$  gases, the maximum intensity in the afterglow was obtained. A strong white-greenish afterglow filled the reaction chamber. When the flow of  $O_2$  was stopped, afterglow did not appear in the reaction chamber even with large flow rate of  $N_2$ .\*

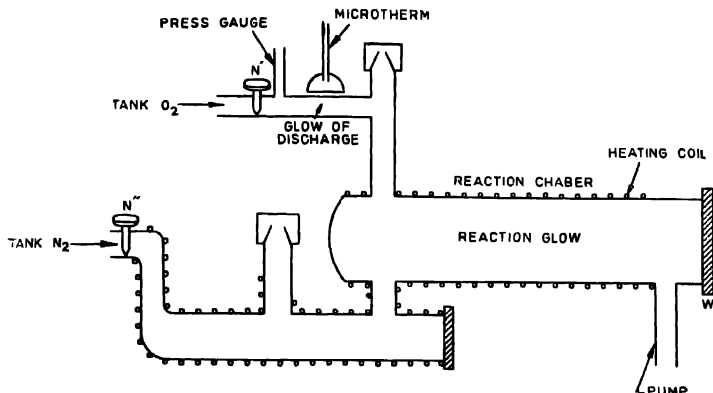


FIGURE 1. Experimental arrangement for the study of the afterglow.

Spectroscopic and photometric observations, and microphotometric analysis of the afterglow are described below.

1. *Spectroscopic*: The spectrum of the afterglow was taken with a Hilger medium quartz spectrograph through the quartz window  $W$  (plate 6). An exposure of 12 hours was given on Kodak F(103)a plate. It was observed that  $N_2$  second positive bands in the range  $3000\text{--}4500\text{ \AA}$  were present.\*\* The bands and their visual intensities are given in table 1.

2. *Photometric observations*: Second positive bands of  $N_2$  at  $3371\text{ \AA}$  and  $3577\text{ \AA}$  were selected by a monochromator described elsewhere (Ghosh *et al* 1969a). Three photometric observations were carried out, namely, variation of intensities of  $3371\text{ \AA}$  and  $3577\text{ \AA}$  with (1)  $N_2$  pressure at a fixed flow rate of  $O_2$ , (2)  $O_2$  pressure at a fixed flow rate of  $N_2$ , and (3) temperature. These observations are described below :

\* Afterglow produced by dissociating  $N_2$  molecules was investigated and was studied in great detail by Young & Black (1966). In the present experimental setup, however, the  $N_2$  gas was not directly under microtherm discharge.

\*\* Actually  $N_2$  second positive bands were observed in the range  $3000\text{--}4500\text{ \AA}$ . The bands above this wavelength region were too weak to be observed.

TABLE 1. N<sub>2</sub> Second positive bands observed in the afterglow of O<sub>2</sub> and N<sub>2</sub> mixture; (B<sup>3</sup>Π<sub>g</sub>—C<sup>3</sup>Π<sub>u</sub>)

Band head (Å)	Intensity (visual)	Transition
3104	VVF	4,3
3116	VF	3,2
3336	F	2,1
3159	S	1,0
3268	VF	4,4
3285	VF	3,3
3309	VVF	2,2
3339	VVF	1,1
3371	VVS	0,0
3501	S	2,3
3537	VS	1,2
3577	VVS	0,1
3642	VVF	4,6
3672	S	3,5
3711	VS	2,4
3755	VVS	1,3
3805	VVS	0,2
3860	VVF	4,7
3895	VF	3,6
3943	S	2,5
3998	VS	1,4
4059	S	0,3
4095	F	4,8
4142	F	3,7
4200	F	2,6
4270	VVF	1,5
4344	VVF	0,4
4355	VVF	4,9

*(v) Variation of intensities of 3371 Å and 3577 Å with N<sub>2</sub> pressure*

The intensity of band at 3371 Å was measured at different pressures in the range 100–650 μ (figure 2) and for the band at 3577 Å, in the range 90–700 μ (figure 3). The flow rate of O<sub>2</sub> was kept constant. It was observed that the intensities of these bands at first rise with N<sub>2</sub> pressure and then, after attaining a maximum in the pressure range 300–400 μ begin to fall. For both these bands, the rise of intensity before reaching maximum values can be represented approximately by  $I = K_1 p$ , where  $I$  is the intensity at a pressure  $p$ ,  $K_1$  is a constant. The fall of intensities after reaching maximum values is given by  $I p = K_2$ , where  $I$ ,  $p$  and  $K_2$  have their usual meanings.

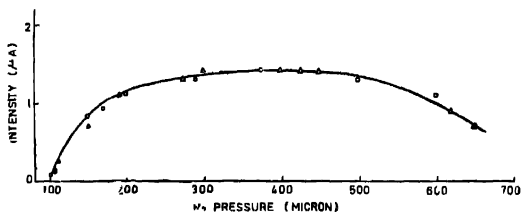


FIGURE 2 The intensity of the band at  $3371\text{\AA}$  is plotted against  $N_2$  pressure at a fixed flow rate of  $O_2$ . Note the flat maximum in the pressure range  $340\text{--}460\mu$

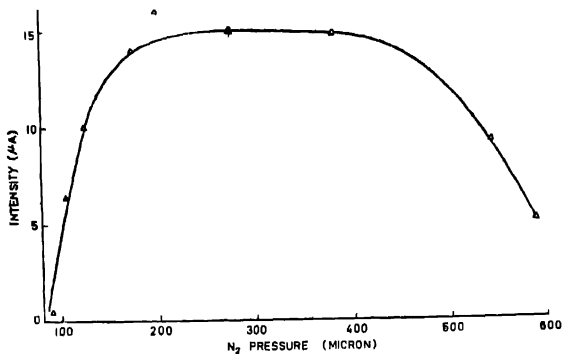


FIGURE 3 The intensity of the band at  $3577\text{\AA}$  is plotted against  $N_2$  pressure at a fixed flow rate of  $O_2$ . Note the flat maximum in the pressure range  $220\text{--}400\mu$ .

(ii) Variation of intensities of  $3371\text{\AA}$  and  $3577\text{\AA}$  with  $O_2$  pressure

Keeping the flow rate of  $N_2$  fixed, the variation of intensities of these bands at different pressures in the range  $85\text{--}200\mu$  (figure 4) and  $100\text{--}450\mu$  (figure 5), respectively, were measured. It was observed that the quenching of these radiations by  $O_2$  was considerable and is strong even at small concentration. The fall of intensities of the bands at  $3371\text{\AA}$  and  $3577\text{\AA}$  with the increase of  $O_2$  pressure can be represented approximately by  $I p^3 = K_3$  and  $I p^4 = K_4$ , respectively, and  $I$ ,  $p$ ,  $K_3$  and  $K_4$  have their usual significances.

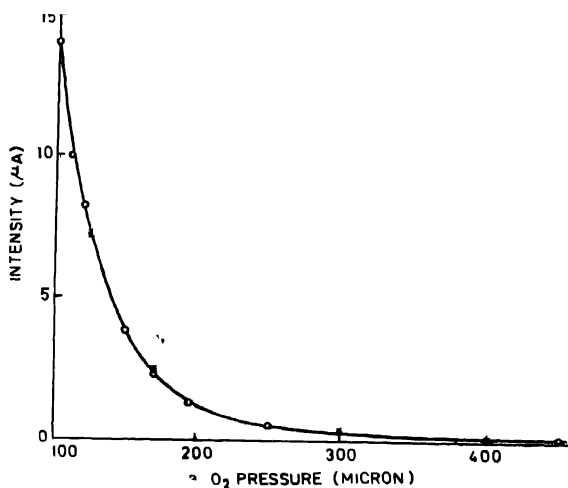


FIGURE 4. The intensity of the band at  $3371\text{\AA}$  is plotted against  $\text{O}_2$  pressure at a fixed flow rate of  $\text{N}_2$ . Note that  $\text{O}_2$  quenches the band considerably.

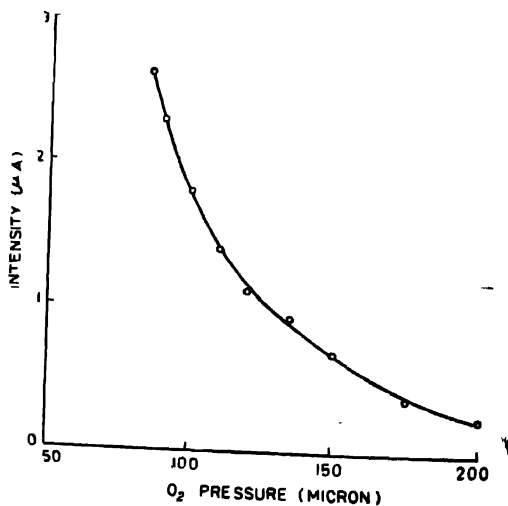


FIGURE 5. The intensity of the band at  $3577\text{\AA}$  is plotted against  $\text{O}_2$  pressure at a fixed flow rate of  $\text{N}_2$ . Note that  $\text{O}_2$  quenches the band considerably.



(iii) Variation of intensities of 3371 Å and 3577 Å with temperature

The intensities of these bands were measured at different temperatures in the range 25–325°C by heating the chamber electrically (figure 6). The temperature of the chamber was measured by a pyrometer (Ghosh *et al* 1969b).

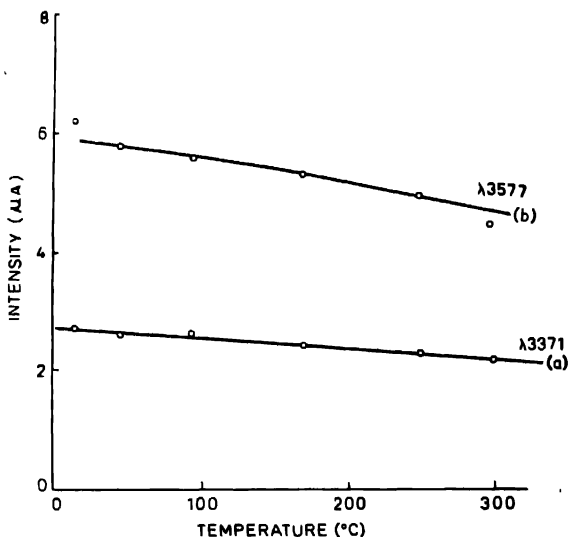


FIGURE 6 The intensities of bands at 3371 Å and 3577 Å are plotted against temperature. The intensity varies slightly with temperature.

It was observed that the effect of temperature on the bands at 3371 Å and 3577 Å is very small. The fall of intensities of these bands is small and can be represented by

$$I = \alpha T + I_0$$

where  $I_0$  and  $I$  are the intensities at room temperature and at  $T^\circ\text{C}$ .  $\alpha$  is a constant and is negative. The values of  $\alpha$  obtained from figure 6 are approximately  $1.84 \times 10^{-3} \mu\text{A}/^\circ\text{C}$  and  $2.92 \times 10^{-3} \mu\text{A}/^\circ\text{C}$  for 3371 Å and 3577 Å respectively.

(iv) Microphotometric analysis

The  $N_2$  second positive bands were scanned from 3000 Å to 5000 Å by a microphotometer described elsewhere (Ghosh *et al* 1969b) (figure 7). By measuring areas covered by the bands, the relative intensities of  $N_2$  second positive bands are obtained and are given in table 2.

TABLE 2. Relative intensities of second positive system of N<sub>2</sub>

Band head (Å)	Transition	Relative Intensity
3576.9	0,1	1.00
3371.3	0,0	0.96
3536.7	1,2	0.75
3159.3	1,0	0.65
3755.4	1,3	0.56
3804.9	0,2	0.55
3136.0	2,1	0.48
4059.4	0,3	0.47
3998.4	1,4	0.47
3943.0	2,5	0.45
3894.6	3,6	0.43
3710.5	2,4	0.41
3285.3	3,3	0.38
3500.5	2,3	0.31
3268.1	4,4	0.30
3857.9	4,7	0.22
3671.9	3,5	0.22
3641.7	4,6	0.18

## CALCULATION OF QUENCHING COEFFICIENTS

The quenching coefficients have been calculated from figures 2 & 3 by utilizing the curves from maximum intensity till it falls to half of its value. The coefficients have been obtained from the formula -

$$K = \frac{A}{n' - 2n_M}$$

where  $A$  = transition probability,

$n'$  = concentration of the quenching species at half intensity, and

$n_M$  = concentration for maximum intensity

The quenching coefficients and quenching cross-sections for the bands at 3371 Å and 3577 Å by N<sub>2</sub> and O<sub>2</sub> are given in table 3

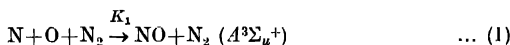
TABLE 3. Quenching coefficients and quenching cross-sections for bands at 3371 Å and 3577 Å

Band head (Å)	Quenching species	Quenching coeff (cm <sup>3</sup> /molecule-sec)	Quenching cross- section (cm <sup>2</sup> )
3371	O <sub>2</sub>	$1.1 \times 10^{-9}$	$5.0 \times 10^{-14}$
3371	N <sub>2</sub>	$1.9 \times 10^{-9}$	$2.2 \times 10^{-15}$
3577	O <sub>2</sub>	$1.3 \times 10^{-9}$	$6.5 \times 10^{-14}$
3577	N <sub>2</sub>	$1.0 \times 10^{-9}$	$5.2 \times 10^{-15}$

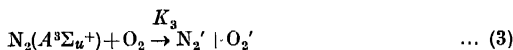
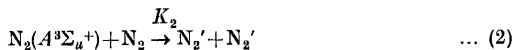
# DISCUSSION

To excite the  $N_2$  second positive bands, high energy (nearly 11 eV) is required. The photometric study carried out in the present investigation suggests the following mechanism for its excitation

N and O atoms may recombine in the presence of  $N_2$  as a third body forming NO molecules. An amount of 6.5 eV energy (dissociation energy of NO, Wilkinson 1963) will be released during the reaction, which will raise  $N_2$  to  $A^3\Sigma_u^+$  state requiring nearly 6.2 eV.



$A^3\Sigma_u^+$  is a metastable state having a lifetime greater than 9 seconds (Nicholls 1964). These excited  $N_2$  molecules may be lost as follows :



where  $N_2'$  and  $O_2'$  are energetic species and  $A$  is the transition probability corresponding to  $N_2$  Vegard-Kaplan bands. At equilibrium, one obtains

$$[N_2(A^3\Sigma_u^+)] = \frac{K_1[O][N][N_2]}{K_2[N_2] + K_3[O_2] + A} \quad \dots (5)$$

Since  $[N]$  and  $[O]$  are proportional to  $[N_2]$  and  $[O_2]$  respectively,

$$[N_2(A^3\Sigma_u^+)] = K \frac{[N_2]^2[O_2]}{A + K_2[N_2] + K_3[O_2]} \quad \dots (6)$$

where  $K = K_1/K_a$  and  $K_b$ .

$K_a$  and  $K_b$  are the rate coefficients for dissociation of  $N_2$  and  $O_2$  molecules. From equation (6), since  $A$  is small, at a small flow rate of  $N_2$ ,  $[N_2(A^3\Sigma_u^+)]$  will be independent of  $O_2$  pressure. On the other hand, if the fixed flow rate of  $O_2$  is small,  $[N_2(A^3\Sigma_u^+)]$  will vary linearly with  $N_2$  pressure.

N atoms can also be removed from the system by the following reaction which is very fast (Schiff 1964)



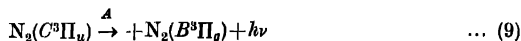
Since in both reactions (1) and (7) N atoms are removed and the flow rate of  $N_2$  used in the experiment is low,  $[N]$  will be small, so much so that it will

limit the production of  $N_2(A^3\Sigma_u^+)$ . In other words, the increase of  $O_2$  pressure will not affect the  $[N_2(A^3\Sigma_u^+)]$ .

The  $N_2(A^3\Sigma_u^+)$  may be excited to  $N_2(C^3\Pi_u)$  state as follows :



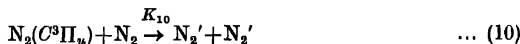
The excited  $N_2$  molecules may be lost as follows :



where  $A$  is the probability for  $B^3\Pi_g - C^3\Pi_u$  transition.

We have already shown in figure 4 and 5 that the second positive bands of  $N_2$  are quenched when  $O_2$  pressure is increased. This can be explained from the fact that in reactions (1) and (7), O atoms remain conserved. There is enough O atoms in the system for the reaction (8) to take place. Increase of  $O_2$  pressure leads to further production of O (O atoms are produced by dissociation of  $O_2$ ) which quenches of the radiation.

$N_2(C^3\Pi_u)$  molecules may be quenched as follows :



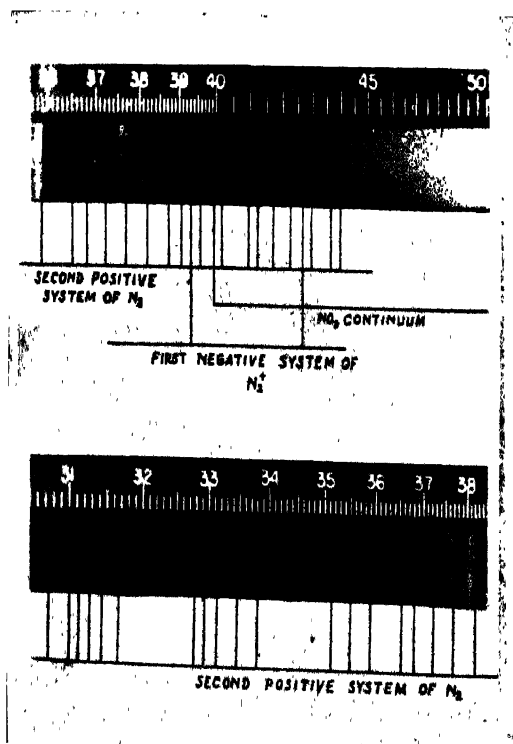
where  $N_2'$ ,  $O_2'$  and  $O'$  have got their usual meanings.

From equations (8) to (12), the intensity at any pressure is given by,

$$I = \frac{K_8[O]^2[N_2(A^3\Sigma_u^+)]}{1 + \frac{K_{10}}{A}[N_2] + \frac{K_{11}}{A}[O_2] + \frac{K_{12}}{A}[O]} \quad \dots (13)$$

As the  $N_2$  second positive bands have allowed transitions (transition probability  $\sim 10^7 \text{ sec}^{-1}$ ) and the quenching terms in the denominator of (13) are  $< 1$  at a small flow rate of  $N_2$  ( $[O_2]$  and  $[O]$  are small). The intensity  $I$  will at first vary linearly with increase of  $N_2$  pressure ( $N_2(A^3\Sigma_u^+)$  is shown above to vary linearly with  $N_2$ ). When  $[N_2]$  is large so much so that  $\frac{K_{10}}{A}[N_2] > 1$ ,  $I$  will be independent of  $[N_2]$  (See the flat part of the curves of figures 2 and 3). However, equation (13) fails to explain decrease of intensity  $I$  in figures 2 and 3.

The quenching coefficients  $K_{10}$  and  $K_{11}$  of bands at  $3371\text{\AA}$  and  $3577\text{\AA}$  are given in table 2. Their values lie in the range  $10^{-8}$ – $10^{-9} \text{ cm}^3/\text{molecule-sec}$ . This agrees with the quenching coefficient ( $10^{-8} \text{ cm}^3 \text{ sec}^{-1}$ ) for CN bands by



Spectrum of the afterglow of  $N_2$  and  $O_2$  mixture showing  $N_2$  second positive bands in the range 3000Å-5000Å

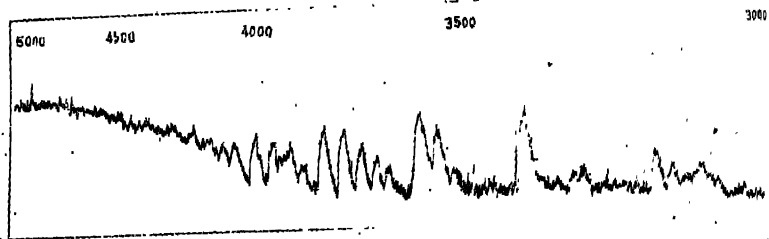


Figure 7. The microphotometer trace of the spectrum of the afterglow in  $N_2$  and  $O_2$  mixture in the range  $3000\text{\AA}$ - $5000\text{\AA}$

CH<sub>2</sub>Cl<sub>2</sub> molecules obtained by Ghosh *et al* (1963), and that of N<sub>2</sub>(A<sup>2</sup>Σ<sub>u</sub><sup>+</sup>) by N atoms (10<sup>-10</sup> cm<sup>3</sup> sec<sup>-1</sup>) obtained by Krassovsky and Shefov (1962) (the quenching by molecules are expected to be larger than by atoms).

Figure 4 shows a slight decrease in the intensities of 3371 Å and 3577 Å bands with the increase of temperature. The decrease may be due to the increase of quenching coefficient with temperature. It was also observed by Ghosh *et al* (1963).

From the investigations carried out in this paper the following conclusions may be drawn.

- (1) For the excitation of second positive bands in the N<sub>2</sub> afterglow, the presence of O is essential.
- (2) The quenching of second positive system by O<sub>2</sub> is much larger compared to that by N<sub>2</sub>.
- (3) Like N<sub>2</sub> first positive bands, these bands have a small negative temperature coefficient.

#### REFERENCES

- Barth C A & Kaplan J., 1957, *J. Chem. Phys.*, **26**, 506.  
 Carrington T., 1959, *J. Chem. Phys.*, **30**, 1087.  
 Chamberlain J. W., 1961, '*Physics of the Aurora and Airglow*,' Academic Press, New York  
 Coster D., Brons H. & Van der Zeil A., 1933, *Z.P.*, **84**, 304.  
 Ghosh S. N., Sharda and Sharma A., 1963, *Proc. Phys. Soc.*, **81**, 713  
 Ghosh S. N., Sahai Y. & Bhutani K. K., 1968, *Indian J. Pure App. Phys.* **6**, 146.  
 Ghosh S. N., Srivastava A. N. & Shukla R. V. 1969a, In course of publication.  
 Ghosh S. N., Srivastava A. N. & Shukla R. V. 1969b, In course of publication.  
 Krassovsky V. I. & Shefov N. N., 1962, *Planet. Space Sci.*, **9**, 883.  
 Krassovsky V. I., Shefov N. N. & Yavin V. I., 1962, *Planet. Space Sci.*, **9**, 83.  
 Mecke R. & Lindau P., 1924, *Phys. Zeit.*, **25**, 277.  
 Nicholls R. W., 1964, *Ann. de Geophys.*, **20**, 144.  
 Philpot J. L., Hughes R. H. & Fan C. Y., 1961, *Phys. Rev.*, **123**, 2084.  
 Prag A. B. & Clark K. C., 1963, *J. Chem. Phys.*, **39**, 799.  
 Schiff H. I., 1964, *Ann. de Geophys.*, **20**, 115.  
 Wilkinson P. G., 1963, *Astrophys. J.*, **138**, 778.  
 Young R. A. & Black G., 1966, *J. Chem. Phys.*, **44**, 3741.

## Effects of external circuit on heat transfer in MHD channel flow

By V. M. SOUNDALGEKAR, *Department of Mathematics,*

B. V. RAO, *Department of Electrical Engineering,*

*Indian Institute of Technology, Bombay (76),*

D. D. HALDAVNEKAR, *Univ. Dept. of Chemical Technology, Bombay-19*

R. S. IYER, *Engineer, Larsen and Toubro, Bombay*

(Received 20 December 1969, revised 19 June 1970)

An analysis of heat transfer in fully developed mhd channel flow has been presented. Closed form solutions in case of (i) two plates at constant temperatures, and (ii) linear variation of temperature along the plates, are derived for temperature, Nusselt number, mean-mixed temperature and the difference between the wall temperature and the mean fluid temperature. Numerical values of the Nusselt number and mean-mixed temperature are entered in tables, whereas, others are shown graphically. The effects of different parameters in different types of channel flows have been discussed.

### NOMENCLATURE

$A$	Temperature gradient	$S$	A non-dimensional number
$B_0$	Magnetic field (applied)	$S_1$	A non-dimensional number
$C_p$	Specific heat at constant pressure	$T$	Temperature
$G$	Temperature	$T_{im}$	Mean mixed temperature
$G^*$	Non-dimensional temperature	$u$	Velocity in $x$ -direction
$I$	Total current		Non-dimensional velocity
$I^*$	Non-dimensional total current		Average velocity
$J^*$	Non-dimensional current density	$V_g$	External generator voltage
$J_z$	Current density	$V_g^*$	Non-dimensional external generator voltage
$K$	Thermal conductivity	$x$	Co-ordinate along the plates
$Nu$	Nusselt number	$2y_0$	Separation between two plates
$M$	Hartmann number	$y$	co-ordinate normal to the $x$ -axis
$P$	Pressure	$z$	Normal to $xy$ -axes
$Pr$	Prandtl number	$\rho$	density
$q$	Heat flux at the plates	$\theta$	Non-dimensional temperature
$Q$	Non-dimensional heat flux	$\sigma$	Electrical conductivity
$R$	Resistance	$\eta$	Non-dimensional transverse axis
$Re$	Reynolds number	$\mu$	Viscosity
$R^*$	Non-dimensional resistance		



## 1. INTRODUCTION

Hartmann (1937) and Hartmann & Lazarus (1937) studied the mhd channel flow under a transverse magnetic field. From technological point of view, the heat transfer aspect of such flow is important. Sutton & Sherman (1965) studied this aspect under the action of the loading parameter, thus distinguishing the channel as an mhd generator, accelerator or flowmeter. The heat transfer has also been studied by Siegel (1958) in open circuit mhd channel flow between non-conducting plates, whereas, between conducting plates, it was discussed independently by Alpher (1961) and Yen (1963). Recently, Soundalgekar (1969) studied the heat transfer aspect of mhd channel flow between conducting walls and under crossed-fields. But to understand the working of the channel in the most general way, the external circuit must also be considered. Such an analysis was recently presented by Hughes & Young (1966) who considered the circuit consisting of a resistance and a generator, and thus characterised the mhd channel flow in different ways. The heat transfer aspect of such a system has not been considered as yet. This provides the motivation to undertake the present study.

In section 2, while presenting the mathematical analysis, two cases are considered :—(1) two plates at different temperatures and (2) linear variation of the temperature along the plates in the direction of the flow. Following Hughes & Young (1966) we have derived the closed form solutions for the velocity, current density and total current. Using these expressions, closed form solutions for temperature, Nusselt number and the mean mixed temperature are derived in case (1) whereas, in case (2) closed form solutions for the temperature, Nusselt number and the difference between wall temperature and mean temperature of the fluid are derived. Numerical values of Nusselt number in cases 1 and 2 and for the mean mixed temperature in case 1 are entered in tables 1 to 3, whereas, other physical quantities are shown on graphs.

In section 3, conclusions are set out.

## 2. MATHEMATICAL ANALYSIS

Here the  $x$ -axis is taken along the centre-line of the channel in the direction of the flow and  $y$ -axis is chosen normal to the  $x$ -axis. The magnetic field is assumed to be applied parallel to the  $y$ -axis. The external circuit is given in figure 1a.

Under these conditions, following Hughes & Young (1966), the expressions for the velocity and the current density for fully developed flow can be derived as follows :

$$u^* = \frac{\coth M}{M} \cdot \frac{1+R^*+M V_g^*}{R^*+M \coth M} \cdot \frac{1-\cosh M\eta}{\cosh M} \quad \dots (1)$$

$$J^* = \frac{(I^* - 1)M}{\sinh M} \cosh M\eta + 1, \quad \dots (2)$$

$$I^* = \frac{V_\theta^* - \left( \frac{1}{M} - \coth M \right)}{R^* + M \coth M}, \quad \dots (2a)$$

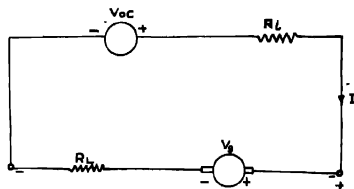


Figure 1a The complete electrical circuit.

where the physical quantities are defined in non-dimensional form as follows :

$$\left. \begin{aligned} u^* &= \frac{u}{(y_0^2/\mu) \left( -\frac{\partial p}{\partial x} \right)} ; \eta = \frac{y}{y_0} ; R^* = \frac{R}{(Z_0/2\sigma x_0 y_0)} ; \\ V_\theta^* &= \frac{V_\theta}{(2y_0^2 z_0 / \sqrt{\sigma \mu}) \left( -\frac{\partial p}{\partial x} \right)} ; M = y_0 B_0 \sqrt{\sigma / \mu} ; \\ I^* &= \frac{I}{\left[ 4x_0 y_0^2 \sqrt{\frac{\sigma}{\mu}} \left( -\frac{\partial p}{\partial x} \right) \right]} ; J^* = \frac{J_z}{(y_0 \sqrt{\sigma / \mu}) \left( -\frac{\partial p}{\partial x} \right)} \end{aligned} \right\} \quad \dots (3)$$

All the physical variables are defined in Nomenclature.

#### 4. THE ENERGY EQUATION

Here we consider two cases :

- (1) Two plates at different temperatures
- (2) Temperature varying linearly along the plates.

Case (1) :

The energy equation for the fully developed flow is now given by

$$K \frac{d^2 T}{dy^2} + \mu \left( \frac{du}{dy} \right)^2 + \frac{J_z^2}{\sigma} = 0 \quad \dots (4)$$

The boundary conditions are

$$T(y_0) = T_1 \quad \text{and} \quad T(-y_0) = T_2 \quad \dots (5)$$

In view of (3), equations (4) and (5) become

$$\frac{d^2\theta}{d\eta^2} + \left( \frac{du^*}{d\eta} \right)^2 + J^{*2} = 0 \quad \dots (6)$$

and

$$\theta(1) = \theta_1, \quad \theta(-1) = \theta_2 \quad \dots (7)$$

where

$$\theta = \frac{K \mu T}{\left[ y_0^2 \left( -\frac{\partial p}{\partial x} \right) \right]^2} \quad \dots (8)$$

Substituting for  $u^*$  and  $J^*$  from (1) and (2) respectively, in (6), simplifying and integrating, the solution, satisfying (7), is given by

$$\begin{aligned} \theta = & \frac{\theta_1 + \theta_2}{2} + A_3(\eta^2 - 1) + A_4(\cosh 2M - \cosh 2M\eta) \\ & + A_5(\cosh M - \cosh M\eta) + \frac{\theta_1 - \theta_2}{2}\eta \end{aligned} \quad \dots (9)$$

where

$$\begin{aligned} A_1 &= \frac{(I^* - 1)M}{\sinh M}, & A_2 &= \frac{1 + R^* + M V_g^*}{R^* \sinh M + M \cosh M}, \\ A_3 &= \frac{A_2^2 - A_1^2 - 2}{4}, & A_4 &= \frac{A_1^2 + A_2^2}{4M^2}, & A_5 &= \frac{2A_1}{M^2} \end{aligned}$$

The temperature profiles are shown in figures 1 to 4 for different values of the parameters  $M$ ,  $R^*$ ,  $V_g^*$  and  $T_1 = \left( \frac{\theta_1 - \theta_2}{2} \right)$ . Hughes & Young (1966)

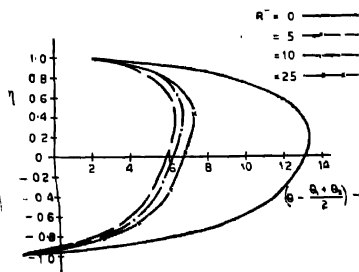


Figure 1. Temperature profiles ;  
 $M=2$ ,  $T_1=4$ ,  $V_g^*=2$ .

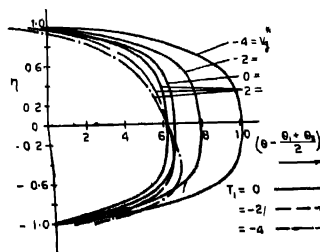


Figure 2. Temperature profiles ;  
 $M=2$ ,  $R^*=10$

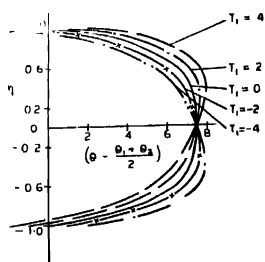


Figure 3. Temperature profiles ; (open circuit case)  $M=2$ .

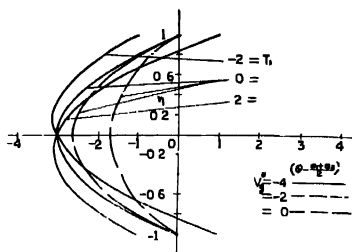


Figure 4. Temperature profiles ;  $M=2, R^*=M/\tanh M$ .

have described in short the interesting case of maximum power transfer between the external circuit and the flow device. The condition for this case as derived by them is that  $R^* = \frac{M}{\tanh M}$ .

The rate of heat transfer expressed in terms of the Nusselt number is given by (Hughes & Young 1966)

$$Nu = \frac{1}{\theta_1 - \theta_2} \left( \frac{d\theta}{d\eta} \right)_{\eta=-1} \quad (10)$$

From (9) and (10) we get,

$$Nu = \frac{M}{\theta_1 - \theta_2} \left[ 2A_4 \sinh 2M + \frac{2(I^* - 1)}{M} \right] - \frac{2A_3}{\theta_1 - \theta_2} + \frac{1}{2} \quad \dots (11)$$

The numerical values of  $Nu$  are entered in table 1. The bulk mean temperature is defined as

$$T_{im} = \frac{\int_{-1}^1 u^* \theta d\eta}{\int_{-1}^1 u^* d\eta} \quad \dots (12)$$

Substituting for  $u^*$  and  $\theta$  from (3) and (9) respectively and simplifying, we obtain

$$T_{im} = \frac{\theta_1 + \theta_2}{2} = \frac{4A_3 \left( \frac{3-M^2}{3M^2} \cosh M - \frac{\sinh M}{M^3} \right) + \frac{2(I^*-1)}{M \sinh M} \left[ 2 \cosh^2 M - \frac{3 \sinh 2M}{2M} + 1 \right] + A_4 \left( 2 \cosh 2M \cosh M + \frac{\sinh 2M \cosh M - 8 \cosh 2M \sinh M}{3M} \right)}{\frac{2(1+R^*+MV_g^*)(M \cosh M - \sinh M)}{M^2(R^* \sinh M + M \cosh M)}} \quad \dots (13)$$

Table 1. Values of Nusselt number (equation 11)

$M$	$R^*$	$\frac{T_1}{V_g}$	-4	-2	2	4
2	5	-4	-15.4304	-31.3609	32.3609	16.4304
		-2	-9.6416	-19.7832	20.7832	10.6416
		0	-6.5056	-13.5112	14.5112	7.5056
		2	-6.0225	-12.5449	13.5449	7.0225
	10	4	-8.1922	-16.8843	17.8843	9.1922
		-4	-11.1074	-22.7149	23.7149	12.1074
		-2	-8.6804	-17.8607	18.8607	9.6804
		0	-7.1640	-14.8280	15.8280	8.1640
		2	-6.5583	-13.6166	14.6166	7.5583
		4	-6.8633	-14.2266	15.2266	7.8633
	4	-4	-483	-966	967	484
		-2	-323	-647	648	324
		0	-214	-430	431	215
		2	-156	-313	314	157
4	5	4	-148	-297	298	149
		-4	9.3963	18.2925	-17.2925	-8.3963
		-2	8.1488	15.7976	-14.7976	-7.1488
		0	6.6514	12.8029	-11.8029	-5.6515
	$R^* = \frac{M}{\tanh M}$	2	5.9043	9.3086	-8.3086	-3.9043
		4	2.9073	5.3147	-4.3147	-1.9073
		-4	-8.1517	-16.8033	17.8033	9.1517
		-2				
	2	$R^* \rightarrow \infty$ (open circuit case)				
4			-263	-528	284	264

The numerical value of  $T_{im} - \frac{\theta_1 + \theta_2}{2}$  are entered in table 2 for all cases.

Table 2. Values of  $T_{im} - \frac{\theta_1 + \theta_2}{2}$  (equation 13),

$M$	$R^*/V_g^*$	-4	-2	0	2	4
2	5	44	33	25	20	17
	10	36	31	26	23	20
4	5	343	250	183	141	124
	10	284	233	193	163	143
2	$M/\tanh M$	27.67	19.72	12.25	5.2716	-1.2324
4	$M/\tanh M$	75	61	47	34	21
	open circuit case	$M$			$T_{im} - \frac{\theta_1 + \theta_2}{2}$	
		2			25	
		4			189	

Case 2 :

The temperature is now assumed to be varying linearly along the walls of the channel. This situation is then governed by the following energy equation

$$\rho C_p u \frac{\partial T}{\partial x} = K \frac{\partial^2 T}{\partial y^2} + \mu \left( \frac{\partial u}{\partial y} \right)^2 + \frac{J^2}{\sigma} \quad \dots (14)$$

The linear variation of temperature along the walls is represented by

$$T = Ax + G(y) \quad \dots (15)$$

Hence equation (14) in view of (15) and (3) reduces to the following non-dimensional form :

$$\frac{d^2 G^*}{d\eta^2} + M^2 \left\{ \left( \frac{du^*}{d\eta} \right)^2 + J^{*2} \right\} - u^* S = 0 \quad \dots (16)$$

where

$$G^* = \frac{K \mu G}{\left[ y_0^2 \left( -\frac{\partial p}{\partial x} \right) \right]^2}, \quad Pr = \frac{\mu C_p}{K}$$

$$Re = \frac{\rho y_0}{\mu} \left[ \frac{y_0^2}{\mu} \left( -\frac{\partial p}{\partial x} \right) \right], \quad S_1 = \left[ \frac{K \mu y_0 A}{y_0^2 \left( -\frac{\partial p}{\partial x} \right)} \right]^2, \quad \dots (16a)$$

$$S = Pr Re S_1.$$

If the fluid and the walls are assumed to be at the same temperature, then the boundary conditions are

$$G^* = 0 \quad \text{at} \quad \eta = \pm 1 \quad \dots (17)$$

Hence the solution of (16), subject to the condition (17) is

$$\begin{aligned} G^* = & \left\{ \frac{A_2 S}{M} \cosh M - M^2 + \frac{M^2}{2} (A_2^2 - A_1^2) \right\} \left( \frac{\eta^2 - 1}{2} \right) \\ & - \left( \frac{A_2 S}{M^3} + 2A_2 \right) (\cosh M\eta - \cosh M) \\ & - \frac{1}{8} (A_2^2 + A_1^2) (\cosh 2M\eta - \cosh 2M) \end{aligned} \quad \dots (18)$$

The temperature profiles for  $G^*$  for different values of  $R^*$ ,  $M$ ,  $S$ ,  $V_\theta^*$  are shown in figures 5 to 8.

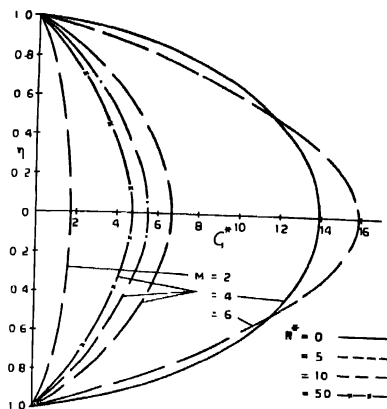


Figure 5. Temperature profiles,  
 $S = 0.2$ ,  $V_\theta^* = 4$

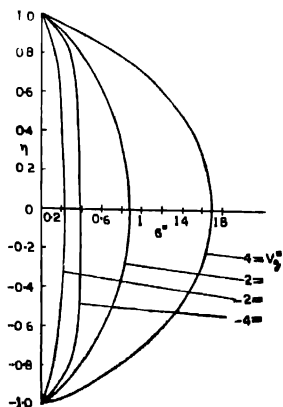


Figure 6. Temperature profiles,  
 $M = 2$ ,  $R^* = 5$ ,  $S = 0.2$

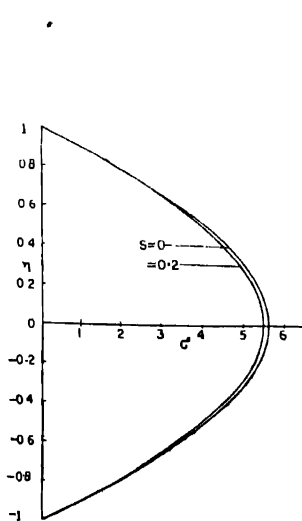


Figure 7. Temperature profiles,  
 $M = 4$ ,  $R^* = 10$ ,  $V_\theta^* = 4$

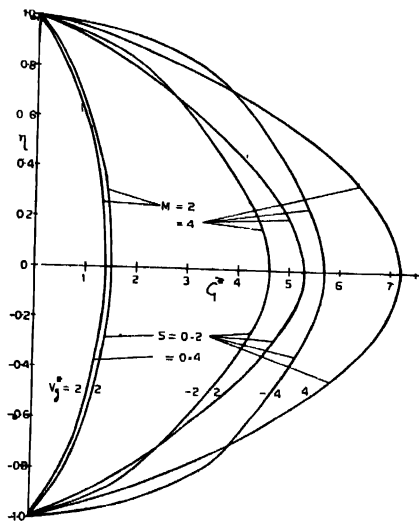


Figure 8. Temperature profiles,  
 $R^* = M \tanh/M$

The rate of heat transfer expressed in terms of the Nusselt number is defined as

$$Nu = \frac{y_0}{G_{y=0}} \left( \frac{dG}{dy} \right)_{y=y_0} = \frac{1}{G_{\eta=0}^*} \left( \frac{dG^*}{d\eta} \right)_{\eta=1} \quad \dots (19)$$

Hence from (18) and (19) we obtain,

$$Nu = \frac{\left[ \left( \frac{A_2 S}{M^2} + 2A_1 M \right) \sinh M + \frac{1}{4}(A_1^2 + A_2^2) M \sinh 2M \right.}{\left[ \left( \frac{A_2 S}{M^2} + 2A_1 \right) (\cosh M - 1) + \frac{1}{8}(A_1^2 + A_2^2) (\cosh 2M - 1) \right.} \quad \dots (20)$$

$$\left. - \left\{ \frac{A_2 S \cosh M}{M} + \frac{M^2}{2} (A_2^2 - A_1^2 - 2) \right\} \right] \left. - \frac{1}{2} \left\{ \frac{A_2 S \cosh M}{M} + \frac{M^2}{2} (A_2^2 - A_1^2 - 2) \right\} \right]$$

The numerical values of  $Nu$  under different conditions are entered in table 3

Knowing  $u^*$  and  $J^*$  from (1) and (2) respectively, the mean temperature gradient  $A$  is found by considering the overall heat balance for a differential length of the channel as

$$A = \frac{\partial T}{\partial x} = \frac{\partial T_m}{\partial x} = \frac{q + \int_0^{y_0} \left[ \mu \left( \frac{\partial u}{\partial y} \right)^2 + \frac{J^2}{\sigma} \right] dy}{y_0 v_a \rho C_p} \quad \dots (21)$$

where  $v_a$  is the average velocity and  $q$  is the heat flux at the plates. Hence by virtue of (3) and (16a), (21) reduces to the following non-dimensional form

$$S = Q + \int_0^1 \left[ \frac{du}{d\eta} + J^{*2} \right] d\eta \quad \dots (22)$$

where

$$Q = \frac{q}{\left[ \frac{y_0^3 \left( -\frac{\partial p}{\partial x} \right)^2}{\mu} \right]}$$

Substituting for  $u^*$  and  $J^*$  from (1) and (3) respectively, in (22) we obtain after simplification

$$S = Q + \frac{A_2^2 + A_1^2}{4M} \sinh M + \frac{A_1^2 - A_2^2}{2} - \frac{2A_1}{M} \sinh M + 1 \quad \dots (23)$$



From the practical point of view, it is important to know the variation of the difference between wall temperature and the mean temperature which is given by

$$\begin{aligned} T_w - T_m &= Ax - \frac{1}{2y_0 v_a} \int_{-y_0}^{y_0} T(x, y) u(y) dy \\ &= -\frac{1}{2y_0 v_a} \int_{-y_0}^{y_0} G(y) u(y) dy \end{aligned} \quad \dots (24)$$

By virtue of (3) and (16a), (24) reduces to the following

$$(T_w - T_m)^* = -\frac{1}{2} \int_{-1}^1 G^* u^* d\eta \quad \dots (25)$$

where

$$(T_w - T_m)^* = \frac{v_a}{\left[ \frac{y_0^2}{\mu} \left( -\frac{\partial p}{\partial x} \right) \right]} \cdot \frac{K\mu(T_w - T_m)}{\left[ y_0^2 \left( -\frac{\partial p}{\partial x} \right) \right]^2}$$

Substituting for  $G^*$  and  $u^*$  from (18) and (1), respectively, in (25), carrying out the integration, we obtain

$$\begin{aligned} (T_w - T_m)^* &= \frac{1 + R^* + M V_g^*}{M \sinh M(R + M \coth M)} \left[ 2 \left( B_1 \frac{M^2 + 6}{2M^2} + D_2 \right) \cosh M \right. \\ &\quad - \frac{2}{M} \left( B_1 \frac{M^2 + 2}{M^2} + D_2 \right) \sinh M + B_2 \frac{2M - \sinh 2M}{2M} \\ &\quad \left. - \frac{B_3}{3M} (\cosh M \sinh 2M + 2 \sinh M \cosh 2M) \right] \end{aligned} \quad \dots (26)$$

where

$$B_1 = \frac{1}{2} \left\{ \frac{A_2 S \cosh M}{M} + \frac{M^2}{2} (A_2^2 - A_1^2 - 2) \right\},$$

$$B_2 = \frac{A_2 S}{M^3} + 2A_1, \quad B_3 = \frac{A_1^3 + A_2^3}{8},$$

$$D_2 = \left( \frac{A_2 S}{M^3} + 2A_1 \right) \cosh M + \frac{1}{8} (A_2^2 + A_1^2) \cosh 2M$$

$$- \frac{1}{2} \left\{ \frac{A_2 S \cosh M}{M} - M^2 + \frac{M^2}{2} (A_2^2 - A_1^2) \right\}$$

$(T_w - T_m)^*$  is calculated from (26) in two different ways. The effects of  $M$ ,  $R^*$ ,  $V_g^*$  and  $S$  have been considered and they have been shown in figure 9-11 and

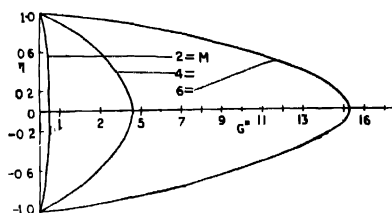


Figure 9. Temperature profiles, (open circuit case)

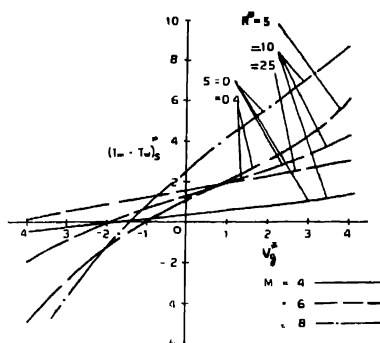


Figure 10.  $(T_m - T_w)_S^*$  vs  $V_g^*$ ;  $M = 4, 6, 8$ .

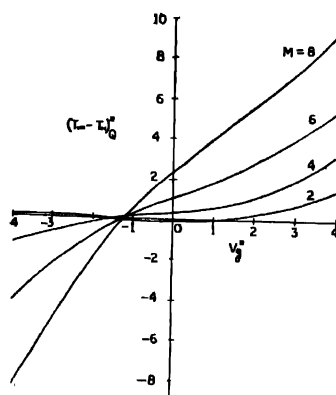


Figure 11.  $(T_m - T_w)_S^*$  vs  $V_g^*$ ;  $R^* = M / \tanh M$ .

it is denoted by  $(T_m - T_w)^* S$ . In figures 12-15 the effects of  $M$ ,  $R^*$ ,  $V_g^*$  and  $Q$  on  $(T_w - T_m)^*$  have been shown and it is denoted now by  $(T_m - T_w)^* Q$ . In this case the expression (23) for  $S$  is substituted in (25) and calculations are carried out for different values of  $Q$ .

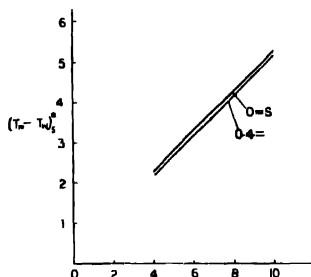


Figure 12. (open-circuit case)  
 $(T_m - T_w)_s^* \text{ vs } M$ ,

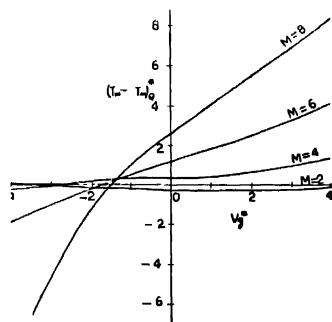


Figure 13.  $(T_m - T_w)_Q^* \text{ vs } V_g^*$ ;  
 $R^* = 10$ ,  $Q = 2$

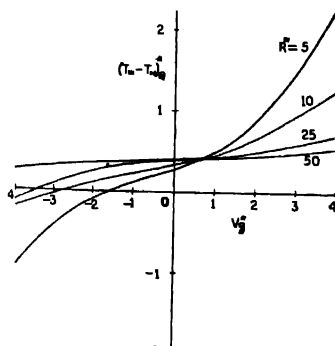


Figure 14.  $(T_m - T_w)_Q^* \text{ vs } V_g^*$ ;  
 $M = 4$ ,  $Q = 4$

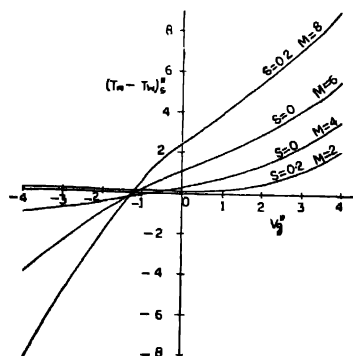


Figure 15.  $(T_m - T_w)_Q^* \text{ vs } V_g^*$ ;  
 $Q = 2$ ,  $R^* = M/\tanh M$ .

### 3. CONCLUSIONS

Now the mhd channel flow described here is characterised as follows :

1. For  $V_g^* = 0$  and  $\partial p/\partial x$  negative, the fluid is flowing in the  $x$ -direction and hence the electric power is flowing into the external circuit provided  $R^* \neq 0$  or  $R^* \neq \infty$ . Such a device is known as a mhd generator.

2 For  $\partial p/\partial x$  negative, the fluid is pumped in the  $x$ -direction if  $V_g^* > 0$  and hence the device is called an mhd accelerator. If  $V_g^* < 0$ , then the electromagnetic body force, due to  $V_g^*$ , opposes the flow in the positive  $x$ -direction and the flow in such a case is called a decelerated flow. In case of an mhd accelerator,  $R^*$  may be interpreted as the internal resistance of the power source.

3.  $R^* \rightarrow \infty$  corresponds to an open circuit channel flow, whereas, for  $R^* = 0$  and  $V_g^* = 0$  corresponds to a short circuit case.

4. In case of an mhd generator, there is an interesting case of the maximum transfer of electrical power. The condition for this case, as derived by Hughes and Young (1966), is that  $R^* = M/\tanh M$ .

With these physical interpretations of the different parameters, in the problem, we have following conclusions in the two cases :

Case (1) :

In this case, the numerical values of the difference between the fluid temperature and the mean of the two wall temperatures is plotted under different conditions. Also in this case,  $T_1$  is half the difference between the two wall temperatures and is positive when the temperature of the upper wall is greater than that of the lower wall and is negative the other way. In figure 1, the effects of the internal resistance in the case of an mhd accelerator on  $\left(\theta - \frac{\theta_1 + \theta_2}{2}\right)$  is shown. It is interesting to note here that  $\left(\theta - \frac{\theta_1 + \theta_2}{2}\right)$  is maximum when  $R^* = 0$ , i.e., when the internal resistance of the power source is zero. But for  $R^* > 0$ , an increase in  $R^*$  leads to an increase in the value of  $\left(\theta - \frac{\theta_1 + \theta_2}{2}\right)$ . In figure 2, the effects of  $V_g^*$  and  $T_1$  on  $\left(\theta - \frac{\theta_1 + \theta_2}{2}\right)$  are shown. We conclude here that for constant  $T_1$ , the temperature is less in case of accelerated flow than that in decelerated flow. Moreover, as  $V_g^*$  decreases,  $\left(\theta - \frac{\theta_1 + \theta_2}{2}\right)$  increases. Regarding the effects of  $T_1$ , the temperature profiles are symmetrical when both the walls are at equal temperatures. But for  $T_1$  negative, i.e., when the temperature of the lower wall is greater than that of the upper wall, the symmetry is distorted and the temperature profiles are deflected towards the wall of higher temperature, which is so because the temperature of the fluid near the wall of higher temperature increases. Figure 4 gives the interesting result which is completely different from the earlier cases. It shows the behaviour of the fluid temperature when there is a maximum transfer of electrical power. In an mhd generator, or accelerator the value of  $\left(\theta - \frac{\theta_1 + \theta_2}{2}\right)$  is found to be negative for all

$T_1$ , from which we can conclude that the temperature of the fluid, at this stage, is less than the mean temperature of the walls.

Case 2 :

In figure 5, the effects of  $M$  and  $R^*$  on the temperature profiles are shown. We observe that an increase in  $M$  leads to an increase in the  $G^*$ , when  $S$ ,  $R^*$  and  $V_g^*$  are constant. However, in this case, an increase in  $R^*$ , the internal resistance of the power source, leads to a decrease in  $G^*$  when  $M$ ,  $S$  and  $V_g^*$  are constant. From figure 6, we observe that temperature in case of an accelerated flow is greater than that in case of decelerated flow. From figure 7, we conclude that an increase in  $S$  leads to a decrease in  $G^*$  when  $M$ ,  $R^*$  and  $V_g^*$  are constant. Figure 8 shows the temperature profiles when  $R^* = M/\tanh M$ . The effects of  $M$ ,  $S$  and  $V_g^*$  are the same as before. In open-circuit case, an increase in  $M$  leads to an increase in  $G^*$ .

Figures 10 to 16 are particularly important from practical point of view for they show the variation of the difference between the mean temperature

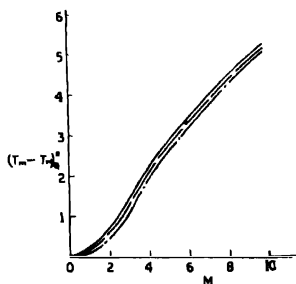


Figure 16.  $(T_m - T_w)_Q^*$  vs  $M$  ; (open circuit case)

and the wall temperatures under different conditions. From figure 10, we conclude that  $(T_m - T_w)_S^*$  increases with increasing  $V_g^*$  in case of an accelerated flow, whereas, it decreases with increasing  $V_g^*$  in case of a decelerated flow. An increase in  $M$  leads to an increase in  $(T_m - T_w)_S^*$  when  $R^*$  and  $S$  are constant. But an increase in  $R^*$  leads to a decrease in  $(T_m - T_w)_S^*$ . An increase in  $S$  leads to a decrease in  $(T_m - T_w)_S^*$ . In figure 11, the values of  $(T_m - T_w)_S^*$ , in case of  $R^* = M/\tanh M$  are plotted against  $V_g^*$ .  $(T_m - T_w)_S^*$  behaves in the same manner as described above for figure 10. In open-circuit case also, the effects of  $M$  and  $S$  on  $(T_m - T_w)_S^*$  are the same as those shown in figure 10.

In figures 13 to 16, the values of  $(T_m - T_w)_Q^*$  are plotted. We observe here also that the effects of  $M$ ,  $R^*$ ,  $V_g^*$  are the same as described above in case of figures 10 to 12.

## Case (1) :

1. From table 1 we conclude that (a) an increase in  $T_1$  leads to a decrease in the value of the Nusselt number. But the rate of heat transfer is less when the temperature of the lower wall is greater than that of the upper wall; (b)  $Nu$  increases with increasing  $V_0^*$  or  $M$ ; (c) in case of an mhd generator,  $R^*$  is the external resistance, whereas,  $R^*$  is the internal resistance of the power source in case of an mhd accelerator. Hence an increase in  $R^*$  leads to an increase in  $Nu$  when  $M$ ,  $T_1$  are constant.

2. From equation 13 and table 2 we conclude that the mean mixed temperature is not affected by the temperature difference of the plates. In case of an mhd generator the mean mixed temperature increases with increasing  $R^*$ . In accelerated flow, the mean mixed temperature increases with increasing  $R^*$ , the resistance of the internal power source, whereas, in decelerated flow, it decreases with increasing  $R^*$ . An increase in  $M$  always leads to an increase in the mean mixed temperature.

## Case (2) (table 3) :

An increase in  $S$ , leads to an increase in the Nusselt number in case of an mhd generator and accelerator, whereas, in an mhd decelerating flow, an increase

Table 3. Values of Nusselt number (equation 20).

$M$	$R^*$	$S/V_0^*$	-4	-2	0	2	4
2	5	0	7.3315	5.6797	3.0841	2.7895	2.9659
		0.2	7.1920	5.8447	3.1859	2.8499	3.0169
		0.4	7.0592	6.0236	3.3031	2.9172	3.0721
	10	0	6.5502	4.6354	3.3809	2.9819	2.9422
		0.2	6.7158	4.8522	3.5133	3.0683	3.0106
		0.4	6.8931	5.1028	3.6673	3.1665	3.0866
	4	0	6.4262	4.7272	3.2647	2.7116	2.9652
		0.2	6.4048	4.7239	3.2697	2.7182	2.9753
		0.4	6.3856	4.7207	3.2749	2.7249	2.9856
4	10	0	5.4307	4.3581	3.4971	3.0131	2.9141
		0.2	5.4246	4.3609	3.5039	3.0211	2.9233
		0.4	5.4184	4.3637	3.5109	3.0293	2.9327
	$M/\tanh M$	0	6.2905	7.0330	2.6099	2.7540	3.1384
		0.2	6.1291	6.8926	2.6881	2.7968	3.1765
		0.4	5.9733	6.7593	2.7335	2.8429	3.2167
	4	0	6.7425	4.8721	3.1862	2.6420	3.0473
		0.2	6.7159	4.8665	3.1907	2.6484	3.0581
		0.4	6.6896	4.8608	3.1953	2.6547	3.0691
Open circuit case							
2		0	3.8053				
		0.2	3.9838				
		0.4	4.1922				
4		0	3.9373				
		0.2	3.9480				
		0.4	3.9588				

in  $S$  leads to a decrease in  $Nu$  when  $R^*$  is small and  $V_g^*$  is large, but for large  $R^*$ ,  $Nu$  increases with increasing  $S$ .  $Nu$  also increases with increasing  $S$  in open-circuit case.

#### ACKNOWLEDGMENTS

We are grateful to the referee whose comments lead to improvement of our paper.

#### REFERENCES

- Alpher R. A. 1961 *Int. J. Heat Mass Transfer*, **3**, 108.  
Hartmann J. 1937 *Hg-Dynamics I, Danske Math-Phys. Medd.*, **15**, No. 6.  
Hartmann H. & Lozarus F. 1937 *Hg-Dynamics II, Danske Math-Phys. Medd.*, **15** No. 7.  
Hughes W. F. & Young F. J. 1966 *The Electromagnetodynamics of Fluids*, J. Wiley and Sons Inc.  
Seigel, R. 1958 *J. Appl. Mech.*, **25**, 415.  
Soundalgekar V. M. 1969 *Proc. Nat. Inst. Sci. India* **35A**, 329.  
Sutton G. W. & Sherman A. 1965 *Engineering Magnetohydrodynamics* (Mc-Graw Hill Co.).  
Yen J. T. 1963 *Tr. ASME, J. Heat Transfer*, **85C**, No. 5, 371.

## Modular spark chamber

SAMIR GHOSH\*, J. P. MUNDRA AND D. MAJUMDAR

*Physical Laboratory, Presidency College, Calcutta*

(Received 9 February 1970)

(Plates—7)

In this paper the construction and operation of three different types of spark chambers are described. In particular, the operations of the modular spark chamber with argon and neon fillings at various pressures lower than one atmosphere are analysed.

### INTRODUCTION

During the last few years spark chambers have been developed with subsequent sophistications as a detector of charged particles. Spark chambers have the unique property of simplicity of operation coupled with the visual manifestation of the path of the charged particles. In this laboratory, so long the charged particles were studied with the help of Wilson's cloud chamber and neon tube hodoscope. Now a modular spark chamber has been developed, experimenting from the primary stage. This spark chamber has the special feature of simplicity of construction and of operation.

### SPARK CHAMBERS

Before this modular spark chamber was developed, two other spark chambers were made in our laboratory with different variable spark gaps and thicknesses of the electrodes. The spark chambers can be constructed without the help of any sophisticated mechanical workshop.

The electrodes of the first spark chamber were made of aluminium sheets of thickness 0.3 mm and individual electrodes were kept apart from one another with the help of perspex spacers. The spark gaps of this 4-gap spark chamber were 5.0 mm and the sensitive area was 117 sq cm. Each pair of two electrodes of same potential were placed facing each other and were kept insulated from each other to facilitate the application of different potentials at different spark gaps and also for connecting different condenser banks to different spark gaps.

The primary difficulty in constructing a spark chamber arises from extraneous sparking at the edges of the electrodes at relatively lower voltages because of sharpness and consequent production of high electric fields at the edges of the electrodes. This difficulty was circumvented by turning the edges of the electrodes in the form of spirals; the spirals being away from the electrodes with opposite potentials (figure 1, plates 7).

---

\* Present address : Department of Radiotherapy, Medical College Hospitals, Cal.-12.



Out of the four sharp edges of the aluminium electrodes the extraneous sparking at two edges, parallel to the axis of the camera, were avoided by this method and the extraneous sparking at voltages, relatively lower than the operating voltage, at two other edges, perpendicular to the axis of the camera, were avoided by placing the electrodes of opposite potentials in criss-cross manner and thereby increasing the distances between the edges. The electrodes were of rectangular shape and the broad-sides of the earthed electrodes were placed facing the long-sides of the high-potential electrodes. In figure 1 (plates 7) this arrangement has been shown. The reflection from the glazing aluminium surfaces was avoided by painting the surfaces with a conducting black paint, taking care that no sharp point is formed thereby. The schematic diagram in figure 2 shows the dimensions of the spark chamber.

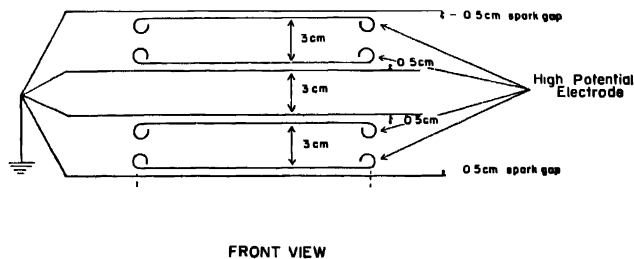


FIGURE 2. The Schematic diagram of Spark Chamber—Model 1.

The whole assembly of this 4-gap spark chamber was placed within an air-tight perspex box, the electrical feedthrough being sealed at the sides of the box. Two nozzles were fitted at two opposite corners of the box for the inlet and outlet of gases. The photography was done from outside this transparent box.

The spark chamber was run first with air inside it and next the air was completely flushed out with argon through the inlet, keeping the outlet open during replacement, and the spark chamber was closed, with argon at atmospheric pressure.

The variations of the threshold voltage (*i.e.*, where the spark appears only in case of passage of heavily ionizing particles) and the breakdown voltage (*i.e.* where the sparking takes place even without the passage of ionizing particles through the sensitive area of the chamber) due to the nature of the gas within the chamber have been studied and the results are given in table 1. The working voltage lies in between threshold and working voltages.

To study the effect of clearing field, potentials of the order of 45 volts and 90 volts were applied in between each pair of opposite electrodes and in opposition to the high-voltage pulses from a 5C22 hydrogen thyratron. The results of these experiments are also incorporated in table 1.

Table 1  
(Spark gap = 5.0 mm)

Gas in chamber	Clearing field, volts	Threshold voltage, kV	Breakdown voltage, kV
Air	0	8.9	9.3
	45	9.1	9.6
	90	9.1	9.6
Argon	0	8.2	8.7
	45	8.2	8.9
	90	8.2	8.9

Table 1 shows that the doubling of the clearing field from 45 V to 90 V has no effect either on the threshold or on the breakdown voltages.

To facilitate the variations of spark gaps and for shortening the space lost due to the spiral formations of the electrodes at the edges, the second spark chamber (Model 2) was constructed with a different design. The electrodes, as before, were made of aluminum and were of thickness 0.55 mm. The sensitive area of the chamber was 175.5 sq cm. The perspex spacers were replaced with glass spacers in the form of tubes and rods. By punching holes at the four corners of the electrodes, these were slid down the glass rods fixed at four corners of the base plate and the spacings in between the electrodes were maintained by sliding glass tubes down the glass rods. The spark gaps could easily be varied by changing the lengths of these glass tubes. The spiral form at the edges of the electrodes was changed to an U-shaped bend with the ends bent inwards (figure 3—plate 7).

In this case also the whole assembly was placed within an air-tight perspex box and experiments performed by filling the chamber with air and argon. The results of these experiments are given in table 2. The effects of varying the clearing field are also shown in this table. These results are for the corresponding spark gap of 3.0 mm.

The gaps in between the electrodes of same potential can be properly utilized for placing in required absorbers for different experiments.

Table 2  
(Spark gap = 3.0 mm)

Gas in chamber	Clearing field, volts	Threshold voltage, kV	Breakdown voltage, kV
argon	0	5.7	6.4
	45	6.1	6.4
	0	5.0	5.9
	45	5.3	6.1

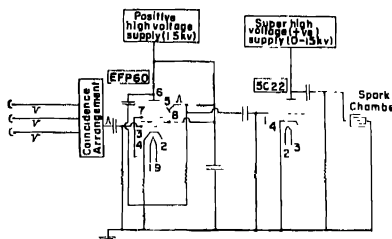


FIGURE 4 Schematic Diagram of the circuit.

Both the above two spark chambers were triggered by charged particles collimated by three GM-counters. The schematic diagram in figure 4 shows the circuit used for the operation of these spark chambers. The coincidence pulses from three GM-counters were fed into the grid of an EFP60 tube giving rise to a 400 V positive pulse at the cathode of the EFP60 and these high-voltage pulses were fed in their turn into the grid of the 5C22 hydrogen thyratron operating at potentials upto 15 kV. The super-high voltage pulses from the hydrogen thyratron were communicated to the high potential electrodes of the spark chambers.

#### MODULAR SPARK CHAMBER

In the next phase of development we have made a 4-gap modular spark chamber of spark gaps 12.4 mm. To avoid the non-uniformity of spark gaps due to the sagging in case of very thin electrodes, we have used aluminium plates of thickness 1.4 mm for intermediate electrodes and the two end electrodes were made out of thicker aluminium plates of thickness 3.4 mm. The end electrodes were made out of thicker plates since these are to withstand the atmospheric pressure when the chamber is evacuated with a vacuum pump to fill it up with argon or neon. The aluminium plates were glued to either sides of perspex frames, made by grooving out the central region from perspex sheets of thickness 12.4 mm. The edges of the electrodes were kept protruding outside in air (figure 5—plate 7).

When the spark chamber is filled with argon or neon the extremities of the electrodes remain in air and since in case of argon or neon the working voltages are much lower than the corresponding working voltages for air for a particular spark gap, there is no possibility of edge effects.

The individual compartments of the 4-gap spark hamber were inter-connected by making small holes in the intermediate electrodes. Since making of holes can give rise to effect, similar to edge effect, because of sharpness around the edges of the holes, the holes were made funnel shaped (figure 6). A glass nozzle was sealed through the side of the last compartment to draw out the air and to fill it up subsequently with argon or neon.



FIGURE 6. Interconnection between chamber gaps.

The same triggering arrangement and operating circuits which have been used in case of operation of the first two spark chambers have also been utilized for the operation of this modular spark chamber. The tracks of charged particles ( $\mu$ -mesons) recorded by this chamber are sufficiently sharp for analysis. Since, as triggering particle collimated cosmic-ray beam has been used, the resolution of the chamber has not been needed to be improved with the help of clearing field.

#### PRESSURE—VOLTAGE RELATION

The dependence of optimum working voltage on pressure of argon within the spark chamber has been studied and the results are shown by the corresponding curve in figure 7.

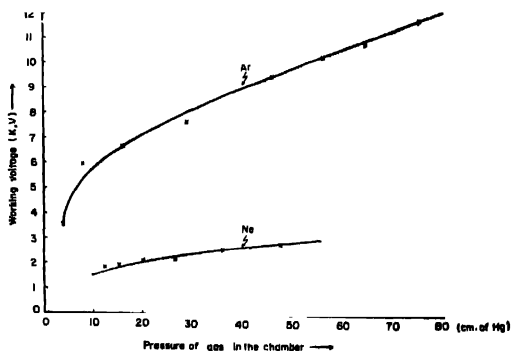


FIGURE 7. Working voltage dependence on Pressure of gas in the chamber.

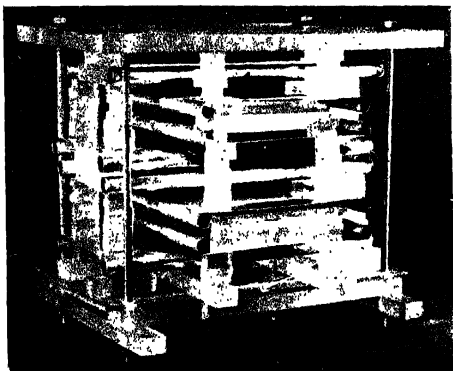


Figure 1. Spark chamber—Model 1.



Figure 3. Spark chamber—Model 2

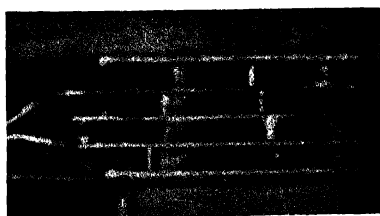


Figure 5. Modular spark chamber



It is observed that in the range of 10 cm to 75 cm of Hg pressure the curve follows the following quadratic equation :—

$$Y = 3.76 + 1.59 \times 10^{-1} X - 7.7 \times 10^{-4} X^2 \quad \dots (1)$$

At lower pressure, about 4 cm of Hg the sparking phenomenon changed into the low pressure discharge phenomenon. It shows that the minimum pressure for the working of the argon-filled spark chamber lies in between 4 and 10 cm of Hg pressure. The construction of this particular modular spark chamber did not permit us to study the dependence of working voltage on pressures of argon higher than the atmospheric pressure. But there is no ground to expect the curve in figure 7 to deviate from its nature at pressures above one atmosphere.

The modular spark chamber was next filled up with pure neon and the dependence of optimum working voltage on pressure was studied and the results were plotted in the corresponding curve in figure 7 for neon. The curve for neon follows the following quadratic equation :—

$$Y = 1.542 + 3.006 \times 10^{-2} X - 7.845 \times 10^{-5} X^2 \quad \dots (2)$$

The curve for neon lies much below the corresponding curve for argon, showing that the working voltage required for neon-filled chambers are much lower than argon-filled chambers.

#### ACKNOWLEDGEMENT

The authors are grateful for the financial support given by the Government of West Bengal, India for this work. They offer sincere thanks to Prof. R. L. Sen Gupta and Prof. P. K. Sen Chaudhury for their interest and encouragement.

#### REFERENCES

Rey C, & Parker S. 1963, *Nuclear Instruments & Methods*, **20**, 173.

## Unsteady hydromagnetic free convection past a vertical flat plate

By IOAN POP

*University of Cluj, Cluj, CP 109, Roumania*

(Received, 17 February 1970)

An investigation of the unsteady boundary layer equations for an electrically conducting fluid past a semi-infinite vertical flat plate in the presence of a uniform transverse magnetic field has been carried out when the plate temperature varies suddenly in time. Expressions for the velocity and temperature distributions have been calculated in the non-dimensional forms. It is found that the skin friction decreases with increases in magnetic field.

### 1. INTRODUCTION

The problem of steady hydromagnetic free convection flow past a semi-infinite vertical flat plate has attracted the attention of many research workers for many years, due to its wide applications in modern technology, and a number of theoretical and experimental results have been obtained by Mori (1959), Sparrow & Cess (1961), Gupta (1962a), Lykoudis (1962), Gupta & Suryaprasada Rao (1965) and D'Sa (1967). Moreover, this problem is easily amenable to experiment in a laboratory. However, the two dimensional unsteady hydromagnetic free convection boundary layer flow past a semi-infinite vertical flat plate has received considerably less attention. To the knowledge of author, the only paper to be due to Gupta (1960b), who applied the method of characteristics to study the effect of horizontal magnetic field on two dimensional unsteady laminar free convection flow past a vertical flat plate undergoing a stepwise change in temperature, has been published so far. Hence the present paper is devoted to a study of the influence of uniform magnetic field in the boundary layer flow past a vertical flat plate when the plate temperature varies suddenly in time. For solving this problem the method of similarity is applied which has its physical meaning in connection with the process of forming the boundary layer. The analysis in the present investigation is confined to low magnetic Reynolds number so that the induced magnetic field is negligible in comparison with the imposed magnetic field.

### 2. FUNDAMENTAL EQUATIONS

Consider a semi-infinite vertical flat plate with  $x$ -axis along the plate measured from the leading edge in the direction against the gravity and  $y$ -axis normal to it. The plate is immersed in an electrically conducting fluid and a uniform magnetic field  $B_0$  is applied along the  $y$ -axis. Then assuming that the



magnetic field induced by the motion can be neglected, the dimensionless equations governing the unsteady boundary layer equations are

$$\begin{aligned}\frac{\partial u}{\partial x} + \frac{\partial v}{\partial y} &= 0, \\ \frac{\partial u}{\partial t} + u \frac{\partial u}{\partial x} + v \frac{\partial u}{\partial y} &= T' + \frac{\partial^2 u}{\partial y^2} - Nu, \\ \frac{\partial T}{\partial t} + u \frac{\partial T}{\partial x} + v \frac{\partial T}{\partial y} &= \frac{1}{Pr} \frac{\partial^2 T}{\partial y^2}.\end{aligned}\quad \dots (1)$$

Here  $u$  and  $v$  are the velocity components in the  $x$  and  $y$  directions respectively,  $t$  the time variable,  $T$  the temperature variable,  $Pr$  the Prandtl number and  $N = \sigma B_0^2 l^3 / \nu \rho$  the interaction parameter. It is noted that the usual assumptions for free convection of constant properties except slight changes in density and negligible viscous dissipation are here retained. The corresponding boundary conditions are

$$\begin{aligned}y = 0 \quad u = v = 0 \quad T = T_w(x) \\ y \rightarrow \infty \quad u \rightarrow 0 \quad T \rightarrow 0\end{aligned}\quad \dots (2)$$

where  $T_w(x)$  is a yet unspecified function of  $x$ .

### 3. SOLUTIONS OF EQUATIONS

If the surface temperature is established impulsively, the initial motion is described by a balance between the viscous term and the time derivative. Define

$$u = \frac{\partial \psi}{\partial y}, \quad v = -\frac{\partial \psi}{\partial x}, \quad \psi = 2\sqrt{t}f(x, \eta, t), \quad \eta = y/2\sqrt{t}, \quad \dots (3)$$

whence, provided  $Pr = 1$ , we get

$$f_{\eta\eta\eta} + 2\eta f_{\eta\eta} + 4tf_{\eta t} + 4t(f_x f_{\eta\eta} - f_\eta f_{\eta x}) = -4tT + 4Ntf_\eta, \quad \dots (4)$$

$$T_{\eta\eta} + 2\eta T_\eta - 4tT_t + 4t(f_x T_\eta - f_\eta T_x) = 0.$$

A solution to equations (4) is sought in the form

$$\begin{aligned}T &= T_0(x, \eta) + T_1(x, \eta)t^3 + \dots, \\ f &= F_0(x, \eta)t + F_1(x, \eta)t^2 + F_2(x, \eta)t^3 + \dots\end{aligned}\quad \dots (5)$$

The  $T_k$  and  $F_k$  satisfy the equations

$$\begin{aligned}T_{0\eta\eta} + 2\eta T_{0\eta} &= 0, \\ F_{0\eta\eta\eta} + 2\eta F_{0\eta\eta} - 4F_{0\eta} &= -4T_0, \\ T_{1\eta\eta} + 2\eta T_{1\eta} - 8T_1 &= 4(F_{0\eta}T_{0x} - F_{0x}T_{0\eta}), \\ F_{1\eta\eta\eta} + 2\eta F_{1\eta\eta} - 8F_{1\eta} &= 4NF_{0\eta}, \\ F_{2\eta\eta\eta} + 2\eta F_{2\eta\eta} - 12F_{2\eta} &= 4NF_{1\eta} + 4(-T_1 + F_{0\eta}F_{0\eta x} - F_{0x}F_{0\eta\eta}).\end{aligned}\quad \dots (6)$$

For solving (6), we take

$$\begin{aligned} T_0 &= T_w \theta_0(\eta), & F_0 &= T_w \zeta_0(\eta), & T_1 &= T_w \frac{dT_w}{dx} \theta_1(\eta), \\ F_1 &= T_w \zeta_1(\eta), & F_2 &= T_w \zeta_{21}(\eta) + T_w \frac{dT_w}{dx} \zeta_{22}(\eta), \end{aligned} \quad (7)$$

so that

$$\begin{aligned} \theta_0'' - 2\eta\theta_0' &= 0, & \zeta_0''' + 2\eta\zeta_0'' - 4\zeta_0' &= -4\theta_0, \\ \theta_1'' - 2\eta\theta_1' - 8\theta_1 &= 4(\zeta_0'\theta_0 - \zeta_0\theta_0'), & \zeta_1'' + 2\eta\zeta_1' - 8\zeta_1' &= 4N\zeta_0', \\ \zeta_1'' + 2\eta\zeta_1' - 12\zeta_1' &= 4N\zeta_1', \\ \zeta_2'' + 2\eta\zeta_2' - 12\zeta_2' &= 4(-\theta_1 + \zeta_0'^2 - \zeta_0\zeta_0''), \end{aligned} \quad (8)$$

which satisfy the following boundary conditions

$$\begin{aligned} \eta = 0: & \quad \theta_0 = 1, & \theta_1 = 0, & \zeta_1 = \zeta_1' = 0, \\ \eta \rightarrow \infty: & \quad \theta_0 \rightarrow 0, & \theta_1 \rightarrow 0, & \zeta_1' \rightarrow 0. \end{aligned} \quad (9)$$

Here the dashes denote differentiation with respect to  $\eta$ . The solutions of (8) subjected to (9) are (Pop, 1969a, b)

$$\begin{aligned} \theta_0(\eta) &= \operatorname{erfc} \eta = \frac{2}{\sqrt{\pi}} \int_{\eta}^{\infty} e^{-\gamma^2} d\gamma, \\ \zeta_0'(\eta) &= -2\eta^2 \operatorname{erfc} \eta + \frac{2}{\sqrt{\pi}} \eta e^{-\eta^2} \\ \theta_1(\eta) &= -\frac{2}{3} \eta^4 \operatorname{erfc}^2 \eta + \frac{1}{3\sqrt{\pi}} \left[ \left( \frac{1}{2}\eta + 5\eta^3 \right) e^{-\eta^2} + \frac{4}{5\sqrt{\pi}} \left( 1 + 4\eta^2 + \frac{4}{3}\eta^4 \right) \right] \\ &\quad \operatorname{erfc} \eta - \frac{1}{\sqrt{\pi}} \eta^2 e^{-2\eta^2} - \frac{4}{15\pi} \left[ 1 + \frac{2}{3\sqrt{\pi}} (5\eta + 2\eta^3) \right] e^{-\eta^2}, \\ \zeta_1'(\eta) &= -\frac{2}{3} N\eta^4 \operatorname{erfc} \eta + \frac{1}{3\sqrt{\pi}} N(2\eta^3 - \eta) e^{-\eta^2}, \quad \dots \quad (10) \\ \zeta_2'(\eta) &= -\frac{4}{45} N^2 \eta^6 \operatorname{erfc} \eta + \frac{2}{45\sqrt{\pi}} N^2 \left( 2\eta^5 - \eta^3 + \frac{3}{2}\eta \right) e^{-\eta^2}, \\ \zeta_2'(\eta) &= \left( \frac{1}{8} + \frac{8}{15\pi} \right) \left[ \frac{8}{15\pi} \left( \frac{33}{4}\eta + 7\eta^3 + \eta^5 \right) e^{-\eta^2} - \left( 1 + 6\eta^2 + 4\eta^4 + \frac{8}{15}\eta^6 \right) \right. \\ &\quad \left. \operatorname{erfc} \eta \right] + \left( \frac{1}{8} + \frac{3}{4}\eta^2 + \frac{1}{4}\eta^4 + \frac{11}{3}\eta^6 \right) \operatorname{erfc}^2 \eta + \left[ \frac{4}{15\pi} \left( 1 + 4\eta^2 + \frac{4}{5}\eta^4 \right) \right] \end{aligned}$$

$$\begin{aligned}
& -\frac{1}{\sqrt{\pi}} \left( \frac{1}{2} \eta + \frac{1}{3} \eta^3 + \frac{2}{5} \eta^5 \right) e^{-\eta^2} - \frac{8}{15\sqrt{\pi}} \eta \left] \operatorname{erfc} \eta + \right. \\
& \left. + \frac{1}{3\pi} (\eta^4 - \frac{1}{2} \eta^2) e^{-\eta^2} + \frac{4}{15\pi} \left[ 1 - \frac{4}{15\sqrt{\pi}} \left( \frac{8}{3} \eta + \eta^3 \right) \right] e^{-\eta^2} \right.
\end{aligned}$$

## CONCLUSION

Now if we consider that the surface temperature is directly proportional to a power of  $x$  (Kelleher & Yang 1968) i.e.,  $T_w = x^n$  then the skin friction at the plate can be written, for  $n = 1$ , as

$$\frac{\pi^{1/2} \tau_w}{x} = t^{1/2} - 0.166 N t^{3/2} + (0.033 N^2 + 0.014) t^{5/2}. \quad \dots (11)$$

The numerical results of (11) at different times and hydromagnetic parameters  $N$  are presented in the table 1 below. It is found that the skin friction

Table 1.  $\pi^{1/2} \tau_w / x$ 

	$N$			
	0	1	1.5	
0.1	0.3160	0.3109	0.3080	0.3059
0.25	0.5004	0.4807	0.4716	0.4636
0.4	0.6334	0.5938	0.5779	0.5628
0.8	0.8989	0.7994	0.7436	0.7376

decreases as the magnetic field increases. Physically this is due to the fact that the magnetic field exerts a retarding influence on the motion of the fluid which implies a reduction in the velocity gradient at the plate and consequently the skin friction is reduced.

In interpreting the results obtained in this paper, it should be borne in mind that the theory is valid for small times.

## REFERENCES

- D'Sa E. R. 1967 *Zeit. Angew. Math. Phys.* **18**, 106  
 Gupta A. S. 1962a *Zeit. Angew. Math. Phys.* **13**, 324.  
 1960b *Appl. Sci. Res.* **9-A**, 319.  
 Gupta A. S. & Suryaprakasarao U. 1965 *J. Phys. Soc. Japan* **20**, 1930.  
 Kelleher M. D. & Yang, K. T. 1968 *Zeit. Angew. Math. Phys.* **19**, 31.  
 Lykoudis P. S. 1962 *Int. J. Heat Mass Transfer* **5**, 23.  
 Mori Y. 1959 *Trans. Japan Soc. Aero. Space Sci.* **2**, 22.  
 Pop I. 1969a *Rozprawy Inzynierskie* **17**, 173. (in Polish)  
 1969b *Indian J. Phys.* **43**.  
 Sparrow E. M. & Coss R. D. 1961 *Int. J. Heat Mass Transfer* **3**, 267.

## $E_2$ transition probabilities in even nuclei

M S RAJPUT AND A. AUGUSTHY

Department of Physics, Aligarh Muslim University  
Aligarh (U.P.), India

(Received 19 December 1969—Revised 31 March 1970)

$E_2$  transition probabilities for  $2^+ \rightarrow 0^+$  ground state transitions of even-even deformed nuclei have been calculated using Davydov and Rostovsky (DR) estimates. The predictions of this model have been compared with the experimental data. From this comparison, it has been found that the DR estimates are closer to the experimental rates. The variations of the ratios  $\frac{B(E_2)_{\text{exp}}}{B(E_2)_{\text{DR}}}$  and  $\frac{B(E_2)_{\text{exp}}}{B(E_2)_{\text{SP}}}$  with nonaxiality parameter ' $\gamma_0$ ' of Davydov and Filippov theory which is a measure of the degree of departure from the axial symmetry, have been studied.

### INTRODUCTION

Systematics of  $E_2$  transition probabilities for  $2^+ \rightarrow 0^+$  ground state transitions in even-even deformed nuclei in the mass region  $150 \leq A \leq 200$  and  $A > 230$  have been studied by several authors. No definite correlation has been found between the experimental and theoretical transition probabilities. Several attempts by Alder *et al* (1956), Coleman (1957), McGowan & Stelson (1961), Curie (1962), Rajput & Sehgal (1967), Schwarzschild (1966) and Rajput (1970) have been made to explain the fastness of these transitions. The various models proposed to explain the fastness of these transitions have confirmed their collective behaviour. The most generally used single particle model predictions have shown that the experimental transition probabilities are larger by a factor ranging from 30 to 300 in the above mass region. In this work we have studied the variations of the ratios of experimental transition probabilities to those theoretically calculated on the basis of the single particle, (Blatt & Weisskopf 1952) as well as the nonaxial collective models (Davydov & Rostovsky 1964), with the nonaxiality parameter  $\gamma_0$  of Davydov and Filippov theory (1958). Davydov and Filippov have suggested a model for deformed nuclei in which they assume that the rotation of the nucleus takes place without change of the intrinsic state. The equilibrium shape of the nucleus is like a triaxial ellipsoid and is determined by the two parameters  $\beta_0$  and  $\gamma_0$ , where  $\beta_0$  is the deformation parameter and  $\gamma_0$  is the nonaxiality parameter. When there is a deviation from axial symmetry, it lowers one of the principal moments of inertia and increases the other. The nucleus rotates about the axis with the largest moment of inertia.

Davydov and Rostovsky (1964) have treated the problem of collective excitations by taking into account the interactions of rotations with  $\beta$  and  $\gamma$  vibrations. The excited states generated in rotation due to the quadrupole vibrations of the nuclear surface are called  $\gamma$  vibrations. When the nucleus passes into the excited states, the shape of the nucleus changes. This increase in deformation increases the moment of inertia and hence causes the centrifugal stretching. Such vibrations are called  $\beta$ -vibrations.

### CALCULATION OF TRANSITION PROBABILITIES

Davydov and Rostovsky (1964) have derived the expressions for the  $E_2$  transition probabilities from one collective state to the other in terms of the usual parameters of DF theory (Davydov & Filippov 1958). The reduced transition probability for  $E_2$  transitions from the ground state to the first  $2^+$  state of ground state rotational band is given by,

$$B(E_2, 0^+ \rightarrow 2^+) = \frac{5e^2 Q_0^2}{16\pi} \left(1 - \frac{1}{S}\right) \left(1 - \frac{2S}{3q^2}\right)^2 \quad \dots (1)$$

$$\text{where } Q_0 = \frac{3ZR_0^2\beta_0}{\sqrt{5\pi}} \quad \dots (2) \quad S = \frac{\epsilon_{22}}{\epsilon_{20}} \quad \dots (3)$$

$$q = \frac{\epsilon_{00}}{\epsilon_{20}} \quad \dots (4) \quad \text{and } R_0 = 1.2 \times 10^{-13} \times A^{1/3} \text{ cm} \quad \dots (5)$$

Here  $\epsilon_{20}$  is the energy of  $2^+$  state of ground state rotational band,  $\epsilon_{22}$  the energy of  $2^+$  state of the  $\gamma$ -vibrational band and  $\epsilon_{00}$  is the energy of  $0^+$  state of the  $\beta$ -vibrational band.  $\beta_0$  is the deformation parameter. The effective values of these parameters have been calculated from the experimentally measured energy levels. The equilibrium deformations  $\beta_0$  used in the calculations were taken from the work of Bes & Szymanski (1961) corrected by Marshack & Rasmussen (1963). Their values were obtained using Nilson levels and including pairing correlations and are in good agreement with experimental ones. Using these relations the transition probabilities have been calculated in 26 cases. The single particle reduced transition probabilities  $B(E_2, 0^+ \rightarrow 2^+)_{SP}$  have been calculated using the relation

$$B(E_2, 0^+ \rightarrow 2^+) = 0.31 A^{4/3} e^2 \times 10^{-52} \text{ cm}^4 \quad \dots (6)$$

The experimental transition probabilities have been compiled from Nuclear Data (1965). In some cases, the transition probabilities have been calculated from  $T_1$  measurements where direct measurements are not available.

## RESULTS AND DISCUSSION

Table I gives the values of the parameters used in the calculations. The column 7 gives the values of transition probabilities calculated using equation 1. We define the factors  $F_{DR}$  and  $F_{SP}$  as follows :

$$F_{DR} = \frac{B(E_2) \exp}{B(E_2)_{DR}}$$

$$F_{SP} = \frac{B(E_2) \exp}{B(E_2)_{SP}}$$

Alder *et al* (1956) studied the systematics of  $E_2$  transition probabilities and pointed out that the interactions of the rotational and vibrational bands are responsible for the enhancement of these probabilities. Nathan & Nilson (1965) further emphasized the occurrence of collective vibrations and their relation with shell structure. The ratio  $\frac{B(E_2) \exp}{B(E_2)_{SP}}$  being always greater than 1, confirms the fact that the first  $2^+$  states are largely collective. Several attempts (Alder *et al* 1956, Coleman 1957, McGowan & Stelson 1961 and Curie 1962) have been made to explain the collective behaviour of these transitions. No definite correlation was found between the experimental data and the proposed systematics. Rajput & Sehgal (1967) found that the enhancement factors of the  $E_2$  transitions for  $2^+$  to  $0^+$  state decreases gradually with the increase in the value of non-axiality parameter  $\gamma_0$  of Davydov & Filippov (1958) theory. Davydov & Rostovsky (1964) have reviewed the DF theory and calculated the transition probabilities taking into account fully the collective excitations of all types.

Experimental values of transition probabilities are compared with Davydov & Rostovsky (1964) and single particle estimates (Blatt & Weisskopf 1952). The theoretical values calculated using DR theory are closer to the experimental values than the single particle values. This indicates the superiority of DR estimates over the single particle estimates.

Further interesting information is obtained when the factors  $F_{DR}$  and  $F_S$  plotted against the nonaxiality parameter  $\gamma_0$  of DF theory. It was reported earlier by Rajput & Sehgal (1967) that the factor  $F_{SP}$  decreases gradually with increase in value of the nonaxiality parameter. But in this work we have observed that the factor  $F_{DR}$  increases slowly with the increase in the value of the nonaxiality parameter. The variations of  $F_{DR}$  and  $F_{SP}$  with nonaxiality parameter  $\gamma_0$  are shown in figure 1. From this figure it is clear that the DR estimates are better approximations than the SP estimates; the two factors follow completely different trends. The variation of the factor  $F_{DR}$  with neutron number is shown in figure 2. The factor increases as the magic number is approached and again decreases as we go away from the magic number.

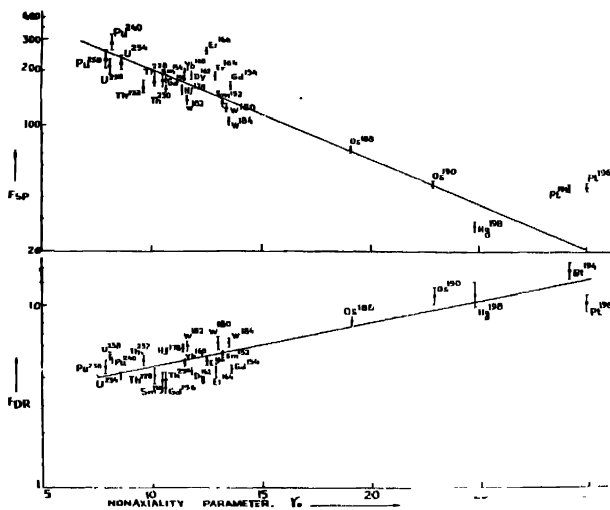


Figure 1. Variation of  $F_{DR}$  and  $F_{SP}$  with nonaxiality parameter  $\gamma_0$

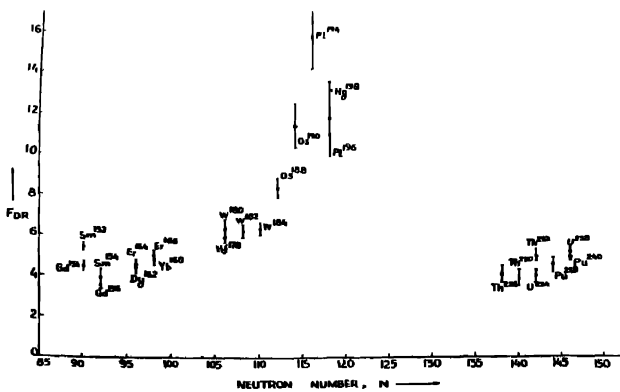


Figure 2. Variation of  $F_{DR}$  with neutron number  $N$ .

Table 1

Nucleus	Energy of of first 2 <sup>+</sup> level (MeV)	S	q	$\beta_0$	$B(E_2)_{\text{exp}}$ $e^2 \times 10^{-48} \text{ cm}^4$	$B(E_2)_{\text{cal}}$ $e^2 \times 10^{-48} \text{ cm}^4$	$F_{DR}$	$F_{SR}$	$\gamma_0$
Sm <sup>152</sup>	0.122	8.90	5.60	0.34	3.40 ± .12	0.629	5.40 ± .20	133 ± 8	13.2
Sm <sup>154</sup>	0.084	14.45	13.73	0.34	4.61 ± .20	1.161	3.90 ± .38	177 ± 12	10.5
Gd <sup>154</sup>	0.123	8.10	5.52	0.33	3.68 ± .20	0.822	4.43 ± .22	167 ± 4	13.6
Gd <sup>156</sup>	0.089	13.00	11.40	0.33	4.68 ± .20	1.134	3.51 ± .15	181 ± 4	10.6
Dy <sup>162</sup>	0.081	10.06	12.71	0.31	5.06 ± .15	1.152	4.39 ± .13	190 ± 9	11.8
Er <sup>164</sup>	0.092	9.40	13.56	0.30	5.20 ± .25	1.171	4.44 ± .26	188 ± 9	12.9
Er <sup>168</sup>	0.081	9.78	18.17	0.29	5.78 ± .20	1.152	5.02 ± .18	246 ± 7	12.5
Yb <sup>168</sup>	0.088	11.21	13.62	0.28	5.43 ± .25	1.122	4.84 ± .22	196 ± 9	11.5
Hf <sup>178</sup>	0.093	12.12	12.80	0.22	4.57 ± .20	0.770	5.93 ± .26	158 ± 6	11.4
W <sup>180</sup>	0.104	7.91	8.77	0.21	4.39 ± .33	0.700	6.26 ± .50	125 ± 5	13.4
W <sup>182</sup>	0.100	12.22	11.38	0.20	4.15 ± .20	0.673	6.17 ± .30	138 ± 7	11.6
W <sup>184</sup>	0.111	8.14	21.00	0.18	3.66 ± .15	0.585	6.26 ± .26	103 ± 4	13.5
Os <sup>196</sup>	0.155	4.08	11.40	0.14	2.75 ± .15	0.332	8.29 ± .46	75 ± 3	19.1
Os <sup>190</sup>	0.137	2.98	18.00	0.12	2.55 ± .25	0.224	11.36 ± 1.11	48 ± 7	22.9
Pt <sup>194</sup>	0.316	1.89	3.85	0.11	1.94 ± .20	0.123	15.83 ± 1.63	46 ± 7	29.2
Pt <sup>196</sup>	0.356	1.91	6.20	0.10	1.27 ± .13	0.116	10.94 ± 1.10	46 ± 5	30.0
Hg <sup>198</sup>	0.412	2.64	4.00	0.08	1.03 ± .10	0.088	11.77 ± 1.76	28 ± 4	24.8
Th <sup>230</sup>	0.058	15.30	14.40	0.22	7.12 ± .75	1.734	4.11 ± .43	17 ± 12	10.1
Th <sup>232</sup>	0.053	13.00	11.90	0.24	7.90 ± .8	2.098	3.85 ± .39	165 ± 4	10.6
Th <sup>234</sup>	0.050	15.80	14.50	0.24	9.70 ± .5	1.942	5.00 ± .26	164 ± 14	9.6
U <sup>234</sup>	0.044	19.40	18.52	0.25	10.00 ± 0.8	2.525	3.96 ± .32	221 ± 21	8.6
U <sup>238</sup>	0.045	23.80	22.20	0.24	12.60 ± 0.6	2.427	5.19 ± .25	211 ± 21	8.1
Pu <sup>238</sup>	0.044	23.20	21.30	0.24	11.50 ± 0.9	2.520	4.57 ± .37	234 ± 25	7.9
Pu <sup>240</sup>	0.044	23.70	20.00	0.24	12.70 ± 0.4	2.526	5.03 ± .15	287 ± 25	8.2



## ACKNOWLEDGEMENT

The authors are very thankful to Dr. M. L. Sehgal for helpful discussions and encouragement. They are also thankful to Prof. Rais Ahmed for his interest in this work, and to the Council of Scientific and Industrial Research, New Delhi, for financial assistance.

## REFERENCES

- Alder K., Bhr A., Huns T., Mottelson B. & Winthor A. 1956 *Rev. Mod. Phys.* **28** 432.  
Bes D. R. & Szymanski Z. 1961 *Nuclear Physics* **28**, 42.  
Blatt J. M. & Weisskopf V. F. 1952 *Theoretical Nuclear Physics* John Wiley & Sons, New York  
Coleman C. F. 1957 *Nuclear Physics* **7**, 488.  
Curie W. M. 1962 *Nuclear Physics* **32**, 574  
Davydov A. S. & Rostovsky V. S. 1964 *Nuclear Physics* **60**, 529  
Davydov A. S. & Filippov G. F. 1958 *Nuclear Physics* **8**, 237  
Grodzins L. 1962 *Physics Letters* **2**, 88  
Funk E. G., Prusk H. J. & Michelich J. W. 1966 *Phys. Rev.* **141**, 1200.  
Marshall E. R. & Rasmussen J. O. 1963 *Nuclear Physics* **43**, 438  
McGowan F. K. & Stelson P. H. 1961 *Phys. Rev.* **132**, 1274  
Nathan O. & Nilson S. G. 1965  *$\alpha$ - $\beta$ - $\gamma$ -ray Spectroscopy*. Edited by K. Siegbahn. N. H. Publ. Co., Amsterdam.  
*Nuclear Data* 1965. Academic Press. New York.  
Rajput M. S. & Sehgal M. L. 1967 *J. Phy. Soc. Japan* **23**, 917  
Rajput M. S. 1970 *Nuovo Orimento* **66A**, 343.  
Schwartzchild A. 1966 *Phys. Rev.* **141**, 1214.

## Capture cross section of 14 MeV neutrons

MANJUSHREE MAJUMDER

Nuclear Physics Laboratory, Bose Institute, Calcutta-9

(Received 15 May 1970)

Radiative capture cross sections for some nuclei round about mass number 100 have been measured for 14.8 MeV neutrons by the activation technique. Sources of systematic errors and the steps taken to control them have been discussed. The results have been compared with those given by Perkin *et al* and Csikai *et al*. Data obtained are very much different from those predicted by the compound nucleus theory.

### INTRODUCTION

Neutron capture by the nucleus is a complicated process. To understand the reaction mechanism, experimental investigations were mostly performed by using thermal neutrons, since they have the larger cross sections, and by studying the gross structure of the capture  $\gamma$ -ray spectra. Nevertheless, total cross sections of  $(n, \gamma)$  reactions of higher energy neutrons, especially 14 MeV neutrons have also been reported by a few workers (Perkin *et al* 1958, Cvelbar *et al* 1966, Csikai *et al* 1967). Comparisons of such data have been made with those obtained from calculations according to simple theoretical reaction models. Experimental cross section values of 14 MeV neutrons, captured by nuclei of mass number higher than 50, are generally, a few orders of magnitude larger than those obtained from calculations according to statistical model (Lane & Lynn 1959). A so called 'semi-direct' capture model (Brown 1964, Clement *et al* 1965) raises the theoretical values in some cases by a few factors of ten, near 14 MeV. But these values also fall shorter by about a factor of ten than the reported experimental values (Csikai *et al* 1967). Moreover, not many experimental values exist for neutrons over 10 MeV of incident energy for any meaningful comparison. Therefore, mainly to supply a set of reasonably accurate experimental values, the following work was undertaken.

The method followed for this work has been the conventional activation measurements. Following such a method, results in the past were presented by Perkin *et al* (1958) and later by Cvelbar *et al* (1966) and Csikai *et al* (1967). Here the values of total cross sections of  $(n, \gamma)$  reactions of 14 MeV neutrons are presented for the following nuclei above mass number 50, viz.  $^{71}\text{Ga}$ ,  $^{75}\text{As}$ ,  $^{127}\text{I}$ ,  $^{138}\text{Ba}$  and  $^{141}\text{Pr}$ .

### EXPERIMENTAL METHOD

The  $\sigma(n, \gamma)_{\text{total}}$  was determined from relative measurements of saturation  $\beta^-$  or  $\beta^+$  activities developed after long neutron-irradiation of sample elements

Generally from a composite decay of 'daughter' element, estimate could be made of the saturation activity of the sought-for isotope developed by  $(n, \gamma)$  reaction. As the neutron source the  $(T-D)$  generator of Bose Institute was used.

*Systematic Errors* : Naturally, when the cross section values are of the order of magnitude of only fractions, or at best a couple of units of millibarns (as predicted by model calculations or previously obtained results, by other workers) one must have to take extreme caution to minimize and/or eliminate every possible error involved. In the present case, errors were held to be composed of the following ones :

- (a) Error due to indefiniteness of the incident neutron energy.
- (b) Error involved in relative  $\beta$ -counting due to mainly the self-interaction of the  $\beta$ -rays.
- (c) Error due to masking caused by activities present from reactions other than  $(n, \gamma)$ ,
- (d) Error due to variation of neutron-flux, which is by far the most serious error.

Procedures followed to eliminate or to minimise the above errors are briefly described here.

(i) The energy spread of incident neutrons were determined knowing exactly the geometry, *i.e.*, from the measured dimension of focal spot on the tritium target and the area and the distance of the sample, and then estimating from the reaction kinetic calculations. The H.T. source of the neutron generator was stabilized and the voltage variation thereby was restricted to within  $\pm 0.1\%$  over 150 KV. This comparatively low H.T. value was used for neutron generation since the spread on the sample was rather large,  $= 30^\circ$ ; hence to restrict the variation within a low limit. 120-150 KV were the compromise values. The large spread was to obtain larger counts, because the approach of sample to source had to be close. The thickness of the sample again was also a compromise, rather then being unduly thick. The effect of this sample thickness is considered separately in (ii). The value of incident neutron energy thus specified was  $14.8 \pm 0.08$  MeV.

Needless to say, the system of irradiation was kept 'clean', having minimum scattering material nearby. For this reason, liquid coolant in the target was dispensed with and forced air cooling was used. This necessitated some inventiveness to prevent fly-out of (generally used) powdered samples, which were irradiated without any cover. No extra backing was used for the thin copper disc of the titanium tritium target foils.

(ii) *Errors in relative  $\beta$ -counting involved* :

In one of the earlier papers published from this laboratory (Mitra & Ghose 1966), the sources of error associated in  $\beta$ -counting of such thick samples, were

discussed and methods to eliminate or minimize them pointed out. However, for the sake of completeness, they are very briefly discussed here. Most of the correction factors involved in thick-sample  $\beta$ -counting were calculated and employed in a straightforward manner, except self-absorption and self-scattering in the sample, which contribute to the largest errors. These self interaction factors were determined by a procedure which was a variation from those adopted by Prestwood & Bayhurst (1959). Overall relative efficiency  $\epsilon_{rel}$  of  $\beta$ -counting was obtained from a semi-empirical relation

$$\epsilon_{rel} = 1 - \exp(-b\bar{E}_{\beta})$$

where  $\bar{E}_{\beta}$  is the average energy of  $\beta$ ,  $b$  is a constant which was experimentally determined for a constant geometry of source and counter during counting. Although such a relation slightly deviates from general, at very low values of  $\bar{E}_{\beta}$ , the deviation was seen to be within a few percent, and the overall relative efficiency of the particular set-up of counting was determined within  $\pm 3\%$  of the total for the  $\bar{E}_{\beta}$ 's encountered in all the cases of our sample activities.

(iii) *Masking caused by other activities :*

It is difficult, in these high mass number elements to get rid of or accurately estimate the lingering activities present due to  $(n, 2n)$  reaction products, since in nearly all the cases, the  $\sigma(n, 2n)$  exceeds the  $\sigma(n, \gamma)$  by a factor of  $10^2-10^3$ , in this neutron energy. However, accurate follow-up of the composite decay curves (figure 1) and reconstruction of the wanted activity from them by adopting a procedure of fitting by least square method, yielded results of desired accuracy. Parallelaactivities of comparable half lives were absent in the chosen samples reactions. The  $(n, 2n)$  caused, in general, increased backgrounds and most of the errors in counting were due to difficulty in estimating the small activity present from large backgrounds.

(iv) *Standards :*

The standard reactions adopted for relative measurements were  $(n, 2n)$  reaction in  $^{63}\text{Cu}$ , adopted value of cross section being  $530 \pm 25$  mb (Mitra & Ghosh, 1966) and  $(n, \alpha)$  reaction in  $^{27}\text{Al}$ , the adopted value for this  $\sigma$  was  $116 \pm 8$  mb. The former reaction was adopted for comparatively short half lives of products and the latter for longer half lives.

(v) *Neutron flux variation :*

Neutron flux was continuously monitored by a heavily biased plastic scintillator detector connected to a sensitive count rate meter and recorder. Flux could be held constant to a deviation of  $\pm 5\%$ .

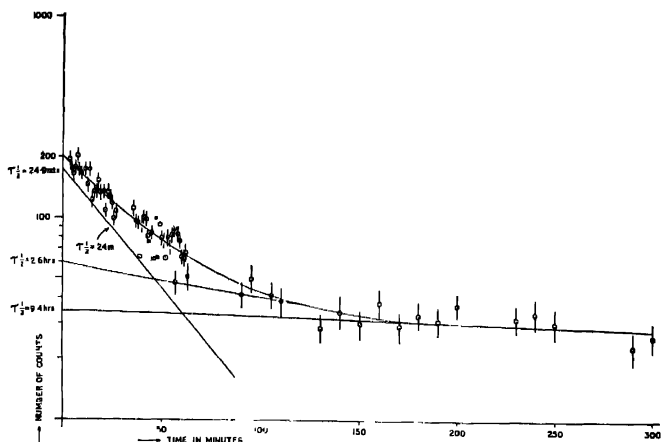


Figure 1. Analysis of the composite decay curve of  $^{127}\text{I}$  to extract different activities.

(vi) *Experimental details :*

Samples were taken in powder form and the chemical form used were respective oxides. Purity of the samples were taken as guaranteed by the manufacturers. The sample holders were in the form of a circular pot of diameter 2.5 cms, in which samples could be pressed to form tablets of maximum thickness 2 mm. Holders were made from pressed graphite. Plastics were not used because of their possible effect of moderating neutron energies to lower values, although during the counting of the long-lived samples, they were often emptied into a plastic pot of same dimensions. Sample to source distance was always maintained to be 4.5 cms in the forward direction. Irradiation was given, keeping the samples inside cadmium boxes. Foils of speeure copper and aluminium as standard materials, were given exact circular diameters as sample-cakes and they were placed above and below the samples. The standard foils were each of  $10\text{mg}/\text{cm}^2$  thickness. A separate correction was made for difference in geometrical dispositions of the sample and target foils towards the neutron source spot.

For iodine samples, during counting, care was taken to ensure that there was no loss by sublimation or that it did not deposit itself on the counter window. For this, a special ice-box was constructed (figure 2) and iodine, after irradiation being transferred in a weighed perspex pot, was housed in the ice-box and counted. Any sublimate depositing on the counter window was checked for, simply by removing the sample and looking for background counts. It was observed that if the ice-box was used, no extra correction was needed for loss of

sample or its deposition on the window, the effects being eliminated. A dry chamber used for 'sample to counter volume' eliminated deposition of moisture on the sample.

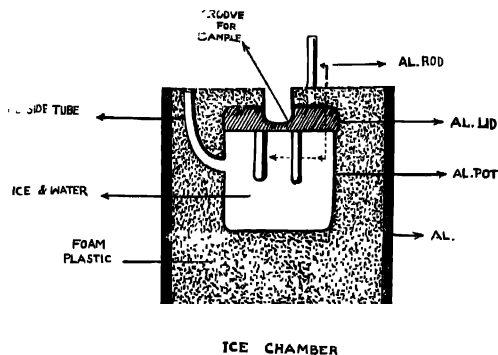


Figure 2. Diagram of ice chamber developed and used during the counting of  $^{127}\text{I}$ .

The counter used was end window  $\beta$ -counter of  $2.4 \text{ mg/cm}^2$  window thickness; sample to counter distance was  $1 \text{ cm}$ .

### RESULTS

The total  $\sigma(n, \gamma)$  was calculated by the usual method, from saturation activities in the sample and the standard, taking into account all the errors discussed above. Ideas of expected half lives were obtained in each case from the data supplied in the table of isotopes by Hollander *et al* (1967), then all re-determined by constructing the full decay curves.

(i) *Irradiation of gallium*: Specpure  $\text{Ga}_2\text{O}_3$  (white powder) was used as sample. Standard in this case was  $^{27}\text{Al}$ , in the form of specpure foil. Sample consists mostly of two isotopes  $^{69}\text{Ga}$  and  $^{71}\text{Ga}$ , in the ratio 39.5 : 60.2. The life-times of generated activities were therefore expected as, 32 secs from  $^{68}\text{Cu}$ , by  $(n, \alpha)$ ; 2.2 mts from  $^{71}\text{Zn}$ , by  $(n, p)$ ; 5.1 mts from  $^{68}\text{Cu}$  by  $(n, \alpha)$ ; 21.1 mts from  $^{70}\text{Ga}$  by  $(n, 2n)$ ; 57 mts from  $^{69}\text{Zn}$  and 68 mts from  $^{68}\text{Ga}$ . These half lives were confirmed by actual follow up of the decay curve. None of them really competes with 14.3 hours activity obtained from  $^{72}\text{Ga}$ . However, a large background due to  $^{68}\text{Ga}$  and  $^{70}\text{Ga}$  was present from which 14.3 hours activity was separated. Multiple irradiation of 2.5 hours each was given for saturation of long time activity.

(ii) *Irradiation of arsenic*:  $^{75}\text{As}$  is a 100% isotope. The activities generated after long irradiation were: 82 mts due to  $^{75}\text{Ge}$  by  $(n, p)$ ; 14.3 hrs due to

$^{72}\text{Ga}$  by  $(n, \alpha)$  and 26.5 hrs due to  $^{76}\text{As}$  by  $(n, \gamma)$ ; sample used was  $\text{As}_2\text{O}_3$  of 99.5% purity.  $^{27}\text{Al}$  ( $n, \alpha$ ) was the standard.

(iii) *Irradiation of iodine* : Iodine metal flakes, pasted in the form of cakes were used as sample.  $^{127}\text{I}$  being a 100% isotope, only activities expected were 9.4 hrs from  $^{127}\text{Te}$ , by  $(n, p)$ ; 13.3 days from  $^{128}\text{I}$  by  $(n, 2n)$ ; 25 mts from  $^{128}\text{I}$  by  $(n, \gamma)$ . From the decay curve, a new activity of 2.6 hrs was recognized and computed. Aagard *et al* (1957) reported such an activity in their study of fission of  $^{126}\text{I}$ . This was recognised as due to the isomerism of 13 days  $(n, 2n)$  product.  $(n, 2n)$  in  $^{63}\text{Cu}$  was the standard.

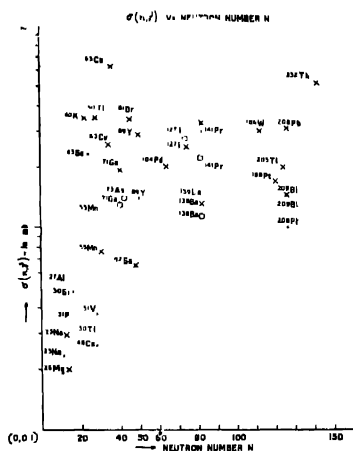


TABLE 1. Capture cross sections for 14.8 MeV neutrons

Reaction	Target	Neutron no. N	$\sigma$ in (mb) $\pm$ counting error	Monitor reaction	Author	Values calculated (compound nucleus theory, Lane 1957)	Particles counted
(1) $^{74}\text{Ga}(n, \gamma)^{75}\text{Ga}$	$\text{Ga}_2\text{O}_3$	40	$1.90 \pm 10\%$ $1.29 \pm 15\%$	$^{27}\text{Al}(n, \alpha)$	Perkin <i>et al</i> (1958) Present author	0.1 mb	$\beta^-$
(2) $^{75}\text{As}(n, \gamma)^{76}\text{As}$	$\text{As}_2\text{O}_3$	42	$1.39 \pm 12\%$	$^{27}\text{Al}(n, \alpha)$	Present author	0.11 mb	$\beta^-$
(3) $^{127}\text{I}(n, \gamma)^{128}\text{I}$	Iodine	74	$2.50 \pm 10\%$ $2.74 \pm 7\%$	$^{63}\text{Cu}(n, 2n)$	Perkin <i>et al</i> (1958) Present author	0.14 mb	$\beta^-$
(4) $^{135}\text{Ba}(n, \gamma)^{136}\text{Ba}$	$\text{BaCO}_3$	82	$1.30 \pm 30\%$ $1.12 \pm 20\%$	$^{63}\text{Cu}(n, 2n)$	Perkin <i>et al</i> (1958) Present author	0.14 mb	$\beta^-$
(5) $^{141}\text{Pr}(n, \gamma)^{142}\text{Pr}$	$\text{Pr}_2\text{O}_3$	82	$3.33 \pm 10\%$ $2.19 \pm 14\%$ $3.00 \pm 10\%$	$^{27}\text{Al}(n, \alpha)$	Perkin <i>et al</i> (1958) Present author Chakraborty <i>et al</i> (1967)	0.14 mb	$\beta^-$



The values of  $\sigma(n, \gamma)$  obtained for all these isotopes are presented in table I, along with the values obtained by other workers.

### DISCUSSION

In all the cases of irradiations, the effects of rarer types of reactions, *viz*  $(n, d)$ ,  $(n, t)$  etc were ignored, since their reported cross sections in the isotopes studied were less than orders of magnitude, as the daughter products are stable or their cross sections have not been reported. It is seen that there is an increasing tendency of the cross sections with increasing mass number, *i.e.*, with increasing number of neutrons. A plot of  $\sigma(n, \gamma)$  vs neutron numbers (figure 3) has been done.

### ACKNOWLEDGEMENTS

The author is grateful to Prof. S M Sircar, Director, Bose Institute for granting her a scholarship. She is grateful to Dr D M Bose, who took constant interest in the work and gave encouragements. Thanks are due to Prof. A M. Ghose Head of the Physics Department for extending to her the facilities of work in the laboratory and to Dr. B Mitra who suggested the problem.

Thanks are also due to Shri B Ghosh and Shri D K. Mitra for their technical assistance and running the generator.

### REFERENCES

- Augard P. & Pappas A. C. 1957 *Jour. Inorg. Chem.* **5**, 105.  
 Bayhurst B. P. & Prestwood R. J. 1959 *Nucleonics*, **17**, 83.  
 Brown G. E. 1964 *Nuclear Phys.* **57**, 339.  
 Clement C. F., Lane A. M. & Rook J. R. 1966 *Nuclear Phys.* **66**, 105.  
 Cetkai J., Reto G., Buczko M., Milligy Z. & Eissa N. A. 1967 *Nucl. Phys.* **A95**, 229.  
 Cvelbar F., Rudoklin A., Mihailovic M., Najzer M. & Ramsak V. 1960 *Proc. Int. Conf. on Nuclear Structure Study with Neutrons*, ed by M. Novo de Mevergnies, P. Van Assche & J. Vervior (North Holland Publishing Company) Amsterdam, 563.  
 Hollander J. M., Lederer C. M. & Perlman I. 1967 *Tables of Isotopes*.  
 Lane A. M. & Lynn J. E., 1957 *Proc. Phys. Soc. (London)* **70A**, 557.  
 Lane A. M. & Lynn J. E. 1959 *Nucl. Phys.* **11**, 646.  
 Mitra B. & Ghosh A. M. 1966 *Nucl. Phys.* **83**.  
 Perkin J. L., Connor L. P. & Coleman R. F. 1958 *Proc. Phys. Soc.* **72**, 505.

## Letters to the Editor

### Near ultra-violet absorption spectrum of meta-methoxy phenol

By C. G. RAMA RAO, B. R. K. REDDY AND P. TIRUVENGANNA RAO

*Department of Physics, Andhra University, Waltair*

(Received 22 July—Revised 23 September 1970)

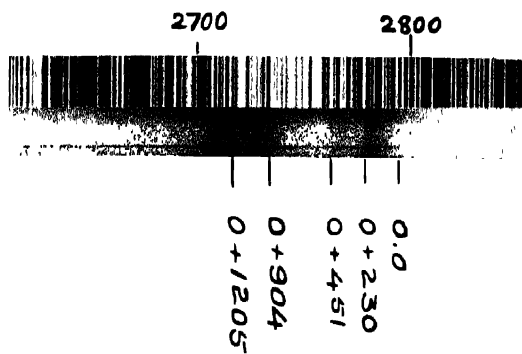
(Plate 10)

The observation of a number of fundamental frequencies characteristic of excited and ground states in the absorption spectrum of phenol in the vapour phase (Matson *et al* 1945) has led to the study of similar properties in substituted phenols. In this context the study of ultra-violet absorption spectrum of meta-methoxy phenol has been taken up

The absorption spectrum of meta-methoxy phenol being redistilled in vacuum, was photographed on a Hilger medium quartz spectrograph having a dispersion of about  $12.6\text{\AA mm}^{-1}$  at  $2800\text{\AA}$ , using a vapour column of 75 cm in the temperature range of  $0^\circ$  to  $90^\circ\text{C}$ . The spectrum thus recorded at  $60^\circ\text{C}$  consists of fairly intense system of bands in the region  $\lambda 2810\text{--}\lambda 2680\text{\AA}$ , as can be seen from plate 10. With an increase of temperature of the vapour column to about  $90^\circ\text{C}$ , a total absorption was observed in this region and no additional bands recorded on the longer wavelength side. The spectrum was also studied taking a thin film of the sample pressed between two quartz plates at the room and liquid oxygen temperatures. The spectrum in the solid state at both the temperatures has indicated only two broad intense bands in the same region where a discrete band system was observed in the vapour state.

The meta-methoxy phenol molecule may be taken as having a  $C_s$  symmetry. Assuming the electronic transition as giving rise to a discrete band system to be an allowed one, the origin of the system is identified at  $35754\text{ cm}^{-1}$ , being the strong band on the longer wavelength side of the spectrum at the minimum possible temperature (about  $30^\circ\text{C}$ ). The remaining bands could be analysed in terms of five upper states 182, 230, 451, 904 and 1205 and two ground states 173 and 149 fundamental frequencies of the molecule. The frequencies together with the visual estimate of intensity of bands and modes of vibration are given in table 1.

A comparison of the shift of the electronic transition upon substitution in ortho, meta and para positions in the methoxy phenols (Suryanarayana & Rao 1956, Sen 1956) with other isomeric disubstituted phenols shows the usual relation  $o- < m- < p-$  and is towards the longer wavelength side of benzene forbidden transition.



Absorption Spectrum of meta-methoxy phenol (vapour at 60°C)



TABLE 1

Band No.	Wave number (cm <sup>-1</sup> )	Difference	Visual intensity	Assignment	Mode of vibration
	35409 <sup>+</sup>				
1	35581	-173	ms	0-173	Totally symmetric vibration. C-OH bending.
2	35605	-149	ms	0-149	
3	35754	0	s	0,0	
4	35936	182	vs	0+182	
5	35984	230	vs	0+230	
6	36044	290	s	0+451-173 or 0+451-149	
7	36107	353	ms	0+2×182	$\alpha_1$ component of 606 $g_1^+$ vibration of benzene. C-C bending.
8	36162	408	ms	0+230+182	
9	36205	451	s	0+451	
10	36658	904	s	0+904	
11	36846 36867*	1092	s	0+904+182	C-H planar bending.
12	36959	1205	s	0+1205	
13	37095	1341	ms	0+451+904	
14	37154	1400	ms	0+1205+182	

<sup>+</sup> Frequencies observed in solid state.

ms - medium strong, s—strong, vs—very strong.

## REFERENCES

- Malsen F. A., Ginsburg N. & Robertson W. W. 1945 *J. Chem. Phys.* **13**, 309.  
 Suryanarayana V. & Ramakrishna Rao V. 1956 *J. Sci. Industr. Res.*, **15B**, 260 and 548.  
 Sen S. K. 1956 *Indian J. Phys.* **30**, 553.

*Indian J. Phys.* 213-244, (1970)

Comment on a note on the linear flow of a viscous incompressible conducting fluid past an infinite flat plate with constant suction in the presence of a transverse magnetic field

By V. V. RAMANA RAO

*Department of Engineering Mathematics, Andhra University, Waltair*

(Received 7 August 1970)

Recently Dube (1969) has studied the effects of the transverse magnetic field and constant suction on the flow of an incompressible electrically conducting fluid when the free-stream velocity varies linearly with time. It should be pointed out that his solutions for velocity and the skin-friction as given by equations

14 and 15 respectively, in his paper are wrong. Also his conclusion on the behaviour of the skin-friction is incorrect. This communication presents the correct solutions for the velocity and the skin-friction. It is further concluded that for a fixed time, the skin-friction decreases with the increase of intensity of the magnetic field

Taking the inverse transform of equation 13 of his paper, we get

$$u = \frac{c}{8} \left[ 8t - 4tc^{\frac{y}{2}} (\sqrt{1+4M^2} - 1) \left\{ e^{-y\sqrt{1+4M^2}} \operatorname{erfc} \left( \frac{y}{4\sqrt{t}} - \sqrt{t(1+4M^2)} \right) + \operatorname{erfc} \left( \frac{y}{4\sqrt{t}} + \sqrt{t(1+4M^2)} \right) \right\} + \frac{yc^{\frac{y}{2}} (\sqrt{1+4M^2} - 1)}{\sqrt{1+4M^2}} \right. \\ \left. \left\{ e^{-y\sqrt{1+4M^2}} \operatorname{erfc} \left( \frac{y}{4\sqrt{t}} - \sqrt{t(1+4M^2)} \right) - \operatorname{erfc} \left( \frac{y}{4\sqrt{t}} + \sqrt{t(1+4M^2)} \right) \right\} \right] \quad \dots (1)$$

The non-dimensional skin-friction  $\tau_0$  is given by

$$\tau_0 = \left( \frac{\partial u}{\partial y} \right)_{y=0} = c \left[ \left( 1 - \frac{\sqrt{1+4M^2}}{2} \right) t + \frac{1}{4\sqrt{1+4M^2}} \operatorname{erf} \{ \sqrt{t(1+4M^2)} \} \right. \\ \left. + \frac{1}{2} \left( \frac{t}{\pi} \right)^{\frac{1}{2}} e^{-(1+4M^2)t} + \frac{t\sqrt{1+4M^2}}{2} \operatorname{erf} \{ \sqrt{t(1+4M^2)} \} \right] \quad \dots (2)$$

The calculated values of the skin-friction from the expression 2 for  $c = 4$ ,  $t = 0, 0.04, 0.09, 0.25$  and  $M = 0, \sqrt{2}$  are given in table 1

Table 1

$M \backslash t$	0	0.04	0.09	0.25
0	0	0.537	0.877	1.720
$\sqrt{2}$	0	0.424	0.667	1.331

From the table it is evident that for a fixed time  $t$ , the skin-friction  $\tau_0$  decreases with the increase of intensity of the magnetic field.

#### REFERENCE

Dube S. N. 1969 *Indian J. Phys.* **43**, 550.

## BOOK REVIEWS

### *Men of Physics—L. D. Landau : Volume 2: Thermodynamics, Plasma Physics and Quantum Mechanics*

D. Ter Haar, Pergamon Press, 1969. Pp 198.

The motivation of these two paper back volumes on Late Professor L. D. Landau, we are told, was "to make the undergraduates familiar with at least some of Landau's works, apart from his text books" and for this purpose the first volume presented eight papers and in this second volume there are ten papers on such varied topics as second order phase transitions, the origin of stellar energy, the multiple production of particles during collision of fast particles; as also, there are papers on more sophisticated topics like conservation laws for weak interactions. The volume is provided with an introduction by Ter Haar, which seeks to clarify the background of the works, the exact nature of the contribution made by Landau and some sort of evaluation of those contributions in the light of later researches. While the reviewer finds the volume quite interesting, he is afraid that it is too high not only for the average undergraduate but even for the more meritorious among them. The book would be of special value to those who are interested in the history of development of science.

A. K. R. C.

### *Topics in Nonlinear Physics—Proceedings of the Physics Session*

International School of Nonlinear Mathematics of Physics A Nato Advanced Study Institute Max Planck Institute for Physics and Astrophysics, (Munich, 1960) Ed. Norman J. Zabusky, Springer—Verlag, 1968.

The Physics Session, of which the present volume gives the proceedings, ran for three weeks. The scope of the school was to survey nonlinear phenomena in different fields of physics and to look for similar concepts and techniques that may be applicable to more than one branch. The opening lecture was a perspective one by Heisenberg entitled 'Nonlinear Problems in Physics'. Heisenberg pointed out that practically every classical problem in Physics involves nonlinear mathematics and it may well be that in the final form quantum theory will also be a nonlinear one. Taking as an example the calculation of the motion of a proton in a proton synchrotron, Heisenberg expresses the suspicion that "nonlinear problems have a certain kind of unpredictability". The way out of this difficulty created by 'Unpredictability' may be to study ensembles of solutions rather than single solutions as is the approach in statistical mechanics.

The following six lectures are on such an advanced level and are on so varied topics that the reviewer finds no other alternative than simply noting their titles and authors: (1) The nonlinear field theories in mechanics by Truesdell giving an axiomatic development of the mechanics and thermodynamics of macroscopic classical non-relativistic continua (2) Introduction to nonequilibrium statistical mechanics by Prigogine (3) Interactions in a classical relativistic plasma by Baus (4) Nonlinear optics by Bloembergen (5) Lectures on homogeneous turbulence by Saffman and lastly (6) Superspace and the nature of quantum geometrodynamics by Wheeler.

The book thus covers a very wide field of advanced classical physics and would undoubtedly be a welcome addition to any library interested in advanced mathematical physics.

A. K. R. C.

*Conference Booklet: High Magnetic Fields and their Applications*  
(Nottingham, 1969)

The Institute of Physics & The Physical Society,  
47, Bolgrave Sq., London SW 1.  
167 pages. 30sh (3.60 dollars)

The booklet is a collection of 30 papers presented at the fourth International Conference on High Magnetic Fields and their Applications held at the University of Nottingham from 17 to 19 September, 1969. The papers, though concise, are successful in indicating the 'wealth and variety' of new problems that are now attacked due to the ready availability of high magnetic fields. Most of the papers appear in a short form, but there are some review papers summarising the recent works accomplished in some well-known laboratories. Eight of the papers deal with the production of high fields utilising Bitter-type magnet and/or superconducting magnet and/or short-duration pulsed magnet, one paper discusses 'embryonic' technological applications to mining, metallurgy and medicine; the rest are devoted mainly to the investigation of electronic and magnetic structure of solids. The papers deal with the band-structure of semi-conductors, semi-metals and metals; electrons, holes, excitons and polarons in crystals; magnetic ordering and phase transitions with reference to exchange interactions between ions in solids; magnetoplasma-phonon interaction; conformations of molecules as revealed by high-field N.M.R. etc. The physical properties of solids studied at high field are (1) reflection and absorption of radiation in UV, visible and infrared region (2) cyclotron resonance (3) antiferromagnetic resonance (4) N.M.R. (5) ultrasonic attenuation (6) laser emission and Raman scattering (7) photo-conductivity (8) oscillatory magnetoresistance and (9) magnetic susceptibility.

The booklet will be a good addition to any Solid State Physics Research Laboratory.

M. C.

*Current Algebra and Phenomenological Lagrange Function.*

Springer Tract in Modern Physics. Ergebnisse der exakten Naturwissenschaften 50  
Springer-Verlag, Berlin. Heidelberg. New York 1969.

The book is a collection of invited papers at the first summer school for Theoretical Physics, University of Karlsruhe (July 22-August 2, 1968). It contains the following articles: (1) Dynamical Groups and their Currents. A Model for Strong Interactions—A. O. Barut. It is a discussion on the differences between the group structure of the multiplets and the group structure of interactions and a review of the general framework of the dynamical group, its special form in cases of the Dirac particle and the H-atom and its application to hadrons. (2) Current Algebra and Light Charges—H. Leutwyler. Starting with a brief review of the basic assumptions involved in current algebra it dwells on the properties of lightlike charges. (3) Introduction to the Lagrangian Method—Volkhard F. Muller. It provides an elementary introduction to the Lagrangian formalism of classical field theory. (4) Introduction to the Method of Current Algebra—H. Pletschmann. The author demonstrates the power of current algebra on two examples, namely the Adler-Weisberger relation and the Mathur-Okubo-Pandit-Callan-Treiman relation. (5) S-Matrix Formulation of Current Algebra—H. Pilkhun. (6) Electromagnetic Mass Difference—J. Rothleitner. It deals on the shift of the energy levels of strongly interacting systems caused by the electromagnetic interaction. (7) Non-leptonic Decays and Mass Differences of Hadrons—B. Stech. The subsequent three articles (8) Current Algebra in the Framework of General Quantum Field Theory, (9) Current Algebra and Renormalizable Field Theories, (10) Introduction to Current Algebra, are by P. Stichel. Starting with a rigorous definition of Equal-Time Commutator, the author investigates the Vacuum-Expectation-value of current commutators and Equal-Time-Commutation Relation in perturbation theory. The last one is a short review of the content of Current Algebra. (11) Realisation of a Compact, connected, semi-simple Lie Group—Julius Wess. This is a comprehensive discussion on the topic. (12) Problems in Vector Meson Theories—W. Zimmermann. The author discusses the model of a massive vector field coupled to a conserved current and models of two vector fields which are coupled to the same current.

N. D. S. G.



# INDIAN JOURNAL OF PHYSICS

VOL. 44

No. 4

AND

VOL. 53

PROCEEDINGS

No. 4

OF THE

INDIAN ASSOCIATION FOR THE CULTIVATION OF SCIENCE

*(Edited in collaboration with the Indian Physical Society).*

**APRIL 1970**

PUBLISHED BY THE

INDIAN ASSOCIATION FOR THE CULTIVATION OF SCIENCE

JADAVPUR, CALCUTTA-32

10

# The $r$ -centroids of diatomic molecules from true potential energy curves

By V. K. VAIDYAN AND C. SANTARAM

Indian Institute of Technology, Madras, India

(Received 23 February 1970—Revised 10 June 1970)

The  $r$ -centroid of a molecular band is defined by  $\int \psi_{v'} r \psi_{v''} dr / \int \psi_{v'} \psi_{v''} dr$  and is an average internuclear separation, which may be associated with the  $v' \rightarrow v''$  transition. For an accurate determination of  $r$ -centroids, a correct estimation of energy values of both electronic states for arbitrary  $r$ -values is necessary. A method to find energy values for any  $r$ -values from the true potential energy curves of a particular electronic state is discussed, which is based on the fact that the internuclear distance  $r$  and the corresponding energy  $V$  can be related by an equation of the form  $y(V) = mx(r) + (C)$ . As illustrations,  $r$ -centroids are evaluated for the first positive, second positive and Vegard-Kaplan bands of  $N_2$ , and the red system of CN. These values are compared with that of Nicholls & Jarman (1956), who calculated it by using Morse function. As expected, since Morse function is a poor approximation for higher vibrational levels, the deviation also increases with large  $v$  and  $\Delta v$  values.

## 1. INTRODUCTION

For the calculation of  $r$ -centroids, a method developed by Nicholls & Jarman (NJ) (1956) is used widely, due to its simplicity compared with the methods involving numerical integration based on RKR potential, which is based on the equation,

$$E_{v'} - E_{v''} = V_1(\bar{r}_{v'v''}) - V_2(\bar{r}_{v'v''}), \quad \dots (1)$$

where  $V_1(r)$  and  $V_2(r)$  are potentials of the upper and lower states respectively,  $E_{v'}$  and  $E_{v''}$  are the vibrational energies concerned. The above relation holds good, only if

- (i)  $V_1(r) - V_2(r)$  is a slowly and smoothly varying function of  $r$  over the significant range of  $\int \psi_{v'} [V_1(r) - V_2(r)] \psi_{v''} dr$ ,
- (ii)  $\mu_A \omega_e \sim 10^4$ ,
- (iii)  $0.01 \text{ \AA} < |r_{e1} - r_{e2}| < 0.25 \text{ \AA}$ ,
- (iv)  $v'$  and  $v''$  do not exceed about 10.

The difference between  $E_{v'}$  and  $E_{v''}$  on the left hand side of equation (1) may be calculated for each band of the system. Values of  $\bar{r}_{v'v''}$  appropriate to these energy differences may then be read from graph of  $[V_1(r) - V_2(r)]$  vs  $r$ , if  $V_1(r)$  and  $V_2(r)$  can be evaluated for different  $r$ -values. To find  $V(r)$ , NJ used Morse function. But it is found that Morse function will not represent the p.e. curves of the electronic states adequately, especially for higher vibrational levels. Hence a method to find  $V(r)$  with sufficient accuracy for any  $r$ -value

within the significant range of the p.e. curve is necessary. In this paper, a method to find the same from *true* p.e. curve of an electronic state is discussed, and consequently the accurate evaluation of  $r$ -centroids.

## 2. THEORETICAL DETERMINATION OF $V(r)$

### 2.1 $E(v, K)$ , a quadratic in $(v + \frac{1}{2})$

For the rotationless state ( $J = 0$ ), the general expression representing energy of an electronic state is

$$Ev = \omega_e(v + \frac{1}{2}) - \omega_e x_e(v + \frac{1}{2})^2 + \omega_e y_e(v + \frac{1}{2})^3 - \omega_e z_e(v + \frac{1}{2})^4 + \dots \quad \dots (2)$$

But for most electronic states,  $Ev$  can be represented fairly accurately by the first two terms of equation (2) after having a least square fitting to constants  $\omega_e$  and  $\omega_e x_e$

To derive an empirical relation connecting  $r$  and  $V$ , one can use the form of Morse function

$$V(r) = D[1 - \exp\{-\alpha(r - r_e)\}]^2, \quad \dots (3)$$

since it satisfies Schrodinger's equation for energy states, which can be represented by a quadratic in  $(v + \frac{1}{2})$ . From equation (3),

$$-\alpha(r - r_e) = \ln[1 \pm \{V(r)/D\}^{\frac{1}{2}}] \quad \dots (4)$$

For the quadratic case,  $D = \omega_e^2/4\omega_e x_e$  (Rees 1947), and since  $\alpha$  and  $r_e$  are constants, one can write equation (4) as

$$\log[\{\omega_e \pm (4\omega_e x_e V)^{\frac{1}{2}}\}/\omega_e] = -\alpha'r + \alpha'r_e, \quad \dots (5)$$

where  $\alpha' = 2.3026\alpha$

$$\text{i.e.,} \quad \log[\omega_e \pm (4\omega_e x_e V)^{\frac{1}{2}}] = -\alpha'r + \alpha'r_e + \log \omega_e.$$

If we replace  $-\alpha'$  by  $m$  and  $(\alpha'r_e + \log \omega_e)$  by  $c$ ,

$$\log[\omega_e \pm (4\omega_e x_e V)^{\frac{1}{2}}] = mr + c. \quad \dots (6)$$

Thus for  $r_{max}$  and  $r_{min}$  sides, one can write the expressions as

$$r > r_e, \quad \log[\omega_e - (4\omega_e x_e V)^{\frac{1}{2}}] = m_+ r_{max} + c_+ \quad \dots (7)$$

$$r < r_e, \quad \log[\omega_e + (4\omega_e x_e V)^{\frac{1}{2}}] = m_- r_{min} + c_- \quad \dots (8)$$

Or,

$$\log[\omega_e + (4\omega_e x_e V)^{\frac{1}{2}}] = m_+' r_{max} + c_+' \quad \dots (9)$$

$$\log[\omega_e - (4\omega_e x_e V)^{\frac{1}{2}}] = m_-' r_{min} + c_-' \quad \dots (10)$$

Alternatively, one can arrive at these relations from the expression of  $f$ , the half width of potential curves, involved in the RKR procedure for calculating the classical turning points of potential curves. For the quadratic case,  $f$  is given by (Vaidyan Santaram 1970a)

$$f = \left( \frac{\hbar}{8\pi^2 \mu c \omega_e x_e} \right)^{\frac{1}{2}} \ln \left[ \frac{\omega_e + (4\omega_e x_e V)^{\frac{1}{2}}}{\omega_e - (4\omega_e x_e V)^{\frac{1}{2}}} \right]^{\frac{1}{2}} \quad \dots (11)$$

But  $f = (r_{max} - r_{min})/2$ , so that equation (11) becomes

$$r_{max} - r_{min} = \left( \frac{\hbar}{8\pi^2 \mu c \omega_e x_e} \right)^{\frac{1}{2}} [\ln\{\omega_e + (4\omega_e x_e V)^{\frac{1}{2}}\} - \ln\{\omega_e - (4\omega_e x_e V)^{\frac{1}{2}}\}]$$

Therefore,

$$\left. \begin{aligned} \log[\omega_e + (4\omega_e x_e V)^{\frac{1}{2}}] &= m r_{max} + c \\ \log[\omega_e - (4\omega_e x_e V)^{\frac{1}{2}}] &= m r_{min} + c \end{aligned} \right\} \quad \dots (12)$$

Equations (7) and (8) or (9) and (10) are the general form of these equations.

Thus by using equations (7) and (8) or (9) and (10) one can find  $V$ -values corresponding to any  $r$ -value within the range of that p.e. curve provided the constants  $m$  and  $c$  are known. These constants can be determined with a knowledge of  $r$ -values evaluated by using RKR method, either by drawing a graph for  $\log [\omega_e \pm (4\omega_e x_e V)^{\frac{1}{2}}]$  vs.  $r$  or, by the method of least squares.

The accuracy of this method has been tested by the authors (1970b) in which true p.e. curves for several electronic states have been constructed using equations (7) and (8) and compared with the RKR data. The agreement was found to be good.

## 2.2 $E(v, K)$ cubic in $v + \frac{1}{2}$

For certain electronic states, it is not possible to represent the whole vibrational term system by a single quadratic in  $(v + \frac{1}{2})$ . But for such states, it can be divided into segments, where each segment consisting of a few vibrational levels, can be represented fairly accurately by suitable choice of  $\omega$  and  $\omega x$ . After such an adjustment, the method outlined in the preceding section can be employed. However, in order to make sure that the segment curve does coincide with the true curve, there must be at least three consecutive vibrational levels in such a segment.

## 3. METHOD

After finding energy values  $V(r)$  corresponding to different  $r$ -values, say with an interval of 0.01 Å for the upper and lower electronic states involved in that transition, one can plot a graph for  $[V_1(r) - V_2(r)]$  vs.  $r$ , over the significant range of  $r$ -values. From this graph, the  $r$ -centroids corresponding to different transitions  $v' \rightarrow v''$  for energy differences  $E_{v'} - E_{v''}$  can be directly read.

## 4. ILLUSTRATIONS

4.1 The  $r$ -centroids of second positive system of  $N_2$ 

Electronic states involved in this transition are  $C^3\pi_u$  and  $B^3\pi_g$ .  $B$  state can be represented adequately by a quadratic in  $(v+\frac{1}{2})$ , while for  $C$  state, it must be divided into two segments, one from  $v=0$  to 2 and other from  $v=2$  to 4. The RKR data for these states are taken from Jain (1964). The  $r$ -centroids obtained by this method is given in table 1, together with that of NJ. The deviation increases with increase of  $v$  and  $\Delta v$ .

Table 1. The  $r$ -centroids and wavelengths of  $N_2$  second positive system  
( $C^3\pi \rightarrow B^3\pi$ )

$v' \backslash v''$		0	1	2	3	4	5	6	7	8	9
0	a i)	1 183	1.148	1.116	1 087	1 061					
	ii)	1 182	1.148	1 116	1.086	1.058					
	b	3371.3	3576.9	3804.9	4059.4	4344					
1	a i)	1.229	1 189	1.154	1.122	1.094	1.067	1.043			
	ii)	1.228	1.189	1.154	1.122	1.092	1.065	1.039			
	b	3159.3	3339	3536.7	3755.4	3998.4	4269.7	4574.3			
2	a i)	1.287	1 235	1.194	1.160	1.128	1.100	1.073	1.049		
	ii)	1 280	1 234	1.195	1 160	1.129	1.099	1.072	1.046		
	b	2976.8	3136.0	3309.0	3500.5	3710.5	3943.0	4200.5	4490.2		
3	a i)		1.294	1 240	1.199	1.165	1.134	1.105	1.079	1 055	1.032
	ii)		1 287	1 241	1.202	1 166	1.135	1 106	1.079	1.054	1.032
	b		2962	3116.7	3285.3	3469	3671.9	3894.6	4141.8	4416.7	4723.3
4	a i)			1 298	1.244	1 203	1.169	1 138	1.110	1.084	1.060
	ii)			1 294	1.247	1.208	1 173	1.141	1.113	1.086	1.061
	b			2953.2	3104.2	3268	3446.0	3641.7	3857.9	4094.8	4355.0

a)  $r$ -centroid: i) Present work ii) Nicholls & Jarman (1956).

b) wavelength.

4.2 The  $r$ -centroids of first positive and Vegard-Kaplan bands of  $N_2$ 

As illustrated above, the  $r$ -centroids are calculated for  $B^3\pi_g \rightarrow A^3\Sigma_u^+$  and  $A^3\Sigma_u^+ \rightarrow X^1\Sigma_g^+$  transitions of  $N_2$ , and are tabulated in tables 2 and 4 respectively. In table 3,  $r$ -values by this new procedure are compared with that of NJ and the deviation is found to increase with increasing values of  $v$  and  $\Delta v$ .

Table 2. The *r*-centroids and wavelengths of N<sub>2</sub> first positive system  
( $B^3\pi \rightarrow A^3\Sigma$ )

$v'$	$v''$	0	1	2	3	4	5	6	7	8	9
0	a)	1.251	1.216	1.185							
	b)	10420									
1	a)	1.298				1.163					
	b)	8911.6									
2	a)	1.351	1.305	1.266							
	b)	7753.2	8722.3	9860							
3	a)	1.412	1.358	1.313	1.274						
	b)	6875.0	7620.2	8541	89599						
4	a)	1.485	1.420	1.366	1.320	1.281					
	b)	6185.2	6788.6	7503	98369.2	9362					
5	a)	1.577	1.493	1.427	1.373	1.328	1.288				1.167
	b)	5032.7	6127	46704.8	7386.6	8302	89133				
6	a)		1.585	1.501	1.435	1.381	1.335				
	b)		9592.9	6069.7	6623.6	7273.3	8047.4				
7	a)			1.594	1.509	1.443	1.389	1.343			
	b)			5553.7	6013.6	6544.8	7164.8	7896.4			
8	a)					1.517	1.451	1.397			
	b)					5959.0	6468.5	7059.0			
9	a)						1.526	1.459	1.405		
	b)						5906	08394.7	6967.8		
10	a)							1.535	1.467		
	b)							5854.4	6322.9		
11	a)								1.544	1.476	
	b)								5804.3	6252.8	
12	a)									1.553	1.485
	b)									5755.2	6185.2

a) *r*-centroids.

b) wavelengths.

Table 3. Comparison of  $r$ -centroids for  $N_2$  first positive bands (Present work with that of Nicholls & Jarman)

Band $v' \rightarrow v''$	$r_{v'v''}$	
	Present work	Nicholls & Jarman
0→0	1.251	1.255
0→1	1.216	1.222
0→2	1.185	1.193
1→4	1.163	1.173
5→9	1.167	1.177
1→0	1.298	1.297
2→0	1.351	1.346
3→0	1.412	1.403
4→0	1.485	1.469
5→0	1.577	1.552

Table 4. The  $r$ -centroids and wavelengths of Vegard-Kaplan bands of  $N_2$  ( $A^3\Sigma \rightarrow X^1\Sigma$ )

$v' \backslash v''$		3	4	5	6	7	8	9	10
0									
a)	1.236	1.256	1.275	1.295	1.315				
b)	2332.8	2461.6	2603.8	2760.6	2935.7				
1									
a)		1.243	1.263	1.282			1.322	1.343	1.366
b)		2377.5	2509.8	2655.5			2997.0	3197.5	3424.6
2									
a)			1.250	1.269	1.289				
b)			2424.2	2560.1	2710.1				

a)  $r$ -centroids, b) wavelengths.4.3 The  $r$ -centroids of CN red system

CN red system is of interest due to the doublet nature of the upper  $A^2\pi$  state. By using Morse function, it is not possible to represent these states, and hence NJ's method fails to give  $r$ -centroids for these two sets of transitions. However, by making use of the new procedure, it is possible to calculate  $r$ -centroids for the bands of both sub-systems, viz.  $A^2\pi_1 \rightarrow X$  and  $A^2\pi_{3/2} \rightarrow X$  and the values thus obtained are given in tables 5 and 6 respectively. Though for small values the difference between the  $r$ -centroids of the corresponding bands in the



two sub-systems is not much, it is appreciable for higher vibrational states. RKR values for classical turning points of these states are taken from Fallon *et al* (1962).

Table 5. The *r*-centroids and wavelengths of CN red system ( $A^3\Pi_1 \rightarrow X^2\Sigma^+$ )

$v'$ \ $v''$	0	1	2	3	4	5	6
0 a)	1.203	1.154					
b)	10933	14074					
1 a)	1.165	1.200					
b)	9148.3	11247					
2 a)	1.130	1.171					
b)	7876.4	9392.5					
3 a)	1.100	1.136					
b)	6927.6	8067					
4 a)	1.072	1.106	1.142				
b)	6191.7	7091	8272				
5 a)	1.046	1.078	1.112	1.148			
b)	5606.7	6332.2	7259	8485			
6 a)	1.022	1.052	1.084	1.118			
b)	5129.7	5730.2	6478.7	7435			
7 a)		1.028	1.058	1.090			
b)		5239.3	5858.2	6631.6			
8 a)			1.034	1.064	1.096		
b)			5347.5	5992.6	6792.5		
9 a)				1.040	1.070	1.102	
b)				5473.3	6133.0	6961	
10 a)				1.018	1.046	1.076	
b)				5043.1	5598.3	6279.4	
11 a)					1.024	1.052	1.082
b)					5155.7	5728.5	6432.7

a) *r*-centroids.

b) wavelengths

Table 6. The  $r$ -centroids and wevelengths of CN red system  
 $(A^2\pi_{3/2} \rightarrow X^2\Sigma^+)$

$v' \backslash v''$	0	1	2	3	4	5	6
0 a)	1.204	1.155					
b)	10970						
1 a)	1 165	1 210					
b)	9174.7						
2 a)	1.130	1.171					
b)	7898.6						
3 a)	1.098	1.136					
b)	6945.4						
4 a)	1 068	1.104	1.142				
b)	6206.1	7110					
5 a)	1.039	1.074	1.110	1.148			
b)	5618.8	6347.0	7273				
6 a)	1.011	1 046	1 080	1.116			
b)		5742.7	6494.1				
7 a)		1.018	1 052	1.086	1.122		
b)		5250.0	5871.3	6648.1			
8 a)			1.025	1.058	1.092		
b)			5354.1	6006.0	6809.2		
9 a)				1.032	1.064	1.099	
b)				5484.9	6146.8		
10 a)					1.039	1.071	
b)					5610.5	6293.7	
11 a)						1.046	1.078
b)							6448.3

a)  $r$ -centroids

b) wavelengths

## 5. GENERAL DISCUSSIONS

The relation connecting  $r$ -centroids and wavelengths, i.e.  $\bar{r}_{v',v''}$  increases or decreases as  $\lambda$  increases or decreases according as  $r_{e1} > r_{e2}$  or  $r_{e1} < r_{e2}$  is found to be true in all cases.

For both first and second positive systems for which comparison is possible, the deviation of the values of  $r$ -centroids calculated from NJ's (1956) method from those of new procedure increases with increasing  $v$  and  $\Delta v$  values. Naturally, this has to be attributed to the poor representation of Morse function for the

higher vibrational states. Hence it can be claimed that the new method yields more accurate values than those of NJ's.

Recently Krupenie & Benesch (1968) have shown that in the case of  $\text{CO}^+$ , *r*-centroids calculated by numerical integration method differs very much from that obtained by NJ's method for some bands in  $A \rightarrow X$  system. We investigated this system by using the present procedure and the results obtained are given in table 7 together with FC factors and *r*-centroids calculated by using numerical integration method.

Table 7. FC factors and *r*-centroids of  $\text{CO}^+ (A^2\pi \rightarrow X^2\Sigma^+)$

$v' \backslash v''$	0	1	2	3	4	5	6
0 a)	0.424-1	0.113	0.167	0.180	0.158	0.122	0.852-1
b) i)	1.177	1.201	1.227	1.253	1.281	1.310	1.342
ii)	1.178	1.202	1.227	1.253	1.280	1.309	1.339
1 a)	0.152	0.193	0.089-1	0.142	0.445-3	0.412-1	0.789-1
b) i)	1.159	1.186	1.210	1.237	1.263	1.291	1.321
ii)	1.161	1.184	1.207	1.270	1.263	1.289	1.317
2 a)	0.251	0.812-1	0.274-1	0.725-1	0.960-1	0.499-1	0.677-2
b) i)	1.144	1.167	1.191	1.216	1.242	1.268	1.296
ii)	1.145	1.167	1.205	1.217	1.240	1.218	1.299
3 a)	0.252	0.524-3	0.107	0.705-1	0.102-2	0.304-1	0.703-1
b) i)	1.130	1.152	1.173	1.199	1.223	1.249	1.276
ii)	1.130	1.147	1.177	1.197	1.239	1.250	1.273
4 a)	0.174	0.921-1	0.857-1	0.355-2	0.763-1	0.582-1	0.400-2
b) i)	1.115	1.137	1.159	1.182	1.206	1.230	1.256
ii)	1.115	1.146	1.159	1.158	1.207	1.227	1.264
5 a)	0.863-1	0.192	0.435-3	0.968-1	0.371-1	0.779-2	0.621-1
b) i)	1.101	1.123	1.144	1.166	1.189	1.213	1.238
ii)	1.101	1.125	1.143	1.170	1.188	1.224	1.238
6 a)	0.321-1	0.177	0.718-1	0.632-1	0.186-1	0.788-1	0.152-1
b) i)	1.088	1.108	1.130	1.150	1.174	1.197	1.211
ii)	1.088	1.110	1.123	1.153	1.162	1.199	1.214

a) FC factors (Krupenie & Benesch)

b) *r*-centroids: (i) Present work (ii) Krupenie & Benesch (1968).

In the case of  $\text{CO}^+$ , Morse function is a good approximation for both *A* and *X* states, as they can be represented adequately by a quadratic equation. Hence NJ's method based on *true* curve and Morse function would yield the same results.

From the table it is evident that the deviation of  $r$ -centroids based on NJ's method from the numerical integration procedure is appreciable only for bands whose FC factors are very small, in other words, the deviation is existing for unobservable bands. For the observed bands, where FC factors are large, there is a good agreement between the two. The deviation of  $r$ -centroids for the non-observed bands can be attributed to the small values of FC factors, and the consequent invalidity of the expression

$$r_{v'v''} = \frac{\int \psi_{v'} r^n \psi_{v''} dr}{\int \psi_{v'} r^{n-1} \psi_{v''} dr}, \quad n = 1, 2, \dots$$

which is one of the conditions to be satisfied for NJ's method. The  $r$ -centroids are of importance in the study of the variation of electronic transition moment with  $r$ . For this study the  $r$ -centroids for the observed bands only need be known along with the experimental band intensities. These can be obtained more easily by the present method with sufficient accuracy.

## 6. CONCLUSION

Thus this new procedure gives a rapid as well as an accurate means to evaluate  $r$ -centroids of diatomic molecules, even for transitions where there is electronic splitting. However, this method is limited to such transitions for which RKR data is available for both upper and lower states.

## REFERENCES

- Fallon R. J., Vanderslice J. T. & Cloney R. D. 1962 *J. Chem. Phys.* **37**, 1097.  
 Jan D. C. 1964 *Proc. Phys. Soc. A*, **83**, 17  
 Krupenie P. H. & Benesch W. 1968 *J. Res. Nat. Bur. Stds. A*, **72**, 495.  
 Nicholls R. W. & Jarmain W. R. 1956 *Proc. Phys. Soc. A*, **69**, 253.  
 Rees A. L. G. 1947 *Proc. Phys. Soc. A*, **59**, 998.  
 Vaidyan V. K. & Santaram C. 1970a *J. Phys. B. (Proc. Phys. Soc.)* **3**, 16.  
 1970b *J. Chem. Phys.* **52**, 3068.

## On motions of test-particles in Kerr metric

By K. D. KROBI

*Mathematical Physics Forum, Cotton College, Gauhati-1, India*

(Received 16 March 1970—Revised 23 June and 16 July 1970)

Motions of test-particles in the  $\theta = \pi/2$  plane of the Kerr metric of a rotating body have been studied here under some specific conditions. Corrections have also been introduced for their spins.

### INTRODUCTION

A particular solution of Einstein's field equations of great interest is Kerr solution (Kerr 1963) which is the only exact solution describing the field exterior to some finite rotating body. The Kerr metric can be written in Schwarzschild-like coordinates (Boyer & Landquist 1967), i.e. coordinates such that when the angular momentum parameter is zero one gets the Schwarzschild metric. Thus we have

$$ds^2 = -(r^2 + \alpha^2 \cos^2 \theta)(r^2 - 2mr + \alpha^2)dr^2 - (r^2 + \alpha^2 \cos^2 \theta)d\theta^2 \\ - [r^2 + \alpha^2 + 2mr\alpha^2 \sin^2 \theta / (r^2 + \alpha^2 \cos^2 \theta)] \sin^2 \theta d\phi^2 \\ - [4mar \sin^2 \theta / (r^2 + \alpha^2 \cos^2 \theta)] dt d\phi + [1 - 2mr / (r^2 + \alpha^2 \cos^2 \theta)] dt^2 \quad \dots (1)$$

Boyer & Price (1965) have shown that "one of the parameters in Kerr's solution (equation 1) can plausibly be related to the angular momentum per unit mass of a uniformly rotating sphere, the other parameter being a measure of the mass of the sphere". Hernandez (1968) has also found a case such that in the Newtonian limit the rotating body in (1) is a uniform density sphere with a moment of inertia  $= 2/5ma^2$  and angular momentum  $= -m\alpha$ .

We propose to study in this paper the motions of test-particles in the  $\theta = \pi/2$  plane of the Kerr metric of a rotating body represented by (1) under some specific conditions. Corrections would also be introduced for their spins.

### ORBITAL EQUATION IN $\theta = \pi/2$ PLANE

Upto second power in  $\alpha$  and first power in  $m/r$ , the Kerr metric (1) is reduced to the form

$$ds^2 = - \left( 1 + \frac{2m}{r} - \frac{\alpha^2}{r^2} \sin^2 \theta \right) dr^2 - (r^2 + \alpha^2 \cos^2 \theta) d\theta^2 - \sin^2 \theta (r^2 + \alpha^2) d\phi^2 \\ - \frac{4m\alpha \sin^2 \theta}{r} dt d\phi + \left( 1 - \frac{2m}{r} \right) dt^2 \quad \dots (2)$$

The approximations made restricts the consideration to distances  $r \gg m$  and to cases where  $\alpha < r$ .

Corresponding to (2), the values of  $g^{11}$ ,  $g^{22}$ ,  $g^{33}$ ,  $g^{34}$  and  $g^{44}$  are obtained. They are

$$\begin{aligned} g^{11} &= - \left( \frac{2m}{r} + \frac{\alpha^2}{r^2} \sin^2 \theta \right) \\ g^{22} &= - \frac{1}{r^2} \left( 1 - \frac{\alpha^2}{r^2} \cos^2 \theta \right) \\ g^{33} &= - \frac{1}{r^2 \sin^2 \theta} \left( 1 - \frac{\alpha^2}{r^2} \right) \quad \dots (3) \\ g^{34} &= \frac{2m\alpha}{r^3} \\ g^{44} &= \left( 1 + \frac{2m}{r} \right) \end{aligned}$$

Now, from (2) and (3), we can obtain the 3-index symbols and write out the  $\theta$ -,  $\phi$ - and  $t$ -equations. The  $\theta$ -equation is

$$\begin{aligned} \frac{d^2\theta}{ds^2} + \frac{\alpha^2 \sin 2\theta}{2r^4} \left( \frac{dr}{ds} \right)^2 + \frac{2}{r} \left( 1 - \frac{\alpha^2}{r^2} \cos^2 \theta \right) \frac{dr}{ds} \frac{d\theta}{ds} - \frac{1}{2} \frac{\alpha^2}{r^2} \sin 2\theta \left( \frac{d\theta}{ds} \right)^2 \\ - \frac{1}{2} \left( 1 + \frac{\alpha^2}{r^2} \sin^2 \theta \right) \sin 2\theta \left( \frac{d\phi}{ds} \right)^2 - \frac{2m\alpha}{r^3} \sin 2\theta \frac{d\phi}{ds} \frac{dt}{ds} = 0. \quad \dots (4) \end{aligned}$$

Let us suppose that the test-particle moves initially in the  $\theta = \pi/2$  plane. Then  $d\theta/ds = 0$ , and  $\cos \theta = 0$  initially, so that  $d^2\theta/ds^2 = 0$ . The particle therefore continues to move in this plane, and we may simplify the  $\phi$ - and  $t$ -equations by putting  $\theta = \pi/2$  throughout.

Then,  $\phi$ - and  $t$ -equations in  $\theta = \pi/2$  plane are

$$\frac{d^2\phi}{ds^2} + \frac{2}{r} \left( 1 - \frac{\alpha^2}{r^2} \right) \frac{dr}{ds} \frac{d\phi}{ds} - \frac{2m\alpha}{r^4} \frac{dr}{ds} \frac{dt}{ds} = 0 \quad (5)$$

$$\frac{d^2t}{ds^2} - \frac{2m\alpha}{r^2} \frac{dr}{ds} \frac{d\phi}{ds} + \left( 1 + \frac{2m}{r} \right) \left( \frac{2m}{r^2} \right) \frac{dr}{ds} \frac{dt}{ds} = 0 \quad (6)$$

For  $\alpha = 0$ , the solutions of (5) and (6) are

$$r^2 \frac{d\phi}{ds} = h_0 \quad (7)$$

$$\left(1 - \frac{2m}{r}\right) \frac{dt}{ds} = c_0 \quad \dots (8)$$

where  $h_0, c_0$  are constants of integration. We now substitute from (7) and (8) in the correction terms of (5) and (6) and obtain the solutions

$$\frac{d\phi}{ds} = \frac{h}{r^2} \left(1 - \frac{2m\alpha}{r} - \frac{c_0}{h} - \frac{\alpha^2}{r^2} \frac{h_0}{h}\right) \quad \dots (9)$$

$$\frac{dt}{ds} = c \left(1 + \frac{2m}{r} - \frac{2m\alpha}{3r^3} \frac{h_0}{c}\right) \quad \dots (10)$$

where  $h, c$  are constants of integration. Writing  $h \approx h_0$  and  $c \approx c_0$  in the correction terms in (9) and (10), we obtain finally

$$\frac{d\phi}{ds} = \frac{h}{r^2} \left(1 - \frac{2m\alpha}{r} - \frac{c}{h} - \frac{\alpha^2}{r^2}\right) \quad \dots (11)$$

$$\frac{dt}{ds} = c \left(1 + \frac{2m}{r} - \frac{2m\alpha}{3r^3} \frac{h}{c}\right) \quad \dots (12)$$

Hence, in the  $\theta = \pi/2$  plane, (2), (11) and (12) give in the usual manner the orbital equation for a test-particle

$$\begin{aligned} \frac{d^2u}{d\phi^2} + u = \frac{m}{h^2} \left\{ 1 + 2\alpha \frac{c}{h} (c^2 - 1) \right\} + \frac{3\alpha^2}{h^2} (c^2 - 1)u \\ + 3m \left( 1 - \frac{8}{3} \alpha \frac{c}{h} \right) u^2 - 4\alpha^2 u^3 \end{aligned} \quad \dots (13)$$

where  $u$  has been substituted for  $1/r$ .

#### ADVANCE OF PERIHELION

The solution of (13), neglecting all terms on the right side except the first, is

$$u = \frac{m}{h^2} \left\{ 1 + 2\alpha \frac{c}{h} (c^2 - 1) \right\} \{1 + e \cos(\phi - \omega)\}. \quad \dots (14)$$

where  $e$  is the eccentricity of the orbit. Now, substituting from (14) on the right side of (13) and finding particular integrals for the terms containing  $\cos(\phi - \omega)$ , the final solution is

$$\begin{aligned} u = \frac{m}{h^2} \left\{ 1 + 2\alpha \frac{c}{h} (c^2 - 1) \right\} \{1 + e \cos(\phi - \omega)\} + \frac{3m\alpha^2 (c^2 - 1)e}{2h^4} \phi \sin(\phi - \omega) \\ + \frac{3m^3 e}{h^4} \left\{ 1 + 4\alpha \frac{c}{h} (c^2 - 1) - \frac{8}{3} \alpha \frac{c}{h} \right\} \phi \sin(\phi - \omega) \\ - \frac{6m^3 \alpha^2 e}{h^4} \phi \sin(\phi - \omega) - \frac{3m^2 \alpha^2 e^3}{2h^4} \phi \sin(\phi - \omega). \end{aligned} \quad \dots (15)$$

This gives for the advance of perihelion per revolution

$$\delta\omega = 2\pi \left[ \frac{3}{2} \frac{\alpha^2}{h^2} (c^2-1) + \frac{3m^2}{h^2} \left\{ 1 + 2\alpha \frac{c}{h} (c^2-1) - \frac{8}{3} \alpha \frac{c}{h} \right\} - \frac{6m\alpha^2}{h^4} - \frac{3}{2} \frac{m^2\alpha^2 c^2}{h^4} \right]. \quad (16)$$

If the test-particle possesses spin angular momentum  $S$  parallel to the angular momentum of the central rotating body, then following Corinaldesi & Papapetrou (1951) and Das (1957), we obtain for small  $S$  from (16)

$$\delta\omega = 2\pi \left[ \frac{3}{2} \frac{\alpha^2}{h^2} (c^2-1) + \frac{3m^2}{h^2} \left\{ 1 + 2\alpha \frac{c}{h} (c^2-1) - \frac{8}{3} \alpha \frac{c}{h} \right\} - \frac{6m^2\alpha^2}{h^4} - \frac{3}{2} \frac{m^2\alpha^2 c^2}{h^4} \right] - \frac{6\pi S m^2}{E h^3} \quad \dots (17)$$

where  $E$  is the total energy of the test-particle.

#### DEFLECTION OF MASSLESS PARTICLES

For massless particles such as photons, gravitons (Synge 1960) and neutrinos, both  $h$  and  $c$  tend to infinity but  $c/h$  is finite. For this case, (13) is reduced to the form

$$\frac{d^2u}{d\phi^2} + u = 2m\alpha \frac{c^3}{h^3} + 3\alpha^2 \frac{c^3}{h^2} u + 3m \left( 1 - \frac{8}{3} \alpha \frac{c}{h} \right) u^2 - 4\alpha^2 u^3 \quad \dots (18)$$

The solution of this equation, neglecting all terms of the right side, is

$$u = \cos \phi / R \quad \dots (19)$$

Now, substituting from (19) on the right side of (18) and finding particular integrals for the different terms, the final solution is

$$\begin{aligned} u = 1/r = 2m\alpha \frac{c^3}{h^3} + \frac{\cos \phi}{R} + \frac{3\alpha^2 c^2}{2Rh^2} \phi \sin \phi \\ + \frac{m}{R^2} \left( 1 - \frac{8}{3} \alpha \frac{c}{h} \right) (\cos^2 \phi + 2 \sin^2 \phi) \\ - \frac{\alpha^2}{R^3} \left\{ \frac{3}{2} \phi \sin \phi + \frac{3}{8} \cos \phi - \frac{1}{4} \cos^3 \phi \right\} \quad \dots (20) \end{aligned}$$

The total deflection of the track of a massless particle is then given by

$$\psi = 2 \left( \frac{R}{r_{\phi \rightarrow \pi/2}} \right) = 2 \left\{ 2m\alpha \frac{c^3}{h^3} + \frac{3}{4} \alpha^2 \frac{c^2}{h^2} \pi + \frac{2m}{R} \left( 1 - \frac{8}{3} \alpha \frac{c}{h} \right) - \frac{3\alpha^2}{4R^2} \pi \right\} \dots (21)$$



If, however, the massless particle possesses spin angular momentum  $S$  parallel to the angular momentum of the (gravitating) rotating body, then, following Corinaldesi & Papapetrou (1951) again, we obtain from (21)

$$\psi = 2 \left\{ 2m\alpha \frac{c^3}{\hbar^3} + \frac{3}{4} \alpha^2 \frac{c^2}{\hbar^2} \pi + \frac{2m}{R} \left( 1 - \frac{8}{3} \alpha \frac{c}{\hbar} \right) - \frac{3\alpha^2}{4R^2} \pi \right\} \left( 1 - \frac{S}{2RE} \right) \quad \dots (22)$$

where  $E$  is the energy of the particle. Since the spin angular momenta of a photon, a graviton and a neutrino are, respectively  $\hbar$ ,  $2\hbar$  and  $\frac{1}{2}\hbar$ , equation (22) shows that for the same values of  $c/\hbar$ ,  $E$  and  $R/\psi$  will be the least for a graviton and greatest for a neutrino.

But for a photon, graviton or neutrino with the spin parallel to their velocities in the  $\theta = \pi/2$  plane,  $\psi$  in this plane is not affected by the spin (Corinaldesi & Papapetrou).

#### ACKNOWLEDGEMENT

Author is grateful to the referee of this paper for suggesting substantial improvements.

#### REFERENCES

- Boyer R. H. & Lindquist R. J. 1967 *J. Math. Phys.* **8**, 265.  
 Boyer R. H. & Price T. G. 1965 *Proc. Camb. Phil. Soc.* **61**, 531.  
 Corinaldesi E. & Papapetrou A. 1951 *Proc. Roy. Soc.* **209**, 259.  
 Das A. 1957 *Prog. Theo. Phys.* **17**, 373.  
 Kerr R. P. 1963 *Phys. Rev. Letters* **11**, 327.  
 Hernandez W. C. 1968 *Phys. Rev.* **167**, 1180.  
 Synge J. L. 1960 *Relativity, The General Theory* 228.

## Generation and properties of multilevel pseudo-random sequences

By N. B. CHAKRABORTI

*Department of Electronics and Electrical Communication Engineering,  
Indian Institute of Technology, Kharagpur, West Bengal*  
and

A. K. MUKHERJEE

*Institute of Radio Physics and Electronics, 92 Acharya Prafulla Chandra Road,  
Calcutta-9, West Bengal. (Received 16 January 1970)*

In this paper generation and properties of multilevel sequences are discussed. The use of phase logic for generating RF multiphase-pseudo-random sequences is described. Application of these codes in communication and schemes for ternary counting and binary-ternary conversion are presented.

### INTRODUCTION

There has been considerable interest in recent years in binary quasi-random sequences with particular reference to their application in radar, communication systems and automatic error-correction circuits.

Pseudo-random sequence (prs) is so-called as it has some important characteristics in common with random noise. These are (i) a complicated looking structure which makes a part of the waveform indistinguishable from a sampled function of noise, (ii) nearly zero average value over a specified period, (iii) a sharp auto-correlation function.

But such sequences are better suited for application in that (i) they can be generated by a perfectly deterministic process, and (ii) the peak factor can be made much lower than that of random noise.

When the sequences are made of presence or absence of a pulse or the positive and negative pulse, or any other set of two distinct states then we call it a binary prs. In multilevel prs similarly, we must have larger number of states which may be pulses of different amplitude, sine or cosine functions with different phases or frequencies or any other recognizable parameters.

It has been suggested (Briggs 1966) that ternary prs can be generated by addition of a binary sequence with its transformed version. Sequences thus obtained are seen to have a spread out correlation function.

In the present paper, techniques of generation of multilevel sequences, which are based on shift-register techniques as employed for generating binary sequences, are described. The two state flip-flops are replaced by multistate devices. The

logic remains still modular but the moduli may be prime or non-prime and take on values of 3, 4, 5, etc. Multistate devices where states signify specified amplitudes are difficult to realize if the number of states exceeds 3. However, if the states are made to signify the phases of a carrier then multistate devices and logical units (e.g., modular adder, multiplier) can quite easily be realized.

Generation of multilevel sequences both on amplitude and phase basis are considered in Section 1. Properties of such sequences are also discussed here. Realization of such sequences both on amplitude and phase basis is discussed in Section 2. Application of such codes in communication and other special purposes and the advantages arising out of their use are discussed in Section 3.

## SECTION 1

### *Multilevel Sequences and Their Properties*

Multilevel sequences having  $n$  levels can be generated, using  $s$ -stage multilevel shift register (Taub 1968) with proper feedback (according to the generating polynomial) to the first stage, which is the modulo- $n$ -sum (Pugh 1967) of the outputs of the appropriate stages multiplied by 1, 2, ... or  $n$ .

The maximum length which can be generated in an  $n$ -level generator is  $L = n^s - 1$ , where  $n$  is the number of levels in the sequence and  $s$  (determining the length) is the degree of the generating polynomial. The polynomial chosen must be irreducible. To find out the irreducible polynomials of a given degree one has only to eliminate the polynomials which can be factorized into polynomials of lower degree. The irreducible polynomials for prime modulo 3, 5 and 7 have been tabulated by Church (1935). It has to be mentioned that an irreducible generating polynomial does not necessarily lead to a maximal length sequence. In other words, the irreducible character is a necessary but not a sufficient condition for generating sequences of maximal length.

The polynomials of modulus-3 give rise to ternary sequences and the polynomials are listed by Elspas (1959). The sequences obtained with these polynomials are presented here in table 1.

To understand the operation of the generator one may consider for example, a ternary function  $D^3 \oplus_3 2D^2 \oplus_3 I = 0$  with the initial condition 012. Here one must

keep in mind that addition and multiplication obey modular logic. With such an arrangement the multistate device will successively go through the states 012, 201, 220, 222, 022, 002, 100, 010, 101, 210, 121, 112, 211, 021, 102, 110, 111, 011, 001, 200, 020, 202, 120, 212, 221, 122, 012, ... Thus after 26 changes the shift registers have come back to the original 012 state and again the sequence is repeated. Thus at the output one will have a repetitive sequence given in the table below.

Table 1

generating polynomial	length	sequences obtained
1. $D^3 \oplus_3 D^2 \oplus_3 2D \oplus_3 1$	26	01200221222010210011211102
2. $D^3 \oplus_3 2D \oplus_3 1$	26	01221202001110211210100222
3. $D^2 \oplus_3 2D^2 \oplus_3 1$	26	01211201110020212210222001
4. $D^3 \oplus_3 2D^2 \oplus_3 D \oplus_3 1$	26	01222120101100211121020220
5. $2D^3 \oplus_3 2D^2 \oplus_3 1$	13	0121001011122, 0212002022211
6. $2D^3 \oplus_3 D \oplus_3 1$	13	0121022111010, 0212011222020
7. $D^3 \oplus_3 D^2 \oplus_3 D \oplus_3 2$	13	0120022122201, 0210011211102
8. $2D^3 \oplus_3 D^2 \oplus_3 D \oplus_3 1$	13	0120201112110, 0210102221220

It is observed that after 13 bits the sequence is an exact repetition of the earlier bits with positions of 1 and 2 interchanged. In the last four polynomials the sequence repeats itself after 13 bits.

If the value of  $s$  is increased to 4, the length of the sequence corresponding to an irreducible generating polynomial may be 5, 10, 16, 20, 40 and 80, i.e., there may be 16 sequences of length 5, 8 sequences of length 10, 5 sequences of length 16, 4 sequences of length 20, 2 sequences of length 40, or a single sequence of length 80. But if the polynomial chosen is reducible then we will have sequences of unequal length depending on the initial conditions of the registers.

When the sequences generated are not of maximal length i.e.,  $L \neq n^s - 1$  all the possible permutations of the states do not occur. The length then obtained corresponds to a subset of the permutation and depends on the initial conditions. The subsets are in general closed on themselves and mutually exclusive.

So far we were discussing the sequences derived from generating polynomials corresponding to prime modulus. But in case of sequences obtained from non-prime modulus such as 'quaternary' or 'sextic' sequences (i.e. the sequences which consist of 4 or 6 different states) even if one chooses the prime polynomial, the length obtained is not equal to  $(n^s - 1)$ , the sequence breaks up into several subsequences depending on the initial conditions.

Table 2 shows the quaternary sequences obtained corresponding to generating polynomials listed. The maximum length for polynomial of degree 3 is 14. There are 4 sequences of length 14 and a single sequence of length 7, totalling 63 possible states. The sum of the lengths of all the possible subsequences of a given generating polynomial is equal to  $n^s-1$ .

Table 2

generating polynomial	length	sequences obtained
$D^3 \oplus_4 D \oplus_4 I$	14	00131230231103, 00313210213301, 01221112120331, 032233332320113, 0022202
	7	
$D^3 \oplus_4 2D \oplus_4 I$	14	01221310100333, 03223130300111, 02113212031121, 02331232013323, 0022202
	7	
$D^3 \oplus_4 3D^2 \oplus_4 I$	14	01211302123112, 03223102321332, 00101312210333, 00303132230111, 0020222
	7	
$D^3 \oplus_4 D^2 \oplus_4 I$	14	01231300103312, 03213100301132, 01330212111221, 03110232333223, 0020222
	7	
$3D^3 \oplus_4 D \oplus_4 I$	14	01223330300313, 03221110100131, 01132302133212, 03312102311232, 0022202
	7	
$3D^3 \oplus_4 3D \oplus_4 I$	14	01223132320311, 03221312120133, 00111230211301, 00333210233103, 0022202
	7	
$3D^3 \oplus_4 D^2 \oplus_4 I$	14	01233300301332, 03211100103112, 01130232313221, 03310212131223, 0020222
	7	
$3D^3 \oplus_4 3D^2 \oplus_4 I$	14	01213302321132, 03231102123312, 00101112230131, 00303332210313, 0020222
	7	

An observation of the sequences shows that the 4 sequences of length 14 corresponding to a fixed polynomial consist of two pairs, a sequence in a pair being obtainable by interchanging the positions of one and three in the other.

Similarly the maximum length for polynomials of degree 4 is 30. Some of these are symmetric with 1 and 3 positions interchanged and others are asymmetric.

### *Properties*

The first point to note is that the sequences have zero or nearly zero average value over a specified length. This is true in case of a prime modulus. This property follows from the fact that the length obtained is the permutation of all the possible sets of states excepting 000 ... 0, the different states occur equal numbers of times to enable the average value to be zero. But in case of non-prime modulo the sequences do not contain all such permutation and so the average value is in general not equal to zero.

The modulo sum of two members of such sequences gives rise to another sequence whether the sequences are generated corresponding to a polynomial of prime or non-prime modulus. The sequences thus obtained are the shifted version of the sequence or its conjugate (*i e.*, the same sequence with 1 or 2 position interchanged in case of ternary and 1 and 3 position interchanged in quaternary). This is in general true for any shift-register generated sequence.

Considering the aperiodic auto-correlations of the sequences of length 13, we see that the side-lobes are 1/8th of the peak. The periodic auto-correlations of such sequences are also found to be of the same character. The cross correlation properties of such sequences are found also to be very good. Unfortunately, however, the correlation properties of sequences of larger length are not that good. This is true for sequences generated corresponding to polynomial of non-prime modulo. They are good enough to be used in connection with correlation detection method. Thus generally, we can say that correlation properties of the multilevel prs's are same as that of binary prs's but the ternary sequences of length 13 have the unique properties of a correlation as described earlier and they may be classified as optimum correlation (Golomb & Scholtz, 1965) ternary prs's. This correlation output is shown in figure 1.

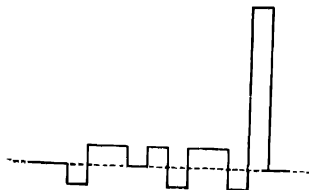


FIGURE 1. Digital matched filter output of a 13 bit ternary prs with digital delay.

The power spectrum of the multilevel prs is of the same nature as that of the binary prs. The minima will occur at a frequency equal to the multiple of the pulse repetition frequency (prf). The first maximum occurs at  $f/k$ , where  $f$  is the prf and  $k$  is the number of bit in the sequence. The other maxima occur at  $\left(\frac{2k+1}{2}\right)f$  and  $k = 1, 2, \dots$

### Error Probabilities in Ternary Decoding

In ternary coding on amplitude basis the three states are 0, 1, and  $-1$ . The decision circuit will include a threshold element with a level of  $|a|$ . The output will be recognised as 1, if input exceeds  $a$  and  $-1$  if the input is less than  $-a$  and otherwise as zero (i.e., it lies between  $-a$  and  $+a$ ). When a zero is sent an error would occur if  $|n_o|$  is greater than  $a$  where  $n_o$  is the inphase component of noise. Similarly if 1 [or  $-1$ ] is sent the error would occur if  $(S+n_o) < a$  [or  $(n_o-S) > -a$ ], where  $S$  is the signal component. If the *a priori* probabilities of the states are represented as  $p(0)$ ,  $p(1)$  and  $p(-1)$  the error probability is

$$P_e = p(0) p_{e(0)} + p(1) p_{e(1)} + p(-1) p_{e(-1)}$$

where  $p_{eA}$  is the error probability when  $A$  is sent.

Now

$$p_{e(1)} = \frac{1}{\sqrt{2\pi}\sigma} \left[ \int_{-\infty}^0 e^{-x^2/2\sigma^2} dx - \int_0^{S-a} e^{-x^2/2\sigma^2} dx \right].$$

$$p_{e(-1)} = p_{e(1)}$$

$$p_{e(0)} = 1 - \frac{2}{\sqrt{2\pi}\sigma} \int_0^a e^{-x^2/2\sigma^2} dx.$$

In figure 2 the variation of error probability with SNR is plotted for different values of the relative threshold  $a/S$ .

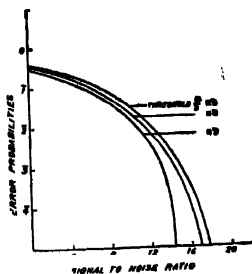


FIGURE 2. Error probabilities of ternary de-coding.

## SECTION 2

*Realization of Such Sequences*

For generating a ternary sequence the same ideas as employed in the case of binary are used. The block diagram of such a system is shown in figure 3. Here  $D$  represents the three level shift register element and  $\bigoplus_3$  represents the mod 3 adder. The multiplying units are represented by  $\overline{x1}$  or  $\overline{x2}$ .

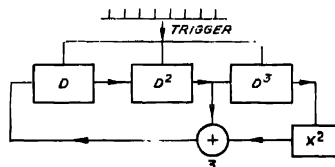


FIGURE 3. Block diagram of 3 level prs generator.

In the diagram the logic is set according to the generating polynomial  $D^3 \bigoplus_3 2D^2 \bigoplus_3 I = 0$  initial condition like 012, 121, 211, or any other permissible set is forced on the ternary shift register. The output of any of the shift register or the mod 3 adder will give the specified sequence.

In general, sequences we require circuits with more than three stable states. These circuits are quite difficult to build and the multi-level logic circuits are not available. So one has to take resort to three or multiphase systems. For these purpose one has to establish equivalents of shift register, multiplier and modulo adder.

A direct method of generating pseudo-random phase shift sequences is to employ rf equivalents to the shift register element or the delay element, the modulo- $p$ -adder and modulo- $p$ -scalar multipliers, and interconnect them according to desired feedback logic. The shift register element would consist of a synchronised oscillator at a frequency of (either a  $n$ -phase oscillator or a subharmonic oscillator of order  $1/n$ ) to which a gated rf input is applied (the duration of the gates (gating time) must be such as to ensure that the phase of the oscillator is locked to the phase of the input after the period of gating). The states or levels here correspond to the different possible phases (mod  $2\pi$ ). The mod- $n$  adder would sum the phases of the inputs. For two inputs this is achieved by multiplying the two inputs.

The inputs and outputs of any element are capable of being at any time in any one of the  $n$  states represented by the digits 0, 1, 2, ...,  $n-1$ . The operations involved are synchronous i.e., the stored digits are forced to change at the same



time as in any clocked system. Ordinarily, the time separation between any two possible transitions is fixed signifying that the clock rate is fixed. There are however, situations when variable prf may be used with profit.

The behaviour of a given linear sequential network of the above type can be described in terms of the associated transfer matrix and the state diagram. The length of the cycle in a given network can be determined from the characteristic polynomial associated with the transfer matrix. One has to find the smallest integer  $k$  such that the characteristic polynomial divides  $X^k - 1$  without a remainder.

The block diagram of a shift register element is shown in figure 4. The input frequency is multiplied 4 times and this is mixed with a frequency which is thrice that of the input. The difference frequency is taken out after passing through a filter. The input is gated and fed to a synchronous oscillator which may be a subharmonic oscillator of order  $1/n$  and can have  $n$  different phases. The phase of the sync. oscillator will be locked to that of the input phase if the input voltage is adequate, the switching time being dependent on input voltage and circuit  $Q$ . It is considered advisable to keep the circuit  $Q$  low during the period of switching and otherwise quite high.

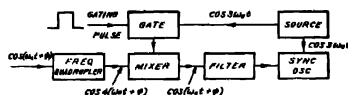


FIGURE 4. RF shift register for three phase system :—Unit phase shift for each circulation.

In multiphase systems multiplication means change of phase. Multiplication by 0 means that the component is absent, by 1 means it remains the same, by 2 means a phase change of  $2\pi/n$ , and so on. This can be incorporated only by extending the idea of shift register as shown in block diagram (figure 5).

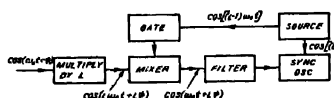


FIGURE 5. Phase multiplier :—Phase of the output  $L$  times the phase of the input.

The  $S$ -ary sequence is multiplied by  $L = 2, 3, \dots$  or  $n$  according to the requirement and mixed with a signal of frequency  $(L-1)\omega t$ . The difference frequency is selected and is fed to the sub-harmonic oscillator. The output of the oscillator will be in same phase as the input to it if the conditions discussed with shift-register are satisfied.

Another basic circuit of importance is the modulo addition circuit, block diagram of which is shown in figure 6. Here the product, of the two inputs  $\cos(\omega_0 t + \phi_1)$  and  $\cos(\omega_0 t + \phi_2)$  is taken and is mixed with a signal of frequency  $\omega_0$ . The output signal phase will be equivalent to the signal whose phase is the sum of the two phases. As the phases are distributed in an equispaced closed field, the sum follows modular logic.

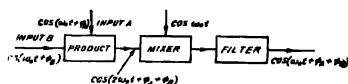


FIGURE 6. Phase adder (modulo) :— The output r.f. carrier phase equivalent to the sum of the two input signal phases.

Now these basic blocks can be connected in the same fashion as stated earlier corresponding to the generating polynomial and we will obtain the desired sequence.

To generate polyphase codes discussed by Frank (1963), one can use the mod- $p$  adder described above in combination with a shift-register in a feedback arrangement. For example if the code is 0,0,0,0; 0,1,2,3; 0,2,0,2; 0,3,2,1; one recognises that it is required to introduce phase advance per bit in the different blocks of length four of amount  $\frac{n}{p} \frac{2\pi}{p}$  for the  $n$ th group. This can be achieved if one of the two inputs to mod-4 adder is obtained from a phase shift type ring counter, the other input being the output of the shift register.

The multi-phase output can, if desired, be modified into multilevel output by multiplying the multiphase voltage with a voltage having selected reference and passing the output through a low pass filter. For example in a ternary system if the phases of the outputs are  $0^\circ$ ,  $120^\circ$ ,  $240^\circ$ , then multiplication by a voltage at a reference phase of  $90^\circ$  will give outputs proportional to 0, 1,  $-1$ .

### SECTION 3

#### *Use of Multilevel Ternary PR Codes for Communication*

Multilevel prs may be employed in any pulse digital modulation system by replacing the single pulse or state by the coded sequence. The additional unit required is a filter matched to the particular sequence.

#### *PCM*

In case of pulse code modulation the analog signal is first converted into a ternary code and then these ternary codes are used as the initial condition of the sequence generator. For analog digital conversion, two types of systems

which are in fact direct extensions of the concepts involving in binary Analog/Digital converter have been found suitable.

In the first system analog signal is used to width modulate a pulse. The greater the amplitude of the sample of the analog signal larger is the width of the pulse. This width modulated pulse is now used to gate a train of clock pulses. Larger the width greater is the number of clock pulses allowed to pass. The number of clock pulses are counted in a ternary system.

The ternary counter is composed of a ring counter of order three. When the last stage of the ring counter is changing from 1 to 0 then only it can change the state of the following ring counter.

The block diagram of the system is shown in figure 7. If  $A_j$  of the system is ON then we will have a 'zero' in the position corresponding to the value of  $j$ .

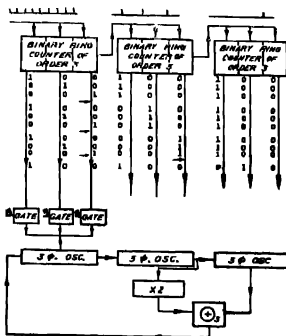


FIGURE 7. A ternary counter.

If  $B_j$  is ON we will have an 'one' in the position denoted by suffix  $j$  and if  $C_j$  is ON we will have a 'two' in the position of the suffix. As an example let us consider 19. Here looking into the ring counter we note that  $B_1 A_2 C_3$  are ON, which can be represented by the ternary number 201. Now these initial conditions can be fed to the shift register generator.

In the other system we must have an idea of the amplitude of the signal. This gives us the knowledge about the digit of pulse the code consists of. For simplicity of discussion let us think that the maximum amplitude is less than 27.

The block diagram of the system is shown in figure 8. The input is first divided by 9 and this is fed to a three state device. The output of the three state device should correspond to the amplitude of the input both qualitatively

and quantitatively. The output is subtracted from the input of the three state device and it is divided by 9 and applied to another three state device. The

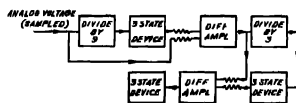


FIGURE 8. Alternative form of ternary counter.

same method is followed in the last stage also, and we get the state of the device as the code corresponding to the amplitude. This may similarly be used as an initial condition of the sequence generator. If the maximum amplitude is more than 27 we have to increase the number of stages accordingly.

### *Binary ternary conversion*

Since most present day data systems use binary mode, a binary to ternary converter would be very useful. At the moment the only technique available is to decode the binary/ternary code and then encode in ternary/binary code.

The decoding scheme is just as in binary. Here we have to select the weighted maximum and then add them up to get the amplitude back.

### *PPM*

Ternary pr codes of length 13 are seen to have a high resolution in time. such codes are useful for ranging. To obtain PPM signal the analog signal is converted into quantised sample of amplitude and these are used to position modulate a series of pulses. The position modulated pulses can be used to trigger the prs generator. Thus the starting point of the sequence will now be proportional to the amplitude of the sample.

The function of the receiver is to decide from the correlator output about the starting time of the pulse.

### *M-ary*

The sequences discussed earlier have little or no cross correlation if the integral is carried over the proper time period. In M-ary modulation one of the  $M$  alternative sequences is transmitted at a given time according to the data. The receiver compares the output of all  $M$  cross correlators and decides. The data signals in such cases are converted into PCM and the code is used as initial condition of the sequence generator. The receiver uses matched filter technique and finds out the maximum matched filter output by comparison.

*Concluding Remarks*

In this paper methods of generation of multilevel sequences both on amplitude and phase state basis have been presented. It has been shown that utilisation of phase logic results in considerable simplification in generation of phase-shift encoded multistate signals and their processing.

## REFERENCES

- Briggs P. A. N. & Godfrey K. R. 1966, *Proc. I.E.E.*, **113**, 1259.  
Church R. 1935, *Annals of Mathematics*, **36**, 198.  
Elspas B. 1959, *IRE Trans. on Circuit Theory*.  
Frank R. L. 1963, *IEEE Trans. on Information Theory*, IT-9, 43.  
Golomb S. W. & Scholtz R. A. 1965, *IEEE Trans. on Information Theory*, IT-11, 533.  
Pugh A. 1967, *Proc. I.E.E.*, **114**, 335.  
Taub D. M. 1968, *Proc. I.E.E.*, **115**, 285.

# Exact partition function of Ising model in magnetism in one, two and three dimensions in nonzero field

By D. D. Das

Department of Physics, Ravenshaw College, Cuttack-3, India

(Received 16 March 1970)

Exact partition function has been obtained for Ising model in one, two and three dimensions in nonzero field and it is shown that transition temperature and spontaneous magnetization do not exist according to our exact calculations with this model.

## INTRODUCTION

It is well known that Ising model (Ising 1925) in one dimension is not ferromagnetic. Two dimensional problem has been solved exactly (Onsager 1944), for non zero field) and also by approximate methods. Approximate calculations have also been carried out in three dimensions (Newell 1953). Two and three dimensional investigations lead to a transition temperature and spontaneous magnetization. Various types of lattice in two dimensions have also been considered. Here the problem has been solved for the linear chain, the two dimensional rectangular net and three dimensional rectilinear paralleloiped lattice as shown in figures 1-3. The results (free energy etc.) of one dimension should follow as a special case of those of two dimensions. Suppose in one dimension we have got one row with  $L$  sites. In two dimensions we have  $M$  rows and  $L$  columns. If  $M = 1$ , one dimension becomes a special case of two dimensions and two dimensional case should be a special case of three dimensions.

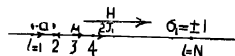


Fig. 1

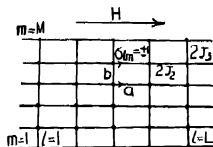


Fig. 2

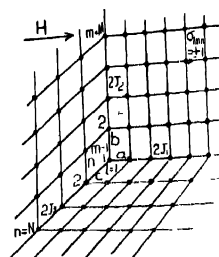


Fig. 3

## FORMULATION OF THE MODEL

A solid consists of crystals. All the crystals behave exactly in the same manner. Inside the crystal along  $X$ -axis there are  $L$  equidistant sites, the distance

between two nearest neighbours being  $a$ , along  $Y$  axis there are  $M$  equidistant sites, the neighbouring distance being  $b$ , along the  $Z$  axis there are  $N$  equidistant sites separated by a distance  $c$ . For one dimension  $M = N = 1$  and for two dimensions  $N = 1$ . In a magnetic field in each site the spin can have two orientations only,  $+1$  and  $-1$ . Interaction between two neighbouring spins along  $X$  axis is measured by  $2J_1$ , along  $Y$  axis by  $2J_2$ , and along  $Z$  axis by  $2J_3$ . In one dimension  $J_2 = J_3 = 0$  and in two dimensions  $J_3 = 0$ . We consider only the nearest neighbour interaction. We represent the spin of the  $(l, m, n)$ th site by  $\sigma_{lmn}$  and  $\sigma_{lmn} = \pm 1$ . The crystal symmetry is defined by  $\sigma_{L+lmn} = \sigma_{lmn}$ ,  $\sigma_{LM+mn} = \sigma_{lmn}$  and  $\sigma_{lmN+n} = \sigma_{lmn}$ . Inside a crystal no site is to be preferred to another site. Statistically all the sites are equivalent. Consider the arbitrary  $(l, m, n)$ th site anywhere in the crystal. In one dimension it will have interaction with two nearest neighbours, in two dimensions with four nearest neighbours and in three dimensions with eight nearest neighbours. Energy of  $l$ th site in one dimension will be given by

$$E_l = -\mu H \sigma_l - J_1 \sigma_l \sigma_{l+1} - J_1 \sigma_l \sigma_{l-1} \quad \dots (1)$$

with  $\sigma_l = \pm 1$ ,  $\sigma_{l+1} = \pm 1$  and  $\sigma_{l-1} = \pm 1$ .

Here  $\mu$  is magnetic moment per site and  $H$  is magnetic field. This will result in eight ( $= 2^3$ ) values of energy :

$$-\mu H - J_1, -\mu H, \mu H - J_1, \mu H, -\mu H, -\mu H + J_1, \mu H \text{ and } \mu H + J_1.$$

In two dimensions the arbitrary  $(l, m)$ th site will have energy given by

$$E_{lm} = -\mu H \sigma_{lm} - J_1 \sigma_{lm} \sigma_{l+1m} - J_1 \sigma_{lm} \sigma_{l-1m} - J_2 \sigma_{lm} \sigma_{lm+1} - J_2 \sigma_{lm} \sigma_{lm-1} \quad \dots (2)$$

The thirty two ( $= 2^5$ ) values of energy will be given by

$$\begin{aligned} &\mu H + 2J_1 + 2J_2, \quad \mu H - 2J_1 + 2J_2, \quad \mu H + 2J_2, \quad \mu H + 2J_2, \quad \mu H + 2J_1 - 2J_2, \\ &\mu H - 2J_1 - 2J_2, \quad \mu H - 2J_2, \quad \mu H - 2J_2, \quad \mu H + 2J_1, \quad \mu H - 2J_1, \quad \mu H, \quad \mu H, \\ &\mu H + 2J_1, \quad \mu H - 2J_1, \quad \mu H, \quad \mu H, \quad \mu H + 2J_1, \quad \mu H - 2J_1, \quad \mu H, \quad \mu H, \quad \mu H + 2J_1, \\ &\mu H - 2J_1, \quad \mu H, \quad \mu H, \quad -\mu H + 2J_1 + 2J_2, \quad -\mu H - 2J_1 + 2J_2, \quad -\mu H + 2J_2, \\ &-\mu H + 2J_1 - 2J_2, \quad -\mu H - 2J_1 - 2J_2, \quad -\mu H - 2J_2, \quad -\mu H - 2J_2, \quad -\mu H - 2J_2, \\ &-\mu H + 2J_1, \quad -\mu H - 2J_1, \quad -\mu H, \quad -\mu H, \quad -\mu H + 2J_1, \quad -\mu H - 2J_1, \quad -\mu H \\ &\text{and } -\mu H. \end{aligned}$$

Some of the energies are of course repeated. Similarly in three dimensions the arbitrary  $(l, m, n)$ th site will have energy given by

$$\begin{aligned} E_{lmn} = &-\mu H \sigma_{lmn} - J_1 \sigma_{lmn} \sigma_{l+1mn} - J_1 \sigma_{lmn} \sigma_{l-1mn} - J_2 \sigma_{lmn} \sigma_{lm+1n} - J_2 \sigma_{lmn} \sigma_{lm-1n} \\ &- J_3 \sigma_{lmn} \sigma_{lmn+1} - J_3 \sigma_{lmn} \sigma_{lmn-1} \quad \dots (3) \end{aligned}$$

There will be 128 ( $= 2^7$ ) energy values.

The total energy of the crystal will be given by  $E = \sum_{l=1}^{L-1} \sum_{m=1}^{M-1} \sum_{n=1}^{N-1} E_{lmn}$

The average energy  $\bar{E}$  will be however  $LMN$  times the average value  $\bar{E}_{lmn}$ .

## PARTITION FUNCTION

The partition function is given by

$$Z = \sum e^{-\frac{E^i}{kT}} \quad \dots (4)$$

where  $k$  is Boltzmann constant,  $T$  is absolute temperature and  $E^i$  is a possible energy value. Free energy is related to partition function by

$$F = -kT \ln Z \quad \dots (5)$$

If  $F_{lmn}$  be free energy per site, total free energy will be given by

$$F = LMN F_{lmn} \quad \dots (6)$$

Let  $Z_{lmn}$  be partition function per site.

$$\begin{aligned} F &= LMN F_{lmn} = -kT \ln Z \\ F_{lmn} &= -\frac{kT}{LMN} \ln Z = -kT \ln (Z)^{\frac{1}{LMN}} \end{aligned} \quad \dots (7)$$

But

$$F_{lmn} = -kT \ln Z_{lmn} \quad \dots (8)$$

So

$$Z_{lmn} = (Z)^{\frac{1}{LMN}} \quad \text{or} \quad Z = (Z_{lmn})^{LMN} \quad \dots (9)$$

Let  $Z_{lmn}$  be given by  $Z_{lmn} = \sum_i e^{-\frac{E_i}{kT}}$

$$\begin{aligned} &= \sum e^{-\frac{E_{lmn}}{kT} (\sigma_{lmn}, \sigma_{l+1mn}, \sigma_{l-1mn}, \sigma_{lm+1n}, \sigma_{lm-1n}, \sigma_{lmn+1}, \sigma_{lmn-1}); \dots (10)} \\ &\sigma_{lmn}, \sigma_{l+1mn}, \sigma_{l-1mn}, \sigma_{lm+1n}, \sigma_{lm-1n}, \sigma_{lmn+1}, \sigma_{lmn-1} = \pm 1 \end{aligned}$$

## THERMODYNAMIC FUNCTIONS

The various thermodynamic functions are related to the free energy. Average energy  $E$ , average magnetic moment  $M$  in magnetic field  $H$ , spontaneous magnetization  $(M)_{H=0}$ , entropy  $S$ , specific heat  $C_v$ , susceptibility  $\chi$ , spin average  $\langle \sigma \rangle$  and spin correlation  $\langle \sigma \sigma' \rangle$  are given by the following relations

$$E = -T^2 \frac{\partial}{\partial T} \left( \frac{F}{T} \right) \quad \dots (11)$$

$$M = - \frac{\partial F}{\partial H}$$

$$(M)_{H=0} = - \left( \frac{\partial F}{\partial H} \right)_{H=0} \quad \dots (12)$$



$$S = - \frac{\partial F}{\partial T} \quad \dots (13)$$

$$C_V = \left( \frac{\partial E}{\partial T} \right)_{H=0} \quad \dots (14)$$

$$\chi = \left( \frac{\partial M}{\partial H} \right)_{H=0} \quad \dots (15)$$

$$\langle \sigma \rangle = \langle \sigma_{lmn} \rangle = - \frac{1}{LMN} \frac{\partial F}{\partial H} \quad \dots (16)$$

$$\langle \sigma \sigma' \rangle_1 = \langle \sigma_{lmn} \sigma_{l+1mn} \rangle = - \frac{1}{LMN} \frac{\partial F}{\partial J_1}$$

$$\langle \sigma \sigma' \rangle_2 = \langle \sigma_{lmn} \sigma_{lm+1n} \rangle = - \frac{1}{LMN} \frac{\partial F}{\partial J_2}$$

$$\langle \sigma \sigma' \rangle_3 = \langle \sigma_{lmn} \sigma_{lmn+1} \rangle = - \frac{1}{LMN} \frac{\partial F}{\partial J_3} \quad \dots (17)$$

# CONSTRUCTION OF PARTITION FUNCTION IN ONE DIMENSION

We immediately get the partition function  $Z_l$  (figure 4)

$$\begin{aligned} Z_l &= \sum_{\sigma_l, \sigma_{l+1}, \sigma_{l-1} = \pm 1} e^{-\frac{El}{kT}} (\sigma_l, \sigma_l, \sigma_{l+1}, \sigma_l, \sigma_{l-1}) \\ &= e^{\frac{\mu H - 2J_1}{kT}} + e^{\frac{\mu H - 2J_1}{kT}} + e^{\frac{-\mu H + 2J_1}{kT}} + e^{\frac{-\mu H - 2J_1}{kT}} + 2e^{\frac{\mu H}{kT} + 2e^{\frac{-\mu H}{kT}}} \\ &= \left( e^{\frac{\mu H}{kT}} + e^{-\frac{\mu H}{kT}} \right) \left( e^{\frac{J_1}{kT}} + e^{-\frac{J_1}{kT}} \right)^2 \\ &= 8 \text{ch} \frac{\mu H}{kT} \text{ch}^2 \frac{J_1}{kT}. \quad \dots (18) \end{aligned}$$

$$Z = 8^L \text{ch}^L \frac{\mu H}{kT} \text{ch}^{2L} \frac{J_1}{kT} \quad \dots (19)$$

## PARTITION FUNCTION IN TWO DIMENSIONS

Easily we get partition function  $Z_{lm}$  (figure 5)

$$\begin{aligned}
 Z_{lm} = & e^{\frac{\mu H + 2J_1 + 2J_2}{kT}} + e^{\frac{\mu H - 2J_1 + 2J_2}{kT}} + 2e^{\frac{\mu H + 2J_2}{kT}} + e^{\frac{\mu H + 2J_1 - 2J_2}{kT}} \\
 & + e^{\frac{\mu H - 2J_1 - 2J_2}{kT}} + 2e^{\frac{\mu H - 2J_2}{kT}} + 2e^{\frac{\mu H + 2J_1}{kT}} + 2e^{\frac{\mu H - 2J_1}{kT}} + 4e^{\frac{\mu H}{kT}} \\
 & + 4e^{\frac{-\mu H}{kT}} + e^{\frac{-\mu H + 2J_1 + 2J_2}{kT}} + e^{\frac{-\mu H - 2J_1 + 2J_2}{kT}} + e^{\frac{-\mu H + 2J_1 - 2J_2}{kT}} \\
 & + e^{\frac{-\mu H - 2J_1 - 2J_2}{kT}} + 2e^{\frac{-\mu H + 2J_1}{kT}} + 2e^{\frac{-\mu H - 2J_1}{kT}} + 2e^{\frac{-\mu H + 2J_2}{kT}} \\
 & + 2e^{\frac{-\mu H - 2J_2}{kT}} \\
 = & \left( e^{\frac{\mu H}{kT}} + e^{-\frac{\mu H}{kT}} \right) \left( e^{\frac{J_1}{kT}} + e^{-\frac{J_1}{kT}} \right)^2 \left( e^{\frac{J_2}{kT}} + e^{-\frac{J_2}{kT}} \right)^2 \\
 = & 32 \operatorname{ch} \frac{\mu H}{kT} \operatorname{ch}^2 \frac{J_1}{kT} \operatorname{ch}^2 \frac{J_2}{kT} \quad \dots (20)
 \end{aligned}$$

$$Z = 32^{LM} \operatorname{ch}^{LM} \frac{\mu H}{kT} \operatorname{ch}^{2LM} \frac{J_1}{kT} \operatorname{ch}^{2LM} \frac{J_2}{kT} \quad \dots (21)$$

## PARTITION FUNCTION IN THREE DIMENSIONS

In a similar manner we get partition function for the three dimensional case.

$$\begin{aligned}
 Z_{lmn} = & \left( e^{\frac{\mu H}{kT}} + e^{-\frac{\mu H}{kT}} \right) \left( e^{\frac{J_1}{kT}} + e^{-\frac{J_1}{kT}} \right)^2 \left( e^{\frac{J_2}{kT}} + e^{-\frac{J_2}{kT}} \right)^2 \left( e^{\frac{J_3}{kT}} + e^{-\frac{J_3}{kT}} \right)^2 \\
 = & 128 \operatorname{ch} \frac{\mu H}{kT} \operatorname{ch}^2 \frac{J_1}{kT} \operatorname{ch}^2 \frac{J_2}{kT} \operatorname{ch}^2 \frac{J_3}{kT} \quad \dots (22)
 \end{aligned}$$

$$Z = 128^{LMN} \operatorname{ch}^{LMN} \frac{\mu H}{kT} \operatorname{ch}^{2LMN} \frac{J_1}{kT} \operatorname{ch}^{2LMN} \frac{J_2}{kT} \operatorname{ch}^{2LMN} \frac{J_3}{kT} \quad \dots (23)$$

We easily observe that by putting  $N = 1$  and  $J_3 = 0$ , free energy for the two dimensional case follows from that of the three dimensional case and by putting  $M = N = 1$  and  $J_2 = J_3 = 0$  (or by putting  $M = 1$  and  $J_2 = 0$  in the two dimensional case) in the three dimensional case we get free energy of

the one dimensional case. It is better if  $L \geq 3$ ,  $M \geq 3$  and  $N \geq 3$ , otherwise we cannot get two neighbours inside a crystal. Normally  $L$ ,  $M$  and  $N$  are large. For sites in extreme position, one of the neighbours is in the neighbouring crystal. If  $L = 2$  say,  $\sigma_{2m}\sigma_{3m} = \sigma_{2m}\sigma_{1m}$  in two dimensions. A crystal can also be possible with  $L < 3$ ,  $M < 3$  and  $N < 3$ .

### RESULTS

One finds that free energy comes out to be a continuous function of temperature and the derivatives of free energy are also continuous. There is no discontinuity in any order derivative of the thermodynamic potential and so in this model a transition temperature is not obtained and also not spontaneous magnetization. The earlier workers do not get a transition temperature and spontaneous magnetization is one dimension, but they get them in two dimensions. In none of our calculations, either in one, two or three dimensional, there is a transition temperature or spontaneous magnetization. This is however not surprising because one dimensional calculations are expected to behave similar to the two dimensional calculations. The experimental results are shown qualitatively in figures 4-8 and theoretical values given qualitatively in figures 9-20.

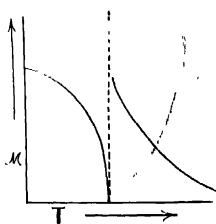


Fig. 4

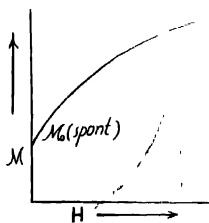


Fig. 5

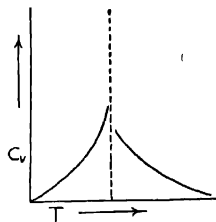


Fig. 6

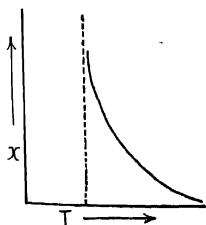


Fig. 7

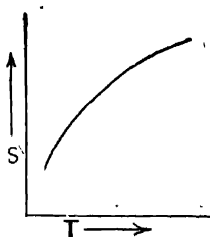


Fig. 8

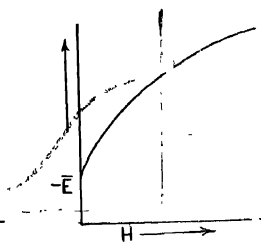


Fig. 9

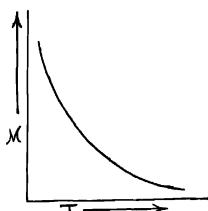


Fig. 10

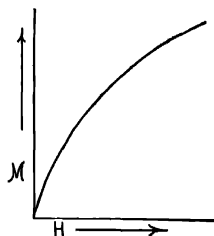


Fig. 11

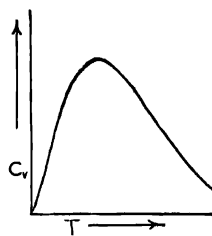


Fig. 12

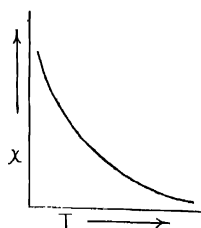


Fig. 13

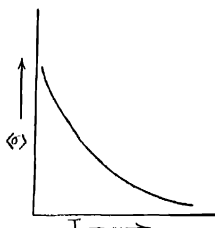


Fig. 14

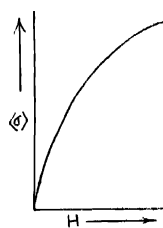


Fig. 15

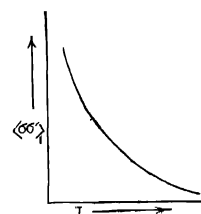


Fig. 16

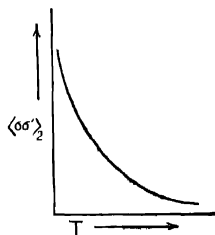


Fig. 17

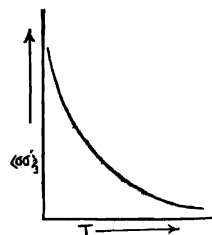


Fig. 18

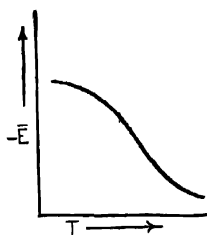


Fig. 19

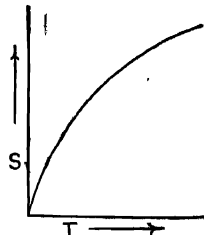


Fig. 20

## CONCLUSION

We have the following expressions for partition functions in various dimensions

$$1 \text{ dimension } Z = 8^L \text{ch}^L \frac{\mu H}{kT} \text{ch}^{2L} \frac{J_1}{kT} \quad \dots (19)$$

$$2 \text{ dimensions } Z = 32^{LM} \text{ch}^{LM} \frac{\mu H}{kT} \text{ch}^{2LM} \frac{J_1}{kT} \text{ch}^{2LM} \frac{J_2}{kT} \quad \dots (21)$$

$$3 \text{ dimensions } Z = 128^{LMN} \text{ch}^{LMN} \frac{\mu H}{kT} \text{ch}^{2LMN} \frac{J_1}{kT} \text{ch}^{2LMN} \frac{J_2}{kT} \text{ch}^{2LMN} \frac{J_3}{kT} \quad \dots (23)$$

If we take

$$Z = \left\{ \sum_{\dots, \sigma_{lmn} = \pm 1,} e^{-\frac{1}{kT} (\mu H \sigma_{lmn} + 2J_1 \sigma_{lmn} \sigma_{l+1mn} + 2J_2 \sigma_{lmn} \sigma_{lmn+1} + 2J_3 \sigma_{lmn} \sigma_{lmn+1})} \right\}^{LMN} \quad \dots (24)$$

the result will be

$$Z = 16^{LMN} \text{ch}^{LMN} \frac{\mu H}{kT} \text{ch}^{LMN} \frac{2J_1}{kT} \text{ch}^{LMN} \frac{2J_2}{kT} \text{ch}^{LMN} \frac{2J_3}{kT} \quad \dots (25)$$

which will not give any qualitative difference.

One may not like to agree with the fact that

$$Z = \left( \sum_{\dots, \sigma_{lmn} = \pm 1, \dots} e^{-\frac{E_{lmn}}{kT}} \right)^{LMN} \quad \dots (26)\text{-I}$$

but one may say

$$\begin{aligned} Z &= \sum_{\dots, \sigma_{lmn} = \pm 1, \dots} e^{-\sum_{l=1, m=1, n=1}^{l=L, m=M, n=N} \frac{E_{lmn}}{kT}} \\ &= \sum_{\dots, \sigma_{lmn} = \pm 1, \dots} e^{\frac{1}{kT} \sum_{l=1, m=1, n=1}^{l=L, m=M, n=N} (\mu H \sigma_{lmn} + 2J_1 \sigma_{lmn} \sigma_{l+1mn} + 2J_2 \sigma_{lmn} \sigma_{lmn+1} + 2J_3 \sigma_{lmn} \sigma_{lmn+1})} \end{aligned} \quad \dots (27)\text{-II}$$

It may be pointed out that the expression II is identical with I for free spins (i.e. if  $J_1 = J_2 = J_3 = 0$ ). However the expression II is a part of the expression I, so there will be no qualitative difference in thermodynamic results. For a ferromagnetic substance at low temperatures with the condition  $\sigma = \pm 1$ , there will be very few spins that will align against the magnetic field with  $\sigma = -1$  and most of the spins will align in the direction of the magnetic field with  $\sigma = +1$ .

The two expressions will differ very little. It may be pointed out that considering the two dimensional cases  $L = 2$ ,  $M = 2$ ,  $N = 1$  (16 terms),  $L = 3$ ,  $M = 2$ ,  $N = 1$  (64 terms) and  $L = 3$ ,  $M = 3$ ,  $N = 1$  (512 terms) as examples, we have evaluated the exact partition function according to expression II. We have calculated free energy, specific heat, magnetization etc. and have found that there is no spontaneous magnetization or discontinuity in the specific heat in the two dimensions. It would appear that the results of Onsager (1944) and Yang (1952) are not so reliable.

The author is thankful to the Ministry of Scientific Research and Cultural Affairs, Government of India, for the award of a Senior Research Scholarship for carrying on this work. He is grateful to Prof. F. C. Auluck, D.Sc., F.N.A. for suggesting the problem.

#### REFERENCES

- Bates L. F. 1951 *Modern Magnetism*.  
Haar D. ter *Statistical Mechanics*.  
Ising E. 1925 *Zeits. f. Physik*, **31**, 253.  
Kaufman B. 1949 *Phys. Rev.* **76**, 1232.  
Kaufmann B. & Onsager L. 1949 *Phys. Rev.* **76**, 1944.  
Newell G. F. & Montroll E. W. 1953 *Rev. Mod. Phys.* **25**, 353.  
Onsager L. 1944 *Phys. Rev.* **65**, 117.  
Schrodinger E. *Statistical Thermodynamics*.  
Yang C. N. 1952 *Phys. Rev.* **85**, 808.

## Neutron bound $S$ -states in Woods-Saxon potential

BY CHHAYA GANGULY

*Department of Theoretical Physics, Indian Association for the Cultivation of Science, Jadavpur, Calcutta-32.*

(Received 31 March 1970 — Revised 17 August 1970).

The  $S$ -wave bound states of neutrons in Woods-Saxon potential have been investigated by calculating the zeros of  $S_0$ -matrix on the negative imaginary axis of the complex  $k$ -plane. Numerical results are presented for the atomic mass  $A = 200$ .

### INTRODUCTION

In the choice of a suitable potential between nucleon and the nucleus, which may take proper account of the general properties of nuclear energy levels, emphasis has so far been given to the analytical convenience. The square-well and harmonic oscillator potentials are quite appealing in this respect since they are amenable to analytical treatment. However, these potentials have severe limitations. The harmonic oscillator potential becomes asymptotically infinite and yields an infinite set of discrete eigenvalues, on the other hand, the square-well potential shows an abrupt change of nuclear potential which is not very realistic. Besides, neither of these potentials gives the proper level sequence. Investigations by Feenberg (1950), Malenka (1952) and others suggest that better level ordering can be obtained if the boundary of the nuclear potential is taken to be diffuse. Malenka has studied the problem of bound states of a heavy nucleus with a potential which has precisely the analytic form of the square-well in the interior region and exponentially diffused form in external region. Green & Lee (1955) have investigated systematically the energy eigenvalue problem with a similar type of spherical-well potential having an exponentially diffused boundary and solved the Schrödinger equation analytically. But these authors have also taken account of the higher angular momentum states by suitably approximating the centrifugal term. The success of the most realistic diffuse potential of Woods-Saxon form (1954) in the scattering problem (Moshbach 1958, Beyster *et al* 1956) have stimulated a number of authors (Ross *et al* 1956, Nemirovskii 1958 and Ghosh & Sil 1960) to apply the same also to the investigations of the bound states of nucleons. Though this form avoids the unrealistic sharp corner of the exponentially diffuse edge potential, it brings some complications in the exact analytical treatment, so that most of its applications have so far been done by numerical integration of the wave equation. Ross *et al* (1956) have used this potential to study numerically some of the upper states of nucleons in nuclei with a spin-orbit interaction, Nemirovskii (1958)

has also dealt numerically the problem of bound states of a neutron in Woods-Saxon potential including the spin-orbit interaction. The analytic solution for the  $S$ -states as given by Lawson (1956) is not of much practical value because of very slow convergence of the series solution. Ghosh & Sil (1960) have solved the wave equation with the above potential by applying the method of Lanczos (1938). They have considered higher angular momentum states with a suitable approximation for the centrifugal term.

In the present paper we have calculated  $S$ -state energy levels for the atomic mass  $A = 200$  with Woods-Saxon potential using the expression for the  $S_0$  matrix as given by Bencze (1966). The results of Ghosh & Sil agree fairly well with those of ours.

### THEORY AND FORMULATION

The interaction potential between the neutron and the nucleus, which is taken to be of Woods-Saxon form, is represented as

$$V(r) = -V_0/[1 + e^{(r-R)/a}]$$

where  $R$  is the nuclear radius and  $a$  the diffusivity parameter. The analytic expression for the  $S_0$ -matrix element with this potential, following Bencze (1966), is

$$S_0(k) = e^{-2k_0 R} \cdot \frac{\Gamma(2ika)}{\Gamma(-2ika)} \times \frac{A \frac{\Gamma(1-2\lambda)}{\Gamma(1-\lambda+ika)\Gamma(-\lambda+ika)} - \frac{\Gamma(1+2\lambda)}{\Gamma(\lambda+ika)\Gamma(1+\lambda+ika)}}{\frac{\Gamma(1+2\lambda)}{\Gamma(1+\lambda-ika)\Gamma(\lambda-ika)} - A \frac{\Gamma(1-2\lambda)}{\Gamma(-\lambda-ika)\Gamma(1-\lambda-ika)}} \quad (1)$$

$$\text{where } A = \left(\frac{b}{1+b}\right)^{2\lambda} (1+b)^{-2ika} \frac{{}_2F_1\left(\lambda+ika, 1+\lambda+ika, 1+2\lambda; \frac{b}{1+b}\right)}{{}_2F_1\left(-\lambda-ika, 1-\lambda-ika, 1-2\lambda; \frac{b}{1+b}\right)}$$

$$\lambda = \pm i\sqrt{k^2 + k_0^2}$$

$$k^2 = \frac{2M}{\hbar^2} E$$

$$k_0^2 = \frac{2M}{\hbar^2} V_0 \quad \text{and} \quad b = \exp(-R/a)$$

$M$  and  $E$  being respectively, the mass and energy of the neutron.  $S_0(k)$  may be written as (Mott & Massey, 1965)

$$S_0(k) = f_0(k)/f_0(-k) \quad \dots (2)$$



where  $f_0(k) = \lim_{r \rightarrow 0} f_0(k, r)$  and  $f_0(\pm k, r)$  are linearly independent solutions of the radial wave equation for the scattering of *S*-wave neutrons

$$\frac{d^2 u_0}{dr^2} + \left[ k^2 - \frac{2M}{\hbar^2} V(r) \right] u_0(r) = 0 \quad \dots (3)$$

and have the asymptotic form

$$f_0(\pm k, r) \sim \exp(\pm ikr)$$

The *S*-wave bound states are determined by the zeros of  $S_0(k)$  corresponding to the zeros of  $f_0(k)$  on the negative imaginary axis of the complex *k*-plane. The redundant zeroes of  $S_0(k)$  on account of the poles of  $f_0(-k)$  on the negative imaginary axis need not be taken into consideration, since these poles do not correspond to the true bound states (Mott & Massey 1965). For numerical computation we note that  $b \sim 10^{-8} b \ll 1$  for the mass number considered, so that the hypergeometric functions reduced to 1 and  $(1+b) \rightarrow 1$ . Writing  $k = -i\kappa$  where  $\kappa$  is positive, we have from (1) and (2) for a bound state at  $-\frac{\hbar^2}{2M} \kappa^2$ ,

$$C - C^* = 0, \text{ i.e., } \text{Im} C = 0 \quad \dots (4)$$

where

$$C = \frac{b^\lambda \Gamma(1-2\lambda)}{\Gamma(1-\lambda+i\kappa a) \Gamma(-\lambda+i\kappa a)}$$

With a simple algebraic manipulation we obtain from equation (4)

$$\cot pR = \eta, \text{ where } \eta = \frac{\mu \cos y + \delta \sin y}{\mu \sin y - \delta \cos y}, \quad \dots (5)$$

in which

$$p = \sqrt{\frac{2M}{\hbar^2} (V_0 - |E|)}, \quad \delta = pa, \mu = \kappa a,$$

and

$$y = \text{Im}[\log \Gamma(1-2i\delta) - 2 \log \Gamma(1+\mu-i\delta)].$$

For the square-well case  $a \rightarrow 0$ . Then we have  $y \propto \delta$ , and hence

$$\cot pR = -\frac{\mu}{\delta} = -\frac{\kappa}{p}$$

or

$$p \cot pR = -\kappa. \quad \dots (6)$$

The expression (6) is identical with the analytic form given by Schiff (1955). The required eigenvalues are found by solving the transcendental equation (5).

## RESULTS AND DISCUSSION

To calculate the  $S$ -state energy levels for the atomic mass  $A = 200$ , we choose the values of the parameters in the potential function as  $V_0 = 52$  Mev,  $R = 1.25 A^{1/3} fm$  and  $a = 0.52 fm$ , which are the same as taken by us in the calculation of the neutron strength function (1967).

Table 1

Levels	E  in Mev	
	Our results	Results due to Ghosh & Sil (1960)
1s	47.98	48.1
2s	36.90	35.5
3s	21.09	20.2
4s	3.69	4.8

In figure 1 we have plotted  $\cot pR$  and  $\eta$  occurring in equation (5) as functions of  $\delta$ . The points of intersection of these two curves give the required energy eigenvalues which are shown in table 1. For comparison we have also given the

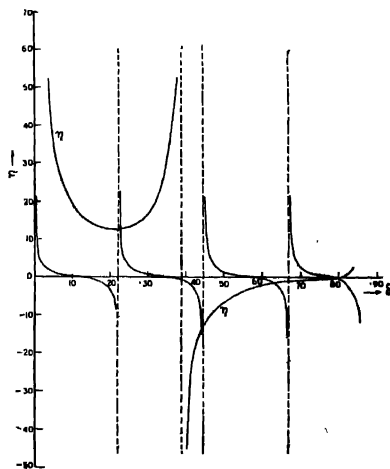


Figure 1.

corresponding eigenvalues as calculated from the energy level diagram given by Ghosh & Sil (1960). The values of the parameters used by these authors are

$$V_0 = 52 \text{ Mev}, \quad R = (1.15 A^{1/3} + 0.4) \times 10^{-13} \text{ cm.}$$

and

$$a = 0.57 \times 10^{-13} \text{ cm.}$$

The author is grateful to Professor D. Basu and Dr. N. C. Sil for many helpful discussions throughout the progress of the work.

#### REFERENCES

- Benezy Gy. 1966 *Nordita Publications* No. 184.  
 Bywater J. R., Walt M. & Salmi E. W. 1956 *Phys. Rev.* **104**, 1319.  
 Feenberg E. 1950 *Phys. Rev.* **77**, 771.  
 Feshbach H. 1958 *Annual Rev. of Nuclear Science* **8**, 88.  
 Ganguly C. & Sil N. C. 1967 *Indian J. Phys.* **41**, 810.  
 Ghosh A. & Sil N. C. 1960 *Nucl. Phys.* **17**, 264.  
 Green A. E. S. & Lee K. 1955 *Phys. Rev.* **99**, 772.  
 Lanczos C. 1938 *Journal of Mathematics and Physics* **17**, 123.  
 Lawson R. D. 1956 *Phys. Rev.* **101**, 311.  
 Malenka B. J. 1952 *Phys. Rev.* **86**, 68.  
 Mott N. F. & Massey H. S. W. 1965 *The Theory of Atomic Collisions*, Oxford Clarendon Press, Third Edition, 138.  
 Nemirovski P. E. 1958 *Soviet Physics JETP* **6**, 573.  
 Ross A. A., Mark H. & Lawson R. D. 1956 *Phys. Rev.* **102**, 1613.  
 Schiff L. I. 1955 *Quantum Mechanics*, McGraw Hill Book Company, Inc., New York. Second Edition.  
 Woods R. D. & Saxon D. S. 1954 *Phys.* **95**, 577.

## A coincidence method for absolute measurement of incident energy of electrons

BY P. K. BHATTACHARYA\* AND M. R. BHIDAY

*Department of Applied Physics, S G.S. Institute of Technology and Science  
17, Park Road, Indore-3, M.P.*

*(Received 3 April, 1970)*

A coincidence method is devised for absolute measurement of energy of electrons upto 5 MeV. The method makes use of the fact that the angle between the scattered and recoil particles is dependent on the relativistic energy of the incident electrons. Using fast coincidence techniques and fast multiparameter analysis system in conjunction with fast directional scintillators like 'Phoswich' to detect the two particles, the method can be made accurate to  $\pm 1\%$ . Employing thin foil targets, multiple scattering ( $Z \simeq 6$ ) and hence, the angular spread in the coincidence peak becomes small. Thus, it is possible to measure the beam energy at the target simultaneously with the scattering cross-section without the necessity of making any change in the experimental set up.

### INTRODUCTION

Electron scattering experiments require an accurate and absolute measurement of energy of incident particles at the target. In addition, it is necessary to monitor the beam energy continuously during the course of an actual run. By using internal conversion electrons, it is possible to achieve the energy measurement with precision (Siegbahn 1965), using well known standard lines. We could have easily decided upon a suitable definition of the position of the line, if the conversion electrons emanated from an 'ideal source', without any inherent errors like Landau energy loss in the foil. However, in most of these cases, conversion lines from different atomic shells have different shapes especially for low energy lines than for high energy lines, thereby limiting the accuracy of tracing the centroid. Thus, even after knowing the energy standards with a high degree of accuracy the method proves to be only relative. Threshold Čerenkov detectors (Bhiday *et al* 1958) have proved to be good alternatives for absolute measurement of the energy of electrons near 5 MeV and have shown their use, also in applications of flux measurements. Unfortunately, the energy resolution for such counters becomes unsatisfactory below 2 MeV due to larger energy losses, while about 5 MeV there is a little change in beta ( $v/c$ ) values of electrons with energy, rendering the Čerenkov method ineffective. The problem of absolute measurement of electron energies

\*Computer programming and associated calculations were done while working in CERN as a Visiting-Scientist with Neutrino Beam Studies Group in The Directorate of Nuclear Physics Apparatus, 1211, Geneva 23, Switzerland.

in the range 2 to 5 MeV becomes important especially when measurements of electron-nuclear or electron-electron scattering cross-sections are to be undertaken. Such experiments are in progress in this laboratory with the help of a 5 MeV Betatron now made available to us to study the effects of (1) exchange terms (Bhabha 1936, Möller 1932), (2) atomic screening constants (Dougal 1964, Koch *et al* 1964), and multiple scattering in various foils

This paper deals with the design of a coincidence method for absolute beam energy measurement and its monitoring and shows feasibility of determination of scattering cross-section in the same experimental set up for the cases of electron-electron, positron-electron and electron-nuclear scattering

## 2. THEORY OF THE METHOD

We shall use the kinematic relations of collisions between two particles, which are relativistic and assume that an incident particle of mass  $m_1$  collides with a free particle of mass  $m_2$ , where, subscripts 0, 1 and 2 hereafter denote quantities related with the incident, scattered and the recoil particles, while subscript  $c$  relates to the corresponding values in barycentric coordinates (*i.e.*, with reference to centre of mass system), shown in figure 1.

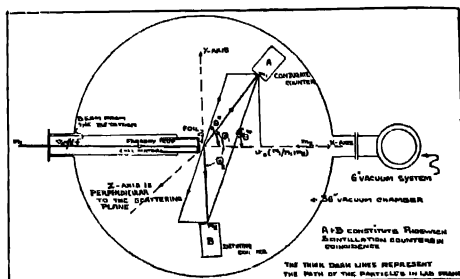


FIGURE 1. Collision kinematics for energy equation.

The momentum and energy relationships form a Lorentz four vector and are held by the equations,

$$cp_c = \gamma_c(cp_x - \beta_c E) \quad \dots (1)$$

$$cp_x = \gamma_c(cp_c + \beta_c E_c) \quad \dots (2)$$

$$E_c = \gamma_c(E - \beta_c cp_x) \quad \dots (3)$$

$$E = \gamma_c(E_c + \beta_c cp_c) \quad \dots (4)$$

$$cp_c = cp_{y,z} \quad \dots (5)$$

and  $c^2 p^2 - E^2 = Q \quad \dots (6)$

whence,  $Q$  is invariant to the frame of reference.

These relations connect  $x$ ,  $y$ , and  $z$  components of the momentum  $p$  and energy  $E$ , where  $p_x$ ,  $p_y$ ,  $p_z$  along with  $E/c^2$  form a four vector. Applying conservation of momentum to the scattered and recoil particles (in C.M. system) we get,

$$m_1^2(\gamma_{c1}^2 - 1) = m_2^2(\gamma_c^2 - 1) \quad \dots (7)$$

where  $\gamma_{c1}$  and  $\gamma_c$  denote the values of  $\gamma = 1/(1-v^2/c^2)^{1/2}$  of  $m_1$  and  $m_2$ . On putting  $\gamma_{c1}$  and  $\gamma_c$  in the relations for momentum of  $m_1$  in barycentric and laboratory (LAB) system and simplifying to evaluate them by substituting  $m_1/m_2 = k$ , we get,

$$(\gamma_{c1}^2 - 1)^{1/2}(1 + \gamma_0 k) = \gamma_c(\gamma_0^2 - 1)^{1/2} \quad \dots (8)$$

On further simplification we obtain,

$$\gamma_{c1} = (\gamma_0 + k)/(1 + 2k\gamma_0 + k^2)^{1/2} \quad \dots (9)$$

$$\gamma_c = (1 + \gamma_0 k)/(1 + 2k\gamma_0 + k^2)^{1/2} \quad \dots (10)$$

From relations (9) and (10) the velocities of  $m_1$  and  $m_2$  can be found reducing to a simple expression,

$$\gamma_c = \gamma_{c1} = [(1 + \gamma_0)/2]^{1/2} \quad \dots (11)$$

in the particular case of  $e-e$  or  $p-e$  scattering, as  $m_1/m_2$  or  $k$  equals unity.

Using equation (2) and combining (5) and (6), one gets resolved components of momenta in  $x$  and  $y$  directions to find ultimately the relationships between angles in the LAB and C.M. systems. We get therefrom,

$$\tan \Theta_2 = -\cot(\theta^*/2)/\gamma_c \quad \dots (12)$$

and

$$\tan \Theta_1 = \sin \theta^*/\gamma_c(\cos \theta^* + k(\gamma_{c1}/\gamma_c)) \quad \dots (13)$$

The negative sign in equation (12) indicates that  $m_2$  recoils on the other side of the collision axis, which can be accurately defined by collimator slits for the Betatron beam which is limited to a spot of a few mm.

To get relationships of LAB angle  $\Theta_1$  and  $\Theta_2$  in terms of  $\theta^*$ , the centre of mass angle of scatter of  $m_1$ , we solve equation (13), a quadratic in  $\cos \theta^*$  using equation (7), and find,

$$\cos \theta^* = \frac{-\gamma_{c1}\gamma_c k \tan^2 \Theta_1 \pm ((1-k^2) \tan^2 \Theta_1 + 1)^{1/2}}{\gamma_c^2 \tan^2 \Theta_1 + 1} \quad \dots (14)$$

The foregoing analysis, if applied to a non-relativistic case, makes the radical zero (or  $\tan^2 \Theta_1 = 1/(k^2 - 1)$ ) and fixes an upper limit to the scattering angle to  $90^\circ$ , as  $\sin \Theta_1 = 1/k = 1$  for identical particle scatters. For  $k < 1$  the roots may be derived using equation (14), whence for  $\Theta_1 > 90^\circ$  more negative root should be chosen and for  $\Theta_1 < 90^\circ$  only the more positive root must be taken. On eliminating  $\theta^*$  from equations (12) and (13) for identical particle case,  $\gamma_{c1} = \gamma_c$ , we obtain an absolute relation for computation of energy as,

$$\tan \Theta_1 \tan \Theta_2 = -\gamma_c^{-2} = -2/(1 + \gamma_0) \quad \dots (15)$$

Assuming  $\Phi = \Theta_1 + \Theta_2$  as the angle between the scattered and recoil particles, we find by proper substitution for  $\tan \Theta_1$  and  $\tan \Theta_2$ ,

$$\tan \Phi = 2/(\beta_c^2 \gamma_c \sin \theta^*) \quad \dots (16)$$

It can be seen from figure 2, that for  $\beta_c = 0.96$  the angle  $\Phi$  rapidly falls down to  $32^\circ$  when  $\theta^* = 90^\circ$ , showing a gradual fall in the angle of scattering between the particles as the incident particle attains relativistic velocity.

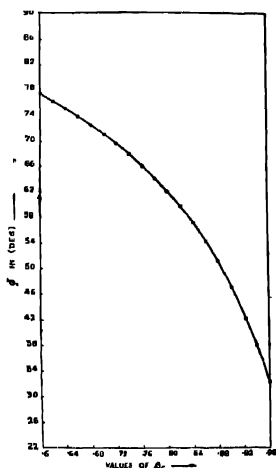


FIGURE 2. Variation of angle  $\Phi$  as a function of  $\beta_c$  for  $\theta^* = 90^\circ$ .

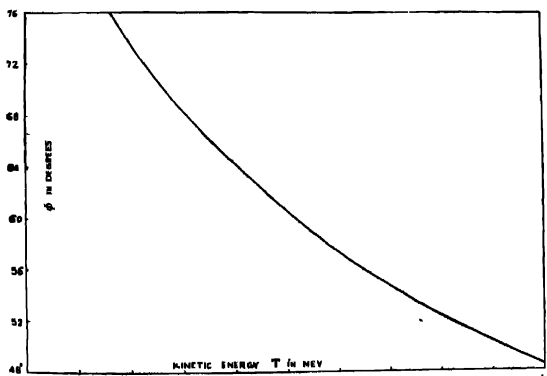


FIGURE 3. Variation of angle  $\Phi$  between the defining and the conjugate counter with energy  $T$  of the incident electrons at the target.

The computations for angle  $\Phi$  from equation (16) using symmetrical detector situation, are plotted in figure 3 for various kinetic energies. Thus, the energy equation can be used to check the accuracy of the beam energy at various stages during the experimental run by devising a multiparameter system in conjunction with a fast coincidence system to measure the coincidence counting rate by fixing the defining counter  $B$  and moving the conjugate  $A$  to a position, where a maximum in coincidence counting rate is found. An accuracy of  $\pm 3\%$  can be achieved for incident energies of the order of 2 MeV for an error of  $\pm 0.5^\circ$  in the measurement of  $\Phi$ . However, it can be seen that the accuracy improves by  $\pm 0.6\%$  at higher energies. This simple method of measuring coincidence in the scattered and recoil particles not only requires a thin foil of low atomic number (terylene, nylon or melinex) as a target but also depends on (1) true  $e-e$  or  $p-e$  scattering, (2) the statistical accuracy of the experiment (*i.e.* true/chance coincidence rate) and (3) energy spread and geometrical resolution of the beam and the detector system.

### 3. FACTORS INFLUENCING PARTICLE ENERGY

Combination of fast and a slow phosphor as 'Phoswich' (Wilkinson 1952) can be used to detect the particles with highly directional properties. Fast phosphors like NE 111, (full width at half maximum = 1.54 ns) plastic scintillators can be combined with slow phosphors like CsI (Tl) to realise a very effective and directional counting by a single photomultiplier. The fast phosphor would give a sharp spike on the leading edge of a gradually falling slope of the pulse due to slow phosphor when electrons pass both the phosphors. This type of 'Phoswich' would, therefore, not only act as an anti-coincidence shield but also allow coupling of a computer system to the coincidence counters (Wiegand 1959), if an appropriate design of a collimator system is put in front of the defining and conjugate counters looking for a compromise between resolution and sensitivity (Hušák and Perinová 1969). Further, by use of such a system no limitations are put on the solid angle of acceptance, even if one prefers to use surface barrier type solid state detectors having a depletion depth suitable to the maximum incident energy. Using an intense beam of electrons (from a 5 MeV Betatron) and thin foil targets, multiple scattering errors become small and take place only in the target plane so that its effects can be readily allowed for by computing the rms angle of scatter. The angular spread in the coincidence peak thus produced, would not be so large as to affect the energy measurement.

### 4. ACCURACY PARAMETERS

We can evaluate the accuracy parameter for the system assuming a particular case of symmetry, whence,  $\Theta_1 = \Theta_2$ , or  $\tan \Phi = 2 \tan \Theta_2 / 1 - \tan^2 \Theta_2 = \tan 2\Theta_2$  and similarly  $\cos 2\Theta_2 = 1 - \tan^2 \Theta_2 / (1 + \tan^2 \Theta_2)$ . From equation (15) we get,



on simplification  $\cos 2\Theta_2 = 1 - (1 - \beta_0^2)^{1/2} / (1 + 3(1 - \beta_0^2)^{1/2}) = A$  say, which on differentiation gives,

$$dA/d\Theta_2 = -2 \sin 2\Theta_2 = -4\beta_0(1 - \beta_0^2)^{-1/2} d\beta_0 / \{1 + 3(1 - \beta_0^2)^{1/2}\}^2 d\Theta_2$$

or 
$$d\beta_0 = \{1 + 3(1 - \beta_0^2)^{1/2}\}^2 \sin 2\Theta_2 d\Theta_2 / 2\beta_0(1 - \beta_0^2)^{-1/2}$$

One can calculate the error in the measurement of the incident beam energy to a near approximation, using the relation  $dT = 0.51(1 - \beta_0^2)^{-3/2} \beta_0 d\beta_0$  for a known inaccuracy of the measurement of angle  $\Theta_2$ . Thus, measurements of angle  $\Phi$  with an accuracy of  $\pm 0.1$  makes the system accurate to  $\pm 1\%$  in the measurement of energy ( $T$ ), using the energy equation with symmetrical detector situation on either side of the beam. However, for simultaneous cross-section measurement with this energy measurement, one can move the conjugate counter to a place near the calculated value of  $\Theta_1$  for a given centre of mass angle in which scattering cross-section is being determined and look for the exact position where coincidence rate becomes maximum.

Calculation for this purpose have been done with the help of CERN computer CDC6400, and authors are highly thankful to Dr. J. B. M. Pattison, group leader for the Neutrino Beam Study Group, and to Dr. V. M. Bhise, Reader in the department of applied mathematics of this Institute for continued interest and discussions.

# REFERENCES

- Bhiday M. R., Jennings R. E. & Kalamus P. I. P. 1958 *Proc. Phys. Soc.* **72**, 973.  
 Bhabha H. J. 1936 *Proc. Roy. Soc.* **A154**, 195.  
 Dougal R. C. 1965 *Proc. Phys. Soc.* **85**, 851.  
 Husák V. & Perinová V. 1969 *Phys. Med. Biol.* **14**, 233.  
 Koch H. W., Motz J. W. & Olsen H. 1964 *Rev. Mod. Phys.* **36**, 881.  
 Moller C. 1932 *Ann. der Phys.* **14**, 531.  
 Seigbahn K. 1965 *Alpha, Beta and Gamma-ray Spectroscopy—I*, 485, North Holland Publishing Co. Amsterdam.  
 Wilkinson D. H. 1952 *Rev. Sci. Instr.* **23**, 414.  
 Wiegand C. 1969 *Proc. Int. Conf. High. Energy. Acc & Instr.* CERN, 581.

# *Letters to the Editor*

*Indian J. Phys.* **44**, 264-265 (1970)

## Modulation effects in NMR.

BY C. RAGHAVENDRA RAO

*Department of Physics, Central College Bangalore University  
Bangalore*

(Received 24 September 1969, Revised 20 November 1969)

While observing NMR absorption lines, it is the usual practice to modulate the absorption line with a sine wave of suitable amplitude and the resulting AC signal whose amplitude is proportional to the first derivative of the line shape function  $g(h)$  is recorded where  $h$  is the value of the magnetic field from the resonance value. The purpose of this note is to show the effect of different types of modulation on the strength of the signal that is recorded.

Let the modulation employed be  $f(t)$  ... (1)

The out-put is proportional to  $g'(h)[h+f(t)]$  ... (2)

where  $g'(h)$  is the first derivative of  $g(h)$  and  $h = H - H_0$

Let  $g(h) = ph$  ... (3)

where  $p$  is a constant (i.e., we assume that the portion of the line traversed by the modulation is linear).

If we use a phase sensitive detector, the out-put  $v$  of the PSD is proportional to the coefficient of  $\sin \omega t$  in (2).

Let us assume that  $f(t)$  the modulation used has a periodicity  $\omega$ .  
Then,

$$f(t) = a_0 + a_1 \sin \omega t + a_2 \sin 2\omega t + a_3 \sin 3\omega t + a_4 \sin 4\omega t + a_5 \sin 5\omega t \quad \dots (4)$$

Expressing  $\sin 2\omega t$ ,  $\sin 3\omega t$  etc in terms of  $\sin \omega t$ , we get

$$f(t) = a_0 + \sin \omega t [(a_1 + 3a_3) + \cos \omega t (2a_2 + 4a_4) - 4a_3 \sin^2 \omega t + 5a_5 \cos^2 \omega t - 8a_4 \cos \omega t \sin^2 \omega t - 8a_5 \sin^2 \omega t \cos^2 \omega t - 7a_5 \sin^2 \omega t + 8a_5 \sin^4 \omega t]$$

Replacing terms within brackets by their averages, we find,

$$v = k(a_1 + a_3 + a_5) \quad \dots (5)$$

where  $k$  is a constant.

*Special cases* : If we use a full square-wave modulation of frequency  $\omega$  and amplitude  $h_m$  we can write,

$$f(t) = \frac{4h_m}{\pi} [\sin \omega t + 1/3 \sin 3\omega t + 1/5 \sin 5\omega t + \dots]$$

$$\therefore v = \frac{322}{165} (kh_m).$$

In a similar way we can show that,  $v = kh_m$  for sinusoidal modulation,  $\frac{161}{165}(kh_m)$  for half square-wave modulation and  $\frac{80.5}{165}(kh_m)$  for saw-tooth type of modulation. Thus we find that we get the strongest signal if we use a full square-wave modulation.

It is enough to consider the first four or five terms in (4) because the different types of modulation that we are thinking of happen to be represented by fairly fast converging Fourier series. But care must be taken to see, while employing square-wave modulation, that  $\omega$  is small so that  $5\omega$  is not large enough to affect the steady state assumptions made in the theory.

The author thanks Prof. K. N. Kuchela for kind interest.

*Indian J. Phys.* 265-267 (1970)

## Vibrational spectra of *o*- and *m*-methylstyrenes

By V. N. VERMA AND KAMALESH SINGH

*Department of Spectroscopy, Banaras Hindu University,  
Varanasi-5 India*

(Received 8 December 1969, revised 26 February 1970)

Styrene is one of the important organic compounds which has attracted the attention of a large number of workers. The infrared, Raman and electronic spectra of styrene have been studied thoroughly by Stair & Colbelt (1935), Williams (1936) and Pitzer *et al* (1946). The infrared absorption spectra of its halogenated derivatives and electronic absorption spectra of the three isomeric methylstyrenes have been studied by Ansari (1968). But in the case of its methyl substituent, no work on infrared and Raman spectra has been reported so far. The present note deals with the infrared spectra of *o*- and *m*-methylstyrenes.

The compounds of L.R. grade quality were supplied by Koch-Light Laboratories, U.K. The infrared traces of the compounds were recorded in the liquid phase on a 13U Perkin Elmer double beam infrared spectrophotometer equipped with NaCl prism using a cell of thickness 0.05 mm.

Both the molecules belong to the  $C_s$  symmetry with the molecular plane as the only symmetry element when we assume the vinyl and methyl groups behaving as a single atom. The 51 normal modes of vibrations are divided as 35  $a'$  (planar) and 16  $a''$  (non-planar). All the vibrations are allowed in infrared and Raman spectra.

In making the assignments, assistance has been taken from comparison with the assignments of benzene by Herzberg (1945), styrene by Stair & Colbelt (1935), isomeric bromostyrenes by Ansari (1968), isomeric methylanilines by Verma (1967) and  $\beta$ -bromostyrene by Singh & Singh (1968). The assignments of observed bands with visual estimates of the relative intensity is presented in table 1.

Table 1. Fundamental vibrational frequencies and their assignments for *o*- & *m*-methylstyrenes

<i>o</i> -methylstyrene (cm <sup>-1</sup> )	<i>m</i> -methylstyrene (cm <sup>-1</sup> )	Species ( <i>C<sub>s</sub></i> )	Assignments
720 (10)	687 (9)	<i>a''</i>	C-C-C bending o.p.
770 (10)	790 (10)	<i>a'</i>	C-CH <sub>3</sub> stretching
867 (1)	883 (4)	<i>a''</i>	C-H bending o.p.
913 (8)	902 (9)	<i>a''</i>	= CH <sub>2</sub> bending o.p.
991 (7)	990 (8)	<i>a''</i>	C-H bending o.p.
1028 (3)	1033 (2)	<i>a'</i>	C-C ring breathing
1057 (2)	1043 (3)	<i>a'</i>	CH <sub>3</sub> rocking
1108 (3)	1095 (3)	<i>a'</i>	C-H bending i.p.
1164 (2)	1159 (3)	<i>a'</i>	C-H bending i.p.
1185 (2)	1168 (3)	<i>a'</i>	C-H bending i.p.
1222 (2)	1194 (1)	<i>a'</i>	C-CH = CH <sub>2</sub> stretching
1280 (2)	1280 (3)	<i>a'</i>	= CH bending i.p. (group-CH = CH <sub>2</sub> )
1310 (1)	1310 (1)	<i>a'</i>	C-C stretching
1390 (4)	1383 (3)	<i>a'</i>	C-H sym. bending in methyl group.
1418 (5)	1418 (3)	<i>a'</i>	= CH <sub>2</sub> bending i.p. (group-CH = CH <sub>2</sub> )
1461 (7)	1448 (4)	<i>a'</i>	C-H asym. bending in methyl group
1487 (8)	1487 (5)	<i>a'</i>	C-C stretching
1562 (1)	1575 (5)	<i>a'</i>	C-C stretching
1590 (1)	1592 (5)	<i>a'</i>	C-C stretching
1624 (7)	1625 (3)	<i>a'</i>	C = C stretching (group-CH = CH <sub>2</sub> )
2872 (sh)	2870 (sh)	<i>a'</i>	C-H sym. stretching in methyl group.
2970 (7)	2952 (5)	<i>a'</i>	C-H asym. stretching in methyl group.
3050 (8)	3032 (6)	<i>a'</i>	= CH stretching (group-CH = CH <sub>2</sub> )

N.B. :—The corresponding intensity is given in the parenthesis.

o.p. = out-of-plane; i.p. = in-plane; sh = shoulder; sym. = symmetric and asym. = asymmetric.

The authors are thankful to Prof. N. L. Singh and Dr. D. K. Rai for interesting discussions. V. N. Verma is grateful to C.S.I.R. (New Delhi) and K. Singh to U.G.C. (New Delhi) for financial assistance.

## REFERENCES

- Ansari B. J. 1968, *Indian J. of Pure & Applied Phys.*, **6**, 289.  
 Herzberg G., 1945, *Infrared and Raman Spectra*, D Van Nostrand Co. Inc, 364.  
 Pitzor K. S., Guttman L. & Westrum E. F., 1946, *J. Amer Chem. Soc.*, **68**, 2209.  
 Singh K. & Singh V. B. 1968, *Current Science*, **137**, No. 18, 425.  
 Stair R. & Colbert W. W. 1935 *J. Res. Natl. Bur. Standards*, **15**, 296.  
 Verma P. K. 1967, *Spectroscopic Studies of Organic Molecules*. Ph.D. Thesis, Banaras Hindu University, India.  
 Williams D., 1936, *Physics*, **7**, 399.

*Indian J. Phys.* **44**, 267-269 (1970)

A preliminary report on the structure of glycoeyamine hemihydrate, diglycine monopicrate and 4-(N-phenyl piperizino)-6-methoxy quinaldine

BY SANKARANANDA GUHA

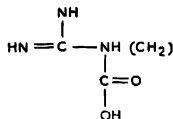
*Indian Association for the Cultivation of Science, Calcutta-32*

(Received 1 September 1970)

The crystal structure determination of several biologically important compounds has been undertaken in this laboratory in order to explain their functions in relation to structure. A preliminary report on the structural study of three of them is presented here.

1. *Glycoeyamine hemihydrate*

Glycoeyamine or guanidoacetic acid having the chemical formula



is an important amino acid. The colourless crystal grows as elongated prism on slow evaporation of an aqueous solution of the compound at room temperature.

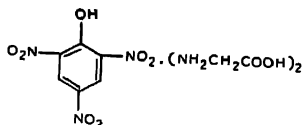
Rotation and Weissenberg X-ray photographs show that the crystal belongs to the monoclinic system with  $a = 5.09\text{\AA}$ ,  $b = 6.16\text{\AA}$ ,  $c = 17.47\text{\AA}$  and  $\beta = 95.2^\circ$ .

The only systematic absences are for  $0k0$  for  $k$  odd and  $h0l$  for  $h+l$  odd, indicating that the space group is  $P2_{1/n}$ . The density of the crystal as determined by floatation method using a mixture of carbon tetrachloride and benzene has been found to be 1.526, while that calculated for 4 molecules of  $\text{HN}=\text{CNHNHCH}_2\text{-COOH}$ .  $\frac{1}{2}\text{H}_2\text{O}$  per unit cell is 1.525.

Complete three-dimensional data have been collected using multiple-film equiinclination Weissenberg technique with  $\text{CuK}\alpha$  radiation. Intensities of the spots have been estimated by visual comparison with a calibrated strip. Spot size (Phillips 1954, 1956), Lorentz and polarization corrections have been applied to the intensity values, after which they have been brought to an absolute scale. The  $E$  value or the normalized structure factor has been calculated for each of the reflections. The structure determination is in progress.

## 2. Diglycine monopicrate

The importance of the first basic amino acid glycine in living systems is well known. All amino acids form additional compounds with various acids. Leven & Van Slyke (1912) described an odd picrate of glycine, *viz.* (glycine)<sub>2</sub> picrate,

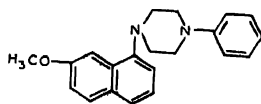


On mixing picric acid and glycine in the ratio of 1 : 1.5 by weight and freezing at  $0^\circ\text{C}$ , yellow tabular crystals of diglycine monopicrate are formed.

The X-ray analysis reveals that the crystal belongs to the monoclinic system. The cell constants are  $a = 15.46\text{\AA}$ ,  $b = 6.92\text{\AA}$ ,  $c = 15.24\text{\AA}$  and  $\beta = 93.2^\circ$ . The only systematic absences are  $0k0$  for  $k$  odd and  $h0l$  with  $l$  odd. The space group is therefore  $P2_{1/c}$ . The observed density of the crystal is 1.55, while that calculated for 4 molecules of  $\text{C}_6\text{H}_2(\text{NO}_2)_3\text{OH}(\text{NH}_2\text{CH}_2\text{COOH})_2$  in the unit cell is 1.54. Complete three dimensional data have been collected and processed as described above. Further work on it is in progress. —

## 3. 4-(*N*-phenyl piperizino)-6-methoxy quinaldine

This compound is very interesting for its medicinal properties. It is an anti-spasmodic agent, both neurologic and musculotropic but it has no action on uterus. Its chemical formula is



and molecular weight 323. The dull light yellow coloured crystal grows as long needles on slow evaporation of a solution of the compound in methanol. The crystal is orthorhombic with  $a = 8.46\text{\AA}$ ,  $b = 13.45\text{\AA}$  and  $c = 16.60\text{\AA}$ . The observed density is 1.14, while that calculated for 4 molecules of  $\text{N}_2\text{C}_{21}\text{OH}_{27}$  per unit cell is 1.13. The only systematic absences are  $0kl$  for  $k+1$  odd,  $h0l$  for  $h$  odd,  $h00$  for  $h$  odd,  $0k0$  for  $k$  odd and  $00l$  for  $l$  odd, indicating the space group to be either  $Pna2_1$  or  $P2_1/n2_1/a2_1/m$ . The latter space group requires 8 molecules per unit cell, and to accommodate only 4 the molecule must have a mirror or 2-fold symmetry which is extremely unlikely in this case. The space group is therefore most probably  $Pna2_1$ . For this crystal also the three dimensional intensity data have been collected and processed. The structure determination is in progress.

The author thanks Dr S. C. Chakravarty of Burdwan University for allowing to collect the X-ray data in his laboratory. His thanks are also due to Dr. R. K. Sen, D.Sc., for encouragement and to the Council of Scientific and Industrial Research, New Delhi, for financial assistance.

#### REFERENCES

- Phillips D. C. 1954 *Acta Cryst.* **7**, 746.  
1956 *Acta Cryst.* **9**, 819.  
Leven P. A. & Van Slyke D. D. 1912 *J. Biol. Chem.* **12**, 285.

## BOOK REVIEWS

### *Physics of Hot Plasma*

Eds B. J. Rye & J. C. Taylor O. P. P. 455 XIV.

*Oliver & Boyd*, Edinburgh, 1970. Price £8.

This book contains the lectures delivered at the 9th 'Scottish Universities' Summer School held at Newbattle Abbey from 28th July to 16th August 1968 and was sponsored jointly by Scottish Universities and NATO. This is a collection of lectures delivered on different aspects of plasma by eminent people in the line, however, topics are arranged in proper sequence, such that the subject is developed most logically. According to present reviewer the following topics are remarkably well covered (a) Kinetic theory of plasma (b) Waves and oscillations (c) Collisionless shocks (d) Collisionless shock waves. This is a welcome edition. This book can be treated as an advanced text and will be useful to research workers and students alike. At a first glance one may think this is a collection of theoretical lectures but actually excellent attempts have been made to demonstrate how theory and experiments are linked up in hot plasma. Kinetic theory of plasma was discussed at length by Prof. W. B. Thomson & C. Oberman; the theory of waves and oscillations by Prof. R. J. Taylor and plasma instabilities by E. G. Harris. The importance of computational problems and numerical methods in plasma physics and controlled thermonuclear research was demonstrated by Prof. J. Killen. Turbulence was discussed by Prof. M. G. Rustidge. The topics which are of current interest 'Collisionless shock' and 'Collisionless shock waves' were discussed by Prof. H. Volk and Prof. J. W. M. Paul. These topics will surely receive more attention (both theoretically and experimentally) in near future. The theoretical and experimental aspects of production of plasma by focussed laser beam were discussed by Prof. S. A. Ramsden. Experiments on the production and confinement of hot plasma was covered by Prof. G. B. F. Niblet while optical diagnostic was given by Prof. U. Ascoli Bartoli. Each topic is followed by an excellent up-to-date bibliography.

B. C.

### *Correlation Effects in Atoms and Molecules*

Advances in Chemical Physics, Vol. XIV,

Edited by R. Lefebvre and C. Moser.

*Interscience Publishers*, 1969, 545 pages

Recently the field theoretic methods are being extensively applied to atoms, molecules and many areas of solid state physics. Calculation of accurate wave functions of many-electron atoms and polyatomic molecules poses formidable computational problems. Hartree-Fock and other self-consistent methods are not suitable to deal with problems such as correlation and co-operative phenomena which are distinctly "many body effects".

The volume under review is a collection of papers which present field theoretic methods used in the calculations of correlation effects in atoms and molecules. Of the 13 papers included in this volume, 8 deal exclusively with atoms and among the rest one is on the electron gas. With the exception of two papers, all deal with the extensions of "traditional" methods such as Hartree-Fock methods and Bethe-Goldstone diagram technique of the many body theory. The exceptions are by B. R. Judd who makes extensive use of group theory and by



V. V. Tolmachev who makes use of angular momentum diagrams which are quite interesting. The Editors hope that this book will encourage the younger generation to work in this most promising yet notoriously difficult and challenging area of physics. In the opinion of the reviewer, this is a very valuable book for those who are carrying out active research work in this field but those who want to have a bird's eye view of the situation will find it difficult to follow most of the book.

A. S. C.

### *Cosmic Electrodynamics*

Piddington—John Wiley & Sons. pages 305.

This book is a valuable addition to the subject which has appeal to both physicists and astrophysicists. After giving a brief historical highlight of the subject, the author proceeds further to present elaborately the various aspects of cosmic electrodynamics, namely cosmic plasmas, sun and solar activity, interplanetary medium, earth's magnetosphere, geomagnetic disturbances, radio galaxies, ionospheric currents and other related phenomena. In the first four chapters the basic principles are discussed. The rest of the chapters are devoted to solar system and other interesting phenomena of geophysics. In many contexts the observational results are described and are explained as far as possible with the existing theories. The chapters on galactic forms and radio galaxies are quite good.

On the whole, this book provides an excellent overview of the current status of many aspects of cosmic electrodynamics. This book will not only be of interest to specialist in the field but will be a very useful monograph for both students and research worker as a text and reference copy.

R. D.

### *Elementary Calculations in Biochemistry and Physiology*

J. A. Barclay and K. White, Churchill, London (1969)—88 + viii pages—20sh

This book, according to the authors, is intended to help "the medical students in preclinical years, the students of human biology in colleges of education and all new students of biochemistry and physiology who find that numerical calculation seems to hinder rather than help the approach to these subjects". Of its 12 chapters, four are devoted to topics of general or mathematical utility—S.I. units, numerical accuracy, errors of observation and calibration curves. These should prove very helpful to students just entering college for courses in chemistry or physiology whose mathematical background is deficient. Five chapters describe elementary calculations concerned with measures of composition, the pH scale, equilibrium constants, electrode measurements and osmotic phenomena. They provide a useful introduction to basic concepts, though the theoretical treatment is at too elementary a level to be of value to students taking degree courses in chemistry in preparation for specialization at the M.Sc. level. In particular, the chapter on electrode measurements appears to be too superficial on the theoretical side. It would have been helpful to have discussed the physical basis and applications of the Nernst equation more fully.

Two chapters on respiration, circulation and work and electrolyte and water balance deal with calculations of interest in physiology. The purpose of the last chapter 'non-calculations' is intriguing; it merely illustrates problems which are insoluble because an essential datum is not available, or are not susceptible to numerical treatment.

The book should be of value chiefly as a preliminary aid to exorcising the fear of even simple mathematical treatment, found so often among students of biology. The style of writing is calculated to hold the interest of the student. There are few misprints—but we may draw attention to the following—p 6, millieron for millimicron in the table of small dimensional units; omission of the equation no.—(6)—from the equation on p. 37; 'relaced' for 'replaced' on p 78, 1.16. The price of 20sh may discourage wide use of the book by those for whom it is meant.

A. N.

### *Electrodynamics of Particles and Plasmas*

By Clemmow and Daugherty, *Addison Wesley Publishing Co.* (1969) 457 pages.

The subject, dealt with in the present book though of recent origin, has developed so much during the past four decades that it indeed appears a difficult task to compress it entirely into a single book. However, Clemmow and Dougherty, who have themselves contributed so significantly to the development of the subject, have done a great service to the readers by writing this book. It will be found useful equally by those who wish to learn the subject and by those who wish to use it as a reference book. The authors have clearly set all the physical principles and given the physical explanations of all the results which they discuss in the book. They have given important references at the end of each chapter, specially those which they refer in the text. They have also given some examples at the end of each chapter so that the reader may check for himself if he has understood what he has learnt in the chapter. This entitles the book to be treated as a text book.

The reviewer has great pleasure in recommending this book to the research workers on this fascinating subject, which has been dealt in the book using both the particle and the continuum descriptions. To some readers the book will look incomplete as far as the discussion of instability and the correlations is concerned but the authors have indicated the texts to which a reader can refer in the case of the first topic and it is difficult to expect them to include all the literature in development in the case of the second topic.

The book contains the following twelve chapters covering about 450 pages :

- 1) Introduction,
- 2) Electro-dynamics
- 3) Čerenkov and Gyro Radiation
- 4) Dynamical Motion of a Point Charge
- 5) Waves in an Ionized Gas : Magneto-Ionic Theory
- 6) Plasma Streams
- 7) Boltzmann's Equation,
- 8) Waves in Ionized Gases : Kinetic Theory
- 9) Waves in Ionized Gases : Kinetic Theory (continued)
- 10) Micro Instabilities
- 11) The Derivation of Magnetohydrodynamics
- 12) Kinetic Equations in Plasmas

In the opinion of the reviewer it is an excellent addition to the library on the subject and the authors deserve hearty congratulations on producing such an useful book.

P. L. B.

# INDIAN JOURNAL OF PHYSICS

VOL. 44

No. 5

AND

VOL. 53

PROCEEDINGS

No. 5

OF THE

INDIAN ASSOCIATION FOR THE CULTIVATION OF SCIENCE

*(Edited in collaboration with the Indian Physical Society).*

**MAY 1970**

PUBLISHED BY THE

INDIAN ASSOCIATION FOR THE CULTIVATION OF SCIENCE

JADAVPUR, CALCUTTA-32



# NON-AQUEOUS TITRATION

A monograph on acid-base titrations in organic solvents

By

PROF. SANTI R. PALIT, D.Sc., F.R.I.C., F.N.I.

DR. MIHIR NATH DAS, D.Phil.

AND

MR. G. R. SOMAYAJULU, M.Sc.

This book is a comprehensive survey of the recently developed methods of acid-base titrations in non-aqueous solvents. Acid-base concept, as developed by Lowry-Brönsted and Lewis is succinctly presented in this slender volume. This subject is divided into two classes, viz. titration of weak bases and titration of weak acids. The method of 'glycolic titration' is described at a great length as also the method of 'acetic titration' including its recent modifications for the estimation of weak bases. Various methods for the titration of weak acids are duly described. A reference list of all pertinent publications is included in this book.

*122 pages with 23 diagrams (1954)*

**Inland Rs. 3 only. Foreign (including postage) \$ 1.00 or 5s.**

*Published by :*

INDIAN ASSOCIATION FOR THE CULTIVATION OF SCIENCE  
JADAVPUR, CALCUTTA-32, INDIA

# PUBLICATIONS OF THE INDIAN ASSOCIATION FOR THE CULTIVATION OF SCIENCE

				Rs. P.
1. RUSSELL, E. J.	..	Methods in Scientific Research	..	0.37
2. JEANS, J. H.	..	The Origin of the Planets	..	0.37
3. ASTON, F. W.	..	Separation of Isotopes	..	0.37
4. LENNARD-JONES, J. E.	..	Interatomic Forces	..	1.50
5. HILL, A. W.	..	The Royal Botanic Gardens, Kew	..	1 50
6. MILLIKAN, R. A.	..	The Educational Aims and Practices of the California Institute of Technology	..	0.37
7. MITRA, S. K.	..	Active Nitrogen—A New Theory	..	2.50
8. WADIA, D. N.	..	Petroleum Resources of India	..	2.50
9. RAY, P.	..	The Theory of Valency and the Structure of Chemical Compounds	..	3 00
10. MUKHERJEE, J. N.	..	The Role of the Electrical Double Layer in the Electro-Chemistry of Colloids	..	1.75
11. ROBINSON, R.	..	Distribution of Anthocyanins	..	1 25
12. CHAPMAN, S.	..	The Earth's Magnetism and its Changes	..	1 00
13. MARK, H.	..	Catalysts in Polymerization Reactions	..	1.50
14. AMALDI, E.	..	Diffraction Effects in the Scattering of Neutrons, Mesons and Electrons by Nuclei	..	1.50
15. FIESER, L. F.	..	Lapinone, A New Antimalarial	..	1.00
16. BOSE, N. K.	..	Fluid Dynamics	..	1.25
17. VENKATARAMAN, K.	..	Constitutional Problems Concerning Vat Dyes	..	1.00
18. ROY, J. N.	..	The Chemical Basis of Some Physiological Actions	..	1.00
19. SHOENBERG, D.	..	Superconductivity	..	1.00
20. PALIT, S. R.	..	Non-Aqueous Titration	..	3.00
21. KRISHNAN, M. S.	..	Iron Ores of India	..	5.00
22. SEN, S. N.	..	Bijnaner Itihas ; Vol. I	..	10.500
		Vol. II	..	12.00
23. SESHADRI, T. R.	..	An Investigation of Plant Drugs and Insecticides	..	1.00
24. BOWEN, E. G.	..	The Formation of Natural and Artificial Rain	..	1 50
25. BANERJI, S. K.	..	Earthquakes in the Himalayan Region	..	3.00
26. MAGNETISM :	..	Report of the Symposium on Magnetism	..	7.00
27. WESTPHAL, DR. ING. E.	..	The Freight Tube Float	..	8.00
28. HIRSCHFELDER, J. O.	..	Molecular Physics and Intermolecular Forces	..	1.25
29. SEN, N. R.	..	The Modern Theory of Turbulence	..	2.00
30. DOUGLAS, A. E.	..	Some Recent Development in Molecular Spectroscopy	..	1.00
31. SHOENBERG, E.	..	Experimental Determination of the Electronic Structure of Metal	..	1.00

## The Raman spectrum of cyclohexyl benzene

By R. N. BAPAT

*Physics Department, Institute of Science, Bombay*

(Received 4 April 1970)

(Plate—9)

The Raman spectrum of cyclohexyl benzene has been studied in the present investigation. About fourteen lines have been recorded. The Raman and infrared spectra of cyclohexyl benzene are discussed in relation with those of benzene and cyclohexane.

### INTRODUCTION

The Raman spectra of benzene and cyclohexane are well known. The cyclohexyl benzene is also known as phenyl cyclohexane or hexahydro-diphenyl. The structure can be represented by the substitution of one of the hydrogen atoms in cyclohexane by a phenyl ring. The infrared spectrum of cyclohexyl benzene is already reported by the author (1962) and it was thought necessary to study the Raman spectrum of the molecule and find the Raman frequencies and discuss the two spectra, since, no previous work has been done on this molecule in this direction.

### EXPERIMENTAL

The Raman spectrum of cyclohexyl benzene was photographed on a three prism Steinheil spectrograph. The Raman source of Steinheil described previously by the author (1959) was used in the present investigation. Experimental details are now well known. An exposure of eight hours with this source was necessary to bring out the details in the spectrum (figure 1). The frequencies of the Raman lines of cyclohexyl benzene are given in table 2 with intensities visually estimated, the strongest line being estimated as ten.

Only principal vibration frequencies of cyclohexyl benzene along with corresponding ones for benzene and cyclohexane are given in the above table. The frequencies are taken from Infrared and Molecular Spectra by Herzberg.

### DISCUSSION

The normal vibrations of the benzene molecule have been worked out by Wilson (1934) who has ascribed it to twenty distinct fundamental frequencies. The benzene molecule is well known to have the shape of a regular plane hexagon and belongs to the symmetry group  $D_{6h}$ . This has been dealt with both theoretically and experimentally by Ingold (1936) and his coworkers. Of the twenty fundamentals of benzene seven (five degenerate and two non degenerate) are

TABLE 1. Principal infrared frequencies of cyclohexane, cyclohexyl benzene and benzene

cyclohexane	cyclohexyl benzene	benzene
	3039 s	3021 s (3044) (Raman)
2933 vvs	2932 vs	—
2841 (?)s	2865* vs	—
	1607* s	(1606) inactive in benzene
	1588 s	(1587) inactive in benzene
	1495 vs	1479 vs
1449 vvs	1449* vs	—
	1177 m	1178 m
	1068	—
	1029* s	1036 vvs
1016 mw	1005	—
	996*	993
	884	—
861 vvs	863 ms	847
	829* m	—
	778*	—
	753	—
	696 vvs	680 s

s-strong, vs-very strong, vvs-very very strong m-medium and mw-medium weak  
 \*common to both Raman and infrared.

TABLE 2. Raman frequencies in  $\text{cm}^{-1}$  of cyclohexyl benzene

cyclohexane	cyclohexyl benzene	benzene	substituent
2937	3068 (5)	3061	
2853	2945 (5)		
	2865 (6)		—C— of cyclohexyl   benzene H
	2795 (6)		
	1607 (5)	1606	
1442	1442 (5)		
	1203 (1)	1178	C—C substituent
1029	1030 (2)		
	999 (10)	991	
	826 (1)	847	
	778 (3)		
	624 (3)	606	
	280 (3)		C—C substituent in plane
	147 (2)		C—C substituent out of plane



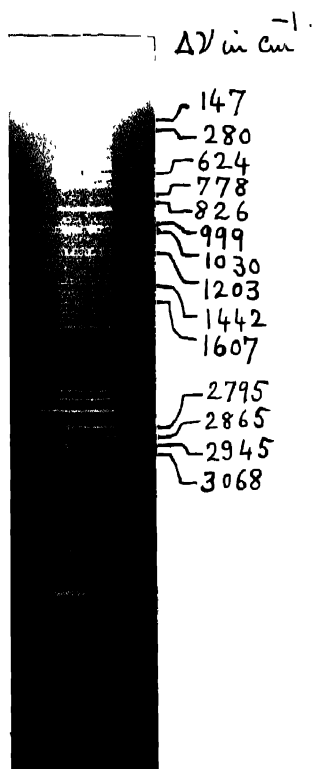


Figure 1. Raman spectrum of cyclohexylbenzene.



allowed in the Raman effect and four fundamentals (three degenerate and one non-degenerate) are allowed in the infrared. Because of the centre of symmetry, fundamentals which are allowed in the Raman effect are forbidden in the infrared and the converse is true.

In cyclohexyl benzene due to the substitution of  $C_6H_{11}$  in place of one of the H atoms of benzene, the symmetry  $D_{6h}$  is reduced to  $C_{2v}$ , if we assume the cyclohexyl group to behave as a single atom. The transformation properties and the selection rules of the various symmetry types of this point group and the number of vibrations of the molecule belonging to each symmetry type are well-known (Sponer 1942). Cyclohexyl benzene may be considered as a monosubstituted benzene.

#### INFRARED SPECTRUM

The principal vibration frequencies of cyclohexyl benzene (Bapat 1962) along with corresponding ones for benzene and cyclohexane are tabulated in table 1. Under the  $C_{2v}$  group all frequencies except the  $A_2$  frequencies are allowed.

In the C—H stretching region a band near  $3039\text{ cm}^{-1}$  obviously corresponds to one of the CH stretching bands of the benzene group. Since the symmetry is reduced it is likely that  $3044\text{ cm}^{-1}$  of Raman spectrum of benzene may be the one which corresponds to  $3030\text{ cm}^{-1}$  in the present case.  $2932$  and  $2865\text{ cm}^{-1}$  bands arise from the CH stretching of the  $CH_2$  group of cyclohexyl part and have been shown to be as such. The prominent band  $1607\text{ cm}^{-1}$  in the present case arises from benzene part and corresponds to either of the  $1606\text{ cm}^{-1}$ ,  $1596\text{ cm}^{-1}$  Fermi doublet in benzene arising from C—C stretching. The shoulder at  $1588\text{ cm}^{-1}$  may correspond to other component; the Raman Spectrum, however does not show a line corresponding to this. The  $1495\text{ cm}^{-1}$  band here corresponds to  $1479\text{ cm}^{-1}$ , C—C stretching band of benzene, whereas the strong band at  $1449\text{ cm}^{-1}$  corresponds to strong band at  $1449\text{ cm}^{-1}$  in cyclohexane corresponding to  $CH_2$  bending vibration.  $1177$  and  $1029\text{ cm}^{-1}$  in the present case correspond to inplane hydrogen bending vibration of benzene. The strong band at  $996\text{ cm}^{-1}$  corresponds to symmetric stretching of benzene ring.  $829$  and  $696\text{ cm}^{-1}$  in the present case correspond to  $847$  and  $680\text{ cm}^{-1}$  out of plane hydrogen bending vibrations of benzene. A very prominent band at  $863\text{ cm}^{-1}$  in the present case corresponds to out of plane hydrogen bending of the cyclohexane group.

It is thus apparent that the whole spectrum can be conveniently divided into more or less distinct groups of bands arising from the cyclohexane and phenyl part. It is observed that the frequencies are not markedly perturbed by the substituent in either part, principally because one is aromatic nucleus with aromatic C—H bonds, whereas the other is an aliphatic saturated ring with cyclic

methylene groups. The two have very distinct characteristic spectra. It is further observed that there are a number of frequencies which are common to infrared and Raman spectra and that cyclohexyl substitution markedly relaxes the selection rules of  $D_{6h}$  group of benzene. The analysis of only the prominent bands is given here. The complete analysis shows that the spectrum can be easily accounted for as a superposition of two spectra when account is taken of the large number of fundamentals.

#### RAMAN SPECTRUM

All the frequencies observed in Raman spectrum of cyclohexyl benzene are recorded in table 2. The table also records the relevant Raman frequencies of benzene and cyclohexane. It is observed that here again all the fundamentals active in the Raman spectrum of benzene are observed.

In the Raman spectrum of benzene the frequency  $991\text{ cm}^{-1}$  appears with great intensity. This can be correlated with the frequency  $999\text{ cm}^{-1}$  present very strongly in cyclohexyl benzene. This may be assigned as corresponding to  $992\text{ cm}^{-1}$  breathing vibration of benzene. It has been observed that the monosubstituted benzenes have a very characteristic Raman band near  $620\text{ cm}^{-1}$  and this has been justified in the present case by the frequency  $624\text{ cm}^{-1}$  present in the Raman spectrum of cyclohexyl benzene and corresponds to  $606\text{ cm}^{-1}$  of benzene. The frequency  $1607\text{ cm}^{-1}$  in cyclohexyl benzene can be correlated with the frequency  $1606\text{ cm}^{-1}$  in benzene. This is one of Fermi doublet at  $1606$  and  $1586\text{ cm}^{-1}$  which is prominent in the Raman spectrum of benzene. It is worth noting that only one component of the doublet appears prominently. Again the frequency  $2945\text{ cm}^{-1}$  in cyclohexyl benzene can be correlated with the frequency  $2937\text{ cm}^{-1}$  in cyclohexane. In the Raman spectrum of benzene there is a strong band at  $3061\text{ cm}^{-1}$  due to the C—H stretching vibration while a similar band is present at  $3068\text{ cm}^{-1}$  in the Raman spectrum of cyclohexyl benzene.

A characteristic band at  $2795\text{ cm}^{-1}$  with apparently no analogue in either case arises from C—H tertiary group at the substituted carbon of cyclohexyl ring. Other frequencies in the Raman spectrum correspond to cyclohexane part. Apart from  $2945$ ,  $2865\text{ cm}^{-1}$  bands which correspond to symmetric and asymmetric stretching vibration of  $\text{CH}_2$  group,  $1442\text{ cm}^{-1}$  corresponding to  $\text{CH}_2$  bending is also shown in cyclohexyl benzene.

In the Raman spectrum the bands  $1203$ ,  $280$  and  $147\text{ cm}^{-1}$  find no analogue in the spectra of either constituent. Apparently because of a monosubstitution, there should be one (phenyl) C—C (substituting) stretching and one each inplane and out of plane bending vibration;  $1203\text{ cm}^{-1}$  possibly does not correspond to  $1178$  of benzene because infrared band at  $1177\text{ cm}^{-1}$  has been assigned to this mode. Thus  $1203\text{ cm}^{-1}$  possibly represents C—C stretching

and 280 and 147 in plane and out of plane substituent bending vibrations. It is important to note that all substituent modes are predominantly Raman active because of close similarity of substituents. Since both phenyl as well as cyclohexane do not have such low frequency vibrations in the range of 280 or 147 and because of the large mass of substituent, the analysis of these is fairly correct.

#### REFERENCES

- Angus W. R., Bailey C. R., Hale J. B., Ingold K. C., Leckie A. H., Raisin C. G.,  
Thomson J. W. & Wilson C. L. 1936 *J. Chem. Soc. Part II*, 971.  
Bapat R. N. 1959 *Indian J. Phys.* **33**, 329.  
1962 *Indian J. Phys.* **36**, 543.  
Sponer H. 1942 *Rev. Mod. Phys.* **14**, 224.  
Wilson E. B. 1934 *Phys. Rev.* **45**, 706.

## Classical distributions of charged dust

By A. K. DATTA

*Physics Department, Bangabasi College, Calcutta, India*

*(Received 17 April 1970)*

The paper considers the equations of classical hydrodynamics and electromagnetism for a distribution of charged dust. Some general theorems and formulae are obtained.

The problem of cosmology has been discussed previously by many authors on the basis of Newtonian mechanics; and the general conclusion reached that while there exists a close parallelism between Newtonian and relativistic cosmologies, there is one important difference in that Newtonian mechanics allows many models which have no analogues in the relativistic theory (Heckmann & Schucking 1955, Raychaudhuri 1957). In recent years there has grown up a considerable literature on the statics and dynamics of charged dust distributions in general relativity, (De 1968, De & Raychaudhuri 1968, Som & Raychaudhuri 1968, Faulkos 1969, Hamoui 1969, Raychaudhuri & De 1970) and it would be of interest to examine how these results, obtained from general relativity, compare with those from Newtonian theory. Indeed, it was pointed out by Som & Raychaudhuri (1968) that there did not exist any classical analogue of an interesting class of solutions obtained by them.

In this preliminary investigation we present some general formulae by considering the coupled system of classical hydrodynamical equations for pressureless charged dust and Maxwell equations.

We have not introduced the ideas of special relativity even—so that we have not considered the electromagnetic energy density as a source of gravitational field and apparently our results can thus be of significance only for weak enough electromagnetic fields and velocities of dust small compared to that of light.

The following results obtained seem to be of interest :

- (i) A formula for the charge density in terms of the electric and magnetic field vectors and the acceleration and vorticity of the dust.
- (ii) The result that, in the absence of magnetic field, the vorticity and electric field are orthogonal.
- (iii) A theorem that if the magnetic field vanishes—the electric flux through any element of area bounded by particles of the dust is a constant of motion.
- (iv) For an irrotational motion in the absence of magnetic fields, the electric field vector is orthogonal to the surfaces defined by constant values of  $(\sigma/\rho)$

(v) A relation between the characteristics of motions (vorticity, acceleration, expansion and shear) and the matter density.

There exists results closely analogous to the above in the relativistic investigations of Raychaudhuri & De (1970).

The basic equations for a distribution of charged dust are :

$$\dot{\rho} + (\rho v_i), i = 0 \quad (11)$$

$$\dot{v}_i + v_{i,k} v_k = -V_{,i} + \sigma/\rho (E_i + 1/c \epsilon_{ikl} v_k H_l) \quad (2)$$

$$V_{,it} = 4\pi\rho \quad (3)$$

$$E_{i,t} = 4\pi\sigma \quad (4)$$

$$H_{i,t} = 0 \quad (5)$$

$$\epsilon_{ikl} E_{l,k} = -\dot{H}_i/c \quad (6)$$

$$\epsilon_{ikl} H_{l,k} = \dot{E}_i/c + 4\pi J_i \quad (7)$$

$$J_i = \sigma v_i \quad (8)$$

$$\frac{1}{2} \epsilon_{ikl} v_{l,k} = \omega_i \quad (9)$$

$\rho, \sigma$  are the matter and charge densities respectively,  $\vec{v}$ , the velocity of the dust,  $\vec{E}$  and  $\vec{H}$  the electric and magnetic field vectors and  $\vec{J}$  the current vector.  $V$  indicates the Newtonian gravitational potential which satisfies Poisson equation (equation (3)), the comma followed by an index indicates differentiation with respect to that coordinate and the Einstein convention of summing over repeated index is used,  $\epsilon_{ikl}$  is the Levi-Civita antisymmetric symbol. The conductivity of the charge is neglected and the dielectric constant and permeability are both put equal to unity and  $\vec{\omega}$  is the vorticity vector.

$$\text{From (1)} \quad \frac{1}{\rho} \frac{D\rho}{Dt} + v_{i,t} = 0 \quad \dots (10)$$

where  $(D/Dt)$  signifies differentiation with the fluid

$$i.e., \quad \frac{D}{Dt} = \frac{\partial}{\partial t} + v_i \cdot \frac{\partial}{\partial x_i} \quad \dots (11)$$

$$\text{Now let} \quad v_{i,t} \equiv \frac{3}{G} \frac{DG}{Dt} \quad \dots (12)$$

$$\text{Then from (10)} \quad \frac{D}{Dt} (\rho G^3) = 0 \quad \dots (13)$$

Again, on taking divergence of (7) and combining with (4) and (12) we get an equation of conservation of charge viz.  $D/Dt(\sigma G^3) = 0$  ... (14)

Now the field vectors as observed by an observer moving with the fluid are given by

$$E_i^* = E_i + 1/c \cdot e_{ikl} v_k H_l \quad \dots (15)$$

$$\text{and} \quad H_i^* = H_i - 1/c \cdot e_{ikl} v_k E_l \quad \dots (16)$$

Taking the divergence of (15) and combining with (9) and (7) we get after a little reduction

$$4\pi\sigma = E_{i,i}^* - 2H_i \frac{\omega_i}{c} - \frac{v_i}{c} \frac{\dot{E}_i}{c} \quad \dots (17)$$

This may be compared with the formula obtained from general relativity

$$4\pi\sigma = E^*_{;a} + E^* v_a - 2H_a \omega^a \quad \dots (18)$$

Similarly from (16), (5), (6), (9) we obtain

$$H^*_{i,i} + 2E_i \frac{\omega_i}{c} - \frac{v_i}{c} \frac{\dot{H}_i}{c} = 0 \quad \dots (19)$$

where again we have the analogous formula in general relativity

$$H^*_{;a} + 2E_a \omega^a + H^a v_a = 0 \quad \dots (20)$$

It may be noted that to our order of approximation  $\frac{v_i \dot{H}_i}{c^2}$  may be replaced by  $\frac{v_i \dot{H}_i^*}{c^2}$  so that for  $H^* = 0$  equation (19) yields

$$E_i \omega_i = 0 \quad \dots (21)$$

Under the condition of no magnetic field we obtain combining with (7), (4), (12) and after a little reduction

$$G^3 \frac{DE_i}{Dt} = G^3 E_i \frac{\partial v_i}{\partial x_i} - E_i G^3 \frac{3}{G} \frac{DG}{Dt} \quad \dots (22)$$

$$\text{or,} \quad \frac{D}{Dt} (E_i G^3) = E_i G^3 \frac{\partial v_i}{\partial x_i}$$

$$\text{or,} \quad \frac{D}{Dt} \left( \frac{E_i}{\rho} \right) = \frac{E_i}{\rho} \frac{\partial v_i}{\partial x_i} \quad \dots (23)$$

Let us now consider two points  $A$  and  $B$  in the dust lying instantaneously on an electric line of force at a distance apart

$$dx_i = \lambda \frac{E_i}{\rho} \quad \dots (24)$$

where  $\lambda$  is a small constant. We have for the difference of velocity at  $A$  and  $B$  for the  $i$ -th component

$$v_{iB} - v_{iA} = \frac{\partial v_i}{\partial x_k} dx_k$$



or, with the help of (23) and (24)

$$v_{iB} - v_{iA} = \lambda \frac{D}{Dt} \left( \frac{E_i}{\rho} \right) \quad (25)$$

Now at an instant later by  $dt$ , when the particles are at  $A^1$  and  $B^1$  we have

$$dx'_i = dx_i + (v_{iB} - v_{iA})dt$$

$$\text{or,} \quad dx'_i = \lambda \left[ \frac{E_i}{\rho} + \frac{D}{Dt} \left( \frac{E_i}{\rho} \right) dt \right] \quad \dots (26)$$

Equation (26) shows that the relation (24) is not affected by the motion. Hence if  $S$  be the area of an element of a tube of force, we have from the conservation of mass  $\rho s dx_i = \text{constant}$  and from (24),  $E_i S = \text{constant}$  i.e., the electric intensity varies inversely as the cross-sectional area of an element of fluid orthogonal to the intensity. Considering the curl of equation (2) and combining with (11), (12), (6) and (15) and after a little reduction we obtain

$$\frac{D}{Dt} (v_{ik} G^2) - \frac{1}{2c} \left( \frac{\sigma}{\rho} \right) \frac{D}{Dt} (H_i G^2) + \frac{G^2}{2} e_{lmn} \left( \frac{\sigma}{\rho} \right)_{,m} E^*_{n,i} = 0 \quad \dots (27)$$

Equation (27) yields in absence of magnetic field and rotation the result that electric field vector is orthogonal to the surfaces defined by constant values of  $(\sigma/\rho)$ .

For the relation (v) we take the divergence of (2) and combine with (3), (4), (7), (9), (12) and after a little reduction we obtain

$$\begin{aligned} 3 \frac{D^2 G}{G Dt^2} = & -4\pi\rho \left( 1 - \frac{\sigma^2}{\rho^2} \right) + \left( \frac{\sigma}{\rho} \right)_{,i} E_i + \left( \frac{\sigma}{\rho} \right)_{,t} e_{ikl} v_k H_l + 2 \left( \frac{\sigma}{\rho} \right) H_t \frac{\omega_t}{c} \\ & - \left( \frac{\sigma}{\rho} \right) \frac{v_t}{c} \frac{\dot{E}_t}{c} - v_{i,k} v_{k,i} + \frac{1}{3} (v_{i,t})^2 \end{aligned} \quad \dots (28)$$

Writing,

$$\begin{aligned} v_{i,k} &= \underline{v_{ik}} + \underline{v_{ik}} \\ v_{k,t} &= \underline{v_{tk}} - \underline{v_{tk}} \end{aligned}$$

$$\text{we have} \quad \frac{1}{3} (v_{i,t})^2 - v_{i,k} v_{k,i} = -\phi^2 + 2\omega^2 \quad \dots (29)$$

where again shear ( $\phi^2$ ) vanishes if and only if  $v_{ik} = \alpha \delta_{ik}$ , i.e., the expansion be isotropic at the point considered and is positive otherwise. We have from (28), (29) and (15) finally,

$$\frac{3}{G} \frac{D^2 G}{Dt^2} = -4\pi\rho \left( 1 - \frac{\sigma^2}{\rho^2} \right) + \left( \frac{\sigma}{\rho} \right)_{,i} E^*_{i,t} + 2 \left( \frac{\sigma}{\rho} \right) H_t \frac{\omega_t}{c} - \phi^2 + 2\omega^2 - \left( \frac{\sigma}{\rho} \right) \frac{v_t}{c} \frac{\dot{E}_t}{c} \quad \dots (30)$$

This may be compared with the general relativity result

$$4\pi\rho\left(1-\frac{\sigma^2}{\rho^2}\right)-E^2\left(1-\frac{\sigma^2}{\rho^2}\right)-H^2=-2\left(\frac{\sigma}{\rho}\right)H^\alpha\omega_\alpha+2(\phi^2-\omega^2) \\ +\frac{\partial^2}{3}+\partial_{,\alpha}v^\alpha+\left(\frac{\sigma}{\rho}\right)_{,\alpha}E^\alpha \quad (31)$$

The author acknowledges his gratitude to Prof. A. K. Raychaudhuri for valuable help and suggestions.

#### REFERENCES

- De U. K. 1968 *J. Phys. A. Gen. Phys.* **1**, 645.  
 De U. K. & Raychaudhuri A. K. 1968a *Proc. Roy. Soc. A* **303**, 97.  
 De U. K. & Raychaudhuri A. K. 1968b *Proc. of 5th International Conf. on Gravitation*, Tbilisi, U.S.S.R.  
 Faulkes M. C. 1969 *Can. J. Phys.* **47**, 1989.  
 Hamoui A. 1969 *Ann. Inst. Henri Poincaré* **10**, 195.  
 Heckmann O. U. E. & Schucking Z. 1955 *Astrophysik* **38**, 95.  
 Raychaudhuri A. K. 1957 *Zeits. für Astrophysik* **43**, 161.  
 Raychaudhuri A. K. & De U. K. 1970 *J. Phys. A* (in press).  
 Som M. & Raychaudhuri A. K. 1968 *Proc. Roy. Soc. A* **304**, 81.

## Theory of operation of the magnetic crescograph

By ARUN KUMAR GUPTA and S. D. CHATTERJEE

*S. and M. Centre, Central Scientific Instruments Organisation,  
Calcutta-13*

(Received 13 May 1970)

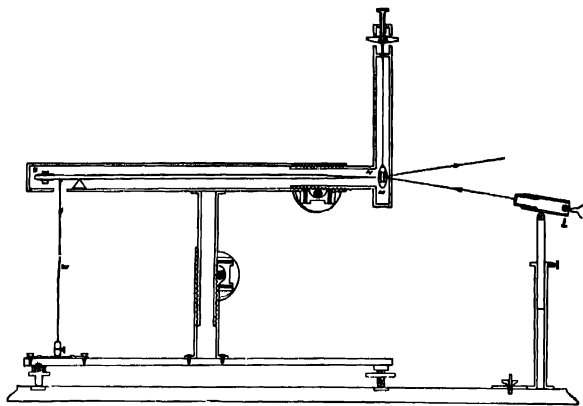
In the formulation of the theory of operation of the magnetic crescograph, the concept of rigid body motion of an astatic pair of magnetic needles has been considered. It has been shown that under existing conditions, there is only one degree of freedom, involving rotation of the astatic pair about a vertical axis. During the course of analysis it has been shown that the sensitivity of the instrument may be altered by a simple horizontal displacement of the suspending fibre holding the astatic pair, from the tip of the magnetic needle.

### INTRODUCTION

During his classical researches on photosynthesis, Bose (1924) devised a special radiometer for the determination of the energy of different rays of the solar spectrum by measuring the elongation of a metallic wire coated with lampblack. The particular spectral ray falling on the wire was absorbed and thus raised the temperature proportionately to the energy of radiation. However, the rise of temperature was excessively feeble, being of the order of  $10^{-5}$  °C; the resulting increase of length was so minute as to be undetectable by any method of magnification then available. Bose got over this difficulty by means of a magnetic device called *Magnetic Crescograph*, by which he obtained a magnification of about  $50 \times 10^6$  times or even higher.

A diagrammatic representation of the apparatus is given in figure 1.  $W$  is a length of zinc wire which becomes lengthened by the rise of temperature produced by absorbed radiation. It is attached by a hook to the short arm of a long magnetic lever, the  $N$ -end of which is lowered by any elongation of the sensitive wire. In front of the  $N$ -end of the magnetic lever is suspended a pair of astatic magnetic needles with an attached mirror. As the  $N$ -pole of the magnetic lever is lowered it produces increasing deflection of the suspended astatic pair, which is magnified by the spot of light reflected from the attached mirror.

Using a prototype of the instrument, Chatterjee & Ghosh (1968) measured the magnetostriction effect in ferrite. More recently, Chatterjee & Gupta (1970) have developed a new method for magnifying galvanometer movements, utilizing a modified version of Bose's original magnetic crescograph. A theoretical treatment of the mode of operation of Bose's original instrument is given below.



### THE MAGNETIC CRESCOGRAPHY

Figure 1

## THEORY OF MAGNETIC CRESCOGRAPH

Let the two magnetic needles  $ns$  and  $n's'$ , each of pole strength  $m$ , be attached to a vertical rigid lamina (as indicated in figure 2) so that their poles are at the positions :

$$\begin{array}{ll} n(+a, 0, +b), & s(+a, 0, -b), \\ n'(-a, 0, -b), & s'(-a, 0, +b), \end{array}$$

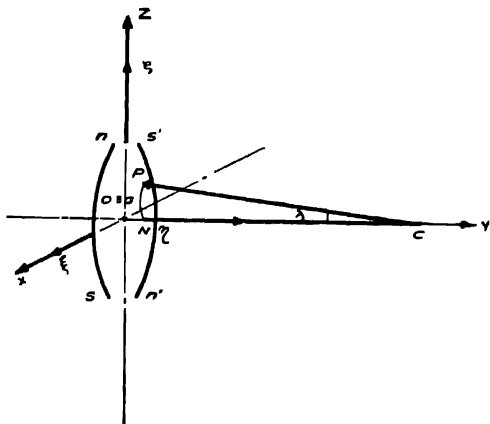


Figure 2

with reference to a body axes frame  $G\xi\eta\zeta$  which is along the principal axes system of the lamina and with its origin at the centre of gravity  $G$ . These positions of the poles with reference to  $G\xi\eta\zeta$  are the same for all positions and orientations of the lamina. A fixed frame of reference  $Oxyz$  is so selected that initially  $Oxyz = G\xi\eta\zeta$  and  $Oz$  is vertical. Let an isolated  $N$ -Pole of strength  $M$  with its initial position with respect to  $Oxyz$  system at  $N(0, +f, 0)$ , be allowed to move in the circle :

$$(y-f-R)^2 + z^2 = R^2$$

about the point  $C(0, f+R, 0)$ , such that at any instant of time  $t$ , its position with respect to fixed frame  $Oxyz$  is  $P[0, f+R(1-\cos\lambda), R\sin\lambda]$ . Due to magnetic attraction and repulsion the vortical lamina containing the magnetic needles will suffer a displacement which is expected to be both translational and rotational

Due to translational motion the centre of gravity  $G$  will be shifted to a new position  $G(x_0, y_0, z_0)$ , as referred to fixed  $Oxyz$ , while rotational displacements are determined by Eulerian angles  $\phi, \theta, \psi$ . If  $(\xi, \eta, \zeta)$  be the position of a point with respect to moving frame  $G\xi\eta\zeta$  and if  $(x, y, z)$  be the position of the same point with respect to fixed frame  $Oxyz$ , then the rule of transformation from  $G\xi\eta\zeta$  system to  $Oxyz$  system is

$$\begin{bmatrix} x \\ y \\ z \end{bmatrix} = \begin{bmatrix} x_0 \\ y_0 \\ z_0 \end{bmatrix} + \begin{bmatrix} \cos\psi \cos\phi & \cos\psi \sin\phi & \sin\psi \sin\theta \\ -\cos\theta \sin\phi \sin\psi & +\cos\theta \cos\phi \sin\psi & \\ -\sin\psi \cos\phi & -\sin\psi \sin\phi & \cos\psi \sin\theta \\ -\cos\theta \sin\phi \cos\psi & +\cos\theta \cos\phi \cos\psi & \\ \sin\theta \sin\phi & -\sin\theta \cos\phi & \cos\theta \end{bmatrix} \begin{bmatrix} \xi \\ \eta \\ \zeta \end{bmatrix} \quad \dots (1)$$

By the rule of transformation (1), the position  $n(a, 0, b)$  with respect to moving frame  $G\xi\eta\zeta$  becomes

$$\begin{aligned} n[x_0 + a(\cos\psi \cos\phi - \cos\theta \sin\phi \sin\psi) + b \sin\psi \sin\theta, \\ y_0 - a(\sin\psi \cos\phi + \cos\theta \sin\phi \cos\psi) + b \cos\psi \sin\theta, \\ z_0 + a \sin\theta \sin\phi + b \cos\theta] \end{aligned}$$

referred to fixed  $Oxyz$  frame, and similar co-ordinates referred to fixed frame  $Oxyz$  for  $s, n', s'$ . Since the instantaneous position of the  $N$ -Pole is  $P[0, f+R(1-\cos\lambda), R\sin\lambda]$  referred to fixed frame  $Oxyz$ , the distance

$$\begin{aligned} P_n = & \{ [x_0 + a(\cos\psi \cos\phi - \cos\theta \sin\phi \sin\psi) + b \sin\psi \sin\theta]^2 \\ & + [(y_0 - R(1-\cos\lambda) - f) - a(\sin\psi \cos\phi + \cos\theta \sin\phi \cos\psi) + b \cos\psi \sin\theta]^2 \\ & + [z_0 - R\sin\lambda + a \sin\theta \sin\phi + b \cos\theta]^2 \}^{\frac{1}{2}} \end{aligned}$$

and similar expressions for  $Pn', Ps, Ps'$ .

Since the magnetic needles form an astatic pair, the geomagnetic field will have no effect on the lamina. The only controlling forces are the torsion generated in the fibre suspending the lamina and the weight  $W$  of the lamina which acts at  $G$  vertically downwards. The deflecting forces are the forces of magnetic attraction and repulsion between the isolated  $N$ -Pole at  $P$  and each of the poles  $n$ ,  $n'$ ,  $s'$ .

To calculate the kinetic and potential energy of the system, the different angular velocities about the principal axes are

- (i)  $(\dot{\phi} \sin \theta \sin \psi + \dot{\theta} \cos \psi)$  about  $G\xi$   
 (ii)  $(\dot{\phi} \sin \theta \cos \psi - \dot{\theta} \sin \psi)$  about  $G\eta$   
 and (iii)  $(\dot{\phi} \cos \theta + \dot{\psi})$  about  $G\xi$ ,

where dot represents the derivative with respect to time  $t$ . If  $\chi$  be the rotation about  $G\xi$ , then

$$\chi = \int_0^t (\dot{\phi} \cos \theta + \dot{\psi}) dt = \psi + \phi \cos \theta + \int_0^t (\dot{\phi} \sin \theta) \cdot \dot{\theta} dt.$$

If  $I_\xi$ ,  $I_\eta$ ,  $I_\zeta$  be the principal moments of inertia of the moving lamina, then the instantaneous kinetic energy is

$$T = \frac{1}{2} \left[ \frac{W}{g} (\dot{x}_0^2 + \dot{y}_0^2 + \dot{z}_0^2) + I_\xi (\dot{\phi} \sin \theta \sin \psi + \dot{\theta} \cos \psi)^2 \right. \\ \left. + I_\eta (\dot{\phi} \sin \theta \cos \psi - \dot{\theta} \sin \psi)^2 + I_\zeta (\dot{\phi} \cos \theta + \dot{\psi})^2 \right]$$

If the suspending fibre be attached to the lamina at  $L(0, 0, p)$  referred to moving frame  $G\xi\eta\zeta$ , then the twist of the fibre is  $\chi$  and the instantaneous potential energy arising due to rotation  $\chi$  is  $\frac{1}{2}c\chi^2$  where  $c$  is the couple per unit angle of twist of the suspending fibre.

If  $V_0$  be the potential energy of the system when it is at rest, then initially the instantaneous potential energy is

$$V = V_0 + Wz_0 + \frac{Mm}{Pn} + \frac{Mm}{Pn'} - \frac{Mm}{Ps} - \frac{Mm}{Ps'} + \frac{1}{2} c\chi^2.$$

Hence the Lagrangian function  $L$  is

$$L = T - V \\ = \frac{1}{2} \left[ \frac{W}{g} (\dot{x}_0^2 + \dot{y}_0^2 + \dot{z}_0^2) + I_\xi (\dot{\phi} \sin \theta \sin \psi + \dot{\theta} \cos \psi)^2 \right.$$

$$+I_n(\dot{\phi} \sin \theta \cos \psi - \dot{\theta} \sin \psi)^2 + I_z(\dot{\phi} \cos \theta + \dot{\psi})^2 \Big] \\ - \left[ V_0 + Wz_0 + \frac{Mm}{P_n} + \frac{Mm}{P_{n'}} - \frac{Mm}{P_s} - \frac{Mm}{P_{s'}} + \frac{1}{2}c\lambda^2 \right].$$

The six co-ordinates,  $x_0, y_0, z_0, \theta, \phi, \psi$  completely describe the motion of the lamina under initial conditions

$$\dot{x}_0 = \dot{y}_0 = \dot{z}_0 = 0 \quad \text{and} \quad \dot{\phi} = \dot{\theta} = \dot{\psi} = 0 \quad \text{at} \quad t = 0,$$

$$\text{and} \quad x_0 = y_0 = z_0 = 0 \quad \text{and} \quad \phi = \theta = \psi = 0 \quad \text{at} \quad t = 0.$$

Lagrange's equations for the co-ordinates  $x_0, y_0, z_0$  are

$$\dot{x}_0 + g \cdot \frac{Mm}{W} \cdot \frac{\partial}{\partial x_0} \left[ \frac{1}{P_n} + \frac{1}{P_{n'}} - \frac{1}{P_s} - \frac{1}{P_{s'}} \right] = 0 \quad \dots \quad (i)$$

$$\ddot{y}_0 + g \cdot \frac{Mm}{W} \cdot \frac{\partial}{\partial y_0} \left[ \frac{1}{P_n} + \frac{1}{P_{n'}} - \frac{1}{P_s} - \frac{1}{P_{s'}} \right] = 0 \quad \dots \quad (ii)$$

$$\ddot{z}_0 + g \cdot \frac{Mm}{W} \cdot \frac{\partial}{\partial z_0} \left[ \frac{1}{P_n} + \frac{1}{P_{n'}} - \frac{1}{P_s} - \frac{1}{P_{s'}} \right] + g = 0 \quad \dots \quad (iii)$$

Integrating the equation (i) with respect to  $x_0$ , the equation (ii) with respect to  $y_0$  and equation (iii) with respect to  $z_0$ , respectively,

$$\frac{1}{2} \dot{x}_0^2 = -g \frac{Mm}{W} [P_n^{-1} + P_{n'}^{-1} - P_s^{-1} - P_{s'}^{-1}]$$

$$\frac{1}{2} \dot{y}_0^2 = -g \frac{Mm}{W} [P_n^{-1} + P_{n'}^{-1} - P_s^{-1} - P_{s'}^{-1}]$$

$$\frac{1}{2} \dot{z}_0^2 = -g \frac{Mm}{W} [P_n^{-1} + P_{n'}^{-1} - P_s^{-1} - P_{s'}^{-1}] - gz_0,$$

the constants of integration vanishing under initial conditions.

#### ONE DEGREE FREEDOM FOR SMALL DISPLACEMENTS

It may be seen that so far as  $x_0, y_0, z_0$  are small in order to satisfy the conditions

$$|x_0| < a + b - \{(a+b)^2 - \frac{1}{2}(a^2 + b^2)\}^{\frac{1}{2}},$$

$$|y_0| < a + b - \{(a+b)^2 - \frac{1}{2}(a^2 + b^2)\}^{\frac{1}{2}} + R.(1 - \cos \lambda) + f,$$

$$|z_0| < a + b - \{(a+b)^2 - \frac{1}{2}(a^2 + b^2)\}^{\frac{1}{2}} + R \sin \lambda,$$

$$\begin{aligned}
P_n^{-1} = F^{-1} \cdot \left[ 1 - \frac{1}{F} \{ a x_0 (\cos \psi \cos \phi - \cos \theta \sin \phi \sin \psi) + b x_0 \sin \psi \sin \theta \right. \\
- a (y_0 - R.1 - \overline{\cos \lambda} - f) \cdot (\sin \psi \cos \phi + \cos \theta \sin \phi \cos \psi) \\
+ b (y_0 - R.1 - \overline{\cos \lambda} - f) \cdot \cos \psi \sin \theta + a (z_0 - R. \sin \lambda) \cdot \sin \theta \sin \phi \\
\left. + b (z_0 - R. \sin \lambda) \cdot \cos \theta \} \right], \text{ approx.}
\end{aligned}$$

and similar approximations for  $P_n'^{-1}$ ,  $P_s^{-1}$ ,  $P_s'^{-1}$ , where

$$F = x_0^2 + (y_0 - R.1 - \overline{\cos \lambda} - f)^2 + (z_0 - R \sin \lambda)^2 + a^2 + b^2.$$

These approximate values show that the expression  $P_n^{-1} + P_n'^{-1} - P_s^{-1} - P_s'^{-1}$  vanishes upto the first order. Hence

$$\frac{1}{2}x_0^2 = 0, \quad \frac{1}{2}y_0^2 = 0, \quad \frac{1}{2}z_0^2 = -gz_0 \quad \text{for all times.}$$

First two equations involving  $\dot{x}_0$  and  $\dot{y}_0$ , under initial conditions, give

$$x_0 = y_0 = 0 \quad \text{for all times,}$$

while the last one involving  $\dot{z}_0$  and  $z_0$  implies that only non-positive values of  $z_0$  are possible. If  $z_0$  be negative,  $G$  will be lowered which means an elongation of the suspending fibre. If the fibre having an unchanged length with its upper end at  $O(0, 0, d)$  referred to fixed frame  $Oxyz$ , and lower end at  $L(0, 0, p)$  in  $G\xi\eta\zeta$ -frame or by (1), at  $L(x_0 + p \sin \psi \sin \theta, y_0 + p \cos \psi \sin \theta, z_0 + p \cos \theta)$  in  $Oxyz$  frame then its present length equals to its initial length,—a condition yielding

$$(x_0 + p \sin \psi \sin \theta)^2 + (y_0 + p \cos \psi \sin \theta)^2 + (d - z_0 - p \cos \theta)^2 = (d - p)^2 \quad (2)$$

Since  $x_0 = y_0 = 0$  this equation (2) reduces to

$$p^2 \sin^2 \theta + (d - z_0 - p \cos \theta)^2 = (d - p)^2$$

For a possible negative value  $z_0$  may be substituted by  $-|z_0|$  and as a result

$$\cos \theta = \frac{2|z_0| \cdot d + 2p \cdot d + |z_0|^2}{2 \cdot p \cdot d + 2|z_0| \cdot p} \leq 1 \quad \text{since } -\pi/2 < \theta < \pi/2.$$

Hence

$$|z_0| [ |z_0| + 2(d - p) ] \leq 0$$

As both  $|z_0|$  and  $d - p$  are positive, the only possibility is

$$|z_0| = 0$$

Therefore,

$$x_0 = y_0 = z_0 = 0 \quad \text{for all times.}$$

In view of this result the relation (2) produces  $\theta = 0$  which further proves

$$\chi = \phi + \psi; \quad \dot{\chi} = \dot{\phi} + \dot{\psi},$$



$$P_n = [a^2 + \{f + R \cdot \overline{1 - \cos \lambda}\}^2 + (b - R \sin \lambda)^2$$

$$+ 2a\{f + R \cdot \overline{1 - \cos \lambda}\} \cdot \sin \chi]^{\frac{1}{2}}$$

and similarly for  $P_s$ ,  $P_{n'}$ ,  $P_{s'}$ .

In this case, the Lagrangian function  $L$  becomes

$$L = \frac{1}{2} I_c \cdot \dot{\chi}^2 - \left[ V_0 + \frac{Mm}{P_n} + \frac{Mm}{P_{n'}} - \frac{Mm}{P_s} - \frac{Mm}{P_{s'}} + \frac{1}{2} c \cdot \chi^2 \right]$$

Lagrange's equation for the co-ordinate  $\chi$  is

$$\frac{d}{dt} \left( \frac{\partial L}{\partial \dot{\chi}} \right) - \frac{\partial L}{\partial \chi} = 0$$

which gives

$$\ddot{\chi} + \beta^2 \dot{\chi} = \frac{Mm}{I_c} [P_n^{-3} + P_{s'}^{-3} - P_{n'}^{-3} - P_s^{-3}] \\ \times a\{f + R(1 - \cos \lambda)\} \cdot \cos \chi$$

$$\text{where } \beta^2 = \frac{c}{I_c} = \frac{4\pi^2}{\tau^2} \quad [\tau = \text{free period of oscillation of the lamina.}]$$

Since the lamina moves in air, there must be a damping term on the left side of the equation and so

$$\ddot{\chi} + 2\alpha \cdot \dot{\chi} + \beta^2 \chi = \frac{Mm}{I_c} [P_n^{-3} - P_{n'}^{-3} + P_{s'}^{-3} - P_s^{-3}] \\ \times a\{f + R \cdot (1 - \cos \lambda)\} \cos \chi \quad \dots (3)$$

$2\alpha$  being the co-efficient of air damping.

For small values of  $\chi$  and so for small values of  $\lambda$ ,  $\cos \chi$  and  $\cos \lambda$ , either of them may be replaced by unity while  $\sin \chi$  and  $\sin \lambda$  by  $\chi$  and  $\lambda$ , respectively.

In this case

$$P_n = [a^2 + f^2 + (b - R\lambda)^2 + 2af\chi]^{\frac{1}{2}}$$

$$P_s = [a^2 + f^2 + (b + R\lambda)^2 + 2af\chi]^{\frac{1}{2}}$$

$$P_{n'} = [a^2 + f^2 + (b + R\lambda)^2 - 2af\chi]^{\frac{1}{2}}$$

$$P_{s'} = [a^2 + f^2 + (b - R\lambda)^2 - 2af\chi]^{\frac{1}{2}}$$

If  $\lambda$  be such as to satisfy

$$|R\lambda| < (a^2 + 2b^2 + f^2)^{\frac{1}{2}} - b,$$

the approximate value of  $P_n^{-3}$  is

$$P_n^{-3} = [a^2 + b^2 + f^2]^{-3/2} \cdot \left[ 1 + \frac{3(bR\lambda - \frac{1}{2}R^2\lambda^2 - af\chi)}{a^2 + b^2 + f^2} \right]$$

and similarly for  $P_s^{-3}$ ,  $P_{n'}^{-3}$  and  $P_{s'}^{-3}$ .

These approximate values indicate that upto the first order of approximation

$$Pn^{-3} + Ps'^{-3} - Pn'^{-3} - Ps^{-3} = \frac{12bR\lambda}{[a^2 + b^2 + f^2]^{5/2}}$$

Hence the equation of motion (3) for the deflection  $\chi$  is,

$$\ddot{\chi} + 2\alpha \dot{\chi} + \beta^2 \chi = \frac{12Mm}{I_c} \cdot \frac{abfR}{[a^2 + b^2 + f^2]^{5/2}} \cdot \lambda \quad \dots (4)$$

provided  $|R\lambda| < (a^2 + 2b^2 + f^2)^{1/2} - b$

This differential equation may be solved and  $\chi$  may be obtained as a function of time  $t$ , provided the actual form of the variable  $\lambda$  as a function of time  $t$  is known.

### SENSITIVITY

Let the final steady value of  $\lambda$  be  $\lambda_f$  and that of  $\chi$  be  $\chi_f$ . Then for final steady state, the equation (4) takes the form

$$\beta^2 \chi_f = \frac{12Mm}{I_c} \cdot \frac{abfR}{(a^2 + b^2 + f^2)^{5/2}} \cdot \lambda_f \quad \dots (4a)$$

which gives

$$S = \frac{\chi_f}{\lambda_f} = \frac{12Mm}{c} \cdot \frac{abfR}{(a^2 + b^2 + f^2)^{5/2}} \quad \dots (5)$$

a quantity which is a measure of the amplifying capacity of the instrument and may be termed as *sensitivity* of the instrument. The expression (5) shows that  $S$  increases with the increase of either of the quantities  $Mm$ ,  $R$  and  $1/c$ . Also  $S$  depends upon the factor

$$\frac{f}{(a^2 + b^2 + f^2)^{5/2}}$$

For given values of  $a$ ,  $b$ ,  $c$ ,  $Mm$  and  $R$ ,  $S$  attains its maximum value

$$S_{max} = \frac{16 \times 12}{25 \cdot \sqrt{5}} \cdot \frac{Mm}{c} \cdot \frac{abR}{(a^2 + b^2)^{3/2}} \quad \dots (6)$$

when  $f = \frac{1}{2}(a^2 + b^2)^{1/2}$ .

In view of the relation (4a), the equation (4) may be written as

$$\ddot{\chi} + 2\alpha \dot{\chi} + \beta^2 \chi = \beta^2 \cdot \chi_f \cdot \frac{\lambda}{\lambda_f} \quad \dots (7)$$

This equation (7) completely describes the motion of the suspended part of the crescograph for small values of  $\chi$  and  $\lambda$ . The equation (5) determines amplification for a particular setting of the instrument. If there be an arrangement for varying the quantity  $f$ , the distance of the centre of gravity  $G$  of the suspended part from the deflecting pole  $N$ , the maximum sensitivity (6) of the instrument may be reached when the particular value  $f = \frac{1}{2}(a^2 + b^2)^{\frac{1}{2}}$  is adjusted.

## REFERENCES

- Dose J. C. 1924 *The physiology of photosynthesis*, p179. Longmans, Green and Co.  
Chatterjee S. D. & Ghosh D. 1968 *Indian J Phys.* **62**, 677.  
Chatterjee S. D. & Gupta A. K. 1970 Unpublished results

## Covalency reduction factors in $D_{4h}$ symmetry and estimation of bonding parameters from magnetic data

BY D. MAJUMDAR AND U. S. GHOSH

*Department of Magnetism,*

*Indian Association for the Cultivation of Science, Jadavpur, Calcutta-32*

*(Received 14 May 1970)*

The expressions for covalency reduction factors for orbital moment and S.O. coupling constant in the case of a complex having  $D_{4h}$  symmetry have been derived in terms of mixing co-efficients of the ligands with the central atom (bonding parameters) and overlap integrals. So far, no explicit expressions for covalency reduction factors in an anisotropic complex have been given, only the isotropic case has been treated. It is known that these anisotropic reduction factors can be obtained from magnetic anisotropy and susceptibility data. It has been shown that the expressions for anisotropic reduction factors along with the magnetic data in the case of complexes having  $D_{4h}$  symmetry provide a simple method to determine the bonding parameters even without the help of epr or hyperfine structure measurements.

### INTRODUCTION

It is now well established that the orbitals of the magnetic electrons of the iron group of ions are not of pure  $3d$ -type and are considerably modified by their admixture with the ligand orbitals. The motions of the electrons actually participating in the bond formation in the co-ordination complexes are polycentric and not monocentric as in the case of the single atom. In other words, charge clouds of such electrons originally belonging to the central atom and surrounding ligands overlap one another resulting in a covalent type of bonding. The consequence of this will bear significantly on some of the properties of the iron group complexes. Since magnetic properties and optical absorption in iron group ions are primarily dependent on the orbitals of the unfilled shell of the central metal atom, these will be modified further if the central orbitals spill over into the ligand orbitals. It is for this reason that the orbital moment and the spin orbit coupling co-efficient of the central metal atom appear to be considerably reduced in the complex from their respective free ion values.

The mathematical formalism to describe the motion of the magnetic electron in the complex employs the method of LCAO-MO as developed by Van Vleck (1935). Following this method Stevens (1953) and Tinkham (1956) obtained expressions for the amount of the aforesaid reduction of the orbital moment and spin orbit coupling co-efficient in an undistorted octahedral complex, in terms of overlap integrals and co-efficients of mixing of the ligand orbitals with those of the central atom, which may be called the *bonding parameters*.

Now a regular  $O_h$  symmetry occurs only in very few complexes and it is more realistic to consider them as distorted. In fact, the magnetic anisotropy of a very large number of iron group complexes, studied in our laboratory, implies that all these complexes are distorted and such distortion will apparently manifest itself in the anisotropies in some other physical properties also. It is reasonable to assume that the covalency overlap of the central atom and ligand orbitals in distorted  $O_h$  complexes should not be treated as isotropic, since the reduction of the degeneracy of the overlapping orbitals is inherently associated with symmetry operations other than cubic. The covalency effect then must partake of the symmetry of the complex.

Expressions for magnetic susceptibility and anisotropy of almost all ions of the iron group have been already derived in this laboratory on the basis of such anisotropic covalency effect. Using these expressions anisotropic covalency reduction factors for orbital moment and S.O. coupling coefficient have also been evaluated with the help of the experimental magnetic anisotropy and susceptibility data. Unfortunately, these anisotropic values cannot be used in Stevens' and Tinkham's expressions for covalency reduction factors deduced in the case of a regular octahedron, to evaluate the bonding parameters. The purpose of this communication is to give similar expressions for square planar and tetragonally distorted octahedral complexes, and to indicate a way to evaluate the bonding parameters in these cases from magnetic anisotropy and susceptibility data. The procedure at the same time throws some light on the nature of the orbitals involved in the bond formation in these complexes.

#### MOLECULAR ORBITALS IN A TETRAGONALLY DISTORTED $XY_6$ COMPLEX

We consider an octahedron distorted along the  $Z$ -axis, the central metal atom being at the origin  $(0, 0, 0)$  and the ligands at  $(\pm a, 0, 0)$ ,  $(0 \pm a, 0)$  and  $(0, 0, \pm b)$ . The local co-ordinate system for describing the ligand orbitals at each ligand site is taken parallel to the central co-ordinate system  $XYZ$ . We consider the most frequent case in the iron group complexes in which the central metal atom has a partly filled  $3d$ -shell with no electron outside it and the ligands have all shells filled upto  $2p$ , with outer shells completely empty. Our interest lies in the molecular orbitals of the magnetic electrons of the central atom which were originally moving in pure  $3d$ -orbit in the free atom. Setting up of the molecular orbitals in a tetragonally distorted hexacoordinated complex is best achieved by considering the point group symmetry of the complex as  $D_{4h}$ . Using the group theoretical method, linear combinations of the  $s$  and  $p$  valence orbitals belonging to the six ligands are constructed in such a way that the combinations transform as the various irreducible representations of  $D_{4h}$  point group. Each of them is then admixed to the corresponding central atom  $3d$ -orbital which spans the same irreducible representation. The antibonding molecular orbitals (denoted by  $\phi$  functions), thus obtained are shown below :

$$A_{1g} : \phi_{z^2} = N_{1g}[d_{z^2} - \lambda_{1g}\{\sigma_x(1) - \sigma_x(4) + \sigma_y(2) - \sigma_y(5)\} - \lambda_{2g}\{\sigma_z(6) - \sigma_z(3)\}] \dots \quad (1)$$

$$B_{1g} : \phi_{x^2-y^2} = N_{2g}[d_{x^2-y^2} - \lambda_{3g}\{\sigma_x(4) - \sigma_x(1) + \sigma_y(2) - \sigma_y(5)\}] \dots \quad (2)$$

$$E_g : \phi_{xz} = N_{1\pi}[d_{xz} - \lambda_{1\pi}\{p_z(1) - p_z(4)\} - \lambda_{2\pi}\{p_x(3) - p_x(6)\}] \dots \quad (3)$$

$$\phi_{yz} = N_{1\pi}[d_{yz} - \lambda_{1\pi}\{p_z(2) - p_z(5)\} - \lambda_{2\pi}\{p_x(3) - p_x(6)\}] \dots \quad (4)$$

$$B_{2g} : \phi_{xy} = N_{2\pi}[d_{xy} - \lambda_{3\pi}\{p_y(1) - p_y(4) + p_x(2) - p_x(5)\}] \dots \quad (5)$$

Since the magnetic electrons of our interest occupy antibonding molecular orbitals, we have used negative sign before  $\lambda$ 's (the mixing co-efficients of the various ligand combinations) in the above expressions (1)–(5). The numbers 1, 2, 3 and 4, 5, 6 appearing with the ligand orbitals  $\sigma$ 's and  $p$ 's refer to the ligands on the positive and negative X, Y, Z axes, respectively. We shall consider the  $p$ 's to be  $2p_\pi$  only and the hybrid  $\sigma$ 's to be made up of  $2p_\sigma$  and  $2s$  only. The  $s$  part of the hybrid is added to the  $p_\sigma$  part with such sign as to reinforce the interior lobe of the  $p_\sigma$  orbital. Further, the  $4s$  orbital of the central metal atom also spans the  $A_{1g}$  representation of  $D_{4h}$ . But we have neglected its mixing with the  $d_{z^2}$  orbital.

$$\text{Thus} \quad \sigma_x(1) = \sin \theta |2p_x(1)\rangle - \cos \theta |2s(1)\rangle \dots \quad (6)$$

$$\text{while} \quad \sigma_x(4) = \sin \theta |2p_x(4)\rangle + \cos \theta |2s(4)\rangle, \quad 0 < \theta < \pi/2 \dots \quad (7)$$

The mixing co-efficients  $\lambda_{i\sigma}$ 's ( $i = 1, 2, 3$ ) depend on the admixtures of  $p_\pi$  and  $s$  in the hybrid and their relation is obtained as follows

$$\begin{aligned} \lambda_{i\sigma}\sigma_x(1) &= \lambda_{i\sigma} \sin \theta |2p_x(1)\rangle - \lambda_{i\sigma} \cos \theta |2s(1)\rangle \dots \quad (8) \\ &= \lambda_{ip_\sigma} |2p_x(1)\rangle - \lambda_{is} |2s(1)\rangle \end{aligned}$$

$$\text{where} \quad \lambda_{ip_\sigma} = \lambda_{i\sigma} \sin \theta \text{ and } \lambda_{is} = \lambda_{i\sigma} \cos \theta; \text{ whence}$$

$$\lambda_{i\sigma}^2 = \lambda_{ip_\sigma}^2 + \lambda_{is}^2 \dots \quad (9)$$

The same relation (9) will be obtained if we start with any other hybrid  $\sigma$  orbital of the ligand instead of  $\sigma_x(1)$ . For directed orbital  $\cos \theta \approx \sin \theta \approx 1/\sqrt{2}$  and  $\lambda_{ip_\pi} \approx \lambda_{is} \approx 1/\sqrt{2}$ .  $\lambda_{i\sigma}$ .

The normalizing constants  $N$ 's appearing in the molecular orbitals (1)–(5) are given by

$$\frac{1}{N_{1\pi}^2} = 1 + 2(\lambda_{1\pi}^2 + \lambda_{2\pi}^2) - 4(\lambda_{1\pi}S_{1\pi} + \lambda_{2\pi}S_{2\pi}) \quad (10)$$

$$\frac{1}{N_{2\pi}^2} = 1 + 4\lambda_{3\pi}^2 - 8\lambda_{3\pi}S_{1\pi} \quad (11)$$

$$\frac{1}{N_{2\sigma}^2} = 1 + 4\lambda_{3\sigma}^2 - 8\lambda_{3\sigma}S_{1\sigma} \quad (12)$$

$$\frac{1}{N_{1\sigma}^2} = 1 + 4\lambda_{1\sigma}^2 + 2\lambda_{2\sigma}^2 - 8/\sqrt{3} \cdot (\lambda_{1\sigma}S_{1\sigma} + \lambda_{2\sigma}S_{2\sigma}) \quad (13)$$

where the overlap integrals of interest are defined by

$$\begin{aligned}
 S_{1\pi} &= \langle p_z(2) | d_{yz} \rangle = \langle p_z(1) | d_{xz} \rangle = \langle p_x(2) | d_{xy} \rangle = \langle p_y(1) | d_{xy} \rangle \\
 &= -\langle p_z(5) | d_{yz} \rangle = -\langle p_z(4) | d_{xz} \rangle = -\langle p_x(5) | d_{xy} \rangle = -\langle p_y(4) | d_{xy} \rangle \\
 S_{2\pi} &= \langle p_x(3) | d_{xz} \rangle = \langle p_y(3) | d_{yz} \rangle = -\langle p_x(6) | d_{xz} \rangle = -\langle p_y(6) | d_{yz} \rangle \\
 S_{1\sigma} &= \langle \sigma_y(2) | d_{x^2-y^2} \rangle = \langle \sigma_x(4) | d_{x^2-y^2} \rangle = \sqrt{3} \langle \sigma_x(1) | d_{z^2} \rangle \\
 &= \sqrt{3} \langle \sigma_y(2) | d_{z^2} \rangle = -\langle \sigma_y(5) | d_{x^2-y^2} \rangle = -\langle \sigma_x(1) | d_{x^2-y^2} \rangle \\
 &= -\sqrt{3} \langle \sigma_x(4) | d_{z^2} \rangle = -\sqrt{3} \langle \sigma_y(5) | d_{z^2} \rangle \\
 S_{2\sigma} &= \sqrt{3}/2 \langle \sigma_x(6) | d_{z^2} \rangle = -\sqrt{3}/2 \langle \sigma_z(3) | d_{z^2} \rangle
 \end{aligned}$$

Because of the anisotropy of the complex we have distinguished between the overlap of the orbitals of the ligands in the  $XY$  plane and that of the ligands in the  $Z$ -direction with the central atom orbital. Moreover, anisotropy of the complex introduces different mixing co-efficients  $\lambda$ 's for different ligand orbital combinations depending upon whether the ligands lie in the  $XY$  plane or along  $Z$ -axis.

It should be noted that the expressions (1)–(5) for molecular orbitals under  $D_{4h}$  point group reduce to those of pure  $O_h$  case if

$$\begin{aligned}
 2\sqrt{3}\lambda_{1\sigma} &= \sqrt{3}\lambda_{2\sigma} = 2\lambda_{3\sigma} = \lambda_{\sigma} \\
 \lambda_{1\pi} &= \lambda_{2\pi} = \lambda_{3\pi} = \lambda_{\pi}
 \end{aligned}$$

and in pure  $O_h$  case  $S_{1\pi} = S_{2\pi} = S_{\pi}$

and  $S_{1\sigma} = S_{2\sigma} = S_{\sigma}$ .

### COVALENCY REDUCTION FACTORS

Covalency reduction factors for the orbital moment in the case of tetragonally distorted octahedral complex are more numerous than in the  $O_h$  case; these are given by the following quantities :

$$k_z(\pi \pi) = \frac{\langle \phi_{yz} | l_z | \phi_{xz} \rangle}{\langle d_{yz} | l_z | d_{xz} \rangle} \quad (14)$$

$$k_x(\pi \pi) = \frac{\langle \phi_{xz} | l_x | \phi_{xy} \rangle}{\langle d_{xz} | l_x | d_{xy} \rangle} = \frac{\langle \phi_{xy} | l_y | \phi_{yz} \rangle}{\langle d_{xy} | l_y | d_{yz} \rangle} = k_y(\pi \pi) \quad (15)$$

$$k_z(\pi \sigma) = \frac{\langle \phi_{xy} | l_z | \phi_{x^2-y^2} \rangle}{\langle d_{xy} | l_z | d_{x^2-y^2} \rangle} \quad (16)$$

$$k_x(\pi \sigma) = \frac{\langle \phi_{yz} | l_x | \phi_{x^2-y^2} \rangle}{\langle d_{yz} | l_x | d_{x^2-y^2} \rangle} = \frac{\langle \phi_{xz} | l_y | \phi_{x^2-y^2} \rangle}{\langle d_{xz} | l_y | d_{x^2-y^2} \rangle} \quad k_y(\pi \sigma) \quad (17)$$

$$k_x(\pi \sigma') \cdot \frac{\langle \phi_{xz} | l_y | \phi_{z^2} \rangle}{\langle d_{xz} | l_y | d_{z^2} \rangle} \quad k_y(\pi \sigma') \quad (18)$$

Covalency reduction factor for the spin orbit coupling co-efficient  $R_i(m, n)$  where  $i$  stands for  $x, y$  and  $z$ ,  $m$  stands for  $\pi$  and  $n$  stands for  $\pi, \sigma$  and  $\sigma'$  are given by similar expressions in which  $l_i$  is simply replaced by  $\zeta l_i$ . The expression for the reduction factors defined above, obtained after calculating the relevant matrix elements occurring in the equations (14)–(18), are given below :

$$k_z(\pi \pi) = 1 - 2\lambda_{1\pi}^2 N_{1\pi}^2 \quad (19)$$

$$k_x(\pi \pi) = k_y(\pi \pi) = N_{1\pi} N_{2\pi} [1 - 4\lambda_{3\pi} S_{1\pi} - 2(\lambda_{1\pi} S_{1\pi} + \lambda_{2\pi} S_{2\pi}) + 2\lambda_{1\pi} \lambda_{3\pi}] \quad (20)$$

$$k_z(\pi \sigma) = N_{2\pi} N_{2\sigma} [1 - 4\lambda_{3\sigma} S_{1\sigma} - 4\lambda_{3\pi} S_{1\pi} - 2\lambda_{3\pi} \lambda_{3\sigma} p_y(1) | \partial/\partial y | s(1) > ] \quad (21)$$

$$k_x(\pi \sigma) = k_y(\pi \sigma) = N_{1\pi} N_{2\sigma} [1 - 4\lambda_{3\sigma} S_{1\sigma} - 2\lambda_{1\pi} S_{1\pi} - 2\lambda_{2\pi} S_{2\pi} - 2\lambda_{1\pi} \lambda_{3\sigma} a < p_z(5) | \partial/\partial z | s(5) > ] \quad (22)$$

$$k_x(\pi \sigma') = k_y(\pi \sigma') = N_{1\pi} N_{1\sigma} [1 - 4\sqrt{3}(\lambda_{1\sigma} S_{1\sigma} + \lambda_{2\sigma} S_{2\sigma}) - 2(\lambda_{1\pi} S_{1\pi} + \lambda_{1\pi} S_{2\pi}) - 2/\sqrt{3} \lambda_{1\pi} \lambda_{3\sigma} a - 2/\sqrt{3} \lambda_{2\pi} \lambda_{2\sigma} a - 2/\sqrt{3} \lambda_{1\pi} \lambda_{1\sigma} a < p_z(5) | \partial/\partial z | s(5) > - 2/\sqrt{3} \lambda_{2\pi} \lambda_{2\sigma} b < p_y(6) | \partial/\partial y | s(6) > ] \quad (23)$$

Here,  $a$  and  $b$  stand for the distances of ligand lying in the  $XY$  plane and along  $Z$  direction, respectively, from the central metal atom. Since the spin orbit coupling is mainly determined by the intense field near the central nucleus, we shall assume that the matrix elements of  $\zeta l_i$  ( $i = x, y, z$ ) between molecular orbital will be simply reduced in proportion to the normalization of the central ion wave functions involved :

$$R_z(\pi \pi) = N_{1\pi}^2 \quad \dots \quad (24)$$

$$R_x(\pi \pi) = R_y(\pi \pi) = N_{1\pi} N_{2\pi} \quad \dots \quad (25)$$

$$R_z(\pi \sigma) = N_{2\pi} N_{2\sigma} \quad \dots \quad (26)$$

$$R_x(\pi \sigma) = R_y(\pi \sigma) = N_{1\pi} N_{2\sigma} \quad \dots \quad (27)$$

$$R_x(\pi \sigma') = R_y(\pi \sigma') = N_{1\pi} N_{1\sigma} \quad \dots \quad (28)$$

We shall apply the above expressions in two cases : (1) tetragonally distorted hexacoordinated  $\text{Fe}^{2+}$  and (2) square planar  $\text{Cu}^{2+}$  complexes. The anisotropic reduction factors for orbital moment and spin orbit coupling coefficient have been obtained from the magnetic susceptibility and anisotropy experiment, and will be used to estimate the bonding parameters using the above expressions for reduction factors.

#### *Application to $\text{Fe}^{2+}$ complex*

Magnetic susceptibility and anisotropy experiments on  $\text{Fe}(\text{NH}_4\text{SO}_4)_2 \cdot 6\text{H}_2\text{O}$  gives the following values of the reduction factors (Pal & Ghosh, in course of publication)

$$\begin{aligned} k_{\parallel} &= k_z(\pi \pi) = 0.90 & R_{\parallel} &= R_z(\pi \pi) = 0.85 \\ k_{\perp} &= k_x(\pi \pi) = k_y(\pi \pi) = 0.80 & R_{\perp} &= R_x(\pi \pi) = R_y(\pi \pi) = 0.77. \end{aligned}$$



The theoretical expressions (19) and (20) contain five independent parameters  $\lambda_{1\pi}$ ,  $\lambda_{2\pi}$ ,  $\lambda_{3\pi}$ ,  $S_{1\pi}$  and  $S_{2\pi}$ ; hence these cannot be evaluated from the above four data. We therefore calculate one of the overlap integrals assuming a particular form of the radial function of the orbitals and knowing the ligand distances from X-ray data (Montgomery *et al* 1967). The three bonding parameters  $\lambda_{1\pi}$ ,  $\lambda_{2\pi}$  and  $\lambda_{3\pi}$  and the other overlap integral can then be easily obtained. A self consistent test of the nature of the orbitals will then be automatically obtained if the latter overlap integral so evaluated agrees with that calculated directly. We have used the Slater orbitals for the purpose. X-ray results show that the ligand  $O^{2-}$  are at 2.086 Å, 2.136 Å and 2.156 Å, apart from the central  $Fe^{2+}$  and the bond angles slightly deviate from  $90^\circ$ . The overlap integral  $S_{2\pi}$  corresponding to the distance 2.086 Å is 0.077 as obtained from graphical interpolation of the values given in Jaffe's tables (1953). Using the experimental values of the above parameters and this value of  $S_{2\pi}$  we finally get

$$\begin{aligned}\lambda_{1\pi} &= 0.24 \\ \lambda_{2\pi} &= 0.29 \\ \lambda_{3\pi} &= 0.41 \\ S_{1\pi} &= 0.033\end{aligned}$$

Jaffe's tables give the values of  $S_{1\pi}$ , for the ligand distances 2.156 Å and 2.136 Å, as 0.067 and 0.069, respectively. Considering the uniaxial approximation, the mean value of  $S_{1\pi}$  is 0.068. In view of the approximations involved and lack of desired accuracy of the experimental results, the agreement is fair.

#### *Application to $Cu^{2+}$ complex*

Magnetic susceptibility and anisotropy measurements on  $CuCa(CH_3COOH)_6H_2O$  (Biswas & Sengupta 1970) give the following values of the reduction factors.

$$\begin{aligned}k_{||} &= k_z(\pi\sigma) = 0.91 & k_{\perp} &= k_x(\pi\sigma) = k_y(\pi\sigma) = 0.78 \\ R_{||} &= R_z(\pi\sigma) = 0.95 & R_{\perp} &= R_x(\pi\sigma) = R_y(\pi\sigma) = 0.84.\end{aligned}$$

X-ray results (Laugs & Hare, 1967) show that four oxygen atoms are coordinated to  $Cu^{2+}$  ion forming a square planar complex and each oxygen atom is about 1.97 Å away from the central copper atom. In the case of planar complex, the ligand nos. 3 and 6 are absent. Hence, the parameter referring to them (i.e.  $\lambda_{2\pi}$ ) will not occur in the expressions (21), (22), (26) and (27). Further, following Tinkham (1956) we assume that  $2p$  and  $2s$  form diagonal hybrids for which  $\lambda_{3s} \approx \lambda_{3p}/\sqrt{2} = \lambda_{3p\sigma}$ . Hence, we have a total of five parameters as in the case of  $Fe^{2+}$  ion and these are  $\lambda_{1\pi}$ ,  $\lambda_{3\pi}$ ,  $\lambda_{3\sigma}$ ,  $S_{1\pi}$  and  $S_{1\sigma}$ . To evaluate them with the help of four experimental data ( $k_{||}$ ,  $k_{\perp}$ ,  $R_{||}$ ,  $R_{\perp}$ ) we follow a procedure similar to that in the case of  $Fe^{2+}$ . Using Slater value of one of the two overlap integrals  $S_{1\pi}$

and  $S_{1\sigma}$ , we treat the other ( $S_{1\pi}$  say) as one of the four unknown parameters to be evaluated from the given four experimental data and then make a consistency test of  $S_{1\pi}$  so evaluated, by comparing it with the Slater value. The Slater value of  $S_{1\sigma}$  is taken from Jaffe's tables remembering that  $S_{1\sigma} = 1/\sqrt{2} (S_{1p\sigma} + S_{1s})$  where  $S_{1p\sigma}$ ,  $S_{1s}$  are the overlap integrals between  $d_{x^2-y^2}$  and  $2p_{\sigma}$ ,  $2s$  ligand orbitals, respectively. Corresponding to a distance of  $1.97 \text{ \AA}$ ,  $S_{1\sigma}$  comes out to be 0.118. Further, using Slater orbital we find that

$$a < 2p_z | \partial/\partial z | 2s \rangle = a < 2p_y | \partial/\partial y | 2s \rangle = \frac{Z^*}{a_0} \cdot \frac{1.97 \text{ \AA}}{4\sqrt{3}} = 2.068.$$

where  $Z^* = 3.85$  is the effective nuclear charge of  $O^{2-}$   $2s2p$  shell, and  $a$  is the metal-ligand distance ( $1.97 \text{ \AA}$ ). With the help of the above Slater values the four parameters  $\lambda_{1\pi}$ ,  $\lambda_{3\pi}$ ,  $\lambda_{1\sigma}$  and  $S_{1\pi}$  are then evaluated from the four experimental data using expressions (21), (22), (26) and (27). Unlike the case of  $Fe^{2+}$ , the expressions in the present case being too complicated compels us to adopt the trial and error method of evaluation of parameters instead of direct solution from the equations. The following values of the parameters give the closest fit to the above reduction factors obtained from the susceptibility and anisotropy data :

$$\lambda_{1\pi} = 0.52$$

$$\lambda_{3\sigma} = 0.01$$

$$S_{1\pi} = 0.048$$

The Slater value of  $S_{1\pi}$  corresponding to a distance of  $1.97 \text{ \AA}$ , obtained by graphical interpolation of the values given in Jaffe's tables is 0.046. Thus, the agreement is found to be surprisingly satisfactory.

The values of the bonding parameters show that the  $\pi$ -bonding is unexpectedly stronger than  $\sigma$  bonding in the complex. Close study of the expressions (21), (22), (10), (11), (12) reveals that the large anisotropy in the reduction factors is solely due to  $\pi$ -bonding i.e., if the  $\pi$ -bonding is completely neglected, the reduction factors  $R_i$ ,  $k_i$  reduce to isotropic expressions which cannot be used to explain the observed anisotropy in the reduction factors. So it is evident that anisotropic reduction factors along with the anisotropic expressions derived in the present paper are very useful in determining the relative importance of  $\sigma$  and  $\pi$  bonding.

## CONCLUSIONS

(1) Expressions for covalency reduction factors for orbital moment and S.O. coupling constant in a complex of  $D_{4h}$  symmetry have been derived in terms of bonding parameters and some integrals involving metal and ligand orbitals

Magnetic measurements of susceptibility and anisotropy provide the values of these reduction factors and hence a simple method to determine the bonding parameters in an anisotropic complex.

(2) The method of evaluation of bonding parameters depends on the type of radial function used to calculate some of the integrals and although lack of correct radial function suitable in the crystal is a limitation of the method, a consistency test for any assumed radial function has been indicated.

(3) In the case of  $O_h$  system, there is only one parameter of each kind  $\pi$  and  $\sigma$ . But when the system is tetragonally distorted as in the case of  $\text{Fe}(\text{NH}_4\text{-SO}_4)_2 \cdot 6\text{H}_2\text{O}$ , the three  $\pi$ -bonding parameters assume widely different values.

(4) In the case of copper complex of  $D_{4h}$  symmetry the anisotropy in the covalency reduction factors is solely brought about by the presence of  $\pi$ -bonding in the system. In the square planar complex of copper calcium acetate it appears that the degree of  $\pi$ -admixture is very high and even surprisingly higher than the  $\sigma$ -admixture.

#### ACKNOWLEDGEMENT

The authors express their sincere thanks to Prof. A. Bose, D.Sc., F.N.A., for useful comments and helpful criticism of the work.

#### REFERENCES

- Biswas P. & Sengupta P. 1970 *Physica Stat. Sol.* **40**, 339.  
 Jaffe H. 1953 *J. Chem. Phys.* **21**, 258.  
 Langs David A. & Hare Curtis R. 1967 *Chem. Communication*, 890.  
 Montgomery H., Chastain R. V., Natt J. J., Witkowska A. M. & Lingafelter F. C. 1967 *Acta Crystallographica* **22**, 775.  
 Pal D & Ghosh D. (*In course of publication*)  
 Stevens K. W. H. 1953 *Proc. Roy. Soc.* **A219**, 542.  
 Tinkham M. 1956 *Proc. Roy. Soc.* **A236**, 549.  
 Van Vleck J. H. 1935 *J. Chem. Phys.* **3**, 803, 807.

## Triple gamma cascade studies in $W^{182}$ from the decay of $Ta^{182}$

By U. S. PANDE and B. P. SINGH

Physics Department, University of Roorkee, Roorkee, India

(Received 20 May 1970)

Triple gamma angular correlation studies have been done in  $W^{182}$  from the decay of  $Ta^{182}$ . The correlation studies have been done keeping two NaI (Tl) detectors in the plane of the table and one perpendicular to it. The third detector detecting the third gamma ray of the cascade was kept at various angles. The correlation function thus obtained are as follows:

For 68 keV-1122 keV-100 keV cascade

$$W(\theta) = 1 + (0.276 \pm 0.0255) P_2(\cos \theta) + (0.0021 \pm 0.0322) P_4(\cos \theta)$$

For 152 keV-1122 keV-100 keV cascade

$$W(\theta) = 1 - (0.131 \pm 0.068) P_2(\cos \theta) + (0.124 \pm 0.082) P_4(\cos \theta)$$

The multipolarities of the 68 keV, 100 keV, 152 keV and 1122 keV gamma radiations have been discussed.

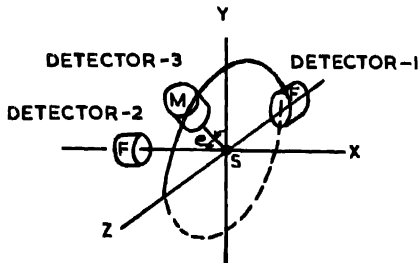
### INTRODUCTION

Decay scheme of  $W^{182}$  following the decay of  $Ta^{182}$  has been studied by many investigators (Lederer *et al* 1965, Nuclear data sheets 1959-65). Recently Korkman & Backlin (1966) and Daniel *et al* (1964) have studied the internal conversion coefficients of transitions in  $W^{182}$ . Gamma-gamma angular correlation studies have been done by El-Nesr *et al* (1961), Hickman & Wiedenbeck (1960) and William & Roulston (1956). Quantum numbers ( $K, I, \pi$ ) for the levels by all these studies are in agreement with those proposed by Alaga *et al* (1955) but there is much controversy regarding the multipole assignments of the transitions. Studies have been made to find the multipolarities by triple gamma angular correlation studies and thus assigning the spin values to the excited levels.

### EXPERIMENTAL SET UP

Three single channel scintillation spectrometers with NaI(Tl) crystals mounted on RCA 6911 photomultiplier tubes and two conventional coincidence circuits are used in these studies. The size of the crystals used are 2.54 cm in length and 2.54 cm in diameter. The resolution of these spectrometers are  $\sim 8\%$  for 661 keV gamma radiation. Two of the detectors are mounted in the plane of the table as shown in figure 1, one of them is fixed and the other movable. The fixed detector detects the first gamma radiation in the cascade in 2 volts channel width (2 volts = 18 keV). The movable detector in the plane of the table detects the 3rd gamma radiation of the cascade in 2 volts channel width at 100 keV in the correlation studies. The third detector is mounted perpendicular to the plane

of the table making an angle of  $90^\circ$  with other two detectors as shown in figure 1 and this detects the 2nd gamma (middle) of the cascade in integral spectrum above 500 keV. The source in the form of powder (metal) was obtained from Bhabha Atomic Research Centre, Trombay and was kept in a cylindrical perspex container ( $3\text{mm} \times 3\text{mm}$ ) mounted on a perspex stand. The source is mounted in the centre at a distance of 4.5 cm from all the three detectors



## NOTE :

Y-Z PLANE IS THE PLANE OF THE TABLE

F = FIXED DETECTOR

M = MOVABLE DETECTOR

Figure 1

Pulses from the fixed detector perpendicular to the plane of the table and the movable detector in the plane are fed to a double coincidence circuit of resolving time of the order of  $2 \times 10^{-7}$  sec. The output of this coincidence unit is the coincidence between 90–108 keV radiation and high energy gamma radiation above 500 keV (with most of the Compton and photopeak distributions). The output of this coincidence unit and the output of the fixed detector (in the plane of the table) which scans the spectrum in one volt channel width are fed to another double coincidence unit whose resolving time is of the order of  $2 \times 10^{-7}$  sec. The block diagram for this arrangement is shown in figure 2. The coincidence output of this unit is the coincidence between the gamma rays forming the triple cascades.

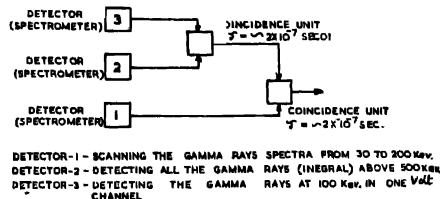


Figure 2

The coincidences along with single spectrum are shown in figure 3. The triple cascades are thus 68 keV—1122keV—100keV and 152keV—1122keV—100keV when the output of the scanning spectrometer is at 68keV and 152keV respectively.

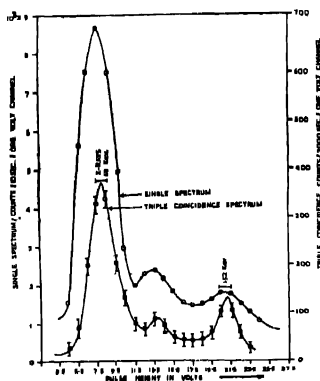


Figure 3

The chance coincidences have been taken by putting delay in one of the input of second coincidence unit. These chance coincidences and calculated chance coincidences given by the expression  $N_c = 2\tau N_1 N_2$  ( $N_c$  = chance coincidence rate,  $N_1$  and  $N_2$  are the input counting rates of the coincidence unit and  $\tau$  is the resolving time) are the same within the statistical error. The ratios of real coincidence and chance coincidence at the peak of 68keV and 152keV are 60 : 40 and 50 : 50, respectively. The angular correlation studies are made keeping the movable detector at various angles of 90°, 120°, 150° and 180°.

#### ANGULAR CORRELATION RESULTS

The angular correlation functions  $W(\theta)$  obtained by the method of least square fit, without applying solid angle correction, are as follows.

For 68keV—1122keV—100keV cascade :

$$W(\theta) = 1 + (0.1566 \pm 0.0141)P_2(\cos \theta) + (0.0118 \pm 0.0179)P_4(\cos \theta)$$

and for 152keV—1122keV—100keV cascade :

$$W(\theta) = 1 - (0.1181 \pm 0.0674)P_2(\cos \theta) + (0.1137 \pm 0.0834)P_4(\cos \theta)$$

$A_2$  and  $A_4$  coefficients are again calculated after subtracting coincidence contribution due to X-ray (52%) as done by El-Nesr *et al* (1962) in 68keV—1122keV—100keV cascade and also considering the attenuation of the correlation coefficient

by the internal fields as observed by Körner *et al* (1963). The correlation function for the above cascade thus is  $W(\theta) = 1 + (0.276 \pm 0.0255)P_2(\cos \theta) + (0.0021 \pm 0.0322)P_4(\cos \theta)$ . Considering the attenuation of the correlation coefficient by the internal field as observed by Körner *et al* (1963) in 152keV–1122keV–100keV cascade, the correlation function is  $W(\theta) = 1 - (0.131 \pm 0.068)P_2(\cos \theta) + (0.124 \pm 0.082)P_4(\cos \theta)$ .

The finite solid angle correction in the above cascades has not been done. This correction has been considered in the calculations of the theoretical values for  $A_2$  and  $A_4$ .

#### THEORETICAL CALCULATIONS FOR ANGULAR CORRELATION COEFFICIENTS

The triple correlation function as given by Ferguson (1965) for the cascade described by the quantum numbers  $a(L_1)$   $b(L_2)$   $c(L_3)$   $d$  with  $a$  taken to be unpolarised ( $a, b, c$  and  $d$  represent spins of the excited levels in sequence and  $L_1, L_2, L_3$  are multiplicarities of the transitions) is

$$W(\Omega_1 \Omega_2 \Omega_3) = (1/4\pi)^{3/2} (-)^{a_1} \alpha \Sigma (-)^{L_1 - L'_1 + k} Z(L_1 b L'_1 b; a k_1) G \left\{ \begin{matrix} c L_2 b \\ c L_2' b \\ 1 \end{matrix} \right\} \quad (1)$$

$$Z_1(L_3 c L'_3 c; d k_3) \delta_1^{r_1} \delta_2^{r_2} \delta_3^{r_3} Q_{k_1} Q_{k_2} Q_{k_3} P_{k_1 k_2 k_3}(\Omega_1 \Omega_2 \Omega_3)$$

with the summation over  $L_1 L'_1 L_2 L'_2 L_3 L'_3 K_1 K_2 K_3$ .  $L_1' L'_2 L'_3$  are interfering multiplicarities in  $L_1, L_2, L_3$  transitions.  $\delta_1^{r_1}, \delta_2^{r_2}, \delta_3^{r_3}$  are the multipole mixing ratios,  $r_1, r_2, r_3$  are the exponents, where  $r_1$  is having the value 0, 1, 2 depending on whether the terms of the type  $(L_1 L_1), (L_1 L'_1), (L'_1 L'_1)$  respectively, and similarly  $r_2$  and  $r_3$  are having value of 0, 1, 2).  $\delta_1^{r_1}$  is given as  $\delta_1^{r_1} = \langle b | L | a \rangle / \langle b | L | a \rangle$ . Similarly  $\delta_2^{r_2}$  and  $\delta_3^{r_3}$  are given.  $Q_{k_1}, Q_{k_2}$  and  $Q_{k_3}$  are the attenuation factors for the detectors which detect the radiations 1, 2 and 3. The tables for  $Z, Z_1$  and  $G$  are given by Ferguson for various combinations of spin values and multiplicarities of gamma-ray transitions. Legendre polynomial  $P_{k_1 k_2 k_3}$  is given by Ferguson under restriction imposed by the geometries in the form  $P_{k_1 k_2 k_3}(\Omega_1 \Omega_2 \Omega_3) = \sum_k \alpha_{k_1 k_2 k_3 k} P_k(\cos \theta)$ . The tables for  $\alpha_{k_1 k_2 k_3 k}$  are also given by Ferguson. Therefore  $W(\Omega_1 \Omega_2 \Omega_3)$  can be written in the form  $W(\theta) = a_0 + a_2 P_2(\cos \theta) + a_4 P_4(\cos \theta)$  and the values of  $a_0, a_2$  and  $a_4$  are written for the coefficients  $P_0(\cos \theta), P_2(\cos \theta)$  and  $P_4(\cos \theta)$  respectively, from equation (1).

Let us consider one of the radiations say  $L_1$  which is a mixture of  $L_1$  and  $(L_1+1)$  multipoles, other two are pure  $L_2$  and  $L_3$ . In that case,  $Z$  along with  $\delta_1^{r_1}$  is written as

$$[Z(L_1 b L_1 b; a k_1) + 2\delta_1 Z(L_1 b L_1 + 1 b; a k_1) + \delta_1^2 Z(L_1 + 1 b L_1 + 1 b; a k_1)]$$

Therefore  $W(\theta)$  has been calculated by taking  $Z(L_1 b L_1 b; a k_1), Z(L_2 b L_1 + 1 b; a k_1)$  and  $Z(L_1 + 1 b L_1 + 1 b; a k_1)$  in equation (1). The values of the triple correlation

coefficients for these three values of  $Z$  in above equation (1) are respectively,  $a_0, a_2, a_4; a_0', a_2', a_4'$  and  $a_0'', a_2'', a_4''$ , which along with mixing parameter can be written as

$$W(\theta) = \{a_0 + a_2 P_2(\cos \theta) + a_4 P_4(\cos \theta)\} + 2\delta_1 \{(a_0' + a_2' P_2(\cos \theta) + a_4' P_4(\cos \theta))\} + \delta_1^2 \{a_0'' + a_2'' P_2(\cos \theta) + a_4'' P_4(\cos \theta)\} \quad \dots (2)$$

We get  $A_2 = \frac{a_2 + 2\delta_1 a_2' + \delta_1^2 a_2''}{a_0 + 2\delta_1 a_0' + \delta_1^2 a_0''}$  after rearranging equation (2) in the form

$[1 + A_2 P_2(\cos \theta) + A_4 P_4(\cos \theta)]$  Similarly we can write  $A_4$ . Defining  $Q = \delta_1^2 / (1 + \delta_1^2)$  and rewriting above expression for  $A_2$  in terms of  $Q$ , we have

$$A_2 = \frac{a_2(1-Q) + 2(\pm)\sqrt{Q(1-Q)}a_2' + Qa_2''}{a_0(1-Q) + 2(\pm)\sqrt{Q(1-Q)}a_0' + Qa_0''}$$

For each value of  $Q$  we shall get two values of  $A_2$  taking either (+) sign with square root or (-) sign with square root. Joining such values one gets the elliptic type of curves. Similar equations and curves are obtained if we consider the mixtures in  $Z_1$  and  $G$ .

#### ANALYSIS OF THE EXPERIMENTAL RESULTS

The level scheme having 68keV—1122keV—100keV triple cascade is given in Nuclear Data Sheets (1959-1965)

$$2 - \frac{68 \text{ keV}}{E_1} \rightarrow 2 + \frac{1122 \text{ keV}}{(M_1 + E_2)?} \rightarrow 2 + \frac{100 \text{ keV}}{E_2} \rightarrow 0$$

where ? indicates uncertainty of  $M_1 + E_2$ .

The multipolarities of the transitions as given above are considered by the conversion coefficient data. Taking this level sequence and 100keV and 68keV to be pure  $E_2$  and  $E_1$  respectively, the mixture in 1122keV is determined by the plot of  $A_2$  versus  $Q$  and the mixture values are  $Q_1 = 0.15 \pm 0.075$  and  $Q_2 = 0.02 \pm 0.015$  as shown in figure 4. Similar analysis was also done for the spin value of 1 and 3 in place of 2 in the above level sequence for 1290keV level. The experimental value for  $A_2$  is too large to account for the data in the plot of  $A_2$  versus  $Q$  either taking 1122 keV as pure  $E_2$  or  $M_1$  or with any mixture of  $M_1$  and  $E_2$  for the spin value 1 and 3

The level sequence having 152keV—1122keV—100keV cascade is given by

$$3 - \frac{152 \text{ keV}}{E_1} \rightarrow 2 + \frac{1122 \text{ keV}}{(M_1 + E_2)?} \rightarrow 2 + \frac{100 \text{ keV}}{E_2} \rightarrow 0. \text{ Taking multipolarity of}$$

100keV to be pure  $E_2$  and 152keV to be pure  $E_1$  the mixture in 1122keV is determined by the plot of  $A_2$  versus  $Q$ . The theoretical value is  $-0.0675$  if we take 1122keV as pure  $M_1$  and  $+0.0377$  if we take 1122keV as pure  $E_2$  while the



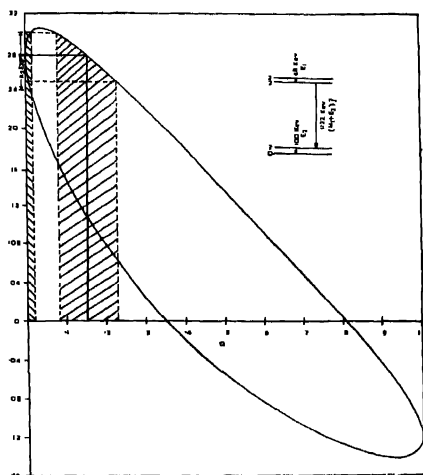


Figure 4

experimental value is  $-0.131 \pm 0.068$ . Therefore it is difficult to take 152keV to be pure  $E_1$  considering 1122keV transition to be pure  $M_1$  or  $E_2$ . Another course left is to take 1122keV as a mixture of  $M_1$  and  $E_2$  as obtained above in 68keV - 1122keV - 100keV cascade. Taking the mean value of the mixture in 1122keV transition as  $M_1 = 85\%$  and  $E_2 = 15\%$  and 100keV to be pure  $E_2$ . The mixture in 152keV is determined by the plot  $A_2$  versus  $Q$  as shown in figure 5. The  $Q$  thus obtained is  $Q_1 = 0.005 \pm 0.015$  and  $Q_2 = 0.89 \pm 0.04$ . But according to the conversion coefficient data 152keV transition is taken pure  $E_1$  (with very little mixture of  $M_2$ ) and therefore the value of  $Q_2 = 0.89 \pm 0.04$  is rejected. This way mixture value  $Q_1 = 0.15 \pm 0.075$  in 1122keV is taken in order to satisfy both the cascades simultaneously. Angular correlation coefficients obtained by  $\gamma\gamma$  angular correlation studies by El-Nesr *et al* (1962), Hickman *et al* (1960) and Williams & Roulston (1956) for 1122keV transition give two sets of mixture values by the method of Arns & Wiedenbeck (1958). The value giving predominantly quadrupole transition is taken and other giving higher percentage of dipole is not considered. But in the present studies the plot of  $A_2$  versus  $Q$  and measured  $A_2(+)$  indicates the higher percentage of  $M_1$  transition.

The multipole assignments on the basis of conversion coefficient data for 68keV and 100keV transition are also pure  $E_1$  and  $E_2$  respectively. 152keV transition should be pure  $E_1$  with a little mixture of  $M_2$  on the basis of conversion coefficient data of Lederer *et al* (1967) and Daniel *et al* (1964) (measured  $\alpha_k = 0.11 \pm 0.02$

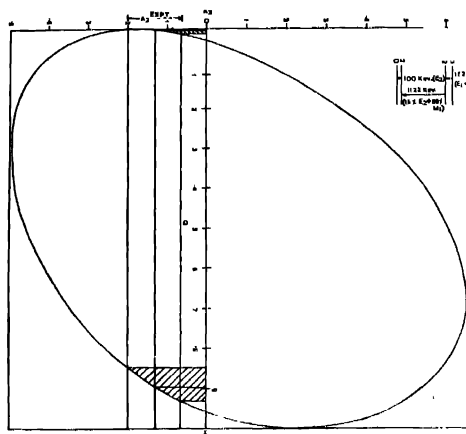


Figure 5

and theoretical value of  $\alpha_k$  for  $E_1 = 0.105$  and  $M_2 = 6.8$ ). In the present measurements the value  $Q_2$  for 152keV is  $M_2/(E_1 + M_2) = 0.005 \pm 0.005$  which shows a little mixture of  $M_2$  in  $E_1$ . It is difficult to account for the measured value of conversion coefficient ( $\alpha_k = 328 \pm 15 \times 10^{-4}$ ) for 1122keV gamma radiation with the mixture of 15%  $E_2$  and 85%  $M_1$  as obtained in the present measurement (considering the theoretical value of conversion coefficient to be for  $E_2 = 0.0029$  and  $M_1 = 0.0060$ ). In case the conversion coefficient value is to be considered for this mixture value, then one way is to consider the reduction in theoretical value of conversion coefficient for  $M_1$  transition by applying the correction in the theoretical value due to finite size effect in  $M_1$  conversion coefficient data as given by Reiner (1958) and Church & Weneser (1960) for  $M_1$  transition between two lowest  $2+$  states

The only quantum numbers ( $I, \pi$ ) as proposed by Alaga *et al* (1955) are satisfied with our experimental results from these two triple cascades angular correlation studies for the levels involved in them.

We are thankful to the Department of Atomic Energy, Government of India for financial help in the research project.

#### REFERENCES

- Alaga G., Alder K., Bohr A. & Mottelson B. R. 1955 *Kgl. Dan Vid. Selsk. Mat. Fys. Medd.* **29**, No. 9.  
 Arns, R. G. & Weidenbock, M. L. 1958 *Phy. Rev.* **111**, 1631.

- Church E. L. and Wensor J. 1960 *Annual Rev. Nucl. Sc.* **10**, 193.
- Daniel H., Huefner J. & Lorenz Th. 1964 *Nucl. Phys.* **56**, 147.
- El-Near M. S. & Bashandy E. 1962 *Ark. Fysik.* **23**, No. 27, 283.
- Ferguson A. J. 1965 *Angular Correlation Methods in Gamma-ray Spectroscopy*, North-Holland Publishing Company, Amsterdam.
- Hickman G. D. & Wiedenbeck M. L. 1960 *Phys. Rev.* **118**, 1049.
- Korkman K. & Backlin A. 1966 *Nucl. Phys.* **82**, 561.
- Körner H. J. Radeloff J. & Bordenotdt E. 1963 *Z. Physik* **172**, 279.
- Lederer C. M., Hollander J. M. & Perlman I. 1965 *Table of Isotopes (sixth edition)*, John Wiley and Sons Inc., New York, London.
- Rainor A. S. 1958 *Nucl. Phys.* **5**, 544
- Williams R. C. & Roulston K. T. 1956 *Can. J. Phys.* **34**, 1087

## Analysis of observed grain density in nuclear emulsions

By R. K. GAUR and A. P. SHARMA

*Department of Physics, Kurukshetra University, Kurukshetra, India*

*(Received 8 March 1969; Revised 12 August 1969 and 14 November, 1969)*

Actually observed grain density, along the tracks of the charged particles in nuclear emulsions, is analysed in terms of primary, secondary and fog grains. An attempt has been made to estimate the contribution of the primary and secondary grain densities theoretically for various values of velocities. The results of our model are compared with those of Patrick & Barkas (1962) and Benton & Heckman (1964). It is concluded that the secondary grain density accounts for nearly 33.5% of the total grain density observed in G-5 emulsions for  $0.08 < \beta < 0.14$  and 23% at minimum ionization. Our theoretical results agree well with the experimentally observed values.

### 1. INTRODUCTION

The signature of charged particles left in nuclear emulsions in the form of tracks can give sufficient information regarding their particulars *e.g.*, velocity, rate of energy loss, charge, kinetic energy and mass. The track parameters in use are grain density  $\delta$ -ray density, tapering length, track width, range and scattering.

Kinoshita (1910) has defined the total grain density in emulsions by the following expression :

$$g = C(1 - e^{-bI}) \quad \dots (1)$$

Where  $C$  is defined as the saturation value of the grain density for heavily ionizing particles and is equal to the available number of silver halide grains ( $g_{max} = N$ ) per hundred micron. The parameter  $b$  is defined as a function of grain sensitivity and its cross-sectional area and also includes the effect of development conditions.  $I$  denotes the specific energy loss which according to Blau (1949) is  $(dE/dR)^{\frac{1}{2}}$  while according to Morand & Rossum (1951) is  $(dE/dR)^{\frac{1}{2}} - a^{\frac{1}{2}}$  ( $a$  representing threshold energy). The magnitudes of exponents  $b$  and  $I$  are not well defined. Patrick & Barkas (1962), Benton & Heckman (1964) and Brown (1953) have given a similar expression for defining primary grain density with different constants.

Experimental observations show that the variation of grain density with specific energy loss for charged particle tracks is a characteristic curve (Fowler 1950, Fowler & Perkins 1951, Powell *et al* 1959, Sharma & Gaur 1968).

The variation at low energy losses has a direct proportionality but at higher values of specific ionization it deviates from linearity and the curve becomes almost flat.

Many workers (Della Corte *et al* 1953, Patrick & Barks 1962, Benton & Heckman 1964, Brown 1953) have pointed out that this actually measured (observed) grain density represents grains of the following types :

- (i) Grains penetrated and affected by a charged particle to the extent that they are rendered developable during the process of development. The number of such grains per  $100\mu\text{m}$  of track length is defined as the primary grain density.
- (ii) Grains not directly traversed by the charged particle, but still made developable during the process of development due to some induced development created in them by the neighbouring grains, or due to the penetration of  $\delta$ -rays projected from the path of the primary particle, are known as secondary grains.
- (iii) Sharma & Gill (1962) have shown that few grains neither affected due to the process (i) nor due to process (ii) are also rendered developable due to the process of undesirable background development. Such grains have been referred as fog grains. They may be due to the radio-active contaminations and impurities etc.

In this paper we have tried to estimate the contribution of the primary and secondary grain densities towards observed grain density. A new scheme for calculating these grains densities is also given.

## 2. EXPERIMENTAL

The measurements were made on MBI-9 scattering microscope having an oil immersion objective of  $90\times$  and a filar micrometer (attached with goniometer) eyepiece of  $15\times$  carrying a fine scale attached with a small drum or rotating head with 100 divisions on its circular scale. The least count of each division for measurements was  $0.1\mu\text{m}$ . The turning stage arrangement for alignment of track was extremely fine. Emulsion stacks exposed to  $1.5\text{ GeV}/\text{CK}^-$ -beam (CERN) and  $4\text{ GeV}/\text{C}\pi^-$ -beam (Berkeley) were used for this purpose.

For measurements well identified  $\pi$ -meson and proton tracks having a dip angle of less than  $10^\circ$  were chosen. Gap density and gap length measurements were made on these tracks. The values of  $\beta$  for various residual ranges were obtained with the help of the tabulated data of Trower (1966).

For determining the grain density, the following expression of Fowler & Perkins (1955) was used.

$$g = \frac{\ln \{H(l_2)/H(l_1)\}}{l_2 - l_1} \quad (2)$$

Where  $g$  is the actual grain density and  $H(l_1)$  and  $H(l_2)$  are the densities of gaps exceeding length  $l_1$  and  $l_2$  respectively.

The variation of observed grain density ( $g$ ) with velocity ( $\beta$ ) in G-5 emulsion is shown in figure 1. The figure indicates that the observed grain density increases rapidly with decreasing values of  $\beta$  at greater velocities but the curve tends to flatten below  $\beta \sim 0.08$ . The dependence of grain density on  $\beta$  is not linear for whole of the region of  $\beta$ , but for  $0.08 < \beta < 0.14$ , the grain density is nearly proportional to the velocity and can be represented by the following empirical relation :

$$g = 4.32 - 14.56\beta \quad (\text{per micron}) \quad (3)$$

A similar type of linear dependence of observed grain density on  $\beta$  is shown by Patrick & Barkas (1962) but with different constants for K-5 emulsions. Benton & Heckman (1964) have approximated from their experimental observations on heavily charged particles, an inverse square dependence of  $g$  on  $\beta$ .

### 3. THEORETICAL

#### 3.1. Calculation of Primary Grain Density :

The development of a grain depends on the amount of latent images or the amount of ionization created in it. The maximum number of holes produced at some specific energy loss ( $dE/dR$ ) in a grain of G-5 emulsion along its diameter (0.27 micron) can be given as : (Sharma & Gaur, 1969)

$$n_0 = 46.55 (dE/dR) \quad \dots (4)$$

where  $dE/dR$  is in Kev/ $\mu m$ .

The total number of holes given by the above relation is not utilized for latent image formation as a fraction of it recombines with electrons during the period of latent image formation. Taking into account the recombination process, the effective number of positive holes ( $n$ ) available for latent image formation in G-5 emulsions is given by the following relation :

$$n = \frac{46.55(dE/dR)}{1 + 0.0777(dE/dR)} \quad (5)$$

In an earlier communication (Sharma & Gaur 1968) it was shown that the probability of development of a grain can be expressed by the following expression:

$$\pi = 1 - e^{-S'} \quad (6)$$

where

$$\begin{aligned} S' = & \gamma e^{-\alpha}(1-\beta)^{-1}[1 + (\alpha-\beta)(1-\beta)^{-1} + \frac{1}{2}(\alpha-\beta)(\alpha-2\beta)(1-\beta)^{-2} + \\ & \frac{1}{6}(\alpha-\beta)(\alpha-2\beta)(\alpha-3\beta)(1-\beta)^{-3} + \frac{1}{24}(\alpha-\beta)(\alpha-2\beta) \\ & (\alpha-3\beta)(\alpha-4\beta)(1-\beta)^{-4} + \dots + \text{negligible terms}] \end{aligned}$$

In the above expression,

$\alpha = \frac{n}{S}$ , ratio of effective number of positive holes and total number of sensitivity centres in a grain.

$\beta = \frac{B}{S}$ , ratio of limiting number of positive holes and total number of sensitivity centres.

and  $r = \alpha/\beta = \frac{n}{B}$ .

Substituting  $S = 2000$ ,  $B = 493$  (Sharma & Gill 1962), we get

$$\begin{aligned} S' = & 1.327ne^{-0.005n}[1 + 6.635 \times 10^{-4}(n-B) + 2.201 \times 10^{-7}(n-B)(n-2B) \\ & + 4.83 \times 10^{-11}(n-B)(n-2B)(n-3B) + 8.075 \times 10^{-15}(n-B) \\ & (n-2B)(n-3B)(n-4B) + \dots \text{negligible terms}] \end{aligned} \quad \dots (7)$$

The primary grain density can be defined as the product of  $\pi$ , the probability of development and the number of grains per  $100\mu m$  (i.e.,  $g_{max}$  or  $N$ ) in the unprocessed emulsion.

Therefore, primary grain density,  $g_p = \pi \times N = N(1 - e^{-S'})$  ... (8)

The value of  $N$  for G-5 emulsion is around 275-300 (Voyvodic 1950 and Sharma & Gill 1962).

### 3.2 Calculation of Secondary Grain Density

For higher values of effective energy loss the primary grain density should approach a saturation value  $g_{max}$  which in case of G-5 emulsion is  $\sim 275$  per hundred micron (Voyvodic 1950). Fowler & Perkins (1955) have shown that the gap length coefficient for relativistic tracks of heavy charge in G-5 emulsion exceeds the maximum value  $g_{max}$  (considered  $3/\mu m$ ) and approaches  $5/\mu m$ . This indicates that apart from primary grains i.e., grains directly affected by the charged particles, few other grains are also developed which also contribute to the gap length coefficient and due to the presence of such grains, the actual grain density exceeds the saturation value  $g_{max}$  ( $3/\mu m$ ). Many workers (Patrick & Barkas 1962, Benton & Heckman 1964, Brown 1953 and Della Corte *et al* 1953) have attempted a separation of the primary and secondary grain densities. These secondary grains are attributed to  $\delta$ -rays.

The observed grain density,  $g$  can be represented as the summation of the three different grain densities i.e.,

$$g = g_p + g_s + g_f \quad (9)$$

Where  $g_p$  is the primary grain density,  $g_s$ , the secondary grain density and  $g_f$ , the grain density due to fog grains. According to the curves of Dodd & Waller

(1951) the value of fog grains is very small say around 5-10 fog grains per  $100\mu\text{m}$ . If we ignore the effect of fog grains in comparison to other grain densities, then

$$g = g_p + g_s$$

$$\text{or} \quad g_s/g = 1 - g_p/g = \phi \quad \dots (10)$$

where  $\phi$  is known as the induction factor and represents the contribution due to the induced or secondary grains towards the observed grain density. The calculated values of  $\phi$  from the above relation are shown in figure 4. From equation (10) we have :

$$g_s = \frac{\phi}{1-\phi} g_p \quad \dots (11)$$

Substituting the value of  $\phi$  in this relation and knowing the value of  $g_p$  at particular specific energy loss or velocity of the particle from equation (8), one can easily calculate the value of secondary grain density.

We shall now calculate the density of such secondary or induced grains produced by  $\delta$ -rays following the procedure considered by Patrick & Barkas (1962) and Benton & Heckman (1964). The range-velocity relation for electrons ( $\beta < 0.3$ ) to a good approximation can be given by

$$R_e = 2.10^2 \beta^{10/3} \quad \dots (12)$$

The grain density at different velocities according to experimental observations is expressed by equation (3) for a singly charged particle in G-5 emulsion. Thus the number of grains due to a  $\delta$ -ray with an initial velocity  $\beta_e$  can be given by :

$$G(\beta_e) = \int_0^{\beta} g \cdot dR_e = 6.66 \times 10^2 \int_0^{\beta} (4.32 - 14.56\beta) \beta^{7/3} d\beta$$

$$\text{or} \quad G(\beta_e) = 0.084 W^{5/3} - 1.36 \times 10^{-2} W^{13/6} \quad \dots (13)$$

where  $W$  is electron energy in Kev. The  $\delta$ -ray density between the energy interval  $W$  and  $W+dw$  due to a particle of charge  $Z_e$  and velocity  $\beta$  is given by the following relation :

$$N(\delta)dw = \frac{2.55 \times 10^{-2} Z_e^2}{\beta^2} \times \frac{dw}{w^2} \quad \dots (14)$$

The number of induced grains,  $g_s$  per hundred micron caused by  $\delta$ -rays can be found by integrating the product of equations (13) and (14) over the energy interval of  $\delta$ -rays from  $w_0$  to  $w_m$  ( $w_0$  and  $w_m$  are the energy limits of  $\delta$ -rays which contribute towards the secondary grain density). The value of  $g$  comes out as :

$$g_s = \frac{0.32 Z_e^2}{\beta^2} (w_m^{2/3} - w_0^{2/3}) - \frac{2.97}{\beta^2} 10^{-2} Z_e^2 (w_m^{7/6} - w_0^{7/6}) \quad \dots (15)$$



The lower limit of  $\delta$ -ray energy ( $w_0$ ) is taken to be 2 Kev (Shapiro 1952, Patrick & Barkas 1962) as discussed in section (3.3). The upper limit of  $\delta$ -ray energy ( $w_m$ ) is taken 22 Kev, as suggested by Barkas (1962) on the basis of their experimental observations on  $^{16}\text{O}$  tracks. Substituting these values of  $w_0$  and  $w_m$  in equation (15), we finally arrive at the following expression :

$$g = \frac{0.97 Z^2}{\beta^2} \text{ (per hundred microns)} \quad (16)$$

The values of secondary grain density calculated from equation (16) are shown in figure 3.

### 3.3 Calculation of Primary Grain Density on the Basis of Barkas Model

The primary grain density has also been calculated by Patrick & Barkas (1962) and Benton & Heckman (1964) using the following expression :-

$$g_p = N(1 - e^{-\lambda I'}) \quad \dots (17)$$

Where  $\lambda$  is a measure of emulsion sensitivity and  $I'$  is the restricted energy loss equal to  $Z^2 i$ , where  $i$  is the energy loss rate of singly charged particle and  $Z^2$ , the mean square effective charge for an energy loss (Barkas 1963). From equation (17) we see that the value of the slope of the curve drawn in  $-\ln(1 - g_p/N)$  and  $I'$  will give us the value of  $\lambda$ . The value of  $g_p$  is taken to be the difference of observed and secondary grain density calculated from equation (16). We have found  $\lambda$  equal to  $3.2 \times 10^{-2} \text{ g/Mev cm}^2$  in case of G-5 emulsion while Benton & Heckman have found its value as  $2.3 \times 10^{-4}$  and  $7.5 \times 10^{-4} \text{ g/Mev cm}^2$  for K-1 and K-0 emulsions respectively. According to Patrick & Barkas (1962),  $\lambda = 0.048 \text{ g/Mev cm}^2$  for K-5 emulsions. Hence equation (17) can be reduced to .

$$g_p = N(1 - e^{-0.032 I'}) \quad \dots (18)$$

Where  $I'$  is the restricted energy loss. We have calculated the restricted energy loss at various velocities with the help of the following relation (Barkas 1963) :

$$I' = \left( \frac{dE}{dR} \right)_{W_1} = \frac{A}{\beta^2} \left[ \frac{\ln 2 m_e C^2 \beta^2 \gamma^2 w_0}{I^2(Z)} - \beta^2 - C' \right] \quad (19)$$

Where  $(dE/dR)$  is the energy loss per unit path length (involving energy transfers of energies less than  $w_0$  per incident collision),  $E$  is the energy of the ionizing particle and  $v = \beta c$  is its velocity,  $A = 0.06705 \text{ Mev cm}^2/\text{g}$  for AgBr,  $m_e$  is the electron rest mass,  $\gamma = (1 - \beta^2)^{-1/2}$ ,  $C'$  is the density effect correction (depending on particle velocity) and has been tabulated by Barkas (1963).  $W_0$  is the upper limit of  $\delta$ -ray energy corresponding to the maximum energy deposited in a single grain,  $I(Z)$  is the mean ionization potential of atoms in the medium (silver bromide) and its value is taken 434 ev as calculated by Sternheimer (1966).

There is some uncertainty about the best value of  $W_0$  and  $I(Z)$ . This may be due to the fact that these constants have only a limited influence on the restricted

energy loss and role of one is partially fulfilled by the other. Shapiro (1952, 1953) found that the ionization loss is not sensitive to the choice of  $W_0$  between 2 and 5 Kev and assumed  $W_0 = 2$  Kev in contradiction to Jongejan's (1959) value (100 Kev). Patrick & Barkas (1962) found a best fit to their data with  $W_0 = 2$  Kev, considering the proposal of Messel & Ritson (1950) that for calculating energy loss the value of  $W_0$  should be taken equal to the energy of the  $\delta$ -ray which has a range equal to the size of the grain. According to Demers (1953) and Lozhkin (1957), the  $\delta$ -rays of 2Kev energy are capable of sometimes causing development of a single grain near the track, hence it is reasonable to take 2 Kev as the minimum  $\delta$ -ray energy capable of broadening the track. Keeping these points in view we have calculated energy loss taking  $W_0 = 2$  Kev as considered by these workers. The values of primary grain density calculated from relation (8) and (18) are shown in figure 2.

## 5. RESULTS AND DISCUSSION

The variation of observed grain density and primary grain density with velocity  $\beta$  are shown in figure 1 and figure 2 respectively. To check the validity of the former variation let us study first the latter one. Curve (a) of figure 2 is based on our calculations from equation (8) while the curve (b) is obtained from equation (18) derived according to the procedure similar to that of Patrick & Barkas (1962).

The variation of secondary grain density  $g_s$  as a function of particle velocity is shown in figure 3. Curve (a) of this figure is generated from the theoretically calculated values of  $g$  (equation 16) assuming that the secondary grains are formed

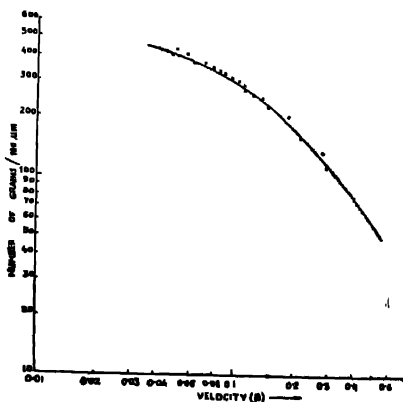


Figure 1. Variation of grain density with velocity  $\beta$ . Solid curve indicates the values of Fowler & Perkins (1951) and  $\times$  points indicate the present work.

by  $\delta$ -rays. Curves (b) and (c) of this figure indicate the variation of the secondary grain density based on the difference of the observed and primary grain densities, the later being calculated on the basis of our model (equation (8)) and that of Barkas (equation (18)) respectively. From figure 3 it is clear that the equation

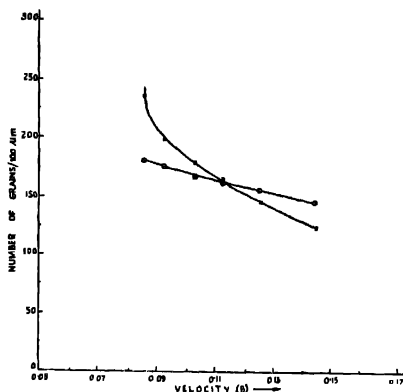


Figure 2. Variation of primary grain density with velocity  $\beta$ .  $\times$  points indicate calculated primary grain density using Barkas model.  $o$  points indicate calculated primary grain density from our model.

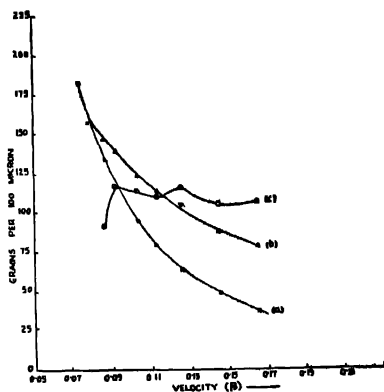


Figure 3. Variation of secondary grain density with velocity. Curve (a) shows secondary grain density calculated on the basis of  $\delta$ -rays. Curves (b) and (c) show the difference of observed and primary grain densities, calculated on the basis of our model (equation 8) and that of Barkas (equation 18) respectively.

(16) fails to describe the production of  $\delta$ -rays for velocities ( $\beta$ )  $< 0.08$  and the secondary grain density continues to increase for lower values of velocity ( $\beta$ ). Similar results were found by Benton & Heckman (1964).

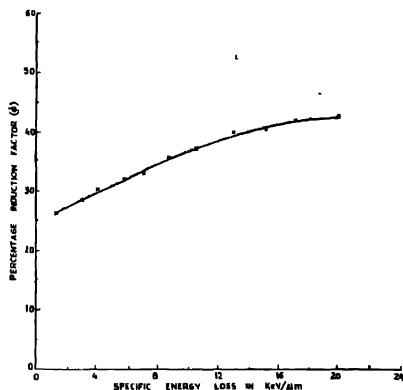


Figure 4. Variation of percentage induction factor with specific ionization.

The percentage contribution of  $g_s$  over  $g$  indicated by the induction factor ( $\phi$ ) for various values of  $(dE/dR)$  Kev/ $\mu$ m is plotted in figure 4. In order to calculate  $\phi$  according to equation (13), the value of  $g_p$  are calculated from equation (8) and the values of  $g$  are taken from figure 1. This indicates that the contribution due to secondary ionization slightly increases at large values of specific energy losses and becomes almost constant. The average value of  $\phi$  estimated from figure 4 is 35% (for  $0.08 < \beta < .014$ ) with the consideration of the fog grains and 32% without fog grains. The mean of these variations is 33.5%. At minimum ionization the contribution of secondary grains due to our model is 23%, which is in contradiction to the results of Nicoletta *et al* (1967) who have shown a contribution of only 10% at minimum ionization but in agreement with the results of Patrick & Barkas (1962) who have shown it as 25%. Benton & Heckman (1964) while studying the secondary grain density have found that the fraction of the observed grain density which is of secondary origin due to  $\delta$ -rays for velocities  $0.08 < \beta < 0.145$ , is nearly constant and equal to  $35 \pm 5\%$  for K-1 and K-0 emulsions and is independent of the atomic number of the charged particles.

In figure 5 we have shown the variation of total grain density with  $\beta$ . Curve (a) shows the variation of observed (experimental) grain density in case of G-5 emulsions. Curve (b) shows the variation of total grain density represented as a sum of primary grain density ( $g_p$ ) calculated on the basis of our model (equation

(8)) and secondary grain density calculated from equation (16). Curve (c) indicates the variation of total grain density represented as a sum of primary grain density calculated on the basis of Barkas model (equation 18) and secondary grain density due to  $\delta$ -rays. These curves indicate that our theoretically calculated values are nearer to the experimental values.

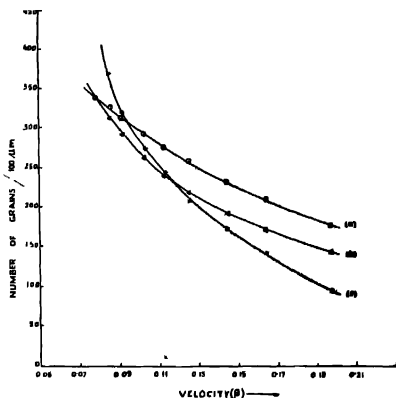


Figure 5. Variation of total grain density with velocity. Curve (a) indicates total observed grain density. Curves (b) and (c) indicate the total grain density, a sum of primary and secondary grain densities, the primary grain density being calculated from our model (equation 8) and from that of Barkas (equation 18) respectively.

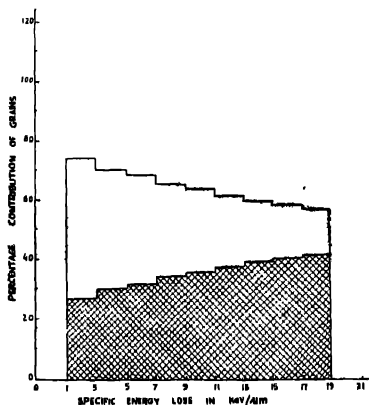


Figure 6. Percentage contribution of primary and secondary grain densities. The shaded area corresponds to the percentage contribution of secondary grain density.

The discrepancy in results may be due to some over-estimation in  $g_s$  calculated from equation (16), because a few secondary grains might have developed as a

result of the joint action of two or more  $\delta$ -rays (Powell *et al* 1959). We have assumed that all these  $\delta$ -rays tend to lie along the trajectory of the particle but there may be a few such  $\delta$ -rays which might go at a certain angle with the trajectory of the particle and may not contribute to the secondary grain density. The grains developed due to such  $\delta$ -rays will not be considered as the part of the particle track.

The percentage contribution of primary and secondary grain density is shown in figure 6 and is in agreement with the results of Patrick & Barkas (1962) and Benton & Heckman (1964).

The authors wish to express their thanks to Miss S. Malik and Miss A. Malik for their help in the scanning. One of the authors (RKG) is grateful to Kurukshetra University authorities for providing financial assistance to him.

#### REFERENCES

- Barkas W. H. 1961 *Phys. Rev.* **124**, 893.  
 Barkas W. H. 1963 *Nuclear Research Emulsions I* (Academy Press, New York).  
 Benton E. V. & Heckman H. H. 1964 *N. Cim.* **32**, 1457.  
 Blau M. 1949 *Phys. Rev.* **75**, 279.  
 Brown L. M. 1953 *Phys. Rev.* **90**, 95.  
 Della Corte M., Ramant M. & Ronchi L. 1953 *N. Cim.*, **10**, 509.  
 Demers P. & Lechno-Wosintynska Z. 1953 *Canad. J. Phys.*, **31**, 480.  
 Dodd E. C. & Waller C. 1951 *Fundamental Mechanism of Photographic Sensitivity* (Butterworths Scientific Publs. London) 266-271.  
 Fowler P. H. 1950 *Phil. Mag.*, **41**, 160.  
 Fowler P. H. & Perkins D. H. 1955 *Phil. Mag.* **46**, 587.  
 1951 *Fundamental Mechanism of Photographic Sensitivity* (Butterworths Scientific Publs. London) 340-345.  
 Jongejans B. 1959 *N. Cim.*, **18**, 625.  
 Kinoshita S. 1910 *Proc. Roy. Soc.* **A83**, 432.  
 Lozhkin O. V. 1957 *Soviet Physics JETP*, **5**, 293.  
 Messel H. & Ritson D. 1950 *Phil. Mag.* **41**, 1129.  
 Morand M. & Rossum L. V. 1951 *Photographic Sensitivity* (Butterworths Scientific Publs. London) 317.  
 Nicoletta C. & Menulty, P. J. & Jain P. L. 1967 *Phys. Rev.* **164**, 1693.  
 Patrick J. W. & Barkas W. H. 1962 *Suppl. N. Cim.* **23**, 1.  
 Powel C. F., Fowler P. H. & Perkins D. H. 1959 *Study of Elementary Particles by the Photographic Method* (Pergamon Press, London)  
 Sharma A. P. & Gaur R. K. 1969 *Indian J. Pure & Appl. Phys.* **7**, 325.  
 1968 *Indian J. of Phys* **42**, 650.  
 Sharma A. P. & Gill P. S. 1962 *Proc. National Inst. of Sciences of India* **28**, 166.  
 Sternheimer R. M. 1966 *Phys. Rev.* **145**, 247.  
 Stiller B. & Shapiro M. M. 1952 *Phys. Rev.*, **87**, 682.  
 Stiller B. & Shapiro M. M. 1953 *Phys. Rev.* **92**, 735.  
 Trower W. P. 1966 *U.C.R.L.* 2426, Vol. II.  
 Voyvodie L. 1950 *Canad. J. Res.*, **A28**, 315.

# Letters to the Editor

*Indian J. Phys.* **44**, 319-322 (1970)

## Elastic scattering of fast electrons by nitrogen-14

BY G. BANERJI

*Department of Theoretical Physics,*

*Indian Association for the Cultivation of Science, Calcutta-32,  
India*

(Received, 8 October 1969)

It was shown (Fregeau & Hofstadter, 1955) for the nucleus of carbon-12 that the assumption of a half-uniform half-Gaussian shell model gives better agreement with experiment than either the uniform or the Gaussian model. The aim of the present note is to calculate the nuclear form factor for nitrogen-14 on the assumption of a parabolic potential and then to obtain the differential elastic electron scattering cross-section.

The differential elastic scattering cross-section of Dirac electrons (energy  $E_0$ ) from a target nucleus of mass  $M$ , containing  $Z$  point protons, each of charge  $e$ , is given (Rose, 1961) in the Born approximation by

$$\frac{d\sigma}{d\Omega} = \left( \frac{d\sigma}{d\Omega} \right)_M |F(q)|^2, \quad (1)$$

where  $F(q)$  is the form factor and  $(d\sigma/d\Omega)_M$  is the relativistic Mott Scattering cross-section for electrons from a massive point nucleus of charge  $Ze$ .

$$\left( \frac{d\sigma}{d\Omega} \right)_M = \left( \frac{Ze^2}{2E_0} \right)^2 \cos^2 \theta/2 \left[ \sin^4 \theta/2 \left( 1 + \frac{2E_0}{Mc^2} \sin^2 \theta/2 \right) \right] \dots (2)$$

in which  $(1 + (2E_0/Mc^2) \sin^2 \theta/2)^{-1}$  denotes the centre-of-mass correction,  $\theta$  being the scattering angle. The form factor is given by,

$$F(q) = \int_v \vec{\rho}(\vec{r}) \exp(i \vec{q} \cdot \vec{r}) d\vec{r} \quad \dots (3)$$

and  $\hbar q$  is the magnitude of the momentum transfer vector given by

$$\hbar q = \frac{2E_0}{c} \sin \theta/2 \left/ \left( 1 + \frac{2E_0}{Mc^2} \sin^2 \theta/2 \right) \right|^{1/2}$$

where  $v$ , is the nuclear volume and  $\vec{\rho}(\vec{r})$  the charge density, and  $\vec{r}$  the radius vector from the centre of the nucleus. The validity of the Born approximation was discussed by Parzen (1950).

For a spherically symmetric charge distribution  $\rho(r) = \rho(r)$  the integration in (3) may be performed to give

$$F(q) = \frac{4\pi}{q} \int_0^\infty \rho(r) \sin(qr) r dr \quad \dots (5)$$

If we consider the infinite parabolic well  $V \propto r^2$ , the nuclear charge distribution is obtained in the analytic form (Buttler, 1968),

$$\rho(r) = \rho(0)(1 + \alpha r^2/a_0^2) \exp(-r^2/a_0^2), \quad \dots (5)$$

where  $\alpha \equiv (Z-2)/3$  and the length parameter  $a_0$  is related to the curvature of the well. Normalization of  $\rho(r)$  as

$$\int_0^\infty \rho(r) 4\pi r^2 dr = 1$$

yields

$$\rho(0) = 2\pi^{-3/2} a_0^{-3} (2+3\alpha)^{-1} \quad \dots (6)$$

The root-mean square radius, weighted according to charge, and defined as

$$a^2 = \int_0^\infty r^2 \rho(r) 4\pi r^2 dr$$

becomes

$$a = [3(2+5\alpha)/\{2(2+3\alpha)\}]^{1/2} a_0. \quad \dots (7)$$

Using (5), (6) and (7) in (4) the expression for  $F$  is obtained as

$$F = [1 - \alpha x^2/\{3(2+5\alpha)\}] \exp[-(2+3\alpha)x^2/\{6(2+5\alpha)\}] \quad \dots (8)$$

in which  $x = qa$ ,

where we have made use of the integral

$$\int_0^\infty e^{-n^2 t^2} \cos nt \, dt = \frac{\sqrt{\pi}}{2n} \exp(-n^2/4m^2). \quad (n > 0).$$

The value of  $x(=qa)$  is varied from 0 to 7 and the form factor calculated in each case. The results are shown in figure 1. It is found that a diffraction zero occurs at  $x = 4.3$ . It is typical of Born approximation from factors for a charge distribution due to an independent particle shell model of a nucleus for an infinite harmonic well potential. The differential scattering cross-section results in the range  $30^\circ$ - $90^\circ$  at an incident electron energy of 400 MeV with the rms radius  $a = 2.48 \times 10^{-13}$  cm for  $N^{14}$  are shown in figure 2. The results of our calculation for the differential cross-section are expected to be reliable excepting the regions in the neighbourhood of the diffraction minimum where the Born approximation is not accurate. In the exact treatment there will be no zero value for the diffraction minimum as obtained in the present calculation.



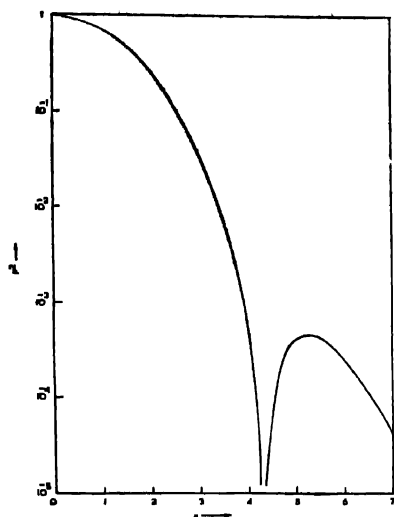
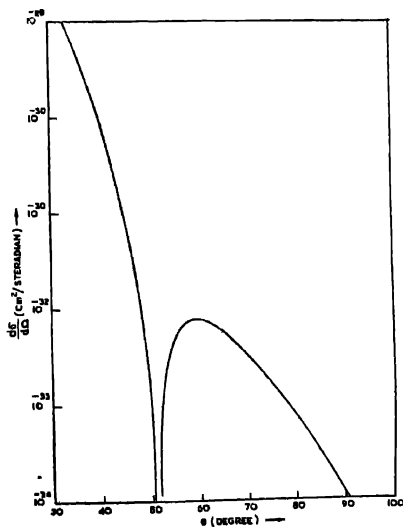
Figure 1. Absolute square of the form factor as a function of  $X$ .

Figure 2. Differential cross-section as a function of scattering angle.

In conclusion, the author thanks Dr. N. C. Sil, Head of the Department of Theoretical Physics, I.A.C.S., Calcutta, for helpful discussions.

#### REFERENCES

- Buttlar H. von 1968, *Nuclear Physics, An Introduction*, Academic Press.  
Fregeau J. H. & Hofstadter R. 1955 *Phys. Rev.* **99**, 1503.  
Parzen G. 1950 *Phys. Rev.* **80**, 261.  
Rose M. E. 1961 *Relativistic Electron Theory*. John Wiley and Sons Inc.

## BOOK REVIEWS

### *Fundamentals of Radiation Protection*

Hugh F. Henry. pp. xviii+485, \$17.50, John Willey, New York.

While the sixties saw nuclear power become a reality the seventies will see it firmly established as one of the major power sources of many nations. At the same time man has suddenly become conscious that this progress is contributing to the fouling of his environment which may one day destroy all plant and animal life. The tragic consequences of atomic explosions at Hiroshima and Nagasaki and the widespread radioactive fallout of subsequent nuclear explosions have left man scared of the biological damage that might show up decades later. As a result of all this, the common man, the worker in the atomic industries and a wide variety of people who come into contact with nuclear and high energy radiations all have to be reassured and taught how to handle them safely. The author has made an attempt to reach all these people in this book on "Fundamentals of Radiation Protection". The beginning chapters are devoted to atomic structure, mass-energy relationships, radiations, artificial and natural radioactivity, nuclear fission, half lives and radioactive equilibrium. These are dealt with in very simple language, deriving equations and defining units of different quantities. The author has defined not only what is kinetic energy and potential energy but even what is energy, which was perhaps not necessary. In chapter II, it is said that the nucleus contains only protons and neutrons but in chapter III it is also stated that beta particles are emitted from the nucleus which the authors should have explained. This could have been done under nuclear stability by discussing the importance of neutron/proton ratio. Since the central theme of the book is how to protect the living tissues from radiations, the author has very rightly discussed the structure of the cell, the chemical constituents of the cell, how different organs have different sensitivity to radiation, and how this injury is repaired in the body. The physical aspects of radiation exposure is one chapter which could have been written better and more readable particularly the subject of density of ionisation.

In chapters VI and VII, the author has dealt with different kinds of exposure to radiation in the course of our normal life and specially for workers in the vicinity of radiation and examined in detail the consequences of such exposure. He has attempted to remove the fear of radiation and stressed some of the beneficial aspects also, like longevity at low exposure levels. In the chapter on 'Genetic Effects of Radiation' the reader is treated to the laws which govern 'inheritance' and how radiation affects them. In the chapter on 'Internal Exposure Evaluations' actual methods of calculations have been illustrated which is of great practical importance.

The book discusses all aspects of personnel monitoring and environment monitoring for radioactivity and the methods to minimise exposure to individuals. It also deals with different kinds of emergencies that can arise in nuclear reactors. They have been illustrated by actual incidents and what was done and what should have been done.

The chapter on Administration is extremely helpful to anyone who is contemplating a health physics programme.

The chapter on 'Nuclear Weapons' is informative to those who are uninitiated in the subject, but would like to know how an atomic explosion takes place. However, the author has tried to justify the American use of nuclear weapons on Japan which is certainly out of place and is a highly controversial issue.

There are some errors and spelling mistakes. In chapter III, p. 31, the equation should be  $^{234}_{90}\text{Th} \rightarrow ^{234}_{91}\text{Pa} + ^0_0\text{e}$ . In page 271, it should be  $\sin^2 \theta/2 = 0.5$  instead of ' $\sin^2 \theta/2$ ' and on page 278, the equation should be  $I = I_0 e^{-\mu x} m^2$  instead of  $I_0 e^{-\mu x} \text{ cm}^2$ . On p. 300, in the last sentence 'emphases' should be 'emphasis' and on p. 313, the end of the first paragraph 'extravagently' should read 'extravagantly'.

The references given at the end of each chapter and the questions are of great help to those who are taking a course in radiation protection. This can serve as a useful text book. The author, on the whole has given an excellent account of the several facets of radiation protection.

K. N. R.

### *The Sixth International Symposium on the Reactivity of Solids*

Edited by Mitchell, De Vries, Roberts and Cannon. pp-852.

Wiley—Interscience.

The proceedings of the Sixth International symposium on the Reactivity of Solids held in Schenectady, New York, U.S.A. from August 25-30, 1968, edited by Mitchell, DeVries, Roberts and Cannon comprise of erudite dissertation of certain topics of solid state chemistry of recent interest. The book presents the various research papers read in the proceedings in a categorised form under eight sectional headings and does not attempt to develop the concepts *ab initio*. The paper entitled "Crystallographic shear and planar faults in solids" read as a Presidential Address by Prof. Wadsley in the first section advances a very ingenious explanation for the behaviour of non-stoichiometric oxides in terms of the localised shear planes and different crystallographic arrangements of the metal-oxygen tetrahedra. The crystal defect such as dislocation, vacancies, interstitials, Wagner defects etc. have been recognised undisputedly as playing a decisive role in many of the gas-solid, liquid-solid, and solid-solid reactions. The phenomena such as catalysis, diffusion, sintering etc. are clear manifestations of the integral part played by these defects in crystalline solids. The paper entitled "Role of crystal structure, defects, and cationic diffusion in the oxidation and reduction processes of iron oxides at low temperature" by Gazzarini *et al* is an immaculate description of the phase transformation relationship of iron oxides utilising the already mentioned ideas of crystal defects. It is not possible to discuss the salient features of all the 79 papers under eight general sections in the limited space available at my disposal. Nevertheless, it can be mentioned that the book entails many interesting discourses of profound scientific interest like decomposition of compounds, corrosion of metals, reaction kinetics of a substance under various physical and chemical environments, crystallo-chemical characteristics of solids in relation to their reactivity, characterisation of ferrites, semiconductors, whiskers, pyrolytic carbon, phase transition of compounds, crystallization of glass, high pressure reaction of solids, etc. Further as this book is a compilation of several works carried out in different laboratories of the world, obviously some gaps, missing links and repetition of the same ideas may creep in the body of the book as a whole, which is unavoidable. However, all these in no way belittle its importance. This book will be very much useful to the researcher in general, particularly to those who are engaged in research pursuit in the aforesaid fields.

B. K. B.

# Indian Journal of Physics, vol 24, 1970

## FORM IV

(See Rule 8)

- |   |  |  |
|---|--|--|
| <p>1. Place of publication</p> <p>2. Periodicity of its publication</p> <p>3. Printer's Name<br/>Nationality<br/>(Address)</p> <p>4. Publisher's Name<br/>Nationality<br/>Address</p> <p>5. Editors' Name<br/>Nationality<br/>Address</p> | <p>Indian Association for the Cultivation of Science, 2 &amp; 3, Raja Subodh Mallick Road, Calcutta-32.</p> <p>Monthly</p> <p>Sri Prokash Chandra Chakraborty<br/>Indian<br/>Eka Press, 204/1, B. T. Road, Calcutta-35.</p> <p>Sri Samarendranath Sen<br/>Indian<br/>Registrar, I. A. C. S. Calcutta-32.</p> <p>As below</p> | <p>Indian Association for the Cultivation of Science, 2 &amp; 3, Raja Subodh Mallick Road, Calcutta-32.</p> <p>Monthly</p> <p>Sri Prokash Chandra Chakraborty<br/>Indian<br/>Eka Press, 204/1, B. T. Road, Calcutta-35.</p> <p>Sri Samarendranath Sen<br/>Indian<br/>Registrar, I. A. C. S. Calcutta-32.</p> <p>As below</p> |
|---|--|--|
- 
- |  |  |  |
|--|--|--|
| <p>1. Prof. F. C. Auluck<br/>Indian<br/>Department of Physics<br/>University of Delhi,<br/>Delhi-7</p> <p>2. Prof. K. Banerjee<br/>Indian<br/>P. O. Naopara<br/>Via Barasat<br/>24-Parganas.</p> <p>3. Prof. D. M. Bose<br/>Indian<br/>Bose Institute<br/>93/1, Acharya Prafulla<br/>C. Road, Calcutta-9.</p> <p>4. Prof. S. N. Bose<br/>Indian<br/>National Professor<br/>22, Iswar Mill Lane<br/>Calcutta-6.</p> <p>5. Prof. S. D. Chatterjee<br/>Indian<br/>91, Ballygunge Place<br/>Calcutta-19,</p> | <p>6. Prof. S. R. Khastgir<br/>Indian<br/>Dept. of Physics,<br/>Visva Bharati<br/>Santiniketan, West Bengal</p> <p>7. Prof. D. S. Kothari<br/>Indian<br/>Department of Physics<br/>Delhi University<br/>Delhi</p> <p>8. Prof. D. N. Kundu<br/>Indian<br/>Director<br/>Saha Institute of Nuclear<br/>Physics<br/>92, Acharya Prafulla Ch.<br/>Road Calcutta-9.</p> <p>9. Dr. B. D. Nag Chowdhuri<br/>Indian<br/>Member, Planning Com-<br/>mission Yojana Bhavan<br/>New Delhi</p> <p>10. Prof. K. R. Rao<br/>Indian<br/>Department of Physics<br/>Andhra University<br/>Waltair</p> | <p>11. Dr. R. Ramanna<br/>Indian<br/>Director, Physical Wing<br/>Bhabha Atomic Research<br/>Centre<br/>Apollo Pior Road<br/>Bombay-6.</p> <p>12. Prof. S. C. Sirkar<br/>Indian<br/>22/1B, South Sinthi Road.<br/>Calcutta-30</p> <p>13. Prof. B. N. Srivastava<br/>Indian<br/>Dept. of General Physics<br/>and X-ray, I. A. C. S.<br/>Calcutta-32</p> <p>14. Prof. A. R. Verma<br/>Indian<br/>Director, National Phy-<br/>sical Laboratory<br/>New Delhi</p> <p>15. Prof. A. Bose (Hon. Sec-<br/>retary)<br/>Indian<br/>Dept. of Magnetism<br/>I. A. C. S.<br/>Calcutta-32</p> |
|--|--|--|
- 
- 6 Names and addresses of individuals who own the newspaper and partners or shareholders holding more than one percent of the total capital.
- India Association for the Cultivation of Science  
2 & 3, Raja Subodh Mullick Road,  
Calcutta-32.

I, Sri Samarendranath Sen, hereby declare that the particulars given above are true to the best of my knowledge and belief.

Dated: 21.6.71

Sd/- Samarendranath Sen  
Signature of Publisher



# INDIAN JOURNAL OF PHYSICS

VOL. 44

No. 6

AND

VOL. 53

PROCEEDINGS

No. 6

OF THE

INDIAN ASSOCIATION FOR THE CULTIVATION OF SCIENCE

*(Edited in collaboration with the Indian Physical Society).*

IJPYAS 44 (6) 325-374 (1970)

**JUNE 1970**

PUBLISHED BY THE  
INDIAN ASSOCIATION FOR THE CULTIVATION OF SCIENCE  
JADAVPUR, CALCUTTA-32





## Use of a logarithmic form of potential in the studies on metals

By J. BEHARI

*Department of Physics, Indian Institute of Technology,  
Hauz Khas, New Delhi-29, India*

(Received, 20 November 1969)

A new logarithmic form of central potential between a pair of atoms is proposed for metals. Calculations on cohesive energies for several FCC, BCC, and HCP metals are reported and are found to be in good agreement with experimental data in all the cases.

### INTRODUCTION

One approach to the theoretical study of the properties of solids is through the assumption of a central pairwise potential function. Unfortunately, the calculation of the potential energy of an assembly of given particles as a function of their mutual distance is very difficult and it has been solved by quantum mechanical methods in a few cases only (Mott & Jones 1936, Seitz 1940, Kuhn & Van Vleck 1950, Kambe 1955, Nikulin 1966). However, if we assume the lattice structure, lattice constant and the lattice energy, a satisfactory explanation can be presented of various lattice dynamical and thermodynamical properties of solids, within the range of approximation, by supposing a force law, provided it resembles the real one in some general features. The parameters of the potential function are determined by fitting it in a narrow region surrounding the equilibrium point, for the structure generally remains unaltered and the density changes slightly even at high pressure and upto the melting point. Most of the properties of the solids are determined by points near the minima of the potential energy curve. Those points, therefore, which are farther away from the minimum point will not affect the results as long as the chosen parameters retain the general feature of the curve. By the same reasoning it can be assumed that  $\phi$  depends on the mutual distance of the particles only, even in those cases where the interatomic forces are not central as, for example in metals.

If  $\phi(r)$  is the energy of interaction of two atoms at a distance  $r$  apart, then for  $\phi(r)$  to represent a true interaction potential in a solid, it must satisfy the following conditions (Girifalco & Weizer 1959) :

- i) The derivative of potential  $\phi(r)$  (*i.e.*  $(\partial\phi/\partial r)$ ) must have attractive nature for large  $r$ , and repulsive for small  $r$ , hence should have minimum at  $r = r_0$  (equilibrium separation).
- ii) The decrease in  $\phi(r)$  with  $r$  should be more rapid than  $r^{-3}$ .

These conditions are consequence of simple physical considerations; the first is due to the existence of condensed phases and the second only confirms that the cohesive energy is finite. The two together mean that the crystal structure be stable under infinitesimal homogeneous deformation.

Born and his collaborators (1940) have made a detailed analysis of the stability of crystal lattices and have given conditions that must be satisfied among the elastic constants. For cubic crystals these are :

iii) All elastic constants are positive,

iv)  $C_{11} - C_{12} > 0$ .

A good potential must have a minimum number of parameters, yet predict the remaining constants with sufficient accuracy as well as being adequately close to the dispersion forces at large distance. For metals, three potential energy functions have been used by different workers;

### 1. The Mie-Gruneisen potential

$$\phi(r) = -\frac{A}{r^n} + \frac{B}{r^m}, \quad (n < m),$$

which assumes that the interatomic force is a superposition of an attracting and a repelling force, both depending on the distance by a simple inverse power function. Gruneisen employed this function in his early investigations on the theory of solids. Furth (1944) and afterwards Dayal & Sharma (1955) and Colo (1959) have discussed the applicability of this function for a number of solids.

### 2. The Morse potential (Morse 1929)

$$\phi(r) = D[e^{-2\alpha(r-r_0)} - 2e^{-\alpha(r-r_0)}],$$

originally suggested for molecules, has also been used for metals (Girifalco & Weizer 1959) where  $\alpha$  is a constant and  $D$  is the dissociation energy.

### 3. Rydberg (1931) proposed the following function for diatomic molecules

$$\phi(r) = -D[1 + b(r-r_0)]e^{-b(r-r_0)}$$

where  $b$  is a constant. This potential has the shape appropriate for a potential function and has been found to give better results than the Morse potential for a good number of diatomic molecules. It has also been successfully applied in the studies of metals (Varshni & Bloore 1963).

Apart from being cumbersome to calculate, Rydberg potential as also Morse suffers from one disadvantage, as being finite for  $r = 0$ . Recently Prakash & Behari (1969) proposed a logarithmic form of potential for the exchange interaction between ions in alkali halides, and it was found that the calculation of

cohesive energy yields an excellent agreement with the experimental data. It removed the physical drawback with the most acceptable Born form ( $ae^{-r/\rho}$ ) viz.  $\phi_{repulsive} = \text{constant}$ , rather than infinity, for  $r = 0$ .

### LOGARITHMIC FUNCTION FOR METALS

In view of this we propose a new form for the potential in metals which satisfies the physical condition at  $r = 0$  and has steeper slope than the exponential form :

$$\phi(r) = -A_1 \log_e[1 + (B_1/r)^n] + A_2 \log_e[1 + (B_2/r)^m]$$

It involves six constants, namely  $A_1$ ,  $B_1$ ,  $A_2$ ,  $B_2$ ,  $n$  and  $m$ . To reduce the number of unknown parameters we have chosen  $B_1 = B_2$ , the ionic radii of the metal in question, which are taken from the work of Pauling (1963).  $n$  and  $m$  are generally chosen from the work of Furth (1944). The remaining two constants  $A_1$  and  $A_2$  are obtained by applying the condition of crystal stability

$$\left(\frac{\partial \phi}{\partial r}\right)_{r=r_0} = 0$$

and the compressibility

$$\left(\frac{\partial^2 \phi}{\partial r^2}\right)_{r=r_0} = \frac{9kr_0}{\beta_0},$$

where  $\beta = \text{compressibility}$ ,  $k$  the structure factor and the zero subscript refers to the values of parameters at absolute zero of temperature. Expressions for  $A_2$  and  $A_1$  are

$$A_2 = \frac{B_2^m m}{r_0^{m+1} + B_2^m r_0} \left[ \frac{9kr_0/\beta_0}{\frac{(m+1)r_0^m + B_2^m}{r_0^{m+1} + B_2^m r_0} - \frac{(n+1)r_0^n + B_1^n}{r_0^{n+1} + B_1^n r_0}} \right]$$

and

$$A_1 = \left( \frac{A_2 B_2^m m}{r_0^{m+1} + B_2^m r_0} \right) \left( \frac{r_0^{n+1} + B_1^n r_0}{B_1^n n} \right).$$

Cohesive energy for a number of FCC, BCC and HCP metals is calculated and found to be in good agreement with the experimental results.

### DISCUSSIONS

It is obvious from the inspection of our form of potential that the condition (i) is satisfied. A finite value of cohesive energy as calculated for various substances also satisfies condition (ii). A first hand calculation of elastic constants also satisfies the condition  $C_{11} - C_{12} > 0$ , both being separately positive.

The choice of the property to be studied at the preliminary stage was dictated by the fact that the cohesive energy of metals has not been studied in detail. Some calculations have been done on alkali and noble metals and as is clear from the data collected in table I that our results show much improvement over the results of earlier workers. Moreover, in the most widely used Morse and Rydberg functional form, cohesive energy is chosen as a known quantity in the determination of the parameters of the potential and hence its direct calculation is not possible. As is evident from the form of potential that any uncertainty in the values of ionic radii does not effect our results appreciably. In fact any other

TABLE I

Substance	Lattice <sup>(a,b)</sup> constant $\times 10^8$ cm	$\beta^{(c)} \times 10^{12}$ cm <sup>2</sup> /dyn.	n	m	Cohesive energy $(-\phi_0)$ (Kg. Cal/mol)		
					Calculated	Experimental <sup>(b)</sup>	Others <sup>(d,e)</sup>
Pb	4.9138	2.31	3	12	46.6	47	
Ag	4.068	0.99	4.5	7	72.6	68.3	58.9
Ni	3.5142	0.53	4	6*	107.8	102.3	
Cu	3.6022	0.72	4	7	78.1	80.8	59.9, 83.7
Al	4.0284	1.34	3*	7	73.9	76.9	
Ca	5.5528	5.70	4	6	39.9	42.1	
Sr	6.0534	8.19	4	6	35.7	39.1	
Pd	3.880	0.53	5	6.5	96.5	90.8	
Pt	3.9142	0.36	5.5	8	128.2	135.0	
Au	4.0626	0.57	5.5	8	88.9	87.3	53.3
Li	3.40	8.7	1.5	6	33.8	38.0	
Na	4.2250	15.6	2	6	26.8	26.0	23.2, 25.9
K	5.2250	35.0	2	6	22.8	21.7	27.9, 24.2
Cs	6.0450	67.0	2	6	18.6	19.1	
Mo	3.1432	0.36	5	7	155.7	157.1	
Cr	2.8818	0.52	5	7	83.8	94.5	
Fe	2.8590	0.59	4	7	89.9	98.9	
Zn	2.659**	1.60	5	7	29.9	31.1	
Cd	2.970**	2.41	6	7	22.64	26.76	
Mg	3.190**	2.95	4	6	40.4	35.3	

\*Values are changed by unity, \*\*Nearest neighbour distance.

(a) Varshni & Bloore, 1963, (b) Kittel 1967, (c) Kittel 1961, (d) Kuhn & Van Vleck 1950, (e) Kambe 1955,

choice of  $B_1$  and  $B_2$  will be equally suitable, provided it satisfies the condition

$$\left(\frac{B_{1,2}}{r}\right)^{n_1 m} = 1.$$

Palladium which does not find a place in studies of Furth (1944) is also included in this list. In general our calculated values are in good agreement with the experimental data.

It is interesting to note that an excellent agreement is obtained in quite complicated cases, such as platinum and molybdenum etc., with this simple two term potential. Difference in our calculated values from the experimental ones may be partly attributed to the uncertainty in the values of compressibility, which is taken from the work of Furth (1944) and data collected by Kittel (1961), and it is referred to at room temperature. The experimental values of the cohesive energies (Kittel 1967) are also at room temperature

It may be pointed out that a similar logarithmic form for the overlap repulsion, adopted between a pair of atoms in solidified noble gases is found to predict the experimental results fairly well (Behari 1969).

#### ACKNOWLEDGMENTS

The author is thankful to Dr. B. B. Tripathi for useful suggestions and discussions during the course of investigation. He also wishes to express his high sense of gratitude to Prof. Krishnaji for encouraging correspondence. Interest of Mr. S. Prakash in the work is thankfully acknowledged

#### REFERENCES

- Behari J. 1969 (unpublished)  
 Born M. 1940 *Proc. Cambridge Phil. Soc.* **36**, 160  
 Cole 1959 *IBM J. Research Develop.* **3**, 126.  
 Dayal B. & Sharma R. S. 1955 *Proc. Phys. Soc.* **B68**, 1949.  
 Furth R. 1944 *Proc. Roy. Soc.* **A183**, 87.  
 Girifalco L. A. & Weizer V. G. 1959 *Phys. Rev.* **114**, 687  
 Kambe K. 1955 *Phys. Rev.* **99**, 419.  
 Kittel C. 1961 *Introduction to Solid State Physics, (Second Edition)* Asia Publishing House, 99.  
 1967 " " " " (Third Edition), John Wiley and Sons, Inc  
 New York, London, Sydney, **29**, 78.  
 Kuhn T. S. & Van Vleck J. H. 1950 *Phys. Rev.* **79**, 382.  
 Morse P. M. 1929 *Phys. Rev.* **34**, 57.  
 Mott N. F. & Jones H. 1936 *The Theory and Properties of Metals and Alloys*.  
 Nikulin V. K. 1966 *Phys. Stat. Solidi* **16**, 125.  
 Pauling L. 1963 *The Nature of the Chemical Bond, (Third Edition)*, Cornell University Press  
 514.  
 Prakash S. & J. Behari 1969 *Indian J. Pure Appl. Phys.* **7**, 709.  
 Rydberg R. 1931 *Z. Physik* **73**, 376.  
 Seitz F. 1940 *The Modern Theory of Solids, Mc-Graw-Hill Book Company Inc. New York and London*, 372.

## Ionization potentials and Rydberg series in Kr I sequence

By M. S. Z. CHAGHTAI and ZAHID ALI

Physics Department, Muslim University, Aligarh (U.P.)

(Received 21 May 1970)

The ionization potentials have been re-evaluated for ZrV and NbVI using Edlén's formula, and quantum defect has been plotted in Rydberg series for the existing energy levels of ZrV, NbVI and MoVII. Uptodate situation of the study in the Kr I sequence is briefly reviewed.

### INTRODUCTION

In the KrI sequence, only the first member has been studied in detail (Moore 1952, 1969). The second member, RbII, was studied some forty years ago by Laporte *et al.* (1931) and only a few transitions to the ground level were reported by Charles (1950, see Moore 1952) in NbVI and MoVII about twenty years ago. One of us (Chaghtai 1969, 1970) recently reported an almost complete set of observable transitions to the ground level in ZrV and NbVI, the former, spectrum for the first time. He also added a few transitions and corrected one reported transition in MoVII. This work permitted evaluation of the series limits of ZrV and re-evaluation of the reported limits of NbVI and MoVII. The iso-electronic diagrams, drawn according to the suggestion of Edlén (Priv. Com.), led to suspect some of the previous identifications in RbII, whereas in ZrV itself one ambiguity was left due to level crossing and meagreness of the data available in the sequence for comparison.

Reader & Epstein (1970) have since then reported some results of their study of this sequence. They have found the first five excited levels in YIV and SrIII, and re-studied RbII, which they have revised and extended, confirming Chaghtai through their re-identification of the transitions from  $4d$  and the identification of these from  $7s$ . This iso-electronic sequence can now be supposed to be known completely for the levels  $4d\ ^1P_1, ^3D_1, ^3P_1$  and  $5s(^1P_1, ^3P_1)$ . The graphs are remarkably smooth except that for  $4d\ ^1P_1$ , which shows some irregularity in the region SrIII to ZrV. This may have arisen due to the suppression of the  $4d\ ^1P_1$  level by the  $nd\ ^4P_1$  levels in YIV in the way Cowan (1968) has discussed theoretically. This anomaly might, however, also suggest the possibility of revising the identification of the transition from this level in YIV.

Chaghtai, (1970), had pointed out the possibility of interchanging his identifications of the transitions from  $5d\ ^1P_1$  and  $6s\ ^3P_1$ . Reader and Epstein (1970), in the light of their above mentioned work, suggest that these levels should of

course be interchanged to fit better in the iso-electronic comparison. This will affect the limit calculations for ZrV. Therefore, it is considered worthwhile to re-calculate these limits using the method of Edlén (1964), as described below. Profiting from this occasion, we have also traced the Rydberg series for the last three observed members of this sequence in order to show the variation of the quantum defect  $\delta$ . More precise values of  $\delta$ , than what can be obtained graphically, are tabulated below in view of their importance in atomic theory (Biberman & Norman 1967, Seaton 1970).

#### RYDBERG SERIES AND LIMIT CALCULATION

Energy levels with the same  $l$ ,  $s$  and  $j$  values in the same spectrum, but with different principal quantum number,  $n$ , constitute a Rydberg series. If  $E_n$  is the energy of a level measured from the ground level,  $T_n$  the term value measured from the ionization limit and  $E_l$  the term value of the ground level, all expressed in  $\text{cm}^{-1}(\text{K})$ , we have the following expression for the term value of a level with principal quantum number  $n$  (effective value  $n^* = n - \delta$ ) of the  $Z$ -th member of an iso-electronic sequence

$$T_n = E_l - E_n = \frac{RZ^2}{n^{*2}}. \quad \dots (1)$$

Supposing the Ritz formula

$$n - n^* \equiv \delta = a + \frac{b}{n^{*2}} \quad \dots (2)$$

to take account of the small but appreciable variation of  $\delta$  with  $n$  in the same Rydberg series, we can expect to evaluate  $E_l$  if at least three members of the Rydberg series are known.

Edlén (1964) has described a method of solving (1) and (2) with  $n_1, n_2$  and  $n_3$ . According to his method, one should begin with an approximate value of  $E_l$ , guessed or extrapolated. Then approximate values of  $T_1, T_2, T_3$  and correspondingly of  $n_1^*, n_2^*, n_3^*$  as well as of  $\delta_1, \delta_2, \delta_3$  can be calculated. The method of successive approximation leads to improvement upon the value of  $E_l$  in each step, till the results are consistent within a desired limit between consecutive steps. Edlén has calculated the correction term for each step to be

$$\Delta T = E_l - E'_l = \frac{2(T_1 - T_2)(\delta_2 - \delta_3) - (T_2 - T_3)(\delta_1 - \delta_2)}{(T_1 - T_2)\left(\frac{n_3^*}{T_3} - \frac{n_2^*}{T_2}\right) - (T_2 - T_3)\left(\frac{n_2^*}{T_2} - \frac{n_1^*}{T_1}\right)} \quad \dots (3)$$

In our case, considerations of accuracy of the term values (about  $10 \text{ cm}^{-1}$ ) coupled with the fact that we are calculating  $E_l$  with the help of  $s$  levels, which are highly penetrating and not totally free from perturbation arising from configuration interaction, do not permit us to give more than four significant figures in the limit

value. The limit of tolerance for the limit evaluations is, therefore, taken to be of the order of  $100 \text{ cm}^{-1}$ .

The evaluated values of the two limits corresponding to  $ns \ ^1P_1$  and  $ns \ ^3P_1$  are adjusted to differ exactly by the already known interval of  $4p^5 \ ^2P_{1/2-3/2}$ . This means that the first limit of the spectra under consideration that we report, is the average of the two evaluations; the second limit is obtained by simply adding to it the  $^2P_{1/2-3/2}$  interval of the next higher spectrum of the elements studied.

#### ZrV

In the KrI sequence, ZrV is situated crucially as regards the crossing of the  $4d$  and  $5s$  levels,  $4d \ ^1P_1$  is situated near  $5s \ ^1P_1$ , and  $5d \ ^1P_1$  near  $6s \ ^3P_1$ , possibly introducing perturbation in both the  $ns$  Rydberg series. The three intervals  $ns \ (^1P_1 - ^3P_1)$  for  $n = 5, 6, 7$  with values  $14755, 15143$  and  $13823 \text{ cm}^{-1}$  compare, of course, well with the  $4p^5 \ (^2P_{3/2} - ^2P_{1/2})$  interval of  $15600 \text{ cm}^{-1}$ , but, in total absence of data on YIV and SrIII, as well as in view of the situation earlier existent in RbII, a second choice of  $11832 \text{ cm}^{-1}$  for the  $6s \ ^1P_1 - ^3P_1$  interval seemed almost as evident.

Reader and Epstein's work (see earlier) has now changed this picture and, relying on their work upon the revision of  $5d$  and  $6s$  levels of RbII, a choice of  $15143 \text{ cm}^{-1}$  for the  $6s \ ^1 - ^3P_1$  interval seems more appropriate. This question will, however, be finally settled in future when the  $5d$  and  $6s$  levels of SrIII and YIV will be completely known.

We have re-evaluated the series limits of ZrV using both choices of  $6s \ ^3P_1$ , and the results are tabulated both in  $\text{cm}^{-1}$  and  $\text{eV}$  (table 1). The quantum

TABLE 1. Ionization potentials

Spectrum		1st limit		2nd limit	
		$\text{cm}^{-1}$	$\text{eV}$	$\text{cm}^{-1}$	$\text{eV}$
ZrV	a	633400	78.14	649000	80.06
	c	631571	77.91	650838	80.29
	a	636800	78.56	652400	80.48
	c	638336	78.75	650838	80.29
NbVI	a	828600	102.22	847799	104.58
	c	830313	102.43	846111	104.38
MoVII	a	1022800	126.17	1046073	129.04

a = adopted value

c = calculated value

a', c' refer to the new assignment of  $^3P_1$   
(see text).



defects calculated using either set of the limit values, have been tabulated (table 2). The limit comes out to be  $636800 \text{ cm}^{-1}$  if  $6s \ ^3P_1$  is taken to be  $473079 \text{ cm}^{-1}$  and  $633400 \text{ cm}^{-1}$  if  $6s \ ^3P_1$  is taken equal to  $476390 \text{ cm}^{-1}$ . The difference of  $3400 \text{ cm}^{-1}$  between these values is small compared to their difference from earlier reported value of  $657600 \text{ cm}^{-1}$ . Therefore, by the present limit calculation, we have in any case improved upon the earlier.

TABLE 2. Quantum defects in ZrV.

Designation	$E(\text{cm}^{-1})$	$T(\text{cm}^{-1})$	$n^*$	$\delta$	$T'(\text{cm}^{-1})$	$n^{*'}$	$\delta'$
$p^5 \ 4d \ ^3P_1$	243590	389810	2.6505	1.3596	393210	2.6410	1.3590
" " $^3D_1$	271455	361945	2.7523	1.2478	365345	2.7386	1.2614
" " $^1P_1$	339676	309324	2.9749	1.0259	312724	2.9580	1.0420
" $5s \ ^3P_1$	328938	304462	3.0000	2.0000	307862	2.9832	2.0168
" " $^1P_1$	343693	305307	2.9958	2.0042	308707	2.9790	2.0210
" $5d \ ^3P_1$	452940	180460	3.8987	1.1013	183860	3.8600	1.1400
" " $^3D_1$	462280	171120	4.0031	0.9969	174520	3.9623	1.0377
" " $^1P_1$	473079	175921	3.9465	1.0535	163721	4.0926	1.9074
" $6s \ ^3P_1$	476390	157010	4.1773	1.8227	176010	3.9465	1.0535
" " $^1P_1$	488222	160778	4.1292	1.8709	164178	4.0865	1.9135
" $7s \ ^3P_1$	533837	99563	5.2240	1.7560	102963	5.1475	1.8525
" " $^1P_1$	547660	101340	5.1960	1.8040	104740	5.0990	1.9010

$T$ ,  $n^*$ ,  $\gamma$ , refer to the old assignment of  $6s \ ^3P_1$  level and to the corresponding limit values, where as  $T'$ ,  $n^{*'}$ ,  $\delta'$  refer to the new assignment (see text).

TABLE 3. Quantum defects in NbVI and MoVII

Designation	Nb VI				Mo VII			
	$E(\text{cm}^{-1})$	$T(\text{cm}^{-1})$	$n^*$	$\delta$	$E(\text{cm}^{-1})$	$T(\text{cm}^{-1})$	$n^*$	$\delta$
$4f^5 \ 4d \ ^3P_1$	274854	553746	2.6698	1.3302	305563	717237	2.7580	1.2620
" " $^3D_1$	306941	521659	2.7495	1.2505	341765	681125	2.8086	1.1914
" " $^1P_1$	384097	463702	2.9147	1.0853	426725	619348	2.9449	1.0551
" $5s \ ^3P_1$	402038	426562	3.0417	1.9583	481292	541508	3.1460	1.8540
" " $^1P_1$	419858	427941	3.0357	1.9643	502919	543154	3.1460	1.8540
" $5d \ ^3P_1$	553869	274731	3.7899	1.2101				
" " $^3D_1$	563215	265385	3.8559	1.1441	668275	354525	3.8910	1.1090
" " $^1P_1$	580289	267510	3.8418	1.1682	688895	357178	3.8784	1.1216
" $6s \ ^3P_1$	587613	240987	4.0472	1.9529	709446	313354	4.1412	1.8588
" " $^1P_1$	601645	241654	4.0427	1.9573	731663	314410	4.1353	1.8647
" $7s \ ^3P_1$	674400	154200	5.0592	1.9408				
" " $^1P_1$	692018	155781	5.0342	1.9658				

*NbVI* and *MoVII* (table 3).

The new limit values of *Nb VI* differ slightly from the earlier ones. They give more smooth Rydberg diagrams, which we report for the first time for this

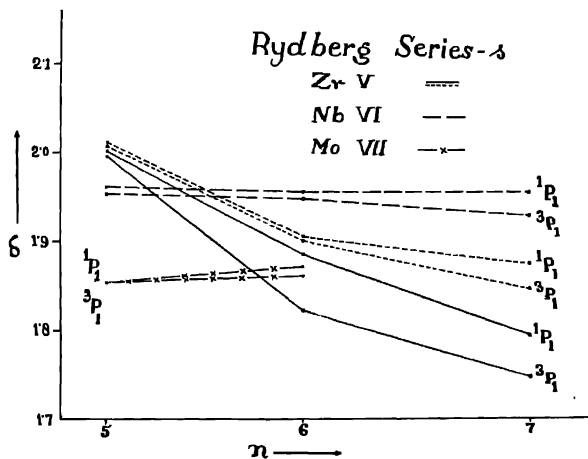


Figure 1

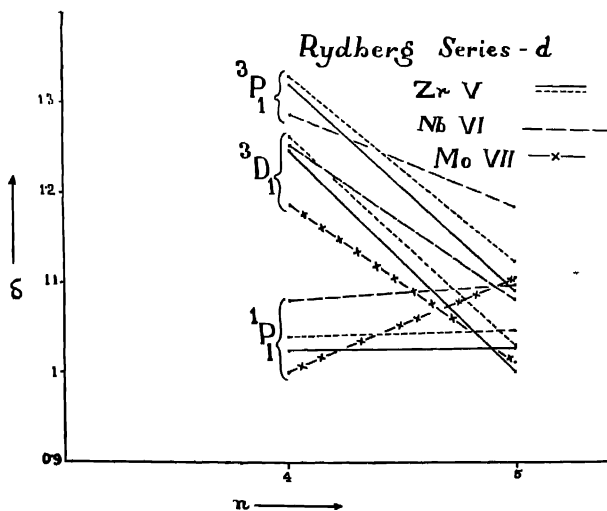


Figure 2

spectrum. In the case of MoVII, the limits have not been re-evaluated because 7s terms are not known in this spectrum. The Rydberg diagrams have been, nevertheless, drawn in order to permit comparison with the neighbouring spectra.

### DISCUSSION

Figures 1 and 2 permit us to examine together the variation of  $\delta$  with  $n$  for the various Rydberg series of the three spectra. The difference between the quantum defect of the  $^1P_1$  and  $^3P_1$  levels of  $ns$  increases rather regularly for higher  $n$  values both in NbVI and ZrV. However, in the case of ZrV, the series perturbation is made evident by the different slopes of 5s—6s and 6s—7s lines. In the case of MoVII, only the 5s, 6s levels are known, but the corresponding  $\delta$ -plots show a close resemblance with the situation in NbVI. This was expected from the absence of 4d—5s interaction in the series from NbVI onwards.

The quantum defects for the much less penetrating  $nd$  levels are naturally much smaller. The behaviour of  $^1P_1$  level is singular, as its quantum defect decreases with bigger  $n$ , contrarily to  $^3P_1$  and  $^3D_1$  levels of  $nd$  system where it increases, and to  $^1,^3P_1$  levels of  $ns$  system where it remains sensibly constant. This tendency of  $\delta$  for  $d^1P_1$  appears to accentuate with higher members of the isoelectronic sequence, where the pressure of 5s levels on 4d  $^1P_1$  disappears. The levels with bigger  $l$  are in general expected to be less penetrating, but the  $^1P_1$  lies much above the other levels in 4d configuration, whereas it lies nearer to them for higher  $n$  members of the Rydberg series. This explains the anomaly.

### ACKNOWLEDGEMENT

We heartily thank Prof. Rais Ahmed for the working facilities provided in his department to carry on this work.

### REFERENCES

- Biberman L. M. & Norman G. E. 1967 *Soviet Uspekhi* **10**, 52.  
 Chaghtai M. S. Z. 1969 *J. Opt. Soc. Am.* **59**, 969.  
     1970 *Physica Scripta*, Stockholm **1**, 31.  
 Charles G. W. 1950 *Phys. Rev.* **77**, 120.  
 Cowan R. D. 1968 *J. Opt. Soc. Am.* **58**, 924.  
 Edlén B. 1964 *Atomic Spectra, Handbuch der Physik* XXVII, 64.  
 Laporte O., Miller G. R. & Sawyer R. A. 1931 *Phys. Rev.* **38**, 843.  
 Moore C. E. 1952 *Atomic Energy Levels*, NBS Circular Vol II, 467.  
     1969 *Bibl. Analysis Opt. Atomic Spectra*, NBS Circular Vol II, 306-2.  
 Seaton M. J. 1970 *Quantum Defect Theory, Comments on Atomic and Molar Physics*,  
     Part D, Vol II, No. 2.

## Electron collision frequency in Martian ionosphere

By D. C. AGARWAL

*J. K. Institute of Applied Physics and Technology  
Allahabad University, Allahabad*

(Received 23 May 1969, revised 5 February 1970)

The results for  $F_2$  region (Bradbury Layer) collision frequency of the Martian atmosphere are presented. It is observed that for this layer, the collision frequency of electrons with neutral constituents are negligible in comparison to that with positive ions. The  $F_2$  region collision frequency is found to be  $7.6 \times 10^6 \text{ sec}^{-1}$ .

### INTRODUCTION

The collision frequency of electrons with neutral and ionized gases of earth's atmosphere is well established. For the Martian atmosphere, it has neither been experimentally nor theoretically deduced. It is the purpose of the present paper to calculate these collision frequency in the Martian ionosphere.

### THEORETICAL CONSIDERATIONS

The collision frequency of electrons with neutral gases depends on (a) the distribution of electron velocities, (b) the variation of electron collision cross-section for each gas with electron velocity and (c) the number densities of the neutral gases present. Thus, collision frequency for mono-energetic electrons,  $\nu_m$  is proportional to the electron-collision cross-section  $\sigma$ , the electron velocity  $v$ , and the density of each gas  $\rho$ , i.e.,

$$\nu_m = \sigma v \rho \quad \dots (1)$$

where,  $\sigma$  is a complex function of  $v$ .

This expression can be rewritten in a simpler form according to Gerson (1961) :

$$\nu_m = 2\sigma N \left[ \frac{(kT)}{3m} \right]^{\frac{1}{2}} \text{ sec}^{-1} \quad \dots (2)$$

where,  $k$  is the Boltzmann's constant,  $T$  is the absolute temperature of the region under consideration,  $m$  is the mass of the electron and  $N$  is the number density of the gas with which the electrons collide.

The argument given above is strictly true only if the electron temperature and the gas temperature are the same. Otherwise, the collision frequency at each height should be increased by the ratio  $T_e/T_g$ , where  $T_e$  is the electron temperature and  $T_g$  is the gas temperature.

According to Nicolet (1953), the collision frequency of electrons with positive ions is given by

$$\nu_{ie} = \left[ 34 + 8.36 \log \frac{T_e^{3/2}}{N_e^{1/2}} \right] N_i \cdot T^{-3/2} \quad \dots (3)$$

where  $T$  is the absolute temperature of the region under consideration,  $N_e$  is the electron density and  $N_i$  is the positive ion density. The expression (3) is valid only if the electron temperature  $T_e$  is same as the ion temperature  $T_i$ . If  $T_e \neq T_i$ , then one should adopt the following expression for  $\nu_{ie}$  (Thrane & Piggott, 1966)

$$\nu_{ie} = [a + b \ln T_e(T_i/N_i)^{1/2}] N_i T_e^{-3/2} \quad \dots (4)$$

where,  $a$  and  $b$  are constants.

Total collision frequency of the  $F_2$  region is the sum of  $\nu_m$  and  $\nu_{ie}$  (Ramana & Rao, 1961) as the collision frequency of electrons with the negative ions is negligible, i.e.,

$$\nu = \nu_m + \nu_{ie} \quad \dots (5)$$

### 3. RESULTS AND DISCUSSIONS

The  $F_2$  region of the Martian ionosphere is at about 128 km high from its surface (Fjeldbo & Eshleman, 1968). For this region, the calculated values of the collision frequency of electrons with neutral and ionized gases are tabulated in table 1. In this calculation, it is assumed that  $T_e = T_i = T_g$  and neutral particle concentrations in  $F_2$  region are taken from Fjeldbo & Eshleman's paper (1968). The positive ion distribution has been taken from Agarwal's paper (1970). From table 1, it is apparent that  $\nu_O$ , the collision frequency of

TABLE 1. Collision frequency of electrons with neutrals and Ions

Neutral gas	Collision frequency of electrons with neutral gas at 128 km	Ionized gas	Collision frequency of electrons with +ve ions at 128 km
CO <sub>2</sub>	$8.2 \times 10^{-2} \text{sec}^{-1}$	CO <sub>2</sub> <sup>+</sup>	$3 \times 10^9 \text{sec}^{-1}$
CO	$8.6 \times 10^{-1} \text{sec}^{-1}$	CO <sup>+</sup>	$2.4 \times 10^8 \text{sec}^{-1}$
O <sub>2</sub>	$2.5 \times 10^{-7} \text{sec}^{-1}$	O <sub>2</sub> <sup>+</sup>	$1.2 \times 10^8 \text{sec}^{-1}$
O	$8.60 \text{sec}^{-1}$	O <sup>+</sup>	$1.0 \times 10^8 \text{sec}^{-1}$

electrons with oxygen atoms is larger than  $\nu_{\text{CO}_2}$ ,  $\nu_{\text{CO}}$  and  $\nu_{\text{O}_2}$ . However, in comparison to the collision frequency of electrons with positive ions  $\nu_O$  is negligible and hence  $\nu = \nu_i$ . Among  $\nu_{\text{CO}_2^+}$ ,  $\nu_{\text{CO}^+}$ ,  $\nu_{\text{O}_2^+}$  and  $\nu_{\text{O}^+}$ , the  $\nu_{\text{CO}_2^+}$  is the largest because of their largest number density in that region.

From table 1,

$$\nu = \nu_{\text{CO}_2} + \nu_{\text{CO}} + \nu_{\text{O}_2} + \nu_{\text{O}} = 7.6 \times 10^8 \text{ sec}^{-1}.$$

As no experimental values of  $\nu$  are available, the calculated value could not be compared with them. It is proposed that  $\nu$  should be determined also by experiments as it would be useful in framing a better theoretical model.

#### REFERENCES

- Agarwal D. C. 1970 *Ind. J Pure and Appl Phys* (In course of publication.)  
 Fjeldbo G. & Eshleman, V R 1968 *Planet. Space. Sci.* **16**, 1035.  
 Gorson N. C. 1961 *J Atmos Terr Phys.* **23**, 1.  
 Nicolet M. 1953 *J. Atmos. Terr. Phys.* **3**, 200  
 Ramana K. V. V. & Rao R. 1961 *Proc IGY Symp. CSIR New Delhi* 149.  
 Thrane E. V. & Piggott W. R. 1966 *J. Atmos. Terr. Phys.* **28**, 721.

## Electronic spectra of 2,4-xyleneol in different states

BY D. MAJIT

*Department of Optics,*

*Indian Association for the Cultivation of Science, Calcutta-32*

*(Received 26 June 1970—Revised 11 August 1970)*

The ultraviolet absorption spectrum of 2,4-xyleneol in vapour state has been recorded and analysed. The spectrum is found to consist of weak absorption bands with the 0,0 band at  $35312\text{ cm}^{-1}$ . The vibrational analysis indicates that the band system of the molecule is due to an allowed transition and the weakness of absorption has been attributed to small migration moment. The spectra of the substance in the liquid and solid states and in a solution of cyclohexane have also been recorded and the observed results discussed.

### INTRODUCTION

The dependence of intensity of bands in the near ultraviolet absorption spectra of polysubstituted benzene compounds on the resultant migration moment was discussed by Sklar (1942). Sponer (1947) reported analysis of absorption spectra of several trichloro- and trimethyl benzenes in vapour state and observed that the intensity of absorption is large for molecules like 1,2,4- $\text{C}_6\text{H}_3\text{X}_3$  molecules, while for molecules like 1,2,3- $\text{C}_6\text{H}_3\text{X}_3$  the intensity is very small and the 0,0 band is absent though the transition is allowed by symmetry. The results are in accord with the idea of Sklar that for 1,2,4- $\text{C}_6\text{H}_3\text{X}_3$  molecule the migration moment vectors add to give a large resultant moment, whereas, for molecules like 1,2,3- $\text{C}_6\text{H}_3\text{X}_3$  this resultant is zero. Sklar's idea was later extended by Platt (1951) to different substituents in benzene and other large ring molecules.

Analyses of absorption spectra of only a few trisubstituted benzene compounds with different substituents (with different X) have been reported in literature. A programme was undertaken to record and analyse the spectra of a few such compounds in vapour state. The results obtained with 2,4-xyleneol and its spectra in liquid and solid states and in solution were recorded, and the observed results are reported in this paper.

### EXPERIMENTAL

The chemically pure sample of 2,4-xyleneol was obtained from B.D.H. The sample was carefully fractionated and proper fraction was distilled under reduced pressure before use.

To study the absorption spectra of 2,4-xyleneol in the vapour phase at different temperatures, absorption cells usually long tubes of different lengths provided

with quartz windows were used. The liquid was kept in a bulb connected to the absorption cell by a side tube. The bulb was placed inside a box heater and the absorption tube was placed inside a cylindrical heater, the temperature of which was kept about  $10^{\circ}\text{C}$  higher than that of the box heater. The absorption tubes together with the attached bulbs were evacuated and sealed off. The best spectrogram was obtained with a 100 cm vapour tube maintained at  $37^{\circ}\text{C}$ . Increase in temperature of the tube did not result in any improvement of intensity of the bands. To identify the 0,0 band and eliminate bands due to  $v-v'$  transition, a 30 cm vapour tube was taken and the temperature of the bulb was varied to obtain different pressures of the absorbing vapour.

The experimental arrangements for studying photographically the absorption spectra of 2,4-xylolol in the liquid state at room temperature, in the solid state at  $-180^{\circ}\text{C}$  and in solution in specpure cyclohexane at  $32^{\circ}\text{C}$  were the same as those used by earlier workers, *viz.* Banerjee (1956), Sirkar & Misra (1959).

The absorption spectra were photographed on Kodak Spectrum Analysis No. 1 film with an Adam Hilger all metal E1 spectrograph (E 478) having dispersion of about  $2.5\text{\AA}/\text{mm}$  in the  $2600\text{\AA}$  region. Iron arc spectrum was also photographed with a Hartmann diaphragm on each film for comparison.

Microphotometric records of the spectra were taken with a Kipp & Zöhen type self-recording Moll microphotometer. The method of determination of the positions of the absorption maxima was the same as that given by Banerjee (1956). The accuracy in the measurements of positions of the absorption peaks was  $\pm 10\text{ cm}^{-1}$  for narrow bands and  $\pm 20\text{ cm}^{-1}$  for broader bands while the uncertainty in the case of broad diffuse bands was much larger.

The Raman spectrum and the state of polarization of Raman lines were photographed in a Fuess glass spectrograph, and the infrared absorption bands of the sample were recorded in the usual way with a Perkin Elmer Model 21 spectrophotometer fitted with rock salt optics (Chattopadhyay & Mukerjee 1967).

## RESULTS

The microphotometric records of the absorption spectra of 2,4-xylolol in the vapour, liquid and solid states and in solution in cyclohexane are reproduced in figures 1 and 2. The positions of the absorption maxima, their relative intensities and probable assignments are given in tables 1, 2 and 3.

The vibrational spectra of 2,4-xylolol were only partially reported by earlier authors. The infrared spectra and the Raman spectra with state of polarization of the lines of this compound were also recorded. These data are included in table 4.



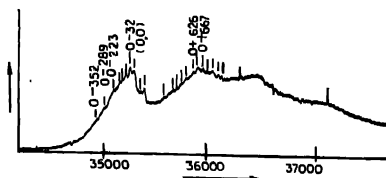


FIGURE 1. Microphotometric records of the ultraviolet absorption spectra of 2, 4-xylénol in the vapour state at 37°C.

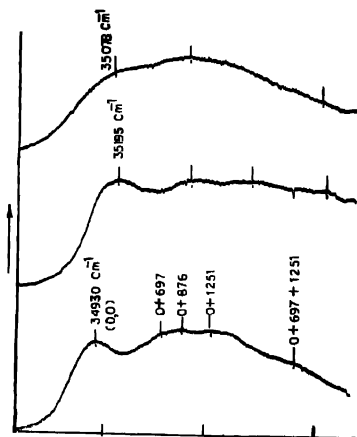


FIGURE 2. Microphotometric records of the ultraviolet absorption spectra of 2, 4-xylénol in different states and in solution.

- a) Liquid state at 26°C
- b) Solid state at -180°C
- c)  $8.5 \times 10^{-4}$ M solution of 2, 4-xylénol in cyclohexane at 32°C

## DISCUSSION

### *The spectrum in the vapour state*

The molecule of 2, 4-xylénol may at most be assumed to belong to  $C_2$  point group, and the electronic transition corresponding to  $A_{1g} - B_{2u}$  transition in benzene would be an  $A' - A'$  transition which is allowed by symmetry of the molecule. The absorption spectrum due to the vapour consists of four groups of bands. Each group consists of several narrow bands degraded towards the red. The

band at  $35312\text{ cm}^{-1}$  in the first group is found to persist with relatively undiminished intensity at lower pressures of the absorbing vapour and has been taken as the 0, 0 band of the system. The bands on the larger wave length side could then be assigned to  $v-o$  and  $v-v$  transitions as indicated in table I.

TABLE I. Ultraviolet absorption spectrum of 2, 4-xyleneol in the vapour state at  $37^\circ\text{C}$

Wave No. in $\text{cm}^{-1}$ of absorption band with intensity	Difference from the 0, 0 band	Assignment
34960 vw	— 352	0—352
35023 w	— 289	0—289
35089 m	— 223	0—223
35310 m	— 158	0—158
35180 m	— 132	0—132
35235 ms	— 77	0— 77 0—289+212
35280 s	— 32	0— 32 0—132+100
35312 s	0	0, 0
35382 vw	70	0+ 70
35412 ms	100	0+100
35437 vw	125	0+125
35524 vw	212	0+212
35582 w	270	0+270
35633 m	321	0+321
35780 w	468	0+468
35832 m	520	0+520
35903 m	591	0+626—32
35938 s	626	0+626
35979 s	667	0+667
36028 w	716	0+626+100
36080 w	768	0+667+100
36134 m	812	0+812
36186 m	874	0+874
36359 ms	1049	0+2×520
36538 m	1226	0+1226
36572 m	1260	0+2×626
36602 w	1290	0+626+676
36804 vw	1492	0+626+874
37202 vvw	1870	0+3×626

TABLE 2. Ultraviolet absorption spectra of 2,4-xyleneol in the liquid and solid states

Liquid at 26°C		Solid at -180°C	
Wave no. in cm <sup>-1</sup> with intensity	Separation between the successive bands in cm <sup>-1</sup>	Wave no. in cm <sup>-1</sup> with intensity	Separation between the successive bands in cm <sup>-1</sup>
35078 (ms)		35195 (s)	
	779		746
35857 (s)		35941 (ms)	
	1160		578
37026 (vs)		36519 (m)	
			728
		37247 (m)	

TABLE 3. Ultraviolet absorption spectrum of  $8.5 \times 10^{-4}$ M solution of 2,4-xyleneol in cyclohexane at 32°C

Wave no. in cm <sup>-1</sup> with intensity	Assignment
34930 (s)	0,0
35627 (s)	0+697
35806 (ms)	0+876
36181 (m)	0+1251
36882 (m)	0+697+1251

It can be seen that the ground state vibrational frequencies 158, 223, 289 and 352 cm<sup>-1</sup> observed in the present work agree reasonably with the Raman shifts 153, 212, 281 and 345 cm<sup>-1</sup>, respectively. The strong band at 35182 cm<sup>-1</sup> on the long wave length side of the 0, 0 band, which could not be assigned to a  $\nu-\nu$  transition, most probably represents a  $\nu-0$  transition involving a fundamental vibrational frequency 132 cm<sup>-1</sup> in the lower state though such a frequency could not be detected in the Raman spectrum. On the short wave length side of the 0, 0 band there is a moderately strong band at 35412 cm<sup>-1</sup>, which may represent a fundamental excited state vibrational frequency 100 cm<sup>-1</sup>, corresponding to the ground state vibrational frequency 132 cm<sup>-1</sup> mentioned above. The correctness of the assignments is probably supported by the fact that there is also a band at 35280 cm<sup>-1</sup> on the long wave length side of the 0, 0 band and separated by 32 cm<sup>-1</sup> from it which may be readily assigned to a  $\nu-\nu$  transition involving the two vibrational frequencies 132 cm<sup>-1</sup> and 100 cm<sup>-1</sup> in the upper and the lower states, respectively. The excited state frequency 70 cm<sup>-1</sup> may represent a suitable torsional mode in the molecule.

TABLE 4. Raman and infrared frequencies of 2, 4-Xylenol at 28°C

Raman shift in $\text{cm}^{-1}$ (Magat, 1936)	Raman shift in $\text{cm}^{-1}$ (present work)	Infrared frequency in $\text{cm}^{-1}$ with intensity (present work)
	153 (1) D	
212 (5)	210 (4) D	
278 (4)	281 (3) D	
348 (5)	345 (5) D	
446 (4) D	448 (5) D	
490 (5)	489 (6) P	
572 (6)	571 (6) P	
717 (8)	721 (10) P	710 (m)
770 (7)	770 (8) P	760 (s)
	810 (0)	804 (vs)
	874 (0)	868 (m)
930 (5)	932 (6) P	924 (m)
1032 (0)	1035 (0)	1005 (m)
		1030 (m)
	1122 (1)	1112 (vs)
	1150 (2) P	1145 (s)
	1190 (1)	1194 (vsb)
1265 (6)	1265 (8) P	1260 (vs)
	1324 (0)	1330 (sb)
1379 (6)	1383 (7) P	1376 (s)
	1417 (1) D	1410 (s)
1449 (1)	1459 (1) D	1452 (s)
	1510 (0)	1505 (vs)
1610 (5)	1600 (2)	1605 (m)
	1614 (8b) D	
2732 (1)	2740 (2) D	
2862 (5)	2875 (4) P	
2917 (10)	2920 (10) P	2925 (s)
3034 (5)	3055 (6) P	3035 (m)
3203 (2)		

As can be seen from tables 1 and 4 that the excited state frequencies observed in the present investigation may be correlated with the observed Raman and infrared frequencies with a fair degree of agreement. The prominent excited state frequencies 520, 626, 667 and  $874\text{ cm}^{-1}$  occur also in combinations. They may be correlated with the ground state frequencies 571, 721, 770 and  $932\text{ cm}^{-1}$ , respectively, all of which arise from symmetric modes belonging to  $a'$ -species, as is

indicated by the fact that the corresponding Raman lines are polarised. The general vibrational structure of the absorption spectrum of the molecule thus conforms to an electronic transition allowed by the symmetry of the molecule.

*The spectra in liquid and solid states and in solution*

In the liquid state 2, 4-xyleneol yields very broad bands without any vibrational structure and only the wave numbers of centres of the bands could be measured very approximately. It may be recalled that in the liquid state, molecules of this compound are associated with each other through intermolecular hydrogen bonding (Banerjee & Mukherjee 1966). This may explain the very large width of bands in the spectrum of the liquid. When the liquid is frozen and cooled to  $-180^{\circ}\text{C}$ , the bands remain broad and structureless.

The bands in the spectrum due to solution of 2, 4-xyleneol in cyclohexane are a little sharper. The bands are somewhat better resolved from each other and the excited state frequencies 697, 876 and  $1251\text{ cm}^{-1}$  (corresponding values observed in vapour spectrum are 667, 874 and  $1226\text{ cm}^{-1}$ , respectively) could be identified.

#### ACKNOWLEDGEMENT

The author expresses his grateful thanks to Dr. S. B. Banerjee for continued guidance throughout the progress of the work, and to Prof. G. S. Kastha, D.Sc., for kind interest. He is also indebted to Sri S. C. Bag for help in the experimental work and to Sri S. Chattopadhyay in recording Raman and infrared spectra.

#### REFERENCES

- Banerjee S. B. 1956 *Indian J. Phys.* **30**, 106.  
Banerjee S. B. & Mukherjee D. K. 1967 *Indian J. Phys.* **41**, 230.  
Chattopadhyay S. & Mukherjee D. K. 1966 *Indian J. Phys.* **40**, 409.  
Mgat M. 1936 *Annual Table of Constants and Numerical Data*  
Platt J. R. 1951 *J. Chem. Phys.* **19**, 263.  
Sirkar S. C. & Misra T. N. 1959 *Indian J. Phys.* **33**, 45.  
Sklar A. L. 1942 *Rev. Mod. Phys.* **14**, 224.  
Spomer H. 1947 *Chem. Rev.* **41**, 281.

# On the energy loss in Čerenkov radiation

By N. D. SEN GUPTA

*Tata Institute of Fundamental Research, Bombay-5*

(Received 30 June 1970)

It is shown that the electromagnetic field energy associated with a charge-particle moving with uniform velocity since infinite remote past in an infinitely extended homogeneous medium is constant. The usual expression for the rate of loss of energy of a particle calculated from the total Poynting flux is shown to be negative of the volume integral of  $c\mathbf{E} \cdot \mathbf{j}$

## INTRODUCTION

In the problem of Čerenkov radiation emitted by a charge-particle moving in a homogeneous medium with uniform velocity greater than the phase velocity of electromagnetic waves in the medium, it is usually assumed that the particle is moving since infinite remote past. In order to obtain the energy emitted by the particle per unit time one calculates the total Poynting flux across a surface enclosing the particle. The total flux is taken to be the rate of loss of energy per unit time. As the particle is moving from infinite remote past, if we take an overall picture of the electromagnetic field associated with the particle, we will find that the field quantities are moving in the forward direction with the same uniform velocity as that of the particle. Since the medium is homogeneous and isotropic the total field energy does not change with time, so long as hysteresis losses are neglected; of course, the total field energy, as in case of a point particle, may be infinite. As a matter of fact, the total flux across the bounded region is nothing but the volume integral of  $-c\mathbf{E} \cdot \mathbf{j}$ . The Poynting theorem states

$$\frac{\partial u}{\partial t} + \nabla \cdot c\mathbf{E} \times \mathbf{H} = -c\mathbf{E} \cdot \mathbf{j} \quad \dots (1)$$

where  $u$  is the energy density

$$u = \frac{\epsilon}{2} \mathbf{E} \cdot \mathbf{E} + \frac{\mu}{2} \mathbf{H} \cdot \mathbf{H} \quad \dots (2)$$

If the total energy,

$$U = \int u d\mathbf{r} \quad \dots (3)$$

(the integral being over the entire space, is independent of time), one obtains on integrating equation (1)

$$\int c\mathbf{E} \times \mathbf{H} \cdot d\mathbf{s} = - \int c\mathbf{E} \cdot \mathbf{j} d\mathbf{r}, \quad \dots (4)$$

In the following section, it is explicitly shown that the usual expression for the rate of energy loss of the particle in the Čerenkov radiation, which is calculated from the total flux of the Poynting vector, is nothing but the right hand side of the above equation. In section 3, it is shown that with the usual expressions for  $\mathbf{E}$  and  $\mathbf{H}$  due to a particle emitting Čerenkov radiation the total field energy  $U$  (equations 2 and 3) is independent of time, i.e.,  $\partial U/\partial t = 0$ . It needs to be emphasized that this is true so long as the particle is assumed to move with uniform velocity from infinite remote past in an infinitely extended homogeneous medium. In the last section, we have tried to point out the difference between the energy flowing across a given section and the energy loss of the particle.

## 2. THE EXPRESSION FOR THE VOLUME INTEGRAL OF $c\mathbf{E} \cdot \mathbf{j}$ .

Let the charge-current due to a particle moving with uniform velocity  $\mathbf{v}$  in a homogeneous isotropic medium with dielectric constant  $\epsilon$  and permeability  $\mu$ , be given by

$$q = q_0 \delta(\mathbf{r} - \mathbf{v}t), \quad \mathbf{j} = \frac{\mathbf{v}}{c} q. \quad \dots (5)$$

The expressions for  $\mathbf{E}$  and  $\mathbf{H}$  due to the particle moving since infinite past are

$$\mathbf{E} = \gamma^2 \nabla \Phi + \frac{1}{u^2} \mathbf{v} \times \mathbf{v} \times \Delta \Phi \quad \dots (6)$$

$$\mathbf{H} = \frac{\epsilon}{c} \mathbf{v} \times \mathbf{E}, \quad \dots (7)$$

$$\text{where} \quad \gamma^2 = \frac{v^2}{u^2} - 1, \quad u^2 = \frac{c^2}{\epsilon\mu}, \quad v = |\mathbf{v}| \quad \dots (8)$$

and

$$\begin{aligned} \Phi = & \frac{q_0}{(2\pi)^3} \int \frac{1}{\epsilon} e^{i\mathbf{k} \cdot (\mathbf{r} - \mathbf{v}t)} \cdot \left\{ \frac{1}{\mathbf{k} \cdot \mathbf{k} - \left( \frac{\mathbf{k} \cdot \mathbf{v}}{u} \right)^2} \right. \\ & \left. + i\pi \frac{\mathbf{k} \cdot \mathbf{v}}{|\mathbf{k} \cdot \mathbf{v}|} \delta \left( \mathbf{k} \cdot \mathbf{k} - \left( \frac{\mathbf{k} \cdot \mathbf{v}}{u} \right)^2 \right) \right\} d\mathbf{k} \quad \dots (9) \end{aligned}$$

(Iwanenko & Sokolov 1953; Sen Gupta 1965, 1968). With these expressions let us now calculate the volume integral of  $c\mathbf{E} \cdot \mathbf{j}$

$$\begin{aligned} c \int \mathbf{E} \cdot \mathbf{j} d\mathbf{r} = & -\frac{iq_0^2}{8\pi^3} \int \frac{\gamma^2}{\epsilon} \mathbf{k} \cdot \mathbf{v} e^{i\mathbf{k} \cdot (\mathbf{r} - \mathbf{v}t)} \cdot \delta(\mathbf{r} - \mathbf{v}t) \\ & \left\{ \frac{1}{\mathbf{k} \cdot \mathbf{k} - \left( \frac{\mathbf{k} \cdot \mathbf{v}}{u} \right)^2} + i\pi \frac{\mathbf{k} \cdot \mathbf{v}}{|\mathbf{k} \cdot \mathbf{v}|} \delta \left( \mathbf{k} \cdot \mathbf{k} - \left( \frac{\mathbf{k} \cdot \mathbf{v}}{u} \right)^2 \right) \right\} d\mathbf{k} d\mathbf{r}. \quad \dots (10) \end{aligned}$$

The first term in the bracket does not contribute (considered as an improper integral), as the presence of the factor  $\mathbf{k} \cdot \mathbf{v}$  makes it an odd function of  $(\mathbf{k} \cdot \mathbf{v})/v$ . The second term may be written as

$$\frac{q_0^2}{8\pi^2} \int \frac{\gamma^2}{\epsilon} |\mathbf{k} \cdot \mathbf{v}| \delta \left( k_1^2 + k_2^2 - \gamma^2 \left( \frac{\mathbf{k} \cdot \mathbf{v}}{v} \right)^2 \right) dk_1 dk_2 d \left( \frac{\mathbf{k} \cdot \mathbf{v}}{v} \right). \quad \dots (11)$$

i)  $\gamma^2 > 0$ , from equation (8),  $v > u$  i.e., the case of Čerenkov radiation, the expression (11) becomes

$$\frac{q_0^2}{8\pi} \int \frac{\gamma^2}{\epsilon} |\mathbf{k} \cdot \mathbf{v}| \cdot d \left( \frac{\mathbf{k} \cdot \mathbf{v}}{v} \right). \quad \dots (12)$$

On writing  $\omega$  for  $\mathbf{k} \cdot \mathbf{v}$  one obtains finally

$$-c \int \mathbf{E} \cdot \mathbf{j} d\mathbf{r} = \frac{q_0^2 v}{4\pi c^2} \int \mu \left( 1 - \frac{u^2}{v^2} \right) \omega d\omega \quad \dots (13)$$

On taking account of the dispersion of the medium the upper limit of the above integral is  $\omega_0$  such that  $u(\omega) > v$  as  $\omega > \omega_0$ . It is exactly the same as the expression which is usually quoted for the rate of loss of energy by the particle calculated from the total Poynting flux (Iwanenko & Sokolov 1953). Hence, we obtain equation (4), which in turn implies that  $\partial U / \partial t = 0$  from equations (1) and (3). In case of non-dispersive medium the integral on the right hand side of (13) is unbounded which is also expected as  $\mathbf{E}$  on the left hand is the self-field and diverges strongly at the position of the charge.

ii)  $\gamma^2 < 0$  i.e.,  $v < u$ , the integral (11) has no contribution. Hence, the volume integral of  $\mathbf{E} \cdot \mathbf{j}$  is zero. It is also well known that the total Poynting flux across a surface enclosing the charge is zero. Thus, we obtain again  $\partial U / \partial t = 0$ .

### 3. THE TOTAL FIELD ENERGY

The field quantities may be better expressed in spherical polar coordinates, with the instantaneous position of the particle as pole and the line of flight of the particle as axis. Thus,

$$\mathbf{E} = \frac{q_0 u^2 \gamma^2}{2\pi \epsilon v^3} \frac{R}{R^3 \left( \cos^2 \theta - \frac{u^2}{v^2} \gamma^2 \right)^{3/2}} \quad \dots (14)$$

i)  $\gamma^2 > 0$ . The expression for the field energy (equations (2) and (3)) integrated over the region of Čerenkov cone is

$$U = \lim_{\substack{\theta' \rightarrow \theta_0 \\ \eta \rightarrow 0}} \frac{q_0^2 u^4 \gamma^4}{4\pi \epsilon v^6} \int_0^{\theta'} d\theta \int_{\eta}^{\infty} \frac{dR}{R^3} \frac{u^2 + v^2 \sin^2 \theta}{\left( \cos^2 \theta - \frac{u^2}{v^2} \gamma^2 \right)^3} \quad \dots (15)$$



where  $\cos \theta_0 = u\gamma/v$ . The upper limit of  $R$  integration does not contribute, the lower limit is divergent but independent of time. Again, the upper limit of  $\theta$  integration is divergent but independent of time.

(ii)  $\gamma^2 < 0$ : The expression (15) is similar, with only change of upper limit of  $\theta$  integration which is now  $\pi$ . Thus, in both the cases

$$\frac{\partial U}{\partial t} = 0. \quad (16)$$

Hence, the total field energy is constant, though, it is unbounded. This divergence is due to the self-energy which depends also on the particle velocity and the electromagnetic properties of the material medium. The fact that the total energy is independent of time is also expected from simple ground as has been noted in the introduction. As the particle is moving with uniform velocity from infinite past, the field quantities are only translated with the same uniform velocity with the evolution of time. Since the total energy, which is obtained by integrating over the whole space, is invariant with respect to this translation, it remains the same.

In the conclusion, we wish to point out that the total Poynting flux gives only the flow across the surface. It is not proper to take this as the rate of loss of energy by the particle due to the radiation. Because the particle can only lose energy to the field and we have shown the total field energy due to a particle moving with uniform velocity ( $v < u$  or  $v > u$ ) since infinite past, is constant. On the other hand, in the usual formulation of the Čerenkov radiation, the particle is assumed to be moving with uniform velocity from infinite past and it is said to be losing energy. Those two statements are in general contradictory. They are agreeable only when the rate of loss of the energy of the particle is zero as we have shown above. It seems a reformulation of the problem of energy loss of the particle is necessary.

#### REFERENCE

- Iwanenko D. & Sokolow A 1949 *Klassischeckaya Teoria Polya*, Moscow and Leningrad; German translation, *Klassische Feldtheorie*—Akademise Verlag, Berlin 1953.  
 Sen Gupta N. D. 1965 *Nuovo Cim.* **37**, 905.  
 Sen Gupta N. D. 1968 *Proc. Phys. Soc. A Ser. 2*, **1**, 340.

## Measurement of diurnal cosmic ray intensity variation at Calcutta with a meson telescope

BY (Mrs) SARAMMA ALEXANDER and S. D. CHATTERJEE\*

*Department of Physics, Jadavpur University, Calcutta-32*

*(Received 22 July 1970)*

The diurnal and semi-diurnal variations of meson intensity have been measured at Calcutta (Geographical latitude  $22^{\circ}32'N$  and longitude  $88^{\circ}20'E$  at sea-level) with a meson telescope.

The diurnal variation has an amplitude of 0.13% with the time-maximum at 10.52 hrs I.S.T which corresponds to 11 hrs. 13 min. local time. Similarly, the semidiurnal variation has been found to have an amplitude of 0.05% corresponding to a time maximum of 16 hrs 10 min local time.

The results have been compared with those obtained at various other places by other workers in the field.

### INTRODUCTION

It is generally recognised that one of the fruitful methods of studying the influence of the solar field on cosmic rays reaching the surface of the earth is by analysing their diurnal and semi-diurnal variations. Since the axis of rotation of the earth and its magnetic axis are inclined to each other, it is reasonable to expect that the anisotropy of cosmic rays incident on the earth will have different phase and amplitude at different stations on the same latitude. The collection of data on various parameters, including the time variations at different localities has been an accepted program in the study of cosmic rays.

The results of the study of data collected for Calcutta (Geographical latitude  $22^{\circ}32'N$  and longitude  $88^{\circ}20'E$ ) during a period of nearly one and a half years during 1967-69, when the solar activity was at its peak for the present cycle, are given here. Another notable feature of scientific interest of Calcutta is its closeness to the Bay of Bengal, where geomagnetic anomaly is present, the significance of which in relation to a number of terrestrial phenomena has not yet been fully explained. For collecting the data under study, a wide angle meson telescope of cubical geometry approximately following IGY specifications has been used. The hourly readings are corrected for atmospheric pressure variations and the corrected readings are subjected to harmonic analysis for the first five Fourier coefficients. Using the first coefficient, the amplitudes and time of maximum for the diurnal and semidiurnal variations are calculated and the results are represented on the harmonic dial.

---

\*Present address: Indian Association for the Cultivation of Science, Jadavpur, Calcutta-32

**EXPERIMENTAL**

A wide angle triple coincidence meson telescope was set up for the present work. It has a cubical geometry of 2 ft  $\times$  2 ft  $\times$  2 ft subtending an angle of 45° with three trays having 15 Geiger counters in each. Between the bottom and middle trays there is a 10 cm thick lead filter. The Geiger counters have been locally fabricated from brass tubes of 2 ft length and 1½ inches diameter with a wall thickness of 1/16 inch and filled with a mixture of argon and ethyl acetate to a pressure of nearly 9 cm of Hg so as to have a working voltage of about 1000 volts. The ends of the brass tubes are closed by means of brass plugs provided with central holes through which pass two narrow glass tubes to which the central filament is fused. Incidentally, the glass tubes also serve the purpose of insulating the central filament from the outer metallic tubes. The different components are assembled together and sealed by means of araldite resin.

Each counter is connected to a quenching unit consisting of 12AT7 uni-vibrators. Fifteen such quenching units are accommodated in one tray and coupled to a cathode-follower tube EF91. The pulses from the three trays are fed to a Rossi coincidence circuit, the output of which is fed to a scaler having a scaling factor of 128. The final scaled output operates a mechanical recorder through a driver unit.

The power supply to the various electronic circuits (except the Geiger counters) are derived from electronically stabilized power packs. The high tension to the counters is obtained directly from a neon stabilized H.T. unit.

The hourly readings of the mechanical recorder along with corresponding times and dates are photographed simultaneously by means of an automatic camera operated by micro-switches and controlled by an external wall clock. The hourly ground pressure is recorded by a micro-barograph.

A negative voltage of nearly 1000 volts, depending upon the requirement of each counter, is fed to the brass tube of the Geiger counter which acts as the cathode. The central filament is connected to the plate of the quenching unit which is kept at a potential of nearly +300 volts when the counter is not working. Different counters having slightly different working voltages, are supplied from a voltage distributor from which any suitable voltage of 1000  $\pm$  400V could be tapped.

The counter usually possesses a plateau of nearly 280 volts and the average life of a counter has been found to be nearly 10 months.

**HARMONIC ANALYSIS OF RESULTS**

Observations have been made for a period of nearly one and a half years starting from December 1967 to April 1969. Since the period under review was characterized by solar activities and geomagnetic disturbances, the readings of

several days have had to be discarded on account of their large fluctuations. Readings for nearly 180 days have accordingly been chosen for the present analysis, which are corrected for the atmospheric pressure effect. A pressure coefficient of  $-0.17\%$  per m.b. has been used for the usual correction. A sample of correlation analysis from a few months' data yielded nearly identical value for the pressure coefficient. The pressure corrected hourly values are next subjected to harmonic analysis for the first five Fourier coefficients from which the amplitude and time of maximum of the diurnal variation and semidiurnal variation are calculated using the following equation :

$$f(M) = \alpha_0 + (\alpha_1 \cos \omega t + \beta_1 \sin \omega t) + (\alpha_2 \cos 2\omega t + \beta_2 \sin 2\omega t) \quad \dots (1)$$

where,  $M$  = the hourly meson count  
 $\alpha_0$  = the constant for the day  
 $\alpha_1, \beta_1$  = the first harmonic coefficients  
 $\alpha_2, \beta_2$  = the second harmonic coefficients  
 $\omega$  = the angular velocity *i.e.*,  $2\pi/24$  in this particular case  
 and  $t$  = time

The first harmonic ( $\alpha_1 \cos \omega t + \beta_1 \sin \omega t$ ) can be rewritten as  $A \sin(\omega t + \epsilon)$ , where  $A$  represents the amplitude which is equal to  $\sqrt{\alpha_1^2 + \beta_1^2}$  and the time of maximum is when  $\omega t + \epsilon = \pi/2$  *i.e.*,

$$\frac{2\pi}{24} + \tan^{-1} \frac{\beta_1}{\alpha_1} = \pi/2 \quad \dots (2)$$

Similarly, the amplitude and time of maximum for the second harmonics are also calculated. The results are represented on a 24 hour harmonic dial for the diurnal variation and a 12 hour harmonic dial for the semidiurnal variation, following Bartels' (1935) method. Probable error circles are drawn on the harmonic dial using Bartel's (1932) method, with the 'centre of the cloud' as the centre and  $P_i = 0.832 M_i$ , as the radius when  $M_i = (\sigma_{\alpha_i}^2 + \sigma_{\beta_i}^2)^{1/2}$  and  $i = 1, 2, 3, \dots$

$$M_i^2 = \frac{\Sigma(x_i^2 + y_i^2)}{N}$$

the average square distance of each point from the centre of the cloud. The number of points within the circle is approximately the same as the number of points outside.

The amplitude of the diurnal of variation has been found to be  $0.13\%$  with the time of maximum at 10.52 hrs I.S.T. which is the same as 11 hrs 13 min local time. The amplitude of the semidiurnal variation is found to be  $0.05\%$  and the time of maximum at 16.10 hrs local time, respectively. Figures 1 and 2 represent the harmonic dials for the diurnal and semi-diurnal variations of cosmic ray intensity at Calcutta.

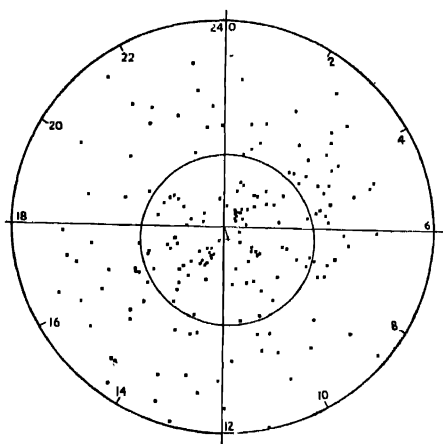


Figure 1. Harmonic dial with circle of standard deviation for diurnal variation of cosmic ray intensity

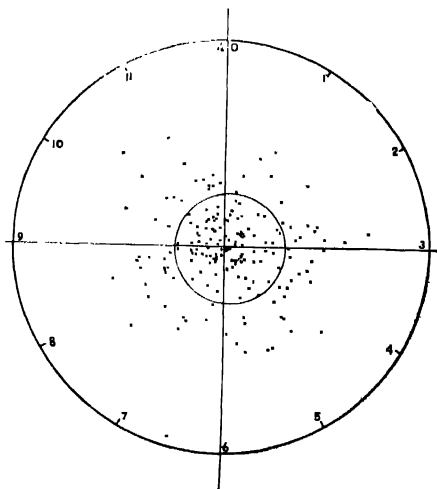


Figure 2. Harmonic dial with circle of standard deviation for the semi-diurnal variation of cosmic ray intensity.

### DISCUSSION

Since only one telescope has been used whose counting rate is scaled down to about 280 hours, the statistical error is found to be rather high.

The theoretical value of the time of maximum is about 18.00 hrs. According to Kane (1967) the geomagnetic bend would shift it by 2-3 hrs earlier in the case of the sea level mesons to about 15.00 hrs. In the present work the time of maximum of the diurnal variation is slightly earlier than the theoretical value which usually falls in the afternoon. One reason for the early occurrence of the time of maximum is that Calcutta is closer to the equator. Sarabhai *et al* (1955) while studying the daily variations at low latitudes using counter telescope data, observed that the time of maximum for diurnal variation comes earlier in lower latitudes. The actual monthly mean value of the amplitude for Ahmedabad varied from 0.22% to 0.71% and the time of maximum varied between 6.00 hrs, and 12 00 hrs. For the semidiurnal component, the amplitude varied between 0.02% to 0.26% while the time of maximum remained widely scattered. Forbush *et al* (1960) studied the diurnal and semi-diurnal variations for a period of 23 years (1937 to 1959) using ionization chamber data from Chetltenham, Huancayo and Christchurch applying statistical methods after correcting for atmospheric variations and got the mean value of the amplitude for the 1st harmonics as 0.12% and time of maximum at 13.48 hrs (L.T.) for Cheltenham, 0.15% and 10.40 hrs (L.T.) for Huancayo and 0.12% and 13.26 hrs (L.T.) for Christchurch, while the second harmonic had the amplitude 0.036% and time of maximum 1.52 hrs for Cheltenham, 0.054% and 2.40 hrs for Christchurch.

Huancayo, being closer to the equator, has the time of maximum shifted towards earlier hours, as compared to other two stations. The present results of 0.13% and 11 hrs 13 min for Calcutta is comparable to Forbush's results for Huancayo which is at a still lower latitude than Calcutta.

Kanno (1961) has studied the data from 45 stations and found that the time of maximum of diurnal variation changes from 9.00 hrs to 18.00 hrs and it increases with the latitude. The effect is very prominent in the case of the sea level stations.

The solar activity during the period under study was very high which also might have contributed to the shift of the time of maximum to earlier hours. It is well known that such phase shifts of the variation take place during magnetically disturbed periods. Sarabhai *et al* (1955), Kane (1963) and Murthy *et al* (1965) observed that during high geomagnetic disturbances the times of maximum were shifted towards the earlier hours. Duggal *et al* (1962) noticed that during disturbed periods the diurnal variation vector had turned around the clock in 8 days.

Another factor that might have possibly influenced our time of maximum is due to the existence of geomagnetic anomaly in the Bay of Bengal (Malurkar, 1954).

The amplitude of the semidiurnal component is so small that many investigators expressed their doubts about its existence. Chatterjee *et al* (1955) obtained

a value of 0.01% and showed that the value is statistically insignificant. Katzman *et al* (1960) studied the nucleonic intensity from 16 stations for a period of 5 years (1955 to 1959) and suggested that the semidiurnal component which was very small in most stations might have been due to the error in calculating the semidiurnal vector. Ahluwalia (1961) studied the data from Ahmedabad and Huancayo by separating the days on the basis of the daily  $C_p$  values and concluded that the low amplitude is due to the large variability of the time of maximum of the semidiurnal variation but that otherwise it is significant and is due to the anisotropy of the primary flux. Venkatesan *et al* (1967) found that the time of maximum for the semidiurnal wave is distributed reasonably well over all hours and suggested its origin as due to the transient changes in intensity. Lactti *et al* (1967) tried to explain the origin of the semidiurnal component as due to the fact that the spiral interplanetary magnetic field is much less highly wound at solar latitudes. According to their hypothesis, the galactic particles arriving along the Sun's polarfield lines may suffer much less modulation than those arriving in the ecliptic plane which would give rise to a second harmonic in the daily variation with the maximum at right angles to the direction of the spiral field.

## REFERENCES

- Bartels J. 1935 *Terr. Mag. Atm. Elec.* **40**, 1.  
 1932 *Terr. Mag. Atm. Elec.*, **37**, 1.  
 Kane R P 1965 *Proc. of 10th Symposium on Cosmic Ray*, Aligarh.  
 Sarabhui V., Desai U. D. & Venkatesan D. 1955 *Phys. Rev.* **99**, 1490.  
 Forbush S E. & Venkatesan D. 1960 *Jour. Geo. Res.* **65**, 2217  
 Kane R. P. 1963 *Nuovo Cim.* **27** (Ser. 10), 14.  
 Kanno T. 1961 *Nature* **192**, 250.  
 Murthy D S. R., Magabhashanam Y & Ramanuja Rao K. 1965 *Proc. Ind. Acad. Sc. (Sec.A)* **62**, 139.  
 Duggal S. P. & Pomerantz M. A. 1962 *Phys. Rev. Letters* **8**, 215.  
 Malurkar S. L. 1954 *Indian Jour. Met. and Geophysics*, **5**, 109.  
 Chatterjee S. D. & Bloom J N. 1955 *Can. Jour Phys.* **33**, 577.  
 Katzman J. & Venkatesan D. 1960 *Can Jour Phys.* **38**, 1011  
 Ahluwalia 1962 *Proc. Phys. Soc.* **80**, Part I, 437  
 Venkatesan D. & Mathew T. 1967 *Can. Jour Phys.* **46**, (Part 4), 794  
 Lactti B. & Quenby J. J. 1967 *Can. Jour. Phys.* **46**, (Part 4), 942.

## The influence of a slowly varying axial magnetic field on the stability of a gravitating cylinder

By P. K. BHAT

*Department of Applied Mathematics, Indian Institute of Science,  
Bangalore-12, India\**

(Received 3 October 1969)

The effect of a slowly varying axial magnetic field on the stability of a gravitating cylinder is considered. In the case of axisymmetric disturbances it is found that whenever the system is unstable the effect of this small inhomogeneity of the field is to add to the instability of the system. Further, an increase in the magnitude of the magnetic field decreases the wave number thereby stabilizing the long wave length disturbances. In the case of two dimensional disturbances it is found that the stability of the system is not influenced by the functional form  $f(r)$ ,  $r$  being the radial co-ordinate, of the axial magnetic field within the cylinder, in the absence of surface currents.

### INTRODUCTION

The problem of the stability of a gravitating cylinder in the presence of a magnetic field has been the subject of extensive study due to its importance in many astrophysical phenomena. Chandrasekhar & Fermi (1953) have discussed the problem subject to the influence of a uniform axial magnetic field. Auluck & Kothari (1957) have investigated the problem in the absence of surface currents for both poloidal and toroidal magnetic fields using the energy method. They find that the effect of the magnetic field is to increase the stability of the system. Chakraborty & Bhatnagar (1960) have investigated the effect of uniform volume current and surface charge on the stability of a self gravitating liquid column using the method of normal modes. They find that the system is unstable against axisymmetric disturbances of all wave lengths lying in some definite interval.

In part *A* of this paper we have studied the stability of an infinitely long incompressible and infinitely conducting gravitating cylinder in the presence of a twisted magnetic field. We have assumed that the axial magnetic field prevailing inside the cylinder varies slowly in space. Applying the method of normal modes we have studied the effect of this small inhomogeneity (in the axial magnetic field) on the longitudinal stability of the system. In part *B* we have discussed the stability of the system against azimuthal disturbances. In this case we have made no assumption on the nature of the axial magnetic field prevailing inside the cylinder.

---

\*Present address : School of Mathematics, Military College of Engineering Dapodi, Poona-31.



### PART-A

#### *Initial state*

We consider the longitudinal stability of an infinite cylinder which is infinitely conducting and self gravitating under the influence of the following magnetic field configurations

$$\vec{H}_0^{(i)} = [0, Br, H_0 - \frac{1}{2}H_1r^2] \quad (r \leq R) \quad \dots \quad (2.1)$$

$$\vec{H}_0^{(o)} = \left[ 0, \frac{BR^2}{r}, H_0 - \frac{1}{2}H_1R^2 \right] \quad (r \geq R) \quad \dots \quad (2.2)$$

where the superscripts (i) and (o) denote the inside and the outside of the cylinder,  $R$  the radius and  $B, H_0$  and  $H_1$  are constants. Taking  $H_0$  as the standard magnetic field,  $R$  as the characteristic length and  $\mu H_0^2$  as the characteristic pressure, (2.1) and (2.2) can be written as

$$\vec{H}_0^{(i)} = [0, \lambda r, 1 - \alpha r^2] \quad (r \leq 1) \quad \dots \quad (2.3)$$

$$\vec{H}_0^{(o)} = [0, \lambda/r, 1 - \alpha], \quad (r \geq 1) \quad \dots \quad (2.4)$$

where  $\lambda = BR/H_0$  and  $\alpha = \frac{1}{2} H_1 R^2/H_0$ . The dimensionless pressure inside the cylinder is given by

$$P_0^{(i)} = \alpha(r^2 - 1) + \alpha^2/2(1 - r^4) + \lambda^2(1 - r^2) + \beta/2(1 - r^2), \quad (r \leq 1) \quad \dots \quad (2.4')$$

where  $\beta = 2\pi G \rho R^2/\mu H_0^2$  and the dimensionless gravitational potentials inside and outside the cylinder are respectively given by

$$\phi_0^{(i)} = \frac{1}{2}(1 - r^2) \quad (r \leq 1) \quad \dots \quad (2.5)$$

and

$$\phi_0^{(o)} = -\ln r. \quad (r \geq 1) \quad \dots \quad (2.6)$$

#### *Linearised Equations*

The equations governing the small perturbation in the physical quantities inside the cylinder are

$$\begin{aligned} \frac{\partial \tilde{v}_r}{\partial t} = & -\frac{\partial \tilde{p}}{\partial r} + (1 - \alpha r^2) \left( \frac{\partial \tilde{H}_r}{\partial z} - \frac{\partial \tilde{H}_z}{\partial r} \right) - \lambda \frac{\partial}{\partial r} (r \tilde{H}_\theta) \\ & + 2\alpha r \tilde{H}_z - 2\lambda \tilde{H}_\theta + \beta \frac{\partial \tilde{\phi}}{\partial r}, \end{aligned} \quad \dots \quad (3.1)$$

$$\frac{\partial \tilde{v}_\theta}{\partial t} = (1 - \alpha r^2) \frac{\partial \tilde{H}_\theta}{\partial z} + 2\lambda \tilde{H}_r, \quad \dots \quad (3.2)$$

$$\frac{\partial \tilde{v}_z}{\partial t} = -\frac{\partial \tilde{p}}{\partial z} - \lambda r \frac{\partial \tilde{H}_\theta}{\partial z} - 2\alpha r \tilde{H}_r + \beta \frac{\partial \tilde{\phi}}{\partial z}, \quad \dots \quad (3.3)$$

$$\frac{1}{r} \frac{\partial}{\partial r} (r \tilde{v}_r) + \frac{\partial \tilde{v}_z}{\partial z} = 0, \quad \dots \quad (3.4)$$

$$\frac{1}{r} \frac{\partial}{\partial r} (r \tilde{H}_r) + \frac{\partial \tilde{H}_z}{\partial z} = 0, \quad \dots \quad (3.5)$$

$$\frac{\partial \tilde{H}_r}{\partial t} = (1 - \alpha r^2) \frac{\partial \tilde{v}_r}{\partial z}, \quad \dots \quad (3.6)$$

$$\frac{\partial \tilde{H}_\theta}{\partial t} = (1 - \alpha r^2) \frac{\partial \tilde{v}_\theta}{\partial z}, \quad \dots \quad (3.7)$$

$$\frac{\partial \tilde{H}_z}{\partial t} = -1/r \frac{\partial}{\partial r} \{r(1 - \alpha r^2) \tilde{v}_r\}, \quad \dots \quad (3.8)$$

$$\nabla^2 \psi + 1/r \frac{\partial \psi}{\partial r} + \frac{\partial^2 \psi}{\partial z^2} = 0, \quad \dots \quad (3.8a)$$

$$\vec{E} + v \times H_0 = 0, \quad \dots \quad (3.8b)$$

where  $\vec{v} = (\tilde{v}_r, \tilde{v}_\theta, \tilde{v}_z)$ ,  $\vec{H} = (\tilde{H}_r, \tilde{H}_\theta, \tilde{H}_z)$ ,  $\tilde{p}$ ,  $\tilde{\phi}$  and  $\vec{E}$  are perturbations in velocity, magnetic field, pressure, gravitational potential and the electric field respectively. It may be noted that for characteristic velocity we have taken the Alfvén velocity.

We assume that the disturbances are of the type  $x = \hat{x}(r) \exp(i\omega t + ikz)$ , where  $\omega$  is the frequency and  $k$  is the wave number, so that the equations (3.1)–(3.8b) reduce to the following form

$$i\omega \hat{v}_r = -\frac{d\hat{p}}{dr} + (1 - \alpha r^2) \left( ik\hat{H}_r - \frac{d\hat{H}_z}{dr} \right) - \lambda \frac{d}{dr} (r\hat{H}_\theta) + 2\alpha r\hat{H}_z - 2\lambda\hat{H}_\theta + \beta \frac{d\hat{\phi}}{dr}, \quad (3.9)$$

$$i\omega \hat{v}_\theta = ik(1 - \alpha r^2)\hat{H}_\theta + 2\lambda\hat{H}_r, \quad (3.10)$$

$$i\omega \hat{v}_z = -ik\hat{p} - ik\lambda r\hat{H}_\theta - 2\alpha r\hat{H}_r + ik\beta\hat{\phi}, \quad (3.11)$$

$$1/r \cdot d/dr \cdot (r\hat{v}_r) + ik\hat{v}_z = 0, \quad (3.12)$$

$$i\omega \hat{H}_r = ik(1 - \alpha r^2)\hat{v}_r, \quad (3.13)$$

$$i\omega \hat{H}_\theta = ik(1 - \alpha r^2)\hat{v}_\theta, \quad (3.14)$$

$$i\omega \hat{H}_z = -1/r \cdot d/dr \cdot \{r(1 - \alpha r^2)\hat{v}_r\}, \quad (3.15)$$

$$\frac{d^2\hat{\phi}}{dr^2} + \frac{1}{r} \frac{d\hat{\phi}}{dr} - k^2\hat{\phi} = 0, \quad \dots \quad (3.15a)$$

$$\vec{\hat{E}} + \vec{v} \times \vec{\hat{H}}_0 = 0. \quad \dots \quad (3.15b)$$

In passing we note that equations (3.6) and (3.8) are equivalent in view of equation (3.5) so we shall drop equation (3.5).

From equations (3.9)—(3.15) we have

$$\begin{aligned} r^2\{\omega^2 - k^2(1 - \alpha r^2)\} \frac{d^2\hat{v}_r}{dr^2} + \{\omega^2 r - k^2 r(1 - \alpha r^2)(1 - 5\alpha r^2)\} \frac{d\hat{v}_r}{dr} \\ + \{k^4 r^2(1 - \alpha r^2)^2 - \omega^2 - \omega^2 k^2 r^2 + k^2(1 - \alpha r^2)(1 + 3\alpha r^2) \\ + \frac{4\lambda^2 k^4 r^2(1 - \alpha r^2)^2}{\omega^2 - k^2(1 - \alpha r^2)}\} \hat{v}_r = 0 \end{aligned} \quad \dots \quad (3.16)$$

We shall assume that  $\alpha$  is very small so that its squares and higher powers can be neglected. Expanding the physical quantities involved in powers of  $\alpha$  we have

$$\begin{aligned} v &= v_0 + \alpha v_1 + O(\alpha^2), \\ \hat{p} &= \hat{p}_0 + \alpha \hat{p}_1 + O(\alpha^2), \\ \dot{H} &= \dot{H}_0 + \alpha \dot{H}_1 + O(\alpha^2), \\ \hat{\phi} &= \hat{\phi}_0 + \alpha \hat{\phi}_1 + O(\alpha^2), \\ \dot{E} &= \dot{E}_0 + \alpha \dot{E}_1 + O(\alpha^2), \\ \omega &= \omega_0 + \alpha \omega_1 + O(\alpha^2). \end{aligned} \quad \dots \quad (3.17)$$

Substituting (3.17) in (3.16) and separating the various order terms we have

$$\frac{d^2\hat{v}_{r0}}{dr^2} + \frac{1}{r} \frac{d\hat{v}_{r0}}{dr} - \left\{ k^2 - \frac{4\lambda^2 k^4}{(\omega_0^2 - k^2)^2} + \frac{1}{r^2} \right\} \hat{v}_{r0} = 0. \quad \dots \quad (3.18)$$

$$\begin{aligned} \frac{d^2\hat{v}_{r1}}{dr^2} + \frac{1}{r} \frac{d\hat{v}_{r1}}{dr} - \left\{ k^2 - \frac{4\lambda^2 k^4}{(\omega_0^2 - k^2)^2} + \frac{1}{r^2} \right\} \hat{v}_{r1} \\ = \frac{4ik^3 r}{(\omega_0^2 - k^2)} \hat{v}_{z0} + \frac{8\lambda^2 k^4}{(\omega_0^2 - k^2)^3} \{\omega_0^2 r^3 + 2\omega_0 \omega_1 + k^2 r^2\} \hat{v}_{r0} \end{aligned} \quad \dots \quad (3.19)$$

*Zeroth order solutions*

$$\hat{v}_{r0} = A I_1(lr) \quad \dots \quad (4.1)$$

where  $A$  is an arbitrary constant of integration,  $I_1$  the modified Bessel function of order unity and  $l^2 = k^2 - \frac{4\lambda^2 k^2}{(\omega_0^2 - k^2)^2}$ .

Now from (3.9)-(3.15), (3.17) and (4.1) we have

$$\left. \begin{aligned} \hat{v}_{\theta 0} &= -\frac{2ik\lambda A}{(\omega_0^2 - k^2)} I_1(lr), \\ \hat{v}_{z0} &= \frac{iAl}{k} I_0(lr), \\ \hat{H}_{r0} &= \frac{kA}{\omega_0} I_1(lr), \\ \hat{H}_{\theta 0} &= -\frac{2i\lambda k^2 A}{\omega_0(\omega_0^2 - k^2)} I_1(lr), \\ \hat{H}_{z0} &= \frac{iAl}{\omega_0} I_0(lr), \\ \hat{p}_0 &= \beta\hat{\phi}_0 + \frac{2i\lambda^2 k^2 Ar}{\omega_0(\omega_0^2 - k^2)} I_1(lr) \\ &\quad - \frac{iA\omega_0 l}{k^2} I_0(lr). \end{aligned} \right\} \quad (4.2)$$

Again from (3.15a) and (3.17) we get

$$\frac{d^2 \hat{\phi}_0}{dr^2} + \frac{1}{r} \frac{d\hat{\phi}_0}{dr} - k^2 \hat{\phi}_0 = 0, \quad \dots \quad (4.3)$$

and

$$\frac{d^2 \hat{\phi}_1}{dr^2} + \frac{1}{r} \frac{d\hat{\phi}_1}{dr} - k^2 \hat{\phi}_1 = 0. \quad \dots \quad (4.3a)$$

Solving (4.3) we get

$$\hat{\phi}_0 = B_1 I_0(lr), \quad \dots \quad (4.4)$$

where  $B_1$  is an arbitrary constant of integration. Similarly from (3.15b), (3.17) and (4.2) we have

$$\left. \begin{aligned} \hat{E}_{r0} &= -\frac{iA\lambda lr}{k} I_0(lr) + \frac{2iA\lambda K}{(\omega_0^2 - k^2)} I_1(lr), \\ \hat{E}_{\theta 0} &= AI_1(lr), \\ \hat{E}_{z0} &= -A\lambda r I_1(lr). \end{aligned} \right\} \quad \dots \quad (4.5)$$

*Solution of first order equations*

From (3.19) and (4.2) we have

$$\frac{d^2 \hat{v}_{r1}}{dr^2} + \frac{1}{r} \frac{d \hat{v}_{r1}}{dr} - \left( l^2 + \frac{1}{r^2} \right) \hat{v}_{r1} = M_1(lr) I_0(lr) + M_2 l^2 r^2 I_1(lr) + M_3 I_1(lr), \quad \dots (5.1)$$

where

$$\left. \begin{aligned} M_1 &= -\frac{4Ak^2}{(\omega_0^2 - k^2)}, \\ M_2 &= \frac{8A\lambda^2 k^4 (\omega_0^2 + k^2)}{(\omega_0^2 - k^2)^3}, \\ M_3 &= \frac{16A\lambda^2 k^4 \omega_0 \omega_1}{(\omega_0^2 - k^2)^3}. \end{aligned} \right\} \quad (5.2)$$

and

Equation (5.1) yields (McLachlan 1934).

$$v_{r1} = M_1' \frac{l^2 r^2}{4} I_1(lr) + M_2' \frac{l^3 r^3}{6} I_2(lr) + M_3' \frac{lr}{2} I_2(lr), \quad \dots (5.3)$$

where

$$M_1' = \frac{M_1}{l^2}, \quad M_2' = \frac{M_2}{l^4} \quad \text{and} \quad M_3' = \frac{M_3}{l^2}.$$

Thus to this order of approximation, we get

$$\hat{v}_r = AI_1(lr) + \alpha \left\{ M_1' \frac{l^2 r^2}{4} I_1(lr) + M_2' \frac{l^3 r^3}{6} I_2(lr) + M_3' \frac{lr}{2} I_2(lr) \right\}. \quad \dots (5.4)$$

Similarly, we can find the other physical variables to this order of approximation.

*Solutions in vacuum*

$$\text{Curl } \vec{\tilde{H}} = 0. \quad \dots (6.1)$$

$$\text{Div } \vec{\tilde{H}} = 0, \quad \dots (6.2)$$

$$\text{Div } \vec{\tilde{E}} = 0, \quad \dots (6.3)$$

$$\text{Curl } \vec{\tilde{E}} = -\frac{\partial \vec{\tilde{H}}}{\partial t}, \quad \dots (6.3)$$

and

$$\Delta^2 \vec{\tilde{\psi}} = 0, \quad \dots (6.4)$$

where  $\vec{\tilde{H}}$ ,  $\vec{\tilde{E}}$  and  $\vec{\tilde{\psi}}$  are the disturbances in the magnetic field, the electric field and the gravitational potential, respectively.

Solving (6.1)–(6.4), we get

$$\begin{aligned}\vec{H} &= [-Ckk_1(kr), 0, iCkk_0(kr)] \\ \vec{E} &= [iDk_1(kr), -\omega Ck_1(kr), Dk_0(kr)],\end{aligned}\quad (6.5)$$

and

$$\hat{\psi} = Ek_0kr$$

where  $C$ ,  $D$  and  $E$  are arbitrary constants of integration.

### Boundary conditions

The equation of the disturbed boundary is  $r = 1 + (\delta r) \exp(i\omega t + ikz)$  and the linearised dynamical and electromagnetic boundary conditions are

$$\begin{aligned}\vec{n} \cdot [\vec{H}] + \vec{n} \cdot [\vec{H}] &= 0, \\ \vec{n} \times [\vec{H}] + \vec{n} \times [\vec{H}] &= \vec{J}^*, \\ \vec{n} \cdot [\vec{E}] + \vec{n} \cdot [\vec{E}] &= \tilde{q}^*, \\ \vec{n} \times [\vec{E}] + \vec{n} \times [\vec{E}] &= \tilde{u}[\vec{H}] + u[\vec{H}], \\ \vec{n}[\vec{p}] + \vec{n}[\vec{p}] &= \vec{J}^* \times \vec{H} + \vec{J}^* \times \vec{H} + \tilde{q}^* \vec{E} + \tilde{q}^* \vec{E}, \\ \tilde{\phi} = \tilde{\psi}, \quad \frac{\partial \tilde{\phi}}{\partial r} &= \frac{\partial \tilde{\psi}}{\partial r} + 2\delta r,\end{aligned}$$

and

$$\vec{n} \cdot \vec{v} + \vec{n} \cdot \vec{v} = u, \quad \dots \quad (7.1)$$

where  $[\ ]$  denotes the jump in the value of a physical quantity in going from the inside of the cylinder to the outside vacuum.  $\vec{n}$ ,  $\vec{J}^*$ ,  $\tilde{q}^*$  and  $u$  denote the unit outward normal to the unperturbed boundary, the surface current density before the disturbance, the surface charge density before the disturbance and the velocity of the unperturbed boundary respectively.  $\vec{n}$ ,  $\vec{J}^*$ ,  $\tilde{q}^*$  and  $\tilde{u}$  denote the perturbations in the unit outward normal, the surface current density, the surface charge density and the velocity of the boundary respectively and  $\vec{H}$  denotes the mean of the magnetic field strength just inside and just outside the cylinder.

The perturbation in the unit normal to the boundary is given by

$$\vec{n} = [0, 0, -ik\delta r \exp(i\omega t + ikz)]. \quad (7.2)$$

After applying the set of boundary conditions (7.1) at the disturbed boundary  $r = 1 + (\tilde{\delta}r) \exp(i\omega t + ikz)$ , we get the following dispersion relations

$$k^2[\beta k_1(k)I_1(l) - 2\beta I_0(k)k_0(k)k_1(k)I_1(l) + \{kk_0(k)I_1(l) + lI_0(l)k_1(l)\}] - \omega_0^2 I_0(l)k_1(k) = 0. \quad \dots (7.3)$$

$$\omega_1 = \left[ 2I_1(l) - \frac{2kk_0(k)I_1(l)}{k_1(k)} - 2lI_0(l) + M_2''\Omega_1 \right] \left[ \frac{2\omega_0 l I_0(l)}{k^2} - M_3''\Omega_2 \right]^{-1} \dots (7.4)$$

where

$$\begin{aligned} M_2'' &= \frac{8\lambda^2 k^4 (\omega_0^2 + k^2)}{(\omega_0^2 - k^2)l^4}, \\ M_3'' &= \frac{16\lambda^2 k^4 \omega_0}{(\omega_0^2 - k^2)^{3/2}}, \\ \Omega_1 &= \frac{l^4(\omega_0^2 - k^2)}{6k^2} \cdot \frac{I_0(l)I_2(l)}{I_1(l)} - \frac{l^4(\omega_0^2 - k^2)}{12k^2} \{3I_1(l) - I_3(l)\}, \\ \Omega_2 &= \frac{l^4(\omega_0^2 - k^2)}{2k^2} \cdot \frac{I_0(l)I_2(l)}{I_1(l)} - \frac{l^4(\omega_0^2 - k^2)}{2k^2} I_1(l). \end{aligned} \quad \dots (7.5)$$

#### DISCUSSION OF RESULTS

We have discussed the following cases

(i)  $\lambda = 0$  :

In this case the azimuthal component of the initial magnetic field is zero. The dispersion relations (7.3) and (7.4) have the following forms respectively,

$$\frac{k}{I_0(k)k_1(k)} [\beta k_1(k)I_1(k) - 2\beta I_0(k)k_0(k)I_1(k)k_1(k) + 1], \quad \dots (8.1)$$

$$\omega_1 = \pm \frac{k}{I_0(k)k_1(k)} \{I_1(k)k_1(k) - 1\} \div$$

$$\left[ \frac{k}{I_0(k)k_1(k)} \{\beta k_1(k)I_1(k) - 2\beta I_0(k)k_0(k)I_1(k)k_1(k) + 1\} \right]^{\dagger} \quad \dots (8.2)$$

From (8.1) it follows that the system is stable for all values of  $k \geq 1.0668$  whatever positive value  $\beta$  may take. In case  $k < 1.0668$  the system is stable if

$$\beta < \left\{ \frac{1}{I_1(k)k_1(k)\{2I_0(k)k_0(k) - 1\}} \right\},$$

and unstable if

$$\beta > \left\{ \frac{1}{I_1(k)k_1(k)\{2I_0(k)k_0(k) - 1\}} \right\}$$

Now (8.2) implies that the effect of the inhomogeneity is to increase the frequency of stable oscillations and if the system is unstable its effect is to increase the growth of instability by a multiple of  $\omega_1$ .

(ii)  $\lambda = 0, \beta = 0$

When the azimuthal magnetic field and the gravitational force are absent, the dispersion relations (7.3) and (7.4) take the forms

$$\omega_0^2 = \left\{ \frac{k}{I_0(k) k_1(k)} \right\}, \quad \dots \quad (8.3)$$

and

$$\omega_1 = \pm \frac{k}{I_0(k) k_1(k)} \{I_1(k) k_1(k) - 1\} \div \left\{ \frac{k}{I_0(k) k_1(k)} \right\}. \quad \dots \quad (8.4)$$

From (8.3) it follows that the system is stable for all real positive values of the wave number  $k$  and (8.4) shows that inhomogeneity adds to stability of the system.

(iii)  $\lambda \neq 0, \beta \neq 0$

We find that  $[\omega_0^2 - \{k^2 \pm 2\lambda k\}]$ , is root of (7.5). This implies that the system is stable for all wave numbers  $k > 2\lambda$  and unstable for all wave numbers  $k < 2\lambda$ . In case  $k > 2\lambda$  the effect of the inhomogeneity of the magnetic field is to add to the stability of the system and if  $k < 2\lambda$  its effect is to enhance the growth rate of instability by a multiple of

$$\omega_1 = \pm \left[ 1 + \frac{k k_0(k)}{k_1(k)} \right] k^2 \div \{k^2 \pm 2\lambda k\}^{\frac{1}{2}}$$

Thus defining a critical wave number  $k^* = \frac{2B}{H_0}$  we find that an increase in the magnitude of the magnetic field decreases the wave number thereby stabilizing long wave length disturbances.

(iv)  $\lambda \neq 0, \beta \neq 0, l \neq 0$

We find that for stable modes the frequency of oscillations is increased by the inhomogeneity of the magnetic field. Further, for such modes we find that (i) for fixed values of  $\lambda$  and  $\beta$  as the wave number  $k$  increases the frequency of stable oscillations also increases, (ii) for fixed  $\lambda$  and  $k$  the frequency increases when  $\beta$  increases, and (iii) for fixed values of  $\beta$  and  $k$  the frequency increases as  $\lambda$  increases (tables 1, 2 and 3).

## PART B

In this part we have studied the disturbances of the type  $X(r) \exp(i\omega t + im\theta)$ , where  $m$  is the azimuthal wave number.



TABLE 1

$k$	$\omega_0^2$	$\omega_1$	$\omega_0^2$	$\omega_1$	$\omega_0^2$	$\omega_1$	$\omega_0^2$	$\omega_1$	$\omega_0^2$	$\omega_1$
	$\beta = 0.0000 \quad \lambda = 0.5000 \quad \beta = 0.0000 \quad \lambda = 0.9000 \quad \beta = 0.0000 \quad \lambda = 2.0000 \quad \beta = 0.0500 \quad \lambda = 0.0500 \quad \beta = 0.0500 \quad \lambda = 0.9000$									
0.1	0.01116	$\pm 0.00121$	0.01208	$\pm 0.00232$	0.01462	$\pm 0.00434$	0.01447	$\pm 0.00325$	0.01778	$\pm 0.00511$
0.3	0.12938	$\pm 0.00152$	0.15901	$\pm 0.00304$	0.18174	$\pm 0.00479$	0.10045	$\pm 0.00479$	0.10876	$\pm 0.00674$
0.5	0.36456	$\pm 0.00185$	0.44593	$\pm 0.00415$	0.66920	$\pm 0.00493$	0.36278	$\pm 0.00613$	0.44355	$\pm 0.00732$
0.7	0.73014	$\pm 0.00217$	0.88208	$\pm 0.00477$	1.30938	$\pm 0.00553$	0.72714	$\pm 0.00679$	0.87957	$\pm 0.00773$
0.9	1.23167	$\pm 0.00278$	1.47011	$\pm 0.00519$	2.15448	$\pm 0.00592$	1.22966	$\pm 0.00715$	1.46848	$\pm 0.00852$
1	1.53619	$\pm 0.00314$	1.82153	$\pm 0.00713$	2.65094	$\pm 0.00789$	1.53524	$\pm 0.00812$	1.82078	$\pm 0.00922$
3	10.93118	$\pm 0.00513$	12.57503	$\pm 0.00755$	17.36081	$\pm 0.00809$	10.93028	$\pm 0.00888$	12.57261	$\pm 0.01213$
5	29.01519	$\pm 0.00554$	32.28381	$\pm 0.00797$	41.51284	$\pm 0.00356$	29.01483	$\pm 0.00905$	32.28772	$\pm 0.01311$

TABLE 2

$k$	$\omega_0^2$	$\omega_1$	$\omega_0^2$	$\omega_1$	$\omega_0^2$	$\omega_1$	$\omega_0^2$	$\omega_1$	$\omega_0^2$	$\omega_1$
	$\beta = 0.0500 \quad \lambda = 2.0000 \quad \beta = 0.5000 \quad \lambda = 0.5000 \quad \beta = 0.9000 \quad \lambda = 0.5000 \quad \beta = 2.0000 \quad \lambda = 0.5000$									
1	0.01464	$\pm 0.00701$	0.02074	$\pm 0.02012$	0.02294	$\pm 0.02325$	0.03094	$\pm 0.03729$	0.11000	$\pm 0.06222$
3	0.13163	$\pm 0.00792$	0.14478	$\pm 0.02373$	0.17193	$\pm 0.04307$	0.25179	$\pm 0.04434$	0.26108	$\pm 0.06715$
5	0.66704	$\pm 0.00832$	0.36136	$\pm 0.03021$	0.44228	$\pm 0.05027$	0.66555	$\pm 0.05213$	0.48381	$\pm 0.07021$
7	1.30721	$\pm 0.00954$	0.70294	$\pm 0.03732$	0.85856	$\pm 0.05797$	1.28836	$\pm 0.06011$	0.74246	$\pm 0.08112$
9	2.15315	$\pm 0.01002$	1.21208	$\pm 0.04013$	1.45424	$\pm 0.08001$	2.14129	$\pm 0.06725$	1.16126	$\pm 0.08993$
1	2.65034	$\pm 0.01052$	1.52666	$\pm 0.04773$	1.81411	$\pm 0.06888$	2.64494	$\pm 0.07002$	1.50004	$\pm 0.09003$
3	17.34406	$\pm 0.01312$	10.92298	$\pm 0.04921$	12.55270	$\pm 0.06929$	17.29678	$\pm 0.07773$	10.90588	$\pm 0.09155$
5	41.50875	$\pm 0.01415$	29.01178	$\pm 0.05013$	32.27862	$\pm 0.07003$	41.47407	$\pm 0.08033$	29.00401	$\pm 0.09312$

TABLE 3

	$\beta = 2.0000$	$\lambda = 0.9000$	$\beta = 2.0000$	$\lambda = 2.0000$
$k$	$\omega_0^2$	$\omega_1$	$\omega_0^2$	$\omega_1$
.1	0.04952	$\pm .07272$	0.05327	$\pm .09099$
.3	0.26404	$\pm .08013$	0.32157	$\pm .10155$
.5	0.54211	$\pm .08688$	0.74436	$\pm .17123$
.7	0.89223	$\pm .09227$	1.31802	$\pm .19773$
.9	1.41130	$\pm .10012$	2.10374	$\pm .21023$
1	1.41130	$\pm .13235$	2.62731	$\pm .26155$
3	12.50422	$\pm .20007$	17.14323	$\pm .29002$
5	32.25507	$\pm .23135$	41.38087	$\pm .31013$

Starting with the magnetic field configuration given by (2.3) and (2.4) we have solved the linearised perturbation equations governing the system. After applying the boundary conditions (7.1) at the perturbed boundary  $r = 1 + (\delta r) \exp(i\omega t + im\theta)$ , we get the following dispersion relation:

$$\omega^2 = (m-1)\{2m\lambda^2 + \beta\}. \quad \dots (9.1)$$

This implies that the system is stable for all wave numbers  $m > 1$ . Further we note that the frequency of stable oscillations does not depend on the axial magnetic field prevailing inside the system. Thus whatever be the functional form  $f(r)$  of the axial magnetic field inside the system, the stability of the system against azimuthal disturbances is not influenced by the same (in the absence of surface currents).

#### ACKNOWLEDGEMENT

The author is thankful to Prof. P. L. Bhatnagar for suggesting the problem and for help and guidance throughout the preparation of this paper.

#### REFERENCES

- Auluck F. C. & Kothari D. S. 1957 *Zeit. fur. Astrophys* **42**, 101.  
 Chakraborty B. B. & Bhatnagar P. L. 1960 *Proc. Nat. Inst. Sci. India*, **26A** (Supple II) 76.  
 Chandrasekhar S. & Fermi E. 1953 *Astrophys. Jour.* **118**, 116.  
 McLachlan N. W. 1934 *Bessel Functions for Engineers*, Oxford University Press.

## Letters to the Editor

*Indian J. Phys.* **44**, 367-368 (1970)

### Dielectric relaxation of 1-and 2-naphthaldehydes from microwave absorption measurements

BY F. F. HANNA AND K. N. ABDEL-NOUR

*Microwave Laboratory, National Research Centre*

*Dokki, Cairo, U.A.R*

(Received 5 August 1970)

$\epsilon'$  and  $\epsilon''$  were measured in benzene solutions at wavelengths 0.22, 3.24, 10 and 25 cm to an accuracy of 2% using apparatus described by Garg *et al* (1965), Laquer & Smyth (1948) and Pitt & Smyth (1959). The static dielectric constant  $\epsilon_0$  was measured at 10 KHz using a Schering bridge. The measurements were carried out at 20°, 40° and 60°C.  $\epsilon_\infty$  is obtained from a Cole-Cole plot and the reduced absorption  $\eta'' = \epsilon''/\epsilon_0 - \epsilon_\infty$  is calculated and plotted against  $\log \lambda$ . The absorption curves obtained were analysed into two Debye terms using a computer IBM 1620. The analysis gives two relaxation times  $\tau_1$  and  $\tau_2$  where  $\tau_1$  belongs to the rotation of the molecule and  $\tau_2$  belongs to that of the group.

Table 1 shows the results obtained which are much higher than the comparative values given. So, the substances were repurified and the measurements repeated using solutions of same concentrations; same results were obtained assuring the given values.

So, the larger values of  $\tau_1$  and  $\tau_2$  in this case may be due to the formation of associates through hydrogen bonding. As the hydrogen bonds in 1-substituted naphthalenes are weaker than the 2-substituted ones, this may be the cause of higher values of  $\tau_1$  and  $\tau_2$  in the 2-naphthaldehyde than those of 1-naphthaldehyde. Also  $\tau_1$  and  $\tau_2$  are very temperature dependent especially in the 2-naphthaldehyde which may be due to the same cause as before. The dipole moment of both molecules were calculated and found to be higher in the case of 2-naphthaldehyde than 1-naphthaldehyde as expected.

It is to be noted that the behaviour of the —CHO group in 1-naphthaldehyde is different from the —OH group in 1-naphthol. It is stated by Knobloch (1965) that in the case of 1-naphthol,  $c''/X$  is not concentration dependent due to the formation of intramolecular hydrogen bridge with the hydrogen atom in the 8th position. While in the case studied here of 1-naphthaldehyde it is clear from the large values of  $\tau_1$  that intermolecular hydrogen bonds are present.

TABLE 1. Relaxation times, dipole moments, activation energy and activation entropy in benzene solutions

Substance	$t^{\circ}\text{C}$					Comparative values at 20°C		$-\frac{\Delta H}{K}$ cal/mole	$\frac{\Delta S}{\text{deg}}$ Cal/mole
		$\tau_1$ P sec	$\tau_2$ P sec			P sec	P sec		
1-Naphthal-									
dehyde	20	40.2	4.80	0.40	2.52	-OH 26.0	2.1 <sup>(a)</sup>	1.25	-6.8
$x = 0.0096$	40	33.5	3.93	0.45		-OCH <sub>3</sub> 24.3	1.7 <sup>(b)</sup>		
mole fraction	60	27.8	2.90	0.50					
2-Naphthal-									
dehydo	20	45.2	8.80	0.30	3.26	-OH 20.6	1.7 <sup>(a)</sup>		
$x = 0.0092$	40	33.4	6.60	0.35		-OCH <sub>3</sub> 19.7	1.1 <sup>(b)</sup>		-3.1
mole fraction	60	24.8	4.50	0.35					

(a) Knoblock (1965), (b) Klages &amp; Knobloch (1960)

The activation energy ( $\Delta H$ ) and activation entropy ( $\Delta S$ ) are calculated (Glastone *et al* 1941) and given in table 1.

## REFERENCES

- Garg S. K., Klip H. & Smyth C. P. 1965 *J. Chem. Phys.* **43**, 2341.  
 Glastone S., Laidler K. & Eyring H. 1941 *The Theory of Rate Process*, New York  
 Klages G. & Knobloch P. 1960 *Z. Naturf.* **209**, 580.  
 Knobloch P. 1965 *Ber. Bunsenges. Physik. Chem.* **69**, 296.  
 Laquer H. L. & Smyth C. P. 1948 *J. Am. Chem. Soc.* **70**, 4097.  
 Pitt D. A. & Smyth, C. P. 1959 *J. Phys. Chem.* **63**, 582.

## Thermodynamic functions of the three isomeric aminophenols

By V. N. VERMA

Department of Spectroscopy, Banaras Hindu University  
Varanasi-5, India

(Received 12 May 1970—Revised 26 February 1971)

Recently the author (1970) studied the vibrational spectra of the three isomeric aminophenols and made a complete assignment of the observed bands. With the help of the assignment of fundamental frequencies of these isomers, the thermodynamic functions have been calculated for an ideal gas for the three aminophenols at one atmosphere under the usual approximation of rigid rotator, harmonic oscillator model and the result is reported in the present communication.

The total energy  $\epsilon$  of the system is given by the simple expression :

$$\epsilon = \epsilon_{trans} + \epsilon_{rot} + \epsilon_{vib} + \epsilon_{elec} \quad \dots (1)$$

Where the subscript *trans* stands for translational, *rot*, for rotational, *vib* for vibrational and *elec* for electronic.

The partition function in terms of energy is given by

$$Q = \sum g_i e^{-\frac{\epsilon_i}{kT}} \quad \dots (2)$$

Where  $g_i$  is the statistical weight,  $k$  is the Boltzmann constant and  $T$  is the absolute temperature.

Hence the total partition function ( $Q_t$ ) is given by

$$Q_t = Q_{trans} + Q_{rot} + Q_{vib} + Q_{elec} \quad \dots (3)$$

The electronic contribution is small and ignored because  $\epsilon_{elec}$  is large compared to  $kT$  at ordinary temperature. For the remaining partition functions, the standard expressions utilized by Colthup (1964) have been used and evaluated.

Considering the substituent groups as single mass point and the molecule a planar one, the principal moments of inertia  $I_x$ ,  $I_y$  and  $I_z$  have been calculated, where  $y$  and  $z$  axes are in the plane of the molecule and the  $x$  axis is perpendicular to the plane. The structural data have been taken from the similar molecules such as phenol by Forest (1966), fluorophenol by Thakur (1968) and benzene by Allen *et al* (1950) because no microwave, electron diffraction or X-ray studies are available in the literature and so bond lengths and bond angles are not known exactly. The idea given by Sutton & Allen (1950) has also been taken into account that there is no appreciable change in the shape and size of the phenyl ring from its magnitude in benzene to benzene derivatives. With these assumptions the calculated moments of inertia for these three molecules are given in table 1.

TABLE 1. Moments of inertia in  $10^{-40}g\text{ cm}^2$  for the three isomeric aminophenols

Moment of inertia ( $I$ )	<i>o</i> -Aminophenol	<i>m</i> -Aminophenol	<i>p</i> -Aminophenol
$I_x$	687	687	697
$I_y$	295	295	145
$I_z$	392	392	552

Under the above assumption *o*- and *m*-aminophenols are classified into  $C_s$  symmetry with external symmetry 1 and *p*-aminophenol into  $C_{2v}$  symmetry with symmetry 2 as used by Herzberg (1945). The calculated values of the  $C_v^0$  (heat capacity),  $(H^0 - E_0^0)/T$  (enthalpy),  $-(G^0 - E_0^0)/T$  (free energy) and  $S^0$  (entropy) at various temperatures ranging from 100-1500°K for the three isomers

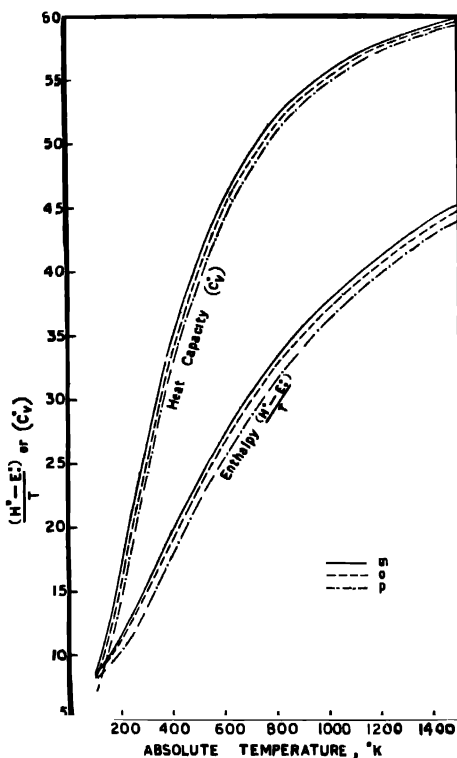


Figure 1. Variation of enthalpy and heat capacity with absolute temperatures for *o*-, *m*- and *p*-aminophenol.

are represented by curves in figures 1 and 2. Here  $E_0^0$  is the energy of one mole of an ideal gas at absolute zero,  $H^0$  is its enthalpy,  $G^0$  is its free energy.

The author is thankful to Prof. Nand Lal Singh for valuable discussions and suggestions.

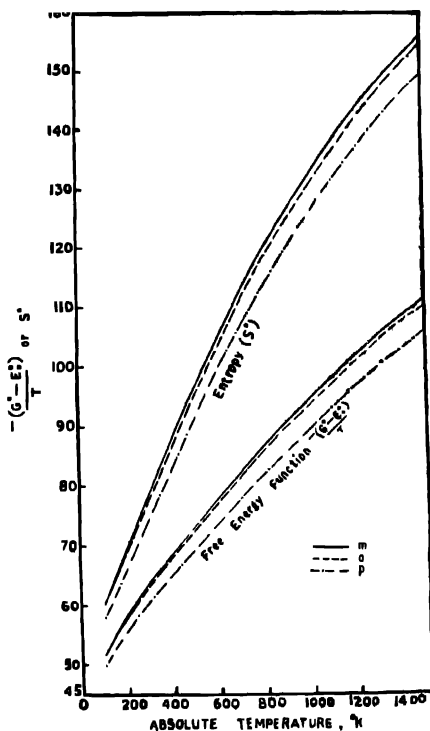


Figure 2. Variation of free energy function and entropy with absolute temperatures for *o*-, *m*- and *p*-aminophenols.

#### REFERENCES

- Allen P. W. & Sutton L. E. 1950 *Acta. Cryst.* **3**, 40.  
 Colthup N. B., Daly L. H. & Wiberley S. E. 1964 *Introduction to Infrared and Raman Spectroscopy* 463 Academic Press Inc. N. Y.  
 Forest H. & Bailey B. P. 1966 *J. Chem. Phys.* **45** 1936.  
 Herzberg G. 1945 *Infrared and Raman Spectra*, 508 D. Van Nostrand Co. Inc. N.Y.  
 Thakur S. N. 1968 *Spectra and Structural Studies of Some Molecules under High Resolution*, Ph.D. Thesis, B.H.U.  
 Verma V. N. & Rai D. K. 1970 *Appl. Spectry*. U.S.A. **24**, 445.

## Transient free convection flow with constant suction

By V. V. RAMANA RAO

Department of Engineering Mathematics, Andhra University, Waltair

(Received 11 August 1970)

The problem of transient free convection flow near a vertical flat plate with constant suction applied perpendicular to the plate is analysed. The transient is induced by a step change in the wall temperature. The solutions for the temperature and the velocity have been obtained by using Laplace transforms. The skin friction at the wall has been evaluated for various times for different values of the suction on which the solution is seen to depend. A steady fall in the skin-friction with increasing suction is noted.

The basic equations which describe the unsteady free convection flow of a viscous incompressible fluid past an infinite flat plate with constant suction in non-dimensional form as shown by Lal (1969) are

$$\frac{\partial u}{\partial t} + v_0 \frac{\partial u}{\partial y} = T + \frac{\partial^2 u}{\partial y^2} \quad \dots (1.1)$$

$$\frac{\partial T}{\partial t} + v_0 \frac{\partial T}{\partial y} = \frac{\partial^2 T}{\partial y^2} \quad \dots (1.2)$$

where the Prandtl number  $\sigma$  is taken as unity.

Appropriate boundary and initial conditions on the velocity and temperature are

$$\left. \begin{aligned} u(y, t) = T(y, t) &= 0, \quad t \leq 0 \quad y \geq 0 \\ u(\infty, t) = T(\infty, t) &= 0, \quad t > 0 \end{aligned} \right\} \quad \dots (1.3)$$

$$\left. \begin{aligned} u(0, t) &= 0, \quad t > 0 \\ T(0, t) &= T_0, \quad t > 0 \end{aligned} \right\} \quad \dots (1.4)$$

Using Laplace transforms with respect to the time variant  $t$  and solving the resultant ordinary differential equations and inverting we obtain in terms of  $\beta$

$$T = \frac{T_0}{2} \left[ e^{-\beta y} \operatorname{erfc} \left( \frac{y}{2\sqrt{t}} - \frac{\beta\sqrt{t}}{2} \right) + \operatorname{erfc} \left( \frac{y}{2\sqrt{t}} + \frac{\beta\sqrt{t}}{2} \right) \right] \quad \dots (1.5)$$

$$u = \frac{T_0 y}{2\beta} \left[ e^{-\beta y} \operatorname{erfc} \left( \frac{y}{2\sqrt{t}} - \frac{\beta\sqrt{t}}{2} \right) - \operatorname{erfc} \left( \frac{y}{2\sqrt{t}} + \frac{\beta\sqrt{t}}{2} \right) \right] \quad \dots (1.6)$$

where  $v_0 = -\beta(\beta$  being positive) since  $v_0$  corresponds to suction.



The non-dimensional skin-friction  $\tau_0'$  is given by

$$\tau_0' = \frac{T_0}{\beta} \operatorname{erfc} \left( \frac{\beta \sqrt{t}}{2} \right). \quad \dots (1.7)$$

The calculated values of  $\tau_0'$  for several values of  $\beta$  and increasing  $t$  are given in the table.

TABLE 1. Values of  $\tau_0'/T_0$

$\beta \backslash t$	0	0.04	0.09	0.25
0	0	0.11284	0.16926	0.28210
1	0	0.11246	0.16800	0.27633
2	0	0.11135	0.16432	0.26025

From the table it is evident that for a fixed time  $t$ , the skin friction  $\tau_0'$  decreases with increasing suction.

#### REFERENCE

Lal K. 1969 *Indian J. Phys.* **43**, 528.

## BOOK REVIEWS

### *Physics of the Solid State*

Edited by S. Balakrishna, M. Krishnamurthy and B. Ramachandra Rao,  
*Academic Press, London & New York (1969) Price 160s.*

This volume has been brought out to commemorate the 40th Birthday of Professor S. Bhagavantam one of the leading scientists of India who has also successfully adorned various important positions of scientific administration. The contributors to the articles are eminent Solid State Physicists from wide geographical range such as London, Toronto, Moscow, Paris, Sydney and various other centres in U.S.A. and India. The subjects also cover quite a wide field including not only diverse modern aspects of Solid State Physics including Crystallography but also such a subject as "Evolution of Oxygen and Nitrogen of Earth's Atmosphere". The editors are to be highly congratulated on their ambitious attempt in bringing out a volume of such diverse interests as well as collecting articles from such a wide geographical area. Many of the articles are from international authorities in the subjects dealt with. The quality of printing and get up are good. The wide nature of the topics and technical nature of the articles are likely to make the volume less useful to the general readers who are interested in Solid State Physics. Those who are not thoroughly acquainted with the topics will have to read other review articles before appreciating the contributions included in this volume on that topic. However, some of the articles are free from this criticism and throw light on interesting new lines of development in a very lucid manner. This volume will serve the limited purpose of catering upto date informations only to specialists of particular domain of Solid State Physics, through the respective review articles of the present publication. However, the readers of this volume will certainly get an idea about the very wide field of physics covered by solid state physics.

R. K. S.

### *Introduction to Quantum Field Theory*

Paul Roman, *J. Wiley and Sons, Inc, N. Y.*, 1969, pp. 634, \$ 18.00.

Paul Roman is a well known author and his 'Advanced Quantum Theory' and 'Theory of Elementary Particles' enjoy a good deal of popularity. The present volume is meant primarily for students taking a course in the subject and anybody with a good knowledge of quantum theory would be able to go through the book. The writing is remarkable for its clarity and although some recent advances or latest application are left out (as the author himself notes) the book would give the reader a sufficient mastery to pursue the researches in the field. An added attraction is the addition of problems at the end of chapters.

The circle of readers that the author has in mind is the students and perhaps that is why he has not given any reference to research papers. However the reviewer considers this to be an unfortunate omission. Besides, there are rather too many printing mistakes (though most of them are trivial) and the reviewer would cite as examples a few occurring in the first few pages :

P5. line below equation (0-3)  $-x_1, -x_2, -x_3$ , should be  $-x^1, -x^2, -x^3$ .

P9. Second line below equation (0-30),  $x \rightarrow 0$  should be  $x \rightarrow \alpha$ .

P12. Eq. (0-41),  $g^{\mu\nu}$  should be  $\epsilon^{\mu\nu}$

A. K. R. G.

# INDIAN JOURNAL OF PHYSICS

**VOL. 44**

**No. 7**

**AND**

**VOL. 53**

**PROCEEDINGS**

**No. 7**

**OF THE**

**INDIAN ASSOCIATION FOR THE CULTIVATION OF SCIENCE**

*(Edited in collaboration with the Indian Physical Society).*

**IJPYAS 44 (7) 375-424 (1970)**

**JULY 1970**

**PUBLISHED BY THE**

**INDIAN ASSOCIATION FOR THE CULTIVATION OF SCIENCE**

**JADAVPUR, CALCUTTA-32**



## Rotational structure in the ${}^1\Pi-{}^1\Sigma^+$ transition of $\text{CS}^{34}$ molecule

A. K. CHAUDHURY, K. N. UPADHYA and S. N. TIHAKUR

Department of Spectroscopy, Banaras Hindu University,  
Varanasi-5

(Received 7 November 1969—Revised 10 May 1970)

(Plates 10—13)

Band spectrum of  $\text{CS}^{34}$  molecule ( $\text{S}_2^{34}$  enriched to 86%) has been photographed by exciting the molecule under microwave discharge. A study of isotope shift in the branches of rotational structures of the bands (0, 0), (0, 1), (2, 1), (3, 2) and (5, 4) of CS molecule is made with  $\text{CS}^{34}$  molecule. A good agreement is found in the calculated and observed shifts. The rotational constants for  ${}^1\Pi$  perturbed state and those of  ${}^3\Sigma^+$  and  ${}^3\Sigma^-$  perturbing states have also been calculated for isotopic molecule.

### INTRODUCTION

$A-X$  band system of CS, lying in 2500-2800 Å region has been very well studied by many workers. Crawford & Shurcliff (1934) performed the rotational analysis of two bands of this system for the first time. Extensive perturbation was observed in the upper state. Howell (1947), after making a comparative study, suggested the possibility of the upper state as  ${}^3\Pi$ . To assign the exact nature of electronic transition, Lagerqvist *et al* (1958) made the detailed rotational analysis of twenty four bands and established the  ${}^1\Pi-{}^1\Sigma^+$  transition for this system. A number of perturbations were observed in  $v' = 0, 1, 2, 3, 4$  and 5 levels of the excited state interpreted as due to the interactions of  ${}^3\Sigma^+$ ,  ${}^3\Sigma^-$  and two singlet states with  ${}^1\Pi$  upper state. Barrow *et al* (1960) recorded in absorption the rotational structure of some of the bands of two forbidden system, viz.  $a'{}^3\Sigma^+-X({}^1\Sigma^+)$  and  $e{}^3\Sigma^+-X({}^1\Sigma^+)$  along with the main system. They observed that  ${}^3\Sigma^+$ ,  ${}^1\Pi$  interaction was in good agreement with the theoretical predictions, while in  ${}^3\Sigma^-$ ,  ${}^1\Pi$  interaction the agreement was poor.

At present the rotational analysis done by Lagerqvist *et al* (1958) for the  $A-X$  system seems to be the most accurate. The regular feature is lost in the rotational structure at many places due to strong perturbations. It has been thought desirable to study the emission bands of  $A-X$  system of CS using highly enriched (86%)  $\text{S}^{34}$  isotope to obtain rotational isotope shift in the branches and to provide an unambiguous check on the validity of perturbations located by Lagerqvist *et al* (1958) in the upper  ${}^1\Pi$  state.

## EXPERIMENTAL

The sample of sulphur 86%  $S_2^{34}$  used in this investigation was obtained from Oak Ridge National Laboratory, Tennessee. Sealed quartz tubes containing traces of sulphur at 2 to 3mm of argon gas were prepared in the manner described by Tomkins & Fred (1957). A Raytheon microtherm oscillator (frequency 2450 Mc/sec) was used to excite the substance placed inside the discharge tube. Trace of carbon as impurity gave rise to the bands of  $CS^{34}$  molecule. The spectrum was recorded in the third order of 10.6 metre concave grating spectrograph with dispersion 0.22 Å/mm. The probable error in the wave number of the lines measured is estimated to be  $\pm 0.05 \text{ cm}^{-1}$  for sharp lines.

## RESULTS

(a) *Determination of Isotopic Shifts*: The vibrational isotope shifts in the bands of this system were measured by Narasimham & Reddy (1966) by taking  $S_2^{34}$  isotopic molecule enriched to 44%. These shifts were verified in the present study also. In addition the rotational isotope shifts in the lines of  $P$ ,  $Q$  and  $R$  branches in the rotational structure of (0, 0), (0, 1), (2, 1), (3, 2) and 5, 4 bands of this system have been obtained. The isotope shifts are calculated from the relation

$$\Delta\nu_r = \nu_r - \nu'_r(1 - \rho^2)[B_e J'(J' + 1) - B'_e J''(J'' + 1)] \quad \dots (1)$$

where  $\rho = \sqrt{\mu/\mu'}$ ,  $\mu$  and  $\mu'$  are the reduced masses of  $S_2^{32}$  and  $S_2^{34}$ . The values of rotational constants  $B_e$  and  $B'_e$  are taken from the rotational analysis of Lagerqvist *et al* (1958) and the microwave spectrum analysis from Mockler & Bird (1955). To this calculated rotational isotope shifts, the vibrational isotope shifts, which is a constant for a band, have been added to get the total calculated isotope shifts. The experimental values are taken directly from wave numbers of the rotational lines for  $CS^{32}$  molecule measured by the previous workers and for  $CS^{34}$  molecule as measured by us. The observed and calculated isotope shifts in  $Q$  branches are given in table 1, and the (0, 0), (0, 1), (2, 1), (3, 2) and (5, 4) bands are plotted against  $J$  in figure 1. The agreement is found to be fairly satisfactory. The rotational structure of these bands are shown in figures 2, 3, 4 and 5. (Plates 10-13).

(b) *Determination of Rotational Constants for Isotopic Molecule  $CS^{34}$* :

For the ground state  $X^1\Sigma^+$ , the rotational constants  $B_e$  and  $\alpha_e$  reported by Mockler & Bird (1955) are used. Thus for the isotopic molecules

$$B'_{e'} = \rho^2 B_e = 0.80690 \text{ cm}^{-1}$$

and

$$\alpha'_{e'} = \rho^3 \alpha_e = 0.00578 \text{ cm}^{-1}$$

These values are found to satisfy the following expression

$$B'_{v'} = 0.80690 - 0.00578 \left( v' + \frac{1}{2} \right) \text{ cm}^{-1} \quad \dots (2)$$

TABLE 1: Vacuum wavenumbers and  $J$  assignments of (0, 0), (0, 1), (2, 1), (3, 2) and (5, 4) bands of  $A-X$  system of  $\text{CS}^{34}$  molecule.

$J$	(0, 0) band of $\text{CS}^{34}$			$Q(J)$ of (0, 0) band of $\text{CS}^{32}$ (Lagerqvist et al 1958)	Total isotope shift in $Q$ branch lines $(\nu_u - \nu_u') + (\nu_r - \nu_r')$	
	$R(J)$	$Q(J)$	$P(J)$		Obs.	Cal.
8		38795.20		38794.49	-0.80	-0.88
9		94.37		93.47	-0.90	-0.90
10		93.41		92.55	-0.86	-0.91
11		92.20		91.51	-0.69	-0.93
12		90.91		90.01	-0.90	-0.94
13		89.61		88.36	-1.25	-0.96
14		87.64		—	—	—
15	38820.80	[85.49 90.49]		[— 89.36]	[— -1.13]	[— -1.00]
16	17.80	88.25		87.00	-1.25	-1.02
17	16.30	86.40		85.21	-1.19	-1.04
18	—	83.93	38760.08	82.84	-1.09	-1.06
19	—	82.16	56.47	80.93	-1.23	-1.08
20	—	[78.98 86.70]	53.00	[77.52 85.57]	[— -1.13]	[— -1.11]
21	—	82.36	49.20	81.17	-1.19	-1.14
22	—	79.08	46.12	78.20	-0.88	-1.17
23	—	77.22	42.66	75.91	-1.31	-1.19
24	—	75.20	38.78	73.72	-1.48	-1.23
25	12.56	73.20	34.88	71.73	-1.47	-1.26
26	11.96	70.93	31.08	69.37	-1.56	-1.29
27	11.20	68.00	27.51	67.22	-1.38	-1.33
28	10.33	66.50	23.90	64.91	-1.59	-1.36
29	09.67	64.12	20.08	62.49	-1.63	-1.40
30	38808.93	38761.90	38716.06	38760.22	-1.68	-1.44
31	07.88	59.40	11.74	57.54	-1.86	-1.48
32	07.00	56.47	07.27	54.97	-1.50	-1.52
33	05.70	53.80	02.82	52.16	-1.64	-1.56
34	04.46	51.07	38698.48	49.28	-1.79	-1.60
35	03.12	48.30	94.44	46.50	-1.80	-1.65
36	01.72	45.10	90.30	43.39	-1.71	-1.70
37	00.17	42.20	85.70	40.38	-1.82	-1.74
38	38798.14	39.30	81.26	37.19	-2.11	-1.79
39	95.76	36.00	76.40	33.88	-2.12	-1.84
40	93.17	32.57	71.36	30.30	-2.27	-1.89
41		28.77	66.31	26.36	-2.14	-1.94
42		24.63		22.54	-2.19	-2.00
43		20.02		18.03	-2.17	-2.06
44		14.80		12.59	-2.29	-2.11
45		10.09				
46		06.00				
47		01.37				
48		38697.10				

TABLE 1 (contd.)

49		[ 92 38					
		702 99					
50		38698.49					
51		94 09					
52		89 58					
53		85 08					
54		80 36					
55		75.54					
56		70 46					
57		65.19					
(0,1) band							
5	37544 35	—					
6	46 66	--	37525 94				
7	46 47	--	23 12				
8	47 43	--	21.60				
9	48 32	37532 90	19 30	37521 80	-11 10	-11.04	
10	49 14	31 95	16 93	20.91	-11 01	-11 05	
11	49 72	30.93	14.61	19.89	-11 04	-11.07	
12	50.35	29 69	12 08	18.59	-11 10	-11.08	
13	-	28.08	09 26	16.90	-11.18	-11 10	
14	-		00 65	—	-	- 11.12	
15	{ -	29.66	03 53	18.60	-11.06	-11.13	
16	59.98						
	57 30	27 50	00 28	16 45	-11 05	-11.16	
17	55.87	25 93	{ 37495 21	14 77	-11 16	-11.18	
			37507.22				
18	---	24 20	01.35	12 99	-11 21	-11 20	
19	--	22 24	37496.43	10.96	-11 28	- 11 22	
20	---	{ 19.30	93.28	{ 07 85	{ -11.45	-11 25	
		{ 26 97		{ 15.55	{ -11.42		
21	--	22 80	89.83	11.51	-11 29	-11.28	
22	---	20 38	86.50	09.04	-11 34	-11 31	
23	---	18 40	83 70	08.08	-11.42	-11 33	
24	---	16 46	79.54	05 13	-11.33	-11.36	
25	---	14 62	76 29	03.21	-11.41	-11 40	
26	--	13 00	72.93	01.33	-11.67	-11 43	
27		37511 16	--	37499 37	-11.79	-11.47	
28	37552.95	09.20	37466.41	97.42	-11.78	-11.51	
29	52.64	07.22	—	95.41	-11.81	-11.54	
30	52.13	05.20		93 30	-11 90	-11.58	
31	51.41	02 90		91.11	-11.79	-11.62	
32	50.75	00.48		88 85	-11.63	-11.66	
33	49.72	37498.21		86.57	-11.64	-11.70	
34	48 80	95 91		84.13	-11.78	-11.74	
35	47.80	93.51		81 71	-11.80	-11.79	
36	46.47	91 00		79.04	-11.96	-11.84	
37	45.66	88.38		76.43	-11.95	-11.88	
38	44.35	85.76		73.67	-12.09	-11.93	
39	42.82	82 51		70.70	-11.81	-11.96	
40	40.68	79 54		67 77	-11.77	-12.03	



TABLE 1 (contd.)

(2,1) band

6		39002.60		39607.97	5.37	5.33
7		01.82		07.20	5.38	5.32
8	39614.11	01.09		06.39	5.30	5.31
9	15.02	00.13		05.46	5.33	5.30
10	—	39599.10	39584.40	04.32	5.22	5.29
11	—	97.83	81.80	03.11	5.28	5.27
12	—	96.26	78.63	01.85	5.59	5.26
13	—	94.88	75.83	00.51	5.63	5.24
14	—	93.70	73.10	39598.80	5.10	6.22
15	—	92.13	70.10	97.11	4.98	5.21
16	15.02	90.27	66.70	95.02	4.75	5.18
17	14.11	87.51	63.40	92.68	5.17	5.16
18	12.76	84.80	59.61	89.67	4.87	5.14
19	10.56	80.81	55.18	85.71	4.90	5.12
20	07.60	75.83	50.70	80.86	5.03	5.09
21	—	90.27	45.42	95.02	4.75	5.06
22	—	84.80	39.00	89.67	4.87	5.03
23	—	80.41	—	85.22	4.81	5.01
24	—	74.96	—	79.71	4.75	4.97
25	—	94.36	—	99.39	5.03	4.94
26	17.31	86.00	—	90.87	4.87	4.91
27	—	78.58	—	83.50	4.92	4.87
28	13.89	73.10	29.83	77.71	4.61	4.83
29	12.35	68.50	24.72	73.16	4.60	4.80
30	39610.56	39564.48	39520.10	39569.63	5.15	4.76
31	08.73	61.38	15.60	66.33	4.95	4.72
32	06.88	58.37	10.60	62.91	4.54	4.68
33	05.60	[54.21 55.77]	05.74	[58.98 60.45]	[4.77 4.63]	4.64
34	03.47	51.02	00.06	56.13	5.11	4.61
35	01.67	47.76	39495.75	52.61	4.85	4.55
36	39599.30	44.17	90.43	48.99	4.82	4.50
37	97.12	40.63	85.18	45.29	4.66	4.46
38	94.88	37.13	80.08	41.51	4.38	4.41
39	92.60	32.99	74.67	37.59	4.60	4.36
40	90.27	29.16	69.40	33.73	4.57	4.31
41	87.51	25.20	—	29.56	4.36	4.26
42	84.80	20.94	—	25.38	4.44	4.20
43	81.85	16.70	—	20.88	4.18	4.14
44	79.11	12.14	—	16.09	3.95	4.09
45	—	07.80	—	12.02	4.22	4.03
46	—	02.98	—	07.11	4.13	3.97
47	—	39498.03	—	01.88	3.85	3.91
48	—	92.36	39496.41	3.78	3.85	3.85
49	—	86.33	90.32	3.99	3.79	3.79
50	—	79.13	82.93	3.80	3.72	3.72

TABLE 1 (*contd.*)

51		{ 69.40 97.60		{ 72.92 500.96	{ 3.53 3.24	3.60
52		85.18		488.95	3.77	
53		76.17		80.16	3.99	3.52
(3,2) band						
8		39360.86		39363.92	3.06	3.02
9		59.80	39346.60	62.89	3.09	3.01
10		58.90	44.67	61.93	3.03	3.00
11		57.60	41.90	60.79	3.19	2.98
12		56.50	38.70	59.61	3.11	2.97
13	39376.29	55.15	35.60	58.26	3.11	2.95
14	76.29	53.60	32.71	56.72	3.12	2.93
15	—	52.20	29.94	55.21	3.01	2.92
16	—	50.60	27.20	53.65	3.05	2.89
17	—	48.80	23.90	51.77	2.97	2.87
18	—	46.91	20.01	49.94	3.03	2.85
19	74.89	44.97	16.37	47.92	2.95	2.83
20	74.08	42.80	13.07	45.74	2.94	2.80
21	73.28	40.01	9.40	43.52	2.91	2.77
22	71.49	38.15	05.30	41.12	2.97	2.74
23	—	35.60	01.45	38.50	2.90	2.72
24	—	33.58	39296.90	36.44	2.86	2.68
25	—	30.76	—	33.54	2.78	2.65
26	69.37	27.71	—	30.46	2.75	2.62
27	67.70	24.32	87.93	27.17	2.85	2.58
28	65.80	20.60	82.90	23.39	2.79	2.54
29	63.80	{ 14.83 27.72	77.64	{ 17.64 30.39	{ 2.81 2.07	2.51
30	61.96	21.16	72.70	23.82	2.66	2.47
31	39358.90	39316.37	39267.70	39319.01	2.64	2.43
32	62.70	12.42	62.89	14.97	2.55	2.39
33	59.30	08.59	56.60	11.14	2.55	2.35
34	56.50	04.81	57.71	07.29	2.48	2.30
35	53.40	00.93	50.59	03.43	2.50	2.26
36	{ 50.56 53.40	39296.90	44.72	39299.21	2.31	2.21
37	50.00	94.70	38.40	96.97	2.27	2.17
38	46.91	89.85	{ 32.00 35.26	91.86	2.01	2.12
39	43.67	85.30	28.80	87.34	2.04	2.07
40	41.11	80.78	22.70	82.82	2.04	2.02
41	38.15	76.01	16.27	78.09	2.08	1.97
42	34.00	71.13		72.90	1.77	1.91
43	29.94	65.60		67.20	1.60	1.85
44	23.12	58.53		60.05	1.52	1.80
45	—	{ 47.32 79.18		{ 48.77 80.81	{ 1.45 1.63	1.74

TABLE 1 (contd.)

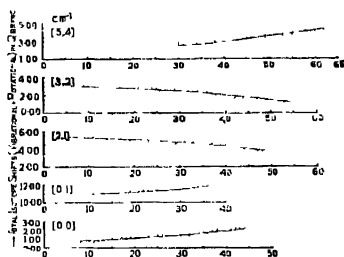
46	—	[31 00 65 60	[32 39 67 20	[1.39 1.60	1.68
47	31.43	56.60	57.96	1.36	1.02
48	24.32	48.83	50.47	1.64	1.56
49	19.10	41.64	43.18	1.54	1.50
50	14.60	[32.00 49.30	[33.17 50.70	1.17 1.40	1.43
51	10.15	37.20	38.53	1.33	1.37
52	06.22	29.66	30.87	1.21	1.30
53	01.45	23.16	24.41	1.25	1.23
54	39296.90	17.30	18.18	0.88	1.15
55	92.80				
56	87.93				
57	83.20				

## (5,4) band

$Q(J)$	$P(J)$	$Q(J)$ , Lager- qvist <i>et al</i> (1958)	Isotope shift obs. calc.		
16	38813.09				
17	09.04				
18	05.58				
19	01.65				
20	38798.11				
21	94.13				
22	89.78				
23	85.74				
24	81.56				
25	76.91				
26	72.43				
27	67.76				
28	62.50				
29	57.63				
30	38795.29	51.76	38792.54	-2.73	-2.57
31	90.91	45.93	88.38	-2.53	-2.61
32	86.30	39.18	83.59	-2.71	-2.65
33	81.50	31.20	78.55	-2.95	-2.69
34	[ 75.61		[ 72.91	-2.70	-2.74
35	[ 68.30		[ 65.82	[-2.48	-2.78
	[ 803.20		[ 800.81	[-2.39	
36	[ 59.45		[ 56.86	[-2.59	-2.83
	[ 92.20		[ 89.36	[-2.84	
37	[ 48.26		[ 45.66	[-2.60	-2.87
	[ 82.36		[ 79.59	[-2.77	
38	[ 38734.57		[ 38731.88	-2.69	-2.92
			[ 71.50		
39	[ 19.10		[ 16.53	[-2.57	-2.97
	[ 67.14		[ 64.56	[-2.58	

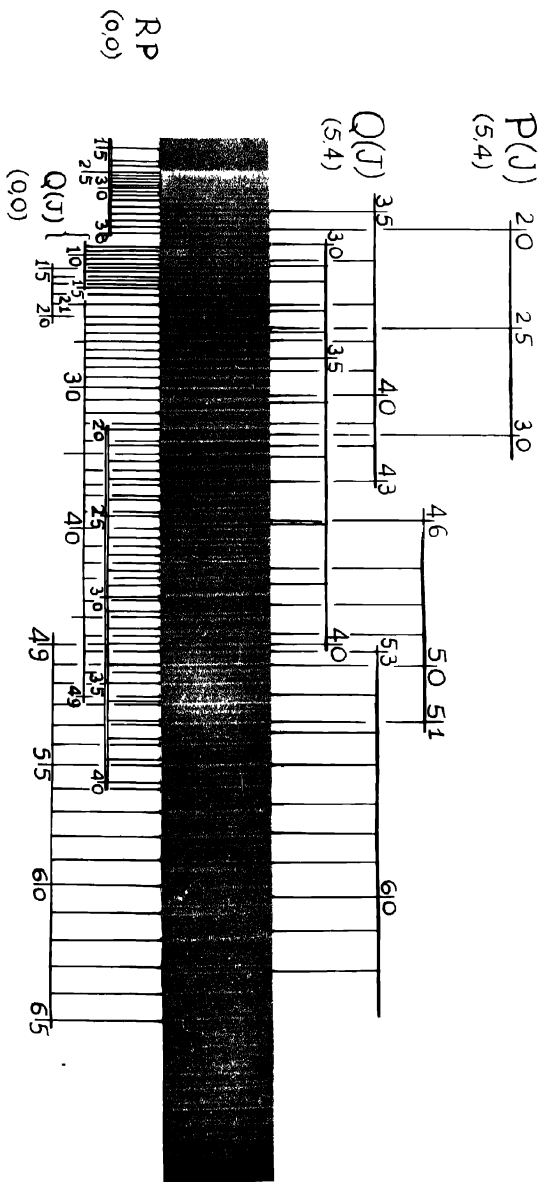
TABLE 1 (contd.)

40	[02 99 61.24	[699.85 758.18	[ -3.14 -3.06	-3.02
41	55.36	52.09	-3.27	-3.07
42	49.05	45.66	-3.39	-3.13
43	41.50	38.42	-3.08	-3.19
44	—	—	—	-3.24
45	—	—	—	-3.30
46	34.80	31.38	-3.42	-3.36
47	23.42	20.50	-2.92	-3.42
48	14.90	12.10	-2.80	-3.48
49	07.20	03.84	-3.36	-3.54
50	38698.30	38694.30	-4.00	-3.61
51	[85.20 —	[82.18 —	[ -3.02 —	-3.67
52	—	—	—	-3.74
53	38701.65	98.04	-3.61	-3.81
54	38691.85	88.07	-3.78	-3.88
55	83.19	79.44	-3.75	-3.95
56	75.54	71.25	-4.29	-4.02
57	68.47	63.78	-3.69	-4.10
58	60.15	55.94	-4.21	-4.17
59	52.40	48.26	-4.14	-4.25
60	44.40	40.29	-4.11	-4.32
61	36.90	32.57	-4.33	-4.40
62	29.10	24.85	-4.25	-4.48

Figure 1. Total isotope shifts plotted against  $J$ .

The rotational constants in  ${}^1\Pi$  upper state were determined from the method used by previous workers by plotting  $\frac{\Delta Q}{2J}$  and  $\frac{\Delta RP}{4J}$  values against  $J$  as shown in figure 6. The two expressions are given by

$$\frac{\Delta Q}{2J} = \frac{Q(J-1) - Q(J)}{2J} = (B_{v'}^i - B_{v''}^i) - 2J^2(D_{v'}^i - D_{v''}^i) \quad \dots (3)$$

Figure 2  $(0,0)$  and  $(5,4)$  bands of  $CS_3$ .

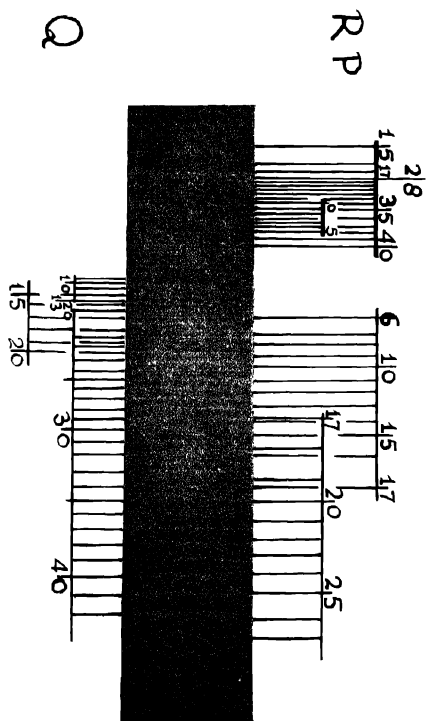


Figure 3. (0,1) band of CS<sub>2</sub>

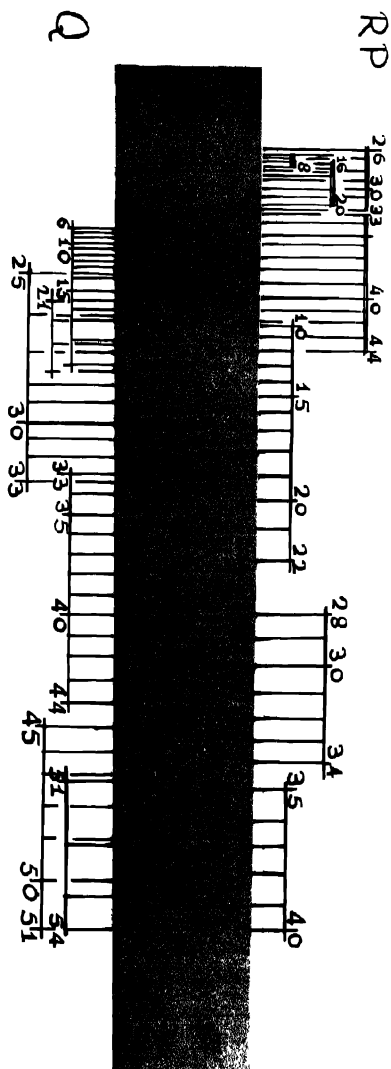


Figure 4. (2,1) band of CS

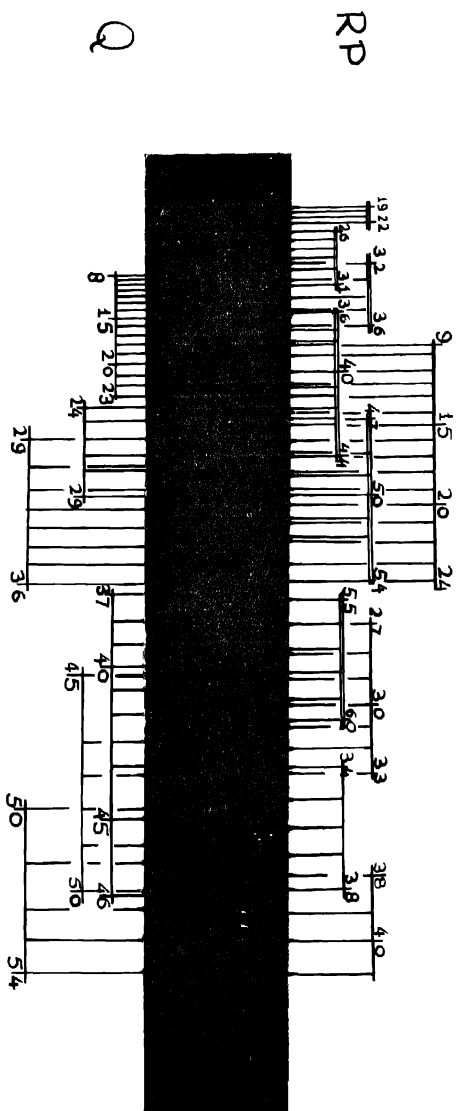
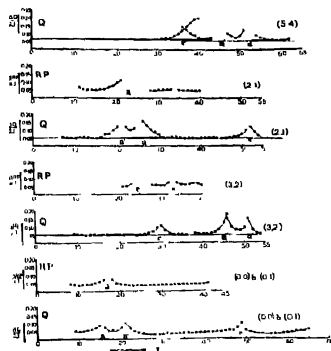


Figure 5. (3,2) band of CS<sup>2</sup>



$$\frac{\Delta RP}{4J} = \frac{R(J-2) - R(J-1) + P(J) - P(J+1)}{4J} = (B_{v''}^i - B_{v'}^i) + 6D_{v''}^i - 2J^2(D_{v''}^i - D_{v'}^i) \dots \quad (4)$$


 Figure 6.  $Q/2J$  &  $RP/4I$  for the upper level plotted against  $J$ .

 $^1\Pi^s\Sigma^+$ —Perturbation indicated with  $c'$ 
 $^1\Pi^s\Sigma^-$ —Perturbation indicated with  $c$ 

As the term  $(D_{v''}^i - D_{v'}^i)$  is very small, the points of graph lie almost on a straight line in unperturbed region. From these graphs  $(B_{v''}^i - B_{v'}^i)$  values are determined, from which  $B_{v'}^i$  can be found, since the values of  $B_{v''}^i$  are known from equation (2). It is found that the values of  $B_{v'}^i$  follow the equation

$$B_{v'}^i = 0.7675 - 0.0062(v' + \frac{1}{2}) - 0.004(v' + \frac{1}{2})^2 \quad \dots \quad (5)$$

The calculated values of  $B_{v'}^i$  from this equation and the graphical representation are shown collectively in table 2. The value of  $B_{e'} (= 0.7675 \text{ cm}^{-1})$  agrees closely with  $0.76745 \text{ cm}^{-1}$ , obtained from the expression  $B_{e'}^i = \rho^2 B_{e'}^i$ . The variations in  $D_{e'}^i$  and  $\alpha_{e'}^i$  are very small and these values remain almost the same.

 TABLE 2 : Rotational constants for  $^1\Pi$  state of  $\text{CS}^{34}$ 

$v'$	$B' (\text{cm}^{-1})$ (from graphical procedure)	$B' (\text{cm}^{-1})$ (calculated)
0	0.7640	0.7643
2	0.7496	0.7498
3	0.7405	0.7409
5	0.7207	0.7213

$$D_{e'}^i = 1.60 \times 10^{-4} \text{ cm}^{-1}, \quad B_{e'}^i = 0.7675 \text{ cm}^{-1}, \quad \alpha_{e'}^i = 0.0062 \text{ cm}^{-1}$$

(c) *Determination of the Rotational Constants for the Perturbing States*

Four  $^1\Pi$ ,  $^3\Sigma^+$  perturbations have been identified in  $v' = 0, 2, 3$  and 5 levels, as shown in table 3. From these perturbations the value  $B'_{3\Sigma^+}$  is obtained using the following equation of Lagerqvist *et al* (1958)

$$B_{3\Sigma^+} = B'_{\Pi} \frac{J_3(J_3+1) - J_1(J_1+1)}{(J_3+1)(J_3+2) - (J_1-1)J_1} \quad \dots (6)$$

TABLE 3. Summary of perturbations

$v'$	$J_e\ ^3\Sigma^-$		$J_{a'}\ ^3\Sigma^+$		$J$		$V_p$	$B'_p$	$C_p + T_e(A\ ^1\Pi)$
	$RP$	$Q$	$RP$	$Q$	$RP$	$Q$			
0			15	17	20.5		$\alpha'$	0.560	38860.00
0	—	47.5	—				$e$		
2			21	23	26		$\alpha' + 3$	0.538	40994.00
2					34	33.5 — 44 5			
2	—	51.5	—				$e + 3$		
2			57	—	—		$\alpha' + 4$		
3	26	30	33				$e + 5$	0.575	42031.00
3					$\sim 24 \sim 24$ $\sim 38 \sim 37$				
3			46	—	50.5		$\alpha' + 5$	0.525	42385.98
5	—	37	—				$e + 7$		
5			46	—	52		$\alpha' + 8$	0.540	44362.00

Since the  $J$  values,  $J_1$ ,  $J_2$  and  $J_3$  correspond to the culmination points and the  $B'_{\Pi}$  are known, the values of  $B'_{3\Sigma^+}$  are determined with the help of equation (6). The values of the energies,  $C_p$  of the perturbing states at  $J = 0$  and above  $J = 0$  in ( $A^1\Pi$ ) states is determined from the equation

$$C_p = (B'' - B^{a'+v})J^2 \quad \dots (7)$$

Only one perturbation of  $^1\Pi$ ,  $^3\Sigma^-$  type has been observed in  $v' = 3$  level. From this the rotational constant  $B_{e+5}$  for  $^3\Sigma^-$  state is obtained. All the molecular constants of the perturbing states  $a'^3\Sigma^+$  and  $e^3\Sigma^-$  are summarised in table 3. The lowest vibrational numbers are designated by  $a'$  and  $e$ , respectively. These constants satisfy the equations for isotopic molecules very well.

(d) *Weak Head at 2575 Å*

It was pointed out by Lagerqvist *et al* (1958) that there is a weak head of (5, 4) band at 2575.9 Å associated with the (0, 0) band. In the present study,

some lines of  $Q$  and  $R$  branches of (5, 4) band have been traced out in the structure of (0, 0) band as shown in figure 6. The agreement of isotopic shifts for these lines are also fairly close. This leads to the conclusion that these lines belong to (5, 4) bands and not due to any impurity.

## ACKNOWLEDGEMENTS

The authors are grateful to Dr C. B. Mayer of Oak Ridge National Laboratory, Tennessee, U.S.A. for providing samples of sulphur  $S_2^{34}$ . Thanks are due to Prof. N. L. Singh and Dr. D. K. Rai for their interest in the work. One of us (AKC) is thankful to Council of Scientific and Industrial Research, New Delhi, for financial assistance.

## REFERENCES

- Barrow R. F., Dixon R. N., Lagerqvist A. & Wright C. V. 1960 *Ark. Phys.* **18**, 543.  
Crawford F. H. & Shureliff W. A. 1934 *Phys. Rev.* **45** 860.  
Howell, H. G. 1947 *Proc. Phys. Soc.* **59**, 107.  
Lagerqvist A., Westerlund H., Wright C. V. & Barrow R. F. 1958 *Ark. Phys.* **14**, 387.  
Mockler R. C. & Bird R. 1955 *Phys. Rev.* **98**, 1837.  
Narasimham N. A. & (Km.) Reddy S. G. 1966 *Current Science* **35**, 485.  
Tomkins F. S. & Fred M. 1957 *J. Opt. Soc. Am.* **47**, 1087.

## Nonlinear interaction of electromagnetic waves in a magnetized electron beam

BY G. S. BAJWA\* and K. M. SRIVASTAVA

*Department of Mathematics, University of Jodhpur, Jodhpur*

*(Received 7 November 1969—Revised 21 March and 3 August 1970)*

The nonlinear interaction of electromagnetic waves in a magnetized electron beam has been investigated. The waves are taken to be propagating across a uniform magnetic field. It has been established here that extraordinary waves are generated when two ordinary and two extraordinary waves interact.

### INTRODUCTION

The phenomenon related to the nonlinear interaction of electromagnetic waves in a plasma plays a basic role (Kroll *et al* 1964, Montgomery 1965) in the study of weak plasma turbulence. The study of coherent interaction of two electromagnetic waves in the ionosphere is an example of the application of this phenomenon in which Blachier & Bouchet (1966) have proposed a scheme of radio communication over a long distance. Etievant *et al* (1968) have discussed the nonlinear interaction of electromagnetic waves in a cold magnetised plasma and shown that (a) interaction of an extraordinary wave with an ordinary wave generates an ordinary wave, and (b) interaction of two ordinary waves generates an extraordinary wave.

In a hot plasma several interaction mechanisms (Clouser 1960) leading to the generation as well as amplification of microwave signals have been suggested. The hot plasma is regarded as of the form of an electron beam whose directed velocity is much greater than the random velocity of the electrons. We have considered the nonlinear interaction of electromagnetic waves propagating across a uniform magnetic field in an electron beam. The nonlinear effects are treated by considering the waves which arise in the linear theory and interact with each other. It is found that for an appropriate choice of these electromagnetic waves a secondary wave is generated.

### FIRST ORDER PERTURBATIONS

In equilibrium, an isotropic plasma consisting of electrons and subjected to a constant uniform magnetic field  $\vec{B} = B\hat{z}$ , may be regarded as a single beam with no perpendicular energy and with a constant zero-order parallel velocity  $\vec{V} = V\hat{x}$ . The basic equations are similar to those of Etievant *et al* (1968). The equations

---

\* Present address: Department of Mathematics, S. G. N. Khalsa College, Sri Ganganagar, Rajasthan.

governing the first order perturbations  $\vec{v}_1, \vec{E}_1, \vec{h}_1$  and  $n_1$  respectively in  $\vec{V}, \vec{E}, \vec{B}$  and  $N$  come out to be

$$\left(\frac{\partial}{\partial t} + \vec{V} \cdot \nabla\right) \vec{v}_1 = -\frac{e}{m} \left( \vec{E}_1 + \frac{\vec{V} \times \vec{h}_1}{c} + \frac{\vec{v}_1 \times \vec{B}}{c} \right), \quad \dots \quad (1)$$

$$\nabla \times \vec{E}_1 = -\frac{1}{c} \frac{\partial \vec{h}_1}{\partial t} \quad \dots \quad (2)$$

$$\nabla \cdot \vec{E}_1 = -4\pi n_1 e \quad \dots \quad (3)$$

$$\nabla \times \vec{h}_1 = \frac{1}{c} \frac{\partial \vec{E}_1}{\partial t} - \frac{4\pi e}{c} (n_1 \vec{V} + N \vec{v}_1); \quad \dots \quad (4)$$

$$\nabla \cdot \vec{h}_1 = 0.$$

In equations (1)–(5), we choose the time dependence of the first order perturbed quantities of the form  $\exp(-i\omega t)$ . On eliminating  $\vec{h}_1$  between equations (1) and (2), we operate successively equation (1) by the operator  $i\omega - \vec{V} \cdot \nabla$ , and obtain

$$i\omega(i\omega - \vec{V} \cdot \nabla)[(i\omega - \vec{V} \cdot \nabla)^2 + \Omega^2] \vec{v}_1 = \frac{e}{m} \vec{\mu} \cdot \vec{P}_1 \quad \dots \quad (6)$$

where

$$\vec{\mu} = \begin{bmatrix} (i\omega - \vec{V} \cdot \nabla)^2 & \Omega(i\omega - \vec{V} \cdot \nabla) & 0 \\ -\Omega(i\omega - \vec{V} \cdot \nabla) & (i\omega - \vec{V} \cdot \nabla)^2 & 0 \\ 0 & 0 & \Omega^2 + (i\omega - \vec{V} \cdot \nabla)^2 \end{bmatrix}, \quad \dots \quad (7)$$

and

$$\vec{P}_n = (i\omega - \vec{V} \cdot \nabla + \nabla \cdot \vec{V}) \vec{E}_n \quad \dots \quad (8)$$

Here  $\Omega = eB/mc$  is the cyclotron frequency and in equation (8) the subscript  $n$  stands for the order of the perturbed quantity.

From equations (2)–(4),  $\vec{v}_1$  when expressed in terms of  $\vec{E}_1$ , comes out to be of the form

$$\vec{v}_1 = \frac{e}{m} \frac{ic^2}{\omega\omega_0^2} \left[ \left( \nabla - \frac{i\omega}{c^2} \vec{V} \right) \cdot \nabla - \nabla^2 - \frac{\omega^2}{c^2} \right] \vec{E}_1. \quad \dots \quad (9)$$

We eliminate  $\vec{v}_1$  between equations (6) and (9) and obtain the dispersion relation

$$\begin{aligned} (i\omega - \vec{V} \cdot \nabla)[(i\omega - \vec{V} \cdot \nabla)^2 + \Omega^2] \left[ \left( \nabla - \frac{i\omega}{c^2} \vec{V} \right) \cdot \nabla - \nabla^2 - \frac{\omega^2}{c^2} \right] \vec{E}_1 \\ = -\frac{\omega_0^2}{c^2} \vec{\mu} \cdot \vec{P}_1 \quad \dots \quad (10) \end{aligned}$$

If the variation of  $\vec{E}_1$  is taken to be of the form  $\vec{e} \exp i(kx - \omega t)$  then the dispersion relation (10) admits of two independent solutions

$$c^2 k^2 = \omega^2 - \omega_0^2, \quad \text{ordinary waves,} \quad \dots \quad (11)$$

$$c^2 k^2 = \omega^2 - \omega_0^2 - \frac{\Omega^2 \omega_0^2}{\alpha^2 - \Omega^2 - \omega_0^2}, \quad \text{extraordinary waves,} \quad \dots \quad (12)$$

where

$$\alpha = (\omega - kV), \quad \omega_0^2 = 4\pi N e^2 / m. \quad \dots \quad (13)$$

From equations (11) and (12), it is evident that two types of waves, ordinary and extraordinary, propagate in a magnetized electron beam.

For propagations perpendicular to the magnetic field the first order perturbations for the extraordinary waves are found to be

$$\begin{aligned} \vec{E}_e &= A(\hat{x} - i a \hat{y}), \quad \vec{v}_e = -\frac{ie}{m} \frac{A}{\omega_0^2} \left[ \alpha \hat{x} + \frac{i}{\Omega} (\alpha^2 - \omega_0^2) \hat{y} \right], \\ \vec{h}_e &= -\frac{ia c k A}{\omega} \hat{z}, \quad n_e = -\frac{ikA}{4\pi e}, \end{aligned} \quad \dots \quad (14)$$

where  $A$  is the normalization factor given by

$$A^2 = \frac{|\epsilon_e|^2}{1 - a^2}, \quad a = \frac{\omega \Omega}{c^2 k^2 + \omega_0^2 - \omega^2}; \quad \dots \quad (14a)$$

and for the ordinary waves we have

$$\vec{E}_o = \epsilon_{\parallel} \hat{z} \vec{V}_o = -\frac{ie}{m\omega} \epsilon_{\parallel} \hat{z}, \quad \vec{h}_o = -\frac{ck}{\omega} c_{\parallel} \hat{y}, \quad n_o = 0. \quad \dots \quad (15)$$

Here in equations (14) and (15), we have omitted the exponential factor  $\exp i(kx - \omega t)$ .

## SECOND ORDER PERTURBATIONS

In a way similar to that adopted for the first order perturbations, we obtain the dispersion relation for the second order perturbations which yields

$$E_x^2 = -\frac{\alpha c^2}{\omega \delta} \left[ i(\alpha^2 \omega_0^2 + (\alpha^2 - \Omega^2)(c^2 k^2 - \omega^2)) J_{sx} - \alpha \Omega \omega_0^2 J_{sy} \right], \quad \dots \quad (16)$$

$$E_y^2 = -\frac{c^2}{\delta} [\Omega \omega_0^2 (\Omega - kV) J_{sx} - i \alpha^2 (\alpha^2 - \Omega^2 - \omega_0^2) J_{sy}], \quad \dots \quad (17)$$

$$E_z^2 = \frac{ic^2 J_{sz}}{\alpha(\alpha^2 - \Omega^2)(c^2 k^2 - \omega^2 + \omega_0^2)}, \quad \dots \quad (18)$$

where

$$\vec{J}_s = \frac{\omega \omega_0^2}{c^2} \frac{m}{e} (i\alpha^2 - \alpha \Omega \hat{z} \times -i\Omega^2 \hat{z} \hat{z}_0) \left[ (\vec{v}_1 \cdot \nabla) \vec{v}_1 + \frac{e}{mc} (\vec{v}_1 \times \vec{h}_1) \right]$$

$$\frac{4\pi e u}{c^2} \alpha (\alpha^2 - \Omega^2) n_1 v_1, \quad \dots (19)$$

$$\delta = \alpha^3 (\alpha^2 - \Omega^2 - \omega_0^2) [\alpha^2 \omega_0^2 + (\alpha^2 - \Omega^2) (c^2 k^2 - \omega^2)] + \alpha^2 \Omega^2 \omega_0^4 (\Omega - kV). \quad \dots (20)$$

Equations (16)–(18) determine the second order electric field, whereas, equation (19) determines the second order current source. The first order terms occurring in equation (19) are given by the set (14) for extraordinary waves and by the set (15) for the ordinary waves.

#### INTERACTION OF TWO ORDINARY WAVES

We choose the subscripts 1 and 2 to distinguish the two interacting ordinary waves and let  $k_{\pm} = k_1 \pm k_2$  etc.

From the set (15) it follows that the first order density for the ordinary waves is zero, therefore only the first term in equation (19) will contribute. In view of the fact that the first order velocity component is directed along the  $z$  axis, from equation (19) it is found that the interaction produces a current source given by

$$\vec{J}_s = \pm \frac{e}{m} \frac{\omega_0^2}{c^2} \frac{\epsilon_{||1} \epsilon_{||2}}{2\omega_1 \omega_2} \alpha_{\pm} k_{\pm} \omega_{\pm} [\alpha_{\pm} \cos(k_{\pm} x - \omega_{\pm} t) \hat{z}$$

$$- \Omega \sin(k_{\pm} x - \omega_{\pm} t) \hat{y}]. \quad \dots (21)$$

Equation (21) establishes that the current source is perpendicular to the magnetic field and therefore the second order wave is an extraordinary wave.

The second order electric field as calculated from equations (16)–(18) and (21), comes out to be

$$\vec{E}_2 = \mp \frac{e}{m} \frac{\Omega}{\delta} \frac{\epsilon_{||1} \epsilon_{||2}}{2\omega_1 \omega_2} \omega_0^2 \alpha_{\pm}^2 k_{\pm} \omega_{\pm} [\omega_0^2 (\Omega - k_{\pm} V) + \alpha_{\pm} (\alpha_{\pm}^2 - \Omega^2 - \omega_0^2)] \hat{y}. \quad (22)$$

#### INTERACTION OF TWO EXTRAORDINARY WAVES

The first order terms for the extraordinary waves are given by the set (14) which reveals that both the terms of equation (19) will contribute. The second

order current source and electric field, calculated from equations (14) and (16)—(19), are given by

$$\vec{J}_2 = \pm \frac{e}{m} \frac{A_1 A_2}{2c^2} \alpha_{\pm} \omega_{\pm} [C_1 \cos(k_{\pm} x - \omega_{\pm} t) \hat{x} - C_2 \sin(k_{\pm} x - \omega_{\pm} t) \hat{y}], \dots \quad (23)$$

$$\vec{E}_2 = \mp \frac{e}{m} \frac{A_1 A_2}{2\delta} \alpha_{\pm} \omega_{\pm} [\Omega \omega_0^2 (\Omega - k_{\pm} V) C_1 + \alpha_{\pm}^2 (\alpha_{\pm}^2 - (\Omega^2 - \omega_0^2)) C_2] \hat{y}, \dots \quad (24)$$

where

$$\begin{aligned} C_1 &= \frac{\lambda_{\pm}}{\omega_0^2} \pm \frac{\Omega^2 \phi + \alpha_{\pm} \psi_{\pm}}{\Omega \omega_1 \omega_2}, \\ C_2 &= \frac{1}{\Omega \omega_0^2} [\alpha_1 \alpha_2 \Omega^2 k_{\pm} \pm (\alpha_{\pm}^2 - \Omega^2) [k_1 (\alpha_2^2 - \omega_0^2) \pm k_2 (\alpha_1^2 - \omega_0^2)] + \alpha_{\pm} \chi] \\ &\quad + \frac{\alpha_{\pm} \phi + \psi_{\pm}}{\omega_1 \omega_2}, \\ \lambda_{\pm} &= \chi - \alpha_1 \alpha_2 \alpha_{\pm} k_{\pm} + (\alpha_{\pm}^2 - \Omega^2) (\alpha_1 k_2 + \alpha_2 k_1), \\ \chi &= \alpha_2 k_1 (\alpha_1^2 - \omega_0^2) + \alpha_1 k_2 (\alpha_2^2 - \omega_0^2), \\ \phi &= \alpha_1 \omega_1 \alpha_2 k_2 + \alpha_2 \omega_2 \alpha_1 k_1 \\ \psi_{\pm} &= \pm [a_1 k_1 \omega_2 (\alpha_2^2 - \omega_0^2) + a_2 k_2 \omega_1 (\alpha_1^2 - \omega_0^2)] \end{aligned} \quad \dots \quad (25)$$

The current source given by equation (23) is perpendicular to the magnetic field, therefore the interaction of two extraordinary waves generates an extraordinary wave. Here the subscripts 1 and 2 distinguish the two interacting extraordinary waves. The quantities  $A$  and  $a$  are given by equation (14a) and  $\delta$  is given by equation (20).

#### INTERACTION OF AN ORDINARY WAVE WITH AN EXTRAORDINARY WAVE

We distinguish the extraordinary wave and the ordinary wave by the subscripts 1 and 2 respectively. For the current source, only the second term of equations (19) contributes and it is found that

$$\vec{J}_s = \pm \frac{e}{m} \frac{A_1 k_1 \epsilon_{\parallel 2}}{2\omega_2 c^2} \alpha_{\pm} \omega_{\pm} (\alpha_{\pm}^2 - \Omega^2) \cos(k_{\pm} x - \omega_{\pm} t) \hat{z}. \quad \dots \quad (26)$$

Equation (26) establishes that the interaction of an ordinary wave with an extraordinary wave generates an extraordinary wave.

In view of equation (11), equation (18) gives an indeterminate value of the second order electric field. This conclusion shows that the consideration of the interaction of an extraordinary wave with an ordinary wave is not possible by this analysis.



ACKNOWLEDGEMENT

This work has been supported by the University of Jodhpur.

REFERENCES

- Blachier B. & Bouchet P. 1966 *Ann. Radioelect.* (France) **21**, 250  
Clouser F. H. 1960 *Symposium of Plasma Dynamics* (Addison-Wesley Publishing Company Inc. ), Chap. 4.  
Etevant C., Fidono I., Ossakow S., Ozizinn E. & Su C. H. 1968 *Phys. Fluids* **11**, 1778  
Kroll N. M., Ron A. & Rostoker N. 1964 *Phys. Rev. Letters* **13**, 83.  
Montgomery D. 1965 *Physica* **31**, 693.

## Cherenkov type of radiation in an anisotropic electron plasma

By R. M. KHAN

*Department of Mathematics, City College, Calcutta*

*(Received 26 February 1970—Revised 26 May and 31 July 1970)*

An exact solution for the electromagnetic field due to a moving line charge through an anisotropic electron plasma in the presence of an external magnetic field is given. Electro-magnetic intensities and radiation are slowly damped due to collision of electrons but the attenuation is very intensive within a certain range of frequency. The wave propagation is mainly transverse to the de magnetic field and there exists other type of radiation along with the Čerenkov radiation

### INTRODUCTION

Kolomenskii (1956) investigated the Čerenkov radiation in an anisotropic electron plasma under an external magnetic field without collision effect. Majumdar (1961) studied a similar problem in a homogeneous electron plasma. He investigated the possibility of other types of radiation in addition to the Čerenkov radiation due to coupling between the longitudinal plasma waves and transverse electro-magnetic waves. Some aspects of the field in a collisionless plasma due to a line source have been considered by Wait (1960), Tuan & Seshadri (1965) and many others.

As a sequel to these works we shall study the interaction of an uniformly moving line charge with the transverse electromagnetic waves in an infinite magneto-electron plasma, which is incompressible but anisotropic in dielectric property, with the low collision frequency. In our case the source is a line charge moving perpendicularly to the external magnetic field. Due to this ideal consideration the problem becomes two-dimensional and the longitudinal wave is trivial. The uniform velocity of the source introduces a cut-off in the frequency range for propagation of waves and the collisions of electrons include damping of the electro-magnetic intensities and radiation. It is found that the radiation is confined between two planes, somewhat similar to Čerenkov cone, and it exists even when the velocity of the source is less than the phase-velocity of light. As a limiting case the expression for radiation in the direction of Čerenkov ray matches with that of Čerenkov radiation due to the motion of a line charge within a homogeneous dielectric medium given by the author (1967). Similar phenomenon may occur in the ionosphere due to some sudden solar disturbances. Moreover, the moving source may be utilized like a test particle to explore the characteristics

of the earth's ionosphere where the charged particles are moving at high speed across the magnetic field.

# PHENOMENOLOGICAL EQUATIONS

We assume that (i) ions are stationary and they neutralize the electrons on the average, (ii) an external magnetic field  $B_0$  is acting in the direction of  $z$ -axis, (iii) a line charge is moving with uniform velocity  $u$  in the direction of  $x$ -axis, and (iv) the collision factor is a small quantity of the first order.

Maxwell's equations for field variables  $\vec{E}$  and  $\vec{H}$  (electric and magnetic vectors) with Fourier transform are

$$\nabla \times \vec{E}(\omega) = -\frac{i\mu\omega}{c} H(\omega) \quad \dots (1)$$

$$\text{and} \quad \nabla \times \vec{H}(\omega) = \frac{i\omega}{c} \vec{D}(\omega) + \frac{4\pi}{c} \vec{j}(\omega). \quad \dots (2)$$

$\mu$  and  $\vec{j}$  are the scalar magnetic permeability, the velocity of light in free space and the current density.  $\vec{D} = (\chi)E$  where  $(\chi)$  is the dielectric tensor described

$$(\chi) = \begin{pmatrix} c_1 & -\epsilon' & 0 \\ \epsilon' & c_1 & 0 \\ 0 & 0 & c_2 \end{pmatrix}$$

$$\left. \begin{aligned} \text{Here } \frac{c_1}{\epsilon} &= 1 - \frac{\omega_p^2}{\omega^2 - \omega_c^2} - i\eta \omega_p^2 \frac{\omega^2 + \omega_c^2}{\omega(\omega^2 - \omega_c^2)^2}, \\ \frac{c_2}{\epsilon} &= 1 - \frac{\omega_p^2}{\omega^2} - i\eta \frac{\omega_p^2}{\omega^3}, \quad \frac{\epsilon'}{\epsilon} = -\frac{i\omega_c \omega_p^2}{\omega(\omega^2 - \omega_c^2)} + \eta \frac{2\omega_c \omega_p^2}{(\omega^2 - \omega_c^2)^2}, \\ \omega_p^2 &= \frac{4\pi N e^2}{\epsilon m}, \quad \omega_c = \frac{e B_0}{m c} \end{aligned} \right\} \dots (3)$$

and  $\epsilon$  is the permittivity of the medium in the limit. The tensor  $(\chi)$  is obtained by the help of the force equation,

$$m \frac{\partial \vec{V}}{\partial t} + m\eta \vec{V} = e \left[ \vec{E} + \frac{\vec{V} \times \vec{B}_0}{c} \right]. \quad \dots (4)$$

$N$ ,  $e$ ,  $m$ ,  $\eta$  and  $\vec{V}$  are the average electron number density, electron charge, mass of an electron, the collision factor and the velocity of the electrons,

In case of  $\vec{j}$ ,  $j_y = 0 = j_z$  and  $j_x = qu\delta(x-ut)\delta(y)$  where  $q$  is the line charge density. By Fourier transform

$$j_x(x, y, \omega) = \frac{1}{2\pi} \int_{-\infty}^{\infty} qu\delta(x-ut)\delta(y)e^{-i\omega t}dt = -\frac{q}{2\pi} e^{-\frac{i\omega x}{u}} \delta(y). \quad (5)$$

The problem thus reduces to a two-dimensional one and all the vector quantities are independent of  $z$ , i.e., the wave propagation is transverse to the applied magnetic field. Moreover, without any inconsistency in the equations (1), (2) and (4) we can assume that  $E_z = 0 = H_x = H_y = V_z$ . It means in effect absence of longitudinal plasma waves.

With the aid of (2) and (3) we have

$$\left. \begin{aligned} E_x(\omega) &= -\frac{ic}{c(\epsilon_1^2 + \epsilon'^2)\omega} \left[ \epsilon_1 \frac{\partial H_z(\omega)}{\partial y} - \epsilon' \frac{\partial H_z(\omega)}{\partial x} - \frac{4\pi}{c} \epsilon_1 j_x(\omega) \right] \\ \text{and } E_y(\omega) &= \frac{ic}{c(\epsilon_1^2 + \epsilon'^2)\omega} \left[ \epsilon' \frac{\partial H_z(\omega)}{\partial y} + \epsilon_1 \frac{\partial H_z(\omega)}{\partial x} - \frac{4\pi}{c} \epsilon' j_x(\omega) \right] \end{aligned} \right\} \quad \dots (6)$$

By (1) and (6) we obtain

$$\frac{\partial^2 H_z(\omega)}{\partial x^2} + \frac{\partial^2 H_z(\omega)}{\partial y^2} + \frac{\mu\epsilon}{c^2} \frac{\epsilon_1^2 + \epsilon'^2}{\epsilon_1} \omega^2 H_z(\omega) = \frac{4\pi}{c} \left\{ \epsilon' \frac{\partial j_x(\omega)}{\partial x} + \frac{\partial j_z(\omega)}{\partial y} \right\} \quad \dots (7)$$

#### FORMAL SOLUTION OF THE EQUATION (7)

Considering Fourier transform with respect to  $y$  in the form  $f(x, y, \omega) = \int_{-\infty}^{\infty} f(x, k, \omega) e^{iky} dk$  and in view of dependence of field components on  $x$  through the phase factor  $e^{-\frac{i\omega x}{u}}$  the equation (7) gives

$$\begin{aligned} H_z(x, k, \omega) &= \frac{i q}{\pi c} \frac{\frac{\epsilon'}{\epsilon_1} \frac{\omega}{u} - k}{\frac{\mu\epsilon}{c^2} \frac{\epsilon_1^2 + \epsilon'^2}{\epsilon_1} \omega^2 - \frac{\omega^2}{u^2} - k^2} e^{-\frac{i\omega x}{u}} \\ H_z(x, y, \omega) &= \frac{i q}{\pi c} \int_{-\infty}^{\infty} \frac{k - \frac{\epsilon'}{\epsilon_1} \frac{\omega}{u}}{k^2 - \left( \frac{\mu\epsilon}{c^2} \frac{\epsilon_1^2 + \epsilon'^2}{\epsilon_1} \omega^2 - \frac{\omega^2}{u^2} \right)} e^{iky - i\omega x/u} dk \quad \dots (8) \end{aligned}$$

Under the assumption about  $\eta$  and for a particular value of  $\omega$  the equation (8) reduces to

$$H_z(x, y, \omega) = \frac{iq}{\pi c} \int_{-\infty}^{\infty} \frac{k - (\eta b_1 - ia_1)}{k^2 - (a^2 - i\eta b)} e^{iky - i(\omega x)^{1/2} k} dk \quad \dots \quad (9)$$

where

$$a_1 = \frac{\omega_c \omega_p^2}{u h_2}, \quad b_1 = \frac{a_1}{h_2} \frac{2\omega^2 - \omega_p^2}{\omega}, \quad a^2 = \frac{\mu \epsilon}{c^2} \frac{h_3}{h_2} - \frac{\omega^2}{u_2},$$

$$b = \frac{\mu \epsilon}{c^2} \frac{\omega \omega_p^2}{h_1}, \quad h_1 = \omega^2 - \omega_c^2, \quad h_2 = \omega^2 - \omega_c^2 - \omega_p^2, \quad h_3 = (\omega^2 - \omega_p^2)^2 - \omega^2 \omega_c^2$$

... (10)

On taking  $a^2 > 0$  and integrating (9) by the residue method

$$H_z(x, y, \omega) = -\frac{q}{c} \left[ 1 - \frac{ia_1}{a} + \eta \xi \right] e^{\psi_1} \quad \text{when } y > 0$$

... (11)

$$\text{and } H_z(x, y, \omega) = -\frac{q}{c} \left[ 1 + \frac{ia_1}{a} - \eta \xi \right] e^{\psi_2} \quad \text{when } y < 0.$$

$$\text{Here } \quad \xi = \frac{b_1}{a} + \frac{ba_1}{2a^3}, \quad \psi_1 = -(\alpha + i\gamma)y - \frac{i\omega x}{u},$$

} ... (12)

$$\psi_2 = (\alpha + i\gamma)y - \frac{i\omega x}{u}, \quad \sqrt{a^2 - i\eta b} = \gamma - i\alpha, \quad \gamma \simeq a, \quad \alpha \simeq \frac{\eta b}{2a}.$$

#### EXPRESSIONS FOR $E$ AND $V$

With the aid of (6) and (11) the following values of  $E_x$  and  $E_y$  are obtained.

$$\text{when } y > 0, \quad E_x(x, y, \omega) = -\frac{iq}{\omega \epsilon a_2} [im_1 + \eta(f_1 + ig_1)] e^{\psi_1}$$

... (13)

$$\text{and } E_y(x, y, \omega) = \frac{iq}{\omega \epsilon a_2} [l_2 + im_2 + \eta(f_2 + ig_2)] e^{\psi_1}.$$

$$\text{When } y < 0, \quad E_x(x, y, \omega) = \frac{iq}{\omega \epsilon a_2} [im_1 + \eta(f_1 - ig_1)] e^{\psi_2}$$

... (14)

$$\text{and } E_y(x, y, \omega) = -\frac{iq}{\omega \epsilon a_2} [l_2 - im_2 + \eta(-f_2 + ig_2)] e^{\psi_2}$$

Here

$$\begin{aligned}
 m_1 &= \frac{h_2}{ah_1} (a^2 + a_1^2), \quad l_2 = \frac{\mu\epsilon}{c^2} \frac{ua_1}{\omega a} \frac{h_2}{h_1}, \\
 n_2 &= \frac{u}{\omega} \frac{h_2}{h_1} \left( \frac{\omega^2}{u^2} - a_1^2 \right), \quad a_2 = \frac{h_3}{\omega^2 h_1^2}, \\
 f_1 &= h_4 - \frac{a_1}{a} h_5 - \frac{\omega_c \omega_p^2}{\omega h} \xi, \quad g_1 = \frac{ah_2}{h} \xi - \frac{a_1}{a} h_4 - h_6, \\
 f_2 &= \frac{\omega_p^2 (\omega^2 + \omega_c^2)}{u h_1^2} + \frac{a_1}{a} h_6 + \frac{\omega_c \omega_p^2 a}{\omega h} \xi - \frac{2h_2 \omega^2 h_7}{a}, \\
 g_2 &= h_6 + \frac{\omega}{u} \frac{h_2}{h_1} \xi + \frac{2\omega_c \omega_p^2}{au^2} h_7, \\
 h_4 &= \frac{b}{2a} \frac{h_2}{h_1} + \frac{a\omega_p^2 (\omega^2 + \omega_c^2)}{\omega h_1^2} - 2a\omega h_2 h_7, \quad h_5 = \frac{2\omega_c \omega_p^2}{u} \left( \frac{1}{h_1^2} + h_7 \right), \\
 h_6 &= \frac{\omega_c \omega_p^2}{h_1} \left( \frac{2a}{h_1} - \frac{b}{2a\omega} \right) + 2a\omega_c \omega_p^2 h_7, \quad h_7 = \frac{\omega_p^2 (\omega^2 + \omega_c^2 - \omega_p^2)}{h_1^2 h_3}.
 \end{aligned} \tag{15}$$

#### THE NATURE OF THE RADIATION

The power radiated by the moving source per unit time is

$$\begin{aligned}
 \dot{S} &= \frac{c}{4\pi} 2Re \int_{-\infty}^{\infty} (\vec{E} \times \vec{H}) dx \\
 &= cu Re \int_{-\infty}^{\infty} (\vec{E}_o \times \vec{H}_o) d\omega.
 \end{aligned}$$

When  $y > 0$ ,  $S_x(\omega) = \frac{q^2 u}{\omega \epsilon a_2} \left[ \frac{a_1 l_2}{a} + m_2 + \eta \left( m_2 \xi + \frac{a_1 f_2}{a} + g_2 \right) \right] e^{-2\pi y}$  (16)

and  $S_y(\omega) = \frac{q^2 u}{\omega \epsilon a_2} \left[ m_1 + \eta \left( m_1 \xi + \frac{a_1 f_1}{a} + g_1 \right) \right] e^{-2\pi y}$  (17)

with the help of (11) and (13).

When  $y < 0$ ,  $S_x(\omega) = \frac{q^2 u}{\omega \epsilon a_2} \left[ \frac{a_1 l_2}{a} + m_2 - \eta \left( m_2 \xi + \frac{a_1 f_2}{a} + g_2 \right) \right] e^{2\pi y}$  (18)

and  $S_y(\omega) = \frac{q^2 u}{\omega \epsilon a_2} \left[ m_1 - \eta \left( m_1 \xi + \frac{a_1 f_1}{a} + g_1 \right) \right] e^{2\pi y}$  (19)

with the help of (11) and (14). Here  $S_y(\omega)$  is in the negative direction of  $y$ -axis.

It is of interest to examine the angular distribution of the radiated energy. The angles between the direction of motion of the line charge and the Čerenkov rays are given by

$$\tan \theta_1 = \frac{S_y(\omega)}{S_x(\omega)} = \frac{u\alpha}{\omega} [1 + \eta\xi_1] \quad \dots \quad (20)$$

and

$$\tan \theta_2 = \frac{u\alpha}{\omega} [1 - \eta\xi_1] \quad (21)$$

according as

$$y > 0 \text{ or } y < 0.$$

Here

$$\xi_1 = \frac{1}{m_1} \left[ m_1\xi + \frac{a_1 f_1}{a} + g_1 - \frac{u\alpha}{\omega m_1} \left( m_2\xi + \frac{a_1 f_2}{a} + g_2 \right) \right].$$

From (20) and (21) it is clear that the intensities of radiation in the two zones of  $y$  make different angles with the line of the moving source.

# CONCLUSION

The equations of electromagnetic intensities and the radiated energy reveal that they are exponentially damped with  $y$ . Since  $\eta$  is very small, the penetration depth  $1/\alpha$  is fairly large and consequently attenuation takes place very slowly. Collisions of electrons are mainly responsible for damping when  $\alpha^2 > 0$ . It is interesting to note that there will be no discrimination in the absolute values of field components, radiation and angular distribution for positive and negative zones of  $y$  unless collisions of electrons are taken into account.

From the equations of (11), (13) and (14) we see that outgoing plane waves will propagate so long as  $\alpha^2 > 0$ . This Čerenkov like condition introduces a cut-off in frequency. In Čerenkov region, i.e., where  $\mu\epsilon\beta^2 - 1 > 0$ , ( $\beta = u/c$ ),  $\alpha^2 < 0$  when  $\omega_1 < \omega < \omega_2$  and consequently there will be almost no wave propagation. The values of  $\omega_1$  and  $\omega_2$  are given by

$$(\omega_2^2, \omega_1^2) = \frac{\{\mu\epsilon\beta^2(2\omega_p^2 + \omega_c^2)\omega_p^2 + \omega_c^2\} \pm \sqrt{[\{\mu\epsilon\beta^2(2\omega_p^2 + \omega_c^2) + \omega_p^2 + \omega_c^2\}^2 - 4\mu\epsilon\beta^2\omega_p^2(\mu\epsilon\beta^2 - 1)]}}{2(\mu\epsilon\beta^2 - 1)}$$

respectively. In the non-Čerenkov region, i.e., where  $\mu\epsilon\beta^2 - 1 < 0$ , the wave propagation as well as emission of radiation exist, if

$$\omega^2 > \frac{\sqrt{[\{\mu\epsilon\beta^2(2\omega_p^2 + \omega_c^2) + \omega_p^2 + \omega_c^2\}^2 - 4\mu\epsilon\beta^2\omega_p^2(1 - \mu\epsilon\beta^2)]} - \{\mu\epsilon\beta^2(2\omega_p^2 + \omega_c^2) + \omega_p^2 + \omega_c^2\}}{2(1 - \mu\epsilon\beta^2)}$$

Those are not in accord with the usual Čerenkov phenomenon.

Here

$$\begin{aligned}
 m_1 &= \frac{h_2}{a h_1} (a^2 + a_1^2), \quad l_2 = \frac{\mu \epsilon}{c^2} \frac{u a_1}{\omega a} \frac{h_2}{h_1}, \\
 m_2 &= \frac{u}{\omega} \frac{h_2}{h_1} \left( \frac{w^2}{u^2} - a_1^2 \right), \quad a_2 = \frac{h_2}{\omega^2 h_1^2}, \\
 f_1 &= h_4 - \frac{a_1}{a} h_5 - \frac{\omega_c \omega_p^2}{u h_1} \xi, \quad g_1 = \frac{a h_2}{h_1} \xi - \frac{a_1}{a} h_4 - h_5, \\
 f_2 &= \frac{\omega_p^2 (\omega^2 + \omega_c^2)}{u h_1^2} + \frac{a_1}{a} h_6 + \frac{\omega_c \omega_p^2 a}{\omega h_1} \xi - \frac{2 h_2 \omega^2 h_7}{u}, \\
 g_2 &= h_6 + \frac{\omega}{u} \frac{h_2}{h_1} \xi + \frac{2 \omega_c \omega_p^2}{a u^2} h_7, \\
 h_4 &= \frac{b}{2a} \frac{h_2}{h_1} + \frac{a \omega_p^2 (\omega^2 + \omega_c^2)}{\omega h_1^2} - 2a \omega h_2 h_7, \quad h_5 = \frac{2 \omega \omega_c \omega_p^2}{u} - \left( \frac{1}{h_1^2} + h_7 \right), \\
 h_6 &= -\frac{\omega_c \omega_p^2}{h_1} \left( \frac{2a}{h_1} - \frac{b}{2a \omega} \right) + 2a \omega_c \omega_p^2 h_7, \quad h_7 = \frac{\omega_p^2 (\omega^2 + \omega_c^2 - \omega_p^2)}{h_1^2 h_3}.
 \end{aligned} \tag{15}$$

#### THE NATURE OF THE RADIATION

The power radiated by the moving source per unit time is

$$\begin{aligned}
 \vec{S} &= \frac{c}{4\pi} 2Re \int_{-\infty}^{\infty} (\vec{E} \times \vec{H}) dx \\
 &= cu Re \int_0^{\infty} (\vec{E}_w \times \vec{H}_w) d\omega.
 \end{aligned}$$

$$\text{When } y > 0, \quad S_x(\omega) = \frac{q^2 u}{\omega \epsilon a_2} \left[ \frac{a_1 l_2}{a} + m_2 + \eta \left( m_2 \xi + \frac{a_1 f_2}{a} + g_2 \right) \right] e^{-2\alpha y} \tag{16}$$

$$\text{and} \quad S_y(\omega) = \frac{q^2 u}{\omega \epsilon a_2} \left[ m_1 + \eta \left( m_1 \xi + \frac{a_1 f_1}{a} + g_1 \right) \right] e^{-2\alpha y} \tag{17}$$

with the help of (11) and (13)

$$\text{When } y < 0, \quad S_x(\omega) = \frac{q^2 u}{\omega \epsilon a_2} \left[ -\frac{a_1 l_2}{a} + m_2 - \eta \left( m_2 \xi + \frac{a_1 f_2}{a} + g_2 \right) \right] e^{2\alpha y} \tag{18}$$

$$\text{and} \quad S_y(\omega) = \frac{q^2 u}{\omega \epsilon a_2} \left[ m_1 - \eta (m_1 \xi + \frac{a_1 f_1}{a} + g_1) \right] e^{2\alpha y} \tag{19}$$

with the help of (11) and (14). Here  $S_y(\omega)$  is in the negative direction of  $y$ -axis.



It is of interest to examine the angular distribution of the radiated energy. The angles between the direction of motion of the line charge and the Čherenkov rays are given by

$$\tan \theta_1 = \frac{S_y(\omega)}{S_x(\omega)} = \frac{ua}{\omega} [1 + \eta \xi_1] \quad \dots \quad (20)$$

and

$$\tan \theta_2 = \frac{ua}{\omega} [1 - \eta \xi_1] \quad \dots \quad (21)$$

according as

$$y > 0 \text{ or } y < 0.$$

Here

$$\xi_1 = \frac{1}{m_1} \left[ m_1 \xi + \frac{a_1 f_1}{a} + g_1 - \frac{ua}{\omega m_1} \left( m_2 \xi + \frac{a_1 f_2}{a} + g_2 \right) \right].$$

From (20) and (21) it is clear that the intensities of radiation in the two zones of  $y$  make different angles with the line of the moving source.

# CONCLUSION

The equations of electromagnetic intensities and the radiated energy reveal that they are exponentially damped with  $y$ . Since  $\eta$  is very small, the penetration depth  $1/\alpha$  is fairly large and consequently attenuation takes place very slowly. Collisions of electrons are mainly responsible for damping when  $a^2 > 0$ . It is interesting to note that there will be no discrimination in the absolute values of field components, radiation and angular distribution for positive and negative zones of  $y$  unless collisions of electrons are taken into account.

From the equations of (11), (13) and (14) we see that outgoing plane waves will propagate so long as  $a^2 > 0$ . This Čherenkov like condition introduces a cut-off in frequency. In Čherenkov region, i.e., where  $\mu\epsilon\beta^2 - 1 > 0$ , ( $\beta = u/c$ ),  $a^2 < 0$  when  $\omega_1 < \omega < \omega_2$  and consequently there will be almost no wave propagation. The values of  $\omega_1$  and  $\omega_2$  are given by

$$(\omega_2^2, \omega_1^2) = \frac{\{\mu\epsilon\beta^2(2\omega_p^2 + \omega_c^2)\omega_p^2 + \omega_c^2\} \pm \sqrt{[\{\mu\epsilon\beta^2(2\omega_p^2 + \omega_c^2) + \omega_p^2 + \omega_c^2\}^2 - 4\mu\epsilon\beta^2\omega_p^2(\mu\epsilon\beta^2 - 1)]}}{2(\mu\epsilon\beta^2 - 1)}$$

respectively. In the non-Čherenkov region, i.e., where  $\mu\epsilon\beta^2 - 1 < 0$ , the wave propagation as well as emission of radiation exist, if

$$\frac{\sqrt{[\{\mu\epsilon\beta^2(2\omega_p^2 + \omega_c^2) + \omega_p^2 + \omega_c^2\}^2 + 4\mu\epsilon\beta^2\omega_p^2(1 - \mu\epsilon\beta^2)] - \{\mu\epsilon\beta^2(2\omega_p^2 + \omega_c^2) + \omega_p^2 + \omega_c^2\}}}{2(1 - \mu\epsilon\beta^2)}$$

These are not in accord with the usual Čherenkov phenomenon.

It is evident from the expressions of electro-magnetic intensities that at a particular frequency radiation is more or less confined between two planes perpendicular to the wave planes parallel to  $(\omega x/u) - \gamma y = 0$  and  $(\omega x/u) + \gamma y = 0$ . One may compare it with the Čerenkov cone. If  $2\theta$  be the angle between the normals to the above planes, then  $\tan \theta \approx ua/\omega$  which is identical with  $\tan \theta_1$  or  $\tan \theta_2$  for the zero value of  $\eta$ .

If we put  $N = 0$  and  $\eta = 0$  in (17), (19), (20) and (21), then the interesting phenomena of Čerenkov radiation by a line charge in an infinite homogeneous dielectric medium are obtained. In this case  $S_y = (\mu\epsilon\beta^2 - 1)q^2/\epsilon$  and  $\tan \theta_1 = \tan \theta = \sqrt{\mu\epsilon\beta^2 - 1}$ . These results have been worked out by the author (1967) for a non-magnetic medium (when  $\mu = 1$ ).

#### REFERENCES

- Khan R. M. 1967 *Indian J. Phys.*, **41**, 226.  
 Kolomenskii A. A. 1956 *Dokl. Akad. Nauk, SSSR*, **106**, 982.  
 Majumdar S. K. 1961 *Proc. Phys. Soc.* **77**, 1100.  
 Tuan H. S. & Seshadri S. R. 1965 *IEEE, AP* **13**, 71.  
 Wait J. R. 1966 *Radio Science* **1**, 641.

## Dielectric function of degenerate plasma at relativistic temperatures

By P. MISRA\* AND K. C. ROY\*\*

*Physics Department, Ravenshaw College, Cuttack, India*

(Received 12 May 1970)

Expressions for the transverse and longitudinal dielectric functions of a degenerate plasma are obtained at relativistic temperatures. The nature of wave propagation is discussed and results compared to those obtained for a degenerate plasma at non-relativistic temperatures (Misra *et al* 1962, 1970).

### INTRODUCTION

Plasmas occurring in stars are at very high temperatures. The temperature of some of the stars is about  $10^8$  °K or even more. For such stars the charged particles constituting the plasma move with very high velocities. It was pointed out by Fowler (1926) that the density of particles in some of these stars (white dwarfs) is so high that even at the relativistic temperatures the plasma is considered as degenerate. Chandrasekhar (1957) studied the properties of such stars using relativistic Fermi-Dirac distribution law and evaluated the integrals using Sommerfeld's (1928) approximate method. Buti (1963) studied the properties of thermonuclear (non-degenerate) plasma using relativistic Boltzmann-Vlasov equation and Maxwell distribution law. Here we use relativistic Boltzmann-Vlasov equation with Fermi-Dirac equilibrium distribution law to obtain explicit expressions for dielectric functions of a degenerate relativistic plasma, evaluating the integrals by Sommerfeld's approximate method.

### DIELECTRIC FUNCTION FROM RELATIVISTIC BOLTZMANN-VLASOV EQUATION

In this section we shall derive formulae for the dielectric function of a relativistic plasma. The relativistic Boltzmann-Vlasov equation is

$$\frac{\partial f(\vec{r}, \vec{p}, t)}{\partial t} + \frac{c \vec{p}}{(p^2 + m^2 c^2)^{3/2}} \cdot \vec{\nabla}_r f(\vec{r}, \vec{p}, t) - e \vec{E}(\vec{r}, t) \cdot \vec{\nabla}_p f = 0 \quad \dots (1)$$

writing  $f(\vec{r}, \vec{p}, t) = n_0 f_0(\vec{p}) + f_1(\vec{r}, \vec{p}, t)$  we obtain the following linearized relativistic B. V. equation :

$$\begin{aligned} \frac{\partial f_1(\vec{r}, \vec{p}, t)}{\partial t} + \frac{c \vec{p}}{(p^2 + m^2 c^2)^{3/2}} \cdot \vec{\nabla}_r f_1(\vec{r}, \vec{p}, t) \\ = n_0 e \vec{E}(\vec{r}, t) \cdot \vec{\nabla}_p f_0(\vec{p}) \end{aligned} \quad \dots (2)$$

---

Present address : \*Samanta Chandra Sekhar College, Puri, Orissa.

\*\*Anugul College, Anugul, Orissa.

A solution is easily obtained by taking the momentum Fourier transform in polar co-ordinates  $(p, \theta, \phi)$  for  $\vec{p}$

$$f_1(\vec{k}, \vec{p}, \omega) = \frac{ien_0 \frac{df_0}{dp} (p^2 + m^2 c^2)^{\frac{1}{2}}}{\omega(p^2 + m^2 c^2)^{\frac{1}{2}} - c p k \cos \theta} \times [E_1 \sin \theta \cos \phi + E_2 \sin \theta \sin \phi + E_3 \cos \theta] \quad \dots (3)$$

The wave number and frequency dependent current density can be expressed as (Gartenhaus 1964)

$$J_a(\vec{k}, \omega) = -ec \int \frac{d\vec{p}}{(p^2 + m^2 c^2)^{\frac{1}{2}}} f_1(\vec{k}, \vec{p}, \omega) \\ \equiv K_{a\beta}(\vec{k}, \omega) E_\beta(\vec{k}, \omega) \quad \dots (4)$$

Using equation (3) in equation (4) we got the following expressions for the transverse and longitudinal response functions

$$K_{tt}(\vec{k}, \omega) = -\frac{i\omega_0^2 c m \omega}{2} \int_0^\infty \int_0^1 \frac{p^3 dp dx (p^2 + m^2 c^2)^{\frac{1}{2}} (1-x^2) \frac{df_0}{dp}}{\omega^2 (p^2 + m^2 c^2)^{\frac{1}{2}} - c^2 p^2 k^2 x^2} \quad \dots (5)$$

and

$$K_{ll}(\vec{k}, \omega) = -i\omega_0^2 c m \omega \int_0^\infty \int_0^1 \frac{p^3 dp dx (p^2 + m^2 c^2)^{\frac{1}{2}} x^2 \frac{df_0}{dp}}{\omega^2 (p^2 + m^2 c^2)^{\frac{1}{2}} - c^2 p^2 k^2 x^2} \quad \dots (6)$$

where

$$\omega_0^2 = \frac{4\pi n_0 e^2}{m} \quad \text{and} \quad x = \cos \theta$$

#### COMPUTATION OF DIELECTRIC FUNCTION FOR RELATIVISTIC FERMI-DIRAC DISTRIBUTION

For relativistic Fermi distribution we shall use

$$n_0 f_0 = \frac{2}{h^3} \frac{1}{\Lambda \exp \left[ \frac{c}{KT} (p^2 + m^2 c^2)^{\frac{1}{2}} \right] + 1} \quad \dots (7)$$

where

$$\frac{1}{\Lambda} = \exp \left[ - \left( \nu + \frac{mc^2}{KT} \right) \right]$$

Expression (5) directly gives the imaginary part of the response function  $K_{tr}(k, \omega)$ ;

$$\text{Im} K_{tr}(\vec{k}, \omega) = \frac{\omega_0^2 z m^3 c \omega}{2 k^3 n_0 h^3 \Lambda} \int_0^\infty \frac{d\theta \operatorname{sh} \theta \exp(Z \operatorname{ch} \theta)}{\left[ \frac{1}{\Lambda} \exp(Z \operatorname{ch} \theta) + 1 \right]^2} \times \\ \left[ \operatorname{sh} 2\theta + \frac{c^2 k^2 \operatorname{sh}^2 \theta - \omega^2 \operatorname{ch}^2 \theta}{\omega c k} \ln \left| \frac{\omega \operatorname{ch} \theta + c k \operatorname{sh} \theta}{\omega \operatorname{ch} \theta - c k \operatorname{sh} \theta} \right| \right] \quad \dots (8)$$

After integrating by parts we get

$$\begin{aligned}\operatorname{Im} K_{\epsilon r}(\vec{k}, \omega) &= \frac{\omega_0^2 m^3 c \omega}{k^2 n_0 b^3 Z} \int_0^{\frac{1}{\Lambda}} \frac{du}{\exp(u)+1} \frac{d\phi(u)}{du} \\ &= \frac{\omega_0^2 m^3 c \omega}{k^2 n_0 b^3 Z} I\end{aligned}\quad (9)$$

where 
$$\frac{d\phi}{du} = \frac{1}{\sinh \theta} \left[ \operatorname{ch} 2\theta + \frac{c^2 k^2 - \omega^2}{\omega c k} \operatorname{sh} 2\theta \times \right.$$

$$\left. \ln \left| \frac{\omega \operatorname{ch} \theta + c k \operatorname{sh} \theta}{\omega \operatorname{ch} \theta - c k \operatorname{sh} \theta} \right| - 1 \right] \quad \dots \quad (10)$$

with

$$u = Z \operatorname{ch} \theta.$$

The integral contained in equation (9) is difficult to evaluate. However, in problems of similar nature a method due to Sommerfeld is extensively used. One expands the integrand round a *stable* value  $u_0 = Z \operatorname{ch} \theta_0$  as

$$I = \phi(u_0) + 2c_2 \phi''(u_0) \quad (11)$$

where

$$c_2 = \frac{\pi^2}{12}.$$

The higher terms of the series cannot be neglected if the ratio of the successive terms is greater than one. We shall study the typical cases at high temperatures when the series converges much faster. From equation (10) we get

$$\begin{aligned}\phi(u_0) &= Z \left[ \frac{\operatorname{sh} 2\theta_0}{2} + \frac{c^2 k^2 \operatorname{sh}^2 \theta_0 - \omega^2 \operatorname{ch}^2 \theta_0}{2ck\omega} \times \right. \\ &\quad \left. \ln \left| \frac{\omega \operatorname{ch} \theta_0 + ck \operatorname{sh} \theta_0}{\omega \operatorname{ch} \theta_0 - ck \operatorname{sh} \theta_0} \right| \right] \quad \dots \quad (12)\end{aligned}$$

and

$$\begin{aligned}\left( \frac{d^2 \phi}{du^2} \right)_{u=u_0} &= \frac{c^2 k^2 - \omega^2}{Zck\omega} \ln \left| \frac{\omega \operatorname{ch} \theta_0 + ck \operatorname{sh} \theta_0}{\omega \operatorname{ch} \theta_0 - ck \operatorname{sh} \theta_0} \right| \\ &+ \frac{2 \operatorname{ch} \theta_0}{Z \operatorname{sh} \theta_0} \left[ 1 + \frac{c^2 k^2 - \omega^2}{\omega^2 \operatorname{ch}^2 \theta_0 - c^2 k^2 \operatorname{sh}^2 \theta_0} \right] \quad \dots \quad (13)\end{aligned}$$

The response function is, from equations (11), (12) and (13)

$$\begin{aligned} \text{Im} K_r(\vec{k}, \omega) = & \frac{\omega_0^2 m^3 c \omega}{n_0 k^3 k^2} \left[ \frac{\text{sh} 2\theta_0}{2} + \frac{c^2 k^2 \text{sh}^2 \theta_0 - \omega^2 \text{ch}^2 \theta_0}{2\omega c k} \times \ln \left| \frac{\omega \text{ch} \theta_0 + c k \text{sh} \theta_0}{\text{ch} \theta_0 - c k \text{sh} \theta_0} \right| \right. \\ & \left. + \frac{\omega_0^2 m^3 c \pi^2 \omega}{6 n_0 k^3 k^2 Z^2} \left[ \frac{c^2 k^2 - \omega^2}{\omega c k} \ln \left| \frac{\omega \text{ch} \theta_0 + c k \text{sh} \theta_0}{\omega \text{ch} \theta_0 - c k \text{sh} \theta_0} \right| \right. \right. \\ & \left. \left. + \frac{2 \text{ch} \theta_0}{\text{sh} \theta_0} \left( 1 + \frac{c^2 k^2 - \omega^2}{\omega^2 \text{ch}^2 \theta_0 - c^2 k^2 \text{sh}^2 \theta_0} \right) \right] \right] \dots \quad (14) \end{aligned}$$

As already noted the formula (11) can be used only when the second term is small compared to the first. This corresponds to the condition

$$\begin{aligned} \pi^2 \left[ \frac{c^2 k^2 - \omega^2}{c k \omega} \ln \left| \frac{\omega \text{ch} \theta_0 + c k \text{sh} \theta_0}{\omega \text{ch} \theta_0 - c k \text{sh} \theta_0} \right| + \frac{2 \text{ch} \theta_0}{\text{sh} \theta_0} \left( 1 + \frac{c^2 k^2 - \omega^2}{\omega^2 \text{ch}^2 \theta_0 - c^2 k^2 \text{sh}^2 \theta_0} \right) \right] \\ \ll 3 Z^2 \left[ \text{sh} 2\theta_0 + \frac{c^2 k^2 \text{sh}^2 \theta_0 - \omega^2 \text{ch}^2 \theta_0}{\omega c k} \ln \left| \frac{\omega \text{ch} \theta_0 + c k \text{sh} \theta_0}{\omega \text{ch} \theta_0 - c k \text{sh} \theta_0} \right| \right] \quad (15) \end{aligned}$$

where  $\theta_0$  is related to the Fermi momentum by the relation

$$\text{sh} \theta_0 = p_0/mc.$$

The condition given in equation (15) is satisfied if

$$p_0 \gg mc$$

provided the temperature is such that

$$\frac{\pi^2 K^2 T^2}{3 c^2 p_0^2} < 1$$

For a relativistic plasma for which  $T > 10^8$  °K the above condition is fulfilled if the plasma is very dense, i.e.

$$n_0 \gg 10^{27}.$$

In other words the plasma becomes highly degenerate. For such a degenerate plasma with  $p_0 \gg mc$ , equation (14) simplifies to

$$\text{Im} K_r(\vec{k}, \omega) = \frac{3 \omega_0^2 \omega^2}{16 \pi c^2 k^3 v_0} \left( 1 + \frac{\pi^2 K^2 T^2}{3 c^2 m^2 v_0^2} \right) \left[ \frac{2 c k}{\omega} + \frac{c^2 k^2 - \omega^2}{\omega^2} \ln \left| \frac{\omega + c k}{\omega - c k} \right| \right]$$

from which we obtain

$$\begin{aligned} \epsilon_r(\vec{k}, \omega) = & 1 - \frac{3 \omega_0^2 \omega}{4 c^2 k^3 v_0} \left( 1 + \frac{\pi^2 K^2 T^2}{3 c^2 m^2 v_0^2} \right) \times \\ & \left[ \frac{2 c k}{\omega} + \frac{c^2 k^2 - \omega^2}{\omega^2} \ln \left| \frac{\omega + c k}{\omega - c k} \right| \right] \dots \quad (16) \end{aligned}$$

An expression for the longitudinal dielectric constant can be obtained by performing analogous computation for  $K_L(\vec{k}, \omega)$ . We shall not go into the details but give the final result as

$$\epsilon_L(\vec{k}, \omega) = 1 + \frac{3\omega_0^2\omega}{2c^2k^2v_0} \left[ 1 + \frac{\pi^2 K^2 T^2}{3m^2 c^2 v_0^2} \right] \times \left[ \frac{2ck}{\omega} - \ln \left| \frac{\omega + ck}{\omega - ck} \right| \right] \quad \dots (17)$$

When the effect of temperature is neglected, the above expressions for the dielectric constants reduce to that obtained by Silin (1960)

#### NATURE OF WAVE PROPAGATION

The analysis of wave propagation in a relativistic plasma is possible with the aid of an expression for the dielectric constant derived in the previous section. Certain interesting conclusions can be drawn without involving ourselves in complex algebraic manipulations, for certain limiting cases

##### Case I

$$\frac{ck}{\omega} < 1 \quad \text{i.e.,} \quad n \simeq \epsilon^{\frac{1}{2}} < 1$$

Under this condition  $\ln$  term in equations (16) and (17) can be expanded in a power series of  $n$  and after simple manipulation we get

$$\epsilon_T(\vec{k}, \omega) = \frac{1 - \frac{\omega_0^2 c}{v_0 \omega^2} \left[ 1 + \frac{\pi^2 K^2 T^2}{3c^2 m^2 v_0^2} \right]}{1 + \frac{\omega_0^2 c}{5\omega^2 v_0} \left[ 1 + \frac{\pi^2 K^2 T^2}{3c^2 m^2 v_0^2} \right]}$$

and

$$\epsilon_L(\vec{k}, \omega) = \frac{1 - \frac{\omega_0^2 c}{\omega^2 v_0} \left[ 1 + \frac{\pi^2 K^2 T^2}{3c^2 m^2 v_0^2} \right]}{1 + \frac{\omega_0^2 c}{5\omega^2 v_0} \left[ 1 + \frac{\pi^2 K^2 T^2}{3c^2 m^2 v_0^2} \right]}$$

It will be seen from the above expressions that both transverse and longitudinal waves can propagate in the plasma under consideration, if their frequency is greater than a limiting frequency, i.e. if

$$\omega > \omega_0 \left[ \frac{c}{v_0} \left( 1 + \frac{\pi^2 K^2 T^2}{3c^2 m^2 v_0^2} \right) \right]^{1/2} \quad \dots (18)$$

This is to be contrasted with that of wave propagation in a non-relativistic degenerate plasma for which wave propagation (Pradhan *et al* 1960, Misra *et al* 1962 and Misra *et al* 1970) is possible if

$$\omega > \omega_0 \left( 1 + \frac{3\pi^2 K^2 T^2}{4m^2 v_0^4} \right)^{1/2} \quad \dots (19)$$

It is interesting to note that if we put  $c = v_0$  in the equation (18) we get approximately the corresponding expression obtained for non-relativistic case,

*Case II*

$$\frac{ck}{\omega} > 1$$

$$\text{i.e., } \epsilon_l \simeq n_l > 1$$

Under this conditions equations (16) and (17) take the simple forms,

$$\epsilon_{tr}(\epsilon_{tr}-1) = -\frac{3\omega_0^2 c}{\omega^2 v_0} \left( 1 + \frac{\pi^2 K^2 T^2}{3m^2 c^2 v_0^2} \right)$$

and

$$\epsilon_l(\epsilon_l-1) = \frac{3\omega_0^2 c}{\omega^2 v_0} \left( 1 + \frac{\pi^2 K^2 T^2}{3m^2 c^2 v_0^2} \right)$$

It will be seen from these equations that longitudinal waves can propagate through the relativistic plasma, whereas, transverse waves cannot do so for  $n < 1$ . Similar results can be obtained for a degenerate non-relativistic plasma. (Misra *et al* 1962).

## ACKNOWLEDGEMENT

The authors are grateful to Prof T. Pradhan of Saha Institute of Nuclear Physics, Calcutta, for suggesting the problem and for guidance. They would also like to thank Sri B. C Roy, Department of Physics, Ravenshaw College for help and comments while the work was in progress.

## REFERENCES

- Buti B. 1963 *Phys. Fluids* **6**, 89.  
 Chandrasekhar S. 1957 *An Introduction to the Study of Stellar Structure*, Dover Publication Inc  
 Fowler R. H. 1926 *M. N.* **87**, 114.  
 Gartenhaus S. 1964 *Elements of Plasma Physics*, p. 107. Holt, Rinehart & Winston, New York.  
 Misra P. & Misra D. 1962 *Indian J. Phys.* **36**, 549.  
 Misra P. 1966 *Indian J. Phys.* **40**, 253  
 Misra P. & Roy S. K. 1969 *Indian J. Phys.* **43**, 534.  
 Pradhan T. & Misra P. 1960 *Phys. Rev.* **119**, 1878  
 Silin V. P. 1960 *Soviet Phys. JETP* **11**, 1130.  
 Sommerfeld A. Z. *Physik* **46**, 1.



# Free convection flow of elastico-viscous liquid from horizontal plate

SHANKAR PRASAD MISHRA

*Post-Graduate Department of Mathematics Utkal University, Orissa*

AND

JYOTIRMOY SINHA ROY

*Department of Applied Mathematics University College of Engineering  
Burla, Sambalpur, Orissa*

(Received 24 June 1970—Revised 12 April 1971)

The free convection flow of an elastico-viscous liquid from a horizontal plate has been studied in this paper. The type of wall temperature distribution and the boundary layer thickness which allow similarity solution are investigated. The effect of elasticity of the liquid and the Prandtl number on the velocity and temperature distributions and the rate of heat transfer from the plate has been studied.

## INTRODUCTION

The phenomenon of natural convection arises in a fluid when temperature changes cause density variations leading to buoyancy forces acting on the fluid elements. This process of heat transfer has many important technological applications. Therefore, in modern times there has been a noticeable increase in interest in free convection problems. Studies on laminar free convection flow and heat transfer of Newtonian fluids have been reported in literature. But little work in this direction seems to have been done in the case of non-Newtonian fluid. Recently, Mishra (1966) has studied the free convection flow of an elastico-viscous liquid past a hot vertical plate. In this paper our aim is to study the free convection flow of an elastico-viscous liquid from a horizontal plate. Similar problems in the Newtonian case have been studied by Sparrow & Minkowycz (1962), Gill & Casal (1962), Hauptmann (1965), Gill *et al* (1965). This problem in the presence of a magnetic field has been studied by Gupta (1966). Free convection flow of a second order fluid from a horizontal plate has been studied by Mishra (1968).

## BASIC EQUATIONS

The equations governing the elastico-viscous fluid model considered here consist of the constitutive equations

$$p_{ik} = -p g_{ik} + p'_{ik}, \quad \dots (1)$$

$$p'^{ik} = 2\eta_0 e^{ik} - 2k_0 \tilde{e}^{ik}, \quad \dots (2)$$

The equations of motion and continuity are

$$\rho \left[ \frac{\partial v^i}{\partial t} + v^j v^i_{,j} \right] = F_i - p_{,i} + p'_{,i} \quad \dots \quad (3)$$

and

$$v_{i,t} = 0. \quad \dots \quad (4)$$

In these equations the term  $\tilde{e}^{ik}$  appearing in (2) is given by

$$\tilde{e}^{ik} = \frac{\partial e^{ik}}{\partial t} + v^m e_{,m}^{ik} - v_{,m}^k e^{im} - v_{,m}^i e^{mk}$$

is the convected derivative of the rate-of-strain tensor  $e^{ik}$  and is defined as

$$2e_{ik} = v_{i,k} + v_{k,i},$$

$v^i$  being the velocity vector,  $p$  is the mean pressure,  $\rho$  is the density of the medium,  $F_i$  is the body force per unit mass in the  $i$ -th direction and  $p_{ik}$  is the stress tensor. The limiting viscosity at small rates of shear is

$$\eta_0 = \int_0^\infty N(\lambda) d\lambda$$

$N(\lambda)$  being the relaxation spectrum as introduced by Walters (1960), and  $g_{ik}$  is the metric tensor of a fixed coordinate system  $x^i$ . This idealized model (2) is a valid approximation of Walter's liquid  $B'$  taking very short memory into account such that terms involving

$$\int_0^\infty \lambda^n N(\lambda) d\lambda \quad (n \geq 2)$$

have been neglected and

$$k_0 = \int_0^\infty \lambda N(\lambda) d\lambda.$$

A detailed description of the model has been given by Walters & Beard (1964). The energy equation, neglecting the dissipation term, which is justified for slow motion as in the case of free convection flow, is

$$u \frac{\partial T}{\partial x} + v \frac{\partial T}{\partial y} = \alpha \frac{\partial^2 T}{\partial y^2}, \quad \dots \quad (5)$$

where  $T$  is the temperature and  $\alpha$  is the thermal diffusivity.

#### BOUNDARY LAYER EQUATIONS

In free convection problems, the thickness of the layer, in which the temperature and velocity differ appreciably from the values at infinity, is found to be small compared with the length of the plate; hence the approximation of the boundary layer theory will be valid. Recently, Beard & Walters (1964) have obtained the boundary layer equations for this class of fluid. Within the boundary layer  $u, \partial u / \partial x, \partial^2 u / \partial x^2, \partial p / \partial x$  are assumed to be of the order unity and  $y$  to be of the order

of the boundary layer thickness. From the equation of continuity (4) we get the  $y$ -component of the velocity to be of the order of the boundary layer thickness. In order that the viscous, elastico-viscous and inertia terms in the modified equations of motion be of the same order of magnitude, it is necessary that

$$\nu = O(\delta^2) \quad \text{and} \quad k_0^* = O(\delta^2)$$

where

$$\nu = \eta_0/\rho \quad \text{and} \quad k_0^* = k_0/\rho.$$

Under these conditions, equations of motion give

$$u \frac{\partial u}{\partial x} + v \frac{\partial u}{\partial y} = F_x - \frac{1}{\rho} \frac{\partial p}{\partial x} + \nu \frac{\partial^2 u}{\partial y^2} - k_0^* \left[ \frac{\partial u}{\partial y} \frac{\partial^2 v}{\partial y^2} + v \frac{\partial^3 u}{\partial y^3} + \frac{\partial}{\partial x} \left( u \frac{\partial^2 u}{\partial y^2} \right) \right], \quad \dots (7)$$

$$0 = F_y - 1/\rho \cdot \partial p / \partial y, \quad \dots (8)$$

$$\text{with the equation of continuity} \quad \partial u / \partial x + \partial v / \partial y = 0 \quad \dots (8a)$$

In the present problem  $F_x = 0$  and  $F_y = -g$ , the acceleration due to gravity, since we study free convection flow from a horizontal plate. We are concerned with the velocity and temperature distributions in the boundary layer over the plate

#### SOLUTION OF EQUATIONS

Since the ambient fluid is at rest, from equation (7) we get

$$\frac{\partial p_\infty}{\partial x} = 0, \quad \dots (9)$$

where the subscript  $\infty$  refers to ambient state. The equation of state is

$$\rho = \rho_\infty [1 - \beta(T - T_\infty)], \quad \dots (10)$$

where  $\beta$ , the coefficient of volume expansion is assumed constant. Hence equation (8) gives

$$-\frac{\partial p}{\partial y} = \rho_\infty g [1 - \beta(T - T_\infty)], \quad \dots (11)$$

which when differentiated with respect to  $x$  gives

$$\frac{\partial^2 p}{\partial x \partial y} = \rho_\infty g \beta \frac{\partial}{\partial x} (T - T_\infty). \quad \dots (12)$$

Integration of equation (12) with respect to  $y$  from  $y$  to  $\delta$  and subsequent use of equation (8) yields.

$$\frac{\partial p}{\partial x} = -\rho_\infty g \beta \int_y^\delta \frac{\partial}{\partial x} (T - T_\infty) dy, \quad \dots (13)$$

where condition at infinity is replaced by the condition at the outer edge of the boundary layer. Substitution of equation (13) in equation (7) leads to

$$u \frac{\partial u}{\partial x} + v \frac{\partial u}{\partial y} = \beta g \frac{\partial}{\partial x} \int_y^\delta (T - T_\infty) dy + \nu \frac{\partial^2 u}{\partial y^2} - k_0^* \left[ \frac{\partial u}{\partial y} \frac{\partial^2 v}{\partial y^2} + v \frac{\partial^3 u}{\partial y^3} + \frac{\partial}{\partial x} \left( u \frac{\partial^2 u}{\partial y^2} \right) \right], \quad \dots \quad (14)$$

where  $\nu = \eta_0 / \rho_\infty$ . This, along with equation (5) and (6) constitute the basic equations of the problem which are to be solved subject to

$$u = v = 0, \quad T = T_w \quad \text{at} \quad y = 0 \quad ] \quad \dots \quad (15)$$

$$u = \frac{\partial u}{\partial y} = 0, \quad T = T_\infty \quad \text{at} \quad y = \delta \quad \dots \quad (16)$$

We solve the boundary layer equation and energy equation by an integral method similar to that of Karman & Pohlhausen. Integration of equation (14) with respect to  $y$  from 0 to  $\delta$  and use of equation (6) lead to

$$\begin{aligned} \frac{\partial}{\partial x} \int_0^\delta u^2 dy &= -\nu \left( \frac{\partial u}{\partial y} \right)_w + \beta g \frac{\partial}{\partial x} \left[ (T_w - T_\infty) \int_0^\delta \frac{(T - T_\infty)}{(T_w - T_\infty)} dy \right] \\ k_0^* &- \left[ \frac{\partial}{\partial x} \int_0^\delta \left( \frac{\partial u}{\partial y} \right)^2 dy + \left( \frac{\partial u}{\partial y} \frac{\partial u}{\partial x} \right)_w + \left( v \frac{\partial^2 u}{\partial y^2} \right)_\delta + 2 \int_0^\delta \frac{\partial u}{\partial x} \frac{\partial^2 u}{\partial y^2} dy \right] \end{aligned} \quad (17)$$

Assuming

$$\theta = \frac{T - T_\infty}{T_w - T_\infty} \quad \text{and} \quad T_w - T_\infty = Nx^n, \quad (18)$$

equation (5) can be written as

$$u \frac{\partial \theta}{\partial x} + v \frac{\partial \theta}{\partial y} + \frac{nu\theta}{x} = \alpha \frac{\partial^2 \theta}{\partial y^2} \quad (19)$$

which when integrated with respect to  $y$  from 0 to  $\delta$  gives

$$\frac{\partial}{\partial x} \int_0^\delta u \theta dy = -\alpha \frac{\partial \theta}{\partial y} - \frac{n}{x} \int_0^\delta u \theta dy \quad (20)$$

We take simple profiles for  $u$  and  $\theta$  satisfying equations (15) and (16) as

$$u = u_1(x) \frac{y}{\delta} \left[ 1 - \frac{y}{\delta} \right]^2 \quad (21)$$

$$\theta = \left[ 1 - \frac{y}{\delta} \right]^2 \quad (22)$$

Substitution of equations (21) and (22) leads to

$$\frac{d}{dx} \left[ \frac{\delta u_1^2}{105} \right] = -\frac{\nu u_1}{\delta} + \frac{1}{12} \beta g N \frac{d}{dx} \left[ x^n \delta^2 \right] - \frac{k_0^*}{10} \left[ \frac{u_1^2}{\delta} \frac{d\delta}{dx} - \frac{7u_1}{\delta} \frac{du_1}{dx} \right] \dots \quad (23)$$

and

$$\frac{1}{30} \left[ \delta \frac{du_1}{dx} + u_1 \frac{d\delta}{dx} \right] = \frac{2\alpha}{\delta} - \frac{\nu u_1 \delta}{30x} \dots \quad (24)$$

Let

$$u_1 = C_1 x^m \quad \text{and} \quad \delta = C_2 x^l, \dots \quad (25)$$

so that equations (23) and (24) become

$$\begin{aligned} \frac{C_1^2 C_2}{105} (l+2m)x^{2m+l-1} &= -\frac{\nu C_1}{C_2} x^{m-l} + \frac{1}{12} \beta g N C_2^2 (2l+n)x^{2l+n-1} \\ &- \frac{k_0^*}{10} \frac{C_1^2}{C_2} (l-7m)x^{2m-l-1} \dots \end{aligned} \quad (26)$$

$$\frac{1}{30} C_1 C_2 (l+m)x^{l+m-1} = \frac{2\alpha}{C_2} x^{-l} - \frac{n C_1 C_2}{30} x^{l+m-1}, \dots \quad (27)$$

Since these equations are valid for all values of  $x$

$$\left. \begin{aligned} 2m+l-1 &= m-l = 2l+n-1 = 2m-l-1 \\ l+m-1 &= -l \end{aligned} \right\} \dots \quad (28)$$

which leads to

$$m = 1, \quad l = 0, \quad n = 2. \dots \quad (29)$$

It is interesting to note that a similarity solution is possible only if the difference between the wall and ambient temperatures varies as the square of the distance from the leading edge along the plate and the boundary layer thickness is uniform all through. Substituting the values of  $l$ ,  $m$  and  $n$  into equations (26) and (27) we get

$$\frac{2}{105} C_1^2 C_2 = -\frac{\nu C_1}{C_2} + \frac{1}{6} \beta g N C_2^2 + \frac{7k_0^* C_1^2}{10C_2}, \quad (30)$$

$$C_1 C_2^2 = 20\alpha. \quad (31)$$

Elimination of  $C_1$  between (30) and (31) gives

$$\lambda^7 - (21P_r + 8)\lambda^2 + R_e = 0 \quad (32)$$

whc

$$\lambda = \left[ \frac{7\beta g N}{40\alpha^2} \right]^{1/5} C_2; \quad R_e = 294k_0^* \left[ \frac{7\beta g N}{40\alpha^2} \right]^{2/5}$$

and  $P_r$  is the Prandtl number  $\nu/\alpha$ . We take in this problem  $P_r = 1/3, 2, 12$ , and 32 so that the equation (32) reduces to

$$\lambda^7 - 15\lambda^2 + R_e = 0 \quad \dots (32a)$$

$$\lambda^7 - 50\lambda^2 + R_e = 0 \quad \dots (33b)$$

$$\lambda^7 - 260\lambda^2 + R_e = 0 \quad \dots (33c)$$

$$\lambda^7 - 680\lambda^2 + R_e = 0 \quad \dots (33d)$$

These equations can have at best two positive roots and one negative root and four roots are imaginary. Negative and the imaginary roots are not to be considered. Table 1 shows the values of  $\lambda$  for different values of  $R_e$  and  $P_r$ . For the viscous case one root is 0.00 which is discarded since the boundary layer thickness is not zero and the roots in the elastico-viscous case which are in correspondence with this root are therefore discarded. Table 1 shows that the boundary layer thickness

TABLE 1. Values of  $\lambda$  for different values of  $P_r$  and  $R_e$ .

$R_e \backslash P_r$	1/3	2	12	32
0.0	1.7187	2.2034	3.0174	3.6944
0.5	1.7123	2.2021	3.0173	3.6943
1.0	1.7062	2.2009	3.0172	3.6943
1.5	1.7035	2.1996	3.0170	3.6942

decreases with the increase in the value of the elastic number. This result agrees with the result by Beard & Walters (1964) but contradicts that by Rajeswari & Rathna (1962). This is because in the Rivlin-Ericksen fluid model the latter authors have taken the memory coefficient to be positive which should be, in fact, negative, as has been proved by Coleman & Markovitz (1964). Davis (1966) has also made the same remark in his paper. But the boundary layer thickness increases with the increase in the value of Prandtl number. With the help of (31) we have

$$\frac{C_1}{20\alpha} \left[ \frac{40\alpha^2}{7\beta g N} \right]^{2/5} = C_1^* = \frac{1}{\lambda_2}$$

Table 2 shows that the value of  $C_1^*$  goes on increasing with the increase in elastic number but decreases as the Prandtl number increases.

Equations (21) and (22) can be written in the forms

$$\frac{u^*}{x^*} = \frac{y^*}{\lambda^3} \left[ 1 - \frac{y^*}{\lambda} \right]^2 \quad \text{and} \quad \theta = \left[ 1 - \frac{y^*}{\lambda} \right]^2 \quad \dots (34)$$

TABLE 2. Values of  $C_1^*$  for different values of  $P_r$  and  $R_0$ 

$R_0 \backslash P_r$	1/3	2	12	32
0.0	0.3385	0.2059	0.1008	0.0734
0.5	0.3411	0.2062	0.1098	0.0734
1.0	0.3435	0.2064	0.1098	0.0734
1.5	0.3447	0.2066	0.1099	0.0735

where

$$x^* = x \left[ \frac{7\beta g N}{40\alpha^2} \right]^{1/5}; \quad y^* = y \left[ \frac{7\beta g N}{40\alpha^2} \right]^{1/5} \quad u^* = \left( \frac{u}{20\alpha} \right) \left[ \frac{40\alpha^2}{7\beta g N} \right]^{1/5}$$

The rate of heat transfer at the wall is given by

$$q = -k \left( \frac{\partial T}{\partial y} \right)_w = \frac{2k(T_w - T_\infty)}{C_2} = \frac{2kNx^2}{C_2}$$

so that the Nusselt number  $N_{u,w} = 2x/C_2 = 2x^*/\lambda$ . ... (35)

Since  $\lambda$  decreases with the increase in the value of the elastic number, the Nusselt number clearly increases with the increase of the elasticity of the liquid. Also, since  $\lambda$  increases with the increase in the value of  $P_r$ , the Nusselt number decreases as Prandtl number increases. Table 3 represents the computed values of  $u^*/x^*$  and  $\theta$ . This table shows that the velocity at any point within a thin liquid layer near the plate increases with the increase in the value of the elastic number. But outside this layer up to the edge of the boundary layer the velocity decreases with the increase in the value of the elastic number. This nature of the profile may be explained from a consideration of the conservation of the mass flux. Since the velocity increases in a thin layer near the plate due to the elasticity of the liquid, the velocity should decrease outside this layer. It can easily be seen from equation (34) that the minimum value of  $u^*$  occurs at  $y = 0$  and at  $y = \lambda$ , that is, at the plate and at the edge of the boundary layer. The maximum value of  $u^*$  occurs at  $\lambda/3$  and its value is  $4/27 \lambda^2$ . Figure 1 shows that the velocity at any point in the boundary layer decreases with the increase in the value of the Prandtl number. Table 4 shows that the elasticity of the liquid decreases with the temperature at any point in the boundary layer. Figure 2 shows that the temperature at any point in the boundary layer increases with the increase in the value of the Prandtl number.

TABLE 3. Velocity distribution for different values of  $R_e$ .  
 $P_r = 2$

$y^* \backslash R_e$	0.00	0.50	1.00
0.00	0.0000	0.0000	0.0000
0.10	0.0084	0.0085	0.0085
0.20	0.0153	0.0154	0.0155
0.30	0.0208	0.0209	0.0210
0.40	0.0249	0.0250	0.0251
0.50	0.0278	0.0279	0.0280
0.60	0.0295	0.0297	0.0298
0.70	0.0303	0.0305	0.0306
0.80	0.0302	0.0303	0.0304
0.90	0.0293	0.0294	0.0295
1.00	0.0278	0.0279	0.0280
1.10	0.0257	0.0258	0.0258
1.20	0.0232	0.0235	0.0233
1.30	0.0204	0.0204	0.0204
1.40	0.0174	0.0173	0.0173
1.50	0.0143	0.0142	0.0142
1.60	0.0112	0.0100	0.0100
1.70	0.0101	0.0091	0.0089
1.80	0.0080	0.0067	0.0062
1.90	0.0052	0.0043	0.0031
2.00	0.0016	0.0009	0.0006



TABLE 4. Temperature distribution for different values of  $R_c$ .  
 $P_r = 2$ .

$y^*$ \ $R_c$	0 0	0 5	1 0	1.5
0.0	1.0000	1.0000	1.0000	1.10000
0.1	0.9114	0.9112	0.9112	0.9110
0.2	0.8270	0.8266	0.8265	0.8262
0.3	0.7466	0.7461	0.7460	0.7456
0.4	0.6704	0.6697	0.6695	0.6691
0.5	0.5983	0.5975	0.5973	0.5967
0.6	0.5302	0.5294	0.5291	0.5285
0.7	0.4662	0.4653	0.4649	0.4644
0.8	0.4064	0.4055	0.4052	0.4044
0.9	0.3508	0.3497	0.3493	0.3486
1.0	0.2992	0.2981	0.2977	0.2970
1.1	0.2517	0.2506	0.2501	0.2495
1.2	0.2083	0.2072	0.2067	0.2061
1.3	0.1690	0.1676	0.1674	0.1668
1.4	0.1338	0.1327	0.1322	0.1317
1.5	0.1027	0.1017	0.1014	0.1008

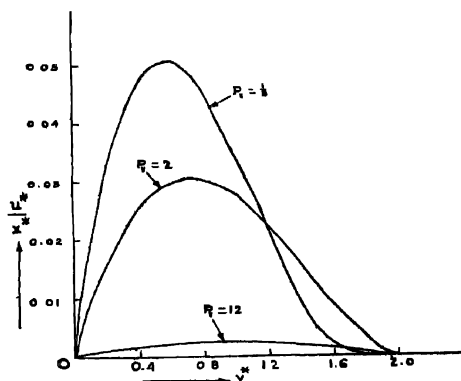


Figure 1. Velocity profiles for different Prandtl numbers.

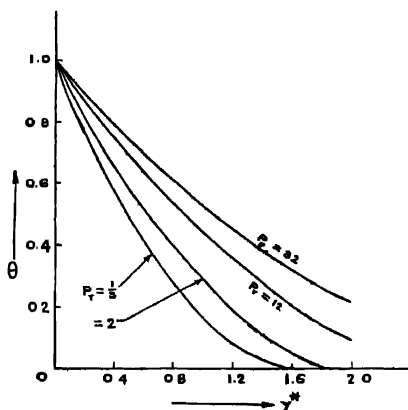


Figure 2 Temperature profiles for different Prandtl numbers.

Gupta (1966) has studied the problem of hydromagnetic free convection flows from a horizontal plate and has obtained the similarity solutions for the velocity and temperature fields. His conclusions are, for a uniform magnetic field

$$T_w - T_\infty = Nx^2; \quad u_1(x) = C_1x; \quad \delta = C_2$$

which we have obtained in our problem in (18), (25) and (29). This gives us an interesting result that the elasticity of the liquid plays some role similar to a magnetic field present at the plate. In this connection reference may also be made to another paper by Gupta (1962).

#### REFERENCES

- Beard D. W. & Walters K. 1964 *Proc. Camb. Phil. Soc.*, **60**, 667.  
 Coleman B. D. & Markovitz H. 1964 *The Physics of Fluids*, **7**, 833.  
 Davis M. H. 1966 *Zamp* **17**, 189.  
 Gill W. N. & Casal E. D. 1962 *J. Amer. Inst. Chem. Engrs.* **8**, 513.  
 Gill W. N., Zeh D. W. & Casal E. D. 1965 *ZAMP* **16**, 539.  
 Gupta A. S. 1962 *ZAMP* **13**, 324.  
 Gupta A. S. 1966 *AIAA Journal* **4**, 1439.  
 Hauptmann, E. G. 1965 *Inter. J. Heat Mass Transfer* **8**, 289.  
 Mishra S. P. 1966 *Indian Chemical Engineer (Trans)* **8**, 28.  
 Mishra S. P. 1966 *Proc. Ind. Acad. Sci.* **LXIV**, 291.  
 Mishra S. P. 1968 *Progress of Mathematics* **2**, 140.  
 Rajeswari G. K. & Rathna S. L. 1962 *ZAMP* **13**, 43.  
 Sparrow E. M. & Minkowycz W. J. 1962 *Inter. Heat Mass Transfer* **5**, 505.  
 Walters Kon 1960 *Quart. J. Mech. Appl. Math* **13**, 444.

## Measurement of the differential elastic scattering cross-section of 662 keV gamma rays in lead

By H. S. SAHOTA AND B. S. SOOD

*Department of Physics, Punjabi University, Patiala, India*

(Received 11 May 1970—Revised 22 December 1970)

Elastic scattering of 662keV gamma rays from cylindrical lead targets has been studied in order to investigate if the scatterer behaves as a homogeneous source of the scattered radiation. It has been observed that for targets with product of linear absorption coefficient and radius of the cylindrical target less than or equal to 0.65 this is essentially true.

The elastic scattering of gamma rays from lead has been studied at an angle  $120^\circ$  in order to verify the assumption (Singh *et al* 1963, Sahota *et al* 1966) that for small values of  $\mu r$  the scatterer behaves as a homogeneous source of radiation scattered from it. The angle  $120^\circ$  was chosen as the elastic scattering of 662 keV gamma rays at this angle consists mainly of Rayleigh scattering, the contribution of nuclear Thomson scattering being much smaller.

The differential cross section of elastic scattering has been measured using a conventional experimental arrangement (Anand & Sood 1965). Gamma rays of 662 keV energy were obtained from a 200mc radioactive source of  $\text{Cs}^{137}$ . The scatterers were in the form of cylinders of different radii but having the same length of 8cm. The elastically scattered gamma rays were counted in a single channel gamma ray spectrometer with a  $5.1\text{ cm} \times 4.4\text{ cm}$  NaI(Tl) crystal. Lead shielding was used to prevent direct radiations from the source reaching the counter. Detector and source were also well shielded to prevent the scattering from walls and surroundings of the detector. Scattering from the scatterer consists mainly of the following :

1. Compton scattering from free and stationary electrons described by Klein & Nishina (1929) .
2. Inelastic scattering from bound electrons having a continuous range of energy extending upto the incident energy minus the binding energy.
3. Elastic scattering having the same energy as that of incident gamma rays.

The separation of the elastic scattering from inelastic scattering was achieved from an analysis of the spectrum of scattered radiation as shown in figure 1. Different fractions of the direct spectrum of 662 keV radiations from a  $\text{Cs}^{137}$  source were subtracted from the elastically scattered spectrum. A lead filter of  $3\text{ gm/cm}^2$  would give the difference spectrum as shown by C. The filter thickness

is sufficient to give a good elastically scattered peak through preferential absorption of  $\gamma$ -rays in lead. The channels were selected to cover a part of the photopeak without appreciable contribution from incoherent scattering events.

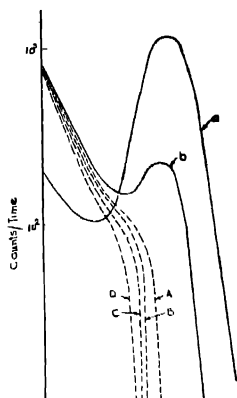


Figure 1. Analysis of elastically scattered spectrum when lead is irradiated with 662keV gamma rays for,  $\theta = 120^\circ$ . (a) Direct spectrum, (b) Elastically scattered spectrum

The determination of differential elastic scattering crosssection with the arrangement described above is done by comparing the counts per unit time in counting rate  $n_a$  in case of coherent scattering is

$$n_a = \frac{s_1}{4\pi} \omega_1 n \frac{d\sigma}{d\Omega} \omega_2 \epsilon_\gamma A, \quad (1)$$

where  $\omega_1$  and  $\omega_2$  are source scatterer and scatterer detector solid angles,  $\frac{d\sigma}{d\Omega}$  is the differential elastic scattering crosssection at the particular angle,  $n$  is the number of target atoms per unit area and  $\epsilon_\gamma A$ , is the effective photopeak efficiency for detection of 662 keV gamma rays. When the scatterer is replaced by a small  $\text{Cs}^{137}$  source  $s_2$ , the number of counts per unit time in the same channels is,

$$n_b = s_2/4\pi \cdot \omega_2 \epsilon_\gamma A, \quad \dots (2)$$

From (1) and (2)

$$d\sigma = n_a/n_b \cdot s_2/s_1 \cdot 1/\omega_1 \cdot 1/n \quad \dots (3)$$

Therefore  $\frac{d\sigma}{d\Omega}$  can be determined if the ratios  $n_a/n_b$ ,  $s_2/s_1$  and the values of  $\omega_1$  and  $n$  are known. The ratio  $n_a/n_b$  was determined from several runs of the experiment on ascertaining the stability of the equipment regarding the shifting of photoppeak after every run. For  $n_b$  the counts were taken for at least three positions of the source to cover the whole size of the cylindrical target. The difference in the counting rate was always within statistical accuracies. The ratio of the source strengths  $s_2/s_1$  was determined by comparing the areas under the photo-peaks in the same geometry. A number of intermediate sources were used as the two sources differed widely in strengths. The accuracy was better than two percent.  $n$  was determined from measurements of dimensions of the target. Measurement of  $\omega_1$  involved size of the target and its distance from the source.

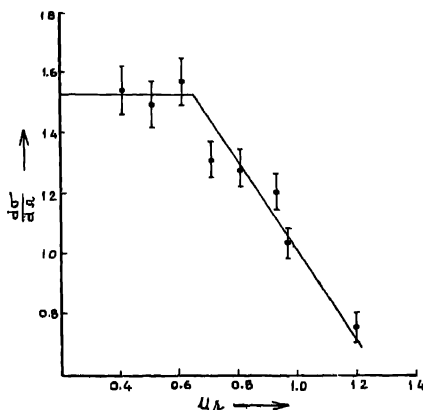


Figure 2. Plot of differential elastic scattering cross section  $d\sigma/d\Omega$  vs  $\mu r$ .

To correct for the absorption in the target due to the radiation incident on and emerging from the target, the formula given by Evans & Evans (1948) for self absorption of  $\gamma$ -rays in the homogeneous source has been used. From a plot of  $d\sigma/d\Omega$  versus  $\mu r$  in figure 2, we observe that the results obtained remain constant within the experimental error upto a value of the product  $\mu r$  equal to 0.65, after which there is a systematic trend in the cross section to fall with the increase in the value of  $\mu r$ . The average value of the cross section from  $\mu r \leq 0.65$  comes out to be  $1.53 \pm 0.08 \text{ mb}$ , which compares favourably with the interpolated value of  $1.6 \pm 0.1 \text{ mb}$  of Anand & Sood (1965). This justifies the assumption that the scatterer behaves as a homogeneous source of radiation for thin scatterers with  $\mu r \leq 0.65$ .

## REFERENCES

- Anand S & Sood B. S. 1965 *Nucl. Phys.* **73**, 368.  
Evans R. D. & Evans R. O. 1948 *Rev. Mod. Phys.* **20**, 305.  
Klein O. & Nishina Y. 1929 *Z. Physik* **52**, 853.  
Sahota H. S., Anand S., Singh M & Sood B. S. 1966, *Nucl. Phys.* **83**, 508.  
Singh M, Anand S. & Sood B. S. 1963 *Ind. J. App. Phys.* **1**, 305.  
Singh M, & Sood B. S. 1965 *Nucl. Phys.* **64**, 502,

# Letters to the Editor

*Indian J. Phys.* **44**, 419-420, (1970)

## Lattice energy and thermal expansion of diatomic crystals

By V. K. DIXIT AND M. N. SHARMA

*Physics Department, Lucknow University, Lucknow-7*

(Received 18 August — Revised 27 October 1970)

In the present work we have computed the cohesive energy and the coefficient of volume expansion of the alkali halide crystals by considering the modified  $V-S$  type of repulsion interaction term of the form  $\lambda \exp(-\mu r^{3/2})$ . Considering the above interaction term in conjunction with the electrostatic, the dipole-dipole and the dipole-quadrupole interaction energy terms, the crystal energy per mole may be expressed as

$$W = -[N\psi(r_0) + \epsilon_0] \quad \dots (1)$$

where  $N$  is the Avogadro's Number,  $\psi(r_0)$  is the lattice energy per cell and  $\epsilon_0$  is the zero point energy per mole. The parameters  $\lambda$  and  $\mu$  have been evaluated employing the Hildebrand's (1931) static lattice conditions. Computed values of the cohesive energy using equation (1) for a few ionic crystals are reported in table 1. The present theoretical values of  $W$  using equation (1) are in better agreement with the observed values than with those calculated by Kachhava & Saxena (1964) using the Gaussian model.

Following Smyth (1955), Kumar (1959) has developed a simple method to compute coefficient of volume expansion  $\alpha_v$ . A general form of Kumar's equation can be expressed as

$$\alpha_v = -\frac{C_p}{2r_0} \frac{\psi'''(r_0)}{[\psi''(r_0)]^2} \sqrt{Z} \quad \dots (2)$$

in which  $r_0$  is the interionic equilibrium separation distance,  $\psi'''(r_0)$  and  $\psi''(r_0)$  refer to the values of third and second derivatives of  $\psi(r)$  at  $r = r_0$  respectively,  $C_p$  the specific heat at constant pressure and  $Z = (Z_c N_c + Z_a N_a)/(N_c + N_a)$  where  $Z_c$ ,  $N_c$  and  $Z_a$ ,  $N_a$  are the charge number of cation and anion, respectively. Substituting the values of  $\psi'''(r_0)$  and  $\psi''(r_0)$  for the modified  $V-S$  model, equation (2) becomes

$$\alpha_v = -\frac{C_p \left[ \frac{6\alpha e^2}{r_0^4} + \frac{336C}{r_0^9} + \frac{720D}{r_0^{11}} + \frac{K}{2} \left( \frac{9b}{2r_0^{3/2}} + \frac{1}{2r_0^3} - \frac{9b^2}{2} \right) \right]}{2r_0 \left[ -\frac{2\alpha e^2}{r_0^3} - \frac{42C}{r_0^8} - \frac{72D}{r_0^{10}} - \frac{K}{2} \left( \frac{1}{r_0^2} - \frac{3b}{r_0^4} \right) \right]^2}, \quad \dots (3)$$

where 
$$K = \left( \frac{\alpha e^2}{r_0} + \frac{6C}{r_0^6} + \frac{8D}{r_0^8} \right)$$

- Hilderbrand J. H. 1931 *Z. Physik* **67**, 127.  
Kachhava C. M. & Saxena S. C. 1964 *Indian J. Phys.* **38**, 388.  
1965 *Indian J. Phys.* **39**, 145.  
Kumar S. 1959 *Proc. Nat. Inst. Sci. India* **A25**, 364.  
Smyth H. T. 1955 *J. Amer. Ceram. Soc.* **38**, 40.



## Gamma-gamma directional correlations of the 552-134 keV cascade in $\text{Re}^{187}$

By M. L. NARASIMHA RAJU, A. KHAYYOOM AND D. L. SASTRY

*The Laboratories for Nuclear Research, Andhra University, Waltair*

*(Received 2 September 1970)*

The level structure of  $\text{Re}^{187}$  is well established (Way *et al* 1965). The 552-134 keV gamma-gamma angular correlation was measured by several authors in the past (Arns *et al* 1960, Gallagher *et al* 1960, Michaelis 1963, Gupta *et al* 1966, Klementovskaya *et al* 1959). Arns *et al* reported a very high positive anisotropy ( $A_2 = 0.316 \pm 0.018$ ,  $A_4 = -0.086 \pm 0.027$ ) whereas Gallagher *et al* found the correlation to be isotropic within 1%. Michaelis and Gupta *et al* observed small negative anisotropy for this correlation, whereas, Klementovskaya *et al* observed small positive anisotropy. In view of the above discrepancies it was felt worthwhile to remeasure the 552-134 keV gamma-gamma angular correlation in  $\text{Re}^{187}$ .

The directional correlation of the above cascade is measured with a conventional slow-fast coincidence scintillation assembly described elsewhere (Narasimha Raju *et al* 1968). The system is checked by measuring the 1.17-1.33 MeV gamma-gamma angular correlation in  $\text{Ni}^{60}$ . The present measurements were done with an effective coincidence resolution of 20 ns. The angular correlation data were collected at three angles  $90^\circ$ ,  $135^\circ$  and  $180^\circ$  and were corrected for the short life of  $\text{W}^{187}$  and chance coincidences. The pooled up counts at the three angles were normalized and the data fitted to the standard polynomial

$$W(\theta) = 1 + A_2 P_2(\cos \theta) + A_4 P_4(\cos \theta)$$

by the method of least squares (Rosc 1953). The angular correlation function after correcting for the geometry of both the detectors is found to be

$$W(\theta) = 1 - (0.028 \pm 0.015) P_2(\cos \theta) + (0.012 \pm 0.017) P_4(\cos \theta)$$

This result is in fairly good agreement with that obtained by Michaelis and Gupta *et al* and differs considerably from the values of Gallagher *et al*, Klementovskaya *et al* and Arns *et al*. The experimental values of  $A_2$  and  $A_4$  coefficients of the earlier authors together with the values of the present work are given in table 1.

The present angular correlation function is consistent with the spin assignment  $5/2$  to the 686 keV level and with the quadrupole content of the 552 keV radiation ( $Q_{552} \leq 0.03$ ) reported by Michaelis and Gupta *et al*.

TABLE 1. The values of the  $A_2$  and  $A_4$  coefficients of the 552-134 keV directional correlation

References	$A_2$	$A_4$
Arns <i>et al</i> (1960)	$+0.316 \pm 0.018$	$-0.086 \pm 0.027$
Gallagher <i>et al</i> (1960)	Isotropic within 1%	
Michaelis (1963)	$-0.034 \pm 0.017$	$-0.007 \pm 0.030$
Klimentovskaya <i>et al</i> (1959)	Small positive anisotropy	
Gupta <i>et al</i> (1966)	$-0.0235 \pm 0.0132$	$+0.0299 \pm 0.0235$
Present work	$-0.028 \pm 0.015$	$0.012 \pm 0.017$

## REFERENCES

- Arns R. C. & Wiedenbeck M. L. 1960 *Nucl. Phys.* **19**, 634.  
 Gallgher C. J., Edwards W. F. & Manning G. 1960 *Nucl. Phys.* **18**, 18.  
 Gupta S. L., Bajaj M. M. & Saha N. K. 1966 *Proc. Nat. Inst. Sci. (India)* **32**, 281.  
 Klementovskaya M. V. & Sharvin J. P. 1959 *Soviet Physics JETP* **36**, 1360.  
 Michaelis W. 1963 *Nucl. Phys.* **45**, 573.  
 Narasimha Raju M. L., Sastry D. L. & Kondraiah E. 1968 *Nuovo Cimento*. **56B**, 29.  
 Rose, M. E. 1953 *Phys. Rev* **91**, 610.  
 Way K. *et al* 1965 *Nuclear Data Sheets*, Edited by K. Way *et al* Academic Press, New York

## BOOK REVIEWS

### *Advances in Plasma Physics, Vol. 2*

Edited by A. Simon and W. B. Thompson, *Interscience Publishers*, 1969;  
pp-vii+211.

The present volume consists of the following three articles:

- 1) Cesium Plasma Research—by N. D'Angelo.
- 2) Wave Phenomena in the Interstellar Plasma—by I. Lerche.
- 3) Shock Waves in Plasma Physics—by C. K. Chu and Robert A. Gross.

There has been an increasing tendency over the last few years for a detailed study of the physical phenomena occurring in a quiescent plasma, as the study is expected to lead to an understanding of the more complicated processes inherent in the plasma of a thermonuclear reactor. One type of such quiescent plasma has been reviewed in the first article, which presents some of the plasma devices as well as the plasma properties in the presence of a magnetic field. Various aspects of the plasma, such as confinement by magnetic fields of different configurations, presence of negative ions, etc. are considered. Although the treatment in certain sections is somewhat sketchy, the relevant references would be of much help to the interested readers. An interesting feature is provided by the speculation on the type of cesium plasma experiments which are likely to be carried out in the near future.

The second article, though the longest one of the volume, is rather restricted in its scope, dealing essentially with a few selected aspects of small amplitude perturbations in the interstellar medium (the composition of which has been described at the outset) by way of comparatively simple model situations. However, the treatment in the limited sphere is quite exhaustive and will surely be helpful to initiate one into the basic hydromagnetics and plasma particle phenomena associated with the subject of astrophysics. It is worth pointing out that the controversial topic of the thermodynamically paradoxical supraluminous waves have been discussed here in detail.

The last article is perhaps the most exciting, as its topic ranges from laboratory shocks to supernova explosions and is, at the same time, intimately connected with thermonuclear research. It starts with a brief introduction to shock waves and gas dynamic shocks including detonation waves. Shock waves in plasma are then presented under the following three headings.

- a) Shock waves in fully ionized plasma—A very interesting item here is the discussion on the so-called collisionless shocks. This discussion is preceded by a single-fluid description of MHD shocks and a multi-fluid description of collisional shocks.
- b) Ionizing shock waves—This study is carried out in the presence of a magnetic field perpendicular, parallel or oblique to the plane of the shock.
- c) High energy shock waves—This covers very strong shock waves namely, thermo-nuclear detonation waves, radiative shocks and shock waves at relativistic speeds; a few examples of astrophysical shock waves are also included.

In conclusion, plasma physicists owe their thanks to the editors for compiling the recent knowledge in a few branches of plasma physics; it is expected that they would add further volumes to this series.

J. B.

*Springer Tracts in Modern Physics*

Vol. 49, Springer-Verlag, Berlin, 1969.

1) *Electron Scattering, Photo-excitation and Nuclear Models*—H. Liberall

Electrons and photons are important tools of investigation of nuclear structure. In this article the author reviews some aspects of the theory of interaction of these particles with nuclei. A brief discussion of the basic mathematical formalism of electron-nuclear interaction is followed by a review of the theories of photoexcitation of the remarkable giant resonance states as well as of states below the giant resonance. For the giant resonance states, the author has given a detailed description of the early Goldhaber-Teller and Steinwedel-Jensen hydrodynamical models and their later extensions. However in contrast the more basic microscopic theory of these states is discussed rather briefly and recent developments, like the continuum shell model theories, find no mention at all.

B. B

2) *Baryon Current Solving SU (3) Charge Current Algebra*—H. Kleinert

The author deals with an attempt to describe the whole of the baryonic spectrum using the local commutation relations of the SU(3) currents at infinite momentum. The approach is partly semiempirical. The mass spectrum of the baryons as well as their electromagnetic form factors are fitted. Apart from the necessity of the notorious space-like states, the agreement with experiment is claimed to be sufficiently good.

G. R

*Thermal Physics*

C. Kittel, John Wiley and Sons, Inc., New York pp. 418 — \$ 10.95

This book makes a refreshingly new approach to thermal physics, i.e. thermodynamics and statistical mechanics. The classical method which has till now been used, in general, leads quickly to the ideal gas laws and expression for the heat capacity of an ideal gas. This advantage is more than off-set by the difficulty in obtaining correct expression for the entropy which is the most important quantity in thermal physics.

In this book, Gibb's approach has been used and the subject matter has been built up from a consistent quantum view point in which the states of the entire system have been considered. In this approach the quantum distribution law are easily derived which in the limit pass to the classical distribution laws to yield expressions for the entropy, gas laws, etc.

Many important applications of thermal physics to the different problems in physics, chemistry, engineering, biology and astrophysics have been given. The more important amongst them are the following : (i) applications of the Fermi-Dirac and Bose-Einstein distribution laws in interpreting various physical phenomena (ii) magnetic properties of solids.

The exposition of the subject matter is clear and the reader is lead step by step to the more advanced topics. The approach used in this book should be used for teaching thermal physics to our students of B.Sc. (Hons.) in Physics.

A. K. B.

# INDIAN JOURNAL OF PHYSICS

VOL. 44

No. 8

AND

VOL. 53

PROCEEDINGS

No. 8

OF THE

INDIAN ASSOCIATION FOR THE CULTIVATION OF SCIENCE

*(Edited in collaboration with the Indian Physical Society).*

IJPYAS 44 (8) 425-474 (1970)

AUGUST 1970

PUBLISHED BY THE  
INDIAN ASSOCIATION FOR THE CULTIVATION OF SCIENCE  
JADAVPUR, CALCUTTA-32



## The binding energy calculation of triton with Faddeev equation in separable approximation

BY GITA PURKAYASTHA, S. N. BANERJEE\* AND N. C. SIL

*Department of Theoretical Physics,  
Indian Association for the Cultivation of Science, Jadavpur, Calcutta-32*

(Received 17 September 1970)

The binding energy of triton has been calculated using Faddeev equation as formulated by Lovelace. Three sets of values have been taken for the parameters occurring in the separable two-body non-local potential with one term only.

### INTRODUCTION

A number of theoretical attempts have been made towards the calculation of the triton binding energy. Variational and other equivalent methods (Rarita & Present 1937, Ohmura & Ohmura 1962, Wagenungen & Kok 1967, Fiedelday *et al* 1968) have been employed with a variety of simple interactions. Amado (1963) and his collaborators (1965) have used a three-body model in which the composite systems have been represented by elementary particles. Treating the Schrodinger equation for the three body problem as a direct eigen value equation, Mitra (1962) has computed the triton binding energy assuming separable potential to act between pairs.

Faddeev (1961) has given a satisfactory theory of non-relativistic three particle systems. For local potentials this involves the solution of a set of coupled integral equations in at least two continuous variables. If separable non-local interactions are assumed instead of local potentials, we have single variable integral equation. We also get single variable integral equation if we employ a Sturmian set of expansion for the two-body  $t$ -matrix. Kharchenko & Sitenko (1963) have used Faddeev equation with two body non-local separable potential. Kharchenko *et al* (1966) have further carried out calculations with two-body local potentials of square well and Hulthen types utilizing a Sturmian set of expansion. Malfliet & Tjon (1969) have calculated the binding energy of triton with two-body local central Yukawa interactions and they have also considered tensor force. Approximating the two-body  $t$ -matrix by one separable term after Noyes (1965) and Kowalski (1965), Humberston *et al* (1968) have obtained the binding energy of triton. Lovelace (1964) has given a practical theory of three particle states based on Faddeev's work. As pointed out by Lovelace if a partial wave is dominated by a bound state or a resonance, then the off-shell  $t$ -matrix can be approximated by a separable term. When this is used as an input in the Faddeev equation, we get a coupled equation in one variable which is amenable to numerical solution.

---

\*Present address : Physics Department, Jadavpur University, Calcutta-32.

The separable approximation, though somewhat unrealistic, enormously simplifies both the bound state and scattering calculation. Further it provides a simple framework in which to investigate the sensitivity of three nucleon properties to the variation of particular two nucleon parameters.

In the present work, we have applied Lovelace formalism to calculate the triton binding energy. As for the intermediate two nucleon states we have considered only the deuteron bound state and used one term separable potential for this interaction. Three sets of two-body parameters have been used in our calculation and their fit to the two-body data of deuteron binding energy, triplet scattering length and recent phase shift ( $^3S$ ) values of MacGregor *et al* (1968) have been studied.

### THEORY

Following Lovelace (1964), the three-body transition operators are defined as

$$U^+_{\alpha\beta}(s) = \sum_{\gamma \neq \alpha} V_\gamma - \sum_{\gamma \neq \alpha} \sum_{\delta \neq \beta} V_\gamma G(s) V_\delta$$

$$U^-_{\alpha\beta}(s) = \sum_{\delta \neq \beta} V_\delta - \sum_{\gamma \neq \alpha} \sum_{\delta \neq \beta} V_\gamma G(s) V$$

where

$$G(s) = [H - sI]^{-1},$$

$H$  is the total Hamiltonian for three-particle system  $V_\alpha$  is the pair potential, where  $\alpha$  takes the values from 0 to 3.  $V_1$ ,  $V_2$  and  $V_3$  are the potentials between particles (2, 3), (1, 3) and (1, 2), respectively and  $V_0$  is equal to 0.

Therefore

$$H = H_0 + V_1 + V_2 + V_3$$

where  $H_0$  is the free Hamiltonian for the three-body system and  $G_0(s) = [H_0 - sI]^{-1}$  is the resolvent of the free Hamiltonian

The Hamiltonian of the various subsystems are

$$H_\alpha = H_0 + V_\alpha$$

The Green's functions of these Hamiltonians are

$$G_\alpha(s) = [H_\alpha - sI]^{-1}$$

These satisfy the second resolvent identity

$$\begin{aligned} G(s) &= G_\beta(s) - \sum_{\delta \neq \beta} G(s) V_\delta G_\beta(s) \\ &= G_\alpha(s) - \sum_{\gamma \neq \alpha} G_\alpha(s) V_\gamma G(s) \end{aligned}$$

We shall define scattering amplitudes for bound states and resonances by

$$\begin{aligned} X_{\alpha n, \beta m}(s) &= \langle \alpha n | G_0(s) U^+_{\alpha\beta}(s) G_0(s) | \beta m \rangle \\ &\quad - Z_{\alpha n, \beta m}(s) [1 + \lambda_{\beta m} \langle \beta m | G_0(s) | \beta m \rangle] \end{aligned} \quad \dots (1)$$



If we take the potentials for bound-state scattering as

$$\langle q_\alpha | Z_{\alpha n, \beta m}(s) | q_\beta \rangle = (1 - \delta_{\alpha\beta}) \langle \alpha n | G_0(s) | \beta m \rangle \quad \dots \quad (2)$$

then the equation for  $X_{\alpha n, \beta m}(s)$  becomes

$$X_{\alpha n, \beta m}(s) = -Z_{\alpha n, \beta m}(s) - \sum_{\gamma r} X_{\alpha n, \gamma r}(s) \hat{\tau}_{\gamma r}(s) Z_{\gamma r, \beta m}(s) \quad \dots \quad (3)$$

For the three-body bound state problem, the equation (2) becomes homogeneous integral equation. For identical particles and triplet two-body state we now have

$$\begin{aligned} \langle q_1 | X_{nm}(s) | q_1 \rangle &= -\langle q_1 | \hat{\tau}_r(s) | q_1' \rangle \langle q_1' | 2Z_{rm}(s) | q_2 \rangle, \\ &\quad \cdot \langle q_2 | X_{n'l}(s) | q_1 \rangle \quad \dots \quad (4) \end{aligned}$$

This homogeneous integral equation should have a solution at an energy equal to binding energy of the three-nucleon system. For equal mass particle  $Z_{rm}$  reduces to

$$\begin{aligned} \langle q_1 | Z_{rm}(s) | q_2 \rangle &= (1 - \delta_{rm}) \frac{g_r(p_1) g_m(p_2)}{p_2^2 + q_2^2 - s - i\epsilon} \cdot \frac{8}{3\sqrt{3}} \\ &= \Lambda_{rm}^{IS} \cdot \frac{1}{2} \int_{-1}^{+1} \frac{8}{3\sqrt{3}} \cdot P_l(\cos \theta) \frac{g_r(p_1) g_m(p_2)}{p_2^2 + q_2^2 - s - i\epsilon} d \cos \theta \quad \dots \quad (5) \end{aligned}$$

where  $\Lambda_{rm}^{IS}$  expresses the dependence of  $Z_{rm}(s)$  on spin and isospin. The subscripts  $r$  and  $m$  in equation (5) each have only one value for triplet two body state. The superscripts  $I, S$  stand for total isotopic spin and spin of the three-body system. For triton  $I = S = \frac{1}{2}$

Assuming the two-body  $S$ -wave potential in momentum space to be non-local and separable of Yamaguchi (1954) form,

$$V(p, p') = \lambda g(p) g(p')$$

We may write the two-body  $S$ -wave  $T$ -matrix which satisfies the Lippmann-Schwinger equation as

$$T(p, p'; s) = g(p) g(p') t(s)$$

where

$$t(s) = \left[ \frac{1}{\lambda} + 4\pi \int_0^\infty \frac{q^2 dq g^2(q)}{q^2 - s - i\epsilon} \right]^{-1}$$

The bound state form factor  $g(p)$  is taken as

$$g(p) = \frac{N_d}{(p^2 + \mu_d^2)}$$

The form factor  $g(p)$  is normalized so that

$$4\pi \int_0^\infty \frac{g^2(p) p^2 dp}{(p^2 + \mu_d^2)^2} = 1$$

The separable potential will have a bound state if there is a point  $k' = -E_d$  for which

$$t(s) = \frac{1}{s + E_D} \left[ 4\pi \int_0^\infty \frac{q^2 dq g^2(q)}{(q^2 + E_d)(q^2 - s - i\epsilon)} \right]^{-1}$$

The operator  $\tau(S)$  is given by the relation

$$\langle q_1 | \tau(s) | q_1' \rangle = \delta_3(q_1 - q_1') t(s - q_1^2)$$

### RESULTS AND DISCUSSIONS

Transforming the integration variable of equation (4) suitably so as to change the limits of the integral to  $\pm 1$  and using the usual Gaussian quadrature formula for integration, we recast the integral equation (4) to the following matrix equation

$$K_{ij}(E_T) X_j(E_T) = X_i(E_T)$$

where  $K_{ij}(E_T)$  is the Kernel of the integral equation for triton binding energy  $E_T$ . We have searched for the poles of the corresponding inverse operator  $[I - K_{ij}(E_T)]^{-1}$  by finding out the zero of the corresponding determinant. This energy for which the determinant vanishes, is the required binding energy of triton. We have calculated triton binding energy for three different sets of values of the two body parameters  $N_d$  and  $\mu_d$  and have studied the sensitivity of triton binding energy with these parameters. The best fit values of the two body parameters occurring in the  $t$ -matrix which is used as input in Faddeev equation, give the binding energy 7.88 Mev as compared with the experimental value 8.48 Mev.

In figures 1, 2 and 3 we have plotted the theoretical triplet phase shift values as well as the absolute errors against laboratory energy for the three sets of parameters.

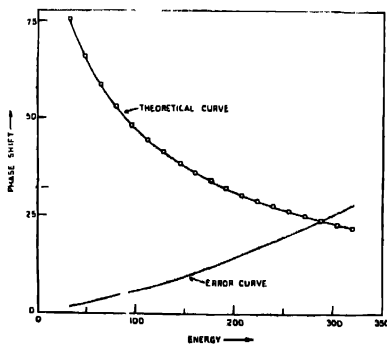


Figure 1. Set 1.

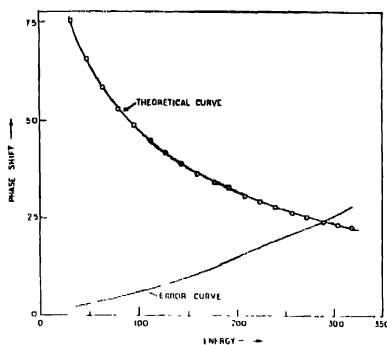


Figure 2. Set 2.

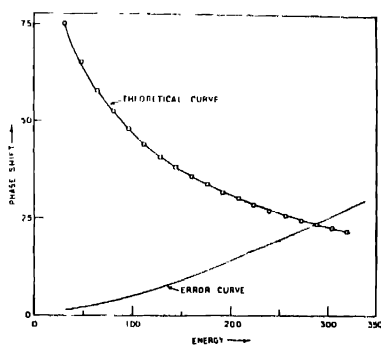


Figure 3. Set 3.

To calculate the absolute errors, we have computed  $\Sigma R^2$  for the three sets where

$$\Sigma R^2 = \sum_{i=1}^{19} [\delta_i^{exp}(E_i) - \delta_i^{theo}(E_i)]^2,$$

$\delta_i^{exp}(E_i)$  and  $\delta_i^{theo}(E_i)$  are the experimental and theoretical values of phase shifts respectively. We have taken the recent experimental phase shifts data of Mac Gregor *et al* (1968).  $\Sigma R^2$  is the sum of the squares of the residuals  $[\delta_i^{exp}(E_i) - \delta_i^{theo}(E_i)]$  at the 19 data points in the range 0 to 320 Mev for  $E_i$ . We have three values of  $\Sigma R^2$  for the three sets of values of the two-body parameters. The minimum value of  $\Sigma R^2$  obviously corresponds to the best fit of the value of the

two-body parameters. In table 1, we have enlisted the three binding energy values of triton and the absolute error values  $\Sigma R^2$  for the three sets. It is seen that the best values of two-body parameters (set 3) yield the binding energy value which compares favourably with the experimental results.

TABLE 1

	$\Sigma R^2$	Triton binding energy
Set 1	4700.8314	7.80
2	4524.20	7.84
3	4386.284	7.88

So far as triton binding energy is concerned we see that a separable approximation to the two-body  $t$ -matrix can reproduce the binding energy, in addition to its added advantage that it simplifies the problem considerably (Lovelace 1964. Harms *et al* 1969).

The authors are thankful to the authorities of C.M.E.R.I Durgapur for extending the facility of using IBM 1620.

## REFERENCES

- Amado R. D. 1963 *Phys. Rev.* **132**, 548.  
 Amado R. D. & Yam Y. Y. 1965 *Phys. Rev.* **140B**, 1291.  
 Faddeev L. D. 1961 *Sov. Phys. JETP* **12**, 1014.  
 Fiedelday H., Erens G., Van wagenningen R., Homan D. H. & Kok L. P. 1968 *Nucl. Phys.* **A113**, 543.  
 Harns E. & Lovinger J. S. 1969 *Phys. Rev. Lett.* **30B**, 449.  
 Humberston J. W., Hall R. L. & Osborn T. A. 1968 *Phys. Rev. Lett.* **27B**, 195.  
 Kharchenko V. F. & Sitenko A. G. 1963 *Nucl. Phys.* **49**, 15.  
 Kharchenko V. F., Sitenko A. G., Kharchenko V. F. & Petrou N. M. 1966 *Phys. Rev. Lett.* **21**, 54.  
 Kowalski K. L. *Phys. Rev. Lett.* **15**, 798.  
 Lovelace 1964 *Phys. Rev.* **135B**, 1225.  
 Mac Gregor M. H., Arndt R. A. & Wright R. M. 1968 *Phys. Rev.* **173**, 1272.  
 Malfliet & Tjon 1969 *Nucl. Phys.* **A127**, 161.  
 Mitra, A. N. 1962 *Nucl. Phys.* **32**, 529.  
 Noyes H. P. 1965 *Phys. Rev. Lett.* **15**, 538.  
 Ohmura H. & Ohmura T. 1962 *Phys. Rev.* **128**, 729.  
 Rarita W. & Present R. D. 1937 *Phys. Rev.* **51**, 788.  
 Wagenningen R. & Kok L. P. 1967 *Nucl. Phys.* **A98**, 303.  
 Yamaguchi Y. 1954 *Phys. Rev.* **95**, 1628.

## Elastic scattering of electrons and positrons by helium atom

By G. BANERJI AND N. C. SIL

*Department of Theoretical Physics,*

*Indian Association for the Cultivation of Science, Jadavpur, Calcutta-32*

*(Received 4 August 1970)*

Calculations of differential and total cross sections for the elastic scattering of electrons and positrons by neutral helium atom have been performed over the range of impact energies 50-700 eV employing the Schwinger variational principle for scattering amplitude. The Hartree-Fock static potential for helium atom has been used in the calculations. The results are compared with the Born approximation calculations and also with experimental findings.

### INTRODUCTION

In the present paper calculations are carried out for the differential and total cross sections of the elastically scattered electrons by helium atom for various energies between 50 and 700 eV, the effects of exchange and polarization are considered to be not so important. The corresponding results for positron scattering are also reported.

Experimental measurements on the elastic collision between electrons and helium atoms have been carried out by several workers (Hughes *et al* 1932, Werner 1933, Vriens *et al* 1968, Bromberg 1969) over a wide range of electron impact energies. A number of theoretical investigations have also been made on the *c*-He elastic scattering. The calculation of scattering cross sections of high energy electrons by helium atom has been performed by Mukherjee (1961) in Born approximation where the use of a refined wave function which includes the correlation function depending on the mutual distance of the atomic electrons has been made. Kim & Inokuti (1968) have used the twenty-term Hylleraas wave function of Hart & Herzberg (1957) in their Born-approximation calculations. Here we apply the Schwinger variational principle for the scattering amplitude (Lippman & Schwinger 1950) to the same collision problem. The static field of helium atom is represented by a linear combination of several Yukawa potentials (Tietz 1965). The form of the trial wave function taken by us has been previously used by Mower (1955) for the calculation of differential cross section in the elastic scattering of electrons from neon atom where it has yielded results very close to the numerical solution.

Unlike other variational principles, Schwinger principle does not require that the trial functions involved should have a particular asymptotic form. This principle has been put in two forms. In one, by making the usual expansions in spherical harmonics an infinite set of independent integral equations and hence

a corresponding set of variational expressions for the phase shifts has been obtained, while in the other, the entire scattering amplitude has been expressed in a stationary form. The calculation of scattering cross section by summing over the individual phase shifts, though accurate, involves a lot of numerical computations, whereas the calculation by the direct estimation of scattering amplitude is intrinsically much simpler.

The choice of the potential as a linear combination of several Yukawa potentials is motivated by the fact that for this potential the integrals occurring in the variational principle can be evaluated in closed form for some suitable trial functions. This evaluation is possible for the relatively simple form of the Fourier transform of the Yukawa potential. For other potentials the variational formulation may not yield closed form expressions for the scattering amplitudes. Unless the integrals can be evaluated in closed form, computations using the Schwinger variational formulation become very tedious and have practically no advantage over exact numerical integration of the differential equation.

#### MATHEMATICAL FORMULATION

The scattering of a particle of mass  $m$  by a potential  $V(\vec{r})$  is described by an exact solution to the integral equation (Mott & Massey 1965)

$$\psi_i(\vec{r}) = e^{ik_i \cdot \vec{r}} + \frac{2m}{\hbar^2} \int G(\vec{r}, \vec{r}') V(\vec{r}') \psi_i(\vec{r}') d\vec{r}', \quad (1)$$

where

$$G(\vec{r}, \vec{r}') = -\frac{1}{4\pi} e^{ik|\vec{r}-\vec{r}'|}$$

is the free space Green function for the Helmholtz equation and  $E = \hbar^2 k^2 / 2m$  is the energy of the incident particle. The vector  $\vec{k}_i = k \hat{n}_i$ , where the unit vector  $\hat{n}_i$  specifies the direction of incidence and the vector  $\vec{r} = r \hat{n}$  is the radius vector which specifies the position of the particle. The amplitude for the scattering from direction  $\hat{n}_1$  to direction  $-\hat{n}_2$  is defined by

$$f(\hat{n}_1, -\hat{n}_2) = -\frac{1}{4\pi} \int e^{ik\hat{n}_2 \cdot \vec{r}} U(\vec{r}) \psi_1(\vec{r}) d\vec{r},$$

where

$$U(\vec{r}) = 2mV(\vec{r})/\hbar^2.$$

For the approximate determination of the scattering amplitude by the Schwinger variational method we take, following Mower (1955), the functional for the scattering amplitude as

$$\begin{aligned} [f(\hat{n}_1, -\hat{n}_2)] = & -\frac{1}{4\pi} \int e^{ik\hat{n}_2 \cdot \vec{r}} U(\vec{r}) \psi_1(\vec{r}) d\vec{r} + \int e^{ik\hat{n}_1 \cdot \vec{r}} U(\vec{r}) \psi_2(\vec{r}) d\vec{r} \\ & - \int \psi_2(\vec{r}) U(\vec{r}) \psi_1(\vec{r}) d\vec{r} + \int \int \psi_2(\vec{r}) U(\vec{r}) G(\vec{r}, \vec{r}') U(\vec{r}') \psi_1(\vec{r}') d\vec{r} d\vec{r}' \quad \dots \quad (2) \end{aligned}$$

where  $\psi_1$  and  $\psi_2$  are trial solutions of (1). Using trial functions of the form

$$\psi_i = C_1 e^{ik\hat{n}_i \cdot \vec{r}} + C_2 e^{-ik\hat{n}_i \cdot \vec{r}}, \quad i = 1, 2$$

the expression (2) for the scattering amplitude is obtained as

$$[f(\hat{n}_1, -\hat{n}_2)] = 2C_1 f_{b1}(\hat{n}_1, -\hat{n}_2) + 2C_2 f_{b1}(\hat{n}_1, \hat{n}_2) \\ - (C_1^2 + C_2^2)[f_{b1}(\hat{n}_1, -\hat{n}_2) - f_{b2}(\hat{n}_1, -\hat{n}_2)] - 2C_1 C_2 [f_{b1}(\hat{n}_1, \hat{n}_2) - f_{b2}(\hat{n}_1, \hat{n}_2)], \quad \dots \quad (3)$$

where

$$f_{b1}(\hat{n}_1, -\hat{n}_2) = -\frac{1}{4\pi} \int e^{ik(\hat{n}_1 + \hat{n}_2) \cdot \vec{r}} U(\vec{r}) d\vec{r} = (-\vec{k}_2 | U | \vec{k}_1) \\ f_{b2}(\hat{n}_1, -\hat{n}_2) = -\frac{1}{4\pi} \iint e^{ik(\hat{n}_1 \cdot \vec{r}' + \hat{n}_2 \cdot \vec{r})} U(\vec{r}) G(\vec{r}, \vec{r}') U(\vec{r}') d\vec{r} d\vec{r}' \quad \dots \quad (4) \\ = \frac{4\pi}{(2\pi)^3} \int \frac{(-\vec{k}_2 | U | \vec{\eta})(\vec{\eta} | U | \vec{k}_1)}{\eta^2 - k^2} d\vec{\eta}$$

are, respectively, the first and second terms in the Born series of approximations to the scattered amplitude. Substituting

$$f_{b1}(\hat{n}_1, \hat{n}_2)/f_{b1}(\hat{n}_1, -\hat{n}_2) = \lambda \text{ and } f_{b2}(\hat{n}_1, -\hat{n}_2)/f_{b1}(\hat{n}_1, -\hat{n}_2) = \mu(\hat{n}_1, -\hat{n}_2)$$

the expression (3) may be rewritten as

$$[f(\hat{n}_1, -\hat{n}_2)] = f_{b1}(\hat{n}_1, -\hat{n}_2)[2C_1 + 2C_2\lambda - (C_1^2 + C_2^2)(1 - \mu(\hat{n}_1, -\hat{n}_2)) \\ - 2C_1 C_2 \lambda (1 - \mu(\hat{n}_1, \hat{n}_2))]$$

Now, adjusting the parameters according to the conditions

$$\partial[f]/\partial C_i = 0, \quad i = 1, 2$$

the scattering amplitude is given by

$$[f(\hat{n}_1, -\hat{n}_2)] = f_{b1}(\hat{n}_1, -\hat{n}_2)[(1 + \lambda^2)(1 - \mu(\hat{n}_1, -\hat{n}_2)) - 2\lambda^2(1 - \mu(\hat{n}_1, \hat{n}_2))]/ \\ [(1 - \mu(\hat{n}_1, -\hat{n}_2))^2 - \lambda^2(1 - \mu(\hat{n}_1, \hat{n}_2))^2] \quad \dots \quad (5)$$

The Hartree—Fock screening factor (Tietz 1965) for neutral atoms can be expressed analytically in the form

$$f(r) = \sum_i \alpha_i e^{-\gamma_i r} \quad (6a)$$

so that the electrostatic scattering potential may be written as

$$V(r) = \frac{Ze^2}{r} f(r). \quad (6b)$$

With this potential the first and second Born scattering amplitudes are obtained from (4) as (Morse & Feshbach 1953, Lewis 1956)

$$f_{b1}(\hat{n}_1, -\hat{n}_2) = -\frac{2mZ}{\hbar^2} \sum_i \frac{\alpha_i}{\gamma_i^2 + 4k^2 \sin^2 \frac{\theta}{2}} \quad \dots \quad (7)$$

$$f_{b2}(\hat{n}_1, -\hat{n}_2) = \frac{4\pi}{(2\pi)^3} \left( \frac{2mZ}{\hbar^2} \right)^2 \sum_{i,j} \frac{\alpha_i \alpha_j}{k^3} M(\gamma_i, \gamma_j)$$

where

$$\begin{aligned} ReM(\gamma_i, \gamma_j) &= \frac{2\pi^2 k^3 T}{T^2 + S^2}, \quad \theta = 0 \text{ and } i = j \\ &= \frac{\pi^2 k^3}{R} \left[ \tan^{-1} \frac{S+R}{T} - \tan^{-1} \frac{S-R}{T} \right], \quad \text{otherwise} \end{aligned}$$

$$\begin{aligned} \text{and} \quad ImM(\gamma_i, \gamma_j) &= \frac{2\pi^2 k^3 S}{T^2 + S^2}, \quad \theta = 0 \text{ and } i = j \\ &= \frac{\pi^2 k^3}{R} \cdot \frac{1}{2} \ln \frac{T^2 + (R+S)^2}{T^2 + (R-S)^2}, \quad \text{otherwise} \end{aligned}$$

with

$$\begin{aligned} R &= [k^2(K^2 + \gamma_i^2 + \gamma_j^2) - T^2 \gamma_i^2 \gamma_j^2] \\ S &= k[K^2 + (\gamma_i + \gamma_j)^2], \quad T = \gamma_i \gamma_j (\gamma_i + \gamma_j) \\ \vec{K} &= \vec{k}_1 + \vec{k}_2, \quad \vec{P} = \vec{k}_1 - \vec{k}_2, \quad \theta = \text{arc cos } (\hat{n}_1, (-\hat{n}_2)). \end{aligned}$$

Using the equations (7) and the definitions of  $\lambda, \mu$ , we can determine the scattering amplitude from the expression (5) and hence the differential cross-sections for the scattering of particles by an atom. The total scattering cross-section  $\sigma$  may be obtained by integration of the differential cross-section through solid angle or by employing the optical theorem

$$\sigma = \frac{4\pi}{k} Imf(\hat{n}_1, \hat{n}_1).$$

## RESULTS AND DISCUSSION

We have calculated the differential and total cross-sections of elastically scattered electrons and positrons having incident energy between 50 and 700 eV by the Schwinger variational method and the Born approximation. Integrations over angles yielding total cross-sections have been performed numerically by Simpson's rule with suitable intervals. The parameters occurring in the expression for the potential (c.f. equations 6a and 6b), which reproduces the Hartree-Fock field of helium atom, are

$$\begin{aligned} \alpha_1 &= 1.0000, & \alpha_2 &= -0.6195, & \alpha_3 &= -0.1846, & \alpha_4 &= 0.6195, & \alpha_5 &= 0.1846 \\ \gamma_1 &= 2.4907, & \gamma_2 &= 3.8530, & \gamma_3 &= 6.1212, & \gamma_4 &= 2.8530, & \gamma_5 &= 5.1212 \end{aligned}$$



The results of our calculation for the differential cross sections are shown in figure 1. We compare our results for the electron scattering for 50 eV and 700

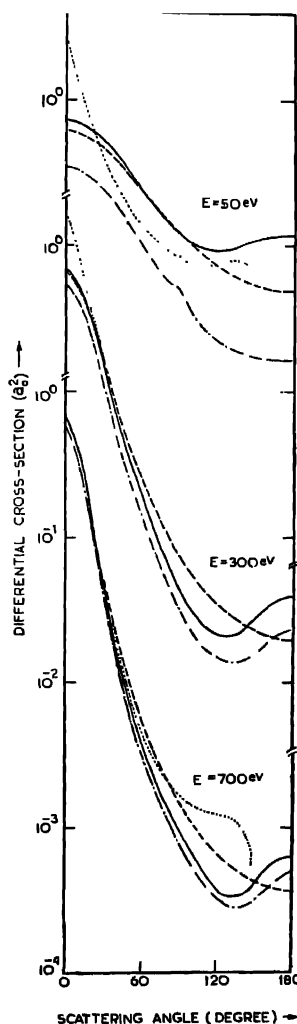


Figure 1. .... experimental findings for electron scattering.  
 ----- Born results  
 ————— variational calculation for electron scattering  
 - . - . - variational calculation for positron scattering.

eV with the experimental data of Hughes *et al* (1932) and that for 300 eV with the experimental data of Vriens *et al* (1968).

At high energies the results for the differential cross-section for electron and positron scattering are nearly the same. But with the decrease of energy there is a marked difference between the two results, as expected. The results for the differential cross-sections for electron scattering obtained by variational calculations are in slightly better agreement with experiment than those calculated by Born-approximation at all energies. In the high energy region ( $E \geq 600$  eV) our theoretical results for the differential cross-sections agree well with the experimental findings for all scattering angles, which contribute appreciably to the total cross-section. For small angle of scattering the ratio of the experimental findings and the corresponding Born results for the differential cross-sections is quite large, more so for low incident energy. In the incident energy region of 300 eV and above, for larger angles, this ratio decreases below unity with the increase of angle. Again with further increase of scattering angle the value of the ratio gradually increases and finally becomes greater than unity. This character is also maintained in the variational calculation.

We obtain the total cross sections for the systems in two ways, by the integration of differential cross sections over the solid angle and by using the optical theorem. In table 1, we have presented these two results of total cross-sections

TABLE 1 Total cross sections  $Q$  (in units of  $\pi a_0^2$ , where  $a_0$  is the Bohr radius) for elastic scattering of electrons and positrons by helium atom

Incident energy (eV)	$Q^*$	$Q$ (Born)	$Q^{**}$		$Q^{***}$	
			electrons	positrons	electrons	positrons
50	0.711005		0.8043	0.3131	0.89298	0.35745
100	0.762	0.410395	0.4063	0.2204	0.46267	0.2672015
150	0.443	0.287944	0.2767	0.1742	0.31380	0.21207
200	0.308	0.221654	0.2111	0.1453	0.23731	0.17507
300	0.190	0.1516999	0.1440	0.1095	0.15929	0.12914
400	0.142	0.1152831	0.1096	$0.8823 \times 10^{-1}$	0.11976	0.102044
500		$0.929577 \times 10^{-1}$	$0.8868 \times 10^{-1}$	$0.7415 \times 10^{-1}$	$0.95901 \times 10^{-1}$	$0.842613 \times 10^{-1}$
600		$0.778729 \times 10^{-1}$	$0.7454 \times 10^{-1}$	$0.6394 \times 10^{-1}$	$0.79957 \times 10^{-1}$	$0.71729 \times 10^{-1}$
700		$0.669988 \times 10^{-1}$	$0.6434 \times 10^{-1}$	$0.5627 \times 10^{-1}$	$0.68549 \times 10^{-1}$	$0.62427 \times 10^{-1}$

\*Experimental results of Vriens *et al* (1968)

\*\*Calculated from the variationally obtained differential cross-sections by integration through the solid angle

\*\*\*Calculated from the variationally obtained amplitude by using the optical theorem

and the corresponding Born results and compared them with the experimental findings of Vriens *et al* (1968). It is seen from the table that at 100 eV and above the cross sections obtained by integration are nearly equal to the Born cross-sections, but the cross-sections obtained by employing the optical theorem are always greater than these two results and closer to experimental findings.

#### ACKNOWLEDGEMENT

The authors thank Dr. S. C. Mukherjee for fruitful discussions. They also thank The Kuljian Corporation (India) Pvt. Ltd., Calcutta, for extending facilities for using their IBM 1130 electronic computer.

#### REFERENCES

- Bromberg J. P. 1969 *J. Chem. Phys.* **50**, No. 9, 3906.  
Hart J. F. & Herzberg, G. 1957 *Phys. Rev.* **106**, 79.  
Hughes A. L., McMillen, J. H. & Webb, G. M. 1932 *Phys. Rev.* **41**, 154.  
Kim Y. K. & Inokuti, M. 1968 *Phys. Rev.* **165**, 39.  
Lewis R. R. 1956 *Phys. Rev.* **102**, 537.  
Lippman B. A. & Schwinger, J. 1950 *Phys. Rev.* **79**, 469.  
Morse P. M. & Feshbach H. 1953 *Methods of Theoretical Physics*, McGraw-Hill Book Co. Inc., New York.  
Mott N. F. & Massey, H. S. W. 1965 *The Theory of Atomic Collisions*, Clarendon Press, Oxford.  
Mower L. 1955 *Phys. Rev.* **99**, 1085.  
Mukherjee S. C. 1961 *Indian J. Phys.* **35**, 333.  
Tietz T. 1965 *Nuovo Cimento* **36**, 1365.  
Vriens L., Kuyatt, C. E. & Mielezarek, S. R. 1968 *Phys. Rev.* **170**, No. 1, 163.  
Weerner S. 1933 *Proc. Roy. Soc.* **A139**, 113.

## On the electrical resistivities of pyrolytic graphite

A. R. SAHA, P. K. BANERJEE AND A.K. DAS

*Department of Electronics and Telecommunication Engineering  
Jadavpur University, Calcutta-32, India*

(Received 23 September 1970—Revised 24 March 1971)

A theoretical formulation of the problem of charge carrier transport in pyrolytic graphite is made and criterion defined when a relaxation time approach for scattering (in addition to normal thermal scattering), originating at the intercrystalline boundary, is justified. Taking into consideration this additional scattering the electrical resistivities (basal plane resistivity  $\rho_a$ , and c-axis resistivity  $\rho_c$ ) of pyrolytic graphite are deducible from single crystal graphite transport parameters. Excellent agreement of the calculated values of resistivities with the experimental ones has been found.

### INTRODUCTION

Pyrolytic graphite (PG) known for a long time has come to lime light only recently because of its application in nuclear and space technology (Bokros 1969). Its electrical properties also have many interesting features for solid state physicists (Reynolds 1968). PG is characterized by largest known anisotropy ( $\rho_c/\rho_a$ ) for materials. Its ( $\rho_c/\rho_a$ ) is found to have values an order of magnitude larger than that of single crystal graphite (Klein 1962) though PG in reality is made up of small single crystals of graphite (crystallites) typically several hundred angstroms in size in the basal plane. In PG deposited at  $T_d \geq 2000^\circ\text{C}$ , these crystallites have a high degree of orientation with almost all the c-axes pointing along the same direction. This composite nature of PG seems to be responsible not only for the difference in its resistivity anisotropy from that of its components (crystallites) but also its dependence of resistivity on temperature. Both  $\rho_c$  and  $\rho_a$  are found experimentally to decrease with temperature like semiconductors, whereas, single crystal graphite is known to have resistivities which increase with temperature like metals.

Mrozowski (1952) attempted to explain the phenomena by assuming that in the energy band structure of PG there must be a bandgap  $E_g$ . He argued that small size of the crystallites may give rise to a bandgap instead of a band overlap as is found in single crystal graphite. But this point of view has never been elaborated in details to be generally acceptable. Several years ago Klein (1964) observed a phenomenological band overlap and an effective mass of electron somewhat different from those of single crystal graphite, which fitted only with the basal plane data for pure, highly graphitized PG.

Our approach presented here shows that electrical resistivity of PG along any direction can be deduced fairly accurately from the charge transport parameters of single crystal graphite after giving due consideration to the effect of finite size of the crystallites.

### THEORETICAL CONSIDERATION

*Formulation of the Problem* Let us imagine a single crystallite within the bulk of PG. It is obvious that it is separated from its adjacent ones by internal surfaces all around. These internal surfaces are really sites of dislocation containing carbon atoms whose  $\sigma$ -electrons are not bonded covalently and thus they are liable to capture mobile  $\pi$ -electrons from the bulk of the crystallite near the surface. Trapping of  $\pi$ -electrons builds a static negative charge on these surfaces, and an induced positive charge of equal amount on to the internal surface of the bulk of the crystallite, so that overall electrical charge neutrality is maintained. The surface space charge layer thus formed produces a local potential field ( $\phi$ ) which repeats in any direction  $j$  at an interval of length  $L_j$ , the crystallite's extension in that direction.

If this macroscopic potential distribution  $\phi(x_j)$  were known, we could, in principle, add this to the atomic potential and solve the Schrodinger equation for wave functions  $\psi_j$  of the entire composite of crystallites with the restriction that the macroscopic potential and macroscopic charge distribution is self-consistent through Poisson's equations. This seems to be the most appropriate procedure to determine the energy band structure of a composite like PG, but unfortunately  $\phi(x_j)$  is not known, apart from the complexity of solving Schrodinger's wave equation when two kinds of potential functions are present.

It has been pointed out by Shockley (1950) that by the application of a small field the wave functions are not seriously distorted but change with time in a manner that can be described as a change of the wave vector  $K$ . This in effect is equivalent to a combination of effective mass approximation with the WKB methods (Schiff 1949) for the solution of the Schrödinger equation, because we have used wave functions which are dependent only on the local kinetic energy at each point. Thus, we may argue that our procedure is subject to the same limits of validity as the WKB method i.e

$$\frac{d\lambda}{dx_j} \ll 4\pi \quad \dots (1)$$

where  $\lambda$  is the electron wavelength. Though we do not know the exact potential function  $\phi(x_j)$  at the intercrystalline boundary, it is reasonable to assume that  $\phi(x_j)$  will be felt over a length  $dx_j$  of the order of a Debye length ( $L_D$ ). Assuming

single crystal's electron and hole concentrations,  $L_D \simeq 5\text{\AA}$  for graphite. So that (1) reduces to

$$d\lambda \ll 4\pi L_D \quad \dots (2)$$

or,

$$\left| \frac{dK}{K} \right| \ll 2|K|L_D \quad (3)$$

Since  $L_D$  is only  $5\text{\AA}$ ,  $|dK/K|$  allowed for the method to be valid, is small indeed. However, in case of PG, we may take the close agreement of the theoretical resistivities, calculated by considering the additional relaxation time for scattering due to the change in  $K$  at the boundary with the experimental values as a proof of the validity of the criterion (3)

*Boundary Scattering Relaxation Time.* With criterion (3) satisfied away from the boundary ( $|x_j| \gg L_D$ ) electron wave function  $\psi_K$  and energy  $\epsilon(K)$  will be that of a single crystal. In case of PG,  $|x_j|$  should refer only to the two dimensions of a crystallite along the basal plane because  $\psi_K$  and  $\epsilon(K)$  of a graphite crystal is mainly determined by the basal plane structure. The interaction between layers through weak Van der Waal force causes only small perturbations in  $\psi(K)$  and  $\epsilon(K)$ . Therefore, when  $|L_{a,b}|$  of a crystallite is much larger than  $L_D$ ,  $\psi(K)$  and  $\epsilon(K)$  of the crystallite may be considered identical with those of a single crystal graphite in spite of the fact that  $|L_c|$  of the crystallite may be comparable to  $L_D$ . The electron in such a crystallite will therefore travel with a velocity  $v_K = 1/\hbar \cdot \nabla_K \epsilon(K)$ . Assuming absence of phonon scattering (which we may take into account separately since the two processes are statistically independent), electron travelling in any direction  $j$  will be scattered, changing its wave vector from  $K_j$  to  $K_j + dK_j$  in a time

$$\tau_j = \frac{L_j}{v_{Kj}} \quad (4)$$

$\tau_j$  values may be different because both  $L_j$  and  $v_{Kj}$  may have values which are not same for all  $x_j$ . However, we may in that case talk of an average crystallite size  $L_j$  and average velocity  $\bar{v}_{Kj}$  and the average time for scattering to occur

$$\bar{\tau}_j = \frac{\bar{L}_j}{\bar{v}_{Kj}} \quad (5)$$

For electrons and holes which take part in the conduction process,  $v_{Kj} = v_{Fj}$  the Fermi-velocity. So that we may rewrite (5) as

$$\bar{\tau}_j = \frac{\bar{L}_j}{v_{Fj}} \quad (6)$$

Now when an electric field  $E$  is applied, a force field  $eE$  operating will cause  $K$  to drift at the rate  $\dot{K} = eE/\hbar$ . When  $E$  is small, change in  $K$  in time  $\bar{\tau}_j$  given by

$\Delta K = \frac{eE}{\hbar} \bar{\tau}_j$  may be considered negligibly small to effect changes in  $v_{Kj}$  and hence

in  $\bar{\tau}_j$  (this situation is usually met). So, under small field condition  $\bar{\tau}_j$  becomes an additional relaxation time in the PG composite.

*Expression for Total Resistivity.* In addition to the above scattering mechanism, there is present the electron-phonon scattering as applicable to the ideal graphite crystal. Let the relaxation time for this be  $\tau_{th}$ . Then we may write according to Matthiessen's rule the total resistivity in any direction  $j$  as

$$\rho_{Tj} = \rho_{sj} + \rho_{tj} \quad \dots (7)$$

where the intercrystalline surface limited resistivity

$$\rho_{sj} = \frac{1}{\frac{ne^2}{m_{ej}^*} \tau_{ej} + \frac{pe^2}{m_{hj}^*} \bar{\tau}_{hj}} \quad \dots (8)$$

and the ideal graphite crystal resistivity

$$\rho_{tj} = \frac{1}{\frac{ne^2}{m_{ej}^*} \tau_{th}^e + \frac{pe^2}{m_{hj}^*} \tau_{th}^h}; \quad \dots (9)$$

$n, p$  are the electron and hole concentrations,  $m_e^*, m_h^*$  are the effective electron and hole masses  $\tau_{th}^e$  and  $\tau_{th}^h$  are the electron and hole thermal relaxation times of ideal single crystal graphite. Combining equations (6) (7) (8) and (9) we obtain

$$\rho_{Tj} = \frac{1}{\frac{ne^2}{m_{ej}^*} \frac{\bar{L}_j}{v_{Ej}^e} + \frac{pe^2}{m_{hj}^*} \frac{\bar{L}_j}{v_{Ej}^h}} + \frac{1}{\frac{n^2 e^2}{m_{ej}^*} \tau_{th}^e + \frac{p^2 e^2}{m_{hj}^*} \tau_{th}^h} \quad \dots (10)$$

## RESULTS

Single crystal graphite transport parameters are tabulated from McClure (1958) Soule, McClure & Smith (1964), the values being accepted as the most accurate, in table 1.

Calculated values of  $\rho_{Ta}$  and  $\rho_{Tc}$  according to equation (10) and the parameters of table 1 are plotted as a function of  $\bar{L}_a$  and  $\bar{L}_c$  in figures 1 and 2 respectively.

For Klein's (1962) deposited sample PG R-40 crystallite size in the basal plane as determined by X-ray analysis corresponds to a value  $\bar{L}_a = 285 \text{ \AA}$ . At  $L_a = 285 \text{ \AA}$  our calculated  $\rho_{Ta}$  according to equation (10) at a temperature of  $300^\circ K$  is

Table 1 Single crystal graphite transport parameters

 $j = a$ , along basal plane.  $j = c$  perpendicular to basal plane

$$\left. \begin{aligned} m_{ea}^* &= 0.03m_0, & m_{ha}^* &= 0.06m_0 \\ m_{ec}^* &= 4.39m_0, & m_{hc}^* &= 17.95m_0 \end{aligned} \right\} m_0 = 9.11 \times 10^{-31} \text{ Kgm.}$$

$n/c_1$			$\times 10^{10}$	cm/sec $\times 10^8$	cm/sec $\times 10^8$	sec $\times 10^{-12}$	sec $\times 10^{-12}$	cm/sec $\times 10^8$	cm/sec $\times 10^8$
4	2	2	1	2.0	0.93	0.54	10	2.2	0.0768
77		2.4	2.3	0.93	0.54	0.8	2.2	0.0768	0.312
300		7.3	7.2	1.5	0.80	0.19	0.33	0.1239	0.0462

$0.449 \times 10^{-3}$  ohm cm. Experimental value of  $\rho_{Ta}$  obtained by Klein for this sample at  $300^\circ\text{K}$  is  $0.452 \times 10^{-3}$  ohm cm. Agreement between experimental and calculated values is therefore excellent. Similar agreement is found at  $77^\circ\text{K}$  and  $4.2^\circ\text{K}$  for this sample.

As a further example, we consider Klein's  $R-7^*$  sample whose  $\bar{L}_a$  is  $700\text{\AA}$ . Again we find agreement between the experimental value  $0.21 \times 10^{-3}$  ohm cm and the calculated value  $0.215 \times 10^{-3}$  ohm cm.

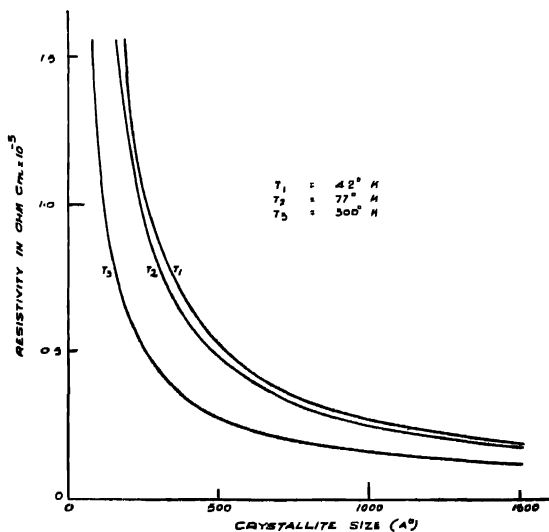


Figure 1. Theoretical basal plane resistivity of PG as a function of crystallite size along the basal plane.



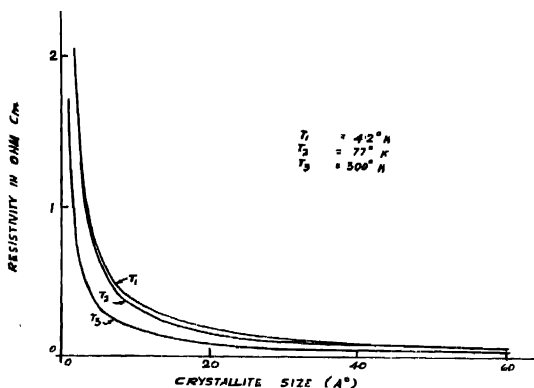


Figure 2. Theoretical *c*-axis resistivity of PG as a function of crystallite size along the *c*-axis.

In order to calculate resistivity along the *c*-axis, we require to know the layer spacing  $\bar{L}_c$ . Klein could not determine  $L_c$  by X-ray analysis because of diffused X-ray reflections. Recently  $\bar{L}_c$  values were determined (Thrower 1969) and are found to have a value of  $\bar{L}_c \approx 5\text{Å}$  for turbostratic graphite (deposited PG are usually turbostratic and since Klein's R-40 is a deposited sample it ought to have turbostratic structure). Putting  $L_c = 5\text{Å}$  in equation (10), we calculated  $\rho_{Tc}$  and obtained a value of 0.65 ohm cm at 77°K. Klein's experimental value of  $\rho_{Tc}$  of R-40 sample at 77°K is also 0.65 ohm cm.

Theoretically Soule, McClure & Smith (1964) found that  $\rho_c/\rho_a = 190$  at 300°K for single crystal graphite. This value of  $\rho_c/\rho_a$  is in reasonable agreement with the experimental values of Primak & Fuchs (1954). On the contrary  $\rho_c/\rho_a$  of PG as measured experimentally (Klein 1964, Saha, Banerjee & Das 1969) is found to have values ranging to several thousands. This is not surprising as can be seen from equation (10). So long  $L_a \ll$  thermal mean free path, anisotropy of PG should increase with the ratio  $\bar{L}_a/L_c$  and both  $\rho_{Tc}$  and  $\rho_{Ta}$  should decrease with increasing temperature.

### CONCLUSION

It is shown here that a unified point of view for the origin of electrical resistivities of single crystal graphite and pyrolytic graphite is permissible so long the intercrystalline space charge layer width is much smaller than crystallites' dimensions in the basal plane. Under this condition energy band structure may be considered to remain invariant but additional scattering of charge carriers occur at the boundary. Also, the long standing confusion (Klein 1962), why PG may

have larger anisotropy in resistivity than single crystal graphite and opposite kind of temperature dependence of resistivity from that of single crystal graphite, is resolved. Besides, the concepts used in this paper may be useful in a general way for elucidating electrical properties of polycrystalline matter in terms of the parameters of its constituent crystallites.

#### ACKNOWLEDGEMENT

The authors gratefully acknowledge the financial support provided by the Council of Scientific and Industrial Research, New Delhi. Thanks are also due to Prof. J S Chatterjee for his interest in the work

#### REFERENCES

- Bokros J. C. 1969 *Chemistry and Physics of Carbon*, Vol. 5, (Edited Walker, P. L.), Marcel Dekker, New York
- Klem G. A. 1962 *Rev. Mod. Phys.* **34**, 56; 1964 *J Appl Phys* **35**, 2947.
- McClure J. W. 1958 *Phys. Rev.* **112**, 715
- Mrozowski S 1952 *Phys. Rev.* **85**, 609
- Primak W. & Fuchs L. H. 1954 *Phys. Rev* **95**, 22.
- Reynolds W. N 1968 *Physical Properties of Graphite*, Elsevier, London.
- Saha A. R., Banerjee P. K. & Das A. K. 1969 *Indian J. Tech* **7**, 221.
- Schiff L. F., 1949 *Quantum Mechanics*, McGraw-Hill, New York, 181.
- Shockley W. 1950 *Electrons and Holes in Semiconductors*, Van Nostrand, New York. 424.
- Soule D. F., McClure J. W. & Smith L. R. 1964 *Phys. Rev* **134A**, 453.
- Thrower P. A. 1969 *Chemistry and Physics of Carbon* (Edited Walker P. L.) Marcel Dekker, New York.
- Wallace P. R. 1947 *Phys. Rev.* **71**, 622.

## Significant structure theory and thermodynamic properties of liquid carbonyl fluoride and trifluorophosphine

BY R. V. GOPALA RAO AND T. NAMMALVAR

*Department of Chemistry, S. V. U. College of Engineering, Tirupati*

(Received 10 September 1970—Revised 19 April 1971)

The significant structure theory has been used to evaluate the thermodynamic properties of the liquid carbonyl fluoride and trifluorophosphine. Since the entropy of fusion in the case of trifluorophosphine was found to be 1.837 e.u., free rotation was assumed even in the solid state. Hence for the 12 degrees of freedom for this molecule three were assigned for rotation three for translation and six for vibrations. In the case of carbonyl fluoride the entropy of fusion is very large (9.903 e.u.) and hence no rotation was assumed in the solid state. Out of the 12 degrees of freedom the solid like part was treated as a six degree Einstein oscillator with the remaining six degrees as vibrations for this molecule. The calculated properties like molar volumes, vapour pressures and entropies which involve the first derivatives of the partition function are in good agreement with experiment. Properties like thermal expansion coefficient, isothermal compressibility and heat capacities which involve the second derivatives of the partition function are also in satisfactory agreement with experiment. This shows that the partition function formulated on the basis of the significant structure theory for the two liquids investigated adequately represents the liquid state properties of the molecules.

### INTRODUCTION

The liquids carbonyl fluoride and trifluorophosphine have been investigated thermodynamically by Pace & Reno (1968), and Pace & Petrella (1962) respectively. The entropy of fusion was found to be 1.837 e.u. in the case of trifluorophosphine and 9.903 e.u. in carbonyl fluoride. The entropy of fusion was found to be very nearly equal to the so-called Communal Entropy which is nearly equal to  $R$ . Hence free rotation in the case of solid trifluorophosphine is assumed. In the case of carbonyl fluoride the entropy of fusion being very large no rotation is assumed in the solid state. Therefore it is important to study these two different molecules with very different entropies of fusion. We report here the thermodynamic properties as derived from the significant structure theory developed by Eyring and his collaborators (1948, 1962, 1966).

According to this theory the liquid is assumed to possess vacancies of molecular size which confer gas-like properties on a neighbouring molecule jumping into the holes and hence a solid-like molecule acquires positional degeneracy equal to the number of neighbouring vacancies. Assuming random distribution of vacancies the mole fractions of gas-like and solid-like molecules are  $(V - V_s)/V$  and  $V_s/V$  respectively. Here  $V$  and  $V_s$  are the molar volumes of the liquid and reference solid respectively.

*Phosphorous trifluoride (Trifluorophosphine PF<sub>3</sub>)*

Out of 12 degrees of freedom for this tetra-atomic molecule three were assigned to rotation, three for translation and six for vibration. Thus the partition function for liquid trifluorophosphine becomes

$$f_{PF_3} = \left[ \frac{e^{E_s/kT}}{(1 - e^{-\theta/T})^3} \frac{\pi^{\frac{1}{2}}}{\sigma} \left( \frac{8\pi^2 kT}{h^2} \right)^{3/2} (I_A I_B I_C)^{\frac{1}{2}} \frac{\pi}{\pi_{i=1}} (1 - e^{-h\nu_i/kT})^{-1} \{1 + n(x-1)e^{-w}\} \right]^{N/\tau}$$

$$\left[ \left( \frac{2\pi mkT}{h^2} \right)^{3/2} \frac{\pi^{\frac{1}{2}}}{\sigma} \left( \frac{8\pi^2 kT}{h^2} \right)^{3/2} (I_A I_B I_C)^{\frac{1}{2}} \frac{\pi}{\pi_{i=1}} (1 - e^{-h\nu_i/kT})^{-1} \frac{eV}{N} \right]^{N(1-1/\alpha)} \dots (1)$$

Here  $x = V/V_s$ ,  $\theta$  is the characteristic temperature of the liquid,  $\sigma$  is the so-called symmetry number which in the present case is equal to 3,  $w = \frac{aE_s}{RT(x-1)}$  and  $\nu_i$  are the characteristic fundamental vibrational frequencies (Pace *et al* 1962) and the rest of the symbols have their usual statistical mechanical significance. The parametric values  $n$ ,  $a$ ,  $\theta$ ,  $V_s$  and  $E_s$  are determined according to Chang's method (Rao & Swamy 1970). While adopting this method  $E_s$  value is varied so as to give the best fit at the melting point. The values so found are:  $n = 11.604$ ,  $a = 7.5963 \times 10^{-4}$ ,  $E_s = 4249.2$  cal/mol,  $V_s = 47.394$  cc/mol,  $\theta = 75.56^\circ\text{K}$ .

*Carbonyl fluoride (COF<sub>2</sub>):*

As pointed out already this substance has a high entropy of fusion (9.903 e.u.) which indicates that there is no free rotation at all in the solid state. Hence out of the 12 degrees of freedom the solid like part is treated as a six degree Einstein oscillator with the remaining six degrees as vibrations. The characteristic vibration frequencies are taken from Pace & Reno (1968). Thus the partition function for liquid carbonyl fluoride can be written as

$$f_{COF_2} = \left[ \frac{e^{E_s/kT}}{(1 - e^{-\theta/T})^6} \frac{\pi}{\pi_{i=1}} (1 - e^{-h\nu_i/kT})^{-1} \{1 + n(x-1)e^{-w}\} \right]^{N/\tau}$$

$$\left[ \left( \frac{2\pi mkT}{h^2} \right)^{3/2} \frac{\pi^{\frac{1}{2}}}{\sigma} \left( \frac{8\pi^2 kT}{h^2} \right)^{3/2} (I_A I_B I_C)^{\frac{1}{2}} \frac{\pi}{\pi_{i=1}} (1 - e^{-h\nu_i/kT})^{-1} \frac{eV}{N} \right]^{N(1-1/\alpha)} \dots (2)$$

Here the symmetry number of the molecule is 2 and the rest of the symbols have been explained already. The parametric values so found are:  $n = 11.07$ ,  $a = 2.5484 \times 10^{-3}$ ,  $E_s = 5739$  cal/mol,  $V_s = 53.931$  c.c./mol,  $\theta = 45.653^\circ\text{K}$ .

#### EVALUATION OF THERMODYNAMIC PROPERTIES OF THE LIQUIDS FROM THE PARTITION FUNCTION

The Helmholtz free energy  $A$  is related to the partition function by the well known equation

$$A = -kT \ln f \dots (3)$$

Hence from equations 1 and 2 we get

$$A = \frac{RT}{x} (\lambda_1 + \lambda_2) - RT(1 - 1/x)(\lambda_3 + \ln x) \quad (4)$$

Here

$$\lambda_1^{\text{PF}_3} = \frac{H_s}{RT} - 3 \ln(1 - e^{-\theta/T}) + \ln f_{\text{rot}}^{\text{PF}_3} - \ln f_{\text{vib}}^{\text{PF}_3} \quad (5)$$

$$f_{\text{rot}}^{\text{PF}_3} = \frac{\pi^{\frac{1}{2}}}{3} \left( \frac{8\pi^2 kT}{h^2} \right)^{3/2} (I_A I_B I_C)^{\frac{1}{2}} \quad \dots \quad (6)$$

$$f_{\text{vib}}^{\text{PF}_3} = \frac{6}{\pi} (1 - e^{-h\nu_i/kT})^{-1} \quad \dots \quad (7)$$

$$\lambda_2^{\text{PF}_3} = \ln [1 + n(x-1)e^{-w}] \quad \dots \quad (8)$$

$$\lambda_3^{\text{PF}_3} = \left\{ \frac{3}{2} \ln \left( \frac{2\pi m kT}{h^2} \right) + \frac{3}{2} \ln \left( \frac{8\pi^2 kT}{h^2} \right) + \frac{1}{2} \ln (I_A I_B I_C) + \frac{1}{2} \ln \pi - \ln \sigma \right. \\ \left. - \sum_{i=1}^6 \ln (1 - e^{-h\nu_i/kT}) + \ln \frac{eV_s}{N} \right\} \quad \dots \quad (9)$$

While in the case of  $\text{COF}_2$  we have

$$\lambda_1^{\text{COF}_2} = \frac{H_s}{RT} - 6 \ln(1 - e^{-\theta/T}) - \sum_{i=1}^6 \ln(1 - e^{-h\nu_i/kT}) \quad (10)$$

while in the case of carbonyl fluoride similar equations as given in (8) and (9) hold good for  $\lambda_2^{\text{COF}_2}$  and  $\lambda_3^{\text{COF}_2}$ . Remembering that  $P = -(\partial A / \partial V)_T$  the Helmholtz free energy is plotted for a given temperature as a function of volume. The volumes at the points of common tangency are the volumes of the corresponding phases and the vapour pressure is given by the slope of the tangent. Except at the triple point a tangent has at most two points of tangency (Eyring *et al* 1964). The volumes and vapour pressures so evaluated are given in tables 1 and 2, and are compared with observed values of Pace & Petrella (1962) and Pace & Reno (1968). A curve of the vapour pressure *versus* temperature is shown in figure 1.

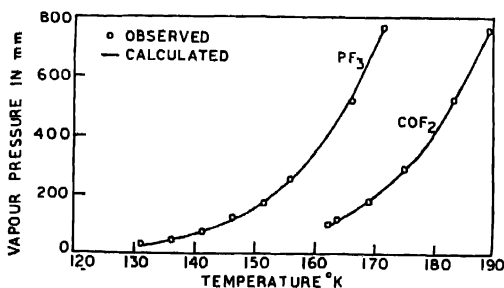


Figure 1. Vapour pressure *vs* temperature.

Table 1. Calculated and observed thermodynamical properties of liquid trifluorophosphine

Temp°K	Volumec/mole	Vapour pressure in mm	$-A/RT$	$S$ cal/mole-deg	$\alpha \times 10^3$ deg $^{-1}$	$\beta \times 10^6$ atm $^{-1}$	$C_p$ cal/mole-deg	
131	49.811	22.201	27.3481	32.5942	1.9806	87.518	12.6051	Calc
	49.223	27.001	—	—	2.5268	—	—	Obs
136	50.24	39.521	26.9254	33.2371	1.9318	90.766	12.7343	Calc
	50.773	44.605	—	—	2.5707	—	—	Obs
141	50.716	67.315	26.544	33.8823	2.0957	104.67	12.8273	Calc
	51.006	71.561	—	—	2.6125	—	—	Obs
146	51.566	109.86	26.1997	34.6747	2.2292	118.34	12.9400	Calc
	51.10	111.68	—	—	2.6368	—	—	Obs
151	51.85	172.57	25.8882	35.1853	2.1255	120.82	13.0156	Calc
	52.79	169.04	—	—	2.6923	—	—	Obs
156	52.608	262.79	25.6068	35.8731	2.5758	157.11	13.0953	Calc
	53.496	250.49	—	—	2.725	—	—	Obs
166	54.03	557.83	25.1228	37.3014	2.5777	181.29	13.6176	Calc
	54.97	517.0	—	—	2.8016	—	—	Obs
171.77	54.504	795.5	24.9488	37.9648	2.6239	190.86	13.8663	Calc
	55.793	760	—	38.041	2.8675	—	—	Obs

Table 2. Calculated and observed thermodynamical properties of liquid carbonyl fluoride

Temp°K	Volumec/mole	Vapour pressure in mm	$-A/RT$	$S$ cal/mole-deg	$\alpha \times 10^3$ deg $^{-1}$	$\beta \times 10^6$ atm $^{-1}$	$C_p$ cal/mole-deg	
161.89	(58.46)	(93.75)	26.1275	29.7296	3.2269	161.26	14.9706	Calc
(M.P.)	58.46	93.75	—	29.730	3.7198	—	—	Obs
163.6	58.89	110.04	26.0429	30.0633	2.9995	156.35	15.0601	Calc
	58.836	109.60	—	—	3.7403	—	—	Obs
169	60.187	177.21	25.6969	41.0058	2.9105	170.58	15.0031	Calc
	60.05	178.6	—	—	3.8123	—	—	Obs
174.94	61.373	286.54	25.3595	31.9082	3.1232	200.98	15.6516	Calc
	61.443	289.89	—	—	3.914	—	—	Obs
182.9	61.697	510.98	24.9613	32.5632	2.9657	197.02	16.2235	Calc
	63.419	520.16	—	—	4.1479	—	—	Obs
188.58	62.669	741.45	24.7097	33.2844	3.1843	226.46	16.5769	Calc
(B.P.)	64.91	76.0	—	33.777	4.2779	—	—	Obs

# ENTROPY OF VAPORIZATION

Molar entropies of the liquid are calculated from the well known equation

$$S = -(\partial A / \partial T)_V \quad \dots (11)$$

The values so calculated are given in the two tables in columns 5 for trifluorophosphine and carbonyl fluoride respectively. The entropy of vaporization is determined as the difference in the entropy of the gas and liquid and the values are :

PF <sub>3</sub>	at 171.77°K	20.4102 (Cal)	20.289 (obs)
COF <sub>2</sub>	at 188.58°K	23.9970 (Cal)	23.17 (obs)

# COMPRESSIBILITY THE LIQUIDS

The isothermal compressibility is given by

$$\beta = -\frac{1}{V} \left( \frac{\partial V}{\partial P} \right)_T = \frac{1}{V \left( \frac{\partial^2 A}{\partial V^2} \right)} \quad \dots (12)$$

Further we have  $P = -(\partial A / \partial V)_T$ . Hence from equation (4) we get

$$P = \frac{RT}{V_s x^2} \left[ -(\lambda_1 + \lambda_2) + x \left( \frac{\partial \lambda_2}{\partial x} \right)_T + \lambda_3 + \ln x + x - 1 \right] \quad \dots (13)$$

Hence we have for the isothermal compressibility of the liquid

$$\frac{1}{\beta} = \frac{-RT}{V_s x^2} \left[ x^2 \frac{\partial^2 \lambda_2}{\partial x^2} - 2x \left( \frac{\partial \lambda_2}{\partial x} \right)_T + 2\lambda_2 - x + 3 - 2(\lambda_3 + \ln x - \lambda_1) \right] \quad \dots (14)$$

This will form a severe test of the partition function since it involves the second derivatives. The values calculated from equation (14) are given in the tables in columns 7 for trifluorophosphine and carbonyl fluoride respectively.

By definition

$$\alpha = \frac{1}{V} \left( \frac{\partial V}{\partial T} \right)_P = -\frac{1}{V} \left( \frac{\partial^2 A}{\partial V \partial T} \right) / \left( \frac{\partial^2 A}{\partial V^2} \right) = \beta \left( \frac{\partial P}{\partial T} \right)_V \quad \dots (15)$$

Hence from equation (13) we get

$$\begin{aligned} \frac{\partial P}{\partial T} = \frac{R}{V_s x^2} & \left[ -(\lambda_1 + \lambda_2) + x \left( \frac{\partial \lambda_1}{\partial x} \right) + \lambda_3 + \ln x + x - 1 - T \left( \frac{\partial \lambda_1}{\partial T} \right) - T \left( \frac{\partial \lambda_2}{\partial T} \right) \right. \\ & \left. + x \left\{ \frac{\partial}{\partial T} \left( \frac{\partial \lambda_2}{\partial x} \right)_T \right\}_V + T \frac{\partial \lambda_3}{\partial T} \right] \quad \dots (16) \end{aligned}$$

The calculated and observed values are given in table 1 and 2 column 6 for trifluorophosphine and carbonyl fluoride respectively.

The heat capacity at constant volume is given by

$$C_V = T \left( \frac{\partial S}{\partial T} \right)_V = \frac{R}{x} \left[ 2T \left( \frac{\partial \lambda_1}{\partial T} \right)_x + T^2 \left( \frac{\partial^2 \lambda_1}{\partial T^2} \right)_x + 2T \left( \frac{\partial \lambda_2}{\partial T} \right)_x + T^2 \left( \frac{\partial^2 \lambda_2}{\partial T^2} \right)_x \right] \\ - R(1-1/x) \left[ 2T \left( \frac{\partial \lambda_3}{\partial T} \right)_x + T^2 \left( \frac{\partial^2 \lambda_3}{\partial T^2} \right)_x \right] \quad (17)$$

and the values obtained are shown in column 8 of the tables.

### DISCUSSION

In both the above liquids, the calculated and observed volumes, vapour pressures and entropies agree very well. The calculated properties like thermal expansion coefficient, isothermal compressibility and heat capacities are also in satisfactory agreement with experiment thereby proving that the partition functions formulated adequately represent the liquid state of the two molecules.

### ACKNOWLEDGEMENT

One of the authors (T.N.) is grateful to the Council of Scientific and Industrial Research, India, for the award of a Research Fellowship during the work.

### REFERENCES

- Chang S., Pak H., Paik W., Park S., Jhon M. S. & Ahn W. S. 1964 *J. Korean Chem. Soc.* **8**, 33.  
 Eyring H., Henderson D., Stover B. J. & Eyring E. M. 1964 *Statistical Mechanics and Dynamics*, John Wiley & Sons Inc., New York, 354.  
 Pace E. L. & Petrella R. V. 1962 *J. Chem. Phys.* **36**, 2991.  
 Pace E. L. & Reno M. A. 1968 *J. Chem. Phys.* **48**, 1231.  
 Rao R. V. G. & Swamy K. N. 1970 *Zent. Physik. Chemie (Neue Folge)* **71**, 218.  
 Eyring H., Henderson D. & Ree T. 1962 *Progress in International Research on Thermodynamics and Transport Properties*. The American Society of Mechanical Engineers, Academic Press, New York 340.  
 Eyring H., Ree T. & Hirai N. 1948 *Proc. Nat. Acad. Sci. (U.S.A.)* **44**, 683.  
 Melaughlin D. R. & Eyring H. 1966 *Proc. Nat. Sci. (U.S.A.)* **55**, 1031.



## Dielectric relaxation of some large aromatic molecules in benzene from microwave absorption measurements

F. F. HANNA and K. N. ABDEL-NOUR

Microwave Laboratory, National Research Centre, Dokki, Cairo, U.A.R.

(Received 5 August 1970)

The dielectric constant ( $\epsilon'$ ) and dielectric loss ( $\epsilon''$ ) of three large aromatic molecules namely  $\alpha$ ,  $\alpha'$ ,  $\alpha'$ , 2, 3, 5, 6-octachloro-*p*-xylene, 9-acetyl anthracene and acridan have been measured at four wavelengths between 0.2 cm and 25 cm and at two or three temperatures between 20° and 60°C. The data have been analysed and two relaxation times have been found in each case. The results obtained are interpreted.

Measurements of  $\epsilon'$  and  $\epsilon''$  are carried out at wavelengths 0.22, 3.24, 10 and 25 cm. to an accuracy of 2%. The apparatus used have been described before by Garg *et al* (1965), Laquer & Smyth (1949), Pitt & Smyth (1959). The static dielectric constant  $\epsilon$  has been measured at 10KHz using General Radio Low Frequency Bridge Type 1615A.

Three large aromatic molecules of grade 'Pure' were measured namely  $\alpha$ ,  $\alpha'$ ,  $\alpha'$ , 2, 3, 5, 6-octachloro-*p*-xylene, acridan (both obtained from Almdrich Chemical Co Inc.) and 9-acetyl anthracene (obtained from K & K Laboratories Inc.). Benzene "Analar" was distilled twice over sodium and used as a solvent. Dilute solutions of the substances under test in benzene were used.

$\epsilon_0$ ,  $\epsilon'$  and  $\epsilon''$  were measured at temperatures ranging between 20° and 60°C with the exception of acridan.  $\epsilon'$  and  $\epsilon''$  for the substances used were plotted in a complex plane (Cole & Cole 1941) and the dispersion step ( $\epsilon_0 - \epsilon_\infty$ ) was obtained for each substance at the different temperatures from these arc plots. As an example, the arc plot of 9-acetyl anthracene at 20°C is given in figure 1. Then the

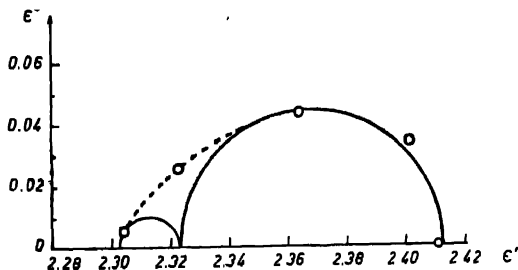


Figure 1. Arc plot for 9-acetyl anthracene in benzene at 20°C (for concentration 0.0099 mole fraction).

reduced absorption  $\eta'' = \frac{\epsilon''}{\epsilon_0 - \epsilon_\infty}$  was calculated for each frequency. The values of  $\eta''$  were plotted against  $\log \lambda$ . The absorption curves obtained were analysed into two Debye terms using the equation

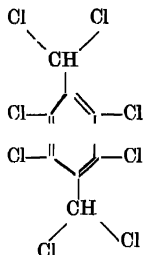
$$\eta'' = (1-G) \frac{\omega\tau_1}{1+\omega^2\tau_1^2} + G \frac{\omega\tau_2}{1+\omega^2\tau_2^2}$$

The numerical analysis has been carried out using a computer IBM 1620.

In case of acridan the variation of  $\epsilon'$  with frequency was very small so that it was difficult to draw the arc plots and hence  $\eta''$  could not be calculated.  $\epsilon''$  was plotted against  $\log f$  and the results were analysed also into two Debye terms. The results of the analyses of all substances are given in table 1.

### DISCUSSION

#### 1. $\alpha, \alpha', \alpha', 2, 3, 4, 6$ -octachloro *p*-xylene :



The measurements were carried out at 20° and 40°C only. It was possible to measure  $c''$  at a wavelength 1.25 cm at 20°C and so  $\eta''$  for this frequency was also calculated. Figure 2 shows the results of analysis at 20°C and 40°C. As shown, the analyses represent the experimental data very well and the absorption curves are found to be composed of two Debye terms having relaxation times  $\tau_1$  and  $\tau_2$ . The availability of the measured values at 2 mm wavelength assure these analyses. The longer relaxation time  $\tau_1$  is that which may be due to the rotation of a molecule of this size as a whole. The short relaxation time  $\tau_2$  is due to a complete rotation of the  $\text{CHCl}_2$  groups. From Stuart & Briegleb model, it is found that no complete rotation of the group is permissible. So, it is concluded that the rotation of the  $\text{CHCl}_2$ -groups is restricted to a slight rotating oscillation by the adjacent Cl-groups. The value of  $\tau_2$  (5.18 psec at 20°C) is comparable with the value 3.72 psec for the  $\text{CH}_2\text{Cl}$ -group in  $\alpha, \alpha'$ , dichloro-*p*-xylene (Purcell *et al* 1960).  $\tau_2$  is very temperature dependent as would be expected for the oscillation of the  $\text{CHCl}_2$  groups while  $G$  does not change much.

TABLE I Dielectric constants, dielectric losses, relaxation times and dipole moments in benzene solutions

Substance	$t^{\circ}\text{C}$	$\epsilon_0$	$\lambda_{\text{cm}}$	$\epsilon'$	$\epsilon''$	$\epsilon_0 - \epsilon_{\infty}$	$\eta'' = \frac{\epsilon' - \epsilon_{\infty}}{\epsilon_0 - \epsilon_{\infty}}$	$\tau_1$ psec	$\tau_2$ psec	$G$	$\mu$
$\alpha, \alpha, \alpha', \alpha', 2, 3, 5, 6$ octachloro <i>p</i> -xylene $x = 0.0336$ mole fraction	20	2.422	0.216	2.320	0.0045	0.102	0.049	84.2	5.18	0.20	1.43
			1.25	2.328	0.0177		0.177				
			3.24	2.339	0.0212		0.206				
			10.00	2.362	0.0403		0.392				
			25.00	2.405	0.0382		0.372				
9-acetyl anthracene $x = 0.0099$ mole fraction	40	2.377	0.216	2.287	0.0079	0.093	0.088	59.5	3.85	0.25	
			3.24	2.300	0.0241		0.258				
			10.00	2.352	0.0371		0.398				
			25.00	2.373	0.0271		0.291				
	20	2.411	0.216	2.304	0.0052	0.108	0.043	65.3	5.10	0.20	2.75
			3.24	2.323	0.0257		0.239				
			10.00	2.364	0.0450		0.417				
			25.00	2.402	0.0340		0.315				
	60	2.320	0.216	2.228	0.0087	0.063	0.093	35.1	4.40	0.30	
			3.24	2.253	0.0331		0.356				
			10.00	2.285	0.0326		0.360				
			25.00	2.317	0.0176		0.188				
Acridan $x = 0.0087$ mole fraction	20	2.308	0.216	2.289	0.0012	—	—	64.9	4.42	0.42	—
			3.24	2.306	0.0026		—				
			10.00	2.308	0.0035		—				
			25.00	2.308	0.0028		—				
							—				
	40	2.280	0.216	2.257	0.0034	—	—	58.9	2.35	0.58	
			3.24	2.267	0.0024		—				
			10.00	2.268	0.0033		—				
			25.00	2.280	0.0023		—				
							—				

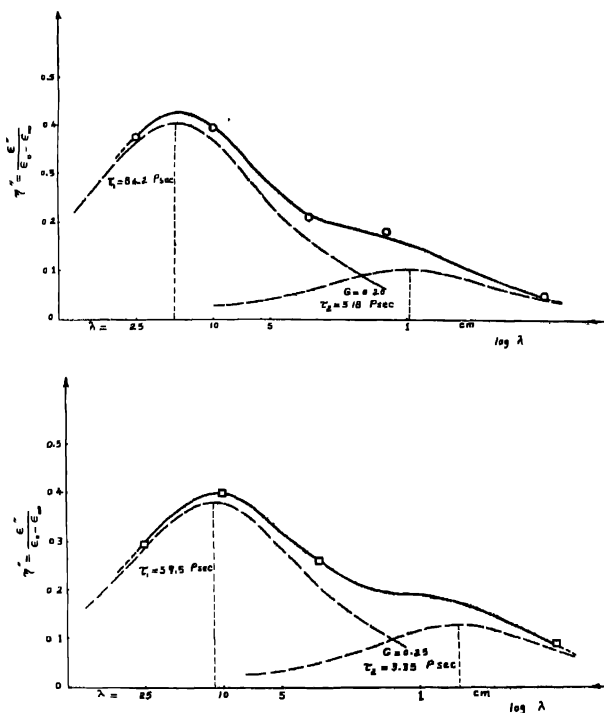
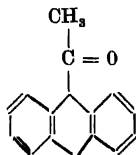


Figure 2. Absorption of  $\alpha, \alpha', \alpha', 2, 3, 5, 0$ -octachloro-*p*-xylene in benzene at 20° and 40°C for concentration 0.0336 mole fraction obtained from the sum of two Debye terms having relaxation times  $\tau_1$  and  $\tau_2$

The dipole moment ( $\mu$ ) was calculated at the two temperatures and was found to be 1.43 D.

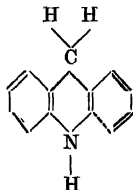
### 2, 9-Acetyl Anthracene



The measurements were carried out in this case at 20° and 60°. It was found in the case of 1-acetyl naphthalene (Fong & Smyth 1963) that the molecule possesses only one relaxation time due to the blocking of the acetyl group by the 8-hydrogen

atom, the acetyl group in 2-acetyl naphthalene is able to rotate having a relaxation time 7.3 psec. Following this interpretation, it is expected that the acetyl-group in the 9-acetyl anthracene will be more blocked by the 1- and 8-hydrogen atom. Anyhow, the relation between  $c'$  and  $c''$  plotted in a complex plane could not be represented by one semicircle. Both absorption curves at 20°C and 60°C are composed of two Debye terms. Figure 1 shows the arc plot obtained at 20°C as an example. The measurements at 2 mm wavelength helped much in obtaining this result. From Stuart & Briegleb model, it is found that the acetyl group may possess a restricted rotation. It is therefore suggested that the longer relaxation time  $\tau_1$ , is to be attributed to the rotation of the molecule as a whole and the shorter relaxation time  $\tau_2$  is due to a restricted orientation of the acetyl group. The values of  $\tau_1$ , shown in table 1, are reasonable for a molecule of that size. The value of  $\tau_2$  (5.10 psec at 20°C) obtained for the restricted rotation of the acetyl group in 9-acetyl anthracene is smaller than the value obtained (7.3 psec at 20°C) for the acetyl-group in 2-acetyl naphthalene which is supposed to have free rotation. As the weight of  $\tau_2$  on the total absorption is not much affected with temperature  $\mu$  is also calculated and is found to be 2.75D.

### 3 Acridan



The measurements were taken at 20° and 40°C. No values of  $(\epsilon_0 - \epsilon_\infty)$  could be obtained due to the very small variation of  $\epsilon'$  with frequency as mentioned before, hence the reduced absorption  $\eta''$  could not be calculated. The values of  $c''$  at each temperature are plotted against  $\log f$ . The measurements of  $\epsilon''$  at 2 mm wavelength (specially at 40°C) show that the absorption cannot be represented by one Debye term. The analysis is carried out as shown in figure 3 using two Debye terms having relaxation times  $\tau_1$  and  $\tau_2$ . The longer relaxation time  $\tau_1$ , which is about the same as that for 9-acetyl anthracene, (molecule being about the same size) could be attributed to the rotation of the whole molecule. This is a reasonable value for a molecule of that size. While the short relaxation time  $\tau_2$  may be due to an internal motion within the molecule. From Stuart & Briegleb model it is seen that the molecule can have an internal motion. This internal motion could not be an orientation but may be due to a tipping over of one of the outer benzene rings. This type of motion, as expected is very temperature dependent.

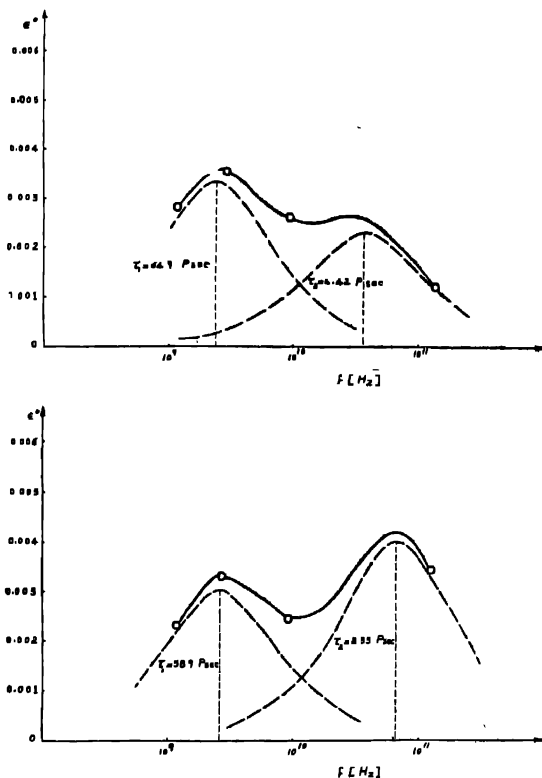


Figure 3. Absorption of acridan in benzene at 20° and 40°C for concentration 0.0087 mole fraction obtained from the sum of two Debye terms having relaxation times  $\tau_1$  and  $\tau_2$ .

#### ACKNOWLEDGEMENT

We thank Prof. Dr. M. Mokhtar, Cairo University, for his kind interest in this work. We also thank Prof. Dr. C. P. Smyth, Princeton University, for allowing Mr. K. N. Abd-El-Nour to take the measurements in his laboratory.

#### REFERENCES

- Cole K. S. & Cole R. H. 1941 *J. Chem. Phys.* **9**, 431.  
 Fong F. K. & Smyth, C. P. 1963 *J. Am. Chem. Soc.* **85**, 1565.  
 Garg S. K., Klip H. & Smyth C. P. 1965 *Chem. Phys.* **43**, 2341.  
 Laquer H. L. & Smyth C. P. 1949 *J. Am. Chem. Soc.* **70**, 4097.  
 Pitt D. A. & Smyth C. P. 1959 *J. Phys. Chem.* **63**, 582.  
 Purcell, W. P., Fish, K. & Smyth, C. P. 1960 *J. Am. Chem. Soc.* **82**, 6299.

# Oscillations of an inhomogeneous bounded plasma

By TUSHAR RAY

Department of Physics, Panskura B. College, Panskura, Midnapore, India

(Received 16 July 1970—Revised 22 December 1970)

Quasi-static waves on a plasma cylinder with radially varying density have been studied. An approximate dispersion relation is derived, with the use of a di-electric tensor which is a local quantity, and is compared with the case of a homogeneous plasma cylinder.

## INTRODUCTION

The study of oscillations of a plasma cylinder is of interest as this configuration has been used in several laboratory experiments (Apel 1969, Barrett *et al* 1968, Wong *et al* 1964). The case of homogeneous magnetoactive plasma confined within a cylindrical conductor has been studied by Lichtenberg & Jayson (1965). These authors have used a di-electric tensor which is correct within the quasi-static approximation and approximation of longitudinal velocity only. Inhomogeneous plasma in the same configuration has been considered by Lee (1969). Here the same problem of inhomogeneous plasma in a metallic cylinder is treated, but with the use of di-electric tensor whose local value is of the form used by Lichtenberg & Jayson, with this exception that only one component plasma is considered and the velocity of streaming neglected. The dispersion relation is derived using quasi-static approximation and reduced for the case of cold plasma also. The results have been compared with the case of a homogeneous bounded plasma.

## DERIVATION OF THE DISPERSION RELATION

A plasma cylinder of radius  $b$  is surrounded by a co-axial cylindrical conducting wall of radius  $a$ . The cross-sectional variation of plasma density is assumed as

$$n(r) = n_0 f(r) \quad \dots (1)$$

with  $f(r) = 1 - r^2/\lambda_1^2$ , so that  $n_0$  is the density on the axis  $r = 0$ , of the cylinder. There is a steady magnetic field  $H$  along this axis.

The di-electric tensor used in this analysis is of the form

$$\bar{\epsilon} \equiv \begin{bmatrix} \epsilon_{rr} & i\epsilon_{r\theta} & 0 \\ -i\epsilon_{r\theta} & \epsilon_{\theta\theta} & 0 \\ 0 & 0 & \epsilon_{zz} \end{bmatrix} \quad \dots (2)$$

$$\begin{aligned}
\text{with } \epsilon_{rr} &= 1 + \frac{\omega_p^2 f(r)}{2^{3/2} K_z \omega_H v_T} [z(\zeta_2) - z(\zeta_1)] = 1 + \tau f(r) \\
\epsilon_{r\theta} &= \frac{\omega_p^2 f(r)}{2^{3/2} K_z \omega_H v_T} [2z(\zeta_3) - z(\zeta_2) - z(\zeta_1)] \quad \} \quad \dots \quad (2A) \\
\epsilon_{zz} &= 1 + \frac{\omega_p^2 f(r)}{K_z^2 v_T^2} [1 + \zeta_3 z(\zeta_3)] = 1 + \tau_0 f(r)
\end{aligned}$$

where  $z(\zeta) = 2ie^{-\zeta^2} \int_{-\infty}^{\zeta} \exp(-t^2) dt$  which is tabulated by Fried & Conte (1961).

$$\begin{aligned}
\zeta_1 &= \frac{\omega + \omega_H}{2^{1/2} K_z v_T}, \quad \zeta_2 = \frac{\omega - \omega_H}{2^{1/2} K_z v_T}, \quad \zeta_3 = \frac{\omega}{2^{1/2} K_z v_T} \\
\omega_p^2 &= \frac{4\pi n_0 e^2}{m}, \quad \omega_H = \frac{eH}{mc}
\end{aligned}$$

Here the Maxwellian velocity distribution with the thermal velocity  $v_T$  and the variation  $\sim e^{i(K_z z - \omega t)}$  are assumed. In using the local value of the dielectric tensor the restriction  $KL < 1$  is imposed,  $K$  being the wave number and  $L$  the characteristic scale length of the plasma density variation. This condition is automatically satisfied for axially propagating quasi-static wave, i.e. for  $K_r = 0$ . In the quasi-static approximation  $\vec{E}$  is derivable from a scalar potential, i.e.

$$\vec{E} = -\nabla\psi$$

Hence the equation  $\nabla \cdot \vec{D} = 0$  becomes

$$\nabla \cdot (\epsilon \nabla \psi) = 0 \quad \dots \quad (3)$$

For the axi-symmetric mode, the equation (3) becomes in the cylindrical polar co-ordinates

$$\frac{d^2\psi}{dr^2} + \frac{1}{r} \frac{d\psi}{dr} + \frac{d}{dr} (\ln \epsilon_{rr}) \cdot \frac{d\psi}{dr} - \frac{\epsilon_{zz}}{\epsilon_{rr}} K_z^2 \psi = 0 \quad \dots \quad (4)$$

Or,

$$u[1 + \tau f(u)] \frac{d^2\psi}{du^2} + \left[ 1 + \tau f(u) + u\tau \frac{df(u)}{du} \right] \frac{d\psi}{du} - u[1 + \tau_0 f(u)] \psi = 0$$

where  $u = rK_z$  and  $f(u) = 1 - \frac{u^2}{\lambda_1^2 K_z^2} = 1 - \frac{u^2}{\lambda^2}$ .



This is a Sturm-Liouville equation which is here solved by the variational method, outlined by Margenau and Murphy (1966). The trial solution is taken as

$$\varphi = \varphi_0 + \frac{1}{2}\varphi_1(K_e^2 b^2 - u^2) = \varphi_0 + \frac{1}{2}\varphi_1(\delta^2 - u)$$

so that

$$\varphi|_{r=b} = \varphi_0,$$

$\varphi_0$  and  $\varphi_1$  are related by the condition

$$\frac{dk(\varphi)}{d\varphi_1} = 0 \quad \dots (5)$$

where

$$k(\varphi) = \int_0^\delta [1 + \tau f(u)] \varphi_1^2 u^2 du + \int_0^\delta [1 + \tau_0 f(u)] \cdot \left[ \varphi_0^2 + \frac{1}{4} \varphi_1^2 (\delta^2 - u^2)^2 + \varphi_0 \varphi_1 (\delta^2 - u^2) \right] u du$$

Outside the plasma column the equation (4) reduces to

$$\frac{d^2 \varphi}{du^2} + \frac{1}{u} \cdot \frac{d\varphi}{du} - \varphi = 0$$

the solution of which is

$$\varphi = AI_0(u) + BK_0(u)$$

where  $I_0$  and  $K_0$  are modified Bessel functions of order zero and,  $A$  and  $B$  are constants. At

$$u = ak_z = \Delta, \quad \frac{d\varphi}{du} = 0$$

Hence in the vacuum region

$$\varphi = \frac{A}{K_0(\Delta)} [K_0(\Delta)I_0(u) - I_0(\Delta)K_0(u)]$$

Again at  $u = \delta$ ,

$$\varphi_{\text{plasma}} = \varphi_{\text{vacuum}}$$

$$\epsilon_{rr}(\delta) \cdot \frac{d\varphi_{\text{plasma}}}{du} = \frac{d\varphi_{\text{vacuum}}}{du}$$

These boundary conditions along with the equation (5) give the dispersion relation as

$$\begin{aligned} & [K_0(\Delta)I_0(\delta) - I_0(\Delta)K_0(\delta)] \left( 1 + \tau - \tau \cdot \frac{\delta^2}{\lambda^2} \right) \cdot \delta \cdot \left[ \frac{1}{4} (1 + \tau_0) - \frac{1}{12} \tau_0 \frac{\delta^2}{\lambda^2} \right] \\ & = [K_0(\Delta)I_0'(\delta) - I_0(\Delta)K_0'(\delta)] \left[ \frac{1}{2} (1 + \tau) - \frac{1}{3} \tau \cdot \frac{\delta^2}{\lambda^2} + \frac{1}{12} (1 + \tau_0) \delta^2 - \frac{1}{48} \tau_0 \delta^2 \cdot \frac{\delta^2}{\lambda^2} \right] \end{aligned}$$

... (6)

## DISCUSSION

For a completely filled wave-guide  $\delta = \Delta$ , and the equation (6) becomes

$$\frac{1}{2} (1 + \tau) - \frac{1}{3} \tau \epsilon^2 + \frac{1}{12} (1 + \tau_0) \cdot \delta^2 - \frac{1}{48} \cdot \tau_0 \delta^2 \cdot \epsilon^2 = 0 \quad \dots (7)$$

where  $\epsilon = \delta/\lambda$  determines the plasma density at the guide-wall. Taking zero density at the guide-wall ( $\epsilon = 1$ ) the equation (7) becomes

$$\delta^2 = -6 \cdot \frac{1 + \tau/3}{1 + 3\tau_0/4} \quad \dots (8)$$

For a homogeneous plasma ( $c = 0$ ) in a cylindrical waveguide the equation (7) becomes

$$\delta^2 = -6 \cdot \frac{1 + \tau}{1 + \tau_0} \quad \dots (9)$$

Case 1. For cold plasma

$$\tau = \frac{\omega_p^2}{\omega_H^2 - \omega^2} \quad \text{and} \quad \tau_0 = -\frac{\omega_p^2}{\omega^2}$$

Taking  $\omega_H/\omega_p = 2$  the relations (8) and (9) are plotted in figure 1. It is found that the stop-band is wider in the case of inhomogeneous plasma.

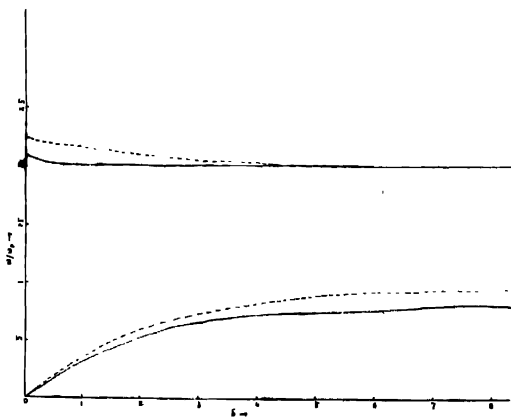


Figure 1

Case 2. For hot plasma, taking  $\omega_H/\omega_p = 2$  and  $v_T/\alpha\omega_p = .072$  the relations (8) and (9) are plotted in figure 2. It is found that as in the case of cold plasma, the values of  $K_z$  for the inhomogeneous hot plasma are slightly higher than for the homogeneous hot plasma, the difference increasing towards the higher frequencies.

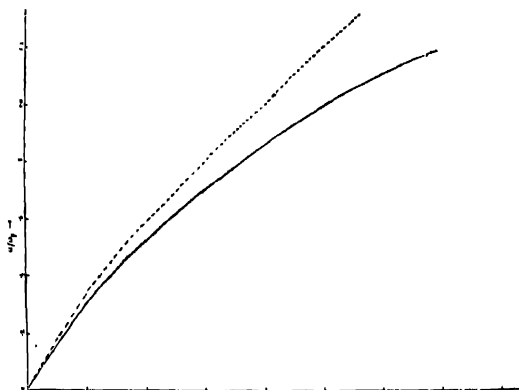


Figure 2

Case 3. Taking  $\Delta = \infty$  the dispersion relation (6) becomes

$$\frac{1}{2} K_0(\delta) \delta \left( 1 + \frac{2}{3} \tau_0 \right) = K_0'(\delta) \left[ \left( 1 + \frac{1}{3} \tau \right) + \frac{1}{6} \left( 1 + \frac{3}{4} \tau_0 \right) \delta^2 \right] \text{ for } \epsilon = 1$$

and  $\frac{1}{2} \delta K_0(\delta) (1 + \tau) (1 + \tau_0) = K_0'(\delta) \left[ (1 + \tau) + \frac{1}{6} (1 + \tau_0) \delta^2 \right] \text{ for } \epsilon = 0$

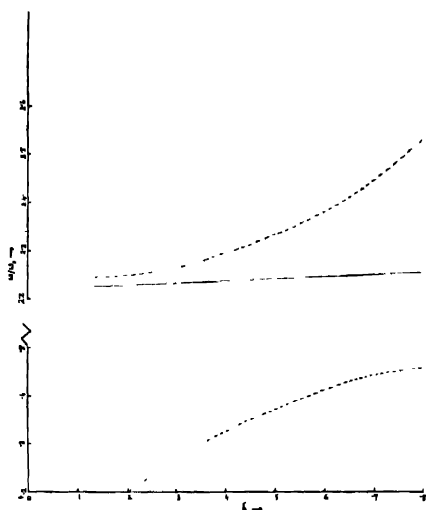


Figure 3



## A note on heat transfer due to the motion of a gradually accelerated plate

BY RAMA SANKAR RATH AND BHIMASEN MAHAPATRA

*Post-Graduate Department of Mathematics, Utkal University, Vani Vihar  
Bhubaneswar-4, Orissa*

(Received 12 May 1970)

Heat transfer due to the motion of a gradually accelerated flat plate in a viscous incompressible fluid is considered. Solutions have been obtained in closed form. It is seen that the thermal boundary layer thickness decreases and that the Nusselt number increases with an increase of the Prandtl number.

### INTRODUCTION

Leslie (1963) considered the motion of a flat plate from rest in an incompressible visco-elastic liquid proposed by Oldroyd (1950) and obtained the velocity profiles for large and small time using series expansions for the velocity and stresses. Rath (1967) solved the same problem for the fluid in which the coefficient of viscosity depends on the three invariants of the rates of deformation.

We have now considered the problem of heat transfer in a viscous incompressible fluid, with constant fluid properties, due to the motion of a flat plate started from rest with an acceleration  $At^4$ . The wall temperature is assumed to be linearly varying with time. Exact solutions have been obtained without considering the dissipation function in the heat balance equation and computations have been carried out for rather small values of Prandtl number in which case we have some justification of neglecting the dissipated heat. Temperature profiles have been drawn for  $Pr = 1, 0.1, 0.01$  and some important conclusions have been drawn from the graphs.

### HEAT BALANCE EQUATION AND ITS SOLUTION

Here we assume that an infinite flat plate occupies the position  $y = 0$  and gradually moves parallel to itself in the  $x$ -direction with an acceleration  $At^4$  starting from rest. The energy equation in the absence of dissipated heat becomes (Schlichting 1966)

$$\rho c \frac{\partial T}{\partial t} = k \frac{\partial^2 T}{\partial y^2} \quad \dots (1)$$

The boundary conditions are

$$\left. \begin{aligned} T(0, t) &= T_w(t) = T_\infty + \lambda t \\ T(\infty, t) &= T_\infty = \text{Constant} \end{aligned} \right\} \quad (2)$$

In the above equations  $\rho$ ,  $c$  and  $k$  denote the density, specific heat and conductivity, all of which are assumed to be constants. Also  $T_w$  and  $T_\infty$  represent the temperatures at the wall and out-side the thermal boundary layer.

We further assume for obtaining similar solutions of the equations (1) and (2), that

$$T - T_\infty = \lambda t \theta(I), \quad I = \frac{y}{2(\nu t)^{1/2}} \quad (3)$$

Transformations (3) reduce equations (1) and (2) to

$$\frac{d}{dI} \left( \frac{2}{I^2} \theta(I) \right) + 2 P_r I \frac{d}{dI} \theta(I) - 4 P_r \theta(I) = 0 \quad (4)$$

where  $P_r = \frac{\mu c}{k}$  = Prandtl number,

and  $I = 0, \quad \theta(I) = 1; \quad I = \infty, \quad \theta(I) = 0 \quad \dots (5)$

The solutions of (4) and (5) are obtained in a closed form as

$$\theta(I) = 2(\pi)^{-1} \{ (2P_r I^2 + 1) \operatorname{erfc}[(P_r)^{1/2} I] - (P_r)^{1/2} I \exp(-P_r I^2) \}$$

where  $\operatorname{erfc}[(P_r)^{1/2} I] = \int_{(P_r)^{1/2} I}^{\infty} \exp(-x^2) dx.$

#### NUSSELT NUMBER

We have according to Newton's law of cooling if  $\alpha$  is the coefficient of heat transfer and  $q$  the quantity of heat exchanged per unit area and unit time,

$$q = \alpha(T_w - T_\infty) = \alpha \lambda t = -k \left[ \frac{\partial T}{\partial y} \right]_{y=0} = -k(\lambda t \theta'_{1/2} (\nu t)^{-1/2})_{I=0} \left[ \theta' = \frac{d\theta(I)}{dI} \right]$$

then  $\alpha = -k \frac{\theta'(0)}{2} (\nu t)^{-1/2}$

Thus we obtain a nondimensional heat transfer co-efficient

$$Nu = \frac{\alpha}{k} (\nu t)^{1/2} \alpha = -\theta'(0) = 4 \left( \frac{P_r}{\pi} \right)^{1/2}$$

#### DISCUSSION

In figure 1 we see that there is an increase in thermal boundary layer thickness as the Prandtl number decreases. The Nusselt number, however, increases with

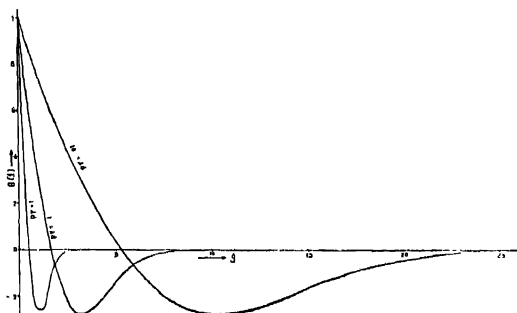


Figure 1. Temperature function.

Prandtl number. It is further seen from the graph that the fluid layer at a distance equal to nearly one-fifth the thermal boundary layer thickness attains the temperature of the fluid outside the thermal boundary layer. In between this layer and the fluid at infinity the fluid temperature falls below  $T_\infty$ , the maximum fall occurring a little before the point halfway between the wall and infinity.

#### REFERENCE

- Leslie F. M. 1962 *Proc. Edin. Math. Soc.* **13** (Series II), 223.  
 Oldroyd J. G. 1950 *Proc. Roy. Soc. A* **200**, 523.  
 Rath, R. S. 1967 *Doctoral Thesis* I.I.T., Delhi  
 Schlichting H. 1968 *Boundary Layer Theory*.

## Spin of 4.8 Mev level of $\text{Be}^8$

By M. K. SAXENA\*

Department of Physics, University of Lucknow, Lucknow

(Received 29 December 1969—Revised 2 June and 31 July 1970)

An ordinary lithium target has been bombarded with 500Kev deuterons from the Cockcroft-Walton high tension machine at the Tata Institute of Fundamental Research, Bombay. The outgoing neutrons were collected on 400 $\mu$  thick Ilford G5 nuclear research emulsion plates at seven angles, viz. 0°, 45° 60°, 90°, 120°, 135° and 150°. The neutron yield at seven angles corresponding to 4.8Mev level of  $\text{Be}^8$  was experimentally found. This value was compared with the predicted neutron yield from the theory of Butler. Of the various curves drawn for the yield at the different values of the proton angular momentum transfer for the curve at  $1_p^1$  showed the closest fit to the observed data. The analysis yields that the spin of the 4.8Mev level of  $\text{Be}^8$  is 0 or 2 and of even parity.

### INTRODUCTION

The spin of the 4.8 Mev level of  $\text{Be}^8$  has been deduced from the consideration of the angular distribution of the neutrons from the nuclear reaction  $\text{Li}+d$ . The experimentally observed angular distribution of neutrons from 500 Kev deuteron bombardment of lithium, has been compared with the various such curves obtained from the theory of Butler (1967) for various values of the proton angular momentum transfer ( $1_p$ ). A comparison of the experimental and calculated values shows the closest fit with  $1_p = 1$ . This gives the spin 0 or 2 and even parity for this level.

### EXPERIMENTAL METHOD

An ordinary lithium target 96 Kev thick on 0.013 cm copper backing, has been bombarded with 500 Kev deuterons from the Cockcroft and Walton high tension machine at the Tata Institute of Fundamental research, Bombay. The outgoing neutrons were collected at seven angles on 400 $\mu$  Ilford G5 nuclear research emulsion plates. The emulsion plates were then processed by the method of "Temperature Cycle" of Dilworth *et al* (1948) and were scanned under Cooke Troughton & Simms Nuclear Research Microscope ( $\times 1200$ ). All the tracks which were produced after the reaction within a solid angle of 5° from the direction of neutrons and originated between 50 $\mu$  to 350 $\mu$  thickness of the emulsion plate and exceed a certain length were measured. The neutron yield in terms of the number of events/ $10^9\mu^3$  at seven angles, corresponding to the 4.8 Mev level, was transferred to the centre of mass system of coordinates by using the formula of Haxby *et al* (1939) and normalised in the forward direction ( $\theta = 0$ ) and plotted on the graph in dashed lines with the statistical variation shown at each angle.

\*Present address : Department of Physics, College of Military Engineering, Poona.



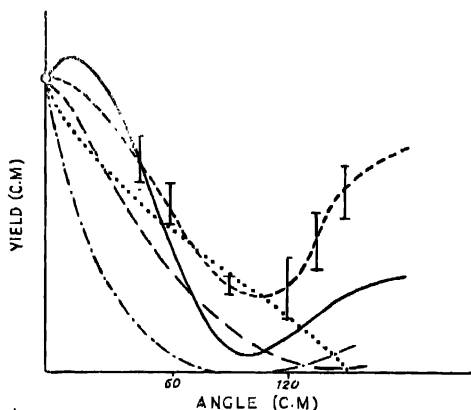


Figure 1

## DISCUSSION OF THE RESULTS

The neutron yield does not show any fore-and-aft symmetry as is expected from Bohr's theory of the formation of the compound nucleus (Evans 1955). The neutron yield shows a pronounced forward maximum, suggesting that the Oppenheimer-Phillips (1935) process of stripping of the nucleus has been mainly responsible for the interaction between the deuteron and the target nucleus. Herein a proton of the deuteron interacts directly with the lithium nucleus and forms the  $\text{Be}^8$  nucleus. The other nucleon of the deuteron, *i.e.*, the neutron goes off with the residual energy and momentum. Though the energetics of the compound nucleus formation and the stripping process are the same, the angular distribution of the outgoing particle is entirely different. An analysis has been made using the theory of Butler (1967). The calculated values of neutron yield for the proton angular momentum transfer values 0, 1, 2 and 3 have been calculated. The data for  $l_p = 0$  has been shown by the dot-dash curve on the figure. The continuous curve shows the data for  $l_p = 1$ . The neutron yield data for  $l_p = 2$  is shown as long dashes. This can be distinguished from the short dash data representing the experimentally observed values having the probable values. The data for  $l_p = 3$  is shown by a dot curve.

The curve for proton angular momentum transfer value  $l_p = 1$  shows the closest fit for the observed data as shown in the figure. It suggests that the proton with an orbital angular momentum value 1 ( $l_p = 1$ ) is directly assimilated in the nucleus of lithium and the outgoing neutrons take the residual energy and the angular momentum. This gives the spin of 4.8 Mev level of  $\text{Be}^8$  to be 0 or 2 and of even parity.

## ACKNOWLEDGEMENT

Thanks are due to Dr. J. P. Sah for his guidance and continuous interest in the work.

Butler S. T., Hewitt R. G. L., McKellar B. H. J. & May R. M. 1967 *Annals of Physics*, **43**(2) 282

Dilworth C. C., Occhialini G. P. S. & Payne R. M. 1948 *Nature*, **163**, 102.

Evans R. D. 1955 *The Atomic Nucleus*, McGraw Hill, New York, 245.

Haxby R. O., Allens J. S. & Williams J. H. 1939 *Phys. Rev.* **55**, 140.

Oppenheimer J. R. & Phillips M. *Phys. Rev.*, 1935 **47**, 835.

# Letters to the Editor

Indian J. Phys. **44**, 469-471 (1970)

## A note on the level structure of $^{190}\text{Au}$

BY M. N. SEETHARAMANATH, B. R. SASTRY AND K. PARTHASARADHI

*The Laboratories for Nuclear Research, Andhra University, Waltair,  
India*

(Received 27 October 1970)

The core-excitation model (de Shalite 1961) was applied with a large degree of success to explain the features of the low-lying levels of  $^{197}\text{Au}$ . In particular, the model successfully accounted for the magnetic moment of the 77 keV ( $1/2_+$ ) state while the models (Ialango *et al* 1967, Kisslinger *et al* 1963) which assumed large single particle admixtures failed to explain it. In the present paper the energy levels as well as the transition rates of  $^{190}\text{Au}$  are treated in this model. In the earlier works on  $^{190}\text{Au}$  (Okano *et al* 1969, Backlin 1967) the applicability of the core-excitation model was discussed in respect of the transition rates only. The spin sequence of the low-lying levels of  $^{190}\text{Au}$  is different from that of the other three oddmass gold isotopes. The correct level sequence is predicted with the present calculation.

As in the case of  $^{197}\text{Au}$ , single particle admixture was allowed in the ground state. The wave functions are written as

$$\begin{aligned} | \frac{3}{2}^+ >_1 &= A | 0 \frac{3}{2} \frac{3}{2} > + \sqrt{1-A^2} | 2 \frac{3}{2} \frac{3}{2} > \\ | \frac{3}{2}^+ >_2 &= -\sqrt{1-A^2} | 0 \frac{3}{2} \frac{3}{2} > + A | 2 \frac{3}{2} \frac{3}{2} > \\ | \frac{5}{2}^+ >_1 &= B | 2 \frac{5}{2} \frac{5}{2} > + \sqrt{1-B^2} | 0 \frac{5}{2} \frac{5}{2} > \\ | J > &= | 2 \frac{5}{2} J > \quad \text{for } J = \frac{1}{2} \text{ and } 7/2 \end{aligned}$$

Using relations of tensor algebra, the formulae for the transitions are written and the results are tabulated in table 1. For calculating the value of  $A^2$ , the BM1( $1/2 \rightarrow 3/2$ ) value is assumed.  $g_p$  is taken to be the Schmidt value and  $g_o$  is taken to be  $Z/A$ .

The core excitation model envisages the low-lying levels of oddmass spherical nuclei as arising from the coupling of the odd  $d_{3/2}$  proton to the even-even core. The coupling results in a core-multiplet which will be degenerate in the absence of an interaction between the particle and the core. The core-particle interaction can in general be represented by a sum of scalar products of irreducible tensors

$$H_{int} = \sum_k f_k (T_c^k \cdot T_p^k)$$

where  $T_c^k$  operates on the degrees of freedom of the core only,  $T_p^k$  operates on the degrees of freedom of the particle and  $f_k$  is the strength of interaction. The allowed values of  $k$  are 0, 1, 2, 3 for  $^{199}\text{Au}$ . Leaving alone  $k=0$  term which causes only a shift of the centre of gravity, the terms which split the multiplet are the  $k=1$  and  $k=3$ . The  $k=2$  term is found to be small and neglected as in the case of  $^{107}\text{Au}$  (Mckinley *et al* 1966). Then the energy levels are given by the expression

$$E(J) = E_0 + \left[ C_1 \left\{ \begin{matrix} 2 & \frac{3}{2} & J \\ \frac{3}{2} & 2 & 1 \end{matrix} \right\} + C_3 \left\{ \begin{matrix} 2 & \frac{3}{2} & J \\ \frac{3}{2} & 2 & 3 \end{matrix} \right\} \right] - 1^{J+1}$$

$$C_k = f_k < J_c \| T_c^k \| J_c > < j_p \| T_p^k \| j_p >$$

where  $E_0$  is the centre of mass parameter. The energies of the 1/2 and 3/2 states are assumed to evaluate  $C_1$  and  $C_3$  starting with a value of  $E_0$  equal to the energy of the first  $2_+$  stato of the neighbouring even-even nucleus. With these values the energies of the remaining states are calculated. The value of  $E_0$  for which the sum of the squares of the deviations of the experimental energies from the theoretical energies is minimum, is assumed to be the best value.

In fact, the energies of the low-lying levels of all the odd  $A$  gold isotopes can be calculated using this model. The low-lying levels of the odd  $A$  gold isotopes may be viewed as resulting from the competition between  $k=1$  and  $k=3$  interactions. The parameter  $C_1$  goes on decreasing and  $C_3$  goes on increasing with increasing neutron number. This behaviour is responsible for the decrease in separation of the 3/2 and 5/2 states and for the reversal of the two states in  $^{199}\text{Au}$ . The calculated and the experimental values are given in table 2.

TABLE 1

	Theory	Experiment
$BM1B[(3/2)_2 - (1/2)]$	0.02675	0.043
$BM1B[(3/2)_2 - (3/2)]$	0.01032	< 0.0052
$BM1B[(7/2) - (5/2)]$	0.01852	~0.001
$BE2B[(5/2) - (3/2)]$	0.0130	> 0.013
$\mu$	0.2153	$0.26 \pm 0.03$
$Q(3/2)$	0.8935	~0.7 for $^{199}\text{Au}$

It can be seen from tables 1 and 2 that the agreement between the experimental and the calculated values is, in general satisfactory. So it may be concluded that the core-excitation model gives a reasonable agreement with experiment in spite of its simplicity.

TABLE 2

TABLE 2. The calculated and experimental values

$J$	$A$	193	195	197	199
1/2	Calculated	0.038	0.061	0.077	0.077
	Exptl.	0.038	0.061	0.077	0.077
3/2	Calculated	0.224	0.241	0.269	0.324
	Exptl.	0.224	0.241	0.269	0.324
5/2	Calculated	0.283	0.297	0.315	0.305
	Exptl.	0.258	0.261	0.279	0.317
7/2	Calculated	0.498	0.504	0.523	0.504
	Exptl.	0.508	0.525	0.548	0.495

Two of the authors (M.N.S. and B.R.S.) are thankful to the Council of Scientific and Industrial Research, New Delhi, for the award of Research Fellowships during the course of the work.

## REFERENCES

- Backlin A. 1967 *Nucl. Phys.* **A103**, 337.  
 De Shalit A. 1961 *Phys. Rev.* **122**, 1530.  
 Iulango G. & Alaga G. 1967 *Nucl. Phys.* **A97**, 600.  
 Kisslinger L. S. & Sorensen R. A. 1963 *Rev. Mod. Phys.* **3S**, 853.  
 McKinley J. M. & Rinard P. M. 1966 *Nucl. Phys.* **79**, 159.  
 Okano O. Kawata Y. Uenara J. & Hayashi T. 1960 *Nucl. Phys.* **A136**, 321

*Indian J. Phys.* **44**, 471-473 (1970)

## Forced convection flow past a plate with variable thermal conductivity

P. C. SINHA

*Department of Mathematics, Indian Institute of Technology,  
Hauz Khas, New Delhi-29*

(Received 17 November 1970—Revised 27 May 1971)

Effect of variable thermal conductivity on heat transfer from a flat plate maintained at a constant temperature has been studied earlier by the author (Sinha 1967). In the present note such effect is considered when the heat flux at the plate surface is prescribed.

The energy equation governing the present problem (Sinha 1967), is

$$\rho C_p \left( Cy \frac{\partial T}{\partial x} \right) = \frac{\partial}{\partial y} \left( k \frac{\partial T}{\partial y} \right). \quad (1)$$

The boundary conditions are

$$\left. \begin{aligned} y = 0 (x > 0); \quad \frac{\partial T}{\partial y} &= -\frac{q}{k}, \\ y \rightarrow \infty; \quad T &\rightarrow T_\infty, \end{aligned} \right\} \quad \dots \quad (2)$$

where  $q$  is the heat flux per unit area of the plate.

With the substitutions

$$\eta = y \left( \frac{C}{9\alpha x} \right)^{1/3}, \quad T = T_\infty + \frac{q}{k} \left( \frac{9\alpha x}{C} \right)^{1/3} H(\eta)$$

and

$$k = k_0[1 + \beta H(\eta)]$$

equation (1) reduces to

$$H'' + 3\eta^2 H' - 3\eta H + \beta(HH'' + H'^2) = 0, \quad \dots \quad (3)$$

where  $k_0$  = thermal conductivity at  $T = T_\infty$ ,  $\alpha = k_0/\rho C_p$ ,  $\beta$  and  $C$  are constants and dashes denote differentiations with respect to  $\eta$ . The new boundary conditions are

$$\left. \begin{aligned} \eta = 0; \quad H' &= -1 \\ \eta \rightarrow \infty; \quad H &\rightarrow 0. \end{aligned} \right\} \quad \dots \quad (4)$$

The solution of equation (3) satisfying (4) is obtained by an integral method due to Epstein (1958), since our aim is to get qualitative results. In this method an appropriate initial form containing some free parameters is assumed for the profiles which are then substituted in the integral equations to obtain new profiles, which are better approximations. The free parameters occurring in the initial profiles are determined by requiring the new profiles to satisfy all the boundary conditions of the problem. Thus satisfying (4),  $H(\eta)$  and  $H'(\eta)$  can be chosen as

$$H'(\eta) = -e^{-a\eta}, \quad H(\eta) = \frac{e^{-a\eta}}{a}, \quad (5)$$

where the free parameter  $a$  is to be evaluated from the boundary condition at infinity. Integration of equation (3) with respect to  $\eta$  from 0 to  $\eta$  yields

$$H'(\eta) = H'(0) - 3\eta^2 H(\eta) + 9 \int_0^\eta \eta H(\eta) d\eta - \beta[H(\eta)H'(\eta) - H(0)]. \quad (6)$$

Substituting (5) in the right-hand side of equation (6) and using (4), we get

$$H_1'(\eta) = - \left( 1 + \frac{\beta}{a} - \frac{9}{a^3} \right) - \frac{9e^{-a\eta}}{a^3} - \frac{9\eta e^{-a\eta}}{a^2} - \frac{3\eta^2 e^{-a\eta}}{a} + \frac{\beta e^{-2a\eta}}{a} \quad \dots \quad (7)$$

The parameter  $a$  can be determined from the condition  $H'(\infty) = 0$ , which suggests that  $a$  should satisfy

$$1 + \frac{\beta}{a} - \frac{9}{a^3} = 0. \quad \dots (8)$$

Equation (7) then reduces to

$$H_1'(\eta) = -\frac{9e^{-a\eta}}{a^3} - \frac{9e^{-a\eta}}{a^2} - \frac{3\eta^2 e^{-a\eta}}{a} + \frac{\beta e^{-2a\eta}}{a}. \quad (9)$$

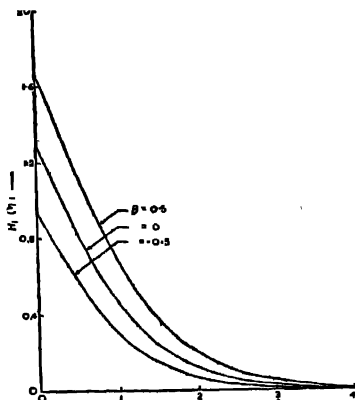


Figure 1. Dimensionless temperature profiles for various values of  $\beta$ .

Integrating (9) with respect to  $\eta$  and using the condition  $H_1(\infty) = 0$ , we obtain

$$H_1(\eta) = \frac{e^{-a\eta}}{a^4} (3a^2\eta^2 + 15a\eta + 24) - \frac{\beta}{2a^3}. \quad \dots (10)$$

The function  $H_1(\eta)$  has been plotted for different values of  $\eta$  and it is found that a linear variation of thermal conductivity with temperature results in a linear variation in the temperature distribution. Similar conclusion has been derived earlier by Sinha (1967).

#### REFERENCES

- Epstein M. 1958 *Ph.D. Thesis, Polytechnic Institute of Brooklyn*.  
 Rao A. K. 1961 *Appl. Sci. Res* **10A**, 141.  
 Sinha P. C. 1967 *ZAMP* **18**, 900.

## BOOK REVIEW

### *Mathematical Methods in Solid State and Superfluid Theory*

Scottish Universities Summer School (1967) Edited by R. C. Clark and G. H. Derrick. *Oliver & Boyd, Edinburgh*, 1969. 77s. pp 400.

The summer school was meant primarily for "theoretical physicists of at least one year's post graduate standing. "However the reviewer feels that most of the reports are at such a level that only fairly experienced workers will be able to utilise them to advantage. A very wide field is covered—there are eight long lectures and seven short report of recent reasearches. The first one, by Lanczos, gives an outline of classical mechanics and then goes on to the discussion of Noether's theorem that an invariance of the Lagrangian with respect to an infinitesimal transformation is associated with a corresponding conservation principle and thus obtains the conservation laws both of mechanical systems and fields. The second lecture is a fairly long discussion of transformation theory by Gross. Baym then takes up the microscopic description of superfluidity and brings out the essential similarity between theories of liquid He and superconductivity. The next lecture by Luttinger on transport theory considers the transport coefficients as tensors and after obtaining Kubo type formulae goes on to a derivation of transport equation using diagram techniques. Valatin's article on 'Density matrix methods and superconductivity theory' discusses the subject matter starting from Hartree-Fock method and then goes on to the magnetic coupling effects in a superconducting film. There are two other main lectures—one on perturbation theory and its application by Brueckner and another on exactly soluble models (discussing Heisenberg chains and two dimensional Ising model) by Lieb. This simple cataloguing of the main lectures and the fact that there are besides seven research reports are perhaps enough to show that the volume will be of great use to a varied group of workers and any library should have a copy if there be an interest in advanced theories of solids and superfluids.

A. K. R. C



# INDIAN JOURNAL OF PHYSICS

Vol. 14

No. 9

AND

Vol. 53

PROCEEDINGS

No. 9

OF THE

INDIAN ASSOCIATION FOR THE CULTIVATION OF SCIENCE

*(Edited in collaboration with the Indian Physical Society).*

IJPYAS 44 (?) 475-520 (1970)

SEPTEMBER 1970

PUBLISHED BY THE  
INDIAN ASSOCIATION FOR THE CULTIVATION OF SCIENCE  
JADAVPUR, CALCUTTA-32



## Spin-1/2 formalism for two-level problems

By H. G. VENKATESH AND L. P. DIXIT

*Birla Institute of Technology, Mesra, Ranchi*

(Received 7 July 1970)

The formalism of the theory of angular momentum (spin-1/2) is the most appropriate for the treatment of the two-level problem (interaction of radiation with a quantum mechanical system with an isolated pair of eigen states of energy). The density matrix and the total Hamiltonian can be expressed as vectors in a co-ordinate system spanned by the basic spin representations related to spin space. The dynamical problem is solved by finding from the equation of motion the spinor transformation  $T$  which effects the rotation of the density operator.

The spin - 1/2 formalism shows the interconnections among the distinctive methods of treating the problem (due to Feynman & Vernon 1957, Dicke 1954, and Lamb 1964). An analytic solution of the mechanical problem of finding the polarization for the transition  $\Delta m = 0$  is presented. Expressions are given for electrical field, power, and oscillation frequency in terms of the one variable, the pulse strength  $\theta_N$  determined by the density  $N$  of molecules interacting with the radiation field in a stationary process. The matrix of interaction containing this parameter is a rotation about the  $z$ -axis in spin-space through the pulse angle  $\theta$  and operates on the initial system vector to produce the system vector at time  $t$ . The latter is a matrix whose elements are the expectation values of the unperturbed Hamiltonian and polarization.

### INTRODUCTION

The two-level problem dealing with spontaneous and induced emission of radiation from an assembly of atoms (or molecules) with an isolated pair of low-lying energy levels has been treated in several ways in order to obtain the emitted power and frequency shifts. Of the four general forms of the equation of motion in quantum mechanics, with which the two-level problem can be treated, namely, those involving the Schrödinger wave function  $\psi$ , the density operator  $\rho$ , the  $T$ -operator, and the Heisenberg variables, only the Heisenberg form seems to have been left out. Some of these methods have been extended and refined to bring out the more detailed, and non-linear aspects of the process (Mohanty 1967, Roy 1969).

There is a very simple form of the dynamical law brought out by Feynman & Vernon (1957) specifically for the two-level problem. This presents the dynamical problem as the motion of a gyroscope (a vector  $\vec{r}$ ) with frequency  $\vec{\omega}$  in  $r$ -space. Dicke (1954) presents no specific form of the equation of motion for the two-level problem. He proceeds on intuitive grounds to deal with an important aspect of the radiative process, namely, the existence of certain exceptional states of the gaseous assembly of  $N$  molecules and shows that in a spontaneous emission

process the intensity of radiation is proportional to  $N^2$  (and not  $N$  as for independent molecules).

By a juxtaposition of Pauli operators with Feynman frequencies and vector  $\rightarrow r$ , one can express the Hamiltonian and density operators respectively as vectors in spin space. One can almost characterize the two-level problem as a spin-1/2 problem. Hints on the application of spin-1/2 formalism to two-level problems have appeared in literature at various times but the authors feel that there is no systematic treatment of the problem from this angle. The purpose of this paper is to present such a treatment and to derive Feynman's solutions *analytically*. Further, the main postulates of Dicke are shown to follow from a general form of the dynamical law. In this way the interconnections between the methods of Lamb (1964), Feynman & Vernon (1957) and Dicke (1954) can be shown.

The system considered is a beam of molecules with an isolated pair of energy levels entering a cavity tuned to the molecular transition frequency, the molecules being all in the state of higher energy just when they enter the cavity at  $t = 0$ . The proper values of the energy are  $E_a$  and  $E_b$ , the molecular transition frequency being  $\omega_0 = \hbar^{-1}(E_a - E_b)$ .

#### SPIN SPACE

Let  $\psi$  represent an arbitrary state of the system

$$\psi = a\psi_a + b\psi_b \quad (1)$$

where the co-efficients satisfy the normalization condition

$$aa^* + bb^* = 1 \quad (2)$$

The matrix

$$T = \begin{pmatrix} a & -b^* \\ b & a^* \end{pmatrix} = \begin{pmatrix} \alpha & \beta \\ \gamma & \delta \end{pmatrix} \quad (3)$$

and its conjugate imaginary

$$\bar{T} = \begin{pmatrix} a^* & b^* \\ -b & a \end{pmatrix} \quad (3a)$$

satisfy  $TT = 1$  in virtue of the normalization (2). Hence  $T$  is unitary. (1) represents the unitary transformation of  $\psi_a$  by  $T$ :

$$\begin{pmatrix} a & -b^* \\ b & a^* \end{pmatrix} \begin{pmatrix} 1 \\ 0 \end{pmatrix} = \begin{pmatrix} a \\ b \end{pmatrix}$$

The elements of the matrix  $T$  are just the Cayley-Klein parameters.

In general the matrix  $T$  transforms a two-component wave function  $\begin{pmatrix} A \\ B \end{pmatrix}$

into another  $\begin{pmatrix} A' \\ B' \end{pmatrix}$  as follows :

$$\left. \begin{aligned} A' &= aA - b^*B = \alpha A + \beta B \\ B' &= bA + a^*B = \gamma A + \delta B \end{aligned} \right\} \quad \dots (4)$$

subject to the condition (2), i.e.,

$$\alpha\delta - \beta\gamma = 1 \quad \dots (2a)$$

A spinor is a two-component quantity defined by the linear transformation (4) subject to (2) (or (2a)) when the co-ordinate system is rotated. The problem of finding  $\psi$  is equivalent to finding a representative of  $T$  involving the interaction which effects a rotation in spin space.

In Euler resolution the general rotation  $T$  is given by the product

$$T = T_\psi T_\theta T_\phi$$

where  $T_\psi$ ,  $T_\theta$ ,  $T_\phi$  are unitary matrices effecting rotations in spin space through the Euler angles,  $\phi$ ,  $\theta$ ,  $\psi$  and are given by

$$\begin{aligned} T_\phi &= I \cos \phi/2 + i\sigma_3 \sin \phi/2 = e^{i\phi/2\sigma_3} \\ T_\theta &= I \cos \theta/2 + i\sigma_1 \sin \theta/2 = e^{i\theta/2\sigma_1} \\ T_\psi &= I \cos \psi/2 + i\sigma_3 \sin \psi/2 = e^{i\psi/2\sigma_3} \end{aligned} \quad \dots (5)$$

The Pauli operators  $\vec{\sigma} = (\sigma_1, \sigma_2, \sigma_3)$  obey the commutation rules

$$\sigma_1\sigma_2 + \sigma_2\sigma_1 = 0; \quad \sigma_1\sigma_2 - \sigma_2\sigma_1 = 2i\sigma_3 \text{ etc.}$$

Also

$$\sigma_1\sigma_2 = i\sigma_3 \text{ etc.}, \quad \sigma_1^2 = \sigma_2^2 = \sigma_3^2 = I$$

They are represented by  $\sigma_1 = \begin{pmatrix} 0 & 1 \\ 1 & 0 \end{pmatrix}$ ,  $\sigma_2 = \begin{pmatrix} 0 & -i \\ i & 0 \end{pmatrix}$ ,  $\sigma_3 = \begin{pmatrix} 1 & 0 \\ 0 & -1 \end{pmatrix}$

Let us denote the unit matrix by  $\sigma_0 = \begin{pmatrix} 1 & 0 \\ 0 & 1 \end{pmatrix}$

#### THE DENSITY MATRIX

The density operator is given by  $\rho(t) = \begin{pmatrix} a^* & a & b^* & a \\ a^* & b & b^* & b \end{pmatrix} \quad \dots (6)$

Introducing a new operator  $\mu(t) = 2\rho(t) - 1$  so that  $\mu(0) = \sigma_3 \quad \dots (7)$

at  $t = 0$ , the dynamical problem reduces to finding the transformed operator

$$\bar{T}T\sigma_3 = \sigma_n = r_1\sigma_1 + r_2\sigma_2 + r_3\sigma_3 \quad \dots (8)$$

where  $\sigma_n$  is the component of  $\sigma$  in a general direction  $n$  with direction cosines  $r_1, r_2, r_3$ . Since

$$1 = T\sigma_3^2\bar{T} = T\sigma_3\bar{T}T\sigma_3\bar{T} = \sigma_n^2$$

$r_1, r_2, r_3$  are also the components of a vector  $\vec{r}$  of unit length

$$r_1^2 + r_2^2 + r_3^2 = 1 \quad \dots (9)$$

Using (3) and (3a) we obtain  $r$  from the transformation (8)

$$\begin{aligned} r_1 &= ab^* + a^*b, \\ r_2 &= i(ab^* - a^*b), \\ r_3 &= aa^* - bb^* \\ r_0 &= 1 = aa^* + bb^* \end{aligned} \quad \dots (10)$$

(9) follows from (10) when the normalization condition is used. The density matrix may then be written as

$$\rho = \frac{1}{2} \begin{pmatrix} 1+r_3 & r_1 - ir_2 \\ r_1 + ir_2 & 1-r_3 \end{pmatrix} = \frac{1}{2}\sigma_0 + \frac{1}{2}(r_1\sigma_1 + r_2\sigma_2 + r_3\sigma_3) \quad \dots (11)$$

and

$$\mu = \begin{pmatrix} r_3 & r_1 - ir_2 \\ r_1 + ir_2 & -r_3 \end{pmatrix} = r_1\sigma_1 + r_2\sigma_2 + r_3\sigma_3 \quad \dots (12)$$

In term of the spin angular momentum  $\vec{S} = \frac{1}{2}\hbar\vec{\sigma}$ ,  $S_0 = \frac{1}{2}\hbar\sigma_0$

$$\rho = \hbar^{-1}(r_1S_1 + r_2S_2 + r_3S_3 + r_0S_0)$$

The form of the matrix  $\mu$  shows that  $\mu$  is a vector of unit length in the space spanned by the unit vectors  $\sigma_1, \sigma_2, \sigma_3$  and rotating under the influence of the radiation field.

### THE HAMILTONIAN

The unperturbed Hamiltonian is represented by the matrix

$$H_0 = \begin{pmatrix} E_a & 0 \\ 0 & E_b \end{pmatrix}$$

If the energies are measured from their mean taken as zero, then

$$H_0 = \frac{1}{2}\hbar\omega_0 \begin{pmatrix} 1 & 0 \\ 0 & -1 \end{pmatrix} = \frac{1}{2}\hbar\omega_0\sigma_3$$

If the system has no permanent electric dipole moment the perturbation is represented by the matrix  $V = \begin{pmatrix} 0 & V_{ab} \\ V_{ba} & 0 \end{pmatrix}$

$$\begin{aligned} \text{Introducing the real quantities} \quad \omega_1 &= \hbar^{-1}(V_{ab} + V_{ba}) \\ \omega_2 &= i\hbar^{-1}(V_{ab} - V_{ba}) \\ \omega_3 &= \omega_0 \end{aligned} \quad \dots (13)$$

We have

$$V = \frac{1}{2}\hbar \begin{pmatrix} 0 & \omega_1 - i\omega_2 \\ \omega_1 + i\omega_2 & 0 \end{pmatrix} = \frac{1}{2}\hbar(\omega_1\sigma_1 + \omega_2\sigma_2) \quad (14)$$

The total Hamiltonian is given by :

$$\begin{aligned} H = H_0 + V &= \frac{1}{2}\hbar(\omega_1\sigma_1 + \omega_2\sigma_2 + \omega_3\sigma_3) \\ &= \frac{1}{2}\hbar \begin{pmatrix} \omega_3 & \omega_1 - i\omega_2 \\ \omega_1 + i\omega_2 & -\omega_3 \end{pmatrix} \end{aligned} \quad (15)$$

#### THE EQUATION OF MOTION

The time development of  $\rho$  is given by

$$i\hbar \frac{\partial \rho}{\partial t} = -(\rho H - H\rho) \quad (16)$$

The commutation rules for  $\sigma_1, \sigma_2, \sigma_3$  lead to the following relation for any two vectors  $\vec{a}$  and  $\vec{b}$

$$(\vec{a} \cdot \vec{\sigma})(\vec{b} \cdot \vec{\sigma}) = \vec{a} \cdot \vec{b} + i(\vec{a} \times \vec{b}) \cdot \vec{\sigma} \quad \dots \quad (17)$$

which gives

$$(a \cdot \sigma)(b \cdot \sigma) - (b \cdot \sigma)(a \cdot \sigma) = 2i(\vec{a} \times \vec{b}) \cdot \vec{\sigma} \quad \dots \quad (17a)$$

Using this relation and substituting for  $\rho$  and  $H$  from (11) and (15) in (16)

$$i\hbar \frac{\partial}{\partial t}(\vec{r} \cdot \vec{\sigma}) = i\hbar(\vec{\omega} \times \vec{r}) \cdot \vec{\sigma}$$

or

$$\frac{\partial \vec{r}}{\partial t} = \vec{\omega} \times \vec{r} \quad \dots \quad (18)$$

This is *Feynman's equation* for the two-level problem. The equation is true for all co-ordinate systems (in spin space) obtained from each other by rotational displacements and for rotating co-ordinate systems.

The interaction process may be regarded as the motion of a vector of unit length in spin space and lends itself to a graphical solution considered by Feynman. The essential step is to transform to some rotating co-ordinate system where the vector  $\vec{r}$  appears to execute a simple precessional motion about the 3-axis, the component of the frequency  $\vec{\omega}$  along the 3-axis being constant and the other two components being zero. The representation of the dynamical law as a unitary transformation (rotation) in spin space automatically leads to the graphical method although we shall adopt here an analytical procedure which is entirely parallel to the graphical method.

## ROTATIONS

Let us denote the four co-ordinate systems here by  $\Sigma_S$  (space-fixed),  $\Sigma_B$  (body-fixed),  $\Sigma_R$  (rotating) and  $\Sigma_P$  (precessional). We pass over to  $\Sigma_R$  by means of  $T_\phi$  effecting a rotation about the 3-axis of  $\Sigma_S$  through an angle  $\phi(t)$ . One can follow the motion of  $\vec{r}$  in  $\Sigma_S$  or regard  $\vec{r}$  as fixed in  $\Sigma_S$  and follow the motion of a co-ordinate system  $\Sigma_B$  relative to  $\Sigma_S$ . Alternatively, one can introduce an intermediate moving  $\Sigma$  i.e.,  $\Sigma_P$  in which  $\vec{r}$  has a simple prescribed motion. Let  $\vec{r}$  precess round the 3-axis of  $\Sigma_P$  with constant angular velocity at a definite angle to it.  $\Sigma_R$  and  $\Sigma_P$  are introduced as a method of getting the solution for  $\vec{r}$ .

We shall denote the components of  $\vec{r}$  in  $\Sigma_R$  by single primes and in  $\Sigma_P$  by double primes and define  $\Sigma_R$  and  $\Sigma_P$  precisely as follows

The transformation to  $\Sigma_R$  is given by

$$(I \cos \phi/2 + i\sigma_3 \sin \phi/2)(r_1\sigma_1 + r_2\sigma_2 + r_3\sigma_3)(I \cos \phi/2 - i\sigma_3 \sin \phi/2) \\ = r_1'\sigma_1 + r_2'\sigma_2 + r_3'\sigma_3$$

which gives

$$r_1' = r_1 \cos \phi - r_2 \sin \phi$$

$$r_2' = r_2 \cos \phi + r_1 \sin \phi$$

Similarly,

$$\omega_1' = \omega_1 \cos \phi - \omega_2 \sin \phi$$

$$\omega_2' = \omega_2 \cos \phi + \omega_1 \sin \phi$$

Since the oscillatory field along 1-axis is a superposition of two oppositely rotating fields and since one of the components, say the clockwise, can be ignored, we have

$$\omega_1' = \frac{1}{2} |\omega_1| \cos(\omega t + \phi), \quad \omega_2' = \frac{1}{2} |\omega_1| \sin(\omega t + \phi)$$

$$\text{If we prescribe for the rotating system } \phi = -\omega \quad \dots \quad (19)$$

We have

$$\omega_2' = 0, \quad \omega_1' = \frac{1}{2} |\omega_1| = \frac{-\mu_{ab}}{\hbar} E_0 \quad \dots \quad (20)$$

To find  $\omega_3'$  we have from (18)

$$\dot{r}_1' = -(\omega_3 + \dot{\phi})r_2' + (\omega_1 \sin \phi + \omega_2 \cos \phi)r_3' \\ = -\omega_3'r_2' + \omega_2'r_3' \quad \dots \quad (21)$$

Hence

$$\omega_3' = \omega_0 - \omega$$

The total angular velocity relative to  $\Sigma_R$  is

$$\Omega = \sqrt{\omega_1'^2 + (\omega_0 - \omega)^2} \quad \dots \quad (22)$$



We obtain the precessional co-ordinate system  $\Sigma_P$  by further rotational displacements  $\theta''$  and  $\psi''$  (about the 1-axis) and then about the new 3''-axis such that the 3''-axis coincides with the resultant angular velocity  $\vec{\Omega}$  in  $\Sigma_R$ . We seek a transform from  $\Sigma_P$  to  $\Sigma_B$

$$\bar{T} = \bar{T}_{\psi''} \bar{T}_{\theta''} \bar{T}_{\phi''} = \bar{T}_{\phi''} \bar{T}_{\theta''} \bar{T}_{\psi''} = T_{-\phi''} T_{-\theta''} T_{-\psi''}$$

$\sigma_3$  is then transformed to

$$\bar{T} \sigma_3 T = \gamma_1'' \sigma_1 + r_2'' \sigma_2 + r_3'' \sigma_3$$

Evaluation of the left hand side using (17) gives

$$r_1'' = \sin \theta'' \sin \psi''; r_2'' = \sin \theta'' \cos \psi''; r_3'' = \cos \theta'' \quad \dots (23)$$

In fact (23) is true for a transformation to any arbitrary coordinate system, the precessional co-ordinate system in particular being defined by

$$\theta'' = \text{constant}, \quad \omega_1'' = \omega_2'' = 0, \quad \omega_3'' = \Omega \quad (24)$$

From (18) and (23)

$$\begin{aligned} \dot{r}_1'' &= r_2'' \dot{\psi}'' = \omega_3'' r_1'' - \omega_1'' r_2'' \\ \dot{r}_2'' &= -r_1'' \dot{\psi}'' = \omega_3'' r_1'' - \omega_1'' r_2'' \\ \dot{r}_3'' &= 0 = \omega_1'' r_2'' - \omega_2'' r_1'' \end{aligned}$$

which leads automatically to

$$\omega_1'' = 0, \quad \omega_2'' = 0, \quad \omega_3'' = -\dot{\psi}'', \quad \dot{\psi}'' = -\Omega t + \delta$$

where  $\delta$  is a phase constant. So that

$$\begin{aligned} r_1'' &= \sin \theta'' \sin (-\Omega t + \delta) \\ r_2'' &= \sin \theta'' \cos (-\Omega t + \delta) \\ r_3'' &= \cos \theta'' \end{aligned} \quad \dots (25)$$

It is easier to write explicit expressions by transforming to  $\Sigma_R$  for evaluation of  $\delta$ . Rotating  $\Sigma_P$  about the 2''-axis through  $\theta''$

$$\begin{aligned} r_3' &= r_3'' \cos \theta'' + r_1'' \sin \theta'' = \cos^2 \theta'' + \sin^2 \theta'' \sin (-\Omega t + \delta) \\ r_1' &= -r_3'' \sin \theta'' + r_1'' \cos \theta'' = -\cos \theta'' \sin \theta'' \{1 - \sin (-\Omega t + \delta)\} \\ r_2' &= r_2'' = \sin \theta'' \cos (-\Omega t + \delta) \end{aligned}$$

The boundary conditions  $r_1' = r_2' = 0$ ,  $r_3' = 1$  at  $t = 0$  give

$$\begin{aligned} \delta &= \pi/2 \\ \psi'' &= -\Omega t + \pi/2 \end{aligned} \quad (26)$$

and

$$\begin{aligned} r_1' &= -\cos \theta'' \sin \theta'' (1 - \cos \Omega t) \\ r_2' &= \sin \theta'' \sin \Omega t \\ r_3' &= \cos^2 \theta'' + \sin^2 \theta'' \cos \Omega t \end{aligned}$$

Again from (18) and the boundary conditions

$$\omega_2' = 0, \quad \sin \theta'' = -\omega_1'/\Omega$$

and from (22)

$$\cos \theta'' = (\omega_0 - \omega)/\Omega \quad (27)$$

Finally,

$$\begin{aligned} r_1' &= \frac{\omega_1'(\omega_0 - \omega)}{\Omega^2} (1 - \cos \Omega t) \\ r_2' &= -\frac{\omega_1}{K} \sin \Omega t \\ r_3' &= 1 - \frac{\omega_1'^2}{\Omega^2} (1 - \cos \Omega t) \end{aligned} \quad (28)$$

This essentially solves the dynamical problem

The angles appearing in Feynman's graphical solution are just the Euler angles and are already built into the spin-1/2 formalism. The relations between the angle (denoted by  $\theta$  by Feynman and Vernon)

$$\Omega t - \Omega L/v = \theta_N = \frac{L}{v} \sqrt{\omega_1'^2 + (\omega_1 - \omega)^2} \quad (29)$$

and the Euler angles  $\psi'', \theta''$  are as follows

$$\theta_N = \pi/2 - \psi'' = -\omega_1' t / \sin \theta''$$

Under conditions of exact tuning  $\omega = \omega_0$  and

$$r_1' = 0, \quad r_2' = -\sin \Omega t, \quad r_3' = \cos \Omega t$$

$$\text{and} \quad \Omega = \omega_1', \quad \Omega t = \omega_1' t = \theta_N = \hbar^{-1} |\mu_{ab}| E_0 t \quad \dots \quad (30)$$

$\theta_N$  is proportional to the pulse strength  $E_0 t$  under exact tuning

#### ELECTROMAGNETIC PART

Dispersion and absorption (or emission) are obtained by treating polarization  $P$  as a complex quantity (for  $\Delta m = 0$  transition)

$$P_e = N(r_1' + ir_2')\mu_{ab}$$

( $N$ , the density of molecules in the cavity) in the Maxwell equation for  $\vec{E}$

$$\nabla^2 \vec{E} - \frac{4\pi\sigma}{c^2} \frac{\partial \vec{E}}{\partial t} - \frac{1}{c^2} \frac{\partial^2 \vec{E}}{\partial t^2} = \frac{4\pi}{c^2} \frac{\partial^2 \vec{P}}{\partial t^2}$$

( $\sigma$  being the conductivity). This leads to the two equations in the stationary case

$$\begin{aligned} -\omega^2 \left[ \epsilon + \frac{4\pi N' \mu_{ab}}{v} \int_0^L f V^{-1} r_1' dz \right] + \omega_c^2 \epsilon &= 0 \\ -\frac{4\pi N' \mu_{ab}}{v} \omega^2 \int_0^L f V^{-1} r_2' dz + \frac{\omega_c \omega}{\theta} \epsilon &= 0 \end{aligned}$$

where the field  $\vec{E}$  in the cavity is given by

$$\vec{E} = \vec{E}_c e(t) e^{i\omega t},$$

$\vec{E}_c$  being the amplitude of the normal mode of the cavity,  $\theta = \omega_c/4\pi\sigma$ ,  $\omega_c$  the frequency of the cavity mode,  $V$  the volume of the cavity,  $f$  the filling factor,  $N'$  the flux of molecules travelling with velocity  $v$

Denoting 
$$A = \frac{4\pi N' \mu_{ab}}{v}$$

$$X = \int_0^L f V^{-1} r_1' dz = f V^{-1} \frac{\omega_1'(\omega_0 - \omega)}{\Omega^2} L \left( 1 - \frac{\sin \theta_N}{\theta_N} \right)$$

$$Y = \int_0^L f V^{-1} r_2' dz = f V^{-1} \frac{\omega_1'}{\Omega^2} v (\cos \theta_N - 1)$$

the two equations are

$$(\omega_c^2 - \omega^2) v - \omega_0^2 A X = 0 \quad (32a)$$

$$v - c - \omega^2 A Y = 0 \quad (32b)$$

Combining these two relations

$$\frac{X}{Y} = Q \frac{\omega_c^2 - \omega^2}{\omega_0^2} = (\omega - \omega_0) \frac{L}{v} \frac{1 - \sin \theta_N / \theta_N}{1 - \cos \theta_N} \quad (33)$$

Since we have  $\omega_c \sim \omega \sim \omega_0$  under actual conditions

$$\frac{\omega - \omega_0}{\omega_c - \omega} = \frac{2Q}{\omega_0} \frac{1}{\tau} \frac{1 - \cos \theta_N}{1 - \sin \theta_N / \theta_N} = a \text{ (say)}$$

where

$$\tau = L/v$$

The frequency shift is then given by

$$\omega - \omega_0 = \frac{a}{1+a} (\omega_c - \omega_0) \quad (34)$$

The electric field is given directly in terms of the oscillation frequency by the definitions

$$\frac{\Omega L}{v} = \theta_N \quad \dots \quad (35)$$

and

$$\omega_1' = \frac{-\mu_{ab}}{\hbar} E_0 = \frac{-\mu_{ab}}{\hbar} V^{-1} c$$

We obtain

$$\epsilon = \frac{\hbar V^2}{\mu_{ab}} \sqrt{\frac{\theta_N^2 v^2}{L^2} - \left(\frac{a}{1+a}\right)^2 (\omega_0 - \omega_c)^2} \quad \dots (36)$$

Under exact tuning of cavity

$$\epsilon = \frac{\hbar V^2}{\tau \mu_{ab} f} \theta_N \quad \dots (37)$$

The parameter  $\theta_N$  itself is determined by the second of the two Maxwell relations in terms of the flux of molecules  $N'$ :

$$\frac{N'}{N_0} = \frac{\theta_N^2}{2(1 - \cos \theta_N)} \quad \dots (38)$$

where

$$N_0' = \frac{\hbar V v^2}{2\pi |\mu_{ab}|^2 L^2 Q f^2} \quad \dots (39)$$

The power emitted under the stationary conditions is obtained by equating the loss to gain. Hence

$$\text{Power} = \frac{\omega W V}{Q} = P$$

The energy density  $W$  is given by

$$W = \epsilon^2/8\pi.$$

From (37) averaging over a periodic time we get under condition of exact tuning

$$W = \frac{\hbar^2 V}{8\pi \tau^2 |\mu_{ab}|^2 f^2} \theta_N^2.$$

From (38)

$$P = \frac{1}{2} N' \hbar \omega (1 - \cos \theta_N) \quad \dots (40)$$

$P$  can also be obtained directly from  $r_3'$ , since by definition

$$P = N' \hbar \omega b b^* = \frac{1}{2} N' \hbar \omega (1 - r_3')$$

(40) is equivalent to Shimoda's result (1957).

#### SUMMARY AND DISCUSSION

The gas has been considered as a system of  $N$  independent molecules so that the total polarisation is taken as  $N$  times the individual dipole moment. Briefly the physical results are given by the equations (34), (36) and (40). The explicit relations of oscillation frequency, electric field and power to molecular flux are pretty complicated but are simple when the former are expressed in terms of the only parameter  $\theta_N$  depending on  $N'$  as in equation (38). Approximate cases can be evaluated.

An exact analytic solution of the two-level problem is possible by the use of the spin-1/2 formalism which is suggested at the very outset by the complex

coefficients  $a$  and  $b$  which give the Cayley-Klein parameters obeying the normalization condition.

The transformation of  $\psi_a$  by the unitary matrix (3) gives the time-dependent state. Under the influence of the radiation the vector  $\sigma_3$  corresponding to the initial state of the system rotates about the origin and acquires the components  $r_1, r_2, r_3$  given by the transformation

$$U\sigma_3\bar{U} = r_1\sigma_1 + r_2\sigma_2 + r_3\sigma_3$$

where  $U$  is unitary and isomorphic with  $T$ . The transformation  $U$  is given by

$$T \rightarrow U = \begin{pmatrix} \sqrt{\frac{1}{2}(1+r_3)} & (r_1 + ir_2)/\sqrt{2(1+r_3)} \\ -\sqrt{\frac{1}{2}(1-r_3)} & (r_1 + ir_2)/\sqrt{2(1-r_3)} \end{pmatrix}$$

Since  $r_1, r_2, r_3$  are also the direction cosines of  $\vec{\mu}$

$$r_1 = \cos \alpha, r_2 = \cos \beta, r_3 = \cos \gamma$$

so that

$$U = \begin{pmatrix} \cos \gamma/2 & \frac{\cos \alpha + i \cos \beta}{2 \cos \gamma/2} \\ -\sin \gamma/2 & \frac{\cos \alpha + i \cos \beta}{2 \sin \gamma/2} \end{pmatrix} \quad \dots \quad (41)$$

This is the familiar rotation of  $\sigma_3$  through an angle  $\gamma$  about some axis in 1-2 plane.

Alternatively the system vector can be kept fixed and the coordinate system rotated by the transformation  $S \rightarrow T$  involving the independent Euler angles. This transformation gives the structure of  $r$  in terms of the Euler angles and suggests the solution of the dynamical problem first in a "precessional" co-ordinate system and then in the rotating system  $\Sigma_R$ . Thus this formalism involves the three familiar representations of the rotation group in two dimensions.

The matrix  $T$  itself effects the transformation  $T\sigma_3\bar{T}$  so that the  $r$ 's are defined in terms of  $a, b$  and hence the reduced density matrix is representable as a vector in spin space. The dynamical problem is to investigate its motion in spin space.

The forces of interaction appear in the transformation matrix  $T$  through the pulse strength  $\theta_N$  given by (30) at exact tuning

$$T \rightarrow S = \begin{pmatrix} \cos \theta_N/2 & -i \sin \theta_N/2 \\ i \sin \theta_N/2 & \cos \theta_N/2 \end{pmatrix} = I \cos \theta_N/2 - i\sigma_1 \sin \theta_N/2 = e^{-i\theta_N/2 \cdot \sigma_1} \quad \dots \quad (42)$$

while the response of the system is given by the transformed vector  $\mu'$  whose elements are the expectation values of the unperturbed Hamiltonian and the polarization,

$$\mu = \begin{pmatrix} \langle H_0 \rangle / \frac{1}{2} N \hbar \omega_0 & \langle P \rangle^* / N |\mu_{ab}| \\ \langle P \rangle / N |\mu_{ab}| & -\langle H_0 \rangle / \frac{1}{2} N \hbar \omega_0 \end{pmatrix} \quad \dots \quad (43)$$

where  $\langle H_0 \rangle = \frac{1}{2} N \hbar \omega_0 r_3$  and the quantities have to be evaluated for exact tuning  $\langle P \rangle$  becomes purely imaginary. The emitted power may be obtained straight away as a difference of energies  $\langle H_0 \rangle$  at  $t = 0$  and  $t = t$

$$P_e = \frac{1}{2} N \hbar \omega_0 - \langle H_0 \rangle = \frac{1}{2} N \hbar \omega_0 (1 - r_3') \quad \dots \quad (44)$$

Thus the spin-1/2 formalism enables one to represent the interaction process as a rotation of  $\sigma_3$  about the 1-axis through the pulse angle  $\theta_N$ , represented by a matrix of interaction.  $-\theta_N$  is none other than the Euler angle  $\theta$  in (5) through which  $\Sigma_B$  is rotated relative to  $\Sigma_S$ .

In fact no explicit reference to rotations in spin space is necessary. The relevant  $T$ -matrix can be obtained by straightforward integration from the equation

$$i \hbar \frac{dT}{dt} = HT$$

$H$  being given by (15).  $r_i$ 's are obtained from the transformation.

$$T\rho(0)\bar{T}$$

It is not surprising that the spin-1/2 formalism is the most appropriate for the treatment of absorption and emission processes. For

$$\sigma_1 \begin{pmatrix} 1 \\ 0 \end{pmatrix} = \begin{pmatrix} 0 \\ 1 \end{pmatrix}, \quad \sigma_2 \begin{pmatrix} 1 \\ 0 \end{pmatrix} = i \begin{pmatrix} 0 \\ 1 \end{pmatrix}$$

$$\sigma_1 \begin{pmatrix} 0 \\ 1 \end{pmatrix} = \begin{pmatrix} 1 \\ 0 \end{pmatrix}; \quad \sigma_2 \begin{pmatrix} 0 \\ 1 \end{pmatrix} = -i \begin{pmatrix} 1 \\ 0 \end{pmatrix}$$

Putting  $\begin{pmatrix} 1 \\ 0 \end{pmatrix} = [+]$  and  $\begin{pmatrix} 0 \\ 1 \end{pmatrix} = [-]$ , we simply have

$$\sigma_1[+] = [-], \quad \sigma_2[\pm] = \pm i[-]$$

Identifying  $[+]$  as the state of the excited atom and  $[-]$  as the normal atom, we note that the Pauli operators  $\sigma_1$  and  $\sigma_2$  are essentially 'transition operators' changing the ground state atom into an excited atom and vice-versa and play the central role in Dicke's formalism.

The gas has been considered as a system of  $N$  independent molecules so that the total polarisation is taken as  $N$  times the individual moment. Another method of treating the gas is to take the product of the  $T$ 's (42) for individual molecules and obtain a transformation for the whole gas, in which certain macroscopic operators will appear. The gas as a system of independent molecules turns out to be a special case. This will be taken up in a subsequent paper.

## ACKNOWLEDGMENT

One of the authors (L.P.D.) gratefully acknowledges the grant of a scholarship under the Research Training Scheme, Government of India

## REFERENCES

- Dicke R. H. 1954 *Phys. Rev.* **93**, 99.  
Feynman R. P. & Vernon Jr. F. L. 1957 *Appl. Phys.* **28**, 49.  
Lamb W. E. 1964 *Phys. Rev.*, **134**, 1429  
Mohanty B. K. 1967 *Indian J. Phys.* **41**, 60.  
Roy N. R. 1969 *Private communication*.  
Shimoda K. 1957 *J. Phys. Soc. Japan* **12**, 1006

## Double-boundary-layer concept in free-convection at high Prandtl numbers

BY SREEDHAN ROY

*Department of Mechanical Engineering, University of Aston,  
Birmingham, England*

(Received 27 July 1970—Revised 6 October 1970)

The double-boundary-layer-concept of Stewartson & Jones (1957) for free-convection at high Prandtl numbers ( $\sigma$ ) is extended. By the method of matched asymptotic expansions it is shown that series-solutions in powers of  $\sigma^{-1}$  exist. Calculations are carried upto terms  $O(\sigma^{-1})$ . The Nusselt number is seen to be in an error of 3.5% compared with exact solutions of Ostrach (1953), for a Prandtl number as low as 1.

### INTRODUCTION

It is well-known that in problems of free-convective heat transfer, from or to a heated surface, the Prandtl number ( $\sigma$ ) of the fluid medium plays a very important role. Mathematically, this role is expressed through the occurrence of this number in the governing non-dimensional partial differential equations. Solutions of these equations have been obtained by different methods. One class of solutions, obtained by integrating the partial differential equations by the integral method of Kármán-Pohlhausen, has an advantage in that they exhibit the Prandtl number dependence explicitly; but at the same time they provide with inaccurate results for skin-friction and heat transfer. Reference may be made to Eckert & Gross (1963) for examples of this type. On the other hand, Ostrach (1953), and Sparrow & Gregg (1958), and others have reduced the partial differential equations through similarity transformations to ordinary differential equations which they solved on high-speed computers. A disadvantage of this technique is that the results have to be tabulated for distinct values of the Prandtl number. A third technique maintaining the advantages of both the methods, *viz.* the accuracy and the explicit Prandtl number dependence has been developed by Le Fevre (1956), and Stewartson & Jones (1957). In fact, Stewartson & Jones in a study of free-convective heat transfer from a vertical flat plate obtained solutions for the extreme case  $\sigma = \infty$ . They introduced a concept of two boundary layers, one of thickness  $O(\sigma^{-1/4})$  in which the temperature difference was brought to zero, and one of thickness  $O(\sigma^{1/4})$  in which the component of the velocity parallel to the surface was brought to zero again.

We shall in this paper extend their work and obtain series-solutions in powers of  $\sigma^{-1}$ , to terms  $O(\sigma^{-1})$ , by means of the method of matched asymptotic expansions (Van Dyke, 1964). We shall call the layers the inner and outer layers respectively.



## MATHEMATICAL FORMULATION

Free-convection from or to a uniformly heated semi-infinite vertical flat surface is governed by the following boundary layer equations

$$\frac{\partial u}{\partial x} + \frac{\partial v}{\partial y} = 0,$$

$$\rho \left( u \frac{\partial u}{\partial x} + v \frac{\partial u}{\partial y} \right) = \mu \frac{\partial^2 u}{\partial y^2} \pm g\rho\beta\theta,$$

$$u \frac{\partial \theta}{\partial x} + v \frac{\partial \theta}{\partial y} = \alpha \frac{\partial^2 \theta}{\partial y^2} \quad \dots \quad (1)$$

$$u = v = 0, \quad \theta = t_w - t_\infty, \quad y = 0,$$

$$u \rightarrow 0, \quad \theta \rightarrow 0 \quad \text{as} \quad y \rightarrow \infty,$$

where  $u, v$  are the velocity components,  $\theta$  is the temperature difference  $(t - t_\infty)$ ,  $x$  is measured from the leading edge along the plate and  $y$  is the distance out perpendicular to the plate, the plus and minus signs apply for heating and cooling of the fluid respectively, and the other symbols have their usual meanings

A similarity solution of (1) is given by

$$\left. \begin{aligned} u &= \frac{\partial \psi}{\partial y}, \quad v = - \frac{\partial \psi}{\partial x}, \\ \phi &= \frac{t - t_\infty}{t_w - t_\infty}, \quad \psi = 2\sqrt{2\nu(Gr_x)^{1/4}}f, \\ Gr_x &= |g\beta x^3(t_w - t_\infty)/\nu^2|, \\ \eta &= \frac{y}{x} \left( \frac{Gr_x}{4} \right)^{1/4}, \end{aligned} \right\} \quad \dots \quad (2)$$

where  $f$  and  $\phi$  are functions of  $\eta$  alone satisfying the equations

$$\frac{d^3 f}{d\eta^3} + 3f \frac{d^2 f}{d\eta^2} - 2 \left( \frac{df}{d\eta} \right)^2 + \phi = 0, \quad \dots \quad (3)$$

and

$$\frac{d^3 \phi}{d\eta^3} + 3\sigma f \frac{d\phi}{d\eta} = 0. \quad \dots \quad (4)$$

The boundary conditions are

$$\left. \begin{aligned} f = \frac{df}{d\eta} &= 0, \quad \phi = 1 \quad \text{at} \quad \eta = 0, \\ \frac{df}{d\eta} &\rightarrow 0, \quad \phi \rightarrow 0 \quad \text{as} \quad \eta \rightarrow \infty. \end{aligned} \right\} \quad \dots \quad (5)$$

## INNER AND OUTER LAYER TRANSFORMATIONS

Following Stewartson & Jones (1957), the appropriate transformations are assumed as follows.

$$\begin{aligned}\zeta_1 &= (3\sigma)^{1/4}\eta, \\ f &= (3\sigma)^{-3/4}F_1(\zeta_1), \\ \phi &= \Phi_1(\zeta_1)\end{aligned}\tag{6}$$

Substituting in (3) and (4) we get

$$F_1'' + \Phi_1 + (3\sigma)^{-1}\{3F_1F_1'' - 2(F_1')^2\} = 0,\tag{7}$$

$$\text{and} \quad \Phi_1'' + F_1\Phi_1' = 0\tag{8}$$

Beyond the inner layer,  $\phi$  becomes exponentially small and  $\frac{df}{d\eta} = O(\sigma^{-1})$ . The outer layer is then introduced to reduce  $\frac{df}{d\eta}$  to zero. In this layer the appropriate transformations are

$$\left. \begin{aligned}\zeta_2 &= \gamma(3\sigma)^{-1/4}\eta, \\ f &= \gamma(3\sigma)^{-1/4}F_2(\zeta_2), \\ \phi &= 0,\end{aligned} \right\} \quad \dots \tag{9}$$

where  $\gamma$  is an arbitrary constant to be specified later. The equation for  $F_2$  is

$$F_2'' + 3F_2F_2'' - 2(F_2')^2 = 0 \quad \dots \tag{10}$$

In the above a prime means differentiation with respect to the appropriate independent variable  $\zeta_1$  or  $\zeta_2$ . It should also be remarked here that the boundary conditions at infinity are redundant for  $F_1$  and those on the surface for  $F_2$ .

Now, applying the method of matched asymptotic expansions we find that series-solutions in the following forms exist

$$\left. \begin{aligned}F_1 &= \sum_{i=0}^{\infty} (3\sigma)^{-i/2}F_{1i}, \\ \Phi_1 &= \sum_{i=0}^{\infty} (3\sigma)^{-i/2}\Phi_{1i}, \\ F_2 &= \sum_{i=0}^{\infty} (3\sigma)^{-i/2}F_{2i},\end{aligned} \right\} \quad \dots \tag{11}$$

together with the boundary conditions:

$$F_{10}(0) = 0, \quad F'_{10}(0) = 0, \quad F''_{10}(\infty) = 0; \quad ]$$

$$F_{20}(0) = 0, \quad F'_{20}(0) = 1, \quad F''_{20}(\infty) = 0;$$

$$F_{11}(0) = 0, \quad F'_{11}(0) = 0, \quad F'''_{11}(\infty) = \gamma^3 F''_{20}(0);$$

$$F_{21}(0) = \lim_{\zeta_1 \rightarrow \infty} \left\{ \frac{1}{\gamma} F_{10}(\zeta_1) - \gamma \zeta_1 \right\}$$

$$F'_{21}(0) = \frac{1}{\gamma^2} \lim_{\zeta_1 \rightarrow \infty} \{ F'_{11}(\zeta_1) - \zeta_1 F''_{11}(\zeta_1) \}, \quad F'_{21}(\infty) = 0;$$

$$F_{12}(0) = 0, \quad F'_{12}(0) = 0, \quad F''_{12}(\infty) = \gamma^3 \lim_{\zeta_1 \rightarrow \infty} \{ F''_{21}(0) + 2\gamma \zeta_1 \}; \quad (12)$$

$$F_{22}(0) = \lim_{\zeta_1 \rightarrow \infty} \left\{ \frac{1}{\gamma} F_{11}(\zeta_1) - \gamma \zeta_1 F'_{21}(0) - \frac{1}{2} \gamma^2 \zeta_1^2 F''_{20}(0) \right\},$$

$$F'_{22}(0) = \lim_{\zeta_1 \rightarrow \infty} \left\{ \frac{1}{\gamma^2} F'_{12}(\zeta_1) - \gamma \zeta_1 F''_{21}(0) - \gamma^2 \zeta_1^2 \right\},$$

$$F''_{22}(\infty) = 0;$$

$$\Phi_{10}(0) = 1, \quad \Phi_{10}(\infty) = 0;$$

$$\Phi_{11}(0) = 0, \quad \Phi_{11}(\infty) = 0;$$

$$\Phi_{12}(0) = 0, \quad \Phi_{12}(\infty) = 0;$$

where  $\gamma^2 = \lim_{\zeta_1 \rightarrow \infty} F'_{10}(\zeta_1)$  [See Appendix].

The equations for  $F$ 's and  $\Phi$ 's are

$$F'''_{10} + \Phi_{10} = 0, \quad (13)$$

$$F'''_{11} + \Phi_{11} = 0, \quad (14)$$

$$F'''_{12} + \Phi_{12} + 3F_{10}F''_{10} - 2(F'_{10})^2 = 0, \quad (15)$$

$$\Gamma_1(\Phi_{10}) = 0, \quad (16)$$

$$\Gamma_1(\Phi_{11}) + \Phi'_{10}F_{11} = 0, \quad (17)$$

$$\Gamma_1(\Phi_{12}) + \Phi'_{10}F_{12} + F'_{11}\Phi'_{11} = 0, \quad (18)$$

$$\Gamma_2(F_{20}) - 2(F'_{20})^2 = 0, \quad (19)$$

$$\Gamma_2(F_{21}) - 4F'_{20}F'_{21} + 3F'_{20}F'_{21} = 0, \quad (20)$$

$$\Gamma_2(F_{22}) - 4F'_{20}F'_{22} + 3F'_{20}F'_{22} + 3F'_{21}F'_{21} - 2(F'_{21})^2 = 0, \quad (21)$$

where  $\Gamma_1$  and  $\Gamma_2$  are the differential operators,

$$\Gamma_1 \equiv \frac{d^2}{d\zeta_1^2} + F_{10} \frac{d}{d\zeta_1}$$

and

$$\Gamma_2 \equiv \frac{d^2}{d\zeta_2^2} + 3F_{20} \frac{d^2}{d\zeta_2^2}.$$

## SOLUTION

Equations (13)–(21), subject to the boundary conditions (12), have been solved on the electronic computer IBM 7094II at The Imperial College, London. The values of the unknown boundary derivatives required to start numerical computations are presented below :

$$\begin{aligned} \gamma &= 0.940347 \\ F''_{10}(0) &= 1.085060, \quad F''_{11}(0) = -0.700126, \quad F''_{12}(0) = 0.861980; \\ \Phi'_{10}(0) &= -0.540229, \quad \Phi'_{11}(0) = 0.245418, \quad \Phi'_{12}(0) = -0.147591; \\ F'_{20}(0) &= 0.0, \quad F'_{20}(0) = 1.0, \quad F'_{20}(0) = -1.540791; \\ F_{21}(0) &= -0.632131, \quad F'_{21}(0) = 1.142751, \quad F''_{21}(0) = -1.654336, \\ F_{22}(0) &= -1.145929, \quad F'_{22}(0) = 2.583852, \quad F''_{22}(0) = -4.087507. \end{aligned} \quad \} \quad (22)$$

## SKIN-FRICTION AND HEAT-TRANSFER

Skin-friction is proportional to  $\left(\frac{d^2f}{d\eta^2}\right)_{\eta=0}$  which is given by

$$\left(\frac{d^2f}{d\eta^2}\right)_{\eta=0} = (3\sigma)^{-1/4}[1.085 - 0.700(3\sigma)^{-1/2} + 0.862(3\sigma)^{-1} + \dots] \quad (23)$$

The rate of heat-transfer is represented by the Nusselt number  $Nu$  that is given by

$$\begin{aligned} Nu &= -\frac{x}{(t_\infty - t_0)} \left(\frac{\partial\theta}{\partial y}\right)_{y=0} \\ &= (\sigma Gr_x)^{-1/4}[0.502 - 0.228(3\sigma)^{-1/2} + 0.137(3\sigma)^{-1} + \dots] \quad \dots \quad (24) \end{aligned}$$

The values of  $Nu (Gr_x)^{1/4}$  calculated from equation (24) for different values of  $\sigma$  are given in the table along with those obtained by Ostrach (1953)

TABLE 1  
Values of the  $Nu (Gr_x)^{-1/4}$

$\sigma$	Roy	Ostrach (1953)
1	0.416	0.401
2	0.517	0.507
10	0.827	0.827
$10^2$	1.547	1.549
$10^3$	2.800	2.805

## REMARKS

(1) It is clear from the table that though our analysis has been developed on the assumption of a large Prandtl number the values of the Nusselt number

compare very favourably with the exact values of Ostrach even for a Prandtl number as low as 1.

(2) The boundary conditions  $F''_{10}(\infty) = 0$ ,  $F_{20}(0) = 0$  and  $F'_{20}(0) = 1$  have been used by Stewartson & Jones (1957). However, they have not given a reason for introducing them. It has been clear that only through the method of matched asymptotic expansions one can deduce these and the other conditions.

(3) The double-boundary-layer concept described here should be applicable to other boundary layer phenomena in free-convection from or to an isothermal surface at high Prandtl numbers. The author has used it in substantiating a conjecture of Gebhart (1962) on dissipation effects in free-convection (Roy 1969).

#### REFERENCES

- Eckert E. R. G. & Gross J. F. 1963 *Introduction to Heat and Mass Transfer*, McGraw Hill.  
 Gebhart B. 1962 *Jour. Fluid Mech.* **14**, 225.  
 Le Fèvre E. J. 1956 *Ninth Intern. Congr. App. Mech.*, Brussels, paper I 168, **4**, 168.  
 Ostrach S. 1953 *N.A.C.A. Rept.* No. 1111.  
 Roy S. 1969 *Int. J. Heat Mass Transfer*, **12**(2), 239.  
 Sparrow E. M. & Gregg J. L. 1958 *NASA Memo* 2-27-59F.  
 Stewartson K. & Jones L. T. 1957 *Jour. Aero. Sci.* **24**, 379.  
 Van Dyke M. 1964 *Perturbation Techniques in Fluid Mechanics*, Academic Press, New York.

#### APPENDIX—MATCHED ASYMPTOTIC EXPANSION

Equations (13)–(21) suggest that series expansions in negative powers of  $\sigma$  exist. Let us consider the equations (13) and (19) and assume that for  $\sigma = \infty$ , the solutions are  $F_{10}$  and  $F_{20}$  and that the next terms are  $K(\sigma)F_{11}$  and  $K(\sigma)F_{21}$  respectively. To find the form of  $K(\sigma)$  we match the solutions for large values of  $\zeta_1$  and for small values of  $\zeta_2$ . Thus

$$\begin{aligned} & (3\sigma)^{-3/4}F_1(\zeta_1) \text{ for large } \zeta_1 \\ & \approx \gamma(3\sigma)^{-1/4}F_2(\zeta_2) \text{ for small } \zeta_2. \end{aligned}$$

Therefore,  $F_{10}(\zeta_1) + K(\sigma)F_{11}(\zeta_1) + \dots$  for large  $\zeta_1$

$$\approx \gamma(3\sigma)^{1/4}\{F_{20}(\zeta_2) + K(\sigma)F_{21}(\zeta_2) + \dots\} \text{ for small } \zeta_2 \quad \dots \quad (\text{A } 1)$$

We now assume that for small  $\zeta_2$ ,  $F_{20}$  and  $F_{21}$  have Taylor-series representations,

$$\left. \begin{aligned} F_{20} &= a_0 + a_1\zeta_2 + a_2\zeta_2^2 + \dots \\ F_{21} &= b_0 + b_1\zeta_2 + b_2\zeta_2^2 + \dots \end{aligned} \right\} \quad (\text{A } 2)$$

Putting from (A.2) into (A.1), and noting that  $\zeta_2 = \gamma(3\sigma)^{-1}\zeta_1$ , we get

$$\begin{aligned} & F_{10}(\zeta_1) + K(\sigma)F_{11}(\zeta_1) + \dots \\ & \sim \gamma\{3\sigma\}^{1/4}[a_0 + \gamma a_1(3\sigma)^{-1}\zeta_1 + \gamma^2 a_2(3\sigma)^{-1}\zeta_1^2 + \dots \\ & + K(\sigma)\{b_0 + \gamma b_1(3\sigma)^{-1}\zeta_1 + \gamma^2 b_2(3\sigma)^{-1}\zeta_1^2 + \dots\}] \text{ as } \zeta_1 \rightarrow \infty \end{aligned} \quad (\text{A } 3)$$

(A.3) shows that

(i)  $a_0 = 0$ , since  $F_{10}$  cannot behave as  $\sigma^1$  as  $\zeta_1 \rightarrow \infty$ , and (ii)  $K(\sigma) = (3\sigma)^{-1}$ . Proceeding in this way it is seen that the third term is proportional to  $(3\sigma)^{-1}$ , and so on. Further, from (A.3) we get,

$$\left. \begin{aligned} F_{10} &\sim \gamma b_0 + \gamma^2 a_1 \zeta_1, \\ F_{11} &\sim \gamma c_0 + \gamma^2 b_1 \zeta_1 + \gamma^3 a_2 \zeta_1^2, \\ &\quad \text{as } \zeta_1 \rightarrow \infty \\ \text{where } F_{22} &= c_0 + c_1 \zeta_2 + \dots & \text{as } \zeta_2 \rightarrow 0 \end{aligned} \right\} \quad (\text{A.4})$$

From (A.2) and (A.4) the boundary conditions for  $F_{10}$  and  $F_{11}$  at  $\zeta_1 = \infty$  and those for  $F_{20}$  and  $F_{21}$  at  $\zeta_2 = 0$  follow. An extension of this matching technique leads to the rest of the boundary conditions.

## Lattice properties of heavier halides<sup>+</sup>—I

By D. C. GUPTA AND M. N. SHARMA

*Department of Physics, Lucknow University, Lucknow*

*(Received 15 September 1970)*

The appropriateness of Born's theory as applied to lighter alkali halides and molecules has been further investigated by considering heavier ionic crystals using a modified Born potential energy function. The values of index of repulsive potential,  $n$ , the repulsive force parameter  $\lambda$ , lattice energy, compressibility and thermal expansion have been calculated and necessary equations derived. The comparison of the experiment with theory reveals that the present simple and direct approach using modified Born model is quite satisfactory to represent various lattice properties. Also the comparison of the results with those obtained employing other models establishes the superiority of the modified Born model.

### INTRODUCTION

Born (1923, 1927) has formulated a theory to describe the various properties of ionic crystals and molecules on the basis of a very simple form of the function expressing interaction potential energy. The correct representation of the potential energy of a set of atoms as a function of the interatomic distances is of fundamental importance. It is well known that the interaction energy of an ionic crystal, in addition to Coulomb energy, consists of terms involving attractive and repulsive energies. In an ionic crystal the charge distribution on each ion has, approximately, spherical symmetry and they interact according to central force law. Thus it seems reasonable to assume that ions of an ionic crystal are of the same electronic structure as the molecules of an inert gas, possessing overlap energy (and Van der Waals energy).

The forces of interaction between ions lead to the formation of the molecules and crystals and at the same time help to determine their properties. For ionic crystals the behaviour of the forces of interaction was studied by Mie (1903), Gruneisen (1912, 1926), Born (1923, 1927), Born & Mayer (1932) and at a later stage by Cubicciotti (1959, 1961), Sharma & Madan (1961, 1962, 1964a, 1964b), Saxena *et al* (1964), Kachhava & Saxena (1965), Gohel & Trivedi (1967), Gupta & Sharma (1969), Chatterjee (1963) and others and has been summarised by Kittel (1956) and Born & Huang (1959). In ionic crystals the interaction consists of (i) an electrostatic term, giving the largest contribution to the total lattice energy (ii) a repulsive term (iii) multipole interactions, like dipole-dipole and dipole-quadrupole interactions, which though small must be taken into account for the sake of completeness and (iv) zero-point energy.

<sup>+</sup>A preliminary note has been published in Indian J. Phys. 43, 358 (1969).

\*Work supported by the University Grants Commission, India.

Many of the properties of liquids and gases have been explained in terms of a commonly used interaction energy function, such as Born potential energy function. This energy function is strictly true for spherical molecules. Thus it is possible to explain a number of properties of ionic crystals on a common basis with the help of this potential energy function. It is reasonable to assume that if we also consider the multipole interactions and zero point energy in conjunction with this potential model (modified Born model) better results may be expected and such an analysis will lead to considerable success.

Now taking into account all the above interactions, the energy of the crystal per unit cell may be expressed as :

$$\psi(r) = -\frac{\alpha e^2}{r} + \frac{\lambda}{r^n} - \frac{C}{r^6} - \frac{D}{r^8} + \epsilon \quad \dots (1)$$

where  $\alpha$  is the Madelung constant,  $e$  the electronic charge,  $r$  the equilibrium inter-ionic distance,  $\lambda$  the repulsive parameter,  $C$  the dipole-dipole interaction parameter,  $D$  the dipole-quadrupole interaction parameter,  $\epsilon$  the zero-point energy and  $n$  the index of the repulsive term

At this juncture, it may be mentioned that the two types of repulsive functions in vogue are an exponential variation with distance and a simple inverse power variation with distance. The results of quantum-mechanical calculations favour the exponential form which is more cumbersome (Cubicciotti 1959, 1961), whereas, the inverse power form has the advantage of greater simplicity (Chatterjee 1963). The exponential form has been used by Born & Mayer (1932), Huggins (1937), and Cubicciotti (1959, 1961), for lighter alkali halides and by Bleick (1934), Mayer (1933), and Mayer & Levy (1933) for heavier halides. It is, therefore, worthwhile to find out whether the simple inverse power law is equally satisfactory for ionic crystals containing heavier ions as less work has been done on these crystals

In the present work, the inverse power form of repulsive term has been adopted and it has been shown that this modified Born potential energy function, too, is equally satisfactory for metal halides. Besides having the advantage of simplicity, its justification lies in the fact that the interionic distance between two ions remains nearly constant being near the value at the potential minimum.

#### DETERMINATION OF POTENTIAL PARAMETERS

The well known equilibrium relations, based on certain assumptions by Hildebrand (1931), about the energy of a lattice are :

$$r \left( \frac{d\psi}{dr} \right)_{r=r_0} = \frac{3vT}{\beta} \left( \frac{1}{V} \frac{\partial V}{\partial T} \right)_P \quad \dots (2)$$

and

$$r^2 \left( \frac{d^2\psi}{dr^2} \right)_{r=r_0} = \frac{9v}{\beta} F_{TP} \quad \dots (3)$$



where

$$F_{T,P} = 1 + \frac{T}{\beta} \left( \frac{\partial \beta}{\partial T} \right)_P + \frac{T}{\beta^2 V} \left( \frac{\partial V}{\partial T} \right)_P \left( \frac{\partial \beta}{\partial P} \right)_T + \frac{2T}{3V} \left( \frac{\partial V}{\partial T} \right)_P$$

$\beta$  is the compressibility,  $\left( \frac{1}{V} \frac{\partial V}{\partial T} \right)_P$  is the thermal expansion coefficient and  $v$  is the volume of the unit cell and is given by  $v = kr^3$ , where  $k$  is the structure constant depending upon the type of crystal lattice.

(a) *The power of repulsive potential*

Combining equations (2) and (3) with equation (1) one obtains,

$$n = \frac{\frac{9kr^3}{\beta} F_{T,P} + 2 \frac{\alpha e^2}{r} + 42 \frac{C}{r^6} + 72 \frac{D}{r^8}}{\frac{\alpha e^2}{r} + \frac{6C}{r^6} + \frac{8D}{r^8} - \frac{3kr^3 T}{\beta} \left( \frac{1}{V} \frac{\partial V}{\partial T} \right)_P} - 1 \quad \dots (4)$$

From an analysis of the crystal structure data, accurate values of the lattice constant are available from which, using the appropriate structural relationship for different cubic lattices, the nearest neighbour distance  $r$  can be obtained. These observed values of  $r$  can be substituted in equation (4) to determine the constant  $n$ , if we have knowledge of  $C$  and  $D$  from other sources. The first term in the numerator and the last term in the denominator are only in the nature of a corresponding term in which experimental values may be used for any selected temperature. If the experimental data for the coefficient of volume expansion, the compressibility and interionic distance be used, the value of  $n$  can be computed from equation (4). These values of  $n$  for several heavier halides have been reported in table 1. The experimental values used for CuCl, CuBr and CuI were obtained from Mayer & Levy (1933), for AgCl, AgBr, AgI, TlCl and TlBr have been taken from Mayer (1933) and for  $\text{NH}_4\text{Cl}$  and  $\text{NH}_4\text{Br}$  from Blicke (1934).

(b) *Repulsive parameter  $\lambda$*

Once the values of the index of the repulsive term,  $n$ , have been evaluated using equation (4), the potential parameters can be evaluated by using the experimental data for different crystal properties.

From equation (1) we at once get

$$\lambda = r^n \left[ \psi(r) + \frac{\alpha e^2}{r} + \frac{C}{r^6} + \frac{D}{r^8} - \epsilon \right] \quad \dots (5)$$

Also, combining equations (1) and (2), we obtain

$$\lambda = \frac{r^n}{n} \left[ \frac{\alpha e^2}{r} + \frac{6C}{r^6} + \frac{8D}{r^8} - \frac{3kr^3}{\beta} T \left( \frac{1}{V} \frac{\partial V}{\partial T} \right)_P \right] \quad (6)$$

and from equations (1) and (3) we get

$$\lambda = \frac{r^n}{n(n+1)} \left[ \frac{9kr^3}{\beta} F_{TP} + \frac{2\alpha e^2}{r} + 42 \frac{C}{r^6} + 72 \frac{D}{r^8} \right]$$

TABLE 1. Potential parameters

Crystal	$n$		$\lambda$		
	Eq (4)	Scitz (1940)	Eq (5)	Eq (6)	Eq (7)
CuCl	9 455	9 000	$5 319 \times 10^{-81.64}$	$7 119 \times 10^{-84.61}$	$7 119 \times 10^{-81.64}$
CuBr	9 704	-	$0 854 \times 10^{-85.03}$	$1 351 \times 10^{-85.03}$	$1 351 \times 10^{-85.03}$
CuI	12 020	-	$0 815 \times 10^{-103.16}$	$1 835 \times 10^{-103.16}$	$1 835 \times 10^{-103.16}$
AgCl	10 009	9.500	$5 973 \times 10^{-88.07}$	$6 952 \times 10^{-88.07}$	$6 952 \times 10^{-88.07}$
AgBr	10 250	-	$0 938 \times 10^{-89.00}$	$1 228 \times 10^{-89.00}$	$1 228 \times 10^{-89.00}$
AgI	10 250	-	$6 762 \times 10^{-90.00}$	$9 822 \times 10^{-90.00}$	$9 822 \times 10^{-90.00}$
TlCl	8 590	10.500	$6 940 \times 10^{-76.72}$	$8 052 \times 10^{-76.72}$	$8 052 \times 10^{-76.72}$
TlBr	8 853	-	$1 239 \times 10^{-77.82}$	$1 409 \times 10^{-77.82}$	$1 409 \times 10^{-77.82}$
NH <sub>4</sub> Cl	8 811	—	—	$8 189 \times 10^{-78.51}$	$8 189 \times 10^{-78.51}$
NH <sub>4</sub> Br	8 613	—	—	$9 770 \times 10^{-77.11}$	$9 770 \times 10^{-77.11}$

The values of  $\lambda$  have been computed separately from equations (5), (6) and (7). It is seen from table 1 that there is a good agreement in the values of the repulsive parameter  $\lambda$  obtained by using the value of  $C$  from optical data and those obtained by using the experimental values of the lattice energy.

## CRYSTAL PROPERTIES

### (a) Interaction energy

Using the expressions (1), (6), and (7), the values of the interaction energies have been calculated and presented in table 2 along with the experimental values for the sake of comparison.

The lattice energy can also be calculated using experimental values of reststrahlen frequency  $\nu_0$ . This method is supposed to be more realistic and accurate as this involves only two measurable quantities,  $\nu_0$  and dielectric constants at static and high frequency regions. If we take the polarization of ions into consideration the equation for force constant can be written as

$$f = \frac{4\pi^2\nu_0^2(\epsilon_0+2)\mu}{(\epsilon_\infty+2)} \quad (8)$$

TABLE 2. Lattice energy and compressibility

Crystal	$\psi(r)$ (K cal./mole)				$\beta (\times 10^{-12} \text{ bars}^{-1})$		
	Observed	Theoretical using eq. (1) and			Observed	Theoretical Using Equation (12)	
		$\lambda$ from Eq. (6)	$\lambda$ from Eq. (7)	Eq. (11) and $f$ from Eq. (8)			
CuCl	221.9 <sup>a</sup>	213.5	213.5	209.7	211.0	2.51 <sup>a</sup>	4.13
CuBr	216.0 <sup>a</sup>	204.4	204.4	196.9	201.9	—	—
CuI	213.4 <sup>a</sup>	199.6	199.6	—	195.6	—	—
AgCl	205.7 <sup>b</sup>	200.4	200.4	211.9	197.5	2.40 <sup>b</sup>	3.20
AgBr	201.8 <sup>b</sup>	193.8	193.8	204.6	190.2	2.75 <sup>b</sup>	4.66
AgI	199.0 <sup>b</sup>	188.0	188.0	—	183.9	—	—
TlCl	170.1 <sup>b</sup>	164.7	164.7	—	161.5	4.90 <sup>b</sup>	6.86
TlBr	165.6 <sup>b</sup>	161.2	161.2	—	157.6	5.30 <sup>b</sup>	7.03
NH <sub>4</sub> Cl	—	160.0	160.0	—	—	—	—
NH <sub>4</sub> Br	—	152.4	152.4	—	—	—	—

<sup>a</sup> Mayer & Levy (1933)<sup>b</sup> Mayer (1933)

where  $\mu$  is the reduced mass per ion pair,  $\epsilon_0$  and  $\epsilon_\infty$  are the static and high frequency dielectric constants, respectively. The experimental values of force constant can be computed using equation (8) if we have a knowledge of experimental values of  $\nu_0$ ,  $c_0$  and  $\epsilon_\infty$ . The force constant  $f$  can also be written as

$$f = \frac{1}{3} \left[ \phi''(r_0) + \frac{2}{r_0} \phi'(r_0) \right] \quad (9)$$

where  $\phi'(r_0)$  and  $\phi''(r_0)$  are the first and second derivatives of  $\phi(r)$  [ $\phi(r)$  contains the rest of the energy  $\psi(r)$  of equation (1) except the electrostatic term  $(-\alpha e^2/r)$ ].

Using equation (1) for  $\phi(r)$  and equation (9) we at once get

$$f = \frac{1}{3} \left[ \frac{\lambda}{r^n} \cdot \frac{n(n-1)}{r^2} - 30 \frac{C}{r^8} - 56 \frac{D}{r^{10}} \right] \quad (10)$$

Now substituting for  $\lambda/r^n$  from equation (1) in equation (10) and solving for  $\psi(r)$  we get

$$\psi(r) = \frac{1}{n(n-1)} \left[ 3fr^2 - \frac{C}{r^6} (n^2 - n - 30) - \frac{D}{r^8} (n^2 - n - 56) \right] + c_0 - \frac{\alpha e^2}{r} \dots \quad (11)$$

The values of  $f$  determined from equation (8) have been used to compute the theoretical values of  $\psi(r)$  on the basis of equation (11) and are presented in table 2 only for a few crystals, which verify the suitability of this method.

(b) *Compressibility*

From the knowledge of  $\lambda$ ,  $C$ ,  $D$  and the lattice energy, we can derive the crystal compressibility which can be compared with the observed values.

Using equation (3) and solving for  $\beta$ , we get

$$\beta = \frac{9kr^3 f_{T,P}}{-\frac{2\alpha e^2}{r} + n(n+1)\frac{\lambda}{r^n} - 42\frac{C}{r^6} - 72\frac{D}{r^8}} \quad (12)$$

Equation (12) enables us to compute  $\beta$  on substituting the value of  $\lambda$  from equation (5) and the values of  $C$  and  $D$  from optical data. The values of  $\beta$  thus obtained are given in table 2, where they have been compared with the experimental values of the crystal compressibility.

(c) *Coefficient of thermal expansion*

In a crystal lattice, the ions oscillate about their equilibrium positions and their amplitudes increase with temperature. Hummel (1950) on this basis has explained the thermal expansion as due to the shifting of equilibrium positions of oscillating ions when their amplitudes become sufficiently large. In view of the effect of ionic vibrations on thermal expansion of solids, many workers have correlated this property with vibration characteristics of ions. Weyl (1955), while discussing simple cubic crystals, has pointed out that expansivity should increase with increasing polarisation of ions.

In the present work, the values of coefficient of thermal expansion on the basis of equation (1) have been calculated in two different ways. We shall take up these methods one by one.

(A) Dividing equation (2) by equation (3), we get

$$\alpha_v = \frac{3f_{T,P}}{rT} \cdot \frac{(d\psi/dr)}{(d^2\psi/dr^2)} \quad \dots \quad (13)$$

and, for the modified Born potential, equation (13) yields

$$\alpha_v = \frac{3f_{T,P}}{T} \cdot \frac{\left[ \frac{\alpha e^2}{r} - \frac{n\lambda}{r^n} + \frac{6C}{r^6} + \frac{8D}{r^8} \right] Z}{\left[ -\frac{2\alpha e^2}{r} + n(n+1)\frac{\lambda}{r^n} - 42\frac{C}{r^6} - 72\frac{D}{r^8} \right]} \quad \dots \quad (14)$$

In the last equation

$$Z = \frac{Z_c N_c + Z_a N_a}{N_a + N_c}$$

where  $Z_c$ ,  $N_c$  and  $Z_a$ ,  $N_a$  are the charge and number of the cation and anion, respectively. This term has been introduced to account for the polarisation effects. The values of  $\alpha_v$  calculated from equation (14), using the values of  $\lambda$  obtained from equation (7), are presented in table 3 along with the experimental values.

TABLE 3. Coefficient of thermal expansion

Crystal	$\alpha_v (\times 10^{-6} \text{ per degree})$			
	Observed	Theoretical using		Kumar (1959)
		Eq. (14)	Eq. (17)	
CuCl	65.40	65.76	—	—
CuBr	62.10	62.30	—	—
CuI	73.50	73.46	—	—
AgCl	98.74	98.73	124.36	94.41
AgBr	104.50	104.38	132.87	95.34
AgI	113.30	113.48	—	—
TlCl	153.80	152.83	181.22	155.40
TlBr	160.40	159.80	—	—
NH <sub>4</sub> Cl	142.00	141.66	—	—
NH <sub>4</sub> Br	161.00	161.57	—	—

(B). Kumar (1959, 1960) has developed a simple method for calculating the coefficient of thermal expansion. According to him,

$$\alpha_v = \left( \frac{3C_p}{2E} \right) \left( \frac{n+4}{n} \right) Z^{\frac{1}{2}} \quad \dots \quad (15)$$

where  $C_p$  and  $E$  are the specific heat at constant pressure and cohesive energy per mole, respectively, and  $Z$  is the same as in equation (14).

A more general form of equation (15) is

$$\alpha_v = -\frac{3C_p}{2r_0} \frac{\psi'''(r_0)}{[\psi''(r_0)]^2} Z^{\frac{1}{2}} \quad \dots \quad (16)$$

where  $r_0$  is the interionic equilibrium separation distance,  $\psi'''(r_0)$  and  $\psi''(r_0)$  refer to values of third and second derivatives, respectively, of  $\psi(r)$  at  $r = r_0$ .

Thus using equation (1) and substituting for  $\psi''(r_0)$  and  $\psi'''(r_0)$  we get

$$\alpha_v = -\frac{3}{2} C_p \frac{\left[ 6 \frac{\alpha e^2}{r} - n(n+1)(n+2) \frac{\lambda}{r^3} + 336 \frac{C}{r^6} + 720 \frac{D}{r^8} \right]}{\left[ -2 \frac{\alpha e^2}{r} + n(n+1) \frac{\lambda}{r^3} - 42 \frac{C}{r^6} - 72 \frac{D}{r^8} \right]^2} Z^{\frac{1}{2}} \dots (17)$$

Using calculated values of  $\lambda$  from equation (7),  $\alpha_v$  has been computed only for AgCl, AgBr and TlCl because for other halides the data for  $C_p$  is not available in literature.

### DISCUSSION

The potential parameters  $n$  and  $\lambda$  for the simple modified Born model have been tabulated in table 1. For a single crystal we get three different sets of potential parameter  $\lambda$  calculated from the three conditions. The use of these parameters to calculate lattice properties will throw some light on the accuracy of experimental data used and the assumed potential model.

The present values of repulsive index  $n$  agree well with those reported by Seitz (1940). The difference is mainly due to the lattice conditions used (equations (2) and (3)) and data taken and also due to additional terms, *i.e.*, dipole-dipole and dipole-quadrupole interactions. These interactions should always be considered especially in the case of heavier ions (Born & Huang 1954).

Table 2 gives the values of interaction energy calculated for two sets of potential parameter  $\lambda$  (equations (6) and (7)). It can be seen that the results obtained are in excellent agreement with the experimental values. The theoretical values of  $\psi(r)$  computed from experimental absorption frequency data compare fairly well with the observed values. The present values of  $\psi(r)$  computed from equations (6) and (7) are in much better agreement than those calculated by Saxena *et al* (1964) using exponential energy function. It is, therefore, clear that the inverse power repulsive form can be used to describe successfully all the classical effects associated with ionic crystals. The authors anticipate that, if a more accurate value of  $F_{TP}$ , be used in calculating the interaction energy, still better agreement with experiment can be obtained.

The values of the compressibility presented in table 2 are fairly accurate and are nearly of the same order as the experimental values.

The thermal expansion values of the crystals calculated from equation (14) along with the experimental values have been presented in table 3. The table also includes values of  $\alpha_v$  calculated from equation (17) for AgCl, AgBr and TlCl and also those reported by Kumar (1959) for these crystals. Values for other crystals could not be given due to nonavailability of experimental data. The present values from equation (14) agree excellently with the experimental values and are better than those of Kumar. However, values calculated presently, from equation (17) following the method of Kumar do not give as good results

for obvious reasons. The agreement between the observed and the theoretical values thus confirms the essential correctness of the theoretical modified Born potential energy model for the ionic lattices.

In view of the simple calculations and the direct approach, it can easily be seen that the modified Born model represents excellently some of the crystal properties reported here and may be considered in preference to the cumbersome models having involved calculations.

#### ACKNOWLEDGEMENTS

The authors are grateful to Dr. B. N. Srivastava, D.Sc., F.N.A. for helpful suggestions and going through the manuscript. The authors are also grateful to Dr. B. G. Gokhale for his interest in the present work. Helpful suggestions and fruitful discussions from Dr. M. C. Saxena and Dr. J. N. Singh are gratefully acknowledged. One of us (D.C.G.) is thankful to State C.S.I.R., U.P. for financial assistance.

#### REFERENCES

- Bleick W. E. 1934 *J. Chem. Phys.* **2** 160  
 Born M. 1923 *Atomtheorie des Festen Zustandes*, Teubner, Leipzig.  
 Born M. 1927 *Handbuch der Physik.*, **24**, 370.  
 Born M. & Huang K. 1959 *Dynamical Theory of Crystal Lattices*, Clarendon Press Ltd., Oxford.  
 Born M. & Mayer J. 1932 *Zeit. f. Phys.* **75**, 1.  
 Chatterjee S. 1963 *Indian J. Phys.* **37**, 105.  
 Cubicciotti D. 1959 *J. Chem. Phys.*, **31**, 1646  
 Cubicciotti D. 1961 *J. Chem. Phys.* **34**, 2189  
 Gohel V. B. & Trivedi M. D. 1967 *Indian J. Pure & Appl. Phys.*, **5**, 265  
 Gruneisen E. 1912 *Ann. Physik* **39**, 257.  
 Gruneisen E. 1926 *Handbuch der Physik* **10**, Part 1. Julius Springer, Berlin.  
 Gupta D. C. & Sharma M. N. 1969 *Indian J. Phys.* **43**, 201.  
 Hildebrand J. H. 1931 *Zeit. f. Phys.* **67** 127  
 Huggins M. L. 1937 *J. Chem. Phys.* **5**, 143.  
 Hummel F. A. 1950 *J. Am. Ceram. Soc.*, **33**, 102.  
 Kachhava C. M. & Saxena S. C. 1965 *Indian J. Phys.* **39**, 145.  
 Kittel C. 1956 *Introduction to Solid State Physics*, John Wiley & Sons, Inc., N.Y.  
 Kumar S. 1960 *Central Glass and Ceramic Research Institute Bulletin*, **7**, 5.  
 Kumar S. 1959 *Proc. Nat. Inst. Sci. India*, **25A** 364.  
 Mayer J. 1933 *J. Chem. Phys.* **1**, 327  
 Mayer J. & Levy R. B. 1933 *J. Chem. Phys.* **1**, 647.  
 Mie G. 1903 *Ann. Physik*, **11**, 657.  
 Saxena S. C., Kachhava C. M. & Mathur S. 1964 *Indian J. Pure & Appl. Phys.* **2**, 338.  
 Seitz F. 1940 *The Modern Theory of Solids*, McGraw-Hill Book Company, N.Y.  
 Sharma M. N. & Madan M. P. 1961 *Indian J. Phys.* **35**, 506.  
 Sharma M. N. & Madan M. P. 1962 *Current Science* **31**, 54.  
 Sharma M. N. & Madan M. P. 1964a *Indian J. Phys.* **38**, 305.  
 Sharma M. N. & Madan M. P. 1964b *Indian J. Phys.* **38**, 231.  
 Weyl W. A. 1955 *Office of Naval Research Techn. Reports* Nos. 64, 65, 66, Pennsylvania State University.

## The emission spectrum of indium monobromide

By A. LAKSHMINARAYANA AND P. B. V. HARNATH

*Spectroscopy Laboratories, Physics Department, Andhra University,  
Waltair*

(Received 23 September 1970—Revised 26 February 1971)

[ Plate—12-13 ]

The emission band spectrum of indium monobromide is excited in a radio frequency discharge from a 1/2kw oscillator. Photographs of the spectra recorded in the first order of 21 ft concave grating spectrograph revealed many more new bands in the region  $\lambda 3980\text{--}\lambda 3560\text{\AA}$ , where two band systems *A* and *B* were reported earlier in absorption. Vibrational analyses of these two band systems are considerably extended to include all the new bands observed in the present investigation. The following vibrational formulae are derived for the *P* heads of  $\text{In}^{70}\text{Br}$  molecule. The two sub-systems are found to be the components of the  $^3\Pi_{0-1} - X^1\Sigma^+$  transition of the  $\text{InBr}$  molecule.

*System A*

$$\nu = 26595.60 + 229.2(\nu' + 1/2) - 1.42(\nu' + 1/2)^2 - 223.1(\nu'' + 1/2) + 0.56(\nu'' + 1/2)^2$$

*System B*

$$\nu = 27379.44 + 225.0(\nu' + 1/2) - 1.53(\nu' + 1/2)^2 - 223.0(\nu'' + 1/2) + 0.59(\nu'' + 1/2)^2$$

### INTRODUCTION

The emission band spectrum of  $\text{InBr}$  was first reported by Patrikain & Hochberg (1933) to consist of a series of bands extending in the regions  $\lambda 3980\text{--}\lambda 3590\text{\AA}$  and  $\lambda 3050\text{--}\lambda 2850\text{\AA}$ . Later Wehrli & Miescher (1934) studied the absorption spectrum of  $\text{InBr}$  in the 2nd order dispersion of a 3-meter grating. The bands in the region  $\lambda 3050\text{--}\lambda 2850\text{\AA}$  were designated as system *C*. The discrete bands in the region  $\lambda 3850\text{--}\lambda 3560\text{\AA}$  were analysed as belonging to two sub-systems *A* and *B* and attributed to  $^3\Pi_0 - X^1\Sigma^+$  and  $^3\Pi_1 - X^1\Sigma^+$  transitions respectively of  $\text{InBr}$ . Following our recent work on the analogous triplet systems of  $\text{AlBr}$  (Lakshminarayana & Haranath 1970a) and  $\text{AlI}$  (Lakshminarayana & Haranath 1970b), it was thought worthwhile to re-investigate the emission spectrum of  $\text{InBr}$  in higher dispersion with the object of gaining more information on the vibrational structure of these band systems. The results of the present investigation are described here.

### EXPERIMENTAL

Pure indium metal pellets are spread inside a translucent silica discharge tube provided with a side tube at one of its ends. A small bulb containing fuming liquid bromine is connected to the side tube through a stopcock. In order to regulate the supply of bromine vapour the tube bulb is immersed in a suitable



low temperature bath. The other end of the discharge tube which is drawn into an adapter is connected to a high vacuum pump through a liquid air trap. The tube is excited by RF discharge from a 500 watt oscillator operating at 30-40MHz. When a regulated supply of bromine is passed over the heated metal a characteristic bluish discharge is observed. Photographs of the spectrum are taken on Hilger  $E_1$  Quartz Littrow spectrograph and in the first order of a 21 ft concave grating spectrograph (dispersion  $1.25\text{\AA}/\text{mm}$ ) Kodak 103-a0 plates are used to record the spectra in the first order of the grating spectrograph giving an exposure of one hour duration.

### RESULTS AND ANALYSIS

Wehrli & Miescher (1934) reported the vibrational analysis of the bands of InBr in the region  $\lambda 3850-3560\text{\AA}$  as belonging to two sub-systems designated as *A* and *B*. The bands of system *A* are observed to be single headed (*P* heads) and attributed to  ${}^3\Pi_0-X{}^2\Sigma^+$  transition while the bands of system *B* were observed to be double headed (*P* and *Q*) and attributed to a  ${}^3\Pi_1-X{}^2\Sigma^+$  transition. When the spectrum was excited in a radio frequency discharge from a 500 watt oscillator it was found that systems *A* and *B* were more extensively developed than in absorption. About 240 bands could be observed in both the systems as against 110 bands observed in absorption. The two systems photographed in the first order of a 21 ft concave grating spectrograph are shown in plate 12, figure 1. It is observed that the higher sequences belonging to both the systems were very well developed in the present emission photographs.

*System A.* The different sequences of system *A* were identified as shown in figure 1. Of these, the bands of sequences  $\Delta v = -3, -4, -5$  and  $-6$  are newly obtained in the present work. In addition some new bands belonging to the other sequences were also observed. As the bands are degraded towards shorter wavelengths the heads are identified as *P* heads. These *P* heads were observed to be double due to the bromine isotope effect. The following vibrational formula was derived for the *P* heads of  $\text{In}^{79}\text{Br}$  molecule

$$\begin{aligned} \nu = 26595.60 + 229.2(v' + 1/2) - 1.42(v' + 1/2)^2 - 223.1(v'' + 1/2) \\ + 0.56(v'' + 1/2)^2 \end{aligned}$$

The vibrational assignments and wavenumbers of the additional bands observed in the present work of this system are shown in table 1a. The agreement between the observed and calculated wavenumbers using the above formula is found to be satisfactory as shown in the last column of table 1a.

*System B.* The different sequences of system *B* were identified as shown in figure 1. Of these, the bands of sequences  $\Delta v = -4, -5$ , are newly obtained in the present work. In addition some more new bands belonging to other sequences

were also observed. The bands of this system which are degraded to shorter wavelengths are observed to be double headed consisting of *P* and *Q* heads. The *P* heads are sharp and line-like while the *Q* heads are broad and diffuse.

Table 1a. The newly observed bands in system *A* of  $\text{In}^{70}\text{Br}$  molecule

Wavenumber $\text{cm}^{-1}$	Intensity	Classification $v', v''$	$\nu_{\text{obs}} - \nu_{\text{cal}}$ $\text{cm}^{-1}$
25321.2	1	5, 11	-0.4
25509.5	1	1, 6	-0.2
25517.4	2	2, 7	-0.6
25523.9	3	3, 8	-0.6
25528.7	3	4, 9	-0.6
25531.9	4	5, 10	-0.5
25726.2	2	1, 5	+0.1
25733.4	3	2, 6	+0.2
25738.3	4	3, 7	-0.3
25741.8	6	4, 8	-0.5
25936.2	4	0, 3	+0.2
25943.8	5	1, 4	+0.2
26727.1	3	13, 12	-2.1
26824.5	9	1, 0; 4, 3	+0.3
26825.9	8	2, 1; 3, 2	-0.3
27044.3	6	4, 2	+0.3
27046.8	6	3, 1	-0.2
27048.0	7	2, 0	-0.3
27187.8	6	11, 8	+0.1

Under the high dispersion used in the present work ( $1.25\text{\AA}/\text{mm}$ ) the bands of  $\Delta v = +1$  and  $+2$  sequences were clearly resolved down to low values of  $v'$  and  $v''$  as shown in figure 2 (plate 13). According to the present vibrational analysis, the vibrational assignments of bands in the  $\Delta v = +1$ ,  $+2$  sequences as reported by Wehrli & Miescher (1934) have to be increased by two units and in  $\Delta v = +3$  sequence by one unit, both in the upper and lower states. The detailed classifications of these bands in the  $\Delta v = +1$  and  $+2$  sequences are shown in Plate 13, figure 2. These vibrational assignments were confirmed by a detailed

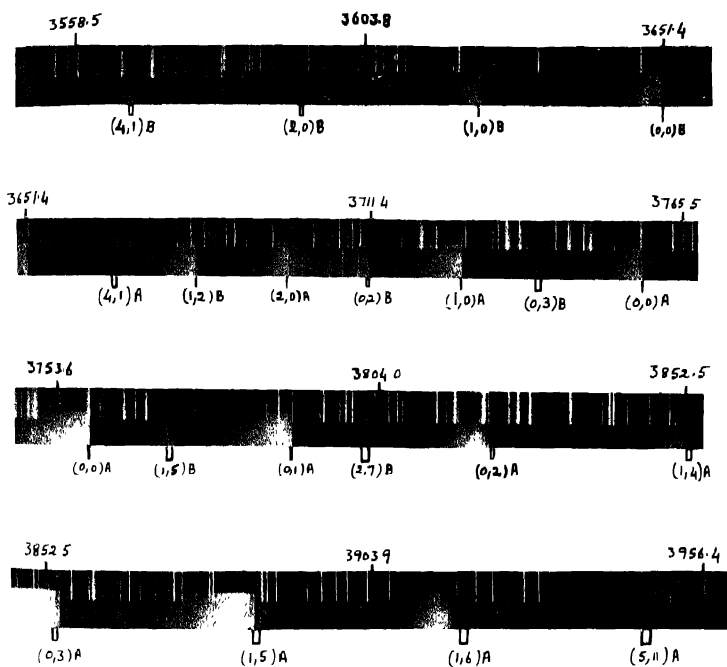


Figure 1. A and B systems of InBr (21 ft concave grating spectrogram)

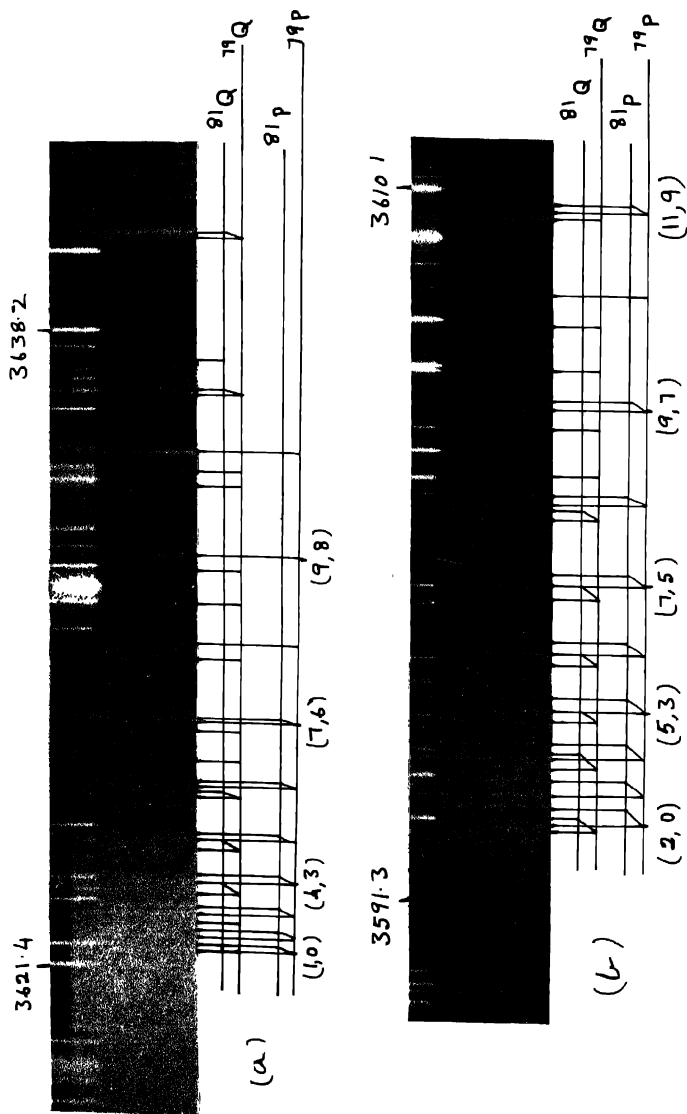


Figure 2. (a). The (1,0) sequence of system B of InBr  
 (b). The (2,0) sequence of system B of InBr

study of the bromine isotopic effect. The following new vibrational quantum formula for the  $P$  heads of  $\text{In } ^{79}\text{Br}$  molecule is derived.

$$\begin{aligned} \nu = & 27379.44 + 225.0(v' + 1/2) - 1.53(v' + 1/2)^2 \\ & - 223.0(v'' + 1/2) + 0.59(v'' + 1/2)^2 \end{aligned}$$

From the present analysis it is observed that  $\omega_e' > \omega_e''$  as in system  $A$  while according to the analysis proposed by Wehrli & Miescher  $\omega_e' < \omega_e''$ . The vibrational frequencies of  $^3\Pi_0$  and  $^3\Pi_1$  levels are close to each other as expected for the components of a  $^3\Pi$  level.

The wavenumbers and their vibrational assignments of  $P$ ,  $Q$  and  $Q'$  heads of the newly observed bands of  $\text{In } ^{79}\text{Br}$  molecule of this system are given in table 1b. A peculiar feature of this system is that in the  $\Delta v = +3$ ,  $+2$  and  $+1$  sequences the bands are degraded towards longer wavelengths while the sequences are degraded to shorter wavelengths. It is observed in some bands with high values of  $v'$  and  $v''$  that the  $Q$  branch tends to form another head which is degraded to longer wavelengths as shown in figure 2. These heads are classified as  $Q'$  heads in table 1b.

As can be seen from the figures 1 and 2, the band heads exhibit well-resolved bromine isotope effect. The observed shifts of the band heads due to the  $\text{In } ^{81}\text{Br}$  molecule from those of the slightly more abundant  $\text{In } ^{79}\text{Br}$  molecule, agree well with those calculated as can be seen from table 2. This isotope study confirms the present changes in the vibrational assignments of some of the bands.

By analogy with similar band systems of the related molecules  $\text{InI}$ ,  $\text{InCl}$  the common lower state of the two sub-systems is identified as ground state  $X^1\Sigma'$  arising from the configuration

$$\dots(z\sigma)^2(y\sigma)^2(w\pi)^4(x\sigma)^2\dots X^1\Sigma'.$$

and the upper  $^3\Pi_{0,1}$  states to the following excited configuration

$$\dots(z\sigma)^2(y\sigma)^2(w\pi)^4(x\sigma) (v\pi) \dots ^3\Pi_r, ^1\Pi.$$

of the  $\text{InBr}$  molecule. Thus the two sub-systems of the  $\text{InBr}$  molecule may be designated as a  $^3\Pi_{0,1} - X^1\Sigma^+$  systems.

Table 1b. The newly observed bands in system *B* of  $\text{In}^{79}\text{Br}$  molecule.

Wavenumber $\text{cm}^{-1}$	Intensity	Classification $v', v''$	Band Head	$\nu_{\text{obs}} - \nu_{\text{cal}}$ $\text{cm}^{-1}$
26292.0	2	2,7	<i>P</i>	-1.1
26505.9	2	1,5	<i>P</i>	+1.1
26723.8	2	2,5	<i>P</i>	+0.1
27532.6	4	9,8	<i>Q'</i>	
27558.4	3	7,6	<i>Q</i>	
27563.5	3	7,6	<i>Q'</i>	
27569.2	5	6,5	<i>P</i>	+0.6
27571.9	3	6,5	<i>Q</i>	
27574.0	2	6,5	<i>Q'</i>	
27581.5	2	5,4	<i>Q</i>	
27588.0	5	4,3	<i>P</i>	+0.3
27590.1	3	4,3	<i>Q</i>	
27594.5	6	3,2	<i>P</i>	+0.1
27596.4	2	3,2	<i>Q</i>	
27599.3	7	2,1	<i>P</i>	+0.1
27602.2	8	1,0	<i>P</i>	0
27749.7	2	9,7	<i>Q'</i>	
27767.9	1	8,6	<i>Q'</i>	
27788.8	3	6,4	<i>Q</i>	
27793.7	1	6,4	<i>Q'</i>	
27797.0	6	5,3	<i>P</i>	+0.5
27800.1	3	5,3	<i>Q</i>	
27809.8	2	4,2	<i>Q</i>	
27814.0	2	3,1	<i>Q</i>	
27815.2	6	3,1	<i>P</i>	+0.2
27821.0	7	2,0	<i>P</i>	0
27822.7	2	2,0	<i>Q</i>	
27954.5	2	9,6	<i>P</i>	+0.2
27975.9	2	8,5	<i>Q</i>	
27993.0	2	7,4	<i>Q</i>	
28007.7	3	6,3	<i>Q</i>	
28019.8	3	5,2	<i>Q</i>	
28028.0	6	4,1	<i>P</i>	+0.2
28030.3	3	4,1	<i>Q</i>	
28036.8	5	3,0	<i>P</i>	0
28039.0	3	3,0	<i>Q</i>	

Table 2. Bromine isotope effect

$v', v''$	Shift (cm <sup>-1</sup> )		$v', v''$	Shift (cm <sup>-1</sup> )	
	Obs.	Cal.		Obs.	Cal.
<i>System A</i>					
5,11	9.4	9.2	4,3	1.6	1.5
1,6	7.5	7.8	3,2	1.5	1.6
2,7	7.4	7.7	2,1	1.5	1.6
3,8	7.1	7.7	1,0	1.6	1.5
4,9	7.3	7.6	12,10	1.7	1.5
5,10	7.5	7.7	11,9	1.7	1.9
1,5	6.2	6.3	10,8	2.1	2.0
2,6	5.6	6.1	9,7	2.4	2.3
4,8	6.3	6.2	8,6	2.4	2.5
0,3	4.8	4.8	7,5	2.6	2.7
1,4	4.8	4.7	6,4	2.9	2.9
2,5	4.8	4.7	5,3	3.1	3.0
3,6	4.5	4.7	4,2	3.5	3.1
0,2	3.3	3.2	3,1	3.2	3.2
1,3	3.2	3.1	2,0	3.2	3.3
2,4	3.0	3.1	11,8	3.2	3.3
3,5	2.9	3.1	10,7	3.5	3.6
4,6	2.9	3.1	9,6	4.2	3.8
0,1	1.6	1.6	8,5	4.3	4.0
1,2	1.6	1.5	7,4	4.3	4.2
2,3	1.7	1.5	6,3	4.5	4.4
8,7	1.1	1.0	5,2	5.0	4.6
7,6	1.5	1.2	4,1	4.7	4.7
6,5	1.5	1.3			
5,4	1.3	1.4			
<i>System B</i>					
2,7	7.1	7.8	8,6	2.1	2.2
1,5	6.8	6.3	7,5	2.4	2.4
1,4	4.9	4.8	6,4	2.7	2.6
2,5	4.7	4.7	5,3	2.9	2.8
0,2	3.4	3.2	4,2	3.2	3.0
1,3	3.3	3.2	3,1	3.1	3.1
7,6	1.3	0.9	2,0	3.3	3.2
6,5	1.2	1.1	9,6	3.8	3.4
5,4	1.2	1.2	8,5	3.3	3.7
4,3	1.6	1.4	7,4	3.7	3.9
3,2	1.3	1.5	6,3	4.3	4.2
2,1	1.6	1.5	5,2	4.5	4.4
1,0	1.6	1.6	4,1	4.6	4.6
9,7	1.6	1.9	3,0	4.8	4.7

## ACKNOWLEDGEMENTS

The authors wish to thank Prof. P. T. Rao for his kind interest in this work. One of the authors (ALN) is grateful to C.S.I.R. for financial support.

## REFERENCES

- Lakshminarayana A. & Haranath P. B. V. 1970a *Curr. Sci.* **39** No 10, 228.  
Lakshminarayana A. & Haranath P. B. V. 1970b *Curr. Sci.* **39**, No 15, 344.  
Petrakou A & Hochberg J. 1933 *Z.P.* **86**, 214.  
Wehrli M & Miescher E 1934 *Helv Phys Acta* **7**, 298.



# Letters to the Editor

*Indian J. Phys.*, **44**, 511-513 (1970).

## Reliability of anode as a reference point of probe potentials in dc gas discharge

By D. R. GUPTA AND G. L. GUPTA

*Department of Physics, University of Jodhpur, Jodhpur*

(Received 17 November 1970)

Langmuir (1923) developed the theory for a plane probe (it can as well be applied to a cylindrical probe) and he used it for the study of the plasma of gas discharge (SPM). When the probe is given sufficiently negative potential the electron current to the probe ( $i_p$ ) under a retarding potential  $V_0$  ( $V - V_s$ ), across the positive ion sheath is given by

$$= i_0 e^{-\frac{-eV_0}{kT_e}} = i_0 e^{-\frac{-e(V - V_s)}{kT_e}} \quad (1)$$

where  $i_0$  is the random plasma electron current to the probe,  $V$  the probe potential,  $V_s$  the plasma potential at the point,  $k$  the Boltzmann's constant,  $e$  the electronic charge and  $T_e$  the electron temperature in degrees absolute. Hence, we have

$$\log_{10} i_p = \text{constant} - \frac{eV}{kT_e} \quad (2)$$

Thus, the semi-logarithmic plot of electron current ( $i_p$ ) vs probe voltage ( $V$ ) is a straight line; the temperature  $T_e$  of the electrons in the plasma may be determined from the slope,  $e/kT_e$  of this line. But in practice the probe voltage is generally referred to one of the electrodes of dc discharge tube (usually the anode which could be called the reference electrode).

The position is entirely different in the case of hf discharges. The electrodes cannot be used as references in view of their alternating potentials. Moreover, external electrodes are used for exciting the discharge. Thus in order to use probe method in hf discharges, it is necessary to introduce an additional electrode, anti-probe ( $A_p$ ) as termed by Beck (1935). Beck and others (1952) have recommended that an anti-probe with large collecting area be used to enable study of broad spectrum of electron velocities.

Johnson & Malter (1950) have described a 'double probe' method (DPM) which is very similar to the use of an extra electrode as the anti-probe for hf discharge. The method has been amply used by Kojima (1953) and others for

the study of hf discharges. From the theory of the double probe method we get,

$$\log_e \left[ \frac{\Sigma I}{i_p} - 1 \right] = -\phi V_d + \log_e \left[ \frac{i_{0A}}{i_{0P}} e^{\phi V_c} \right] \quad \dots (3)$$

putting  $\Gamma = \frac{\Sigma I}{i_p} - 1$  and  $\sigma = \frac{i_{0A}}{i_{0P}} e^{\phi V_c}$

we have,  $\log_{10} \Gamma = -\phi V_d + \log_{10} \sigma$  (4)

where  $\Sigma I$  is the total positive ion current to the probe system,  $\phi$  is  $e/k.T_e$ ,  $V_d$  the differential voltage applied to the system,  $V_c$  the difference in potentials between the plasmas surrounding  $P$  and  $A$ ,  $i_p$  the electron current received by the probe. Thus the plot of  $\log_{10} \Gamma$  against  $V_d$  is a straight line whose slope is  $e/k.T_e$  from which the electron temperature can be determined.

Experiments have been carried by Gupta (1956) in dc plasma of neon gas in the pressure range of  $3.6$  to  $67 \times 10^{-2}$  mm Hg using a tungsten wire probe of length  $3.45$  cm and diameter  $0.22$  mm. Observations are recorded for probe currents ( $i$ ) by varying probe voltage ( $V$ ) for different values of discharge currents and voltages. A sample characteristic is shown in figure 1 for the gas pressure

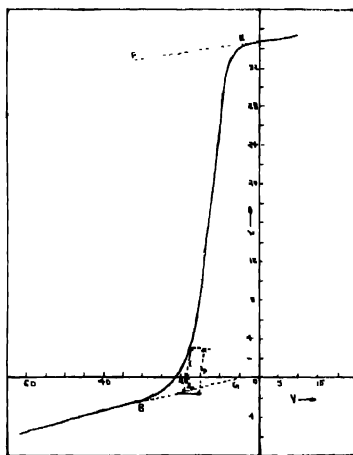


Figure 1. Graph showing probe potential  $V$  vs probe current  $i_p$ .

$0.096$  mm with discharge current of  $50$  mA and voltage  $50$  V. The electron current  $i_p$  to the probe at probe potential  $V$  is determined by adding the value of  $I_p$  (positive ion current to the probe as read from extrapolated line BG) to the actual value of probe current  $i_p$  at the corresponding voltage. Figure 2(a) shows the corresponding

sample plot of  $\log_{10} i_p - V$  curve which is fairly linear but bends near  $-13.5V$  giving the value of the space potential. From the slope of the line the electron temperature  $T_e$  has been calculated and found to be  $45,000^\circ K$ .

Now we apply DPM theory to our system considering the anode as anti-probe of the double probe system. The values of total positive ion current to the probe system,  $\Sigma I$  for different values of probe voltages are found from figure 1 by reading the total current between the extrapolated lines BG and EF, which is actually equal to the sum of  $I_p$  and  $I_A$  positive ion current to the probe and the anode current, respectively. The corresponding values of  $\log_{10}(\Sigma I/i_p - 1)$  are computed and the plot is made for  $\log_{10} T - V$  as shown in figure 2(b) which is mostly linear without any bend in a comparatively wider voltage range in contrast to figure 2(a). The electron temperature  $T_e$  is calculated from the slope of this line and found to be  $42,000^\circ K$ .

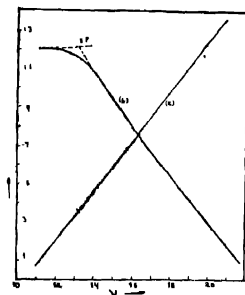


Figure 2. (a) Graph showing probe potential  $V$  vs  $\log_{10} i_p$   
(b) Graph showing probe potential  $V$  vs  $\log_{10} T_e$

The values of electron temperature  $T_e$  found by two different approaches (SPM and DPM theories) of analysis of  $i - V$  curves for dc gas discharge are found to agree well. Hence it can be said that the anode has served as a true reference point in dc discharge and the double probe technique could be used for analysis of dc discharge also. Further this technique enables the use of greater portion of  $i - V$  curve for analysis of electrons of wider velocity range to furnish parameters of dc gas discharge.

## REFERENCES

- Beck 1935 *Zeit. f. Physik*, **79**, 355.  
Gupta G. L. 1956 *Raj. Univ. Phys. Sc. Studies*, I & II, 34 and 51.  
Johnson & Maltor 1950 *Phys. Rev.* **80**, 58  
Kojima, Takayama & Shimauchi 1953 *Phys. Soc. Japan* **8**, 55.  
Langmuir & Mott-Smith 1923 *Gen. Elec. Rev.* **26**, 731.  
Mehra G. K. 1952 *Thesis, Univ. of Bombay*.

## Effect of rubber ingredients on its dielectric properties

By F F HANNA, A. A YEHIA AND A. ABOU-BAKR

National Research Centre, Tahrir Street, Dokki, Cairo. U A.R.

(Received 20 November 1970)

Natural and synthetic rubbers, specially butyl rubber, are widely used in cable industry. It is worthy to study the effect of conventional rubber ingredients added stepwise to raw rubber on the dielectric constant  $\epsilon'$  and dielectric loss  $\epsilon''$ .

Butyl rubber was chosen for this study as it is a non-polar copolymer with low degree of unsaturation (Clark 1962). Thus, it is heat, ozone and weather resisting rubber and has excellent insulating properties. Moreover, raw butyl rubber can be shaped easily into air-bubble-free discs needed for the measurements.

Five rubber formulations were prepared as shown in table 1, for this study.  $\epsilon'$  and  $\epsilon''$  were measured at frequencies between 60Hz/s and 10<sup>2</sup>Hz/s in the same way described before (Hanna & Ghoneim 1970). The results obtained are illustrated in figure 1. These results show that the addition of sulphur and accelerators MBT+TMTD (formula 2) decrease  $\epsilon'$  slightly in the whole frequency region, which may be due to the cross linking by the curing system used. Also  $\epsilon''$  is much increased in the low frequency region and then decreased a little in the high frequency region (curve 2). The increase at low frequency region may be due to the interfacial polarization (Smyth 1955) arising from the existence of more than one phase. The addition of stearic acid (formula 3) increases  $\epsilon'$  to some extent specially in the low frequency region, while  $\epsilon''$  is very much increased in the whole frequency regions (curve 3). This behaviour may

TABLE I

Formula no	1	2	3	4	5
Ingredients					
Butyl rubber	100	100	100	100	100
Sulphur	—	1.5	1.5	1.5	1.5
TMTD	—	1	1	1	1
MBT	—	0.5	0.5	0.5	0.5
Stearic acid	—	—	3	3	—
Zinc oxide	—	—	—	5	5

be attributed to the polarity of the carboxylic group in stearic acid. The addition of zinc oxide (formula 4) changes markedly the dielectric properties (curve 4). It is found that  $\epsilon'$  is decreased to about the same value as samples 1 and 2.  $\epsilon''$  is also decreased to a value somewhat higher in the low frequency region but is lower in the high frequency region than that of raw rubber. This may be explained as due to the formation of zinc salt which is less polar than stearic acid itself. The addition of zinc oxide in the absence of stearic acid (formula 5) shows dielectric loss not much different from formula 4 in the low frequency region but are somewhat higher in the high frequency region, while  $\epsilon'$  remains the same as formula 1. This may assist the suggestion that the polarity of the carboxylic group in stearic acid is the cause of the large increase in  $\epsilon''$ .

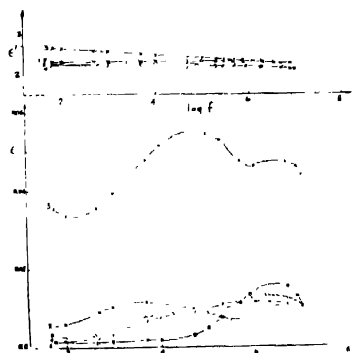


Figure 1. Dielectric constant  $\epsilon'$  and dielectric loss  $\epsilon''$  for the 5 samples given in table 1.

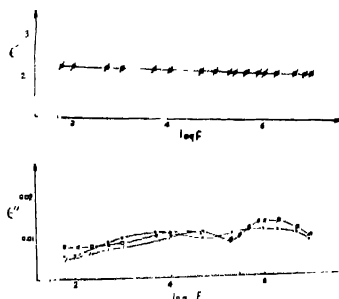


Fig. 2.  $\epsilon'$  and  $\epsilon''$  for sample 2 using different cure time (—○— 10 min, —●— 15 min, —/— 24 min)

The rubber vulcanizate obtained by formula 4 has good physico-mechanical properties, e.g. samples vulcanized at 160°C for 10 minutes give tensile strength 106 kg/cm<sup>2</sup>, elongation 730%, modulus 300% elongation 9kg/cm<sup>2</sup> and permanent set 5%.

The effect of cure time on  $\epsilon'$  and  $\epsilon''$  was also studied. Three cure times were used namely 10, 15 and 25 minutes. As shown in figure 2,  $\epsilon'$  does not change with the cure time, while  $\epsilon''$  is changes slightly. Since the cure time affects mainly the physico-mechanical properties of vulcanizates, it is recommended to use the cure time which gives optimum physico-mechanical properties, as its effect on the dielectric properties is negligible.

This study leads to the conclusion that the ingredients which are normally added to improve the physical properties of raw rubber, specially in the described proportions, do not practically change the dielectric properties

We should like to thank Prof Dr. R. N. Sedra, Cairo University, for his kind interest in this work. The facilities offered to us by the Transport and Engineering Co. in preparing these samples are very much appreciated.

#### REFERENCES

- Clark F. M. 1962 *Insulating Materials for Design and Engineering* New York, 923  
 Hanna F. F. & Ghoneim A. M. 1970 *Z. Phys. Chem.* (In the press).  
 Smyth C. P. 1955 *Dielectric Behaviour and Structure* New York 188.

*Indian J. Phys.* **44**, 516-518, (1970)

### Comparison of experimental and theoretical pair cross-sections near the threshold

By J. RAMA RAO, M. SRIRAMACHANDRA MURTY AND K. PARTHASARADHI

*The Laboratories for Nuclear Research, Andhra University,*

*Waltair, India*

(Received 4 December 1970)

It is well known that the experimental pair cross-sections of gamma rays very near the threshold are not in agreement with the predicted values from Bethe-Heitler theory (1934) or with the extrapolated values from Jaeger & Hulme (1936) calculations. Recently, however, more accurate theoretical pair cross-sections are reported by Overbo *et al* (1968) claiming a better agreement with the experimental values near the threshold. In the present communication a comparison is made of experimental cross-sections at 1.119 MeV reported by

Rama Rao *et al* (1963) with Overbo's (1968) theory. In addition, the pair cross-sections in germanium recently reported by Yamazaki *et al* (1965) are compared with Overbo's theory with a view to test its validity near the threshold.

Rama Rao *et al* (1963) measured the pair cross-sections absolutely at the energy 1.119 MeV in eight elements from copper to lead, using a coincidence method. Yamazaki *et al* (1965) determined the pair cross-sections in germanium in the energy range 1.007 to 2.754 MeV by using a Ge(Li) crystal both as the target as well as detector. These latter cross-sections were measured relatively and then normalized to the Jaeger & Hulmes' (1936) value at 2.754 MeV which is 4% higher than the Bethe-Heitler (1934) value. It must be noted that this method implies the agreement between the experimental value and the theoretical value of Jaeger & Hulme at 2.754 MeV in germanium. The experimental values of Yamazaki *et al* and those of Rama Rao *et al* along with the theoretical values of Overbo *et al* are given in tables 1 and 2.

It can be seen from the table 1 that the agreement between theory and experiment is satisfactory from 2.754 MeV down to 1.5 MeV. Below this energy there is deviation. The deviation cannot, however, be ascribed to an error arising from normalization procedure since the discrepancy increases with atomic number. It may also be noted that the theoretical values are always smaller than the experimental values wherever there is a discrepancy. The inclusion of screening correction, neglected in the theory of Overbo *et al*, would however, still decrease the theoretical cross-section. The trend of deviation, increasing with atomic number toward the pair threshold, suggests that adequate refinements are necessary in the theory of Overbo *et al* in these directions.

TABLE 1 Experimental pair cross-sections in germanium (millibarns per atom)

Energy (MeV)	Experimental Value	Theoretical Value (Overbo <i>et al</i> 1968)
1.007	$0.342 \pm 0.029$	0.266
1.115	$1.38 \pm 0.10$	1.14
1.173	$4.66 \pm 0.17$	3.85
1.278	$15.6 \pm 0.5$	13.5
1.332	$24.8 \pm 0.8$	21.0
1.368	$30.7 \pm 1.0$	26.6
1.407	$37.7 \pm 2.1$	33.1
1.477	$55.7 \pm 2.5$	47.3
1.596	$78.3 \pm 4.2$	75.0
1.837	$153 \pm 7$	145.0
2.185	$263 \pm 10$	246.0
2.318	$284 \pm 8$	282.0
2.754	$451 \pm 14$	447.0

TABLE 2. Pair cross-sections of 1.119 MeV gamma rays  
(millibarns per atom)

Element	Experimental Value	Theoretical Value (Overbo <i>et al</i> 1968)
Cu	1.42 $\pm$ 0.09	1.02
Zr	2.95 $\pm$ 0.18	2.16
Rh	3.90 $\pm$ 0.23	2.79
Sn	5.00 $\pm$ 0.3	3.43
Ta	11.40 $\pm$ 0.6	6.3
Pt	13.20 $\pm$ 0.7	6.92
Au	13.40 $\pm$ 0.7	7.0
Pb	14.80 $\pm$ 0.7	7.24

## ACKNOWLEDGEMENTS

One of the authors (M.S.R.) is grateful to the C.S.I.R. Government of India, for the award of a Government Research Fellowship.

## REFERENCES

- Bethe H. A. & Hottler W. 1934 *Proc. Roy. Soc.* **A146**, 83.  
 Jaeger J. C. & Hulme, H. R. 1936 *Proc. Roy. Soc.* **A153**, 443.  
 Overbo I., Mork K. J. & Olsen H. A. 1968 *Phys. Rev.* **175**, 1978.  
 Rama Rao J. Lakshminarayana V. & Swami Jnanananda 1963 *Proc. Phys. Soc.* **A81**, 949.  
 Yamazaki T. & Hollander J. M. 1965 *Phys. Rev.* **140B**, 630.

*Indian J. Phys.* **44**, 518-519 (1970).

# Some comments on exact partition function of Ising model in Magnetism in one, two and three dimensions in non-zero field

By V. P. DESAI

*Saha Institute of Nuclear Physics, Calcutta-9*

(Received 6 September 1971)

In a recent paper on Ising model, Das (1970) comes to the surprising conclusion that Onsager's (1944) and Yang's (1952) results of two dimensional Ising model are not reliable! A closer look at the paper reveals that Das's approach to the problem is basically erroneous. The basic fallacy in



his approach is that he considers *finite crystals*. The partition function for a finite crystal is an *analytic function* of temperature and as such its derivatives will not show discontinuity (Onsager 1944, Wannier 1959). Hence the author does not find any phase transition in two or three dimensional finite crystals. Mere imposition of periodic boundary conditions will not ensure that the crystal is infinite. Periodic boundary conditions only eliminate the surface effects. The correct way to calculate exactly the partition function would be to write down the partition function and then let the number of atoms, number of rows of atoms or number of layers of atoms (depending on whether one is interested in one, two or three dimensions) go to infinity, after which only, one should try to derive the thermodynamic properties from the partition function. This limiting process is very complicated which requires special mathematical methods such as the matrix method or the combinatorial methods in the case of two and three dimensional crystals. The author is wrong in assuming that one can obtain the behaviour of one or two dimensional crystals from that of three dimensional crystals, because the three dimensional problem is the most complicated one and, therefore, as yet unsolved. There is absolutely no ground to believe that the behaviour of one, two and three dimensional crystals are similar.

## REFERENCES

- Das D. D., 1970 *Ind. J. Phys.* **44**, 144  
Onsager L. 1944 *Phys. Rev.* **65**, 117.  
Wannier G. H. 1959 *Elements of Solid State Theory*, Cambridge University Press.  
Yang C. N. 1952 *Phys. Rev.* **85**, 808.

## BOOK REVIEW

### *Advances in plasma physics, Vol. 3*

Edited by A. Simon and W. B. Thompson,  
*Interscience Publishers, 1969, pp. 249. \$ 14.95*

The present volume is the third in a series which aims at providing review articles on advances in the several branches of plasma physics and forming, in this way, a channel of communication among plasma physicists in various disciplines.

This volume consists of the following three articles.

- 1 Kinetic Theory of Plasma Waves in a Magnetic Field—by David E. Baldwin, Ira B. Bernstein and M. P. H. Weenink.
- 2 Electron Distribution Functions in Weakly Ionized Plasmas—by Ira B. Bernstein
3. Classical Plasma Phenomena from a Quantum Mechanical Viewpoint—by E. G. Harris.

The leading article summarizes the important techniques and results relating to the kinetic theory of wave phenomena in a magnetized plasma. It deals first with small-amplitude waves in an infinite homogeneous plasma and considers a few limiting cases, such as the limit of low temperature and small magnetic field propagation parallel and perpendicular to the magnetic field, etc., the treatment being marked by some interesting mathematical approaches. The effects of boundaries and density gradients are gradually introduced; in this connection the problem of resonances in plasma columns is well discussed and the method of geometric optics is developed to give the synchrotron radiation from a hot magnetoplasma. A helpful feature of the article is the presentation of concise bibliographic notes at the end of each section.

The second article is a comparatively short one, presenting a new approach to an old problem. The electron-neutral collision term is expanded in powers effectively of  $m/m'$ , the ratio of the electron to neutral mass, and the result is used to give a perturbation solution of the electron Boltzmann equation, which permits derivation of the usual transport coefficients. The treatment is particularly suitable for dealing with boundary conditions. The full Boltzmann equation, encompassing the effect of inelastic processes and charged particle encounters, is briefly discussed.

The third and last article is perhaps the most interesting one in the volume. The dielectric tensor of plasma is derived quantum mechanically, and the linear theory of wave propagation in plasma is discussed. This is followed by the quantization of the electromagnetic field in a dispersive medium. Waves in a plasma are considered as consisting of quasiparticles (plasmas, phonons, photons, etc.) interacting with the particles of the plasma and with each other. Nonlinear effects in plasma, particularly of small magnitude, are thoroughly discussed in this light. It is worth noting that the quantum mechanical calculations are, in some cases, more straightforward and less difficult than the corresponding classical calculations.

Although the contents of the present volume in the review series are undoubtedly theoretical in nature, the articles would have been more comprehensive and the purpose of the series served better if surveys of the experimental work, wherever pertinent, were included. However, the articles contain authoritative discussions on basic phenomena of plasma physics and the volume can, therefore, be recommended to all concerned with the subject.

J. B.

# INDIAN JOURNAL OF PHYSICS

VOL. 44

No. 10

AND

VOL. 53

PROCEEDINGS

No. 10

OF THE

INDIAN ASSOCIATION FOR THE CULTIVATION OF SCIENCE

*(Edited in collaboration with the Indian Physical Society).*

IJPYAS 44 (10) 521-568 (1970)

OCTOBER 1970

PUBLISHED BY THE  
INDIAN ASSOCIATION FOR THE CULTIVATION OF SCIENCE  
JADAVPUR, CALCUTTA-32



## Potential function for diatomic molecules

By S. M. MIRAJKAR

Science College, Satara

(Received 15 July 1970—revised 11 September 1970)

A new potential function for diatomic molecules is suggested and its Schrodinger equation has been solved by the method of Pekeris (1934). Values of anharmonicity and rotation-vibration coupling constants have been calculated by the method suggested by Varshni (1957). The results have been compared with experimental values and also with those calculated by different authors.

### INTRODUCTION

Potential energy function for diatomic molecules is given by comparison with experimental data. Comparative study of various potential functions was made by Varshni (1957), Manning (1935), Steele *et al* (1962) and Levine (1966). Considering some applications of the potential functions, the solution of corresponding Schrodinger equation and determination of the wave functions becomes necessary. The solution of Schrodinger equation has been possible in a few cases (Kratzer 1920, Morse 1929, Manning 1935, Eisenhart 1948, Tietz 1963, Wojtczak 1965). In some cases the solution is very complex.

As suggested by Landau (1959) the potential function can be obtained by the combination of centrifugal energy and electrical interaction energy of the nuclei screened by electrons. Based on this suggestion of Landau, Wojtczak (1965) proposed that the potential energy function should reach asymptotically to a finite value for  $x \rightarrow \infty$ , and to  $\infty$  as  $x \rightarrow 0$ . He therefore suggested the following form for P.E. function :

$$V(x) + D_e \left( \frac{T}{x^2} + \frac{Zf(x)}{x} + 1 \right)$$

where  $T$  and  $Z$  are arbitrary constants,  $f(x)$  is screening function, variable  $x = r/r_e$  and  $V(x)$  is some function of  $x$ . The P.E. function should also satisfy Varshni conditions.

The function having a simpler solution and comparable results of  $\omega_e$ ,  $\omega_e x_e$  and  $\alpha_e$ , are described here. The new function has been arrived at by giving simple values for screening function  $f(x)$  and the function  $V(x)$ . This has been done by semiempirical logic and the following form for P.E. function has been arrived at :

$$V = D_e + \frac{A}{r} + \frac{Ar_e}{r^2} - \frac{3A}{\alpha r_e^2} e^{-\alpha(r-r_e)} \quad \dots \quad (a)$$

where  $D_e$  is dissociation energy,  $A$  is a constant determined to satisfy Varshni condition,  $r_e$  is equilibrium separation between nuclei, and  $\alpha$  is a parameter the value of which determines the percentage accuracy of the results of  $\omega_e x_e$  and  $\alpha_e$ . The present discussion is divided into two parts. In the first, it is assumed that  $\alpha r_e = 3/2$  and then in the second part a generalization like  $\alpha r_e = \delta$  has been attempted. The Schrödinger equations for both first and second general part have been solved. From the general solution, it appears that  $\omega_e$  is the same for all values of  $\delta$  but  $\omega_e x_e$  and  $\alpha_e$  depend on  $\delta$ . Results of  $\omega_e x_e$  have been obtained and tabulated for values of  $\delta$  ranging from  $\delta = 1.5$  to  $\delta = 2$  (table 4). The percentage errors in  $\omega_e x_e$  for ZnH and HCl have been calculated at various  $\delta$ 's (table 5). It indicates that percentage error in the value of  $\omega_e x_e$  depends on  $\delta$  and for a group of molecules there exists a particular value of  $\delta$  at which there is near coincidence between experimental and calculated values of  $\omega_e x_e$ . It appears that  $\delta$  which produces near coincidence may be a function of atomic numbers of nuclei and the quantum numbers of the electrons in outermost shells.

Out of the two methods to test the validity of function, *viz.* (1) Matching of values of  $\omega_e$ ,  $\omega_e x_e$  and  $\alpha_e$  with the experimental values, (2) Percentage deviation of suggested potential from R.K.R. potential, (Steele *et al*) the first method is used to check the validity of suggested function.

Our function satisfies the following Varshni conditions

$$(dV/dr)_{r=r_e} = 0 \quad \dots (1)$$

$$(V)_{r=0} = \infty \quad \dots (2)$$

$$(V)_{r=\infty} \equiv 0 \quad \dots (3)$$

$$\left( \frac{d^2 V}{dr^2} \right)_{(r=r_e)} = k_e \quad \dots (4)$$

### Part I

It is assumed here that  $\alpha r_e = 3/2$ .

$$\text{From (4)} \quad A = \frac{2}{7} k_e r_e^3 \quad \dots (5)$$

According to Varshni (1957), vibration-rotation coupling constant is given by

$$\alpha_e = - \left( \frac{x r_e}{3} + 1 \right) \frac{6 B_e^2}{\omega_e} \quad \dots (6)$$

$$\text{and} \quad \omega_e x_e = \left( \frac{5}{3} X^2 - Y \right) \frac{2.1078.10^{-16}}{\mu_A} \quad \dots (7)$$

From (a) 
$$X = \left( \frac{V'''}{V''} \right)_{r=r_e} = -\frac{93}{14} \frac{1}{r_e}$$

$$Y = \left( \frac{V'''}{V''} \right)_{r=r_e} = \frac{1071}{28r_e^2}$$

Substituting these values

$$\omega_e x_e = \frac{74.47}{\mu_A r_e^2} 10^{-16} \quad \dots (8)$$

and 
$$\alpha_e = 7.285 B_e^2 \quad \dots (9)$$

Values calculated from (8) and (9) are compared with other values given in tables 1 and 2

TABLE 1

Diatom	$\omega_e x_e$ (calculated)	$\omega_e x_e$ (experimental)	$\omega_e x_e$ (Morse)
H <sub>2</sub>	268.6	117.99	179.00
ZnH	29.52	55.14	4.72
CdH	24.01	46.3	5.16
HgH	24.53	83.01	3.31
CH	63.84	64.3	72.55
OH	83.30	82.81	96.12
HF	92.51	90.06	122.305
HCl	46.76	52.05	56.27
HBr	37.42	45.21	42.14
HI	28.95	39.73	40.50
Li <sub>2</sub>	2.973	2.59	1.425
Na <sub>2</sub>	0.6837	0.726	0.092
K <sub>2</sub>	0.2481	0.35	0.00389
N <sub>2</sub>	8.884	14.456	14.756
P <sub>2</sub>	1.341	2.8	1.895
O <sub>2</sub>	6.393	12.073	11.263
SO	3.133	6.116	4.325
Cl <sub>2</sub>	1.077	4.00	2.8
Br <sub>2</sub>	0.3569	1.146	0.1927
I <sub>2</sub>	0.1650	0.6127	0.3159
ICl	0.5041	1.465	1.054
CO	8.539	13.46	14.97
NO	7.526	13.97	12.79

SOLUTION OF SCHRÖDINGER EQUATION [WHEN  $\alpha r_e = 3/2$ ]

Morse (1929) solved wave equation for nuclear motion. This wave equation was originally suggested by Born and Oppenheimer (1927). By separating  $r, \theta$  and  $\phi$  dependent parts, Morse obtained the following equation for radial function  $R(r)$ .

$$\frac{d^2 R}{dr^2} - \frac{J(J+1)}{r^2} R + \frac{8\pi^2 \mu}{h^2} [W - E(r)] R = 0$$

TABLE 2

Diatom	$\alpha_e$ experimental	
H <sub>2</sub>	2 993	6.13
ZnH	0.25	0.2022
CdH	0.21	0.1505
HgH	0 312	0.1617
CH	0 534	0.5322
OH	0.714	0 6901
HF	0.7705	0.7716
HCl	0 3019	0.2732
HBr	0 226	0.1974
HI	0 183	0.1354
Li <sub>2</sub>	0.00704	0 009385
Na <sub>2</sub>	0 00079	0.001095
K <sub>2</sub>	0 000219	0.0002483
N <sub>2</sub>	0.0187	0 01247
P <sub>2</sub>	0 00142	0.0008584
O <sub>2</sub>	0.015	0.009640
SO	0.00562	0.003250
Cl <sub>2</sub>	0 0017	0.0007663
Br <sub>2</sub>	0.000275	0 0001475
I <sub>2</sub>	0.000117	0.00004749
ICl	0.00053	0 0002474
CO	0 01748	0 001251
NO	0.0178	0 01111

Changing the notation,  $R = S$ ,  $E(r) = V$  and  $W = E$ , the equation for radial function becomes

$$\frac{d^2 S}{dr^2} - \frac{J(J+1)}{r^2} S + \frac{8\pi^2 \mu}{h^2} [E - V] S = 0$$



When the value of  $V$  from equation (a) is put in the above, the following equation is obtained.

$$\frac{d^2S}{dr^2} - \frac{J(J+1)}{r^2} S + \frac{8\pi^2\mu}{h^2} \left( E - D_e - \frac{A}{r} - \frac{Ar_e}{r^2} + \frac{3A}{\alpha r_e^2} e^{-\alpha(r-r_e)} \right) S = 0$$

$$\text{Let } B = \frac{h^2 J(J+1)}{8\pi^2 \mu r_e^2}, \text{ and } y = e^{-\alpha(r-r_e)}$$

$$\therefore \frac{r_e}{r} \approx 1 + \frac{1}{\alpha r_e} \left[ (y-1) - \frac{(y-1)^2}{2} \right] + \frac{1}{\alpha^2 r_e^2} (y-1)^2$$

$$\therefore \left( \frac{r_e}{r} \right)^2 \approx 1 + \frac{2}{\alpha r_e} \left[ (y-1) - \frac{(y-1)^2}{2} \right] + \frac{3}{\alpha^2 r_e^2} (y-1)^2$$

$$\therefore y^2 \frac{d^2S}{dy^2} + y \frac{dS}{dy} + \frac{8\pi^2\mu}{\alpha^2 h^2} [C_0 + C_1 y + C_2 y^2] S = 0 \quad (10)$$

where

$$C_0 = E - D_e - \frac{A}{r_e} \left( 1 - \frac{3}{2\alpha r_e} + \frac{1}{\alpha^2 r_e^2} \right) - \frac{A}{r_e} \left( 1 - \frac{3}{\alpha r_e} + \frac{3}{\alpha^2 r_e^2} \right) - B \left( 1 - \frac{3}{\alpha r_e} + \frac{3}{\alpha^2 r_e^2} \right) \quad (11)$$

when

$$\alpha r_e = 3/2, \quad C_0 = E - D_e - \frac{7}{9} \frac{A}{r_e} - \frac{B}{3}$$

Similarly

$$C_1 = -\frac{A}{r_e} \left( \frac{2}{\alpha r_e} - \frac{2}{\alpha^2 r_e^2} \right) - \frac{A}{r_e} \left( \frac{4}{\alpha r_e} - \frac{6}{\alpha^2 r_e^2} \right) + \frac{3A}{\alpha r_e^2} - B \left( \frac{4}{\alpha r_e} - \frac{6}{\alpha^2 r_e^2} \right), \quad (12)$$

For

$$\alpha r_e = 3/2, \quad C_1 = \frac{14A}{9r_e};$$

$$C_2 = -\frac{A}{r_e} \left( -\frac{1}{2\alpha r_e} + \frac{1}{\alpha^2 r_e^2} \right) - \frac{A}{r_e} \left( -\frac{1}{\alpha r_e} + \frac{3}{\alpha^2 r_e^2} \right) - B \left( -\frac{1}{\alpha r_e} + \frac{3}{\alpha^2 r_e^2} \right). \quad \dots \quad (13)$$

For

$$\alpha r_e = 3/2, \quad C_2 = -\frac{7A}{9r_e} - \frac{2}{3} B.$$

When the following substitutions are made in (10), equation (14) is obtained.

$$S = e^{-z/2} \cdot z^{b/2} u \quad \text{where} \quad z = 2dy$$

$$d^2 = -\frac{8\pi^2 \mu C_2}{\alpha^2 \hbar^2}$$

$$b^2 = -\frac{32\pi^2 \mu}{\alpha^2 \hbar^2} C_0$$

$$K = \frac{8\pi^2 \mu}{\alpha^2 \hbar^2} \frac{C_1}{2d} = -\frac{b+1}{2}$$

$$\therefore \frac{d^2 u}{dz^2} + \frac{du}{dz} \left( \frac{b+1}{z} - 1 \right) + \frac{k}{z} u = 0. \quad \dots (14)$$

Put

$$u = \Sigma a_n z^n \text{ in (14).}$$

This gives

$$a_{n+1} = a_n \frac{n-K}{n(n+1) + (b+1)(n+1)}$$

The series should be finite and terminate at  $n$ -th term.

$$\therefore n = K$$

$$\therefore \frac{8\pi^2 \mu}{\alpha^2 \hbar^2} \frac{C_1}{2d} - \frac{b+1}{2} = n$$

$$\therefore C_0 = \frac{C_1}{d} (n+1/2) - \frac{\alpha^2 \hbar^2}{8\pi^2 \mu} (n+1/2)^2 - \frac{8\pi^2 \mu}{\alpha^2 \hbar^2} (C_1/2d)^2 \quad \dots (15)$$

When the value of  $C_0$  is introduced in the above, the value of  $E$  is given in the following form .

$$E = \left( \frac{14}{9} \frac{A}{r_e} \right) \frac{1}{d} (n+1/2) - \frac{\alpha^2 \hbar^2}{8\pi^2 \mu} (n+1/2)^2 + \frac{1}{3} \frac{\hbar^2 J(J+1)}{8\pi^2 \mu r_e^2} + D_e + \frac{7}{9} \frac{A}{r_e} - \frac{8\pi^2 \mu}{\alpha^2 \hbar^2} \frac{1}{4d^2} \left( \frac{14}{9} \frac{A}{r_e} \right)^2.$$

Substituting  $d$  and expanding the first and last terms

$$\begin{aligned} \frac{E}{ch} &= \frac{\alpha}{\pi c} \sqrt{\frac{7A}{18\mu r_e}} (n+1/2) - \frac{3\alpha \hbar^2 r_e}{56\pi^2 \mu r_e^2 A c} \sqrt{\frac{7A}{18\mu r_e}} J(J+1)(n+1/2) \\ &\quad - \frac{\alpha^2 \hbar}{8\pi^2 \mu c} (n+1/2)^2 + \frac{\hbar J(J+1)}{8\pi^2 \mu r_e^2 c} + \frac{D_e}{ch} \end{aligned}$$

Introduce value of  $A$  from (5) in the coefficient of  $(n+1/2)$  in the first term which represents  $\omega_e$  of diatomic molecule so that,

$$\frac{\alpha}{\pi c} \sqrt{\frac{7A}{18\mu r_e}} = \omega_e = \frac{1}{2\pi c} \sqrt{\frac{k_e}{\mu}}.$$

Above formula of  $\omega_e$  is the same as that obtained by other considerations. Values calculated from this are compared with experimental ones and given in table 3

TABLE 3

Diatom	$\omega_e$ calculated	$\omega_e$ experimental
H <sub>2</sub>	4390	4395
ZnH	1603	1607.6
CdH	1429	1430
HgH	1387	1387.1
CH	2859	2861
OH	3732	3735
HF	4134	4138.5
HCl	2986	2989.7
HBr	2647	2649.7
HI	2308	2309.5
Li <sub>2</sub>	351.1	351.43
Na <sub>2</sub>	159.1	159.23
K <sub>2</sub>	92.53	92.64
N <sub>2</sub>	2357	2359.6
P <sub>2</sub>	779.8	780.43
O <sub>2</sub>	1579	1580.4
SO	1123	1123.7
Cl <sub>2</sub>	563.5	564.9
Br <sub>2</sub>	546.4	546.2
I <sub>2</sub>	214.4	214.6
ICl	119.1	119.18
CO	2168	2170.2
NO	1902	1904

## Part 11

*Generalisation of  $\alpha$* 

It is assumed here that in general  $\alpha r_e = \delta$ .

From (a), (6) and (7)

$$x = \frac{3}{r_e} \left( \frac{-10 + \delta^2}{8 - 3\delta} \right) \quad \dots \quad (16)$$

$$y = \frac{1}{r_e^2} \frac{144 - 3\delta^3}{8 - 3\delta} \quad \dots \quad (17)$$

$$\omega_e x_e = \left[ \frac{5}{3} x^2 - y \right] \frac{2.1078 \cdot 10^{-16}}{\mu_A}$$

From (16) and (17)  $\omega_e x_e$  assumes following form

$$\omega_e x_e = \left[ \frac{348 + 432\delta - 300\delta^2 + 24\delta^3 + 6\delta^4}{(8 - 3\delta)^2} \right] \frac{2.1078}{\mu_A r_e^2} 10^{-16} \quad \dots \quad (18)$$

The value of  $\omega_e x_e$  changes with  $\delta$  in the manner shown in the following table 3A.

TABLE 3A

$\delta$	$\omega_e x_e \times \mu_A r_e^2 \times 10^{16}$
1.5	74.47
1.6	83.97
1.7	96.12
1.8	111.1
1.85	120.3
1.9	131.0
2	158.1

TABLE 4. Variation of  $\omega_e x_e$  with  $\delta$ 

$\delta =$	1.5	1.6	1.7	1.8	1.85	1.9	2	
Mol.	$\omega_e x_e$ calc.	$\omega_e x_e$ calc.	$\omega_e x_e$ calc.	$\omega_e x_e$ calc.	$\omega_e x_e$ calc.	$\omega_e x_e$ calc.	$\omega_e x_e$ calc.	$\omega_e x_e$ exptl.
H <sub>2</sub>	268.6	302.8	346.6	400.7	433.8	472.6	570.2	117.97
ZnH	29.52	33.29	38.11	44.06	47.68	51.95	62.69	55.14
CdH	24.01	27.07	30.98	35.82	38.77	42.24	50.95	46.3
HgH	24.53	27.67	31.66	36.61	39.63	43.17	52.08	53.01
CH	63.84	71.97	82.39	95.26	103.1	112.3	135.5	64.3
OH	83.30	93.91	107.5	124.3	134.5	146.6	176.8	82.81
HF	92.51	104.3	119.4	138	149.4	162.8	196.3	90.06
HCl	46.76	52.71	60.34	69.76	75.51	82.26	99.24	52.05
HBr	37.42	42.19	48.29	55.84	60.43	65.85	79.43	45.21
HI	28.95	32.63	37.36	43.19	46.76	50.93	61.41	39.73
Li <sub>2</sub>	2.973	3.352	3.837	4.436	4.801	5.231	6.311	2.59
Na <sub>2</sub>	0.6837	0.7709	0.8824	1.021	1.104	1.203	1.452	0.726
K <sub>2</sub>	0.2481	0.2799	0.3203	0.3703	0.4099	0.4367	0.5209	0.35
N <sub>2</sub>	8.884	10.02	11.47	13.25	14.35	15.63	18.66	14.456
P <sub>2</sub>	1.341	1.511	1.726	2.00	2.165	2.358	2.845	2.8
O <sub>2</sub>	6.393	7.207	8.250	9.539	10.32	11.25	13.57	12.072
SO	3.133	3.533	4.043	4.676	5.060	5.513	6.651	6.116
Cl <sub>2</sub>	1.077	1.214	1.390	1.607	1.740	1.895	2.287	4.00
Br <sub>2</sub>	0.3569	0.4024	0.4606	0.5325	0.5763	0.6279	0.7675	1.146
I <sub>2</sub>	0.1650	0.1860	0.2129	0.2461	0.2665	0.2902	0.3501	0.6127
ICI	0.5041	0.5683	0.6506	0.7521	0.8141	0.8869	1.070	1.465
CO	8.539	9.627	11.03	12.75	13.81	15.03	18.12	13.46
NO	7.526	8.486	9.714	11.23	12.15	13.24	15.98	13.97

General Solution of Schrödinger equation when  $\alpha r_e = \delta$ 

From (10)

$$y^2 \frac{d^2 S}{dy^2} + y \frac{dS}{dy} + \frac{8\pi^2 \mu}{\alpha^2 \hbar^2} [C_0 + C_1 y + C_2 y^2] S = 0$$

The values of  $C_0$ ,  $C_1$ ,  $C_2$  in the present case ( $\alpha r_e = \delta$ ), can be obtained from (11), (12) and (13).

$$C_0 = E - D_e - \frac{A}{r_e} \left( 2 - \frac{9}{2\delta} + \frac{4}{\delta^2} \right) - B \left( 1 - \frac{3}{\delta} + \frac{3}{\delta^2} \right) \quad \dots (19)$$

$$C_1 = -\frac{A}{r_e} \left( \frac{3}{\delta} - \frac{8}{\delta^2} \right) - B \left( \frac{4}{\delta} - \frac{6}{\delta^2} \right) \quad \dots \quad (20)$$

$$C_2 = -\frac{A}{r_e} \left( -\frac{3}{2\delta} + \frac{4}{\delta^2} \right) - B \left( -\frac{1}{\delta} + \frac{3}{\delta^2} \right) \quad \dots \quad (21)$$

Introduction of  $C_0$ ,  $C_1$ ,  $C_2$  and  $d$  in (15) and corresponding expansion gives

$$\begin{aligned} \frac{E}{Ch} = & \frac{\alpha}{\pi C} \left[ \frac{A}{2\mu r_e} \left( \frac{-3}{2\delta} + \frac{4}{\delta^2} \right) \right]^{\frac{1}{2}} (n+1/2) \\ & + \frac{h^2}{8\pi^2 \mu r_e^2} \frac{\alpha}{\pi C} \left[ \frac{A}{2\mu r_e} \left( \frac{-3}{2\delta} + \frac{4}{\delta^2} \right) \right] \frac{\left( \frac{3}{\delta} - \frac{3}{\delta^2} \right)}{\frac{A}{r_e} \left( \frac{3}{\delta} - \frac{8}{\delta^2} \right)} (n+1/2) J(J+1) \\ & - \frac{\alpha^2 h}{8\pi^2 \mu C} (n+1/2)^2 + \frac{A}{r_e Ch} \left( 2 - \frac{3}{\delta} \right) + \frac{D_e}{Ch} + \frac{hJ(J+1)}{8\pi^2 \mu r_e^2 C} \end{aligned}$$

The coefficient of  $(n+1/2)$  in first term on the right hand side is

$$\omega_e = \frac{\alpha}{\pi C} \left[ \frac{A}{2\mu r_e} \left( \frac{-3}{2\delta} + \frac{4}{\delta^2} \right) \right]^{\frac{1}{2}} \quad .$$

The value of force constant is given by  $K_e = (8-3\delta) A/r_e^3$  in this case. When it is introduced in the above value of  $\omega_e$ , usual form for  $\omega_e$  is obtained, which is  $\omega_e = 1/2\pi C \cdot \sqrt{K_e/\mu}$ . It suggests that  $\omega_e$  is independent of  $\delta$ , but  $\omega_e x_e$  and  $\alpha_e$  depend on  $\delta$ .

TABLE 5. Variation of percentage error in  $\omega_e x_e$  with  $\delta$  for ZnH and HCl

$\delta$	Percentage error in $\omega_e x_e$ for ZnH                      HCl	
1.5	-46.47	-10.16
1.6	-39.5	+ 1.3
1.7	-30.08	+16.0
1.8	-20.09	+34.1
1.85	-13.54	+45.1
1.9	- 5.79	+58.1
2	+13.7	+90.6

## REFERENCES

- Born M. & Oppenheimer J. R. 1927 *Ann. d. Physik* **84**, 457.  
Eisenhart L. P. 1948 *Phys. Rev.* **74**, 87.  
Kratzer Z. 1920 *Phys.* **3**, 289.  
Landau L. & Lifschitz E. 1959 *Quantum Mechanics*, Pergamon Press, London, Paris.  
Levine I. N. 1966 *Jour. Chem. Phys.* **45**, No. 3,  
Manning M. F. 1935 *Phys. Rev.* **49**, 161.  
Morso P. M. 1929 *Phys. Rev.* **4**, 57.  
Pekeris C. I. *Phys. Rev.* **45**, 98  
Steele D. Lippincott E. R. & Vandershice, J. T. 1962 *Rev. Mod. Phys* **34** 239.  
Tietz T. J. 1963 *Chem. Phys.* 3036.  
Varshni Y. 1957 *Rev. Mod. Phys.* **29**, 664.  
Wojtczak L. 1965 *Acta Phys. Polonica*, **27**, 233.

## Line and continuum spectra of H.F. at Alibag during quiet and disturbed periods

By A. K. SEN

*Colaba Observatory, Bombay-5, India*

*(Received 22 December 1970)*

The nature of spectral lines and continuum spectra in the wavelength range 5 min to 185 min has been investigated for two periods, one of relative magnetic calm and the other disturbed. Spectra of digitized (2.5 min) Horizontal Intensity at Alibag suggest that during disturbances significant fluctuations occur in the range of 37.0 min to 185.0 min. These are ascribed to the variation in the mean level of the solar wind. From the computed power law it is noticed that the functional dependence of the continuum power on the frequency is almost the same for quiet and disturbed periods. The level of the continuum, however, is about  $5\frac{1}{2}$  times higher during the disturbed period.

### INTRODUCTION

In the course of a study of the magnetic data by spectrum analysis in the period range of 40 days to 5.5 years, Currie (1966) suggested that the continuum spectrum often provides information about the physical mechanisms that generate a time series. According to Banks (1969) continuum spectrum is generated by a real geophysical process and is not the result of instrumental noise or a function of the local observatory environment. To investigate the spectrum it is necessary to use sufficient length of data of any observatory. But the data are often vitiated by noise, such as, due to instrumental, scaling or reading errors or due to errors in copying, calculating, printing and rounding-off of the data.

The old and established observatory at Alibag (dip  $24^{\circ}.4N$ ) has a collection of excellent magnetic data extending over several decades. The continuum spectra of horizontal intensity of the earth's magnetic field during a period of low solar activity have been computed from a selection of samples from this data for quiet and disturbed periods. As short period fluctuations are known to become prominent during disturbed conditions the present analysis has been made to cover the wavelengths from 5 min to 185 min. To facilitate comparison an analysis restricted to quiet day data, has also been done. The functional dependence of the power density of the null continuum over the frequency has been computed for quiet and disturbed periods.

For adequate resolution 2.5 min digitized data of Alibag, made available by World Data Centre, have been used. Two series, one each for quiet and disturbed periods have been considered. The data used for computations for quiet and disturbed periods have been confined to the same month and year so that the



seasonal and solar cycle characteristics remain the same. Using Bartel's diagram three days from September 12 to September 14, 1964 were selected as a sample of a quiet period, the index  $A_p$  being 2 on each of those days. Three days, from September 7 to September 9, 1964 were selected as a sample of a disturbed period, the index  $A_p$  these days being 28, 23 and 16. Each series consisted of 1728 data points extending over a period of 72 hours. Following the procedure outlined by Blackman & Tukey (1959) autospectra were computed with a maximum lag of 300. Prior to computations a high pass digital filter was applied to each series to eliminate long period (diurnal and semi-diurnal) variations. Trend-free series,  $Y_t$ , were computed from the series of digitized data,  $X_t$ , by the linear transformation :

$$Y_t = \sum_{k=-n}^n W_k X_{t+k}$$

where  $W_k$  was the  $k$ -th weight of the filtering function and  $n = 100$ . The response of the filter was nearly unity for periods shorter than 187 minutes. Its response was zero for wave length of 625 minutes and above. From the autocorrelations computed in the course of power spectrum analysis the noise characteristic of the series was tested. The lag-one serial correlation coefficient  $r_1$  differed significantly from zero and the relations  $r_2 \simeq r_1^2$ ,  $r_3 \simeq r_1^3$ , etc, were satisfied where  $r_2$  and  $r_3$  were the serial correlation coefficients of lag 2 and lag 3. The null continuum was, thus, assumed as that of Markov red noise, as outlined in Tech. Note No. 79. Assuming that  $r_1$  was an unbiased estimate of the spectrum, the null continuum was computed from the following relationship :

$$s_k = \bar{s} \left[ \frac{1 - r_1^2}{1 + r_1^2 - 2r_1 \cos \frac{\pi k}{m}} \right]$$

where  $\bar{s}$  was the average of all raw spectral estimates,  $m$  = number of lags and  $k = 0, 1, 2, \dots, m$ . 95 per cent confidence line of the continuum was computed for each spectrum with chi-square values corresponding to the number of degrees of freedom  $(2N - M/2)/M$  where  $N$  was the number of data points and  $M$  was the maximum lag. The line spectra, null continua and 95 per cent confidence lines of the null continuum are shown in figures 1 & 2. As the continuum decreased asymptotically with increasing frequency, the power law for each series was determined by the relation  $P = Af^{-\alpha}$  where  $P$  was the power density of the null continuum corresponding to the frequency  $f$ ,  $\alpha$  the functional dependence and  $A$ , a constant.

## RESULTS

From the spectral estimates of the data for the quiet period it is noticed that peaks significant at 95 per cent level occur at the periods of 34.1, 30.6, in the

bandwidth of 26.8 and 25.9 min and at 18.3 min. The power density of the null continuum has a functional dependence  $f^{-\alpha}$  on frequency where  $\alpha = 1.65$  and constant  $A_q = 0.12 \times 10^{-4}$ . For the disturbed periods spectral peaks significant at 95 per cent confidence level occur in the wavelength from 166.7 to 150 mμ and

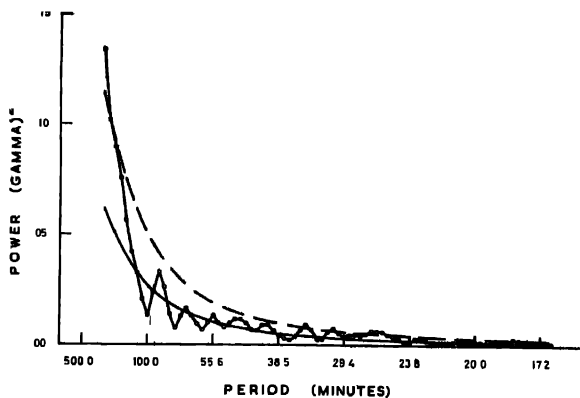


Figure 1. Spectra of Alibag H. F. during Quiet period. The line, joining the circles represents the line spectrum. The continuous line is the null continuum and the broken line represents 95 percent confidence line of the null continuum.

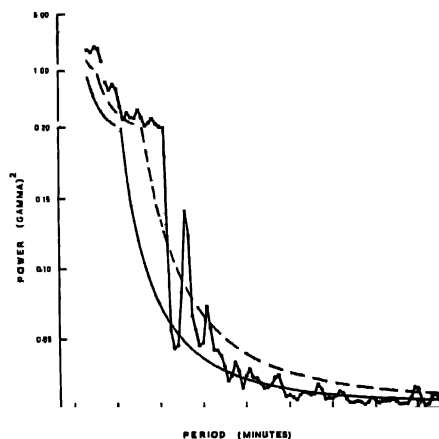


Figure 2. Spectra of Alibag H. F. during Disturbed period. The line joining the circles represents the line spectrum. The continuous line is the null continuum and the broken line represents 95 percent confidence line of the null continuum.

at wavelengths of 107.1, 83.3, 71.4, 60.0, 44.1, 37.5, 15.3 and around 11.0 m $\mu$ . The power density of the null continuum has a functional dependence  $f^{-\alpha}$  on frequency where  $\alpha = 1.72$  and constant  $A_d = 0.66 \times 10^{-4}$ .

## DISCUSSION

According to Parker (1967) the longer period fluctuations of the magnetic field are due to the variations in the mean level of the solar wind. From both the spectra it is observed that in the low frequency range the number of spectral peaks significant at 95 per cent confidence level are higher during disturbed period. This is to be expected because larger variations over mean level of the enhanced solar wind can be expected only during disturbances. From the investigation of periodic fluctuations in the geomagnetic field during 36 storms in 1958, Pai & Sarabhai (1964) observed that the most common periods were 40-50 min. Some fluctuations had periods as large as 60 to 80 min. Best & Grafe (1969) from their studies of proton flare events between August 27 and September 7, 1966 suggested that for  $H$  and  $D$  components at Honolulu, the spectral density peaks occur around 100-120 min. They also noticed spectral peaks at 50 to 60 min and 90 to 120 min at Niemegk and Sitka. Bhargava & Rao (1970) studied the fluctuations in the period range of 6-150 min for the statistical properties of world-wide fluctuations during disturbed periods at several stations and observed a peak around 120 min. They also obtained shorter period secondary oscillations with periods around 25 and 37 min. From this investigation it is noticed that significant spectral peaks also occur in the period range of 150 to 166.7 min and around 11 and 15 min. It is also noticed that, for both quiet and disturbed periods, the functional dependence of continuum power on frequency is almost same, being 1.65 and 1.72. These constants are slightly lower than the constant of about 2.0 obtained by Mason (1963) from his study on spectra for  $D$ ,  $H$  and  $Z$  of 4 disturbed days of 3 stations for periods in the range 6-120 min.

Although the functional dependence of power on frequency is almost equal in both the series, the level of the continuum during disturbed period is about  $5\frac{1}{2}$  times higher than that of quiet period as noticed from the ratio of  $A_d$  to  $A_q$ . This may be ascribed to the intensification of solar wind during the disturbed period. Currie (1966) pointed out that at some observatories no semi-annual or annual lines were observed in the spectra and this indicated that Observatory noise was severe resulting in the continuum power levels being higher than the line spectra. From this study it is noticed that during disturbances the continuum level is slightly higher than the line spectrum towards the high frequency end of the spectrum (from 7.7 min to 5 min). This feature is, however, absent during quiet period. This result suggests that the contribution of the instrumental noise to the continuum is negligible. That the continuum level is higher than the line spectrum only during disturbed period could be ascribed to either noise during

disturbances or rounding-off error of the data, a feature likely to be more effective during disturbed periods.

#### ACKNOWLEDGEMENT

The author is grateful to Shri B. N. Bhargava, Director, Colaba and Alibag Observatories for suggesting the problem and guidance during the course of this investigation. The author is thankful to the Director General of Observatories Lodi Road, New Delhi for giving permission to publish this paper.

#### REFERENCES

- Banks R. J. 1969 *Geophys. J. Res.* **17**, 457.  
Best A. & Grafe A. 1969 *Arbeiten Zum Proton Flareprojekt der Beobachtungs-Periode 1966*, Berlin  
Bhargava B. N. & Rao D. R. K. 1970 *Planet. Space Sci.* **18**, 1381.  
Blackman R. B. & Tukey J. W. 1959 *The Measurement of Power Spectra*, Dover Publ., New York.  
Curcio R. G. 1966 *J. Geophys. Res.* **71**, 4579.  
Mason R. G. 1963 *Marine Phys. Lab, Scripps Inst. of Oceanogr. Rep No. 63-13*.  
Pai G. L. & Sarabhai V. A. 1964 *Planet. Space. Sci.* **12**, 855.  
Parker E. N. 1967 *Phys Geomag. Pheno-II*. Academic Press, New York and London.  
*Tech. Note. No 79, 1966 World Meteorological Organization.*

## The effect of salinity on the apparent dielectric constant values of rock specimens

By S RANGACHARI

*Department of Physics, Indian School of Mines, Dhanbad, Bihar*

(Received 20 November 1970—Revised 4 May 1971)

Dielectric constant values of two rock specimens saturated with aqueous sodium chloride solution at various concentrations have been measured at various frequencies in the range 1 MHz to 24 MHz and a significant rise in the values has been noticed with the decrease of frequency and increase of concentration. An attempt has been made to fit these data into an empirical relation and to explain the increase.

### INTRODUCTION

Determination of the dielectric properties of natural-state rocks is beset with many difficulties both in measurement and in interpretation of results. The relative permittivity data obtained so far show a dispersion with change of frequency far in excess of theoretical predictions due probably to the existence of dispersing mechanisms not yet understood. Among factors affecting the dielectric properties of such rocks may be mentioned composition, structure, porosity, water-content, salinity, temperature and pressure. For an understanding of their dielectric behaviour it is therefore necessary to study the effects of these factors within wide limits.

The pore-fluids in rocks are known to contain dissolved salts and organic matter. Measurements of the dielectric constant, loss tangent and the electrical conductivity of natural-state rocks at various frequencies, temperatures and levels of water content have been reported by many workers (Keller & Licastro 1950; Howell & Licastro 1961; Scott *et al* 1967 and Singh & Jha 1965). At frequencies above about 10 MHz, many mechanisms known to operate at low frequencies are rendered inoperative and the observed permittivity values decrease drastically. Only the large values at low and medium frequencies are of interest in the present study. In the present work the frequencies between 1 MHz and 24 MHz have been chosen with a view to avoid large errors in measurement at lower frequencies due to polarization at the electrodes while retaining the dispersive mechanisms referred to above. Metallic film electrodes and a Q-meter have been used in these measurements to study the effect of salinity on the dielectric constant of natural rock specimens.

### APPARATUS USED

A Q-meter, by Messrs. Advance Ltd. of England, was used for this purpose. The sample holder was a completely covered and earthed brass box with one insulated electrode of 2.54 cm diameter. The two electrode surfaces to be in contact

with the specimen were carefully polished plane and parallel to within 1/20 mm and arranged one above the other as viewed through a microscope. To reduce the edge effects, the specimens were made of diameters less than that of the insulated electrode by about twice the specimen thickness as recommended by Von Hippel (1956) and the edge of the insulated electrode was bevelled. The connection between the Q-meter and the sample holder was effected through a specially prepared coaxial line of low capacitance and loss, having a length of about 30 cm

#### PREPARATION OF THE SAMPLE AND METHOD OF MEASUREMENT

Specimens were prepared from core-samples of homogeneous rock (very fine-grained carbonaceous shale from Jharia near Dhanbad, India) with low porosity. They were lathed down to the required diameter and flats were sliced out, having thicknesses slightly larger than the required value, using a copper disc saw imbedded with diamond bits. The flat faces were then polished to the required thickness and checked to be within 1/50 mm. Thin aluminium foil was used as the electrode material and pasted on the specimen in the manner recommended (Von Hippel 1956) and held tightly in the sample holder. This system was considered sufficient for the kind of measurement undertaken. At each chosen frequency the standard capacitor of the Q-meter, which is capable of an accuracy of 0.2 pF, was adjusted for resonance. This procedure was followed with and without the specimen in position. The relative permittivity was calculated as the ratio of the capacity of the condenser, with the specimen forming the medium, to the capacity of the same system with air as dielectric. Loss tangent values could not be measured as these were found somewhat larger than what might be measured accurately with the apparatus, especially below 6 MHz. The reliability of the instrument was first tested using discs of paraffin wax and polythene and the values obtained agreed very closely with those quoted in standard handbooks, which were well within the accuracy of 5 percent, claimed for the measurements.

With any given specimen, three kinds of measurements were made with the specimen (a) remaining completely dry, (b) saturated with pure distilled water and (c) saturated with pure aqueous solution of sodium chloride at concentrations of 2.5, 5.0, 7.5, and 10.0 percent by weight.

After the specimen was washed with pure benzene and dried, it was saturated with distilled water and dried several times to remove any dissolved salts. Finally the disc was dried thoroughly in a hot air oven. Measurements were made on the sample quickly after cooling it in anhydrous calcium chloride. Sides of the disc were not covered as readings obtained were found materially to be the same during dry summer days with or without cover. Next the specimen was saturated with distilled water by forcing water into its pores with a vacuum pump. Immediately

after placing the specimen in the holder, readings were obtained every 15 minutes for one hour, and every one hour for 6 hours thereafter and the change in the readings, if any, was observed as the specimen dried. It was found that initially the loss values were large and changing, though the capacity values remained almost steady. After a period of one to two hours depending on the atmospheric conditions, both the loss and the capacitance values were found to remain steady for several hours. The initial changes were attributed to the conductivity of the liquid adhering to the sides. The steady values were recorded. In the third stage, the specimen was dried as aforesaid and then saturated with 2.5 percent aqueous solution of sodium chloride in the same manner as with distilled water and data obtained. The specimen was then left in distilled water for several days with frequent renewal of water to ensure that all the salt was removed. The removal was assumed to be complete when the readings obtained agreed with those at the second step described above. The same procedure was followed before using solutions of other concentrations. All the data were obtained between temperature limits of 30°C and 36°C. Lastly, readings were also obtained with the specimens saturated with 10 percent aqueous solution of cane sugar for the reason given in the discussion of results. The data are presented in the table and graphs.

#### DISCUSSION

As may be found from the table and curves, the dielectric constant data show three kinds of change. (a) At any frequency, d.e.c. increases with increasing concentration and tends to a steady value. (b) At any given concentration of the salt in the pore fluid d.e.c. decreases with increasing frequency and rapidly so from 6 to 1 MHz. (c) In the case of the specimen saturated with distilled water and 2.5 percent solution, it is found that there is a slight fall and then a rise in d.e.c. values as the frequency decreases from 24 MHz. This change is barely noticeable in the case of 5 percent and hardly so in 10 percent solution.

The change (a) closely resembles the change in electrical conductivity of aqueous sodium chloride solution as its concentration increases and is as to be expected. The change (b) is also known to take place but the significance in this case is that it is more than if the pore fluid were distilled water. Though the permittivity values may be increased by the presence of ions in a solid, this increase is expected to appear only at much higher frequencies. Interfacial effects are stated to contribute to the large d.e.c. values at the frequencies of observation (Smyth 1955). Thus the presence of ions at interfaces in rock specimens seems to accentuate the effect very considerably. This seems to be particularly noticeable below 3 MHz whereas, above 6 MHz there is only a nominal increase. That the ions do play an important part becomes apparent if one compares the permittivity values of the specimens with those obtained when they are saturated with solutions in water containing non-ionizing solutes, *e.g.*, sugar. Data for a

Table 1. Dielectric constants of two rock samples, dry and saturated with various pore fluids, and of two materials used for standardization.

Freq. in MHz	Specimens obtained from core samples of hard, fine-grained carbonaceous shale from Jharia near Dhanbad										Spec 2																																																																																																																																																																																																																																																																																																																																																																																																																																																																																																																																																																																																																																																																																																																																																																																																																																																																																																																																																																																																																																																																																																																																																																																																																																																																																																																																																		
	Specimen 1 (Observed)				Specimen 2 (Observed)				Calculated from empirical relation				Poly- thene fin disc																																																																																																																																																																																																																																																																																																																																																																																																																																																																																																																																																																																																																																																																																																																																																																																																																																																																																																																																																																																																																																																																																																																																																																																																																																																																																																																																																
	Dry Dist.		Salt Soln.		Dry Dist.		Salt Soln.		Dist.		Salt Soln.		disc.																																																																																																																																																																																																																																																																																																																																																																																																																																																																																																																																																																																																																																																																																																																																																																																																																																																																																																																																																																																																																																																																																																																																																																																																																																																																																																																																																
	water	2.5%	5.0%	7.5%	10.0%	water	2.5%	5.0%	7.5%	10.0%	water	2.5%	5.0%	7.5%	10.0%																																																																																																																																																																																																																																																																																																																																																																																																																																																																																																																																																																																																																																																																																																																																																																																																																																																																																																																																																																																																																																																																																																																																																																																																																																																																																																																																														

These values are calculated on the assumption that the frequency-dependent term in the empirical relation remains inoperative. The relation itself is taken to be valid only for specimens containing some pore fluid.



specimen saturated with 10 percent aqueous solution of cane sugar have been obtained and presented in the table. It may be seen that these values differ insignificantly from those for distilled water.

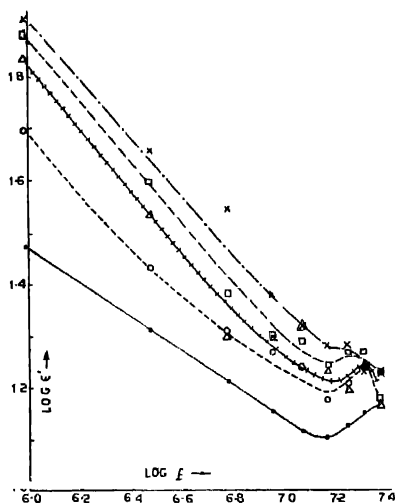


Figure 1. Curves are indicated as: —●— distilled water, —○— 2.5%  
 ++△++ 5% ; —□— 7.5% ; × — 10%

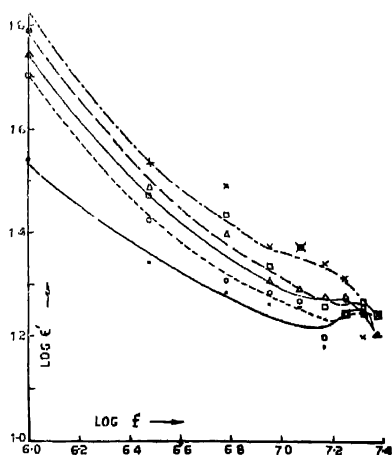


Figure 2. Curves are similarly indicated as in figure 1

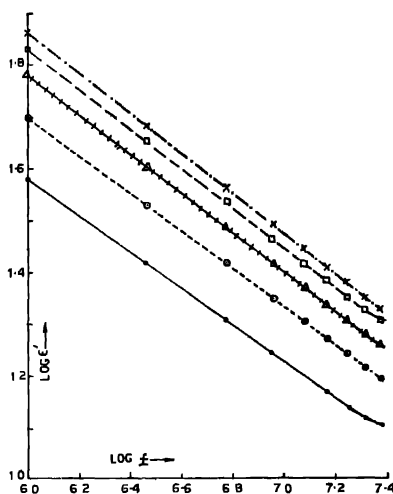


Figure 3. Curves are indicated as in figure 1

No comprehensive theory for the dielectric behaviour of moist rocks seems to be available wherefrom one can calculate even approximately the d.e.c. and other properties if the physical conditions of the rock specimen are known. However, Scott *et al* (1967) have given empirical relations for rough calculations of these values. Briefly, they have taken a very large number of specimens and obtained data with varying water-contents and frequencies. The graphical presentation of the data has to be a log-log plot, a trial relation with unknown constants is chosen, the data are fed into a computer to obtain a good fit and the constants are obtained from the computer. This has been done for a first and a second order fit. In this work under report, the coefficients of the first order equation have been suitably changed and a term has been added to take salinity into account through  $n$ , the normality of the solution. The effort appears to have been successful to the extent that the relation gives the trend of the changes. The values calculated from the empirical relation given below are also presented in the table and graphs.

The empirical relation used is,

$$\log k = 0.75 + 4.7 \log (1+w) - 0.35 \log f + \frac{2.1}{\log f} (1 - 1/\exp n).$$

where,  $k$  is the dielectric constant of the specimen,  $w$ , the water content by volume,  $f$  the frequency and  $n$  is the normality of the solution used.

The dispersion due to ions at the interfaces seems to vanish at frequencies above 9 MHz or so, and other complicating effects are also in evidence at the higher frequencies. The empirical relation assumes dispersion at all frequencies and so the curves representing the calculated values are spread out even at 24 MHz. Below about 6 MHz, the empirical relation gives nearly the same trend as curves depicting the observed values. However, it is recognised that more data with more specimens at lower frequencies are needed to make the equation more meaningful. Such measurements are in progress and will be reported shortly.

#### CONCLUSION

The salinity of the pore fluid in natural-state rocks does have a pronounced effect on the d.e.c. values, especially below a certain frequency which may depend on the specimen. The very large values of the observed d.e.c. are likely to be due to the presence of ions in the interfaces. Any theory on the dielectric properties of natural-state rocks may not be complete without including the effect of salinity of the pore fluids explicitly or implicitly.

#### ACKNOWLEDGEMENT

The author is grateful to Dr J. Singh, Senior Professor and Head of the Department of Applied Geophysics, Indian School of Mines, Dhanbad, for kindly providing with samples and the Q-meter, and for helpful discussions. He is also grateful to Prof S. N. Mitra, Professor and Head of the Department of Physics and Mathematics, Indian School of Mines, for his constant encouragement.

#### REFERENCE

- Howell B. F. & Lucastro P. H. 1961 *American Mineralogist*, **46**, 269.  
Keller G. V. & Lucastro P. H. 1950 *Bull. U.S. Geol. Survey*, **No. 1052H**.  
LeFevre 1953 *Dipole Moments*, 3rd edn, Methuen Monograph.  
Scott J. et al 1967 *Jour Geophys. Research* **20**, No. 20.  
Singh J. & Jha B. P. 1965 *Jour Ind Geophys Union* **2**, 65.  
Singh J. & Jha B. P. *Jour. Pure & Appl. Geophys.* (in press).  
Smyth C. P. 1955 *Dielectric Behaviour and Structure*, McGraw Hill.  
Von Hippel A. R. 1956 *Dielectric Materials and Applications*, Chapman Hall.

## Flow of a power law fluid in a rotating straight pipe.—I : Determination of flow field

BY KANAKA RAJU

*Department of Applied Mathematics, Indian Institute of Science,  
Bangalore-12, India*

(Received 18 August 1970)

A steady flow of a power law fluid in a rotating straight pipe of circular cross-section is discussed in the present paper. The flow field consists of a primary axial flow and a secondary swirling flow in the meridian plane. It is found that at low rotational speeds the swirl flow induced due to the rotation is weak and symmetrical about the plane of rotation in any cross-section. As the rotation increases an almost shear free central region and a boundary layer type flow at the offside end of the cross-section develop. Figures 1 to 6 depict these results.

### 1. INTRODUCTION

Non-Newtonian fluids are found to be better heat transport media than the conventional Newtonian fluids as pointed out by Fraas & Ozisik (1965). Therefore the heat transfer phenomena in the flow of non-Newtonian fluids are of importance and need thorough investigation. Many of the coolers use rotating devices and intrinsic cooling of rotating devices themselves are of great importance. Hence the study of flow of a non-Newtonian fluid in rotating pipes is of practical importance. The temperature distribution in any coolant is governed not only by the heat conduction but is very much dependent on the flow behaviour of the fluid as well as convective effects as seen from Raju & Rathna (1970). We first study the flow field of a power law fluid in a rotating straight pipe of circular cross-section in this part and consider the heat and mass transfer in a subsequent paper. We have chosen power law fluids because amongst the class of non-Newtonian fluids they have the minimum number of empirical constants in their constitutive equation. Also many realistic fluids can be approximated by power law fluids. For instance, blood plasma can be treated as a power law fluid with flow behaviour index,  $n = 0.92$  and many other high polymer solutions also behave similarly.

The corresponding flow in a rotating straight pipe for viscous incompressible Newtonian fluids for small angular speeds of rotation was first investigated by Barua (1954). He found that the flow field consists of a primary axial flow and a weak swirling secondary flow. This resembles the flow generated in a curved pipe studied extensively by Dean (1927) and others. These investigations utilize mainly the perturbation technique. Recently, a different approach to this problem has been made by Jones & Walters (1967). They determine the flow in the

neighbourhood of the axis of rotation assuming that the meridional flow is shear free, following Dean & Hurst (1959). Because of this limitation, even though they obtain simpler equations and approximate flux, their solution is not valid away from the axis. Especially it does not satisfy the boundary conditions. But the heat transfer phenomena critically depend on the behaviour of the swirl flow near the boundary, as shown earlier by Raju & Rathna (1970), owing to the fact that the convective heat transfer is not negligible. Consequently, the perturbation technique developed by Barua gives better results though restricted to small rotational speeds.

We determine the swirl flow induced by the rotation of the pipe in a primary pressure driven axial shear flow as a power series in rotational speed in the next section. We give a detailed discussion of the flow field later on. In part 2 we determine the temperature field and study the behaviour of Nusselt number with Dean's number as well as rotation.

#### FORMULATION OF THE PROBLEM

As given by Tomita (1959), the constitutive equation for a power law fluid is

$$T = -pI + \mu_p \odot E \quad \dots (2.1)$$

where  $T$  is the stress tensor,  $E$  is the rate of strain tensor,  $\mu_p$  a constant and

$$\odot = |E_{11}^2 + E_{22}^2 + E_{33}^2 + 2(E_{12}^2 + E_{23}^2 + E_{31}^2)|^{\frac{n-1}{2}}, \quad \dots (2.2)$$

$n$  being the flow behaviour index.

Consider the steady flow of the above fluid in a straight pipe rotating uniformly with an angular speed  $\Omega$ . For simplicity of expressions, we refer the motion to a Cartesian frame of reference fixed in the pipe and rotating with it, such that the  $X$ -axis is along the axis of rotation and the  $Z$ -axis is along the axis of the pipe. The equations of continuity and momentum are

$$\frac{\partial U}{\partial X} + \frac{\partial V}{\partial Y} = 0 \quad \dots (2.3)$$

$$U \frac{\partial U}{\partial X} + V \frac{\partial U}{\partial Y} = - \frac{\partial}{\partial X} (P/\rho) + \nu_p \left[ \odot \nabla^2 U + E_{xx} \frac{\partial \odot}{\partial X} + E_{xy} \frac{\partial \odot}{\partial Y} \right] \dots (2.4)$$

$$-2\Omega W + U \frac{\partial V}{\partial X} + V \frac{\partial V}{\partial Y} = - \frac{\partial}{\partial Y} (P/\rho) + \nu_p \left[ \odot \nabla^2 V + E_{xy} \frac{\partial \odot}{\partial X} + E_{yy} \frac{\partial \odot}{\partial Y} \right] \dots (2.4)$$

$$2\Omega V + U \frac{\partial W}{\partial X} + V \frac{\partial W}{\partial Y} = - \frac{\partial}{\partial Z} (P/\rho) + \nu_p \left[ \odot \nabla^2 W + E_{xz} \frac{\partial \odot}{\partial X} + E_{yz} \frac{\partial \odot}{\partial Y} \right] \dots (2.6)$$

where  $U(X, Y)$ ,  $V(X, Y)$  and  $W(X, Y)$  are the velocity components in the directions of  $X$ ,  $Y$  and  $Z$ , respectively and  $\nu_p = \mu_p/\rho$ . The boundary conditions are

$$U = V = W = 0 \text{ on } F(X, Y) = 0, \quad \dots (2.7)$$

where  $F(X, Y) = 0$  is the equation to the cross-section of the pipe. We introduce the stream function  $\psi$  by

$$U = -\frac{\partial \psi}{\partial Y}; \quad V = \frac{\partial \psi}{\partial X} \quad \dots (2.8)$$

Substituting (2.8) in (2.4) to (2.6) and eliminating the pressure gradient term, we obtain

$$\begin{aligned} & \left[ \frac{\partial \psi}{\partial X} \cdot \frac{\partial}{\partial Y} - \frac{\partial \psi}{\partial Y} \cdot \frac{\partial}{\partial X} \right] \left( \frac{\partial^2 \psi}{\partial X^2} + \frac{\partial^2 \psi}{\partial Y^2} \right) - 2\Omega \frac{\partial W}{\partial X} \\ &= \nu_p \left[ \Theta \nabla^4 \psi + \frac{\partial \Theta}{\partial X} \left\{ 2 \frac{\partial^3 \psi}{\partial X \partial Y^2} + 2 \frac{\partial^3 \psi}{\partial X^3} \right\} + \frac{\partial \Theta}{\partial Y} \left\{ 2 \frac{\partial^3 \psi}{\partial Y^3} + 2 \frac{\partial^3 \psi}{\partial X^2 \partial Y} \right\} \right. \\ & \quad \left. + 4 \frac{\partial^2 \Theta}{\partial X \partial Y} \cdot \frac{\partial^2 \psi}{\partial X \partial Y} + \left( \frac{\partial^2 \psi}{\partial X^2} - \frac{\partial^2 \psi}{\partial Y^2} \right) \left( \frac{\partial^2 \Theta}{\partial X^2} - \frac{\partial^2 \Theta}{\partial Y^2} \right) \right] \quad (2.9) \end{aligned}$$

and

$$\nu_p \left[ \Theta \nabla^2 W + \frac{\partial \Theta}{\partial X} \frac{\partial W}{\partial X} + \frac{\partial \Theta}{\partial Y} \frac{\partial W}{\partial Y} \right] = -C + \frac{\partial(\psi, W)}{\partial(X, Y)} + 2\Omega \frac{\partial \psi}{\partial X} \quad \dots (2.10)$$

where  $C = \frac{1}{\rho} \frac{\partial P}{\partial z}$ , is the given constant axial pressure gradient. To study the flow in a circular pipe of radius  $a$  we transform to cylindrical polar coordinates defined by

$$\left. \begin{aligned} Z &= R \sin \theta \\ Y &= R \cos \theta \\ Z &= Z \end{aligned} \right\} \quad \dots (2.11)$$

Further, let

$$\begin{aligned} R &= ar; \quad \psi = \bar{U}a\bar{\psi}; \quad W = \bar{W}w; \\ \Theta &= \bar{W}a^{n-1}\Theta_1 \end{aligned} \quad \dots (2.12)$$

where  $\bar{U}$  and  $\bar{W}$  are characteristic velocities given by

$$\left. \begin{aligned} \bar{U} &= \frac{2\Omega a^{n+1}}{\nu_p} \left( \frac{Ca^{n+1}}{\nu_p} \right)^{\frac{2-n}{n}} \\ \bar{W} &= \left( \frac{Ca^{n+1}}{\nu_p} \right)^{\frac{1}{n}} \end{aligned} \right\} \quad \dots (2.13)$$

We expand the flow field in the form

$$\left. \begin{aligned} W &= w_0(r) + \frac{\bar{U}}{K\bar{W}} w_1(r, \theta) + \left(\frac{\bar{U}}{K\bar{W}}\right)^2 w_2(r, \theta) + \dots \\ \frac{\psi}{K} &= \left(\frac{\bar{U}}{K\bar{W}}\right) \psi_1(r, \theta) + \left(\frac{\bar{U}}{K\bar{W}}\right)^2 \psi_2(r, \theta) + \dots \end{aligned} \right\} \dots \quad (2.14)$$

where the non-dimensional constant  $K$  is given by

$$K = \frac{Ca}{\bar{W}^2}. \quad \dots \quad (2.15)$$

Substituting (2.11) and (2.14) in (2.9) and (2.10) and comparing equal powers of  $\frac{\bar{U}}{K\bar{W}}$ , we get the equations satisfied by various order terms.

The differential equation for  $w_0(r)$  is

$$\left[ \left( \frac{dw_0}{dr} \right)^2 \right]^{\frac{n-1}{2}} \left[ n \frac{d^2 w_0}{dr^2} + \frac{1}{r} \frac{dw_0}{dr} \right] = -1, \quad \dots \quad (2.16)$$

with the boundary condition

$$w_0 = 0, \text{ on } r = 1. \quad \dots \quad (2.17)$$

The well known solution of (2.16) is

$$w_0(r) = \frac{1}{2^{1/n}} \cdot \frac{n}{n+1} \cdot (1-r^{1+1/n}), \quad \dots \quad (2.18)$$

which is the solution of the pressure driven axial flow. We call this the primary motion of the problem. It is of interest to note that for  $n = 1$ , this reduces to Poiseuille flow.

The differential equation for  $\psi_1$  is of the form

$$\begin{aligned} & \frac{\partial^4 \psi_1}{\partial r^4} + \frac{2n-1}{n^2} \cdot \frac{1}{r^3} \cdot \frac{\partial \psi_1}{\partial r} - \frac{2n-1}{n^2} \cdot \frac{1}{r^2} \cdot \frac{\partial^2 \psi_1}{\partial r^2} + \frac{2n-1}{n} \cdot \frac{2}{r} \cdot \frac{\partial^3 \psi_1}{\partial r^3} \\ & - \frac{1}{n} \cdot \frac{2}{r^3} \cdot \frac{\partial^3 \psi_1}{\partial r \partial \theta^2} + \frac{2}{r^2} \cdot \frac{\partial^4 \psi_1}{\partial r^2 \partial \theta^2} + \frac{1}{r^4} \cdot \frac{\partial^4 \psi_1}{\partial \theta^4} + \frac{n^2+4n-1}{n^2} \cdot \frac{1}{r^4} \cdot \frac{\partial^2 \psi_1}{\partial \theta^2} \\ & = \sin \theta \cdot \left[ \frac{r}{2} \right]^{\frac{2-n}{n}}, \quad \dots \quad (2.19) \end{aligned}$$

with the boundary conditions

$$\frac{\partial \psi_1}{\partial r} = \frac{\partial \psi_1}{\partial \theta} = 0 \quad \text{on } r = 1, \quad \dots \quad (2.20)$$

Solving

$$\psi_1 = g(r) \sin \theta \quad \dots (2.21)$$

where

$$g(r) = A'r + B'r^s + C'r^{2/n+3} \quad \dots (2.22)$$

and

$$\left. \begin{aligned} A' &= C' \left[ \frac{2+2n-n(s-1)}{n(s-1)} \right] \\ B' &= -C' \left[ \frac{2+2n}{n(s-1)} \right] \\ C' &= \frac{1}{2^{(2-n)/n}} \cdot \frac{n^4}{4(n+1)(3n+1)(n^2+4n+1)} \\ s &= \frac{n+1}{2n} + \sqrt{\frac{(\sqrt{17}n-1)^2 + 2n(\sqrt{17}-1)}{2n}} \end{aligned} \right\} \quad \dots (2.23)$$

With (2.18) and (2.21), it can be seen that  $w_1$  satisfies the differential equation,

$$nr^2 \frac{\partial^2 w_1}{\partial r^2} + (2n-1)r \frac{\partial w_1}{\partial r} + \frac{\partial^2 w_1}{\partial \theta^2} = -\frac{1}{2^{(2-n)/n}} \left[ A'r^{\frac{2+n}{n}} + B'r^{s+2/n} + C'r^{\frac{4}{n}+3} \right] \cos \theta. \quad \dots (2.24)$$

the boundary condition being

$$w_1 = 0, \text{ on } r = 1. \quad \dots (2.25)$$

The solution for  $w_1$  is

$$w_1 = F(r) \cos \theta. \quad \dots (2.26)$$

$F(r)$  is given by

$$\begin{aligned} F(r) &= \left[ \frac{r^{1/n}}{2^{(2-n)/n}} \right] \cdot \left[ \frac{nA'}{2(n+1)^2} (1-r^{1+1/n}) + \frac{nB'(1-r^{s+1/n})}{(ns+1)(ns+2+n)} \right. \\ &\quad \left. + \frac{nC'}{12(n+1)^3} (1-r^{3/n+3}) \right] \quad \dots (2.27) \end{aligned}$$

where  $A'$ ,  $B'$ ,  $C'$  and  $s$  are given in (2.23).

This gives the solution up to the first order in the rotation parameters. We have carried out the analysis to the second order terms as well. The expressions are complicated and lengthy. The order of magnitude of successive terms decreases very rapidly and the principal features of the flow are given by first order term itself.



## DISCUSSION OF THE RESULTS

In order to study the solution (2.18), (2.21) and (2.26) we consider in detail three flow behaviour indices,  $n = 0.8$  (psuedoplastic),  $n = 1.0$  (Newtonian) and  $n = 1.2$  (dilatant) which cover almost the whole range of power law fluids met with in practice. For instance blood plasma can be treated as a psuedoplastic liquid with  $n = 0.92$ . Secondly, we consider the cases of very small and fairly high rotational speeds. The velocity profiles are drawn for low rotational speeds in figures 1, 3 and 5, and for high rotational speeds in figures 2, 4 and 6 for  $n = 0.8, 1.0$  and  $1.2$ .

The secondary meridional flow is symmetrical about the plane of rotation in any cross-section. At low rotational speeds the swirl flow generated is weak. But as the rotational speed increases an almost shearfree region develops in the central region with a boundary layer type flow at the offside end of the cross-section towards which the coriolis force acts. The swirl flow detaches from the boundary and flows inside at the onside end of the cross-section. These conclusions are evident from the figures as well. This action of coriolis force is similar to the effect of centrifugal force due to curvature of a bent pipe, studied earlier by McConalogue & Srivastava (1968) for Newtonian fluids and by Raju & Rathna (1970) for power law fluids. Here this force is proportional to rotational speed and the pressure driven axial flow, and consequently not as strong as in the case of curvature effect, where it is proportional to square of the axial flow.

In all figures broken lines refer to  $\psi = \text{constant}$  and unbroken lines to  $W = \text{constant}$ .

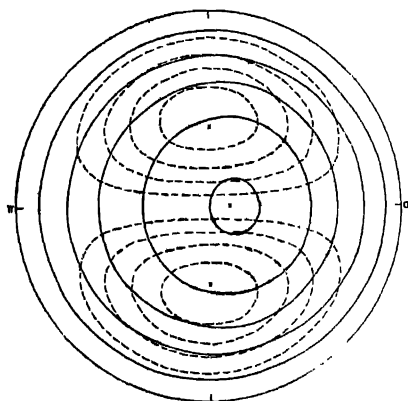


Figure 1. Secondary flow field for the Newtonian fluid at low rotational speeds ( $n = 1.0$ ).

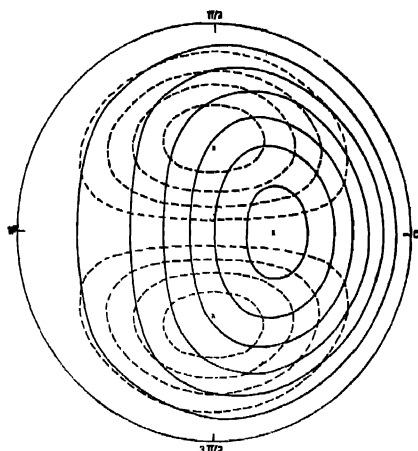


Figure 2. Secondary flow field for the Newtonian fluid at high rotational speeds ( $n = 1.0$ ).

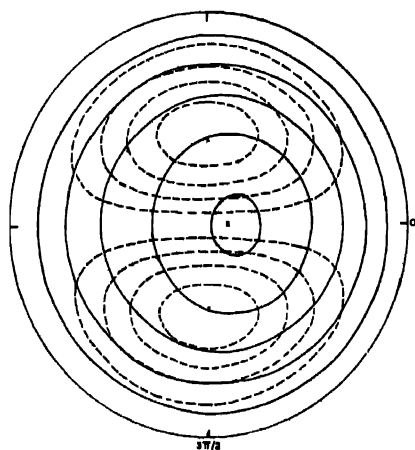


Figure 3. Secondary flow field for a dilatant fluid at low rotational speeds ( $n = 1.2$ ).

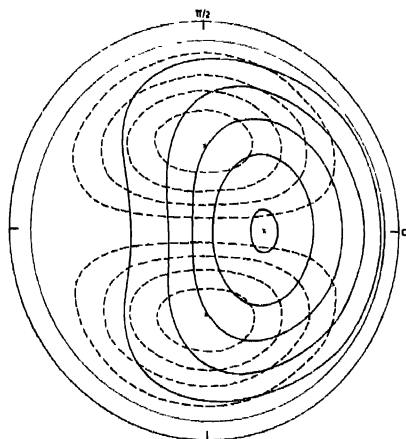


Figure 4. Secondary flow field for a dilatant fluid at high rotational speeds ( $n = 1.2$ ).

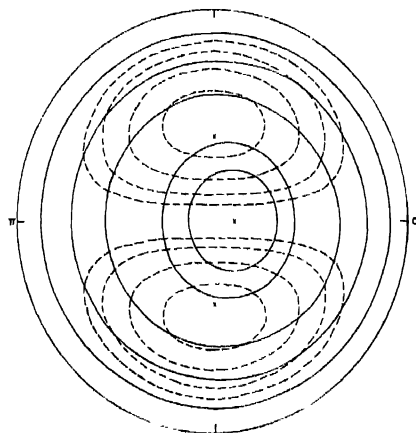


Figure 5. Secondary flow field for a pseudoplastic fluid at low rotational speeds ( $n = 0.8$ ).

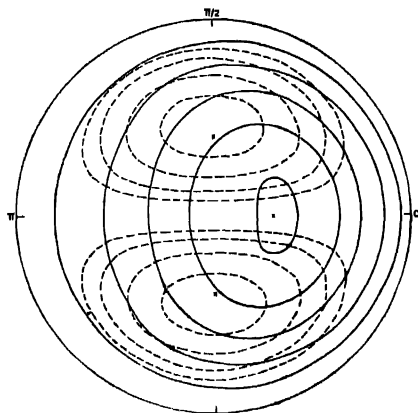


Figure 6. Secondary flow field for a pseudoplastic fluid at high rotational speeds ( $n = 0.8$ ).

The following table gives the relative maxima of the axial speeds and positions where they occur.

TABLE 1

$n$	Low rotational speeds		High rotational speeds	
	$W_{max}$	Point of occurring	$W_{max}$	Point of occurring
0.8	0.4474	$r = 0.1$	0.5163	$r = 0.3$
1.0	0.5098	$r = 0.1$	0.6390	$r = 0.3$
1.2	0.5650	$r = 0.1$	0.7664	$r = 0.3$

It is seen that the  $W_{max}$  increases with the increasing values of  $n$  which may be explained by considering the fact that the pseudoplastic fluids ( $n = 0.8$ ) sustain less strain and dilatant fluids ( $n = 1.2$ ) sustain more strain. We notice that the point, where  $W_{max}$  occurs, shifts towards the offside as the rotation increases, but there is no variation in its occurrence with the flow behaviour index,  $n$ . This behaviour of flow field has great significance in the convective heat transfer pattern that develops.

## ACKNOWLEDGEMENT

The author conveys his thanks to Dr. S. L. Rathna for her kind help and to Dr. C. Devanathan for useful discussions in the preparation of the paper. He also thanks the Council of Scientific and Industrial Research, New Delhi, for financial assistance.

## REFERENCES

- Barua S. N. 1954 *Proc. Roy. Soc.* **227A**, 133.  
Dean W. R. 1927 *Phil. Mag.* **4**, 208.  
Dean W. R. & Hurst J. M. 1959 *Mathematika* **6**, 77.  
Fraas A. P. & Ozisik M. N. 1965 *Heat Exchanger Design*, John Wiley and Sons Inc., New York.  
Jones J. R. & Walters T. S. 1967 *ZAMP* **18**, 774.  
McConologue D. J. & Srivastava R. S. 1968 *Proc. Roy. Soc.* **307A**, 37.  
Raju Kanaka K. Rathna, S. L. 1970 *Jour. Ind. Inst. Sci.*, **52**, 34.  
Tomita Y. 1959 *Bull. J. S. M. E.* **2**, 469.

## Propagation of oblique shock waves in the troposphere

By V. P. SINGH

*Terminal Ballistics Research Laboratory, Chandigarh*

AND

PREM KUMAR

*Indian Institute of Technology, Delhi*

(Received 20 November 1970—Revised 21 April 1971)

Propagation of the shock waves, when propagated at a constant angle to the vertical, in the troposphere, is discussed. In a special case, the results of an earlier paper are deduced.

### INTRODUCTION

Propagation of shock waves in the earth's atmosphere in the vertical direction was discussed by Singh (1969), in which the model of Mitra (1952) was used with minor changes. It was found that the shock velocity increases as the shock front propagates in the vertically upward direction. In the isothermal part of the atmosphere, the increase in shock velocity is smaller, but larger in layers where the temperature decreases. At a height of 78.44 km the fluid velocity behind the shock front becomes greater than the escape velocity. In this paper, we generalize the idea of previous work for oblique shock waves. Propagation of shock wave is considered only in the troposphere. Curvature of the earth is neglected, so that density, pressure and temperature of the atmosphere are varying in planes parallel to the surface of the earth. We consider the component of the shock front making angle  $\theta$  to the vertical, so that the planes of variation of thermodynamical parameters are inclined at an angle  $\theta$  to the shock surface which is assumed to be plane.

It is found that the rate of increase of shock velocity decreases as  $\theta$  increases, being the maximum in vertical direction. In figure 2, the variation of shock velocity is shown for  $\theta = 0, \pi/6, \pi/4$  as the shock propagates in the troposphere. In figure 3 the shock envelope at different intervals of time is drawn.

### FORMULATION OF THE PROBLEM

If we take the point of explosion as origin and denote it by O,  $r_0$  the radius vector,  $\theta$  the angle made by the radius vector to the vertical and  $g_0$  the acceleration due to gravity at a distance  $r_0$  from the origin, then

$$g_\theta = g_s \left( \frac{R_0}{R_0 + r_0 \cos \theta} \right)^2 \quad \dots (1)$$

where  $g_s$  the value of  $g_0$  at the surface of the earth, and  $R_0$  the radius of the earth

We assume that there is an explosion at the point O, which is on the surface of the earth. Shock wave created by the explosion propagates in all directions. We consider the component of the shock which propagates along the radius vector  $r_0$  and inclined at an angle  $\theta$  to the vertical. For simplicity we assume that the shock front is plane.

Let  $p_s, \rho_s, T_s$ , and  $p_0, \rho_0, T_0$  be the pressure, density and absolute temperature at the surface of the earth and at a radial distance  $r_0$ , and  $u, U, p, \rho, r, \bar{R}, t$ , and  $g$  be the dimensionless fluid velocity, shock velocity, gas pressure, density, radius vector, earth's radius, time, and acceleration due to gravity, given by Singh (1969) in equation (4). Then equations of motion in terms of dimensionless parameters are given by

$$\left. \begin{aligned} \frac{\partial \rho}{\partial t} + u \frac{\partial \rho}{\partial r} + \rho \frac{\partial u}{\partial r} &= 0 \\ \frac{\partial u}{\partial t} + u \frac{\partial u}{\partial r} + \frac{1}{\rho} \frac{\partial p}{\partial r} + \left( \frac{\bar{R}}{\bar{R} + r \cos \theta} \right)^2 \cos \theta &= 0 \\ \frac{\partial}{\partial t} (p \rho^{-\gamma}) + u \frac{\partial}{\partial r} (p \rho^{-\gamma}) &= 0 \end{aligned} \right\} \quad \dots (2)$$

In equilibrium conditions the variation of pressure in the atmosphere is given by

$$\frac{dp}{p} = - \left( \frac{\bar{R}}{\bar{R} + r \cos \theta} \right)^2 \frac{\cos \theta}{T} dr \quad \dots (3)$$

where  $T$  is the dimensionless absolute temperature such that at the surface of the earth

$$p_s = R \rho_s T_s \quad \dots (4)$$

$R$  being the gas constant. Here we have assumed that there is no wind in the troposphere

When shock created at point O reaches the distance  $\xi$ , jump conditions across the shock front at  $r = \xi$  are, (Pai, 1959, Singh 1969)

$$\left. \begin{aligned} \rho_2(u_2 - U) &= -\rho U \\ p_2 - p &= \rho u_2 U \\ \frac{\gamma}{\gamma-1} \frac{p_2}{\rho_2} + \frac{(u_2 - U)^2}{2} &= \frac{\gamma}{\gamma-1} \frac{p}{\rho} + \frac{U^2}{2} \end{aligned} \right\} \quad \dots (5)$$

where  $p_2, \rho_2, u_2$  are the values of  $p, \rho, u$  behind the shock front and  $\gamma$  being adiabatic gas constant. Quantities behind the shock front are functions of  $\xi$  and  $t$  whereas, ahead the shock front they are functions of  $\xi$  alone,  $\xi$  being the shock position. It is assumed that fluid velocity  $u$  in front of the shock is zero. Solving relations (5) for  $u_2, p_2, \rho_2$  in terms of Mach number  $M$ , defined as

$$M = U/(\gamma p/\rho)^{\frac{1}{2}}$$

we get

$$\left. \begin{aligned} u_2(\xi, t) &= \frac{2c}{(\gamma+1)} \{M-M^{-1}\} \\ p_2(\xi, t) &= \frac{\gamma p}{(\gamma+1)} f(M) \\ \rho_2(\xi, t) &= \frac{(\gamma+1)\rho M^2}{g(M)} \end{aligned} \right\} \quad \dots (6)$$

where

$$\left. \begin{aligned} f(M) &= \left\{ 2M^2 - \frac{\gamma-1}{\gamma} \right\} \\ g(M) &= \{2 + (\gamma-1)M^2\} \\ c^2 &= \gamma p / \rho \end{aligned} \right\} \quad \dots (7)$$

To visualize the problem we must know four unknown variables  $u_2$ ,  $p_2$ ,  $\rho_2$  and  $M$  in terms of  $p$ ,  $\rho$ . To relate these four variables we have three jump conditions (6). One extra relation between these four variables is required, which we get from the rule devised by Whitham (1958). According to the rule, we write equations of motion just behind the shock front along the positive characteristic axis. In this equation we substitute the expressions for  $u_2$ ,  $p_2$ ,  $\rho_2$  from (6).

Equation of motion along the positive characteristic axis, just behind the shock front is

$$dp_2 + \rho_2 c_2 du_2 + \frac{\rho_2 c_2}{u_2 + c_2} \left( \frac{\bar{R}}{\bar{R} + \xi \cos \theta} \right)^2 \cos \theta d\xi = 0 \quad \dots (8)$$

where  $\xi$  is the shock position. Using relations (6) in (8) and after some simplifications we get,

$$\begin{aligned} 2\{(M^2+1)h(M) + 2M^2\} \frac{dM}{M} + f(M) \frac{dp}{p} + 2(M^2-1)h(M) \frac{dc}{c} \\ + \left( \frac{\bar{R}}{\bar{R} + \xi \cos \theta} \right)^2 \frac{(\gamma+1)^2 M^2 h(M) \cos \theta d\xi}{c^2 \{2(M^2-1) + \sqrt{\gamma f g}\}} = 0 \end{aligned} \quad \dots (9)$$

where,

$$h(M) = \sqrt{\frac{\gamma f(M)}{g(M)}} \quad \dots (10)$$

Relation (9) gives the variation of  $M$ , if  $p$  and  $c$  are known. If the variation of absolute temperature is known, the pressure can be found from (3) and thus  $M$  can be calculated from (9).



We discuss below the variation of  $M$  as the shock propagates in the troposphere. As the height of troposphere is very small compared to the radius of the earth, our assumption, that the earth's surface round the location is plane, is justified.

#### SHOCK WAVES IN THE TROPOSPHERE

In the troposphere, which extends upto a height of 10 kilometers above the equator, the gases are in adiabatic equilibrium. In this region the variation of pressure and the equation of state in terms of dimensionless parameters  $p$ ,  $\rho$ , can be written as

$$\frac{1}{\rho} \frac{dp}{dr} = - \left( \frac{\bar{R}}{\bar{R} + r \cos \theta} \right)^2 \cos \theta \quad \dots (11)$$

$$p = \rho^\gamma \quad \dots (12)$$

Combining (11) and (12) we get after some simplifications

$$\frac{\gamma}{\gamma-1} \frac{d\rho^{\gamma-1}}{dr} = - \left( \frac{\bar{R}}{\bar{R} + r \cos \theta} \right)^2 \cos \theta \quad \dots (13)$$

Integrating (13) from the surface of the earth, where  $r = 0$ ,  $\rho = 1$  to the current point  $r$ , where density is  $\rho$ , we get,

$$\rho = \left[ 1 - \frac{\gamma-1}{\gamma} \frac{\bar{R} r \cos \theta}{\bar{R} + r \cos \theta} \right]^{\frac{1}{\gamma-1}} \quad \dots (14a)$$

From this we can easily get pressure  $p$  and temperature  $T$  as follows

$$p = \left[ 1 - \frac{\gamma-1}{\gamma} \frac{\bar{R} r \cos \theta}{\bar{R} + r \cos \theta} \right]^{\frac{\gamma}{\gamma-1}} \quad \dots (14b)$$

$$T = \left[ 1 - \frac{\gamma-1}{\gamma} \frac{\bar{R} r \cos \theta}{\bar{R} + r \cos \theta} \right] \quad \dots (14c)$$

Substituting the values of  $p$  and  $c$  at  $r = \xi$  from equations (14) and (17) in equation (9) after some simplifications we get

$$\frac{2}{M} \frac{dM}{d\xi} = K_s(M) \frac{\left( \frac{\bar{R}}{\bar{R} + \xi \cos \theta} \right)^2 \cos \theta}{\left[ 1 - \frac{\gamma-1}{\gamma} \frac{\bar{R} \xi \cos \theta}{\bar{R} + \xi \cos \theta} \right]} \quad \dots (15)$$

where

$$K_s(M) = K_1(M) + \frac{\gamma-1}{2\gamma} K_2(M). \quad \dots (15a)$$

$$K_1(M) = \frac{\left\{ f(M) - \frac{(\gamma+1)^2/\gamma M^2 h(M)}{2(M^2-1) + \sqrt{\gamma f g}} \right\}}{\{(M^2+1)h(M) + 2M^2\}} \quad \dots (15b)$$

$$K_2(M) = \frac{2(M^2-1)h(M)}{\{(M^2+1)h(M) + 2M^2\}} \quad \dots (15c)$$

In figure 1, we have drawn the value of  $K_3(M)$  *versus*  $M$ , for  $\gamma = 1.4$ . It is found that the variation of  $K_3(M)$  is small for  $M \geq 3$ , as compared to the variations of  $M$ .

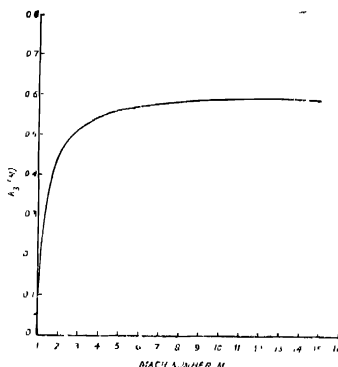


Figure 1. Variation of  $K_3(M)$  *versus*  $M$ .

From figure 1, it is seen that  $K_3(M)$  increases sharply as  $M$  increases from 1 to 3, having values 0 and 0.5156 at  $M = 1$  and 3, respectively. When  $M$  increases from 3 onward, its variation becomes negligible. We take the value of  $M$  at the surface of earth as equal to 4. Thus if we take  $K_3(M)$ , which no doubt is a function of  $M$ , as a constant and evaluate  $M$  from equation (15), the error is less than 2%. This error decreases as  $M$  increases. This fact can easily be seen from figure 1, where the curve showing the variation of  $K_3(M)$ , becomes a straight line as  $M$  becomes greater than 4.

Thus we neglect the variations in  $K_3(M)$  in the process of integration of the equation (15). Integrating (15) and taking  $K_3(M)$  as a constant during integration, we get,

$$M = M_s \left[ 1 - \frac{\gamma-1}{\gamma} \frac{\bar{R} \xi \cos \theta}{\bar{R} + \xi \cos \theta} \right] - \frac{\gamma}{\gamma-1} \frac{K_3}{2} \quad \dots (16)$$

where  $M_s$  is the values of  $M$  at  $\xi = 0$ . From (16), (14) and the definition of  $M$ , we get shock velocity  $U$ , given by,

$$U = \sqrt{\gamma} M_s \left[ 1 - \frac{\gamma-1}{\gamma} \frac{R \xi \cos \theta}{R + \xi \cos \theta} \right]^{-\left( \frac{\gamma K_s}{\gamma-1} - 1 \right) / 2} \quad (17)$$

Relations (16) and (17) give the variation of Mach number and the shock velocity as the shock propagates along the radial distance at an angle  $\theta$  to the vertical. In figure 2, we have drawn the variation of shock velocity *versus* dimensionless

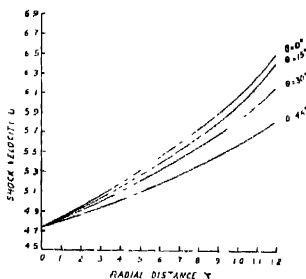


Figure 2 Variation of shock velocity  $U$  *versus* the radial distance  $\xi$ .

shock position  $\xi$  for  $\theta = 0, \pi/6, \pi/4$ . It is seen that the rate of increase of shock velocity decreases with the increase of  $\theta$

Equation (17) can be written as,

$$\Delta \xi = \sqrt{\gamma} M_s \left[ 1 - \frac{\gamma-1}{\gamma} \frac{R \xi \cos \theta}{R + \xi \cos \theta} \right]^{-\left( \frac{\gamma K_s}{\gamma-1} - 1 \right) / 2} \Delta t \quad \dots (18)$$

where

$$\frac{d\xi}{dt} = U$$

From (18) we can compute the distance  $\xi$  at a particular time  $t$ . In figure 3, we have drawn the shock envelop at different time intervals after the explosion. All the figures are drawn in the dimensionless parameters.

## CONCLUSION

In figure 2 we have plotted the variation of shock velocity in non-dimensional form. Here we have used the following data to nondimensionalize.  $g_s = 981$  cm/sec<sup>2</sup>,  $p_s = 10^6$  dynes/cm<sup>2</sup>,  $\rho_s = 1.3 \times 10^{-3}$  gm/cm<sup>3</sup>,  $\alpha = 1275.3 \times 10^{-9}$  cm<sup>-1</sup>. From computations we find that the shock velocity at a distance 9.4 km is 1.807,

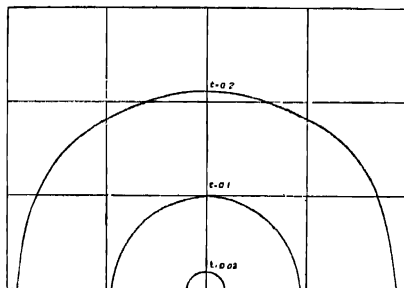


Figure 3. Position of shock front at dimensionless times 0.02, 0.1, 0.2 the origin being the point of explosion.

1.783, 1.712, 1.614 km/sec for  $\theta = 0, \pi/12, \pi/6, \pi/4$ , respectively. It is seen that the rate of increase of shock velocity is less for larger values of  $\theta$ .

In figure 3 we have drawn the shock envelope at time intervals of 0.5655, 2.8275, 5.6550 seconds, respectively. It is shown that in a specific time the distance covered by the shock wave decreases as  $\theta$  increases from 0 to  $\pi/2$ , being maximum for  $\theta = 0$ . In all the above calculations, the initial shock velocity is taken to be 1.313 km/sec

#### ACKNOWLEDGEMENT

One of us (VPS) is thankful to Col. G. S. Sawhney, Director, Terminal Ballistic Research Laboratory Chandigarh, for his permission to publish the work. Thanks are due to the referee for very useful comments.

#### REFERENCE

- Mitra S. K. 1952 *Upper Atmosphere*, Asiatic Society, Calcutta.  
 Pai S. I. 1959 *Introduction to the Theory of Compressible Flow*, D. Van Nostrand Co., N.Y.  
 Singh V. P. 1969 *Indian J. Phys.* **43**, 519.  
 Whitham G. B. 1958 *J. Fluid Mech.* **4**, 337.

## Letters to the Editor

*Indian J. Phys.* **44**, 561-564 (1970)

### Crystal and molecular structure of piperidine hydrochloride

By J. K. DATTA GUPTA AND N. N. SAHA

*Crystallography and Molecular Biology Division,  
Saha Institute of Nuclear Physics, Calcutta-9*

(Received 2 March 1971)

The structure of piperidine in the form of its different hydrohalides has been undertaken by us as a part of our major program on the structure and functions of biomolecules. The present communication deals with the structure determination of piperidine hydrochloride by heavy atom technique

Single crystals were grown by slow evaporation of an aqueous solution of this compound at room temperature. The crystals thus grown are needle shaped, the needle axis being parallel to *b*-axis. The unit cell dimensions as revealed by Weissenberg, oscillation and rotation photographs taken about *b*- and *a*-axes, using  $\text{CuK}\alpha$  radiation are :

$$\begin{aligned}a &= 9.68 \text{ \AA} \\b &= 7.40 \text{ \AA} \\c &= 9.67 \text{ \AA} \\ \alpha = \beta = \gamma &= 90^\circ\end{aligned}$$

Systematic absences of reflections in Weissenberg photographs indicate that the space group may be either *Pbcm* or *Pbc2<sub>1</sub>*. Three dimensional analysis at a later stage confirmed that the space group is *Pbcm*. Density data ( $\rho_m = 1.14$  gm/cc,  $\rho_{cal} = 1.16$  gm/cc) indicate that there are four formula units ( $\text{C}_5\text{H}_{11}\text{N.HCl}$ ) per unit cell. Multiple-film equi-inclination Weissenberg technique was used to record intensities on layers *h0l* to *h6l* and *0kl*. The position of the heavy atom (chlorine) in the unit cell was located from three dimensional Patterson synthesis. Three dimensional Fourier synthesis was computed with the phase of the heavy atom on CDC 3600 at T.I.F.R., Bombay, using the program written by Blount. A spoke and bead model was constructed which satisfied the stereochemistry.

Refinement was carried out by the method of full matrix least squares using the modified (Srikanta) program of Busing, Martin & Levy (1962) with isotropic temperature factors. The discrepancy factor  $R = \frac{\sum ||F_o| - |F_c||}{\sum |F_o|}$  at this stage was 0.14.

The structure was further refined using individual anisotropic temperature factors for the non-hydrogen atoms,  $R$ -value at this stage being 0.11. A three-dimensional difference Fourier synthesis using all the reflections revealed the hydrogen atom positions. Structure factor calculations including the hydrogen atoms were carried out and the final value is 0.094. The atomic parameters and anisotropic temperature factors for the atoms are given in table 1 and intramolecular bond lengths and bond angles are given in table 2. The

TABLE 1  
*a) Atomic parameters*

Atom	$x/a$	$y/b$	$z/c$
Cl	0.17334	0.03633	0.25
N	0.14296	0.45723	0.25
C(1)	0.34000	0.49669	0.11550
C(2)	0.19292	0.54043	0.12009
C(3)	0.40814	0.58508	0.25
C(1')	0.34690	0.49669	0.38450
C(2')	0.19292	0.54043	0.37991

*b) Anisotropic temperature coefficients\**

		$\rho_{22}$	$\rho_{33}$	$\rho_{12}$	$\rho_{13}$	$\rho_{23}$
Cl	0.00546	0.00980	0.00923	-0.00015	0.0000	0.0000
N	0.00418	0.02505	0.00327	-0.00078	0.0000	0.0000
C(1)	0.01202	0.03416	0.01866	0.00378	0.00188	0.00137
C(2)	0.01064	0.03139	0.00765	0.00592	-0.00049	0.00123
C(3)	0.00684	0.01344	0.03608	0.00312	0.0000	0.0000

\* In the expression  $T = \exp[-(\beta_{11}h^2 + \beta_{22}k^2 + \beta_{33}l^2 + 2\beta_{12}hk + 2\beta_{13}hl + 2\beta_{23}kl)]$

TABLE 2. Intramolecular bond lengths and bond angles

Bond length (Å)	Bond angle (degree)
Cl—N	3.088
N—C(2)	1.478
C(1)—C(2)	1.525
C(1)—C(3)	1.569
Cl—N—C(2)	112
N—C(2)—C(1)	105
C(2)—C(1)—C(3)	105
C(1)—C(3)—C(1')	112

pipridine ring has been found to assume a chair configuration. A mirror parallel to  $xy$  plane at  $z = 1/4$  passes through the molecule. Atoms Cl, N, C(3) lie on the mirror and C(1'), C(2') (figures 1 and 2) are mirror images of C(1) and C(2). The

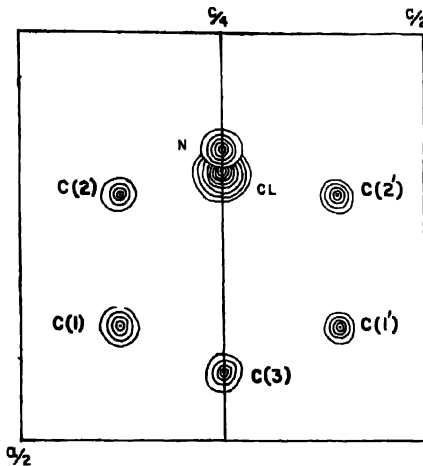


Figure 1. Piperidine hydrochloride molecule viewed along  $b$ -axis

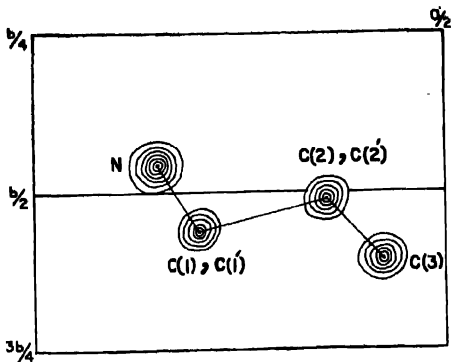


Figure 2. Piperidine hydrochloride molecule viewed along  $c$ -axis

molecules as viewed down *b* and *c*-axes are shown in figure 1 and figure 2, respectively. The molecules are held together by a three-dimensional net work of hydrogen bonds of the type N-H ... Cl, as can be seen from figure 3, a projection down *c*-axis.

At the final stage of the structural solution of this compound, our attention was drawn to a paper on this compound published by Rerat (1960) with *R* value of 0.26. In his refinement of the structure, anisotropic temperature factors were not used. The hydrogen atom positions also were not located. His findings, *e.g.* bond lengths and bond angles, differ considerably from ours. The detailed paper will be published elsewhere.

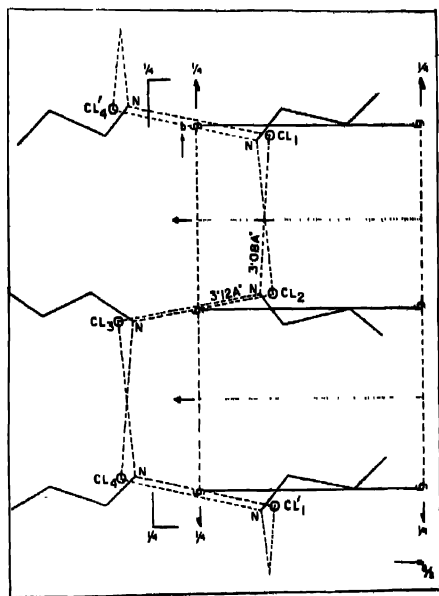


Figure 3. Intermolecular packing projected down *c*-axis.

#### REFERENCES

- Busing W. R., Martin, K. O. & Levy H. A. 1962 *Least Squares Refinement (XFLS) Programme*  
 Rerat Par C. 1960 *Acta Cryst.* **13**, 72,



## A note concerning second and third order optical and magneto-optical activity

BY DEBASHIS MUKHERJEE AND MIHIR CHOWDHURY

*Presidency College, Calcutta-12*

(Received 22 May, 1971)

Recently the optical rotatory dispersion (ORD) and circular dichroism (CD) and their magnetic analogues—the magneto-optical rotatory dispersion (MORD) and magnetic circular dichroism (MCD) have received considerable interest in spectral investigations of molecular structure (Buckingham & Stephens 1966). For light of very high intensity, *e.g.* a laser beam, the molecular response to the light is nonlinear and this gives rise to multiphoton absorption and harmonic generation (Armstrong *et al* 1962). We have looked into the significance of bi-photonic absorption and second harmonic generation in relation to optical and magneto-optical rotations, and have derived expressions for the latter.

We have used the formalism of quantized field and have decomposed the electric and the magnetic field vector of the light in terms of Fourier components and Creation and Annihilation operators (Heitler 1953). The expressions for rotation of the plane of polarization of the incident light and its ellipticity are obtained as the expectation values of the corresponding Stokes operators (Jauch & Rohrlich 1955). In our description of the near-resonance processes, the generalised perturbation theory of Heitler & Ma (1949) revived by Hameka (1962) was used. The process of second harmonic generation does not conserve the total number of photons, and therefore, we have resorted to an oscillatory coherent wave-packet description of the incident light.

Our main conclusions are as follows :

- 1) The optical and magneto-optical rotations should show a dispersion anomaly at the second harmonic frequency corresponding to the biphotonic absorption band.

The general expression for the complex rotation is given by

$$\hat{\rho}_{non-linear} = \frac{8\pi^2 I \omega N}{\hbar^2 c} \sum_{l,l',m} A_{l,l',m} \frac{\omega(2\omega^2 + 2\omega_l \omega_{l'} + \omega_l \omega_m + \omega_{l'} \omega_m) \text{Im}(\tilde{D}_{ll'm} + \tilde{M}_{ll'm})}{(\omega^2 - \omega_l^2 + i\omega_l \gamma_l)(\omega^2 - \omega_{l'}^2 + i\omega_{l'} \gamma_{l'})} \\ - \frac{i(\omega_m \omega^2 + \omega_m \omega_l \omega_{l'} + 2\omega^2 \omega_l + 2\omega^2 \omega_{l'}) \text{Re}(\tilde{D}_{ll'm} + \tilde{M}_{ll'm})}{(4\omega^2 - \omega_m^2 + 2i\omega_m \gamma_m)}$$

Here  $I$  is the intensity of the incident light beam of frequency  $\omega$ ;  $\omega_l$ ,  $\omega_{l'}$  and  $\omega_m$  are excitation energies for states  $l$ ,  $l'$  and  $m$ , respectively;  $\gamma_l$ ,  $\gamma_{l'}$  and  $\gamma_m$  are the corresponding band-widths; and  $\bar{A}$  denotes averaging with respect to molecular orientations. The matrix elements  $\tilde{D}_{l'm}$  and  $\tilde{M}_{l'm}$  are given by

$$\tilde{D}_{l'm} = D_{yxx} + D_{xyx}$$

$$\tilde{M}_{l'm} = M_{jyx} + M_{syjx} + M_{xyjy} + M_{yjjx} - M_{jxx} - M_{xjx}$$

where

$D_{\alpha\beta\gamma\delta}$  and  $M_{\alpha\beta\gamma\delta}$  are the abbreviations of

$$\langle \alpha | D_\alpha | l \rangle \langle l | D_\beta | m \rangle \langle m | D_\gamma | l' \rangle \langle l' | D_\delta | a \rangle \text{ and}$$

$$\langle \alpha | M_\alpha | l \rangle \langle l | D_\beta | m \rangle \langle m | D_\gamma | l' \rangle \langle l' | D_\delta | a \rangle \text{ respectively.}$$

Quantities like  $D_\alpha$  and  $M_\alpha$  denote the component of electric and magnetic dipole operators, respectively, and  $|a\rangle$  the ground state of the molecules.

(2) The third order optical birefringence is observable only for molecules lacking planes of reflection symmetry, and third order optical rotation is observable only for molecules lacking planes of reflection symmetry and/or inversion symmetry—the requirements being the same as those for linear birefringence and optical activity, respectively. These follow from the symmetries of matrix-elements  $\tilde{D}_{l'm}$  and  $\tilde{M}_{l'm}$ .

(3) If an intense polarized light beam, containing a small amount of coherently matched similarly polarised second harmonic, is allowed to pass through a substance along or perpendicular to the direction of the magnetic field, a magneto-optical rotation of the second harmonic may occur due to the production of a second harmonic polarised perpendicular to the incident beam.

(4) An optical rotation of a generated second harmonic should occur for a set-up as in (3) in the absence of a magnetic field for crystals lacking centre of inversion symmetry, the conditions being the same as those for second harmonic generation.

(5) The above non-linear effects will be observable at high photon densities ( $\approx 10^{23}$ ) achievable with laser source.

The dispersion curves for the above non-linear processes contain contribution from states which are ordinarily inaccessible due to the forbiddenness of the ordinary transitions. In addition, the high-lying excited states might be located by observing the dispersion anomaly of the inducing light due to third order optical and Faraday rotation. The linear dispersion anomaly in this case may be very difficult to observe because of technical difficulties to be faced at short wave lengths.

The details of the derivation and expressions for the above-mentioned non-linear effects will be published soon

#### REFERENCES

- Armstrong J. A., Bloembergen N., Ducuing J. & Pershan P. S. 1962 *Phys. Rev.* **127**, 1918.  
Buckingham A. D. & Stephens P. J. 1966 *Ann. Rev. Phys Chem.* and references therein.  
Hammett H. F. 1962 *J. Chem. Phys.* **36**, 2540  
Heitler W. 1953 *The Quantum Theory of Radiation*, Oxford University Press.  
Heitler W. & Ma S. T. 1949 *Proc. Roy. Irish Acad.* **52**, 100.  
Jauch J. & Rohrlich F. 1955 *Electrons and Photons*, New York.

## BOOK REVIEW

### *The Structure and Chemistry of Solid Surfaces*

Edited by Gabor A. Somorjai, *John Wiley & Sons Inc., New York, London, Sydney, Toronto*, 1969 (pp 1573+XXIV), price \$ 37.50

The Inorganic Material Research Division of Lawrence Radiation Laboratory organized several symposia on material science during the last couple of years. The International Conference on "The Structure and Chemistry of the Solid Surfaces" held at the University of California, Berkeley during June 17-21, 1968 was the fourth in the series. The total number of papers presented was about 84 and the present book is the photo offset lithographic reproduction of the above papers. The above topic has attained new importance in recent times and hence a co-ordinated approach, both from theoretical and experimental points of view, especially on recent advances in the study of surface structure, chemistry of solid surfaces, nature of adsorbed layers, electronic and atomic structures of clean surface, etc. is no doubt a timely one. Numerous experimental results by LEED technique, field ion and field emission microscopy, electron spectroscopy, molecular beam scattering method, ellipsometry, etc were presented at the above Conference. Majority of the papers, however, deals with LEED technique, a very powerful tool, for the study of surface layer of clean single crystals, and also of the adsorbed layers formed by exposure to different environments. The authors emphasised not only the importance of the technique but also the pitfalls involved due to the complexities in interpretations of LEED patterns. The theoretical approach mainly concerns with the energetic conditions of surfaces of clean as well as adsorbed layers. Some of the papers are quite exhaustive and the length varies from 20-50 pages in a number of cases. One important technique namely HEED method has however been completely left out of the scope of present conference probably due to the paucity of time.

This book will be an asset to anyone interested in the surface structure and its chemistry and must be kept in all libraries. Considering the volume of this book, contributions from so many well-known authors and the quality of reproduction, the price is not high, though it may be well beyond the purse of an individual.

A. G

# INDIAN JOURNAL OF PHYSICS

VOL. 44

No. 11

AND

VOL. 53

PROCEEDINGS

No. 11

OF THE

INDIAN ASSOCIATION FOR THE CULTIVATION OF SCIENCE

*(Edited in collaboration with the Indian Physical Society).*

IJPYAS 44 (11) 569-616 (1970)

NOVEMBER 1970

PUBLISHED BY THE  
INDIAN ASSOCIATION FOR THE CULTIVATION OF SCIENCE  
JADAVPUR, CALCUTTA-32



## Interaction of electromagnetic field with matter (angular momentum basis)

By B. S. RAJPUT

*Department of Physics, Kurukshetra University, Kurukshetra*

(Received 22 December 1970)

Reduced expansions of electromagnetic fields are derived in terms of irreducible representations of proper, orthochronous, inhomogeneous Lorentz group in angular momentum basis. The second quantized expansions, derived by replacing photon wavefunctions and their complex conjugates by annihilation and creation operators in the reduced expansion, are given in terms of vector spherical harmonics with annihilation and creation operators as amplitudes. For calculating the interaction Hamiltonian, when electromagnetic field is coupled to an atom, the second quantized expansion of three components transverse electromagnetic vector potential is used to avoid fictitious photons of helicity other than  $\pm j$  (spin) and subsidiary state vector condition and to overcome the difficulty of vanishing amplitude for emission or absorption of photon as  $p \rightarrow 0$ . The selection rules, derived in the relativistically quantized manner, are identical with already known selection rules for classical radiation fields, except that here the photon takes or supplies angular momentum to conserve the total angular momentum of the system.

### INTRODUCTION

It has been shown by Koba, Tati & Tomonago (1947) and Schwinger (1948) that to pass over from the Heisenberg representation to the interaction representation, the supplementary condition due to Fermi for the electromagnetic field has to be modified by adding a charge term because this condition involves one difficulty that there is no normalized state which satisfies it, as shown by Ma (1949) and Belinfante (1949). To overcome this difficulty, Gupta (1950) has given a new treatment for the longitudinal part of the electromagnetic field where an indefinite metric has been used for scalar photons. Weinberg (1965) preferred to avoid indefinite metric and photons of helicity other than  $\pm j$  (spin) by treating them as the rough conclusions of the fact that no symmetric tensor fields of rank  $j$  can be constructed from the creation and annihilation operators of massless particles of spin  $j$ . He further proved that the most general covariant field that can be constructed from such operators cannot represent real photon interaction because they give the amplitudes for emission and absorption of massless particles which vanish as  $p^j$  for momentum  $p \rightarrow 0$ .

The transformation of the first order Lorentz gauge formulation into the radiation gauge was done by Schwinger (1963) by decomposing the complementary fields into longitudinal and transverse fields and by eliminating the longitudinal fields (spin-zero components) from the physical quantities. This elimination of

longitudinal fields is always advantageous for the physical system containing photons, as proved by Weinberg (1964) that the zero mass has a special kind of dynamical self-consistency for spin-1 (transverse part) which it would not have for zero-spin (longitudinal part).

To avoid the use of fictitious photons of helicity other than  $j$  or the indefinite metric and subsidiary state-vector conditions and to overcome the difficulty of vanishing amplitude for emission or absorption of photons as  $p \rightarrow 0$ , we use here the three components transverse electromagnetic vector potential, curl of which gives the fields, for the study of interaction of electromagnetic fields. For this purpose we use our results of reduction of electromagnetic fields, in linear (Rajput 1970a) and angular (Rajput 1969a) momentum basis, to the irreducible representation of proper, orthochronous, inhomogeneous Lorentz group. These results have been derived by using our results for the reductions of antisymmetric tensor (Rajput 1969b, 1969c) scalar (Rajput 1969d) and three-components vector (Rajput 1969e) fields. Using these results, we also derived the reductions of generalized electromagnetic fields in presence of magnetic monopoles, for zero (Rajput 1970b) and nonzero (Rajput & Singh 1970) mass systems. In all these reduced expansions we decomposed the complementary fields into longitudinal and transverse parts, and omitted the longitudinal and scalar parts by setting them equal to zero for the physical systems.

To second quantize the electromagnetic fields the photon wavefunctions and their complex conjugates, in their reduced expansions on angular momentum basis, are replaced by annihilation and creation operators. Using these second quantized reduced expansions the interaction Hamiltonian, for the study of interaction of electromagnetic fields with atom, has been calculated. The selection rules derived here are identical to those derived by Blatt-Weiskopf (1952) and Rose (1957) for classical fields, except that here the photon takes or supplies the angular momentum in order to conserve the total angular momentum of the atomic system. The probability of the emission of a photon by an atom is proved proportional to  $(n+1)$  where  $n$  is the number of photons of a given kind in the interacting field. This explains the spontaneous emission, since the probability for no photon in the system is different from zero. Using similar procedure we have derived similar results for linear momentum representation in an earlier paper (Rajput 1970c). Our procedure, in contrast with that of Davydov (1965), is completely relativistic where photon wavefunctions are introduced explicitly.

#### REDUCTION OF ELECTROMAGNETIC FIELDS IN ANGULAR MOMENTUM BASIS

In the angular momentum basis a wavefunction is given in terms of magnitude of linear momentum  $p$ , the total angular momentum quantum number  $k$ , the quantum number  $m$  of  $J_z$  (the  $z$ -components of angular momentum) and the helicity  $\lambda$ . In this basis the reduced expansions of electric and magnetic fields are defined as (Rajput 1969a),



$$\begin{aligned}
\vec{E}(\mathbf{x}, t) &= E_1(\mathbf{x}, t) + E_1^*(\mathbf{x}, t) \\
\vec{H}(\mathbf{x}, t) &= H_1(\mathbf{x}, t) + H_1^*(\mathbf{x}, t)
\end{aligned}
\quad \dots \quad (1)$$

where

$$\begin{aligned}
E_1(\mathbf{x}, t) &= -4\pi/(3\pi)^{\frac{1}{2}} \sum_{\lambda=\pm 1} \sum_{\beta=0, \pm 1} \vec{\chi}(\beta) \sum_{k=1}^{\infty} \sum_{m=-k}^k (i)^{k+1+\beta-\lambda} \exp\{i\pi(\lambda-m/2)\} \\
&\times Y_k^{m,\lambda}(\theta, \phi) Y_1^{\beta,\lambda*}(\theta, \phi) Y_k^{m0}(\hat{\theta}, \hat{\phi}) Y_k^{m,0*}(\theta, \phi) \\
&\times \int dp/p \cdot j_k(pr) F(p, k, m, \lambda) \exp(-ipt)
\end{aligned}
\quad \dots \quad (2)$$

and

$$\begin{aligned}
H_1(\mathbf{x}, t) &= -4\pi/(3\pi)^{\frac{1}{2}} \sum_{\lambda=\pm 1} \sum_{\beta=0, \pm 1} \vec{\chi}(\beta) \sum_{k=1}^{\infty} \sum_{m=-k}^k \lambda(i)^{k-\lambda+\beta} \exp\{i\pi(\lambda-m/2)\} \\
&\times Y_k^{m,\lambda}(\theta, \phi) Y_1^{\beta,\lambda*}(\theta, \phi) Y_k^{m,0}(\hat{\theta}, \hat{\phi}) Y_k^{m,0*}(\theta, \phi) \\
&\times \int dp/p \cdot j_k(pr) F(p, k, m, \lambda) \exp(-ipt)
\end{aligned}
\quad \dots \quad (3)$$

where  $F(p, k, m, \lambda)$  is the wavefunction of the photon and  $\vec{\chi}(\beta)$  is a vector having the following components

$$\begin{aligned}
\vec{\chi}(\beta) &= (2)^{\frac{1}{2}}(1, i\beta, 0) \quad \text{for } \beta = \pm 1 \\
\vec{\chi}(0) &= -i(0, 0, 1) \quad \text{for } \beta = 0
\end{aligned}$$

$Y_k^{m,\lambda}(\theta, \phi)$  etc in equation (3) are the generalized spherical harmonics for  $\theta, \phi$  as the polar angles of the linear momentum vector  $\vec{p}$  given by

$$\vec{p} = p(\sin \theta \cos \phi, \sin \theta \sin \phi, \cos \theta). \quad \dots \quad (5)$$

$j_k(pr)$ , for  $r = |\mathbf{x}|$ , is spherical Bessel function of order  $k$ , and  $\hat{\theta}, \hat{\phi}$  are the polar angles of the vector  $\vec{x}$ .

Using the transposition theorem of generalized spherical harmonics we have

$$Y_k^{m-\beta,0*}(\theta, \phi) = (i)^{2\beta-2m} Y_k^{0,m-\beta}(\theta, \phi)$$

$$Y_1^{\beta,\lambda}(\theta, \phi) = (i)^{2\beta-2\beta} Y_1^{\lambda,\beta}(\theta, \phi),$$

and

$$Y_m^{\lambda,m}(\theta, \phi) = (i)^{2\lambda-2m} Y_k^{\lambda,m*}(\theta, \phi)$$

Substituting these results in equation (2) we get

$$\begin{aligned} E_1(\vec{x}, t) = & -4(\pi/3)^{\frac{1}{2}} \sum_{\lambda=\pm 1} \sum_{\beta=0, \pm 1} \vec{\chi}(\beta) \sum_{k=1}^{\alpha} \sum_{m=-k}^k (i)^{k+\beta+\lambda+1-m} \\ & \times Y_{k,\lambda,m}^*(\theta, \phi) Y_{1,\lambda,\beta}(\theta, \phi) Y_{k,m-\beta,0}(\hat{\theta}, \hat{\phi}) Y_{k,0,m-\beta}(\theta, \phi) \\ & \times \int dp/p \cdot j_k(pr) F(p, k, m, \lambda) \exp(-ipt) \quad \dots (6) \end{aligned}$$

On expanding the product and using the orthogonality relations for the generalized spherical harmonics, we get

$$\begin{aligned} Y_{k,0,m-\beta}(\theta, \phi) Y_{1,\lambda,\beta}(\theta, \phi) = & \sum_{J=|k-1|}^{k+1} \left[ \frac{3(2k+1)}{4\pi(2J+1)} \right]^{\frac{1}{2}} (k, m-\beta, 1, \beta | k, 1, J, m) \\ & \times (k, 0, 1, \lambda | k, 1, J, \lambda) Y_{J,\lambda,m} \quad \dots (7) \end{aligned}$$

and

$$\int_0^{2\pi} d\phi \int_0^{2\pi} d\theta \sin \theta Y_{j,m,n}^*(\theta, \phi) Y_{j',m',n}(\theta, \phi) = \delta_{j,j'} \delta_{m,m'} \quad \dots (8)$$

In equation (7) Clebsch-Gordan coefficients are used in the form  $(j, m, j', m' | j, j', J, M)$ .

When equations (7) and (8) are substituted in equation (6) it reduces to,

$$\begin{aligned} E_1(\vec{x}, t) = & (2)^{\frac{1}{2}} \sum_{\lambda} \sum_{k=1}^{\alpha} \sum_{m=-k}^k (i)^{k-m+1} \\ & \times [Y_{k,\lambda,m}(\theta, \phi) \int p dp j_k(pr) F(p, k, m, \lambda) \exp\{-ipt\} \\ & - i\lambda\{k/(2k+1)\}^{\frac{1}{2}} Y_{k,k+1,m}(\theta, \phi) \int p dp j_{k+1}(pr) F(p, k, m, \lambda) \exp\{-ipt\} \\ & + i\lambda\{(k+1)/(2k+1)\}^{\frac{1}{2}} Y_{k,k-1,m}(\theta, \phi) \int p dp j_{k-1}(pr) F(p, k, m, \lambda) \exp\{-ipt\}] \quad \dots (9) \end{aligned}$$

where the vector spherical harmonics  $Y_{k,k',m}(\theta, \phi)$  are defined as

$$Y_{k,k',M}(\theta, \phi) = \sum_{m,\beta} (i)^{\beta+1} \vec{\chi}(\beta) Y_{k,m-\beta,0}(\hat{\theta}, \hat{\phi}) (k', m, 1, \beta | k', 1, k, M)$$

In deriving equation (10) we have used the values of Clebsch-Gordan coefficients. In a similar manner the reduction of magnetic field also can be derived as the following expression

$$\begin{aligned} H_1(\vec{x}, t) = & (2)^{\frac{1}{2}} \sum_{\lambda} \sum_{k=1}^{\alpha} \sum_{m=-k}^k (i)^{k-m} \\ & \times [\lambda Y_{k,k,m}(\theta, \phi) \int p dp j_k(pr) F(p, k, m, \lambda) \exp\{-ipt\} \\ & - i\{k/(2k+1)\}^{\frac{1}{2}} Y_{k,k+1,m}(\theta, \phi) \int p dp j_{k+1}(pr) F(p, k, m, \lambda) \exp\{-ipt\}, \\ & + i\{(k+1)/(2k+1)\}^{\frac{1}{2}} Y_{k,k-1,m}(\theta, \phi) \int p dp j_{k-1}(pr) F(p, k, m, \lambda) \exp\{-ipt\}] \quad (10) \end{aligned}$$

The three-dimensional vector potential  $\vec{A}(\vec{x}, t)$  of electromagnetic field is given by

$$\begin{aligned} E(\vec{x}, t) &= -\frac{\partial}{\partial t} \vec{A}(\vec{x}, t) \\ H(\vec{x}, t) &= \text{curl } \vec{A}(\vec{x}, t) \end{aligned} \quad (11)$$

Using equations (9) and (10) in equation (11) the reduction of electromagnetic potential to the irreducible representation of inhomogeneous, orthochronous, proper Lorentz group in angular momentum basis can be derived as the following expansion

$$\begin{aligned} A_1(\vec{x}, t) &= (2)^{\frac{1}{2}} \sum_{\lambda=\pm 1} \sum_{k=1}^{\infty} \sum_{m=-k}^k (i)^{k-m} \\ &\times [Y_{k,k,m}(\theta, \phi) \int dp j_k(p) F(p, k, m, \lambda) \exp(-ipt) \\ &- i\lambda \{k(2k+1)\}^{\frac{1}{2}} Y_{k,k-1,m}(\theta, \phi) \int dp j_{k-1}(p) F(p, k, m, \lambda) \exp(-ipt) \\ &+ i\lambda \left\{ \frac{k+1}{2k+1} \right\}^{\frac{1}{2}} Y_{k,k-1,m}(\theta, \phi) \int dp j_{k-1}(p) F(p, k, m, \lambda) \exp(-ipt)] \dots \quad (12) \end{aligned}$$

where

$$A_1(\vec{x}, t) + A_1^*(\vec{x}, t) = A(\vec{x}, t)$$

The vector spherical harmonic  $Y_{k,k,m}(\theta, \phi)$  in equations (9) and (10) which corresponds to the angular momentum quantum number  $k$  of total angular momentum  $J$  and the parity  $(-1)^{J+1}$  can be considered as transverse magnetic vector spherical function. The transverse electrical vector spherical function which corresponds to angular quantum number  $(k+1)$  and parity  $(-1)^{J+1}$  can be considered as

$$Y_{k,k+1,m}(\theta, \phi) = 1/(2J+1)^{\frac{1}{2}} [J(J+1)^{\frac{1}{2}} Y_{k,k+1,m}(\theta, \phi) + (J+1)(J)^{\frac{1}{2}} Y_{k,k-1,m}(\theta, \phi)]$$

The longitudinal and scalar functions, which are derived from the scalar electromagnetic vector and the fourth component of vector electromagnetic potential corresponding to  $\lambda = 0$  in the reduction, do not contribute at all so far so as physical effects are concerned.

#### SECOND QUANTIZATION OF ELECTROMAGNETIC FIELDS IN ANGULAR MOMENTUM BASIS

To second quantize the electromagnetic fields in the angular momentum representation; the photon wavefunction  $F(p, k, m, \lambda)$  and its complex conjugate in the reduced expansions of  $\vec{E}(\vec{x}, t)$  and  $\vec{H}(\vec{x}, t)$  are replaced by annihilation and

creation operators  $b(p, k, m, \lambda)$  and  $b^*(p, k, m, \lambda)$ , respectively. These operators satisfy the following commutation rules

$$\begin{aligned} [b(s), b(s')] &= [b^*(s), b^*(s')] = 0 \\ [b(s), b^*(s)] &= \delta(p-p')\delta_{k,k'}\delta_{m,m'} \end{aligned} \quad \dots \quad (13)$$

where  $s$  denotes the collection of variables  $p, k, m$  and  $\lambda$ . In terms of these operators the Hamiltonian  $H$  and number of operator  $N$  are given as follows

$$\begin{aligned} H &= 1/2 \sum_{\lambda} \int [b^*(s)b(s) + b(s)b^*(s)] dp \\ &= \sum_{\lambda} \int [b^*(s)b(s) + 1/2] dp \\ &= \sum_{\lambda} \int [n(s) + 1/2] dp \end{aligned} \quad \dots \quad (14)$$

$$\begin{aligned} N &= (2)^{-1} \sum_{\lambda} \int [b^*(s)b(s) + b(s)b^*(s)] \frac{dp}{p} \\ &= \sum_{\lambda} \int [b^*(s)b(s) + 1/2] \frac{dp}{p} \\ &= \sum_{\lambda} \int [n(s) + 1/2] \frac{dp}{p} \end{aligned} \quad \dots \quad (15)$$

where  $n(s) = b^*(s)b(s)$  is the operator of the number of photons with variables denoted by  $s$ . The poynting vector operator  $\vec{P}$  can also be expressed in terms of annihilation and creation operators, as follows

$$\begin{aligned} \vec{P} &= e \vec{\epsilon} (8\pi)^{-3} \sum_{\lambda} 1/2 \int [b^*(s)b(s) + b(s)b^*(s)] dp \\ &= e \vec{\epsilon} (8\pi)^{-3} \sum_{\lambda} \int [b^*(s)b(s) + 1/2] dp \\ &= e \vec{\epsilon} (8\pi)^{-3} \sum_{\lambda} \int [n(s) + 1/2] dp \end{aligned}$$

where  $\vec{\epsilon}$  is unit vector in the direction of  $\vec{P}$ .

The  $n$ -particle basis vector for second quantization, in the angular momentum basis, is given by

$$|s_1, s_2, \dots, s_n\rangle = \frac{b^*(s_1)b^*(s_2) \dots b^*(s_n)}{(n!)^{1/2}} |0\rangle \quad \dots \quad (16)$$

where  $|0\rangle$  designates the vacuum state.

For the photons with well defined quantum state the equation (16) reduces to

$$|s_1, s_2, \dots, s_n\rangle = \frac{b^{*n}(s)}{(n!)^{1/2}} |0\rangle$$

The annihilation and creation operators act upon these basis vectors (kets) in the following manner

$$b^*(s) |s_1, s_2, \dots, s_n\rangle = \{n(s)+1\}^{\frac{1}{2}} |s_1, s_2, \dots, s_n, s\rangle \quad \dots \quad (17)$$

$$b(s) |s_1, s_2, \dots, s_n\rangle = \{n(s)\}^{\frac{1}{2}} |s_1, s_n, \dots, s_{n-1}\rangle \quad \dots \quad (18)$$

#### INTERACTION OF ELECTROMAGNETIC FIELD WITH ATOM

The number of photons in the system containing electrical charge is not constant as the photons can be emitted or absorbed. Here we study the interaction between the electromagnetic fields and an atom assuming that the system is at rest.

Neglecting the interaction, the Hamiltonian  $H_0$  of the system (atom and the field) is the sum of radiation and atomic Hamiltonians

$$H_0 = H_a + H_{rad}$$

where  $H_a$  is the Hamiltonian of the atomic system and  $H_{rad}$  is field Hamiltonian operator given by equation (14).

The interaction Hamiltonian for the present case is of the form  $\vec{A}(x, 0) \cdot \vec{v}$ , where  $\vec{v}$  is a polar vector which is a function of atomic dynamical variables. The vector  $\vec{v}$  may also be regarded as a first rank tensor, the average value of which for initial and final atomic states gives current density. Using this value of interaction Hamiltonian operator form, we can study the emission and absorption of photon by an atomic system.

*Emission* Let the initial state  $|\psi_i\rangle$  of the system without interaction be considered as containing the atom and  $n(s)$  photons, and the final state  $|\psi_f\rangle$  after the interaction as containing the atom and  $\{n(s)+1\}$  photons. Thus in the interaction the atom emits one photon with momentum  $p$ , other quantum numbers being  $k$ ,  $m$  and parity  $\pi$ . Then

$$|\psi_f\rangle = |V\rangle |\psi_i\rangle \quad \dots \quad (19)$$

where  $|V\rangle$  is the field state containing  $n(s)$  photons and  $|\psi_i\rangle$  designates the initial atomic state with quantum numbers  $k_i, m_i$  and  $\pi_i$  for the total angular momentum,  $z$ -component of angular momentum and parity, respectively.

$$|\psi_f\rangle = |s\rangle |\psi_f\rangle \quad \dots \quad (20)$$

where  $|s\rangle$  is the field state containing  $\{n(s)+1\}$  photons and  $|\psi_f\rangle$  designates the final atomic state with corresponding quantum numbers  $k_f, m_f$  and  $\pi_f$ .

The matrix element of interest for emission is given by

$$\begin{aligned}
 & \langle \psi_I | A(\vec{x}, 0) \cdot \vec{v} | \psi_F \rangle \\
 &= \langle \psi_f | \langle s | A_1^*(\vec{x}, 0) \cdot \vec{v} | V \rangle | \psi_I \rangle \\
 &= (2)^{1/2} (-i)^{k-m} \{n(s)+1\}^{1/2} j_k(pr) \langle \psi_f | Y_{k,k,m}^*(\theta, \phi) \cdot \vec{v} | \psi_I \rangle \\
 &+ i\lambda \{k/(2k+1)\}^{1/2} j_{k+1}(pr) \langle \psi_f | Y_{k,k+1,m}^*(\theta, \phi) \cdot \vec{v} | \psi_I \rangle \\
 &- i\lambda \{(k+1)/(2k+1)\}^{1/2} j_{k-1}(pr) \langle \psi_f | Y_{k,k-1,m}^*(\theta, \phi) \cdot \vec{v} | \psi_I \rangle
 \end{aligned} \quad (21)$$

where we have used equation (17) from which it is clear that only  $A_1^*(\vec{x}, 0)$  part of  $A(\vec{x}, 0)$  contributes to interaction Hamiltonian for emission, while the other part, *i.e.*  $A_1(\vec{x}, 0)$  contributes to the Hamiltonian for absorption. The matrix element given by equation (21) consists of the terms like

$$\langle \psi_f | Y_{k,k',m}^*(\theta, \phi) \cdot \vec{v} | \psi_i \rangle, \quad (k' = k, k \pm 1)$$

which can also be written in terms of quantum numbers of the initial and final states as follows

$$k_f, m_f, \pi_f | Y_{k,k',m(\pi)}^*(\theta, \phi) \cdot \vec{v} | k_i, m_i, \pi_i \rangle \quad (22)$$

where

$$Y_{k,k',m(\pi)}^* \cdot \vec{v} \text{ is an irreducible tensor of rank } k.$$

Applying Wigner-Eckart theorem, it is clear that only those matrix elements like (22) are nonvanishing for which following selection rules are satisfied

$$k_i = k_f + k, k_f + k - 1, \dots, |k_f - k| \quad \dots \quad (23)$$

$$m_i = m_f + m \quad \dots \quad (24)$$

The parity of irreducible tensor  $Y_{k,k',m(\pi)}^* \cdot \vec{v}$  is  $(-1)^{J+1} \pi_v$  for electric multipole and  $(-1)^J \pi_v$  for magnetic multipole where  $\pi_v$  (the parity of the vector  $\vec{v}$ ) is  $(-1)$  since it changes sign under reflection of coordinates and the operator for it anticommutes with parity operator. Thus the parity selection rules for photon emission are derived as

$$\begin{aligned}
 \pi_f \pi_i &= (-1)^J \quad \text{for electrical transition} \\
 \pi_f \pi_i &= (-1)^{J+1} \quad \text{for magnetic transition}
 \end{aligned} \quad \dots \quad (25)$$

The probability for the emission per unit time in the transition from  $|\psi_f\rangle$  to  $|\psi_F\rangle$  is proportional to the square of the matrix element (21). Hence, it is proportional to  $\{n(s)+1\}$ , which is nonvanishing even for  $n(s) = 0$ . The quantization of the electro-magnetic field thus explains the occurrence of spontaneous

**Absorption.** For absorption we consider the transition from the initial state  $|\psi_I\rangle$  given by equation (19) to final state  $|\psi_{f'}\rangle$  of the system containing the atom and  $\{n(s)-1\}$  photons

$$|\psi_{f'}\rangle = |s'\rangle |\psi_f'\rangle \quad \dots \quad (26)$$

where  $|s'\rangle = |s_1, s_2 \dots s_{n-1}\rangle$

The matrix element of interest in this case is

$$\begin{aligned} & \langle \psi_{f'} | \langle s' | A_1(\vec{x}, 0) \cdot \vec{v} | V \rangle | \psi_i \rangle \\ &= (2)^{1/2} \{n(s)\}^{1/2} p(i) k^{-m} | j_k(pr) \langle \psi_f | Y_{k,k,m}(\theta, \phi) \cdot \vec{v} | \psi_i \rangle \\ & - i\lambda \{k/(2k+1)\}^{\frac{1}{2}} j_{k+1}(pr) \langle \psi_f | Y_{k,k+1,m}(\theta, \phi) \cdot \vec{v} | \psi_i \rangle \\ & + i\lambda \{(k+1)/(2k+1)\}^{\frac{1}{2}} j_{k-1}(pr) \langle \psi_f | Y_{k,k-1,m}(\theta, \phi) \cdot \vec{v} | \psi_i \rangle \quad \dots \quad (27) \end{aligned}$$

By a similar method as discussed for emission, we get the following selection rules for absorption

$$k_f = k_i + k, k_i + k - 1, \dots, |k_i - k| \quad \dots \quad (28)$$

$$m_f = m_i + m \quad \dots \quad (39)$$

The probability for absorption is proportional to the number of photons of a given kind in the initial state

### DISCUSSION

The reduction of electromagnetic fields to the irreducible representations of proper orthochronous inhomogeneous Lorentz group in angular momentum basis is given by equations (9) and (10) in terms of the wavefunctions of particles of zero mass and spin-1 (transverse photons). On replacing the photon wavefunctions and their complex conjugates in these reduced expansions by annihilation and creation operators, a covariant second quantized theory is obtained in purely relativistic manner. The second quantized operator  $\vec{A}(\vec{x}, t)$  derived in this manner is a covariant quantized analogue to the expansion in multipole of classical theory due to Blatt & Weisskopf (1952). This quantized reduced expansion of  $\vec{A}(\vec{x}, t)$  in terms of vector spherical harmonics, with annihilation and creation operator as the amplitudes, is used for calculating the interaction Hamiltonian to avoid the use of fictitious photons of helicity other than  $\pm j$  (spin) and to overcome the difficulty of vanishing the amplitudes for photon emission and absorption as the momentum  $p \rightarrow 0$  (Weinberg 1965).

The probability of photon emission is proportional to the square of the matrix element given by equation (21) and thus, consists of two terms. The first term is independent of the number of photons in the electromagnetic field before emission and gives rise to spontaneous emission because it is nonvanishing even if there

is no photon initially. The second term, which is proportional to the number of photons in the interacting field, gives rise to certain induced emission. The probability of absorption of a photon, given by the square of matrix element in equation (27), depends on the energy of absorbed photon and is proportional to the number of photons in the interacting electromagnetic field. The ratio of the probability of photon emission to that of its absorption is, therefore, proportional to  $\{n(s)+1\}/\{n(s)\}$

The selection rules for emission and absorption of photons by atoms are identical to those derived by Blatt & Weisskopf (1952) classically and to those derived by Davydov (1965) non-relativistically, except that here the photon takes or supplies angular momentum, in order to conserve the total angular momentum of the system. We thus get the parallelism between the classical and quantum theories of radiation in angular momentum basis. The similarity of the selection rules verifies the validity of reduction of electromagnetic fields given in equation (9) and (10) to the irreducible representation of proper, orthochronous inhomogeneous Lorentz group on angular momentum basis because in calculating the interaction Hamiltonian we have used the reduced expansion of  $A(\vec{x}, t)$  derived from these expansions. Moreover, this similarity of the selection rules for interaction of electromagnetic fields with atom suggests the use of this relativistic quantized procedure in the study of interactions of electromagnetic field with molecules, nuclei and elementary particles. The procedure being a relativistic one will prove itself more advantageous and straightforward.

#### REFERENCES

- Belinfante F. J. 1940 *Phys. Rev.* **76**, 226.  
 Blatt J. M. & Weisskopf V. F. 1952 *Theoretical Nuclear Physics, Appendix B*.  
 Davydov A. 1965 *Quantum Mechanics* (Translated, edited with addition by D. Ter Haar). 571  
 Gupta S. N. 1950 *Proc. Phys. Soc.* **A63**, 681  
 Koba Z., Tai T. & Tomonago S. 1947 *Prog. Theo. Phys.* **2**, 101.  
 Ma S. T. 1949 *Phys. Rev.* **75**, 535.  
 Rajput B. S. 1969a *Indian J. Pure Appl. Phys.* **7**, 823.  
 Rajput B. S. 1969b *Indian J. Phys.* **43**, 135.  
 Rajput B. S. 1969c *Indian J. Phys.* **43**, 439.  
 Rajput B. S. 1969d *Indian J. Pure Appl. Phys.* **7**, 720.  
 Rajput B. S. 1969e *Indian J. Phys.* **43**, 602.  
 Rajput B. S. 1970a *Nuovo Cimento* **66A** 517.  
 Rajput B. S. 1970b *Indian J. Pure Appl. Phys.* **8**, 297  
 Rajput B. S. 1970c *Nuovo Cimento* **2B**, 45.  
 Rajput B. S. & Singh R. N. 1970 *Indian J. Pure Appl. Phys.* **8**, 439.  
 Rose M. E. 1957 *Elementary Theory of Angular Momentum* (New York).  
 Schwinger J. 1948 *Phys. Rev.* **74**, 1439.  
 Schwinger J. 1963 *Phys. Rev.* **130**, A02.  
 Weinberg S. 1964 *Phys. Rev.* **135B**, 1049.  
 Weinberg S. 1965 *Phys. Rev.* **138B**, 988.



## Response of a moving-coil galvanometer in a vacuum tube circuit

BY S. D. CHATTERJEE and ARUN KUMAR GUPTA

*Indian Association for the Cultivation of Science, Jadavpur,  
Calcutta-32*

(Received 11 February 1971)

The nature of response of a moving-coil galvanometer to an exponentially decreasing input voltage pulse in a VTVM circuit has been theoretically analysed. The output pulse, as revealed by the galvanometer deflection consists of the following two components :

- (i) first component decreases exponentially with time;
- (ii) second component varies sinusoidally with time, having constant amplitude, provided the effect of galvanometer damping is negligible. However, when the damping is effective, the amplitude of the oscillatory component decreases exponentially with time

These findings have been experimentally verified as far as practicable.

### INTRODUCTION

It is customary to use a high-impedance device for measuring voltage and a low impedance device for measuring current. However, for measurement of very small voltages and currents, just the reverse is true, since power is required to operate the instrument. For example, if the number of turns per unit cross-section is changed in a galvanometer coil, the quantity that is held constant for a given deflection is the power (*i.e.*  $I^2R$  or  $E^2/R$ ). Hence high current sensitivity requires a high-resistance coil, and high voltage sensitivity requires a low-resistance coil.

For the most sensitive galvanometer made the power per unit deflection is approximately  $10^{-10}W$ . Thus the best voltage sensitivity is about  $10^{-9}V$  (for  $R \approx 10$  ohms) and the best current sensitivity is about  $10^{-11}$  amp (for  $R \approx 1000$  ohms)

For measurements of currents smaller than about  $10^{-10}$  or  $10^{-11}$  amp, a galvanometer becomes impractical, and an electrometer, which is essentially a voltage measuring instrument with a sensitivity of the general order of 1 mv per scale deflection, can be used in conjunction with a shunt resistor of  $10^{12}$  ohms to obtain a sensitivity of  $10^{-15}$  amp. Alternatively, a simple nonfeedback type electronic amplifier consisting of an electrometer type tube with a sensitive galvanometer as the plate load may be used. The grid current for large bias voltages is made very small for proper tube design and may be about  $10^{-16}$  amp for the best tubes. The fundamental circuit, is a single-tube dc amplifier, in which the ionisation

current or photo-electric current passes through a grid-leak resistance ( $\sim 10^{12}$  ohms) and the resulting voltage alters the grid potential of the electrometer tube. The consequent change in plate current is read on the galvanometer. Montgomery & Montgomery (1940) have discussed the circuit diagram of a vacuum tube electrometer when used in conjunction with an Ionization Chamber. Swann (1946) has published the replica of a cosmic ray nuclear burst as recorded by such an arrangement. Weisz & Ramsey (1942) have used a more elaborate arrangement to study the ionizing capacity of individual particles of cosmic ray ionization. The charge produced by each discharge in a proportional counter is converted into a voltage pulse, which is amplified by a three stage linear amplifier and fed into a vacuum-tube voltmeter consisting of a type-38 tube. Finally the pulse is recorded photographically by the amount of deflection of a galvanometer, whenever a ray passes through a path in the proportional counter tube which is defined by three trays of GM counters in a telescopic arrangement.

Detailed analysis of the influence of the time-constants of various coupling stages of a linear amplifier has been worked out by Wilson (1941) and Chatterjee (1944). Lewis (1942) has also indicated the distorted form of an ionization chamber pulse, after three-stage amplification by a R-C coupled linear amplifier.

It may be noted, however, that in almost all the cases cited above, the galvanometer has been used merely as an indicating instrument, whose deflection has been assumed to be proportional to the amplitude of the input pulse. No account has been taken of the influence of the galvanometer constants in influencing the size and the wave-form of the output pulse. These factors have now been taken into consideration in determining the nature of response of a moving coil galvanometer in a vacuum-tube circuit whose input is a transient pulse simulating an Ionization Chamber pulse. The relevant circuit is actually that of a valve tube voltmeter (VTVM). Since a voltage sensitive galvanometer is essentially a low resistance instrument, it cannot be used in a high impedance circuit. And so a single-stage dc electronic amplifier is used to amplify the signal and to match a high input impedance to that of a sensitive d'Arsonval type galvanometer. In our present set up, the galvanometer has been transformer coupled to the plate load of the vacuum tube in order to avoid the balancing of plate-current for zero adjustment.

#### THEORETICAL CONSIDERATIONS

A galvanometer has been transformer coupled to the plate load of the vacuum tube (triode) as shown in figure 1. A transient voltage pulse,

$$e = e_0 e^{-t/\tau}$$

where  $t$  = time and  $\tau$  = time-constant of the grid-system, has been applied between the grid and the filament of the triode,

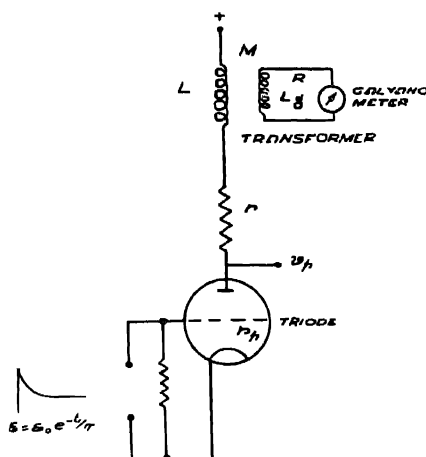


Figure 1. Basic vacuum tube circuit.

Assuming that plate current  $i_p$  and plate voltage  $v_p$  represent changes from steady current conditions,

$$i_p = \frac{v_p}{r_p} + \mu e \quad \dots (1)$$

where  $r_p$  = plate resistance of the tube and  $\mu$  = amplification factor.

The plate of the triode consists of a protective resistance  $r$  in series with the primary of an air-core transformer, while the secondary is coupled to a moving coil galvanometer.

#### (a) Basic equations

Now, if  $L$  be the co-efficient of self-inductance of the primary and  $L_g$  that of the galvanometer circuit and  $M$  the mutual inductance, then the governing equations are the following

$$L \frac{di_p}{dt} + M \frac{di_g}{dt} + r i_p + v_p = 0 \quad \dots (2)$$

and

$$L_g \frac{di_g}{dt} + M \frac{di_p}{dt} + R i_g = 0 \quad \dots (3)$$

where  $i_g$  = current in the galvanometer circuit,  $R$  = total resistance in the galvanometer circuit,

Eliminating  $di_p/dt$  between the equations (2) and (3) and then substituting  $v_p$  by the value as obtained from equation (1)

$$(LL_g - M^2) \frac{di_g}{dt} + LR i_g - M(r + r_p)i_p = -M\mu\epsilon_0 e^{-t/\tau} \quad \dots (4)$$

Differentiating equation (4) and then eliminating  $di_p/dt$  with the help of equation (3),

$$A \cdot \frac{d^2 i_g}{dt^2} + B \cdot \frac{di_g}{dt} + C i_g = \frac{M\mu\epsilon_0}{\tau} e^{-t/\tau} \quad \dots (5)$$

where

$$A = LL_g - M^2$$

$$B = LR + (r + r_p) \cdot L_g$$

$$C = (r + r_p) \cdot R$$

(b) *Solution for  $i_g$  with large plate resistance  $r_p$*

It will, at this stage, be desirable to make such approximations as will apply to the present case. The quantity  $r_p$  is of the order of  $10^5$  ohms. There is no need for  $r$  to have more than a protective significance. In view of this large value of  $r_p$ , the auxiliary equation of the equation (5) will have the roots

$$-\frac{R}{L_g} \text{ and } -\frac{r_p}{L - \frac{M^2}{L_g}}$$

while the dominant term in the denominator of the particular integral will be

$$r_p(R\tau - L_g\tau)$$

Thus, determination of complementary function and particular integral under the above specification leads the solution of equation (5) into the form :

$$i_g = \frac{M\mu\epsilon_0}{r_p(R\tau - L_g)} \left[ e^{-t/\tau} + \alpha \cdot e^{-\frac{Rt}{L_g}} + \beta \cdot e^{-\frac{r_p t}{L - \frac{M^2}{L_g}}} \right] \quad \dots (6)$$

and

$$\frac{di_g}{dt} = \frac{M\mu\epsilon_0}{r_p(R\tau - L_g)} \cdot \left[ -\frac{e^{-t/\tau}}{\tau} - \alpha \frac{R}{L_g} e^{-\frac{Rt}{L_g}} - \beta \frac{r_p}{L - \frac{M^2}{L_g}} \cdot e^{-\frac{r_p t}{L - \frac{M^2}{L_g}}} \right] \quad \dots (7)$$

At  $t = 0$ ,  $i_g = 0$  and  $i_p = 0$

Hence from equation (6)

$$1 + \alpha + \beta = 0, \quad \dots (8)$$

and from the equations (4) and (7),

$$\left(\frac{di_g}{dt}\right)_{t=0} = -\frac{M\mu\epsilon_0}{L L_g - M^2} = -\frac{M\mu\epsilon_0}{r_p(R\tau - L_g)} \left[ \frac{1}{\tau} + \frac{\alpha R}{L_g} + \frac{\beta r_p}{1 - \frac{M^2}{L_g}} \right]$$

$$\approx -\frac{M\mu\epsilon_0}{R\tau - L_g} - \frac{\beta}{L - \frac{M^2}{L_g}} \text{ (approximately)}$$

since  $r_p$  is large.

Therefore,

$$\beta = \frac{R\tau}{L_g} - 1$$

$$\alpha = -(\beta + 1) = -\frac{R\tau}{L_g} \quad \text{by equation (8).}$$

Substituting these values of  $\alpha$  and  $\beta$  in equation (6)

$$i_g = \frac{M\mu\epsilon_0}{r_p(R\tau - L_g)} \left[ e^{-t/\tau} - \frac{R\tau}{L_g} \cdot e^{-Rt/L_g} + \left( \frac{R\tau}{L_g} - 1 \right) e^{-L_g r_p t / (L L_g - M^2)} \right] \quad \dots (9)$$

### (c) Galvanometer deflection with negligible damping

Due to the current  $i_g$ , the galvanometer coil would be deflected through an angle  $\theta$ . If  $R$  be large enough so that the damping in the galvanometer circuit is negligible, then the differential equation giving  $\theta$ , is

$$K \frac{d^2\theta}{dt^2} + C\theta = \frac{JG^1}{r_p} \frac{M\mu\epsilon_0}{(R\tau - L_g)} \left[ e^{-t/\tau} - \frac{R\tau}{L_g} e^{-Rt/L_g} + \left( \frac{R\tau}{L_g} - 1 \right) e^{-r_p L_g t / (L L_g - M^2)} \right] \quad \dots (10)$$

where  $K$  = moment of inertia of the suspended system and  $JG^1$  galvanometer constant.

Solving this equation (10) under the initial conditions viz ,

$$\text{at } t = 0, \quad \theta = 0 \quad \text{and} \quad \frac{d\theta}{dt} = 0$$

and introducing the quantity  $\tau_g$  defined by  $\tau_g = \frac{L_g}{R}$ , the deflection  $\theta$  is,

$$\theta = \frac{W}{4\pi^2} \left[ \frac{e^{-t/\tau}}{1 + \frac{T^2}{4\pi^2\tau^2}} - \frac{\frac{\tau}{\tau_g} e^{-t/\tau_g}}{1 + \frac{T^2}{4\pi^2\tau_g^2}} + \frac{\sin\left(\frac{2\pi t}{T} - \phi_1\right)}{\left(1 + \frac{T^2}{4\pi^2\tau^2}\right)^{\frac{1}{2}}} - \frac{\frac{\tau}{\tau_g} \sin\left(\frac{2\pi t}{T} - \phi_2\right)}{\left(1 + \frac{T^2}{4\pi^2\tau_g^2}\right)^{\frac{1}{2}}} \right] \quad \dots (11)$$

where  $T$  = free period of the galvanometer,

$$\tan \phi_1 = \frac{2\pi\tau}{T}, \quad \tan \phi_2 = \frac{2\pi\tau_g}{T}$$

and

$$W = \frac{4\pi^2 \cdot JG^{\frac{1}{2}} \cdot M\mu\epsilon_0}{Cr_p(R\tau - L_g)}$$

The solution (11) has been written on neglecting the term which involves the large quantity  $\tau_p^2$  in the denominator. The equation (11) gives  $\theta$  as a function of time  $t$ ; its maximum occurs when

$$\frac{d\theta}{dt} = 0,$$

i.e. when

$$-\frac{\frac{1}{\tau} e^{-t/\tau}}{1 + \frac{T^2}{4\pi^2\tau^2}} + \frac{\frac{1}{\tau_g} \left(\frac{T}{\tau_g}\right) e^{-t/\tau_g}}{1 + \frac{T^2}{4\pi^2\tau_g^2}} + \frac{\frac{2\pi}{T} \cos\left(\frac{2\pi t}{T} - \phi_1\right)}{\left(1 + \frac{T^2}{4\pi^2\tau^2}\right)^{\frac{1}{2}}} - \frac{\frac{2\pi\tau}{T\tau_g} \cos\left(\frac{2\pi t}{T} - \phi_2\right)}{\left(1 + \frac{T^2}{4\pi^2\tau_g^2}\right)^{\frac{1}{2}}} = 0.$$

In view of the complexity of the expression, it is probably better to obtain the maximum by plotting  $\theta$  against  $t$ .

Now

$$\frac{W}{4\pi^2} = \frac{JG^{\frac{1}{2}} \cdot M\mu\epsilon_0}{Cr_p(R\tau - L_g)}$$

Since  $G$  represents the resistance of the galvanometer coil and  $R$  the resistance of the secondary of the transformer,

$$R = R_c + G$$

and so

$$\frac{W}{4\pi^2} = \frac{J \cdot \mu \epsilon_0}{cr_p \tau} \cdot \left( \frac{G^2 \cdot M}{R_c + G - \frac{L_g}{\tau}} \right)$$

Also for a given coil space in the secondary and a fixed primary,  $L_g$  is proportional to the square of the number of turns and so to  $R_c$ ; hence  $L_g/\tau$  becomes equal to  $gR_c$ , where  $g$  is the constant of proportionality.

Also  $M$  is proportional to  $R_c^{\frac{1}{2}}$ . Thus for a given resistance  $R_1$  of the primary coil,  $G = R_c(1-g)$  for a maximum and the maximum is proportional to  $R_c^{\frac{1}{2}}/R_c^{\frac{1}{2}}$ , and so, is independent of  $R_c$ . Of course,  $\theta$  involves  $G$  and  $R_c$  other than through  $W$ . However, the importance of  $G$  and  $R$  relationship lies in  $W$ .

Now,  $JG^{\frac{1}{2}}$  is the coefficient of current in the expression for couple per unit angle of twist. Hence for a deflection  $\delta\theta$  due to a current  $\delta i_g$ ,

$$c\delta\theta = JG^{\frac{1}{2}} \cdot \delta i_g.$$

If  $\sigma$  be the current sensitivity of the galvanometer, then

$$\sigma = \lim_{\delta i_g \rightarrow 0} \frac{\delta\theta}{\delta i_g} = \frac{JG^{\frac{1}{2}}}{c},$$

and so

$$\frac{W}{4\pi^2} = \frac{\sigma M \mu \epsilon_0}{r_p R \tau \left( 1 - \frac{\tau_g}{\tau} \right)}$$

This looks as though  $\theta$  tends to become infinite as  $\tau_g$  approaches  $\tau$ ; but it may be noted also that as  $\tau_g$  approaches  $\tau$ , the quantity inside the square bracket in equation (11) tends to become zero. It is of interest to inspect the order of

$$\frac{\sigma M \mu \epsilon_0}{r_p R \tau}.$$

If  $\sigma$  be of the order of  $10^9$ ,  $\mu \approx 10^3$  and  $\epsilon_0 \approx 10^{-5}$ , thus remembering that  $r_p = 10^5$  and  $\tau = 10^{-1}$ , it may be seen that

$$\frac{\sigma M \mu \epsilon_0}{r_p R \tau} \approx \frac{10^9 \times 10^3 \times 10^{-5}}{10^5 \times 10^{-1}} \cdot \frac{M}{R} = 1000 \frac{M}{R}.$$

(d) *Galvanometer deflection after a long interval of time*

It is interesting to note the amplitude of oscillation long after the incident pulse had been applied to the input terminals i.e. at  $t = \infty$ .

At  $t = \infty$ , as follows from equation (11),

$$\theta_{\infty} = \frac{\sigma M \mu \epsilon_0}{r_p R \tau \left(1 - \frac{\tau_g}{\tau}\right)} \left[ \left( \frac{x}{1+x^2} - \frac{y^2/x}{1+y^2} \right)^2 + \left( \frac{1}{1+x^2} - \frac{y/x}{1+y^2} \right)^2 \right] \sin(\zeta - \phi)$$

where  $\tan \phi = \frac{\frac{1}{1+x^2} - \frac{y/x}{1+y^2}}{\frac{x}{1+x^2} - \frac{y^2/x}{1+y^2}}$

$$x = \frac{T}{2\pi\tau}, y = \frac{I}{2\pi\tau_g}, \zeta = \frac{2\pi t}{T}$$

and  $\frac{y}{x} = \frac{\tau}{\tau_g}$

( $x$  and  $y$  are constants but  $\zeta$  varies with time  $t$ ).

Hence the amplitude of  $\theta_{\infty}$  is

$$|\theta_{\infty}| = \frac{\sigma M \mu \epsilon_0}{r_p R \tau \left(1 - \frac{\tau_g}{\tau}\right)} \left[ \frac{1}{1+x^2} + \frac{y^2/x^2}{1+y^2} - 2 \frac{(y^2+y/x)}{(1+x^2)(1+y^2)} \right]^{\frac{1}{2}} \quad \dots (12)$$

It is of interest to investigate  $|\theta_{\infty}|$  for different values of  $y$  and  $x$ .

*Case I*

Let  $y/x = 1 + \eta$ , such that  $\eta^2$  is negligible. If  $y = 1$ , the result is indeterminate. Substituting this in equation (12) and remembering that  $\eta$  is small,

$$|\theta_{\infty}| = \frac{\sigma M \mu \epsilon_0}{r_p R \tau_g \eta} \left[ \frac{2\eta \left( 1 - \frac{x^2}{1+x^2} - \frac{1}{1+x^2} \right)}{1+x^2} \right]^{\frac{1}{2}}$$

The radical vanishes, as it should, to the first order.

*Case II*

Let  $y/x = 10$ ,  $x = 2$ ,  $y = 20$ .

Substituting these in equation (12)

$$\begin{aligned} |\theta_{\infty}| &= \frac{\sigma M \mu \epsilon_0}{r_p R \tau (0.9)} \left[ \frac{1}{5} + \frac{100}{(1+400)} - \frac{2(400+10)}{5(1+400)} \right]^{\frac{1}{2}} \\ &= \frac{\sigma M \mu \epsilon_0}{r_p R \tau (0.9)} \cdot [0.2 + 0.25 - 0.4]^{\frac{1}{2}} \quad \text{approximately.} \end{aligned}$$



Therefore

$$\frac{|\theta_{\infty}|}{\frac{\sigma M \mu \epsilon_0}{r_p R \tau}} = \frac{2.23}{9}$$

Furthermore, let  $y/x = 10$ ,  $x = 4$ ,  $y = 40$

In this case, by substitution in equation (12)

$$|\theta_{\infty}| = \frac{\sigma M \mu \epsilon_0}{r_p R \tau (0.9)} \left[ \frac{1}{17} + \frac{1600}{16(1+1600)} - \frac{2(1600+40/4)}{(1+16)(1+1600)} \right] \\ = \frac{\sigma M \mu \epsilon_0}{r_p R \tau (0.9)} \left( \frac{1}{16^2} \right) \quad \text{approximately}$$

Hence

$$\frac{|\theta|}{\frac{\sigma M \mu \epsilon_0}{r_p R \tau}} = \frac{0.625}{9}$$

Hence it is important to have  $x$  not so large. Remembering that where  $T$  = free period of the galvanometer and  $\tau$ , the time-constant of the grid system, it is advantageous to have the free period of the galvanometer to be small and the time constant of the grid system correspondingly large.

*Note:* By making  $y/x$  very small, the quantity inside the square bracket in equation (12), may be approximated to  $[1(1+x^2)]^{\frac{1}{2}}$ . This is reasonable because it is equivalent to lengthening  $\tau$  to some extent although the external factor  $1-\tau_g/\tau$  is admittedly affected.

#### (c) Conclusion

The expression for  $\theta$  in equation (11) suggests that the galvanometer deflection is a consequence of two components. (i) One of these decreases exponentially with time, and (ii) the other varies sinusoidally with time, provided the galvanometer damping factor is negligibly small.

The exponential component dominates so long as the time  $t$  is comparable with the time constant of the grid system and also with the time constant of the galvanometer circuit.

After a long interval, only the sinusoidal component persists. The amplitude of this component depends upon the following:

- (i) time constant  $\tau$  of the grid system
- (ii) free period  $T$  of the galvanometer
- (iii) time constant  $\tau_g$  of the galvanometer-circuit.

The amplitude may also be increased by decreasing the quantities  $T/2\pi\tau$  and  $\tau/\tau_g$ . Since  $T$  is fixed for a given galvanometer, it is advantageous to increase both  $\tau$  and  $\tau_g$ , to get a larger amplitude. Furthermore, it may be seen that the quantity inside the square bracket in equation (12) is maximum when  $T' = 2\pi\sqrt{\tau\tau_g}$  i.e. when the free-period of the galvanometer is  $2\pi$  times the geometric mean of the time constants of the grid system and the galvanometer circuit.

It has been mentioned earlier that an increase in  $\tau_g$  is an advantage. This can be done by decreasing the resistance  $R$  in the galvanometer circuit. However, if  $R$  be diminished beyond a certain limit, the damping factor in the galvanometer will prevail which will nullify the equation (10) governing the galvanometer motion

(f) *Solution without approximations*

In the foregoing derivation, the solution for the galvanometer deflection  $\theta$  has been obtained under the following assumptions :

(i) the plate resistance  $r_p$  of the vacuum tube is large in comparison with similar elements in the circuit;

and (ii) the damping factor in the galvanometer circuit is negligibly small.

These approximations have been removed in the following steps. For the sake of simplicity it will be convenient to adopt the following notations :

$$g_0 = 1 - \frac{M^2}{LL_g}$$

$$\frac{1}{\lambda_1} = \frac{B}{2A} - \left( \frac{B^2}{4A^2} - \frac{C}{A} \right)^{\frac{1}{2}}$$

$$\frac{1}{\lambda_2} = \frac{B}{2A} + \left( \frac{B^2}{4A^2} - \frac{C}{A} \right)^{\frac{1}{2}}$$

$$\frac{1}{\lambda_0} = \frac{1}{\lambda_2} - \frac{1}{\lambda_1} = 2 \left( \frac{B^2}{4A^2} - \frac{C}{A} \right)^{\frac{1}{2}}.$$

$\tau$  = time constant of grid system,  $\tau_g = L_g/R$ ,  $\tau_p = L/(r+r_p)$ .

$T_1$  = time constant of galvanometer circuit with  $L_g$  coupled to  $L$  as in use.

$T'$  = damped galvanometer period divided by  $2\pi$ .

$T$  = undamped galvanometer period divided by  $2\pi$ .

In terms of these notations, the solution of the equation (5), under the initial conditions, viz.;

$$\text{at } t = 0, i_g = 0, i_p = 0, \text{ and } \left( \frac{di_g}{dt} \right)_{t=0} = -\frac{M\mu\epsilon_0}{g_0LL_g}$$

$$\text{is } i_g = \frac{M\mu\epsilon_0}{h_0} \left[ e^{-t/\tau} + \alpha \cdot e^{-t/\lambda_1} + \beta \cdot e^{-t/\lambda_2} \right] \quad \dots (13)$$

where  $h_0 = R(r+r_p)\tau \left[ 1 - \frac{\tau_g}{\tau} - \frac{\tau_p}{\tau} + \frac{\tau_p \tau_g}{\tau^2} \cdot g_0 \right]$ ,

$$\alpha = \lambda_0 \left( \frac{1}{\tau} - \frac{1}{\lambda_2} - h \right),$$

$$\beta = \lambda_0 \left( h + \frac{1}{\lambda_1} - \frac{1}{\tau} \right) - 1.$$

$$h = \frac{h_0}{g_0 L L_g}.$$

Taking into consideration the damping of the galvanometer, the deflection  $\theta$  arising due to  $i_g$ , satisfies the differential equation

$$K \frac{d^2 \theta}{dt^2} + b \frac{d\theta}{dt} + c\theta = \frac{JG^t \cdot M\mu\epsilon_0}{h_0} \left[ e^{-t/\tau} + \alpha \cdot e^{-t/\lambda_1} + \beta \cdot e^{-t/\lambda_2} \right]$$

where  $JG^t$  is the co-efficient of  $i_g$  in the expression of couple and  $b$ , a constant. In view of the relations

$$T^2 = K/c, \text{ and } b = \frac{2K}{T_1} = 2c \frac{T^2}{T_1},$$

the above equation of motion becomes

$$\frac{d^2 \theta}{dt^2} + 2 \frac{d\theta}{T_1 dt} + \frac{1}{T^2} \theta = -\frac{JG^t \cdot M\mu\epsilon_0}{h_0} \left[ e^{-t/\tau} + \alpha e^{-t/\lambda_1} + \beta e^{-t/\lambda_2} \right]$$

This equation when solved under the initial conditions viz.,

at  $t = 0, \theta = 0$  and  $\frac{d\theta}{dt} = 0$ ,

gives the solution

$$\begin{aligned} \theta = \frac{\sigma M \mu \epsilon_0}{h_0} & \left[ e^{-t/\tau} + \left( \frac{T'}{\tau} - \frac{T'}{T_1} \right) \cdot e^{-t/T_1} \sin \frac{t}{T'} - e^{-t/T_1} \cos \frac{t}{T'} \right. \\ & + \alpha \frac{e^{-t/\lambda_1} + \left( \frac{T'}{\lambda_1} - \frac{T'}{T_1} \right) \cdot e^{-t/T_1} \sin \frac{t}{T'} - e^{-t/T_1} \cos \frac{t}{T'}}{1 - \frac{2T^2}{\lambda_1 T_1} + \frac{T^2}{\lambda_1^2}} \\ & \left. + \beta \frac{e^{-t/\lambda_2} + \left( \frac{T'}{\lambda_2} - \frac{T'}{T_1} \right) e^{-t/T_1} \sin \frac{t}{T'} - e^{-t/T_1} \cos \frac{t}{T'}}{1 - \frac{2T^2}{\lambda_1 T_2} + \frac{T^2}{\lambda_2^2}} \right] \quad \dots (14) \end{aligned}$$

provided  $T_1 > T$ ,

where  $\sigma = \frac{JG_1}{c} = \lim_{\delta i_g \rightarrow 0} \frac{\delta \theta}{\delta i_g}$  = galvanometer sensitivity,

$$\frac{1}{\lambda_1} = \frac{1}{2g_0} \left[ \frac{1}{\tau_g} + \frac{1}{\tau_p} - \left\{ \frac{1}{\tau_g^2} + \frac{1}{\tau_p^2} + \frac{2-4g_0}{\tau_p \tau_g} \right\}^{\frac{1}{2}} \right],$$

$$\frac{1}{\lambda_2} = \frac{1}{2g_0} \left[ \frac{1}{\tau_g} + \frac{1}{\tau_p} + \left\{ \frac{1}{\tau_g^2} + \frac{1}{\tau_p^2} + \frac{2-4g_0}{\tau_p \tau_g} \right\}^{\frac{1}{2}} \right]$$

It may be observed that the quantities  $\lambda_0$ ,  $\lambda_1$ ,  $\lambda_2$  are practically always concerned with the ratios such as  $T/\lambda_1$ , etc., and so should be calculated in these terms.

Thus,

$$\frac{T}{\lambda_1} = \frac{1}{2g_0} \left[ \frac{T}{\tau_g} + \frac{T}{\tau_p} - \left\{ \frac{T^2}{\tau_g^2} + \frac{T^2}{\tau_p^2} + (2-4g_0) \frac{T^2}{\tau_p \tau_g} \right\}^{\frac{1}{2}} \right]$$

and so on

The expression for  $\theta$  in equation (14) shows that the galvanometer deflection consists of two components :

(i) one decreases exponentially with time,

and (ii) the other is damped during an oscillatory motion.

In the earlier analysis where the damping has been neglected, the oscillatory component persists and exhibits a steady amplitude. But in the present case, where damping effect dominates, the amplitude of the oscillatory component decreases exponentially with time. As the damping of the galvanometer is decreased by increasing the total resistance  $R$  of the galvanometer circuit, the rate of decrease of the amplitude of deflection of the coil diminishes.

#### EXPERIMENTAL ARRANGEMENT

Figure 2, is a diagrammatic representation of the experimental arrangement. Initially the key  $K$  is closed and a negative voltage  $(-v)$ , equal to PD across the potentiometer wire, is applied to the grid terminal of the triode vacuum tube. The condenser  $G_1$  is also charged to the same potential  $(-v)$ . When the key  $K$  is opened, the condenser  $C_1$  discharges through the resistance  $R_1$  and the grid voltage rises exponentially towards zero with a time constant  $\tau = R_1 C_1 = 10$  milliseconds approximately. The shape of the voltage pulse, recorded with a Tektronix CRO is shown in figure 3A.

Due to the exponentially varying input voltage applied to the grid, the primary current in the transformer varies with time. Consequently an emf is induced

in the transformer secondary and a current flows in the galvanometer circuit. The shape of the current pulse as revealed by the voltage drop across the resistance  $R$  in the secondary circuit is shown by the oscillogram pattern in figure 3B. It may be noted that the output current pulse does not correspond with the sharp exponential incident voltage pulse pattern. The complexity of the nature of the galvanometer current pulse has already been discussed in an earlier section.

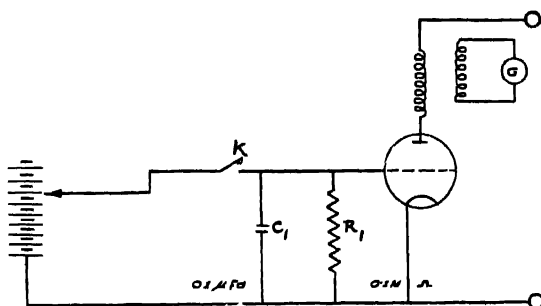


Figure 2. Schematic experimental arrangement.

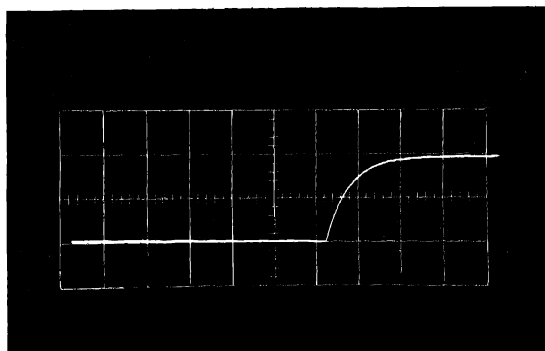


Figure 3A Oscillogram of input voltage pulse.

The actual experimental set up for recording the galvanometer deflections is schematically represented in figure 4. Light from a straight-filament lamp is focussed by means of an adjustable system of lenses so that after reflection at the galvanometer mirror, a luminous vertical line is formed on the cylindrical lens. The latter focusses this light on a narrow horizontal slit behind which a sensitive photographic paper is smoothly drawn at constant speed.

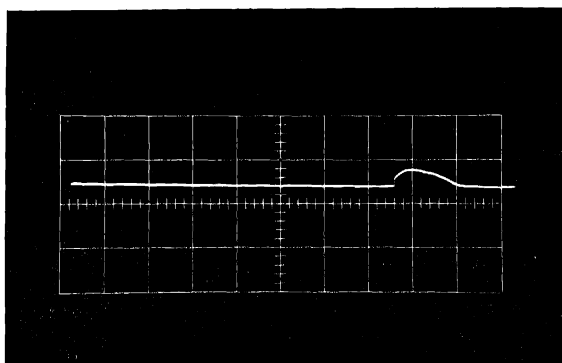
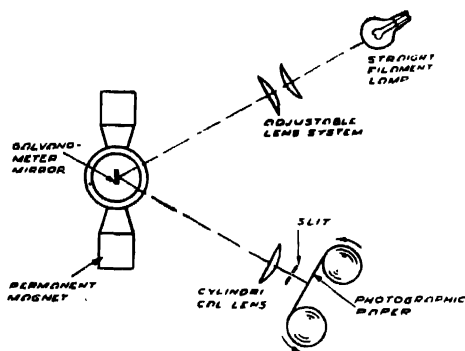


Figure 3B. Oscillogram of current pulse in the galvanometer.



#### RECORDING SYSTEM

Figure 4. Galvanometer deflection recording arrangement.

Figure 5A, is a photographic record of the resultant deflection when the galvanometer is slightly underdamped, while figure 5B represents the case when the damping factor is reduced by increasing the total resistance in the galvanometer circuit. The oscillatory motion of the galvanometer spot of light associated with its logarithmic decrement is recognizable in figure 5B.

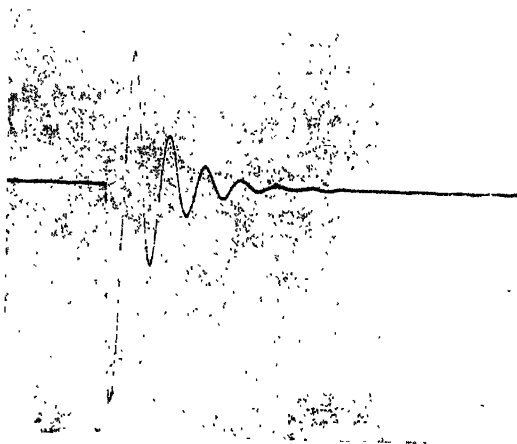


Figure 5A. Photographic record of 'slightly underdamped' galvanometer deflection.

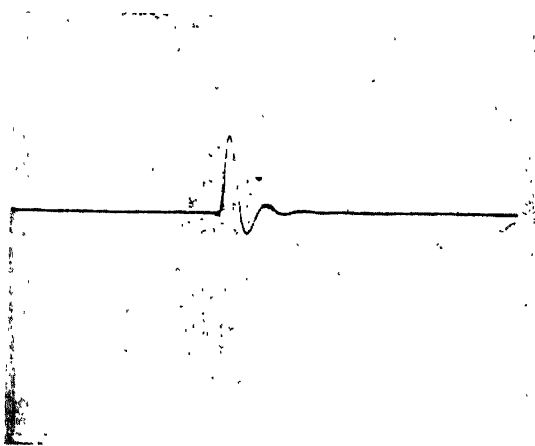


Figure 5B. Photographic record 'undamped' galvanometer deflection

Finally, the total resistance of the galvanometer circuit is made equal to its critical damping resistance. The galvanometer deflections can now be easily recorded. Figure 6 represents the calibration curve for transient pulses measured in our experimental set up. It may be noted that the calibration curve is no longer a straight line as the input pulse is increased in magnitude. This may be due to the distortion introduced by transformer coupling and the consequence of attenuating factors enunciated in earlier equations.

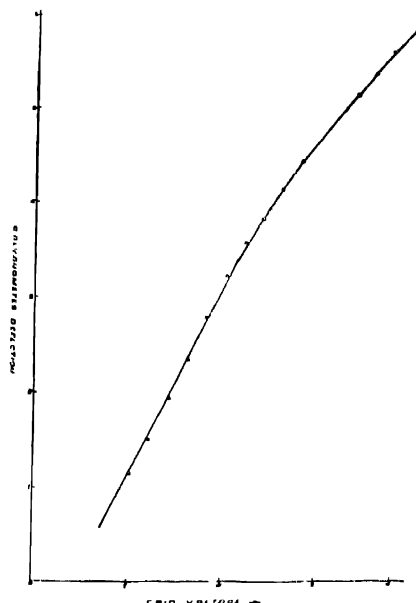


Figure 6. Calibration curve for transient input voltage pulses.

#### ACKNOWLEDGEMENT

The first author wishes to offer his respectful homage to the memory of late Dr. W. F. G. Swann, Director, Bartol Research Foundation of the Franklin Institute, who suggested the mathematical formulation of the problem more than a decade ago.

We are also grateful to the National Professor S. N. Bose, F.R.S. for his kind interest in this work.



REFERENCES

- Chatterjee S. D. 1944 *Ind. J. Phys.* **28**, 269.  
Lewis W. B. 1942 *Electrical Methods of Counting*, Cambridge University Press.  
Montgomery C. G. & Montgomery D. D. 1940 *Jour. Frank Inst.* **229**, 596.  
Swann W. F. G. 1946 *Rep. Prog. Phys.* **10**, 31.  
Weisz P. & Ramsey W. E. 1942 *Rev. Sci. Inst.* **13**, 258.  
Wilson 1941 *Proc. Roy. Soc.* **A177**, 382.

# Dielectric function of a magnetoactive degenerate plasma at relativistic temperature\*

By P. MISRA

Department of Physics, S.C.S. College, Puri

AND

K. C. ROY

Department of Physics, Anugul Science College, Anugul

(Received 13 March 1971)

Using relativistic Boltzmann-Vlasov equation, expression for the frequency and wave-number dependent dielectric function of a degenerate electron plasma is derived in presence of a steady magnetic field, which is valid at temperatures satisfying the condition  $mc^2 \ll KT$ . The result is compared with those obtained for a plasma under different physical conditions.

## INTRODUCTION

In this paper the dielectric constant of a degenerate plasma in presence of a uniform magnetic field is derived in a manner similar to our earlier work (Misra *et al* 1970). The expression is valid in the extreme relativistic limit, i.e.  $KT \gg mc^2$ , and for the case when the imposed steady magnetic field is parallel to the wave-number vector.

## DIELECTRIC FUNCTION OF A MAGNETOACTIVE RELATIVISTIC PLASMA

The linearised relativistic Boltzmann-Vlasov equation in presence of an external magnetic field can be written as

$$\frac{\partial \vec{f}(r, p, t)}{\partial t} + \frac{c \vec{p}}{(p^2 + m^2 c^2)^{3/2}} \cdot \nabla_r \vec{f}_1(r, p, t) + n_0 e \vec{E}(r, t) \cdot \nabla_p \vec{f}_0(p) - \frac{e(\vec{p} \times \vec{B})}{(p^2 + m^2 c^2)^{3/2}} \cdot \nabla_p \vec{f}_1(r, p, t) \quad \dots (1)$$

whose space-time Fourier transform, in a polar co-ordinate system  $(p, \theta, \phi)$  for  $\vec{p}$  with  $\vec{B}$  and  $\vec{k}$  along  $z$  axis, gives

$$f_1(k, p, \omega) = -\frac{n_0 A}{B} (p^2 + m^2 c^2)^{3/2} \frac{\partial f_0}{\partial p} \times \left( (E_1 \sin \theta \frac{A \sin \phi - \cos \phi}{A^2 + 1} - E_2 \sin \theta \frac{A \cos \phi + \sin \phi}{A^2 + 1} - E_3 \cos \theta \right) \quad \dots (2)$$

\*A part of the work was done at the Ravenshaw College, Cuttack

where

$$A = \frac{eB}{i[cpk \cos \theta - \omega(p^2 + m^2 c^2)^{\frac{1}{2}}]}$$

When equation (2) is substituted in the wavenumber and frequency dependent current density (Gartenhaus 1964)

$$\begin{aligned} J_{\alpha}(\vec{k}, \omega) &= -ec \int d\vec{p} \frac{p_{\alpha} f_1(\vec{k}, \omega, \vec{p})}{(p^2 + m^2 c^2)^{\frac{1}{2}}} \\ &\equiv K_{\alpha\beta}(\vec{k}, \omega) E_{\beta}(\vec{k}, \omega) \end{aligned} \quad \dots \quad (3)$$

we get the following expressions for the Response functions

$$K_{11} = K_{22} = - \frac{\pi n_0 e c}{B} \int_0^{\infty} \int_0^{\pi} \frac{A p^3 \sin^3 \theta dp d\theta}{A^2 + 1} \frac{\partial f_0}{\partial p} \quad \dots \quad (4)$$

$$K_{12} = -K_{21} = - \frac{\pi n_0 e c}{B} \int_0^{\infty} \int_0^{\pi} \frac{A^2 p^3 \sin^3 \theta d\theta dp}{A^2 + 1} \frac{\partial f_0}{\partial p} \quad \dots \quad (5)$$

$$K_{33} = - \frac{2\pi n_0 e c}{B} \int_0^{\infty} \int_0^{\pi} A \left( \frac{\partial f_0}{\partial p} \right) p^3 \cos^2 \theta \sin \theta dp d\theta \quad \dots \quad (6)$$

After some elementary calculations equations (4), (5) and (6) become,

$$K_{tr}(\pm) = - \frac{i\omega_0^2 m c}{2} \int_0^{\infty} \int_0^1 \frac{dp dx p^3 [\omega(p^2 + m^2 c^2)^{\frac{1}{2}} \pm eB] (1 - x^2)}{[\omega(p^2 + m^2 c^2)^{\frac{1}{2}} \pm eB]^2 - c^2 p^2 k^2 x^2} \times \frac{\partial f_0}{\partial p} \quad (7)$$

and

$$K_l = - i\omega_0^2 \omega m c \int_0^{\infty} \int_0^1 \frac{dp dx p^3 (p^2 + m^2 c^2)^{\frac{1}{2}} x^2}{\omega^2 (p^2 + m^2 c^2) - c^2 p^2 k^2 x^2} \frac{\partial f_0}{\partial p} \quad \dots \quad (8)$$

where  $K_{tr}(\pm) = K_{11} \pm K_{13}$  and  $K_l = K_{33}$ . From the equation (8) it is clear that in a relativistic plasma the longitudinal mode is also not affected by the magnetic field. Using the equation (7) in the relation,

$$\epsilon_{tr} = 1 - \frac{4\pi i K_{tr}(\vec{k}, \omega)}{\omega^2}$$

we can obtain the expression for the dielectric function.

## EVALUATION OF DIELECTRIC CONSTANT FOR RELATIVISTIC FERMI DISTRIBUTION

Using the value of equilibrium relativistic Fermi distribution,  $f_0$  in equation (7) we have

$$\begin{aligned} \text{Im} K_{tr}(\pm) = & \frac{\omega_0^2 m}{k^2 K T n_0 h^3 \Lambda} \times \\ & \int_0^\infty \frac{p^2 dp [\omega(p^2 + m^2 c^2)^{\frac{1}{2}} \pm eB] \exp \left[ \frac{c}{KT} (p^2 + m^2 c^2)^{\frac{1}{2}} \right]}{\left[ \frac{1}{\Lambda} \exp \left\{ \frac{c}{KT} (p^2 + m^2 c^2)^{\frac{1}{2}} \right\} + 1 \right]^2 (p^2 + m^2 c^2)^{\frac{1}{2}}} \times \\ & \left[ 1 + \frac{c^2 k^2 p^2 - [\omega(p^2 + m^2 c^2)^{\frac{1}{2}} \pm eB]^2}{2ckp[\omega(p^2 + m^2 c^2)^{\frac{1}{2}} \pm eB]} \ln \left| \frac{\omega(p^2 + m^2 c^2)^{\frac{1}{2}} \pm eB - c p k}{\omega(p^2 + m^2 c^2)^{\frac{1}{2}} \pm eB + c p k} \right| \right] \quad \dots \quad (9) \end{aligned}$$

where  $n_0 f_0(p) = \frac{2}{h^3} \left[ \frac{1}{\Lambda} \exp \left\{ \frac{c}{KT} (p^2 + m^2 c^2)^{\frac{1}{2}} \right\} + 1 \right]^{-1}$

and  $\frac{1}{\Lambda} = \exp \left[ -(\nu + \frac{mc^2}{KT}) \right]$

It can easily be shown that for  $c \rightarrow \infty$  and  $B = 0$  equation (9) reduces to the corresponding non-relativistic equation given by Misra *et al* (1962) in equation (12)

The integrals occurring in equation (9) cannot be analytically carried out. However, for temperatures,  $KT \gg mc^2$ , approximate analytical forms can be obtained by using Sommerfeld's method (1928) of integration as was done in our earlier work (Misra *et al* 1970), and we give the final result

$$\begin{aligned} \epsilon_{tr} = & 1 - \frac{3\omega_0^2}{2ck^2 v_0^3} \left[ \frac{v_0(\omega v_0 \pm \Omega c)}{\omega} \right. \\ & + \frac{c^2 k^2 v_0^2 - (\omega v_0 \pm \Omega c)^2}{2ck\omega} \ln \left| \frac{\omega v_0 \pm \Omega c + ckv_0}{\omega v_0 \pm \Omega c - ckv_0} \right| \\ & - \frac{\pi^2 \omega_0^2 K^2 T^2}{2k^2 v_0^3 m^2 c^3} \left[ 1 + \frac{c^2 k^2 - \omega^2}{2ck\omega} \ln \left| \frac{\omega v_0 \pm \Omega c + ckv_0}{\omega v_0 \pm \Omega c - ckv_0} \right| \right. \\ & \left. \left. + \frac{c(\omega c \pm \Omega v_0)[(c^2 k^2 - \omega^2)v_0 \pm \Omega c \omega]}{\omega[(\omega v_0 \pm \Omega c)^2 - c^2 k^2 v_0^2]v_0} \right] \right] \quad \dots \quad (10) \end{aligned}$$

where we have taken  $\Omega = \frac{eB}{mc}$  and  $c \ll v_0 = \left( \frac{3n_0}{8\pi} \right)^{\frac{1}{3}} \left( \frac{h}{m} \right)$ . In the limit of vanishing  $B$ , the expression for  $\epsilon_{tr}$  coincides with that obtained for the magnetic field free case (Misra *et al* 1970). Further if we put  $c = v_0$  in equation (10), the temperature independent term becomes identically equal to that obtained for non-relativistic case given by Misra *et al* (1969) in equation (5).

# DISCUSSION OF THE RESULT

Propagation of electromagnetic waves can be analysed with the aid of equation (10). As the expression is complicated and lengthy we discuss only the nature of propagation in certain limiting cases.

$$\text{Case I} \quad \frac{v_0 ck}{\omega v_0 \pm \Omega c} < 1$$

$$\text{Case II} \quad \frac{\omega v_0 \pm \Omega c}{v_0 ck} < 1$$

The first case is satisfied for  $ck < \omega$  and  $\omega v_0 > \Omega c$ . With this approximation and simple calculation, we get

$$\begin{aligned} \epsilon_{tr} &= 1 - \frac{\omega_0^2 c}{\omega(\omega v_0 \pm \Omega c)} \left[ 1 + \frac{\pi^2 K^2 T^2}{2m^2 r^2 v_0^2} \left( 1 + \frac{\omega^2}{k^2 v_0^2} \right) \right] \\ &\simeq 1 - \frac{\omega_0^2 c}{\omega(\omega v_0 \pm \Omega c)} \end{aligned}$$

We see from this equation that waves with frequencies for which

$$\omega(\omega v_0 \pm \Omega c) < \omega_0^2 c$$

cannot propagate through the relativistic degenerate plasma. Whereas the corresponding condition for a non-relativistic degenerate plasma is given by  $\omega(\omega \pm \Omega) < \omega_0^2$ , (Misra *et al* 1969).

The second case is satisfied for  $\omega v_0 \sim \Omega c$  as well as for  $\omega$ , for which  $ck > \omega$ . Under this approximation we get

$$\begin{aligned} \epsilon_{tr} &= 1 - \frac{3\omega_0^2 c(\omega v_0 \pm \Omega c)}{c^2 k^2 v_0^2 \omega} \\ &\quad - \frac{\pi^2 \omega_0^2 K^2 T^2}{2k^2 v_0^3 m^2 c^3} \left[ 1 + \frac{(c^2 k^2 - \omega^2)(\omega v_0 \pm \Omega c)}{c^2 k^2 \omega v_0} \right] \end{aligned}$$

Since the term containing temperature is small we can write

$$\epsilon_{tr}(\epsilon_{tr} - 1) \simeq - \frac{3\omega_0^2 c(\omega v_0 \pm \Omega c)}{\omega^3 v_0^2}$$

where

$$\epsilon_{tr} \simeq \frac{ck}{\omega}$$

From the above equation it is clear that for the extraordinary wave, when

$$\omega v_0 = \Omega c, \quad \epsilon_{tr} = 1$$

$$\omega v_0 > \Omega c, \quad \epsilon_{tr} < 1$$

and

$$\omega v_0 < \Omega c, \quad \epsilon_{tr} > 1$$

The equation (12) is to be compared with the corresponding equation for the non-relativistic plasma, which is quoted below from Misra *et al* (1969),

$$\epsilon_{tr}(\epsilon_{tr}-1) \simeq \frac{3\omega_0^2 c^2 (\omega \pm \Omega)}{m^2 \eta^2}$$

We then conclude that the imposition of a strong magnetic field makes plasma transparent to very low frequency electromagnetic waves which in the absence of the field cannot be propagated. The same conclusion can be made from equation (12) with the difference that magnetic field necessary to make the plasma transparent will be  $v_0/c$  times greater than that required for the non-relativistic case.

The authors are grateful to Prof. T. Pradhan of Saha Institute of Nuclear Physics, Calcutta. for suggesting the problem and for his guidance

#### REFERENCES

- Gartenhaus S. 1964 *Elements of Plasma Physics*, 107, Holt, Rinehart and Winston, New York  
 Misra P. & Misra D. 1962 *Indian J. Phys* **36**, 540.  
 Misra P. & Ray S. K. 1969 *Indian J. Phys.* **43**, 534.  
 Misra P. & Roy K. C. 1970 (*To be published in Indian J. Phys*)  
 Sommerfeld A. 1928 *Z. f. Physik* **46**, 1.

## Magnetic properties of bismuth telluride ( $\text{Bi}_2\text{Te}_3$ ) crystals

BY S. R. GUHA THAKURTA AND A. K. BOSE

*Department of Magnetism, Indian Association for the Cultivation of  
Science, Calcutta-32, India*

(Received 20 March 1971)

Rhombohedral single crystals of  $\text{Bi}_2\text{Te}_3$  (both *p* and *n* types) were prepared by horizontal zone melting apparatus set up here. The magnetic susceptibility along both the principal crystallographic directions were measured over the temperature range  $90^\circ$  to  $650^\circ\text{K}$ . The magnetic susceptibility due to carriers was separated out from the observed susceptibility. From this the energy gaps in both the principal directions were calculated and compared with values obtained from electrical measurements.

### INTRODUCTION

Various properties such as the electrical and thermal conductivities, Hall effect, Seebeck effect and magneto-resistance etc., of bismuth telluride ( $\text{Bi}_2\text{Te}_3$ ), the thermoelectrically important semiconductor, have been studied by a number of workers (Shigetomi *et al* 1956, Satherwaite *et al* 1957, Goldsmid 1957, Mansfield *et al* 1958, Drabble *et al* 1958, Delves *et al* 1961, Caywood *et al* 1970).

But investigations on its magnetic properties are rather scanty. Matyas (1958) measured the magnetic susceptibility of polycrystalline  $\text{Bi}_2\text{Te}_3$  over the temperature range of  $100^\circ$  to  $500^\circ\text{K}$  and found it to be diamagnetic, its susceptibility being temperature independent. Mansfield (1959) measured the principal diamagnetic susceptibilities of  $\text{Bi}_2\text{Te}_3$  single crystals over the temperature range of  $100^\circ$  to  $600^\circ\text{K}$  and found that the diamagnetic susceptibilities (the principal susceptibilities as well as the average value) are temperature dependent. But he could not separate the carrier susceptibility from the observed susceptibility and therefore could not discuss his observations in relation to the existing theories of magnetic properties of charge carriers. Van Deynse *et al* (1969) measured the susceptibility of  $\text{Bi}_2\text{Te}_3$  crystals from  $1.3^\circ$  to about  $300^\circ\text{K}$ . Obviously their measurements are confined to the extrinsic region only, and therefore not expected to throw any light on the intrinsic behaviour of the substance. We have therefore undertaken to study the magnetic properties of both *n* and *p* type single crystals of  $\text{Bi}_2\text{Te}_3$  over the temperature range  $90^\circ$  to  $650^\circ\text{K}$ . An account of these measurements are given in the present communication.

### EXPERIMENTAL

#### *Preparation of the crystals*

The crystals were prepared in the laboratory by the horizontal zone melting process in an apparatus set up by us. The apparatus is a modified form of the

one described by Cressel & Powel (1957). It consists of various components, viz. a speed adjustable (within the range 0.4 to 10 cms/hour) moving furnace, two water-cooled steel muffles to adjust the zone width, accompanying vacuum system, inert gas flushing system etc. The different parts of the unit are diagrammatically represented in figure 1.

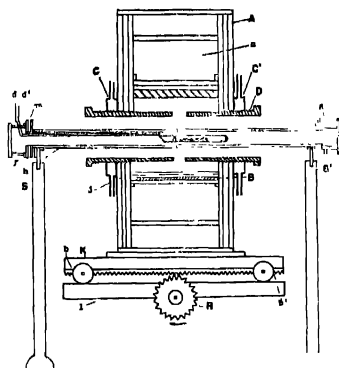


Figure 1. Schematic diagram of the horizontal zone-melt crystal growing furnace.

- |                             |  |
|-----------------------------|--|
| A—Furnace housing           | a—Quartz crucible with molten zone                           |
| B—Nichrome element          | b, b'—Ball race  |
| C, C'—Water cooled jacket   | m—Gas inlet  |
| D—Adjustable muffle         | j—Porcelain tube   |
| d, d'—Thermocouple elements | K—Saddle trolley   |
| e, e'—Glass windows         | l—Precision bed  |
| f—Gas outlet                | n—Thermal insulation   |
| g—Brass end closure         | S, S'—Adjustable holder                                      |
| h—Silica tube               | R—Electric motor driven wheel<br>(with gear-down attachment) |

For the preparation of  $\text{Bi}_2\text{Te}_3$ , we used 99.98% pure Bi and 99.97% pure Te. We purified further the Bi and Te components separately by the zone-melting process. A quantity of Bi was put in a quartz ampoule of about 5 cms length and 1 cm bore which was sealed after evacuation to  $\sim 10^{-5}$  mm of Hg. The furnace with zone width 3 mm was made to pass over the charge of Bi ten times in one direction only at the rate of 0.5 cm/hr. The temperature of the zone was kept at some value higher than the melting point ( $271.3^\circ\text{C}$ ) of Bi. The parts of the ingot which had solidified first had the highest degree of purity. But Te being similarly treated, evaporated and condensed on the inner surface of the ampoule. We therefore kept Te in the ampoule in an argon gas atmosphere (the pressure was slightly less than the atmospheric pressure) and purified it in the usual way. Bi and Te



thus refined were put in requisite proportions in a similar quartz ampoule which was sealed after being filled with argon gas at a pressure slightly lower than the atmospheric pressure. The ampoule was then placed inside the silica tube over which the furnace with the same zone width can traverse lengthwise. The furnace was now allowed to traverse the ingot ten times in one direction only at the rate of 0.5 cm/hr. The temperature of the melt was kept at about 650°C. After these operations were over, the ampoule was broken and the single crystal obtained from the ingot. For *p*-type specimens a slight excess of Bi ( $\sim 0.2\%$ ) and for *n*-type that of iodine ( $\sim 0.2\%$ ) were used as dopants. The specimens were then chemically analysed and tested by X-rays.

The basic unit cell is rhombohedral but for electrical and magnetic work the corresponding hexagonal unit cell is frequently used. We have found from our X-ray data,  $a = 4.384\text{\AA}$  and  $c = 30.487\text{\AA}$ , the three fold axis or the *c*-axis of the hexagonal system is normal to the direction of crystal growth.

### *Magnetic Measurement*

The crystals are of uniaxial type with easy cleavage, the *c*-axis being perpendicular to the cleavage plane. Therefore for the anisotropy as well as absolute susceptibility measurements, observations with the cleavage plane vertical would be sufficient.

#### (i) *Anisotropy*

A single crystal of Bi<sub>2</sub>Te<sub>3</sub> with a perfect cleavage plane was chosen and its mass measured with a Mettler microbalance (least count  $5 \times 10^{-8}$  gm). It was attached with its cleavage plane vertical at one end of a calibrated quartz fibre, the other end being fixed to a graduated torsion head. The entire system was so placed that the crystal remained suspended inside a homogeneous horizontal magnetic field. The anisotropy of the crystal was then measured by the usual "null method" developed in this laboratory (Dutta, 1954).

#### (ii) *Susceptibility*

For the measurement of susceptibility, the crystal was suspended with its cleavage plane vertical by a quartz fibre, from the free end of the arm of a jewel pivoted microbalance (Das 1963) and placed in a horizontal magnetic field with a vertical gradient, such that the magnetic force remained constant over an appreciable region (Sucksmith 1939, Dutta-Ray 1955). The magnetic force on the sample when the field was switched on was balanced by an electrodynamic balancing device (Das 1963) attached at the other end of the balance beam.

All measurements were made in dark and vacuum. For low temperature measurements the crystal remained inside the experimental chamber of a gas flow liquid oxygen cryostat (Bose 1947), the temperature of the chamber being recorded by a calibrated copper-constantan thermocouple. For measurements at high temperatures the crystal was kept within the experimental chamber

of a cylindrical furnace non-inductively wound on the outside with nichrome wire. The temperature in this case was measured by calibrated chromel-alumel thermocouple.

### RESULTS AND DISCUSSIONS

The crystal suspended with the cleavage plane vertical ( $c$ -axis horizontal) was found to set with this plane along the magnetic field and its susceptibility was diamagnetic. Therefore  $\chi_{\perp}$ , the susceptibility per unit mass in the cleavage plane was algebraically greater than  $\chi_{\parallel}$ , that along the  $c$ -axis. Therefore the measured anisotropy was  $\chi_{\perp} - \chi_{\parallel}$  and the susceptibility measured  $\chi_{\perp}$ .

The values of  $\chi_{\perp} - \chi_{\parallel}$ ,  $\chi_{\perp}$  and  $\chi_{\parallel}$  at different temperatures are given in figure 2. The values of  $\bar{\chi}$  the average susceptibility, and  $\chi_{\perp}/\chi_{\parallel}$  the ratio of susceptibilities, at 300°K of various authors including the present are given in table 1.

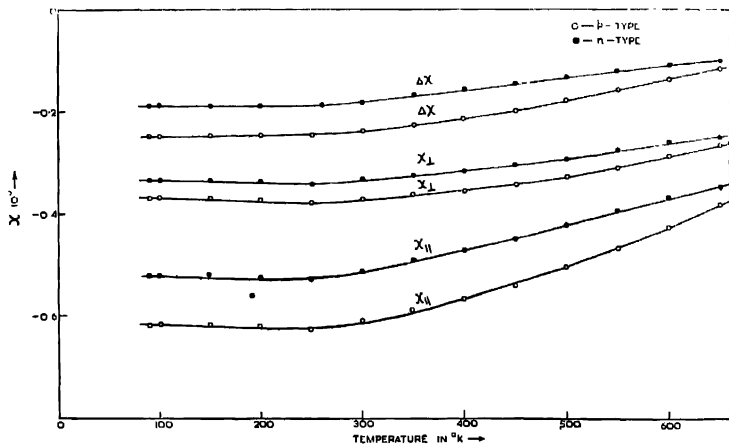


Figure 2. The variation of mass susceptibility of  $\text{Bi}_2\text{Te}_3$  with temperature.

It is observed from our results plotted in the figure 2 that both  $\chi_{\perp} - \chi_{\parallel}$  and  $\chi_{\perp}$  numerically increase with the lowering of temperature and ultimately attain a temperature independent value.

Now with the increase of temperature the thermally excited free carriers increase exponentially; but from the nature of the curve (figure 2), it is found that the total diamagnetic susceptibility gradually decreases with the increase of temperature, suggesting thereby that contributions due to the excited free carriers is paramagnetic, which can be separated as follows.

Table 1

Author	Mean mass susceptibility at 300° $\bar{\chi} \times 10^6$	Anisotropy ratio ( $\chi_{II}/\chi_L$ ) at 300°K	Susceptibility of carriers
Matyas (1958)	-0.402		
Mansfield (1958)	-0.462		Paramagnetic
Van Deynse <i>et al</i> (1969)	-0.485	1.63	
Present Authors	-0.451 ( <i>p</i> -type) -0.392 ( <i>n</i> -type)	1.64 ( <i>p</i> -type) 1.54 ( <i>n</i> -type)	Paramagnetic

The observed susceptibility  $\chi$  of a semiconducting system may be assumed to be composed of  $\chi_L$  the lattice susceptibility,  $\chi_c$  the susceptibility due to free carriers, and  $\chi_I$  the susceptibility due to impurity centres (impurity atoms or lattice defects).

Algebraically,

$$\chi = \chi_L + \chi_c + \chi_I. \quad (1)$$

$\chi_L$  was thought to be a diamagnetic term which is essentially temperature independent. But Krumhansl & Brooks (1956) have shown that this should also include a paramagnetic term, somewhat analogous to the high frequency Van Vleck paramagnetism, but having a small temperature dependence of the same order as that of the band gap, which, however, for ordinary temperatures may be neglected.  $\chi_c$  contains two temperature dependent terms: a paramagnetic term due to the spin of free carriers and a diamagnetic term due to their orbital motions in a magnetic field.  $\chi_I$  also contains two terms: a temperature independent diamagnetic contribution of the core and valence electrons of the impurity atoms and a paramagnetic temperature dependent term due to the net magnetic moment. Therefore in our case  $\chi$  may be written as

$$-\chi = \pm \chi_0 \pm \chi_c(T) + \chi_I(T) \quad (2)$$

where  $\chi_0$  is the temperature independent susceptibility arising out of all the different contributions and  $\chi$  the observed susceptibility.

Now assuming a simple Curie law for the temperature variation of  $\chi_I$  and plotting  $\chi T$  against  $T$ , we could find the contribution of  $\chi_I$  at different temperatures (which in our case was actually found to be very small, a fact also evident from the temperature independence of  $\chi$  at low temperatures). It may be pointed out in this connection that the effect of  $\chi_I$  which arises out of the ionized and non-ionized impurity centres, is generally considered negligible and from electrical

measurements it was found that the impurities were all ionized even below  $100^{\circ}\text{K}$ . Mansfield (1958) neglected the effect due to impurity. From the low temperature portion of the curve obtained by plotting  $\chi_{obs}$  vs  $T$  (figure 2), after eliminating  $\chi_I$ ,  $\chi_0$  could be found and it appeared to be diamagnetic. Subtracting  $\chi_0$  and  $\chi_I$  from  $\chi_{obs}$  we obtained  $\chi_c$ , the contribution due to free carriers which obviously is paramagnetic, and increases with the temperature.

Now it is well known (Busch & Mooser 1953) that the charge-carrier susceptibility of a semiconductor in the intrinsic range is given by

$$\chi_c = AT^{\frac{1}{2}}e^{-E_g/2kT}; \quad (3)$$

where  $A$  is a constant containing the appropriate effective masses of carriers,  $E_g$  the activation energy and the rest of the symbols have their usual significance. Plotting  $\log \chi_c T^{-\frac{1}{2}}$  against  $1/T$ , the resulting curve (figure 3) is found to have a straight portion within the temperature range  $400^{\circ}$  to  $650^{\circ}\text{K}$ , which we know from our electrical conductivity measurements to be well within the intrinsic region.

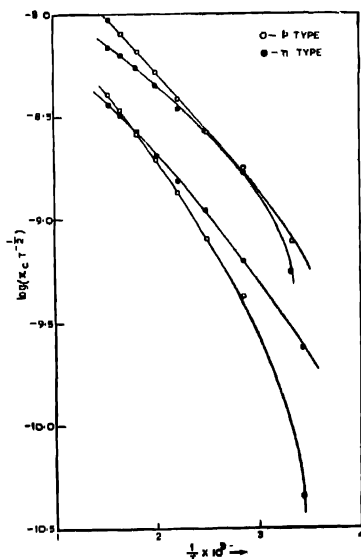


Figure 3.  $\log(\chi_c T^{-\frac{1}{2}})$  as a function of temperature

Uppercurves refer to the cases when the magnetic field is parallel to the  $c$ -axis.

Lowercurves refer to the cases when the magnetic field is perpendicular to the  $c$ -axis

From the slope of the straight line portion  $E_g$ 's were calculated and from the intercept the values of  $A$  were determined. The values of these parameters for different directions and for both  $p$ - and  $n$ -type specimens are given in table 2.

Table 2

	Crystallographic direction	By magnetic measurements		By electrical measurements
		$A \times 10^8$	$E_g$ in eV	$E_g$ in eV
$p$ -type $\text{Bi}_2\text{Te}_3$	Along $c$ -axis	5.89	0.21	0.20
	Perpendicular to $c$ -axis	2.24	0.21	0.20
$n$ -type $\text{Bi}_2\text{Te}_3$	Along $c$ -axis	4.17	0.19	0.20
	Perpendicular to $c$ -axis	1.91	0.19	0.20

The corresponding values of  $E_g$  obtained from electrical conductivity measurements are indicated in table 2. It is observed that the values of  $E_g$  obtained from two measurements may be considered to compare, in general, well with each other.

It is found from figure 3 that the curve deviates from linearity at lower temperatures. This may be due to the predominance of the effect of a constant number of extrinsic carriers in the valence or conduction band (due to very small activation energy, all the impurity centres are ionized at very low temperature and this remains constant till the intrinsic carriers are set free). Within the purely extrinsic region of our measurements i.e., below  $250^\circ\text{K}$ , where the carrier numbers as pointed out above are constant, the carrier susceptibility is an admixture of degenerate and non-degenerate regions.

A complete discussion of these effects as also the evaluation of the different fundamental parameters involved in  $A$ , requires the development of a theory for single crystals, which has recently been worked out here and calculations are in progress. This will be published in a subsequent paper.

#### ACKNOWLEDGMENT

The authors wish to express their best thanks to Shri A. K. Dutta for suggesting the problem and his constant guidance. They are also thankful to Professor A. Bose for his interest in the work.

## REFERENCES

- Bose A. 1947 *Indian J. Phys.* **21**, 275.  
Busch G. & Mooser E. 1953 *Helv Phys. Acta* **26**, 611.  
Caywood L. P. Jr. & Miller G. R. 1970 *Phys. Rev.* **B2**, 3209.  
Cressel J. G. & Powel J. A. 1957 *Prog. in Semiconductors*, **2**, 137 Heywood & Company, London.  
Das D. 1963 *Indian J. Phys* **37**, 582.  
Dolys R. T., Bowley A. E., Hazelden D. W. & Goldsmid H. J. 1961 *Proc. Phys. Soc.* **78**, 838.  
Drabble J. R., Groves R. D. & Wolfe R. 1958 *Proc. Phys. Soc.* **71**, 430.  
Dutta S. K. 1956 *D. Phil. Thesis* (Calcutta University).  
Dutta Roy S. K. 1955 *Indian J. Phys* **29**, 429.  
Goldsmid H. J. 1958 *Proc. Phys. Soc.* **71**, 633.  
Krumhansl J. A. & Brooks H. 1956 *Bull. Amer. Phys. Soc.* **1**, 117.  
Mansfield R. 1959 *Proc. Phys. Soc.* **74**, 599.  
Mansfield R. & Williams W. 1958 *Proc. Phys. Soc.* **72**, 733.  
Matyas M. 1958 *Czech. J. Phys* **8**, 309.  
Satterthwaite C. B. & Ure R. W. 1957 *Phys. Rev.* **108**, 1164.  
Shigetomi S. & Mori S. 1956 *J. Phys. Soc. Japan* **11**, 915.  
Sucksmith W. 1939 *Proc. Roy. Soc.* **A107**, 551.  
Van Deynse N., Van Itterboek A. & Dekeyser R. 1969 *Z. Angew. Phys.* **26(2)**, 174.

## Letters to the Editor

Indian J. Phys. 44, 609-610 (1970).

### Search for nuclear penetration in the internal conversion process of the 53 keV transition in $^{144}\text{Pr}$ .

H. S. SAHOTA

Physics Department, Punjabi University, Patiala

(Received 12 May 1971)

Of the 33, 53 and 133 keV transition depopulating the 133 keV level in  $^{144}\text{Pr}$ , 53 keV should have an  $M_1$  hindrance of 7 compared to single particle estimates. Geiger *et al* (1960) from careful analysis of  $L$  subshell ratios established the multipolarity of this transition as  $M_1$  with less than 0.2%  $E_2$ . Since retardation is a common condition for nuclear penetrations we thought of making a search for them. However, the  $K$ -conversion coefficient for this transition is far from accurately determined. The findings of different groups as well as the same group using different techniques differ widely. Geiger *et al* (1961) from the combined  $K$  80- $\gamma$  and  $K$  133- $\gamma$  results obtained a value for  $\alpha_K = 3.7 \pm 1.0$ , while from the  $L_1$  80- $\gamma$  coincidence spectrum results they obtained a value of  $\alpha_K = 8.6 \pm 1.8$  and a still higher value of  $\alpha_K = 10 \pm 3$  from their  $\gamma$  80- $\gamma$  coincidence measurements. Iwashita *et al* (1963) found a value of  $\alpha_K = 5.6$ .

Mangal & Trehan (1969) from their scintillation spectrometer singles and sum peak coincidence measurements found an  $\alpha_K$  value of  $9.4 \pm 1.0$ . We thus decided to re-evaluate this conversion coefficient for studying the penetrations. The  $\gamma$ -ray intensities were taken from the work of Potnis *et al* (1970) determined with a solid state detector. The electron intensities from the work of Geiger *et al* (1960) were used.

Since for the 53 keV transition only  $L$  subshell intensities have been reported we have used the following method for finding the  $K$ -shell electron intensity. From the  $K$  and  $L$  electron intensities for the 133 and 80 keV transitions we find that the  $K/L$  ratios are 7.2 and 7.4 respectively, for these transitions with errors of about 5 and 10 percent. We took the theoretical (Hager & Seltzer 1968)  $K/L$  ratio of 7.2 for the 53 keV transition energy and  $M_1$  multipolarity and from the  $L$  shell intensity after Geiger *et al* (1960) arrived at the  $K$  shell intensity for this transition as  $14.8 \pm 2.2$ . Using the theoretical conversion coefficient for the 133 keV pure  $M_1$  transition from the work of Hager & Seltzer (1968) as  $\alpha_K = 0.495$ , the conversion coefficient for 53 keV transition turns out to be  $\alpha_K = 6.8 \pm 1.6$ . Hager & Seltzer (1969) give the following relation for the lowest order magnetic conversion involving penetrations.

$$\beta_{M_1}^K(\lambda) = \beta_{M_1}^K(\lambda = 1)(1 + B_1\lambda + B_2\lambda^2)$$

where  $\beta_{M_1}^K (\lambda = 1)$  is the conversion coefficient without penetrations  $B_1$  and  $B_2$  are penetration coefficients for magnetic multipole conversion coefficients and  $\lambda$  is the penetration factor defined as ratio of penetration matrix element to the gamma ray matrix element. Taking the values of the quantities  $\beta_{M_1}^K (\lambda = 1)$ ,  $B_1$  and  $B_2$  from the work of Hager & Seltzer (1968, 1969) and giving different values to  $\lambda$  we plot a graph between  $\beta_{M_1}^K (\lambda)$  and  $\lambda$ .

From the graph corresponding to our value of the conversion coefficient determined above we find  $\lambda$  essentially equal to unity. Thus the conversion process is taking place without any dynamic nuclear effects present in it. This is confirmed from the study of the  $L_1$  and  $L_2$  conversion coefficients as well.

The author is thankful to Professor B. S. Sood for useful facilities and encouragement in his work.

#### REFERENCE

- Geiger J. S., Graham R. L. & Evans G. T. 1960 *Nucl. Phys.* **16**, 1.  
1961 *Nucl. Phys.* **28** 387.  
Hager R. S. & Seltzer E. C. 1968 *Nuclear Data* **A4**, 1.  
1969 *Nuclear Data* **A6**, 1.  
Iwashita T., Inamura T., Ikemoto Y. & Kugeyama S. 1963 *J. Phys. Soc. Japan* **18**, 1358.  
Mangal P. C. & Trohan P. N. 1969 *J. Phys. Soc. Japan* **27**, 1.  
Potins V. R., Agin G. P. & Mandeville C. E. 1970 *J. Phys. Soc. Japan* **29**, 539

*Indian J. Phys.* **44**, 610-612 (1970)

### Binding energy of hyper nuclei from $K^-$ -capture

BY T. ROY AND I. K. DAFTRI

*Department of Physics, Jadavpur University, Calcutta-32*

(Received 4 March 1971)

(Plate-16)

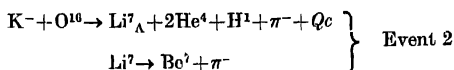
Experimental determinations of binding energies of hypernuclei have been made during the last decade. Yet there are reports of some observed uncertainties in the binding energies of hypernuclei. Thus it seems desirable to find the binding energies of hypernuclei just to increase the statistics and sharpen the mean values.

In this note a study is made of mesic decays of hyperfragments produced by  $K^-$ -reaction at rest in an emulsion which yields data on the binding energies of  $Li^7_\Lambda$  and  $B^{10}_\Lambda$ . The average binding energies of  $Li^7_\Lambda$  and  $B^{10}_\Lambda$  was found to be 5.92 MeV and 8.90 MeV which agree with the binding energies summarized by Levisetti & Slater (1963), Slater (1959), and Gilbert (1956) as 5.5 MeV and 8 MeV.

During a systematic scanning of an emulsion plate  $4.3' \times 4.3' \times 400\mu$  thick exposed to  $K^-$ -particle beam, with momenta 800 MeV/c at the CERN Proton



synchrotron, a number of events have been observed among which the case of  $\text{Li}^7\Lambda$  h.f. and  $\text{B}^{10}\Lambda$  h.f. are mentioned here. These are designated as event 1 and event 2 respectively.



In event 1 as shown in the plate 16  $K^-$ -particle is captured by  $\text{O}^{16}$  nucleus at the point A.  $\text{Li}^7\Lambda$  h.f. produced decays at rest and gives the  $\text{Bo}^7$  track AB. Prongs (T1) and (T3) represent the negative pions. (T4) and (T5) represent the  $\text{He}^4$  particles and prong (T2) the  $\text{H}^1$  particle. Also during the production of new particles some energy is lapsed in the formation of  $\delta$ -rays which is represented by  $Q_c$  in the above reaction. These data are given in table 1.

Table 1

Track	Identity	Range (microns)	Energy (Mev)	Momentum (Mev/c)
(T2)	$\text{H}^1$	1112.10	14.45	28.738
(T1)	$\pi^-$	480.10	4.08	2.399
(T3)	$\pi^-$	648.20	4.80	2.760
(T4)	$\text{He}^4$	1492.11	38.85	51.899
(T5)	$\text{He}^4$	488.00	20.43	27.931

The identities of different prongs were obtained from ionization, range measurements and from end point of each prong

The above reaction satisfies (a) conservation of charge and (b) conservation of energy. The momentum unbalance of the reaction is  $45.93 \pm 1.2$  Mev/c.

The binding energy is most conveniently computed from the equation

$$m_{f'} + m_{\Lambda} - B_{\Lambda} = \sum_i m_i + Q = m_f \quad \dots (1)$$

where the various  $m$ 's are the rest energies of particles involved in the event, and  $Q$  is the total kinetic energy release.  $f'$  represents the core of nucleus in which the particle  $\Lambda^0$  is bound,  $f$  is the h.f. whose binding energy we want to find out and  $i$  labels as decay particles.

$$\begin{aligned} f &= m_{f'} + m_{\Lambda} - m(\pi^-) \\ &= 5562.30 + 1091.92 - 120.50 \\ &= 6533.72 \end{aligned} \quad (2)$$

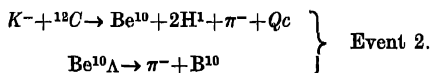
$$\begin{aligned} Q_0 &= f - \sum_i m_i \\ &= 6533.72 - 6486.16 \\ &= 67.56 \text{ Mev.} \end{aligned}$$

$$\begin{aligned} B_{\Lambda} &= Q - Q_0 \\ &= 73.20 - 67.56 \\ &= 5.64 \text{ Mev} \end{aligned}$$

The binding energy found from other events has been found in the same manner and is as follows.

Possible identification $\text{Li}^7\Lambda$	Expected $B(\text{Mev})$ 5.5	Experimental $B(\text{Mev})$ 5.64, 6.49, 5.65
--	------------------------------------	---

Average binding energy of  $\text{Li}^7\Lambda$  is found to be 5.92 Mev.



The event 2 as shown in plate is the case of  $\text{Be}^{10}\Lambda$  which is produced when a  $K^-$ -particle beam is captured by the  $\text{C}^{12}$  nucleus in the emulsion and decays at rest to give  $\text{B}^{10}$  and negative  $\pi$ -meson. Prongs (*B*) and (*C*) represent the  $\pi^-$  mesons. (*D*) and (*F*) are  $\text{H}^1$  particles, and prong (*HE*) represents the  $\text{B}^{10}$  nucleus. The data are given below.

Table 2

Track	Identity	Range (microns)	Energy (Mev)	Momentum (Mev/c)
( <i>B</i> )	$\pi^-$	2368.01	10.31	6.4139
( <i>C</i> )	$\pi^-$	188 00	2 36	0.9536
( <i>D</i> )	$\text{H}^1$	2312.00	22 52	44.1926
( <i>F</i> )	$\text{H}^1$	7496 01	44 39	86 8433

The above reaction obeys the energy and charge conservation. The momentum unbalance has been found to be  $58.51 \pm 1.2$ .

The binding energy is found in the same manner as in the previous case. binding energy turns out to be 8.64 Mev.

We thank the CERN Emulsion Plate Division for sending suitable plates for our work.

#### REFERENCES

- Gilbert C. 1956 *Phys. Rev* **103**, 248,  
 Levisetti R. & Slater W. E. 1963 *Nuovo Cimento* **15**, 181.  
 Slater W. E. 1958 *Nuovo Cimento Supp.* **10**, 1.  
 1959 *Nuovo Cimento* **21**, 213,

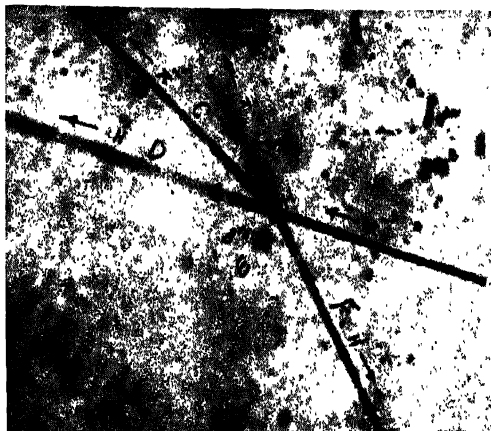


Figure 1. Event 1.

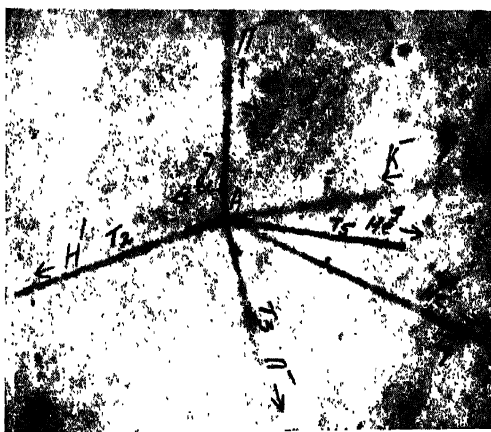


Figure 2. Event 2.



# A report on the crystal structure of 5-benzene sulphonamido 3-phenyl 1-2-4-triazole

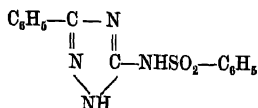
BY DILIP KUMAR NAG and SANKARANANDA GUHA

*Department of Magnetism,*

*Indian Association for the Cultivation of Science, Calcutta-32*

(Received 16 April 1971)

Crystal structure determination of 5-benzene sulphonamido 3-phenyl 1-2-4-triazole has been undertaken in order to get an insight into the biological activities of the compound. It has a remarkable hypoglycemic activity, i.e. it reduces blood sugar. Its chemical formula is



The compound crystallizes as transparent thin elongated plates. The crystals are very brittle, but quite stable at normal conditions of humidity and temperature. Rotation and Weissenberg X-ray photographs showed that the crystal belongs to the monoclinic system with  $a = 14.55 \text{ \AA}$ ,  $b = 5.87 \text{ \AA}$ ,  $c = 16.42 \text{ \AA}$ , and  $\beta = 99.6^\circ$ . The only systematic absences were for  $0k0$  with  $k$  odd and  $h+l$  odd for  $(h0l)$ . This indicates that the space group is  $P2_{1/n}$ . The density of the crystal as measured by the floatation method using a mixture of benzene and carbon tetrachloride is 1.46, while the calculated value for 4 molecules of  $\text{C}_{14}\text{N}_4\text{O}_2\text{SH}_{12}$  per unit cell is 1.44.

Three dimensional intensity data were collected for  $hkl$  with  $k = 0$  to 4 and for  $hk0$  using multiple-film equi-inclination Weissenberg technique with  $\text{CuK}_\alpha$  radiation. The intensity values of the spots were estimated by visual comparison with a calibrated strip, and corrected for Lorentz, polarization and spot size effects (Phillips 1954, 1956). They were then brought to an absolute scale (Wilson 1942).

The  $b$ -axis being much shorter than the other two, attempts were made to derive the structure from the zero layer data along this axis. Two Patterson syntheses, one unsharpened and the other sharpened by multiplying the  $F^2$  values by the zero layer  $LP^{-1}$  function, were calculated. From the sharpened Patterson synthesis it was observed that the peaks due only to one benzene ring are quite prominent around the origin, suggesting its orientation, if it is assumed that the ring is almost parallel to the  $ac$ -plane. This showed that the two benzene

rings at the two ends of the molecule have nearly the same orientation. But the  $S-S$  peak which should be heavy, could not be located uniquely even in this sharpened synthesis. Attempts were also made to obtain the structure from a series of minimum functions derived from the unsharpened synthesis. Three dimensional analysis of the structure is now in progress.

The authors are thankful to Dr. B. K. Paul of the Bengal Immunity Research Institute, Calcutta, for supplying a few crystals of the compound. Thanks are also due to Professor A. Bose and Dr. R. K. Sen for encouragement and discussion and also to the Council of Scientific and Industrial Research, New Delhi, for financial assistance.

#### REFERENCES

- Phillips D. C. 1954 *Acta Cryst.* **7**, 746.  
1956 *Acta Cryst.* **9**, 819.  
Wilson A. J. C. 1942 *Nature* **150**, 152.

## BOOK REVIEWS

### *Physics—Part 1 and 2*

Edited by David Halliday and Robert Resnick.

Wiley Eastern Private Ltd., New Delhi, Price Rs. 13.50 per volume.

This book has been published with the assistance of the joint Indian American Text Book Programme and is a carefully revised and expanded edition of the authors' famous text book "Physics for Students of Science and Engineering" "first published in 1969".

The first volume contains Mechanics, Fluid Statics and Dynamics, Gravitation, Heat and Thermodynamics and the second volume contains Magnetism, Electricity and Light. The mathematical level in these volumes assumes the knowledge of a first course in Calculus. In specific problems vector algebra has been used, whenever this has been proved very fruitful. The authors have tried to reveal the underlying unity of the different branches of Physics. Throughout the text they have used wave picture, resonance etc. in Mechanics, Sound, Electromagnetism, Optics and Atomic Physics. They have discussed the limitations of the classical theories and introduced new ideas applicable in a broader domain. In fact the authors have preferred the topics and examples with modern flavour, wave-particle duality, the uncertainty principle, the complementarity principle and the correspondence principle, etc. The book contains some excellent tables of some fundamental and derived constants, terrestrial data, solar system, fundamental particles etc. Large number of theoretical and numerical problems, with a wide choice of level of difficulty and area of interest, have been provided at the end of each chapter.

This book has no chapter on Nuclear Physics which would have been very useful to the students for which it is meant.

The book may be considered as an excellent reference book for students of degree course of our universities and should be considered as an asset to every library.

P. K. B.

*Phase Transformation**American Society for Metals**Seminar Coordinator—H. I. Aaronson*

Park Ohio, Seminar held October 1968, Published 27.8.70.

Price 24.7/- pp. 632.

The publication is the outcome of a seminar on phase transformation organized by the American Society for Metals in 1968. Phase transformation is a phenomenon which is of interest not only to the metallurgists but also to the geologists, chemists and solid state physicists. In view of its importance in understanding the properties of materials, and also this phenomenon being of interdisciplinary nature, the publication of the book is an welcome addition in this field. The crystallography of martensitic transformation has been elucidated by the efforts of a very active group of scientists mainly during the last two decades. Similarly an insight into the mechanism of diffusion and nucleation involved in such phase transformation has also been developed through the continuous efforts of a large number of active research workers. Articles presented in the book deals with the studies on the crystallography, the kinetics and nucleations of the various types of phase transformations, e.g., martensitic, bainitic, massive transformation, order disorder transformation etc.

The book discusses the recent experimental results on phase transformations and compares these results with the predictions of the theories. The articles clearly show that though in a number of cases the quantitative agreement between the two is quite impressive, there are a few cases of disagreement and the complete understanding of the basic principles leading to phase transformation is still to be reached. The authors have taken care to discuss these areas of disagreement and in some cases indicated the directions which the experimentalists should focus their attention for the development of the theories. While presenting the experimental results, the authors of the articles have reproduced a number of surface reliefs and electron micro-graphs which are very spectacular and impressive. The articles also contain a very useful list of references which are almost up to date. Though the book is meant to benefit the active research workers in this field, the new entrants in this field will also benefit by this almost exhaustive list of references.

The printing and the reproduction of the photographs are excellent. The book will certainly be a very useful addition to any modern library. The American Society for metals is to be congratulated for bringing out such an elegant and useful publication on an interdisciplinary topic like the phase transformations.

*R. K. S.*



# INDIAN JOURNAL OF PHYSICS

VOL. 44

No. 12

AND

VOL. 53

PROCEEDINGS

No. 12

OF THE

INDIAN ASSOCIATION FOR THE CULTIVATION OF SCIENCE

*(Edited in collaboration with the Indian Physical Society).*

IJPYAS 44 (12) 617-666 (1970)

DECEMBER 1970

PUBLISHED BY THE  
INDIAN ASSOCIATION FOR THE CULTIVATION OF SCIENCE  
JADAVPUR, CALCUTTA-32



## Entry-length flow in a vertical cooled pipe

By S. N. SINGH AND R. N. PANDEY

*Department of Mathematics, Banaras Hindu University, Varanasi-5*

(Received 8 February 1971)

A treatment of the flow and heat transfer due to free convection in the entry region of a cooled vertical pipe, which is open at both ends, has been given. The analysis is based on the Lighthill method. Further in the analysis, velocity and temperature profiles have been assumed, which satisfy all the boundary conditions. Parameters involved in the profiles have been calculated by assuming series solution. In the analysis, we have defined a new non-dimensional number  $M$ , which happens to be a function of boundary layer nondimensional thickness  $\delta$ . This number has an influence over the fluid flow in the boundary layer region. A value of  $M$  has been obtained for which vertical displacement  $Q$  is the maximum, on taking only first two terms of  $Q$ . It has been observed that there is a deceleration of flow in the vicinity of the wall in boundary layer region due to cooling of the wall and increasing the Rayleigh number. For  $R = 0(10^3)$ , there is a reversal of flow in the vicinity of the wall.

### INTRODUCTION

Ostrach (1954) obtained an expression for buoyancy forces on the fluid within the pipe relative to the cooled fluid at the same level outside the pipe. In this it will be better to regard the fluid as moving only under the influence of a pressure gradient and relative buoyancy forces within. Ostroumov (1958) has given an extensive treatment of the natural convection in cylindrical channels in terms of Bessel & Neumann functions. Lighthill (1953) has given an analysis of the flow through a cylindrical pipe in which one end is closed and the wall of the pipe maintained at a constant temperature, the body forces acting in the direction of the closed end. It has been considered here that at the open end there is an orifice which supplies fluid. The flow of fluid depends upon the parameter  $l/R$ , for given Prandtl and Rayleigh numbers. When  $l/R$  is small, the flow is like free convection about a flat plate, but when  $l/R$  is large, the flow is not like free convection. In his treatment, he has used the integral method and in case of similarity regime he finds that the flow fills the whole of the tube for a particular value of  $l/R$ . Different authors have adopted this technique in the case of free convection in combined flow to slightly varied physical situations. Martin (1967) has performed experiments of heat transfer due to natural convection in a long extremely cooled vertical cylinder with uniform wall temperature, containing heat generating fluid in a laminar flow (with Prandtl number equal to or greater than unity). Takhar (1967) has given a treatment for the entry length flow in a vertical heated open pipe. He finds that at Rayleigh numbers greater than  $10^3$ , the flow in the middle

of the pipe becomes stagnant. This analysis cannot produce satisfactory results before the boundary layer fills the whole of the tube.

In the present paper, an attempt has been made to study the flow in entrance region of a vertical pipe which has both its ends open and is being cooled with (i) a constant temperature at the wall and (ii) the wall temperature decreasing exponentially as a function of vertical height. It has been taken for granted that; (a) kinematic viscosity and thermal conductivity are approximately constant and Boussinesque approximation holds; (b) velocity and temperature profiles are assumed so as to satisfy the initial and boundary conditions; (c) the equations of motion, continuity and heat conduction have been integrated to find out the various parameters involved in the analysis with the help of the equations at the axis and at the walls; (d) the momentum and thermal boundary layer thicknesses are assumed to be equal; (e) The parameter  $Q$  in the assumed profiles gives the vertical displacement outside the boundary layer thickness.

It is seen that boundary layer fills the entire tube so as to give the fully developed flow through the pipe, and a reversal of the flow occurs at the cooling Rayleigh number greater than  $10^3$ . Graph has been plotted between

$$M = \frac{\beta_1 v^2}{\sigma \beta^2 g a^3}$$

and the boundary layer thickness  $\delta$ .

It seems that the analysis may prove useful to engineering problems on free convection in the entrance region of the pipe.

#### ANALYSIS

The equations of motion here are similar to differential equations of free convection except that the pressure no longer takes the hydrostatic value. The flow is assumed to be of boundary layer type, which means that gradient of a quantity along the pipe is small as compared to the pressure gradient in the radial direction. Keeping this in view, we have the equations of :

conservation of mass

$$\frac{\partial u}{\partial z} + \frac{1}{r} \frac{\partial(rv)}{\partial r} = 0,$$

conservation of momentum

$$\left( u \frac{\partial u}{\partial z} + v \frac{\partial u}{\partial r} \right) = -\frac{\partial p}{\partial z} + \mu \left( \frac{\partial^2 u}{\partial r^2} + \frac{1}{r} \frac{\partial u}{\partial r} \right) - \rho g,$$

$$0 = -\frac{1}{\rho} \frac{\partial p}{\partial r}$$

and conservation of heat

$$u \frac{\partial T}{\partial z} + v \frac{\partial T}{\partial r} = k \left[ \frac{\partial^2 T}{\partial r^2} + \frac{1}{r} \frac{\partial T}{\partial r} \right]$$

where  $u, v$  are the axial and radial velocities  $k$  and  $\mu/\rho$  ( $=\nu$ ) are the thermal diffusivity and the coefficient of kinematic viscosity, respectively. The initial and boundary conditions are

$$(i) \quad r = a, \quad u = 0 = v, \quad T = T_w \text{ for all } z > 0$$

$$(ii) \quad z = 0, \quad u = u_0, \quad v = 0, \quad T = T_0 \text{ for all } r > 0.$$

Let  $T_w$  and  $T_0$  be the temperature of the wall and that of the fluid at the entry, respectively. Let us assume that the wall temperature is of the form

$$T_w = T_0 - \Delta T f(z), \quad \text{where} \quad \Delta T = T_w - T_0.$$

Further, the variation of all physical properties are ignored except the density involved in the buoyancy term. Also the viscous dissipation and work done against gravity field are neglected. Thus we have for the density in the buoyancy term

$$\rho = \rho_{T_w} + \left( \frac{\partial \rho}{\partial T} \right)_{T_w} (T - T_w) + \frac{1}{2!} \left( \frac{\partial^2 \rho}{\partial T^2} \right)_{T_w} (T - T_w)^2 + \dots \quad (2)$$

which can be regarded as Taylor equation of state.

Introducing coefficient of volume expansion at  $T_w$  as

$$\beta = -\frac{1}{\rho} \left( \frac{d\rho}{dT} \right)_{T_w} \text{ and the quantity } \beta_1 = \frac{1}{\rho} \left( \frac{\partial^2 \rho}{\partial T^2} \right)_{T_w},$$

we can write (2) as

$$-\rho = -\rho_w - \beta \rho (T_w - T) - \frac{\beta_1 \rho}{2} (T_w - T)^2.$$

Substituting this in (1), we get

$$u \frac{\partial u}{\partial z} + v \frac{\partial u}{\partial r} = - \left( \frac{1}{\rho} \frac{\partial p}{\partial z} + g \right) + \nu \left( \frac{\partial^2 u}{\partial r^2} + \frac{1}{r} \frac{\partial u}{\partial r} \right) - g \beta (T_w - T) - \frac{g \beta_1}{2} (T_w - T)^2.$$

The temperature  $\Delta T = T_w - T_0$  defines a cooling Rayleigh number

$$Ra = \frac{\beta g a^3 \Delta T}{k \nu}.$$

If we introduce the non-dimensional quantities as  $r = aR, z = aZ$ ,

$$u = \frac{k}{a} U, \quad v = \frac{k \nu}{a}, \quad L \frac{k \nu}{a^3} = - \left( \frac{1}{\rho} \frac{dp}{dZ} + g \right), \quad T = T_w + \frac{\Delta T}{Ra} \Theta,$$

$$M = \frac{\beta_1 \nu^2}{\sigma \beta^2 g a^3},$$

We have the equations of mass, momentum and heat as

$$\frac{\partial U}{\partial Z} + \frac{1}{R} \frac{\partial(RV)}{\partial R} = 0 \quad \dots (3)$$

$$\frac{1}{\sigma} \left[ \frac{1}{2} \frac{\partial}{\partial Z} U^2 + V \frac{\partial U}{\partial R} \right] = L + \frac{1}{R} \frac{\partial}{\partial R} \left( \frac{\partial}{\partial R} UR \right) - \frac{1}{2} M \Theta^2 + \Theta \quad \dots (4)$$

$$\frac{\partial P}{\partial R} = 0$$

$$-Ra U \frac{df}{dZ} + \left( U \frac{\partial \Theta}{\partial Z} + V \frac{\partial \Theta}{\partial R} \right) = \frac{1}{R} \frac{\partial}{\partial R} \left( R \frac{\partial \Theta}{\partial R} \right) \quad \dots (5)$$

subject to the conditions

$$\left. \begin{aligned} R=1, \quad Z > 0, \quad U = V = \Theta = 0, \quad \text{at the wall} \\ R > 0, \quad Z = 0, \quad U = U_0, \quad V = 0, \quad \Theta = -Ra, \quad \text{at the entry} \end{aligned} \right\} \quad \dots (6)$$

where  $U_0$  is the non-dimensional velocity at the entry along  $Z$ -direction.

Integrating (3), (4), (5) over a cross-section subject to the conditions (6), we get

$$\left. \begin{aligned} \int_0^1 RU dR &= \frac{1}{2} U_0 \\ \frac{1}{2\sigma} \cdot \frac{d}{dZ} \int_0^1 RU^2 dR &= \frac{L}{2} + \left( \frac{\partial U}{\partial R} \right)_{R=1} + \int_0^1 R \Theta dR - \frac{1}{2} M \int_0^1 \Theta^2 R dR \\ \text{and } -\frac{1}{2} Ra U_0 \frac{df}{dZ} + \frac{d}{dZ} \int_0^1 RU \Theta dR &= \left( \frac{\partial \Theta}{\partial R} \right)_{R=1} \end{aligned} \right\} \quad \dots (7)$$

and the equations

$$\left. \begin{aligned} \frac{1}{2\sigma} \frac{\partial}{\partial Z} U^2 &= L + \frac{1}{R} \frac{\partial}{\partial R} \left( \frac{\partial}{\partial R} UR \right) + \Theta - \frac{1}{2} M \Theta^2, \\ U \frac{\partial \Theta}{\partial Z} &= \frac{1}{R} \frac{\partial}{\partial R} \left( R \frac{\partial \Theta}{\partial R} \right) \end{aligned} \right\} \quad \dots (8)$$

at the axis of the pipe, and

$$\left. \begin{aligned} 0 &= L + \frac{1}{R} \frac{\partial}{\partial R} \left( R \frac{\partial U}{\partial R} \right) \\ 0 &= \frac{1}{R} \frac{\partial}{\partial R} \left( R \frac{\partial \Theta}{\partial R} \right) \end{aligned} \right\} \quad \dots (9)$$

at the wall.

Here, we shall assume the velocity and temperature profiles of Kerman—Pohlhausen type, which satisfies the conditions given in (6). These profiles are :

$$U = \begin{cases} PU_0 & (\delta < X < 1) \\ PU_0 \left\{ 1 - \left( 1 - \frac{X}{\delta} \right)^2 \left( 1 - \frac{OX}{\delta} \right) \right\} & (0 < X < \delta) \end{cases} \quad \dots (10)$$

$$\Theta = \begin{cases} Ra & (\delta < X < 1) \\ Ra \left\{ 1 - \left( 1 - \frac{X}{\delta} \right)^2 \right\} & (0 < X < \delta) \end{cases}$$

where  $\delta$  corresponds to a boundary layer of non-dimensional thickness, enclosing a potential core of radius  $\delta_1 = 1 - \delta$  and  $X = 1 - R$ . Here, we have two cases depending upon the way the pipe is cooled.

*Case I.*

When the temperature of the wall is constant the equation (5) becomes

$$U \frac{\partial \Theta}{\partial Z} + V \frac{\partial \Theta}{\partial R} = \frac{1}{R} \frac{\partial}{\partial R} \left( R \frac{\partial \Theta}{\partial R} \right)$$

*Case II.*

When the wall temperature decreases exponentially, i.e., when  $T_w = T_0 - \Delta T \exp(\alpha X)$ , where  $\alpha$  is a small quantity.

On using (8) and (10) we can find the value of  $L$ . Hence substituting the values given in (10) and the value of  $L$  in (7), we obtain for case I

$$P[5(6 - 4\delta + \delta^2) + Q\delta(5 - 2\delta)] = 30 \quad \dots (11)$$

$$\begin{aligned} & \frac{U_0^2}{840\sigma} \frac{d}{d\delta} [P^2\{14(15 - 28\delta + 8\delta^2) + 4Q\delta(21 - 10\delta) + Q^2\delta(8 - 3\delta)\}] \\ & = \left\{ \frac{-\delta(4 - \delta)}{12} Ra - \frac{Z + Q}{\delta} PU_0 - \frac{M}{60}(4\delta^2 - 14\delta + 15) \right\} \frac{d\delta}{dZ} \quad \dots (12) \end{aligned}$$

and

$$\frac{d}{d\delta} [P\{14(15 - 14\delta + 4\delta^2) + Q\delta(21 - 10\delta)\}] = \left( \frac{-840}{U_0\delta} \right) \frac{dZ}{d\delta} \quad \dots (13)$$

We see that for  $\delta = 0$ ,  $P = 1$ ,  $Q = 0$  at  $E = 0$ .

Obviously,  $\delta = 0$  is a singularity for the above equations, for which we have to find the values of  $P$  and  $Q$  in the neighbourhood of  $\delta = 0$  by considering series solution in terms of  $\delta$ . Thus

$$\begin{aligned} P &= 1 + a_1\delta + a_2\delta^2 + \dots \\ Q &= d_1\delta + d_2\delta^2 + \dots \end{aligned}$$

On substituting these values in (11), (12) and (13) and comparing the coefficients of various powers of  $\delta$ , we obtain

$$P = 1 + .666\delta + (.016M - .033)\delta^2 + \frac{(6M^2 - 548.6M + .24M^3 - 747.3Ra + 4705.4 + 60.6MRa)\delta^3}{1500 + 157.5M} + \dots$$

$$Q = (1.86 - M)\delta + (20.07 - .17M - .01M^2 - 3.3Ra)\delta^2 + \dots$$

Now to find  $Z$ , substituting the values of  $P$  and  $Q$  in either of (12) and (13), we have

$$Z = \frac{1}{30}[\delta^2 + (1.01 - .033M)\delta^3 + \dots]$$

#### Case II.

When the temperature of the wall decreases exponentially (with  $\alpha$  as a small number), we have the treatment exactly similar to the case I. Now we obtain after simplification

$$= [P\{14(15 - 14\delta + 4\delta^2) + Q\delta(21 - 10\delta)\}]$$

$$= \left[ -\frac{840}{U_0\delta} + 210\alpha \right] \frac{dZ}{d\delta}$$

the equation (11) and (12), and

$$Z = .033\delta^2 + (.101 + .005\alpha - .003M)\delta^3 + \dots$$

Thus, we have  $P$ ,  $Q$  and  $Z$  in terms of the boundary layer thickness  $\delta$ .

Now from the analysis of the problem, we have,

$$\text{Nusselt number} = \frac{4}{\delta}$$

$$\text{Heat flux at the wall} \left( \frac{\partial \Theta}{\partial Z} \right)_{Z=0} = \frac{2Ra}{\delta},$$

$$\text{Skin friction at the wall} \left( \frac{\partial U}{\partial Z} \right)_{Z=0} = PU_0 \left( \frac{2+Q}{\delta} \right).$$

#### DISCUSSION

We observe that due to cooling of the wall, the fluid in the vicinity of the wall in the boundary layer region becomes decelerated. This deceleration of the fluid also depends upon the cooling Rayleigh number  $Ra$ . As  $Ra$  increases fluid goes on decelerating and ultimately when it becomes greater than  $10^3$ , the reversal of flow occurs in the fluid in the vicinity of wall.



Further, in the case of the pipe the flow is due to its continuity. It is noted that in free convection, the adverse pressure gradient is confined to the boundary layer produced by buoyancy forces, but in the case of forced convection, this takes place in the main stream also

We see that for  $M = 0$ ,  $Ra = 0$ , the boundary layer fills the whole of the tube for  $Z = 0.045$ , but at increasing  $Ra$  this value decreases, we easily see that at

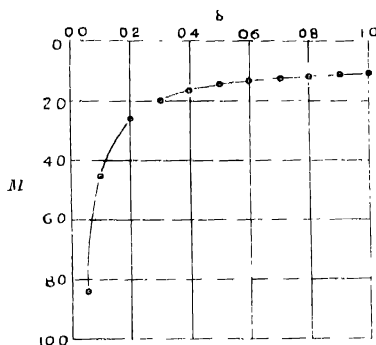


Figure 1

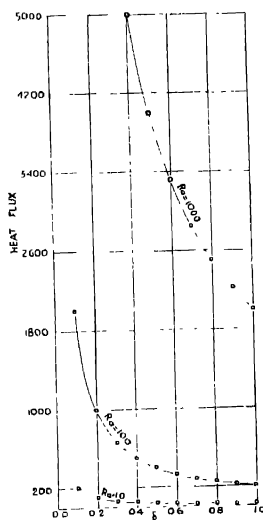


Figure 2

$Ra = O(10^3)$ , the value of  $Z$  is approximately 0.004. The value of  $M$ , for which  $Q$  is maximum upto the first two terms, comes out to be

$$M = \frac{-6.79\delta - 3.88}{\delta},$$

which shows that this depends upon  $\delta$ . The graph of  $M$  vs  $\delta$  is shown in figure 1.

Also, we see that Nusselt number is a function of  $\delta$ ; heat flux at the wall and the skin friction at the wall are functions of  $Ra$  and  $\delta$ .

The graph of heat flux vs  $\delta$  for fixed  $Ra$  is shown in figure 2.

#### REFERENCES

- Lighthill M J. 1953 *Q. J. Mech. Appl. Math.* **6**, 398  
 Martin B. W. 1967 *Proc. Roy. Soc.* **A301**, 327  
 Ostrach S. 1954 *NACA Tech. Note* 3141  
 Ostroumov G. A. 1958 *NACA Tech. Mem.* (Translation) 1407  
 Takhar H. S. 1967 *Proc. Jap. Soc. Mech. Engrs.*, Semi-International Symposium, Paper No. 201, 1-8.

## Stability of a Homopolar device

By P. K. BHAT\* AND M. P. SRIVASTAVA†

*Department of Applied Mathematics, Indian Institute of Science,  
Bangalore-12*

(Received 3 October 1969—Revised 8 September 1971)

In this paper we have studied the problem of instability in a Homopolar device. We consider a plasma shell of finite thickness and of infinite conductivity to be in steady state in the presence of a space varying magnetic field such as found in Ixion device. The instabilities for such a device have been studied by normal mode technique both for axisymmetric and azimuthal disturbances. It has been found that the system is unstable in zeroth order of the perturbation parameter  $\beta$  for an axisymmetric disturbance. Further, the effect of slow rotation and slowly varying magnetic field is to increase the growth rate of instability. The system is unstable in the zeroth order for the azimuthal disturbance. The first order dispersion relation shows that the effects of low intensity ring currents is to increase the growth rate of instability. Further, the increase of rotation decreases the growth rate of instability.

### INTRODUCTION

The study of instabilities encountered in plasma systems is of considerable importance in connection with fusion devices and in astrophysical context. A number of investigations has been made by several authors under varying assumptions to get a magnetic trap which confines a plasma for sufficiently long time. The study of instabilities of such devices is also very important in order to find if these devices are useful for controlled fusion.

In the present paper we have studied the instabilities which set in an idealized laboratory device known as Ixion or Homopolar device. In this a plasma shell of very small resistivity is immersed in radial electric and axial magnetic fields which decrease as the radial coordinate increases. The effect of crossed fields is to give each particle a drift perpendicular to both electric and magnetic fields. An experimental and theoretical speculation of this device for containment has been made by Boyer *et al.* (1958). They have shown that particle containment is improved by the centrifugal force of crossed field rotation which has the tendency to keep the particles away from the axis. Further, Anderson *et al.* (1958) have also investigated the characteristics of this experimental device. Perkins

Present Addresses : \* School of Mathematics, Military College of Engineering, Dapodi, Poona-31.

† Department of Physics, Delhi University, Delhi-7.

& Post (1963) while investigating the MHD stability of a cylindrical plasma have found that the system is unstable whenever rotation is present. Verma & Verma (1965) have also investigated the stability of a rotating plasma cylinder and have shown that rotation has a stabilizing influence.

In the present investigation we have applied the usual normal mode technique to study the stability of the device. In section 2 we have recorded the steady state. In the subsequent sections we have recorded the solutions for axisymmetric and azimuthal disturbance and the corresponding dispersion relations obtained after using the required boundary conditions which are discussed in detail in the last two sections.

## 2 STEADY STATE

The non-dimensional magnetic field in the steady state is given by

$$\mathbf{B}^{(i)} = [0, 0, (1 - \beta/r^2)^{1/4}], \quad 1 \leq r \leq m$$

$$\mathbf{B}^{(o)} = [0, 0, H_1], \quad 0 \leq r \leq 1$$

and

$$\mathbf{B}^{(o)} = [0, 0, H_2], \quad r \geq m$$

where the superscripts *i* and *o* stand for inside and outside of the plasma device, respectively. The electric field inside the plasma region is

$$\mathbf{E}^{(i)} = [K/r, 0, 0], \quad 1 \leq r \leq m$$

and outside the plasma region it is zero. *K* is the rotation parameter and *m* is the ratio of the outer to inner radius. The corresponding pressure and velocity can be calculated through the momentum equation and generalized Ohm's law. It is found that due to the presence of electric field in the radial direction inside the plasma region the azimuthal component of the velocity is non-zero.

## 3 AXISYMMETRIC DISTURBANCES

We perturb the steady state described in section 2 in an axisymmetric manner and assume that these disturbances are so small that their squares and products can be neglected. In order to investigate the stability of such a system we assume that these perturbed quantities vary with time and *z*-coordinate exponentially *i.e.*, as  $e^{i\omega t + ilz}$  where  $\omega$  is the angular frequency and *l* is the axial wave number. We denote the amplitudes of the perturbations in velocity, pressure, magnetic field and the electric field, respectively, by  $\mathbf{v}$ ,  $\tilde{p}$ ,  $\tilde{\mathbf{b}}$  and  $\tilde{\mathbf{e}}$ . We consider  $\beta$  to be small and treat it as an expansion parameter so that

$$\mathbf{X} = \mathbf{X}_0 + \beta \mathbf{X}_1 + \dots \quad (3.1)$$

where  $X$  is taken as  $\mathbf{v}$ ,  $\tilde{\eta}$ ,  $\mathbf{b}$ ,  $\mathbf{e}$  and  $\omega$ . In view of (3.1) and using the governing momentum and Maxwell's equations, we obtain the following equation for  $v_{r0}$  in the zeroth order after linearization

$$\frac{d^2 v_{r0}}{dr^2} + \frac{1}{r} \frac{dv_{r0}}{dr} - (l^2 + 1/r^2) v_{r0} = 0 \quad (3.2)$$

This equation has been obtained on the approximation of slow rotation such that  $K$  can be treated to be of the same order as  $\beta$ . After solving (3.2) for  $v_{r0}$  and making use of the resulting solution in the remaining set of equations we find the following zeroth order solutions

$$\begin{aligned} v_{r0} &= AI_1(lr) + BK_1(lr), \\ v_{\theta 0} &= 0, \\ v_{z0} &= i[A I_0(lr) - BK_0(lr)], \\ b_{r0} &= \frac{l}{\omega_0} [AI_1(lr) + BK_1(lr)], \\ b_{\theta 0} &= 0, \\ b_{z0} &= \frac{il}{\omega_0} [AI_0(lr) - BK_0(lr)], \\ p_0 &= -\frac{l\omega_0}{l} [AI_0(lr) - BK_0(lr)] \\ e_{r0} &= 0, \\ e_{\theta 0} &= AI_1(lr) + BK_1(lr), \\ e_{z0} &= 0, \end{aligned} \quad (3.3)$$

where  $A$  and  $B$  are arbitrary constants of integration. The governing differential equation for  $v_{r1}$  is given by

$$\frac{d^2 v_{r1}}{dr^2} + \frac{1}{r} \frac{dv_{r1}}{dr} - \left( l^2 + \frac{1}{r^2} \right) v_{r1} = \frac{l^3}{i^3(\omega_0^2 - l^2)} [AI_0(lr) - BK_0(lr)], \quad (3.4)$$

Solving (3.4) and taking care of the set of equations involving other physical quantities, we obtain the following set of first order solutions

$$\begin{aligned} v_{r1} &= A_{11}I_1(lr) + B_{11}K_1(lr) + K_1(lr)I_1 - I_1(lr)I_2, \\ v_{\theta 1} &= 0, \\ v_{z1} &= i[A_{11}I_0(lr) - B_{11}K_0(lr) - K_0(lr)I_1 - I_0(lr)I_2], \end{aligned}$$

$$\begin{aligned}
b_{r1} &= \frac{1}{\omega_0} \left[ lA_{11}I_1(lr) + lB_{11}K_1(lr) + lK_1(lr)I_1 - lI_1(lr)I_2 \right. \\
&\quad \left. - \frac{l}{4r^2} \{AI_1(lr) + BK_1(lr)\} - \frac{\omega_1 l}{\omega_0} \{AI_1(lr) + BK_1(lr)\} \right], \\
b_{\theta 1} &= 0, \\
b_{z1} &= \frac{il}{\omega_0} \left[ A_{11}I_0(lr) - B_{11}K_0(lr) - lI_0(lr)I_2 - lK_0(lr)I_1 \right. \\
&\quad \left. + \frac{1}{2r^2 l} \{AI_0(lr) + BK_1(lr)\} - \left( \frac{1}{4r^2} + \frac{\omega_1}{\omega_0} \right) \{AI_0(lr) - BK_0(lr)\} \right], \\
p_1 &= \frac{1}{il} \left[ \omega_0 \{A_{11}I_0(lr) - B_{11}K_0(lr) - lK_0(lr)I_1 - lI_0(lr)I_2\} \right. \\
&\quad \left. + \omega_1 \{AI_0(lr) - BK_0(lr)\} + \frac{l}{2r^3 \omega_0} \{AI_1(lr) + BK_1(lr)\} \right], \\
e_{r1} &= -\frac{b_{z0}}{r},
\end{aligned}$$

$$e_{\theta 1} = A_{11}I_1(lr) + B_{11}K_1(lr) + lK_1(lr)I_1 - lI_1(lr)I_2 - \frac{1}{4r^2} [lI_1(lr) + BK_1(lr)],$$

and

$$e_{z1} = -\frac{b_{r0}}{r} \quad (3.5)$$

where  $A_{11}$ ,  $B_{11}$  are arbitrary constants and the integrals  $I_1$  and  $I_2$  are given by

$$I_1 = \int^r I_1(x) \frac{l^4}{x^2(l^2 - \omega_0^2)} \{AI_0(x) - BK_0(x)\} dx$$

and

$$I_2 = \int^r K_1(x) \frac{l^4}{x^2(l^2 - \omega_0^2)} \{AI_0(x) - BK_0(x)\} dx.$$

#### 4. SOLUTIONS IN VACUUM

We have to solve Maxwell's field equations in the outside and inside vacua. The set of zeroth order solutions is

$$\begin{aligned}
&\left. \begin{aligned} b_{r0} &= lCI_1(lr), & b_{\theta 0} &= 0, & b_{z0} &= ilCI_0(lr), \\ e_{r0} &= -iEI_1(lr), & e_{\theta 0} &= \omega_0 CI_1(lr), & e_{z0} &= EI_0(lr) \end{aligned} \right\} 0 \leq r \leq 1 \\
&\text{and} \\
&\left. \begin{aligned} b_{r0} &= -lDK_1(lr), & b_{\theta 0} &= 0, & b_{z0} &= ilDK_0(lr), \\ e_{r0} &= iFK_1(lr), & e_{\theta 0} &= -\omega_0 DK_1(lr), & e_{z0} &= FK_0(lr) \end{aligned} \right\} r \geq m \quad (4.1)
\end{aligned}$$

where  $C$ ,  $D$ ,  $E$  and  $F$  are arbitrary constants of integration. The set of first order solutions is

$$\left. \begin{aligned} b_{r1} &= C_{11}I_1(lr), & e_{r1} &= -iE_{11}I_1(lr) \\ b_{\theta 1} &= 0, & e_{\theta 1} &= \omega_0 C_{11}I_1(lr) + \omega_1 C I_1(lr) \\ b_{z1} &= iC_{11}I_0(lr), & e_{z1} &= E_{11}I_0(lr) \end{aligned} \right\} 0 \leq r \leq 1$$

and

$$\left. \begin{aligned} b_{r1} &= -D_{11}lK_1(lr), & e_{r1} &= iF_{11}K_1(lr) \\ b_{\theta 1} &= 0, & e_{\theta 1} &= -\omega_0 D_{11}K_1(lr) - \omega_1 D K_1(lr) \\ b_{z1} &= iD_{11}K_0(lr), & e_{z1} &= F_{11}K_0(lr) \end{aligned} \right\} r > m \quad (4.2)$$

where  $C_{11}$ ,  $D_{11}$ ,  $E_{11}$  and  $F_{11}$  are arbitrary constants of integration.

## 5. TWO-DIMENSIONAL DISTURBANCES

Starting with the steady state described in section 2 we have applied small amplitude disturbances of the type  $\exp(i\omega t + in\theta)$  to the system where  $n$  is the wave number and  $\omega$  is the angular frequency. After adopting the same procedure as done earlier but keeping  $K$  finite we obtain the following set of solutions:

(i) *Zeroth order solutions*

$$v_{r0} = \left( Ar^{n-1} + \frac{B}{r^{n+1}} \right),$$

$$v_{\theta 0} = i \left( Ar^{n-1} - \frac{B}{r^{n+1}} \right),$$

$$v_{z0} = 0,$$

$$b_{r0} = b_{\theta 0} = b_{z0} = 0$$

$$p_0 = i \left( \frac{K}{r^2} - \frac{\omega_0}{n} \right) \left( Ar^n - \frac{B}{r^n} \right),$$

$$e_{r0} = i \left( -Ar^{n-1} + \frac{B}{r^{n+1}} \right),$$

$$e_{\theta 0} = v_{r0},$$

$$e_{z0} = 0.$$

(5.1)

(ii) *First order solutions*

$$v_{11} = Cr^{n-1} - \frac{D}{r^{n+1}} - r^{-n-1}I_3 + r^{n-1}I_4,$$

$$v_{\theta 1} = i \left( Cr^{n-1} - \frac{D}{r^{n+1}} - r^{-n-1}I_3 + r^{n-1}I_4 \right),$$

$$v_{z1} = 0,$$

$$b_{r1} = b_{\theta 1} = 0,$$

$$b_{z1} = \frac{i}{2} \left( \frac{Ar^{n-2} + Br^{-n-2}}{\omega_0 r^2 - nK} \right)$$

$$p_1 = \left( \frac{iK}{r} - \frac{i\omega_0 r}{n} \right) \left( Cr^{n-1} - \frac{D}{r^{n+1}} + r^{-n-1}I_3 + r^{n-1}I_4 \right)$$

$$+ \left( \frac{iK}{4r^3} - \frac{i\omega_0 r}{n} \right) \left( Ar^{n-1} - \frac{B}{r^{n+1}} \right)$$

$$+ \frac{iK}{2n} \left( Ar^{n-1} + \frac{B}{r^{n+1}} \right) + \frac{nr}{2K} R(r).$$

$$e_{r1} = -i \left[ \frac{R(r)}{2} - \frac{Ar^{n-3}}{4} + \frac{B}{4r^{n+3}} + Cr^{n-1} - \frac{D}{r^{n+1}} + r^{-n-1}I_3 + r^{n-1}I_4 \right],$$

$$e_{\theta 1} = -\frac{1}{4r^2} (Ar^{n-1} + Br^{-n-1}) + (Cr^{n-1} + Dr^{-n-1} - r^{-n-1}I_3 + r^{n-1}I_4),$$

$$e_{z1} = 0 \quad (5.2)$$

where,

$$I_3 = \int x^n R(x) dx,$$

$$I_4 = \int x^{-n} R(x) dx$$

and

$$R(r) = \frac{Ar^{n-3} + Br^{-n-3}}{\left( n - \frac{\omega_0 r^2}{K} \right)}.$$



## 6. SOLUTIONS IN VACUUM

Solving Maxwell's field equations in the outside vacuum we obtain the following sets of zeroth and first order solutions

(i) Zeroth order solutions

$$\left. \begin{aligned} b_{10} &= -iE_0 r^{n-1}, & b_{\theta 0} &= E_0 r^{n-1}, & b_{z0} &= 0, \\ c_{r0} &= -iM_0 r^{n-1}, & c_{\theta 0} &= M_0 r^{n-1}, & c_{z0} &= \frac{iE_0 \omega_0 r^n}{n} \end{aligned} \right\} 0 \leq r \leq 1$$

and

$$\left. \begin{aligned} b_{10} &= iE_0 r^{-n-1}, & b_{\theta 0} &= E_0 r^{-n-1}, & b_{z0} &= 0 \\ c_{r0} &= iN_0 r^{-n-1}, & c_{\theta 0} &= N_0 r^{-n-1}, & c_{z0} &= -\frac{i\omega_0 E_0 r^{-n}}{n} \end{aligned} \right\} r \geq m \quad (6.1)$$

(ii) First order solutions

$$\left. \begin{aligned} b_{11} &= -iE_1 r^{n-1}, & b_{\theta 1} &= E_1 r^{n-1}, & b_{z1} &= 0 \\ c_{r1} &= -iM_1 r^{n-1}, & c_{\theta 1} &= M_1 r^{n-1}, & c_{z1} &= \frac{i\omega_0}{n} (\omega_1 E_0 + \omega_0 E_1) \end{aligned} \right\} 0 \leq r \leq 1$$

and

$$\left. \begin{aligned} b_{r1} &= iE_1 r^{-n-1}, & b_{\theta 1} &= E_1 r^{-n-1}, & b_{z1} &= 0, \\ c_{r1} &= iN_1 r^{-n-1}, & c_{\theta 1} &= N_1 r^{-n-1}, & c_{z1} &= -\frac{i\omega_0}{n} (\omega_0 E_1 + \omega_1 E_0) \end{aligned} \right\} r \geq m \quad (6.2)$$

## 7. DISPERSION RELATIONS FOR AXISYMMETRIC DISTURBANCE AND DISCUSSION ON THEM

After applying the boundary conditions at the the perturbed surfaces  $r = 1 + (\delta r) \exp(i\omega t + iz)$  and  $r = m + (\delta r) \exp(i\omega t + iz)$  we obtain the following zeroth and first order dispersion relations, respectively

$$\begin{aligned} & \omega_0^4 [K_0(ml)K_1(l)I_0(l)I_1(l) - I_0(ml)K_1(ml)I_1(l)K_0(l)] \\ & + \omega_0^2 [K_0(ml)K_1(ml)\{-l^2 I_0(l)I_1(l) + l^2 H_2^2 I_0(l)I_1(l)\} \\ & + l^2 I_0(l)I_1(l)\{H_2^2 K_0(ml)K_1(ml) - K_0(ml)K_1(ml)\} \\ & + l^2 I_0(ml)K_1(ml)\{K_0(l)I_1(l) + H_1^2 I_0(l)K_1(l)\}] \\ & + \{l^2 H_2^2 K_0(ml)K_1(ml) - l^2 K_0(ml)K_1(ml)\} \\ & \times \{l^2 H_1^2 I_0(l)I_1(l) - l^2 I_0(l)I_1(l)\} \\ & - \{l^2 K_0(l)I_1(l) + l^2 H_1^2 I_0(l)K_1(l)\} \\ & \times \{l^2 I_0(ml)K_1(ml) + l^2 H_2^2 I_1(ml)K_0(ml)\}] = 0 \end{aligned}$$

i.e.,

$$a\omega_0^4 + b\omega_0^2 + c = 0 \quad (7.1)$$

and

$$\omega_1 = f(\omega_0, l, H_1, H_2, m). \quad (7.2)$$

We shall calculate  $\omega_0$  from (7.1) for given values of  $l$ ,  $m$ ,  $H_1$  and  $H_2$  and the corresponding  $\omega_1$  from (7.2) which gives the effect of small rotation and the slow space variation of magnetic field. We have discussed the following cases :

(a) *Large wave-number disturbances* :—In this case (7.1) reduces to

$$(\omega_0')^4 - (1 + H_1^2)(\omega_0')^2 + (H_1^2 + 1)(H_2^2 + 1) = 0, \quad (7.3)$$

where  $\omega_0 = \omega_0' l$  and  $H_2^2 = H_1^2 + K^2(1 - 1/m^2)$ . From (7.3) we find that the system is always unstable. Further the effect of slow rotation and slowly varying field is to increase the growth rate of instability.

(b) *Small wave number disturbances* :—In this case (7.1) gives two growing modes and two decaying modes. Therefore the system is unstable. From (7.2) we find that the inhomogeneity in the magnetic field enhances the growth rate of instability by a multiple of  $\omega_1$ .

Thus a Homopolar device is unstable against axisymmetric disturbances.

#### 8. DISPERSION RELATIONS FOR AZIMUTHAL DISTURBANCE AND DISCUSSION ON THEM

After using the boundary conditions we obtain the following dispersion relations of zeroth and first order respectively :

$$\begin{aligned} & \omega_0^4 \{m^{2n+4} - m^4\} + \omega_0^3 \{-nK(3 + H_1)m^{2n+4} - nK(3 + H_2)m^{2n+2} \\ & + nK(3 - H_2)m^2 + nK(3 - H_1)m^4\} + \omega_0^2 \{(3n^2K^2 - 2nK^2)m^{2n+4} \\ & + n^2K^2(3 + H_1)(3 + H_2)n^2k^2 + (3n^2k^2 + 2nK^2)m^{2n} - (n^2k^2 - 2nK^2) \\ & - n^2K^2(3 - H_1)(3 - H_2)m^2 - (n^2K^2 + 2nK^2)m^4\} + \omega_0 \{-nK(3 + H_2) \\ & \times (3n^2K^2 - 2nK^2)m^{2n+2} - nK(3n^2K^2 + 2nK^2)(3 + H_1)m^{2n} \\ & + nK(n^2K^2 - 2nK^2)(3 - H_1) + nK(n^2K^2 + 2nK^2)(3 - H_2)m^2\} \\ & + \{K^4(9n^4 - 4n^2)m^{2n} - K^4(n^4 - 4n^2)\} = 0, \end{aligned} \quad (8.1)$$

and

$$\omega_1 = F(\omega_0, n, H_1, H_2, m, K) \quad (8.2)$$

We shall find  $\omega_0$  from the zeroth order dispersion relation and  $\omega_1$  from the first order dispersion relation. We have discussed the following cases :

(i) From the zeroth order dispersion relation we find that in general if we express it in the form

$$a\omega_0^4 + 4b\omega_0^3 + 6c\omega_0^2 + 4d\omega_0 + e = 0. \quad (8.3)$$

the discriminant of the reducing cubic given by;

$$\Delta \equiv \{I_3 - 27J^2\}, \quad (8.4)$$

where

$$I = \{ac - 4bd + 3c^2\} \quad (8.5)$$

and

$$J = \{ace - 2bdc - ad^2 - eb^2 - c^3\}, \quad (8.6)$$

is less than zero for  $m = 1, 2$ ,  $H_1 = 1, 2$ ,  $K = 0.5, 5$  for  $n = 1, 2, 3$  modes. This shows that it has two real and two complex roots. Thus the system is unstable in the zeroth order approximation.

From the first order dispersion relation we note that the effects of low intensity ring currents is to increase the growth rate of instability. Further as  $K$  increases the growth rate of instability decreases.

(ii) For purely imaginary roots of the zeroth order dispersion relation we set  $\omega_0 = i\alpha$  and obtain

$$\alpha = \pm \sqrt{\frac{\{nK^2(3-H_2)(n-2)m^{-n-2} + nK^2(3-H_1)(n-2)m^{-n-4} - nK^2(3n-2) \times (3+H_2)m^{n-2} - nK^2(3+H_1)(3n-2)m^{n-4}\}}{\{(3-H_2)m^{-n-2} + (3-H_1)m^{-n-4} - (3+H_2)m^{n-2} - n(3+H_1)m^n\}}} \quad (8.7)$$

where

$$\begin{aligned} & \alpha^1(m^n - m^{-n}) - \alpha^2\{nK^2(3n+2)m^{n-4} + nK^2(3n-2)m^n \\ & + n^2K^2(3+H_1)(3+H_2)m^{n-2} - nK^2(n-2)m^{-n-4} - nK^2(n+2)m^{-n} \\ & + n^2K^2(H_1-3)(3-H_2)m^{-n-2}\} + \{n^2K^4(9n^2-4)m^{n-4} \\ & - n^2K^4(n^2-4)m^{-n-4}\} = 0 \end{aligned} \quad (8.8)$$

Thus whenever (8.8) is satisfied, we have one unstable mode. Moreover,  $\omega_1$  will increase the growth rate of instability by a fraction of  $\beta$ .

## CONCLUSIONS

By using the normal mode technique we get more insight of the problem as compared to that of Energy Principle. It was extremely difficult to solve the differential equation satisfied by perturbed quantities in the axisymmetric disturbance for general rotation. However, we got a reasonably good physical picture even when  $K$  is of the order of perturbation parameter. The equations involved in  $\theta$ -disturbance could be solved for general rotation and we find that both the stable and unstable modes were present. Thus, as usual we conclude that the net effect of the  $\theta$ -disturbance is to bring instability in the device.

## ACKNOWLEDGMENT

The authors are extremely grateful to Prof. P. L. Bhatnagar for encouragement, help and guidance throughout the preparation of this paper. One of us (M.P.S.) wishes to thank Council of Scientific and Industrial Research for the financial assistance.

## REFERENCES

- Anderson O. A., Baker W. R., Bratenahl A., Furth H. P., Iso Jr, J., Kunkel W. B., & Stone J. M. 1958. *Proc. II Int United Nations Int Conf. on Peaceful Uses of Atomic Energy* **32**, 155.
- Boyer K., Hammel J. E., Longmire C. L., Nagle D., Ribe F. L., & Rosenfeld W. B. 1958 *Proc. II Int United Nations Int. Conf. on Peaceful Uses of Atomic Energy* **31**, 319.
- Perkins W. A. & Post R. F. 1963 *Phys. Fluids* **6**, 1537.
- Verma P. & Verma Y. K. 1965 *Zett. fur Physik* **182**, 238.

## Quadrupole hyperfine effects in microwave spectrum of $\text{SF}_6\text{Cl}$

BY K. S. R. MURTY\* AND A. K. MOHANTY

Department of Physics, G. M. College, Sambalpur, Orissa

(Received 7 March 1970—Revised 24 September 1970)

The hyperfine structures of the absorption lines having frequencies 25,543.85 Mc/s and 35,670.59 Mc/s observed in the microwave spectrum of  $\text{SF}_6\text{Cl}$  using a Stark Modulation Spectrometer and identified with transitions  $J\ 7 \leftarrow 6$ , of  $^{32}\text{SF}_6\ ^{35}\text{Cl}$  and  $J\ 10 \leftarrow 9$  of  $^{32}\text{SF}_6\ ^{37}\text{Cl}$ , respectively, have been studied in details. The hyperfine structures could be interpreted as due to the combined effects mainly of nuclear quadrupole interaction and subsidiarily of the centrifugal distortion due to rotation. The best fit was obtained with quadrupole coupling constant  $eqQ = -81.5 \pm 5$  Mc/s and the centrifugal distortion constant  $D_{JK} = 0.0026 \pm 0.005$  Mc/s for the  $^{35}\text{Cl}$  nucleus in  $^{32}\text{SF}_6\ ^{35}\text{Cl}$  and  $eqQ = -64.23 \pm 5$  Mc/s and  $D_{JK} = 0.0026 \pm 0.0005$  Mc/s for the  $^{37}\text{Cl}$  nucleus in  $^{32}\text{SF}_6\ ^{37}\text{Cl}$ . These values of the quadrupole coupling constant have been used for a discussion on the *s*-, *d*-, and ionic characters of chemical bond.

### INTRODUCTION

The quadrupole hyperfine structure in the absorption lines of the rotational spectrum of  $\text{SF}_6\text{Cl}$  in the frequency range 29,193 Mc/s—29,198 Mc/s has been studied in details using a Stark Modulation Spectrometer. The transitions involved were identified as  $J\ 8 \leftarrow 7$ . The correlation of observation and calculation made by taking the value of quadrupole coupling constant  $eqQ = -81.5 \pm 5$  Mc/s and centrifugal distortion constant  $D_{JK} = 0.0026 \pm 0.0005$  Mc/s were reported by Kewly, *et al* (1960). In this work corresponding calculations for  $J\ 7 \leftarrow 6$  transition for  $^{32}\text{SF}_6\ ^{35}\text{Cl}$  and  $J\ 10 \leftarrow 9$  transition for  $^{32}\text{SF}_6\ ^{37}\text{Cl}$  are made and compared with the experimental observations made earlier by Murty (1961).

### EXPERIMENTAL

The absorption spectrum of  $\text{SF}_6\text{Cl}$  in the frequency range 20,000–30,000 and 35,000–37,000 Mc/s was studied at Cambridge by Murty (1961) using a Stark Modulation Microwave Spectrometer.

The hyperfine structure of the lines having frequencies 25,543.85 Mc/s was identified with transition  $J\ 7 \leftarrow 6$  for the  $\text{SF}_6\ ^{35}\text{Cl}$  isotope and correlation between the observation and calculation is shown in table 1.

\* Department of Physics, Ravenshaw College, Cuttack-3, Oris

TABLE 1  $J \leftarrow 6$  transition  $^{32}\text{SF}_6^{35}\text{Cl}$ .

$K$	$K' + J$	$K'$	Frequency in Mc/s	
			Calculated	Observed
0	17/2	15/2	25,544.08	25,544.13
	15/2	13/2	25,544.08	..
	13/2	11/2	25,543.41	25,543.85
	11/2	9/2	25,543.40	..
1	17/2	15/2	25,544.17	25,544.13
	15/2	13/2	25,543.81	25,544.13
	13/2	11/2	25,543.27	25,543.85
	11/2	9/2	25,543.63	25,543.85
2	17/2	15/2	25,544.36	25,543.85
	15/2	13/2	25,543.00	25,543.03
	13/2	11/2	25,542.83	25,543.03
	11/2	9/2	25,544.23	25,544.13
3	17/2	15/2	25,544.94	25,545.66
	15/2	13/2	25,541.67	25,541.82
	13/2	11/2	25,542.09	25,541.82
	11/2	9/2	25,545.37	25,545.66
4	17/2	15/2	25,545.61	25,545.66
	15/2	13/2	25,539.80	—
	13/2	11/2	25,541.18	25,541.82
	11/2	9/2	25,546.90	25,547.03
5	17/2	15/2	25,546.49	25,547.03
	15/2	13/2	25,537.39	25,537.88
	13/2	11/2	25,539.77	—
	11/2	9/2	25,548.87	25,549.75
6	17/2	15/2	25,547.54	25,547.03
	15/2	13/2	25,534.45	25,534.92
	13/2	11/2	25,538.17	25,537.88
	11/2	9/2	25,551.28	25,551.25

Starting from  $eqQ$  value obtained for  $^{35}\text{Cl}$  nucleus in  $^{32}\text{SF}_6^{35}\text{Cl}$  and using the ratio of the quadrupole moment of  $^{35}\text{Cl}$  nucleus and  $^{37}\text{Cl}$  nucleus given by

$$\frac{Q_{35}}{Q_{37}} = 1.2688$$

a value of  $-64.23 \pm 5$  Mc/s is obtained for the quadrupole coupling constant for  $^{37}\text{Cl}$  nucleus. Assuming the change in  $D_{jk}$  to be negligibly small for the isotopic substitution of  $^{35}\text{Cl}$  by  $^{37}\text{Cl}$  the frequencies of the components of  $J \leftarrow 10 \leftarrow 9$  transi-

values and calculated values is shown in table 2. The intensities of lines in the transitions are less than in the corresponding transitions for  $^{32}\text{SF}_6$ ,  $^{35}\text{Cl}$  because of the lower relative natural abundance of  $^{37}\text{Cl}$  isotope. It is only because the frequencies in this transitions are higher and the absorption increases with frequencies, that the nuclear quadrupole effect could be observed in the transitions of this molecular species. Calculations for values of  $K$  lower than 6 are not included in the table as the shifts are much too small and are certainly within the broad central peak observed. The correlation is good particularly for the extreme components.

 TABLE 2.  $J\ 10 \leftarrow 9$  transition of  $^{32}\text{SF}_6$ ,  $^{37}\text{Cl}$ 

$K$	$F \rightarrow I$	$F$	Frequencies in Mc/s	
			Calculated	Observed
6	23/2	21/2	35,670.23	35,670.60
	21/2	19/2	35,667.30	35,666.74
	19/2	17/2	35,667.28	35,666.74
	17/2	15/2	35,670.79	35,670.60
7	23/2	21/2	35,670.07	35,670.60
	21/2	19/2	35,665.30	—
	19/2	17/2	35,665.15	35,666.74
	17/2	15/2	35,670.92	35,670.60
8	23/2	21/2	35,669.87	35,670.60
	21/2	19/2	35,663.61	35,663.54
	19/2	17/2	35,664.82	—
	17/2	15/2	35,671.05	35,670.60
9	23/2	21/2	35,669.65	35,670.60
	21/2	19/2	35,661.75	35,661.90
	19/2	17/2	35,663.25	35,663.54
	17/2	15/2	35,671.20	35,670.60

#### INTERPRETATION OF QUADRUPOLE COUPLING CONSTANT

The value of quadrupole constant for the  $^{35}\text{Cl}$  nucleus made use of in this investigation is  $-81.5 \pm 5$  Mc/s and in table 3 are collected the values for this constant in different molecules. In cases where the coupling constants are known in solid phase the values are put in a separate column. They are obtained from observations of pure quadrupole resonance (Livingstone 1951, Dailey 1951 and Nave *et al.* 1968).

The quantity  $eqQ$  involves a nuclear property  $Q$  and a molecular property  $q$ . Knowledge of  $eqQ$  and one of these enables one to determine the other. The quantity  $q$  can be estimated if the charge distribution over the molecule is known;

TABLE 3.  $eqQ$  for  $^{35}\text{Cl}$  in some molecules

Molecules	$eqQ$			
	Solid	Reference	Gas	Reference
Cl (atomic)			-109.6	Townes & Schawlow 1955
FCI			-146.0	
ICl			-82.5	
ClCN			-83.3	
Cl <sub>2</sub>			1	
CH <sub>3</sub> Cl	68.40	(Livingstone 1951)	-74.74	Nordsieck 1940, Newell 1950, Ishigur 1948
CH <sub>2</sub> Cl <sub>2</sub>	-72.47	(Dailey 1960)	-78.40	"
CHCl <sub>3</sub>	-76.98	"	-82.9	"
CCl <sub>4</sub>	-81.85	"	-87.9	"
CHF <sub>2</sub> Cl	-70.50	"		
CF <sub>3</sub> Cl	-77.50	"		
CHFCl <sub>2</sub>	-73.53	"		
CF <sub>2</sub> Cl <sub>2</sub>	-78.16	"		
CFCl <sub>3</sub>	-79.63	"		
CF <sub>2</sub> BrCl	-73.35	"		
PCl <sub>3</sub>	-52.40	(Nave <i>et al</i> 1968)	-53.3 ± 1.0	(Nave <i>et al</i> 1968)
POCl <sub>3</sub>	-57.97	"	-55.4 ± 1.2	"

but the charge distribution involves knowledge of wave functions for the electron in the molecule. Accurate calculation of  $q$  has been made only for the case of hydrogen deuteride (Nordsieck 1940) as accurate wave functions are known only for hydrogen molecule. Somewhat less accurate self consistent field molecular orbital (SCFMO) wave functions are available for a few other molecules. But, so far as the interpretation of nuclear quadrupole coupling constant is concerned, one has to be content with the semi-empirical approach that forms the basis of the theory of Townes & Dailey (1949). They have given the following relations between  $eqQ$  in a diatomic molecule and the atomic  $eqQ_{310}$  which is obtained from the atomic data.

The quadrupole coupling constant for an atom forming a hybrid bond with a negative ionic character is

$$eqQ = (-1 + s - d)(1 - i)eqQ_{310}$$

For the partially ionic bond

$$eqQ = [(-1 + s - d)(1 - i) + 2(1 + e)i]eqQ_{310}$$

$s$ ,  $d$  and  $i$  are the amounts of  $s$ -,  $d$ -, and ionic characters in the bond and  $(1 + e)$  is the ratio of the interaction between a valence  $p$  electron and the nucleus



when the atom is positively ionic and neutral. The value of  $e$  is known and tabulated for various elements (Dailey & Townes 1955).

The measurements of quadrupole effects, however, cannot determine the three quantities  $s$ ,  $d$  and  $i$ . Consequently, reasonable assumptions concerning  $s$ , and  $d$ , are to be made in order to determine the value of  $i$ . Townes & Dailey (1949) arrived at a purely empirical rule, "Cl, Br and I bonds are considered to have 15 percent  $s$ -character, whenever halogen is bonded to an atom which is more electropositive than the halogen, by as much as 0.25 units; otherwise no hybridization is allowed". In the diatomic molecules considered by them, they put the limit of  $d$ -character at about 5 percent. The ionicity arrive at from these considerations plotted against the electronegativity difference between the bonding atoms gives an  $s$ -shaped curve. Gordy (1955), however, has different views on hybridization of orbitals.

The length of S-Cl bond in  $\text{SF}_5\text{Cl}$  is very nearly the sum of single bond covalent radii for sulphur and chlorine (Pauling 1960). So it is reasonable to assume that the double bond character is not present in the bond. Hydrolysis of  $\text{SF}_5\text{Cl}$  indicates that chlorine is positive. The positive nature of the chlorine atom is supported from the observation that  $\text{SF}_5\text{Cl}$  is a powerful oxidising agent. If chlorine is positive two  $p$ -electrons must be missing from a  $p_o$  ( $m = 0$ ) orbital. With two missing  $p_o$  electrons,  $\text{Cl}^+$  should have a value of  $q = -2q^+_{310}$ . Here  $q^+_{310}$  refers to  $\text{Cl}^+$  atom and may be different from  $q_{310}$  for the natural atom, even though the difference is not expected to be considerable. In the diatomic molecule  $\text{FCl}$ , where chlorine is positive,  $eqQ$  observed has a value, 146 Mc/s. This is considerably lower than  $-2q_{310}$ , and is evidently due to the ionicity of the bond.

Considering the expression for the ratio of  $eqQ$  and  $eqQ_{310}$  in the case of a positive ion, it is found that in the case of  $\text{SF}_5\text{Cl}$  the value of  $s-d$  must be high and ionicity low. The following table 4 gives a few sets of values of ionicity and  $(s-d)$  that are consistent with the ratio.

Table 4

$i$	$(s-d)$
0	0.26
0.1	0.54
0.2	0.89
0.23	1

The upper limit set for these calculations for the ionicity of the bond is 0.23, but it should be lower than that, because otherwise  $(s-d)$  becomes unreasonably high.

## REFERENCES

- Dailey B. F. 1960 *J. Chem. Phys.* **33**, 1641  
Dailey B. P. & Townes C. H. 1955 *J. Chem. Phys.* **23**, 118.  
Goudy W. 1955 *Disc. Faraday Society* **19**, 14  
Ishiguro E. 1948 *J. Phys. Soc. Jap.* **3**, 129  
Kewley R., Murty K. S. R. & Sugden T. M. 1960 *Trans. Faraday Society* **56**, No. 456  
Livingstone R. 1951 *J. Chem. Phys.* **19**, 1434  
Murty K. S. R. 1961 *Ph.D. Thesis*, Cambridge University  
Nave C. R., Weatherly T. L. & Williams Q. 1968 *J. Chem. Phys.* **49**, 1413.  
Newell G. F. 1950 *Phys. Rev.* **78**, 711  
Nordsieck A. 1940 *Phys. Rev.* **58**, 310  
Pauling L. 1960 *The Nature of the Chemical Bond* (Cornell Univ. Press)  
Townes C. H. & Dailey B. P. 1949 *J. Chem. Phys.* **17**, 782  
Townes C. H. & Schawlow A. L. 1955 *Microwave Spectroscopy*, McGraw Hill

## A new logarithmic form of overlap repulsion for the heavier salts

By K. P. PANDE, K. D. MISRA AND M. N. SHARMA

*Department of Physics, University of Lucknow, Lucknow-7*

(Received 16 April 1970)

The various lattice properties of metal halides containing heavier ions have been studied on the basis of a modified new logarithmic form  $4 \log(1 + B/b^6)$  for overlap repulsion. The necessary equations for the potential parameters  $A$  and  $B$  have been derived using the room temperature lattice conditions. These parameters have been utilized to compute the cohesive energies, force constants, reststrahlen frequencies and Debye characteristic temperatures. It is inferred that the theoretical values of these lattice properties compare well with observed values and are much better than the other computed values reported earlier. The present approach serves to justify the adequacy of the chosen potential energy function for the heavier salts also.

### INTRODUCTION

The theory of ionic crystals was first developed by Born and later extended by Born & Mayer (1932) and others. The cohesive energy of ionic crystals consists of the Coulomb interaction which gives rise to Madelung's energy, the short range repulsive potential energy, the dipole-dipole and dipole-quadrupole interaction energies and the zero point energy.

The need for a repulsive potential in order to maintain a stable crystal was recognized long before the advent of quantum mechanics and in order to facilitate the computation of cohesive energy of ionic crystals, Born and other workers adopted an empirical repulsive potential of the form  $\lambda/r^n$ , where  $\lambda$  and  $n$  are constants to be determined by the condition of thermodynamic equilibrium of the crystal lattice.

After the advent of quantum mechanics Born & Mayer (1932) introduced an exponential form  $\lambda \exp(-r/\rho)$  where  $\lambda$  and  $\rho$  were taken as potential parameters. These forms for repulsive potential are not quite adequate. The Born form is a fair approximation for short range of  $r$  only, whereas in the Born & Mayer (1932) form  $\rho$  is chosen quite arbitrarily for different crystals and the constant  $\lambda$  has ionic radii dependence. Keeping in view the limitations of these repulsive potential forms, Prakash & Behari (1969) have recently suggested a new logarithmic form for repulsive potential and successfully calculated the cohesive energies of alkali halide crystals at 0°K. In the present work we have modified the logarithmic form of the overlap repulsion by taking into account

the dipole-quadrupole interaction energy term, because Van der Waal's potential shows a systematic tendency to increase for salts of heavier ions

#### EVALUATION OF POTENTIAL PARAMETERS

Taking into account all the above interaction energy terms, the cohesive energy per unit cell in an ionic crystal may be written as

$$\psi(r) = -\frac{\alpha e^2}{r} + A \log_e \left(1 + \frac{B}{r^9}\right) - \frac{C}{r^6} - \frac{D}{r^8} + \epsilon \quad (1)$$

where  $\alpha$  is the Madelung's constant,  $e$  the electronic charge,  $r$  the interionic distance,  $A$  and  $B$  the potential parameters.  $C$  and  $D$  Van der Waal's interaction constants and  $\epsilon$  the zero point energy

The potential parameters  $A$  and  $B$  are evaluated from the room temperature equilibrium lattice conditions due to Hildebrand (1931).

$$\left(r \frac{d\psi}{dr}\right)_{r=r_0} = \frac{3vT\alpha_v}{\beta} \quad (2)$$

and

$$\left(r^2 \frac{d^2\psi}{dr^2}\right)_{r=r_0} = \frac{9v}{\beta} F_{T,P} \quad (3)$$

where  $\beta$  is the compressibility,  $\alpha_v$  the thermal expansion,  $T$  the absolute scale room temperature and  $v$  the volume per ion pair given by  $v = V/N = kr_0^3$  in which  $k = 2$  for f.c.c. crystals,  $k = 1.54$  for b.c.c. crystals and  $k = 3.2$  for crystals having zinc blende structure.  $F_{T,P}$  is a correction term which is taken to be equal to unity due to non-availability of data required for its computation.

Equations (1), (2) and (3) give

$$A = \frac{1}{9} \left( \frac{\alpha e^2}{r_0} + \frac{6C}{r_0^6} + \frac{8D}{r_0^8} - \frac{3vT\alpha_v}{\beta} \right) \left( 1 + \frac{r_0^9}{B} \right) \quad (4)$$

and

$$B = \frac{8\alpha e^2 r_0^7 + 18Cr_0^2 + 8D - 3vr_0^8(10T\alpha_v + 3)/\beta}{\frac{\alpha e^2}{r_0^2} + \frac{36C}{r_0^7} + \frac{64D}{r_0^6} + \frac{3v}{\beta r_0}(T\alpha_v + 3)} \quad (5)$$

#### COMPUTATION OF CRYSTAL PROPERTIES

##### (1) Cohesive energies

The values of  $A$  and  $B$  computed on the basis of equations (4) and (5) have been utilized for the theoretical determination of  $\psi(r)$  from equation (1) which are presented in table 1.

Table 1 Values of Cohesive Energies

Crystal	$\psi(r)$ (K cal/mol)			
	Expt.	Theor. eq. (1)	Theor. (c)	Theor. (d)
NH <sub>4</sub> Cl	—	164.1	—	—
NH <sub>4</sub> Br	—	156.9	—	—
CuCl	221.9 <sup>a</sup>	214.9	211.0	216.9
CuBr	216.0 <sup>a</sup>	204.8	201.9	—
CuI	213.4 <sup>a</sup>	197.2	195.6	194.5
AgCl	205.7 <sup>b</sup>	200.6	197.5	197.9
AgBr	201.8 <sup>b</sup>	193.3	190.2	190.5
AgI	199.0 <sup>b</sup>	186.9	183.9	—
TlCl	170.1 <sup>b</sup>	166.8	161.5	168.2
TlBr	165.6 <sup>b</sup>	159.2	157.6	162.4

(a) Mayer &amp; Levy (1933)

(b) Mayer (1933).

(c) Saxena &amp; Kachhava (1961)

(d) Mathur &amp; Singh (1967)

## (2) Reststrahlen frequencies

Krishnan & Roy (1951) and Born & Huang (1954) have given the following relation for the force constant in terms of potential parameters,

$$f = \frac{1}{3} \left[ \phi''(r_0) + \frac{2}{r_0} \phi'(r_0) \right] \quad (6)$$

in which  $\phi'(r)$  and  $\phi''(r)$  are the first and second derivatives of  $\phi(r)$ , ( $\phi(r)$  contains the rest of energy in  $\psi(r)$ , except the Coulombian term  $-\alpha e^2/r$ ). Using equation (6) in conjunction with equation (1), the expression for the force constant can be derived as

$$f = \frac{3AB(8r_0^9 - B)}{r_0^2(B + r_0^9)^2} - \frac{10C}{r_0^8} - \frac{56D}{3r_0^{10}} \quad (7)$$

Now if we consider the polarization of positive ions with respect to the lattice of negative ions, the reststrahlen frequency can be computed from the equation

$$\nu = (2\pi)^{-1} [f(\epsilon_\infty + 2)]^{1/2} [\mu(\epsilon_0 + 2)]^{-1/2} \quad (8)$$

where  $\mu$  is reduced mass per ion pair,  $\epsilon_0$  and  $\epsilon_\infty$  are the static and high frequency dielectric constants, respectively. The calculated values of  $f$  from equation (7) have been used to compute  $\nu_0$  on the basis of equation (8) and are tabulated in table 2.

Table 2. Values of Force Constants and Reststrahlen Frequencies

Crystal	$f \times 10^{-4}$ Eq. (7)	$\nu_0 \times 10^{-12}$ cm/sec.		
		Expt.	Theor. eq. (8)	Theor. <sup>(c)</sup>
NH <sub>4</sub> Cl	2 756	—	4.20	—
CuCl	9.065	5.67 <sup>a</sup>	5 31	5 344
CuBr	8.137	5.27 <sup>a</sup>	4 67	4 692
AgCl	7 095	3 09 <sup>b</sup>	3 99	4.168
AgBr	6.422	2.40 <sup>b</sup>	3.06	3.086
TlCl	3.241	1.89 <sup>b</sup>	1.85	1.909
TlBr	3.089	1 43 <sup>b</sup>	1 38	1.591

(a) Born &amp; Huang (1954)

(b) Jones *et al* (1961).

(c) Srivastava &amp; Madan (1967)

## (3) Debye Characteristic Temperature

A number of relations have been given for  $\Theta_D$  in terms of compressibility and lattice energy by Joshi & Mitra (1960) and Srivastava & Madan (1967). It is seen that their results are at variance when compared with experimental results. However, in the present work a relation has been suggested for  $\Theta_D$  in terms of the various lattice properties. If the value of force constant  $f$  is computed from equation (7), the value of  $\Theta_D$  can be easily obtained from the equation

$$\Theta_D = h(2\pi k)^{-1} [f(\epsilon_\infty + 2)]^{1/2} [\mu(\epsilon_0 + 2)]^{-1/2} \quad (9)$$

where  $h$  is the Planck's constant and  $k$  the Boltzman's constant. The theoretical values of  $\Theta_D$  for a few metal halides have been presented in table 3, where these

Table 3. Values of Debye Characteristic Temperatures

Crystal	$\Theta_D$ in °K				
	Expt.	Theor. eq. (9)	Theor. <sup>(a)</sup>	Theor. <sup>(b)</sup>	Theor. <sup>(c)</sup>
NH <sub>4</sub> Cl	—	204	—	—	—
CuCl	—	255	255	—	—
CuBr	—	224	222	—	—
AgCl	183	191	198	136	—
AgBr	144	147	147	128	—
TlCl	—	89	89	—	157, 123, 125, 164.
TlBr	—	66	65	109	123, 114, 117

(a) Sharma (1969).

(b) Reddy (1963).

(c) Mitra &amp; Joshi (1960).

have been compared with the experimental values as well as with the calculated values from other methods. The present values of  $\Theta_D$  are in excellent agreement with observed values and are in a much better fit with the values obtained from other determinations.

#### DISCUSSIONS

The theoretical values of  $\psi(r)$  (table 1) using the logarithmic form of repulsion interaction in terms of various lattice properties are in excellent agreement with the experimental results when compared with the theoretical values of Saxena & Kachhava (1964) who employed the Born-Mayer potential energy function, and with those of Mathur & Singh (1967) using Varshni & Shukla (1961) potential model which neglect the dipole-dipole and dipole-quadrupole interactions.

The computed values of  $\nu_0$  (table 2) show a superiority over the theoretical values of Srivastava & Madan (1967) employing the repulsion interaction term of the form  $\lambda e^{-r/\rho}$  neglecting the contribution of dipole-dipole and dipole-quadrupole interaction terms, which are quite important for crystals containing heavier ions, when compared with observed values of  $\nu_0$ . In view of the present simple approach using a more accurate potential model, the present results are comparable to the results obtained from the study of frequency *versus* wave vector dispersion curves.

The calculated values of  $\Theta_D$  for AgCl, AgBr are in better agreement with the observed values of  $\Theta_D$  as compared with the calculated values of Reddy (1963). Unfortunately for other crystals observed data are not available, therefore we can predict the correctness of theoretical values of  $\Theta_D$  for  $\text{NH}_4\text{Cl}$ , CuCl, CuBr, TiCl, and TiBr on this basis. The authors feel that the old and incomplete experimental data for  $\Theta_D$  need thorough revision for these crystals. The salts considered here have different characteristics from the alkali halides. These salts have a high value of attractive Van der Waal's potential so that the contribution due to dipole-quadrupole interaction is quite significant for them.

#### ACKNOWLEDGEMENTS

The authors are thankful to Dr. B. G. Gokhale for his keen interest in the present work. Two of them (K.P.P. and K.D.M.) are grateful to the Council of Scientific and Industrial Research and University Grants Commission, New Delhi, for providing financial assistance.

#### REFERENCES

- Born M. & Mayer J. E. 1932 *Zeits f. Physik*. **75**, 1.  
 Born M. & Huang K. 1954 *Dynamical Theory of Crystal Lattices*, Clarendon Press, Oxford.  
 Jones G. O., Martin D. H., Mawer P. A. & Periy C. H. 1961 *Proc. Roy. Soc.* **A261**, 10.

- Kittel C 1956 *Introduction to Solid State Physics*, John Wiley and Sons Inc. New York.
- Mathur V K & Singh S. P. 1967 *Phil. Mag* **16**, 1299
- Mayer J E. & Levy B B 1933 *J. Chem Phys* **1**, 647.
- Mayer J. E. 1933 *J. Chem Phys*, **1**, 270
- Mitra S S & Joshi S. K. 1960 *Physica* **26**, 825
- Prakash S. & Behari J. 1969 *Ind J. Pure. Appl. Phys* **7**, 709
- Reddy P. J 1963 *Physica* **29**, 63.
- Saxena S C & Kachhava C M 1964 *Ind. J Pure Appl Phys* **2**, 338.
- Sharma M N. 1969 *J Phys Soc. Japan* **227. No. 6**, 1691
- Srivastava S P & Madan M P 1967 *J Phys Soc Japan* **23**, 1433
- Varshni Y P & Shukla R C. 1961 *J. Chem. Phys* **35**, 582.



## Hydromagnetic source flow

By M. A. A KHAN AND R. B. SRIVASTAVA

*Department of Mathematics and Astronomy, Lucknow University,  
Lucknow-7*

*(Received 17 November 1970)*

The steady flow of a viscous incompressible and electrically conducting fluid between two parallel coaxial rotating disks with a transverse magnetic field has been analysed when the two disks are rotating with the same velocity and there is a source at the centre. The velocity of the fluid relative to the disks is supposed to be small.

### 1. INTRODUCTION

The steady laminar source flow between two parallel disks rotating in the same direction with the same constant angular velocity has been studied by Kreith & Peube (1965, 1966) and Broiter & Pohlhausen (1962). Recently Khan (1968) studied the effect of porosity on the laminar source flow between two disks rotating with the same velocity. Further Khan (1969) extended the problem of Kreith & Peube to hydromagnetics and calculated the effect of uniform transverse magnetic field for the two cases, *viz.*,

- (i) when the applied transverse magnetic field is small,
- and (ii) when the rotational Taylor numbers of the two disks are small

In the present paper an attempt has been made to analyse the flow of a viscous, incompressible and electrically conducting fluid in presence of a constant transverse magnetic field, when there is no restriction on the strength of the magnetic field (but the induced field, is neglected), or on the rotational Taylor numbers of the two disks, but it has been supposed that the velocity of the fluid relative to the velocities of the disks is small. Source flow problems of this type are of interest in the design of viscosity pumps (Hasinger & Kohrt 1963, Rice 1963), rotating heat exchangers (Clark & Bromley 1961), air thrust bearings (Grassam & Powell 1964), multiple disk turbines (Armstrong 1952, Gurbert 1960), in calculating the loss of lift in ground effect on VOLT aircraft with centrally located downward pointing jet, and in the design of radial diffusers, particularly with reference to the design of efficient internal ducts in annular jet ground effect machines.

## 2. BASIC EQUATIONS AND BOUNDARY CONDITIONS

Let us take the axis of rotation of the two disks as  $z$ -axis and let the two disks be situated at  $z = \pm a$ . Consider the flow of an incompressible fluid between two parallel rotating disks with the source at the centre.

The governing non-dimensional hydromagnetic equations of motion in cylindrical polar coordinates are

$$u \frac{\partial u}{\partial r} + w \frac{\partial u}{\partial z} - \frac{v^2}{r} = -\frac{\partial p}{\partial r} + \frac{\partial}{\partial r} \left( \frac{\partial u}{\partial r} + \frac{u}{r} \right) + \frac{\partial^2 u}{\partial z^2} - Mu, \quad (2.1)$$

$$u \frac{\partial v}{\partial r} + w \frac{\partial v}{\partial z} + \frac{uv}{r} = \frac{\partial}{\partial r} \left( \frac{\partial v}{\partial r} + \frac{v}{r} \right) + \frac{\partial^2 v}{\partial z^2} - Mr, \quad (2.2)$$

$$u \frac{\partial w}{\partial r} + w \frac{\partial w}{\partial z} = -\frac{\partial p}{\partial z} + \frac{\partial^2 w}{\partial r^2} + \frac{1}{r} \frac{\partial w}{\partial r} + \frac{\partial^2 w}{\partial z^2}, \quad (2.3)$$

and the equation of continuity

$$\frac{\partial}{\partial r}(ru) + \frac{\partial}{\partial z}(rw) = 0 \quad (2.4)$$

where the non-dimensional quantities are defined as

$$r = \frac{\bar{r}}{\sqrt{\nu/\omega}}, \quad z = \frac{\bar{z}}{\sqrt{\nu/\omega}}, \quad u = \frac{\bar{u}}{\sqrt{\nu\omega}},$$

$$v = \frac{\bar{v}}{\sqrt{\nu\omega}}, \quad w = \frac{\bar{w}}{\sqrt{\nu\omega}}, \quad p = \frac{\bar{p}}{\rho\nu\omega}, \quad M = \frac{\sigma B_0^2}{\rho\omega}$$

If the two disks rotate with angular velocity  $\omega$  and the strength of the source is  $Q$ , the boundary conditions are

$$\left. \begin{aligned} u &= 0 \\ v &= r \\ w &= 0 \end{aligned} \right\} \text{ at } z = \pm \alpha \quad (2.5)$$

$$r \int_{-\alpha}^{+\alpha} u dz = K. \quad (2.6)$$

where  $\alpha = \frac{a}{\sqrt{\nu/\omega}}$  and  $K = \frac{Q\omega^{\frac{1}{2}}}{2\pi\nu^{\frac{3}{2}}}$

## 3 SOLUTION OF THE PROBLEM

It is convenient to introduce instead of  $v$ , which is the non-dimensional tangential velocity in the fixed system of coordinates, the non-dimensional tangential velocity relative to the disks

$$V = v + r.$$

Substituting  $v = V + r$  in the equations of motion and assuming that the velocity of fluid relative to the disks is small (this condition is well satisfied for large  $\text{radn}$ ), so that the quadratic terms are negligible, we obtain

$$-2V + r = -\frac{\partial p}{\partial r} + \frac{\partial}{\partial r} \left( \frac{\partial u}{\partial r} + \frac{u}{r} \right) + \frac{\partial^2 u}{\partial z^2} - Mu, \quad (3.1)$$

$$2u = \frac{\partial}{\partial r} \left( \frac{\partial V}{\partial r} + \frac{V}{r} \right) + \frac{\partial^2 V}{\partial z^2} - M(V + r), \quad (3.2)$$

$$0 = -\frac{\partial p}{\partial z} + \frac{1}{r} \frac{\partial}{\partial r} \left( r \frac{\partial w}{\partial r} \right) + \frac{\partial^2 w}{\partial z^2} \quad (3.3)$$

and the no-slip boundary conditions then become

$$\left. \begin{aligned} u(r, \pm\alpha) &= 0, \\ v(r, \pm\alpha) &= 0, \\ w(r, \pm\alpha) &= 0 \end{aligned} \right\} \quad (3.4)$$

The equation of continuity (2.4) is satisfied by introducing a stream function  $\psi$  defined by

$$u = \frac{1}{r} \frac{\partial \psi}{\partial z}, \quad w = -\frac{1}{r} \frac{\partial \psi}{\partial r} \quad (3.5)$$

The solution can then be expressed in the form

$$u = rf'_{-1} + f'_0 + \frac{f'_1}{r} + \frac{f'_2}{r^2} + \frac{f'_3}{r^3} + \dots + \frac{f'_n}{r^n} + \dots, \quad (3.6)$$

$$V = rf_{-1} + f_0 + \frac{f_1}{r} + \frac{f_2}{r^2} + \frac{f_3}{r^3} + \dots + \frac{f_n}{r^n} + \dots, \quad (3.7)$$

$$w = -2f_{-1} - \frac{f_0}{r} + \frac{f_2}{r^3} + \dots + \frac{(n-1)f_n}{r^{n+1}} + \dots, \quad (3.8)$$

$$p = r^2 h_{-2} + rh_{-1} + h_0 + h_1 \log r + \frac{h_2}{r} + \frac{h_3}{r^2} + \dots + \frac{h_n}{r^{n-1}} + \dots, \quad (3.9)$$

Substituting these values of  $u$ ,  $V$ ,  $w$  and  $p$  in equations (3.1) to (3.3) and equating terms in like powers of  $r$  on both sides, we get an infinite system of simultaneous ordinary differential equations. The first five systems are

$$(I) \quad \begin{cases} f'''_{-1} + 2g_{-1} + 1 = 2h_{-2} + Mf'_{-1}, \\ g''_{-1} - 2f'_{-1} = M(g_{-1} + 1), \\ h'_{-2} = 0. \end{cases}$$

$$(II) \quad \begin{cases} f'''_0 + 2g_0 = h_{-1} + Mf'_0, \\ g''_0 - 2f'_0 = Mg_0, \\ h'_{-1} = 0. \end{cases}$$

$$(III) \quad \begin{cases} f'''_1 + 2g_1 = h_1 + Mf'_1, \\ g''_1 - 2f'_1 = Mg_1, \\ h'_1 = 0. \end{cases}$$

$$(IV) \quad \begin{cases} f'''_2 + 2g_2 = -h_2 + f'_0 + Mf'_2, \\ g''_2 + 2f'_2 = g_0 + Mg_2, \\ h'_2 = f''_0 \end{cases}$$

$$(V) \quad \begin{cases} f'''_3 + 2g_3 = 2h_3 + Mf'_3, \\ g''_3 - 2f'_3 = Mg_3, \\ h'_3 = 0 \end{cases}$$

Solving system (I) and applying boundary conditions, we have

$$\begin{aligned} f'_{-1}(z) &= A_1 \cosh(z\sqrt{r} \cos \theta/2) \cos(z\sqrt{r} \sin \theta/2) \\ &\quad + B_1 \sinh(z\sqrt{r} \cosh \theta/2) \sin(z\sqrt{r} \sin \theta/2) - \frac{2Mh_{-2} + M}{M^2 + 4}, \end{aligned}$$

$$\begin{aligned} g_{-1}(z) &= A_1 \sinh(z\sqrt{r} \cos \theta/2) \sin(z\sqrt{r} \sin \theta/2) \\ &\quad - B_1 \cosh(z\sqrt{r} \cosh \theta/2) \cos(z\sqrt{r} \sin \theta/2) + \frac{4h_{-2} - (M^2 + 2)}{M^2 + 4}, \end{aligned}$$

where  $r = \sqrt{M^2 + 4}$ ,  $\theta = \tan^{-1} 2/M$  and  $A_1$ ,  $B_1$  and  $h_{-2}$  are constants given by

$$\begin{aligned}
 A_1 = & 2 \left[ \frac{2Mh_{-2} + M}{M^2 + 4} \right] [\cos \theta/2 \cosh(\alpha\sqrt{r} \cos \theta/2) \sin(\alpha\sqrt{r} \sin \theta/2) \\
 & - \sin \theta/2 \sinh(\alpha\sqrt{r} \cos \theta/2) \cos(\alpha\sqrt{r} \sin \theta/2) \\
 & - \alpha\sqrt{r} \sinh(\alpha\sqrt{r} \cos \theta/2) \sin(\alpha\sqrt{r} \sin \theta/2)] \\
 & + [\cos \theta/2 \sin(2\alpha\sqrt{r} \sin \theta/2) - \sin \theta/2 \sinh(2\alpha\sqrt{r} \cos \theta/2)], \\
 B_1 = & -2 \left[ \frac{2Mh_{-2} + M}{M^2 + 4} \right] [\sin \theta/2 \cosh(\alpha\sqrt{r} \cos \theta/2) \sin(\alpha\sqrt{r} \sin \theta/2) \\
 & + \cos \theta/2 \sinh(\alpha\sqrt{r} \cos \theta/2) \cos(\alpha\sqrt{r} \sin \theta/2) \\
 & - \alpha\sqrt{r} \cosh(\alpha\sqrt{r} \cos \theta/2) \cos(\alpha\sqrt{r} \sin \theta/2)] \\
 & - [\cos \theta/2 \sin(2\alpha\sqrt{r} \sin \theta/2) - \sin \theta/2 \sinh(2\alpha\sqrt{r} \cos \theta/2)], \\
 h_{-2} = & \left\{ \frac{2M^2 + 4}{M^2 + 4} - \frac{2M}{M^2 + 4} \left[ \frac{\cos \theta/2 \sinh(2\alpha\sqrt{r} \cos \theta/2) + \sin \theta/2 \sin(2\alpha\sqrt{r} \sin \theta/2)}{-\alpha\sqrt{r} \{ \cosh(2\alpha\sqrt{r} \cos \theta/2) + \cos(2\alpha\sqrt{r} \sin \theta/2) \}} \right. \right. \\
 & \left. \left. - \frac{\cos \theta/2 \sin(2\alpha\sqrt{r} \sin \theta/2) - \sin \theta/2 \sinh(2\alpha\sqrt{r} \cos \theta/2)}{\cos \theta/2 \sin(2\alpha\sqrt{r} \sin \theta/2) - \sin \theta/2 \sinh(2\alpha\sqrt{r} \cos \theta/2)} \right] \right\} \\
 & - \left\{ \frac{8}{M^2 + 4} + \frac{4M}{M^2 + 4} \left[ \frac{\cos \theta/2 \sinh(2\alpha\sqrt{r} \cos \theta/2) + \sin \theta/2 \sin(2\alpha\sqrt{r} \sin \theta/2)}{-\alpha\sqrt{r} \{ \cosh(2\alpha\sqrt{r} \cos \theta/2) + \cos(2\alpha\sqrt{r} \sin \theta/2) \}} \right. \right. \\
 & \left. \left. - \frac{\cos \theta/2 \sin(2\alpha\sqrt{r} \sin \theta/2) - \sin \theta/2 \sinh(2\alpha\sqrt{r} \cos \theta/2)}{\cos \theta/2 \sin(2\alpha\sqrt{r} \sin \theta/2) - \sin \theta/2 \sinh(2\alpha\sqrt{r} \cos \theta/2)} \right] \right\}
 \end{aligned}$$

Putting  $M = 0$ , the values of  $f'_{-1}(z)$ ,  $g_{-1}(z)$  and  $h_{-2}$  reduce to those obtained by Kreith & Peube (1965)

Solving the system (II) we have

$$f_0 = g_0 = h_{-1} = 0$$

On solving system (III) we have

$$\begin{aligned}
 f'_1(z) = & A_2 \cosh(z\sqrt{r} \cos \theta/2) \cos(z\sqrt{r} \sin \theta/2) \\
 & + B_2 \sinh(z\sqrt{r} \cos \theta/2) \sin(z\sqrt{r} \sin \theta/2) - \frac{Mh_1}{M^2 + 4}, \\
 g_1(z) = & A_2 \sinh(z\sqrt{r} \cos \theta/2) \sin(z\sqrt{r} \sin \theta/2) \\
 & - B_2 \cosh(z\sqrt{r} \cos \theta/2) \cos(z\sqrt{r} \sin \theta/2) + \frac{2h_1}{M^2 + 4},
 \end{aligned}$$

where

$$\begin{aligned}
 A_2 = & \left[ \frac{2Mh_1}{M^2+4} \right] [\cos \theta/2 \cosh(\alpha\sqrt{r} \cos \theta/2) \sin(\alpha\sqrt{r} \sin \theta/2) \\
 & - \sin \theta/2 \sinh(\alpha\sqrt{r} \cos \theta/2) \cos(\alpha\sqrt{r} \sin \theta/2) \\
 & - \left\{ \alpha\sqrt{r} + \frac{K\sqrt{r}}{2} \left( \frac{M^2+4}{Mh_1} \right) \right\} \sinh(\alpha\sqrt{r} \cos \theta/2) \sin(\alpha\sqrt{r} \sin \theta/2)] \\
 & - [\cos \theta/2 \sin(2\alpha\sqrt{r} \sin \theta/2) - \sin \theta/2 \sinh(2\alpha\sqrt{r} \cos \theta/2)], \\
 B_2 = & - \left[ \frac{2Mh_1}{M^2+4} \right] [\sin \theta/2 \cosh(\alpha\sqrt{r} \cos \theta/2) \sin(\alpha\sqrt{r} \sin \theta/2) \\
 & + \cos \theta/2 \sinh(\alpha\sqrt{r} \cos \theta/2) \cos(\alpha\sqrt{r} \sin \theta/2) \\
 & - \left\{ \alpha\sqrt{r} + \frac{K\sqrt{r}}{2} \left( \frac{M^2+4}{Mh_1} \right) \right\} \cosh(\alpha\sqrt{r} \cos \theta/2) \cos(\alpha\sqrt{r} \sin \theta/2)] \\
 & + [\cos \theta/2 \sin(2\alpha\sqrt{r} \sin \theta/2) - \sin \theta/2 \sinh(2\alpha\sqrt{r} \cos \theta/2)], \\
 h_1 = & K\sqrt{r} \{ \cosh(2\alpha\sqrt{r} \cos \theta/2) + \cos(2\alpha\sqrt{r} \sin \theta/2) \} \\
 & + \left[ \frac{K}{M^2+4} \{ \cos \theta/2 \sin(2\alpha\sqrt{r} \sin \theta/2) - \sin \theta/2 \sinh(2\alpha\sqrt{r} \cos \theta/2) \} \right. \\
 & \left. + \frac{2M}{M^2+4} \{ \cos \theta/2 \sinh(2\alpha\sqrt{r} \cos \theta/2) + \sin \theta/2 \sin(2\alpha\sqrt{r} \sin \theta/2) \right. \\
 & \left. - \alpha\sqrt{r} \{ \cosh(2\alpha\sqrt{r} \cos \theta/2) + \cos(2\alpha\sqrt{r} \sin \theta/2) \} \right].
 \end{aligned}$$

Putting  $M = 0$ , the values of  $f'_1(z)$ ,  $g_1(z)$  and  $h_1$  again reduce to those obtained by Kreith & Peube (1965)

On solving other systems we have

$$f'_n = g_n = 0, \quad (n = 2, 3, \dots)$$

Table 1.  $\alpha = 1$

$z$	$1/Kf'_1(z)$	$M = 0$	$M = 1$	$M = 10$
0.0		0.7278	0.7236	0.6658
0.1		0.7216	0.7177	0.6628
0.2		0.7031	0.6997	0.6535
0.3		0.6716	0.6695	0.6369
0.4		0.6265	0.6259	0.6111
0.5		0.5669	0.5678	0.5736
0.6		0.4915	0.4941	0.5203
0.7		0.3988	0.4026	0.4464
0.8		0.2872	0.2916	0.3414
0.9		0.1549	0.1584	0.1972
1.0		0.0000	0.0000	0.0000

## 4. DISCUSSION

Curves have been drawn showing the variation of  $f'_{-1}(z)$ ,  $g_{-1}(z)$  and  $g_1(z)$  with  $z$  when  $\alpha = 1$  and  $M = 0, 1$  and  $10$ . The variation of  $f'_{-1}(z)$  with  $z$  is shown in table 1.

From figure 1, it is seen that for the magnetic case ( $M = 1$ ) the value of  $f'_{-1}(z)$  is zero at the two disks. It increases rapidly as the non-dimensional

VARIATION OF  $f'_{-1}(z)$  WITH  $z$

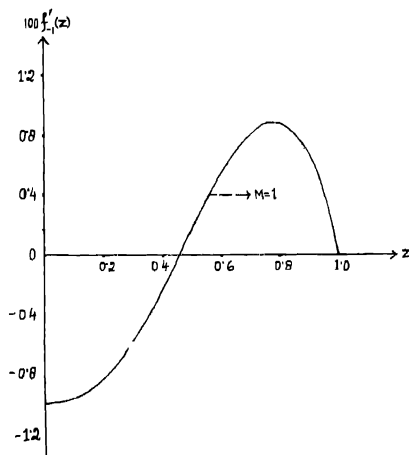


Figure 1

distance from the disks increases from 0 to  $\pm 0.22$ . It attains its greatest value at  $z \simeq 0.78$ . The value then decreases rapidly and again attains zero value at  $z \simeq \pm 0.45$ . It then becomes negative and its numerical value increases in the same manner till it becomes almost constant in the small region midway between the two disks. The curve showing the variation of  $f'_{-1}(z)$  with  $z$  is of an oscillatory nature and is symmetrical about  $z = 0$ .

For the non-magnetic case *i.e.*, when  $M = 0$ ,  $f'_{-1}(z)$  is zero throughout the region between the two disks. We, therefore, infer that the magnetic field increases the value of  $f'_{-1}(z)$  in the regions bounded by  $z \simeq (0.45, 1)$  and  $z \simeq (-0.45, -1)$  while it damps the value of  $f'_{-1}(z)$  in the region  $z \simeq (0.45, -0.45)$ .

Again from table 1 it is observed that the variation of  $f'_1(z)$  with  $z$  for the magnetic and non-magnetic cases is almost the same *i.e.*, the effect of magnetic field on the value of  $f'_1(z)$  is very small. The magnetic field increases and decreases the value of  $f'_1(z)$  in the same regions as it does in the case of  $f'_{-1}(z)$ .

From the above discussion we infer that when  $M = 1$ , the effect of magnetic field is to increase the radial velocity in the regions bounded by  $z \simeq (0.45, 1)$  and  $z \simeq (-0.45, -1)$ , while it damps it in the region bounded by  $z \simeq (0.45, -0.45)$ .

VARIAION OF  $g_{-1}(z)$  WITH  $z$

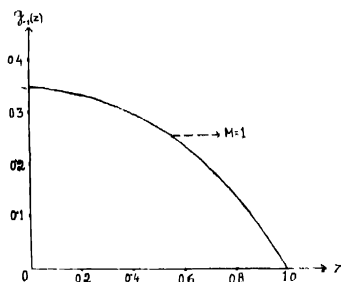


Figure 2

VARIAION OF  $g_1(z)$  WITH  $z$

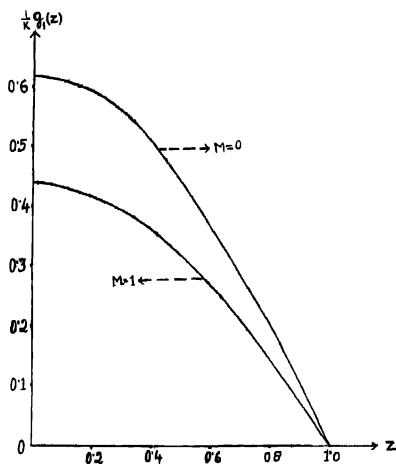


Figure 3

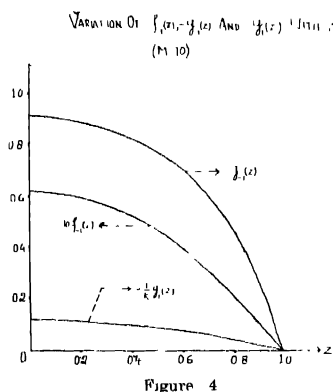
From figures 2 and 3 we observe that the pattern of variation of  $g_{-1}(z)$  and  $g_1(z)$  with  $z$  is almost the same. It is seen that the transverse velocity  $V$  relative



to the disks is always negative and its amplitude is maximum in the region midway between the two disks. It decreases to zero as  $z$  increases from  $z = 0$  to  $z = \pm 1$ . It is obvious from the two figures that the effect of magnetic field is to damp the transverse velocity.

Hence we see that when  $M = 1$ , the effect of magnetic field is similar to that found by Khan (1969) when the transverse magnetic field is small.

Again from figure 4 we see that when  $M = 10$ , the effect of magnetic field is to damp the radial as well as the transverse velocity throughout the region between the two disks.



Hence we may conclude that for small and moderate values of the magnetic parameter  $M$ , the effect of magnetic field is to increase the radial velocity in the region near the two disks, while it damps it in the region midway between the two disks. However, for large values of  $M$  the effect of magnetic field is to damp the radial velocity for every region between the two disks. The effect of the magnetic field on transverse velocity is to damp it for all values of the magnetic parameter  $M$ . The damping effect is large for large values of  $M$  and small for small values of the magnetic parameter.

#### ACKNOWLEDGEMENT

The authors are highly obliged to Professor Ram Ballabh for his kind help and valuable guidance in the preparation of this paper, and to the Council of Scientific and Industrial Research, New Delhi, for awarding them fellowships.

## REFERENCES

- Armstrong H. J. 1952 *An Investigation of the Performance of a Modified Tesla Turbine : M.S Thesis* Mechanical Engineering Department, Georgia Institute of Technology.
- Brentner M. C & Pohlhausen K 1962 *Report No ARL-62-318* Aeronautical Research Laboratory, Wright-Patterson Air Force Base, Ohio.
- Clark R. L & Bromley L. A. 1961 *Chem. Engg. Progress* **57**, 64.
- Graessum N. J & Powell J. W 1964 *Gas Lubricated Bearings*. Butterworth, Washington, D.C.
- Gumbert E. L 1960 *An Investigation of a Turbine with a Suitable Disc. M.S. Thesis*. Engineering Science Department, Arizona State University
- Hasinger S. H. & Kohrt L. A. 1963 *Trans. ASME, Ser.A, Jour. Engg. for Power* **85**, 201
- Khan M. A. A. 1958 *Jour. de Mecanique* **7**, 575; 1969 *ibid* **8**, No. 3.
- Kreith F & Peube J. L. 1965 *C.R. Academie (Paris)* **260**, 5184.
- Peube J. L. & Kreith F 1966 *Jour de Mecanique* **5**, 261
- Rice W. 1963 *Trans. ASME, Ser.A, Jour. Engg. for Power* **85**, 191

# Letters to the Editor

*Indian J. Phys.* **44**, 657-660 (1970).

## Infrared spectrum of dichlorosilicon-phthalocyanine

By S. C. MATHUR AND JAI SINGH

*Physics Department, Indian Institute of Technology,*

*New Delhi, India*

AND

A. C. KRUPNICK

*George C. Marshall Space Flight Center*

*Huntsville, Alabama, U.S.A.*

*(Received 7 June 1971)*

Phthalocyanines belong to an important class of organic photo- and semi-conductors. Besides they are involved in a very important group of biological molecules, chlorophyll and hemoglobin in particular. There is extensive literature on the infrared spectra, between  $4,000\text{ cm}^{-1}$  and  $400\text{ cm}^{-1}$  of  $\alpha$ - and  $\beta$ -polymorphic forms of various phthalocyanines (Gurnovich *et al* 1963; Sidorov & Kotlyar 1961).

Bloor *et al* (1964) have pointed out the major differences between the spectra of metal free and metal phthalocyanines. However, the spectra of metal phthalocyanines are in general very similar to those of the parent. In dichlorosilicon phthalocyanine ( $\text{SiCl}_2\text{Pc}$ ) the central metal atom has two chlorine atoms linked to it. Thus it differs from other metal phthalocyanines, and the situation is quite similar to uranyl phthalocyanine [ $\text{UO}_2\text{Pc}$ ]. The purpose of this note is to report the infrared and far infrared spectra of  $\text{SiCl}_2\text{Pc}$  and to confirm that in the molecule the two chlorine atoms in fact remain attached to the silicon atom. The material under investigation was prepared by heating phthalonitrile, tetrachlorosilane and quinoline in a sealed Carius tube for several hours. The crystalline compound was isolated from the tars by washing with dimethyl formamide and acetone. The method yielded good single crystals of dichlorosilicon-phthalocyanine. Nitrogen analysis: theoretical 18.33 analysed 18.37.

The spectra of the  $\text{SiCl}_2\text{Pc}$  prepared as KBr pellets, were recorded from  $4,000\text{ cm}^{-1}$  to  $300\text{ cm}^{-1}$  on a Perkin Elmer model 521 infrared spectrophotometer, and from  $300\text{ cm}^{-1}$  to  $100\text{ cm}^{-1}$  on a Perkin Elmer model 301 F.I.R. Spectrophotometer. Using the numbering system of Sidorov and Kotlyar (1961) we have

listed various bands of  $\text{SiCl}_2\text{Pc}$ . We have also included in these tables the spectra of  $\text{UO}_2\text{Pc}$  as reported by Bloor *et al* (1964). The I.R. spectrum of dichlorosilicon-phthalocyanine is very similar to  $\text{UO}_2$ - and metal-phthalocyanines (Bloor *et al* 1964) except that some of the bands are slightly shifted in position. The notable difference from metal-phthalocyanines are the strong bands in dichlorosilicon phthalocyanine in the  $600\text{ cm}^{-1}$  and  $350\text{ cm}^{-1}$  region. The situation seems to arise from a shift in the symmetry of the molecule. It is well known (Gurnovich *et al* 1963)

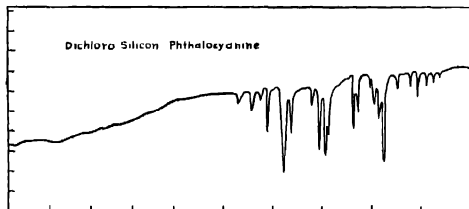


Figure 1. I.R. Spectrum of dichloro-silicon phthalocyanine

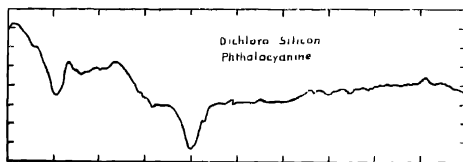


Figure 2. F.I.R. Spectrum of dichloro-silicon phthalocyanine

that in the case of porphyrins one should expect five bands corresponding to N-H vibrations if the symmetry of the molecule is  $C_{2v}$  but only three if the symmetry is  $D_{2h}$ . Therefore, the increase in the number of absorption bands in the case of dichlorosilicon and uranyl phthalocyanines may be due to departure from  $D_{4h}$  molecular symmetry of metal phthalocyanines. This departure is expected towards lower symmetry. This seems reasonable if one remembers that the spectrum of  $\text{SiCl}_2\text{Pc}$  and  $\text{UO}_2\text{Pc}$  are essentially similar to each other and both have two extra atoms besides the central metal atom. However, with the limited evidence it is not possible to assign any specific symmetry to the molecule.

Metal-ligand stretching and bending frequencies are usually few in number, and have been assigned below  $300\text{ cm}^{-1}$ . Our spectra in the  $300\text{ cm}^{-1}$ - $100\text{ cm}^{-1}$  region is the second reported for any of the phthalocyanine. It shows only two clear bands at  $122\text{ cm}^{-1}$  and  $180\text{ cm}^{-1}$ . The bands at  $130\text{ cm}^{-1}$ ,  $142\text{ cm}^{-1}$ ,  $240\text{ cm}^{-1}$  and  $248\text{ cm}^{-1}$  are only speculative and cannot be established firmly. Looking at the spectra reported by Bloor *et al* (1964) along with those reported here one may guess that  $122\text{ cm}^{-1}$  band is a Si-N band and the one at  $180\text{ cm}^{-1}$  is due to Cl-Si-Cl bending frequency.

TABLE 1 Infrared spectra bands in  $\text{cm}^{-1}$

Band No	UO <sub>2</sub> Pc <i>Bloor et al</i>	SiCl <sub>2</sub> Pc	Band No.	UO <sub>2</sub> Pc <i>Bloor et al</i>	SiCl <sub>2</sub> P
32	1605	1605	17a		
31a	1575		17b	1030	1060
31b	1520	1528	16	1020	
31c			15	960	
30a	1510		14	930	912
30b	1490		13	900	880
29			12	868	
28		1171	12		805
27a		1128	9	775	781
27b	1410		8	765	759
37c	1350		7	727	
26	1331	1332	6a	720	731
25			6b	712	
24	1300wk		5	704	
23a	1285	1288	4a	675	
23b			1b	640	644
22a			4c	620	
22b			3		575
21	1150	1162	2a		532
20a			2b	460	464
20b	1120	1120	1a	415	427
19					381
18	1072	1080			

TABLE 2. Far infrared spectra bands in  $\text{cm}^{-1}$

UO <sub>2</sub> Pc <i>Bloor et al</i>	SiCl <sub>2</sub> Pc	UO <sub>2</sub> Pc <i>Bloor et al</i>	SiCl <sub>2</sub> Pc
306	304	244	230*
—	283*	—	180 (Cl-Si-Cl Band)
278s		164ms	—
—		147ms	122
258	250*		

Abbreviations: s-strong, ms-moderately strong.

\*These peaks are very weak and cannot be confirmed beyond doubt.

We wish to thank the National Academy of Science, National Research Council and NASA George C. Marshall Space Flight Center for supporting the work. Our special thanks are due to Sara H. Corbitte for help in taking the I.R. Spectra and to Dr. T. K. Mookherji for helpful discussions.

## REFERENCES

- Bloor J. E., Schlubitz J., Walden C. C. & (in part) Demerdache A. 1964 *Canad. J. Chem.* **42**, 2201  
 Gurnovich G. P., Sevchenko A. N. & Solv'ev K. N. 1963 *Soviet Phys. Usp.* (English Translation) **6**, 173.  
 Sidorov A. N. & Kotlyar I. P. 1961 *Opt. Spectry. U.S.S.R.* (English Translation) **XI**, 175.

*Indian J. Phys.* **44**, 660-663, (1970)

## Crystal and molecular structure of *p*-dimethylamino-benzaldehyde hydrobromide

BY J. K. DATTA GUPTA and N. N. SAHA

*Crystallography and Molecular Biology Division,  
 Saha Institute of Nuclear Physics, Calcutta-9*

(Received 2 March 1971)

*p*-Dimethylaminobenzaldehyde ( $C_9H_{11}NO$ ) is a biologically important compound. Among its various biological functions mention may be made of its special role in differentiating between true scarlet fever and serum eruptions. The structural analysis of this compound in the form of its different hydrohalides and metal complexes has been undertaken by us with an ultimate view to correlate the structural features with biological functions. This short communication deals with the crystal structure of *p*-dimethylaminobenzaldehyde hydrobromide.

The compound was prepared in our laboratory by treating *p*-dimethylaminobenzaldehyde with 30% HBr. Single crystals were grown by slow evaporation of an aqueous solution of this compound between 35°-40°C. The crystals thus grown are needle shaped, *c*-axis being parallel to needle axis. As the crystal was found to be unstable under normal atmospheric condition, it was placed in a sealed thin walled glass capillary while taking X-ray photographs. The crystals belong to monoclinic space group  $P2_1/c$  having unit cell dimensions

$$a = 12.65 \text{ \AA}$$

$$b = 10.20 \text{ \AA}$$

$$c = 7.42 \text{ \AA}$$

$$\beta = 90^\circ 30'$$

Density data ( $\rho_m = 1.54 \text{ gm/cc}$ ,  $\rho_c = 1.59 \text{ gm/cc}$ ) indicate that there are four formula units of  $(C_9H_{11}NO)HBr$  per unit cell. Multiple-film equi-inclination Weissenberg technique was used to collect three-dimensional intensity data for layers

$hk0$  to  $hk5$  and  $h0l$ . The positions of four heavy atoms (bromine) in the unit cell were located from Patterson synthesis projected along  $c$ - and  $b$ -axes. Three dimensional Fourier synthesis was computed with phases of the heavy atom on CDC 3600 using the program written by Blount. A spoke and bead model was constructed at this stage satisfying the stereochemistry

Refinement was carried out by the full matrix least squares method using isotropic temperature factors. Program used was the modified (Srikanta) one of

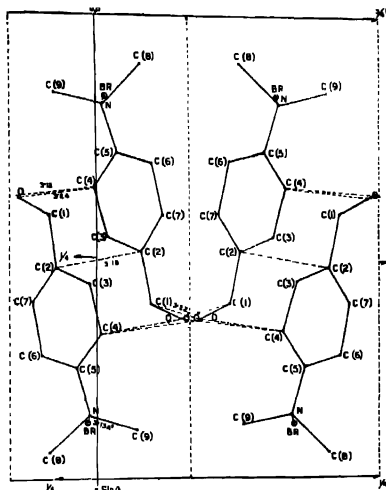


Figure 1. *p*-Dimethylaminobenzaldehyde hydrobromide molecule viewed along  $b$ -axis.

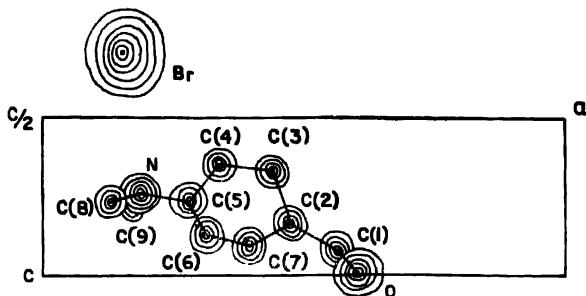


Figure 2. Intermolecular packing projected along  $c^*$ -axis.  $o'$  and  $o''$  refer to the oxygen atoms of the molecules above and below the paper respectively.

Busing, Martin & Levy (1962) A few cycles of refinement brought the discrepancy factor  $R = \frac{\sum ||F_o| - |F_c||}{\sum |F_o|}$  down to 0.16. Further refinement was made using anisotropic temperature factors for the non-hydrogen atoms and the  $R$  value at this stage was 0.11. A difference Fourier synthesis computed at this stage revealed the positions of hydrogen atoms. Taking the contribution of hydrogen atoms, the  $R$  value was 0.10. Atomic parameters and the intramolecular bond lengths are given in tables 1 and 2, respectively. The molecule as viewed down  $b$ -axis has been shown in figure 1. Amino nitrogen atom has tetragonal configuration and is bonded to the benzene ring, two methyl groups and the bromine atom. The bond between the amino nitrogen and bromine atom is a hydrogen bond of the type  $N-H \cdots Br$ , length being  $3.13 \text{ \AA}$ . Least squares and best plane calculations show that the angle between the plane containing dimethyl group  $-N \begin{matrix} \swarrow CH_3 \\ \searrow CH_3 \end{matrix}$  and the plane of the benzene ring is  $61^\circ$ , whereas the aldehyde group  $-C \begin{matrix} \nearrow O \\ \searrow H \end{matrix}$  is almost coplanar with the benzene ring. In a similar structure of Wurster's red bromide (Tanaka *et al* 1968) the dimethyl-amino group is perfectly coplanar with the benzene ring. The molecules are held together in space by a number of Van der Waals bonds between carbon atoms and oxygen atom of adjacent molecules. Three dimensional packing of the molecules is shown in figure 2. A paper in details will be published elsewhere shortly.

TABLE 1. Atomic Parameters

a) *Fractional co-ordinates*

Atom	$x/a$	$y/b$	$z/c$
Br	0.16113	0.02253	0.31758
O	0.62371	0.22132	0.99875
N	0.17272	0.02105	0.73858
C(1)	0.59546	0.14497	0.88826
C(2)	0.48982	0.11714	0.85915
C(3)	0.45969	0.03155	0.72883
C(4)	0.35603	-0.00447	0.68238
C(5)	0.27976	0.05755	0.78086
C(6)	0.30310	0.15014	0.90431
C(7)	0.41073	0.17619	0.94685
C(8)	0.09388	0.12191	0.80171
C(9)	0.15305	-0.11201	0.78936



## (b) Anisotropic temperature coefficients\*

Atom		$\beta_{22}$	$\beta_{33}$	$\beta_{12}$	$\beta_{23}$
Br	0.00482	0.01012	0.01088	-0.00057	-0.00034
O	0.00504	0.00928	0.01968	-0.00289	0.00249
N	0.00064	0.00159	0.00769	0.00048	0.00041
C(1)	0.00192	0.01304	0.00665	0.00056	-0.00264
C(2)	0.00431	0.00601	0.01805	0.00048	0.00050
C(3)	0.00205	0.01087	0.01146	0.00192	0.00095
C(4)	0.00504	0.00719	0.00843	-0.00013	0.00065
C(5)	0.00377	0.00428	0.01632	-0.00076	0.00151
C(6)	0.00035	0.00954	0.00627	-0.00140	-0.00042
C(7)	0.00511	0.00902	0.00610	0.00029	0.00462
C(8)	0.00944	0.00888	0.05073	-0.00384	-0.00033
C(9)	0.00828	0.01257	0.01663	0.00444	0.00205

\*In the expression  $T = \exp[-(\beta_{11}h^2 + \beta_{22}k^2 + \beta_{33}l^2 + 2\beta_{12}hk + 2\beta_{13}hl + 2\beta_{23}kl)]$

TABLE 2. Intramolecular bond lengths and bond angles

Bond length (Å)		Bond angles (degrees)	
Br—N	3.127	Br—N—C(5)	105
O—C(1)	1.184	Br—N—C(8)	106
N—C(5)	1.436	Br—N—C(9)	105
N—C(8)	1.510	C(8)—N—C(9)	116
N—C(9)	1.431	C(8)—N—C(5)	112
C(1)—C(2)	1.381	C(9)—N—C(5)	110
C(2)—C(3)	1.355	C(6)—C(5)—N	122
C(2)—C(7)	1.341	C(4)—C(5)—N	116
C(3)—C(1)	1.402	C(1)—C(5)—C(6)	122
C(4)—C(5)	1.370	C(7)—C(6)—C(5)	119
C(5)—C(6)	1.347	C(3)—C(4)—C(5)	114
C(6)—C(7)	1.420	C(2)—C(7)—C(6)	121
		C(2)—C(3)—C(4)	126
		C(7)—C(2)—C(3)	115
		C(1)—C(2)—C(3)	120
		C(1)—C(2)—C(7)	123
		O—C(1)—C(2)	121

## REFERENCES

- Busing W. R., Martin K. O. & Levy H. A. 1962 *Least Squares Refinement (XPLS) Program*  
 Tanaka J. & Sakabe, N. 1968 *Acta Cryst.* **B24**, 1315

## BOOK REVIEWS

### *Lectures on Quantum Mechanics*

Edited by Gordon Baym, Published by W. A. Benjamin, New York

Pp xi + 594, 1969.

The present book consisting of a self-contained course in quantum mechanics, starting from the first principles to elementary relativistic one-particle mechanics, is suitable mainly at the postgraduate level of the Indian Universities. The author, presumes preliminary knowledge of the introductory concepts and basic postulates of quantum mechanics which are now-a-days taught at the graduate level of many Indian Universities and the book opens directly with a discussion on photon polarization to bring out the essential features of superposition and properties of quantum mechanical states. Although suitable mainly for the postgraduate students the book contains a number of advanced topics which are probably beyond the present postgraduate curriculum of the Indian Universities. The reviewer is particularly happy to note that the topic on second quantization which is usually treated in brief in many modern text books has been given careful and extensive consideration by the author. The author appears to concentrate more on the mathematical methods without using too complicated mathematics and the physics of quantum mechanics has been very skillfully demonstrated in the applications of the quantum mechanical methods for tackling various problems of atomic, nuclear, solid state and chemical physics. It is here and a few other topics where the book probably goes beyond the postgraduate level of the Indian Universities. The inclusion of topics like neutral K-mesons, Cooper pairs, Brillouin-Wigner perturbation theory, spin resonance, Clebsch-Gordan technique, irreducible tensor operators, spatially directed orbitals, hybridization, Lamb shift etc, although extends the standard of the book to an advanced level mainly on the application side, will undoubtedly interest the new workers in the field of both theoretical physics and chemistry.

*U. S. G.*

*Solenoid Magnet Design :*

*The magnetic and mechanical aspects of resistive and superconducting systems .*

D. Bruce Montgomery, pp. 312, \$ 13.95, 1969.

Wiley-Interscience, a division of John Wiley & Sons, New York.

The present volume deals with the design of magnets involving air core coils only. Such coils are divided into three categories, steady state dissipative coils, steady state non-dissipative (superconducting) coils and transient pulse field coils. The different relations between current and central field for coils of various shapes and distributions of currents have been developed as also the relations between current and other basic design parameters like energy, coil volume, magnetic stresses, cooling requirements and current density. The relations between the central field and fields at all other points have also been discussed from the stand point of analysis and synthesis. In addition to the formulae and design charts necessary for designing air core magnets, which are copiously incorporated in the book, it also includes a discussion of the relative importance of the design variables, through formulation, graphs and examples, which will evidently be of much use in particular design. It is obvious from above that the book is a highly useful one for designers of air core magnets.

The author of the book, a wellknown and experienced worker in the field and who has taken great pains in bringing out this volume, should certainly be congratulated.

A. K. D.

*Glass Lasers*

Edited by K. Patek.

Ilife Publications, 1970, 217 pages, £ 6.50.

The book deals with the science of glass lasers. The treatment is balanced, clear and free from irrelevant details. Part 1 discusses electronic spectra of free and doped rare earth ions, energy transfers, non-radiative transitions, and some systematizations regarding structure of glasses. Mathematical deductions have been avoided in the discussion of theories, and the basic ideas and deduced results have been put in a concise form that will be very handy for experimental spectroscopists. The results on emission from doped glasses obtained upto 1967 have been summarized. Part 1 will be of general interest, while Parts 2 and 3 are meant for those connected with the development of optically-pumped lasers. In part 3 the emphasis has been on the theories behind the design of the glass laser that might help the research workers in this field.

M. C.

## ERRATA

Vol. 44, No. 2 p. 129, 2nd para, 3rd line, read "(Plates 3-5)" after "respectively".  
In *Contents* Read "Plate 1" after 2nd article, "Plate 2" after 4th article, "Plates 4-5" after 6th article.

Vol. 44, No. 3 p. 212, beneath date of receipt, and also 2nd para, 6th line, read "Plate 8" instead of "Plate 10".

Vol. 44, No. 5, p. 273, 2nd para, 5th line, read "Plate 9" after "figure 1".


Vol. 44, No. 7, p. 376, 2nd para, last line, read "10-13" after "Plates" instead of "10-13"

Vol. 44, No. 9, p. 504 under heading, date of receipt, read "Plates 14-15" instead of "12-13".

p. 505, 2nd para, 10th line, read "plate 14" instead of "12".

p. 506, last line, read "Plate 15" instead of "13".

*Contents* read "Plates 14-15" instead of "12-13".

Vol. 44, No. 11, p. 593, interchange  Blocks of Figs. 5A and 5B.

Application of Rao's rule to liquified inert gases, 1970, *Indian Journal of Physics*, **44**, No. 2, p. 141 by A. Qadeer, M. N. Sharma and A. S. Varma.

1. Equation (5) i.e.,  $\frac{MC^{\frac{1}{2}}}{d} = R$  for helium should be read as  $\frac{MC^{2/7}}{d} = R$
2. Equation (6) i.e.,  $\frac{MC^{1/3}}{d} = R$  for argon should be read as  $\frac{MC^{2/7}}{d} = R$
3. The value of  $\lambda$  for liquid helium in table I is 3.50 and not 2.0724
4. The value of  $\lambda$  for liquid argon in table I is 3.50 and not 3.0012

The reference of Bergmann L., 1956, *Ultrasonics*, **1L**, has been taken from the book, *Application of Ultrasonics in Molecular Physics* by V. F. Nozdrev (Gordon and Breach 1963) page 225.

## ADDENDUM

Vibrational transition probabilities of the BO $\alpha$ -system, by A. P. Walvekar, *Indian J. Phys.* 1969, **43**, 742.

## ACKNOWLEDGEMENT

The work presented in this paper forms the Ph.D. thesis submitted by the author and accepted by the Karnatak University, Dharwar. The author conveys his grateful thanks to Dr. N. R. Tawde for his guidance and sustained interest in the work.

## INSTRUCTIONS TO AUTHORS FOR PREPARATION OF MANUSCRIPTS

Original scientific papers on all branches of Physics and allied subjects are accepted for publication in INDIAN JOURNAL OF PHYSICS. Short notes, not exceeding in length two printed pages of the Journal, are also accepted for publication. Mss. for publication, in duplicate, should be sent to the Honorary Secretary, Indian Journal of Physics, Indian Association for the Cultivation of Science, Jadavpur, Calcutta-32. These should be type-written with double spacing on one side of good quality bond paper with sufficient margins. Each paper should have a title, the name and full address of the author or authors and an abstract. References in the body of the text should be given by quoting the name of author and year of publication within parentheses; for example, "Thermal transformation..... was studied by Bernal *et al* (1959), and Das Gupta (1960);" or "Thermal decomposition..... studied by different workers (Cuthbert *et al* 1947, Weiden 1954)." The full references should be given at the end under the head REFERENCES, arranged alphabetically by surname followed by initials of the authors, year of publication, standard abbreviated name of journal, the volume and the page; e.g., Perkins H. D. 1950 *Proc. Roy. Soc. A* 203, 309. If more than one paper by the same author occur in the same year, whether in the same journal or not, these should be chronologically signified, both in the text and in the REFERENCES by adding a, b, c, etc., to the year. Positions for figures and diagrams and tables should be indicated in the margin. Line diagrams should be drawn with black Indian ink on white Bristol board, white art paper or good quality tracing paper backed with white paper, and interior of the diagrams should contain minimum number of index letters (bold capital style) or numerals (Roman type). Wherever possible different graphs in the same diagram should be differentiated by full line, dotted line, dashed line, crosses, circles, squares etc. Full captions of all figures with serial numbers should be given in a separate sheet. Numerals for scales and description of coordinates in graphs should be written clearly by the side. Diagram, with index letters and numerals inside them, should be drawn preferably three times the size intended to be reproduced. Photoprints should be contrasting on hard glossy white paper.

MATHEMATICAL SYMBOLS, SUBSCRIPTS AND SUPERSCRIPTS MUST BE CLEAR AND UNAMBIGUOUS. REPETITION OF A COMPLICATED EXPRESSION SHOULD BE AVOIDED BY REPRESENTING IT AS A WHOLE BY A SINGLE DISTINGUISHING SYMBOL. GREEK LETTERS AND UNUSUAL SYMBOLS SHOULD BE EXPLAINED IN THE MARGIN IN WORDS. Fractional exponents should be used instead of root signs. Tables and figures should be numbered by Arabic numerals. Authors should provide a short title of the paper for use on top right hand page of the print. Logarithms of  $N$  to the base ten may be written as  $\log N$ , natural logarithms as  $\ln N$ ; any other base should be specifically indicated. The language of the papers should be concise and clear. The results should be incorporated as far as possible either in the form of graphs or tables, NOT BOTH. The number of tables, diagrams and photographs should not be more than what is absolutely necessary, in view of the fact that the reproduction of these is very costly. If these exceed 20% of the pages of text the authors may be asked to pay for the excess cost.

The galley proof sent to the authors with editorial queries should be carefully checked and corrected to save considerable expense, trouble and delay. Extensive changes or additions should not be made in the proof. Any additional remarks may be made in proof at end of the paper under the head 'Note added in proof'. Authors are supplied with TWENTYFIVE copies of reprints of the paper without cover, free of cost. The cost of additional reprints is Rs. 5/- per page for 50 copies (in minimum units of 25). Authors should return the Reprints Order Form duly filled in, along with the proof sent to them. For obvious reasons no request for additional reprints can be entertained after the final print has gone through the press. The corrections of proofs must be made according to standard press practice.

## CONTENTS

Indian Journal of Physics

Vol. 44, No. 12

December 1970

Pages

SINGH S. N. AND PANDREY R. N.

Entry-length flow in a vertical coiled pipe

617-624

BHAT P. K. AND SRIVASTAVA M. P.

Stability of a Homopolar device

625-634

MURTY K. S. R. AND MOHANTY A. K.

Quadrupole hyperfine effects in microwave spectrum of  $\text{SF}_6\text{Cl}$ 

635-640

PANDE K. P., MISRA K. D. AND SHARMA M. N.

A new logarithmic form of overlap repulsion for the heavier salts

641-646

KHAN M. A. A. AND SRIVASTAVA B. B.

Hydromagnetic source flow

647-658

## LETTERS TO THE EDITORS

MATHUR S. C., SINGH JAI AND KRUPNICK A. C

Infrared spectrum of dichlorosilicon-phthalocyanine

657-660

DATTI GUPTA J. K. AND SAHA N. N.

Crystal and molecular structure of p-dimethyl-amino-benzaldehyde hydrobromide

660-683

## BOOK REVIEWS

684-685

## ERRATA AND ADDENDUM

686